Title

Harnessing Cyclic Alkynes for the Synthesis of Heterocyclic Compounds and Nickel-Catalyzed C–C Bond Forming Reactions From Amide Derivatives

Author

Medina, Jose Miguel

Publication Date

2017

Peer reviewed|Thesis/dissertation

UNIVERSITY OF CALIFORNIA

Los Angeles

Harnessing Cyclic Alkynes for the Synthesis of Heterocyclic Compounds and Nickel-Catalyzed C–C Bond Forming Reactions From Amide Derivatives

A dissertation submitted in partial satisfaction of the

requirements for the degree Doctor of Philosophy

in Chemistry

by

Jose Miguel Medina

2017

ABSTRACT OF THE DISSERTATION

Harnessing Cyclic Alkynes for the Synthesis of Heterocyclic Compounds and Nickel-Catalyzed C–C Bond Forming Reactions From Amide Derivatives

by

Jose Miguel Medina

Doctor of Philosophy in Chemistry

University of California, Los Angeles, 2017

Professor Neil Kamal Garg, Chair

This dissertation describes synthetic endeavors aimed at harnessing the reactivity of arynes and cyclic alkynes toward the synthesis of heterocycles. Arynes and cyclic alkynes are highly reactive intermediates that act as electrophilic arene and alkyne surrogates. Additionally, this dissertation outlines the strategic activation of the amide C–N bond using nickel catalysis. This recently discovered mode of reactivity is strategically employed for the generation of molecular complexity.

Chapter One describes a systematic experimental and computational study of a particularly important class of arynes, 3-halobenzynes. Our efforts show that aryne distortion, rather than steric factors or charge distribution, are responsible for the regioselectivities observed in 3-halobenzyne trapping reactions. Experiments also validate the synthetic utility of 3-

halobenzynes for the synthesis of heterocycles, using a tandem aryne trapping / cross-coupling sequence involving 3-chlorobenzyne.

Chapter Two outlines synthetic studies pertaining to two heterocyclic aryne intermediates: the 2,3-pyridyne and the 4,5-pyrimidyne. 2,3-pyridyne generation and trappings were used to access a variety of functionalized pyridines in a regioselective manner. Additionally, synthetic routes to two isomeric silyltriflates, which were intended to serve as precursors to the 4,5-pyrimidyne, are disclosed. Subsequent 4,5-pyrimidyne generation and trapping experiments were ultimately unfruitful.

Chapter Three reports on the synthesis of poly(benzonorbornadiene) polymers via a strategic blend of benzyne chemistry and ROMP. Through a comparative study, we demonstrate that substitution at the benzylic / allylic position prevents oxidative deformation and polymer decomposition, yet does not inhibit polymerization by common ruthenium catalysts with good control over molecular weight dispersity.

Chapter Four illustrates the strategic use of cyclohexyne and the more elusive intermediate, cyclopentyne, as efficient tools for the synthesis of new heterocyclic compounds with high sp^3 character. Experimental and computational studies of the first 3-substituted cyclohexyne are also described. The observed regioselectivities are explained by the distortion / interaction model.

Chapter Five describes the generation of the first 3,4-piperidyne and its use as a building block for the synthesis of highly decorated piperidines. Experimental and computational studies of this intermediate are disclosed, along with comparisons to the well-known 3,4-pyridyne aromatic analogue. Additionally, the distortion / interaction model is used to explain the observed regioselectivities.

Chapter Six pertains to the generation of two oxacyclic intermediates, the 4,5-benzofuranyne and the 3,4-oxacyclohexyne. In situ trapping of these intermediates affords an array of heterocyclic scaffolds. Across all trapping reactions performed, product distributions are consistent with predictions made with the distortion / interaction model. Oxygen-containing strained intermediates were also found to react with higher selectivities when compared to their corresponding nitrogen-containing analogues.

Chapter Seven depicts the first non-decarbonylative Mizoroki–Heck reactions of imides. The transformation relies on the use of nickel catalysis and proceeds with sterically hindered tri- and tetrasubstituted olefins to yield products containing quaternary centers. Moreover, a diastereoselective variant of this reaction demonstrates its utility for accessing adducts bearing vicinal stereocenters. Our results demonstrate that amide derivatives can be used as building blocks for the assembly of complex scaffolds.

The dissertation of Jose Miguel Medina is approved.

Kendall N. Houk

Jennifer M. Murphy

Neil Kamal Garg, Committee Chair

University of California, Los Angeles

2017

"Energy and persistence conquer all things…"

– Benjamin Franklin

For my parents and brothers: Marco, Sara, Daniel, and Diego

TABLE OF CONTENTS

LIST OF FIGURES

CHAPTER ONE

CHAPTER TWO

CHAPTER FOUR

CHAPTER FIVE

CHAPTER SIX

CHAPTER SEVEN

LIST OF SCHEMES

CHAPTER TWO

CHAPTER FOUR

CHAPTER FIVE

CHAPTER SIX

LIST OF TABLES

CHAPTER ONE

CHAPTER TWO

CHAPTER THREE

CHAPTER FOUR

CHAPTER FIVE

CHAPTER SIX

CHAPTER SEVEN

LIST OF ABBREVIATIONS

Å	angstrom
$[\alpha]_D$	specific rotation at wavelength of sodium D line
Ac	acetyl, acetate
AcOH	acetic acid
α	alpha
APCI	atmospheric pressure chemical ionization
app.	apparent
aq.	aqueous
atm	atmosphere
Bn	benzyl
br	broad
Boc	*tert*-butoxycarbonyl
Bu	butyl
n-Bu	butyl (linear)
t-Bu	*tert*-butyl
c	concentration for specific rotation measurements
°C	degrees Celsius
calcd	calculated
cat.	catalytic
Cbz	carboxybenzyl
COD	1,5-cyclooctadiene

CSA	camphorsulfonic acid
d	doublet, day(s)
DABCO	1,4-diazabicyclo[2.2.2]octane
dba	dibenzylideneacetone
DCE	1,2-dichloroethane
dd	doublet of doublets
DFT	Density functional theory
DIC	*N,N*′-diisopropylcarbodiimide
DMAP	4-dimethylaminopyridine
DME	dimethoxyethane
DMF	*N*,*N*-dimethylformamide
DMI	1,3-dimethyl-2-imidazolidinone
DMSO	dimethyl sulfoxide
dr	diastereomeric ratio
ee	enantiomeric excess
equiv	equivalent
ESI	electrospray ionization
Et	ethyl
g	gram(s)
h	hour(s)
HMDS	hexamethyldisilane
HRMS	high resolution mass spectroscopy
Hz	hertz

IR	infrared (spectroscopy)
IPr	1,3-bis(2,6-di-i-propylphenyl)imidazol-2-ylidene
i-Pr	iso-propyl
J	coupling constant
L	liter
LDA	lithium diisopropylamide
M	molecular mass
m	multiplet or milli
m	meta
m/z	mass to charge ratio
μ	micro
Me	methyl
MHz	megahertz
min	minute(s)
mol	mole(s)
mp	melting point
MS	molecular sieves
NBS	*N*-bromosuccinimide
NMR	nuclear magnetic resonance
o	ortho
p	para
PPA	polyphosphoric acid
Ph	phenyl

pH	hydrogen ion concentration in aqueous solution
PhH	benzene
ppm	parts per million
i-Pr	isopropyl
PSI	pounds per square inch
pyr	pyridine
q	quartet
rt	room temperature
R_f	retention factor
s	singlet
sat.	saturated
SIPr	1,3-bis(2,6-di-i-propylphenyl)-4,5-dihydroimidazol-2-ylidine
t	triplet
TBAF	tetrabutylammonium fluoride
TBAI	tetrabutylammonium iodide
TBS	*tert*-butyldimethylsilyl
TBSCl	*tert*-butyldimethylsilyl chloride
TES	triethylsilyl
Tf	trifluoromethanesulfonyl (trifyl)
TFA	trifluoroacetic acid
THF	tetrahydrofuran
TLC	thin layer chromatography

TMEDA	tetramethylethylenediamine
TMS	trimethylsilyl
TMSCl	trimethylsilyl chloride
TMSOTf	trimethylsiyl triflate
Ts	*p*-toluenesulfonyl (tosyl)
TS	transition state
tt	triplet of triplets
UV	ultraviolet
λ	wavelength

ACKNOWLEDGEMENTS

First and foremost, I'd like to thank Professor Neil K. Garg for being an amazing mentor and advisor. I am tremendously grateful for his role in my development and growth throughout grad school. From helping me put together professional documents and oral presentations, to giving me specific advise regarding research projects, his guidance, mentorship, and support have been instrumental. The operating standards set by him undoubtedly made me a better scientist. He encouraged me to always put my best foot forward and not settle for less. This is something very valuable that I will carry with me for the rest of my life.

I'd like to thank Professors Kendall N. Houk and Heather D. Maynard for our fruitful collaborations. The opportunity to closely interact with them has increased my appreciation for other scientific disciplines and also fostered a sense of community within the Chemistry department. I would also like to acknowledge the members of my thesis committee, Professors Kendall N. Houk, Yi Tang, and Jennifer M. Murphy for providing support and taking the time to serve on my committees.

Professors Simone Aloisio, Blake Gillespie, and Philip Hampton encouraged me to pursue Chemistry as an undergraduate student at CSU, Channel Islands. Their enthusiasm in the classroom was inspirational and a major contributor in my decision to pursue a graduate level education. In particular, I am extremely thankful to Professor Philip Hampton for his support in and out of the laboratory. Phil is incredibly kind, patient, and committed to his role as a mentor. I am very fortunate and grateful to have benefitted from his advice and support.

The projects that contributed to my thesis would have not been possible without the hard work and perseverance of my teammates: Travis C. McMahon, Bryan J. Simmons, Moritz K. Jackl, Robert B. Susick, Tejas K. Shah, Jesus Moreno, and Sophie Racine. I also had the

opportunity to work with talented students from the Houk and Maynard laboratories. I'd like to thank Gonzalo Jiménez-Osés (Houk lab), Joel L. Mackey (Houk lab), Yun-Fang Yang (Houk lab), and Jeong Hoon Ko (Maynard lab) for their time, expertise, and patience in addressing my questions and concerns. I learned a great deal from our interactions and I hope they did as well.

The people I've had the pleasure of working with over the past five years are people I consider great colleagues and life-long friends. The constant guidance and moral support I received from them were paramount in getting me through the unique challenges posed by graduate school. When I joined the lab as a clueless first-year, I had the pleasure of overlapping with the lone survivor of Neil's second graduating class, Alex Huters. I still remember the excitement in lab when Alex finished welwit B. As a timid young student still wondering what I had gotten myself into, the most intimidating class by far was the third graduating class. Grace Chiou seemed to walk around lab with a sense of unshaken confidence. Amanda Silberstein was always hard at work but she knew when to play around in lab, like the time she successfully hid under her desk from Mike Corsello. As the safety officer, Adam Goetz taught me how to appropriately set up my first hydrogenation reaction. He was very stoic, but could not disguise his love for popcorn.

Stephen Ramgren was quite an interesting character. He was always confident in his chemistry knowledge and made this very apparent during group meetings. Our relationship evolved quickly. At first he seemed a bit distant, but once the dust settled he became a great mentor and friend. I benefitted greatly from working next to him for over two years and I am very thankful for that. I now look forward to meeting his dog and drinking beers when I settle in San Diego.

Another fellow lab member currently residing in San Diego is Joel Smith. Joel will go down as the most knowledgeable and creative lab member I overlapped with and I look forward to catching up with him as well. Noah Fine Nathel was very supportive and understanding. As my first student mentor, he was always patient and willing to help me through the problems I encountered early in lab. Evan Styduhar had great taste in music and brewed amazing beer. Tejas Shah was a happy-go-lucky computer wiz who helped me with countless technology related problems and his partner in crime, Liana Hie, was someone I could look up to for motivation on those days I felt particularly sluggish.

Then there is my graduating class: Nick Weires, Mike Corsello, and Jesus Moreno. We went through the journey together and made it out alive! I am thankful to have worked in the same room with all three of them at some point in my time at UCLA. I started out in 5235 with Nick who was the most enthusiastic and energetic of us four. I will always remember our matching mustaches, the mustache party (good times), and the long conversations we used to have over beers at Weyburn. Also, fun fact, Nick and I were almost murdered at a movie theater once.

The next room I worked at really became my home away from home. 5229 is where the toughest and most stressful days of grad school happened. Fortunately I didn't have to struggle alone, Mike-bud and I got through a lot together. We pulled an overnighter once writing our first-year reports, characterizing way too many compounds, and eating hot pockets. We listened to good music, made amazing friends, and shared hilarious jokes that resulted in tears from time to time. Grad school would not have been the same without Mike and I'm very grateful we got to know each other. During my last year I worked in 5234 with Jesus Moreno. Our most memorable moments were certainly at music festivals and concerts around LA. Watching bands like Tame

Impala (three times), Local Natives, and BRMC was a lot of fun, almost as much fun as working on our nickel-Heck project. Our graduating class was very special. I cherish the opportunity I had to learn from Nick, Mike, and Jesus, and I look forward to seeing where life takes them in their personal and professional pursuits.

The next graduating class had the first group of students I could theoretically mentor: Emma Baker-Tripp, Junyong Kim, and Elias Picazo. I didn't get to work in the same room as Emma, but I did enjoy our conversations and going to see scary movies. She frequently brought home-baked pastries to lab, making everyone's day a little bit sweeter. During my 5th year I had the great pleasure of working across Junyong, aka Juney. He never failed to amaze the entire room with his beautiful singing voice rivaled only by Adele herself. The occasional bursts of singing (featuring Lucas Morrill) lightened the mood in the room and were always entertaining. Prior to me joining 5234, I spent most days working right next to Elias. Over time Eli became one of my very best friends and the best little bud (LB) I could ask for. I enjoyed our talks about recent events, music, funny Internet memes/videos, our friends, family, and chemistry. We also explored LA clubs and bars along with Dalton and Rocky (WOES for life, haha). I really enjoyed getting to know Eli and having some of his personality rub off on me. I look forward to being one of the groomsman at his wedding.

The next three students were not only great lab mates, but also fellow 14D Teaching Assistants. Barhopping with Neil around Westwood, dinner with the UA's, and running into our own students at Cabo Cantina were good times I'll look back on and cherish. Bryan Simmons is one of the funniest and most sarcastic guys around. He came up with the best holiday party gift ideas (family picture and face cardboard cutout). Spending a lot of time together in 5229, I quickly discovered he's a softy despite the tough guy persona. Joyann Barber is a really bright

and cheerful person, a talented roller-skater and a big fan of Piology. Her attention to detail made her one of my favorite proofreaders in lab. Lucas Morrill is a passionate singer and beer enthusiast. I'm particularly proud of my role as "wingman" in him meeting a fellow Peruvian, Evelyn. Going out for drinks, making a fool out of myself trying to dance, and getting kicked out of gay bars together was fun (thanks Tejas).

I am also fortunate to overlap with some younger students full of energy and optimism. Jacob Dander, Michael Yamano, and Robert Susick are very close friends and always fun to be around. Jacob and I for some reason are on essentially identical bathroom schedules and we also have similar hobbies. I really enjoy our quality conversations about chemistry, politics, and other shenanigans. Michael is very energetic and always up for trying new things, while Rob is more centered and level headed. They seem to balance each other well, which came in handy during our Vegas trip. I'll miss our Spike ball tournaments and hanging out in and out of lab.

Last but not least, the first years: Sarah Anthony, Margeaux Miller, Tim Boit, and Melissa Ramirez. I am very optimistic and confident in their class, as the four of them are hard working, motivated, and eager to learn. Sarah and Margeaux are the cutest pair of best friends, even cuter than first-year Nick and Mike. Sarah's personality is contagious (in a good way). She is very outgoing and always smiling, even when chemistry is not going so well. Margeaux is more on the shy side of the spectrum. She kindly makes me feel useful by asking for my opinion on things. Tim can be a bit absent-minded at times, which I find amusing, but he is also very intelligent and motivated. And of course, I also really enjoyed getting to know Melissa during my last year in lab.

The undergraduate students I worked with helped keep the lab young and lively. Sarah Anthony, Ashley Pournamdari, JJ Hwang, and Alane Co are talented and determined students

with bright futures ahead. I'd also like to thank the postdocs I got to work with Travis McMahon, Marie Hoffmann, Evan Darzi, and Sophie Racine. The knowledge and friendships they shared with me meant a lot.

Finally, all my accomplishments in grad school would not have been possible without the support of my family and friends. Generally speaking, the worst part about graduate school is how time consuming it can be. I'd like to thank the special people in my life for being understanding of this, and I hope they agree that my last five years at UCLA were well spent. In particular, I'd like to give a special thanks to my parents, Marco and Sara, for all the love and support they provide for my brothers and I. The many sacrifices they have made for us opened many doors and I am extremely grateful for that. Lastly, I'd like to thank my brothers, Daniel and Diego, for being great siblings and always being supportive.

Chapter One is a version of Medina, J. M.; Mackey, J. L.; Garg, N. K.; Houk, K. N. *J. Am. Chem. Soc*. **2014**, *136*, 15798–15805. Medina was responsible for the experimental work. Mackey was responsible for the computational work.

Chapter Two is a version of Medina, J. M.; Jackl, M. K.; Susick, R. B.; Garg, N. K. *Tetrahedron* **2016**, *72*, 3629–3634. Medina, Jackl, and Susick were responsible for the experimental work.

Chapter Three is a version of Medina, J. M.; Ko, J. H.; Maynard, H. D.; Garg, N. K. *Macromolecules* **2017**, *50*, 580–586. Medina and Ko were responsible for the experimental work.

Chapter Four is a version of Medina, J. M.; McMahon, T. C.; Jiménez-Osés, G.; Houk, K. N.; Garg, N. K. *J. Am. Chem. Soc*. **2014**, *136*, 14706–14709. Medina and McMahon were responsible for the experimental work. Jiménez-Osés was responsible for the computational work.

Chapter Five is a version of McMahon, T. C.; Medina, J. M.; Yang, Y.-F.; Simmons, B. J.; Houk, K. N.; Garg, N. K. *J. Am. Chem. Soc*. **2015**, *137*, 4082–4085. McMahon, Medina, and Simmons were responsible for the experimental work. Yang was responsible for the computational work.

Chapter Six is a version of Shah, T. K.; Medina, J. M.; Garg, N. K. *J. Am. Chem. Soc*. **2016**, *138*, 4948–4954. Shah and Medina were responsible for the experimental work.

Chapter Seven is a version of Medina, J. M.; Moreno, J.; Racine, S.; Du, S.; Garg, N. K. *Angew. Chem., Int. Ed.* [Online early access]. DOI: 10.1002/anie.201703174R1. Medina, Moreno, Racine, and Du were responsible for the experimental work.

BIOGRAPHICAL SKETCH

Education:

University of California, Los Angeles, CA

- Ph.D. in Organic Chemistry, anticipated Spring 2017
- Advanced to Candidacy, 09/05/2014
- Cumulative GPA: 3.9/4.0

CSU, Channel Islands, Camarillo, CA

- B.S. in Chemistry, minor in Math – Fall 2011
- *Magna Cum Laude*; Cumulative GPA: 3.8/4.0
- Chemistry Program Honors

Professional and Academic Experience:

Graduate Research Assistant - University of California, Los Angeles, CA

- November 2012 – present; Advisor: Prof. Neil K. Garg.
- Systematically studied the regioselectivities of reactions of 3-halobenzynes and demonstrated the synthetic utility of 3-halobenzynes as building blocks.
- Developed synthetic methods for the synthesis of heterocycles and validated the distortion / interaction model for predicting regioselectivities in reactions of non-aromatic strained alkynes.
- Established routes to the first 3,4-azacyclohexyne and 3,4-oxacyclohexyne precursors and synthesized various piperidine- and dihydropyran-fused heterocycles.
- Discovered the nickel-catalyzed Heck cyclization of activated amides for the synthesis of ketones bearing quaternary stereocenters.

Graduate Teaching Assistant - University of California, Los Angeles, CA

- Undergraduate organic chemistry discussion sections (Winter 2012, Spring 2012, Fall 2012, and Spring 2013).

Undergraduate Research Assistant - CSU, Channel Islands, Camarillo, CA

- Synthesized a series of water-soluble curcumin analogues under the tutelage of Prof. Philip D. Hampton (Fall 2010 – Spring 2012).

Undergraduate Research Assistant - CSU, Channel Islands, Camarillo, CA

- Chemistry and Math courses (Fall 2010 – Spring 2012).

Honors and Awards:

- 2010 Merck Index Award for Outstanding Student, CSU Channel Islands, 2010
- Graduation Honors: *Magna Cum Laude*, CSU Channel Islands, 2012
- Chemistry Program Honors, CSU Channel Islands, 2012
- UCLA NSF AGEP Competitive Edge Award, UCLA, 2012
- Eugene V. Cota-Robles Research Fellowship, UCLA, 2012 – 2016
- Glenn T. Seaborg Symposium 1st Place Poster Prize, UCLA, 2015
- UCLA Travel Grant, UCLA, 2016
- UCLA Dissertation Year Fellowship, UCLA, 2016
- Majeti–Alapati Fellowship, 2016

Publications:

7. **Mizoroki–Heck Cyclization of Amide Derivatives for the Introduction of Quaternary Centers.** Jose M. Medina,† Jesus Moreno,† Sophie Racine, Shuaijing Du, and Neil K. Garg. *Angew. Chem., Int. Ed.* [Online early access]. DOI: 10.1002/anie.201703174R1. (†These authors contributed equally).

6. **Expanding the ROMP Toolbox: Synthesis of Air-Stable Benzonorbornadiene Polymers by Aryne Chemistry.** Jose M. Medina,† Jeong Hoon Ko,† Heather D. Maynard, and Neil K. Garg. *Macromolecules* **2017***, 50,* 580–586. (†These authors contributed equally).

5. **Expanding the Strained Alkyne Toolbox: Generation and Utility of Oxygen-Containing Strained Alkynes.** Tejas K. Shah,† Jose M. Medina,† and Neil K. Garg. *J. Am. Chem. Soc*. **2016**, *138*, 4948–4954. (†These authors contributed equally).

4. **Synthetic Studies Pertaining to the 2,3-Pyridyne and 4,5-Pyrimidyne.** Jose M. Medina, Moritz K. Jackl, Robert B. Susick, and Neil K. Garg. *Tetrahedron* **2016**, *72*, 3629–3634.

3. **Generation and Regioselective Trapping of a 3,4-Piperidyne for the Synthesis of Functionalized Heterocycles.** Travis C. McMahon,† Jose M. Medina,† Yun-Fang Yang, Bryan J. Simmons, K. N. Houk, and Neil K. Garg. *J. Am. Chem. Soc.* **2015**, *137*, 4082–4085. (†These authors contributed equally).

2. **The Role of Aryne Distortions, Steric Effects, and Charges in Regioselectivities of Aryne Reactions.** Jose M. Medina,† Joel L. Mackey,† Neil K. Garg, and K. N. Houk. *J. Am. Chem. Soc.* **2014**, *136*, 15798–15805. (†These authors contributed equally).

1. **Cycloadditions of Cyclohexynes and Cyclopentyne.** Jose M. Medina,† Travis C. McMahon,† Gonzalo Jiménez-Osés, K. N. Houk, and Neil K. Garg. *J. Am. Chem. Soc*. **2014**, *136*, 14706–14709. (†These authors contributed equally).

Presentations:

5. **Cyclic Alkynes as Useful Synthetic Building Blocks.** Jose M. Medina,* and Neil K. Garg. Oral, 252nd ACS National Meeting and Exposition, Philadelphia Convention Center, Philadelphia, PA, United States, August 2016.

4. **Cyclic Alkynes as Useful Synthetic Building Blocks.** Jose M. Medina,* Travis C. McMahon, Bryan J. Simmons, and Neil K. Garg. Poster, 251st ACS National Meeting and Exposition, San Diego Convention Center, San Diego, CA, United States, March 2016.

3. **Strained Alkynes as Useful Synthetic Building Blocks.** Jose M. Medina,* Tejas K. Shah, Robert B. Susick, and Neil K. Garg. Poster, 29th Annual Glenn T. Seaborg Symposium, UCLA, CA, United States, October 2015.

2. **Cyclic Alkynes and Allenes as Useful Synthetic Building Blocks.** Jose M. Medina,* Travis C. McMahon, Evan D. Styduhar, Bryan J. Simmons, Joyann S. Barber, Gonzalo Jiménez-Osés, K. N. Houk, and Neil K. Garg. Poster, 28th Annual Glenn T. Seaborg Symposium, UCLA, CA, United States, November 2014. *1st Place Poster Prize Winner*

1. **Regioselectivities in Reactions of Haloarynes.** Jose M. Medina,* Joel L. Mackey, K. N. Houk, and Neil K. Garg. Poster, 27th Annual Glenn T. Seaborg Symposium, University of California, Los Angeles, CA, United States, October 2013.

CHAPTER ONE

The Role of Aryne Distortion, Steric Effects, and Charges in Regioselectivities of Aryne Reactions

Jose M. Medina, Joel L. Mackey, Neil K. Garg, and K. N. Houk

J. Am. Chem. Soc. **2014**, *136*, 15798–15805.

1.1 Abstract

The distortion / interaction model has been used to explain and predict reactivity in a variety of reactions where more common explanations, such as steric and electronic factors, do not suffice. This model has also provided new fundamental insight into regioselectivity trends in reactions of unsymmetrical arynes, which in turn, has fueled advances in aryne methodology and natural product synthesis. This article describes a systematic experimental and computational study of one particularly important class of arynes, 3-halobenzynes. 3-Halobenzynes are useful synthetic building blocks whose regioselectivities have been explained by several different models over the past few decades. Our efforts show that aryne distortion, rather than steric factors or charge distribution, are responsible for the regioselectivities observed in 3-haloaryne trapping experiments. We also demonstrate the synthetic utility of 3-halobenzynes for the efficient synthesis of functionalized heterocycles, using a tandem aryne trapping / cross-coupling sequence involving 3-chlorobenzyne.

1.2 Introduction

The fundamental understanding of molecular reactivity continues to fuel countless aspects of scientific discovery. One model for understanding reactivity that has recently received great attention is the distortion / interaction model.[1,2,3,4,5,6] The premise of this model, which is also known as the activation–strain model according to Bickelhaupt,[7] divides the activation energy of a bimolecular process into two components: the energy needed to distort reactants to the transition state geometry and the energy of interaction between the distorted fragments. The distortion / interaction model has provided fundamental new insight into chemical reactivity, and has been used to understand and predict reactivities and selectivities in an array of chemical processes, including Diels–Alder, 1,3-dipolar and bioorthogonal cycloadditions,[1] palladium-catalyzed cross-couplings,[2] C–H functionalizations,[3] and epoxidation reactions.[4]

We have recently explored the application of the distortion / interaction model to explain regioselectivity patterns observed in the reactions of certain arynes, especially heterocyclic arynes such as indolynes.[5,6] Although historically avoided because of their high reactivities, a revival of interest in the chemistry of benzynes has occurred in recent decades and benzyne itself may now be exploited in a variety of efficient transformations.[8] Garnering an improved understanding of the reactivity of substituted benzynes should not only facilitate their use in complexity-generating reactions, but may also explain reactivity trends observed over several decades of prior study.

One particular class of substituted benzynes known to react with significant regioselectivities are 3-substituted benzynes (**1.1**, Figure 1.1).[8,9] More specifically, when X is an inductively electron-withdrawing group (e.g., methoxy or halide), nucleophilic attack at C1 is preferred.[10] This leads to the formation of *meta*-substituted products **1.2** rather than *ortho*-

substituted adducts **1.3**. This has been explained by several models. In the *Charge-Controlled Model*,[11] the X group polarizes the triple bond, and nucleophilic addition occurs at the site of greatest positive charge.[12] A related model, based on NBO electron densities of in-plan π-orbitals has been advocated by Ikawa, Akai, and coworkers.[9c,d] Alternatively, nucleophilic attack at C1 might be dictated by steric effects (*Steric Model*).[3] Finally, our groups have shown that the regioselectivities of reactions of hetarynes and other arynes are controlled by *Aryne Distortions*, where a substituent causes a geometrical distortion such that the geometry of the aryne resembles the transition state for nucleophilic attack on one of the carbons.[5] Each of these models provides a useful mnemonic to predict aryne regioselectivities, but the importance of the different factors emphasized by each of these models has not been unambiguously determined. We report a systematic experimental and theoretical study of 3-substituted arynes **1.1**, where X = halide or methoxy, which demonstrates that regioselectivities for these arynes are predominantly controlled by aryne distortions. Moreover, we showcase the synthetic utility of 3-haloarynes for the efficient synthesis of heterocyclic compounds using a tandem aryne trapping / cross-coupling sequence.

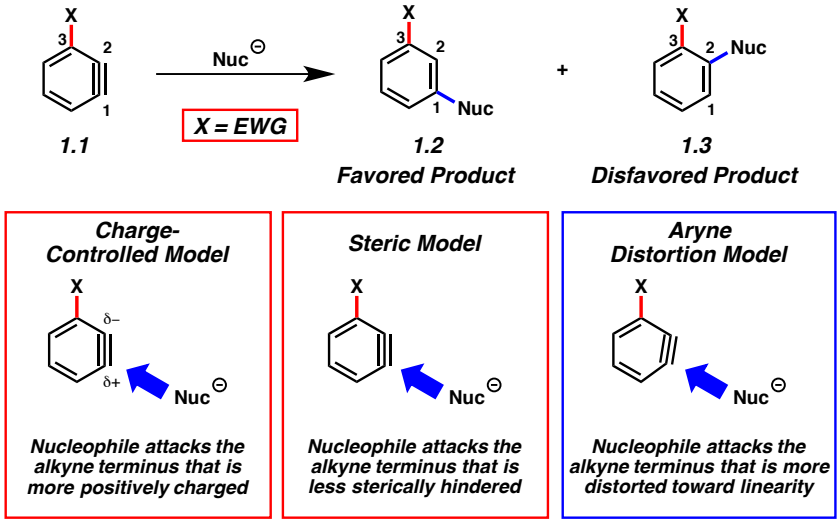

Figure 1.1. Charge-controlled, steric, and aryne distortion models

1.3 Results and Discussion

1.3.1 Aryne Distortion Versus Steric Factors

We first performed computational geometry optimizations of the 3-substituted benzynes **1.1a–1.1e** shown in Figure 1.2. Calculations were carried out using DFT methods (B3LYP/6-311+G(d,p) and LANL2DZ for Br and I atoms). We also studied these arynes and reactants with M06-2X and MP2 and these results are reported and discussed in the Experimental Section.[13,14,15,16] The Experimental Section also provides structural and charge information for each substituted benzyne. Methoxybenzyne (**1.1a**) is well known to react with a high degree of regioselectivity for attack at C1[8] and serves as a useful point of comparison to the corresponding haloarynes **1.1b–1.1e**. Regarding the *Aryne Distortion Model*, a simplified view of this model allows one to make predictions based on an analysis of an optimized geometry of the aryne.[5b,17] The 3-methoxybenzyne (**1.1a**) shows significant distortion; there is a 15° difference in internal angles between C1 and C2. Nucleophilic addition is favored at the more linear terminus, C1, as the transition state distortion energy for attack at this site is lowest.[4] Halobenzynes **1.1b–1.1e** are

all distorted in a similar manner and are all predicted to undergo preferential attack at C1. The degree of regioselectivity is expected to decrease as a function of the electronegativity of the halide going from 3-fluorobenzyne (**1.1b**) to 3-iodobenzyne (**1.1e**), as a consequence of decreased distortion. Although reactions of 3-haloarynes are well known in the literature,[1,18] a systematic study of reactions involving **1.1b**–**1.1e** has not been performed previously.

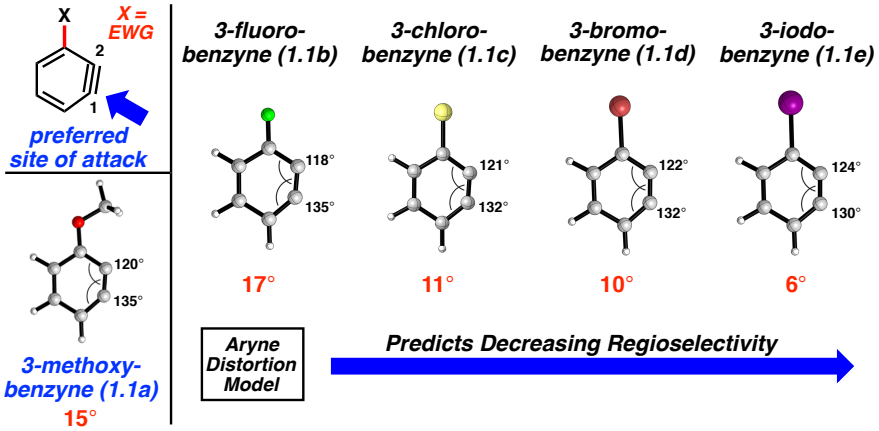

Figure 1.2. Geometry-optimized structures of **1.1a–1.1e** (B3LYP) and regioselectivity predictions for nucleophilic attack based on the aryne distortion model

The regioselectivities of reactions of **1.1a**–**1.1e** using *N*-methylaniline as the trapping agent were determined using both computations and experiments (Table 1.1). The results vary from exclusive attack at C1 for OMe and F, high selectivity with Cl, and less pronounced selectivity with Br and I. Transition state modeling was performed using DFT calculations (B3LYP) for the addition of *N*-methylaniline to C1 or C2 for each aryne. The $\Delta\Delta G^{\ddagger}$ values predict that nucleophilic addition to 3-methoxybenzyne (**1.1a**) and 3-fluorobenzyne (**1.1b**) should be highly regioselective (entries 1 and 2). Decreased regioselectivity was predicted for **1.1c**–**1.1e** (entries 3–5), consistent with the *Aryne Distortion Model* (see Figure 1.2). After

accessing suitable silyltriflate precursors **1.4a–1.4e**, [19, 20] we verified the computational predictions experimentally.[21] The *Steric Model* was deemed inconsequential based on our results and a comparison to A-values, which are 0.15 (fluoride), 0.43 (chloride), 0.38 (bromide), and 0.43 (iodide).[22] The highest selectivity for attack at C1 is observed for the smallest substituent, fluoro **1.4b**. Consequently steric effects are not dictating regioselectivities in reactions of 3-halobenzynes. Previous studies of 3-silylarynes have also shown that steric effects can be outweighed by other factors (i.e., distortion),[6,9a,9b] despite the fact that trialkylsilyl groups have A-values greater than 2.

Table 1.1. Addition of *N*-Methylaniline to Various Benzynes[a]

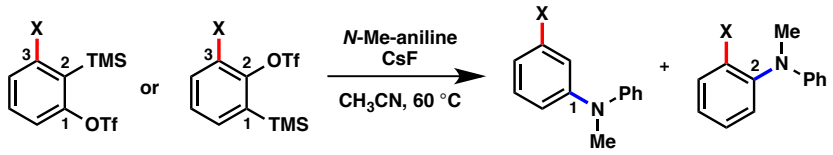

1.4a *1.4b–e* *1.2a–e* *1.3a–e*

Entry	*1.4a–e*	*Computations (ratio 1.2 : 1.3)*	*Yield (ratio 1.2 : 1.3)[b]*
1[a]	***1.4a*** **X = OMe**	**ΔΔG‡ = 5.2 kcal/mol** ***(>500 : 1)***	**94%** ***(1.2a formed exclusively)***
2	***1.4b*** **X = F**	**ΔΔG‡ = 4.1 kcal/mol** ***(>500 : 1)***	**80%** ***(1.2b formed exclusively)***
3	***1.4c*** **X = Cl**	**ΔΔG‡ = 2.4 kcal/mol** ***(57 : 1)***	**66%** ***(>20 : 1)***
4	***1.4d*** **X = Br**	**ΔΔG‡ = 1.4 kcal/mol** ***(11 : 1)***	**67%** ***(13 : 1)***
5	***1.4e*** **X = I**	**ΔΔG‡ = 1.7 kcal/mol** ***(19 : 1)***	**57%** ***(9 : 1)***

[a] Conditions: see experimental section. Computed ratios obtained from Boltzmann factors using B3LYP/6-31G(d) free energies including Conductor-Like Polarizable Continuum Model (CPCM) solvation by CH_3CN. [b] Experimental yields and ratios are the average of three experiments and were determined by ^1H NMR analysis using hexamethylbenzene as an external standard.

The same conclusion was drawn for the trapping of arynes **1.1a**–**1.1e** in azide cycloaddition reactions (Table 1.2).[23] Consistent with computational predictions, 3-methoxybenzyne (**1.1a**) and 3-fluorobenzyne (**1.1b**) react with high regioselectivity (entries 1 and 2, respectively). A sequential decrease in regioselectivity was observed for reactions of arynes **1.1c**–**1.1e**, as the electron-withdrawing effects of the halide substituents decrease from F to Cl to Br to I (entries 3–5, respectively).[24]

Table 1.2. Cycloaddition of Benzylazide with Various Benzynes[a]

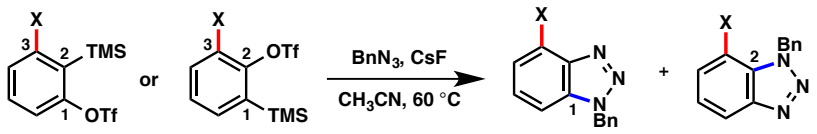

1.4a *1.4b–e* *1.5a–e* *1.6a–e*

Entry	*1.4a–e*	*Computations (ratio 1.5 : 1.6)*	*Yield (ratio 1.5 : 1.6)*[b]
1[a]	***1.4a*** X = OMe	ΔΔG‡ = 3.4 kcal/mol *(292 : 1)*	94% *(1.5a formed exclusively)*
2	***1.4b*** X = F	ΔΔG‡ = 2.5 kcal/mol *(71 : 1)*	68% *(1.5b formed exclusively)*
3	***1.4c*** X = Cl	ΔΔG‡ = 1.4 kcal/mol *(10 : 1)*	53% *(16 : 1)*
4	***1.4d*** X = Br	ΔΔG‡ = 1.2 kcal/mol *(8 : 1)*	45% *(12 : 1)*
5	***1.4e*** X = I	ΔΔG‡ = 0.9 kcal/mol *(5 : 1)*	43% *(6 : 1)*

[a] Conditions: see experimental section. Computed ratios obtained from Boltzmann factors using B3LYP/6-31G(d) free energies including CPCM solvation by CH_3CN; methylazide was used as a model for benzylazide to simplify computational studies. [b] Experimental yields and ratios are the average of three experiments and were determined by ^1H NMR analysis using hexamethylbenzene as an external standard.

1.3.2 The Role of Charges

Having ruled out the importance of the *Steric Model*, we next assessed the role of charges, which have often been used to explain aryne regioselectivities.[3] Indeed it is quite natural

to think of the greater negative charge at the carbon with the smallest angle because that carbon will have more s character in the orbital involved in the in-plane π bond. However, we will argue here that this charge polarization is insufficient to account for observed regioselectivities.

The charge on an atom is not an observable parameter, and there have been different definitions made of charges on atoms. Each of these depends on the definition of the boundaries separating atoms in molecules. Charges derived from a natural bond orbital analysis have been found to be very useful,[25] and we use NBO charges here. Figure 1.3 shows computed Natural Bond Orbital (NBO) charges of *ortho*-benzyne (**1.7**), which were obtained computationally using B3LYP/6-311+G(d,p). The charges found on the triple bond carbons of *ortho*-benzyne (**1.7**) are +0.02. This charge is negligible, and the high electrophilic reactivity of benzyne is not a result of charge effects. For comparison, NBO charges were computed at the same level of theory for acetone. A charge of 0.57 was found for the electrophilic carbon, in agreement with its polarized double bond. Acetone is, however, much less reactive than the nonpolar benzyne, so the magnitude of charge is not an index of reactivity. We next studied the charges of substituted arynes that might have polarized triple bonds to determine if the charges are related to regioselectivity.

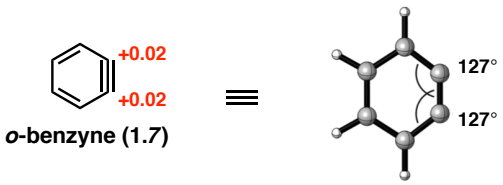

Figure 1.3. Geometry-optimized structures and NBO charges for *o*-benzyne (**1.7**) (B3LYP)

Since many authors use charges for qualitative interpretations, it behooves us to provide a quantitative assessment of such a model and not just invoke the view that theoreticians deny the validity of atomic charges. The charges of 3-fluorobenzyne (**1.1b**) are shown in Figure 1.4. The geometry-optimized structure reveals NBO charges of +0.14 and –0.11 for C1 and C2 respectively. To determine if this charge polarization could be reasonable for the observed regioselectivities, a simple Coulombic interaction model was devised. A point charge of –1 was placed in the benzyne plane at a distance of 2.4 Å from C1. This model is an exaggeration in the localization of charge, but is the extreme case of an anionic nucleophile. The position of the nucleophile charge bisects the C6–C1–C2 angle at C1. The distance between the point charge and C2 is 3.1 Å in this model. Coulomb's law was used to compute the net interaction energy between the point negative charge and benzyne with these charges.[26] This gives an attractive energy of 0.2 kcal/mol at C1 using a dielectric constant of 36, which is appropriate for acetonitrile. The corresponding analysis with a point negative charge 2.4 Å from C2 and a dielectric constant of 36 gives an interaction energy of 0.0 kcal/mol. The electrostatic energy difference for the two modes of attack differ by 0.2 kcal/mol, whereas moderate to high regioselectivities are observed in reactions of all 3-halobenzynes, in addition to computed energy differences that are typically several kcal/mol. We conclude that electrostatic effects are nearly negligible, and in any case too small to explain the regioselectivities. Furthermore, the explanation of regioselectivities of reactions such as cycloadditions by electrostatic effects have long been discredited.[27]

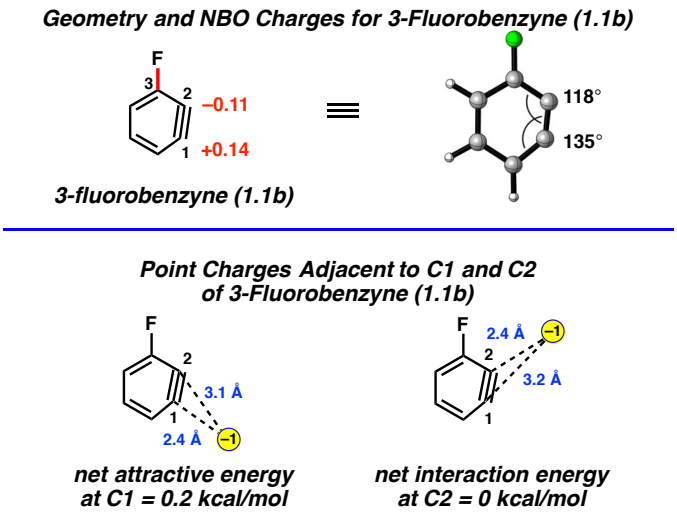

Figure 1.4. Geometry-optimized structure and NBO charges for 3-fluorobenzyne (**1.1b**) (B3LYP) and point charge analysis

We also calculated the electrostatic potentials for interaction of a charge with the full 3-fluorobenzyne (**1.1b**) to compare to our simple Coulombic model, again with a dielectric constant of 36, for acetonitrile. These values are 0.0 kcal/mol at C1 and repulsive by 0.2 kcal/mol at C2. The 0.2 kcal/mol preference for attak at C1 is favored in both models and is not enough to explain the observed regioselectivities. We also performed calculations of this type for 3-chlorobenzyne (**1.1c**). While our simple Coulombic model predicts a 0.1–0.2 kcal/mol preference for attack at C1 (with the charge placed anywhere from 2.0-2.4 Å from the carbon being attacked), the full electrostatic potential calculation predicts a modest 0.2–0.3 kcal/mol preference for attack at C1.

Two additional calculations involving **1.1b** were performed to probe the origin of the small charge polarization shown from NBO charges or electrostatic potentials (Figure 1.5). First, we replaced the F substituent with H, but maintained the geometry of **1.1b**. Despite not having the electron-withdrawing substituent, significant charge polarization was observed (+0.10 for C1

and –0.05 for C2) in the distorted molecule. The negative charge is preferred on C2, the carbon with the smaller angle and greater s character in the in-plane π bond. Additionally, calculations were performed on **1.1b**, but with the geometry restricted to that of benzyne (i.e., 127° internal angle at C1 and C2). Charges of +0.07 and –0.05 for C1 and C2, respectively, were observed. Here the charge polarization due to pure induction without rehybridization is one-half that observed when there is geometrical relaxation. Figure 1.5 also shows color-coded electrostatic potentials on the isodensity surfaces for benzyne (**1.7**) and 3-fluorobenzyne (**1.1b**), in addition to those for benzyne constrained to the 3-fluorobenzyne geometry and for 3-fluorobenzyne constrained to the benzyne geometry. These geometrical constraints have a meaningful influence on the relative electrostatic potential at C1 and C2.

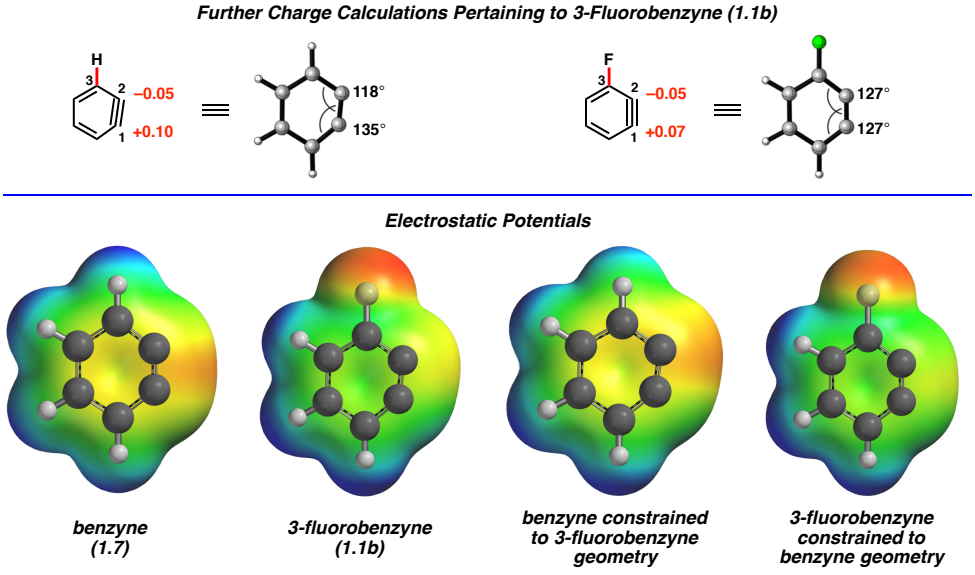

Figure 1.5. NBO charges for **1.1b** separated based on distortion or inductive effects. Electrostatic potentials of benzyne (**1.7**) and 3-fluorobenzyne (**1.1b**). Also shown are electrostatic potentials for benzyne with 3-fluorobenzyne geometry and 3-fluorobenzyne with benzyne geometry (red indicates the lowest electrostatic potential energy, whereas blue indicates the highest)

These findings show that the aryne distortion and inductive effects are synergistic factors contributing to the overall charge polarization. Of course, there is no geometrical distortion until a substituent is added. This geometrical distortion and the small charge polarization are caused by the electronegativity of the substituent. According to Bent's Rule,[28] the bond from C2 to C3 of the aryne will involve a hybrid orbital on C2 with more p character than that on C3. This releases electron density to C3 and its attached electronegative atom. This decreases the C2 bond angle from its natural 127° (see Figure 1.3) toward 90°. The in-plane π orbital between C1 and C2 is polarized toward C2 since C2 will have more s character.

A similar charge analysis was performed for 3-trimethylsilylbenzyne (**1.8**), as shown in Figure 1.6.[6,29] Notably, the distortion and partial charges for **1.8** are reversed in comparison to 3-haloarynes. The charges at C1 and C2 are –0.04 and +0.09, respectively. By replacing the trimethylsilyl group with H, but maintaining the geometric constraints found in **1.8**, the charge distribution was found to be similar (–0.03 and +0.07 at C1 and C2, respectively). Most of the polarization is the result of distortion and rehybridization codified in Bent's rule. Finally, we gauged the electronic influence of the trimethylsilyl group on charge by performing calculations on **1.8** but with the undistorted geometry of benzyne. Only small charges of –0.01 and +0.04 at C1 and C2, respectively, were observed.

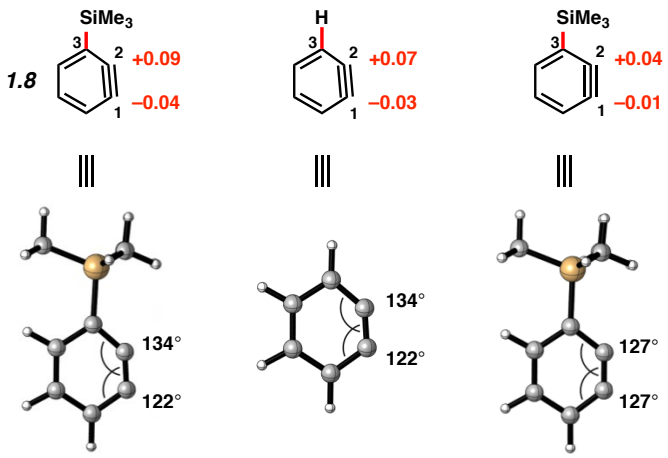

Figure 1.6. Geometry-optimized structure and NBO charges for 3-trimethylsilylbenzyne (**1.8**), in addition to charge distribution due to distortion or inductive effects

These results underscore that the geometrical distortion present in unsymmetrical arynes, and rehybridization that accompanies this distortion, largely contributes to observed charge polarization. The small degree of charge polarization is not the sole cause of the observed regioselectivites, and we conclude that the *Charge-Controlled Model* is not sufficient to explain the regioselectivities observed in these unsymmetrical aryne reactions, particularly in the case of 3-halobenzynes. It does, of course, give a qualitatively correct prediction about selectivity, and might be considered a useful mnemonic for this reason. However, it is an example of the "right answer for the wrong reason."

Ikawa, Akai, and coworkers have shown that there is a qualitative correspondence between the NBO electron density of the in-plane aryne π-orbital and the regioselectitivity of nucleophilic attack.[9c,d] Attack occurs at the site of lower NBO electron density. This is presumably related to the lesser closed-shell repulsion that occurs upon overlap of the occupied orbitals of the nucleophile and aryne.

1.3.3 Transition State Analysis and Aryne Distortion

In previous articles,[5] we have shown that the reactant distortion controls regioselectivites by influencing the distortion energies for attack at C1 vs C2. Figure 1.7 shows the geometry of the transition state for methyl azide attack on benzyne (**1.7**). As described earlier, the nucleophilic attack of N1 of the azide occurs at the relatively more linear angle on the benzyne where the π orbital has more p character. The 131° angle is similar to that in benzyne itself (i.e., 127°). The weaker interaction is at the carbon with the angle of 121°.

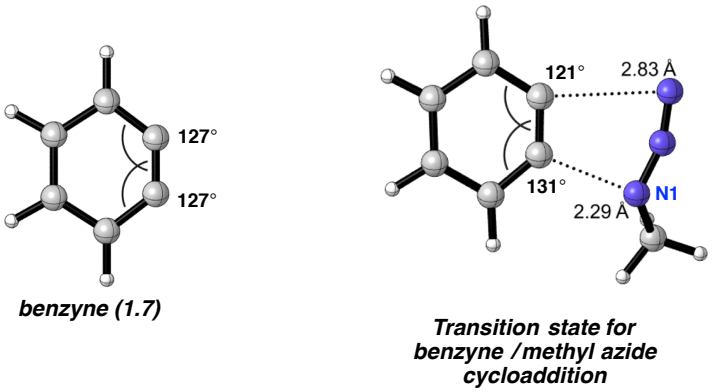

Figure 1.7. Benzyne internal angles and transition state for methyl azide / benzyne cycloaddition

The regioselectivity trends for the reactions of halobenzynes are explained by analysis of the competing transitions states, as shown in Figure 1.8 for 3-fluorobenzyne (**1.1b**) and 3-chlorobenzyne (**1.1c**). In the case of 3-fluorobenzyne (**1.1b**), **TS1** and **TS3** are favored over **TS2** and **TS4**, respectively. The aryne distortion[5] in each of the favored transition states closely resembles the distortion already present in the ground state of aryne **1.1b**. Initial bond formation occurs at C1; the π orbital at this site possesses greater p-character due to the aryne distortion. In the preferred transition states **TS1** and **TS3**, the distortion caused by fluorine is slightly increased

by the attacking azide, but fluorine and the azide are distorting in conflicting manners for the disfavored transition state, **TS4**.

The reactions involving 3-chlorobenzyne (**1.1c**) are analogous. **TS5** and **TS7** are favored over **TS6** and **TS8**, respectively due to the distortion present in **1.1c**. As the atomic radius and A-values for Cl (79 pm and 0.43, respectively) are significantly larger compared to those of F (42 pm and 0.15, respectively), steric effects should be considered as well in the disfavored transition states, **TS6** and **TS8**. Comparisons of **TS2** and **TS6** show that the trajectories for approach of the *N*-Me-aniline nucleophile is nearly identical; additionally, the forming C–N bond distances are nearly the same in both cases (2.12 Å and 2.16 Å, respectively). As such, there is no evidence for steric replusions by chlorine in **TS2** or **TS6**. The comparision of **TS4** and **TS8** reveal slightly different transition states, but the shorter distance of the forming C–N bond at C2 in **TS8** (2.52 Å in **TS4** vs. and 2.35 Å in **TS8**) suggests that steric effects are not a major controlling factor in the reaction of 3-chlorobenzyne. Moreover, as mentioned earlier, if steric factors were the guiding factor in reactions of 3-halobenzynes, a higher preference for reaction at C1 would be expected in trapping experiments of 3-chlorobenzyne (**1.1c**) than with 3-fluorobenzyne (**1.1b**). Experimentally and computationally the opposite trend is observed. We can conclude that although steric factors and charge distribution can make small contributions to the observed regioselectivities, the aryne distortion and the associated transition state distortion play key roles in determining regioselectivity in these trapping experiments.

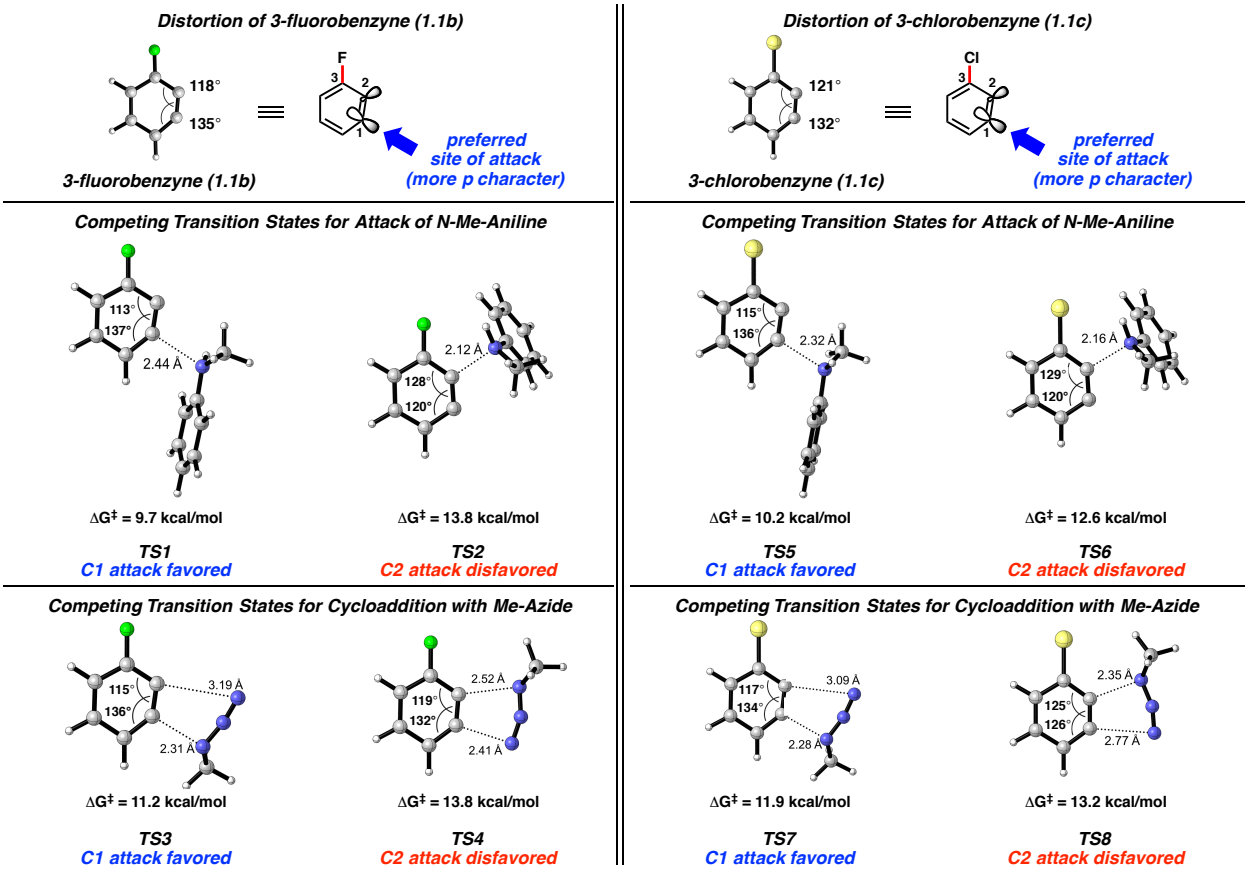

Figure 1.8. Competing transition states for the addition of *N*-methylaniline and methyl azide to 3-fluorobenzyne (**1.1b**) and 3-chlorobenzyne (**1.1c**). Transition states were located using B3LYP/6-311+G(d)

1.3.4 Efficient Synthesis of Heterocyclic Scaffolds

Although trapping experiments of 3-haloarynes have been reported,[8,18] the general synthetic utility of these species has remained underexplored. We hypothesized that 3-halosilyltriflates (and, in turn, the corresponding arynes) could serve as valuable building blocks for the synthesis of functionalized heterocycles. Specifically, it was envisioned that a sequence involving aryne cycloaddition[30] and subsequent metal-catalyzed cross-coupling[31] could allow for the conversion of aryne precursors **1.4** to decorated heterocycles **1.10** in just two steps. In this scenario, the halide would first be used to govern aryne distortion; cycloaddition of the aryne

would then give rise to a heterocyclic product **1.9** with regiocontrol. Finally, the halide would be used as a cross-coupling partner to construct a new C–C or C–N bond and deliver products **1.10**.

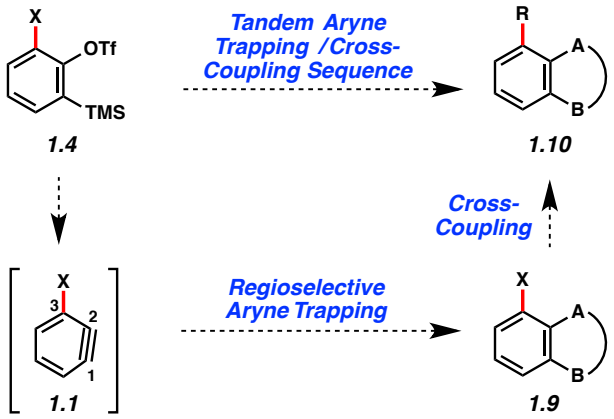

Figure 1.9. Tandem aryne trapping / cross-coupling sequence

We elected to synthesize C4-substituted benzotriazoles as a means to validate the sequence suggested in Figure 1.9. C4-substituted benzotriazoles have been studied as drug candidates, for example in the search for JNK1 inhibitors.[32] As described earlier, the 3-haloarynes readily undergo cycloaddition with benzylazide to give benzotriazole products bearing halide substituents with significant regioselectivities (see Table 1.2). As a challenging test for the cross-coupling part of the sequence, we chose chlorobenzotriazole **1.5c** as the test substrate. Although cross-couplings of aryl chlorides are generally less common compared to couplings of aryl bromides and iodides, conditions for aryl chloride couplings are available. In fact, nickel catalysis can be used for aryl chloride couplings using conventional ligands, including readily available phosphines.[33] As shown in Figure 1.10, **1.5c** could be employed in the Ni-catalyzed Suzuki–Miyaura coupling with heteroaryl boronic acids.[34] The transformation proceeds in the green solvent 2-Me-THF, and gives products **1.11a** and **1.11b** in good yields.

Additionally, the Ni-catalyzed amination [35] of **1.5c** proceeded smoothly to produce aminobenzotriazoles **1.12a** and **1.12b**, also in synthetically useful yields. It should be emphasized that the Ni-catalyzed C–C and C–N bond formations: a) utilize air-stable precatalysts, and thus are carried out on the benchtop, b) are tolerant of the benzotriazole motif, and c) are tolerant of a variety of other heterocycles, as demonstrated by the formation of products **1.11a**, **1.11b**, **1.12a**, and **1.12b**. Therefore, our results not only validate the utility of 3-haloarynes for the construction of functionalized heterocycles, but also showcase the growing value of nickel catalysis in modern cross-coupling reactions.[33]

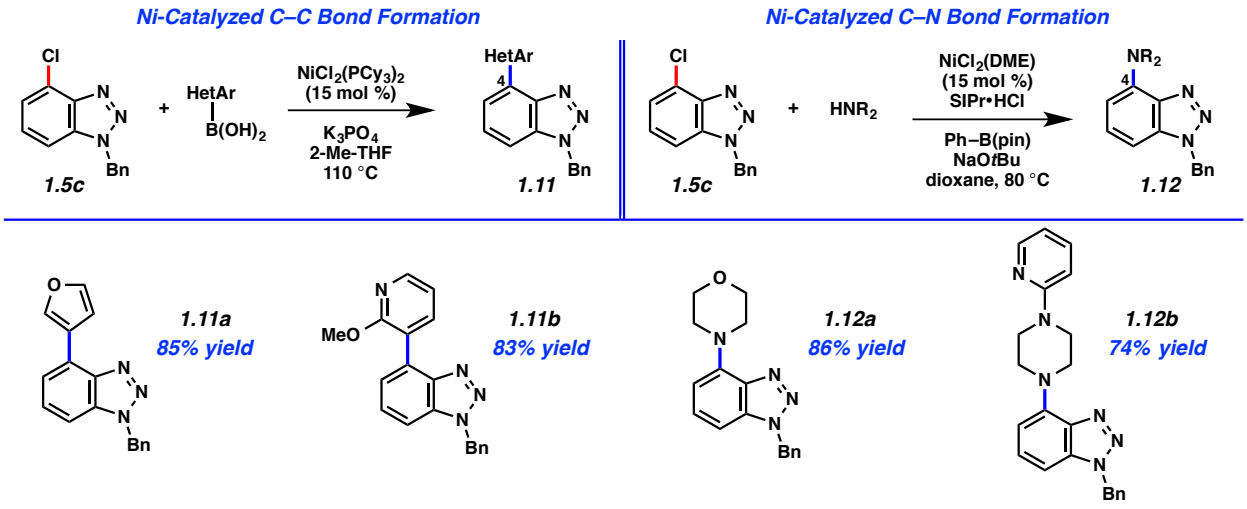

Figure 1.10. Nickel-catalyzed C–C and C–N bond forming reactions for the synthesis of functionalized benzotriazoles **1.11** and **1.12**

1.4 Conclusion

We have compared three commonly used models for rationalizing regioselectivity in reactions of 3-haloarynes. Our experimental and computational study shows that regioselectivity in these systems is explained by the *Aryne Distortion Model*. Moreover, by virtue of the tandem

aryne trapping / cross-coupling sequence developed, we have demonstrated the synthetic utility of 3-haloarynes for the assembly of functionalized heterocyclic compounds. We expect that these studies of reactivity, regioselectivity, and synthetic applications will help propel the use of unsymmetrical arynes in complexity-generating transformations.

1.5 Experimental Section

1.5.1 Materials and Methods

Unless stated otherwise, reactions were conducted in flame-dried glassware under an atmosphere of nitrogen using anhydrous solvents (freshly distilled or passed through activated alumina columns). All commercially obtained reagents were used as received unless otherwise specified. Cesium fluoride (CsF) was obtained from Strem Chemicals and stored on the bench-top at ambient temperature under an N_2 atmosphere. 2,6-Dibromophenol was obtained from Combi-Blocks, Inc. *N*-Phenyl-bis(trifluoromethanesulfonimide) was obtained from Oakwood Products, Inc. Finely powdered anhydrous K_3PO_4 was obtained from Acros Organics. 3-Furanylboronic acid was obtained from Combi-Blocks, Inc. 2-Methoxypyridine-3-boronic acid was obtained from Frontier Scientific. 2-Methyltetrahydrofuran (2-Me-THF), anhydrous, was obtained from Acros Organics. $NiCl_2$(DME) and $NiCl_2(PCy_3)_2$ were obtained from Strem Chemicals. NaO*t*Bu was obtained from Alfa Aesar. Morpholine, 2-pyridylpiperazine, SIPr•HCl, and Ph–B(pin) were obtained from Sigma Aldrich and Alfa Aesar. The following reagents were distilled prior to use: Trifluoromethanesulfonic anhydride (Tf_2O), pyridine, and *tert*-butyldimethylsilyl trifluoromethanesulfonate (TBSOTf). Trimethylsilyl chloride (TMSCl) and tetramethylethylenediamine (TMEDA) were stirred over CaH_2 for 1 h prior to distillation. Dioxane was distilled over sodium benzophenone ketyl. Diethylamine (Et_2NH) was dried over

KOH and then passed over basic Brockman Grade I 58 Å Al_2O_3 (Activity 1). 1,8-Diazabicycloundec-7-ene (DBU), and *N*-methylaniline were dried over 3 Å molecular sieves and then passed over basic Brockman Grade I 58 Å Al_2O_3 (Activity 1) prior to use. *n*-Pentane was dried over $MgSO_4$ prior to use. Reaction temperatures were controlled using an IKAmag temperature modulator and, unless stated otherwise, reactions were performed at room temperature (rt, approximately 23 °C). Thin-layer chromatography (TLC) was conducted with EMD gel 60 F254 pre-coated plates (0.25 mm) and visualized using a combination of UV light and potassium permanganate staining. Silicycle Siliaflash P60 (particle size 0.040–0.063 mm) was used for flash column chromatography. ^{1}H NMR and 2D-NOESY spectra were recorded on Bruker spectrometers (at 300 MHz, 400 MHz, or 500 MHz) and are reported relative to deuterated solvent signals. Data for ^{1}H NMR spectra are reported as follows: chemical shift (δ ppm), multiplicity, coupling constant (Hz) and integration. ^{13}C NMR spectra were recorded on Bruker spectrometers (at 125 MHz) and are reported relative to deuterated solvent signals. Data for ^{13}C NMR spectra are reported in terms of chemical shift and, when necessary, multiplicity, and coupling constant (Hz). IR spectra were recorded on a Perkin-Elmer 100 spectrometer and are reported in terms of frequency of absorption (cm^{-1}). High-resolution mass spectra were obtained on Waters LCT Premier with ACQUITY LC and Thermo Scientific™ Exactive Mass Spectrometers with DART ID-CUBE.

1.5.2 Experimental Procedures

1.5.2.1 Synthesis of 3-Fluorobenzyne Precursor 1.4b

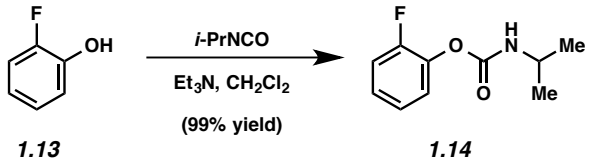

1.13 *1.14*

Fluorocarbamate 1.14. To a stirred solution of 2-fluorophenol (**1.13**) (0.95 mL, 10.6 mmol) in CH_2Cl_2 (35 mL) was added *i*-PrNCO (1.56 mL, 15.9 mmol, 1.5 equiv), followed by Et_3N (0.30 mL, 2.1 mmol, 0.2 equiv). The solution was stirred at 23 °C for 12 h and then quenched with saturated aqueous $NaHCO_3$ (20 mL). The layers were separated, and the aqueous layer was extracted with CH_2Cl_2 (3 x 20 mL). The organic layers were combined and washed with brine (50 mL), and then dried over $MgSO_4$. Evaporation of the solvent under reduced pressure afforded the crude product, which was further purified by flash chromatography (20:1 Hexanes:EtOAc) to furnish carbamate **1.14** (2.09 g, 99% yield) as a white solid. Spectral data match those previously reported.[36]

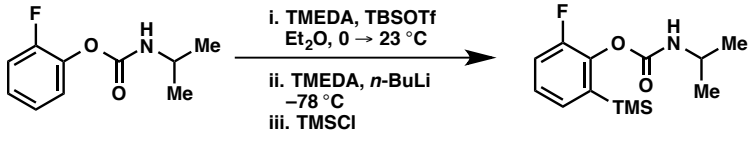

1.14 (93% yield) *1.15*

Fluorosilylcarbamate 1.15. To a solution of fluorocarbamate **1.14** (2.09 g, 10.5 mmol) in diethyl ether (100 mL) at 0 °C was added TMEDA (1.77 mL, 11.8 mmol, 1.1 equiv), followed by a solution of TBSOTf in *n*-pentane (1.30 M, 8.70 mL, 11.8 mmol, 1.1 equiv). The mixture was allowed to stir at 0 °C for 5 min and was then warmed to 23 °C over 30 min. Additional

TMEDA (3.22 mL, 21.4 mmol, 2.0 equiv) was added and the reaction was cooled to –78 °C. A solution of *n*-BuLi in hexanes (2.20 M, 9.75 mL, 21.4 mmol, 2.0 equiv) was added dropwise over 70 min. The mixture was stirred at –78 °C for an additional 1 h and then neat TMSCl (4.76 mL, 37.5 mmol, 3.5 equiv) was added dropwise over 35 min. The resulting mixture was stirred at –78 °C for 85 min, quenched with saturated aqueous $NaHSO_4$ (60 mL), and allowed to warm to 23 °C over 45 min with vigorous stirring. The organic layer was separated, washed successively with 1 M $NaHSO_4$ (60 mL) and brine (60 mL), and then dried over Na_2SO_4. Evaporation under reduced pressure afforded crude product, which was further purified by flash chromatography (95:5 Hexanes:EtOAc) to afford **1.15** (2.62 g, 93% yield) as a white solid. Spectral data match those previously reported.[36]

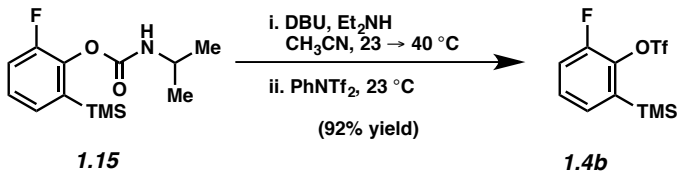

1.15 *1.4b*

Fluorosilyltriflate 1.4b. To a solution of fluorosilylcarbamate **1.15** (2.62 g, 9.7 mmol) in CH_3CN (100 mL) was added DBU (2.20 mL, 14.6 mmol, 1.5 equiv) and Et_2NH (1.20 mL, 11.7 mmol, 1.2 equiv). The resulting mixture was placed in an oil bath maintained at 40 °C for 45 min and then allowed to cool to 23 °C. Next, a solution of $PhNTf_2$ (5.20 g, 14.6 mmol, 1.5 equiv) in CH_3CN (30 mL) was added via cannula over 20 min. After stirring for 2 h, the reaction mixture was washed successively with saturated aqueous $NaHSO_4$ (2 x 60 mL) and 10% aqueous NaOH (2 x 60 mL), and then dried over Na_2SO_4. Evaporation under reduced pressure afforded the crude product, which was further purified by flash chromatography (200:1 Hexanes:Et_2O) to provide fluorosilyltriflate **1.4b** (2.83 g, 92% yield) as a colorless oil. **1.4b**: R_f 0.52 (10:1 Hexanes:Et_2O);

^{1}H NMR (400 MHz, $CDCl_3$): δ 7.36–7.28 (m, 2H), 7.26–7.21 (m, 1H), 0.41 (s, 9H); ^{13}C NMR (125 MHz, $CDCl_3$): δ 153.4 (d, *J* = 254.2), 140.8 (d, *J* = 11.8), 137.3 (d, *J* = 3.1), 131.0 (d, *J* = 4.3), 129.4 (d, *J* = 6.6), 118.9 (q, *J* = 320.3, CF_3), 118.5 (d, *J* = 19.4), 0.4; IR (film): 2961, 1604, 1578, 1420, 1269, 1207 cm^{-1}; HRMS-ESI (*m/z*) $[M - H]^-$ calcd for $C_{10}H_{11}F_4O_3SSi$, 315.01288; found, 315.01429.

1.5.2.2 Synthesis of 3-Chlorobenzyne Precursor 1.4c

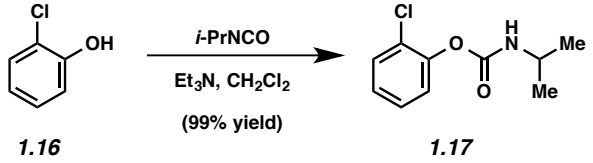

1.16 *1.17*

Chlorocarbamate 1.17. To a stirred solution of 2-chlorophenol (**1.16**) (1.37 g, 10.6 mmol) in CH_2Cl_2 (35 mL) was added *i*-PrNCO (1.56 mL, 15.9 mmol, 1.5 equiv), followed by NEt_3 (0.30 mL, 2.1 mmol, 0.2 equiv). The solution was stirred at 23 °C for 12 h and then quenched with saturated aqueous $NaHCO_3$ (20 mL). The layers were separated, and the aqueous layer was extracted with CH_2Cl_2 (3 x 20 mL). The organic layers were combined and washed with brine (50 mL), and then dried over $MgSO_4$. Evaporation of the solvent under reduced pressure afforded the crude product, which was further purified by flash chromatography (20:1 Hexanes:EtOAc) to furnish chlorocarbamate **1.17** (2.29 g, 99% yield) as a white solid. Spectral data match those previously reported.[37]

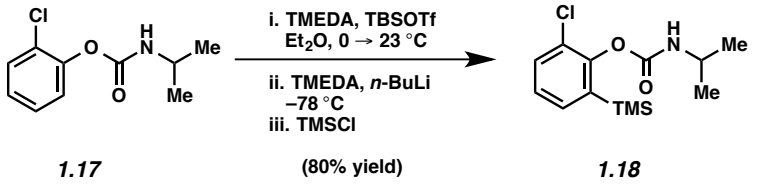

1.17 (80% yield) *1.18*

Chlorosilylcarbamate 1.18. To a solution of chlorocarbamate **1.17** (2.29 g, 10.5 mmol) in diethyl ether (105 mL) at 0 °C was added TMEDA (1.77 mL, 11.8 mmol, 1.1 equiv), followed by a solution of TBSOTf in *n*-pentane (1.30 M, 8.70 mL, 11.8 mmol, 1.1 equiv). The mixture was allowed to stir at 0 °C for 5 min and was then warmed to 23 °C over 30 min. Additional TMEDA (3.22 mL, 21.4 mmol, 2.0 equiv) was added and the reaction was cooled to –78 °C. A solution of *n*-BuLi in hexanes (2.20 M, 9.75 mL, 21.4 mmol, 2.0 equiv) was added dropwise over 70 min. The mixture was stirred at –78 °C for an additional 1 h and then neat TMSCl (4.76 mL, 37.5 mmol, 3.5 equiv) was added dropwise over 35 min. The resulting mixture was stirred at –78 °C for 85 min, quenched with saturated aqueous $NaHSO_4$ (60 mL), and allowed to warm to 23 °C over 45 min with vigorous stirring. The organic layer was separated, washed successively with 1 M $NaHSO_4$ (60 mL) and brine (60 mL), and then dried over Na_2SO_4. Evaporation under reduced pressure afforded crude product, which was further purified by flash chromatography (95:5 Hexanes:EtOAc) to afford chlorosilylcarbamate **1.18** (2.39 g, 80% yield) as a white solid. Spectral data match those previously reported.[37]

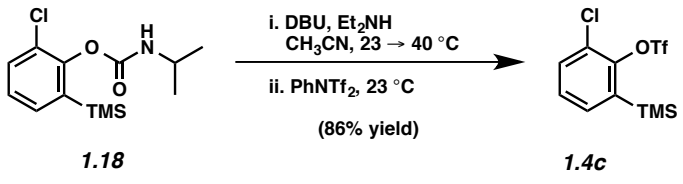

1.18 (86% yield) *1.4c*

Chlorosilyltriflate 1.4c. To a solution of chlorosilylcarbamate **1.18** (2.39 g, 8.36 mmol) in CH_3CN (100 mL) was added DBU (1.87 mL, 12.5 mmol, 1.5 equiv) and Et_2NH (1.04 mL, 10.0

mmol, 1.2 equiv). The resulting mixture was placed in a heating bath maintained at 40 °C for 45 min and then allowed to cool to 23 °C. Next, a solution of $PhNTf_2$ (4.48 g, 12.5 mmol, 1.5 equiv) in CH_3CN (30 mL) was added via cannula over 20 min. After stirring for 2 h, the reaction mixture was washed successively with saturated aqueous $NaHSO_4$ (2 x 60 mL) and 10% aqueous NaOH (2 x 60 mL), and then dried over Na_2SO_4. Evaporation under reduced pressure afforded the crude product, which was further purified by flash chromatography (100% Hexanes) to provide chlorosilyltriflate **1.4c** (2.16 g, 86% yield) as a colorless oil. **1.4c**: R_f 0.55 (200:1 Hexanes:Et_2O); ^{1}H NMR (400 MHz, $CDCl_3$): δ 7.50 (dd, J = 7.8, 1.6, 1H), 7.46 (dd, J = 7.5, 1.6, 1H), 7.31 (t, J = 7.8, 1H), 0.41 (s, 9H); ^{13}C NMR (125 MHz, $CDCl_3$): δ 148.3, 137.7, 135.0, 132.6, 129.0, 127.6, 118.7 (q, J = 320, CF_3), 0.0; IR (film): 2958, 1556, 1397, 1254, 1208 cm^{-1}; HRMS-ESI (*m/z*) $[M + H]^+$ calcd for $C_{10}H_{13}ClF_3O_3SSi$, 332.99898; found, 332.99871.

1.5.2.3 Synthesis of 3-Bromobenzyne Precursor 1.4d

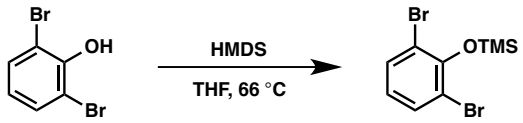

1.19 *1.20*

Silylether 1.20. Silylether **1.20** was prepared following the general procedure described by Díaz.[38] To a solution of 2,6-dibromophenol (**1.19**) (1.09 g, 4.3 mmol) in THF (5 mL) was added HMDS (1.81 mL, 8.7 mmol, 2.0 equiv). The reaction vessel was sealed and placed in an aluminum heating block maintained at 66 °C for 24 h. After cooling to 23 °C, evaporation of the solvent under reduced pressure afforded crude **1.20** as a colorless oil, which was used in the subsequent step without further purification.

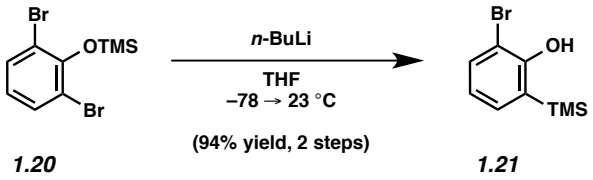

1.20 *1.21*

Bromosilylphenol 1.21. Compound **1.21** was prepared following a modification of the procedure described by Booker.[39] Silylether **1.20** (1.40 g, 4.3 mmol) was dissolved in THF (43 mL) and cooled to –78 °C. A solution of *n*-BuLi in hexanes (2.20 M, 1.97 mL, 4.3 mmol, 1.0 equiv) was added dropwise over 15 min. After stirring at –78 °C for 1 h, the solution was removed from the bath and allowed to warm to 23 °C. After stirring for an additional 4.5 h, the reaction was quenched with saturated aqueous NH_4Cl (30 mL). The biphasic mixture was further diluted with Et_2O (50 mL). The layers were separated, and then the aqueous layer was extracted with Et_2O (3 x 50 mL). The combined organic layers were washed with H_2O (50 mL), and then dried over $MgSO_4$. Evaporation of the solvent under reduced pressure afforded the crude product, which was further purified by flash chromatography (100% Hexanes) to afford **1.21** (1.02 g, 94% yield, 2 steps) as a colorless oil. Spectral data match those previously reported.[39]

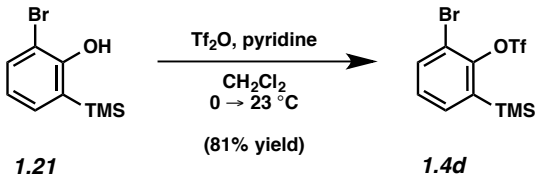

1.21 *1.4d*

Bromosilyltriflate 1.4d. Bromosilyltriflate **1.4d** was prepared following a modified procedure described by Shimizu.[40] To a solution of bromosilylphenol **1.21** (1.00 g, 4.1 mmol) in CH_2Cl_2 (15 mL) at 0 °C was added Tf_2O (1.02 mL, 6.1 mmol, 1.5 equiv) followed by pyridine (1.64 mL, 20.4 mmol, 5.0 equiv). The reaction was stirred at 0 °C for 5 min and then at 23 °C for 16 h. The

reaction was quenched with saturated aqueous $NaHCO_3$ (20 mL). The layers were separated, and the aqueous layer was extracted with hexanes (3 x 20 mL). The combined organic layers were washed with brine (50 mL), and then dried over $MgSO_4$. Evaporation of the solvent under reduced pressure afforded the crude product, which was further purified by flash chromatography (100% Hexanes) to afford bromosilyltriflate **1.4d** (1.25 g, 81% yield) as a colorless oil. Spectral data match those previously reported.[41]

1.5.2.4 Synthesis of 3-Iodobenzyne Precursor 1.4e

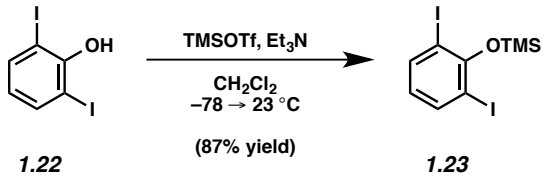

Chlorocarbamate 1.17. To a solution of 2,6-diiodophenol (**1.22**)[42] (2.63 g, 7.6 mmol) in CH_2Cl_2 (20 mL) at –78 °C was added Et_3N (5.90 mL, 42.0 mmol, 5.5 equiv) followed by TMSOTf in *n*-pentane (3.80 M, 16.8 mL, 38.0 mmol, 5.0 equiv) over 20 min. The reaction was stirred at –78 °C for 1 h. After warming to 23 °C, the mixture was loaded directly onto a silica gel column and purified by flash chromatography (100% Hexanes) to afford **1.23** (2.76 g, 87% yield) as a colorless oil. **1.23**: R_f 0.60 (100% Hexanes); ^{1}H NMR (300 MHz, C_6D_6): δ 7.44 (d, J = 7.8, 2H), 5.82 (t, J = 7.9, 1H), 0.44 (s, 9H); ^{13}C NMR (125 MHz, C_6D_6): δ 156.5, 140.2, 125.1, 89.8, 2.8; IR (film): 2954, 1542, 1432, 1267, 1253, 1076 cm^{-1}; HRMS-ESI (*m/z*) $[M + H]^+$ calcd for $C_9H_{13}I_2OSi$, 418.88195; found, 418.88285.

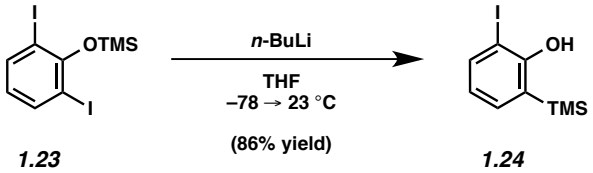

1.23 *1.24*

Iodosilylphenol 1.24. Iodosilylphenol **1.24** was prepared following a modification of the procedure described by Booker.[39] Silylether **1.23** (3.40 g, 8.1 mmol) was dissolved in THF (85 mL) and cooled to –78 °C. A solution of *n*-BuLi in hexanes (2.54 M, 3.20 mL, 8.1 mmol, 1.0 equiv) was added dropwise over 15 min. After stirring at –78 °C for 2 h, the solution was removed from the bath and allowed to warm to 23 °C. After stirring for an additional 4.5 h, the reaction was quenched with H_2O (20 mL) and the biphasic mixture was further diluted with Et_2O (50 mL). The layers were separated, and the aqueous layer was extracted with Et_2O (3 x 50 mL). The combined organic layers were washed with brine (50 mL), and then dried over $MgSO_4$. Evaporation of the solvent under reduced pressure afforded the crude product, which was further purified by flash chromatography (100% Hexanes) to afford **1.24** (2.05 g, 86% yield) as a colorless oil. **1.24**: R_f 0.50 (100% Hexanes); ^{1}H NMR (300 MHz, $CDCl_3$): δ 7.66 (dd, J = 7.9, 1.6, 1H), 7.32 (dd, J = 7.2, 1.5, 1H), 6.66 (t, J = 7.6, 1H), 5.45 (s, 1H), 0.30 (s, 9H); ^{13}C NMR (125 MHz, $CDCl_3$): δ 158.7, 139.5, 135.8, 126.5, 122.3, 87.1, -1.1; IR (film): 3491, 2954, 1576, 1416, 1319, 1229 cm^{-1}; HRMS-ESI (*m/z*) $[M - H]^-$ calcd for $C_9H_{12}IOSi$, 290.9665; found, 290.9714.

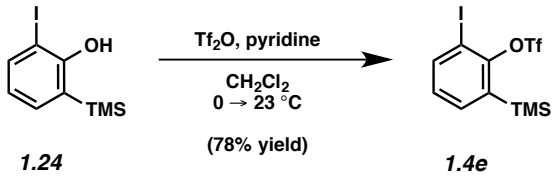

1.24 *1.4e*

Iodosilyltriflate 1.4e. Iodosilyltriflate **1.4e** was prepared following the general procedure described by Shimizu.[40] To a solution of **1.24** (2.05 g, 7.0 mmol) in CH_2Cl_2 (25 mL) at 0 °C was added Tf_2O (1.80 mL, 10.6 mmol, 1.5 equiv) followed by pyridine (2.83 mL, 35.2 mmol, 5.0 equiv). The reaction was stirred at 0 °C for 5 min and then at 23 °C for 16 h. The reaction was quenched with saturated aqueous $NaHCO_3$ (20 mL). The organic layers were separated, and the aqueous layer was extracted with hexane (3 x 20 mL). The organic layers were combined and washed with brine (50 mL), and then dried over $MgSO_4$. Evaporation of the solvent under reduced pressure afforded the crude product, which was further purified by flash chromatography (100% Hexanes) to afford iodosilyltriflate **1.4e** (2.33 g, 78% yield) as a colorless oil. **1.4e**: R_f 0.50 (100% Hexanes); ^{1}H NMR (300 MHz, $CDCl_3$): δ 7.92 (dd, J = 7.7, 1.7, 1H), 7.54 (dd, J = 7.4, 1.7, 1H), 7.07 (t, J = 7.6, 1H), 0.38 (s, 9H); ^{13}C NMR (125 MHz, $CDCl_3$): δ 151.2, 142.6, 137.6, 137.0, 129.4, 118.6 (q, J = 319.6, CF_3), 90.0, 0.3; IR (film): 2957, 1574, 1544, 1401, 1384, 1206 cm^{-1}; HRMS-ESI (*m/z*) $[M + H]^+$ calcd for $C_{10}H_{13}F_3IO_3SSi$, 424.9346; found, 424.9342.

1.5.2.5 *N*-Methylaniline Trapping Experiments

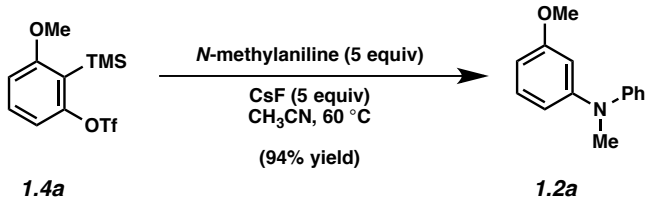

Representative Procedure (Preparation of adduct 1.2a is used as an example). 1.2a (Table 1.1, entry 1) To a stirred solution of silyltriflate **1.4a** (21.0 mg, 0.064 mmol) and *N*-methylaniline (34.5 μL, 0.320 mmol, 5.0 equiv) in CH_3CN (2.50 mL) was added CsF (51.0 mg,

0.320 mmol, 5.0 equiv). The reaction vessel was sealed and placed in an aluminum heating block maintained at 60 °C for 2 h. After cooling to 23 °C, the heterogeneous reaction mixture was filtered over silica gel (EtOAc eluent). Evaporation under reduced pressure afforded the crude product **1.2a** and the yield was determined by ^{1}H NMR analysis using hexamethylbenzene as an external standard (94% yield, average of three experiments). An analytical sample of **1.2a** was isolated as a colorless oil by preparative thin layer chromatography (95:5 Hexanes:EtOAc). Spectral data match those previously reported.[43]

Any modifications of the conditions shown in this representative procedure are specified in the following schemes, which depict all of the results shown in Table 1.1.

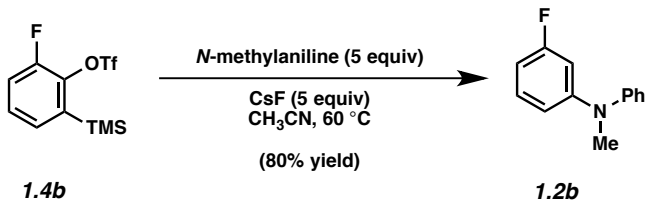

1.4b *1.2b*

1.2b (Table 1.1, entry 2). The yield was determined by ^{1}H NMR analysis using hexamethylbenzene as an external standard (80% yield, average of three experiments). An analytical sample of **1.2b** was isolated as a colorless oil by preparative thin layer chromatography (95:5 Hexanes:EtOAc). **1.2b**: R_f 0.62 (95:5 Hexanes:EtOAc); ^{1}H NMR (500 MHz, $CDCl_3$): δ 7.36–7.32 (m, 2H), 7.17–7.12 (m, 3H), 7.10 (tt, *J* = 7.3, 1.2, 1H), 6.65 (ddd, *J* = 8.4, 2.4, 0.9, 1H), 6.58 (dt, *J* = 12.1, 2.4, 1H), 6.53 (tdd, *J* = 8.3, 2.5, 0.8, 1H), 3.30 (s, 3H); ^{13}C NMR (125 MHz, $CDCl_3$): δ 163.8 (d, *J* = 245.8), 150.9 (d, *J* = 10.4), 148.4, 130.1 (d, *J* = 10.0), 129.7, 123.9, 123.8, 112.9 (d, *J* = 2.6), 106.1 (d, *J* = 21.4), 104.3 (d, *J* = 24.7), 40.4; IR (film):

2917, 1616, 1590, 1492, 1348, 1259 cm^{-1}; HRMS-ESI (*m/z*) $[M + H]^+$ calcd for $C_{13}H_{13}FN$, 202.10265; found, 202.10178.

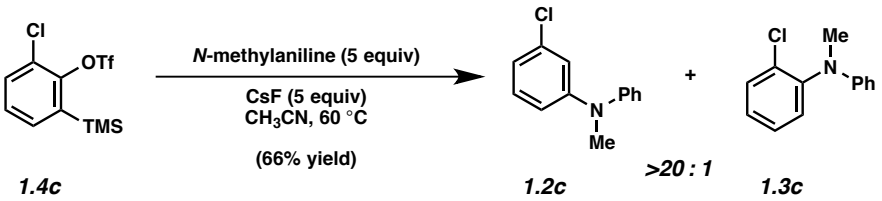

1.2c and 1.3c (Table 1.1, entry 3). The yield and product ratio were determined by ^1H NMR analysis using hexamethylbenzene as an external standard (>20:1 ratio of **1.2c:1.3c**, 66% yield, average of three experiments). Analytical samples of **1.2c** and **1.3c**, both isolated as colorless oils, were obtained by preparative thin layer chromatography (95:5 Hexanes:EtOAc). **1.2c**: R_f 0.50 (95:5 Hexanes:EtOAc); ^1H NMR (500 MHz, $CDCl_3$): δ 7.36–7.32 (m, 2H), 7.15–7.07 (m, 4H), 6.89 (t, *J* = 2.1, 1H), 6.83 (ddd, *J* = 7.9, 2.0, 0.9, 1H), 6.78 (ddd, *J* = 8.4, 2.4, 0.9, 1H), 3.30 (s, 3H); ^{13}C NMR (125 MHz, $CDCl_3$): δ 150.4, 148.4, 134.9, 130.1, 129.7, 123.6, 123.5, 119.6, 117.6, 115.9, 40.4; IR (film): 3063, 2881, 2814, 1583, 1561, 1494 cm^{-1}; HRMS-ESI (*m/z*) $[M + H]^+$ calcd for $C_{13}H_{13}ClN$, 218.07310; found, 218.07204. Spectral data for **1.3c** match those previously reported.[44]

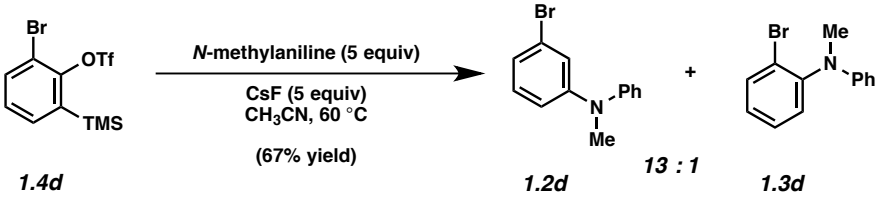

1.2d and 1.3d (Table 1.1, entry 4). To yield and product ratio were determined by ^1H NMR analysis using hexamethylbenzene as an external standard (13:1 ratio of **1.2d:1.3d**, 67% yield, average of three experiments). Analytical samples of **1.2d** and **1.3d**, both isolated as colorless

oils, were obtained by preparative thin layer chromatography (95:5 Hexanes:EtOAc). **1.2d**: R_f 0.52 (95:5 Hexanes:EtOAc); ^{1}H NMR (500 MHz, $CDCl_3$): δ 7.36–7.32 (m, 2H), 7.13–7.04 (m, 5H), 6.98 (br d, *J* = 7.8, 1H), 6.82 (dd, *J* = 8.3, 2.3, 1H), 3.30 (s, 3H); ^{13}C NMR (125 MHz, $CDCl_3$): δ 150.5, 148.3, 130.4, 129.7, 123.6, 123.4, 123.1, 122.6, 120.5, 116.4, 40.4; IR (film): 3062, 2880, 2813, 1582, 1560, 1495 cm^{-1}; HRMS-ESI (*m/z*) [M + H]$^+$ calcd for $C_{13}H_{13}BrN$, 262.02259; found, 262.02160. Spectral data for **1.3d** match those previously reported.[45]

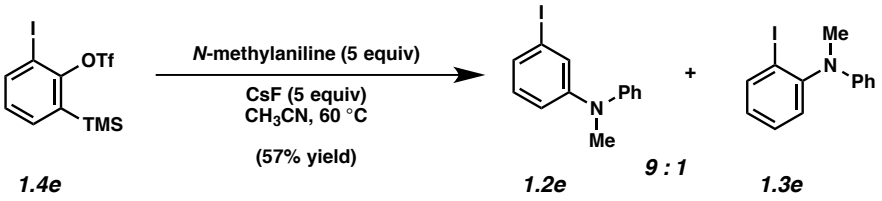

1.2e and 1.3e (Table 1.1, entry 5). The yield and product ratio were determined by ^{1}H NMR analysis using hexamethylbenzene as an external standard (9:1 ratio of **1.2e:1.3e**, 57% yield, average of three experiments). Analytical samples of **1.2e** and **1.3e**, both isolated as colorless oils, were obtained by preparative thin layer chromatography (95.5 Hexanes:EtOAc). **1.2e**: R_f 0.55 (95:5 Hexanes:EtOAc); ^{1}H NMR (500 MHz, $CDCl_3$): δ 7.35–7.31 (m, 2H), 7.26 (app. t, *J* = 2.0, 1H), 7.20 (ddd, *J* = 7.6, 1.6, 1.1, 1H), 7.11–7.06 (m, 3H), 6.93 (dd, *J* = 7.6, 7.6, 1H), 6.87 (ddd, *J* = 8.3, 2.3, 1.0, 1H), 3.29 (s, 3H); ^{13}C NMR (125 MHz, $CDCl_3$): δ 150.4, 148.3, 130.5, 129.7, 128.9, 126.8, 123.4, 123.0, 117.5, 95.1, 40.4; IR (film): 3059, 2877, 2812, 1577, 1555, 1476 cm^{-1}; HRMS-ESI (*m/z*) [M + H]$^+$ calcd for $C_{13}H_{13}IN$, 310.00872; found, 310.01013. Spectral data for **1.3e** match those previously reported.[46]

1.5.2.6 Benzylazide Trapping Experiments

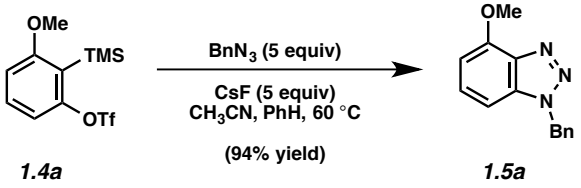

1.4a *1.5a*

Representative Procedure (Preparation of adduct 1.5a is used as an example). 1.5a (Table 1.2, entry 1). To a stirred solution of silyltriflate **1.4a** (19.6 mg, 0.060 mmol) in CH_3CN (2.50 mL) was added a solution of benzylazide[47] in benzene (0.80 M, 0.38 mL, 0.300 mmol, 5.0 equiv) followed by CsF (48.0 mg, 0.300 mmol, 5.0 equiv). The reaction vessel was sealed and placed in an aluminum heating block maintained at 60 °C for 2 h. After cooling to 23 °C, the reaction mixture was filtered over silica gel (EtOAc eluent). Evaporation under reduced pressure afforded the crude product **1.5a** and the yield was determined by ^{1}H NMR analysis using hexamethylbenzene as an external standard (94% yield, average of three experiments). An analytical sample of **1.5a** was isolated as a colorless oil by preparative thin layer chromatography (9:1 Hexanes:EtOAc). Spectral data match those previously reported.[48]

Any modifications of the conditions shown in this representative procedure are specified in the following schemes, which depict all of the results shown in Table 1.2

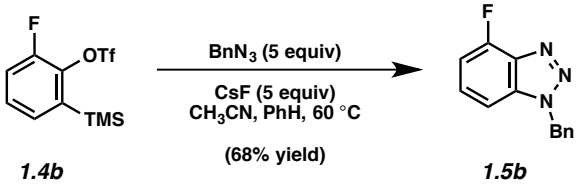

1.4b *1.5b*

1.5b (Table 1.2, entry 2). The yield was determined by ^{1}H NMR analysis using hexamethylbenzene as an external standard (68% yield, average of three experiments). An analytical sample of **1.5b** was isolated as amorphous solids by preparative thin layer chromatography (9:1 Hexanes:EtOAc). **1.5b**: R_f 0.23 (9:1 Hexanes:EtOAc); ^{1}H NMR (500 MHz, $CDCl_3$): δ 7.37–7.31 (m, 4H), 7.29–7.26 (m, 2H), 7.13 (dd, *J* = 8.4, 0.5, 1H), 7.00 (ddd, *J* = 10.1, 7.8, 0.5, 1H), 5.85 (s, 2H); ^{13}C NMR (125 MHz, $CDCl_3$): δ 153.6 (d, *J* = 259.5), 136.8 (d, *J* = 19.0), 135.8 (d, *J* = 6.5), 134.4. 129.2, 128.8, 128.4 (d, *J* = 6.9), 127.7, 108.7 (d, *J* = 17.2), 105.9 (d, *J* = 5.0), 52.7; IR (film): 3088, 3033, 1632, 1594, 1509, 1495 cm^{-1}; HRMS-ESI (*m/z*) [M + H]$^{+}$ calcd for $C_{13}H_{11}FN_3$, 228.09315; found, 228.09291.

The structure of **1.5b** was confirmed by a 2D-NOESY experiment, as the following interaction was observed:

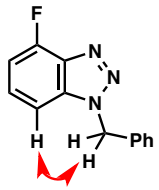

1.5b

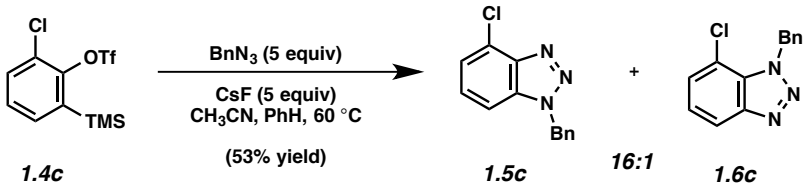

1.4c ***1.5c*** ***16:1*** ***1.6c***

1.5c and 1.6c (Table 1.2, entry 3). The yield and product ratio were determined by ^{1}H NMR analysis using hexamethylbenzene as an external standard (16:1 ratio of **1.5c:1.6c**, 53% yield, average of three experiments). Analytical samples of **1.5c** and **1.6c**, both isolated as amorphous solids, were obtained by preparative thin layer chromatography (7:2:1

Hexanes:EtOAc:Benzene). **1.5c**: R_f 0.25 (9:1 Hexanes:EtOAc); ^{1}H NMR (500 MHz, $CDCl_3$): δ 7.37–7.29 (m, 5H), 7.28–7.23 (m, 3H), 5.85 (s, 2H); ^{13}C NMR (125 MHz, $CDCl_3$): δ 144.2, 134.4, 134.2, 129.2, 128.8, 128.1, 127.7, 125.7, 124.0, 108.6, 52.8; IR (film): 3068, 1610, 1580, 1561, 1495, 1456 cm^{-1}; HRMS-ESI (*m/z*) $[M + H]^+$ calcd for $C_{13}H_{11}ClN_3$, 244.06360; found, 244.06295. **1.6c**: R_f 0.45 (7:2:1 Hexanes:EtOAc:Benzenes); ^{1}H NMR (500 MHz, $CDCl_3$): δ 7.99 (dd, *J* = 8.4, 0.8, 1H), 7.42 (dd, *J* = 7.6, 0.9, 1H), 7.32–7.24 (m, 6H), 6.15 (s, 2H); ^{13}C NMR (125 MHz, $CDCl_3$): δ 147.9, 136.2, 130.2, 129.0, 128.4, 128.3, 127.4, 124.9, 119.1, 116.1, 53.0; IR (film): 3067, 2918, 1575, 1497, 1456, 1442 cm^{-1}; HRMS-ESI (*m/z*) $[M + H]^+$ calcd for $C_{13}H_{11}ClN_3$, 244.06360; found, 244.06316.

The structure of **1.5c** was confirmed by a 2D-NOESY experiment, as the following interaction was observed:

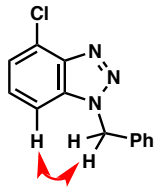

1.5c

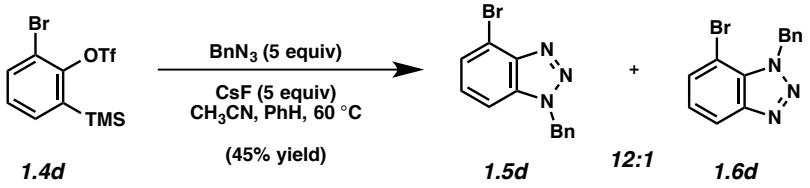

1.4d *1.5d* *12:1* *1.6d*

1.5d and 1.6d (Table 1.2, entry 4). To yield and product ratio were determined by ^{1}H NMR analysis using hexamethylbenzene as an external standard (12:1 ratio of **1.5d:1.6d**, 45% yield, average of three experiments). Analytical samples of **1.5d** and **1.6d**, both isolated as amorphous solids, were obtained by preparative thin layer chromatography (7:2:1

Hexanes:EtOAc:Benzene). **1.5d**: R_f 0.25 (9:1 Hexanes:EtOAc); ^{1}H NMR (500 MHz, $CDCl_3$): δ 7.51 (dd, *J* = 7.0, 1.2, 1H), 7.35–7.28 (m, 4H), 7.27–7.22 (m, 3H), 5.85 (s, 2H); ^{13}C NMR (125 MHz, $CDCl_3$): δ 145.5, 134.4, 133.8, 129.2, 128.8, 128.4, 127.7, 127.2, 113.7, 109.2, 52.9; IR (film): 3067, 3033, 1608, 1580, 1490, 1455 cm^{-1}; HRMS-ESI (*m/z*) $[M + H]^+$ calcd for $C_{13}H_{11}BrN_3$, 288.01309; found, 288.01228. **1.6d**: R_f 0.35 (7:2:1 Hexanes:EtOAc:Benzene); ^{1}H NMR (500 MHz, $CDCl_3$): δ 8.04 (dd, *J* = 8.2, 0.8, 1H), 7.62 (dd, *J* = 7.5, 0.8, 1H), 7.33–7.28 (m, 3H), 7.24–7.21 (m, 3H), 6.19 (s, 2H); ^{13}C NMR (125 MHz, $CDCl_3$): δ 147.6, 136.4, 131.9, 131.5, 128.9, 128.3, 127.2, 125.3, 119.7, 102.6, 52.6; IR (film): 3034, 1607, 1569, 1496, 1455, 1436 cm^{-1}; HRMS-ESI (*m/z*) $[M + H]^+$ calcd for $C_{13}H_{11}BrN_3$, 288.01309; found, 288.01250.

The structure of **1.5d** was confirmed by a 2D-NOESY experiment, as the following interaction was observed:

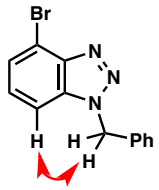

1.5d

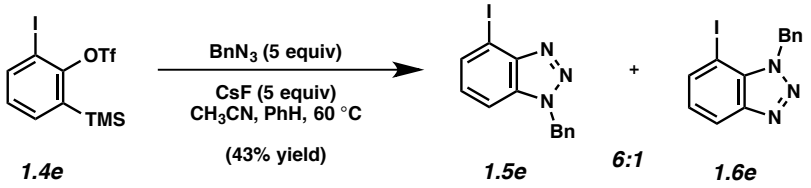

1.4e ***1.5e*** ***6:1*** ***1.6e***

1.5e and 1.6e (Table 1.2, entry 5). The yield and product ratio were determined by ^{1}H NMR analysis using hexamethylbenzene as an external standard (6:1 ratio of **1.5e:1.6e**, 43% yield, average of three experiments). Analytical samples of **1.5e** and **1.6e**, both isolated as colorless oils, were obtained by preparative thin layer chromatography (7:2:1 Hexanes:EtOAc:Benzene).

1.5e: R_f 0.30 (7:2:1 Hexanes:EtOAc:Benzene); ^{1}H NMR (500 MHz, $CDCl_3$): δ 7.76 (dd, *J* = 7.3, 0.8, 1H), 7.33–7.28 (m, 4H), 7.26–7.23 (m, 2H), 7.13 (dd, *J* = 8.4, 7.3, 1H), 5.83 (s, 2H); ^{13}C NMR (125 MHz, $CDCl_3$): δ 147.1, 133.4, 132.6, 131.6, 128.2, 127.7, 127.5, 126.7, 109.0, 84.8, 52.0; IR (film): 1573, 1487, 1456, 1433, 1248 cm^{-1}; HRMS-ESI (*m/z*) $[M + H]^+$ calcd for $C_{13}H_{11}IN_3$, 335.99922; found, 335.99803. **1.6e**: R_f 0.35 (7:2:1 Hexanes:EtOAc:Benzene); ^{1}H NMR (500 MHz, $CDCl_3$): δ 8.09 (dd, *J* = 8.4, 0.9, 1H), 7.92 (dd, *J* = 7.4, 0.8, 1H), 7.33–7.27 (m, 3H), 7.16 (br d, *J* = 7.4, 2H), 7.09 (dd, *J* = 8.3, 7.4, 1H), 6.22 (s, 2H); ^{13}C NMR (125 MHz, $CDCl_3$): δ 145.6, 138.2, 135.4, 133.0, 128.0, 127.2, 126.0, 124.8, 119.7, 70.5, 50.8; IR (film): 3031, 2950, 1601, 1561, 1494, 1484, 1455 cm^{-1}; HRMS-ESI (*m/z*) $[M + H]^+$ calcd for $C_{13}H_{11}IN_3$, 335.99922; found, 335.99835.

The structure of **1.5e** was confirmed by a 2D-NOESY experiment, as the following interaction was observed:

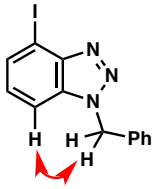

1.5e

1.5.2.7 Derivatization Using Cross-Coupling

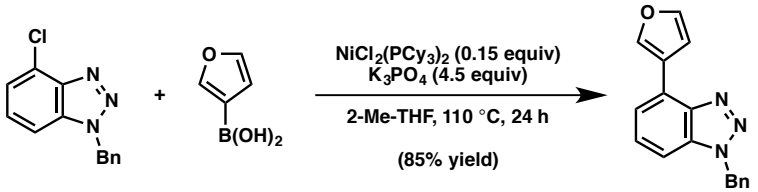

1.5c *1.25* *1.11a*

1.11a (Figure 1.10). The cross-coupling was performed using a general procedure reported by our laboratory.[49] To a 4 mL vial was added anhydrous powdered K_3PO_4 (79.0 mg, 0.370 mmol, 4.5 equiv) and a magnetic stir bar. The vial was then flame-dried under reduced pressure and allowed to cool under N_2. $NiCl_2(PCy_3)_2$ (8.5 mg, 0.012 mmol, 0.15 equiv), boronic acid **1.25** (23.0 mg, 0.205 mmol, 2.5 equiv), and triazole **1.5c** (18.3 mg, 0.075 mmol, 1.0 equiv) were added. The vial was then evacuated and backfilled with N_2. To the vial, 2-Me-THF (0.6 mL) was added and the vial was sealed with a Teflon-lined screw cap. The mixture was stirred at 23 °C for 1 h, and then at 110 °C for 24 h in a preheated aluminum block. After cooling the reaction vessel to 23 °C, the reaction was diluted with 1 M aqueous HCl (1 mL). The layers were separated and the aqueous layer was extracted with EtOAc (3 x 2 mL). The combined organic layers were then dried over $MgSO_4$, filtered by passage through a plug of silica gel (EtOAc eluent, 12 mL), and concentrated under reduced pressure. The crude residue was purified by preparative thin layer chromatography (3:1 Hexanes:EtOAc) to afford **1.11a** (17.5 mg, 85% yield) as a colorless oil: R_f 0.48 (3:1 Hexanes:EtOAc); ^{1}H NMR (500 MHz, $CDCl_3$): δ 8.74 (app. s, 1H), 7.56 (t, J = 1.7, 1H), 7.46 (dd, J = 7.2, 0.9, 1H), 7.40 (dd, J = 8.2, 7.3, 1H), 7.36–7.27 (m, 5H), 7.22 (dd, J = 8.2, 0.9, 1H), 7.05 (dd, J = 1.8, 0.8, 1H), 5.86 (s, 2H); ^{13}C NMR (125 MHz, $CDCl_3$): δ 143.9, 143.4, 143.3, 134.9, 133.5, 129.1, 128.6, 127.8, 127.7, 125.0, 121.9, 120.3,

108.7, 107.9, 52.4; IR (film): 3034, 1611, 1519, 1456, 1164 cm^{-1}; HRMS-ESI (*m/z*) $[M + H]^+$ calcd for $C_{17}H_{14}N_3O$, 276.11314; found, 276.11239.

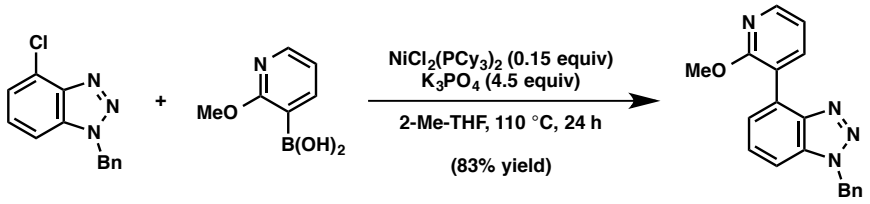

1.5c ***1.26*** ***1.11b***

1.11b (Figure 1.10). The cross-coupling was performed using a general procedure reported by our laboratory.[49] To a 4 mL vial was added anhydrous powdered K_3PO_4 (79.2 mg, 0.370 mmol, 4.5 equiv) and a magnetic stir bar. The vial was then flame-dried under reduced pressure and allowed to cool under N_2. $NiCl_2(PCy_3)_2$ (8.4 mg, 0.012 mmol, 0.15 equiv), boronic acid **1.26** (32.0 mg, 0.205 mmol, 2.5 equiv), and triazole **1.5c** (17.9 mg, 0.074 mmol, 1 equiv) were added. The vial was then evacuated and backfilled with N_2. To the vial, 2-Me-THF (0.6 mL) was added and the vial was sealed with a Teflon-lined screw cap. The mixture was stirred at 23 °C for 1 h, and then at 110 °C for 24 h in a preheated aluminum block. After cooling the reaction vessel to 23 °C, the mixture was diluted with 1 M aqueous HCl (1 mL). The layers were separated and the aqueous layer was extracted with EtOAc (3 x 2 mL). The combined organic layers were then dried over $MgSO_4$, filtered by passage through a plug of silica gel (EtOAc eluent, 12 mL), and concentrated under reduced pressure. The crude residue was further purified by preparative thin layer chromatography (3:1 Hexanes:EtOAc) to afford **1.11b** (19.2 mg, 83% yield) as a colorless oil: R_f 0.23 (3:1 Hexanes:EtOAc); ^1H NMR (500 MHz, $CDCl_3$): δ 8.25 (dd, *J* = 4.9, 2.0, 1H), 8.20 (dd, *J* = 7.3, 2.0, 1H), 7.63 (app. d, *J* = 7.3, 1H), 7.45 (app. t, *J* = 7.9, 1H), 7.36–7.28 (m, 6H), 7.08 (dd, *J* = 7.4, 5.0, 1H), 5.88 (s, 2H), 3.98 (s, 3H); ^{13}C NMR (125 MHz, $CDCl_3$): δ 161.2, 146.7, 145.0, 141.0, 134.9, 133.4, 129.1, 128.9, 128.6, 127.8, 127.3, 125.1, 119.9, 117.1,

109.1, 53.8, 52.5; IR (film): 2949, 1577, 1464, 1396, 1257 cm^{-1}; HRMS-ESI (*m/z*) $[M + H]^+$ calcd for $C_{19}H_{17}N_4O$, 317.13969; found, 317.13870.

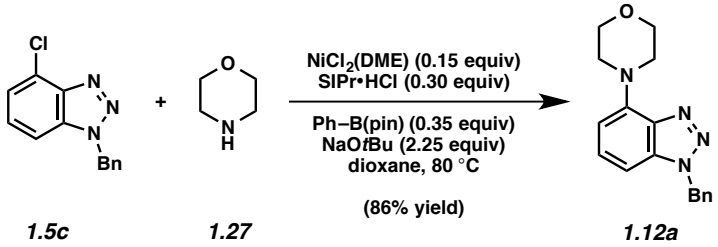

1.5c ***1.27*** ***1.12a***

1.12a (Figure 1.10). The cross-coupling was performed using a general procedure reported by our laboratory.[50] A 4 mL vial containing a magnetic stir bar was flame-dried under reduced pressure and allowed to cool under N_2. The vial was then charged with $NiCl_2$(DME) (2.9 mg, 0.013 mmol, 0.15 equiv), SIPr•HCl (10.7 mg, 0.025 mmol, 0.30 equiv), Ph–B(pin) (5.9 mg, 0.029 mmol, 0.35 equiv), anhydrous powdered NaO*t*Bu (17.7 mg, 0.185 mmol, 2.25 equiv), and triazole **1.5c** (19.3 mg, 0.079 mmol, 1 equiv). The vial was then evacuated and backfilled with N_2. Subsequently, dioxane (0.45 mL) and morpholine (**1.27**) (13 μL, 0.148 mmol, 1.8 equiv) were added successively. The resulting mixture was stirred for 1 min and the vial was then sealed with a Teflon-lined screw cap. The mixture was allowed to stir at 23 °C for 1 h, and then at 80 °C for 16 h in a preheated aluminum block. After cooling the reaction vessel to 23 °C, the mixture was filtered by passage through a plug of silica gel (EtOAc eluent, 12 mL) and concentrated under reduced pressure. The crude residue was purified by preparative thin layer chromatography (3:1 Hexanes:EtOAc) to afford **1.12a** (20.0 mg, 86% yield) as a white solid: Mp: 112–114 °C; R_f 0.27 (3:1 Hexanes:EtOAc); ^{1}H NMR (500 MHz, $CDCl_3$): δ 7.34–7.22 (m, 6H), 6.82 (dd, *J* = 8.2, 0.5, 1H), 6.51 (d, *J* = 7.6, 1H), 5.79 (s, 2H), 3.98 (app. t, *J* = 4.7, 4H), 3.74 (app. t, *J* = 4.7, 4H); ^{13}C NMR (125 MHz, $CDCl_3$): δ 143.6, 139.2, 135.1, 134.9, 129.0, 128.7,

128.4, 127.6, 106.2, 100.7, 67.1, 52.2, 49.9; IR (film): 2960, 2853, 1603, 1510, 1239 cm^{-1}; HRMS-ESI (*m/z*) $[M + H]^+$ calcd for $C_{17}H_{19}N_4O$, 295.15534; found, 295.15426.

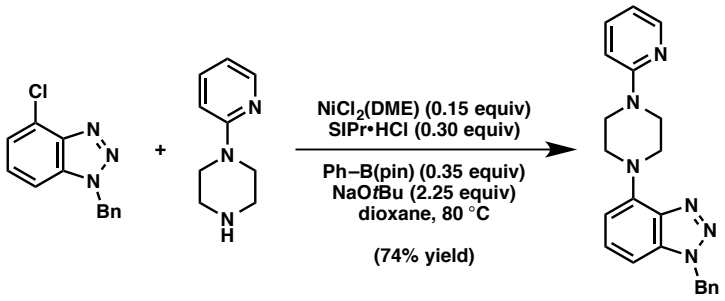

1.5c ***1.28*** ***1.12b***

1.12b (Figure 1.10). The cross-coupling was performed using a general procedure reported by our laboratory.[50] A 4 mL vial containing a magnetic stir bar was flame-dried under reduced pressure and allowed to cool under N_2. The vial was then charged with $NiCl_2$(DME) (2.8 mg, 0.013 mmol, 0.15 equiv), SIPr•HCl (10.7 mg, 0.025 mmol, 0.30 equiv), Ph–B(pin) (6.1 mg, 0.029 mmol, 0.35 equiv), anhydrous powdered NaO*t*Bu (17.5 mg, 0.185 mmol, 2.25 equiv), and triazole **1.5c** (20.7 mg, 0.084 mmol, 1 equiv). The vial was then evacuated and backfilled with N_2. Subsequently, dioxane (0.45 mL) and piperazine **1.28** (24.1 mg, 0.148 mmol, 1.8 equiv) were added successively. The resulting mixture was stirred for 1 min and the vial was then sealed with a Teflon-lined screw cap. The mixture was allowed to stir at 23 °C for 1 h, and then at 80 °C for 16 h on a preheated aluminum block. After cooling the reaction vessel to 23 °C, the mixture was filtered by passage through a plug of silica gel (EtOAc eluent, 12 mL), and concentrated under reduced pressure. The crude residue was further purified by preparative thin layer chromatography (3:1 Hexanes:EtOAc) to afford **1.12b** (22.5 mg, 74% yield) as a white solid: Mp: 118–120 °C; R_f 0.22 (3:1 Hexanes:EtOAc); ^{1}H NMR (500 MHz, $CDCl_3$): δ 8.23 (ddd, *J* = 4.9, 2.0, 0.8, 1H), 7.52 (ddd, *J* = 8.8, 7.2, 2.0, 1H), 7.34–7.23 (m, 6H), 6.82 (d, *J* = 8.0, 1H), 6.73 (d, *J* = 8.5, 1H), 6.66 (ddd, *J* = 5.5, 4.9, 0.6, 1H), 6.56 (d, *J* = 7.6, 1H), 5.80 (s, 2H), 3.92–3.86

(m, 4H), 3.85–3.79 (m, 4H); ^{13}C NMR (125 MHz, $CDCl_3$): δ 159.7, 148.2, 143.4, 139.3, 137.7, 135.1, 134.9, 129.0, 128.8, 128.4, 127.6, 113.7, 107.4, 106.6, 100.4, 52.2, 49.3, 45.4 ; IR (film): 3006, 2835, 1592, 1436, 1235 cm^{-1}; HRMS-ESI (*m/z*) $[M + H]^+$ calcd for $C_{22}H_{22}N_6$, 371.19787; found, 371.19664.

1.5.3 Computational Methods

1.5.3.1 Computational Details

All reported energies in the paper are Gibbs free energies. Low frequencies (less then 100 cm^{-1}) have been corrected using the method discussed in a recent Truhlar paper.[51] All reactants were optimized to their ground state with a tight convergence criteria and a frequency calculation was performed with an ultrafine integration grid to verify no imaginary frequencies. Transition states for methyl azide were optimized to a saddle point with a tight convergence criteria and then a frequency calculation was performed with an ultrafine integration grid to verify only one imaginary frequencies and the correct saddle point was obtained. The transition state for attack of N-methylaniline is a variational transition state. It was obtained by doing a bond scan from 1.8Å out to 3.2Å with a step size of 0.04Å. At each of these points, the structure was optimized tight convergence citeria with only the distance between the nitrogen of *N*-methylaniline and either the *meta* or *ortho* carbon of the aryne fixed. Frequencies were computed at each of these points with an ultrafine integration grid and a free energy reaction coordinate was obtained.

1.5.3.2 Summary of Steric, Charge, and Distortion Models

The general trends predicted by the distortion model correlate to both experimental results and computed transition state energies. The steric model predicts the opposite trend. The charge model incorrectly predicts the regioselectivity for **1.1e** (Figure 1.11).

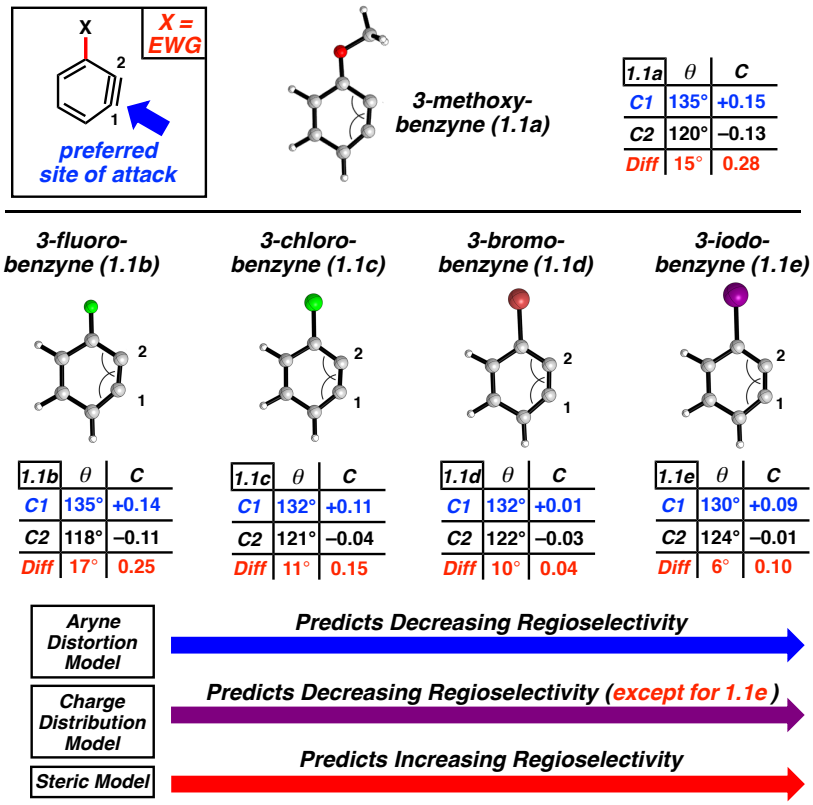

Figure 1.11. Geometry-optimized structures of **1.1a**–**1.1e** (B3LYP), internal angles (θ), NBO charges (C), and predictions based on the aryne distortion, charge distribution, and steric models

1.5.3.3 Point Charge Analysis

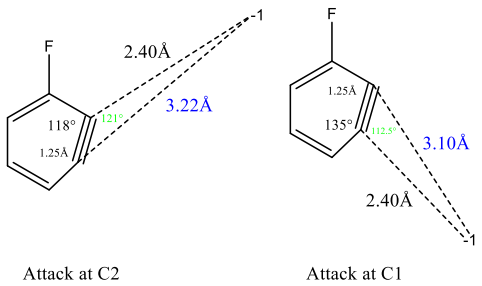

To determine the distance of the point charge to the more distal carbon, the law of cosines must be used. To use the law of cosines, two sides and the angle between them are needed. The two sides used are the 2.4Å and the alkyne bond length. To obtain the angle in between these sides, we bisect the alkyne angle with the point charge, allowing the angle labeled in green to be calculated by subtracting 180 from ½ of the alkyne angle. Once the sides are known and the angle, we use the equation shown below.

Point charge attacking at C2

$$c^2 = a^2 + b^2 - 2 * a * b * \cos\gamma$$

$$c^2 = 1.25^2 + 2.4^2 - 2 * 1.25 * 2.4 * \cos 121$$

$$c^2 = 7.3225 - -3.0902$$

$$c^2 = 10.4127$$

$$c = 3.22$$

Point charge attacking at C1

$$c^2 = a^2 + b^2 - 2 * a * b * \cos\gamma$$

$$c^2 = 1.25^2 + 2.4^2 - 2 * 1.25 * 2.4 * \cos 112.5$$

$$c^2 = 7.3225 - -2.2961$$

$$c^2 = 9.6186$$

$$c = 3.10$$

Now that we know the distance of the point charge to both carbons of the alkyne, we can use Coulombs law to determine the attractive or repulsive energy felt by the point charge at each attack. The equations are shown below.

Coulomb's Law:

$$E = 332\frac{q_1 * q_2}{\epsilon * r_{q1q2}}$$

Attack at C2:

Interaction between point charge and C2

$$E = 332\frac{-1 * -0.11}{36 * 2.40}$$

$$E = 0.42 \text{ kcal/mol}$$

Interaction between point charge and C1

$$E = 332\frac{-1 * 0.14}{36 * 3.22}$$

$$E = -0.40 \text{ kcal/mol}$$

Attack at C1:

Interaction between point charge and C2

$$E = 332\frac{-1 * -0.11}{36 * 3.10}$$

$$E = 0.33 \text{ kcal/mol}$$

Interaction between point charge and C1

$$E = 332\frac{-1 * 0.14}{36 * 2.40}$$

$$E = -0.54 \text{ kcal/mol}$$

For attack at the C2 position the net energy is 0.0 kcal/mol. The attack at the C1 position is net attractive by 0.2 kcal/mol.

1.5.3.4 M06-2X Discussion

Due to no electronic barrier for *N*-methylaniline attacking at the *meta* position for fluorobenzyne (**1.1b**), a bond scan was performed to get the free energy pathway or variational transition state. When done with B3LYP, a transition state was found in which the energy converged at a transition state as *N*-methylaniline approached fluorobenzyne and then decreased to the products. Frequencies were studied to assure that the only imaginary frequency was nucleophilic attack. This was performed for the *ortho* pathway as well and similar behavior was observed, however with M06-2X the energies did not converge on a transition state, instead they became erratic, as the imaginary frequency that was calculated was no longer that of a nucleophilic attack of *N*-methylaniline to the benzyne. Regioselectivities computed at the B3LYP level of theory have done a good job of estimating not only the trend in decreasing regioselectivities as the angle distortion decreases, but also the magnitude of the selectivity as stated in the paper.

1.5.3.5 Angles of Alkynes Computed at Several Levels of Theory

B3LYP and M06-2X agree well with each other and follow the trend of F- and OMe-substituents having the greatest angle distortions, thus the greatest regioselectivities, and as we move down the halogens, that selectivity is eroded. The calculations at MP2 also have the correct trend with F- and OMe- displaying the greatest distortion of the alkyne angles, but moving down the halogens shows little to no distortion from benzyne but experimental there is selectivity. We

previously have seen similar subtle variations in distortion using MP2.[52] It appears that B3LYP does a good job of getting angle distortion correct and should be sufficient when performing calculations on reactants to predict selectivities.

	B3LYP 6-311+g(d,p)		M06-2X 6-311+g(d,p)		MP2 6-311+g(d,p)	
Reactant Angles	**Ortho**	**Meta**	**Ortho**	**Meta**	**Ortho**	**Meta**
Methoxybenzyne	120°	135°	119°	136°	123°	131°
Fluorobenzyne	118°	135°	117°	136°	122°	130°
Chlorobenzyne	121°	132°	121°	133°	125°	128°
Bromobenzyne	122°	132°	121°	133°	126°	127°
Iodobenzyne	124°	130°	124°	131°	127°	127°
TMSbenzyne	134°	122°	134°	122°	130°	125°

1.5.3.6 Cartesian Coordinates for Reactants and Transition States

Cartesian coordinates for the optimized structures have been previously reported.[53]

1.6 Spectra Relevant to Chapter One:

The Role of Aryne Distortion, Steric Effects, and Charges in Regioselectivities of Aryne Reactions

Jose M. Medina, Joel L. Mackey, Neil K. Garg, and K. N. Houk

J. Am. Chem. Soc. **2014**, *136*, 15798–15805.

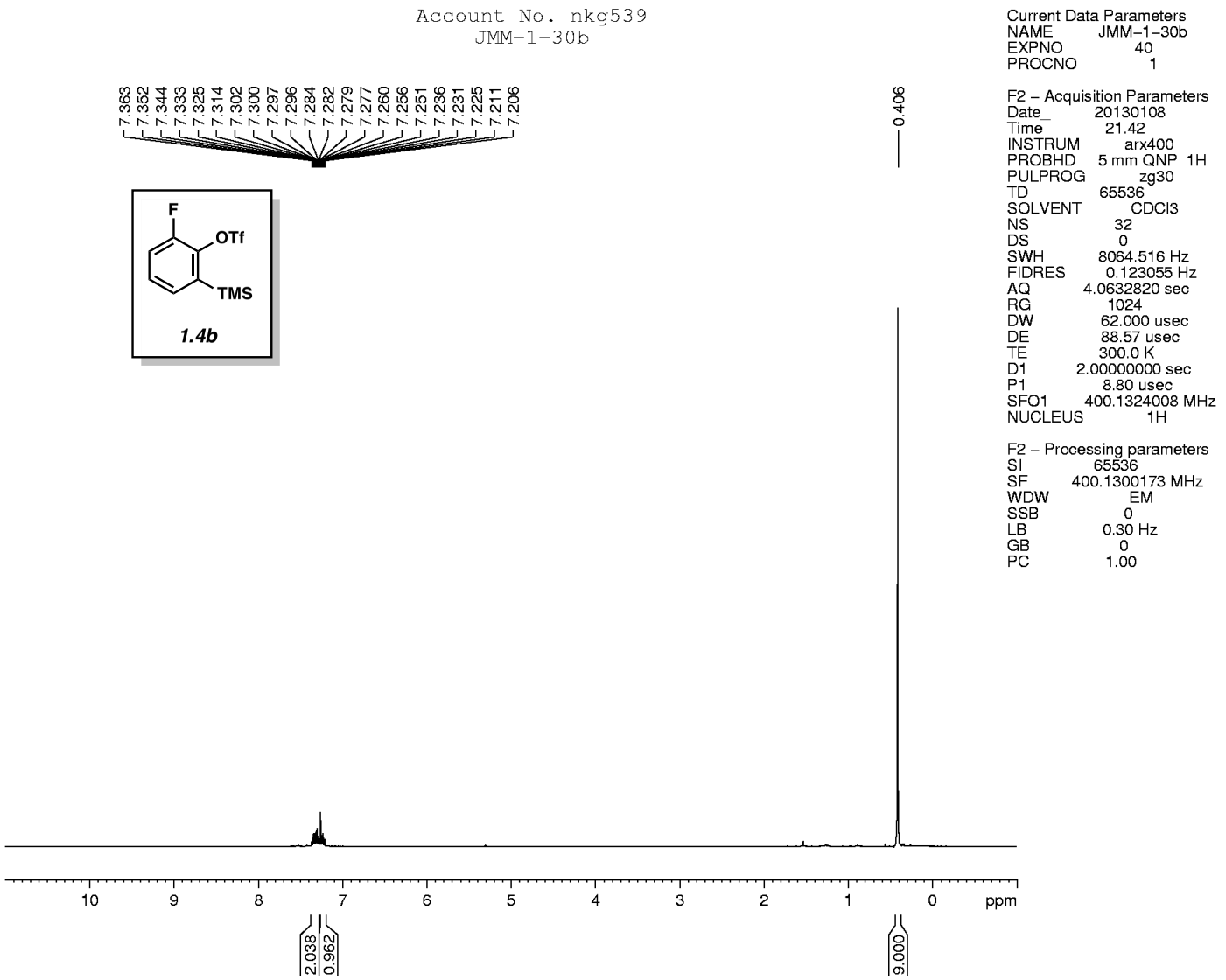

Figure 1.12. ^{1}H NMR (400 MHz, $CDCl_3$) compound **1.4b**

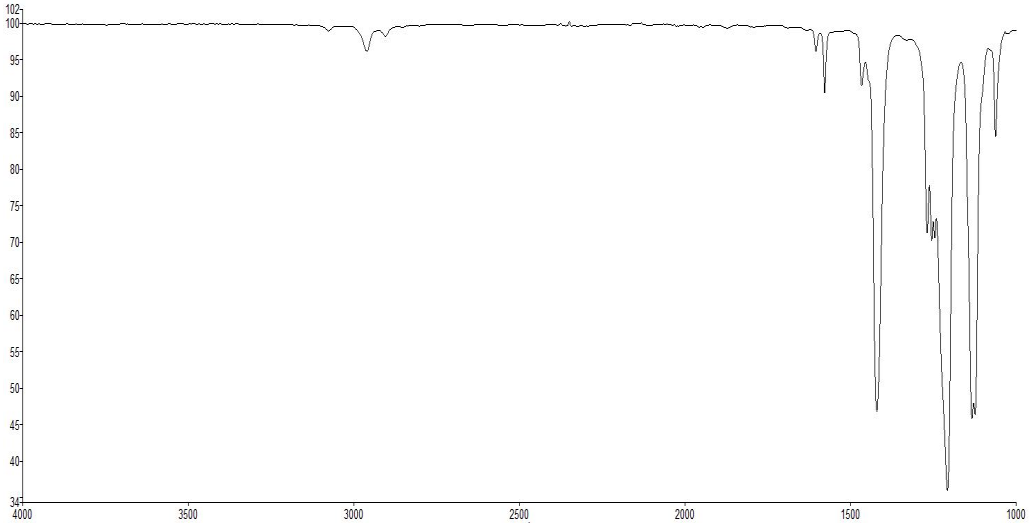

Figure 1.13. Infrared spectrum of compound **1.4b**

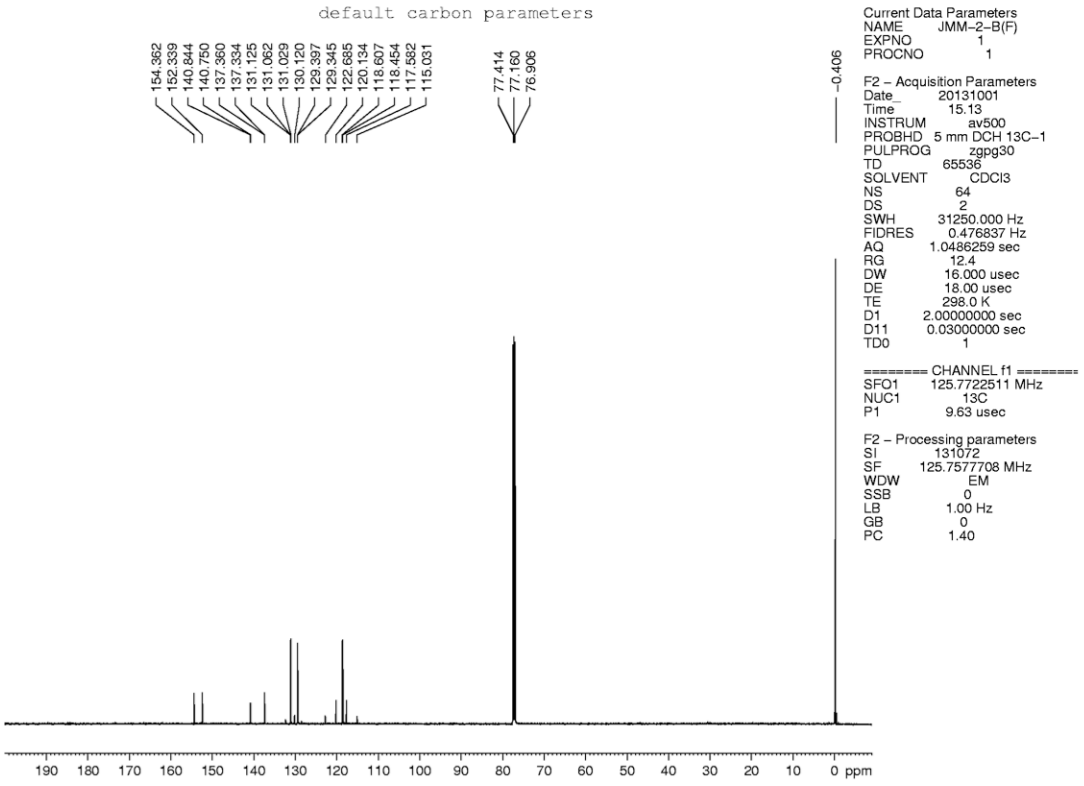

Figure 1.14. ^{13}C NMR (125 MHz, $CDCl_3$) of compound **1.4b**

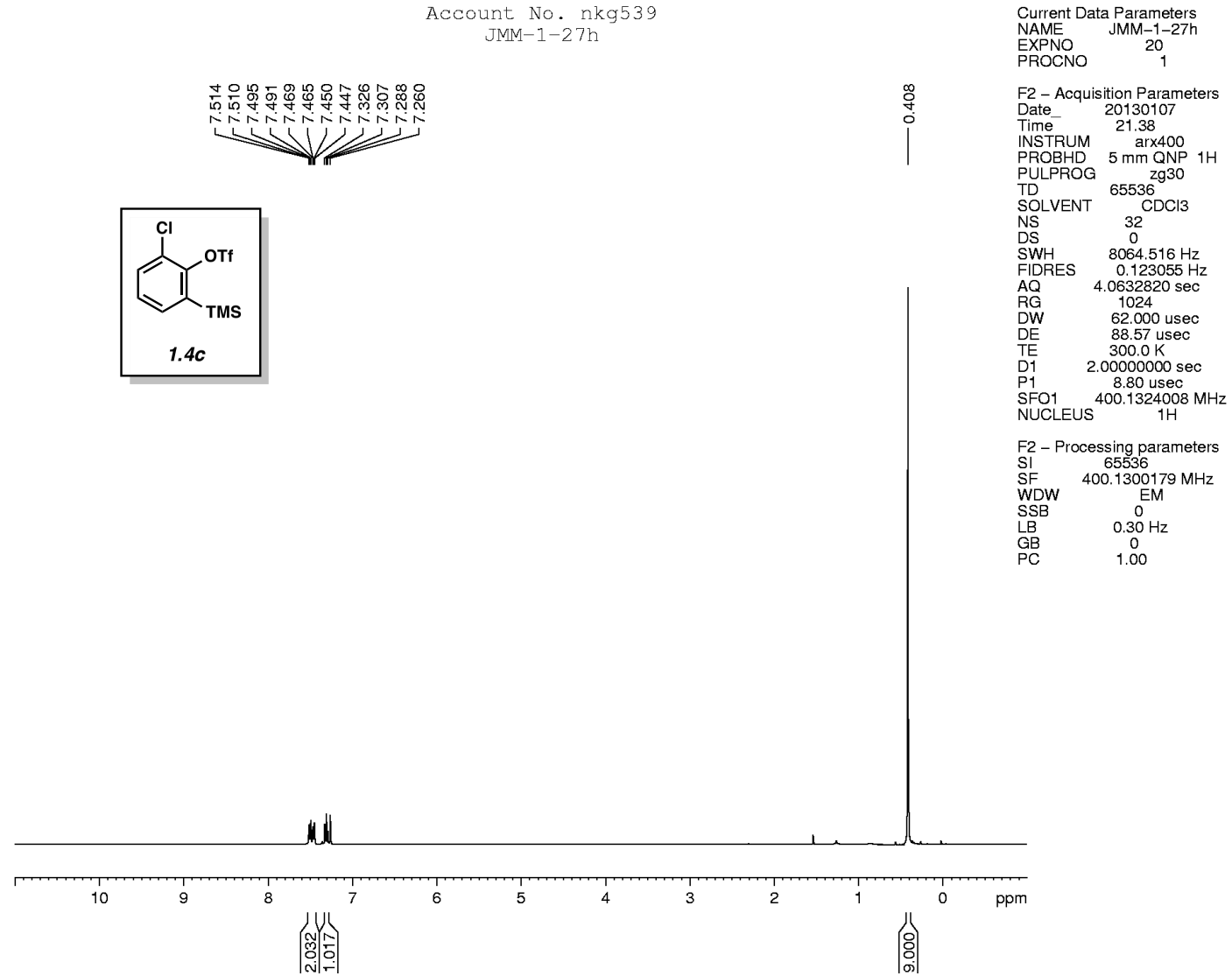

Figure 1.15. ^{1}H NMR (400 MHz, $CDCl_3$) compound **1.4c**

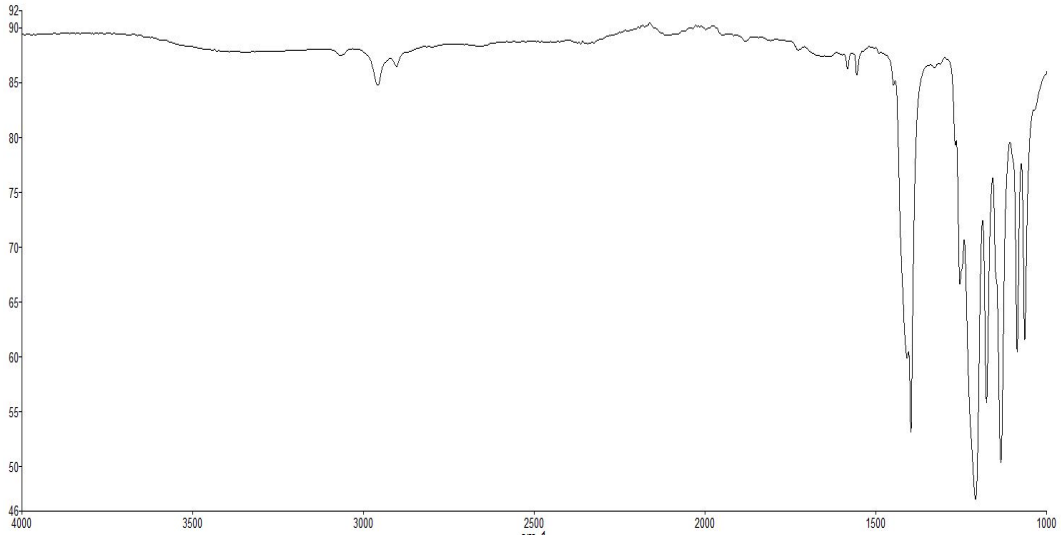

Figure 1.16. Infrared spectrum of compound **1.4c**

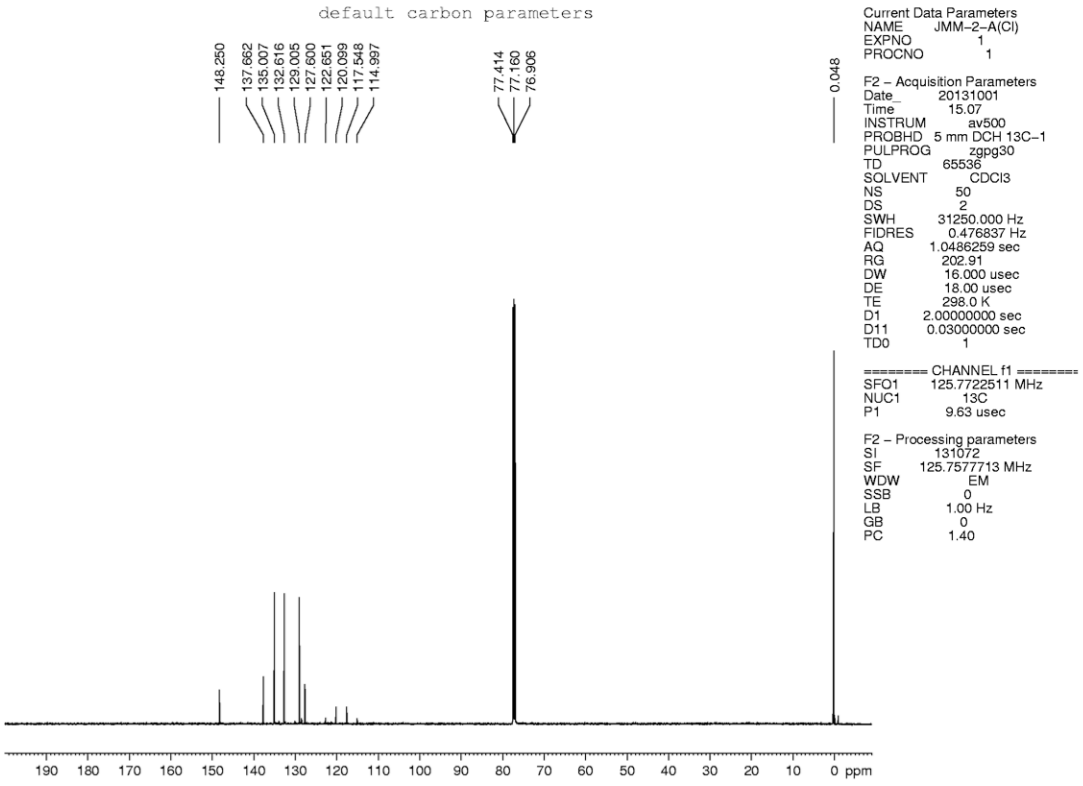

Figure 1.17. ^{13}C NMR (125 MHz, $CDCl_3$) of compound **1.4c**

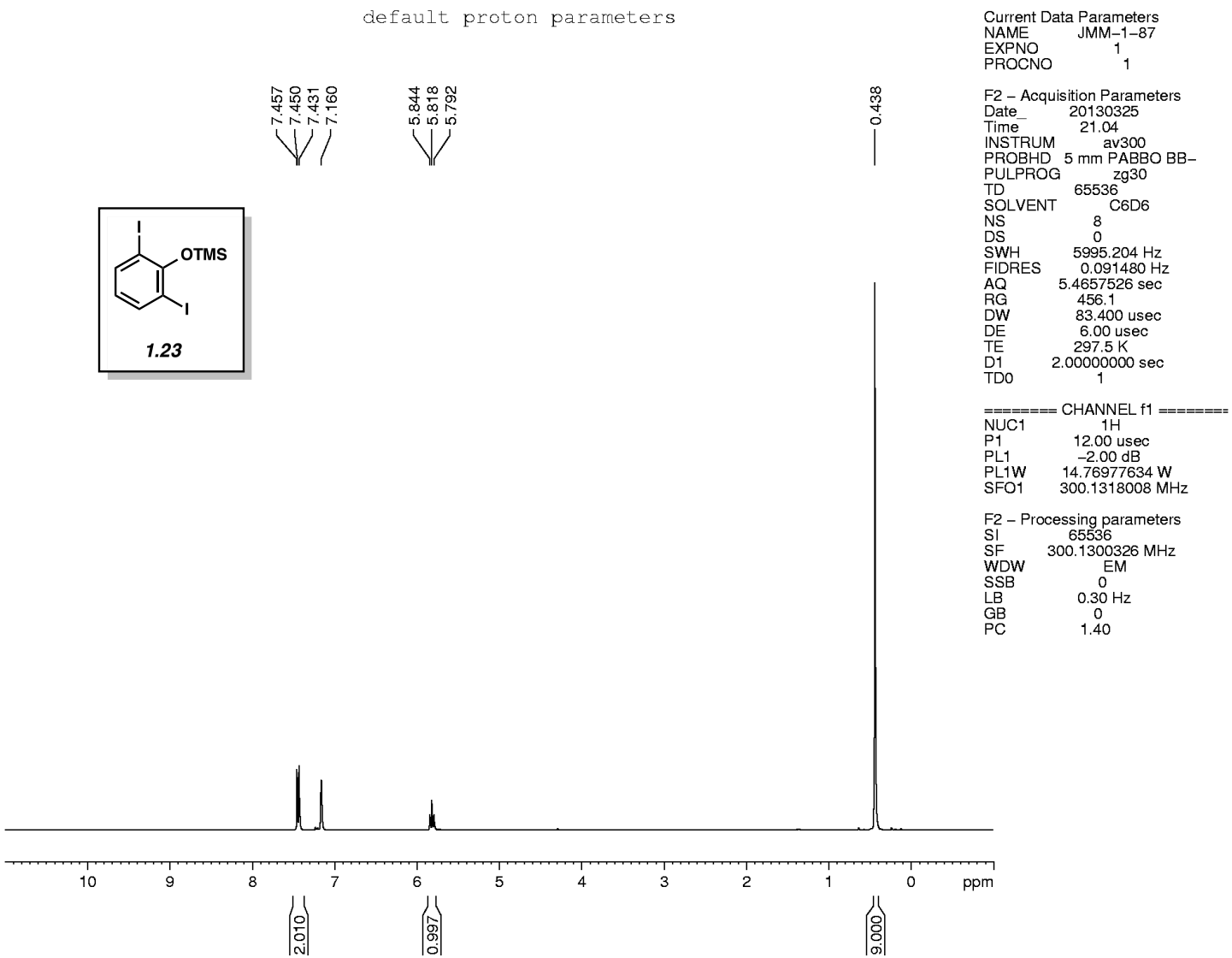

Figure 1.18. ^{1}H NMR (300 MHz, C_6D_6) compound **1.23**

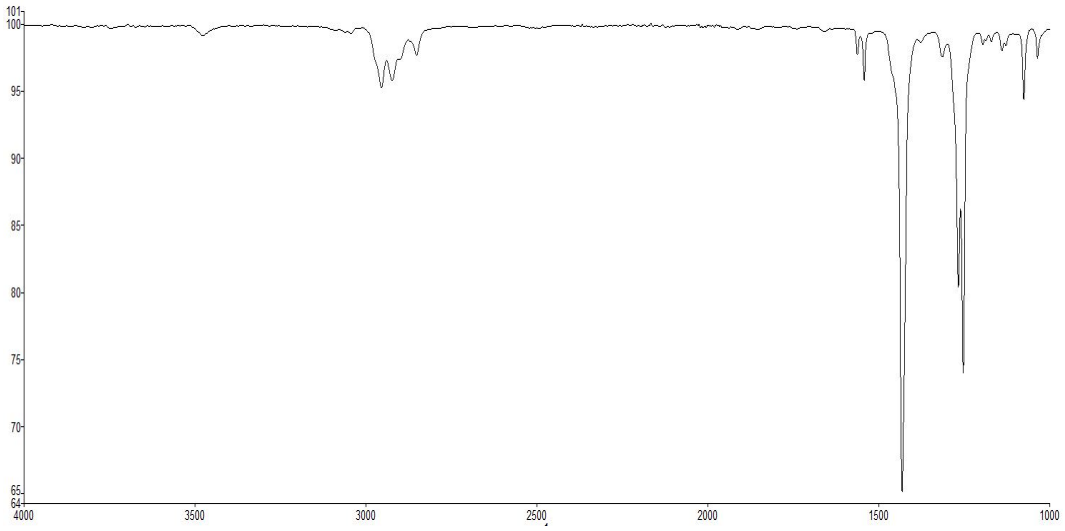

Figure 1.19. Infrared spectrum of compound **1.23**

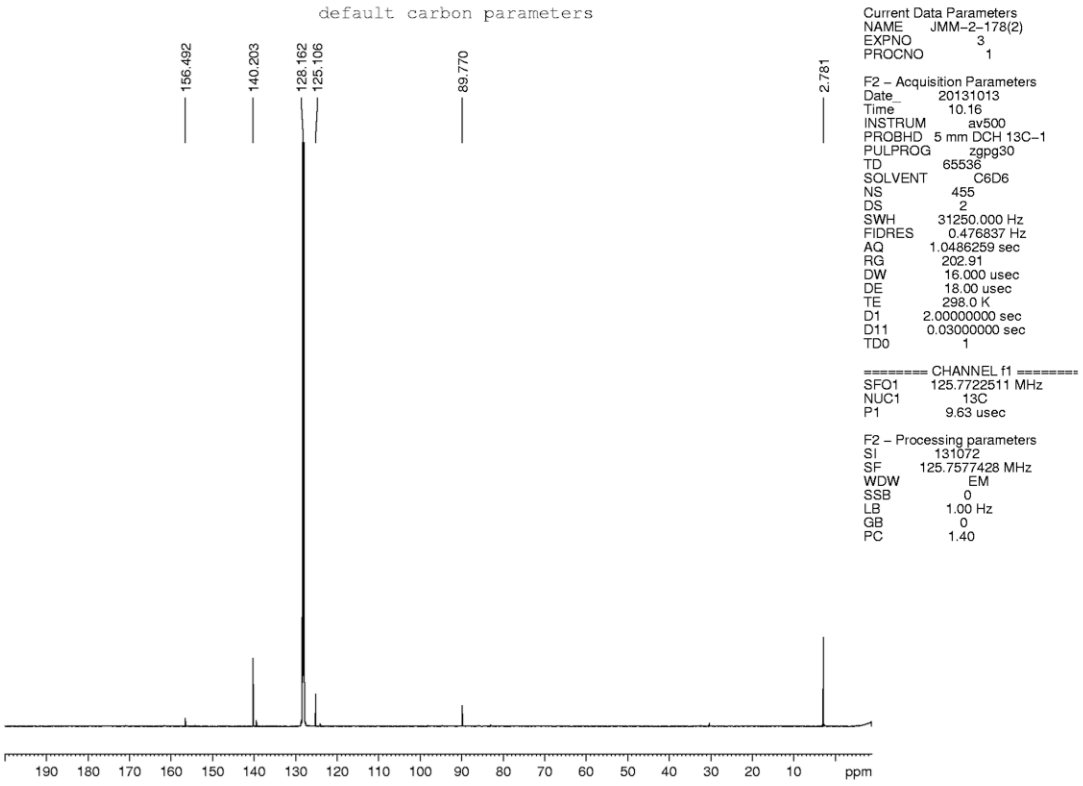

Figure 1.20. ^{13}C NMR (125 MHz, C_6D_6) of compound **1.23**

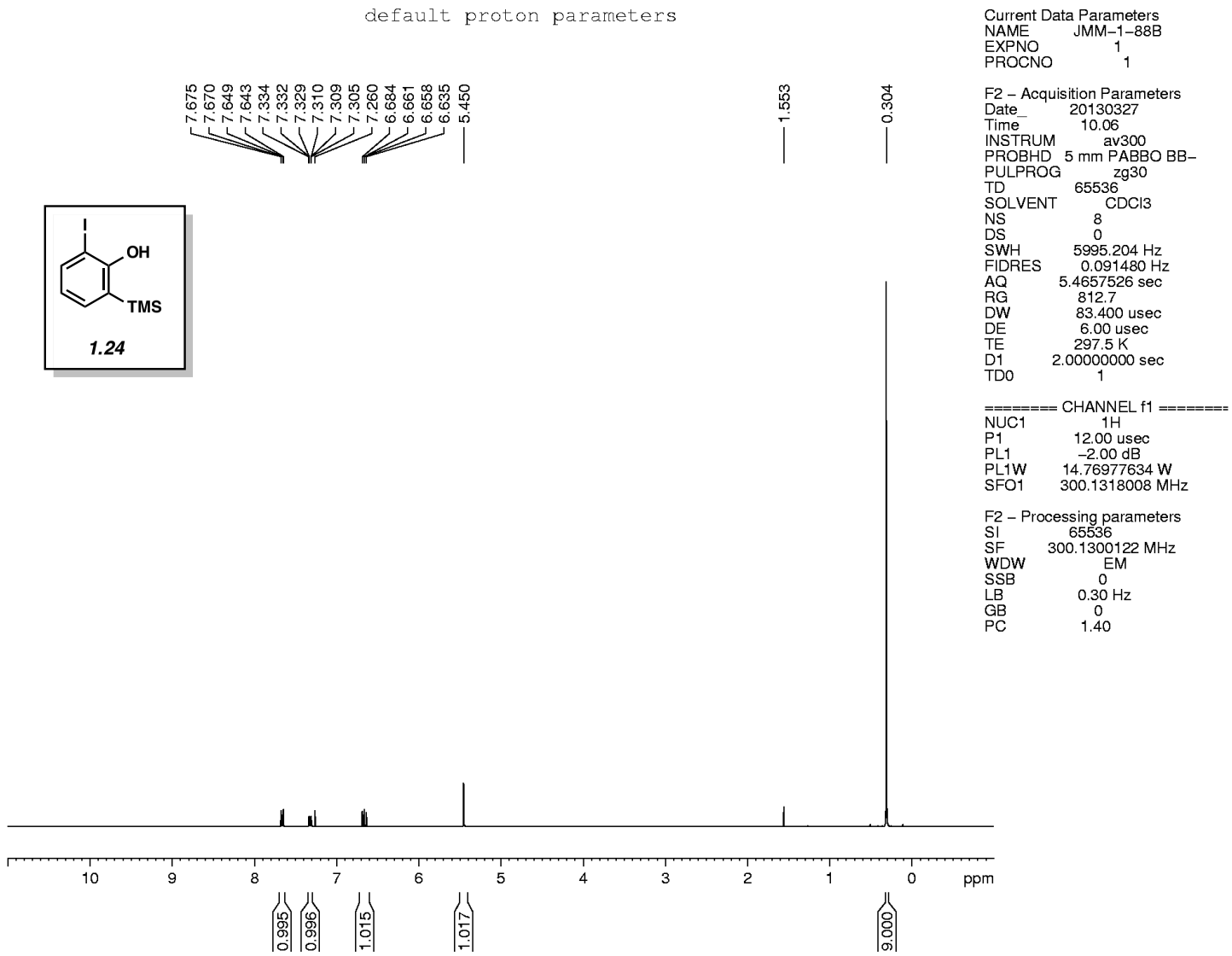

Figure 1.21. ^{1}H NMR (300 MHz, $CDCl_3$) compound **1.24**

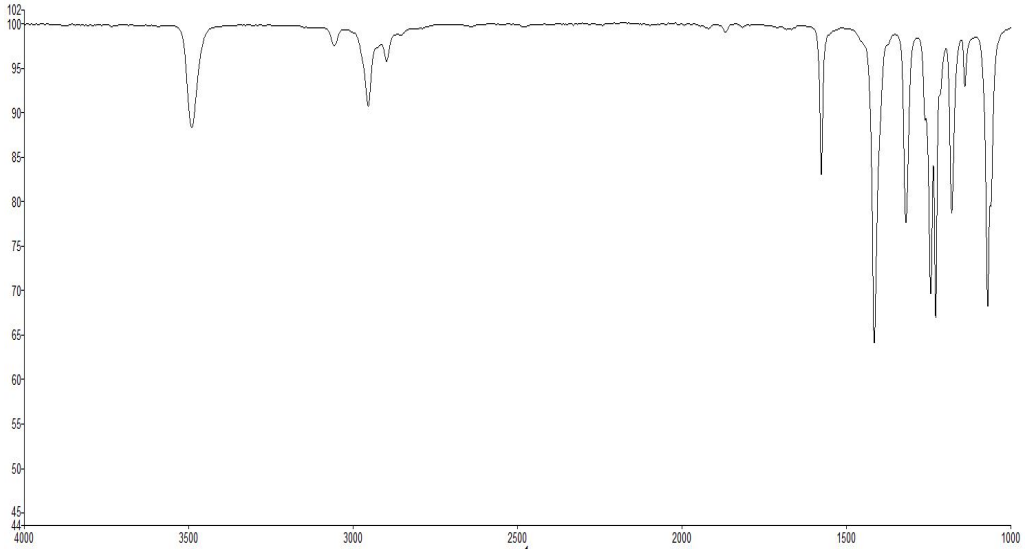

Figure 1.22. Infrared spectrum of compound **1.24**

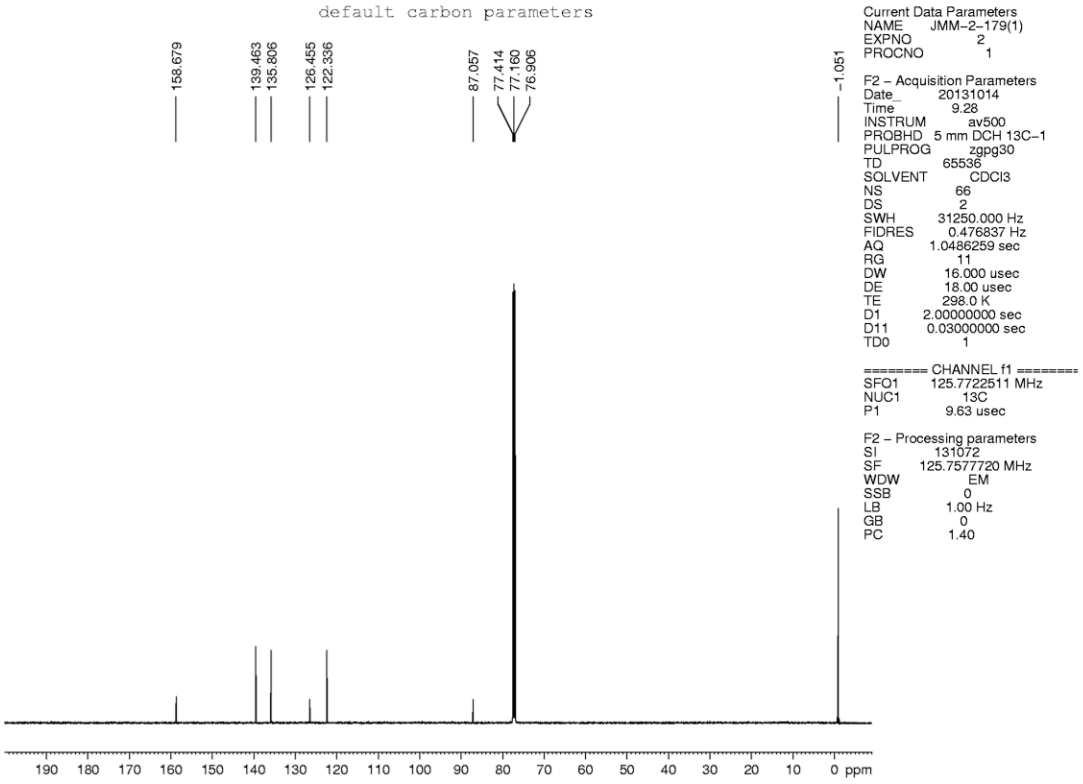

Figure 1.23. ^{13}C NMR (125 MHz, $CDCl_3$) of compound **1.24**

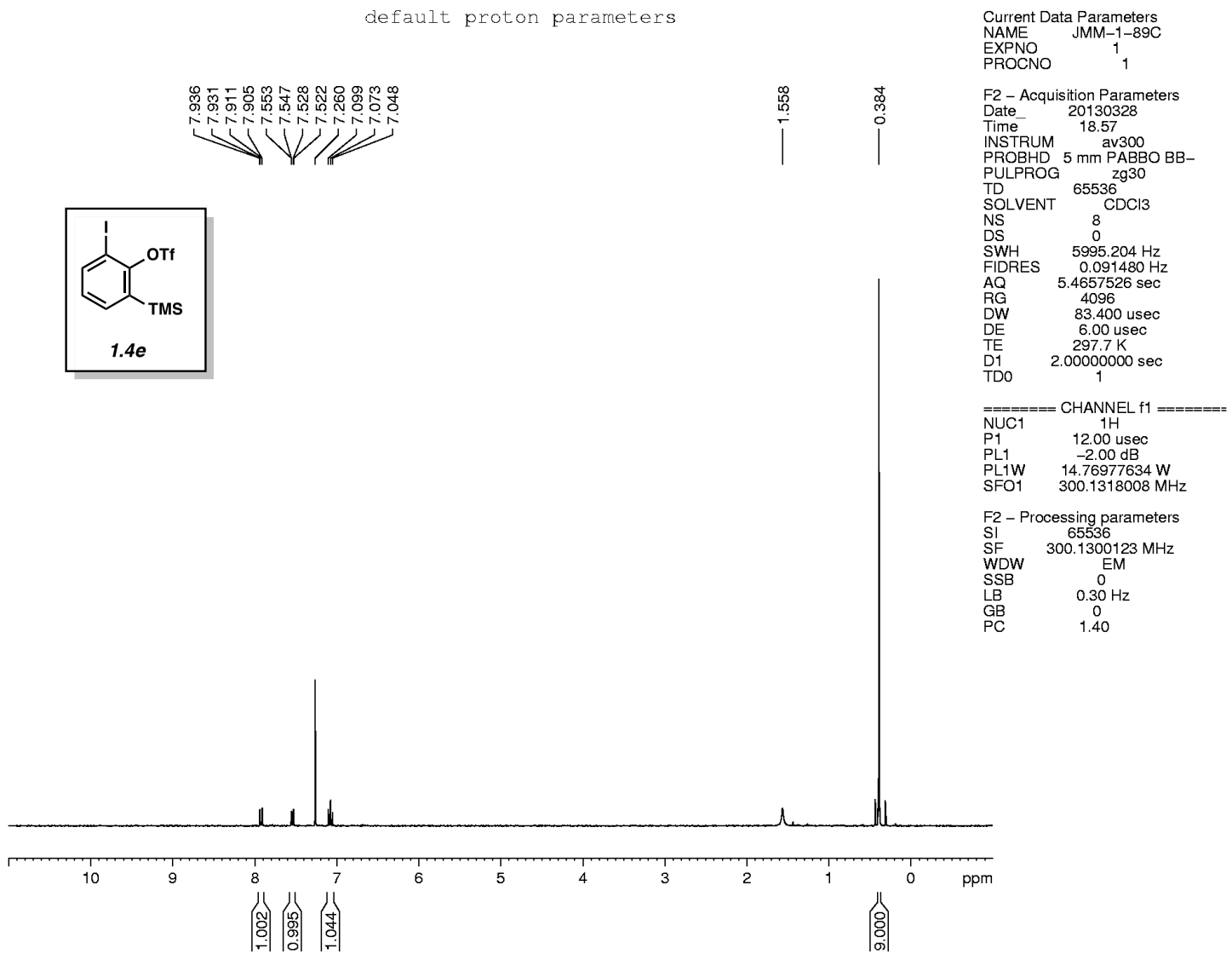

Figure 1.24. ^{1}H NMR (300 MHz, $CDCl_3$) compound **1.4e**

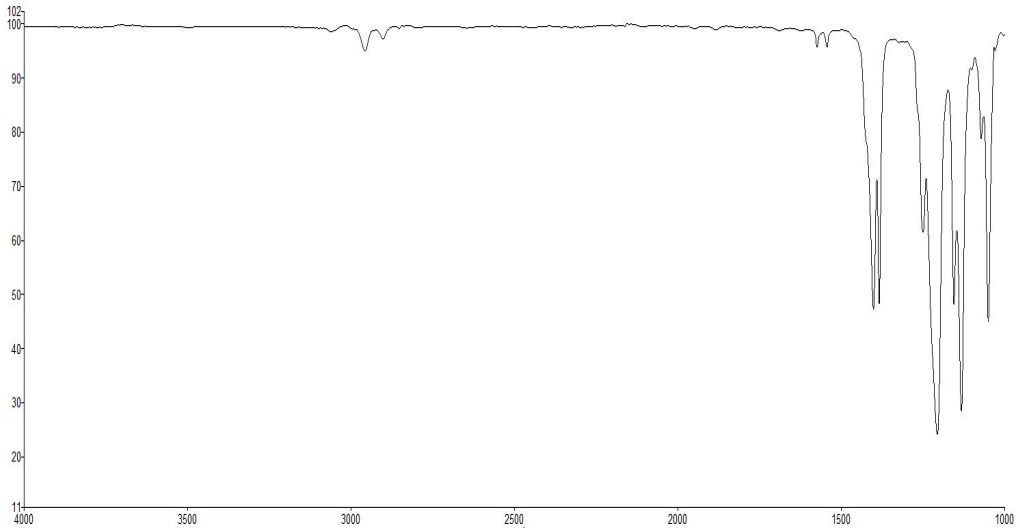

Figure 1.25. Infrared spectrum of compound **1.4e**

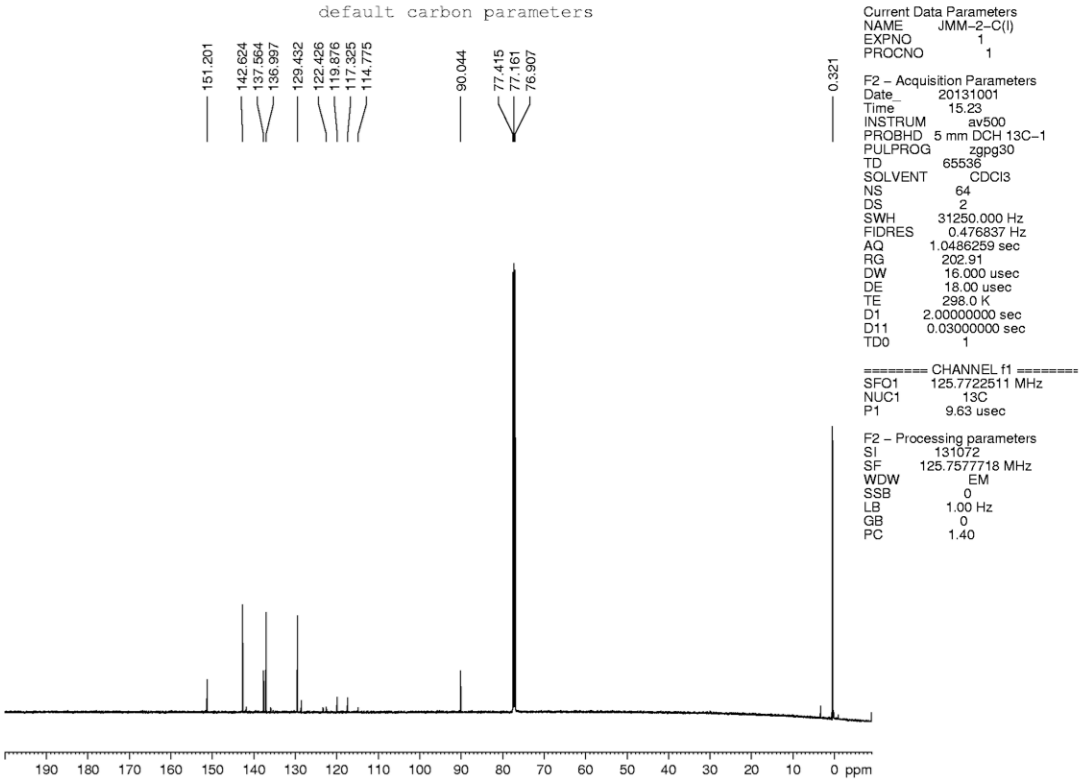

Figure 1.26. ^{13}C NMR (125 MHz, $CDCl_3$) of compound **1.4e**

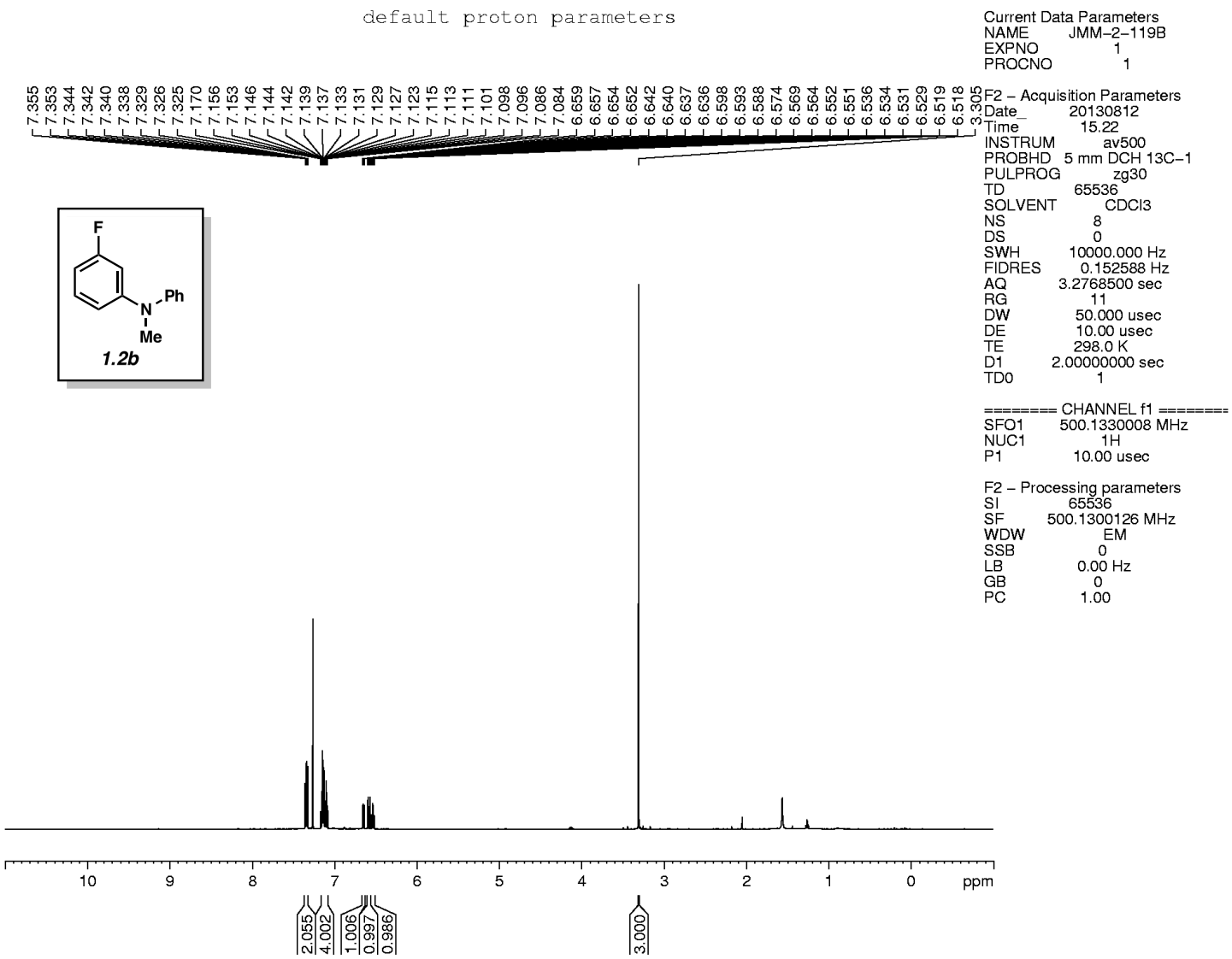

Figure 1.27. ^{1}H NMR (500 MHz, $CDCl_3$) compound **1.2b**

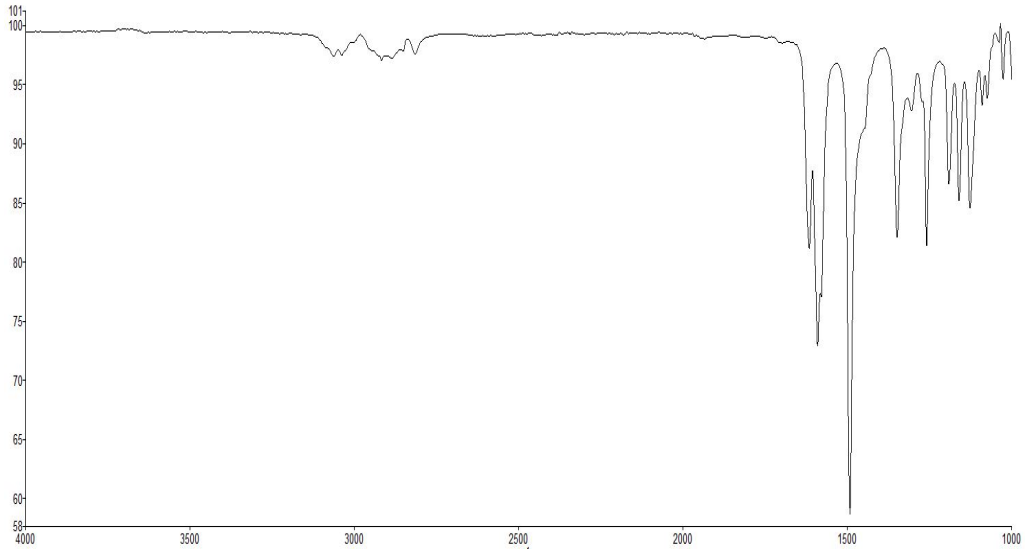

Figure 1.28. Infrared spectrum of compound **1.2b**

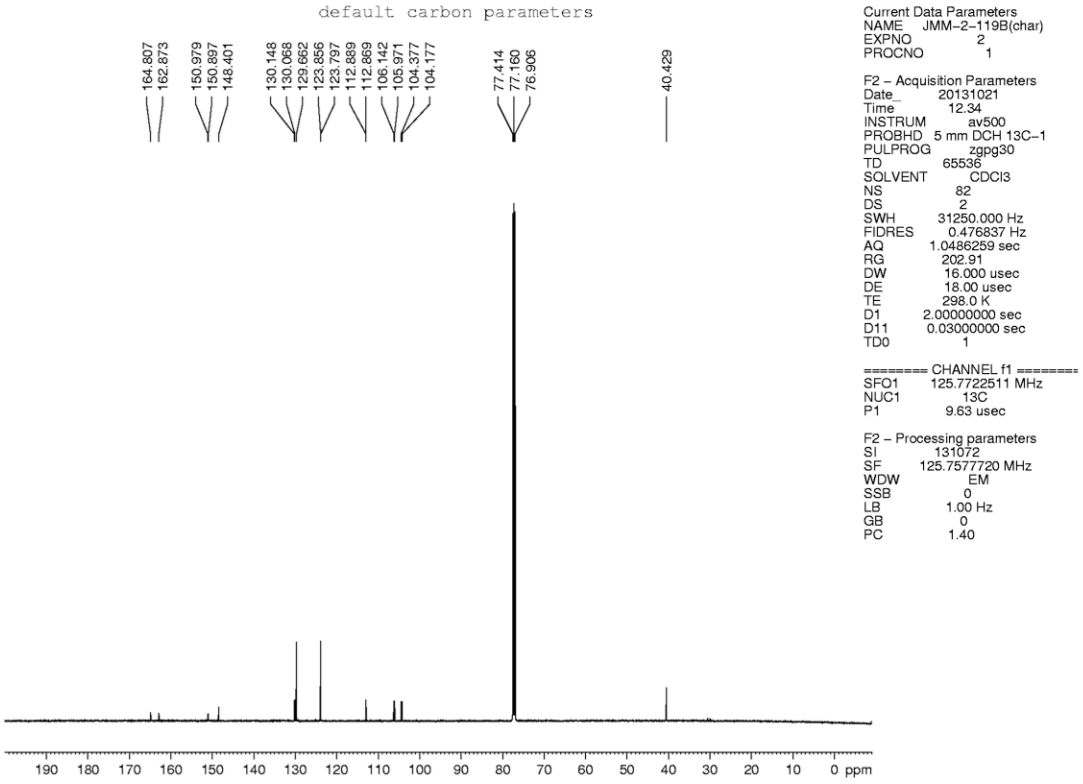

Figure 1.29. ^{13}C NMR (125 MHz, $CDCl_3$) of compound **1.2b**

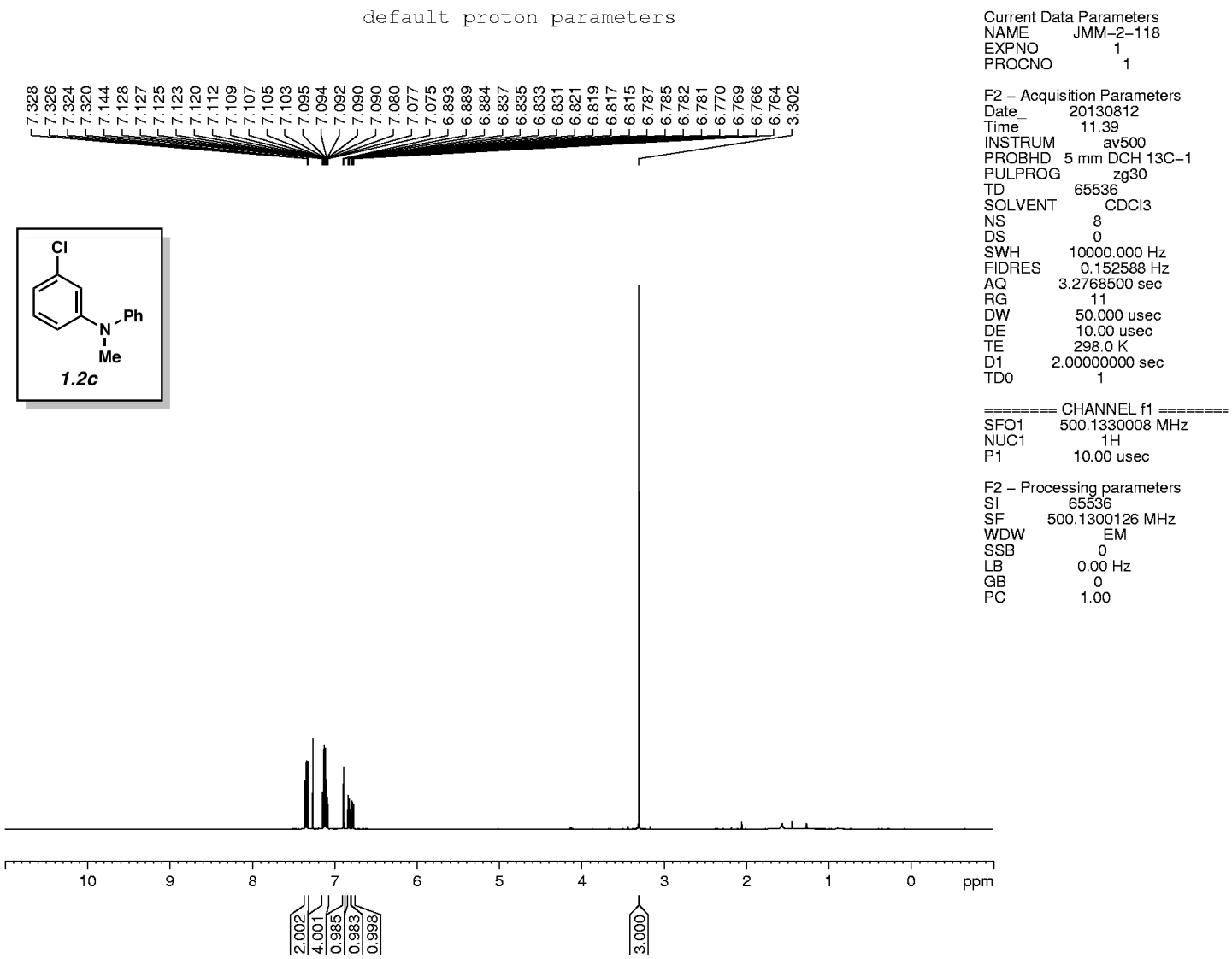

Figure 1.30. ^{1}H NMR (500 MHz, $CDCl_3$) compound **1.2c**

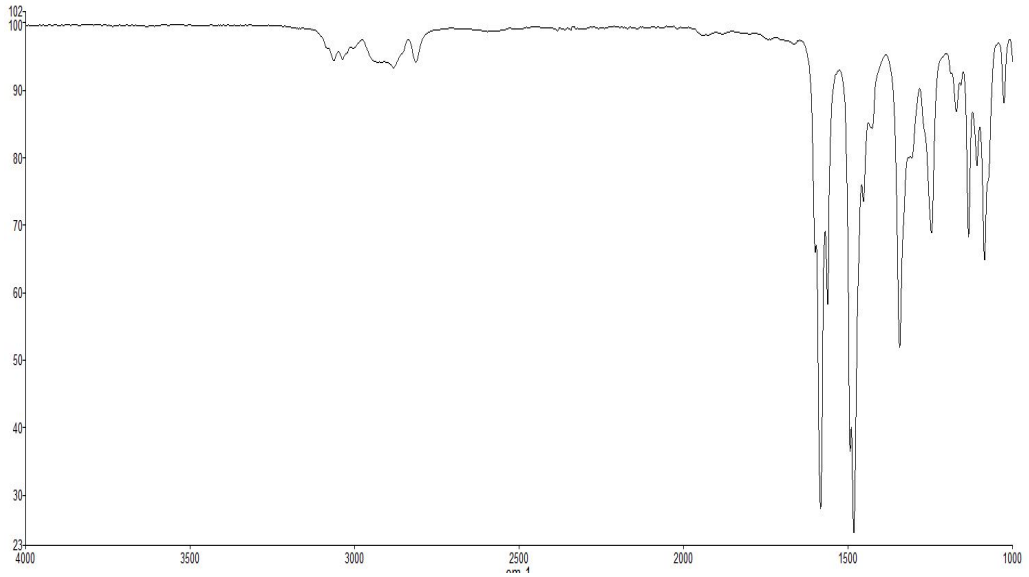

Figure 1.31. Infrared spectrum of compound **1.2c**

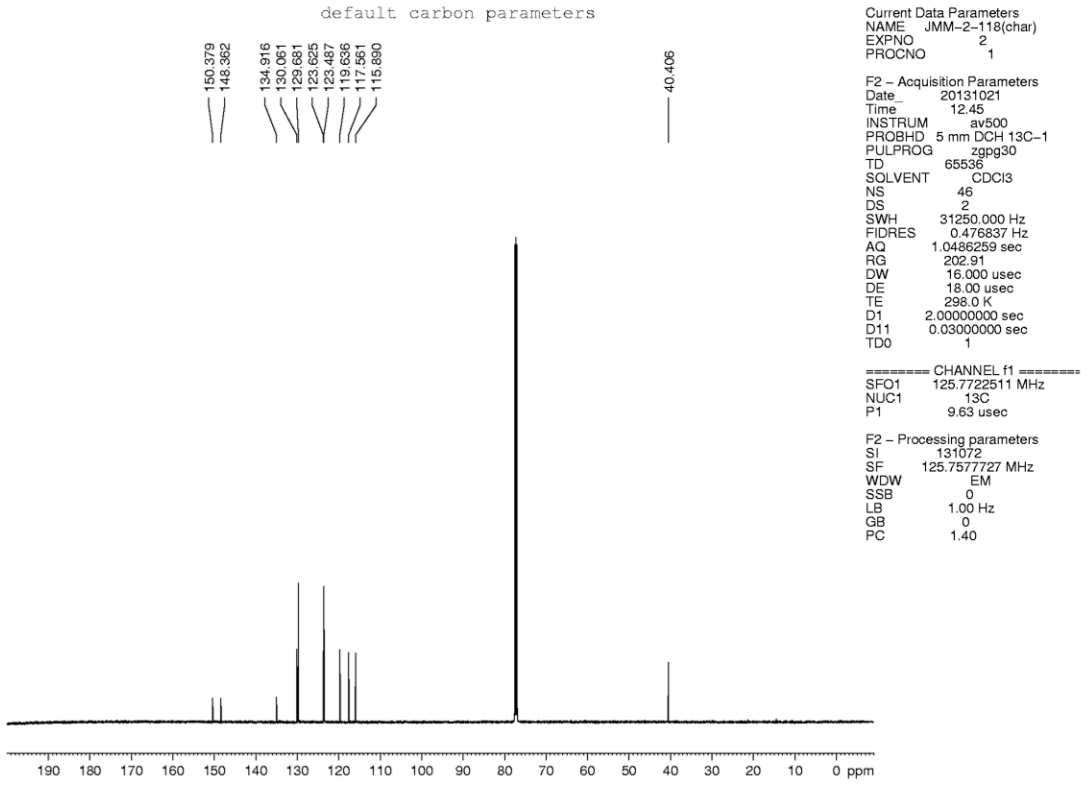

Figure 1.32. ^{13}C NMR (125 MHz, $CDCl_3$) of compound **1.2c**

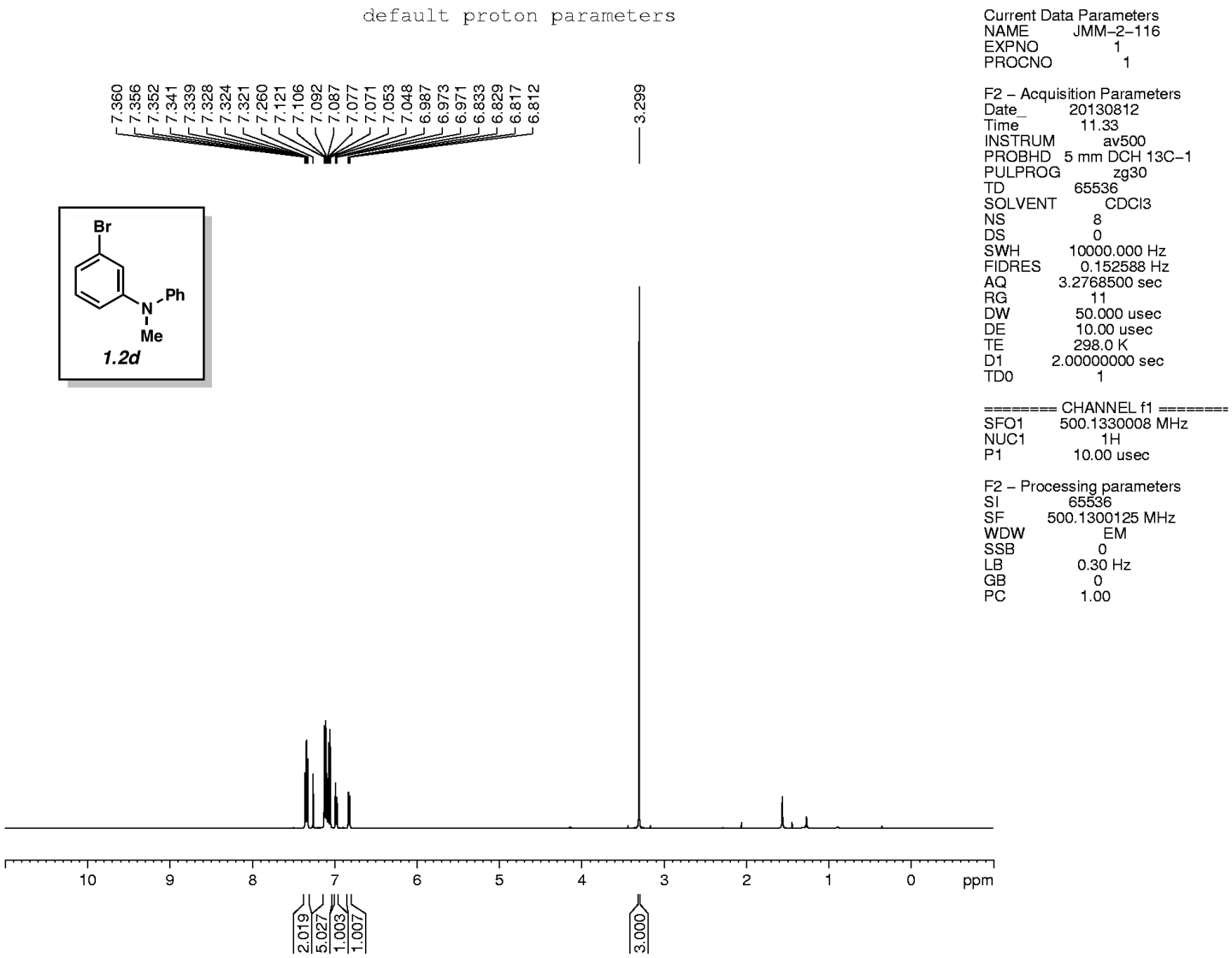

Figure 1.33. ^{1}H NMR (500 MHz, $CDCl_3$) compound **1.2d**

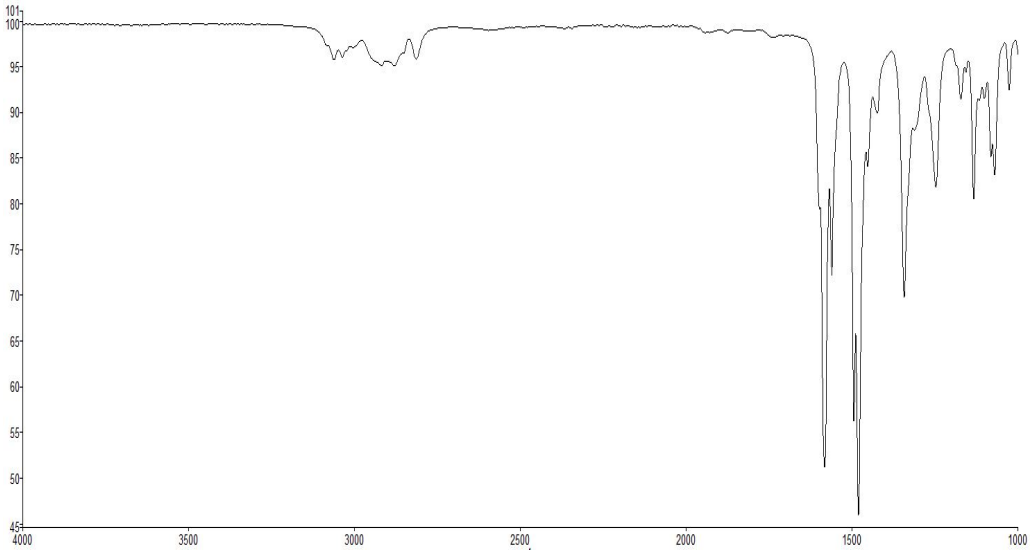

Figure 1.34. Infrared spectrum of compound **1.2d**

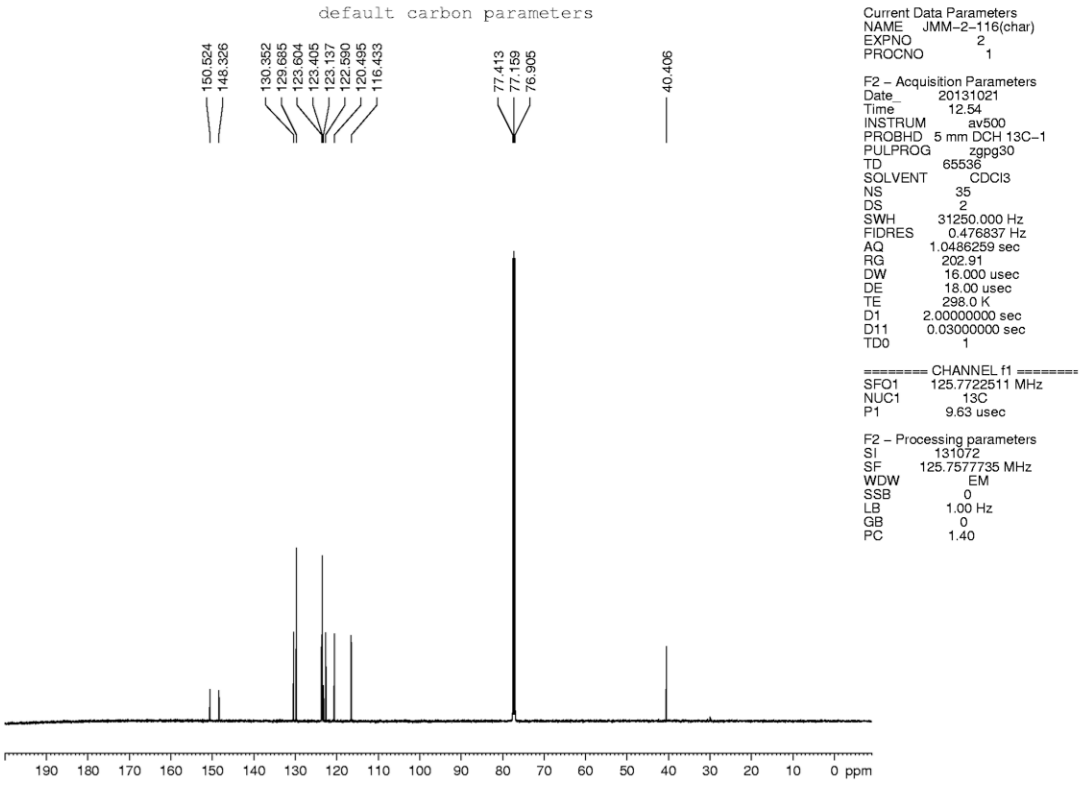

Figure 1.35. ^{13}C NMR (125 MHz, $CDCl_3$) of compound **1.2d**

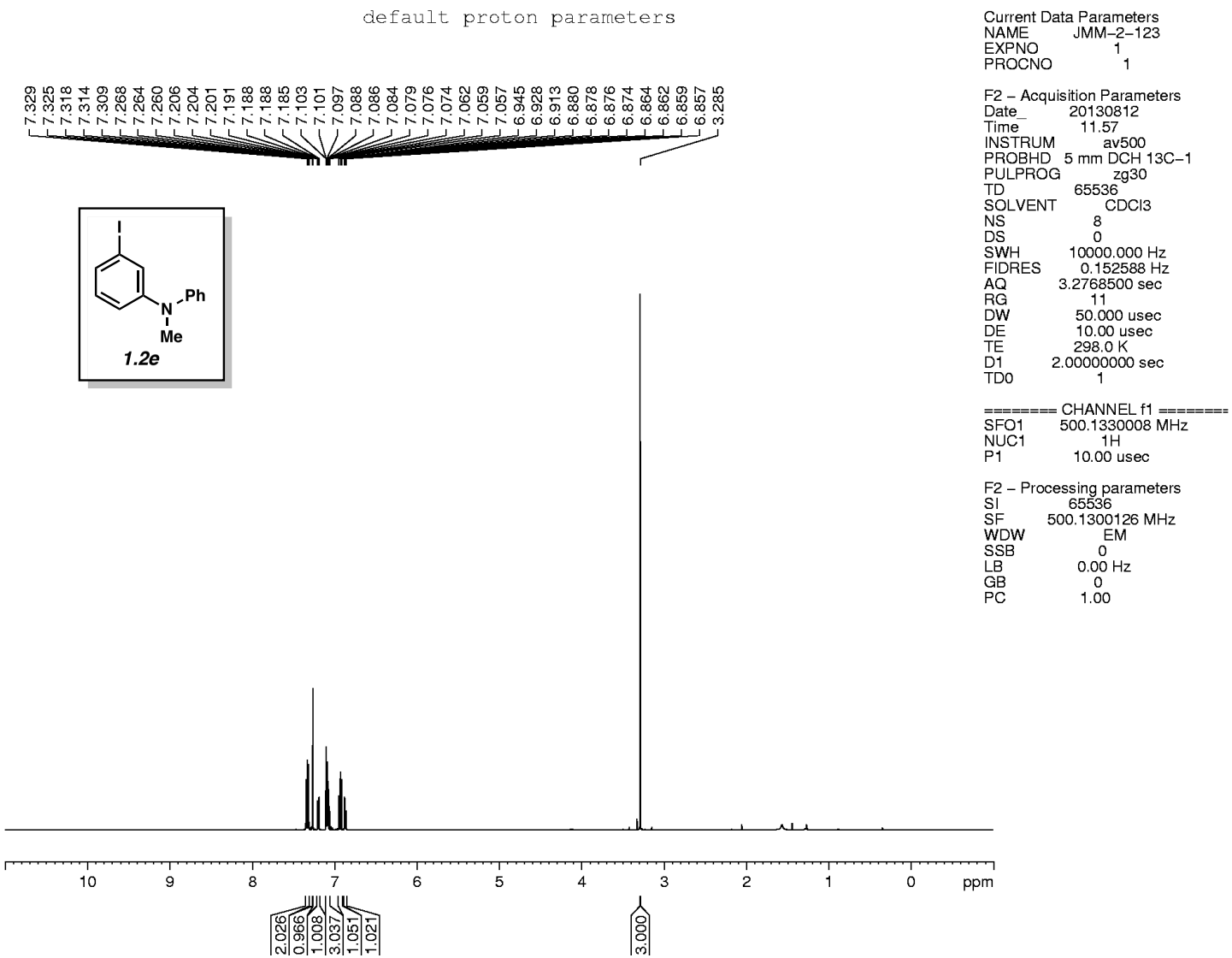

Figure 1.36. ^{1}H NMR (500 MHz, $CDCl_3$) compound **1.2e**

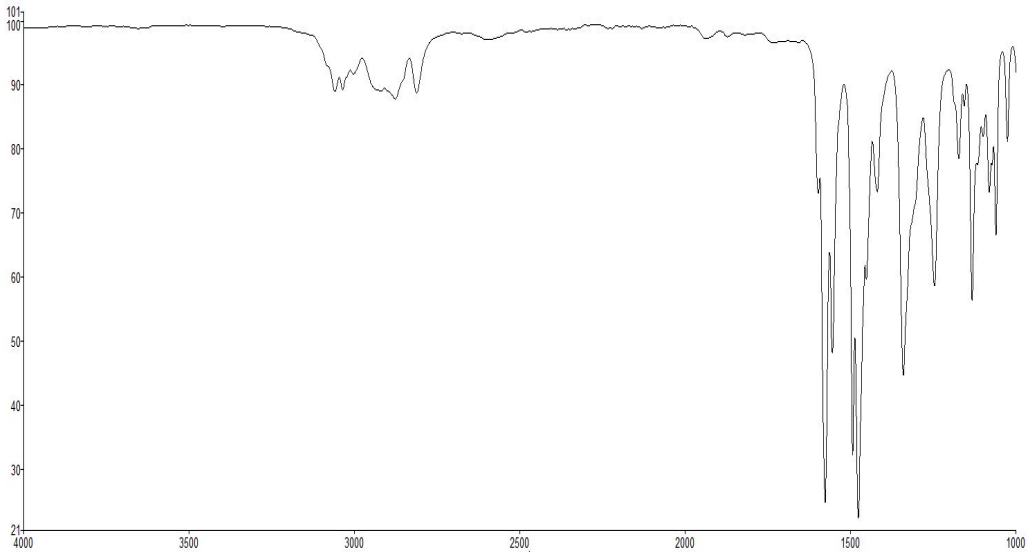

Figure 1.37. Infrared spectrum of compound **1.2e**

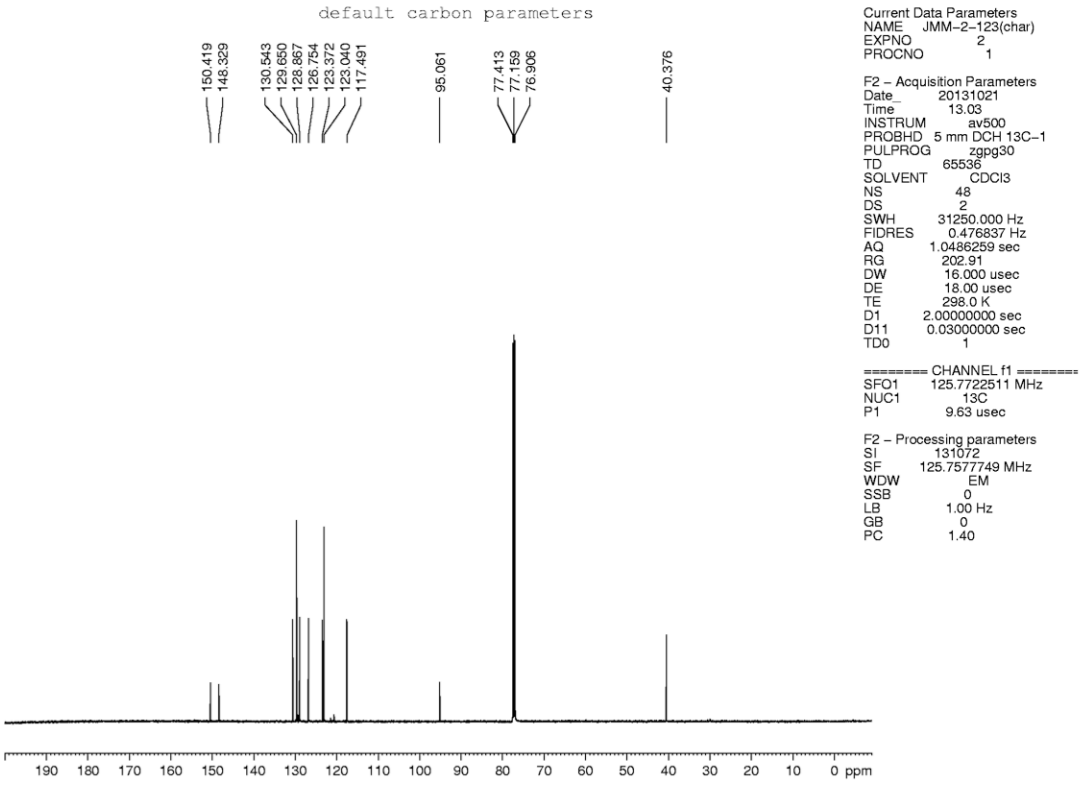

Figure 1.38. ^{13}C NMR (125 MHz, $CDCl_3$) of compound **1.2e**

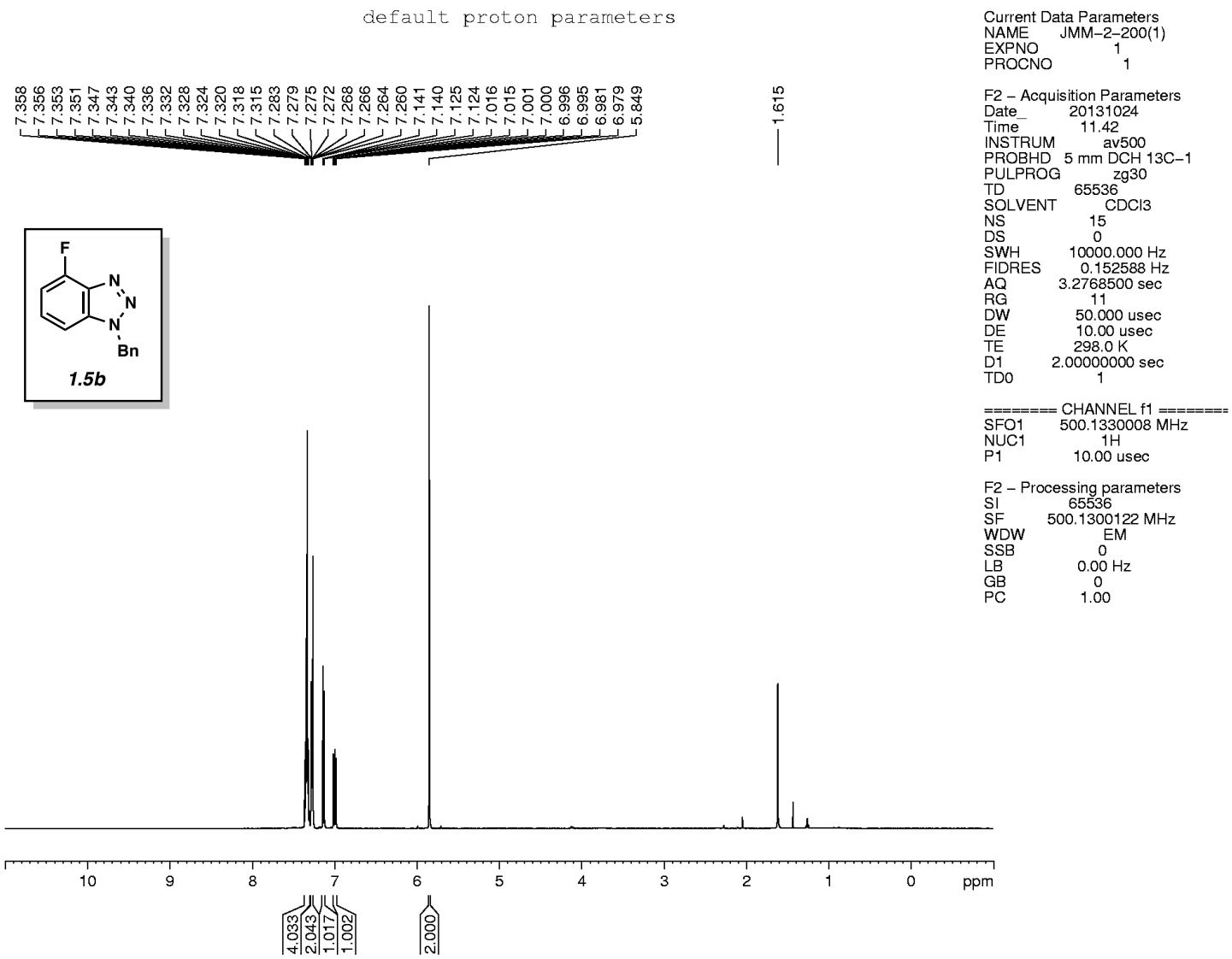

Figure 1.39. ^{1}H NMR (500 MHz, $CDCl_3$) compound **1.5b**

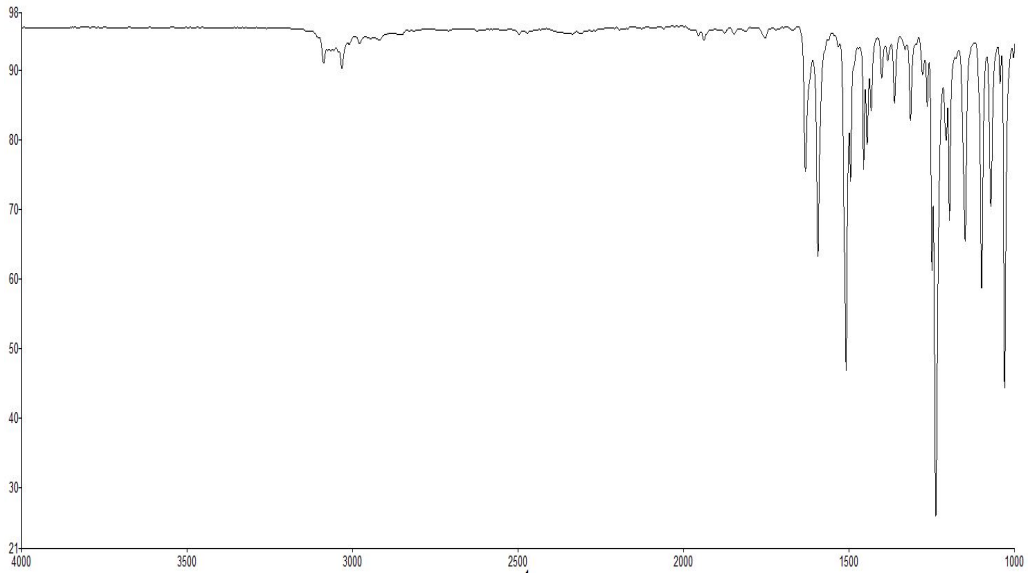

Figure 1.40. Infrared spectrum of compound **1.5b**

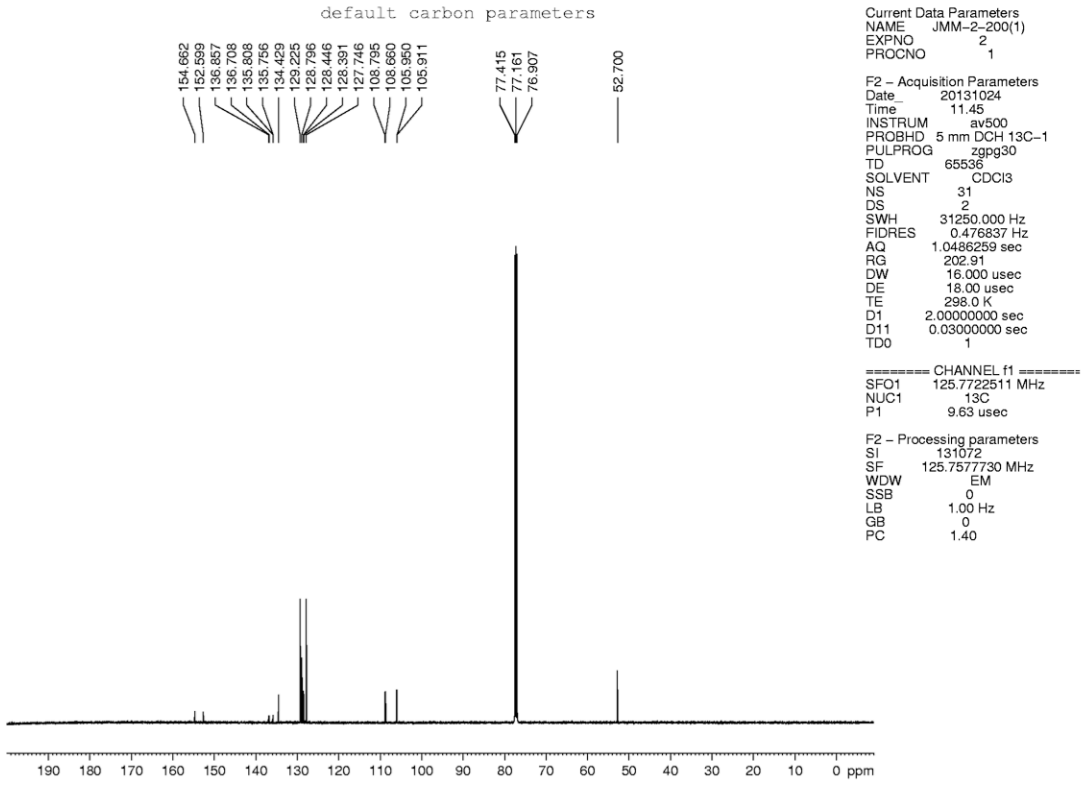

Figure 1.41. ^{13}C NMR (125 MHz, $CDCl_3$) of compound **1.5b**

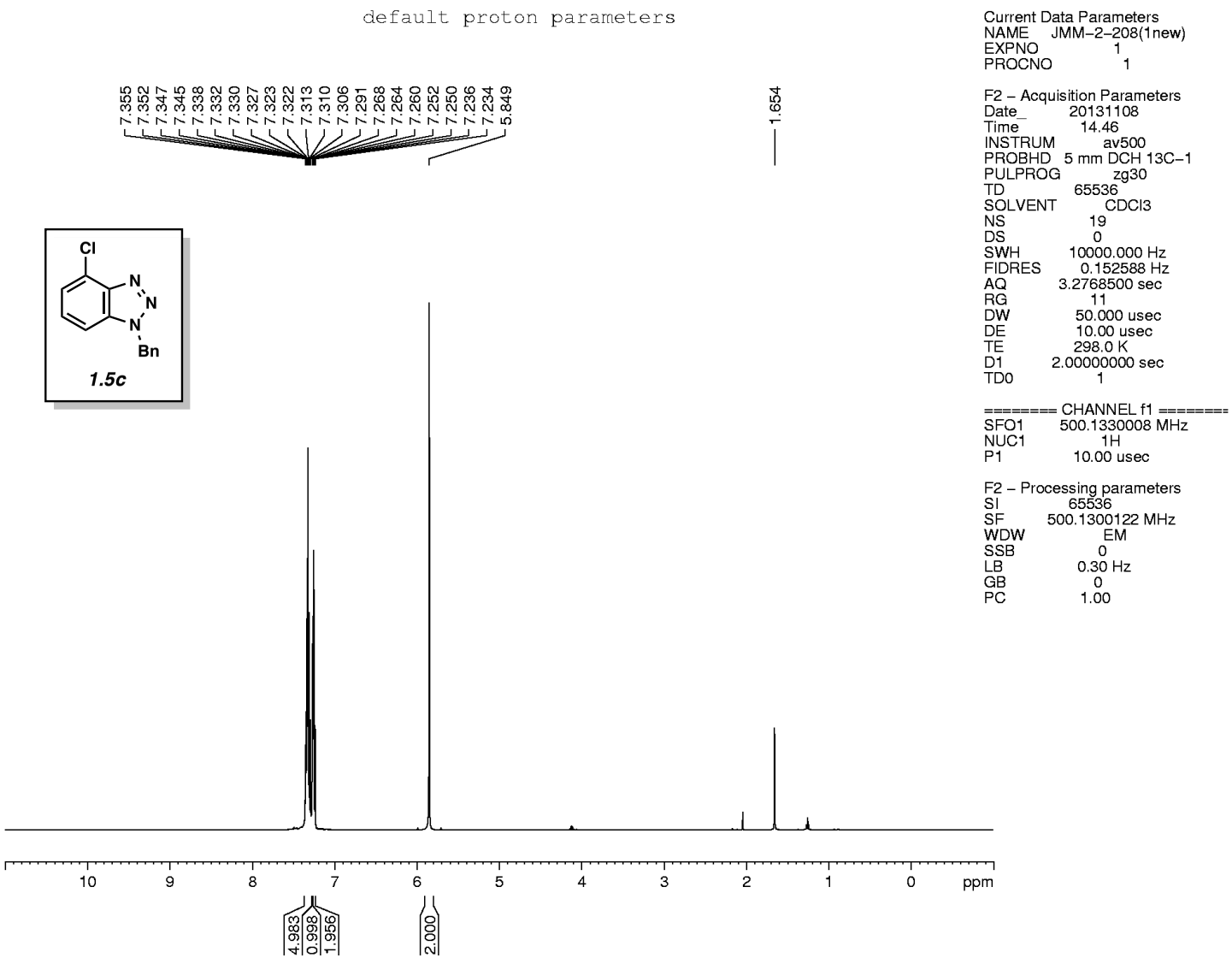

Figure 1.42. ^{1}H NMR (500 MHz, $CDCl_3$) compound **1.5c**

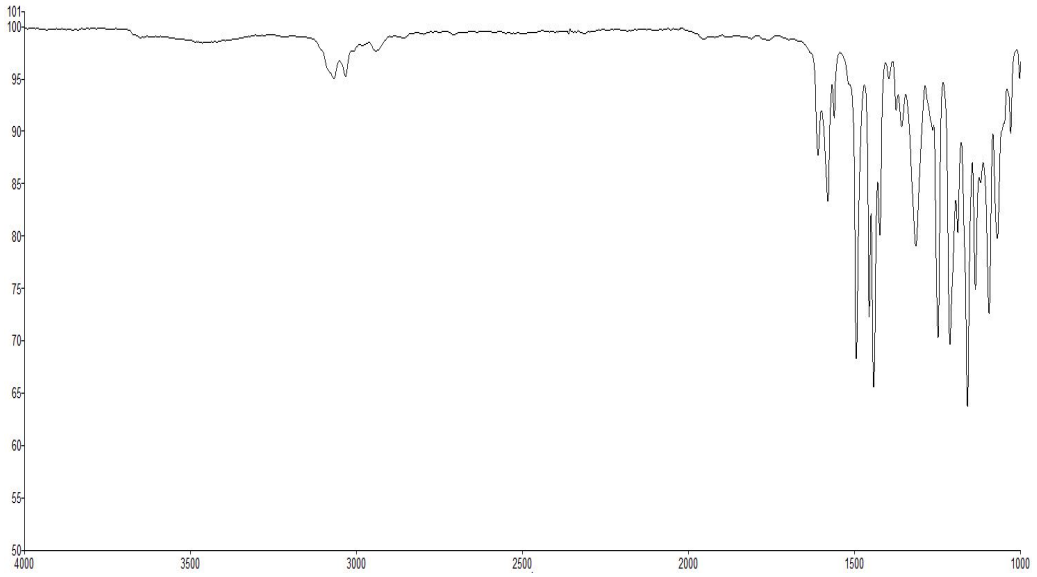

Figure 1.43. Infrared spectrum of compound **1.5c**

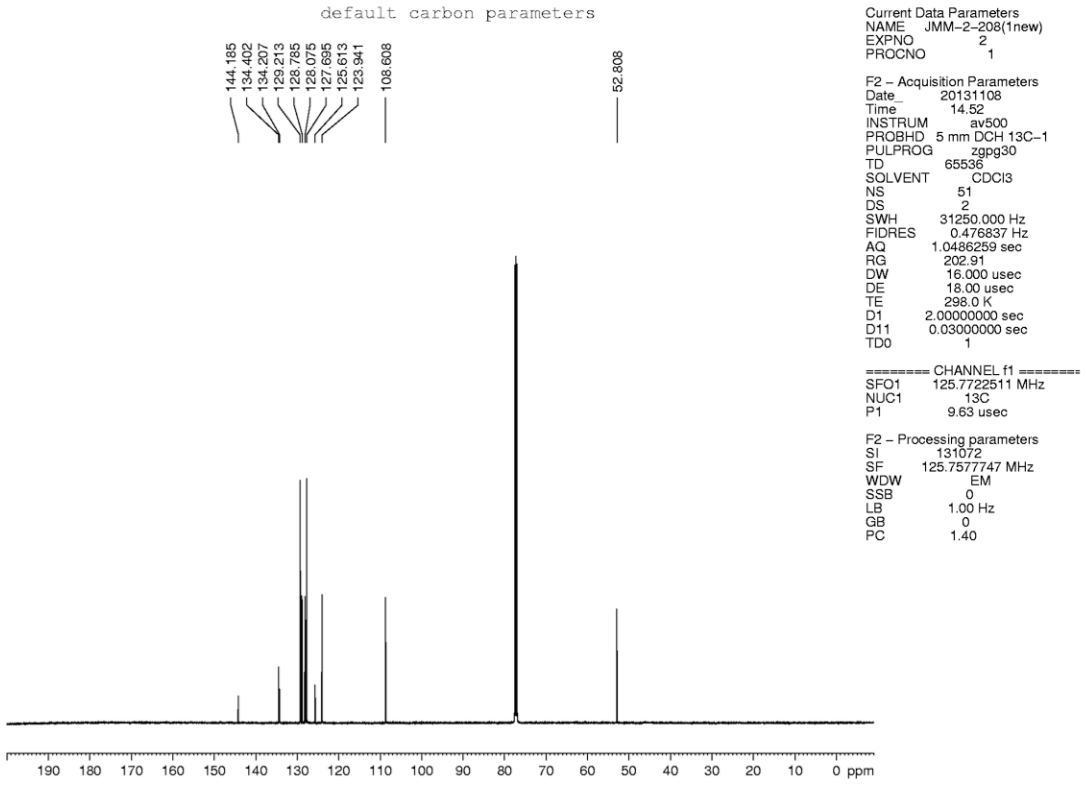

Figure 1.44. ^{13}C NMR (125 MHz, $CDCl_3$) of compound **1.5c**

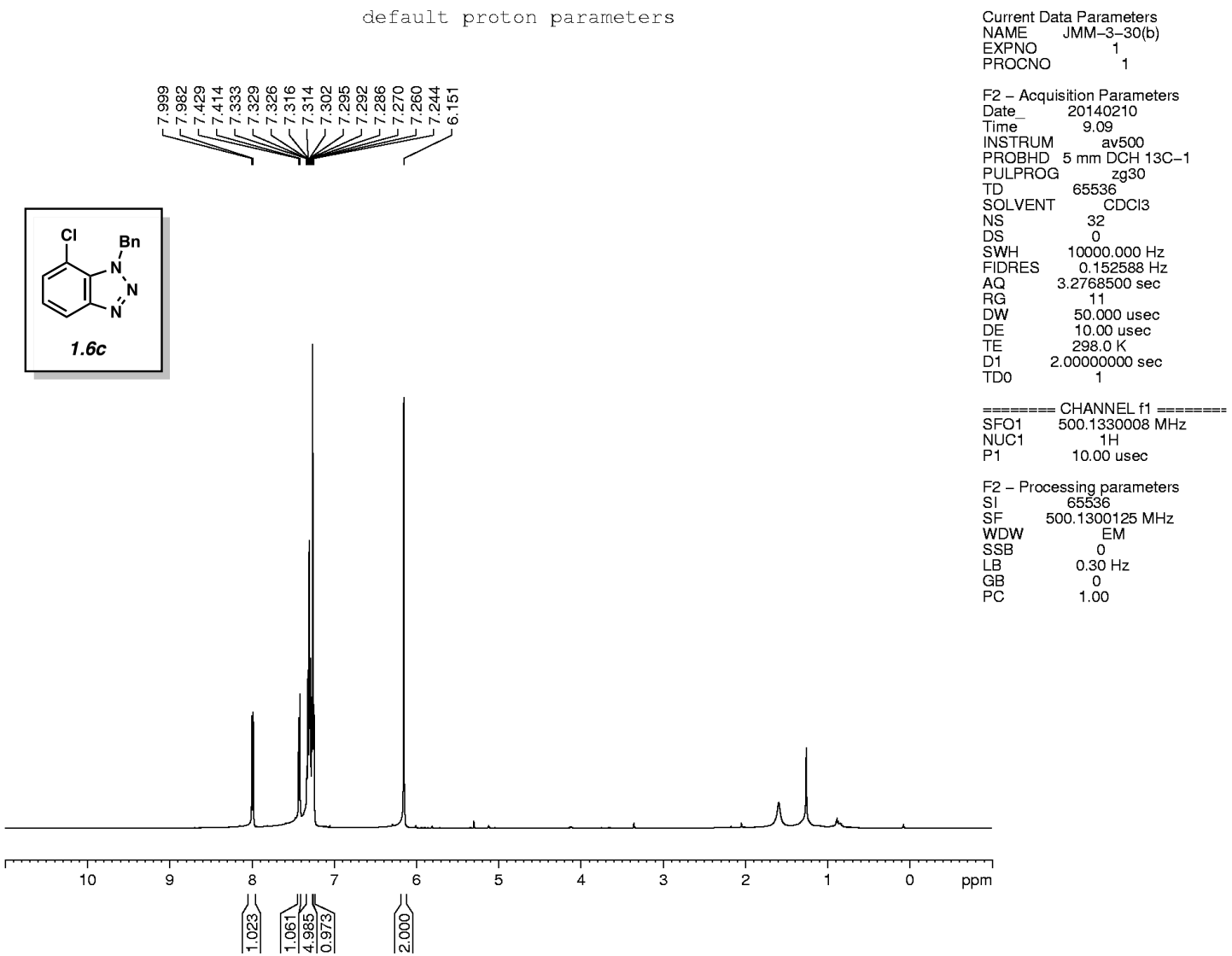

Figure 1.45. ^{1}H NMR (500 MHz, $CDCl_3$) compound **1.6c**

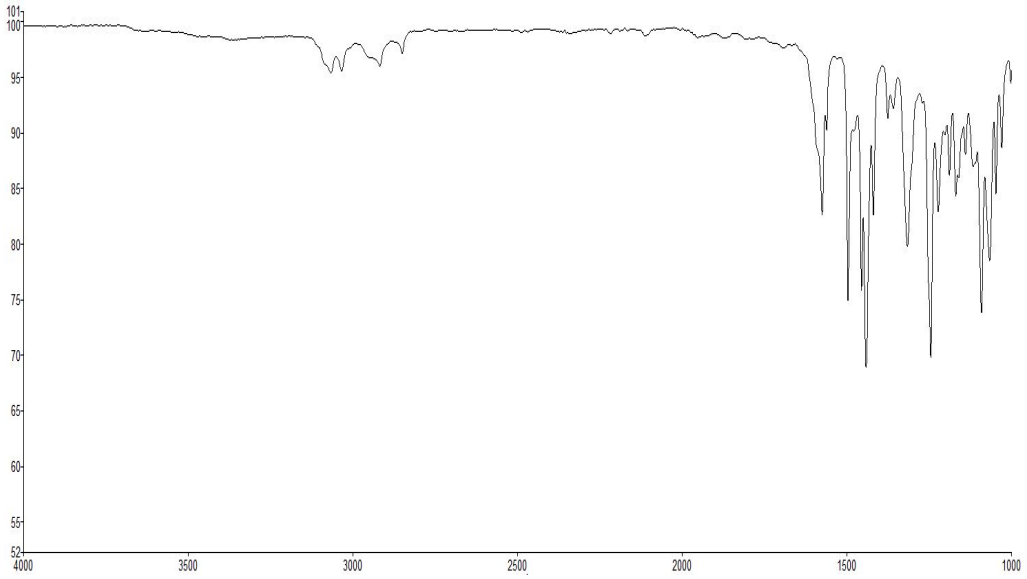

Figure 1.46. Infrared spectrum of compound **1.6c**

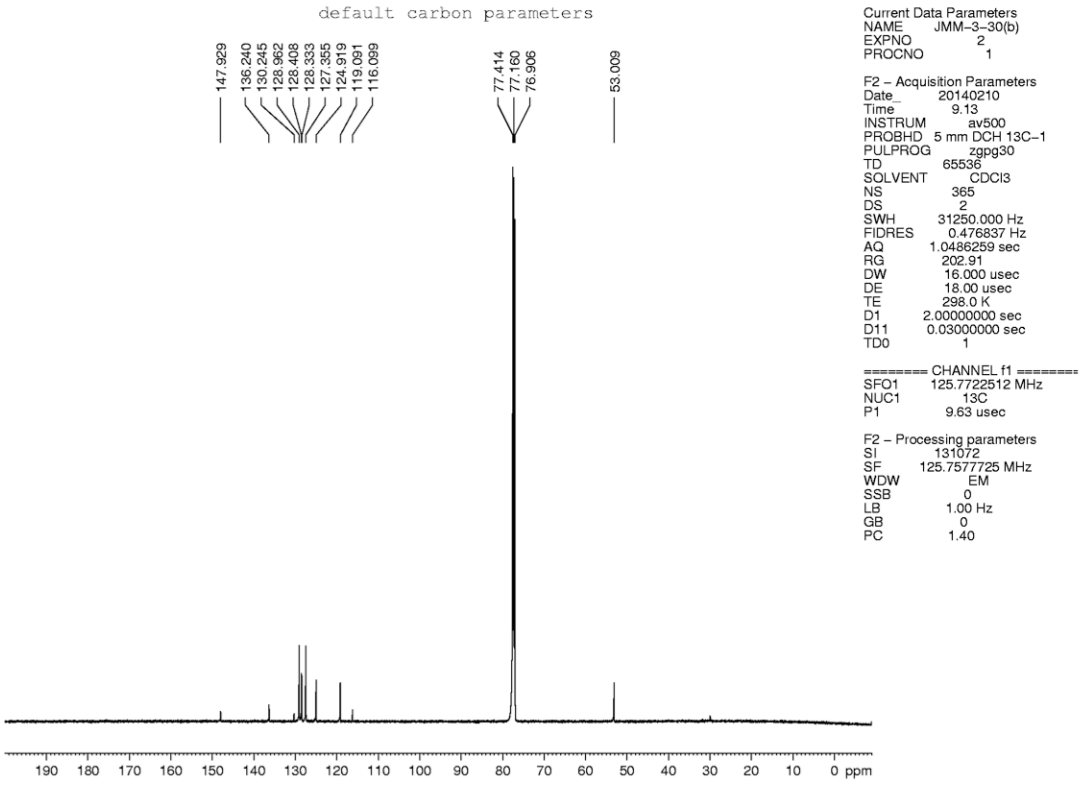

Figure 1.47. ^{13}C NMR (125 MHz, $CDCl_3$) of compound **1.6c**

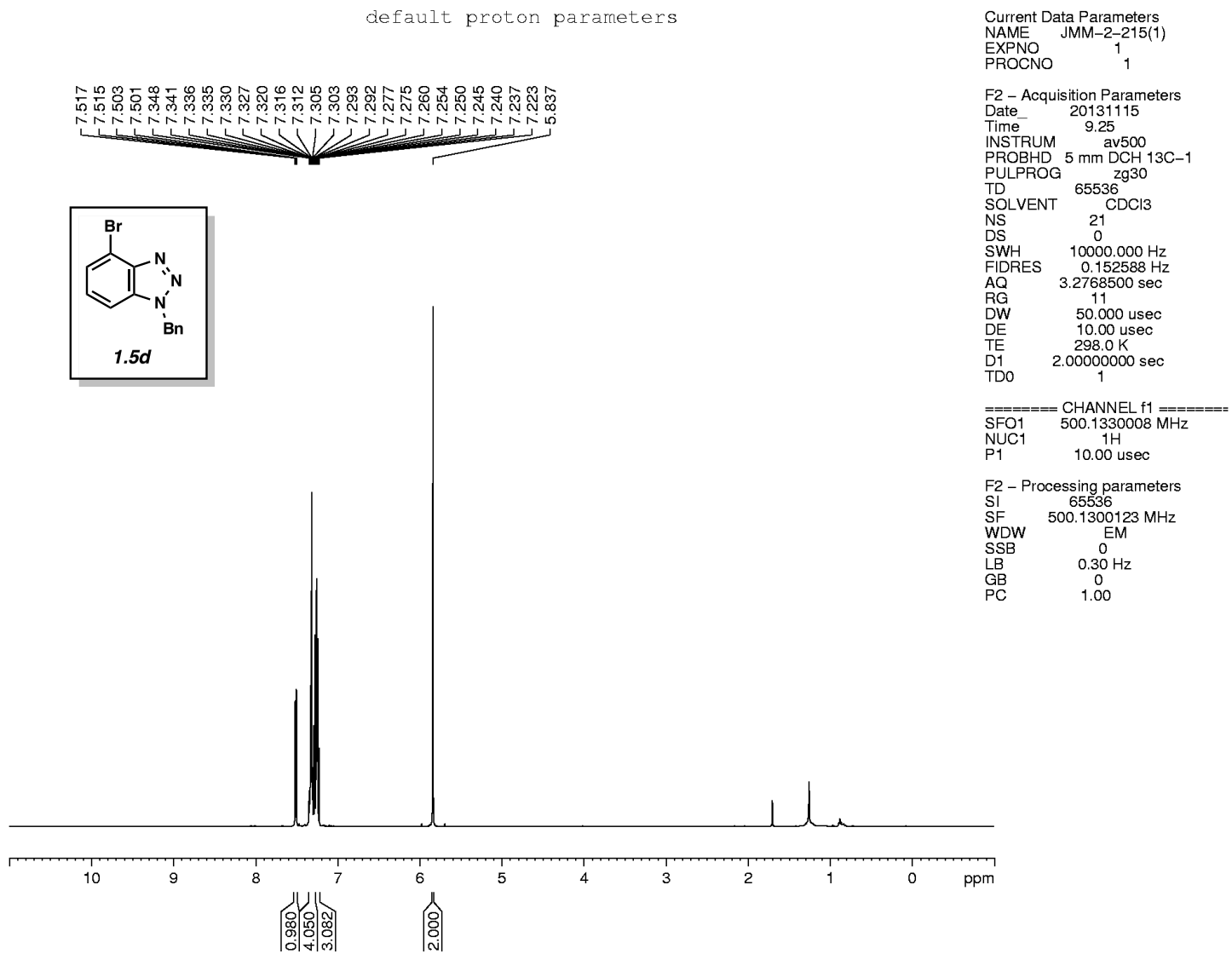

Figure 1.48. ^{1}H NMR (500 MHz, $CDCl_3$) compounds **1.5d**

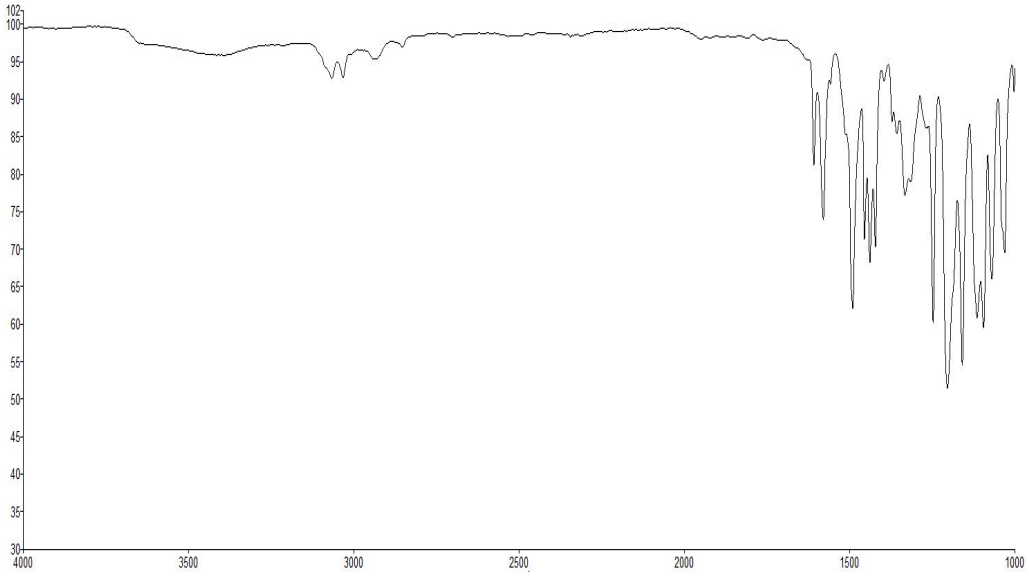

Figure 1.49. Infrared spectrum of compounds **1.5d**

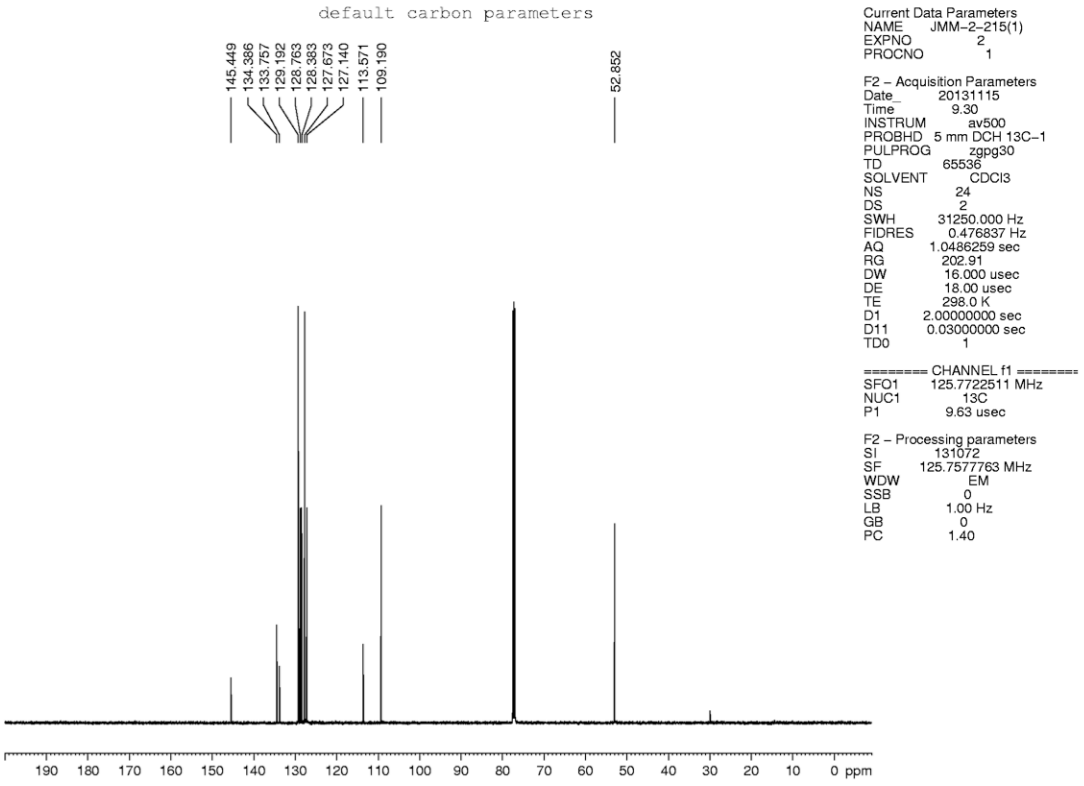

Figure 1.50. ^{13}C NMR (125 MHz, $CDCl_3$) of compounds **1.5d**

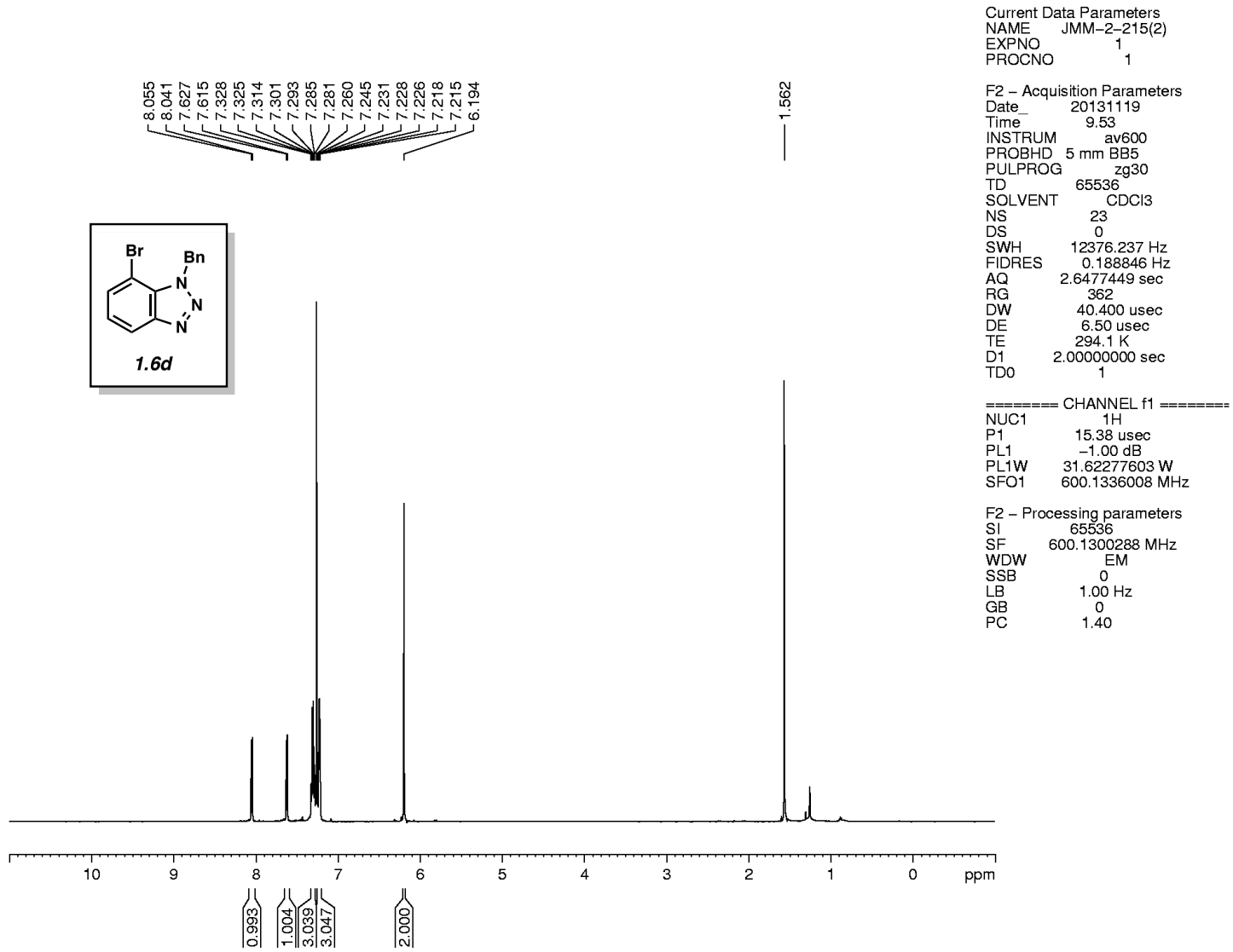

Figure 1.51. ^{1}H NMR (600 MHz, $CDCl_3$) compounds **1.6d**

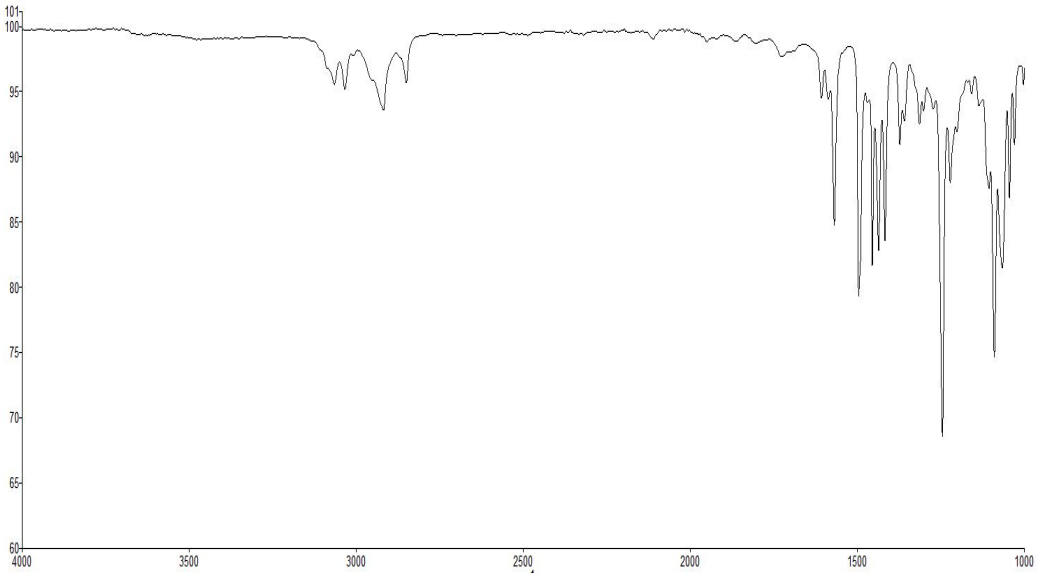

Figure 1.52. Infrared spectrum of compound **1.6d**

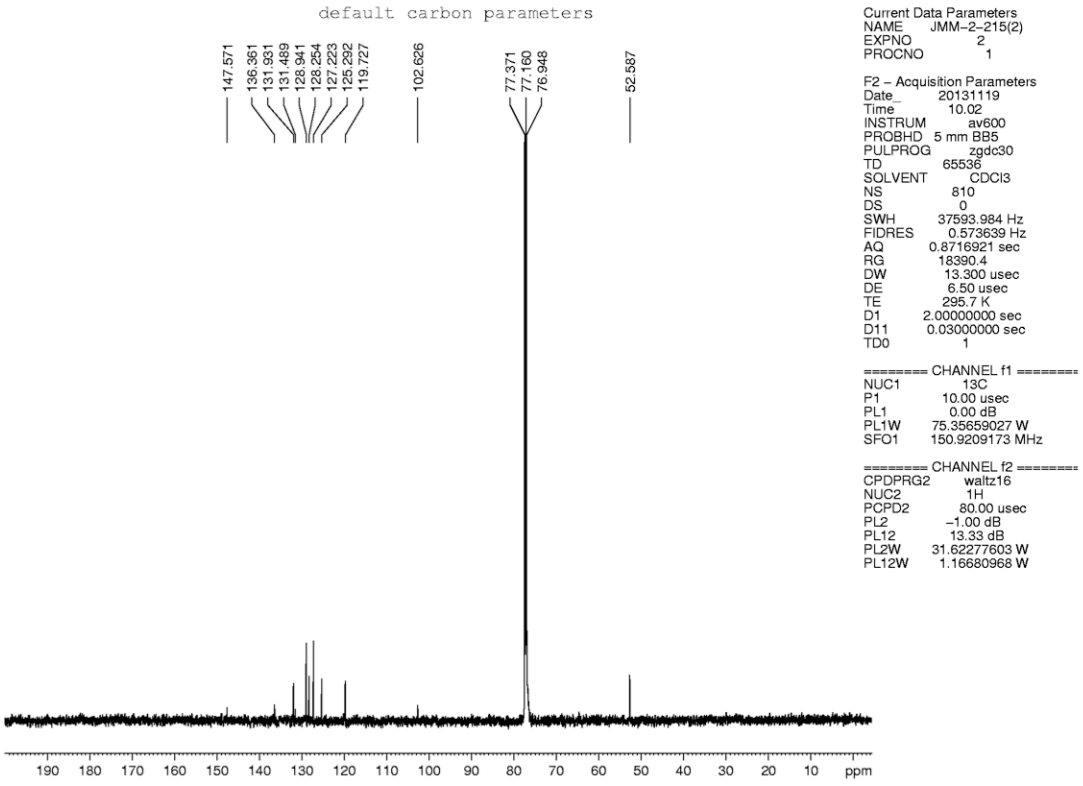

Figure 1.53. ^{13}C NMR (150 MHz, $CDCl_3$) of compounds **1.6d**

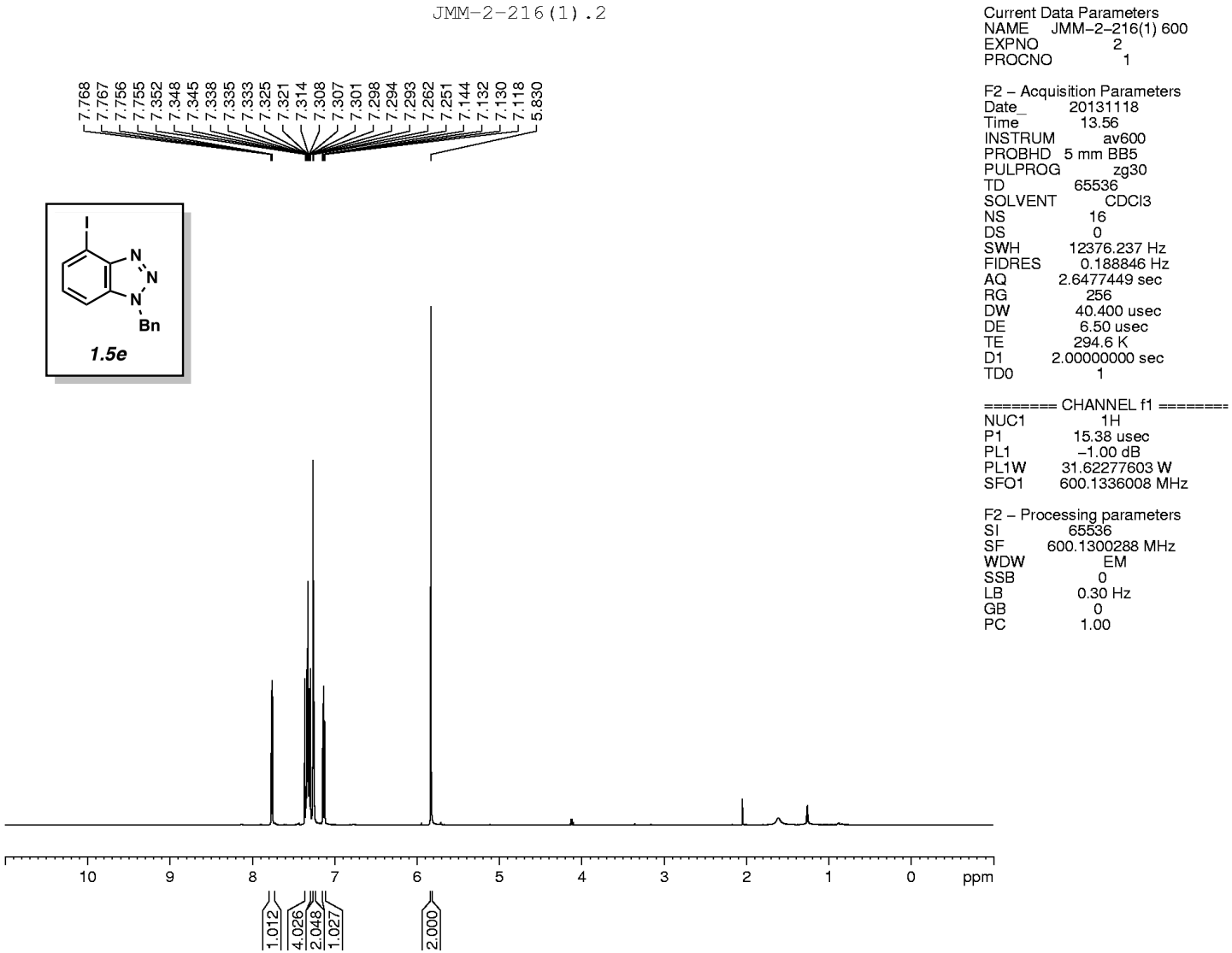

Figure 1.54. ^{1}H NMR (600 MHz, $CDCl_3$) compound **1.5e**

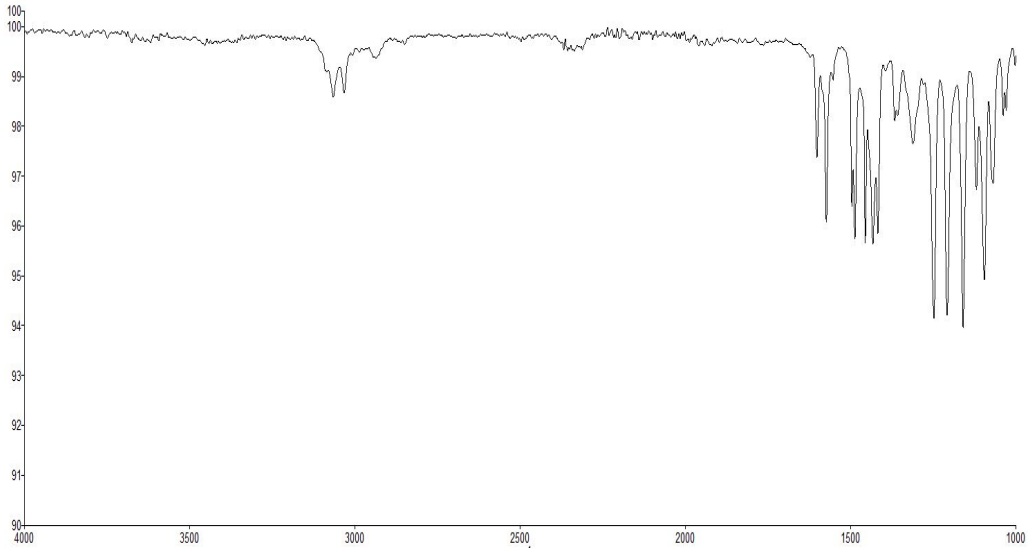

Figure 1.55. Infrared spectrum of compound **1.5e**

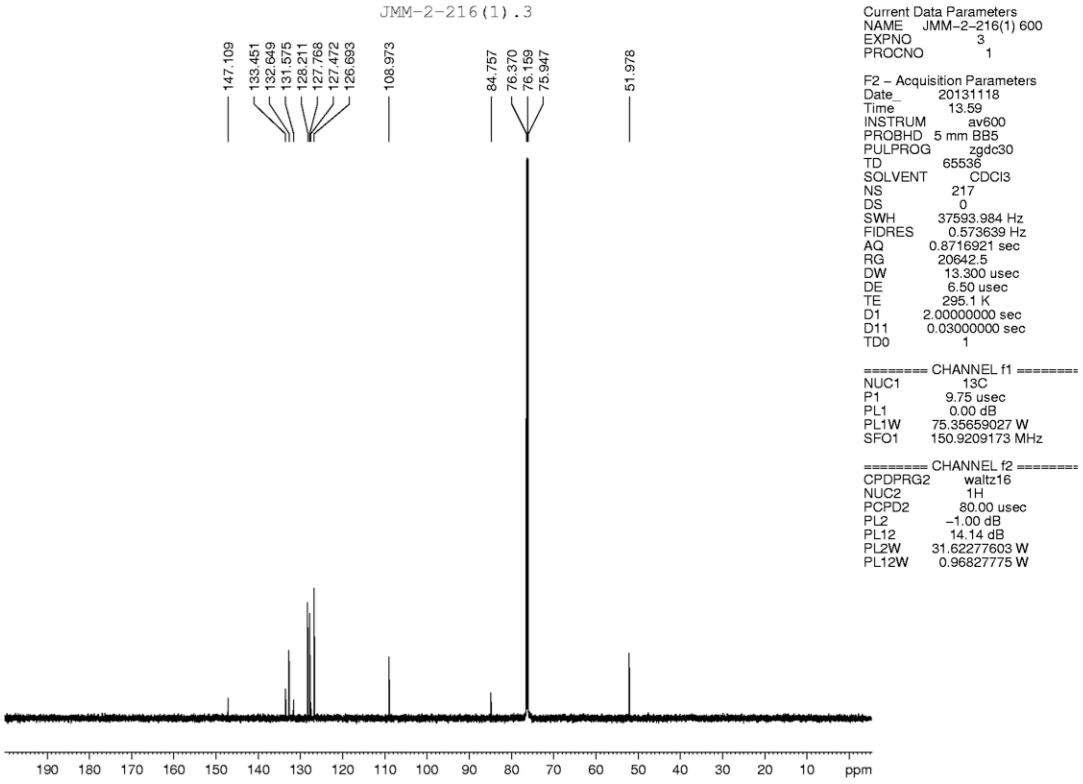

Figure 1.56. ^{13}C NMR (150 MHz, $CDCl_3$) of compound **1.5e**

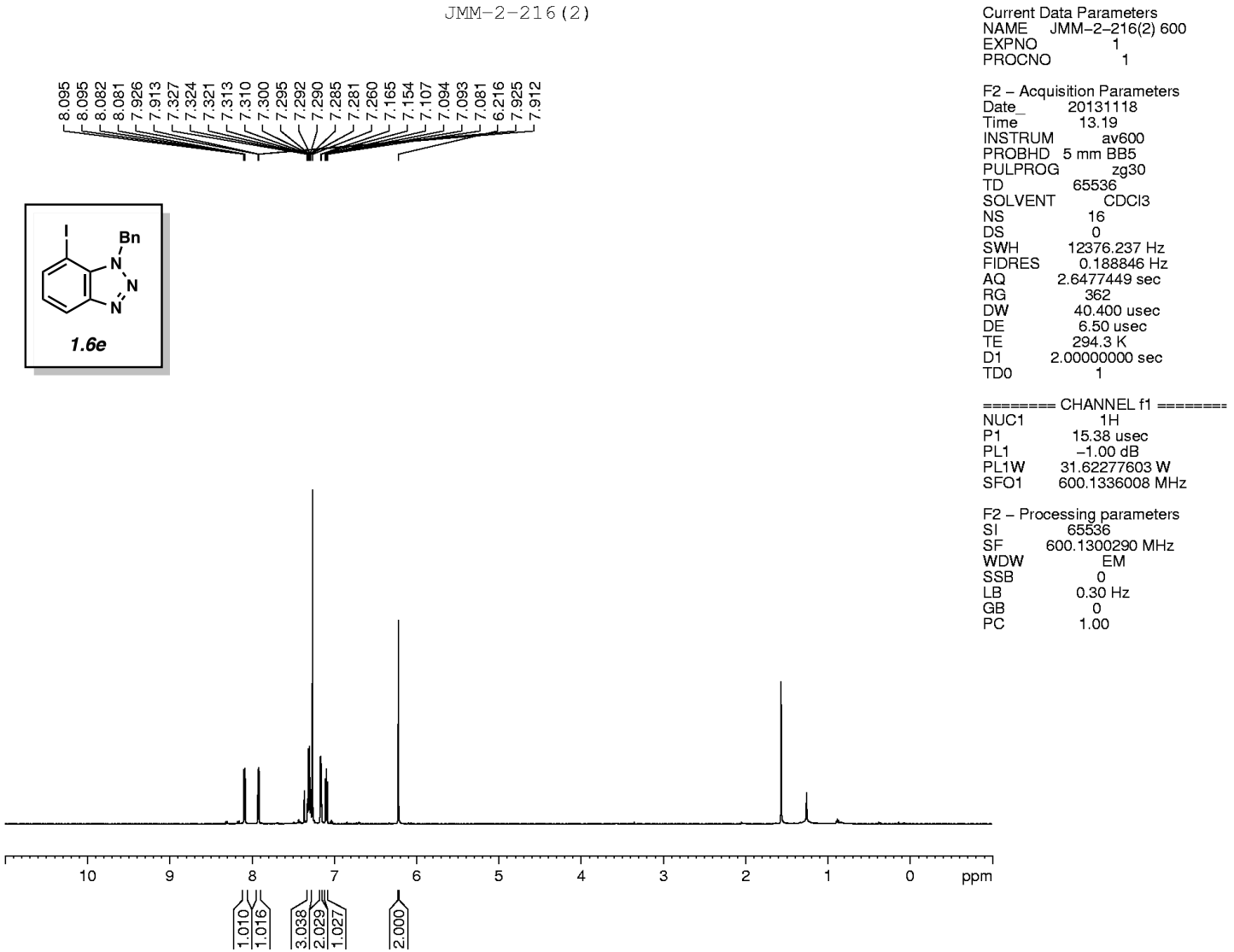

Figure 1.57. ^{1}H NMR (600 MHz, $CDCl_3$) compound **1.6e**

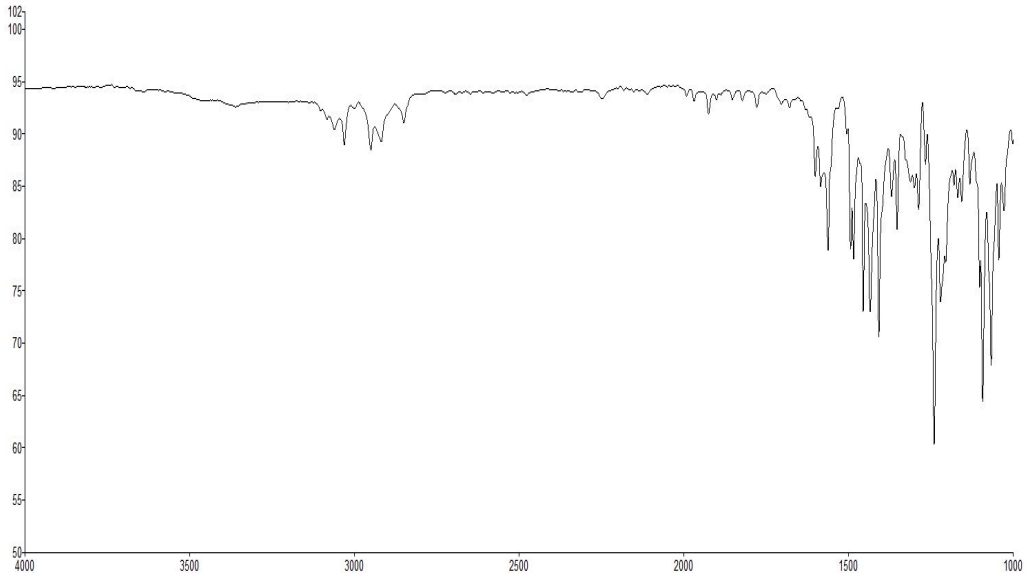

Figure 1.58. Infrared spectrum of compound **1.6e**

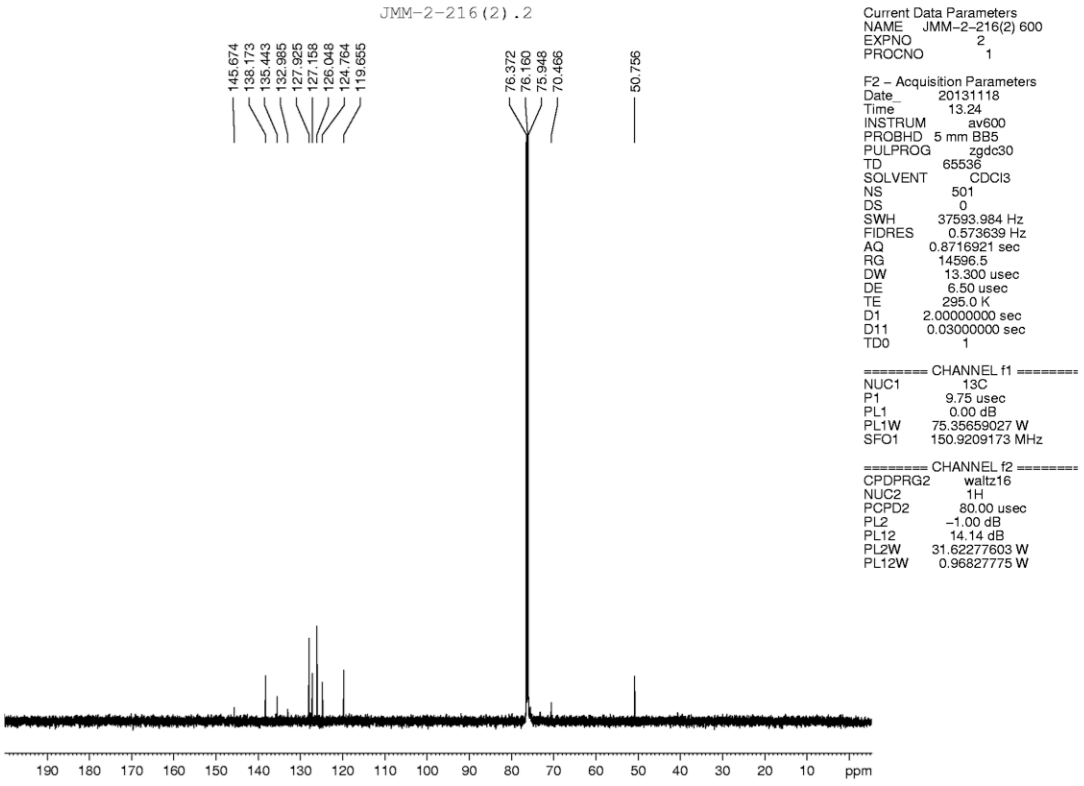

Figure 1.59. ^{13}C NMR (150 MHz, $CDCl_3$) of compound **1.6e**

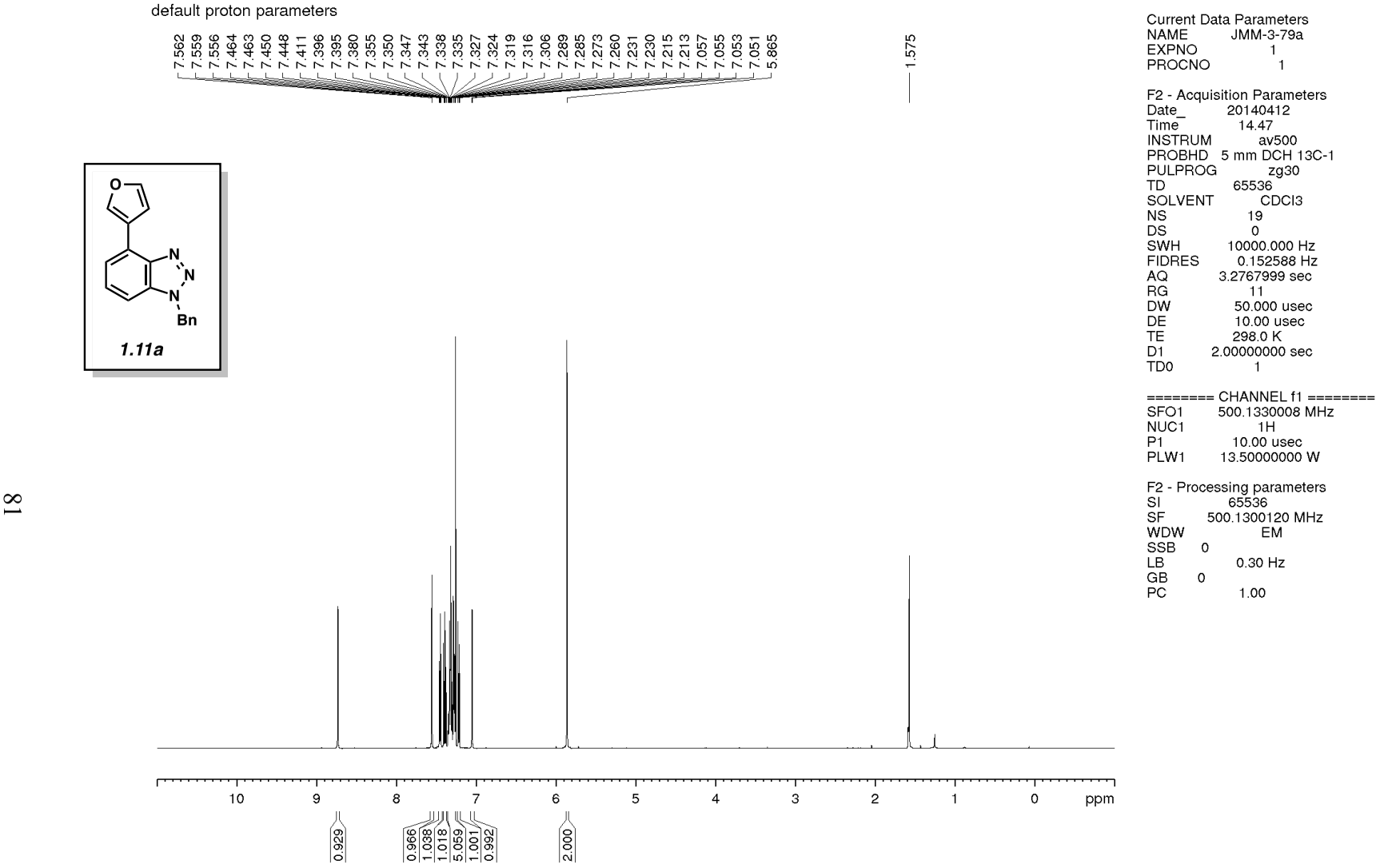

Figure 1.60. ^{1}H NMR (500 MHz, $CDCl_3$) compound **1.11a**

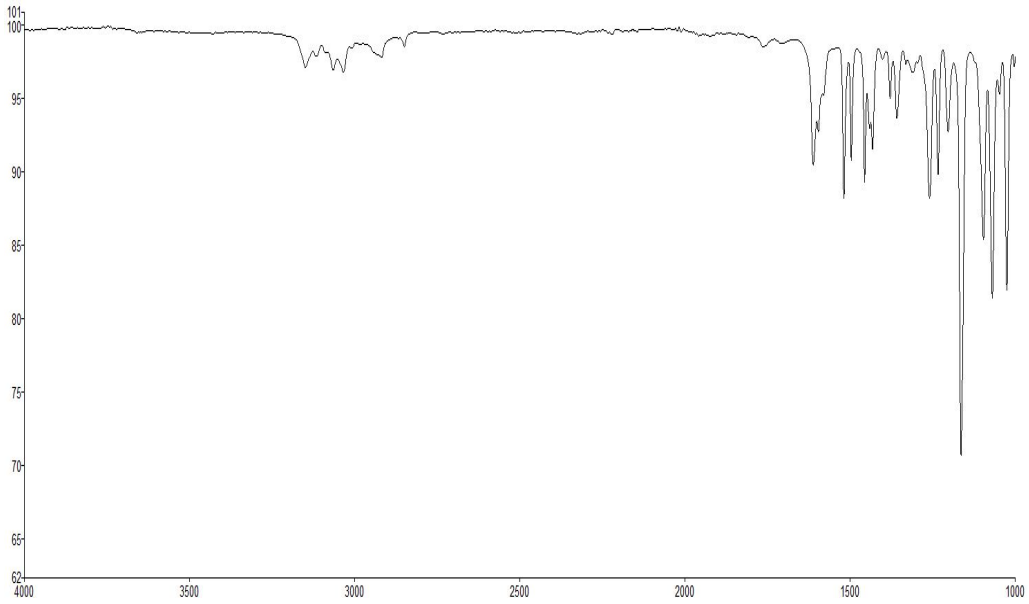

Figure 1.61. Infrared spectrum of compound **1.11a**

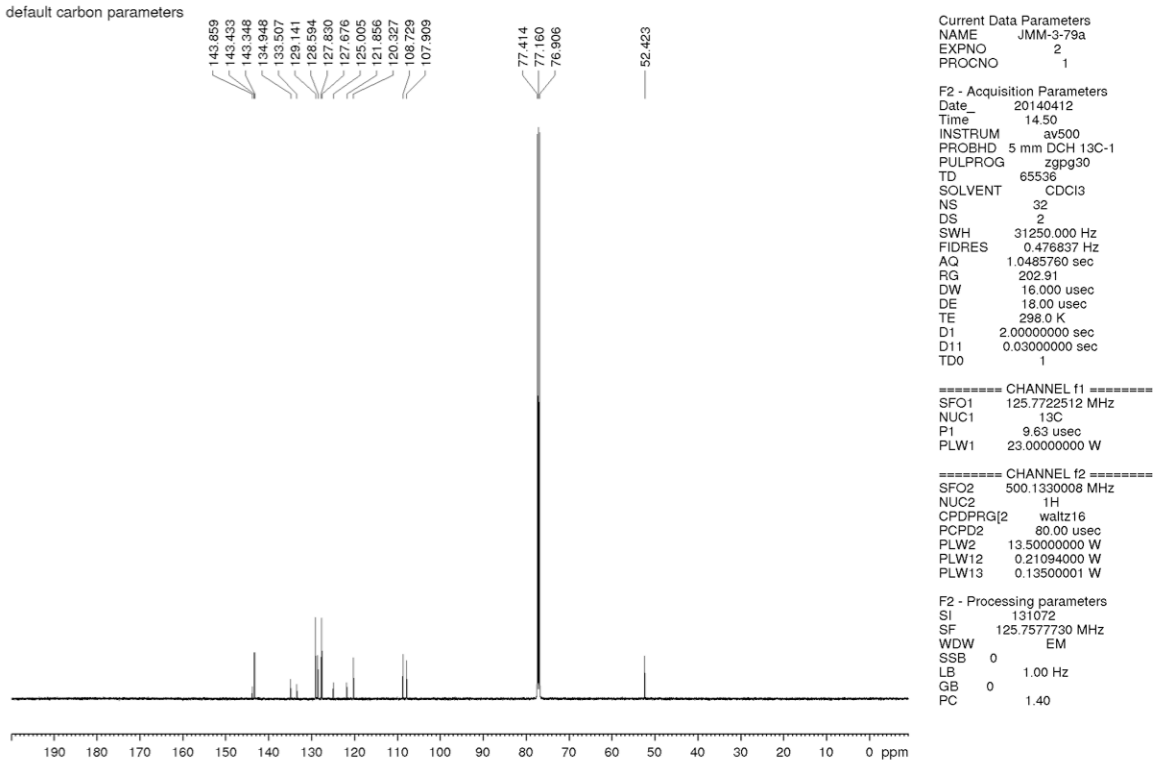

Figure 1.62. ^{13}C NMR (125 MHz, $CDCl_3$) of compound **1.11a**

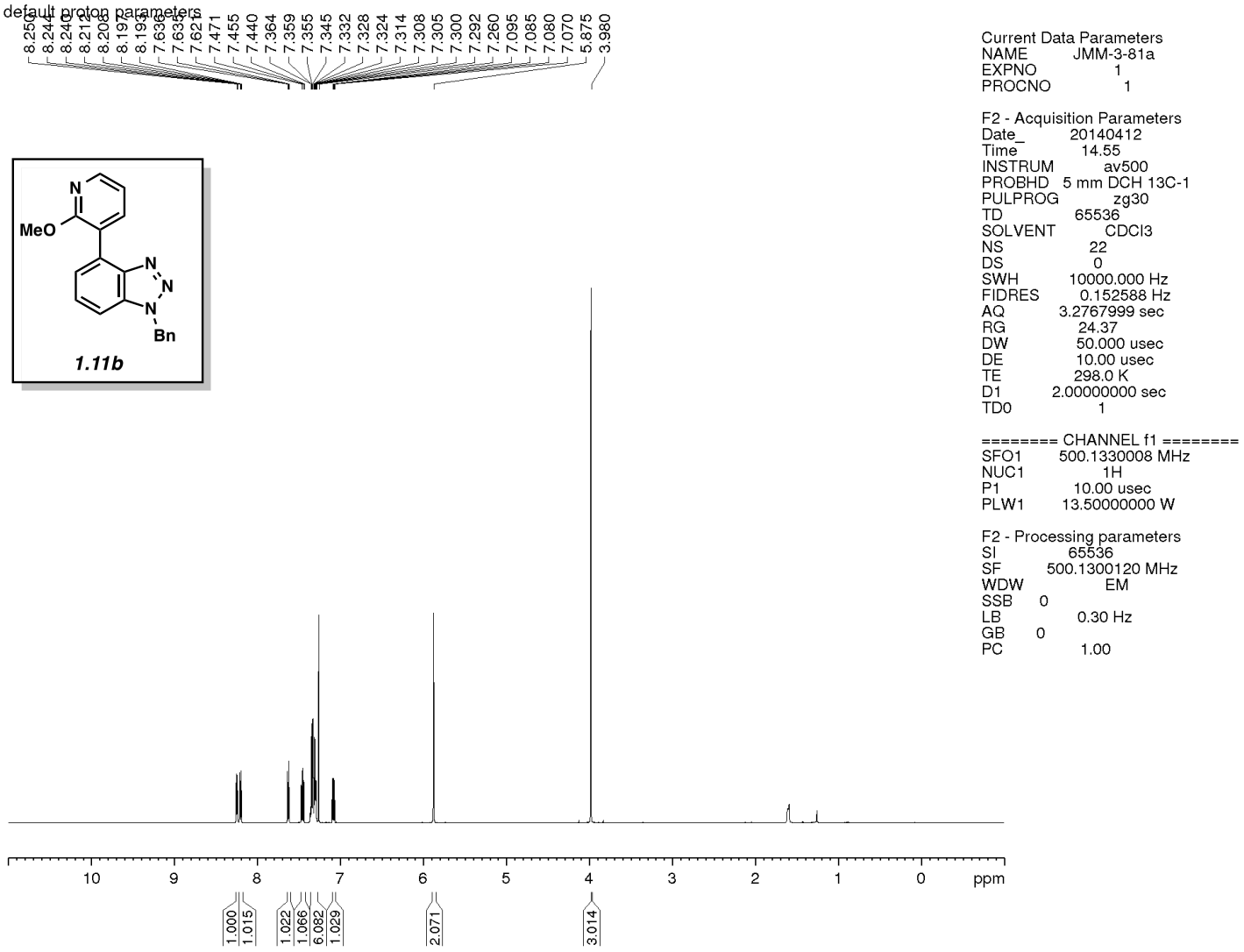

Figure 1.63. ^{1}H NMR (500 MHz, $CDCl_3$) compound **1.11b**

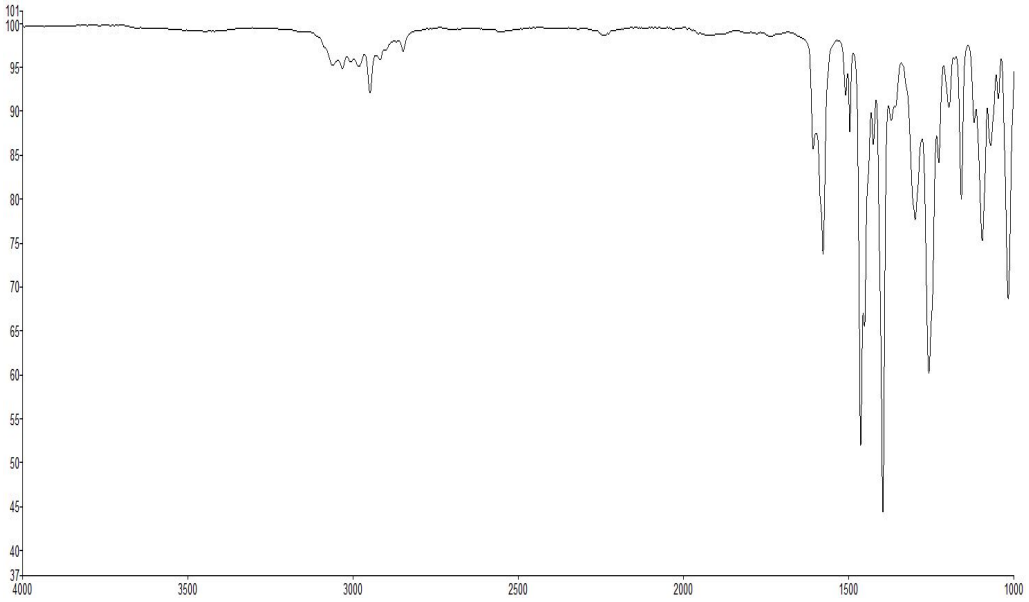

Figure 1.64. Infrared spectrum of compound **1.11b**

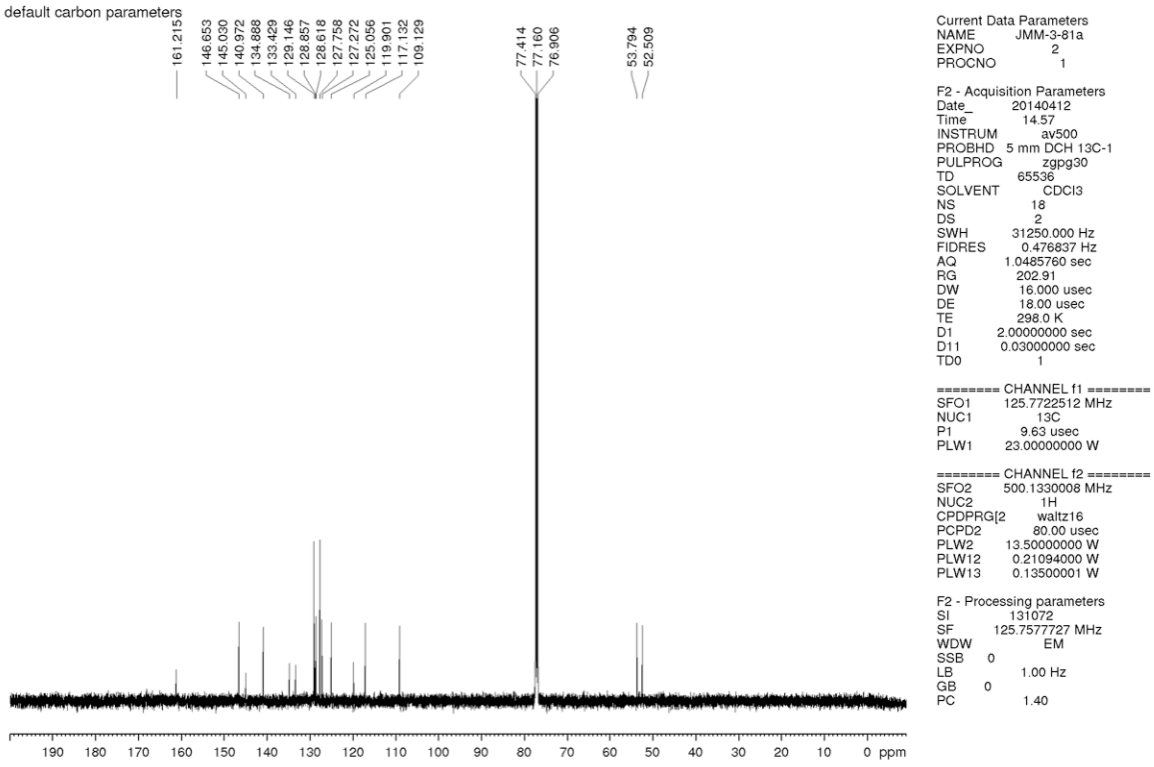

Figure 1.65. ^{13}C NMR (125 MHz, $CDCl_3$) of compound **1.11b**

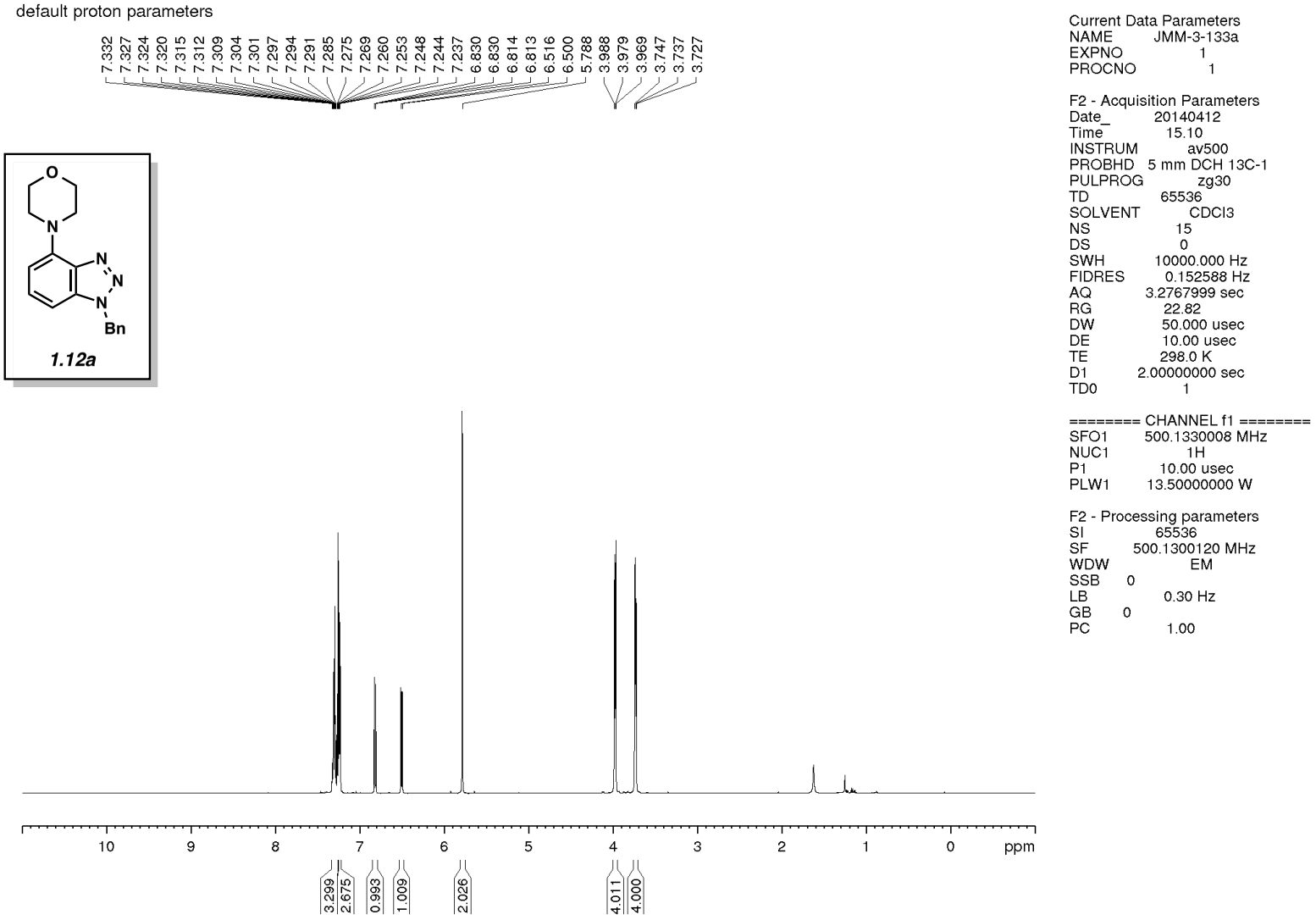

Figure 1.66. ^{1}H NMR (500 MHz, $CDCl_3$) compound **1.12a**

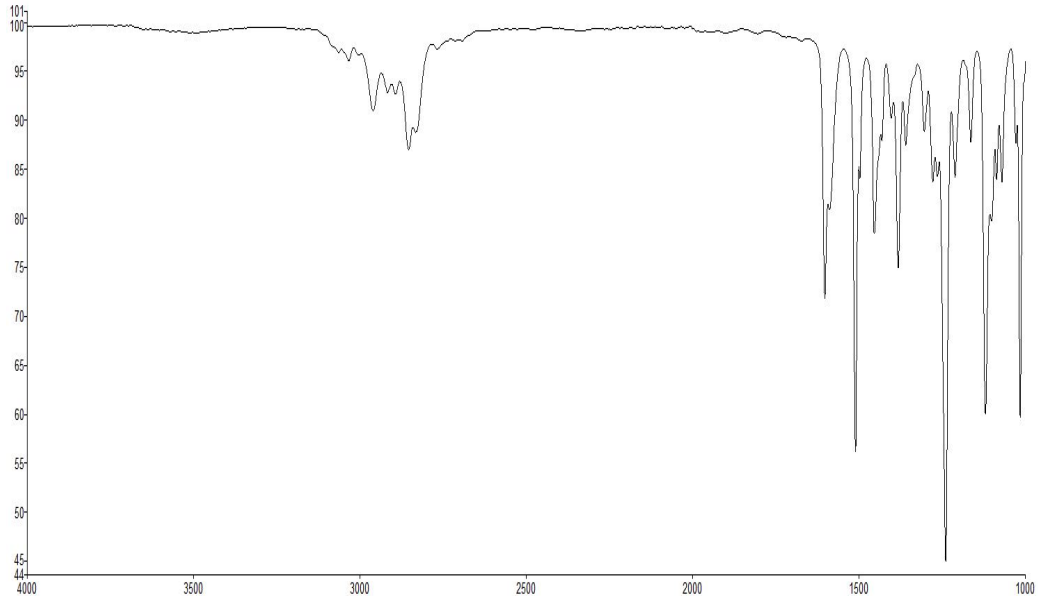

Figure 1.67. Infrared spectrum of compound **1.12a**

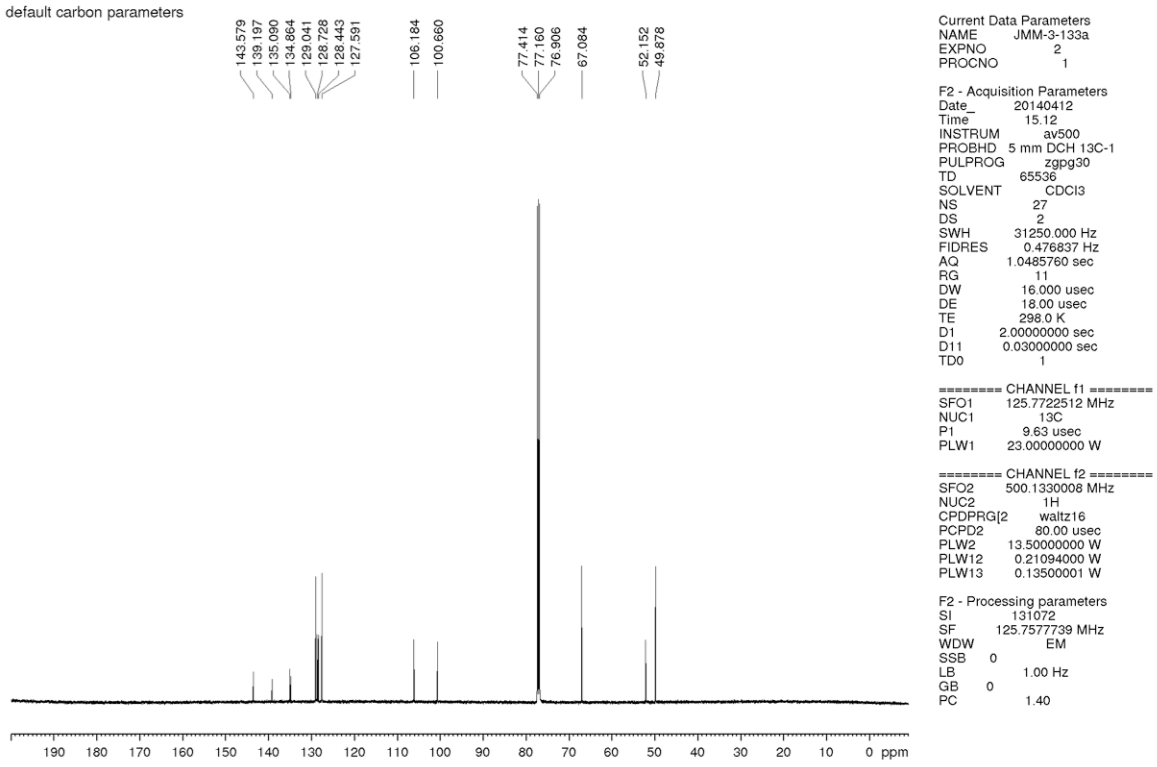

Figure 1.68. ^{13}C NMR (125 MHz, $CDCl_3$) of compound **1.12a**

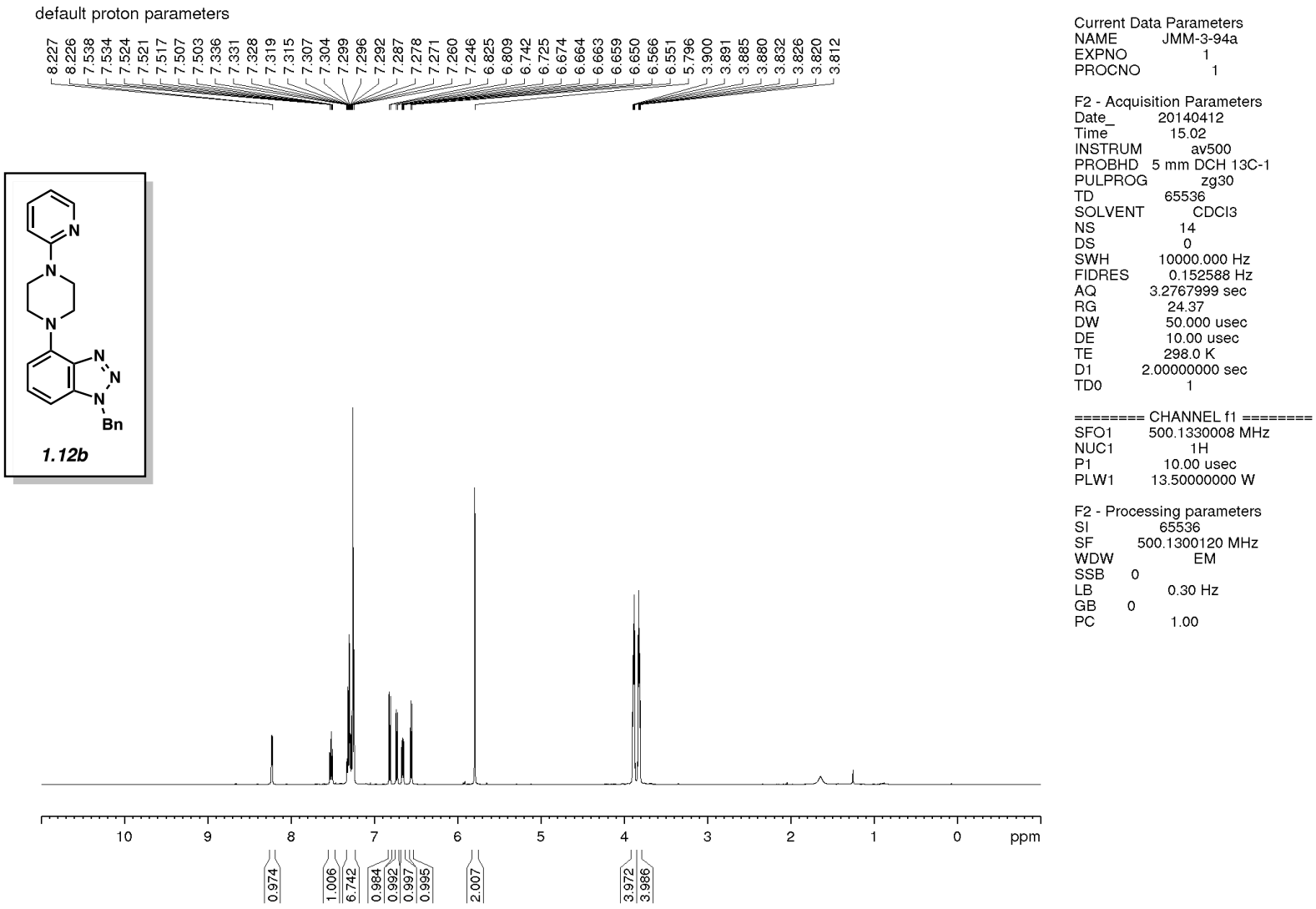

Figure 1.69. ^{1}H NMR (500 MHz, $CDCl_3$) compound **1.12b**

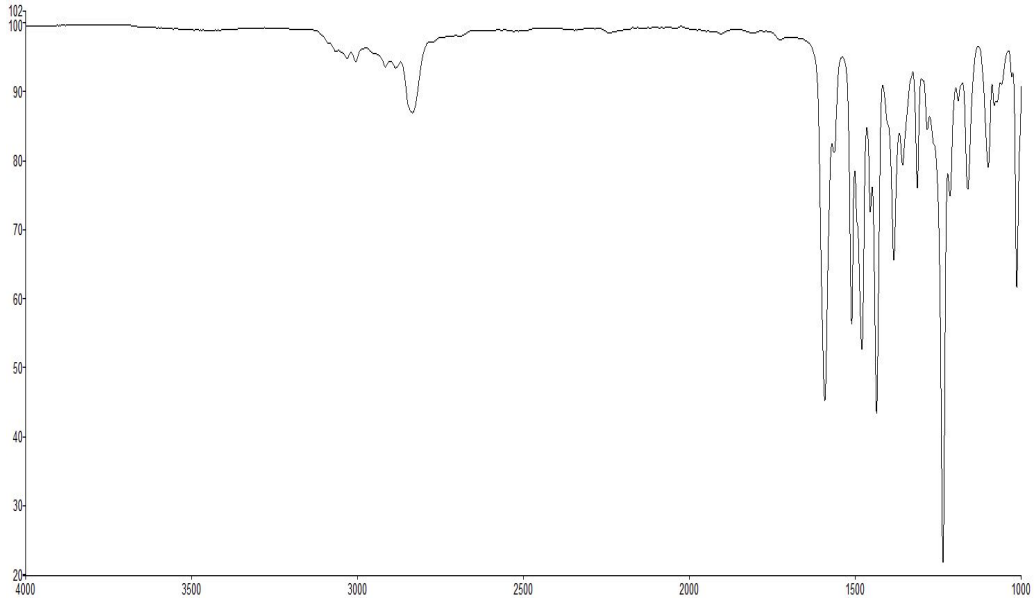

Figure 1.70. Infrared spectrum of compound **1.12b**

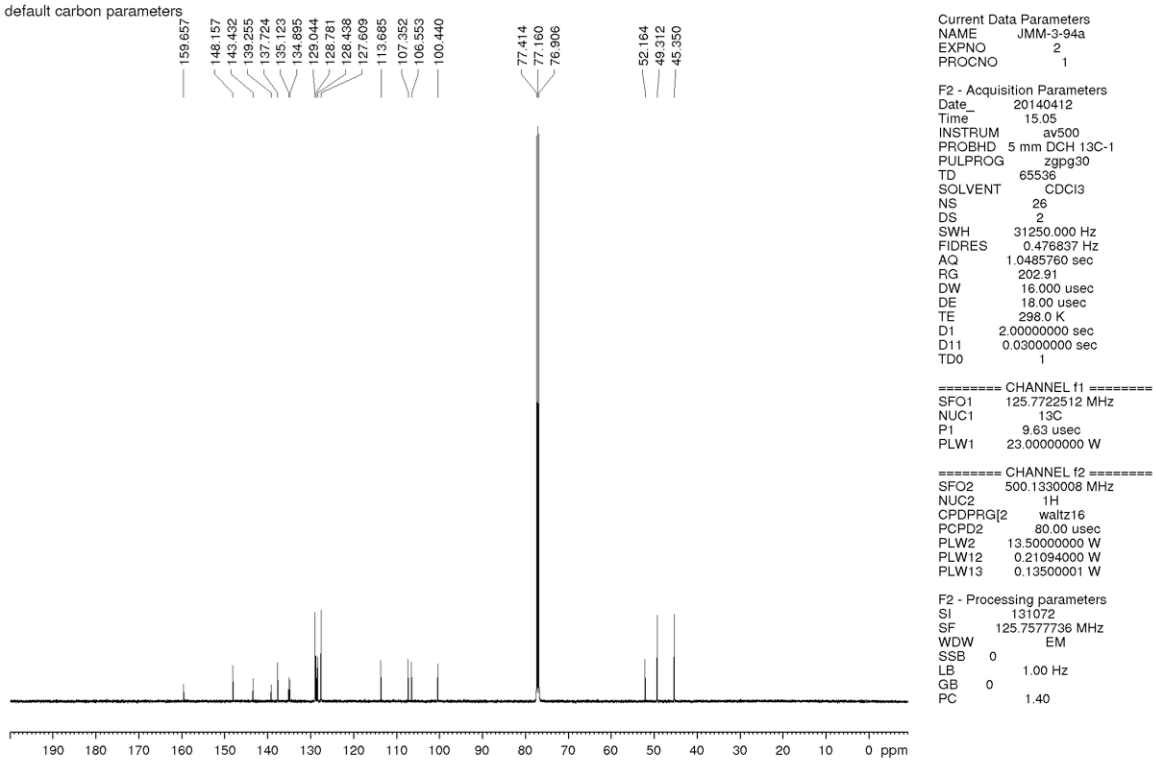

Figure 1.71. ^{13}C NMR (125 MHz, $CDCl_3$) of compound **1.12b**

1.7 Notes and References

(1) For the application of distortion energies to regioselectivity of cycloaddition reactions, see: (a) Ess, D. H.; Houk, K. N. *J. Am. Chem. Soc.* **2007**, *129*, 10646–10647. (b) Ess, D. H.; Houk, K. N. *J. Am. Chem. Soc.* **2008**, *130*, 10187–10198. (c) Lam, Y.-h.; Cheong, P. H.-Y.; Blasco Mata, J. M.; Stanway, S. J.; Gouverneur, V.; Houk, K. N. *J. Am. Chem. Soc.* **2009**, *131*, 1947–1957. (d) Hayden, A. E.; Houk, K. N. *J. Am. Chem. Soc.* **2009**, *131*, 4084–4089. (e) Schoenebeck, F.; Ess, D. H.; Jones, G. O.; Houk, K. N. *J. Am. Chem. Soc.* **2009**, *131*, 8121–8133. (f) Osuna, S.; Houk, K. N. *Chem. Eur. J.* **2009**, *15*, 13219–13231. (g) Paton, R. S.; Kim, S.; Ross, A. G.; Danishefsky, S. J.; Houk, K. N. *Angew. Chem. Int. Ed.* **2011**, *50*, 10366–10368. (h) Lan, Y.; Wheeler, S. E.; Houk, K. N. *J. Chem. Theory Comput.* **2011**, *7*, 2104–2111. (i) Liang, Y.; Mackey, J. L.; Lopez, S. A.; Liu, F.; Houk, K. N. *J. Am. Chem. Soc.* **2012**, *134*, 17904–17907. (j) Gordon, C. G.; Mackey, J. L.; Jewett, J. C.; Sletten, E. M.; Houk, K. N.; Bertozzi, C. R. *J. Am. Chem. Soc.* **2012**, *134*, 9199–9208. (k) Lopez, S. A.; Munk, M. E.; Houk, K. N. *J. Org. Chem.* **2013**, *78*, 1576–1582. (l) Lopez, S. A.; Houk, K. N. *J. Org. Chem.* **2013**, *78*, 1778–1783. (m) Kamber, D. N.; Nazarova, L. A.; Liang, Y.; Lopez, S. A.; Patterson, D. M.; Shih, H.-W.; Houk, K. N.; Prescher, J. A. *J. Am. Chem. Soc.* **2013**, *135*, 13680–13683. (n) Liu, F.; Paton, R. S.; Kim, S.; Liang, Y.; Houk, K. N. *J. Am. Chem. Soc*. **2013**, *135*, 15642–15649. (o) Yang, J.; Liang, Y.; Šečkutė, J.; Houk, K. N.; Devaraj, N. K. *Chem. Eur. J.* **2014**, *20*, 3365–3375. (p) Hong, X.; Liang, Y.; Griffith, A. K.; Lambert, T. H.; Houk, K. N. *Chem. Sci.* **2014**, *5*, 471–475. (q) Liu, F.; Liang, Y.; Houk, K. N. *J. Am. Chem. Soc.* **2014**, *136*, 11483–11493. (r) Cao, Y.; Liang, Y.; Zhang, L.; Osuna, S.; Hoyt, A.-L. M.; Briseno, A. L.; Houk, K. N. *J. Am. Chem. Soc.* **2014**, *136*, 10743–10751. (s) Hong, X.; Liang, Y.; Brewer, M.; Houk, K. N. *Org. Lett.* **2014**, *16*, 4260–4263.

(2) For the application of distortion energies to regioselectivity of palladium-catalyzed cross coupling reactions, see: (a) Legault, C. Y.; Garcia, Y.; Merlic, C. A.; Houk, K. N. *J. Am. Chem. Soc.* **2007**, *129*, 12664–12665. (b) Garcia, Y.; Schoenebeck, F.; Legault, C. Y.; Merlic, C. A.; Houk, K. N. *J. Am. Chem. Soc.* **2009**, *131*, 6632–6639.

(3) For the application of distortion energies to understanding selectivities in C–H functionalization reactions, see: (a) Zou, L.; Paton, R. S.; Eschenmoser, A.; Newhouse, T. R.; Baran, P. S.; Houk, K. N. *J. Org. Chem.* **2013**, *78*, 4037–4048. (b) Green, A. G.; Liu, P.; Merlic, C. A.; Houk, K. N. *J. Am. Chem. Soc.* **2014**, *136*, 4575–4583.

(4) For the application of the distortion / interaction model to explain stereoselectivity in epoxidation reactions, see: Kolakowski, R. V.; Williams, L. J. *Nat. Chem.* **2010**, *2*, 303–307.

(5) For early studies and reviews regarding the aryne distortion model, see: (a) Cheong, P. H.-Y.; Paton, R. S.; Bronner, S. M.; Im, G.-Y. J.; Garg, N. K.; Houk, K. N. *J. Am. Chem. Soc.* **2010**, *132*, 1267–1269. (b) Im, G.-Y. J.; Bronner, S. M.; Goetz, A. E.; Paton, R. S.; Cheong, P. H.-Y.; Houk, K. N.; Garg, N. K. *J. Am. Chem. Soc.* **2010**, *132*, 17933–17944. (c) Bronner, S. M.; Goetz, A. E.; Garg, N. K. *Synlett* **2011**, *18*, 2599–2604. (d) Goetz, A. E.; Garg, N. K. *J. Org. Chem.* **2014**, *79*, 846–851.

(6) For the application of the aryne distortion model to 3-silylbenzynes, see: Bronner, S. M.; Mackey, J. L.; Houk, K. N.; Garg, N. K. *J. Am. Chem. Soc.* **2012**, *134*, 13966–13969.

(7) (a) van Zeist, W.-J.; Bickelhaupt, F. M. *Org. Biomol. Chem.* **2010**, *8*, 3118–3127. (b) Fernández, I.; Cossío, F. P.; Bickelhaupt, F. M. *J. Org. Chem.* **2011**, *76*, 2310–2314. (c) Fernández, I.; Bickelhaupt, F. M. *J. Comput. Chem.* **2012**, *33*, 509–516. (d) Fernández, I.; Sola,

M.; Bickelhaupt, F. M. *Chem. Eur. J.* **2013**, *19*, 7416–7422. (e) Fernández, I.; Bickelhaupt, F. M. *Chem. Soc. Rev.* **2014**, *43*, 4953–4967.

(8) For pertinent reviews, see references 5c, 5d, and the following: (a) Pellissier, H.; Santelli, M. *Tetrahedron* **2003**, *59*, 701–730. (b) Wenk, H. H.; Winkler, M.; Sander, W. *Angew. Chem. Int. Ed*. **2003**, *42*, 502–528. (c) Sanz, R. *Org*. *Prep. Proced. Int*. **2008**, *40*, 215–291. (d) Chen, Y.; Larock, R. C. In *Modern Arylation Methods*; L. Ackermann, Wiley-VCH: Weinheim, 2009; pp 401–473. (e) Tadross, P. M.; Stoltz, B. M. *Chem. Rev*. **2012**, *112*, 3550–3577. (f) Gampe, C. M.; Carreira, E. M. *Angew. Chem. Int. Ed*. **2012**, *51*, 3766–3778. (g) Yoshida, H.; Takaki, K. *Synlett* **2012**, *23*, 1725–1732. (h) Dubrovskiy, A. V.; Markina, N. A.; Larock, R. C. *Org. Biomol. Chem*. **2013**, *11*, 191–218. (i) Wu, C.; Shi, F. *Asian J. Org. Chem*. **2013**, *2*, 116–125. (j) Hoffmann, R. W.; Suzuki, K. *Angew. Chem. Int. Ed.* **2013**, *52*, 2655–2656. (k) Bhunia, A.; Biji, A. T. *Synlett* **2014**, *25*, 608–614.

(9) For studies of 3-silylarynes or 3-borylbenzynes, which are not the major focus of the current study, see reference 6 and the following: (a) Ikawa, T.; Nishiyama, T.; Shigeta, T.; Mohri, S.; Morita, S.; Takayanagi, S.-i.; Terauchi, Y.; Morikawa, Y.; Takagi, A.; Ishikawa, Y.; Fujii, S.; Kita, Y.; Akai, S. *Angew. Chem. Int. Ed.* **2011**, *50*, 5674–5677. (b) Ikawa, T.; Takagi, A.; Goto, M.; Aoyama, Y.; Ishikawa, Y.; Itoh, Y.; Fujii, S.; Tokiwa, H.; Akai, S. *J. Org. Chem.* **2013**, *78*, 2965–2983. (c) Takagi, A.; Ikawa, T.; Kurita, Y.; Saito, K.; Azechi, K.; Egi, M.; Itoh, Y.; Tokiwa, H.; Kita, Y.; Akai, S. *Tetrahedron* **2013**, *69*, 4338–4352. (d) Takagi, A.; Ikawa, T.; Saito, K.; Masuda, S.; Ito, T.; Akai, S. *Org. Biomol. Chem.* **2013**, *11*, 8145–8150.

(10) For a recent study of a 3-alkoxycyclohexyne, see: Medina, J. M.; McMahon, T. C.; Jiménez-Osés, G.; Houk, K. N.; Garg, N. K. *J. Am. Chem. Soc.* **2014**, *136*, 14706–14709.

(11) For examples involving the *Charge Distribution* and *Steric Models* to rationalize regioselectivities in trapping experiments of 3-substituted arynes, see: (a) Kessar, S. V. In *Comprehensive Organic Synthesis*; Trost, B. M.; Fleming, I. Eds.; Pergamon Press: Oxford, England, 1991; Vol. 4, pp 483–515. (b) Liu, Z.; Larock, R. C. *J. Org. Chem.* **2006**, *71*, 3198–3209. (c) Liu, Z.; Larock, R. C. *Org. Lett*. **2003**, *5*, 4673–4675. (d) Tadross, P. M.; Gilmore, C. D.; Bugga, P.; Virgil, S. C.; Stoltz, B. M. *Org. Lett.* **2010**, *12*, 1224–1227. (e) Yoshida, H.; Sugiura, S.; Kunai, A. *Org. Lett.* **2002**, *4*, 2767–2769. (f) Hamura, T.; Ibusuki, Y.; Sato, K.; Matsumoto, T.; Osamura, Y.; Suzuki, K. *Org. Lett*. **2003**, *5*, 3551–3554.

(12) In a somewhat related sense, it has also been argued that the presence of an adjacent inductively withdrawing group causes regioselectivity in aryne reactions due to stabilization of the developing carbanion, which we would be formed upon nucleophilic addition to the substituted benzyne. However, arynes undoubtedly react through very early transition states with low enthalpic barriers, so this explanation is inadequate.

(13) Calculations shown are at the B3LYP/6-311+G(d,p) level of theory and LANL2DZ for the Br and I atoms with tight convergence criteria and an ultrafine integration grid. Angles were also calculated at this level of theory. See the Experimental Section for calculations of angles of reactants and TSs with M06-2X and MP2. Because the potential energy surface of the reaction of **1.1b** has no maximum, a variational transition state search was performed to locate a saddle point. Although B3LYP overestimates the regioselectivities, it predicts the correct trend in reactivity.

(14) (a) Becke, A. D. *J. Chem. Phys*. **1993**, *98*, 5648–5652. (b) Lee, C.; Yang, W.; Parr, R. G. *Phys. Rev. B* **1988**, *37*, 785–789. (c) Vosko, S. H.; Wilk, L.; Nusair, M. *Can. J. Phys*. **1980**, *58*,

1200–1211. (d) Stephens, P. J.; Devlin, F. J.; Chabalowski, C. F.; Frisch, M. J. *J. Phys. Chem*. **1994**, *98*, 11623–11627.

(15) (a) Hay, P. J.; Wadt, W. R. J. *J. Chem. Phys*. **1985**, *82*, 270–283. (b) Wadt, W. R. J.; Hay, P. J. *J. Chem. Phys*. **1985**, *82*, 284–298. (c) Hay, P. J.; Wadt, W. R. J. *J. Chem. Phys*. **1985**, *82*, 299–310.

(16) Gaussian 09, Revision D.01, Frisch, M. J.; Trucks, G. W.; Schlegel, H. B.; Scuseria, G. E.; Robb, M. A.; Cheeseman, J. R.; Scalmani, G.; Barone, V.; Mennucci, B.; Petersson, G. A.; Nakatsuji, H.; Caricato, M.; Li, X.; Hratchian, H. P.; Izmaylov, A. F.; Bloino, J.; Zheng, G.; Sonnenberg, J. L.; Hada, M.; Ehara, M.; Toyota, K.; Fukuda, R.; Hasegawa, J.; Ishida, M.; Nakajima, T.; Honda, Y.; Kitao, O.; Nakai, H.; Vreven, T.; Montgomery, J. A., Jr.; Peralta, J. E.; Ogliaro, F.; Bearpark, M.; Heyd, J. J.; Brothers, E.; Kudin, K. N.; Staroverov, V. N.; Kobayashi, R.; Normand, J.; Raghavachari, K.; Rendell, A.; Burant, J. C.; Iyengar, S. S.; Tomasi, J.; Cossi, M.; Rega, N.; Millam, M. J.; Klene, M.; Knox, J. E.; Cross, J. B.; Bakken, V.; Adamo, C.; Jaramillo, J.; Gomperts, R.; Stratmann, R. E.; Yazyev, O.; Austin, A. J.; Cammi, R.; Pomelli, C.; Ochterski, J. W.; Martin, R. L.; Morokuma, K.; Zakrzewski, V. G.; Voth, G. A.; Salvador, P.; Dannenberg, J. J.; Dapprich, S.; Daniels, A. D.; Farkas, Ö.; Foresman, J. B.; Ortiz, J. V.; Cioslowski, J.; Fox, D. J. Gaussian, Inc., Wallingford CT, 2009.

(17) (a) Bronner, S. M.; Goetz, A. E.; Garg, N. K. *J. Am. Chem. Soc.* **2011**, *133*, 3832–3835.

(18) For select examples of studies pertaining to 3-haloarynes, see ref 17a and the following: (a) Biehl, E. R.; Nieh, E.; Hsu, K. C. *J. Org. Chem*. **1969**, *34*, 3595–3599. (b) Moreau-Hochu, M. F.; Caubere, P. *Tetrahedron* **1977**, *33*, 955–959. (c) Ghosh, T.; Hart, H. *J. Org. Chem*. **1988**, *53*, 3555–3558. (d) Hart, H.; Ghosh, T. *Tetrahedron Lett*. **1988**, *29*, 881–884. (e) Wickham, P. P.;

Reuter, K. H.; Senanayake, D.; Guo, H.; Zalesky, M.; Scott, W. J. *Tetrahedron Lett*. **1993**, *34*, 7521–7524. (f) Gokhale, A.; Scheiss, P. *Helv. Chem. Acta* **1998**, *81*, 251–267. (g) Goetz, A. E.; Garg, N. K. *Nat. Chem.* **2013**, *5*, 54–60. (h) Hendrick, C. E.; McDonald, S. L.; Wang, Q. *Org. Lett*. **2013**, *15*, 3444–3447. (i) Kirkham, J. D.; Delaney, P. M.; Ellames, G. J.; Row, E. C.; Harrity, J. P. A. *Chem. Commun*. **2010**, *46*, 5154–5156.

(19) Using Kobayashi's strategy, silyltriflates readily undergo conversion to the corresponding arynes upon treatment with fluoride sources; see: Himeshima, Y.; Sonoda, T.; Kobayashi, H. *Chem. Lett.* **1983**, *12*, 1211–1214.

(20) Silyltriflate **1.4a** was obtained from commercial sources. The syntheses of silyltriflates **1.4b–1.4e** are described in the Experimental Section. For an alternative synthesis of **1.4c**, see: (a) Hall, C.; Henderson, J. L.; Ernouf, G.; Greaney, M. F. *Chem. Commun*. **2013**, *49*, 7602–7604. For the prior synthesis of **1.4d**, see: (b) Dai, M.; Wang, Z.; Danishefsky, S. J. *Tetrahedron Lett*. **2008**, *49*, 6613–6616.

(21) For the addition of heteroatom nucleophiles to benzynes generated from silyltriflate precursors, see reference 11d.

(22) Although the atomic radii increase steadily from F to I, the corresponding A-values only increase from F to Cl, and then remain nearly constant for Cl, Br, and I. This is due to the increased C–X bond length as atom size increases.

(23) (a) Shi, F.; Waldo, J. P.; Chen, Y.; Larock, R. C. *Org. Lett*. **2008**, *10*, 2409–2412. (b) Campbell-Verduyn, L.; Elsinga, P. H.; Mirfeizi, L.; Dierckx, R. A.; Feringa, B. L. *Org. Biomol. Chem*. **2008**, *6*, 3461–3463.

(24) Given that reaction yields are not quantitative, and that computational free energies have some standard error, the predicted and experimental ratios should be taken with a grain of salt. Nonetheless, the general trends seen in the experimental and computation data of Tables 1.1 and 1.2 entirely correlate to predictions made by the aryne distortion model (i.e., highest selectivity is observed and calculated for the most distorted 3-haloaryne, **1.1b**, whereas the lowest selectivity is observed and calculated with the least distorted 3-haloaryne, **1.1e**).

(25) Weinhold, F.; Landis, C. R *Discovering Chemistry with Natural Bond Orbitals*; John Wiley & Sons, Inc: Hoboken, New Jersey, 2012.

(26) The net attractive energy was calculated by separately determining the Coulombic interactions between the point charge and C1 and C2, using the aforementioned calculated NBO charges for **1.1b**, and then adding these values.

(27) Houk, K. N. *Acc. Chem. Res.* **1975**, *8*, 361–369.

(28) Bent, H. *Chem. Rev.* **1961**, *61*, 275-311.

(29) Although not the main focus of this study, it should be noted that steric effects are important in reactions of other unsymmetrical arynes, such as 3-silylbenzynes; for further discussion, see references 6 and 9.

(30) An array of aryne cycloaddition reactions are available in the literature using silyltriflate precursors; see reference 8.

(31) (a) Hassan, J.; Sevignon, M.; Gozzi, C.; Schulz, E.; Lemaire, M. *Chem. Rev*. **2002**, *102*, 1359–1469. (b) *Topics in Current Chemistry*, Vol. 219; Miyaura, N., Ed.; Springer Verlag: New York, 2002. (c) *Metal-Catalyzed Cross-Coupling Reactions*; Diederich, F., Meijere, A., Eds.; Wiley-VCH: Weinheim, 2004. (d) Corbet, J.; Mignani, G. *Chem. Rev*. **2006**, *106*, 2651–2710. (e)

Negishi, E. *Bull. Chem. Soc. Jpn*. **2007**, *80*, 233–257. (f) *Application of Transition Metal Catalysis in Drug Discovery and Development: An Industrial Perspective*; Shen, H. C., Crawley, M. L., Trost, B. M., Eds.; John Wiley & Sons, Inc.: Hoboken, NJ, 2012.

(32) Gong, L.; Jahangir, A.; Reuter, D. C. US Patent US2010160360A1, 2010.

(33) For recent reviews regarding Ni-catalyzed cross-couplings, see: (a) Rosen, B. M.; Quasdorf, K. W.; Wilson, D. A.; Zhang, N.; Resmerita, A.-M.; Garg, N. K.; Percec, V. *Chem. Rev*. **2011**, *111*, 1346–1416. (b) Li, B.-J.; Yu, D.-G.; Sun, C.-L.; Shi, Z.-J. *Chem. Eur. J*. **2011**, *17*, 1728–1759. (c) Mesganaw, T.; Garg, N. K. *Org. Process Res. Dev*. **2013**, *17*, 29–39. (d) Tasker, S. Z.; Standley, E. A.; Jamison, T. F. *Nature* **2014**, *509*, 299–309.

(34) For our previous studies of Ni-catalyzed Suzuki–Miyaura couplings, see: (a) Quasdorf, K. W.; Tian, X.; Garg, N. K. *J. Am. Chem. Soc*. **2008**, *130*, 14422–14423. (b) Quasdorf, K. W.; Riener, M.; Petrova, K. V.; Garg, N. K. *J. Am. Chem. Soc*. **2009**, *131*, 17748–17749. (c) Quasdorf, K. W.; Antoft-Finch, A.; Liu, P.; Silberstein, A. L.; Komaromi, A.; Blackburn, T.; Ramgren, S. D.; Houk, K. N.; Snieckus, V.; Garg, N. K. *J. Am. Chem. Soc*. **2011**, *133*, 6352–6363.

(35) For our previous studies of Ni-catalyzed amination reactions, see: (a) Mesganaw, T.; Silberstein, A. L.; Ramgren, S. D.; Fine Nathel, N. F.; Hong, X.; Liu, P.; Garg, N. K. *Chem. Sci*. **2011**, *2*, 1766–1771. (b) Ramgren, S. D.; Silberstein, A. L.; Yang, Y.; Garg, N. K. *Angew. Chem. Int. Ed*. **2011**, *50*, 2171–2173.

(36) Kauch, M.; Hoppe, D. *Synthesis* **2006**, *10*, 1578–1589.

(37) Kauch, M.; Hoppe, D. *Can. J. Chem*. **2001**, *79*, 1736–1746.

(38) Díaz, M.; Cobas, A.; Guitian, E.; Castedo, L. *Eur. J. Org. Chem*. **2001**, 4543–4549.

(39) Booker, J. E. M.; Boto, A.; Churchill, G. H.; Green, C. P.; Ling, M.; Meek, G.; Prabhakaran, J.; Sinclair, D.; Blake, A. J.; Pattenden, G. *Org. Biomol. Chem*. **2006**, *4*, 4193–4205.

(40) Shimizu, M.; Mochida, K.; Hiyama, T. *Angew. Chem. Int. Ed*. **2008**, *47*, 9760–9764.

(41) Please see Ref. 20b

(42) Boughton, B. A.; Hor, L.; Gerrard, J. A.; Hutton, C. A. *Bioorg. Med. Chem*. **2012**, *20*, 2419–2426.

(43) Lee, D.-H.; Taher, A.; Hossain, S.; Jin, M.-J. *Org. Lett*. **2011**, *13*, 5540–5543.

(44) Heiries, S.; Chartoire, A.; Slawing, A. M. Z.; Nolan, S. P. *Organometallics* **2012**, *31*, 3402–3409.

(45) Andrew, T. L.; Swager, T. M. *J. Org. Chem*. **2011**, *76*, 2976–2993.

(46) Please see Ref. 11b

(47) Alvarez, S. G.; Alvarez, M. T. *Synthesis* **1997**, 413–414.

(48) Please see Ref. 23a

(49) Ramgren, S. D.; Hie, L.; Ye, Y.; Garg, N. K. *Org. Lett*. **2013**, *15*, 3950–3953.

(50) Hie, L.; Ramgren, S. D.; Mesganaw, T.; Garg, N. K. *Org. Lett*. **2012**, *14*, 4182–4185.

(51) Ribeiro, R. F.; Marenich, A. V.; Cramer, C. J.; Truhlar, D. G. *J. Phys. Chem. B* **2011**, *115*, 14556–14562.

(52) Goetz, A. E.; Bronner, S. M.; Cisneros, J. D.; Melamed, J. M.; Paton, R. S.; Houk, K. N.; Garg, N. K. *Angew. Chem. Int. Ed.* **2012**, *51*, 2758–2762.

(53) Medina, J. M.; Mackey, J. L.; Garg, N. K.; Houk, K. N. *J. Am. Chem. Soc*. **2014**, *136*, 15798–15805.

CHAPTER TWO

Synthetic Studies Pertaining to the 2,3-Pyridyne and 4,5-Pyrimidyne

Jose M. Medina, Moritz K. Jackl, Robert B. Susick, and Neil K. Garg

Tetrahedron **2016**, *72*, 3629–3634.

2.1 Abstract

We report synthetic studies pertaining to two heterocyclic aryne intermediates: the 2,3-pyridyne and the 4,5-pyrimidyne. First, a 2,3-pyridyne precursor was readily accessed from 2-pyridone using a known procedure. Subsequently, 2,3-pyridyne generation and trapping were used to access several functionalized pyridines in a regioselective manner. In addition, we report synthetic routes to two isomeric silyltriflates, which were intended to serve as precursors to the 4,5-pyrimidyne. Consecutive 4,5-pyrimidyne generation and trapping experiments were ultimately deemed unfruitful. We expect these findings will promote the use of 2,3-pyridyne and other heterocyclic arynes as building blocks for the synthesis of functionalized heterocycles.

2.2 Introduction

The synthesis of heterocycles continues to be a vital area of research. Heterocycles, especially *N*-containing compounds, are commonly seen in a variety of important molecules including medicines, natural products, and agrochemicals.[1] One exciting approach to the synthesis of decorated heterocycles involves the trapping of in-situ generated heterocyclic arynes, commonly referred to as hetarynes.[2,3] This strategy was well studied several decades ago,[4] but only led to modest synthetic utility.

More recently, the chemistry of heterocyclic arynes has undergone a revival. Methodological studies pertaining to indolynes[5,6] and 3,4-pyridynes[7] have been disclosed and several silyltriflate precursors to these intermediates are now commercially available.[8] Moreover, heterocyclic arynes have been used to synthesize several natural products (e.g., **2.1**–**2.4**, Figure 2.1).[2,9,10] One particularly attractive subclass of heterocyclic arynes are those that possess one or more nitrogen atoms in a 6-membered ring (e.g., **2.5**–**2.7**). The successful generation and trapping of such species via cycloaddition processes would provide a powerful means to build medicinally privileged scaffolds, including compounds that may be difficult to access by other means.

We have been particularly interested in the chemistry of pyridynes and pyrimidynes, each of which are classes of heterocyclic arynes with an interesting history. The 3,4-pyridyne (**2.5**) was first generated in 1955[11] and has subsequently been the subject of numerous investigations, including one by our own laboratory.[7] The 3,4-pyridyne and substituted versions can now be used to access polysubstituted pyridines in a controlled and predictable way by virtue of the aryne distortion model,[5,12] using robust silyltriflate precursors.[7] Similarly, the 2,3-pyridyne (**2.6**) has been known for several decades.[13] In more recent efforts, Walters and Shay reported the

synthesis of a silyltriflate precursor to **2.6**.[14] In turn, a few examples where **2.6** can be used in Diels–Alder reactions or other annulations are available.[14,15,16,17,18,19] The least well-studied of our targets is the 4,5-pyrimidyne (**2.7**). Substituted derivatives have been accessed by dehydrohalogenation under strongly basic reaction conditions or by oxidation of an aminotriazole precursor.[20] Prior experiments involving 4,5-pyrimidynes have led to amination or low yields of annulated products.[20]

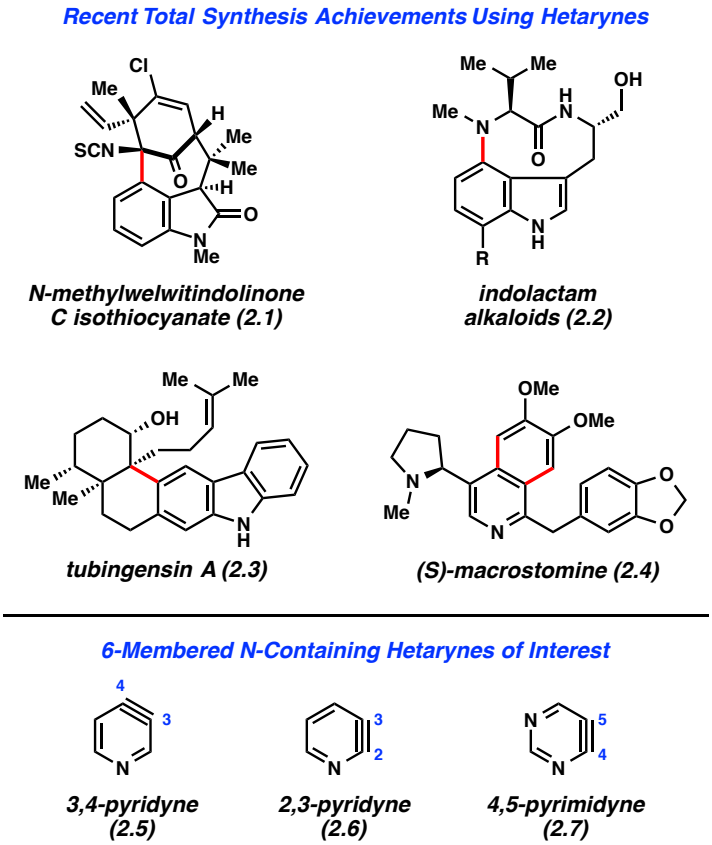

Figure 2.1. Natural products **2.1**–**2.4** and heterocyclic arynes **2.5**–**2.7**

Given the earlier promising results involving the 2,3-pyridyne (**2.6**) and 4,5-pyrimidyne (**2.7**), we sought to further expand the utility of these intermediates for the synthesis of

functionalized heterocycles. Herein, we report new trapping experiments involving pyridyne **2.6**, in addition to efforts toward 4,5-pyrimidyne (**2.7**).

2.3 Results and Discussion

2.3.1 Synthesis of 2,3-Pyridyne Precursor

To study annulations of 2,3-pyridyne, it was first necessary to prepare a suitable silyltriflate precursor. Thus, silyltriflate **2.10** was synthesized using a known procedure (Scheme 2.1).[14] Beginning from 2-pyridone (**2.8**), a lithiation and silylation sequence provided silylhydroxypyridine **2.9**. Subsequent reaction with triflic anhydride furnished silyltriflate **2.10**. This high-yielding two-step sequence provides a reliable method to access **2.10** in multigram quantities. It should be noted that **2.10** is now also commercially available.[21]

Scheme 2.1. Synthesis of Silyltriflate **2.10**

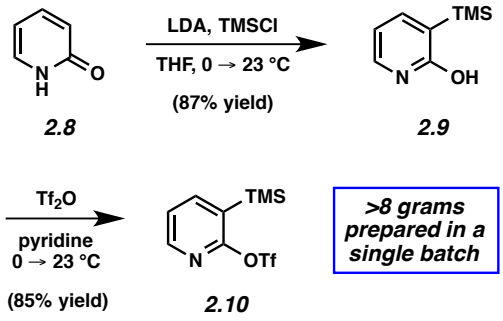

2.3.2 Generation & Trapping of 2,3-Pyridyne

Silyltriflate **2.10** was examined in nucleophilic trapping experiments as shown in Table 2.1. Trapping with morpholine (**2.12**) led to the formation of **2.13** in 55% yield (entry 1), whereas use of imidazole (**2.14**) as the trapping agent delivered **2.15** in 63% yield (entry 2). In

both cases, the 2-substituted pyridine products were obtained, with no evidence of the formation of 3-substituted adducts. This regioselectivity trend is consistent with prior observations[2c] and predictions made by the aryne distortion model.[12c]

Table 2.1. Trapping of 2,3-Pyridyne **(2.6)** with Nucleophiles

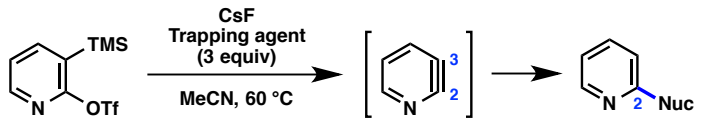

2.10 *2.6* *2.11*

Entry	*Trapping agent*	*Product*	*Yield*[a]
1	 *2.12*	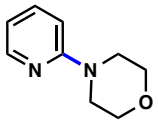 *2.13*	*55%*
2	 *2.14*	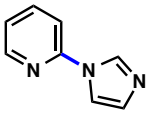 *2.15*	*63%*

[a] Reported yields are the average of two experiments and are based on the amounts of isolated product.

We were delighted to find that silyltriflate **2.10** could also be employed in cycloaddition reactions (Table 2.2). For example, interception of pyridyne **2.6** by benzylazide (**2.17**)[22] furnished annulated product **2.18**, albeit only in low yield (entry 1). Alternatively, trapping with nitrone **2.19**[23] provided the unusual heterocycle **2.20** (entry 2). We also tested an azomethine imine cycloaddition[24] using **2.21**, which gave rise to tricycle **2.22** in 42% yield (entry 3). More synthetically useful yields were obtained when dimethylurea **2.23**[16] was utilized in the trapping experiments. This reaction gave fused bicyclic pyridine derivative **2.24** in 75% yield (entry 4).

In all cases, only one regioisomer of annulated product was detected, indicative of preferential nucleophilic attack occurring at C2 of the 2,3-pyridyne intermediate.

Table 2.2. Annulation Reactions of 2,3-Pyridyne **(2.6)**

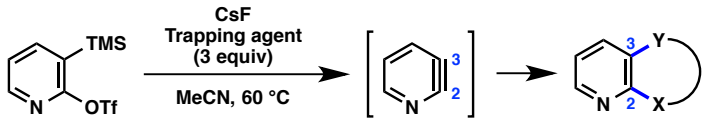

2.10 *2.6* *2.16*

Entry	*Trapping agent*	*Product*	*Yield*[a]
1	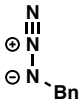 *2.17*	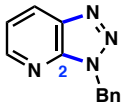 *2.18*	*20%*
2	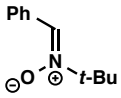 *2.19*	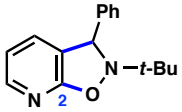 *2.20*	*33%*
3	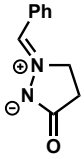 *2.21*	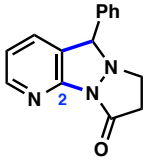 *2.22*	*42%*
4	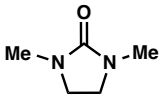 *2.23*	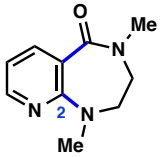 *2.24*	*75%*

[a] Reported yields are the average of two experiments and are based on the amounts of isolated product.

Despite the success of the aforementioned trapping experiments, it should be noted that silyltriflate **2.10** could not be employed successfully in other attempted 2,3-pyridyne trapping

experiments (Figure 2.2). For example, the use of nitrile oxide precursor **2.25**, diazoester **2.26**, or enamide **2.27** in attempted annulations led only to decomposition. Similarly, efforts to utilize sydnone **2.28** in a Diels–Alder trapping or β-ketoester **2.29**[25] in a formal (2+2) cycloaddition were unsuccessful. Nonetheless, the knowledge gained from our 2,3-pyridyne studies should enable the judicious use of **2.10** in synthetic applications.

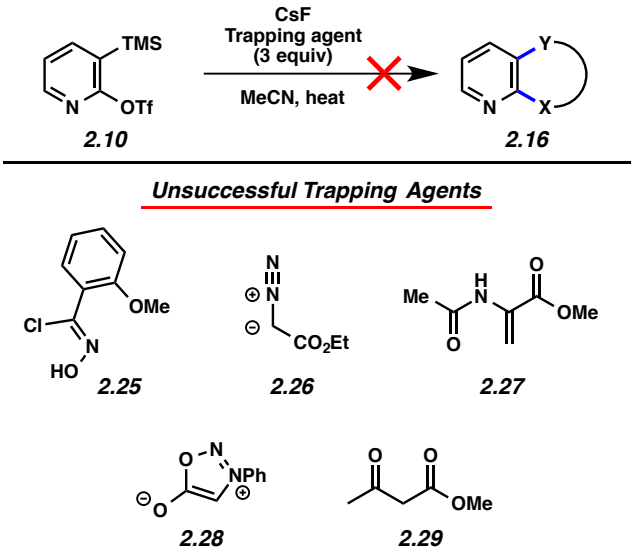

Figure 2.2. Unsuccessful cycloadditions using silyltriflate **2.10**

2.3.3 Synthesis of 4,5-Pyrimidyne Precursors & Trapping Experiments

As noted earlier, we were also eager to expand the limited scope of 4,5-pyrimidyne trapping experiments.[20] As such, we pursued the notion suggested in Scheme 2.2. Specifically, we envisioned that 4,5-pyrimidyne (**2.7**) could be prepared in situ from silyltriflate **2.30** or its constitutional isomer **2.31**.

Scheme 2.2. Approaches to 4,5-Pyrimidyne **2.7** from Silyltriflate Precursors **2.30** and **2.31**

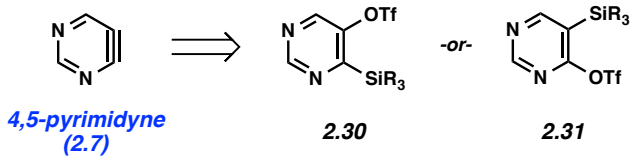

In our initial approach, we sought to access a silyltriflate precursor from known benzyloxypyrimidine **2.32**[26] (Scheme 2.3). As such, 5-benzyloxypyrimidine (**2.32**) was synthesized from the corresponding commercially available bromide using an Ullman coupling.[26] With **2.32** in hand, extensive efforts were put forth to effect silylation. It was ultimately found that the desired triethylsilylated product **2.33** could be obtained using a one-pot procedure involving mixing of **2.32** with TESCl, followed by low temperature lithiation, with in situ silylation.[27] From **2.33**, debenzylation and subsequent triflation delivered the desired silyltriflate **2.34**. Eager to attempt pyrimidyne generation, **2.34** was subjected to a battery of experiments involving variation of fluoride sources, trapping agents, and other reaction conditions. Unfortunately, no products indicative of pyrimidyne formation were observed. Instead, it was found that **2.34** was prone to readily undergo thia-Fries rearrangement in the presence of fluoride sources. For example, treatment of **2.34** with CsF in acetonitrile gave **2.35** as the major product.[28] Greaney and coworkers have also observed thia-Fries rearrangement in attempted aryne generation from silyltriflate precursors.[29]

Scheme 2.3. Synthesis of Silyltriflate **2.34** and Undesired Fries Rearrangement

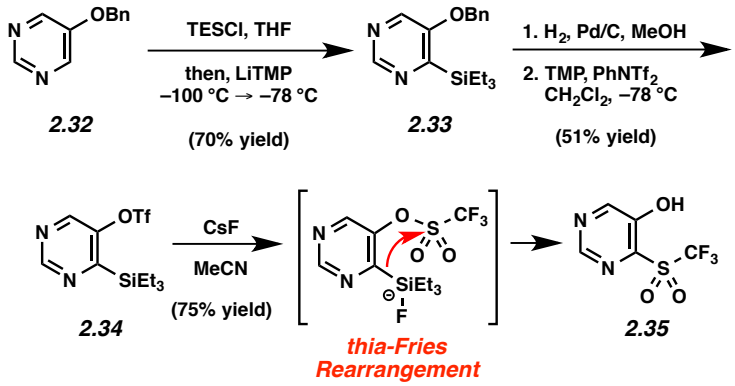

With our initial efforts thwarted, we pursued the synthesis of an isomeric silyltriflate, as shown in Scheme 2.4. 2-Pyrimidone (**2.36**) was found to undergo lithiation/silylation using a protocol similar to the one described previously to access pyridyne precursor **2.10** (see Scheme 2.1). Subsequent triflation of the remaining hydroxyl group furnished silyltriflate **2.37**.[30]

Scheme 2.4. Synthesis of Silyltriflate **2.37**

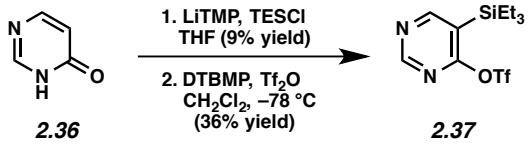

With the desired isomeric silyltriflate **2.37** available in just two steps from commercially available material, we pursued pyrimidyne generation and trapping (Figure 2.3). Thus, **2.37** was exposed to fluoride sources (e.g., CsF) in the presence of trapping agents. However, in all attempts, we were unable to observe any of the desired cycloaddition adducts. Instead, only substantial non-specific decomposition or formation of 2-pyrimidone was observed.[31]

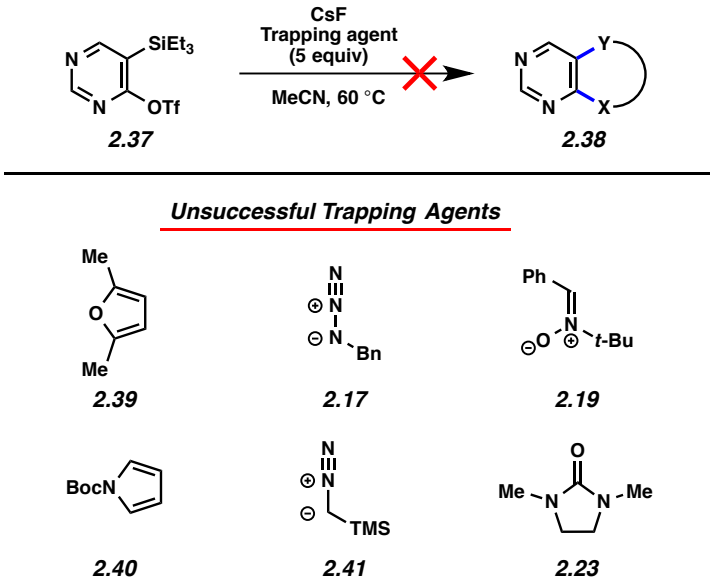

Figure 2.3. Unsuccessful attempts to generate and trap the 4,5-pyrimidyne from silyltriflate **2.37**

2.4 Conclusion

In summary, we have performed studies pertaining to two interesting heterocyclic aryne intermediates: 2,3-pyridyne and 4,5-pyrimidyne. We have shown that 2,3-pyridyne can be employed in various trapping experiments involving nucleophiles or cycloaddition partners. Several of the products obtained are unique scaffolds that would arguably be difficult to access by other means. In addition, we have developed synthetic routes to two plausible silyltriflate precursors to the 4,5-pyrimidyne, although no evidence of pyrimidyne formation was noted in attempted trapping experiments. We expect our findings will promote the use of 2,3-pyridyne and other strained heterocyclic intermediates in the synthesis of functionalized heterocycles.

2.5 Experimental Section

2.5.1 Materials and Methods

Unless stated otherwise, reactions were conducted in flame-dried glassware under an atmosphere of nitrogen using anhydrous solvents (freshly distilled or passed through activated alumina columns). All commercially obtained reagents were used as received unless otherwise specified. Cesium fluoride (CsF) was obtained from Strem Chemicals. Trifluoromethanesulfonic anhydride (Tf_2O), trimethylsilyl chloride (TMSCl), and triethylsilyl chloride (TESCl) were obtained from Oakwood Products, Inc. and distilled before use. *N*-tert-butyl-α-phenylnitrone and methyl 2-acetamidoacrylate were obtained from Alfa Aesar. Ethyl diazoacetate, (trimethylsilyl) diazomethane (1M in Et_2O), 2,5-dimethylfuran, imidazole, and *N*-Boc-pyrrole were obtained from Sigma Aldrich. Morpholine was obtained from Spectrum Chemical and distilled before use. Reaction temperatures were controlled using an IKAmag temperature modulator and, unless stated otherwise, reactions were performed at room temperature (rt, approximately 23 °C). Thin layer chromatography (TLC) was conducted with EMD gel 60 F254 pre-coated plates (0.25 mm) and visualized using a combination of UV light and potassium permanganate staining. Preparative thin layer chromatography (TLC) was conducted with EMD gel 60 F254 pre-coated plates (0.5 mm) and visualized using UV light. Silicycle Siliaflash P60 (particle size 0.040–0.063 mm) was used for flash column chromatography. ^{1}H NMR spectra were recorded on Bruker spectrometers (500 MHz) and are reported relative to deuterated solvent signals. Data for ^{1}H NMR spectra are reported as follows: chemical shift (δ ppm), multiplicity, coupling constant (Hz) and integration. ^{13}C NMR spectra were recorded on Bruker spectrometers (125 MHz) and are reported relative to deuterated solvent signals. Data for ^{13}C NMR spectra are reported in terms of chemical shift and, when necessary, multiplicity, and coupling constant (Hz). IR spectra

were obtained using a Perkin-Elmer 100 spectrometer or a Perkin-Elmer UATR two spectrometer, and are reported in terms of frequency absorption (cm^{-1}). High-resolution mass spectra were obtained on Waters LCT Premier with ACQUITY LC and Thermo Scientific™ Exactive Mass Spectrometers with DART ID-CUBE.

2.5.2 Experimental Procedures

2.5.2.1 Trapping Experiments of 2,3-Pyridyne

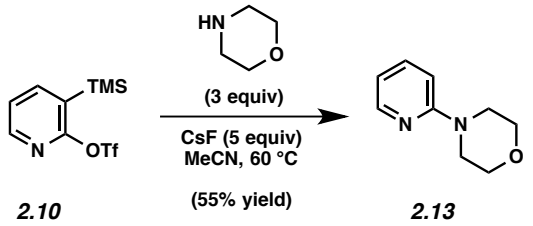

2.10 *2.13*

Representative Procedure for 2,3-Pyridyne Trappings. Adduct 2.13 (Table 2.1, Entry 1). To a stirred solution of silyltriflate **2.10**[14] (51.1 mg, 0.172 mmol, 1.0 equiv) and morpholine (48.0 μL, 0.516 mmol, 3.0 equiv) in MeCN (7.0 mL) was added CsF (128 mg, 0.840 mmol, 5.0 equiv). The reaction vessel was sealed and placed in a preheated aluminum heating block maintained at 60 °C for 2 h. After cooling to 23 °C, the reaction mixture was filtered over silica gel (EtOAc eluent, 12 mL). Evaporation under reduced pressure and further purification by preparative thin layer chromatography (2:1 hexanes:EtOAc) afforded **2.13** as a colorless oil (55% yield, average of two experiments). **2.13**: R_f 0.48 (3:1 hexanes:EtOAc); ^{1}H NMR (500 MHz, $CDCl_3$): δ 8.19 (ddd, *J* = 4.9, 2.0, 0.8, 1H), 7.49 (ddd, *J* = 9.0, 7.2, 2.0, 1H), 6.65 (ddd, *J* = 7.2, 4.9, 0.8, 1H), 6.62 (d, *J* = 8.7, 1H), 3.82 (t, *J* = 5.0, 4H), 3.49 (t, *J* = 5.0, 4H); ^{13}C NMR (125 MHz, $CDCl_3$): δ 159.7, 148.1, 137.6, 113.9, 107.0, 66.9, 45.7; IR (film): 1593, 1481, 1437, 1376, 1312, 1243 cm^{-1}; HRMS-ESI (*m/z*) $[M + H]^+$ calcd for $C_9H_{12}N_2O$, 165.1022; found 165.1024.

Any modifications of the conditions shown in this representative procedure are specified in the following schemes, which depict all of the results shown in Tables 2.1 and 2.2.

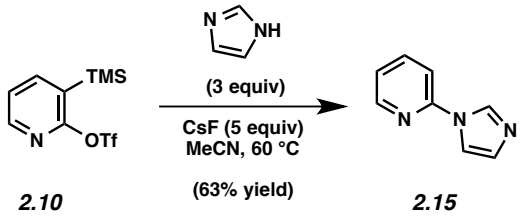

Adduct 2.15 (Table 2.1, Entry 2). Purification by preparative thin layer chromatography (6:3:1 EtOAc:PhH:MeOH) afforded **2.15** (63% yield, average of two experiments) as a light orange oil. **2.15**: R_f 0.62 (9:1 EtOAc:MeOH); ^{1}H NMR (500 MHz, $CDCl_3$): δ 8.49 (ddd, *J* = 4.9, 1.8, 0.9, 1H), 8.35 (s, 1H), 7.83 (dt, *J* = 7.5, 1.8, 1H), 7.65 (s, 1H), 7.36 (d, *J* = 8.2, 1H), 7.24 (ddd, *J* = 7.5, 4.9, 0.8, 1H), 7.20 (s, 1H); ^{13}C NMR (125 MHz, $CDCl_3$): δ 149.4, 149.3, 139.1, 135.1, 130.9, 122.1, 116.3, 112.5; IR (film): 1598, 1578, 1487, 1444, 772, 738 cm^{-1}; HRMS-ESI (*m/z*) $[M + H]^+$ calcd for $C_8H_7N_3$, 146.0713; found 146.0714.

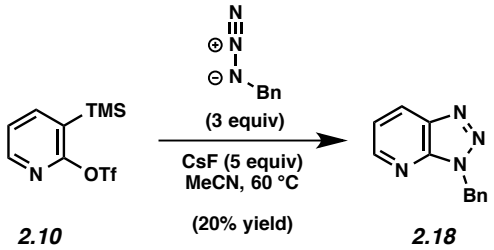

Adduct 2.18 (Table 2.2, Entry 1). Purification by preparative thin layer chromatography (3:1 hexanes:EtOAc) afforded **2.18** (20% yield, average of two experiments) as a light yellow oil. **2.18**: R_f 0.35 (3:1 hexanes:EtOAc); ^{1}H NMR (500 MHz, $CDCl_3$): δ 8.69 (dd, *J* = 4.5, 1.4, 1H), 8.37 (dd, *J* = 8.2, 1.4, 1H), 7.46 (d, *J* = 7.2, 2H), 7.36–7.28 (m, 4H), 5.92 (s, 2H); ^{13}C NMR (125 MHz, $CDCl_3$): δ 150.5, 145.8, 137.2, 135.2, 129.0, 128.7, 128.5, 128.4, 120.0, 50.6; IR (film):

3032, 2927, 2852, 1591, 1216 cm^{-1}; HRMS-ESI (*m/z*) $[M + H]^+$ calcd for $C_{12}H_{11}N_4$, 211.0978; found 211.0974.

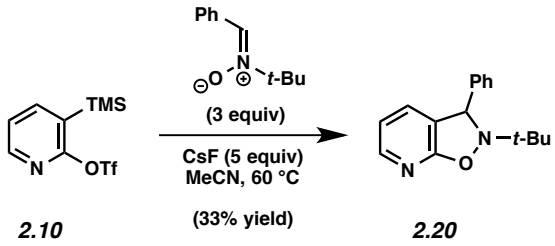

Adduct 2.20 (Table 2.2, Entry 2). Purification by preparative thin layer chromatography (3:1 hexanes:EtOAc) afforded **2.20** (33% yield, average of two experiments) as an amorphous white solid. **2.20**: R_f 0.52 (3:1 hexanes:EtOAc); ^{1}H NMR (500 MHz, $CDCl_3$): δ 8.04 (d, *J* = 5.0, 1H), 7.42 (d, *J* = 7.2, 2H), 7.35 (t, *J* = 7.2, 2H), 7.28 (tt, *J* = 7.2, 1.2, 1H), 7.19 (dt, *J* = 7.3, 1.3, 1H), 6.74 (dd, *J* = 7.3, 5.0, 1H), 5.62 (s, 1H), 1.20 (s, 9H); ^{13}C NMR (125 MHz, $CDCl_3$): δ 165.1, 147.9, 143.0, 132.8, 128.9, 127.9, 127.4, 123.0, 116.8, 66.3, 61.4, 25.5; IR (film): 1604, 1420, 1282, 1270, 775, 739 cm^{-1}; HRMS-ESI (*m/z*) $[M + H]^+$ calcd for $C_{16}H_{18}N_2O$, 255.1492; found 255.1492.

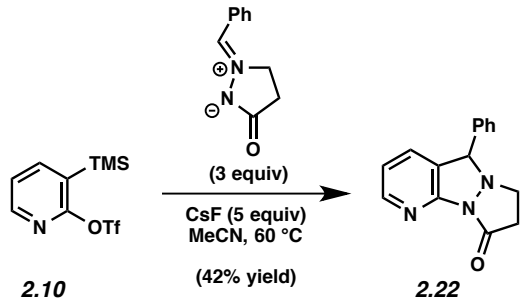

Adduct 2.22 (Table 2.2, Entry 3). Purification by preparative thin layer chromatography (95:5 EtOAc:MeOH) afforded **2.22** (42% yield, average of two experiments) as a colorless amorphous solid. **2.22**: R_f 0.48 (95:5 EtOAc:MeOH); ^{1}H NMR (500 MHz, $CDCl_3$): δ 8.32 (dt, *J* = 5.1, 1.1,

1H), 7.44–7.38 (m, 5H), 7.18 (dt, J = 7.5, 1.3, 1H), 6.94 (dd, J = 7.5, 5.1, 1H), 5.16 (s, 1H), 3.64–3.60 (m, 1H), 3.19–3.06 (m, 2H), 2.89–2.83 (m, 1H); ^{13}C NMR (125 MHz, $CDCl_3$): δ 163.2, 148.8, 148.5, 137.6, 132.5, 129.2, 129.1, 128.8, 128.4, 119.7, 73.5, 52.5, 36.9; IR (film): 1708, 1597, 1460, 1430, 1388, 1308 cm^{-1}; HRMS-ESI (m/z) [M + H]$^+$ calcd for $C_{15}H_{13}N_3O$, 252.1131; found 252.1126.

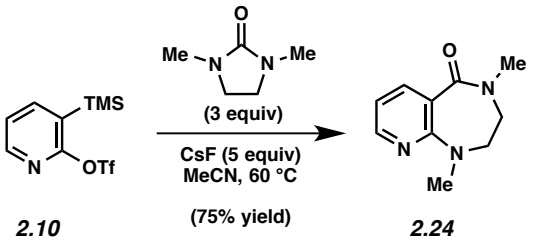

Adduct 2.24 (Table 2.2, Entry 4). Purification by preparative thin layer chromatography (95:5 EtOAc:MeOH) afforded **2.24** (75% yield, average of two experiments) as a colorless oil. **2.24**: R_f 0.45 (95:5 EtOAc:MeOH); ^{1}H NMR (500 MHz, $CDCl_3$): δ 8.29 (dd, J = 4.9, 2.0, 1H), 8.01 (dd, J = 7.6, 2.0, 1H), 6.76 (dd, J = 7.6, 4.9, 1H), 3.61–3.57 (m, 2H), 3.57–3.52 (m, 2H), 3.18 (s, 3H), 3.05 (s, 3H); ^{13}C NMR (125 MHz, $CDCl_3$): δ 169.2, 155.7, 150.9, 140.7, 119.4, 114.6, 56.3, 48.1, 38.9, 35.6; IR (film): 1633, 1504, 1408, 1385, 1247, 1208 cm^{-1}; HRMS-ESI (m/z) [M + H]$^+$ calcd for $C_{10}H_{13}N_3O$, 192.1131; found 192.1131.

2.5.2.2 Synthesis of 4,5-Pyrimidyne Precursors

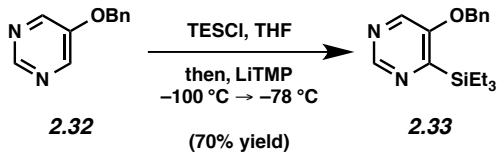

Pyrimidine 2.33 (Scheme 2.3). To a stirred solution of freshly distilled tetramethylpiperidine (1.97 g, 14.0 mmol, 1.4 equiv) in THF (50 mL) at 0 °C was added *n*-BuLi in hexanes (2.3 M, 5.65 mL, 13.0 mmol, 1.3 equiv). The resulting solution was allowed to stir at 0 °C for 30 min. A separate flask was charged with 5-benzyloxypyrimidine **2.32** (2.00 g, 10.0 mmol, 1.0 equiv), TESCl (4.53 g, 30.0 mmol, 3.0 equiv), and THF (50 mL). The resulting solution was cooled to –100 °C and the LiTMP solution was added dropwise via cannula over 20 min. The resulting solution was warned to –78 °C and allowed to stir for 3.5 h. The solution was then allowed to warm to 0 °C and quenched with saturated NH_4Cl (25 mL). The volatiles were removed under reduced pressure and EtOAc (75 mL) was added. The organic phase was separated and the aqueous layer was extracted with EtOAc (3 x 50 mL). The combined organic layers were dried with $MgSO_4$ and concentrated under reduced pressure. The resulting oil was further purified by column chromatography (5:1 hexanes:EtOAc) to yield pyrimidine **2.33** (2.09 g, 70% yield) as a colorless oil. **2.33**: R_f 0.41 (3:1 hexanes:EtOAc); ^{1}H NMR (500 MHz, $CDCl_3$): δ 8.95 (s, 1H), 8.24 (s, 1H), 7.42–7.34 (m, 5H), 5.12 (s, 2H), 0.95–0.91 (m, 9H), 0.91–0.86 (m, 6H); ^{13}C NMR (125 MHz, $CDCl_3$): δ 165.5, 158.4, 151.7, 137.6, 135.7, 128.9, 128.6, 127.7, 70.6, 7.5, 3.0; IR (film): 2953, 2874, 1558, 1456, 1397, 1284 cm^{-1}; HRMS-ESI (*m/z*) $[M + H]^+$ calcd for $C_{17}H_{25}N_2OSi$, 301.1731; found 301.1729.

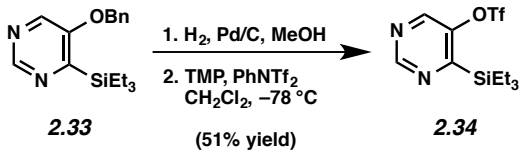

2.33 (51% yield) *2.34*

Silyltriflate 2.34 (Scheme 2.3). To a stirred solution of pyrimidine **2.33** (1.00 g, 3.33 mmol, 1.0 equiv) in dry MeOH (20 mL) was added 10% Pd/C (350 mg, 0.330 mmol, 0.1 equiv). The resulting mixture was placed under an atmosphere of H_2 (balloon) and was allowed to stir at 23

°C for 2 h. The mixture was filtered over celite (MeOH eluent). Evaporation of the solvent under reduced pressure afforded the crude alcohol intermediate, which was used in the subsequent step without further purification.

The alcohol intermediate (510 mg, 2.43 mmol, 1.0 equiv) was dissolved in dry CH_2Cl_2 (7 mL) and freshly distilled tetramethylpiperidine (282 mg, 9.72 mmol, 4.0 equiv) was added dropwise over 10 min. The resulting solution was cooled to –78 °C and a solution of $PhNTf_2$ (714 mg, 2.92 mmol, 1.2 equiv) in CH_2Cl_2 (7 mL) was added dropwise over 15 min. The resulting solution was stirred at –78 °C for 2 h and was then quenched with saturated $NaHCO_3$ (10 mL). The organic layer was separated and the aqueous layer was extracted with CH_2Cl_2 (3 x 20 mL). The combined organic layers were dried with $MgSO_4$ and concentrated under reduced pressure. The resulting oil was further purified by column chromatography (30:1 hexanes:EtOAc) to yield silyltriflate **2.34** as a colorless oil (581 mg, 51% yield, 2 steps). **2.34**: R_f 0.70 (3:1 hexanes:EtOAc); ^{1}H NMR (500 MHz, $CDCl_3$): δ 9.26 (s, 1H), 8.64 (s, 1H), 0.97 (br s, 15H); ^{13}C NMR (125 MHz, $CDCl_3$): δ 169.7, 156.7, 152.4, 147.0, 118.5 (q, J = 318.2, CF_3), 7.3, 3.0; IR (film): 2960, 2880, 1565, 1428, 1386, 1211 cm^{-1}; HRMS-ESI (*m/z*) $[M + H]^+$ calcd for $C_{11}H_{18}F_3N_2O_3SSi$, 343.0754; found 343.0748.

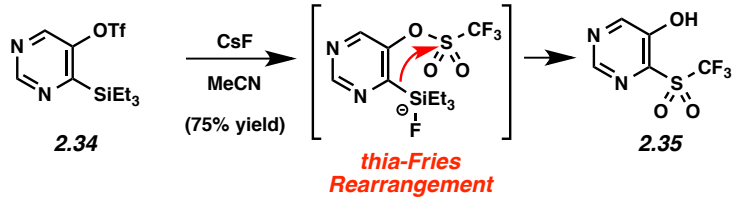

Alcohol 2.35 (Scheme 2.3). To a stirred solution of silyltriflate **2.34** (130 mg, 0.380 mmol, 1.0 equiv) in MeCN (3.8 mL) was added CsF (173 mg, 1.14 mmol, 3.0 equiv). The reaction vessel was sealed and placed in a preheated aluminum heating block maintained at 60 °C for 2 h. After

cooling to 23 °C, the reaction mixture was filtered over celite (MeOH eluent, 12 mL). Evaporation under reduced pressure and further purification by preparative thin layer chromatography (100:10:1 CH_2Cl_2:MeOH:Et_3N) afforded **2.35** as a colorless oil (75% yield). **2.35**: R_f 0.76 (MeCN); ^{1}H NMR (500 MHz, MeOD): δ 8.28 (s, 1H), 8.08 (s, 1H); ^{13}C NMR (125 MHz, MeOD): δ 165.6, 161.0, 142.0, 137.6, 122.5 (q, J = 327.9, CF_3); IR (film): 3349, 1643, 1575, 1510, 1445, 1341 cm^{-1}; HRMS-ESI (*m/z*) $[M - H]^-$ calcd for $C_5H_2F_3N_2O_3S$, 226.9733; found 226.9750.

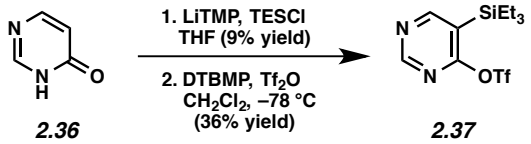

Silyltriflate 2.37 (Scheme 2.4). To a stirred solution of freshly distilled tetramethylpiperidine (1.02 g, 7.20 mmol, 1.4 equiv) in THF (10 mL) at 0 °C was added *n*-BuLi in hexanes (2.3 M, 2.94 mL, 6.80 mmol, 1.3 equiv). The resulting solution was stirred at 0 °C for 30 min. A separate flask was charged with 2-pyrimidone **2.36** (500 mg, 5.20 mmol, 1.0 equiv), TESCl (1.97 g, 13.0 mmol, 2.5 equiv), and THF (16 mL). The resulting solution was cooled to 0 °C and the LiTMP solution was added dropwise via cannula over 20 min. The resulting solution was warmed to 23 °C and allowed to stir for 24 h. The solution was then quenched with saturated NH_4Cl (10 mL). The volatiles were removed under reduced pressure and EtOAc (30 mL) was added. The organic phase was separated and the aqueous layer was extracted with EtOAc (3 x 20 mL). The combined organic layers were dried with $MgSO_4$ and concentrated under reduced pressure. The resulting oil was further purified by column chromatography (1:2 to 1:4 hexanes:EtOAc) to yield an alcohol intermediate (100 mg, 9% yield (unoptimized)) as a colorless oil.

The alcohol intermediate (90.0 mg, 0.430 mmol, 1.0 equiv) was dissolved in dry CH_2Cl_2 (2 mL) and DTBMP (96.0 mg, 0.470 mmol, 1.1 equiv) was added. The resulting solution was cooled to –78 °C and Tf_2O (133 mg, 0.470 mmol, 1.1 equiv) was added dropwise over 5 min. The resulting solution was allowed to stir at –78 °C for 2 h and was then quenched with saturated $NaHCO_3$ (1 mL). The organic layer was separated and the aqueous layer was extracted with CH_2Cl_2 (3 x 3 mL). The combined organic layers were dried with $MgSO_4$ and concentrated under reduced pressure. The resulting oil was further purified by column chromatography (40:1 hexanes : EtOAc) to yield silyltriflate **2.37** as a colorless oil (55 mg, 36% yield). **2.37**: R_f 0.52 (5:1 hexanes : EtOAc); ^{1}H NMR (500 MHz, $CDCl_3$): δ 9.14 (d, J = 1.2, 1H), 7.29 (d, J = 1.2, 1H), 0.99 (t, J = 7.2, 9H), 0.92–0.86 (m, 6H); ^{13}C NMR (125 MHz, $CDCl_3$): δ 184.2, 162.2, 158.2, 118.6 (q, J = 320.6, CF_3), 117.0, 7.2, 2.6; IR (film): 2959, 2880, 1579, 1511, 1428, 1211 cm^{-1}; HRMS-ESI (*m/z*) $[M + H]^+$ calcd for $C_{11}H_{18}F_3N_2O_3SSi$, 343.0754; found 343.0755.

2.6 Spectra Relevant to Chapter Two:

Synthetic Studies Pertaining to the 2,3-Pyridyne and 4,5-Pyrimidyne

Jose M. Medina, Moritz K. Jackl, Robert B. Susick, and Neil K. Garg

Tetrahedron **2016**, *72*, 3629–3634.

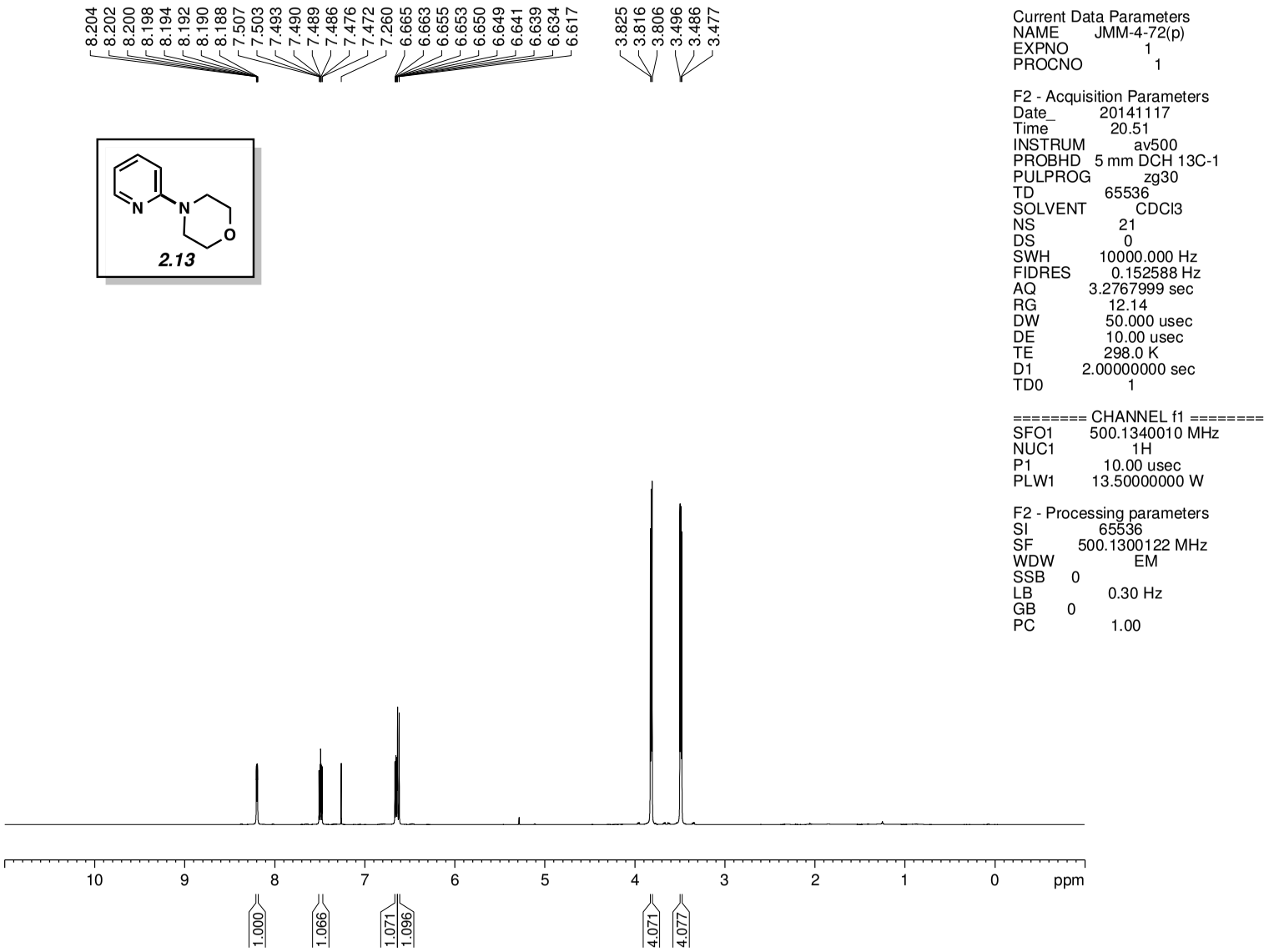

Figure 2.4. ^{1}H NMR (500 MHz, $CDCl_3$) compound **2.13**

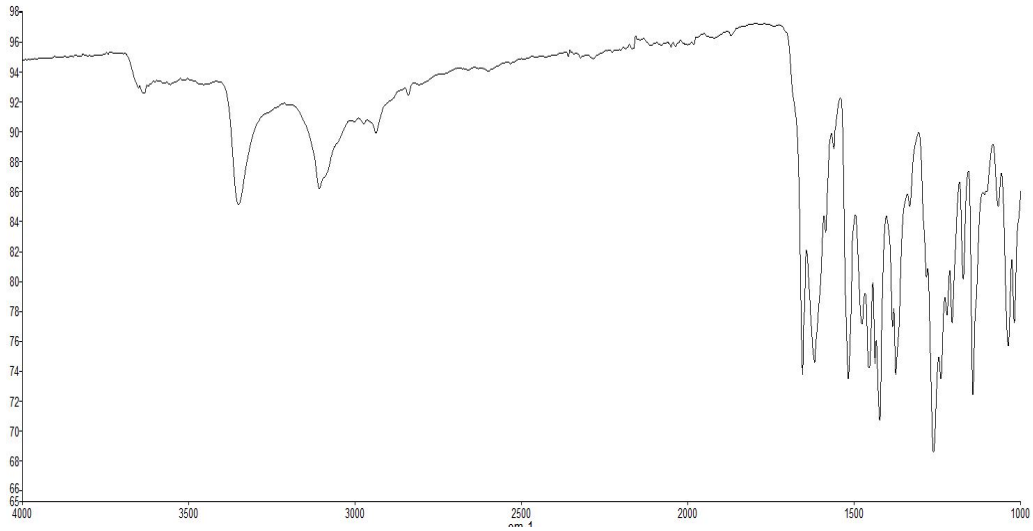

Figure 2.5. Infrared spectrum of compound **2.13**

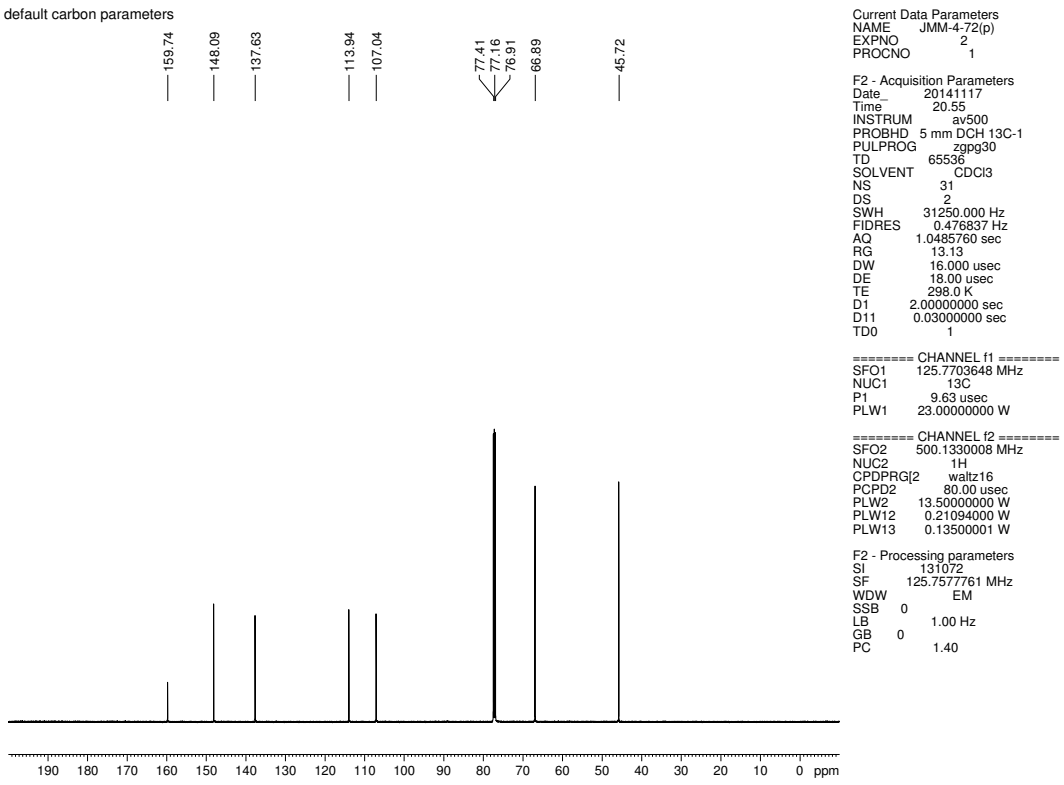

Figure 2.6. ^{13}C NMR (125 MHz, $CDCl_3$) of compound **2.13**

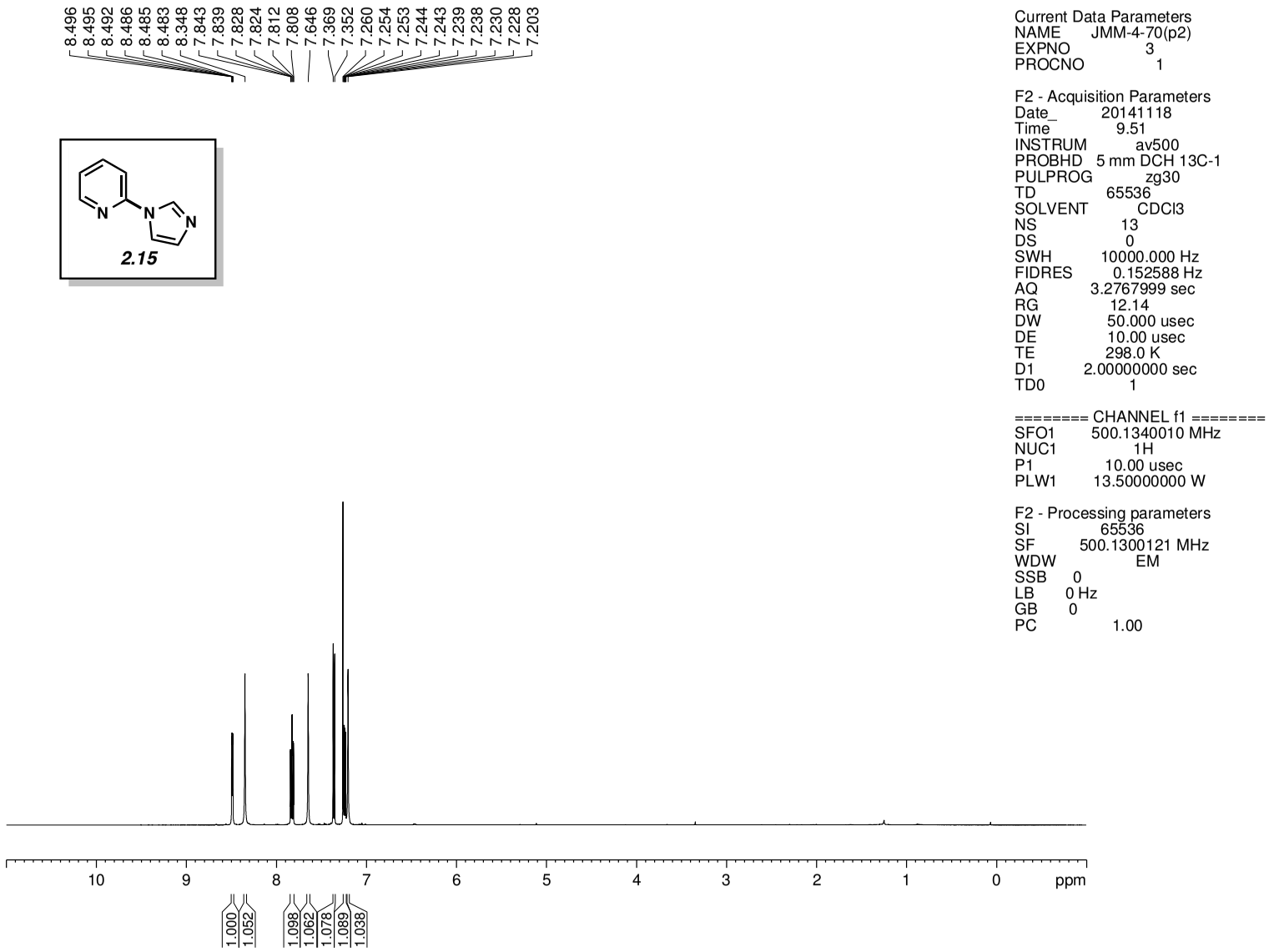

Figure 2.7. ^{1}H NMR (500 MHz, $CDCl_3$) compound **2.15**

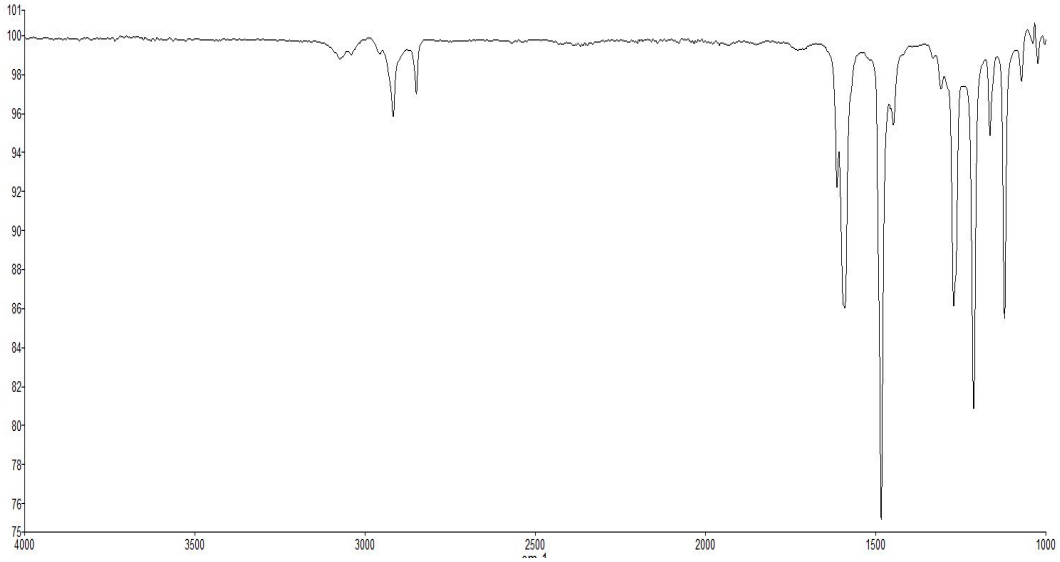

Figure 2.8. Infrared spectrum of compound **2.15**

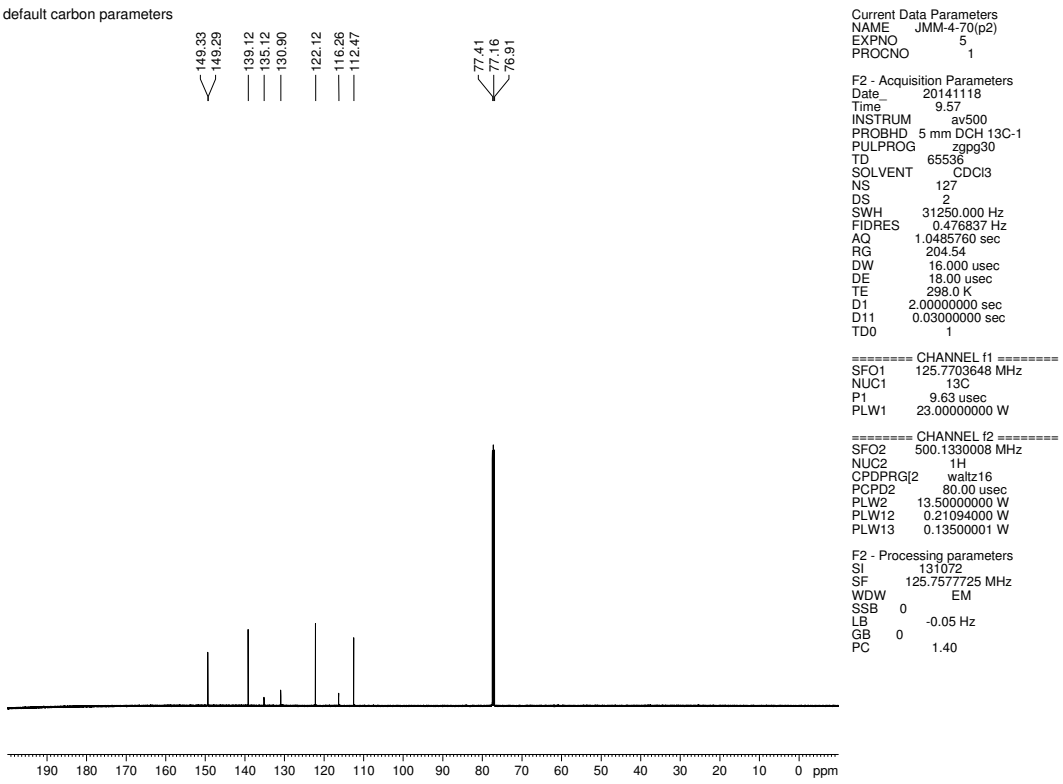

Figure 2.9. ^{13}C NMR (125 MHz, $CDCl_3$) of compound **2.15**

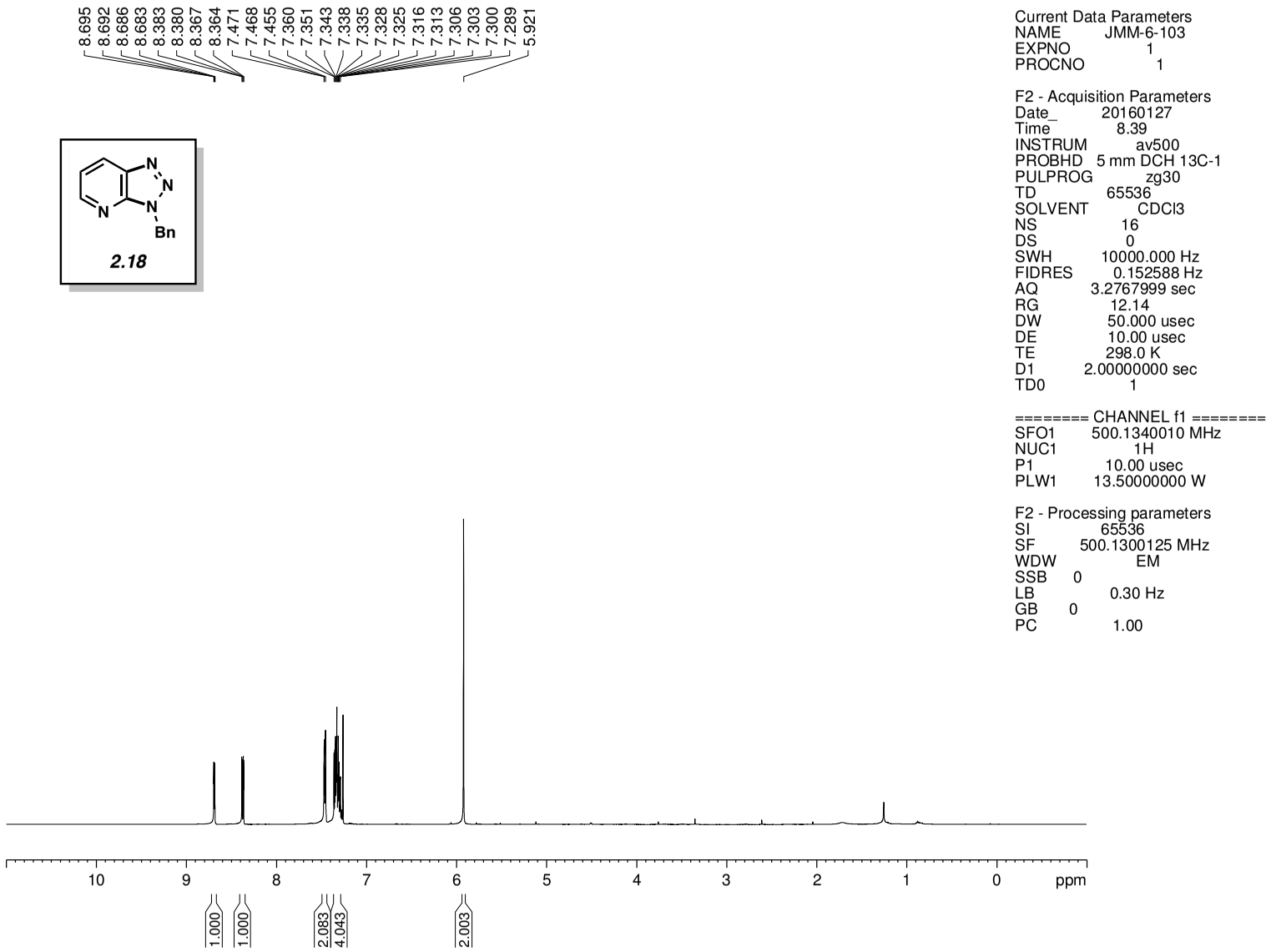

Figure 2.10. ^{1}H NMR (500 MHz, $CDCl_3$) compound **2.18**

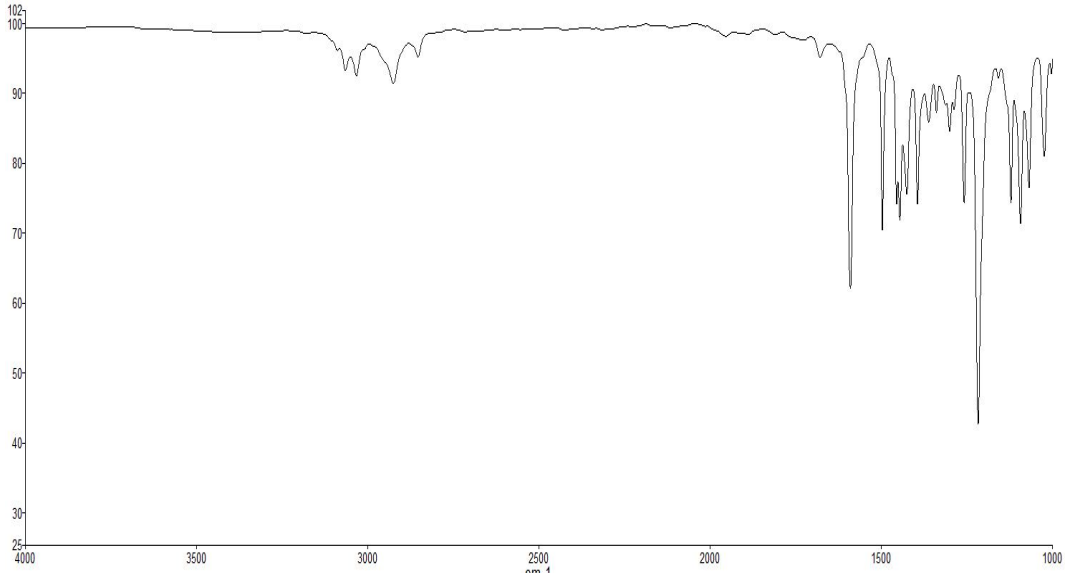

Figure 2.11. Infrared spectrum of compound **2.18**

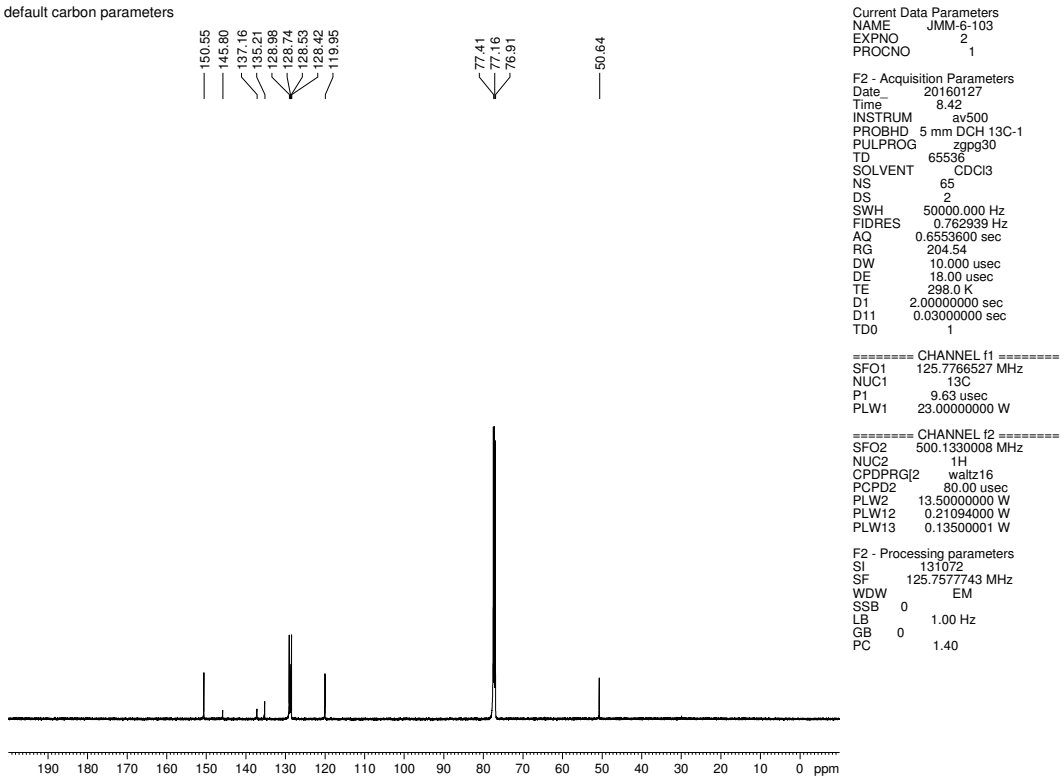

Figure 2.12. ^{13}C NMR (125 MHz, $CDCl_3$) of compound **2.18**

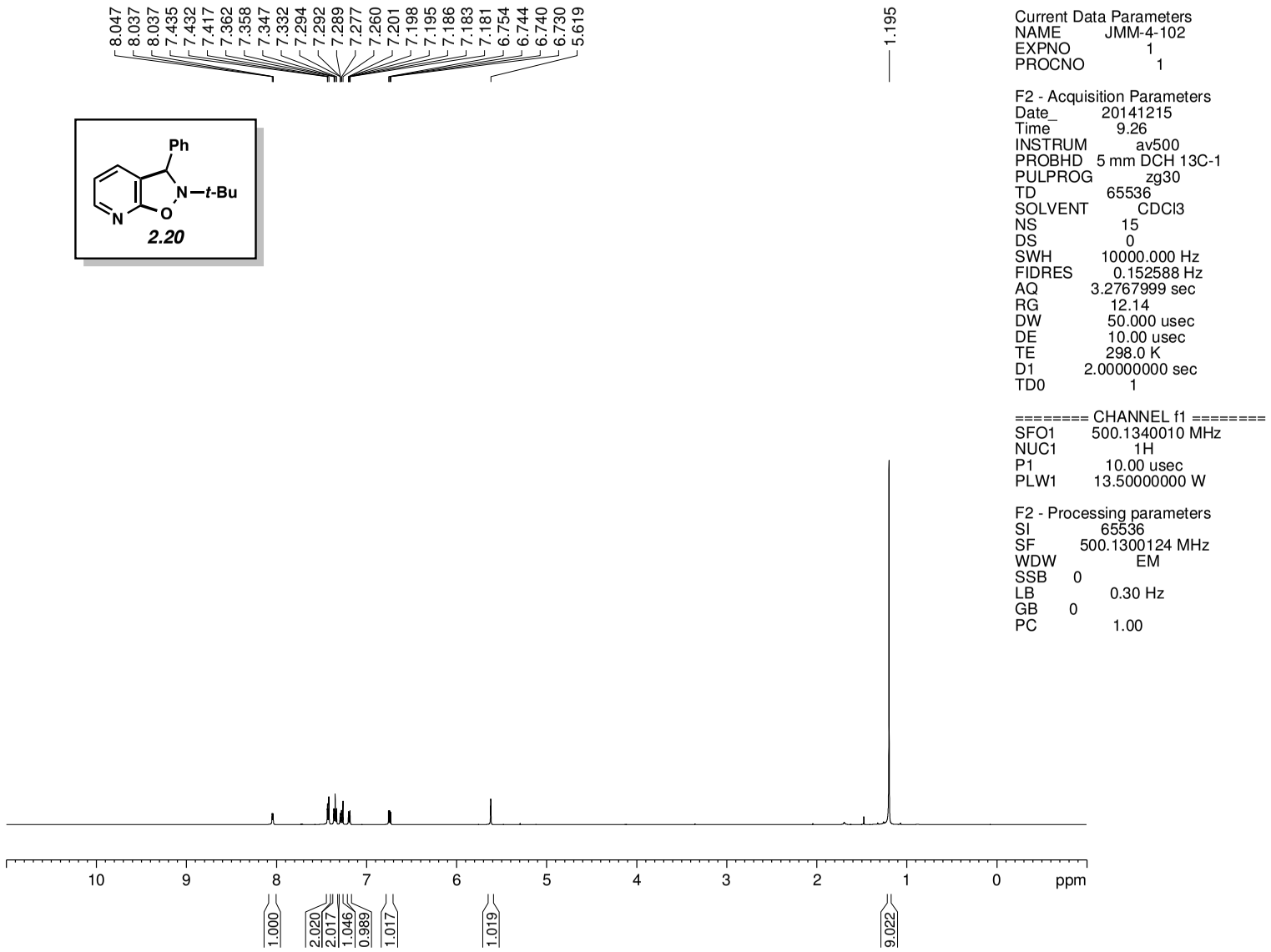

Figure 2.13. ^{1}H NMR (500 MHz, $CDCl_3$) compound **2.20**

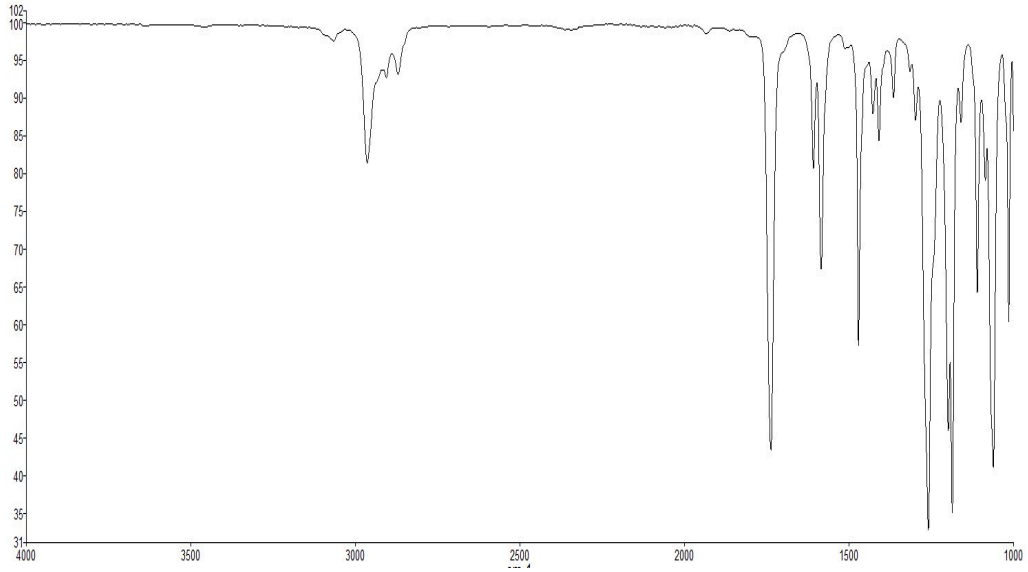

Figure 2.14. Infrared spectrum of compound **2.20**

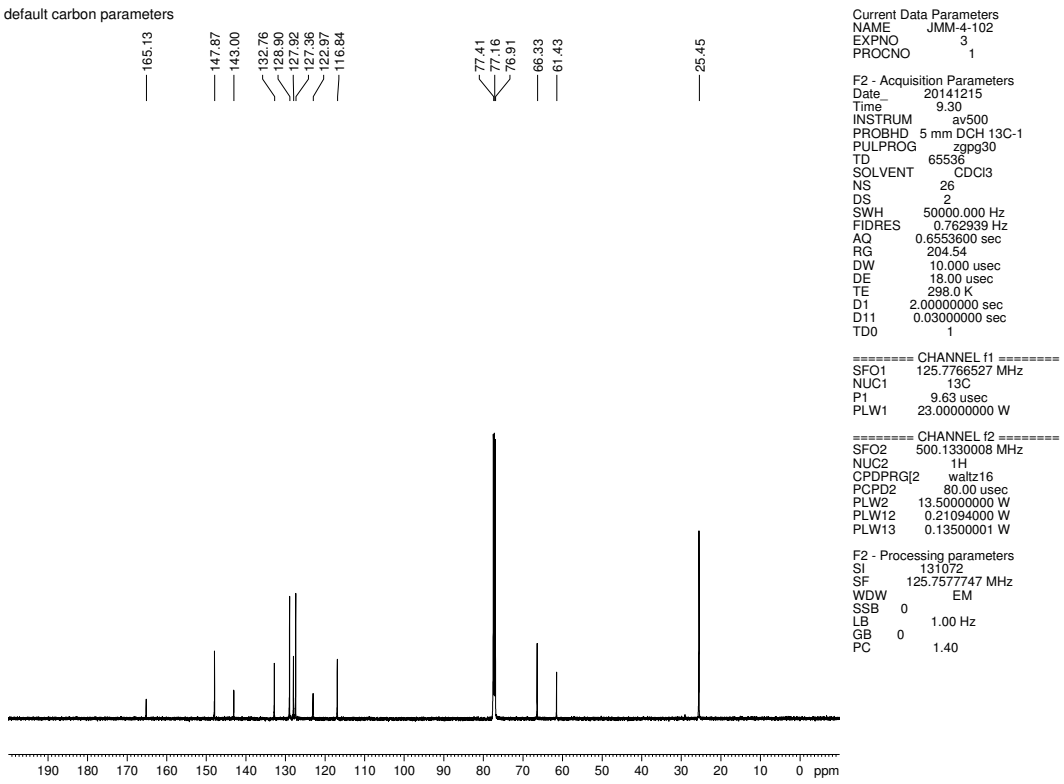

Figure 2.15. ^{13}C NMR (125 MHz, $CDCl_3$) of compound **2.20**

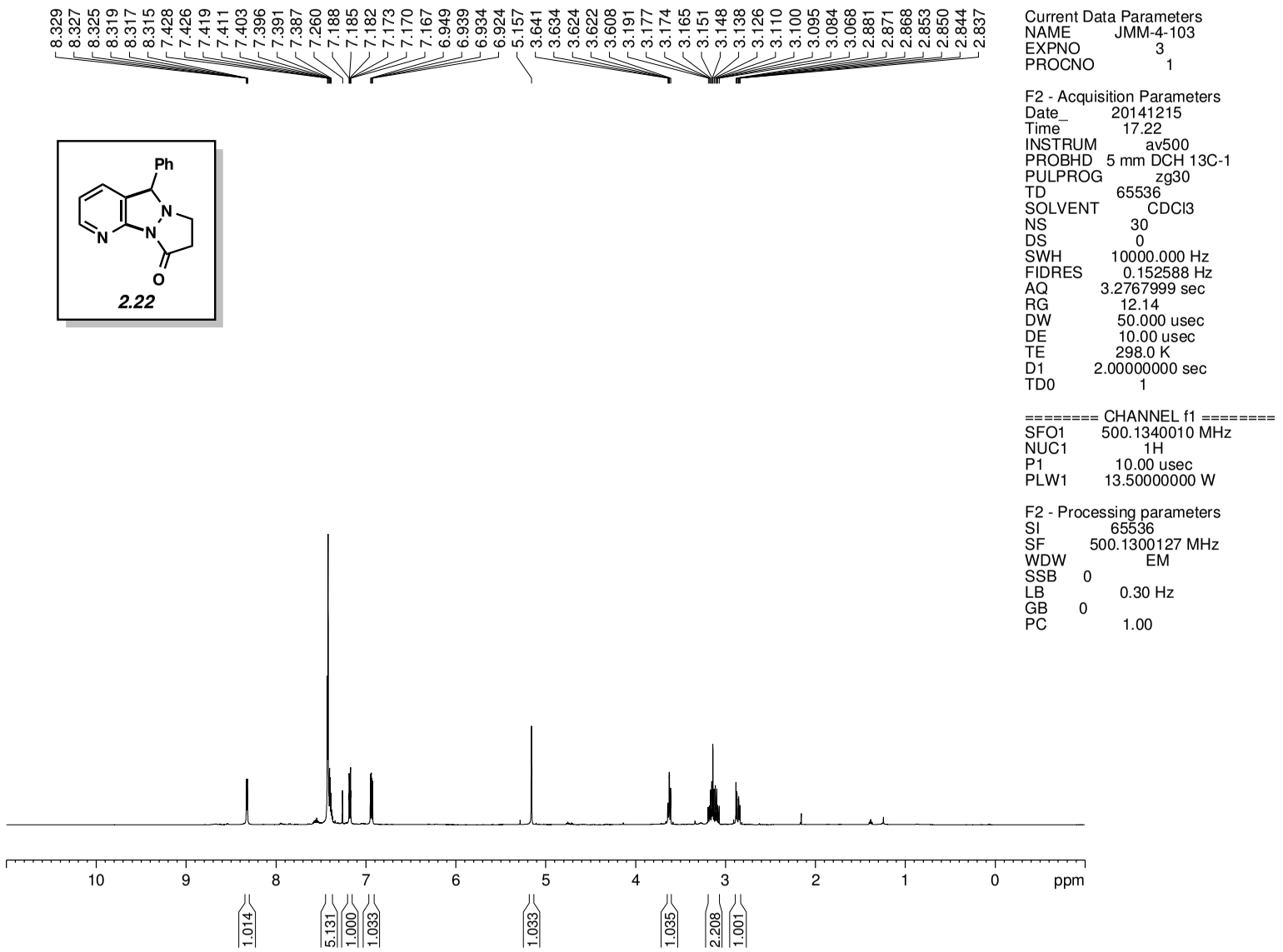

Figure 2.16. ^{1}H NMR (500 MHz, $CDCl_3$) compound **2.22**

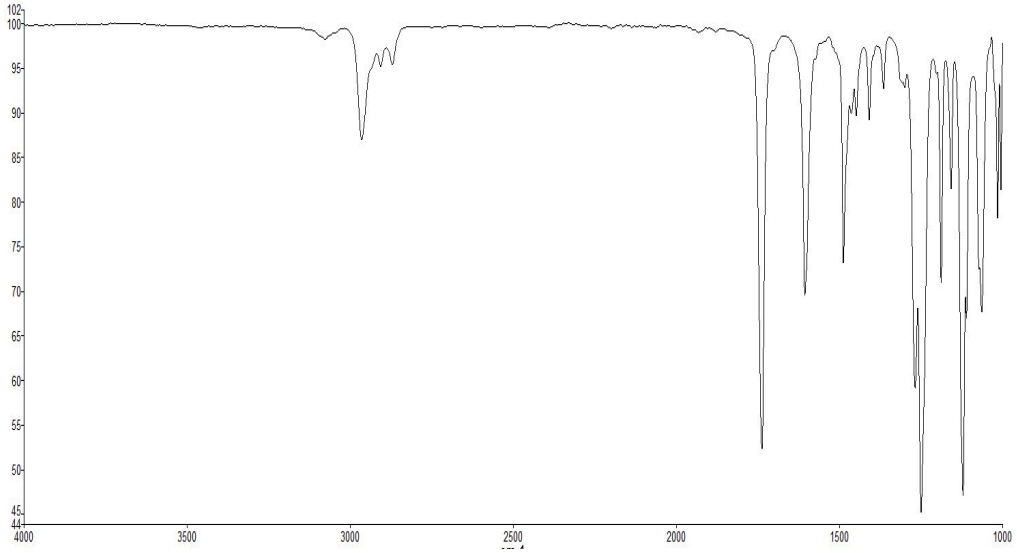

Figure 2.17. Infrared spectrum of compound **2.22**

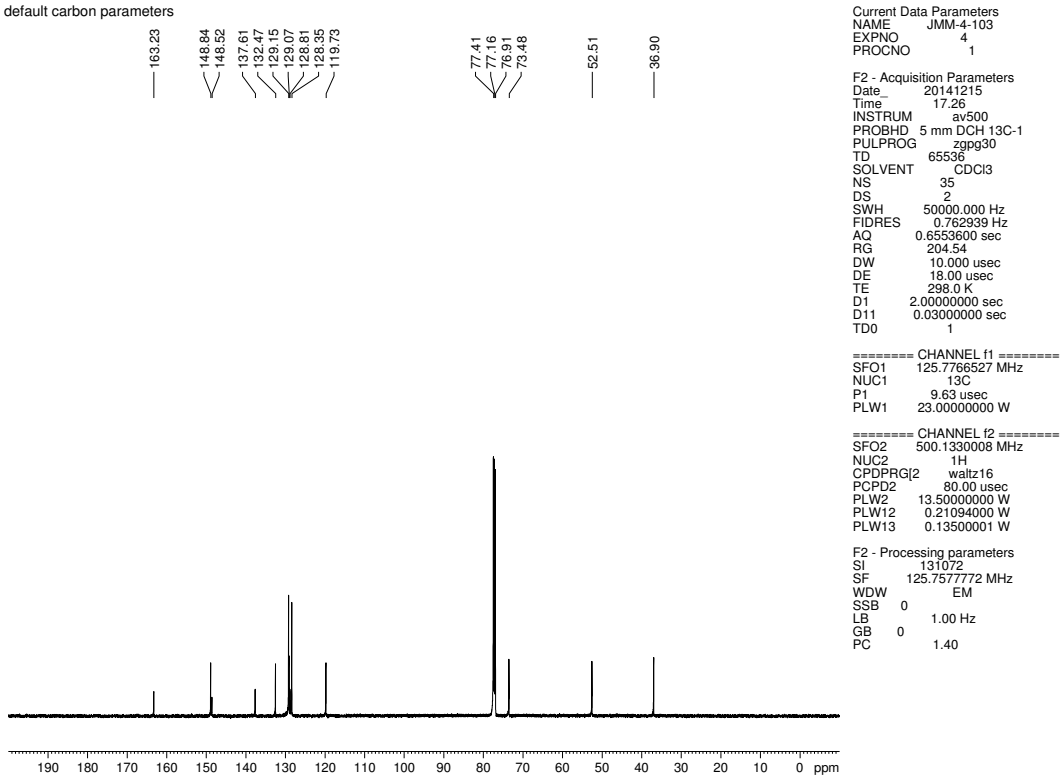

Figure 2.18. ^{13}C NMR (125 MHz, $CDCl_3$) of compound **2.22**

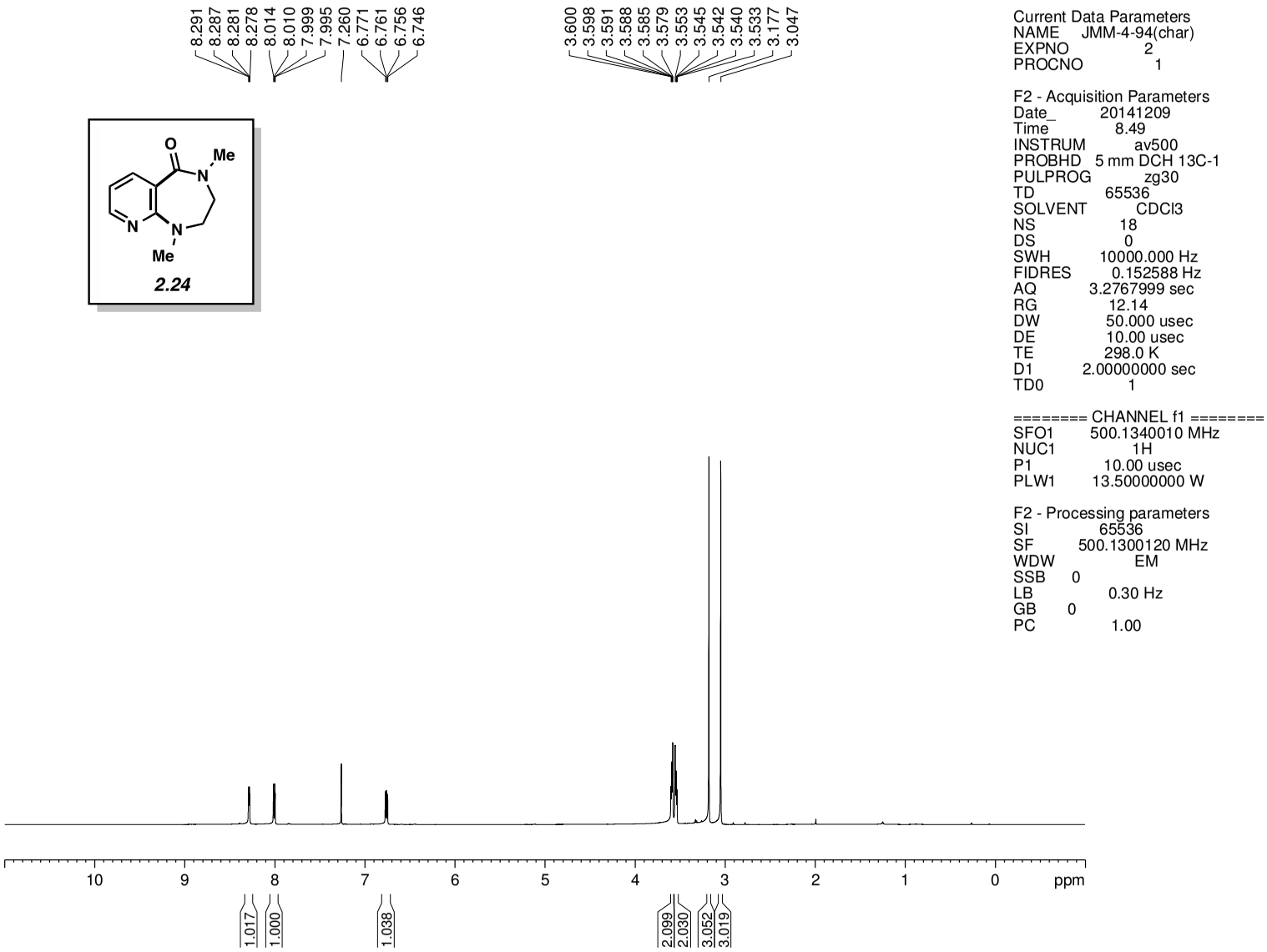

Figure 2.19. ^{1}H NMR (500 MHz, $CDCl_3$) compound **2.24**

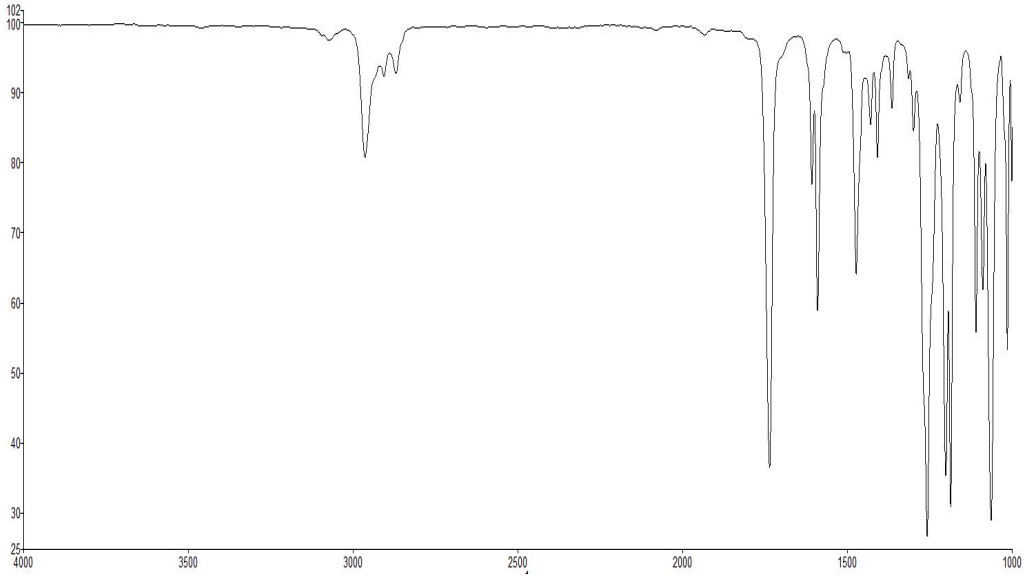

Figure 2.20. Infrared spectrum of compound **2.24**

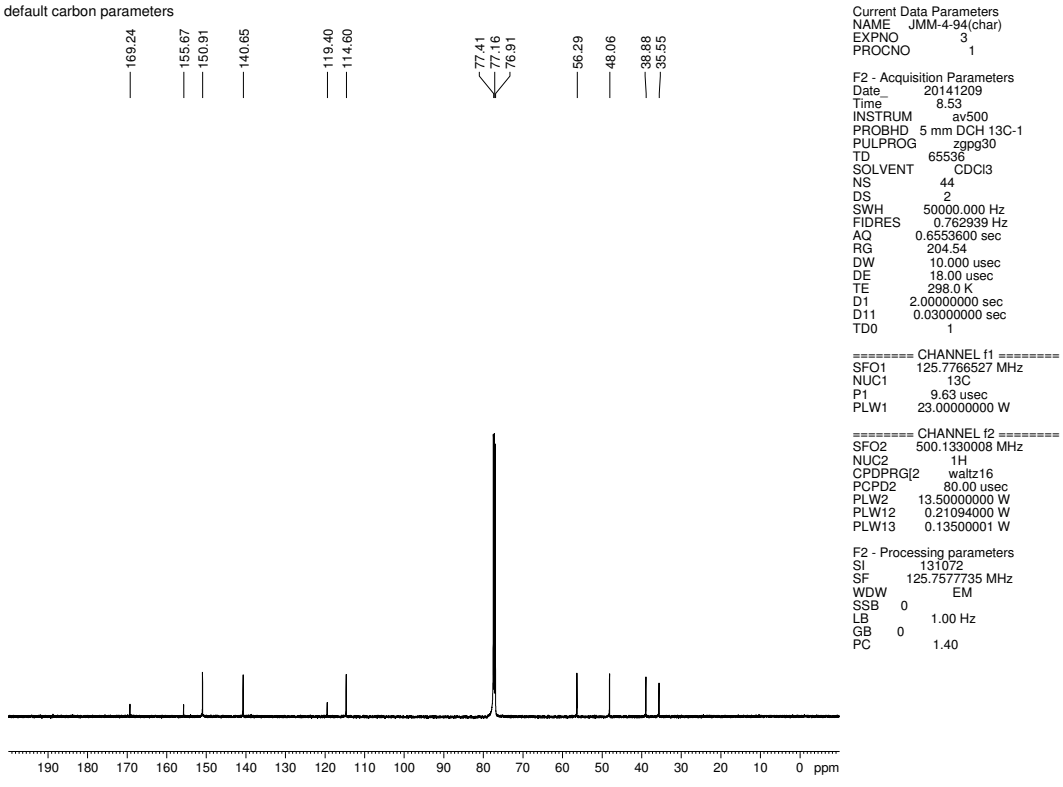

Figure 2.21. ^{13}C NMR (125 MHz, $CDCl_3$) of compound **2.24**

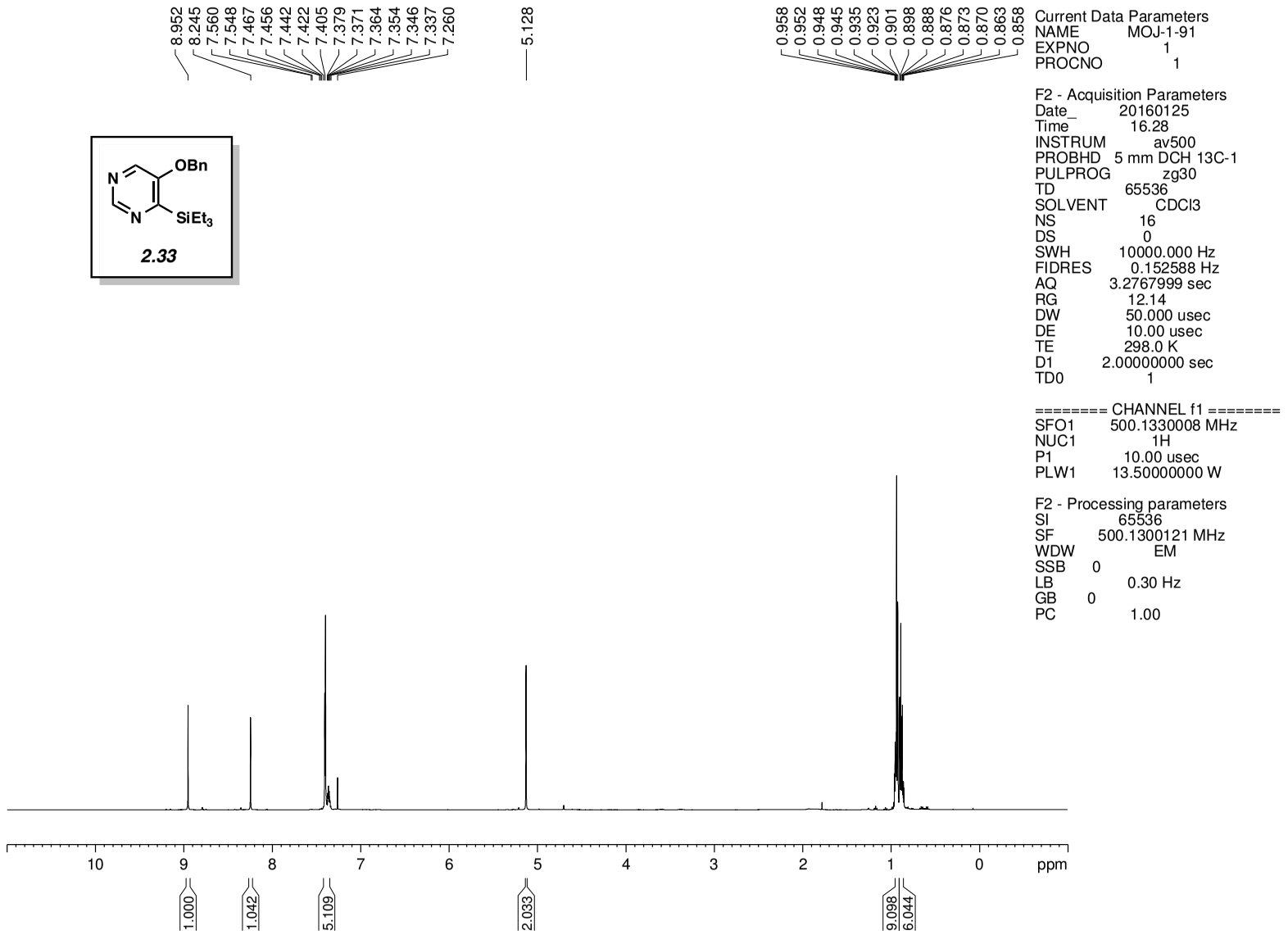

Figure 2.22. ^{1}H NMR (500 MHz, $CDCl_3$) compound **2.33**

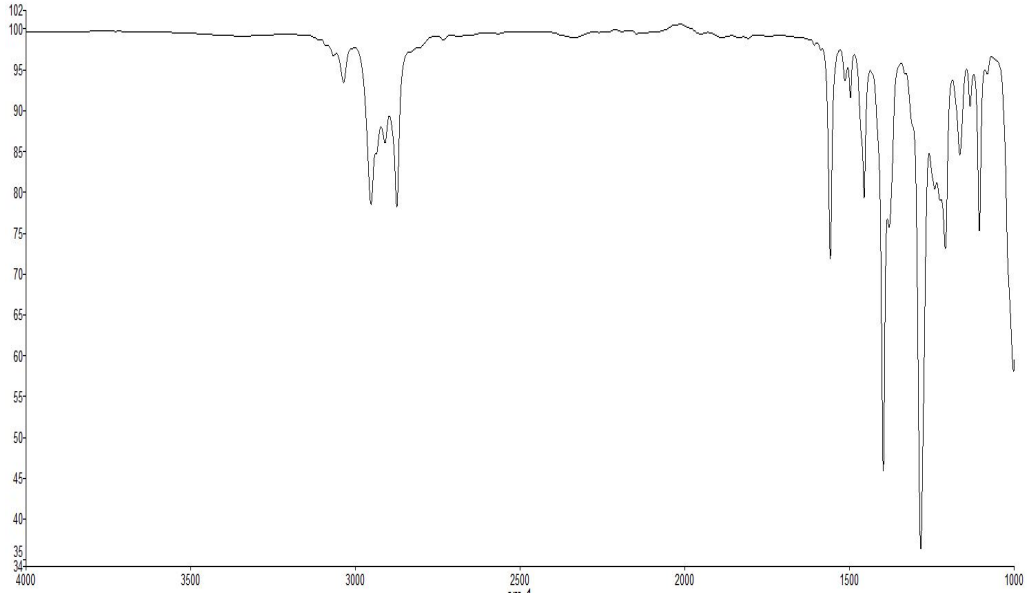

Figure 2.23. Infrared spectrum of compound **2.33**

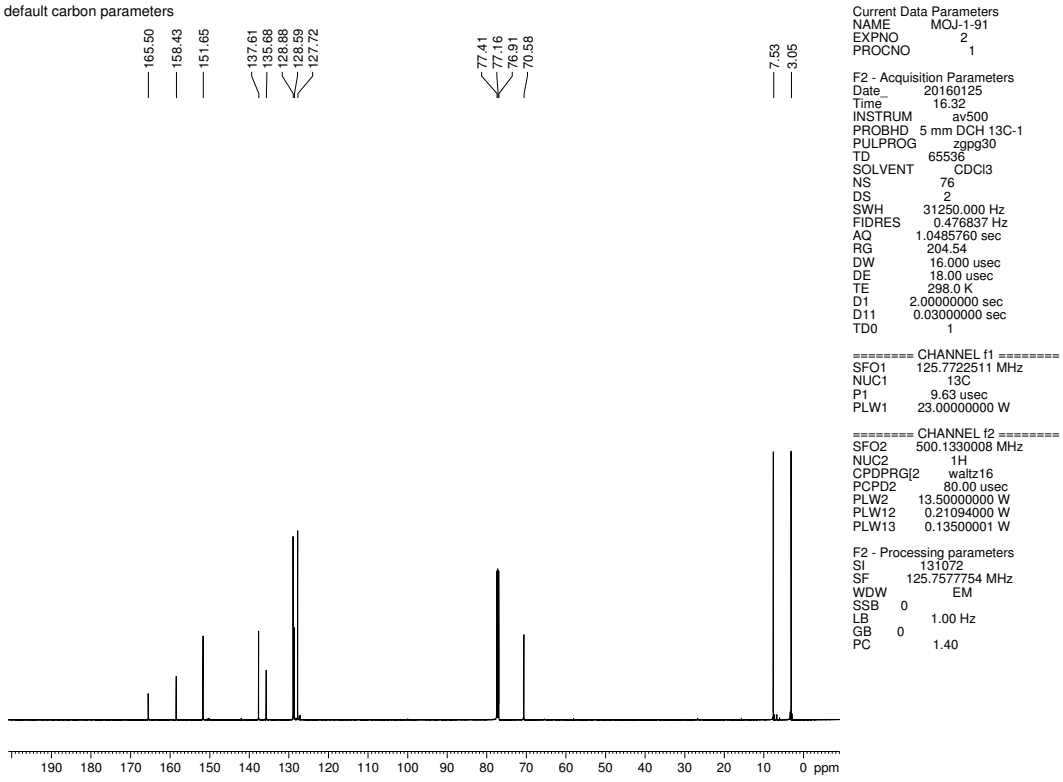

Figure 2.24. ^{13}C NMR (125 MHz, $CDCl_3$) of compound **2.33**

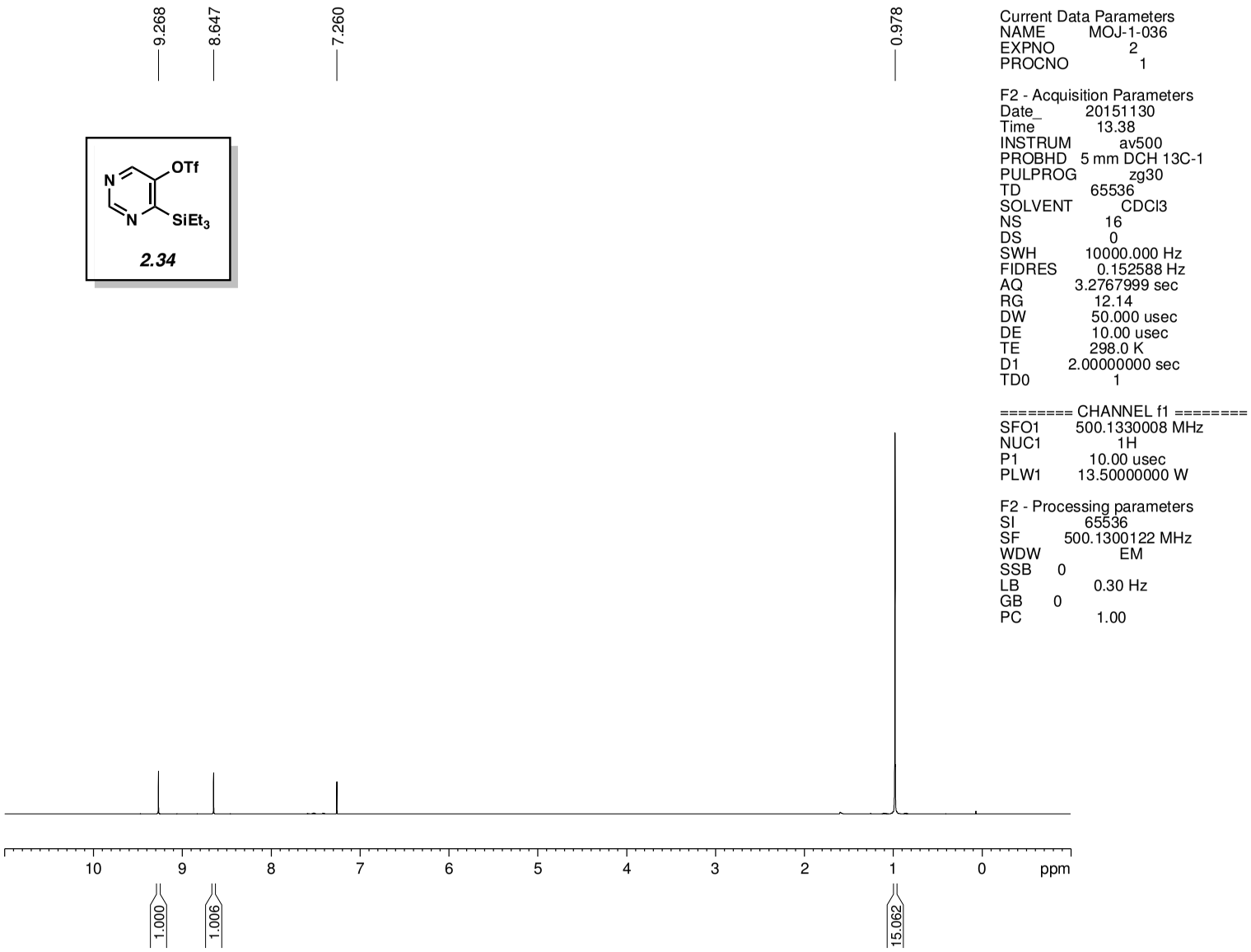

Figure 2.25. ^{1}H NMR (500 MHz, $CDCl_3$) compound **2.34**

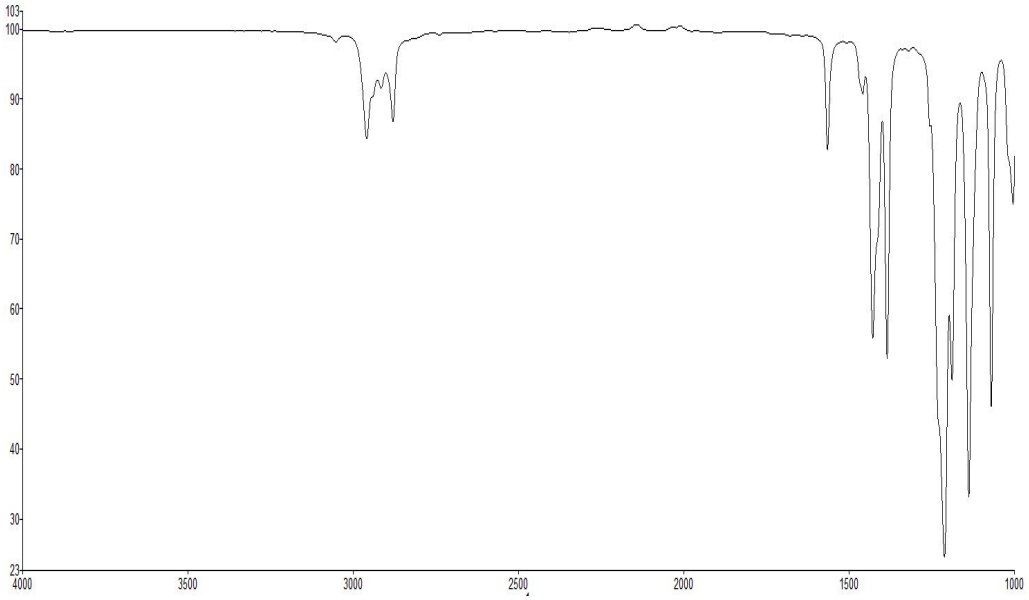

Figure 2.26. Infrared spectrum of compound **2.34**

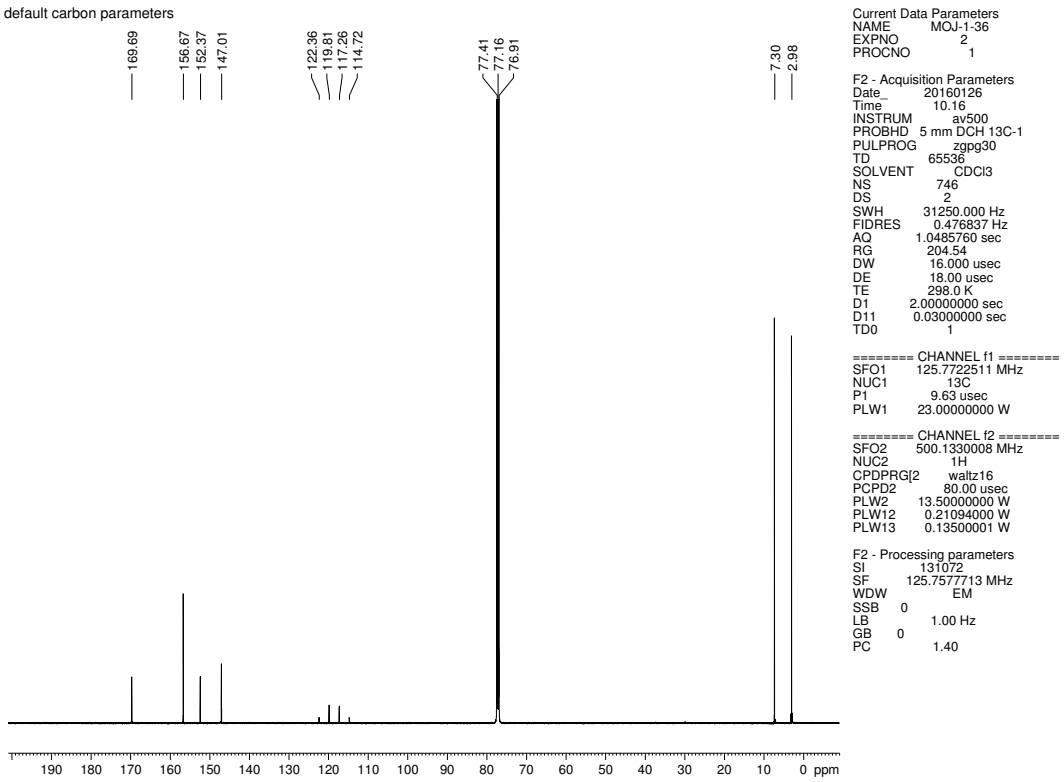

Figure 2.27. ^{13}C NMR (125 MHz, $CDCl_3$) of compound **2.34**

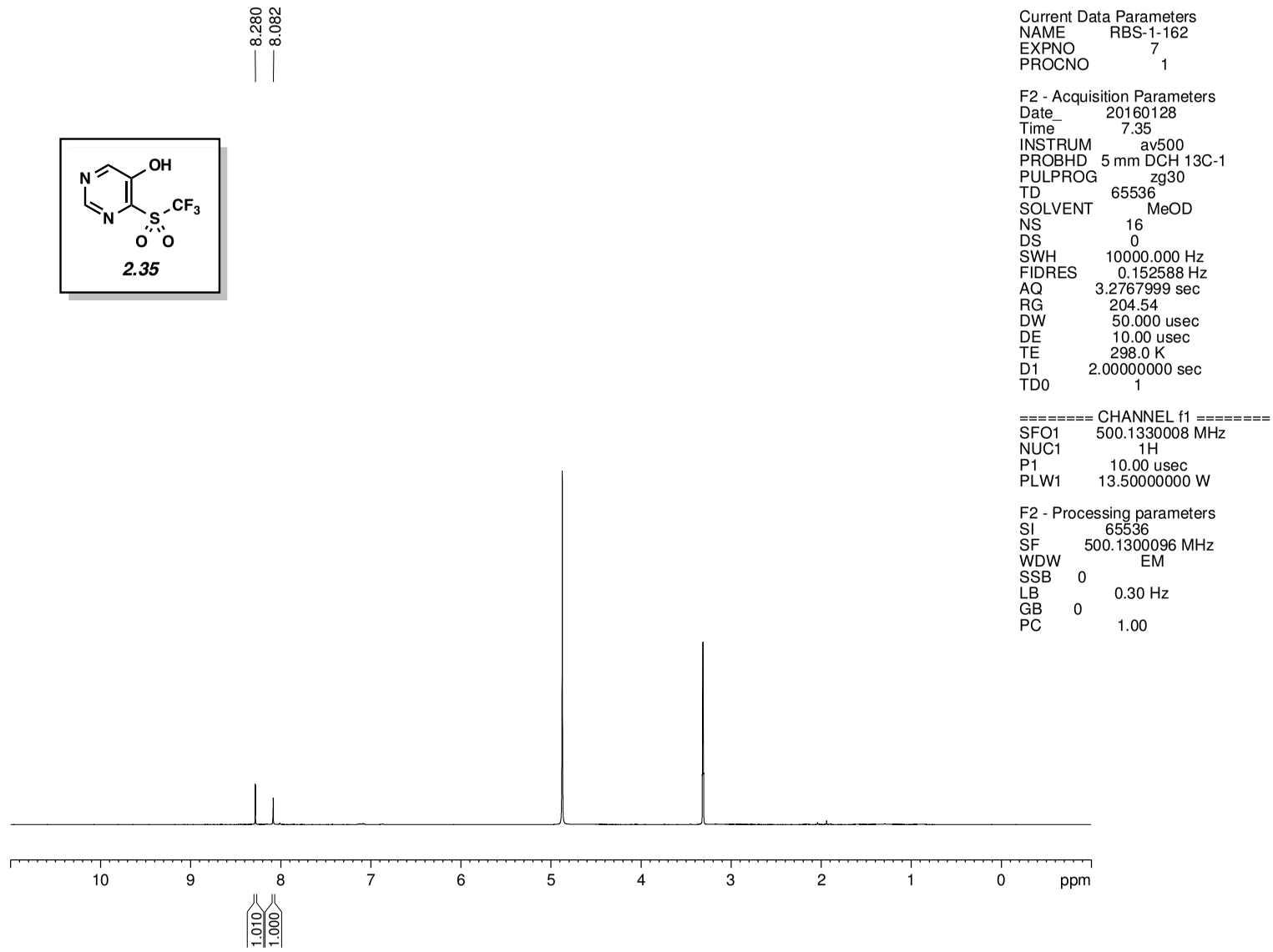

Figure 2.28. ^{1}H NMR (500 MHz, MeOD) compound **2.35**

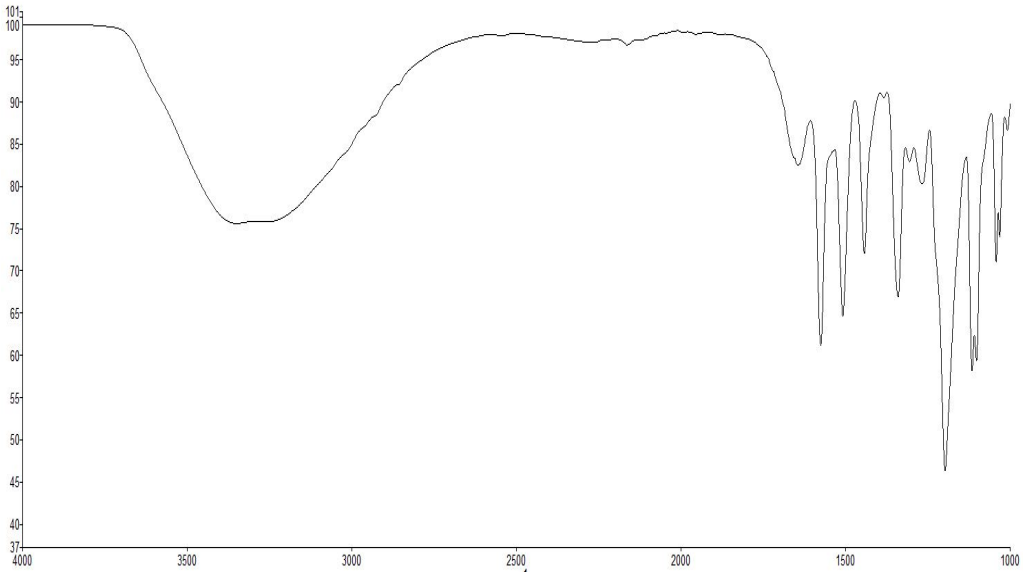

Figure 2.29. Infrared spectrum of compound **2.35**

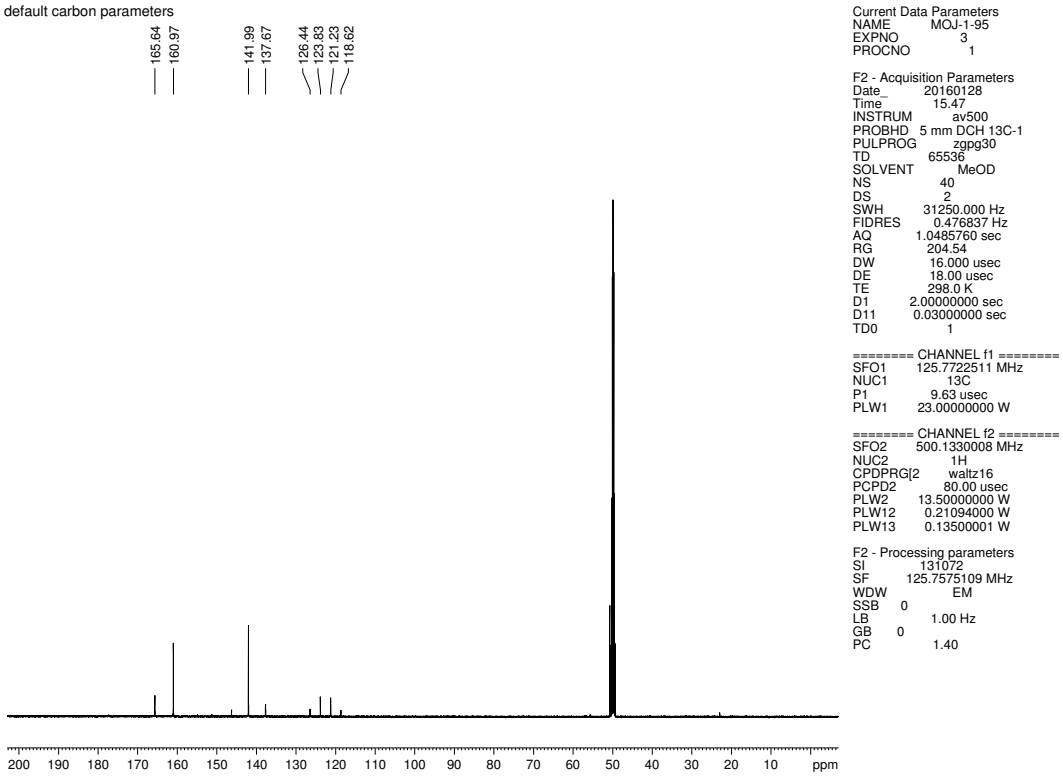

Figure 2.30. ^{13}C NMR (125 MHz, MeOD) of compound **2.35**

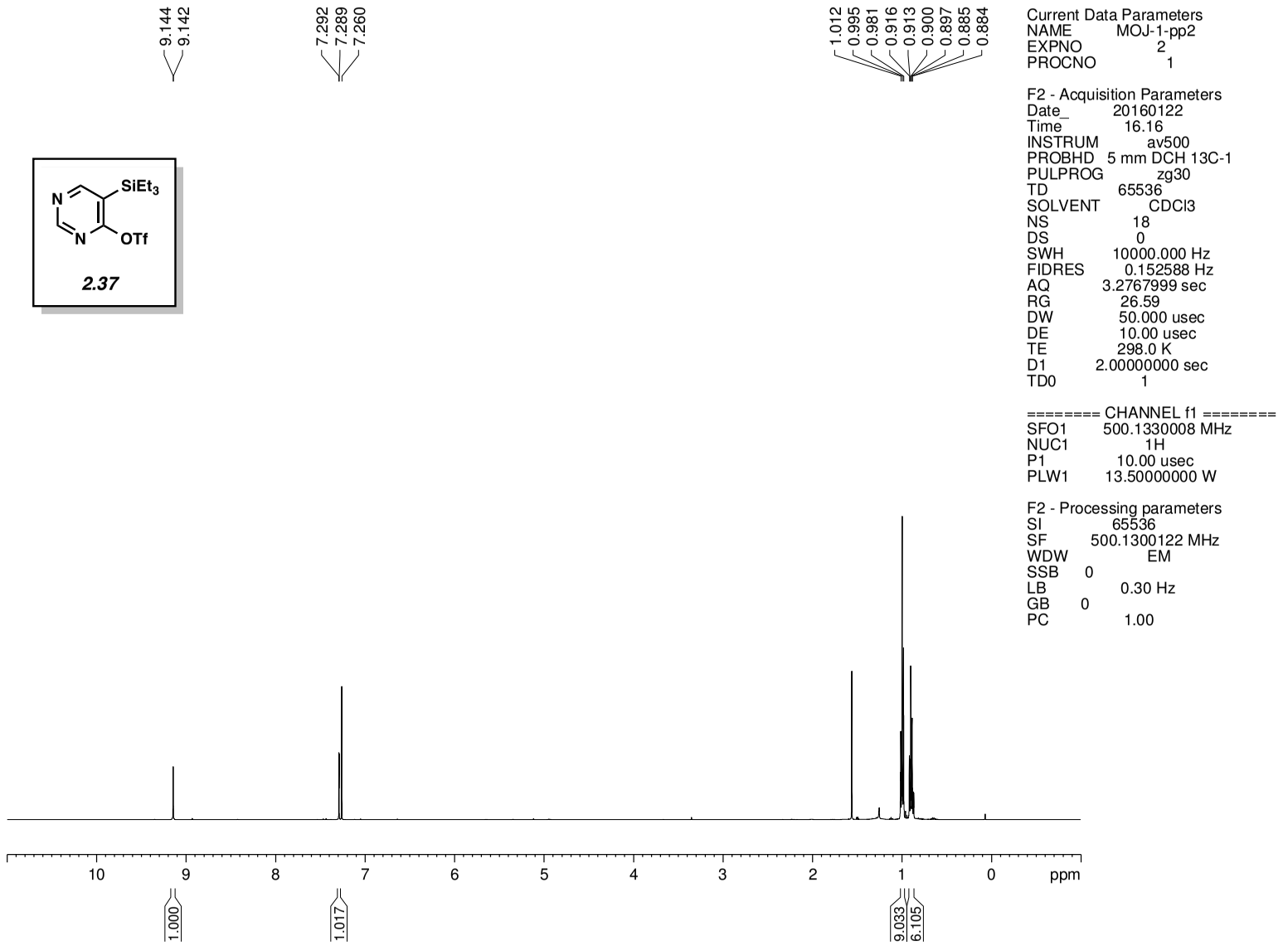

Figure 2.31. ^{1}H NMR (500 MHz, $CDCl_3$) compound **2.37**

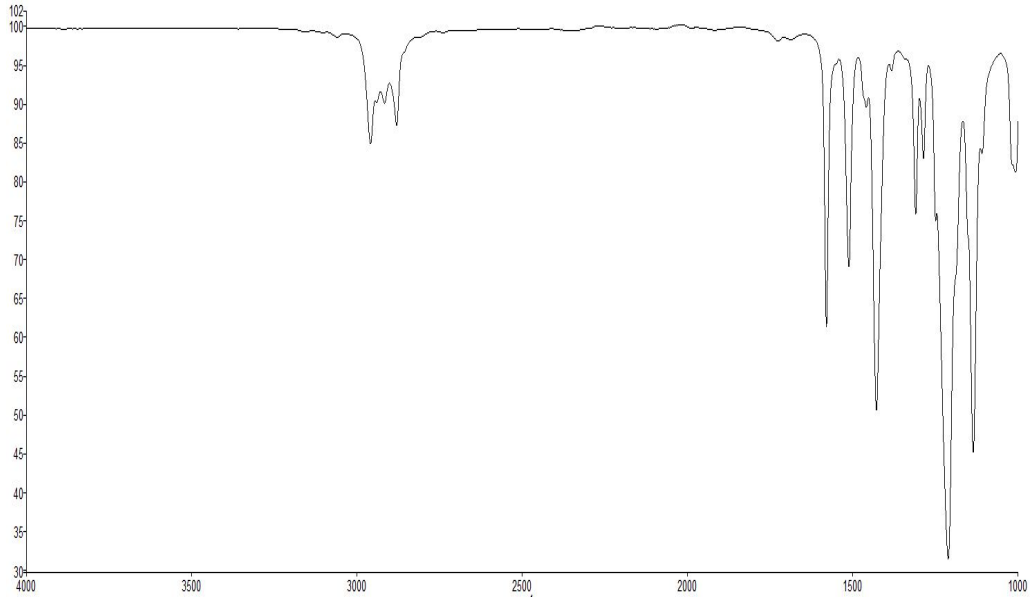

Figure 2.32. Infrared spectrum of compound **2.37**

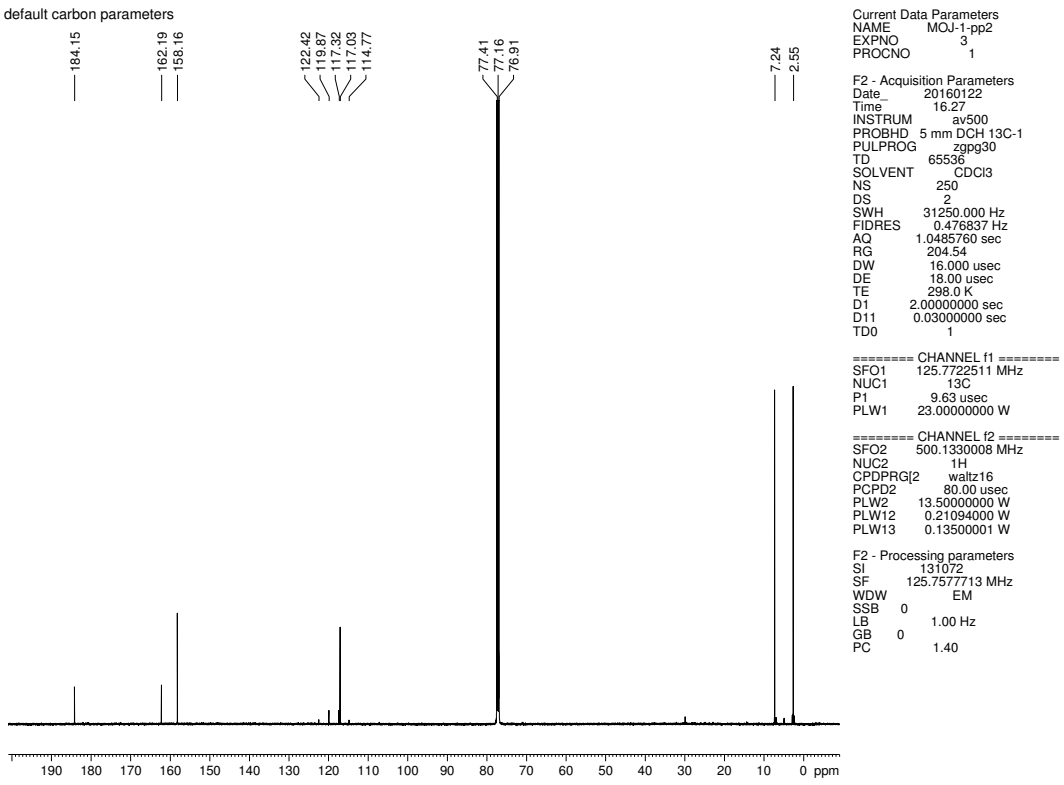

Figure 2.33. ^{13}C NMR (125 MHz, $CDCl_3$) of compound **2.37**

2.7 Notes and References

(1) (a) Vitaku, E.; Smith, B. R.; Smith, D. T.; Njardarson, J. T. http://njardarson.lab.arizona.edu/sites/njardarson.lab.arizona.edu/files/Top%20US%20Pharmaceutical%20Products%20of%202013.pdf (accessed January 25, 2016). (b) McGrath, N. A.; Brichacek, M.; Njardarson, J. T. *J. Chem. Educ.* **2010**, *87*, 1348–1349. (c) Dinges, J., Lamberth, C., Eds. *Bioactive Heterocyclic Compounds Classes: Agrochemicals*; Wiley-VCH: Weinheim, 2012. (d) Gilchrist, T. L. *J. Chem. Soc., Perkin Trans. 1* **1999**, 2849–2866.

(2) For reviews of hetarynes, see: (a) Bronner, S. M.; Goetz, A. E.; Garg, N. K. *Synlett* **2011**, 2599–2604. (b) Goetz, A. E.; Garg, N. K. *J. Org. Chem.* **2014**, *79*, 846–851. (c) Goetz, A. E.; Shah, T. K.; Garg, N. K. *Chem. Commun*. **2015**, *51*, 34–45.

(3) For reviews of arynes, see: (a) Pellissier, H.; Santelli, M. *Tetrahedron* **2003**, *59*, 701–730. (b) Wenk, H. H.; Winkler, M.; Sander, W. *Angew. Chem., Int. Ed.* **2003**, *42*, 502–528. (c) Sanz, R. *Org. Prep. Proced. Int.* **2008**, *40*, 215–291. (d) Tadross, P. M.; Stoltz, B. M. *Chem. Rev.* **2012**, *112*, 3550–3557. (e) Gampe, C. M.; Carreira, E. M. *Angew. Chem., Int. Ed.* **2012**, *51*, 3766–3778. (f) Bhunia, A.; Yetra, S. R.; Biju, A. T. *Chem. Soc. Rev.* **2012**, *41*, 3140–3152. (g) Yoshida, H.; Takaki, K. *Synlett* **2012**, 1725–1732l. (h) Dubrovskiy, A. V.; Markina, N. A.; Larock, R. C. *Org. Biomol. Chem.* **2013**, *11*, 191–218. (i) Wu, C.; Shi, F. *Asian J. Org. Chem.* **2013**, *2*, 116–125. (j) Hoffmann, R. W.; Suzuki, K. *Angew. Chem., Int. Ed.* **2013**, *52*, 2655–2656.

(4) (a) Kauffmann, T. *Angew. Chem. Int. Ed.* **1965**, *4*, 543–618. (b) Reinecke, M. G. *Tetrahedron* **1982**, *38*, 427–498.

(5) (a) Bronner, S. M.; Bahnck, K. B.; Garg, N. K. *Org. Lett.* **2009**, *11*, 1007–1010. (b) Cheong, P. H.-Y.; Paton, R. S.; Bronner, S. M.; Im, G-Y. J.; Garg, N. K.; Houk, K. N. *J. Am. Chem. Soc.*

2010, *132*, 1267–1269. (c) Im, G-Y. J.; Bronner, S. M.; Goetz, A. E.; Paton, R. S.; Cheong, P. H.-Y.; Houk, K. N.; Garg, N. K. *J. Am. Chem. Soc.* **2010**, *132*, 17933–17944. (d) Bronner, S. M.; Goetz, A. E.; Garg, N. K. *J. Am. Chem. Soc.* **2011**, *133*, 3832–3835. (e) Pareek, M.; Fallon, T.; Oestreich, M. *Org. Lett.* **2015**, *17*, 2082–2085. (f) Picazo, E.; Houk, K. N.; Garg, N. K. *Tetrahedron Lett*. **2015**, *56*, 3511–3514.

(6) (a) Buszek, K. R.; Luo, D.; Kondrashov, M.; Brown, N.; VanderVelde, D. *Org. Lett.* **2007**, *9*, 4135–4137. (b) Brown, N.; Luo, D.; VanderVelde, D.; Yang, S.; Brassfield, A.; Buszek, K. R. *Tetrahedron Lett.* **2009**, *50*, 63–65. (c) Buszek, K. R.; Brown, N.; Luo, D. *Org. Lett.* **2009**, *11*, 201–204. (d) Garr, A. N.; Luo, D.; Brown, N.; Cramer, C. J.; Buszek, K. R.; VanderVelde, D. *Org. Lett.* **2010**, *12*, 96–99. (e) Brown, N.; Luo, D.; Decapo, J. A.; Buszek, K. R. *Tetrahedron Lett.* **2009**, *50*, 7113–7115. (f) Thornton, P. D.; Brown, N.; Hill, D.; Neuenswander, B.; Lushington, G. H.; Santini, C.; Buszek, K. R. *ACS Comb. Sci.* **2011**, *13*, 443–448. (g) Nerurkar, A.; Chandrasoma, N.; Maina, L.; Brassfield, A.; Luo, D.; Brown, N.; Buszek, K. R. *Synthesis* **2013**, *45*, 1843–1852.

(7) For a recent study, see: Goetz, A. E.; Garg, N. K. *Nat. Chem.* **2013**, *5*, 54–60; see also references therein.

(8) http://www.sigmaaldrich.com/technical-documents/articles/technologyspotlights/heterocyclic-aryne-precursors.html (accessed January 25, 2016).

(9) For recent examples of total syntheses using hetarynes, see: (a) Huters, A. D.; Quasdorf, K. W.; Styduhar, E. D.; Garg, N. K. *J. Am. Chem. Soc.* **2011**, *133*, 15797–15799. (b) Quasdorf, K. W.; Huters, A. D.; Lodewyk, M. W.; Tantillo, D. J.; Garg, N. K. *J. Am. Chem. Soc.* **2012**, *134*, 1396–1399. (c) Styduhar, E. D.; Huters, A. D.; Weires, N. A.; Garg, N. K. *Angew. Chem. Int. Ed.*

2013, *52*, 12422–12425. (d) Weires, N. A.; Styduhar, E. D.; Baker, E. L.; Garg, N. K. *J. Am. Chem. Soc.* **2014**, *136*, 14710–14713. (e) Bronner, S. M.; Goetz, A. E.; Garg, N. K. *J. Am. Chem. Soc.* **2011**, *133*, 3832–3835. (f) Fine Nathel, N. F.; Shah, T. K.; Bronner, S. M.; Garg, N. K. *Chem. Sci.* **2014**, *5*, 2184–2190. (g) Goetz, A. E.; Silberstein, A. L.; Corsello, M. A.; Garg, N. K. *J. Am. Chem. Soc.* **2014**, *136*, 3036–3039. (h) Buszek, K. R.; Brown, N.; Luo, D. *Org. Lett.* **2009**, *11*, 201–204. (i) Enamorado, M. F.; Ondachi, P. W.; Comins, D. L. *Org. Lett.* **2010**, *12*, 4513–4515.

(10) Arynes have also been used in the synthesis of medicinal agents and to access the fungicide Isopyrazam®. For references, see: (a) Carroll, F. I.; Robingson, T. P.; Brieaddy, L. E.; Atkinson, R. N.; Marscarella, S. W.; Damaj, M. I.; Martin, B. R.; Navarro, H. A. *J. Med. Chem.* **2007**, *50*, 6383–6391. (b) Shah, F.; Tao, Y.; Tang, C.-Y.; Zhang, F.; Wu, X.-Y. *J. Org. Chem.* **2015**, *80*, 8122–8133. (c) Schleth, F.; Vettiger, T.; Rommel, M.; Tobler, H. WO2011131544 A1, 2011.

(11) Levine R.; Leake, W. W. *Science* **1955**, *121*, 780.

(12) (a) Bronner, S. M.; Mackey, J. L.; Houk, K. N.; Garg, N. K. *J. Am. Chem. Soc.* **2012**, *134*, 13966–13969. (b) Goetz, A. E.; Bronner, S. M.; Cisneros, J. D.; Melamed, J. M.; Paton, R. S.; Houk, K. N.; Garg, N. K. *Angew. Chem. Int. Ed.* **2012**, *51*, 2758–2762. (c) Medina, J. M.; Mackey, J. L.; Garg, N. K; Houk, K. N. *J. Am. Chem. Soc.* **2014**, *136*, 15798–15805.

(13) Martens, R. J.; den Hertog, H. J. *Tetrahedron Lett.* **1962**, *3*, 643–645.

(14) Walters, M. A.; Shay, J. J. *Synth. Commun.* **1997**, *27*, 3573–3579.

(15) Fang, Y.; Larock, R. C. *Tetrahedron* **2012**, *68*, 2819–2826.

(16) Yoshida, H.; Shirakawa, E.; Honda, Y.; Hiyama, T. *Angew. Chem. Int. Ed.* **2002**, *41*, 3247–3249.

(17) Nguyen, T. D.; Webster, R.; Lautens, M. *Org. Lett*. **2011**, *13*, 1370–1373.

(18) Saito, N.; Nakamura, K.-i.; Shibano, S.; Ide, S.; Minami, M.; Sato, Y. *Org. Lett*. **2013**, *15*, 386–389.

(19) Lopchuk, J. M.; Gribble, G. W. *Tetrahedron Lett*. **2014**, *55*, 2809–2812.

(20) (a) van der Plas, H. C.; Smit, P.; Koudijs, A. *Tetrahedron Lett*. **1968**, *9*, 9–13. (b) Tielemans, M.; Areschka, V.; Colomer, J.; Promel, R. *Tetrahedron* **1992**, *48*, 10575–10586.

(21) Several silyltriflate aryne and hetaryne precursors are available from Aldrich Chemical Co., Inc. The 2,3-pyridyne precursor **2.10** is available under catalog number L511641.

(22) Shi, F.; Waldo, J. P.; Chen, Y.; Larock, R. C. *Org. Lett*. **2008**, *10*, 2409–2412.

(23) Matsumoto, T.; Sohma, T.; Hatazaki, S.; Suzuki, K. *Synlett* **1993**, 843–846.

(24) Shi, F.; Mancuso, R.; Larock, R. C. *Tetrahedron Lett*. **2009**, *50*, 4067–4070.

(25) Tambar, U. K.; Stoltz, B. M. *J. Am. Chem. Soc*. **2005**, *127*, 5340–5341.

(26) Nara, S. J.; Jha, M.; Brinkhorst, J.; Zemanek, T. J.; Pratt, D. A. *J. Org. Chem*. **2008**, *73*, 9326–9333.

(27) For lithiation and silylation of pyrimidynes, see: (a) Nishiwaki, T. *Tetrahedron* **1966**, *22*, 2401–2412. (b) Ple, N.; Turck, A.; Couture, K.; Queguiner, G. *J. Org. Chem*. **1995**, *60*, 3781–3786. (c) Wada, A.; Yamamoto, J.; Kanatomo, S. *Heterocycles* **1987**, *26*, 585–589.

(28) We also prepared the nonaflate derivative of **2.34**; however, attempted pyrimidyne generation from this substrate also led to the formation of the corresponding alcohol.

(29) For the thia-Fries rearrangement in attempts to generate arynes, see: (a) Hall, C.; Henderson, J. L.; Ernouf, G.; Greaney, M. F. *Chem. Commun.* **2013**, *49*, 7602–7604. (b) Zhao, Z.; Messinger, J.; Schon, U.; Wartchow, R.; Butenschon, H. *Chem. Commun*. **2006**, 3007–3009. (c) Rasheed, O. K.; Hardcastle, I. R.; Raftery, J.; Quayle, P. *Org. Biomol. Chem*. **2015**, *13*, 8048–8052.

(30) Because **2.37** was deemed an unsuitable precursor to the 4,5-pyrimidyne, the synthetic route to **2.37** was not further optimized.

(31) At present, it is unclear why the silyltriflate approach to the 4,5-pyrimidyne is unsuccessful.

CHAPTER THREE

Expanding the ROMP Toolbox: Synthesis of Air-Stable Benzonorbornadiene Polymers by Aryne Chemistry

Jose M. Medina, Jeong Hoon Ko, Heather D. Maynard, and Neil K. Garg

Macromolecules **2017**, *50*, 580–586.

3.1 Abstract

Benzonorbornadiene polymers synthesized by ring-opening metathesis polymerization (ROMP) are typically prone to oxidation at the benzylic / allylic position under ambient conditions. Accordingly, the use of benzonorbornadiene polymers in practical applications has remained limited. In this manuscript, we report the synthesis of poly(benzonorbornadiene) polymers using a strategic blend of benzyne chemistry and ROMP. Through a comparative study, we show that substitution at the benzylic / allylic position prevents oxidative deformation, yet does not inhibit polymerization by common ruthenium catalysts with good control over molecular weight dispersity. We expect the benzyne / ROMP reaction sequence will allow easy access to air-stable benzonorbornadiene polymers for various applications.

3.2 Introduction

Since its original discovery, ring-opening metathesis polymerization (ROMP) has enabled ready access to well-defined polymers for numerous industrial applications including drug delivery,[1,2] electronic materials,[3,4] and nanostructures.[5,6] This process typically relies on strained monomers, such as norbornene and cyclopentene, to provide the thermodynamic driving force necessary to achieve ring opening and promote polymerization. In particular, norbornene and its related analogues have proven to be ideal substrates for ROMP. The energy stored as ring strain (~27.2 kcal / mol) allows for facile ring opening and promotes the subsequent polymerization, while substituents prevent the secondary metathesis of the polymer backbone.[7] In fact, norbornenes are the most frequently used substrates for ROMP.[8]

Despite the widespread utility of norbornenes in various synthetic applications, norbornadienes fused to a benzene ring, or benzonorbornadienes, have been rarely investigated. As a result, the potential utility of the resulting polymers have been largely overlooked. El-Saafin and Feast first reported the synthesis of poly(benzonorbornadiene) (**3.1**, Figure 3.1) in 1982.[9,10] In their study, this polymer was found to be susceptible to oxidation under ambient conditions. Molecular oxygen was thought to facilitate oxidation of the benzylic / allylic position, which then led to intermolecular cross-linking, chain scission, and the ultimate formation of ill-defined materials. Similar studies on related systems by the groups of Grubbs[11] and Schrock[12,13] further suggested that polymers containing a C–H bond at the readily oxidized benzylic / allylic position undergo rapid decomposition, rendering the polymers unstable and of limited utility.

To evade the problem of poly(benzonorbornadiene) stability, one approach is to chemically alter the resulting polymer to essentially mask the troublesome functional groups, thus avoiding the undesired reactivity (Figure 3.1, *Solution A*). In fact, the Swager group opted to

hydrogenate the olefins in the benzonorbornadiene polymer backbone to give **3.2**, in order to prevent oxidation and improve polymer solubility.[14] This strategy proved effective for further electrochemical polymerization and cross-linking of the polymers to form conducting materials. However, the hydrogenation reaction was shown to change the polymer properties such as glass transition temperatures and oxidation onset values.

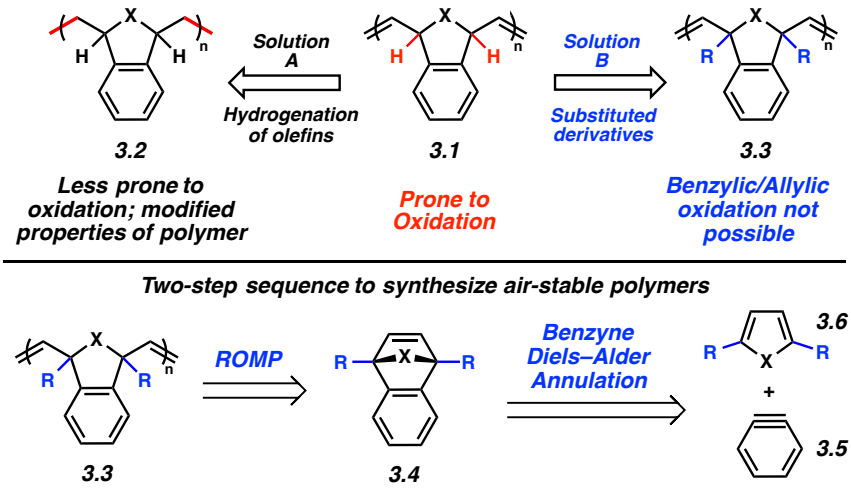

Figure 3.1. Possible solutions to poly(benzonorbornadiene) oxidation problem

An alternative solution for the synthesis of air-stable poly(benzonorbornadiene) involves substituting the benzylic / allylic position that is otherwise prone to oxidation with an unreactive substituent (R = alkyl group) (Figure 3.1, *Solution B*). Ideally, the substituents would be introduced prior to ROMP, thus allowing for the synthesis of polymers without further chemical modification. Such a strategy would not only complement the approach taken by Swager, but could also allow for the potential utilization of the intact double bonds for post-polymerization modification.[15,16,17,18] To test this general strategy, we envisioned accessing substituted polymers **3.3** (Figure 3.1) via ROMP of monomers **3.4**. The success of this approach hinged on the

development of an efficient route to access various monomers **3.4**. For this purpose, we sought to utilize the Diels–Alder trapping of benzyne (**3.5**) with cyclic dienes **3.6**. Although historically avoided due to their high reactivity, arynes have recently been employed in chemical synthesis,[19,20,21,22,23,24,25,26,27,28,29,30,31,32,33,34,35,36,37,38,39,40,41,42] albeit with only limited applications in polymer chemistry.[43,44,45,46] Herein, we report the use of a benzyne annulation / ROMP reaction sequence to furnish well-defined poly(benzonorbornadiene) derivatives, including two that are stable to oxidation.

3.3 Results and Discussion

3.3.1 Synthesis of Benzonorbornadiene Monomers

The benzonorbornadiene monomers **M3.1**–**M3.4** were easily synthesized using the commercially available benzyne precursor **3.7**,[47] as summarized in Table 3.1. Whereas **M3.3** and **M3.4** would later be used to access air-stable polymers, the less substituted monomers, **M3.1** and **M3.2**, were targeted for comparative purposes. Silyltriflate **3.7** was exposed to CsF in the presence of cyclic diene trapping partners in acetonitrile at 60 °C. This simple protocol promotes an elimination reaction to give the benzyne intermediate (**3.5**), which is subsequently trapped in Diels–Alder cycloadditions to give monomers **M3.1**–**M3.4** in excellent yields. Several features of this approach should be noted: (a) the reactions are operationally trivial to perform and generally do not require the rigorous exclusion of water or oxygen; (b) the benzyne trapping allows for the formation of two new carbon–carbon bonds and two tertiary stereocenters in a single transformation, and (c) purification of the desired monomers is straightforward using chromatography.

Table 3.1. Benzonorbornadiene Monomers **M3.1–M3.4** Synthesized by Aryne Chemistry

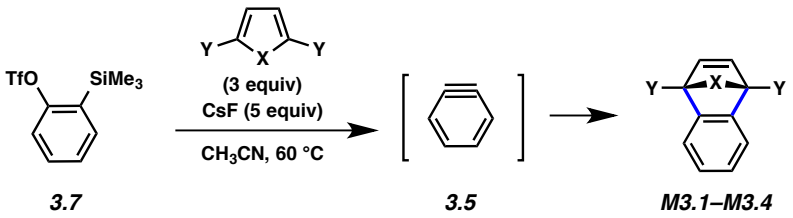

3.7 *3.5* *M3.1–M3.4*

Entry	*Trapping agent*	*Product*		*Yield*
1			*M3.1*	99%
2			*M3.2*	94%
3	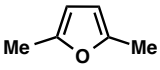	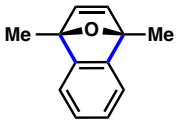	*M3.3*	99%
4	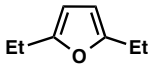	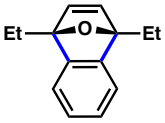	*M3.4*	91%

3.3.2 Synthesis & Properties of Benzonorbornadiene Polymers

The results of polymerization studies are shown in Table 3.2. Monomers **M3.1–M3.3** were readily polymerized using the first-generation Grubbs catalyst in toluene at room temperature (entries 1–9) at various monomer to catalyst ratios. Initially we observed that ROMP of benzonorbornadiene **M3.1** resulted in polymers **P3.1** with moderate dispersities (Đ = 1.60 – 1.73, Experimental Section Figure 3.5b). Based on the aforementioned precedents, we suspected that polymers **P3.1** were highly sensitive to molecular oxygen and readily oxidized at the benzylic / allylic position when exposed to air. Since the polymers were stored in the freezer and thus exposed to ambient oxygen prior to analysis, we theorized that this was the origin of the

observed molecular weight distributions. To test this hypothesis, we took freshly polymerized samples directly from the glove box and dissolved them in chloroform immediately before analyzing by gel permeation chromatography (GPC). Even with this precaution, the traces of **P3.1** exhibited shoulder peaks (Figure 3.2a); however the dispersities of the polymers (Đ = 1.15 – 1.20, Table 3.2) were much smaller than those of the stored samples. It is also interesting to note that the molecular weight of **P3.1** decreased after incubation in air (Table 3.4) suggesting chain scission. El-Saafin and Feast had postulated that molecular oxygen reacts at the benzylic / allylic of poly(benzonorbornadiene) to produce a peroxy radical and that oxidation of the polymer both degrades and cross-links the polymer;[9] the GPC data for **P3.1** supports this hypothesis.

The oxygen-containing analogue **M3.2** resulted in ill-defined polymers with high dispersities even when analyzed immediately after polymerization (Figure 3.5c). The light scattering (LS) trace significantly differed from the refractive index (RI) trace and showed larger molecular weight species that eluted prior to the main peak (Figure 3.5c). It should be noted that LS is more sensitive to higher molecular weight species than RI,[48,49,50] and thus the high molecular weight shoulder is more pronounced in the LS trace. Continued exposure of the sample to air resulted in further deformation of the LS trace, and a second distinct peak appeared near the 10 min mark on the chromatogram (Figure 3.5d). Comparison of **P3.1** and **P3.2** GPC traces suggested that **P3.2** underwent more significant oxidation (Figure 3.5a vs. 3.5c), implying that **P3.2** is especially prone to oxidation and will likely oxidize immediately upon contact with air. To compare the relative oxidation potentials of **P3.1** and **P3.2**, energies of monomer units were computed by density functional theory (DFT) calculations.[51] Results show that the oxidation potential of **P3.2** is 0.238 V higher than that of **P3.1**, which supports the experimental

observation that **P3.2** oxidizes more readily than **P3.1** (see Calculation of Oxidation Potential section in the Experimental Section).

It was also noted that the main peaks from the **P3.2** chromatogram had higher dispersity values (Figure 3.2b, Đ = 1.83 – 2.00) than those observed for fresh **P3.1** (Figure 3.2a, Đ = 1.15 – 1.20). It has been previously reported that monomer **M3.2** is roughly 19 times more reactive than monomer **M3.1**.[52] Assuming similar rates of initiation (k_i) for the first-generation Grubbs catalyst in the ROMP of **M3.1** and **M3.2**, this increased reactivity likely leads to a high propagation rate (k_p) and low k_i / k_p ratio that consequently results in the observed higher dispersities for **M3.2**.

Table 3.2. ROMP of Monomers **M3.1–M3.4** Using Grubbs Catalysts

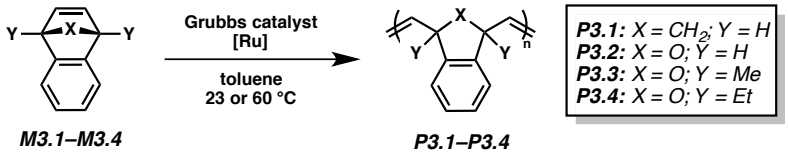

M3.1–M3.4 *P3.1–P3.4*

Entry	*Catalyst*	*Monomer*	*[M] / [I]*	*M_n (theo)*	*M_n*	*Đ*
1	G1	M3.1	50	7.1 kDa	11.8 kDa	1.16
2	G1	M3.1	150	21.3 kDa	31.6 kDa	1.15
3	G1	M3.1	300	42.6 kDa	53.0 kDa	1.20
4	G1	M3.2	50	7.2 kDa	15.7 kDa[a]	1.83[a]
5	G1	M3.2	150	21.6 kDa	38.4 kDa[a]	1.86[a]
6	G1	M3.2	300	43.3 kDa	50.6 kDa[a]	2.00[a]
7	G1	M3.3	50	8.6 kDa	5.4 kDa	1.14
8	G1	M3.3	150	25.8 kDa	25.2 kDa	1.14
9	G1	M3.3	300	51.7 kDa	54.0 kDa	1.17
10	G3	M3.4	50	10.0 kDa	17.4 kDa	1.11
11	G3	M3.4	150	30.0 kDa	46.4 kDa	1.12
12	G3	M3.4	300	60.1 kDa	162.0 kDa	1.07

[a] Major peak calculated from RI trace

Grubbs 1
G1

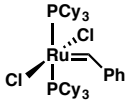

Grubbs 3
G3

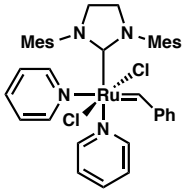

Whereas the unsubstituted polymers **P3.1** and **P3.2** were highly susceptible to oxidation, polymers **P3.3** and **P3.4** (bearing alkyl substituents at the benzylic / allylic positions) did not exhibit such discrepancy between RI and LS traces, suggesting that benzylic substitution effectively prevents oxidation. For the dimethyl-substituted monomer **M3.3**, the substitution attenuates the reactivity of the system, allowing for well-controlled polymerizations with narrow dispersity (Đ = 1.14 – 1.17) for all molecular weights tested (Figure 3.2c). Effective polymerization of monomer **M3.4** required the use of the more reactive third-generation Grubbs catalyst and higher reaction temperatures (60 ^{o}C) (Table 3.2, entries 10–12) to give polymers with low dispersity values (Figure 3.2d, $Đ$ = 1.07 – 1.12).

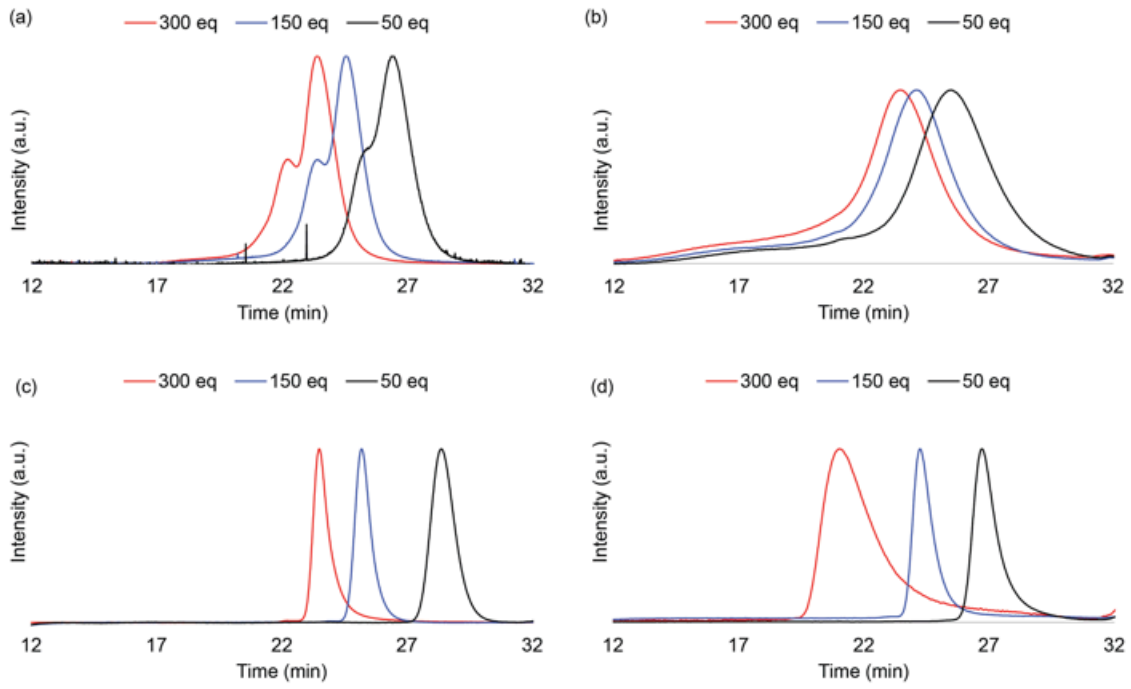

Figure 3.2. SEC-MALS Chromatograms of polymers (a) **P3.1** and (b) **P3.2** show broad overlapping peaks. Chromatograms of polymers (c) **P3.3** and (d) **P3.4** show well-defined peaks

In order to verify that alkyl substitution at the benzylic / allylic positions results in polymers that are stable to oxidation, we analyzed polymers **P3.1**–**P3.4** by elemental analysis (Table 3.3). Benzonorbornadiene polymer **P3.1** was detected to contain 0.37 oxygen atoms per repeat unit. This represents direct evidence for the incorporation of oxygen to the polymer once it is exposed to air. Similarly, oxabenzonorbornadiene polymer **P3.2** was found to contain 1.32 oxygen atoms per repeat unit. The instrumental error in the measurement of oxygen is 0.30%. The data indicates that both unsubstituted polymers have higher oxygen-content than we would normally expect (>30% more oxygen). In stark contrast, polymers **P3.3** and **P3.4** both contained the expected number of oxygen atoms per repeat unit, suggesting that substitution at the benzylic / allylic positions successfully suppressed the oxidation pathway.

Table 3.3. Elemental Analysis Data for Polymers **P3.1–P3.4**

Polymer	*Element*	*% observed*	*# of atoms per unit observed*	*# of atoms per unit theoretical*
P3.1	Carbon	88.70	11	11
	Hydrogen	7.27	10.74	10
	Oxygen	3.96	0.37	0
P3.2	Carbon	80.38	10	10
	Hydrogen	5.58	8.27	8
	Oxygen	14.14	1.32	1
P3.3	Carbon	83.54	12	12
	Hydrogen	7.09	12.14	12
	Oxygen	9.46	1.02	1
P3.4	Carbon	83.89	14	14
	Hydrogen	7.93	15.77	16
	Oxygen	8.08	1.01	1

To further confirm the oxidation of **P3.1** and **P3.2**, the polymer samples were subjected to Fourier-transform infrared spectroscopy (FT-IR) analysis (Figure 3.3). Upon oxidation and incorporation of an OH group, the FT-IR spectrum is expected to show a broad alcohol or

peroxide O–H stretch in the 3600–3200 cm^{-1} range. Polymer **P3.1** shows a small broad peak at 3400 cm^{-1} (Figure 3.3a), in good agreement with the IR spectrum previously reported for the poly(benzonorbornadiene).[10] The same indicative stretch (3400 cm^{-1}) is more pronounced in polymer **P3.2** (Figure 3.3b), and it is completely absent in the cases of polymers **P3.3** and **P3.4** (Figure 3.3c and 3.3d). Taken together with the elemental analysis data, these experimental findings confirm that benzonorbornadiene monomers with benzylic / allylic substitution give air-stable polymers.

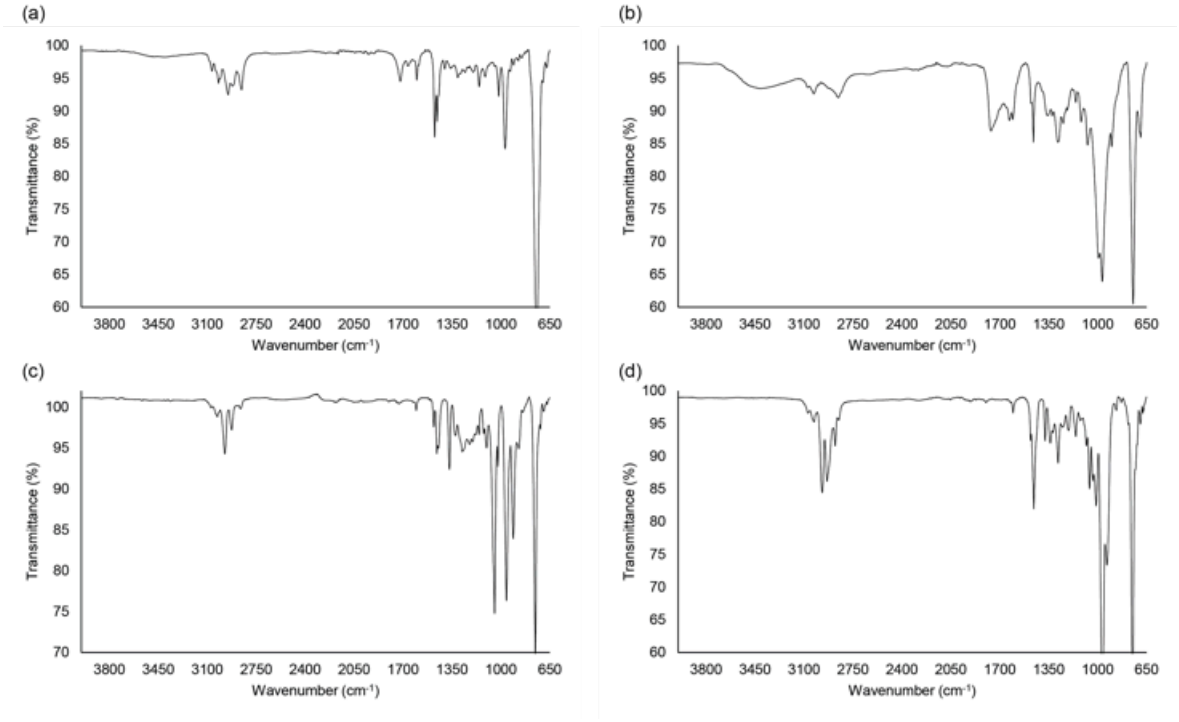

Figure 3.3. FT–IR spectra: (a) **P3.1**, (b) **P3.2**, (c) **P3.3**, (d) **P3.4**

Having determined the relative stability to oxygen of non-substituted (**P3.1** and **P3.2**) and substituted (**P3.3** and **P3.4**) polymers, we measured the glass transition temperatures (T_g) by dynamic scanning calorimetry (DSC) (Figure 3.4). Polymers **P3.1** and **P3.3** each have a high T_g

(**P3.1**: 155.40 °C and **P3.3**: 151.99 °C), whereas the diethyl-substituted polymer **P3.4** has a lower T_g (93.58 °C). This drastic decrease in glass transition temperature, related to the longer alkyl substituent (methyl vs. ethyl), has been previously attributed to the internal plasticization effect.[53,54] Longer alkyl substituents are thought to disrupt intermolecular interactions between polymer chains, thereby reducing the thermal barrier required to reach the glass transition threshold. For polymer **P3.2** (Figure 3.4b), Schrock and coworkers have previously reported a T_g of 167 ^{o}C.[13] Interestingly, we do not observe a T_g in the –50 to 250 °C range. We suspect that the polymer cross-linked through the oxidation pathway prior to analysis, which would restrict polymer chain motion that causes the onset of glass transition.[55] As cross-linking would make the microstructure of the polymer highly heterogeneous, the glass transition of the polymer may be altered to different extents, ultimately leading to broadening of T_g such that it is not detectable.

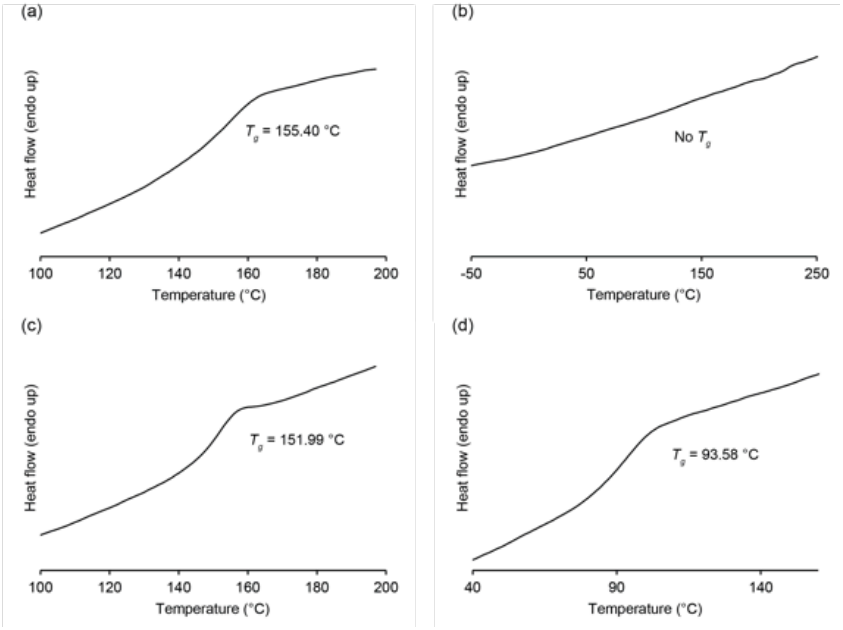

Figure 3.4. DSC curves, (a) **P3.1**, (b) **P3.2** (not detected), (c) **P3.3**, and (d) **P3.4**

3.4 Conclusion

We have successfully demonstrated an efficient approach for the synthesis of air-stable benzonorbornadiene polymers. Monomers were synthesized in high yields using benzyne Diels–Alder reactions involving a commercially available benzyne precursor. Subsequently, ruthenium-based Grubbs catalysts were used to promote ROMP, giving polymers with good control over molecular weight dispersity. This approach complements more commonly used strategies for handling unstable materials, such as post-polymerization modifications. We anticipate that this report will stimulate further efforts to utilize arynes in the synthesis of polymers, in addition to benzonorbornadiene polymers in materials applications.

3.5 Experimental Section

3.5.1 Materials and Methods

Unless stated otherwise, reactions were conducted in flame-dried glassware under an atmosphere of nitrogen using anhydrous solvents (freshly distilled or passed through activated alumina columns). All commercially obtained reagents were used as received unless otherwise specified. Cesium fluoride (CsF) was obtained from Strem Chemicals and stored on the bench-top at ambient temperature under a N_2 atmosphere. 2-(Trimethylsilyl)phenyl trifluoromethanesulfonate, dicyclopentadiene, and 2,5-dimethylfuran were obtained from Sigma Aldrich. Furan was obtained from Alfa Aesar. First-generation and second-generation Grubbs catalysts were obtained from Materia Inc. Third-generation Grubbs catalyst was synthesized from the second-generation catalyst according to literature precedent.[56] Reaction temperatures were controlled using an IKAmag temperature modulator and, unless stated otherwise, reactions were performed at room temperature (rt, approximately 23 °C). Thin-layer chromatography

(TLC) was conducted with EMD gel 60 F254 pre-coated plates (0.25 mm) and visualized using a combination of UV light and potassium permanganate staining. Silicycle Siliaflash P60 (particle size 0.040–0.063 mm) was used for flash column chromatography. ^{1}H NMR spectra were recorded on Bruker spectrometers (at 400 MHz, or 500 MHz) and are reported relative to deuterated solvent signals. Data for ^{1}H NMR spectra are reported as follows: chemical shift (δ ppm), multiplicity, coupling constant (Hz) and integration. ^{13}C NMR spectra were recorded on Bruker spectrometers (at 125 MHz) and are reported relative to deuterated solvent signals. Data for ^{13}C NMR spectra are reported in terms of chemical shift and, when necessary, multiplicity, and coupling constant (Hz). IR spectra were recorded on a Perkin-Elmer 100 spectrometer and are reported in terms of frequency of absorption (cm^{-1}). High-resolution mass spectra were obtained on Waters LCT Premier with ACQUITY LC and Thermo Scientific^{TM} Exactive Mass Spectrometers with DART ID-CUBE.

3.5.2 Analytical Techniques

Gel permeation chromatography (GPC) was conducted on a Shimadzu HPLC Prominence-i system equipped with a UV detector, Wyatt DAWN Heleos-II Light Scattering detector, Wyatt Optilab T-rEX RI detector, one MZ-Gel SDplus guard column, and two MZ-Gel SDplus 100 Å 5 μm 300 x 8.0 mm columns. Chloroform ($CHCl_3$) at 40 °C was used as the eluent (flow rate: 0.70 mL/min). For polymers **P3.1**, **P3.3**, and **P3.4**, dn/dc was calculated by the Astra 6.0 software and used for calculation of molecular weights. For **P3.2**, near-monodisperse poly(styrene) standards (Polymer Laboratories) were employed for calibration and molecular weights were calculated from refractive index. Infrared absorption spectra were recorded on a PerkinElmer FT-IR equipped with an ATR accessory. Elemental analysis was conducted through

Midwest Microlab, Inc., on an Exeter Analytical CE-440. For each polymer series, equal amounts of samples were combined from all equivalents (50, 150, and 300 equiv) and submitted for analysis. The samples were vacuum dried overnight prior to the elemental analysis. Differential scanning calorimetry was conducted on a DSCQ200 calorimeter (TA Instruments) equipped with a RSC 90 electric freezing machine, using approximately 5 mg of dried polymer sample (150 equiv as the representative sample) in an aluminum pan under a dry nitrogen flow at a heating/cooling rate of 10 °C/min, with a total of two cycles from –80 to 200 °C.

3.5.3 Experimental Procedures

3.5.3.1 Synthesis of Benzonorbornadiene Monomers M3.1–M3.4

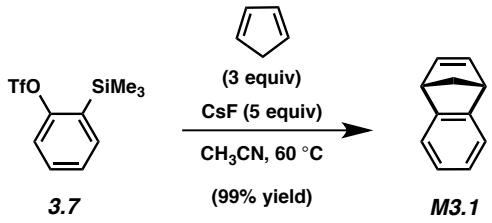

Representative Procedure: Cyclopentadiene Diels-Alder monomer M3.1 (Table 3.1, Entry 1). Cyclopentadiene was purified as follows: a 250 mL round bottom flask containing a stir bar was attached to a Vigreux column. The Vigreux column was fitted with a short-path distillation head, which in turn, was connected to a Schlenk tube. The apparatus was flame-dried, and then the 250 mL round bottom flask was charged with dicyclopentadiene (100 mL). The apparatus was purged with N_2, and the 250 mL round bottom flask was heated to 220 °C. After several hours, approximately 50 mL of cyclopentadiene was collected in the Schlenk tube, which was submerged in a –78 °C bath (acetone/dry ice). The distillate was stored at –80 °C.

To a stirred solution of silyltriflate **3.7** (500 mg, 1.68 mmol) and cyclopentadiene (705 μL, 8.38 mmol, 5 equiv) in CH_3CN (17 mL) was added CsF (1.3 g, 8.38 mmol, 5 equiv). The reaction vessel was sealed and placed in an aluminum heating block maintained at 60 °C for 16 h. After cooling to 23 °C, the reaction mixture was filtered over silica gel (EtOAc eluent). Evaporation under reduced pressure afforded crude **M3.1**. The crude residue was further purified by column chromatography (hexanes) to afford **M3.1** (239 mg, 99% yield) as a colorless oil: Spectral data matched those previously reported.[57]

Any modifications of the conditions shown in this representative procedure are specified in the following schemes, which depict all of the results shown in Table 3.1

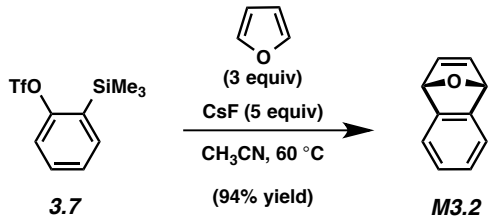

Furan Diels-Alder monomer M2 (Table 3.1, Entry 2). To a stirred solution of silyltriflate **3.7** (500 mg, 1.68 mmol) and furan (370 μL, 5.03 mmol, 3 equiv) in CH_3CN (17 mL) was added CsF (1.3 g, 8.38 mmol, 5 equiv). The crude residue was purified by column chromatography (95:5 hexanes:EtOAc) to afford **M3.2** (227 mg, 94% yield) as a colorless oil: Spectral data matched those previously reported.[58]

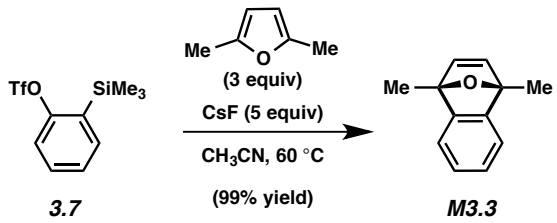

2,5-Dimethylfuran Diels-Alder monomer M3.3 (Table 3.1, Entry 3). To a stirred solution of silyltriflate **3.7** (500 mg, 1.68 mmol) and 2,5-dimethylfuran (555 µL, 5.03 mmol, 3 equiv) in CH_3CN (17 mL) was added CsF (1.3 g, 8.38 mmol, 5 equiv). The crude residue was purified by column chromatography (95:5 hexanes:EtOAc) to afford **M3.3** (289 mg, 99% yield) as a faint yellow oil: Spectral data matched those previously reported.[59]

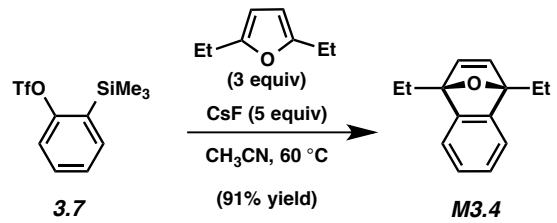

2,5-Diethylfuran Diels-Alder monomer M3.4 (Table 3.1, Entry 4). To a stirred solution of silyltriflate **3.7** (500 mg, 1.68 mmol) and 2,5-diethylfuran (625 mg, 5.03 mmol, 3 equiv) in MeCN (17 mL) was added CsF (1.3 g, 8.38 mmol, 5 equiv). The crude residue was purified by column chromatography (99:1 hexanes:EtOAc) to afford **M3.4** (305 mg, 91% yield) as a faint orange oil. **M3.4**: R_f 0.63 (9:1 hexanes:EtOAC); ^{1}H NMR (500 MHz, $CDCl_3$): δ 7.15–7.10 (m, 2H), 6.99–6.93 (m, 2H), 6.79 (s, 2H), 2.40–2.32 (m, 2H), 2.30–2.22 (m, 2H), 1.19 (t, J = 7.53, 6H); ^{13}C NMR (125 MHz, $CDCl_3$): δ 152.6, 146.0, 124.7, 119.0, 92.5, 22.5, 9.2; IR (film): 3069, 2970, 2937, 1452, 1379, 1291 cm^{-1}; HRMS-ESI (m/z) $[M + H]^+$ calcd for $C_{14}H_{17}O$, 201.12739; found, 201.12732.

3.5.3.2 Synthesis of Benzonorbornadiene Polymers P3.1–P3.4

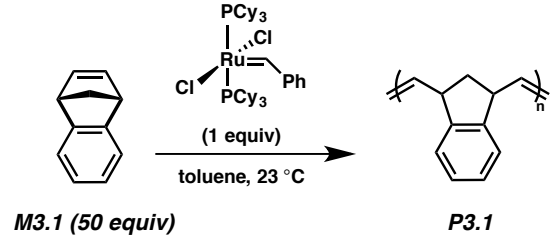

Representative Procedure: Polymerization P3.1 (50 equiv) (Table 3.2, Entry 1). A 1-dram vial containing a magnetic stir bar was flame-dried under reduced pressure, and then allowed to cool under N_2. The vial was charged with monomer **M3.1** (20.0 mg, 0.14 mmol, 50 equiv), and the vial was flushed with N_2. The vial was taken into a glove box and the monomer was dissolved in toluene (100 μL).

In the glovebox, a separate vial was charged with Grubbs first-generation catalyst (5.9 mg) and toluene (230 μL). A 90 μL aliquot of the resulting solution (2.3 mg Grubbs 1st gen. cat., 2.8 μmol, 1 equiv) was then added to the monomer **M3.1** solution while stirring vigorously. The reaction mixture was allowed to stir at 23 °C for 24 h. The vial was then removed from the glove box and the reaction was quenched with ethyl vinyl ether (10 μL, 0.1 mmol). The polymer was then precipitated by dropwise addition into a scintillation vial containing 15 mL of MeOH kept at –20 °C. The precipitated polymer was recovered and freeze-dried from benzene to afford **P3.1** (50 equiv). ^{1}H NMR (400 MHz, CD_2Cl_2) δ: 7.56–6.93 (4H), 5.88–5.41 (2H), 4.35–4.09 (1H), 3.93–3.60 (1H), 2.74–2.43 (1H), 1.92–1.64 (1H). M_n (MALS): 5.8 kDa, $Đ$ = 1.16.

Any modifications of the conditions shown in the representative procedure in the manuscript are specified in the following schemes, which depict all of the results shown in Table 3.2

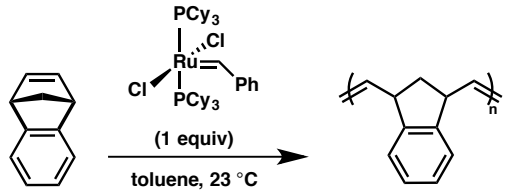

M3.1 (150 equiv) *P3.1*

P3.1 (150 equiv) (Table 3.2, Entry 2). ^{1}H NMR (400 MHz, CD_2Cl_2) δ: 7.66–7.04 (4H), 5.85–5.43 (2H), 4.33–4.00 (1H), 3.92–3.55 (1H), 2.74–2.39 (1H), 1.89–1.61 (1H). M_n (MALS): 10.8 kDa, $Đ$ = 1.15.

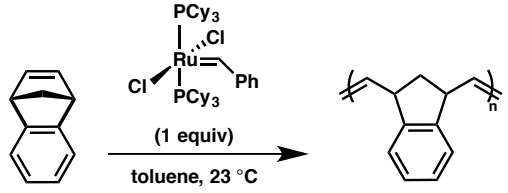

M3.1 (300 equiv) *P3.1*

P3.1 (300 equiv) (Table 3.2, Entry 3). ^{1}H NMR (400 MHz, CD_2Cl_2) δ: 7.41–7.09 (4H), 5.80–5.46 (2H), 4.32–4.04 (1H), 3.92–3.59 (1H), 2.74–2.38 (1H), 1.90–1.61 (1H). M_n (MALS): 17.4 kDa, $Đ$ = 1.20.

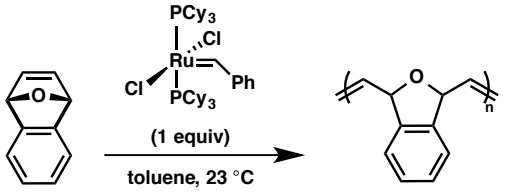

M3.2 (50 equiv) *P3.2*

P3.2 (50 equiv) (Table 3.2, Entry 4). ^{1}H NMR (400 MHz, CD_2Cl_2) δ: 7.45–7.11 (4H), 6.27–5.91 (2H), 5.89–5.54 (2H). M_n (PS standards): 15.7 kDa, $Đ$ = 1.83.

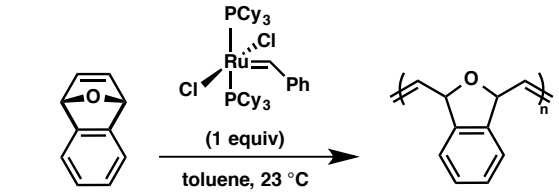

M3.2 (150 equiv) *P3.2*

P3.2 (150 equiv) (Table 3.2, Entry 5). ^{1}H NMR (400 MHz, CD_2Cl_2) δ: 7.45–7.08 (4H), 6.28–5.94 (2H), 5.91–5.56 (2H). M_n (PS standards): 38.4 kDa, $Đ$ = 1.86.

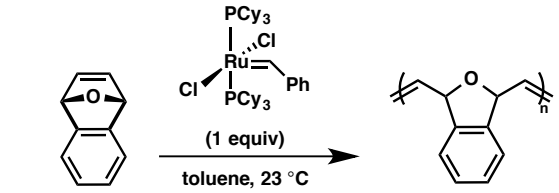

M3.2 (300 equiv) *P3.2*

P3.2 (300 equiv) (Table 3.2, Entry 6). ^{1}H NMR (400 MHz, CD_2Cl_2) δ: 7.44–7.09 (4H), 6.33–5.93 (2H) 5.92–5.54 (2H). M_n (PS standards): 50.6 kDa, $Đ$ = 2.00.

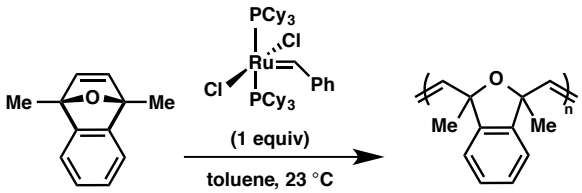

M3.3 (50 equiv) *P3.3*

P3.3 (50 equiv) (Table 3.2, Entry 7). ^{1}H NMR (400 MHz, CD_2Cl_2) δ: 7.35–6.89 (4H), 6.13–5.84 (2H), 1.70–1.40 (6H). M_n (MALS): 5.4 kDa, $Đ$ = 1.14.

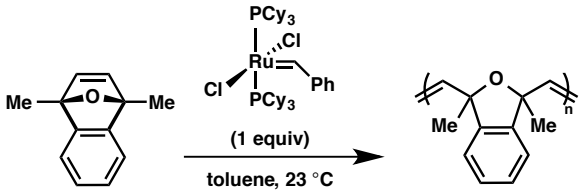

M3.3 (150 equiv) *P3.3*

P3.3 (150 equiv) (Table 3.2, Entry 8). ^{1}H NMR (400 MHz, CD_2Cl_2) δ: 7.35–6.90 (4H), 6.10–5.86 (2H), 1.67–1.40 (6H). M_n (MALS): 25.2 kDa, $Đ$ = 1.14.

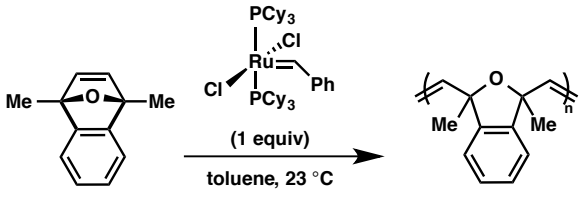

M3.3 (300 equiv) *P3.3*

P3.3 (300 equiv) (Table 3.2, Entry 9). ^{1}H NMR (400 MHz, CD_2Cl_2) δ: 7.37–6.87 (4H), 6.08–5.88 (2H), 1.69–1.46 (6H). M_n (MALS): 54.0 kDa, $Đ$ = 1.17.

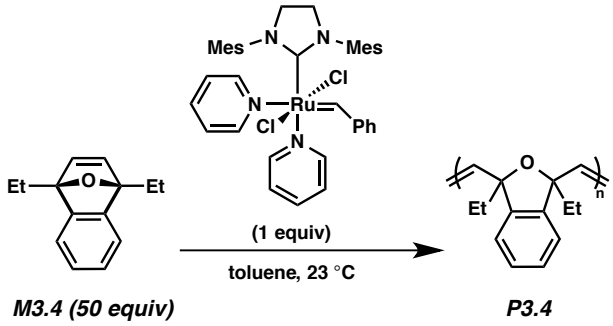

M3.4 (50 equiv) *P3.4*

P3.4 (50 equiv) (Table 3.2, Entry 10). ^{1}H NMR (400 MHz, CD_2Cl_2) δ: 7.25–7.01 (2H), 7.01–6.82 (2H), 6.13–5.85 (2H), 1.99–1.80 (2H), 1.80–1.62 (2H), 1.02–0.77 (6H). M_n (MALS): 17.4 kDa, $Đ$ = 1.11.

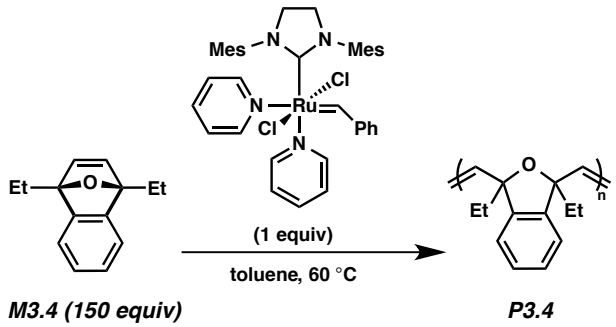

M3.4 (150 equiv) *P3.4*

P3.4 (150 equiv) (Table 3.2, Entry 11). A 1-dram vial containing a magnetic stir bar was flame-dried under reduced pressure, and then allowed to cool under N_2. The vial was charged with monomer **M3.4** (20.2 mg, 0.10 mmol, 150 equiv), and the vial was flushed with N_2. The vial was taken into a glovebox.

In the glovebox, a separate vial was charged with Grubbs third-generation catalyst (4.5 mg) and toluene (560 μL). A 60 μL aliquot of the resulting solution (0.48 mg Grubbs 3rd gen. cat., 0.67 μmol, 1 equiv) was then added to the monomer **M3.4** (neat) while stirring vigorously. The reaction mixture was allowed to stir at 60 °C for 24 h. The vial was then removed from the glovebox and the reaction was quenched with ethyl vinyl ether (10 μL, 0.1 mmol). The polymer was then precipitated by dropwise addition into a scintillation vial containing 15 mL of MeOH kept at –20 C. The precipitated polymer was recovered and freeze-dried from benzene to afford **P3.4** (150 equiv). ^{1}H NMR (400 MHz, CD_2Cl_2) δ: 7.14–6.99 (2H), 6.99–6.84 (2H), 6.09–5.92 (2H), 1.94–1.80 (2H), 1.80–1.65 (2H), 0.97–0.79 (6H). M_n (MALS): 46.4 kDa, $Đ$ = 1.12.

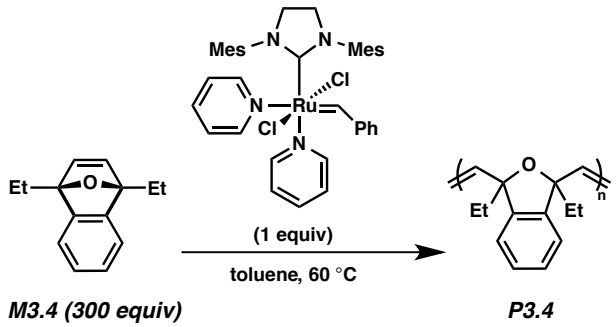

M3.4 (300 equiv) *P3.4*

P3.4 (300 equiv) (Table 3.2, Entry 12). A 1-dram vial containing a magnetic stir bar was flame-dried under reduced pressure, and then allowed to cool under N_2. The vial was charged with monomer **M3.4** (20.4 mg, 0.10 mmol, 300 equiv), and the vial was flushed with N_2. The vial was taken into a glovebox.

In the glovebox, a separate vial was charged with Grubbs third-generation catalyst (3.2 mg) and toluene (800 μL). A 60 μL aliquot of the resulting solution (0.24 mg Grubbs 3rd gen. cat., 0.33 μmol, 1 equiv) was then added to the monomer **M3.4** (neat) while stirring vigorously. The reaction mixture was allowed to stir at 60 °C for 24 h. The vial was then removed from the glovebox and the reaction was quenched with ethyl vinyl ether (10 μL, 0.1 mmol). The polymer was then precipitated by dropwise addition into a scintillation vial containing 15 mL of MeOH kept at –20 C. The precipitated polymer was recovered and freeze-dried from benzene to afford **P3.4** (300 equiv). ^{1}H NMR (400 MHz, CD_2Cl_2) δ: 7.13–7.02 (2H), 7.01–6.84 (2H), 6.05–5.92 (2H), 1.94–1.78 (2H), 1.78–1.64 (2H), 0.95–0.77 (6H). M_n (MALS): 162 kDa, $Đ$ = 1.07.

3.5.3.3 Further Evidence for P3.1 & P3.2 Decomposition

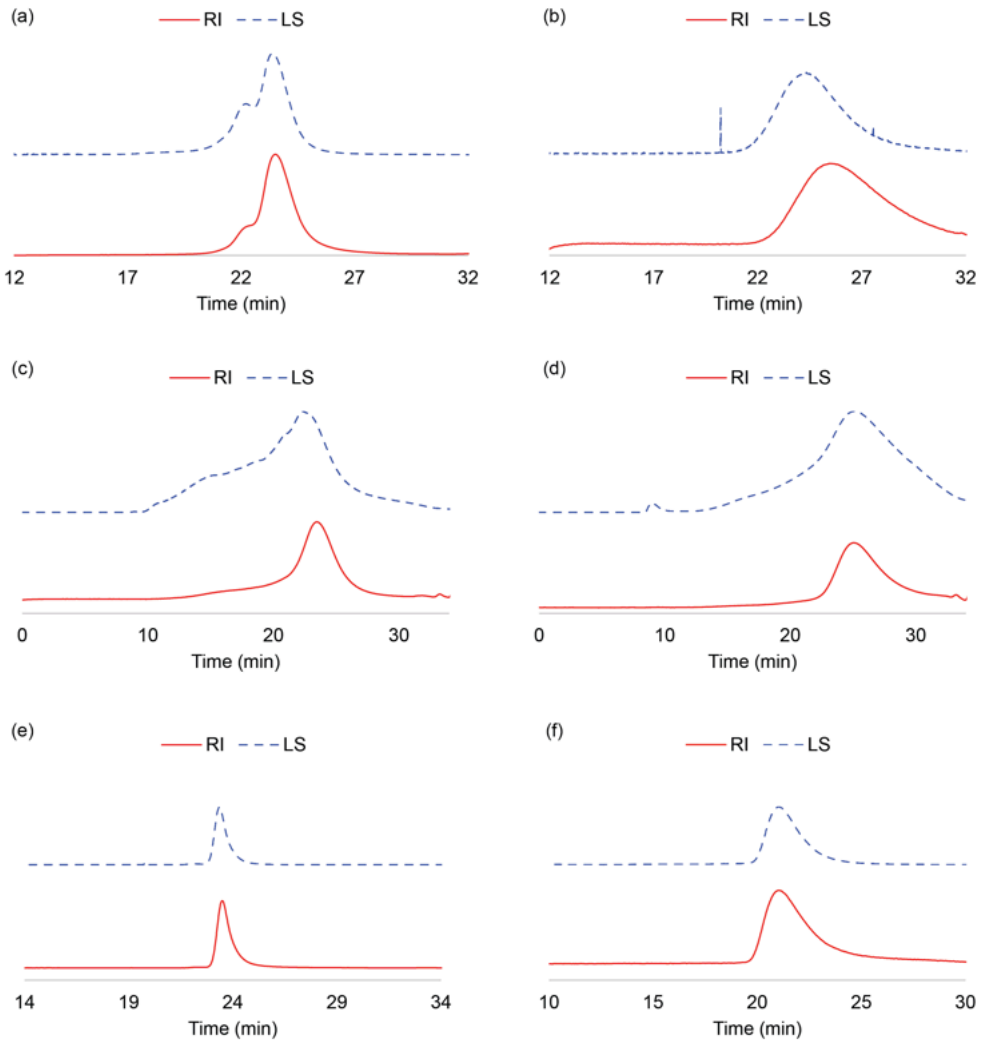

Figure 3.5. Comparison of RI and LS traces of benzonorbornadiene polymers. (a) **P3.1** immediately after polymerization, (b) **P3.1** after incubation in air, (c) **P3.2** immediately after polymerization, (d) **P3.2** after incubation in air, (e) **P3.3**, and (f) **P3.4**

Table 3.4. Molecular Weight of **P3.1** After Incubation in Air

[M] / [I]	*M_n (theo)*	*M_n*	*Đ*
50	7.1 kDa	5.8 kDa	1.73
150	21.3 kDa	10.8 kDa	1.62
300	42.6 kDa	17.4 kDa	1.60

3.5.3.4 Calculation of Oxidation Potentials for P3.1 & P3.2

Oxidation potential calculation for **P3.1** and **P3.2** were calculated as reported by Nicewicz et al.[60] Briefly, neutral and cation radical structures for respective model compounds **P3.1'** and **P3.2'** were optimized using B3LYP/6-31+G(d,p) in the gas phase with Gaussian 09 and their energies were computed.

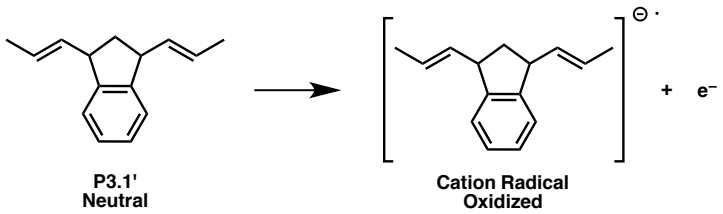

G_{298}(neutral) = –581.928047 Hartree

G_{298}(oxidized) = –581.626248 Hartree

$\Delta G^0_{1/2}$ = (–581.928047 – (–581.626248 Hartree)) × 627.5 kcal mol^{-1} Hartree^{-1} = –189.4 kcal mol^{-1}

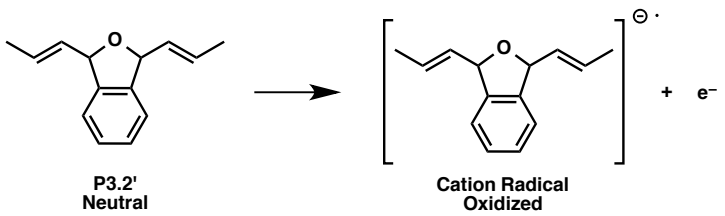

G_{298}(neutral) = –617.841918 Hartree

G_{298}(oxidized) = –617.531377 Hartree

$\Delta G^0_{1/2}$ = (–617.841918 – (–617.531377 Hartree)) × 627.5 kcal mol^{-1} Hartree^{-1} = –194.9 kcal mol^{-1}

The obtained free energies were transformed into oxidation potential by the following equation:

$$E^{0,\text{calc}}_{1/2} = -\frac{\Delta G^0_{1/2}}{n_e \mathcal{F}} - E^{0,\text{SHE}}_{1/2} + E^{0,\text{SCE}}_{1/2}$$

where n_e = number of electrons (one electron in the oxidation of interest), $\mathcal{F}$ = Faraday's constant (23.061 kcal mol^{-1} V^{-1}), $E^{0,\text{SHE}}_{1/2}$ and $E^{0,\text{SCE}}_{1/2}$ are the potential of the standard hydrogen electrode and the saturated calomel electrode, respectively.

Taking the difference in oxidation potential of **P3.1'** and **P3.2'** cancels out the electrode potentials $E^{0,\text{SHE}}_{1/2}$ and $E^{0,\text{SCE}}_{1/2}$ to yield the following expression:

$$\Delta E^{0,\text{calc}}_{\frac{1}{2}} = E^{0,\text{calc}}_{\frac{1}{2}}(\mathbf{P3.2'}) - E^{0,\text{calc}}_{\frac{1}{2}}(\mathbf{P3.1'})$$

$$= -\frac{\Delta G^0_{\frac{1}{2}}(\mathbf{P3.2'}) - \Delta G^0_{\frac{1}{2}}(\mathbf{P3.1'})}{n_e \mathcal{F}} = -\frac{-194.9 - (-189.4)\ \text{kcal mol}^{-1}}{1 \times 23.061\ \text{kcal mol}^{-1}\ \text{V}^{-1}} = 0.238\ \text{V}$$

3.5.3.5 Cartesian Coordinates for Computed Structures

Cartesian coordinates for the computed structures have been previously reported.[61]

3.6 Spectra Relevant to Chapter Three:

Expanding the ROMP Toolbox: Synthesis of Air-Stable Benzonorbornadiene Polymers by Aryne Chemistry

Jose M. Medina, Jeong Hoon Ko, Heather D. Maynard, and Neil K. Garg

Macromolecules **2017**, *50*, 580–586.

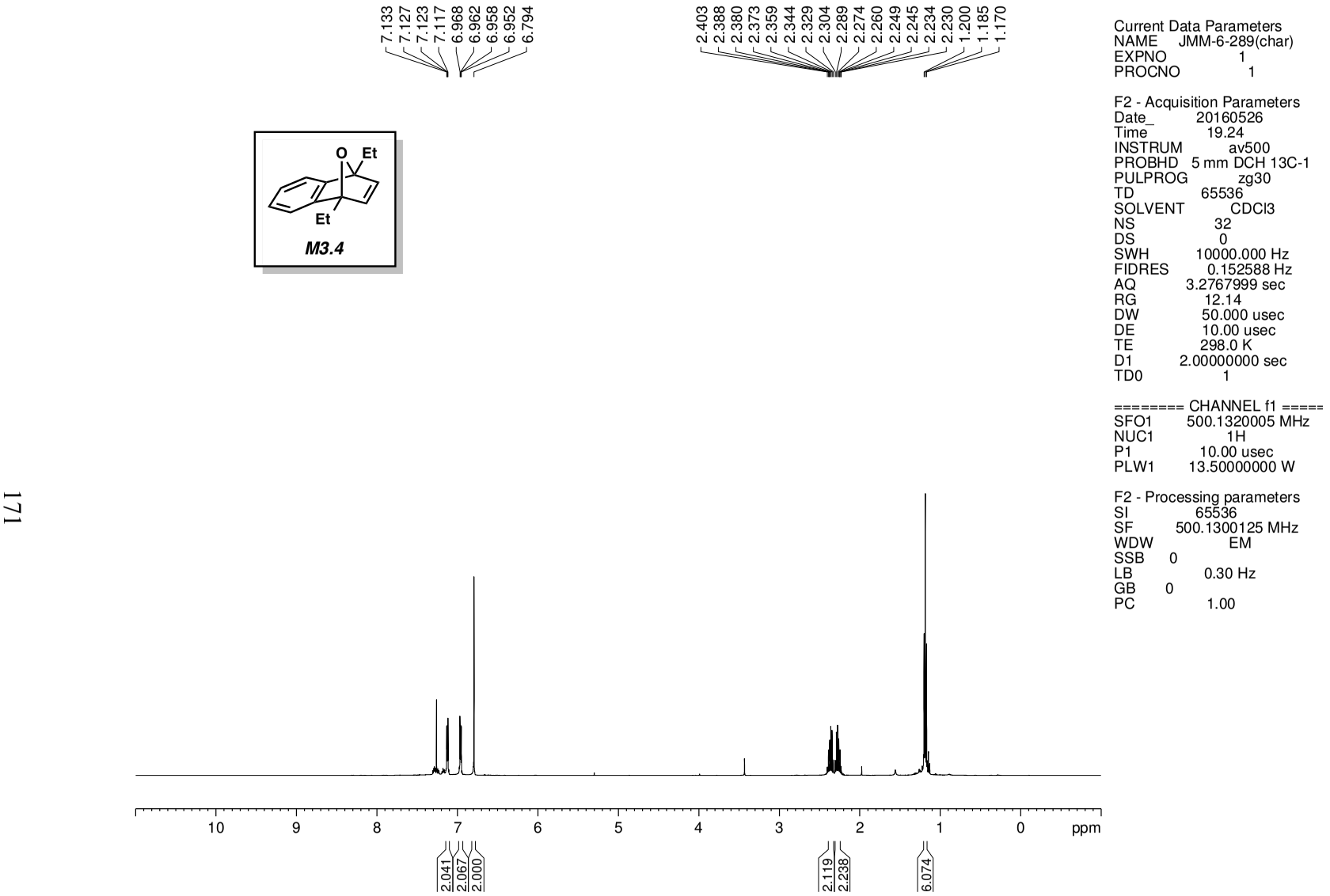

Figure 3.6. ^{1}H NMR (500 MHz, $CDCl_3$) compound **M3.4**

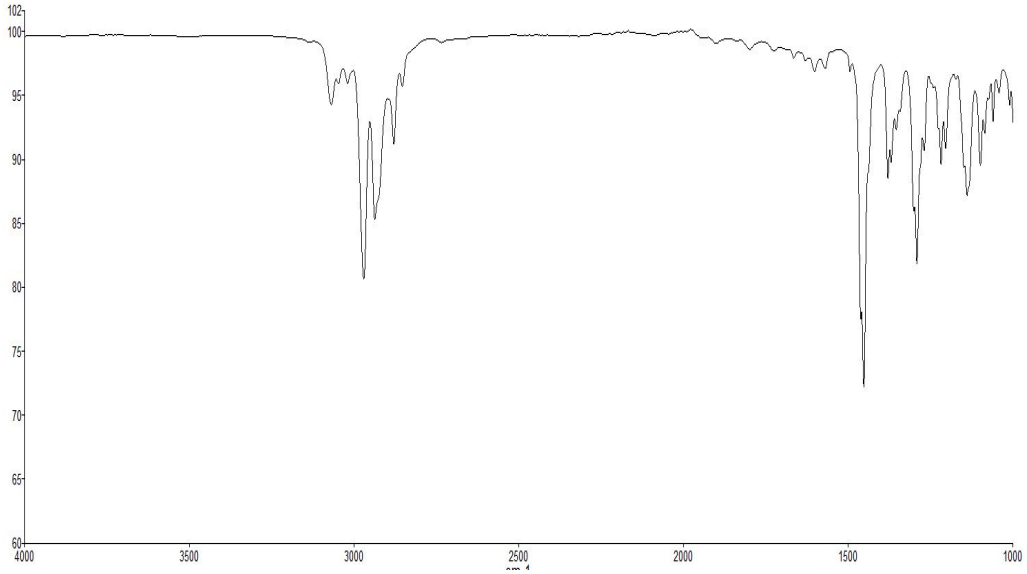

Figure 3.7. Infrared spectrum of compound **M3.4**

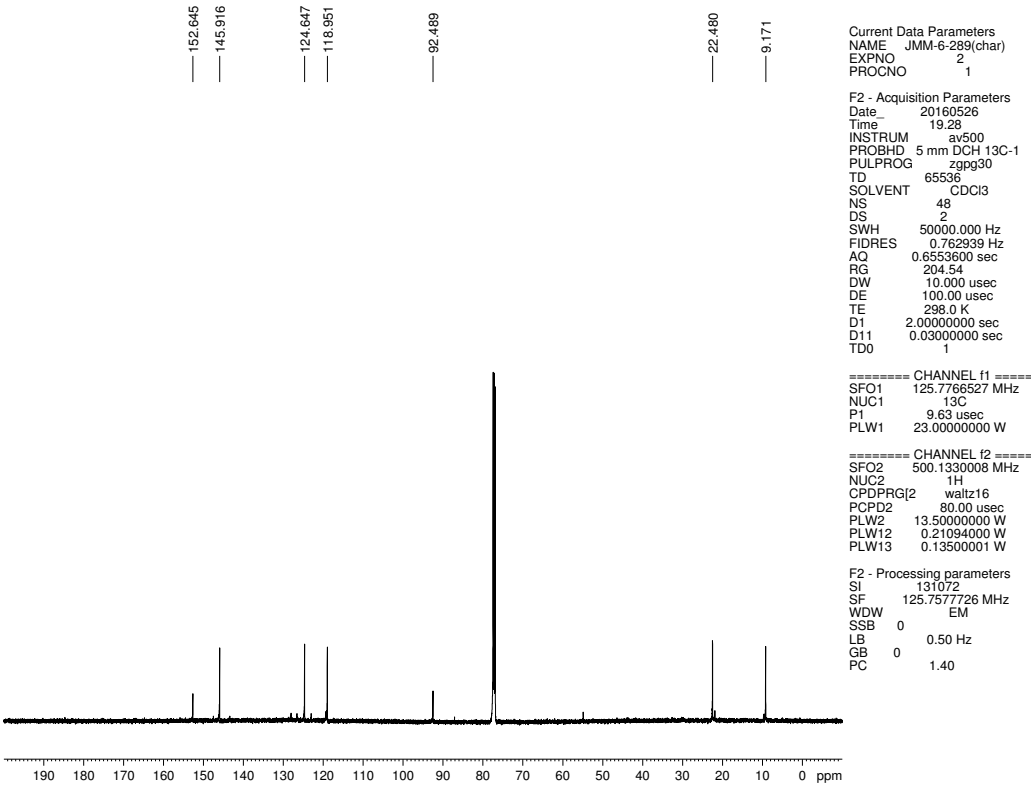

Figure 3.8. ^{13}C NMR (125 MHz, $CDCl_3$) of compound **M3.4**

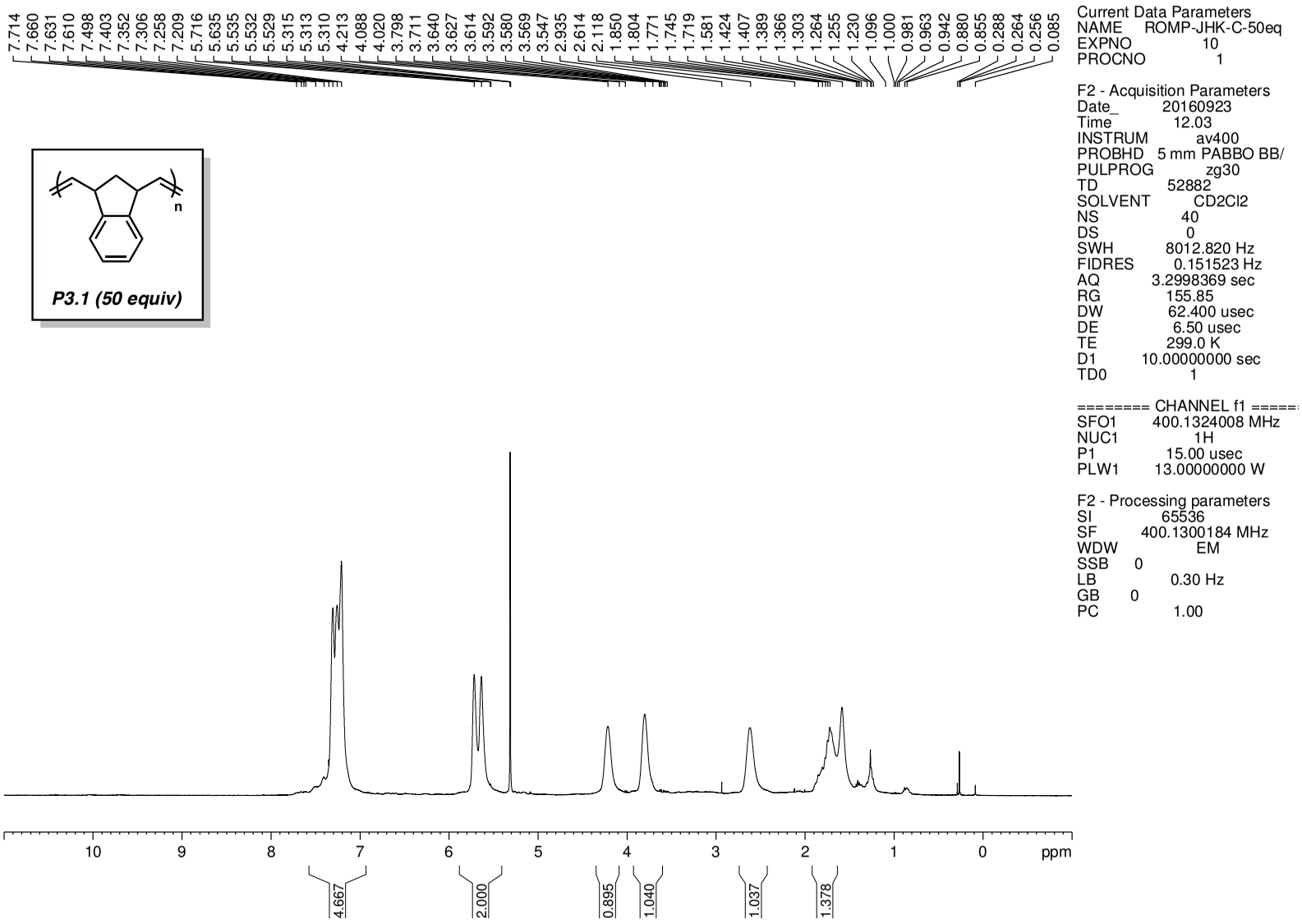

Figure 3.9. ^{1}H NMR (400 MHz, CD_2Cl_2) compound **P3.1 (50 equiv)**

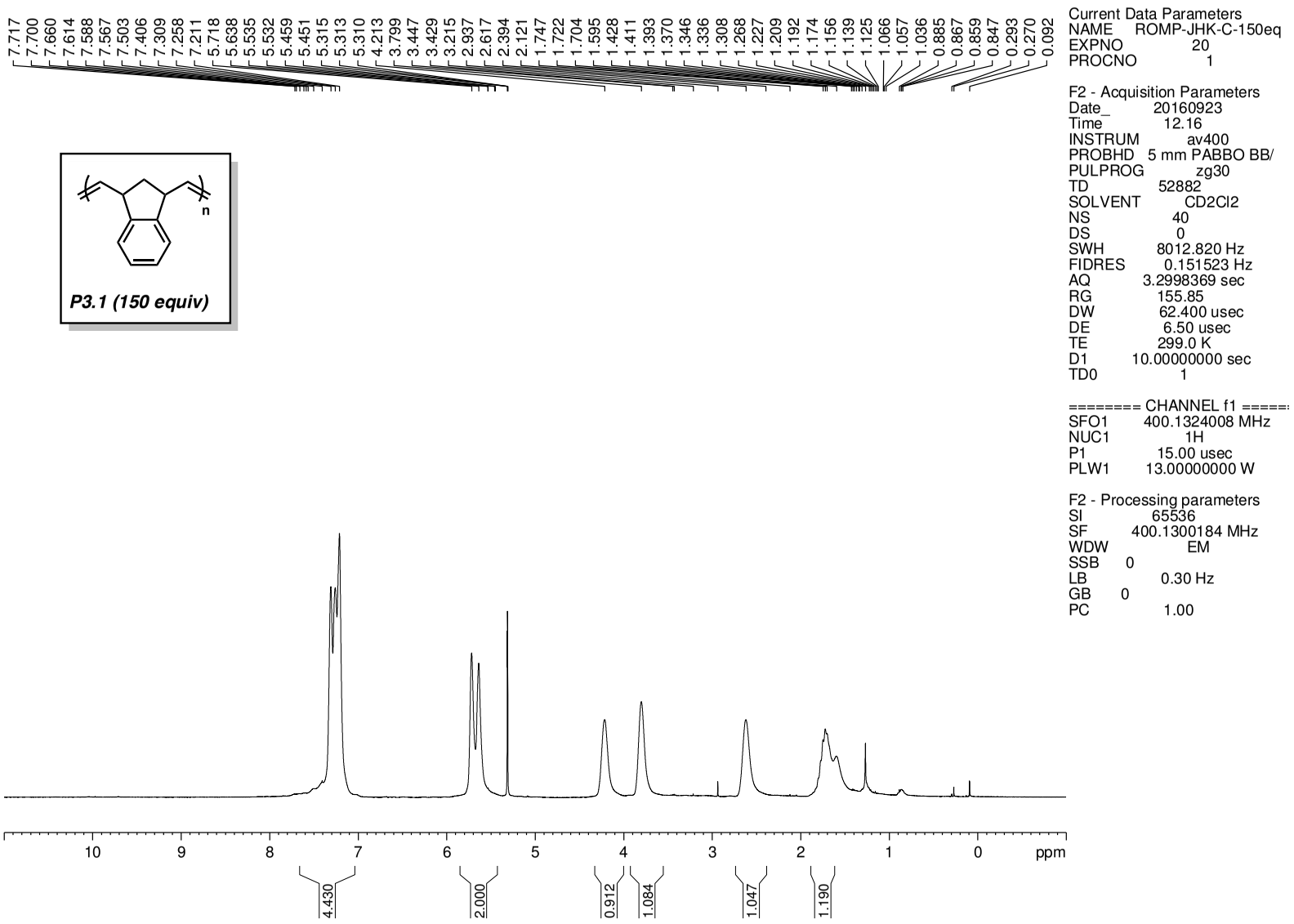

Figure 3.10. ^{1}H NMR (400 MHz, CD_2Cl_2) compound **P3.1 (150 equiv)**

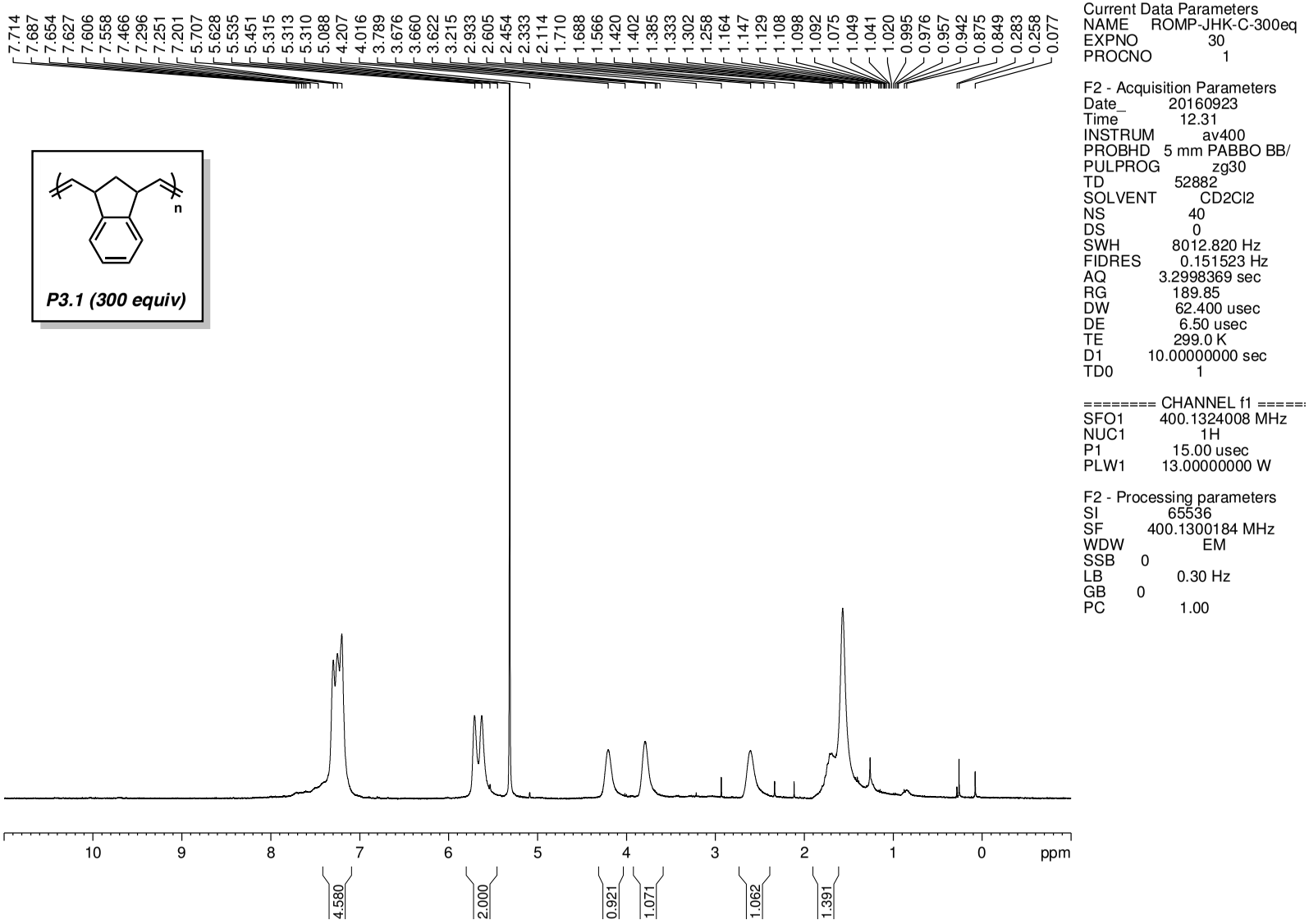

Figure 3.11. ^{1}H NMR (400 MHz, CD_2Cl_2) compound **P3.1 (300 equiv)**

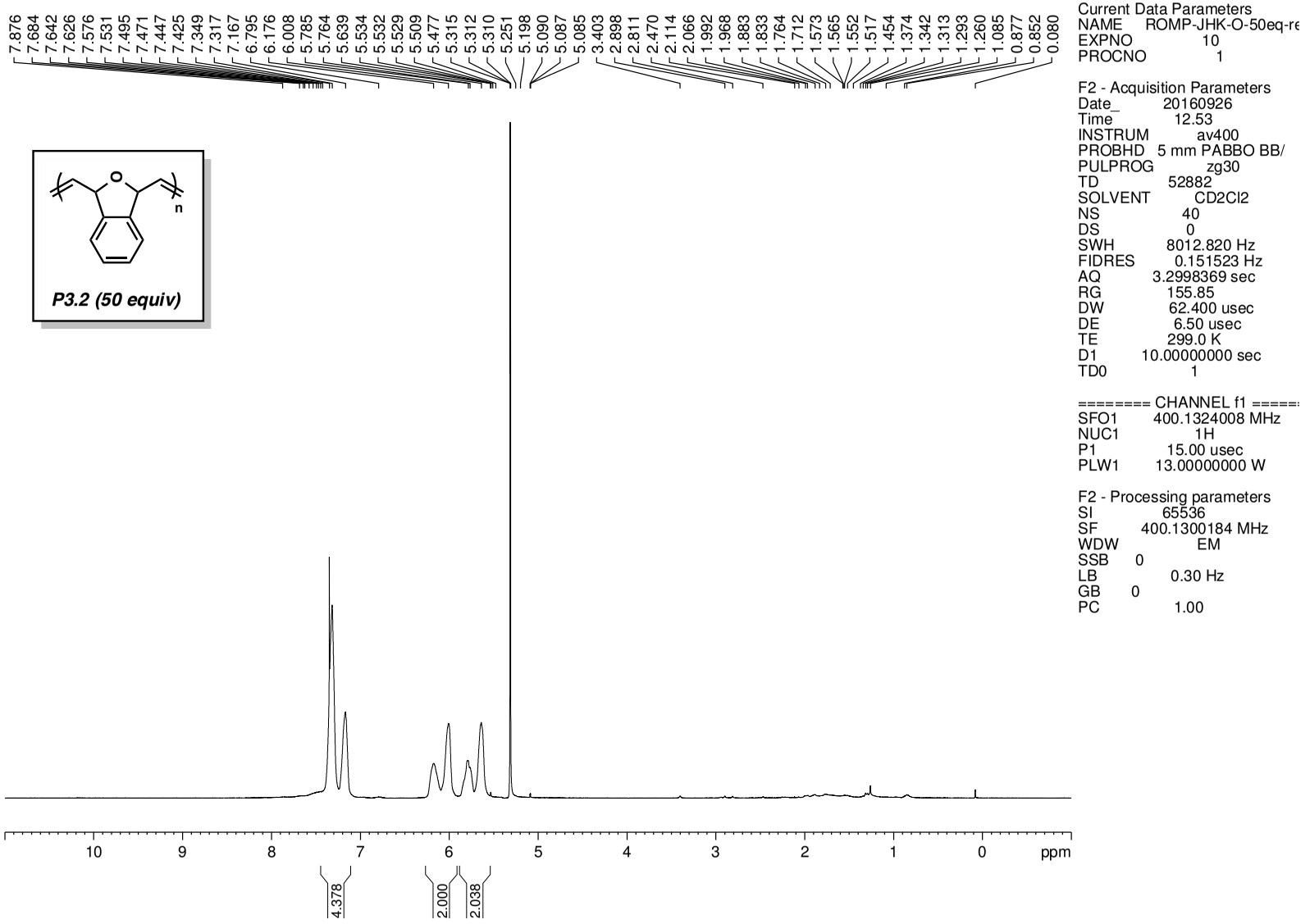

Figure 3.12. ^{1}H NMR (400 MHz, CD_2Cl_2) compound **P3.2 (50 equiv)**

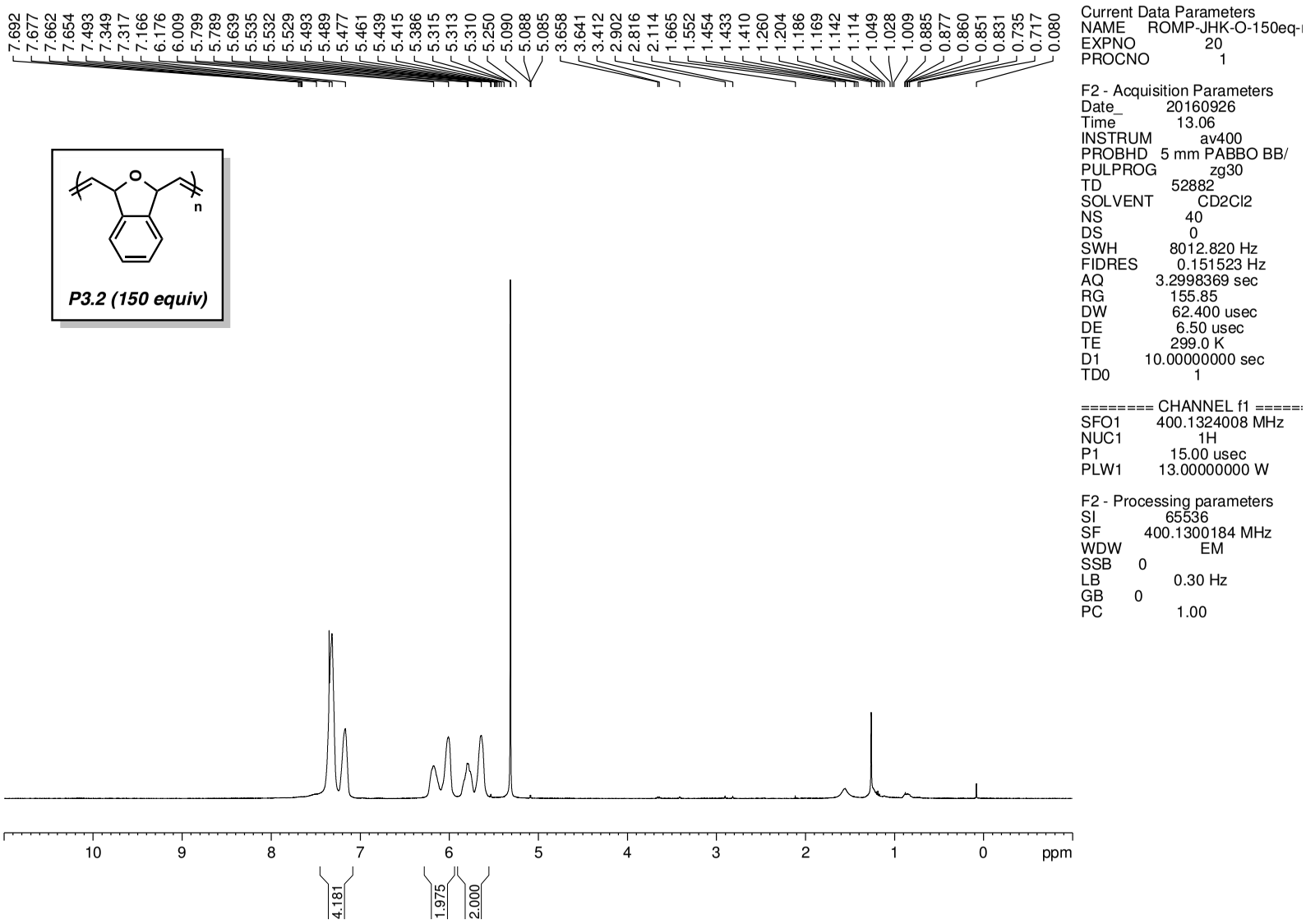

Figure 3.13. ^{1}H NMR (400 MHz, CD_2Cl_2) compound **P3.2 (150 equiv)**

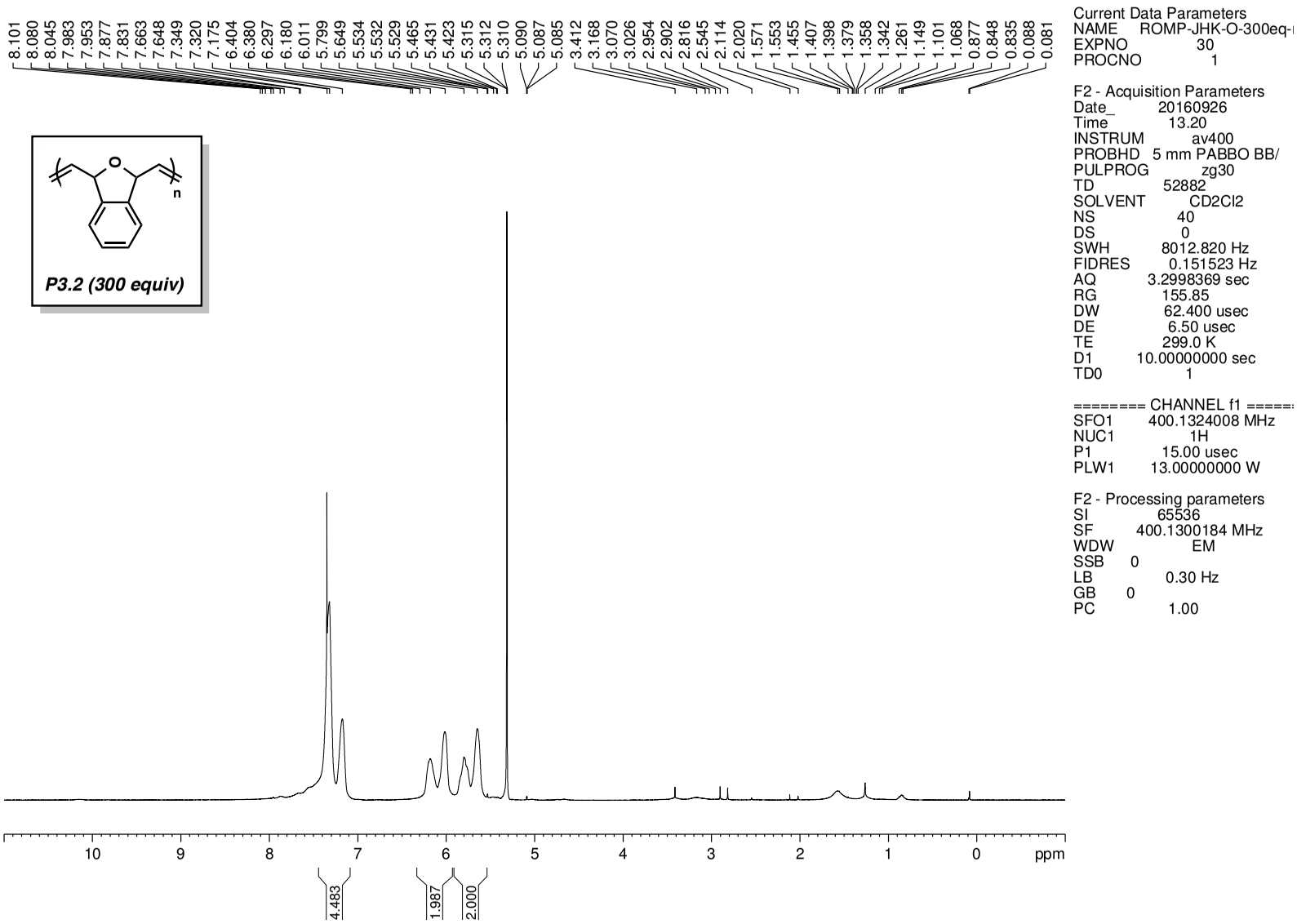

Figure 3.14. ^{1}H NMR (400 MHz, CD_2Cl_2) compound **P3.2 (300 equiv)**

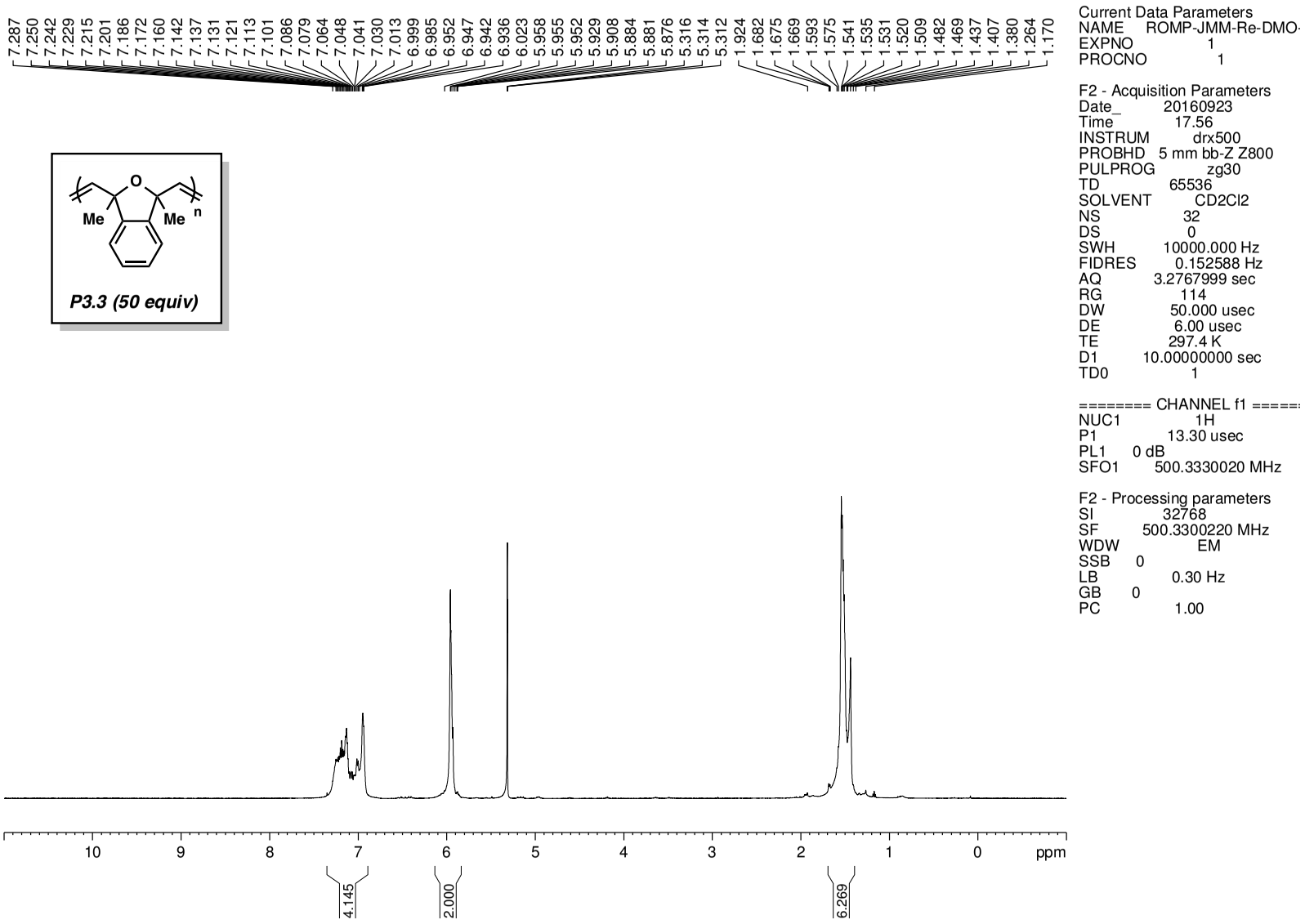

Figure 3.15. ^{1}H NMR (500 MHz, CD_2Cl_2) compound **P3.3 (50 equiv)**

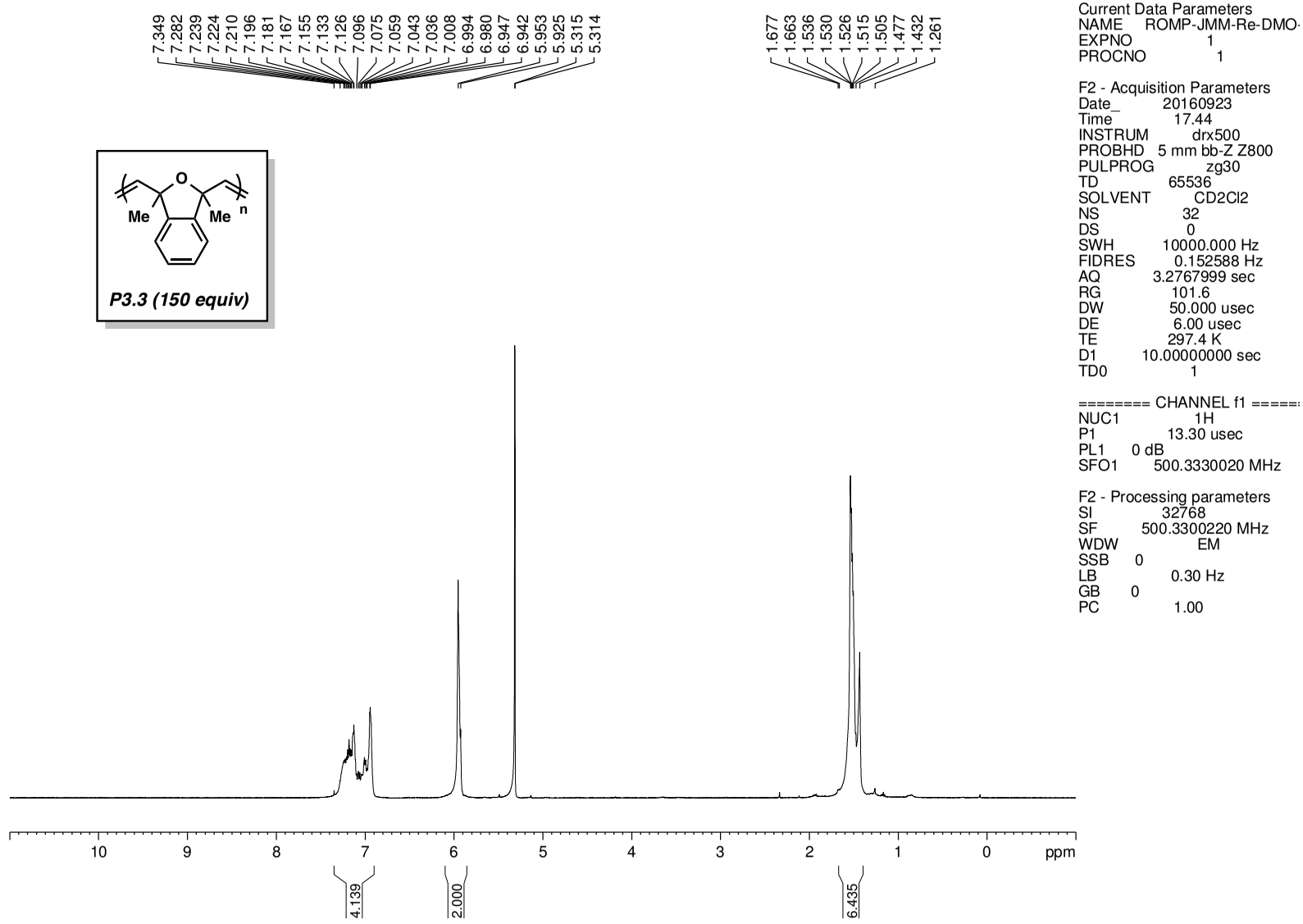

Figure 3.16. ^{1}H NMR (500 MHz, CD_2Cl_2) compound **P3.3 (150 equiv)**

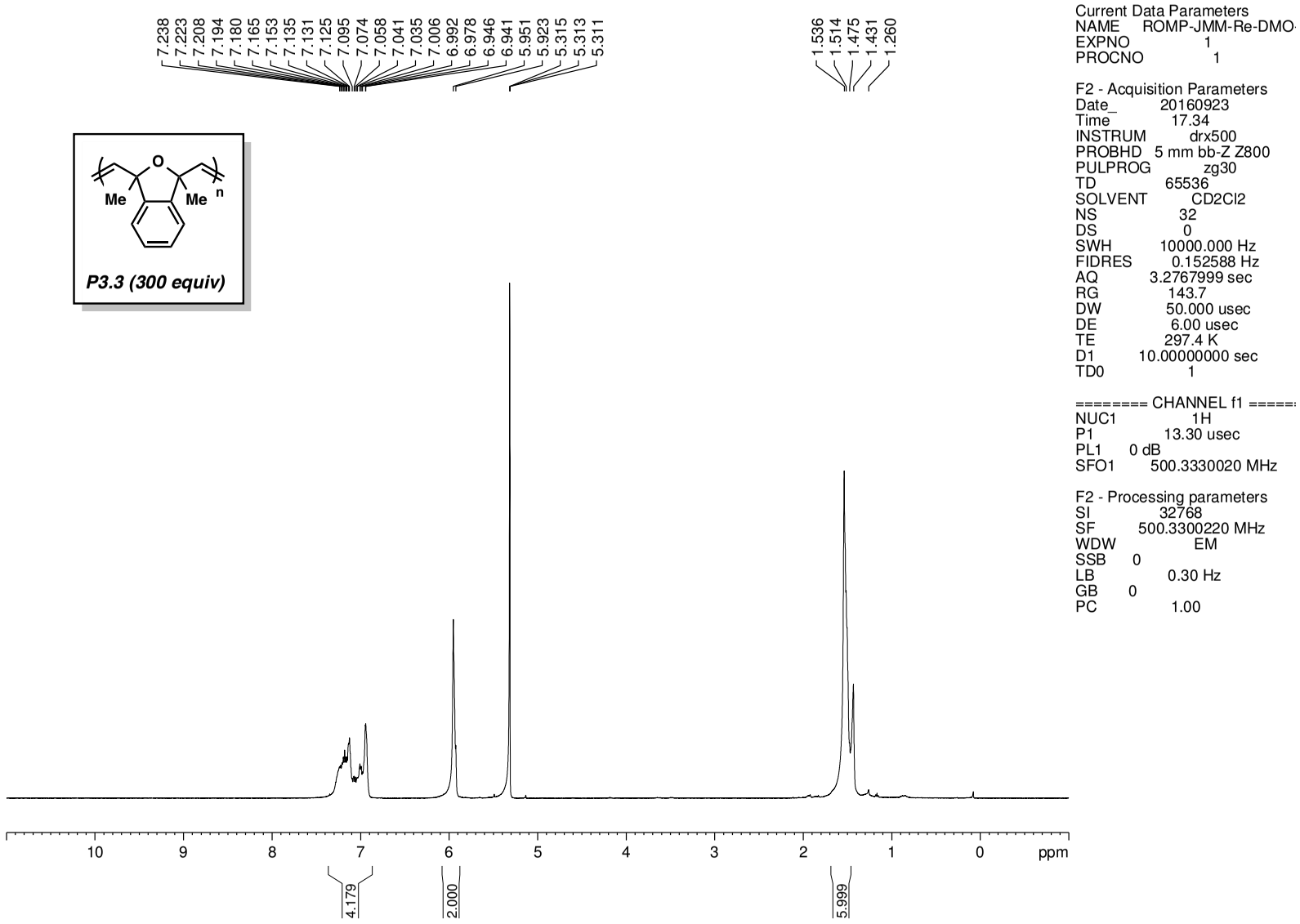

Figure 3.17. ^{1}H NMR (500 MHz, CD_2Cl_2) compound **P3.3 (300 equiv)**

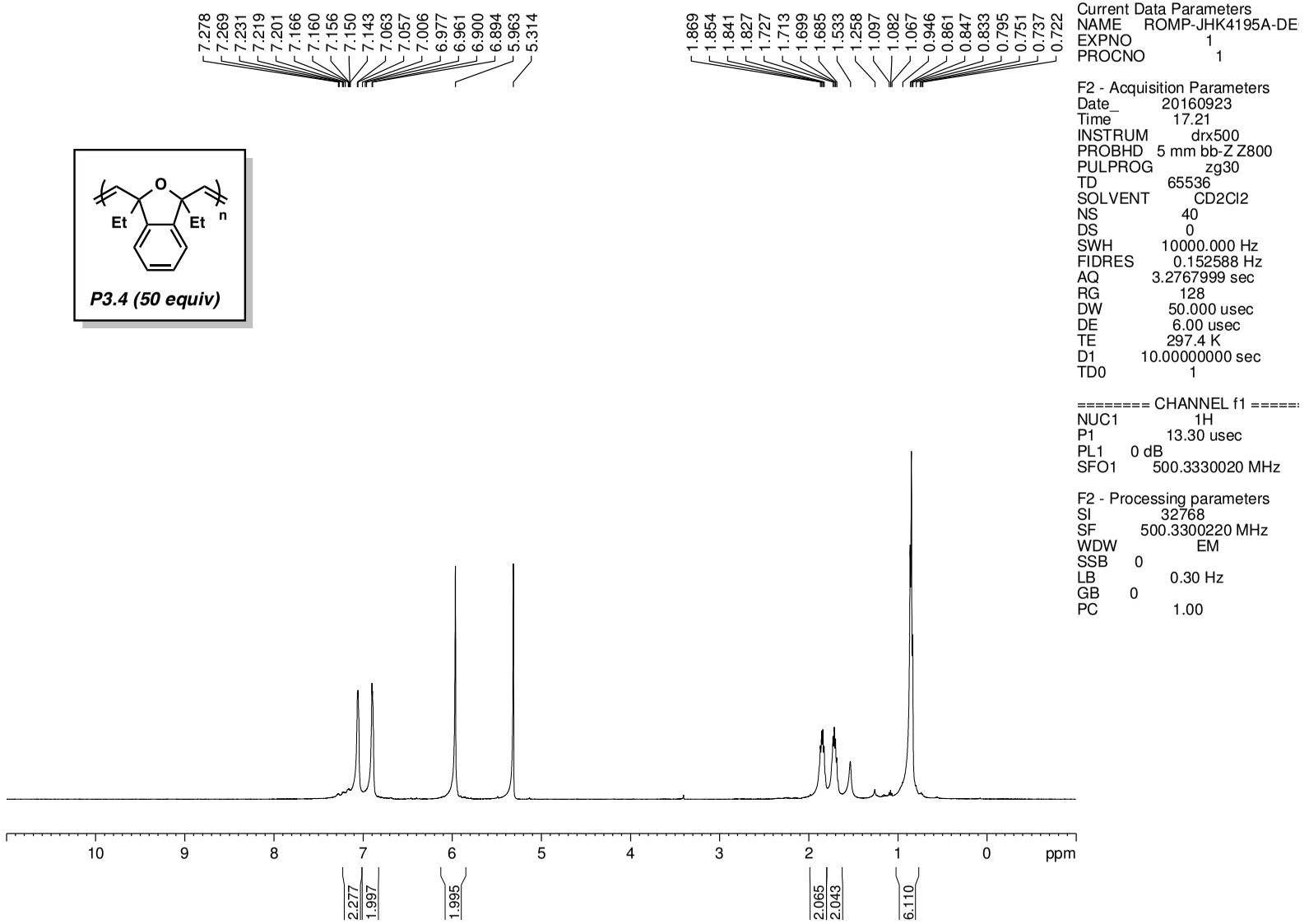

Figure 3.18. ^{1}H NMR (500 MHz, CD_2Cl_2) compound **P3.4 (50 equiv)**

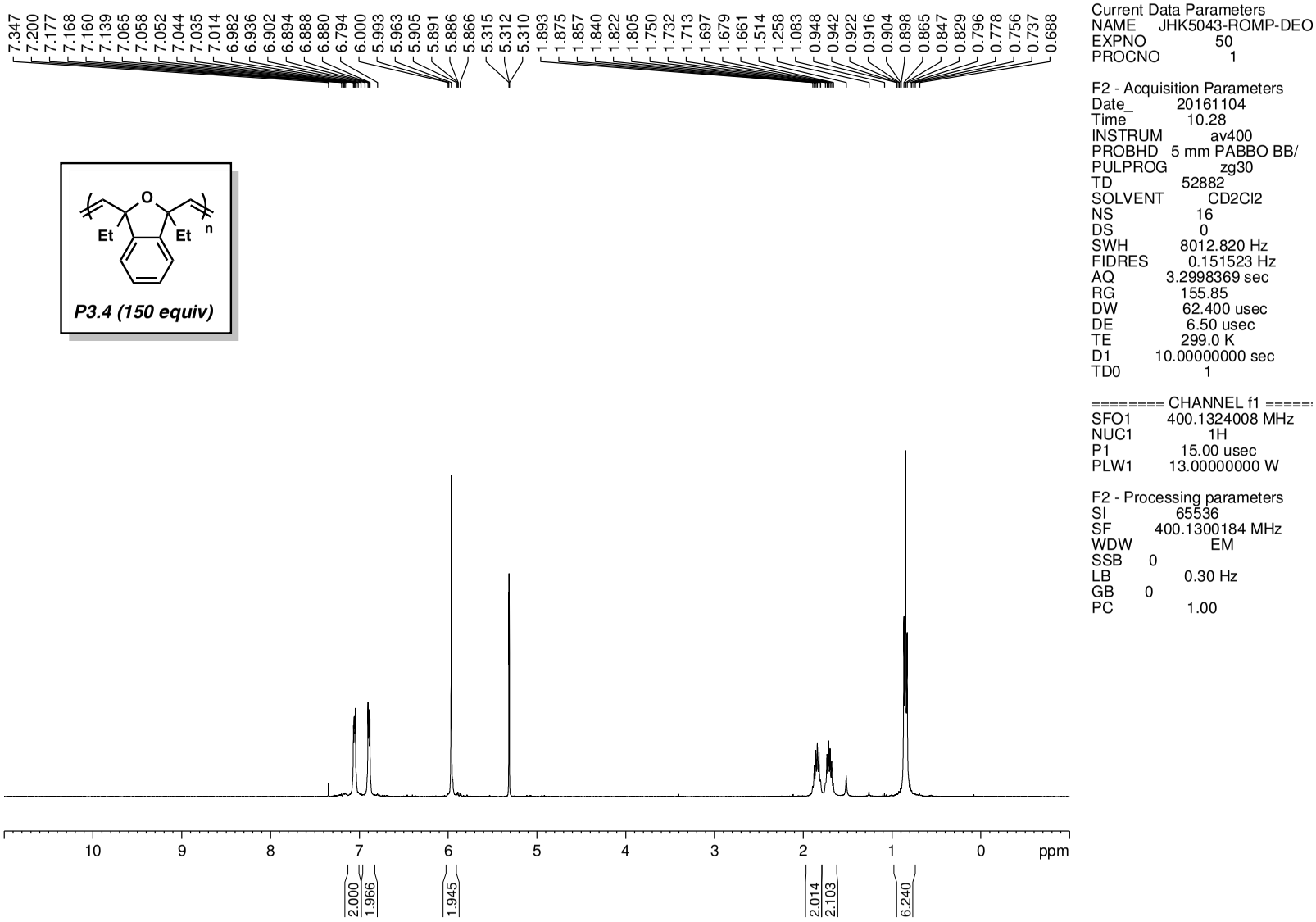

Figure 3.19. ^{1}H NMR (400 MHz, CD_2Cl_2) compound **P3.4 (150 equiv)**

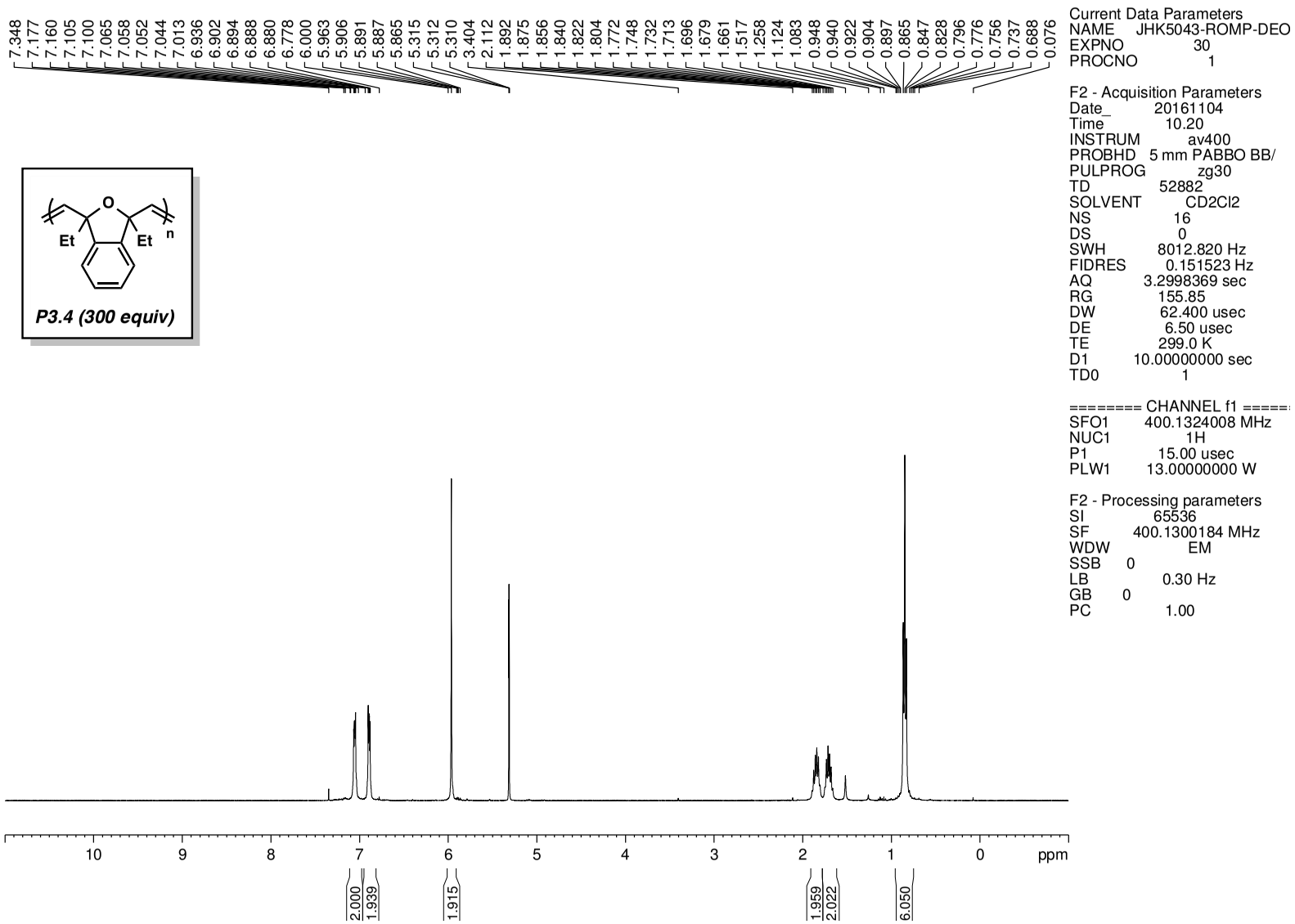

Figure 3.20. ^{1}H NMR (400 MHz, CD_2Cl_2) compound **P3.4** **(300 equiv)**

3.7 Notes and References

(1) Callmann, C. E.; Barback, C. V.; Thompson, M. P.; Hall, D. J.; Mattrey, R. F.; Gianneschi, N. C. *Adv. Mater.* **2015**, *27*, 4611–4615.

(2) Liao, L.; Liu, J.; Dreaden, E. C.; Morton, S. W.; Shopsowitz, K. E.; Hammond, P. T.; Johnson, J. A. *J. Am. Chem. Soc.* **2014**, *136*, 5896–5899.

(3) Rutenberg, I. M.; Scherman, O. A.; Grubbs, R. H.; Jiang, W.; Garfunkel, E.; Bao, Z. *J. Am. Chem. Soc.* **2004**, *126*, 4062–4063.

(4) Long, T. M.; Swager, T. M. *J. Am. Chem. Soc.* **2003**, *125*, 14113–14119.

(5) Yoon, K.-Y.; Lee, I.-H.; Kim, K. O.; Jang, J.; Lee, E.; Choi, T.-L. *J. Am. Chem. Soc.* **2012**, *134*, 14291–14294.

(6) Miyake, G. M.; Piunova, V. A.; Weitekamp, R. A.; Grubbs, R. H. *Angew. Chem., Int. Ed.* **2012**, *51*, 11246–11248.

(7) Schleyer, P. v. R.; Williams Jr, J. E.; Blanchard, K. *J. Am. Chem. Soc.* **1970**, *92*, 2377–2386.

(8) Leitgeb, A.; Wappel, J.; Slugovc, C. *Polymer* **2010**, *51*, 2927–2946.

(9) El-Saafin, I. F.; Feast, W. J. *J. Mol. Catal.* **1982**, *15*, 61–73.

(10) El-Saafin, I. F., Ph.D. Dissertation, Durham University, 1981.

(11) Cannizzo, L. F.; Grubbs, R. H. *Macromolecules* **1988**, *21*, 1961–1967.

(12) Bazan, G.; Khosravi, E.; Schrock, R. R.; Feast, W.; Gibson, V.; O'Regan, M.; Thomas, J.; Davis, W. *J. Am. Chem. Soc.* **1990**, *112*, 8378–8387.

(13) Bazan, G. C.; Oskam, J. H.; Cho, H. N.; Park, L. Y.; Schrock, R. R. *J. Am. Chem. Soc.* **1991**, *113*, 6899–6907.

(14) Kang, H. A.; Bronstein, H. E.; Swager, T. M. *Macromolecules* **2008**, *41*, 5540–5547.

(15) Wolfberger, A.; Rupp, B.; Kern, W.; Griesser, T.; Slugovc, C. *Macromol. Rapid Commun.* **2011**, *32*, 518–522.

(16) Durmaz, H.; Butun, M.; Hizal, G.; Tunca, U. *J. Polym. Sci., Part A: Polym. Chem.* **2012**, *50*, 3116–3125.

(17) van Hensbergen, J. A.; Burford, R. P.; Lowe, A. B. *J. Polym. Sci., Part A: Polym. Chem.* **2013**, *51*, 487–492.

(18) Lowe, A. B. *Polym. Chem.* **2014**, *5*, 4820–4870.

(19) Kauffmann, T. *Angew. Chem., Int. Ed. Engl.* **1965**, *4*, 543–557.

(20) Reinecke, M. G. *Tetrahedron* **1982**, *38*, 427–498.

(21) Pellissier, H.; Santelli, M. *Tetrahedron* **2003**, *59*, 701–730.

(22) Wenk, H. H.; Winkler, M.; Sander, W. *Angew. Chem., Int. Ed.* **2003**, *42*, 502–528.

(23) Sanz, R. *Org. Prep. Proced. Int.* **2008**, *40*, 215–291.

(24) Bronner, S. M.; Goetz, A. E.; Garg, N. K. *Synlett* **2011**, *18*, 2599–2604.

(25) Tadross, P. M.; Stoltz, B. M. *Chem. Rev.* **2012**, *112*, 3550–3577.

(26) Gampe, C. M.; Carreira, E. M. *Angew. Chem., Int. Ed.* **2012**, *51*, 3766–3778.

(27) Bhunia, A.; Yetra, S. R.; Biju, A. T. *Chem. Soc. Rev.* **2012**, *41*, 3140–3152.

(28) Yoshida, H.; Takaki, K. *Synlett* **2012**, *23*, 1725–1732.

(29) Dubrovskiy, A. V.; Markina, N. A.; Larock, R. C. *Org. Biomol. Chem.* **2013**, *11*, 191–218.

(30) Wu, C.; Shi, F. *Asian J. Org. Chem.* **2013**, *2*, 116–125.

(31) Goetz, A. E.; Garg, N. K. *J. Org. Chem.* **2014**, *79*, 846–851.

(32) Goetz, A. E.; Shah, T. K.; Garg, N. K. *Chem. Commun.* **2015**, *51*, 34–45.

(33) Shah, T. K.; Medina, J. M.; Garg, N. K. *J. Am. Chem. Soc.* **2016**, *138*, 4948–4954.

(34) Medina, J. M.; Mackey, J. L.; Garg, N. K.; Houk, K. N. *J. Am. Chem. Soc.* **2014**, *136*, 15798–15805.

(35) Bronner, S. M.; Mackey, J. L.; Houk, K. N.; Garg, N. K. *J. Am. Chem. Soc.* **2012**, *134*, 13966–13969.

(36) Bronner, S. M.; Goetz, A. E.; Garg, N. K. *J. Am. Chem. Soc.* **2011**, *133*, 3832–3835.

(37) Picazo, E.; Houk, K. N.; Garg, N. K. *Tetrahedron Lett.* **2015**, *56*, 3511–3514.

(38) Im, G.-Y. J.; Bronner, S. M.; Goetz, A. E.; Paton, R. S.; Cheong, P. H.-Y.; Houk, K. N.; Garg, N. K. *J. Am. Chem. Soc.* **2010**, *132*, 17933–17944.

(39) Goetz, A. E.; Garg, N. K. *Nat. Chem.* **2013**, *5*, 54–60.

(40) Bronner, S. M.; Bahnck, K. B.; Garg, N. K. *Org. Lett.* **2009**, *11*, 1007–1010.

(41) Cheong, P. H.-Y.; Paton, R. S.; Bronner, S. M.; Im, G.-Y. J.; Garg, N. K.; Houk, K. N. *J. Am. Chem. Soc.* **2010**, *132*, 1267–1269.

(42) Medina, J. M.; McMahon, T. C.; Jiménez-Osés, G.; Houk, K. N.; Garg, N. K. *J. Am. Chem. Soc.* **2014**, *136*, 14706–14709.

(43) Mizukoshi, Y.; Mikami, K.; Uchiyama, M. *J. Am. Chem. Soc.* **2015**, *137*, 74–77.

(44) Ihara, E.; Kurokawa, A.; Koda, T.; Muraki, T.; Itoh, T.; Inoue, K. *Macromolecules* **2005**, *38*, 2167–2172.

(45) Ito, S.; Takahashi, K.; Nozaki, K. *J. Am. Chem. Soc.* **2014**, *136*, 7547–7550.

(46) Sibi, M. P. S., S.; Zimmermann, N.; Serum, E.; Ma, G.; Moorthy, R.; Kalliokoski, K. U. S. Patent 2016022943, Jun. 16, 2016.

(47) Himeshima, Y.; Sonoda, T.; Kobayashi, H. *Chem. Lett.* **1983**, *12*, 1211–1214.

(48) MacRury, T.; McConnell, M. *J. Appl. Polym. Sci.* **1979**, *24*, 651–662.

(49) Podzimek, S. *J. Appl. Polym. Sci.* **1994**, *54*, 91–103.

(50) Ganachaud, F.; Monteiro, M. J.; Gilbert, R. G.; Dourges, M.-A.; Thang, S. H.; Rizzardo, E. *Macromolecules* **2000**, *33*, 6738–6745.

(51) Roth, H. G.; Romero, N. A.; Nicewicz, D. A. *Synlett* **2016**, *27*, 714–723.

(52) Amir-Ebrahimi, V.; Rooney, J. J. *J. Mol. Catal. A: Chem.* **2004**, *212*, 107–113.

(53) Simril, V. *J. Polym. Sci.* **1947**, *2*, 142–156.

(54) Khosravi, E.; Feast, W.; Al-Hajaji, A.; Leejarkpai, T. *J. Mol. Catal. A: Chem.* **2000**, *160*, 1–11.

(55) Jenekhe, S. A.; Roberts, M. F. *Macromolecules* **1993**, *26*, 4981–4983.

(56) Love, J. A.; Morgan, J. P.; Trnka, T. M.; Grubbs, R. H. *Angew. Chem., Int. Ed.* **2002**, *41*, 4035–4037.

(57) Wang, B. Y.; Turner, D. A.; Zujović, T.; Hadad, C. M.; Badjić, J. D. *Chem. Eur. J.* **2011**, *17*, 8870–8881.

(58) Kitamura, T.; Yamane, M.; Inoue, K.; Todaka, M.; Fukatsu, N.; Meng, Z.; Fujiwara, Y. *J. Am. Chem. Soc*. **1999**, *121*, 11674–11679.

(59) Sumida, Y.; Kato, T.; Hosoya, T. *Org. Lett*. **2013**, *15*, 2806–2809.

(60) Roth, H. G.; Romero, N. A.; Nicewicz, D. A. *Synlett* **2016**, *27*, 714–723.

(61) Medina, J. M.; Ko, J. H.; Maynard, H. D.; Garg, N. K. *Macromolecules* **2017**, *50*, 580–586.

CHAPTER FOUR

Cycloadditions of Cyclohexynes and Cyclopentyne

Jose M. Medina, Travis C. McMahon, Gonzalo Jiménez-Osés,

K. N. Houk, and Neil K. Garg

J. Am. Chem. Soc. **2014**, *136*, 14706–14709.

4.1 Abstract

We report the strategic use of cyclohexyne and the more elusive intermediate, cyclopentyne, as a tool for the synthesis of new heterocyclic compounds. Experimental and computational studies of a 3-substituted cyclohexyne are also described. The observed regioselectivities are explained by the distortion / interaction model.

4.2 Introduction

The study of small rings containing triple bonds has been a topic of vast interest for over a hundred years.[1] Following a provocative report in 1902 suggesting the intermediacy of an aryne,[2] chemists probed the viability of benzyne (**4.1**, Figure 4.1) and related intermediates. Roberts, in 1953, validated the existence of benzyne (**4.1**),[3] which can be used today in a host of synthetic applications.[1] Perhaps the next most well-studied classes of strained alkynes are cyclooctynes (e.g., **4.2**) and thiacycloheptynes, which have proven useful in bioorthogonal reactions by Bertozzi, Boons, and others.[4] In contrast, cyclohexyne (**4.3**)[5] and cyclopentyne (**4.4**)[6] have seen only sparse use in synthetic applications. Breakthroughs in the manipulation of cyclohexyne include formal C–C bond insertions reported by the laboratories of Stoltz and Carreira,[7,8] in addition to Diels–Alder reactions as shown by the groups of Guitián and Du Bois.[9] The use of cyclopentyne has been limited to [2+2] and Diels–Alder cycloadditions.[10]

Despite the relatively limited use of **4.3** and **4.4** in synthetic applications for the construction of C–C bonds, we envisioned harnessing these strained intermediates to construct new bicyclic heterocyclic scaffolds. Heterocycles are prevalent in drugs, natural products, and other compounds of tremendous importance.[11] Thus, new methods for their synthesis, especially previously inaccessible compounds, remain highly sought after. As suggested in Figure 4.1, cycloadditions involving **4.3** or **4.4** would provide heterocycles **4.5** or **4.6**, respectively. Despite the simplicity of this approach, there are no examples of the trapping of cyclohexyne or cyclopentyne to construct heterocycles with one or more newly formed C–X bonds (where X=heteroatom). In addition, we sought to prepare a substituted cyclohexyne **4.7** and probe regioselectivities in both nucleophilic trapping and cycloaddition reactions. We have previously explained regioselectivities in reactions of substituted benzynes and hetarynes using the

distortion / interaction model,[12] but this model has not been tested on the non-aromatic cyclohexyne derivatives. Herein, we demonstrate the synthetic utility of **4.3** and **4.4** for the construction of bicyclic heterocycles, and also explain the regioselectivities seen in reactions of the first 3-substituted cyclohexyne using the distortion / interaction model.

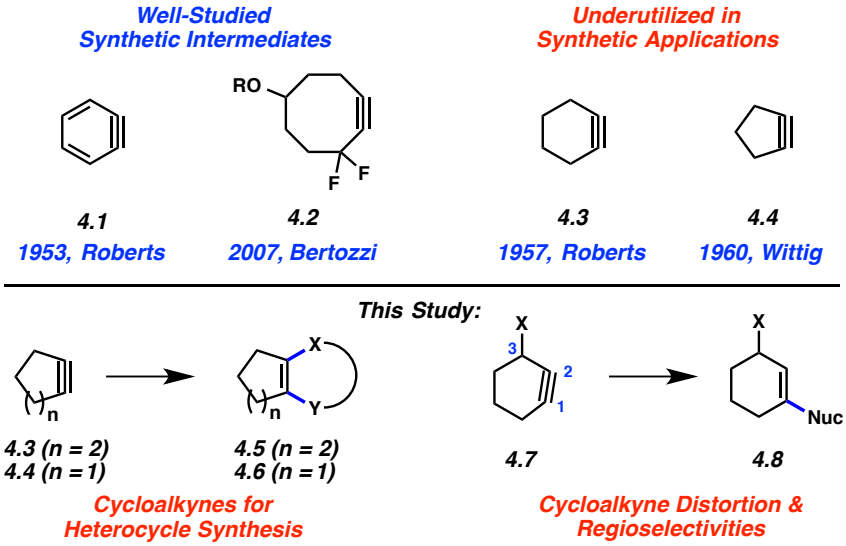

Figure 4.1. Well-studied cyclic alkynes **4.1**–**4.2**, cyclohexyne (**4.3**), cyclopentyne (**4.4**), and objectives of the present study

4.3 Results and Discussion

4.3.1 Generation & Trapping of Cyclohexyne (4.3)

To initiate our study, we opted to generate cyclohexyne in situ from the corresponding silyltriflate, **4.9** (Table 4.1). Silyltriflate **4.9** was first synthesized in 1998,[9a] but has seen limited use, for example, in Diels–Alder reactions and formal C–C bond insertion reactions.[7a,9,13,14] We were delighted to find that treatment of silyltriflate **4.9** with CsF in the presence of a variety of trapping agents delivered heterocyclic products in synthetically useful yields. Specifically, triazoles and pyrazoles were obtained by the trapping of azide and diazo coupling partners,

respectively (entries 1–3).[15] An *N*-Ph pyrazole was accessed using a sydnone cycloaddition (entry 4). We also explored nitrone and nitrile oxide cycloadditions, which provided isoxazoline- and isoxazole-containing products, respectively (entries 5–6). Moreover, additional new trapping experiments to forge 6-membered heterocycles from cyclohexyne are provided in the Experimental Section. It should be emphasized that in contrast to many common methods for heterocycle synthesis, particularly benzyne trapping, the products obtained from cyclohexyne trapping possess more aliphatic character. Being able to access "higher fraction sp^3" compounds is an important direction in contemporary drug discovery.[16]

Table 4.1. Cycloaddition Reactions of **4.3** to Construct 5-Membered Heterocycles

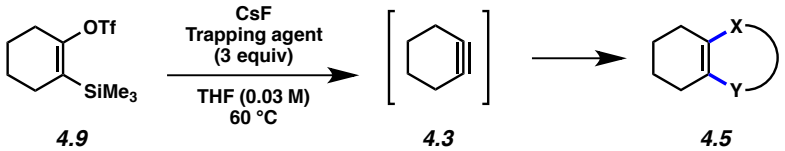

4.9 *4.3* *4.5*

Entry	*Trapping agent*	*Product*	*Yield*[a]
1	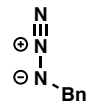	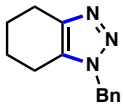	*94%*[b]
2	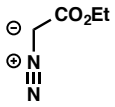	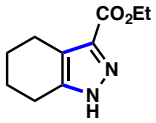	*98%*
3	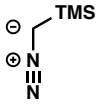	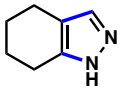	*82%*[c]
4	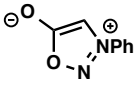	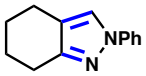	*82%*
5	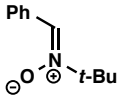	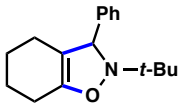	*61%*
6	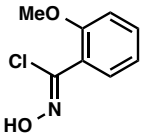	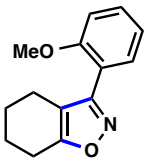	*90%*

[a] Reported yields are the average of two experiments and are based on the amount of isolated products. [b] Benzene was used as a cosolvent. [c] Et_2O was used as a cosolvent.

4.3.2 Generation & Trapping of Cyclopentyne (4.4)

Encouraged by our success in building heterocycles from cyclohexyne, we performed trapping experiments of the less well-studied intermediate, cyclopentyne (**4.4**), using silyltriflate **4.10** (Table 4.2).[17] Although silyltriflate **4.10** has been synthesized previously,[18] no successful trapping experiments involving **4.10** have been reported. Thus, **4.10** was treated with CsF in acetonitrile in the presence of various trapping agents. Most trapping agents gave only low yields

or none of the desired products; however, benzyl azide and sydnone partners could be employed to deliver triazole and pyrazole products, respectively (entries 1–2). Additionally, we found that trapping of **4.4** with a cyclic dimethylurea[19] generated a unique product possessing a [5,7]-fused ring system (entry 3).[20] Despite the limited scope of trapping agents that can be used to intercept **4.4**, these studies validate the notion that cyclopentyne can be used in reactions beyond [2+2] and Diels–Alder cycloadditions, and may react through non-radical pathways.

Table 4.2. Trapping Experiments of Cyclopentyne (**4.4**)

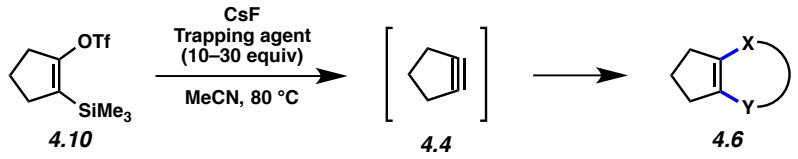

4.10 *4.4* *4.6*

Entry	*Trapping agent*	*Product*	*Yield*[a]
1	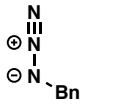	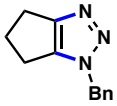	*49%*
2	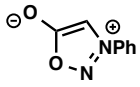	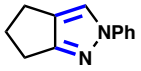	*59%*
3	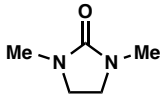	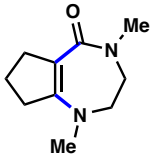	*61%*

[a] Reported yields are the average of two experiments and are based on the amount of isolated products.

4.3.3 Prediction of Regioselectivities Based on the Distortion / Interaction Model

Figure 4.2 shows the optimized structures of cyclohexyne (**4.3**) and cyclopentyne (**4.4**) (see the Experimental Section for computational details).[21] The minimum energy conformer of cyclopentyne is slightly puckered and shows C_s symmetry, in agreement with previous studies.[22] The large angle-strain of this structure is revealed by the large deviation of the internal ring

angles (116°) from the ideal linear disposition of alkynes. The strain has been calculated to be *ca.* 74 kcal mol^{-1}.[22] Such a large strain distorts the in-plane π bond in a way that cyclopentyne has ~10% calculated diradical character.[23] The more relaxed internal angle in cyclohexyne (132°) causes a smaller, but still significant strain, estimated as *ca.* 44 kcal mol^{-1}.[22] Cyclohexyne (**4.3**) possesses a C_2-symmetric structure that resembles the well-known half-chair structure of cyclohexene.[22a,24]

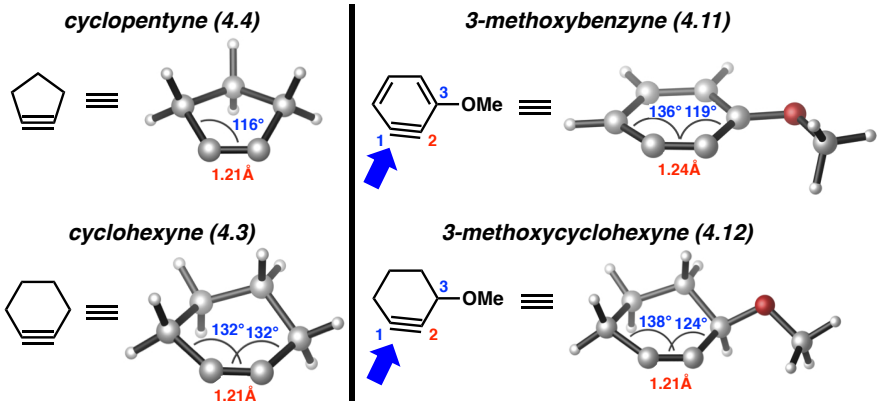

Figure 4.2. Optimized structures of **4.3**, **4.4**, **4.11**, and **4.12** obtained using PCM(THF)/M06-2X/6-311+G(2d,p)

We also compared 3-methoxybenzyne (**4.11**) to its non-aromatic counterpart, 3-methoxycyclohexyne (**4.12**) (Figure 4.2). In the case of **4.11**, as we have previously described,[12a,b] the inductively withdrawing methoxy group at C3 distorts the aryne significantly. Nucleophilic trapping occurs at C1, the more linear aryne terminus whose reactive orbital possesses more *p* character, uniformly with high degrees of regioselectivity. Interestingly, 3-methoxycyclohexyne (**4.12**) bears similar distortion, with internal angles at C1 and C2 being calculated as 138° and 124°, respectively.[25] Much like the distortion seen in **4.11**, the distortion in **4.12** is attributed to the inductively withdrawing nature of the C3 methoxy group that causes

rehybridization of C2 (Bent's Rule, see Experimental Section for further discussion).[26] Consequently, we predict that nucleophilic addition to 3-alkoxycycloalkynes should occur with a significant preference for attack at C1, the more linear alkyne terminus.

4.3.4 Generation & Trapping of C3-Substituted Cyclohexyne 4.14

To test our prediction, we prepared benzyloxysilyltriflate **4.13**, the first C3-substituted cyclohexyne precursor, and performed trapping experiments (Figure 4.3).[27] When silyltriflate **4.13** was treated with CsF in the presence of imidazole, adduct **4.15** was obtained exclusively, which arises via attack at C1 of cyclohexyne **4.14**. Similarly, trapping with benzylazide gave a 5.1 to 1 ratio of cycloadducts **4.16** and **4.17**, which is consistent with a preference for initial bond formation occurring between the more nucleophilic terminus of the azide[28] and C1 of **4.14**.

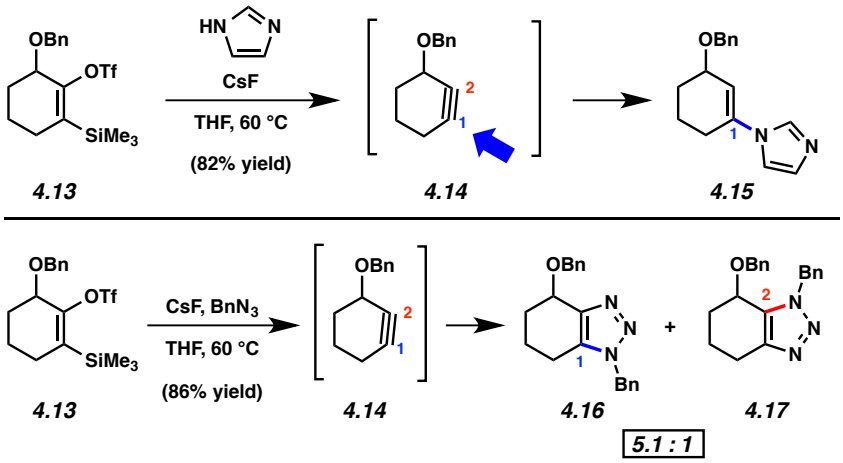

Figure 4.3. Experimental results validate regioselectivity predictions in reactions of 3-substituted cyclohexyne **4.14**

4.3.5 Comparison of Transition States for Nucleophilic Addition and Cycloaddition

Figure 4.4 shows the calculated competing transition states, **TS4.1**–**TS4.4**, for the reactions shown in Figure 4.3.[29] In agreement with the observed selectivity, attack by imidazole at C1 is highly preferred (*ca.* 3 kcal mol^{-1}) because 3-methoxycyclohexyne (**4.12**) is pre-distorted toward the preferred transition state, **TS4.1**. Similarly, in the azide cycloaddition, **TS4.3** is favored over **TS4.4**, although the calculated regioselectivity is overestimated. It is important to note the systematic increase in distortion energy (ΔE^{dist}), the cost of altering the substrate geometry toward the transition state, of the 3-methoxycyclohexyne moiety in **TS4.2** and **TS4.4**, which accounts for most of the calculated energy differences between competing transition states. As a common feature of distortion-controlled reactions, the interaction energies (ΔE^{int}), or in other words, the stabilization due to orbital overlap between the reacting fragments in the transition state, is nearly identical when comparing competing transition states. It is notable that this trend is observed for both the imidazole and azide trapping agents, despite their different electronic properties.

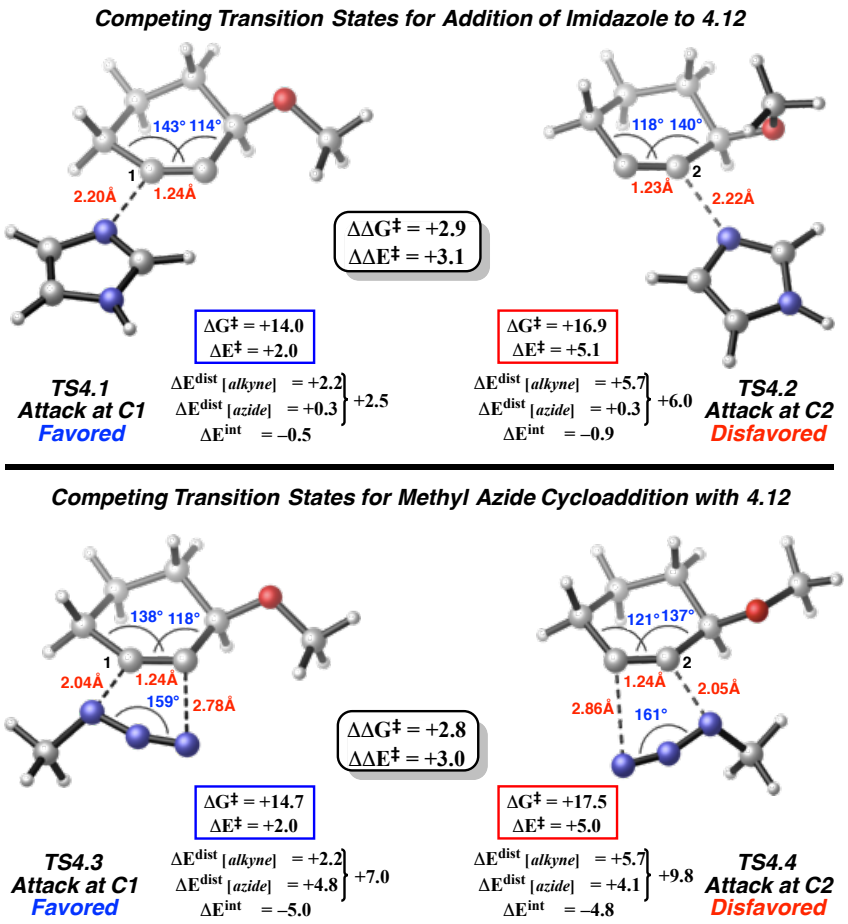

Figure 4.4. Optimized transition states for reactions with imidazole and methyl azide to **4.12** using PCM(THF)/M06-2X/6-11+G(2d,p). Energies are provided in kcal mol^{-1}

4.3.6 Synthesis of Highly Functionalized Heterocycles

In addition to serving as a probe to assess the distortion / interaction model, benzyloxycyclohexyne **4.14** can also be used to access highly functionalized heterocycles. As shown in Scheme 4.1, triazole **4.16**, prepared from the benzylazide cycloaddition of **4.14** (Figure 4.3), was converted to azide **4.18** through an uncommon functionalization of a pseudobenzylic benzyloxy group.[30] Subsequent reduction and pyrrole formation provided triazolopyrrole **4.19**.

Scheme 4.1. Elaboration of Benzyloxycyclohexyne **4.16** to Triazolopyrrole **4.19**

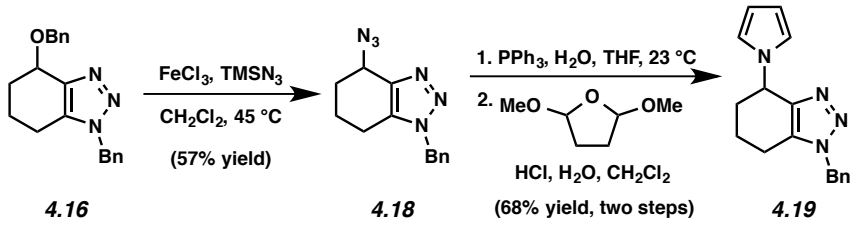

4.16 *4.18* *4.19*

4.4 Conclusion

In summary, we have demonstrated that cyclohexyne and the more elusive intermediate, cyclopentyne, serve as effective tools for the synthesis of new heterocyclic compounds. We have also shown that the distortion / interaction model correctly predicts regioselectivities in reactions of the first 3-substituted cyclohexyne. This validates the distortion / interaction model as a powerful predictive tool for gauging cycloalkyne regioselectivities, just from the reactant's structure, while also providing the impetus for the further exploration of highly strained cycloalkynes as valuable synthetic building blocks.

4.5 Experimental Section

4.5.1 Materials and Methods

Unless stated otherwise, reactions were conducted in flame-dried glassware under an atmosphere of nitrogen using anhydrous solvents (freshly distilled or passed through activated alumina columns). All commercially obtained reagents were used as received unless otherwise specified. Cesium fluoride (CsF) was obtained from Strem Chemicals. *N*-phenyl-bis(trifluoromethanesulfonimide) was obtained from Oakwood Products, Inc. *N*-tert-butyl-α-phenylnitrone, 1,3-dimethyl-2-imidazolidinone, and methyl 2-acetamidoacrylate were obtained

from Alfa Aesar. Methyl thiolsalicylate was obtained from Acros Organics. Ethyl diazoacetate, L-selectride (1 M in THF), and (trimethylsilyl)diazomethane (1 M in Et_2O) were obtained from Sigma Aldrich. *Caution: (trimethylsilyl)diazomethane is a flammable liquid that is very toxic when inhaled. Inhalation can cause pulmonary edema. It may be harmful if ingested or absorbed through the skin. It causes respiratory tract, skin, and eye irritation.* Trimethylsilyl chloride (TMSCl) was distilled over CaH_2 prior to use. Reaction temperatures were controlled using an IKAmag temperature modulator and, unless stated otherwise, reactions were performed at room temperature (rt, approximately 23 °C). Thin-layer chromatography (TLC) was conducted with EMD gel 60 F254 pre-coated plates (0.25 mm) and visualized using a combination of UV light and potassium permanganate staining. Silicycle Siliaflash P60 (particle size 0.040–0.063 mm) was used for flash column chromatography. ^{1}H NMR and 2D-NOESY spectra were recorded on Bruker spectrometers (at 500 MHz) and are reported relative to deuterated solvent signals. Data for ^{1}H NMR spectra are reported as follows: chemical shift (δ ppm), multiplicity, coupling constant (Hz) and integration. ^{13}C NMR spectra were recorded on Bruker spectrometers (at 125 MHz) and are reported relative to deuterated solvent signals. Data for ^{13}C NMR spectra are reported in terms of chemical shift and, when necessary, multiplicity, and coupling constant (Hz). ^{19}F NMR spectra were recorded on Bruker spectrometers (at 376 MHz) and reported in terms of chemical shift. IR spectra were obtained using on a Perkin-Elmer 100 spectrometer and are reported in terms of frequency of absorption (cm^{-1}). High-resolution mass spectra were obtained on Waters LCT Premier with ACQUITY LC and Thermo Scientific™ Exactive Mass Spectrometers with DART ID-CUBE.

4.5.2 Experimental Procedures

4.5.2.1 Cyclohexyne Trapping Experiments

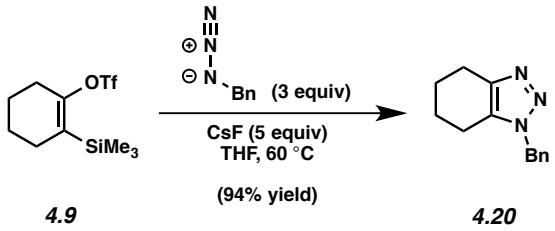

4.9 *4.20*

Representative Procedure (Preparation of triazole 4.20 is used as an example).

4.20 (Table 4.1, Entry 1). To a stirred solution of silyltriflate **4.9**[31] (52.0 mg, 0.172 mmol) and benzylazide (0.8 M in PhH, 640 μL, 0.512 mmol, 3.0 equiv) in THF (5.90 mL) was added CsF (0.130 g, 0.857 mmol, 5.0 equiv). The reaction vessel was purged with N_2 gas, sealed, and placed in a preheated aluminum heating block maintained at 60 °C for 24 h. After cooling to 23 °C, the reaction mixture was filtered over silica gel (EtOAc eluent, 12 mL). Evaporation under reduced pressure and further purification by preparative thin layer chromatography (3:2 EtOAc : hexanes) afforded triazole **4.20** as a white amorphous solid (94% yield, average of two experiments). R_f 0.30 (3:2 EtOAc : hexanes); ^{1}H NMR (500 MHz, $CDCl_3$): δ 7.34–7.27 (m, 3H), 7.19–7.17 (app. d, J = 7.5, 2H), 5.41 (s, 2H), 2.72 (app. t, J = 5.0, 2H), 2.40 (app. t, J = 5.2, 2H), 1.78–1.72 (m, 4H); ^{13}C NMR (125 MHz, $CDCl_3$): δ 144.0, 135.1, 132.1, 129.0, 128.3, 127.6, 51.9, 22.6, 22.5, 22.0, 20.2; IR (film): 2934, 2855, 1586, 1497, 1456, 1440 cm^{-1}; HRMS-ESI (*m/z*) $[M + H]^+$ calcd for $C_{13}H_{16}N_3$, 214.1339; found, 214.1332.

Any modifications of the conditions shown in this representative procedure are specified in the following schemes, which depict all of the results shown in Tables 4.1 and additional examples

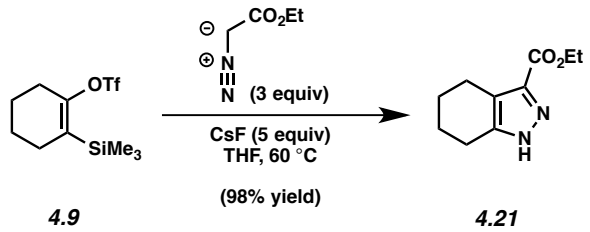

4.9 *4.21*

4.21 (Table 4.1, Entry 2). Purification by preparative thin layer chromatography (1:1 hexanes : EtOAc) afforded pyrazole **4.21** as a faint yellow oil (98% yield, average of two experiments). R_f 0.40 (1:1 hexanes : EtOAc); ^{1}H NMR (500 MHz, $CDCl_3$): δ 11.55 (br s, 1H), 4.34 (q, J = 7.0, 2H), 2.72 (t, J = 5.9, 2H), 2.68 (t, J = 5.9, 2H), 1.85–1.67 (m, 4H), 1.34 (t, J = 7.1, 3H); ^{13}C NMR (125 MHz, $CDCl_3$): δ 162.2, 145.3, 135.8, 119.6, 60.6, 23.0, 22.7, 22.2, 21.6, 14.4; IR (film): 2934, 2855, 1714, 1442, 1256, 1143 cm^{-1}; HRMS-ESI (*m/z*) $[M - H]^-$ calcd for $C_{10}H_{13}N_2O_2$, 193.0972; found, 193.0981.

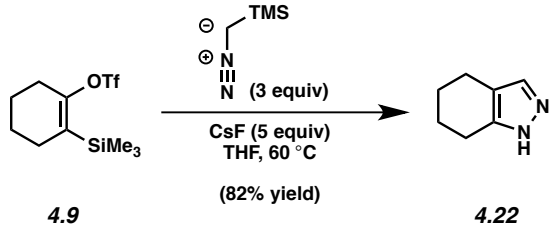

4.9 *4.22*

4.22 (Table 4.1, Entry 3). Purification by preparative thin layer chromatography (2:1 EtOAc : hexanes) afforded pyrazole **4.22** as a colorless oil (82% yield, average of two experiments). R_f 0.20 (2:1 EtOAc : hexanes); ^{1}H NMR (500 MHz, $CDCl_3$): δ 10.16 (br s, 1H), 7.30 (s, 1H), 2.68 (t, J = 6.1, 2H), 2.54 (t, J = 6.1, 2H), 1.86–1.78 (m, 2H), 1.78–1.70 (m, 2H); ^{13}C NMR (125 MHz, $CDCl_3$): δ 143.5, 132.2, 115.2, 23.6, 23.3, 22.2, 20.6; IR (film): 3155, 3103, 2923, 2849, 1593, 1444 cm^{-1}; HRMS-ESI (*m/z*) $[M + H]^+$ calcd for $C_7H_{11}N_2$, 123.0917; found, 123.0914.

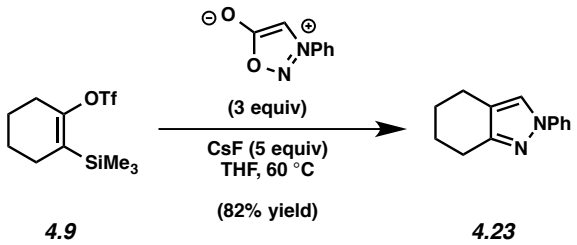

4.23 (Table 4.1, Entry 4). The sydnone trapping agent was synthesized using a known procedure.[32] Purification by preparative thin layer chromatography (9:1 hexanes : EtOAc) afforded pyrazole **4.23** as a faint orange oil (82% yield, average of two experiments). R_f 0.55 (9:1 hexanes : EtOAc); ^{1}H NMR (500 MHz, $CDCl_3$): δ 7.62 (dd, J = 8.7, 1.0, 2H), 7.61 (s, 1H), 7.40 (tt, J = 7.2, 1.8, 2H), 7.20 (tt, J = 7.3, 1.0, 1H), 2.78 (t, J = 6.4, 2H), 2.62 (t, J = 6.4, 2H), 1.89–1.83 (m, 2H), 1.81–1.75 (m, 2H); ^{13}C NMR (125 MHz, $CDCl_3$): δ 151.4, 140.6, 129.4, 125.6, 123.8, 118.7, 118.3, 23.6, 23.6, 23.5, 20.8; IR (film): 2928, 2855, 1598, 1570, 1504, 1376 cm^{-1}; HRMS-ESI (*m/z*) $[M + H]^+$ calcd for $C_{13}H_{15}N_2$, 199.1230; found, 199.1227.

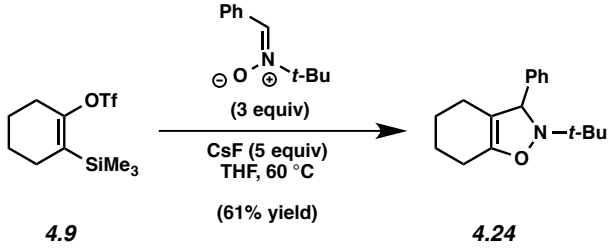

4.24 (Table 4.1, Entry 5). Purification by preparative thin layer chromatography (9:1 hexanes : EtOAc) afforded isoxazoline **4.24** as a colorless oil (61% yield, average of two experiments). R_f 0.65 (9:1 hexanes : EtOAc); ^{1}H NMR (500 MHz, $CDCl_3$): δ 7.36–7.28 (m, 4H), 7.22 (app. tt, J = 6.4, 1.7, 1H), 4.88 (s, 1H), 2.21–2.07 (m, 2H), 1.86–1.78 (m, 1H), 1.70–1.58 (m, 3H), 1.58–1.52 (m, 2H), 1.11 (s, 9H); ^{13}C NMR (125 MHz, $CDCl_3$): δ 148.0, 143.8, 128.4, 127.5, 127.1, 106.5,

70.6, 60.3, 25.2, 22.8, 22.7, 21.4, 21.2; IR (film): 2972, 2932, 1724, 1453, 1361, 1211 cm^{-1}; HRMS-ESI (*m/z*) $[M + H]^+$ calcd for $C_{17}H_{24}NO$, 258.1852; found, 258.1851.

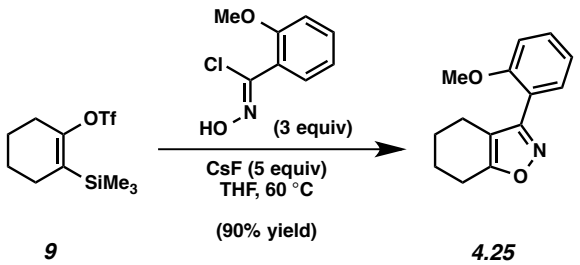

4.25 (Table 4.1, Entry 6). The chloro-oxime trapping agent was synthesized using a known procedure.[33] Purification by preparative thin layer chromatography (9:1 hexanes : EtOAc) afforded isoxazole **4.25** as a faint yellow oil (90% yield, average of two experiments). R_f 0.40 (9:1 hexanes : EtOAc); ^1H NMR (500 MHz, $CDCl_3$): δ 7.47 (dd, *J* = 7.5, 1.7, 1H), 7.41 (ddd, *J* = 8.3, 7.4, 1.7, 1H), 7.02 (dt, *J* = 7.5, 1.0, 1H), 6.98 (d, *J* = 8.3, 1H), 3.84 (s, 3H), 2.74 (tt, *J* = 6.4, 1.5, 2H), 2.39 (tt, *J* = 6.4, 1.5, 2H), 1.94–1.86 (m, 2H), 1.77–1.70 (m, 2H); ^{13}C NMR (125 MHz, $CDCl_3$): δ 167.8, 159.8, 157.4, 131.1, 131.0, 120.8, 118.9, 113.5, 111.1, 55.5, 22.9, 22.8, 22.3, 20.7; IR (film): 2937, 2856, 1634, 1604, 1510, 1470 cm^{-1}; HRMS-ESI (*m/z*) $[M + H]^+$ calcd for $C_{14}H_{16}NO_2$, 230.1176; found, 230.1179.

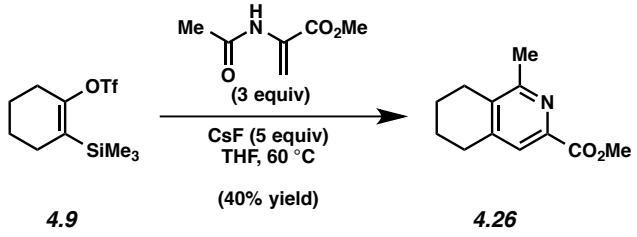

4.26. Purification by preparative thin layer chromatography (9:1 hexanes : EtOAc) afforded tetrahydroisoquinoline **4.26** as a colorless oil (40% yield, average of two experiments). R_f 0.10

(9:1 hexanes : EtOAc); ^{1}H NMR (500 MHz, $CDCl_3$): δ 7.71 (s, 1H), 3.96 (s, 3H), 2.78 (t, J = 6.4, 2H), 2.66 (t, J = 6.4, 2H), 2.51 (s, 3H), 1.89–1.85 (m, 2H), 1.80–1.76 (m, 2H); ^{13}C NMR (125 MHz, $CDCl_3$): δ 166.6, 157.8, 146.9, 143.8, 135.6, 124.1, 52.8, 29.5, 26.5, 22.8, 22.6, 21.9; IR (film): 2935, 1741, 1717, 1590, 1436, 1214 cm^{-1}; HRMS-ESI (*m/z*) [M + H]$^+$ calcd for $C_{12}H_{16}NO_2$, 206.1176; found, 206.1173.

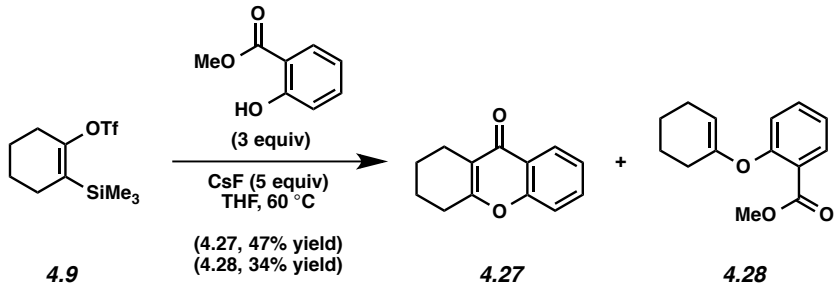

4.27 and 4.28. Purification by preparative thin layer chromatography (9:1 hexanes : EtOAc) afforded adducts **4.27** (47% yield, average of two experiments) and **4.28** (34% yield, average of two experiments) as colorless oils. **4.27**: R_f 0.22 (9:1 hexanes : EtOAc); ^{1}H NMR (500 MHz, $CDCl_3$): δ 8.19 (dd, J = 8.0, 1.7, 1H), 7.59 (ddd, J = 8.6, 7.1, 1.7, 1H), 7.36 (dd, J = 8.6, 0.6, 1H), 7.33 (ddd, J = 8.1, 7.1, 1.1, 1H), 2.66 (tt, J = 6.4, 1.5, 2H), 2.57 (tt, J = 6.4, 1.5, 2H), 1.90–1.84 (m, 2H), 1.78–1.73 (m, 2H); ^{13}C NMR (125 MHz, $CDCl_3$): δ 177.8, 163.9, 156.0, 133.0, 125.8, 124.5, 123.3, 118.5, 117.7, 28.3, 22.0, 21.8, 21.1; IR (film): 2943, 2872, 1638, 1622, 1609, 1468 cm^{-1}; HRMS-ESI (*m/z*) [M + H]$^+$ calcd for $C_{13}H_{13}O_2$, 201.0910; found, 201.0910. **4.28**: R_f 0.55 (9:1 hexanes : EtOAc); ^{1}H NMR (500 MHz, $CDCl_3$): δ 7.82 (dd, J = 7.8, 1.7, 1H), 7.44 (ddd, J = 8.2, 7.3, 1.7, 1H), 7.10 (dt, J = 7.6, 1.1, 1H), 7.06 (dd, J = 8.2, 1.1, 1H), 4.84 (tt, J = 3.9, 1.2, 1H), 3.88 (s, 3H), 2.26–2.21 (m, 2H), 2.07–2.00 (m, 2H), 1.78–1.72 (m, 2H), 1.61–1.55 (m, 2H); ^{13}C NMR (125 MHz, $CDCl_3$): δ 166.6, 155.6, 154.2, 133.3, 131.7, 123.0, 122.9, 120.8, 105.5,

52.2, 26.9, 23.7, 23.0, 22.4; IR (film): 2932, 2843, 1733, 1716, 1602, 1227 cm^{-1}; HRMS-ESI (*m/z*) $[M + H]^+$ calcd for $C_{14}H_{17}O_3$, 233.1172; found, 233.1174.

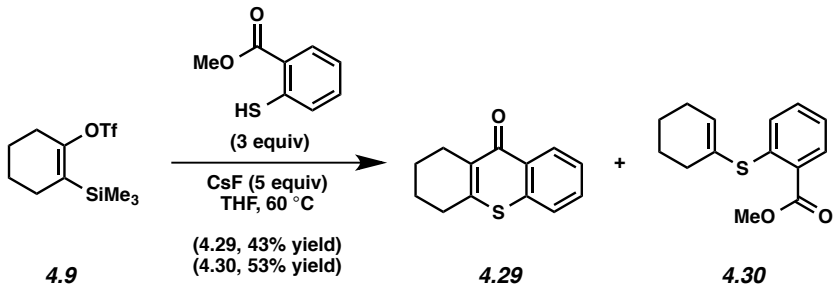

4.29 and 4.30. Purification by preparative thin layer chromatography (9:1 hexanes : EtOAc) afforded adducts **4.29** (43% yield, average of two experiments) and **4.30** (53% yield, average of two experiments) as colorless oils. **4.29**: R_f 0.25 (9:1 hexanes : EtOAc); ^1H NMR (500 MHz, $CDCl_3$): δ 8.49 (dd, *J* = 8.1, 1.4, 1H), 7.54–7.44 (m, 3H), 2.73–2.65 (m, 4H), 1.88–1.80 (m, 4H); ^{13}C NMR (125 MHz, $CDCl_3$): δ 180.1, 147.4, 137.2, 131.5, 130.9, 130.5, 129.0, 127.0, 125.7, 31.3, 24.8, 22.4, 22.2; IR (film): 3065, 2934, 2867, 1605, 1581, 1548 cm^{-1}; HRMS-ESI (*m/z*) $[M + H]^+$ calcd for $C_{13}H_{13}OS$, 217.0682; found, 217.0682. **4.30**: R_f 0.55 (9:1 hexanes : EtOAc); ^1H NMR (500 MHz, $CDCl_3$): δ 7.93 (dd, *J* = 7.9, 1.5, 1H), 7.38 (ddd, *J* = 8.1, 7.3, 1.5, 1H) 7.24 (dd, *J* = 8.1, 0.8, 1H), 7.14 (ddd, *J* = 8.4, 7.9, 1.2, 1H), 6.39–6.37 (m, 1H), 3.91 (s, 3H), 2.27–2.23 (m, 2H), 2.18–2.15 (m, 2H), 1.75–1.70 (m, 2H), 1.68–1.63 (m, 2H); ^{13}C NMR (125 MHz, $CDCl_3$): δ 167.0, 141.4, 139.6, 132.2, 131.4, 130.1, 127.8, 127.2, 124.3, 52.2, 30.4, 27.3, 23.8, 21.6; IR (film): 2931, 1717, 1588, 1562, 1434, 1249 cm^{-1}; HRMS-ESI (*m/z*) $[M + H]^+$ calcd for $C_{14}H_{17}O_2S$, 249.0944; found, 249.0945.

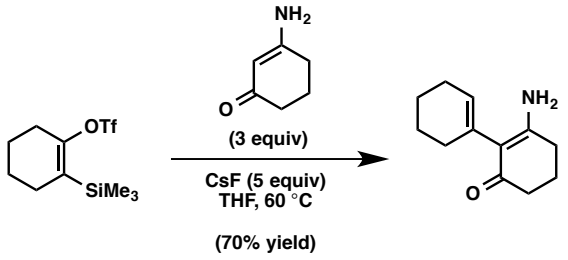

4.9 *4.31*

4.31. Purification by preparative thin layer chromatography (1:1 hexanes : EtOAc) afforded adduct **4.31** as an amorphous white solid (70% yield, average of two experiments). R_f 0.10 (1:1 hexanes : EtOAc); ^{1}H NMR (500 MHz, $CDCl_3$): δ 5.53–5.50 (m, 1H), 4.80 (br s, 2H), 2.40 (t, *J* = 6.1, 2H), 2.31 (t, *J* = 6.1, 2H), 2.12–2.07 (m, 2H), 2.07–1.98 (m, 2H), 1.96–1.90 (m, 2H), 1.72–1.66 (m, 2H), 1.65–1.59 (m, 2H); ^{13}C NMR (125 MHz, $CDCl_3$): δ 194.8, 159.4, 133.7, 127.9, 115.3, 37.0, 29.1, 28.3, 25.6, 23.1, 22.3, 21.5; IR (film): 3449, 3303, 3164, 2928, 1529, 1405 cm^{-1}; HRMS-ESI (*m/z*) $[M + H]^+$ calcd for $C_{12}H_{18}ON$, 192.1383; found, 192.1376.

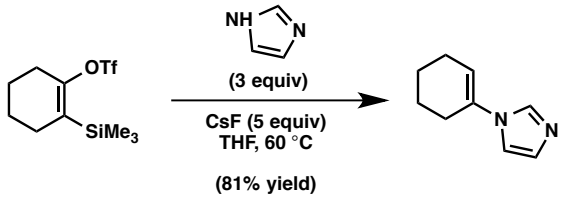

4.9 *4.32*

4.32. Purification by preparative thin layer chromatography (1:1 hexanes : EtOAc) afforded adduct **4.32** as a colorless oil (81% yield, average of two experiments). R_f 0.15 (1:1 hexanes : EtOAc); ^{1}H NMR (500 MHz, $CDCl_3$): δ 7.64 (s, 1H), 7.06 (d, *J* = 9.8, 2H), 5.83–5.79 (m, 1H), 2.44–2.38 (m, 2H), 2.22–2.15 (m, 2H), 1.85–1.78 (m, 2H), 1.69–1.62 (m, 2H); ^{13}C NMR (125 MHz, $CDCl_3$): δ 134.6, 133.9, 129.4, 116.7, 116.5, 27.4, 24.2, 22.5, 21.8; IR (film): 3390, 3115, 2931, 2861, 1673, 1490 cm^{-1}; HRMS-ESI (*m/z*) $[M + H]^+$ calcd for $C_9H_{12}N_2$, 149.1073; found, 149.1070.

4.5.2.2 Synthesis of Cyclopentyne Precursor & Trapping Experiments

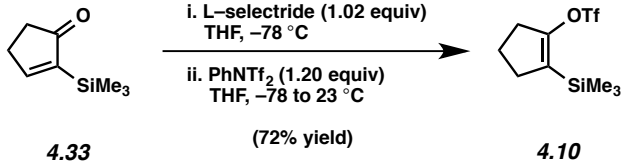

4.33 *4.10*

Silyl triflate 4.10. To a solution of known silyl enone **4.33**[34] (0.963 g, 67.2 mmol, 1 equiv) in THF (22 mL) at –78 °C was added L-selectride (1 M in THF, 6.37 mL, 6.37 mmol, 1.02 equiv) dropwise over 5 min. The reaction was stirred for 3 h, then a solution of $NPhTf_2$ (2.68 g, 7.49 mmol, 1.2 equiv) in THF (6.2 mL) was added over 5 min. The reaction was allowed to slowly warm to room temperature and was then stirred for 15 h. The reaction was quenched with saturated aqueous ammonium chloride (20 mL). The layers were separated and the aqueous layer was extracted with EtOAc (3 × 20 mL). The combined organic layers were washed with brine (50 mL), dried over Na_2SO_4, and concentrated *in vacuo* to provide the crude product, which was purified by flash chromatography (hexanes) to afford silyl triflate **4.10** (1.30 g, 72% yield) as a colorless oil. R_f 0.52 (hexanes); ^{1}H NMR (500 MHz, $CDCl_3$): δ 2.65–2.69 (m, 2H), 2.40–2.44 (m, 2H), 1.97–2.03 (m, 2H), 0.16 (s, 9H); ^{13}C (125 MHz, $CDCl_3$): δ 155.0, 130.5, 118.6 (q, J = 319.8), 32.6, 32.5, 22.2, –1.7; ^{19}F NMR (376 MHz, $CDCl_3$): δ -74.3, IR (film): 2959, 2902, 2857, 1638, 1418, 1315, 1288, 1250, 1204, 1142, 1122, 1068 cm $^{-1}$; HRMS-ESI (*m/z*) $[M + H]^+$ calcd for $C_9H_{16}F_3O_3SSi$, 289.0536; found, 289.0525.

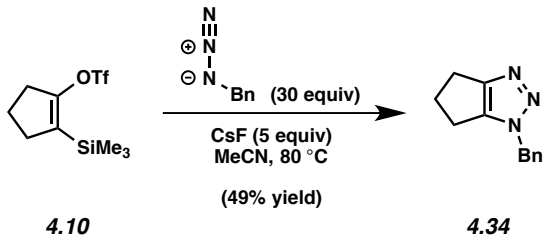

4.34. Silyl triflate **4.10** (65.4 mg, 0.227 mmol, 1 equiv) was added to a flame-dried vial. In a separate flame-dried vial, benzylazide (0.8 M in benzene, 8.5 mL, 6.8 mmol, 30 equiv) was added and the benzene was removed *in vacuo*. The neat benzylazide was then transferred to the vial containing **4.10** with MeCN (0.91 mL). CsF (0.172 g, 1.13 mmol, 5 equiv) was added and the vial was capped and heated to 80 °C in a pre-heated aluminum heating block. After heating for 6 d, the reaction was cooled to room temperature and filtered through a small plug of silica gel (EtOAc eluent, 10 mL). The solvent was removed *in vacuo* and the crude material was purified by flash chromatography (3:1→1:1 hexanes : EtOAc) to provide triazole **4.34** (49% yield, average of two experiments) as a white solid. R_f 0.39 (1:1 hexanes : EtOAc); Mp: 71.4–73.2 °C; ^{1}H NMR (500 MHz, $CDCl_3$): δ 7.33–7.37 (m, 3H), 7.24–7.26 (m, 2H), 5.41 (s, 2H), 2.72–2.74 (m, 2H), 2.51–2.57 (m, 2H), 2.38–2.41 (m, 2H); ^{13}C (125 MHz, $CDCl_3$): δ 156.8, 142.1, 134.7, 129.1, 128.7, 128.3, 53.3, 30.4, 22.7, 21.8; IR (film): 3063, 3032, 2978, 2955, 2937, 2921, 2866, 1572, 1495, 1452, 1373, 1275, 1230, 1176, 1084, 1059 cm $^{-1}$; HRMS-ESI (*m/z*) $[M + H]^+$ calcd for $C_{12}H_{14}N_3$, 200.1182; found, 200.1174.

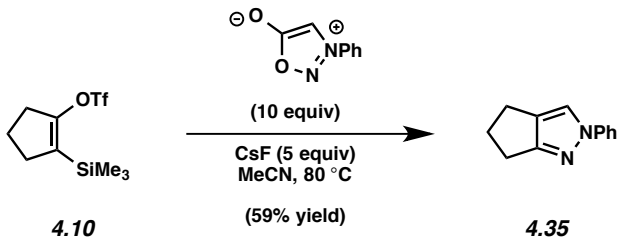

4.35. To a solution of silyl triflate **4.10** (50.4 mg, 0.175 mmol, 1 equiv) in MeCN (1.4 mL) in a flame-dried vial was added the sydnone (0.283 g, 1.75 mmol, 10 equiv), and CsF (0.133 g, 0.874 mmol, 5 equiv). The vial was capped and heated to 80 °C in a pre-heated aluminum block. After stirring for 17 h, the reaction was cooled to room temperature and filtered through a small plug of silica gel (EtOAc eluent, 10 mL). The solvent was removed *in vacuo* and the crude material was purified by flash chromatography (39:1→19:1 hexanes : EtOAc) to afford pyrazole **4.35** (59% yield, average of two experiments) as a white solid. R_f 0.36 (9:1 hexanes : EtOAc); Mp: 74.9–75.6 °C; ^{1}H NMR (500 MHz, $CDCl_3$): δ 7.61–7.63 (m, 2H), 7.53 (s, 1H), 7.38–7.42 (m, 2H), 7.19–7.26 (m, 1H), 2.79–2.82 (m, 2H), 2.70–2.73 (m, 2H), 2.42–2.47 (m, 2H); ^{13}C (125 MHz, $CDCl_3$): δ 164.0, 141.1, 129.5, 127.4, 125.6, 120.6, 118.7, 30.1, 24.7, 23.2; IR (film): 3109, 3051, 2962, 2947, 2866, 2853, 1598, 1577, 1504, 1460, 1440, 1376, 1212, 1036 cm^{-1}; HRMS-ESI (*m/z*) $[M + H]^+$ calcd for $C_{12}H_{13}N_2$, 185.1073; found, 185.1065.

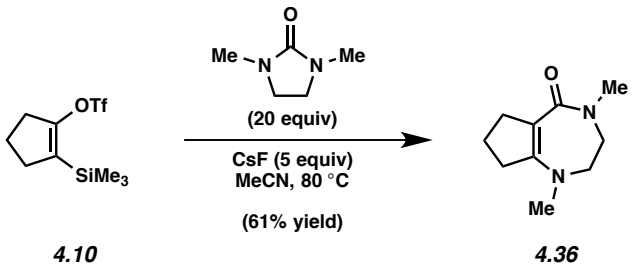

4.10 *4.36*

4.36. To a solution of silyl triflate **4.10** (44.8 mg, 0.155 mmol, 1 equiv) in MeCN (0.62 mL) in a flame-dried vial was added DMI (0.34 mL, 3.11 mmol, 20 equiv) and CsF (0.118 g, 0.777 mmol, 5 equiv). The vial was capped and heated to 80 °C in a pre-heated aluminum block. After stirring for 23 h, the reaction was cooled to room temperature and filtered through a small plug of silica gel (EtOAc eluent, 10 mL). The solvent was removed *in vacuo* and the crude product was purified by flash chromatography (EtOAc→49:1→19:1 CH_2Cl_2 : MeOH) to afford vinylogous

urea **4.36** (61% yield, average over two experiments) as a colorless oil. R_f 0.34 (9:1 CH_2Cl_2 : MeOH); ^{1}H NMR (500 MHz, $CDCl_3$): δ 3.45–3.46 (m, 2H), 3.31–3.33 (m, 2H), 2.98 (s, 3H), 2.89 (s, 3H), 2.73 (t, *J* = 7.3, 2H), 2.60 (t, *J* = 7.6, 2H), 1.75 (p, *J* = 7.5, 2H); ^{13}C (125 MHz, $CDCl_3$): δ 168.9, 152.1, 101.4, 55.6, 49.2, 41.1, 36.6, 36.4, 34.5, 20.6; IR (film): 2938, 2845, 1587, 1574, 1560 1490, 1431, 1404, 1305, 1204, 1090 cm $^{-1}$; HRMS-ESI (*m/z*) $[M + H]^+$ calcd for $C_{10}H_{17}N_2O$, 181.1335; found, 181.1327.

4.5.2.3 Synthesis of 3-Benzyloxy-Cyclohexyne Precursor

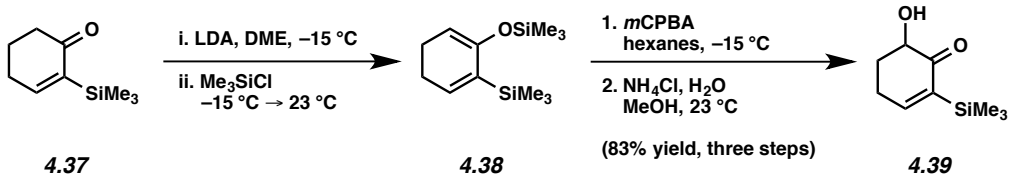

4.37 ***4.38*** ***4.39***

Hydroxy-silylenone 4.39. To a solution of *i*Pr_2NH (0.5 mL, 3.57 mmol, 1.2 equiv) in DME (7.4 mL) at –15 °C was added *n*–BuLi (2.52 M in hexanes, 1.3 mL, 3.27 mmol, 1.1 equiv). The reaction was stirred for 20 min, then known ketone **4.37**[34] (0.500 g, 2.97 mmol, 1 equiv) in DME (3.5 mL) was added. After stirring for 30 min at –15 °C, TMSCl (0.75 mL, 5.94 mmol, 2 equiv) was added and the mixture was allowed to warm to room temperature. After stirring for 2 h, the solvent was removed *in vacuo*. The residue was suspended in pentane (15 mL), filtered and concentrated *in vacuo* to give silyl enol ether **4.38**, which was used in the next step without further purification.

Silyl enol ether **4.38** was dissolved in hexanes (5 mL) and added to a mixture of *m*CPBA (77%, 0.732 g, 4.24 mmol, 1.1 equiv) in hexanes (42 mL) at –15 °C. The reaction was allowed to warm to room temperature, stirred for 2 h, and then filtered and concentrated *in vacuo*. The

residue was dissolved in MeOH (5 mL) and saturated aqueous ammonium chloride (5 mL) was added. After stirring for 25 min, saturated aqueous sodium bicarbonate (20 mL) was added. The layers were separated and the aqueous layer was extracted with EtOAc (3 × 20 mL). The combined organic layers were washed with brine (40 mL), dried over Na_2SO_4 and concentrated *in vacuo* to give a crude oil. Purification by flash chromatography (9:1 hexanes : EtOAc) provided α–hydroxy-silylenone **4.39** (0.457 g, 83% yield) as a yellow oil. R_f 0.27 (9:1 hexanes : EtOAc); ^{1}H NMR (500 MHz, $CDCl_3$): δ 7.06–7.08 (m, 1H), 4.09 (dd, *J* =13.8, 5.7, 1H), 3.82 (bs, 1H), 2.47 (m, 2H), 2.28–2.33 (m, 1H), 1.72–1.81 (m, 1H), 0.09 (s, 9H); ^{13}C (125 MHz, $CDCl_3$): δ 203.2, 159.1, 139.1, 72.5, 31.3, 27.5, –1.5; IR (film): 3483, 2954, 2899, 2870, 2824, 1664, 1591, 1457, 1423, 1332, 1246, 1167, 1144, 1113, 1076 cm $^{-1}$; HRMS-ESI (*m/z*) $[M + H]^+$ calcd for $C_9H_{17}O_2Si$, 185.0992; found, 185.0989.

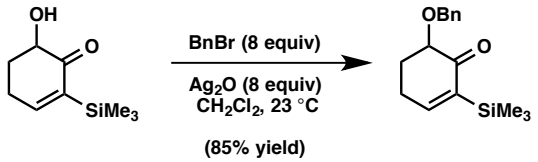

4.39 *4.40*

4.40. Hydroxy-silylenone **4.39** (1.00 g, 5.43 mmol, 1 equiv) was dissolved in CH_2Cl_2 (22 mL) and BnBr (5.2 mL, 43.41 mmol, 8 equiv) and Ag_2O (10.06 g, 43.41 mmol, 8 equiv) were added. After stirring for 14 h at room temperature, the reaction was filtered through celite (CH_2Cl_2 eluent, 30 mL) and concentrated *in vacuo*. The crude product was purified by flash chromatography (benzene→99:1→49:1 benzene : EtOAc) to give benzyloxy-silylenone **4.40** (1.269 g, 85% yield) as a white solid. Mp: 56.5–59.5 °C; R_f 0.60 (9:1 hexanes : EtOAc); ^{1}H NMR (500 MHz, $CDCl_3$): δ 7.38 (app. dd, *J* = 7.3, 1.4, 2H), 7.34 (app dt, *J* = 7.3, 1.8, 2H), 7.28 (app. tt, *J* = 6.5, 2.1, 1H), 7.06 (ddd, *J* = 3.9, 3.0, 0.6, 1H), 4.87 (d, *J* = 11.9, 1H), 4.60 (d, *J* =

11.9, 1H), 3.89 (dd, J = 11.0, 4.6, 1H), 2.57 (dq, J = 19.4, 4.4, 1H), 2.46–2.36 (m, 1H), 2.21 (dq, J = 13.2, 4.4, 1H), 2.14–2.03 (m, 1H), 0.17 (s, 9H); ^{13}C NMR (125 MHz, $CDCl_3$): δ 201.5, 157.3, 140.8, 138.4, 128.4, 127.9, 127.7, 78.7, 72.1, 29.6, 26.9, -1.3; IR (film): 3031, 2953, 1749, 1673, 1593, 1338 cm^{-1}; HRMS-ESI (*m/z*) $[M + H]^+$ calcd for $C_{16}H_{23}O_2Si$, 275.1462; found, 275.1453.

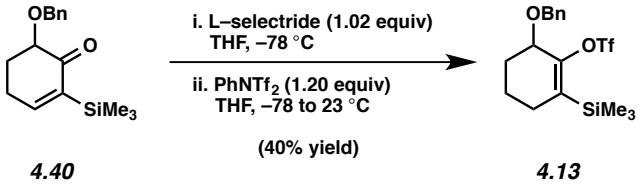

4.40 ***4.13***

Benzyloxy-silyltriflate 4.13. To a solution of benzyloxy-silylenone **4.40** (0.148 mg, 0.541 mmol, 1 equiv) in THF (2.2 mL) at –78 °C was added L-selectride (1 M in THF, 552 μL, 0.552 mmol, 1.02 equiv) dropwise over 5 min. The reaction was stirred for 3 h at –78 °C, then a solution of $NPhTf_2$ (233 mg, 0.649 mmol, 1.20 equiv) in THF (0.5 mL) was added dropwise over 5 min. The reaction was allowed to slowly warm to 23 °C and was stirred for an additional 15 h. The reaction was then quenched with saturated NH_4Cl (4 mL). The layers were separated and the aqueous layer was extracted with EtOAc (3 × 4 mL). The combined organic layers were washed with brine (5 mL), dried over Na_2SO_4 and concentrated *in vacuo*. Further purification by column chromatography with basic Brockman Grade I 58 Å Al_2O_3 (Activity 1) as the stationary (hexanes) afforded benzyloxy-silyltriflate **4.13** (88.6 mg, 40% yield) as a colorless oil. R_f 0.80 (9:1 hexanes : EtOAc); ^{1}H NMR (500 MHz, C_6D_6): δ 7.34 (d, J = 7.6, 2H), 7.19–7.12 (m, 2H), 7.08 (t, J = 7.6, 1H), 4.32 (dd, J = 46.3, 10.9, 2H), 4.16 (app. t, J = 4.2, 1H), 1.91 (dt, J = 17.9, 4.2, 1H), 1.77–1.61 (m, 2H), 1.53–1.41 (m, 1H), 1.30 (app. tt, J = 12.3, 3.3, 1H), 1.16–1.04 (m, 1H), 0.15 (s, 9H); ^{13}C (125 MHz, CD_2Cl_2): δ 152.9, 138.7, 134.1, 128.6, 128.3, 128.0, 118.8 (q, J

= 332.0), 73.4, 70.9, 29.3, 28.2, 17.9, -1.3; IR (film): 3210, 3035, 2950, 2868, 1643, 1401 cm $^{-1}$; HRMS-ESI (*m/z*) $[M + H]^+$ calcd for $C_{17}H_{24}O_4SSiF_3$, 409.1111; found, 409.1094.

4.5.2.4 Trapping Experiments of 3-Benzyloxy-Cyclohexyne

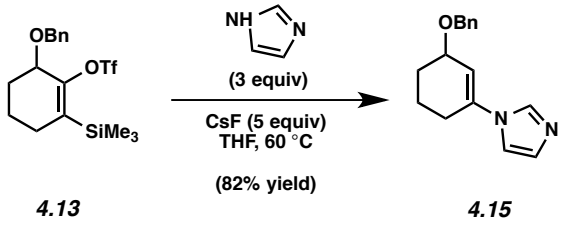

4.13 *4.15*

Imidazoyl-cyclohexene 4.15 (Figure 4.3). To a solution of silyl triflate **4.13** (51.6 mg, 0.126 mmol, 1 equiv) in THF (5.1 mL) in a flame-dried vial was added imidazole (25.8 mg, 0.379 mmol, 3 equiv) and CsF (95.9 mg, 0.632 mmol, 5 equiv). The vial was capped and heated to 60 °C in a pre-heated aluminum block. After stirring for 17.5 h, the reaction was cooled to room temperature and filtered through a small plug of silica gel (EtOAc eluent, 10 mL). The solvent was removed *in vacuo* and the crude product was purified by flash chromatography (3:1 EtOAc : hexanes) to afford imidazoyl-cyclohexene **4.15** as a colorless oil (82% yield, average of two experiments). R_f 0.50 (EtOAc); ^{1}H NMR (500 MHz, $CDCl_3$): δ 7.70 (s, 1H), 7.36–7.27 (m, 5H), 7.12 (s, 1H), 7.07 (s, 1H), 5.92 (m, 1H), 4.65 (d, *J* = 11.8, 1H), 4.57 (d, *J* = 11.8, 1H), 4.18–4.15 (m, 1H), 2.53–2.48 (m, 1H), 2.44–2.38 (m, 1H), 2.06–2.01 (m, 1H), 1.88–1.74 (m, 3H); ^{13}C NMR (125 MHz, $CDCl_3$): δ 138.6, 136.9, 134.6, 129.8, 128.6, 127.8, 127.8, 116.5, 115.7, 71.7, 70.7, 27.7, 27.3, 18.6; IR (film): 3396, 3117, 2942, 2866, 1669, 1491, 1454, 1392, 1292, 1246, 1073 cm^{-1}; HRMS-ESI (*m/z*) $[M + H]^+$ calcd for $C_{16}H_{19}N_2O$, 255.1492; found, 255.1483.

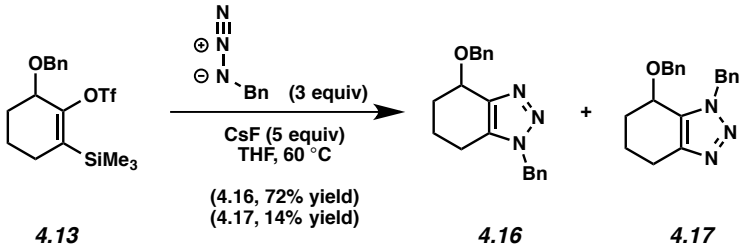

Triazoles 4.16 and 4.17 (Figure 4.3). Silyl triflate **4.13** (50.7 mg, 0.124 mmol, 1 equiv) was added to a flame-dried vial. In a separate flame-dried vial benzylazide (0.8 M in benzene, 0.47 mL, 0.37 mmol, 3 equiv) was added and the benzene was removed *in vacuo*. The neat benzylazide was then transferred to the vial containing **4.13** with THF (5.0 mL). CsF (0.094 g, 0.62 mmol, 5 equiv) was added and the vial was capped and heated to 60 °C in a pre-heated aluminum heating block. After 21 h, the reaction was cooled to room temperature and filtered through a small plug of silica gel (EtOAc eluent, 10 mL). The solvent was removed *in vacuo* and the crude product was purified by flash chromatography (5:3:2 hexanes : EtOAc : benzene) to provide triazole **4.16** (72% yield, average over two experiments) as a colorless oil and triazole **4.17** (14% yield, average over two experiments) as a colorless oil. Triazole **4.16**: R_f 0.47 (5:3:2 hexanes : EtOAc : benzene); ^{1}H NMR (500 MHz, $CDCl_3$): δ 7.19–7.42 (m, 10H), 5.49 (d, J = 15.4, 1H), 5.40 (d, J = 15.4, 1H), 4.88 (d, J = 12.0, 1H), 4.80 (d, J = 12.0, 1H), 4.70 (t, J = 3.6, 1H), 2.55 (ddd, J = 16.5, 5.8, 3.0, 1H), 2.29 (ddd, J = 16.5, 10.5, 6.0, 1H), 2.11–2.16 (m, 1H), 1.99–2.08 (m, 1H), 1.77–1.83 (m, 1H), 1.65–1.71 (m, 1H); ^{13}C (125 MHz, $CDCl_3$): δ 144.2, 138.8, 134.7, 133.9, 129.1, 128.4, 128.4, 127.9, 127.7, 127.5, 10.7, 67.9, 52.0, 29.4, 20.2, 18.1; IR (film): 3063, 3031, 2946, 2866, 1605, 1586, 1497, 1455, 1436, 1314, 1237, 1208, 1116, 1089, 1070, 1047, 1028 cm $^{-1}$; HRMS-ESI (*m/z*) $[M + H]^+$ calcd for $C_{20}H_{22}N_3O$, 320.1757; found, 320.1744. Triazole **4.17**: R_f 0.35 (5:3:2 hexanes : EtOAc : benzene); ^{1}H NMR (500 MHz, $CDCl_3$): δ 7.39–7.27 (m, 8H), 7.04–7.03 (m, 2H), 5.64 (d, J = 15.1, 1H), 5.31 (d, 15.1, 1H), 4.65

(d, J = 11.3, 1H), 4.40 (t, J = 4.7, 1H), 4.39 (d, J = 11.3, 1H), 2.84 (dt, J = 16.0, 5.5, 1H), 2.69 (ddd, J = 16.0, 8.3, 5.6, 1H), 2.09–2.03 (m, 1H), 2.01–1.93 (m, 1H), 1.88–1.82 (m, 1H), 1.80–1.74 (m, 1H); ^{13}C (125 MHz, $CDCl_3$): δ 145.8, 137.8 135.3, 131.6, 128.9, 128.8, 128.2, 128.2, 128.1, 127.6, 70.4, 67.9, 52.4, 27.9, 22.1, 19.5; IR (film): 3064, 3031, 2943, 2861, 1587, 1497, 1455, 1358, 1311, 1198, 1159, 1072 cm $^{-1}$; HRMS-ESI (*m/z*) $[M + H]^+$ calcd for $C_{20}H_{22}N_3O$, 320.1757; found, 320.1745.

4.5.2.5 Derivatization of Triazole 4.16

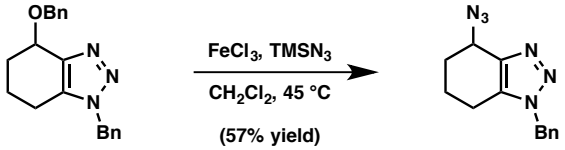

4.16 *4.18*

Azide 4.18 (Scheme 4.1). Triazole **4.16** (24.6 mg, 0.077 mmol, 1 equiv) in CH_2Cl_2 (0.39 mL) was added to a vial containing $FeCl_3$ (18.7 mg, 0.116 mmol, 1.5 equiv). $TMSN_3$ (61 μL, 0.462 mmol, 6 equiv) was then added and the vial was capped and heated to 45 °C. After stirring for 18 h, the vial was cooled to room temperature and water (1 mL) was added. The layers were separated and the aqueous layer was extracted with CH_2Cl_2 (3 × 1 mL). The combined organic layers were washed with brine (3 mL), dried over Na_2SO_4, filtered, and concentrated *in vacuo*. The crude product was purified by preparative thin layer chromatography (5:3:2 hexanes : EtOAc : benzene) to provide azide **4.18** (11.2 mg, 57% yield) as a white solid. R_f 0.40 (5:3:2 hexanes : EtOAc : benzene); Mp: 53.4–55.1 °C; ^{1}H NMR (500 MHz, $CDCl_3$): δ 7.37–7.31 (m, 3H), 7.21–7.19 (m, 2H), 5.52 (d, J = 15.4, 1H), 5.43 (d, J = 15.4, 1H), 4.83 (t, J = 4.1, 1H), 2.56–2.51 (m, 1H), 2.35–2.29 (m, 1H), 1.98–1.80 (m, 4H); ^{13}C (125 MHz, $CDCl_3$): δ 142.1, 134.5,

133.9, 129.2, 128.7, 127.7, 53.0, 52.3, 29.2, 20.0, 18.6; IR (film): 3064, 3033, 2949, 2866, 2096, 1587, 1497, 1456, 1436, 1240, 1091, 1071 cm $^{-1}$; HRMS-ESI (*m/z*) $[M + H]^+$ calcd for $C_{13}H_{15}N_6$, 255.1353; found, 255.1347.

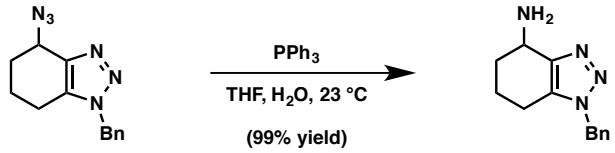

4.18 ***4.41***

Amine 4.41 (Scheme 4.1). Water (21 μL, 1.18 mmol, 10 equiv) was added to a mixture of azide **4.18** (30 mg, 0.118 mmol, 1 equiv) and PPh_3 (93 mg, 0.354 mmol, 3 equiv) in THF (1.2 mL) at room temperature. After stirring for 18 h, the reaction was concentrated *in vacuo*. The crude material was purified by flash chromatography (EtOAc→9:1 CH_2Cl_2 : MeOH) to afford amine **4.41** (26.5 mg, 99% yield) as a white solid. R_f 0.21 (9:1 CH_2Cl_2 : MeOH); Mp: 89.6–91.6 °C; ^{1}H NMR (500 MHz, $CDCl_3$): δ 7.35–7.30 (m, 3H), 7.19–7.18 (m, 2H), 2.43 (s, 2H), 4.19 (t, J = 5.6, 1H), 2.50 (bs, 2H), 2.46–2.35 (m, 2H), 2.06–1.95 (m, 2H), 1.76–1.69 (m, 1H), 1.60–1.54 (m, 1H); ^{13}C (125 MHz, $CDCl_3$): δ 147.3, 134.8, 132.4, 129.1, 128.5, 127.7, 52.1, 44.6, 32.1, 20.2, 19.9; IR (film): 3361, 3063, 3032, c2932, 2860, 1586, 1497, 1456, 1303, 1242, 1204, 1098, 1074 cm $^{-1}$; HRMS-ESI (*m/z*) $[M + H]^+$ calcd for $C_{13}H_{17}N_4$, 229.1448; found, 229.1449.

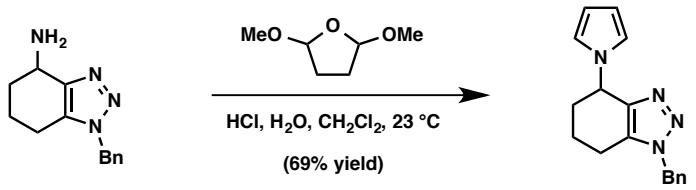

4.41 ***4.19***

Triazolopyrrole 4.19 (Scheme 4.1). To a vial containing HCl (0.1 M in H_2O, 0.22 mL) was added 2,5-dimethoxytetrahydrofuran (28.4 μL, 0.219 mmol, 4 equiv) and the mixture was heated to 100 °C. After 30 min, the vial was cooled to room temperature and the mixture was added to a solution of amine **4.41** (11.8 mg, 0.055 mmol, 1 equiv) in CH_2Cl_2 (0.55 mL). The reaction was stirred at room temperature for 15 h, then aqueous sodium hydroxide (1 M in H_2O, 1 mL) was added. The solution was extracted with CH_2Cl_2 (3 × 1 mL). The combined organic layers were washed with brine (2 mL), dried over Na_2SO_4, filtered and concentrated *in vacuo*. The crude product was purified by flash chromatography (3:2 hexanes : EtOAc) to provide triazolopyrrole **4.19** (10.5 mg, 69% yield) as a white solid. R_f 0.46 (1:1 hexanes : EtOAc); Mp: 168.4–170.6 °C; ^{1}H NMR (500 MHz, $CDCl_3$): δ 7.37–7.34 (m, 3H), 7.23–7.21 (m, 2H), 6.61 (t, *J* = 2.2, 2H), 6.14 (t, *J* = 2.2, 2H), 5.53 (d, *J* = 15.3, 1H), 5.47 (d, *J* = 15.3, 1H), 5.41 (t, *J* = 4.8, 1H), 2.57 (dt, *J* = 16.5, 5.2, 1H), 2.40 (dt, *J* = 16.5, 7.5, 1H), 2.18–2.13 (m, 1H), 2.10–2.03 (m, 1H), 1.85–1.80 (m, 2H); ^{13}C (125 MHz, $CDCl_3$): δ 142.3, 134.6, 134.3, 129.2, 128.7, 127.7, 119.8, 108.2, 52.3, 51.3, 31.8, 20.0, 19.0; IR (film): 3096, 3064, 3033, 2930, 2864, 1587, 1488, 1455, 1434, 1277, 1247, 1089, 1072 cm $^{-1}$; HRMS-ESI (*m/z*) $[M + H]^+$ calcd for $C_{17}H_{19}N_4$, 279.1604; found, 279.1599.

4.5.3 Computational Methods

All calculations were carried out with the meta-hybrid M06-2X[35] functional and 6-311+G(2d,p) basis set. Full geometry optimizations and transition structure (TS) searches were carried out with the Gaussian 09 package.[36] Thermal and entropic corrections to energy were calculated from vibrational frequencies. The nature of the stationary points was determined in each case according to the appropriate number of negative eigenvalues of the Hessian matrix from the frequency calculations. Scaled frequencies were not considered. Mass-weighted intrinsic reaction

coordinate (IRC) calculations were carried out using the Gonzalez and Schlegel scheme[37] in order to ensure that the TSs indeed connected the appropriate reactants and products. Bulk solvent effects were considered implicitly during optimization through the IEF-PCM polarizable continuum model[38] as implemented in Gaussian 09. The parameters for tetrahydrofuran were used to calculate solvation free energies (ΔG_{solv}). The possibility of different conformations was taken into account for all structures. Gibbs free energies (ΔG) were used for the discussion on the relative stabilities of the considered structures. Cartesian coordinates, electronic energies, entropies, enthalpies, Gibbs free energies, and lowest frequencies of the different conformations of all structures are provided.

4.5.3.1 Bent´s Rule & Alkyne Distortion Determine Regioselectivity of Nucleophilic Addition

Henry Bent stated in 1961 that *"atomic s character concentrates in orbitals directed toward electropositive substituents"*. The rationale for this rule is that bonds between elements of different electronegativities are polarized in a way that the electron density will be shifted towards the more electronegative element. Due to the inherent higher stability of *s* orbitals, the hybrid orbitals from the more electronegative atoms will increase their *s* character in order to stabilize the withdrawn electron density. To compensate for this shift in electron density, the less electronegative atoms will direct hybrid orbitals with an increased *p* character toward the more electronegative atoms to which they are bound, without a significant energy penalty. As a result, the hybrid orbitals that constitute these polarized bonds deviate from ideal sp^n (n = 1, 2 or 3) hybridizations, which translates into distorted geometries.

In restrained alkynes bearing an electron-withdrawing substituent, such as 3-methoxycyclohexyne, the C2–C3 is polarized as revealed by the increment in the atomic charge (Δq) at C2 with respect to cyclohexyne (Figure 4.5); following Bent´s rule, the σ-bonding orbitals (*sp*) at C2 possess more *p* character, which translates into a more compressed internal angle (124º) with respect to cyclohexyne (132º). In turn, the *sp* σ-bonding orbitals of C1 rehybridize to increase their *s* character, which causes the internal angle to be more linear (138º) with respect to cyclohexyne (132º). This change in geometry is associated with a very slight polarization of the C1–C2 bond and an increase of the *p* character of the reacting orbital and a slightly greater contribution of C1 to the LUMO, but, more importantly, involves a pre-distortion of the reactant towards the geometry that is required to achieve the transition state for nucleophilic addition. For the *distal* attack, only minimal geometric and electronic changes are required to reach the saddle point in the potential energy surface, resulting in a generally early transition state and low activation barrier (Figures 4.4 and 4.6). Conversely, attack at the *proximal* position, besides minor electrostatic and steric repulsions, requires a complete redistribution of the electron density and modification of the geometry (*i.e.* distortion) to reallocate the developing negative charge in the C1; this reaction pathway is thus associated to a normally late transition state and a high activation barrier (Figures 4.4 and 4.6). Another benefit for regioselectivity is the stabilization of the negative charge of the developing anion at C2, whose non-bonding orbital has an increased *s* character, upon nucleophilic attack at C1.

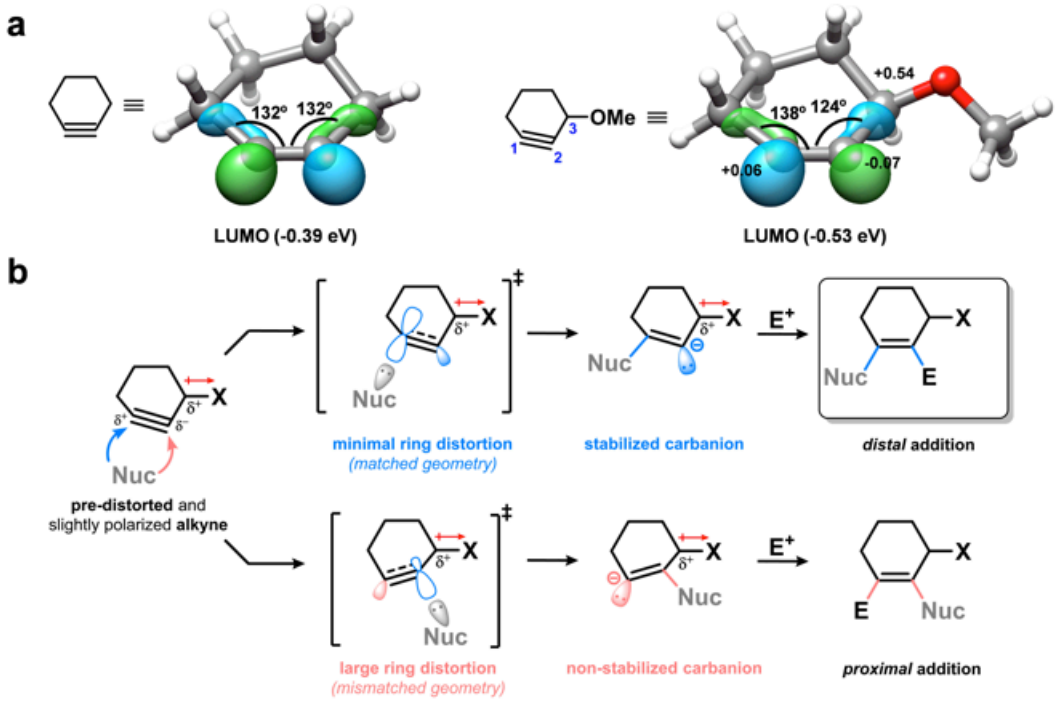

Figure 4.5. a) Structures and isosurface representation of the LUMO of cyclohexyne and 3-methoxycyclohexyne calculated at the PCM(THF)/M06-2X/6-311+G(2d,p) level. Incremental atomic charges (NPA) with respect to cyclohexane are shown. b) Distortion-accelerated regioselective nucleophilic addition at the *distal* position (C1) of strained cycloalkynes

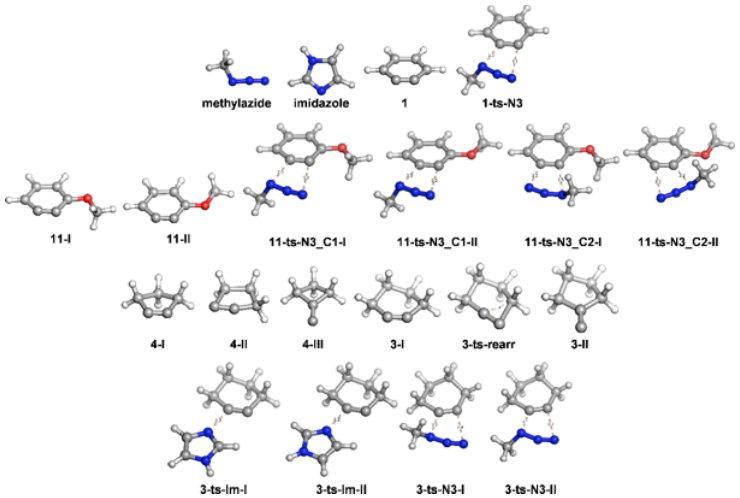

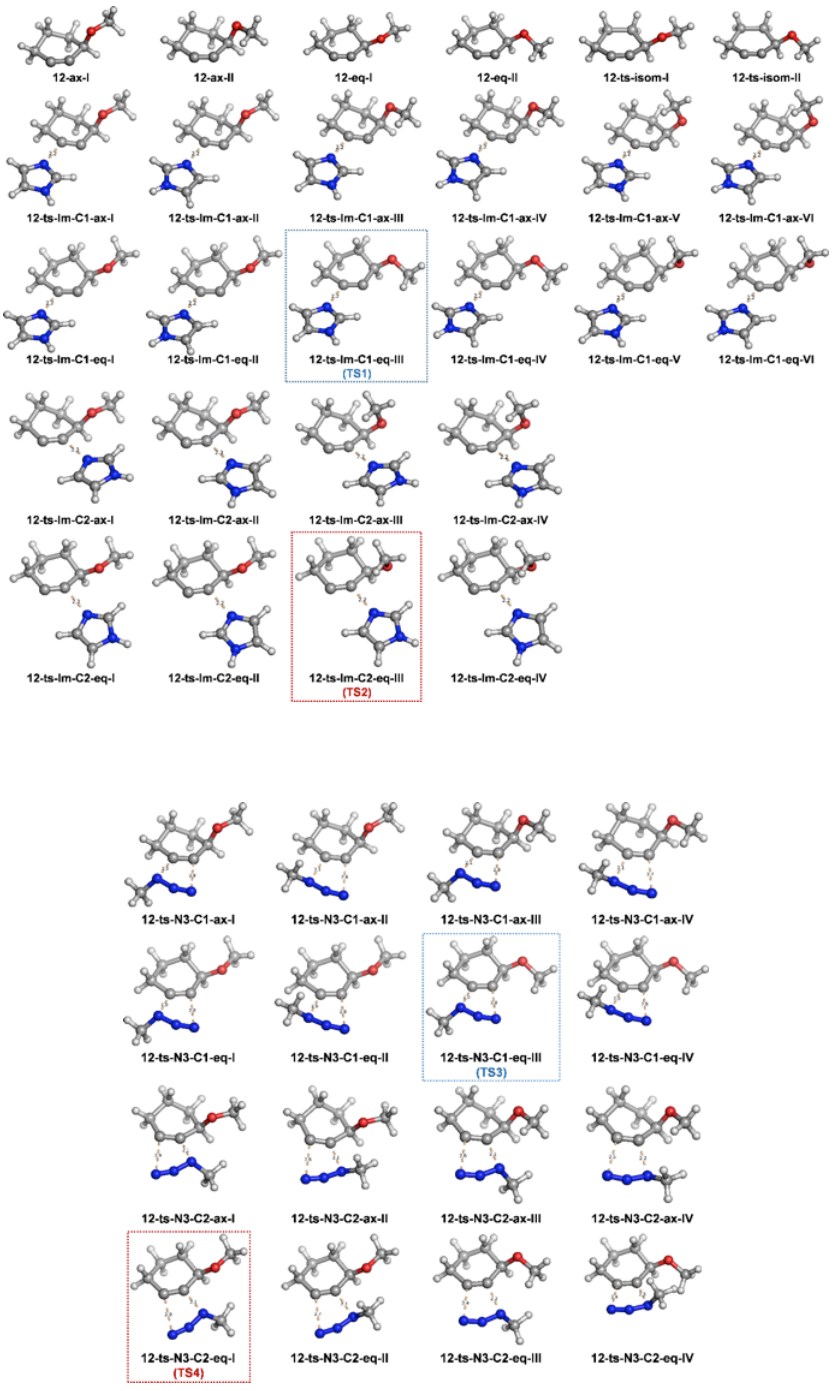

Figure 4.6. **Geometries calculated at the PCM(THF)/M06-2X/6-311+G(2d,p) level.** The minimum energy transition states for 3-methoxycyclohexyne are labeled as TS4.1–TS4.4 as shown in Figure 4.4

4.5.3.2 Table 4.3. Energies, Enthalpies, Free Energies, and Entropies of the Structures Calculated at the PCM(THF)/M06-2X/6-11+G(2d,p) level

Structure	E_0	E_0+ZPE	H	S	G	Lowest freq.
	(Hartree)[a]	(Hartree)[a]	(Hartree)[a]	(cal mol^{-1} K^{-1})[b]	(Hartree)[a]	(cm^{-1})
methylazide	–204.069524	–204.018649	–204.013286	67.2	–204.045233	105.8
imidazole	–226.202555	–226.130419	–226.125799	64.9	–226.156640	573.7
1	–230.878167	–230.802434	–230.797046	68.9	–230.829767	393.9
1-ts-N3	–434.950394	–434.822419	–434.811989	97.9	–434.858514	–116.3
11-I	–345.400552	–345.291894	–345.283997	82.2	–345.323071	88.1
11-II	–345.397789	–345.288702	–345.280992	81.1	–345.319529	100.3
11-ts-N3_C1-I	–549.475642	–549.315051	–549.301834	113.2	–549.355610	–22.2
11-ts-N3_C1-II	–549.472332	–549.311289	–549.298277	112.0	–549.351475	–65.0
11-ts-N3_C2-I	–549.468182	–549.306996	–549.294232	109.0	–549.346033	–258.2
11-ts-N3_C2-II	–549.468606	–549.307182	–549.294315	110.1	–549.346617	–127.0
4-II	–193.938760	–193.847196	–193.840924	74.8	–193.876483	18.2
4-I	–193.931905	–193.839749	–193.833657	71.2	–193.867484	166.4
4-III	–193.934091	–193.843322	–193.837020	73.5	–193.871964	64.2
3-I	–233.294602	–233.172350	–233.165836	73.6	–233.200822	220.2
3-ts-rearr	–233.266845	–233.145944	–233.139629	73.5	–233.174555	–279.9
3-II	–233.274581	–233.153708	–233.146671	79.2	–233.184308	22.6
3-ts-N3-I	–437.358527	–437.183951	–437.172698	99.9	–437.220178	–254.5
3-ts-N3-II	–437.358352	–437.183755	–437.172485	100.1	–437.220035	–262.7
3-ts-Im-I	–459.490404	–459.294913	–459.284066	100.3	–459.331718	–149.5
3-ts-Im-II	–459.489721	–459.294291	–459.283418	100.6	–459.331231	–149.6
12-ax-I	–347.804816	–347.649578	–347.640560	87.4	–347.682085	76.6
12-ax-II	–347.808374	–347.652964	–347.644036	86.6	–347.685177	91.2
12-eq-I	–347.805789	–347.650487	–347.641527	87.0	–347.682843	77.7

12-eq-II	–347.809663	–347.654307	–347.645385	86.5	–347.686470	101.3
12-ts-isom-I	–347.794583	–347.639455	–347.630927	85.7	–347.671634	–195.1
12-ts-isom-II	–347.797951	–347.642836	–347.634293	85.8	–347.675050	–189.8
12-ts-N3-C1-ax-I	–551.869777	–551.662152	–551.648313	113.7	–551.702345	–232.6
12-ts-N3-C1-ax-II	–551.869730	–551.662041	–551.648227	113.4	–551.702127	–238.6
12-ts-N3-C1-ax-III	–551.873313	–551.665602	–551.651815	113.3	–551.705641	–248.6
12-ts-N3-C1-ax-IV	–551.873040	–551.665315	–551.651532	113.3	–551.705373	–255.8
12-ts-N3-C1-eq-I	–551.872162	–551.664584	–551.650777	113.5	–551.704692	–215.3
12-ts-N3-C1-eq-II	–551.872052	–551.664345	–551.650636	112.5	–551.704111	–215.3
12-ts-N3-C1-eq-III	–551.875995	–551.668317	–551.654566	112.9	–551.708230	–228.1
12-ts-N3-C1-eq-IV	–551.875920	–551.668118	–551.654438	112.5	–551.707867	–231.7
12-ts-N3-C2-ax-I	–551.870525	–551.662842	–551.649073	112.8	–551.702648	–199.5
12-ts-N3-C2-ax-II	–551.871266	–551.663722	–551.649931	112.9	–551.703574	–212.5
12-ts-N3-C2-ax-III	–551.871594	–551.663903	–551.650166	112.8	–551.703737	–290.4
12-ts-N3-C2-ax-IV	–551.870128	–551.662248	–551.648653	111.6	–551.701666	–315.8
12-ts-N3-C2-eq-I	–551.871229	–551.663389	–551.649739	111.3	–551.702638	–211.7
12-ts-N3-C2-eq-II	–551.870799	–551.663099	–551.649324	112.9	–551.702944	–254.1
12-ts-N3-C2-eq-III	–551.870263	–551.662308	–551.648696	111.8	–551.701819	–340.1
12-ts-N3-C2-eq-IV	–551.869761	–551.661668	–551.648058	112.1	–551.701326	–351.3
12-ts-Im-C1-ax-I	–574.002341	–573.773880	–573.760421	114.7	–573.814916	–136.3
12-ts-Im-C1-ax-II	–574.001586	–573.773181	–573.759691	115.1	–573.814384	–137.7
12-ts-Im-C1-ax-III	–574.005826	–573.777163	–573.763818	113.3	–573.817653	–140.7
12-ts-Im-C1-ax-IV	–574.005155	–573.776492	–573.763141	113.4	–573.817012	–139.9
12-ts-Im-C1-ax-V	–574.002596	–573.773656	–573.760443	112.6	–573.813920	–144.4
12-ts-Im-C1-ax-VI	–574.001827	–573.772935	–573.759692	113.0	–573.813401	–144.6
12-ts-Im-C1-eq-I	–574.005167	–573.776671	–573.763283	113.7	–573.817317	–130.2
12-ts-Im-C1-eq-II	–574.004410	–573.775909	–573.762522	113.8	–573.816572	–128.6

12-ts-Im-C1-eq-III	–574.009116	–573.780513	–573.767187	112.9	–573.820843	–134.7
12-ts-Im-C1-eq-IV	–574.008479	–573.779863	–573.766533	113.1	–573.820249	–131.7
12-ts-Im-C1-eq-V	–574.006685	–573.778075	–573.764687	113.9	–573.818796	–135.3
12-ts-Im-C1-eq-VI	–574.006004	–573.777504	–573.764062	114.8	–573.818605	–133.5
12-ts-Im-C2-ax-I	–574.002396	–573.774125	–573.760587	114.9	–573.815185	–122.8
12-ts-Im-C2-ax-II	–574.002866	–573.774556	–573.761054	114.4	–573.815409	–121.7
12-ts-Im-C2-ax-III	–574.003910	–573.775438	–573.762030	113.8	–573.816099	–122.4
12-ts-Im-C2-ax-IV	–574.003894	–573.775305	–573.761943	113.2	–573.815751	–119.8
12-ts-Im-C2-eq-I	–574.002460	–573.774222	–573.760689	114.7	–573.815201	–116.9
12-ts-Im-C2-eq-II	–574.002531	–573.774280	–573.760734	115.1	–573.815434	–119.5
12-ts-Im-C2-eq-III	–574.004123	–573.775543	–573.762113	113.8	–573.816198	–129.3
12-ts-Im-C2-eq-IV	–574.004223	–573.775521	–573.762168	112.7	–573.815730	–129.0

[a] 1 Hartree = 627.5 kcal mol^{-1}. [b] Thermal corrections at 298.15 K.

4.5.3.3 Cartesian Coordinates of the Structures Calculated at the PCM(THF)/M06-2X/6-311+G(2d,p) level

Cartesian coordinates for the optimized structures have been previously reported.[39]

4.6 Spectra Relevant to Chapter Four:

Cycloadditions of Cyclohexynes and Cyclopentyne

Jose M. Medina, Travis C. McMahon, Gonzalo Jimenez-Oses,

K. N. Houk, and Neil K. Garg

J. Am. Chem. Soc. **2014**, *136*, 14706–14709.

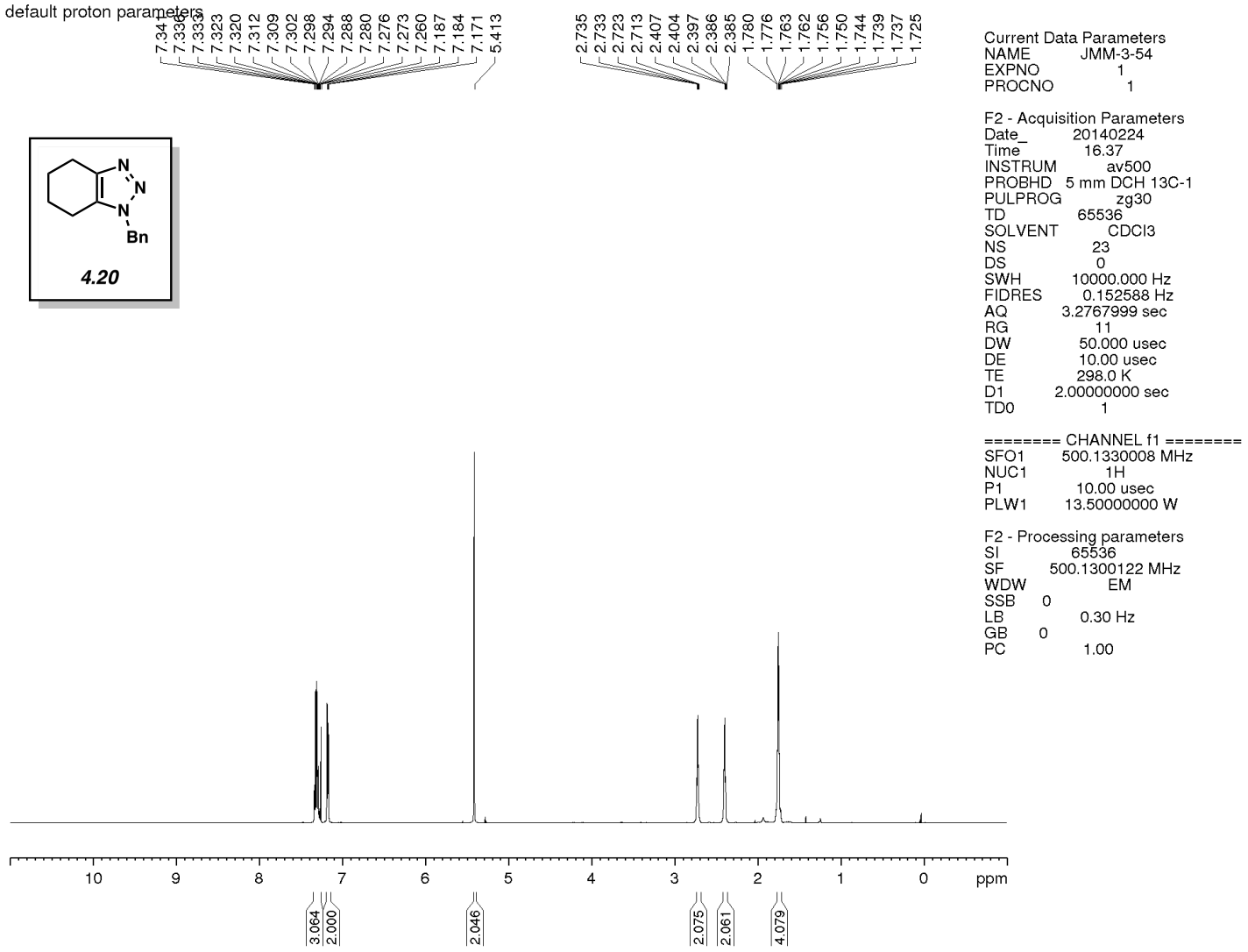

Figure 4.7. ^{1}H NMR (500 MHz, $CDCl_3$) compound **4.20**

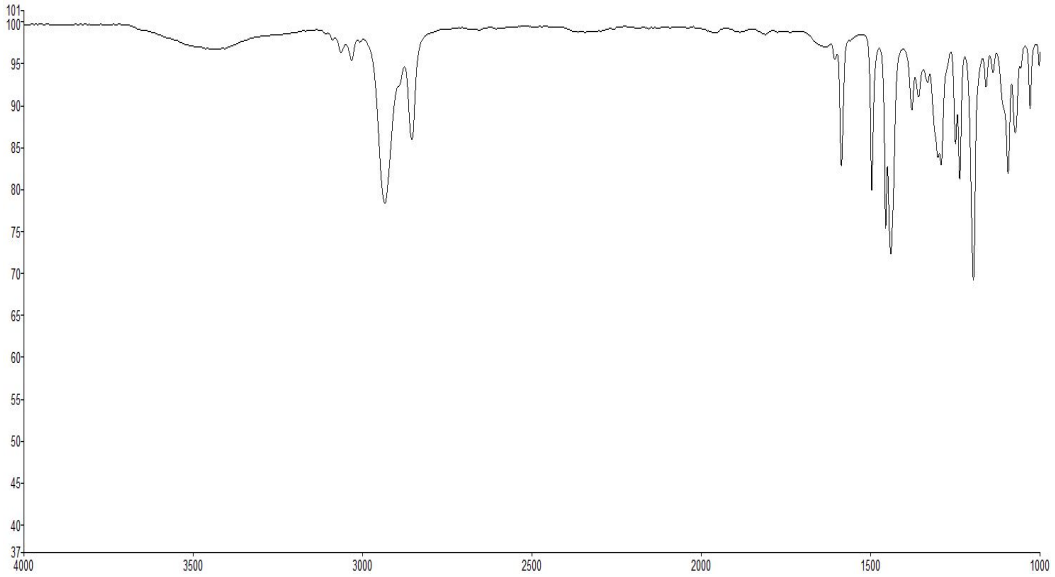

Figure 4.8. Infrared spectrum of compound **4.20**

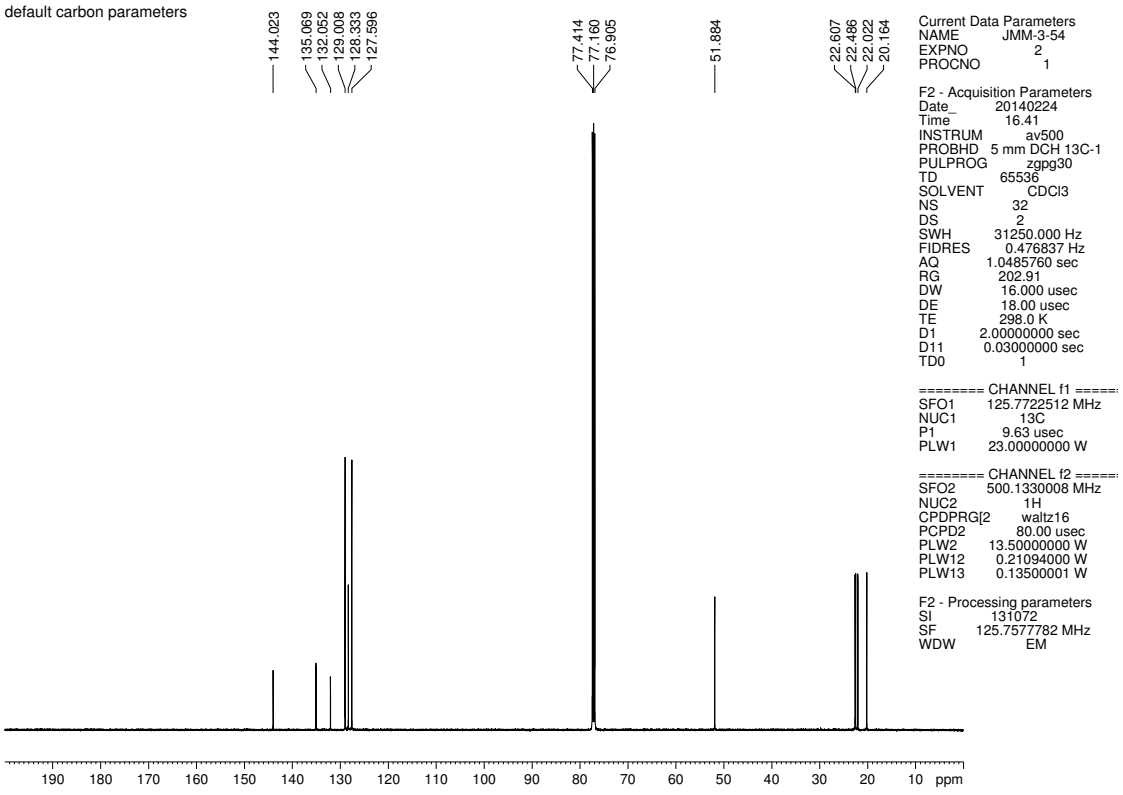

Figure 4.9. ^{13}C NMR (125 MHz, $CDCl_3$) of compound **4.20**

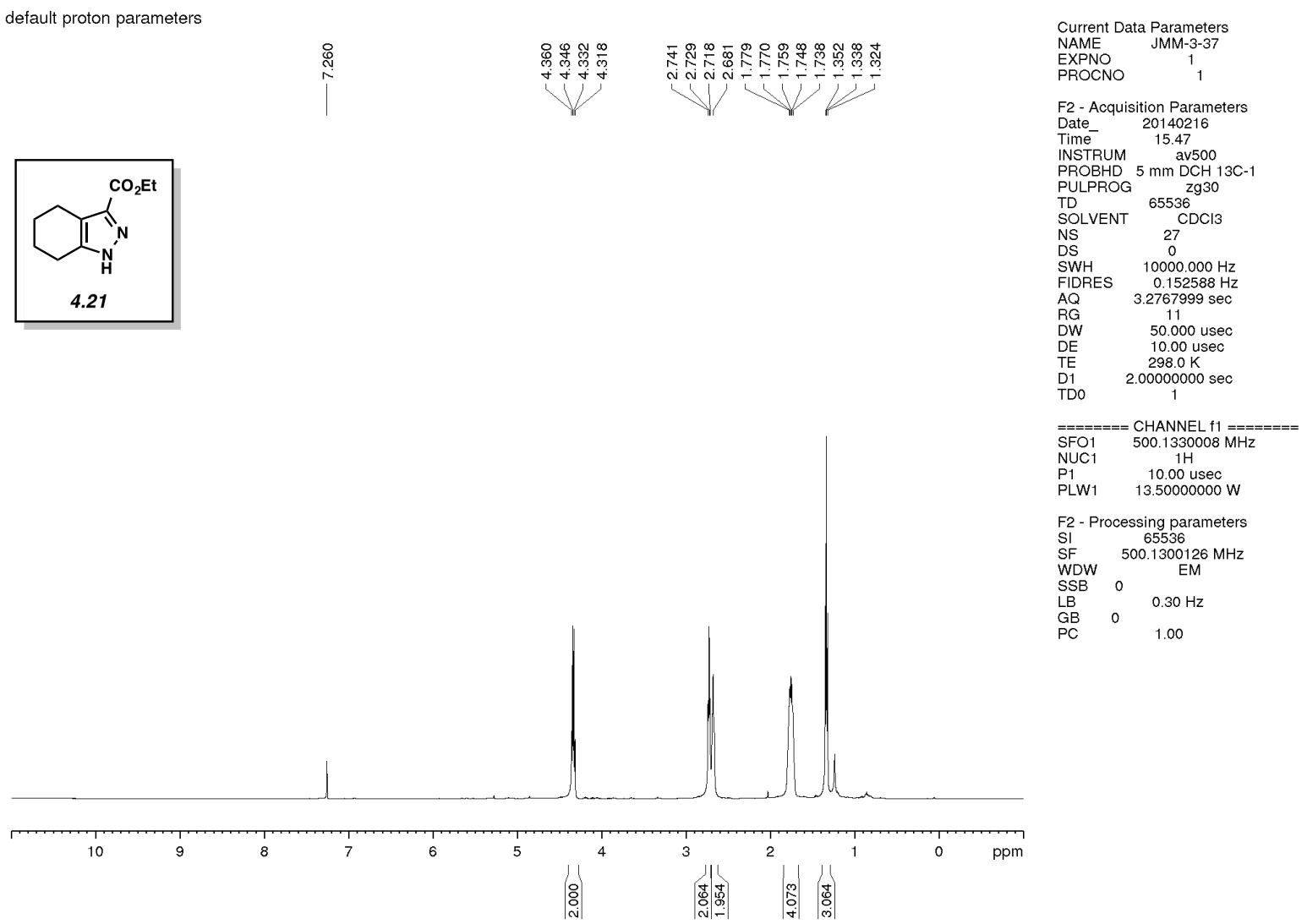

Figure 4.10. ^{1}H NMR (500 MHz, $CDCl_3$) compound **4.21**

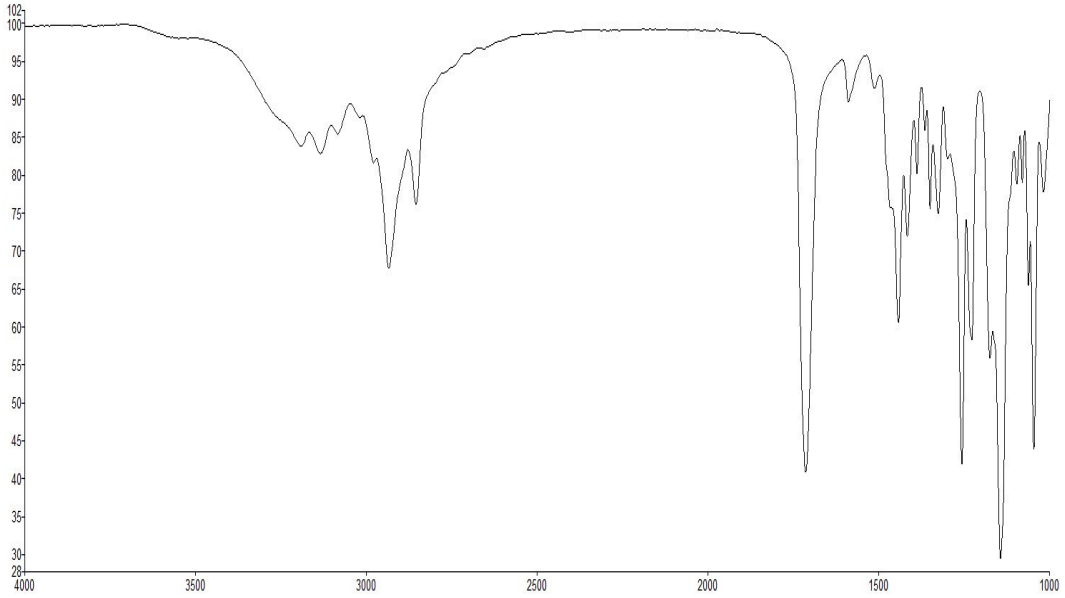

Figure 4.11. Infrared spectrum of compound **4.21**

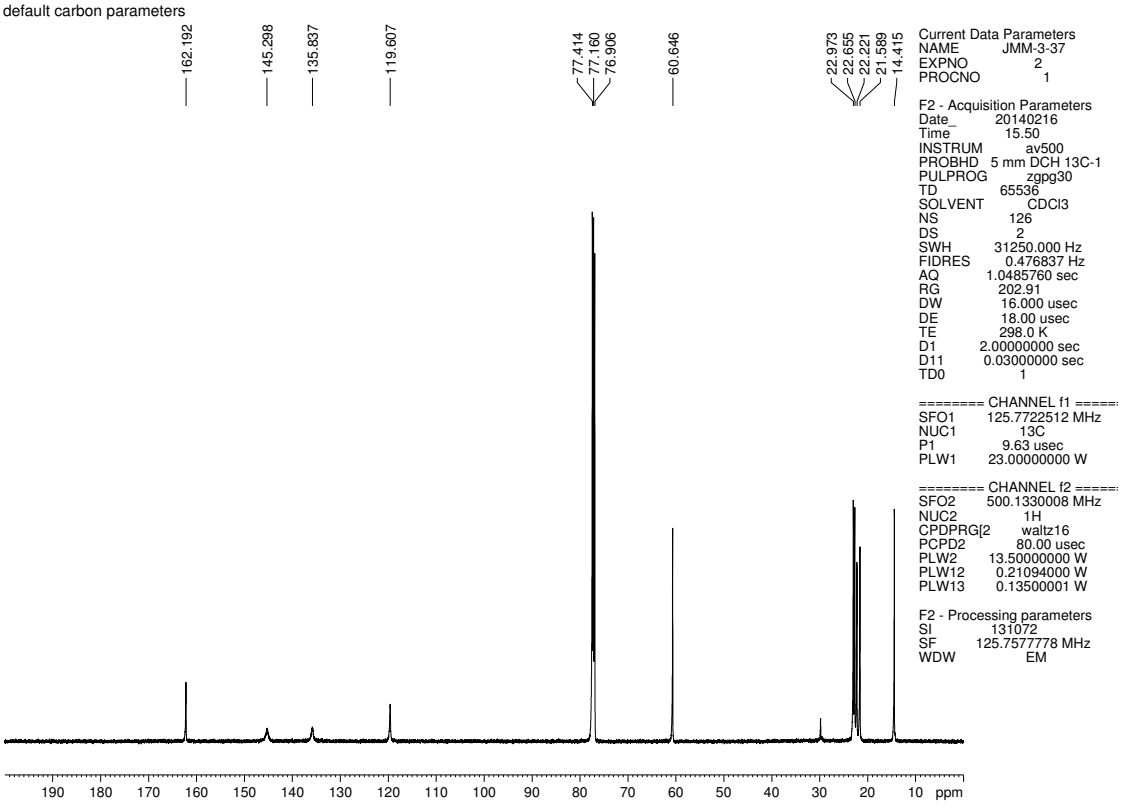

Figure 4.12. ^{13}C NMR (125 MHz, $CDCl_3$) of compound **4.21**

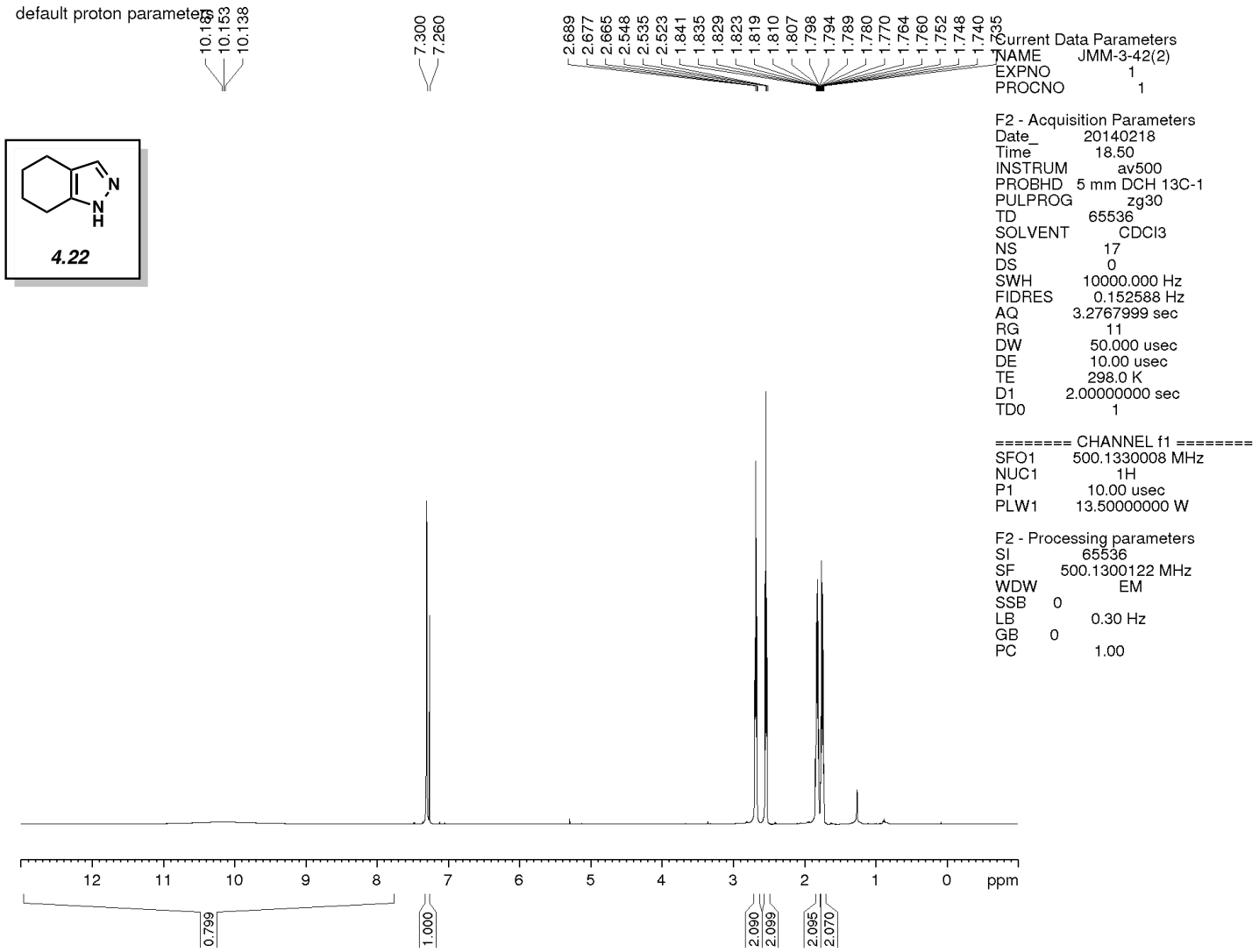

Figure 4.13. ^{1}H NMR (500 MHz, $CDCl_3$) compound **4.22**

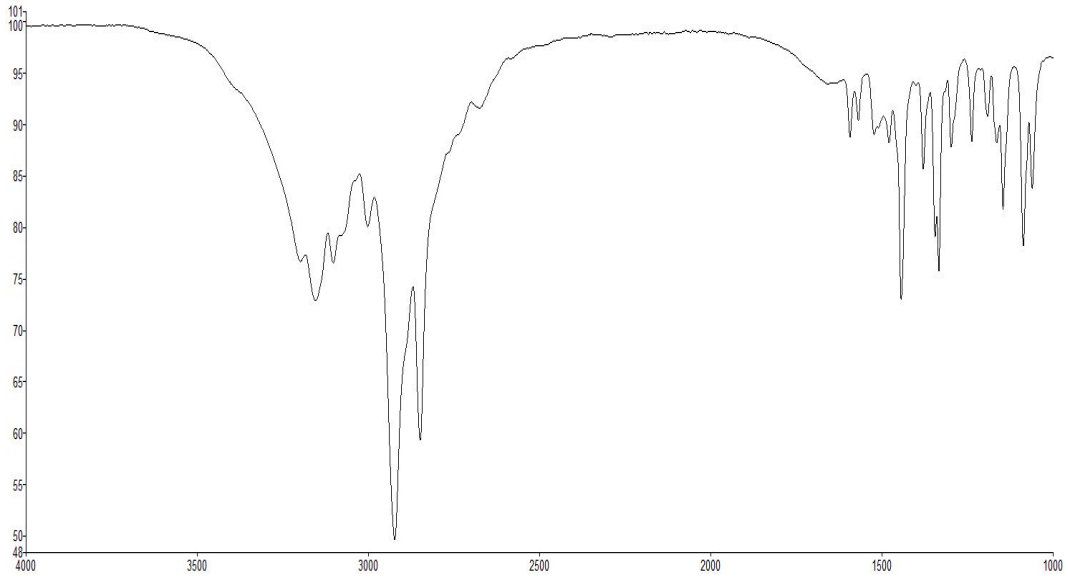

Figure 4.14. Infrared spectrum of compound **4.22**

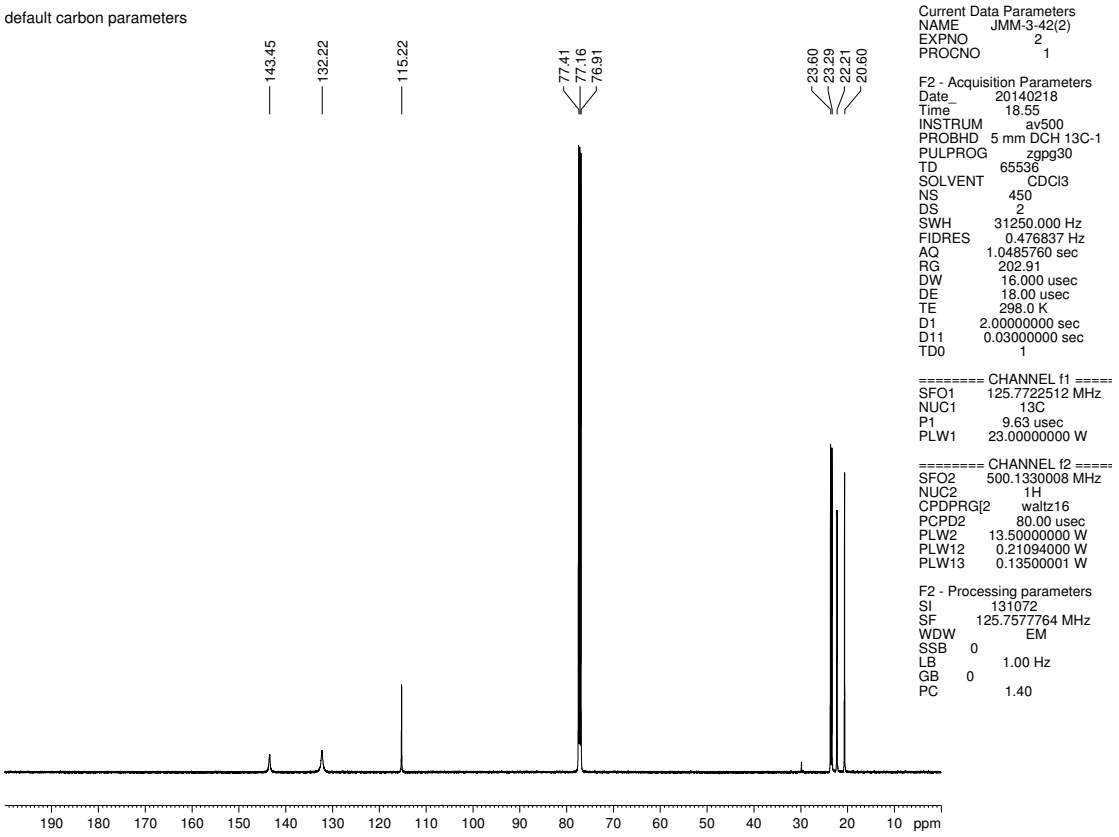

Figure 4.15. ^{13}C NMR (125 MHz, $CDCl_3$) of compound **4.22**

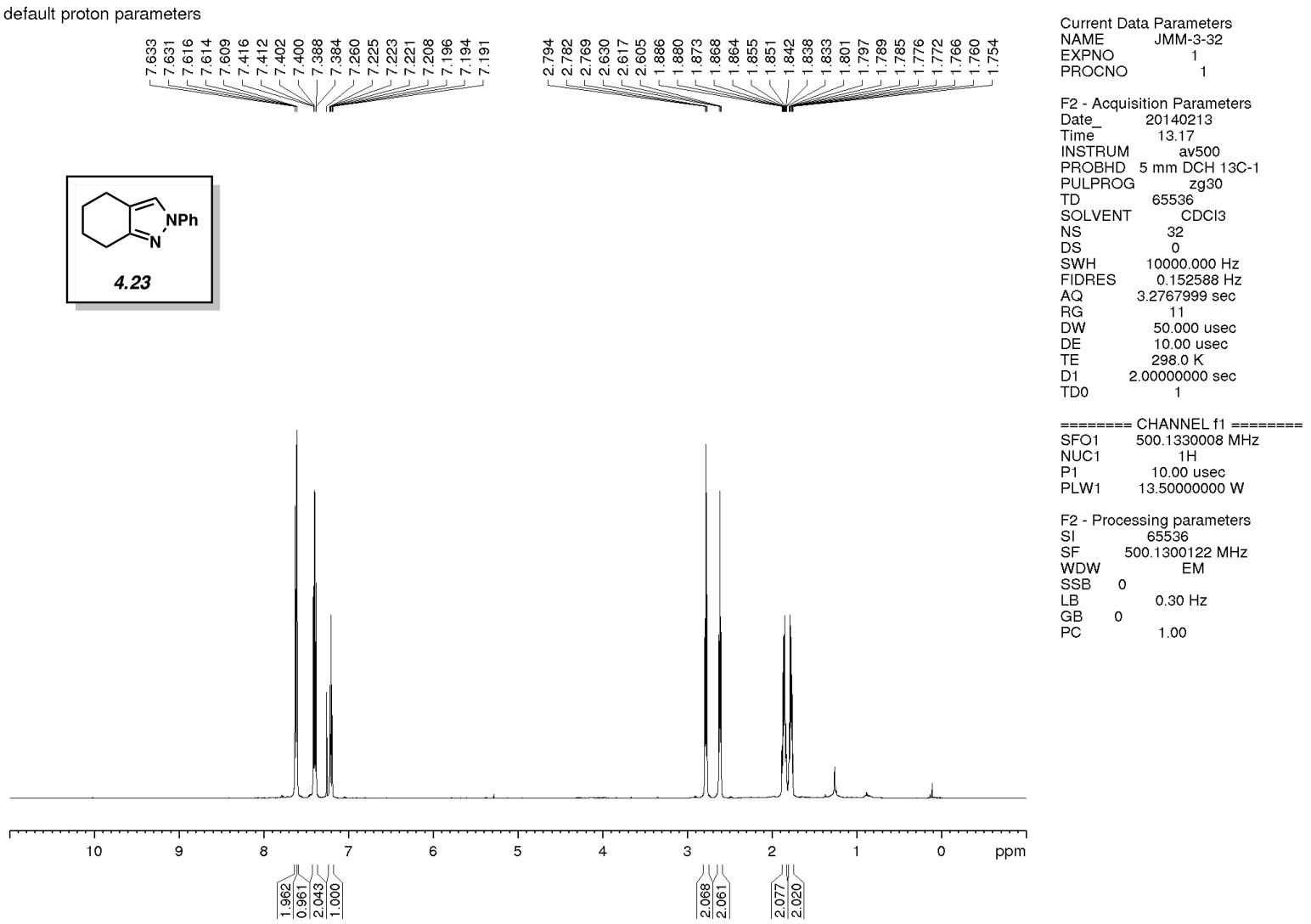

Figure 4.16. ^{1}H NMR (500 MHz, $CDCl_3$) compound **4.23**

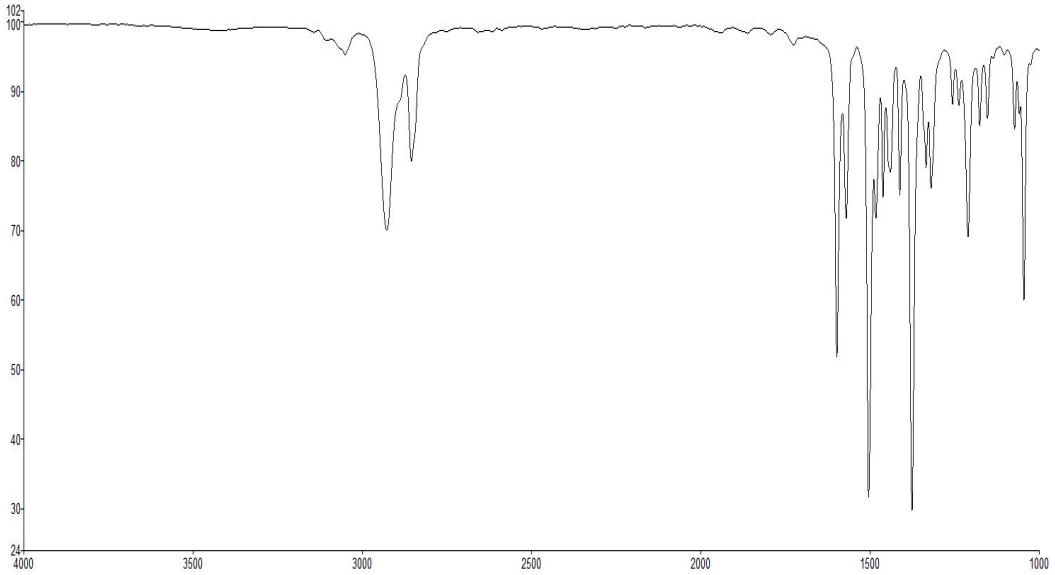

Figure 4.17. Infrared spectrum of compound **4.23**

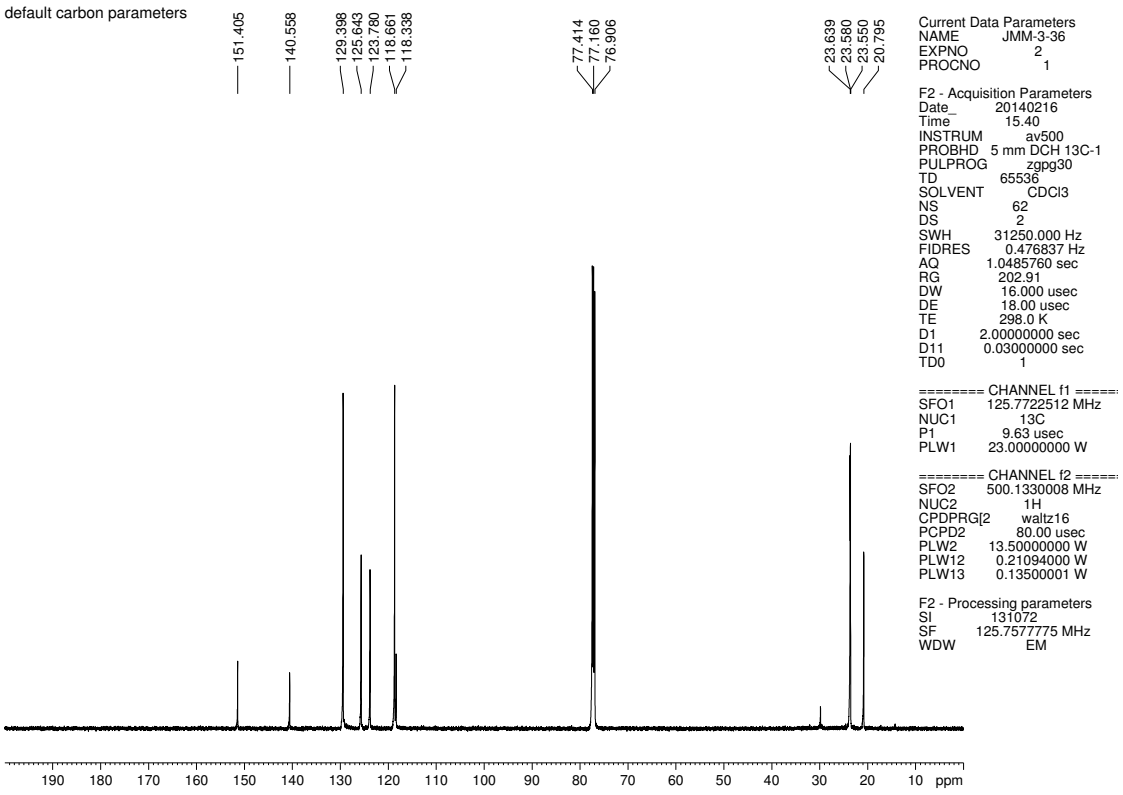

Figure 4.18. ^{13}C NMR (125 MHz, $CDCl_3$) of compound **4.23**

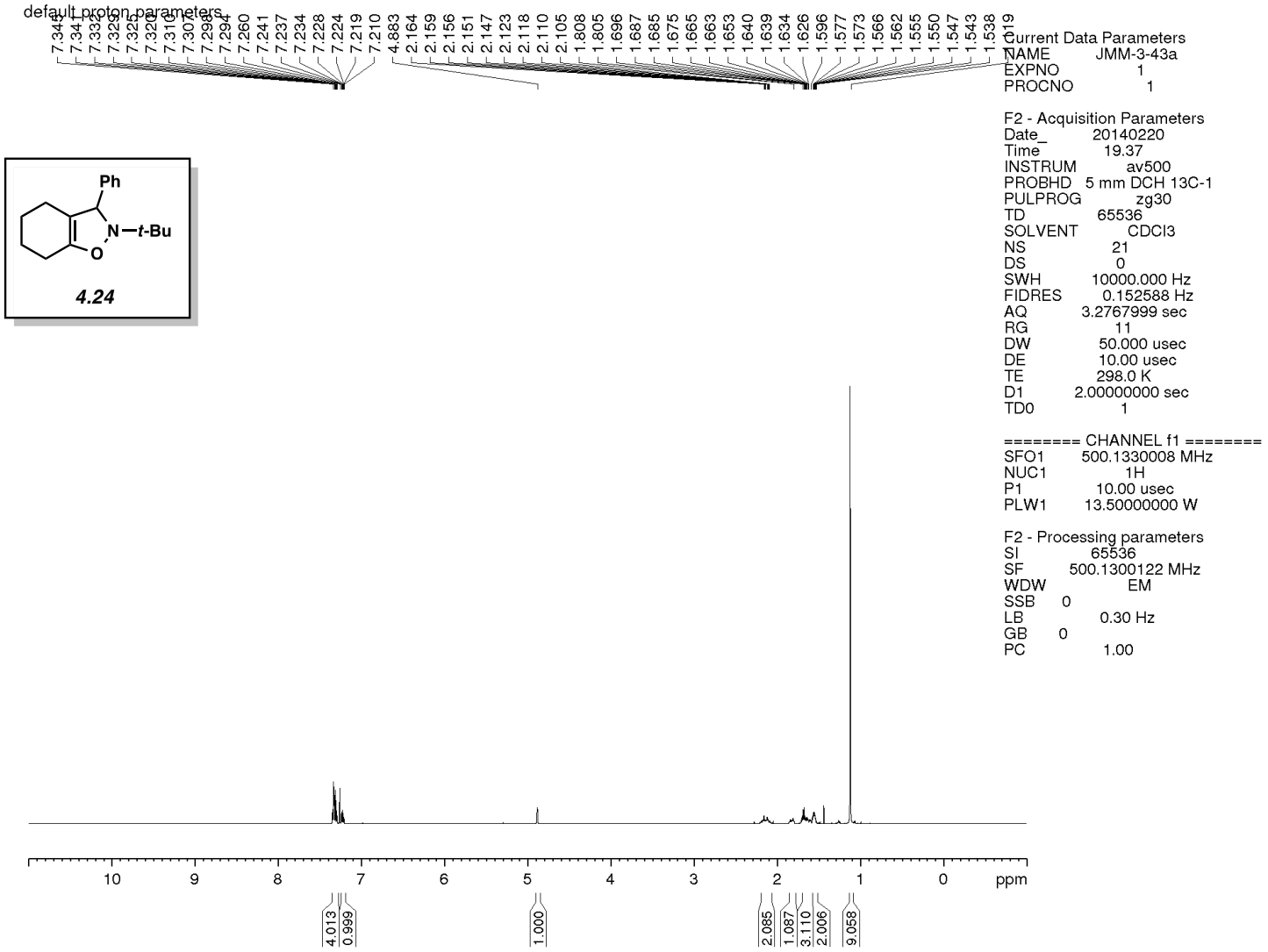

Figure 4.19. ^{1}H NMR (500 MHz, $CDCl_3$) compound **4.24**

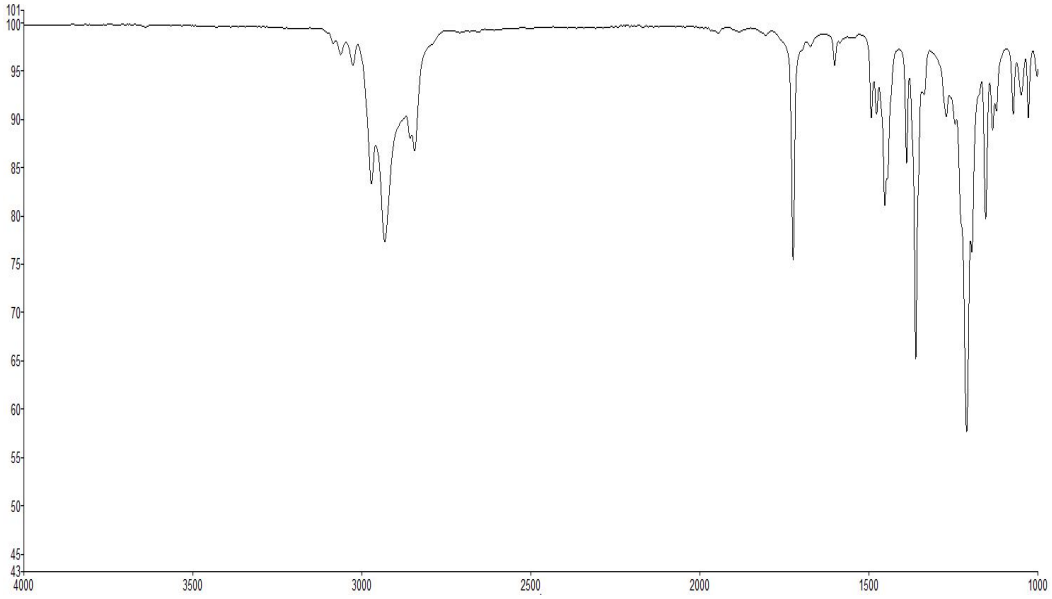

Figure 4.20. Infrared spectrum of compound **4.24**

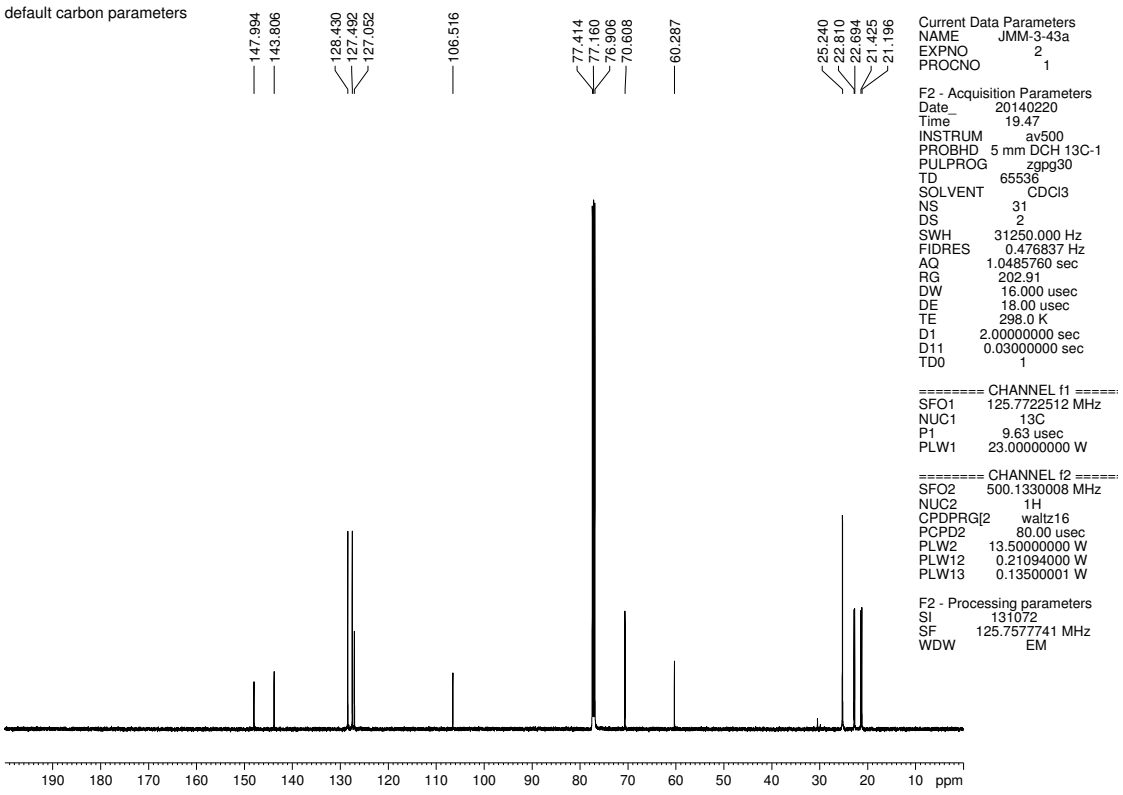

Figure 4.21. ^{13}C NMR (125 MHz, $CDCl_3$) of compound **4.24**

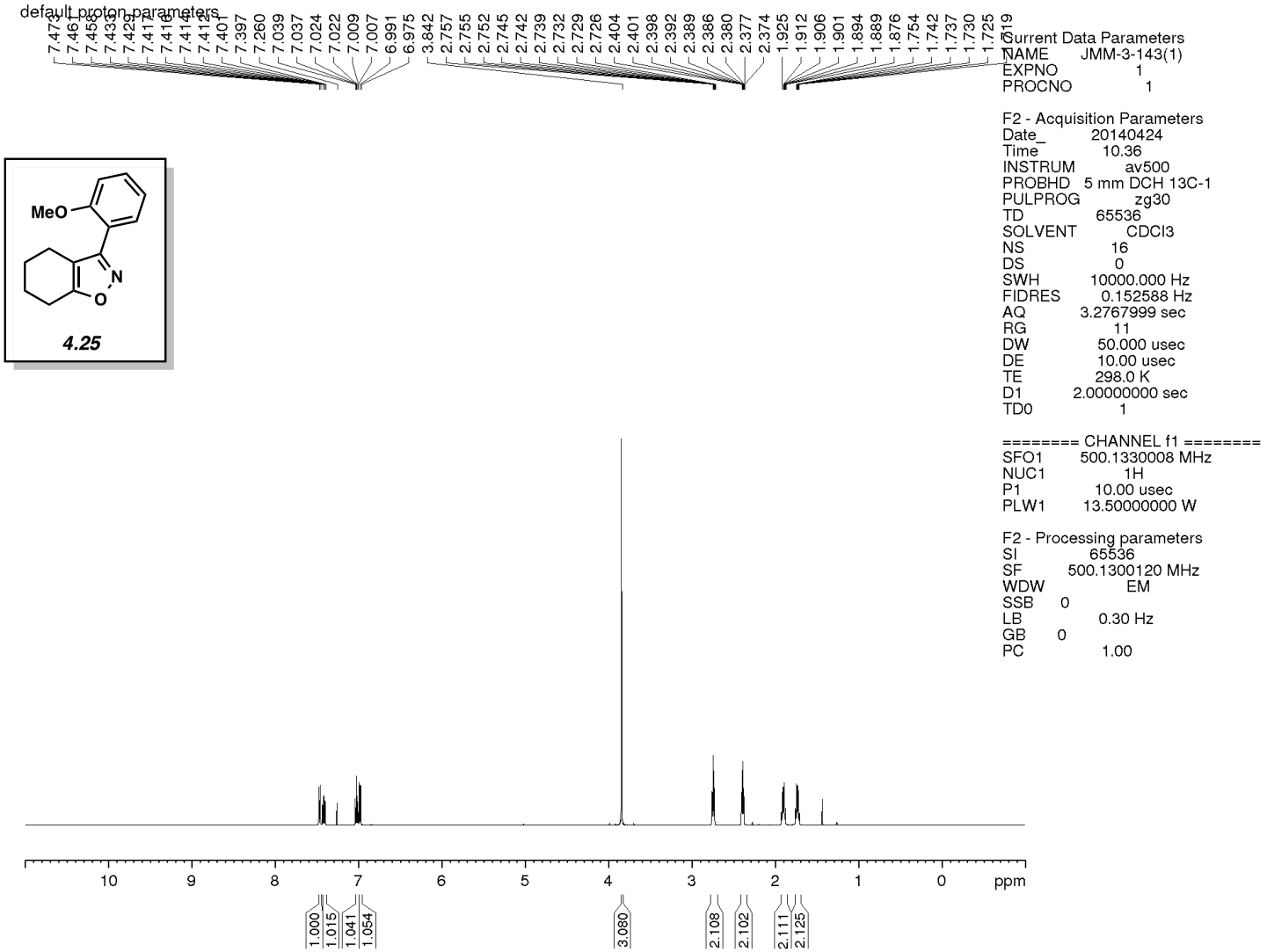

Figure 4.22. ^{1}H NMR (500 MHz, $CDCl_3$) compound **4.25**

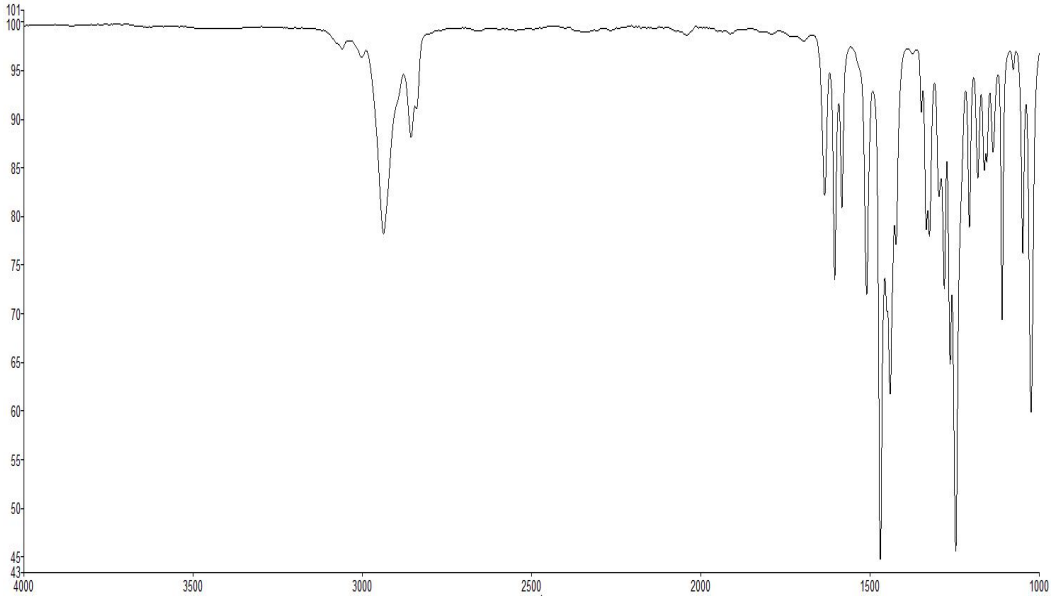

Figure 4.23. Infrared spectrum of compound **4.25**

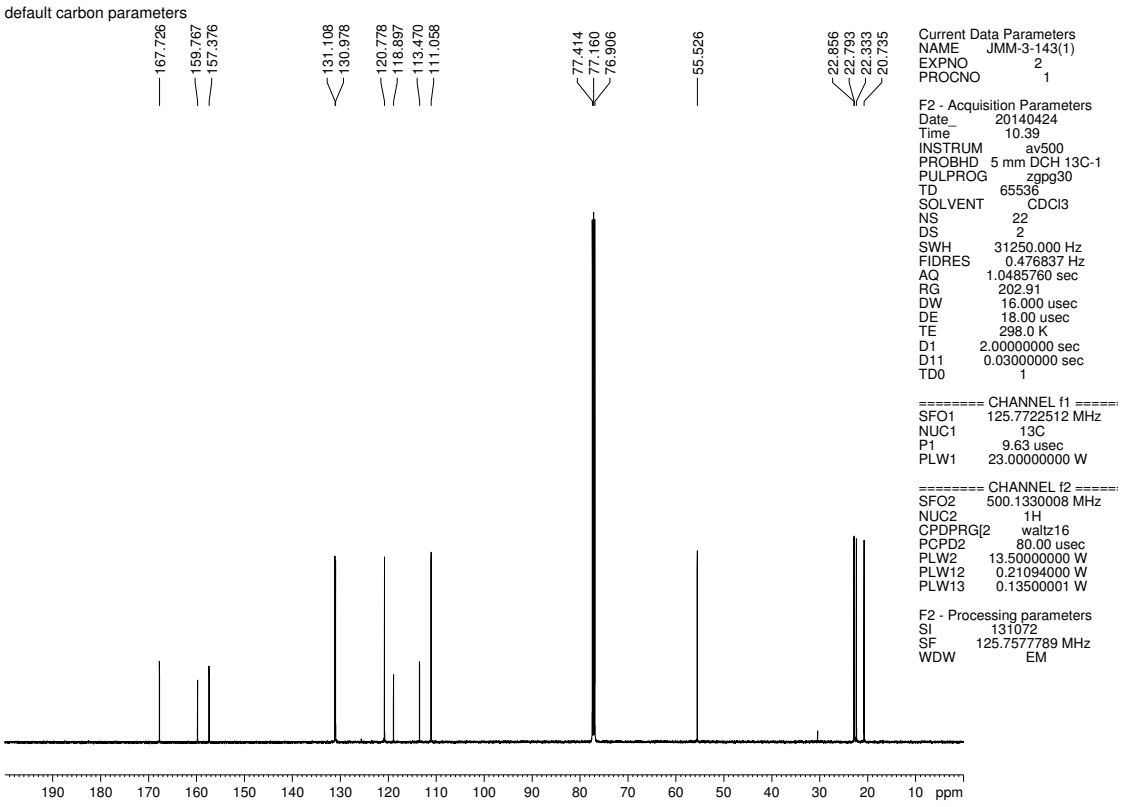

Figure 4.24. ^{13}C NMR (125 MHz, $CDCl_3$) of compound **4.25**

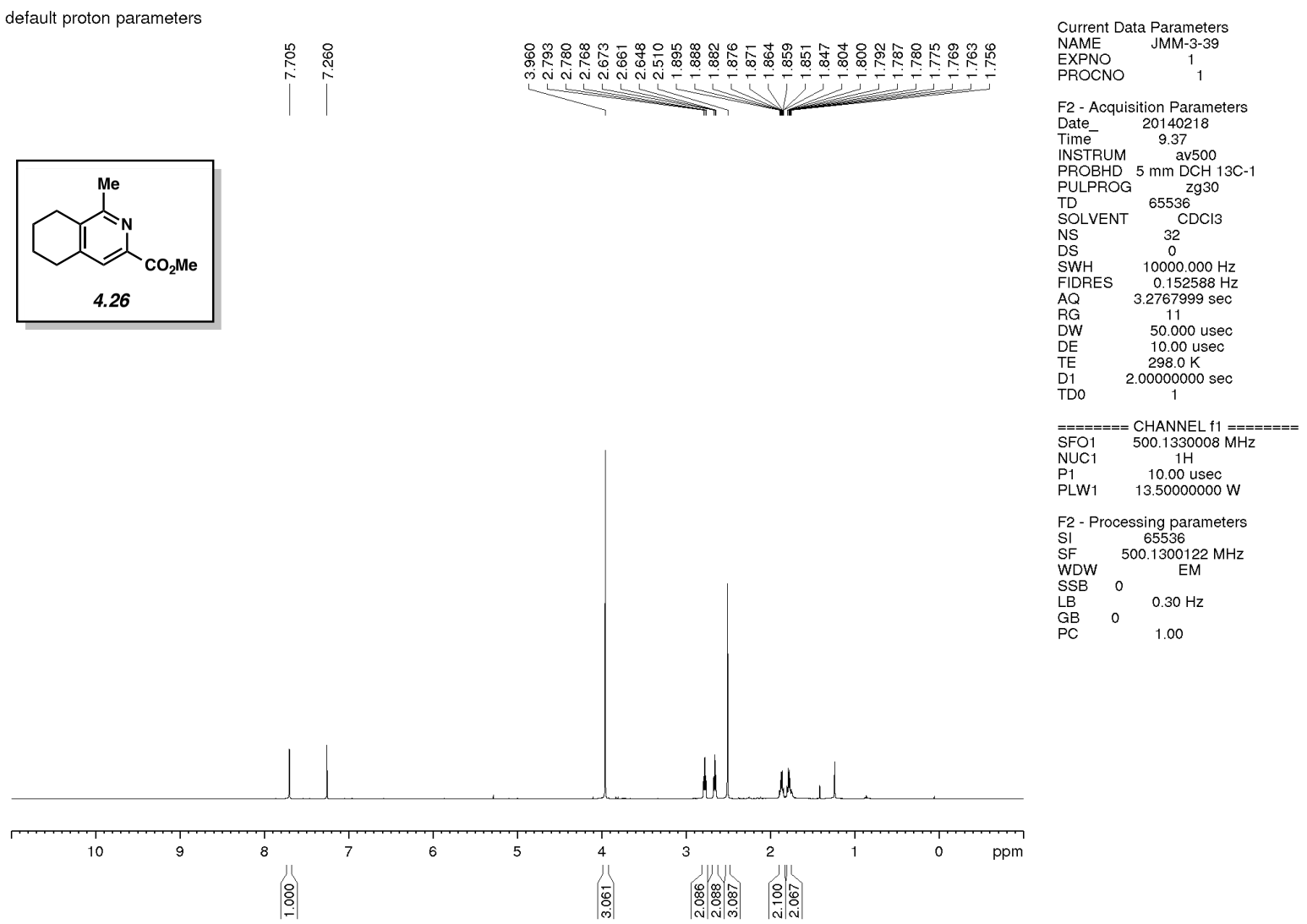

Figure 4.25. ^{1}H NMR (500 MHz, $CDCl_3$) compound **4.26**

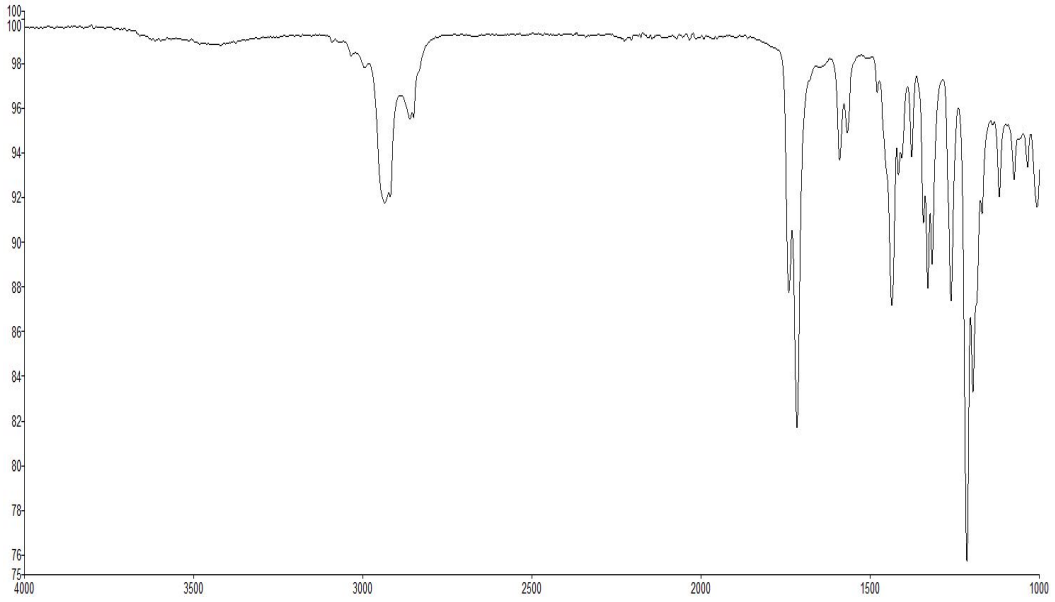

Figure 4.26. Infrared spectrum of compound **4.26**

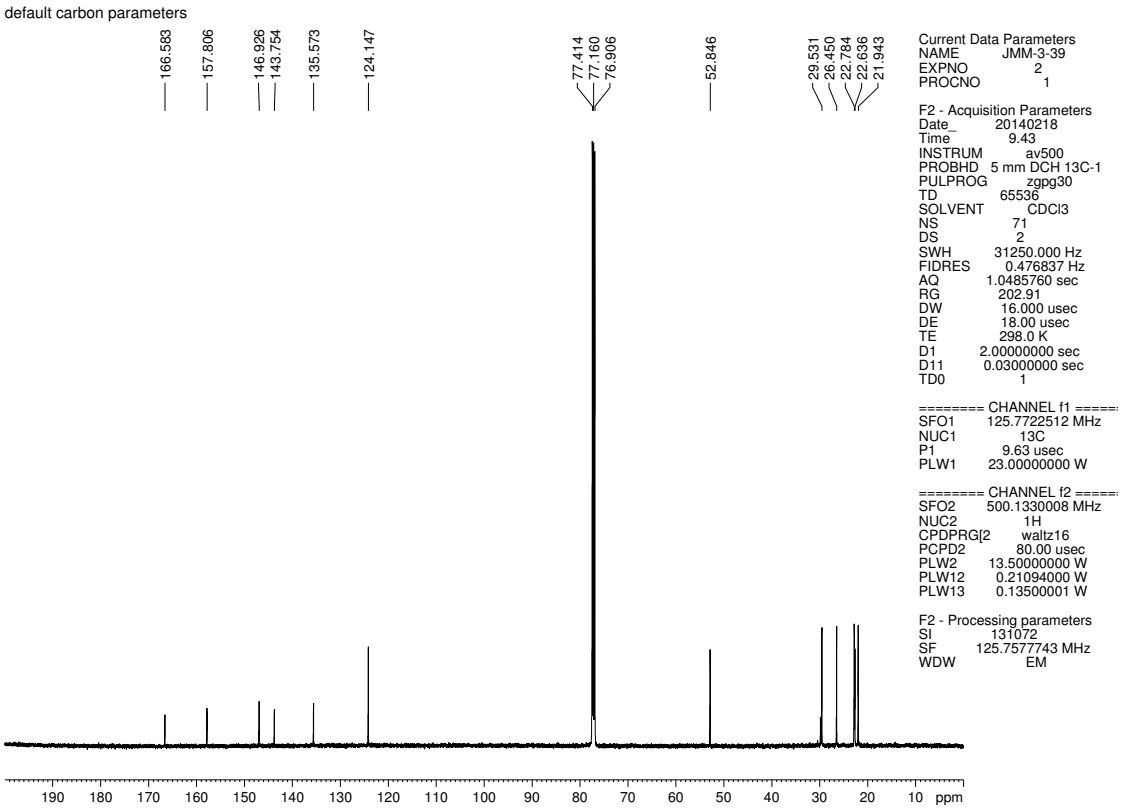

Figure 4.27. ^{13}C NMR (125 MHz, $CDCl_3$) of compound **4.26**

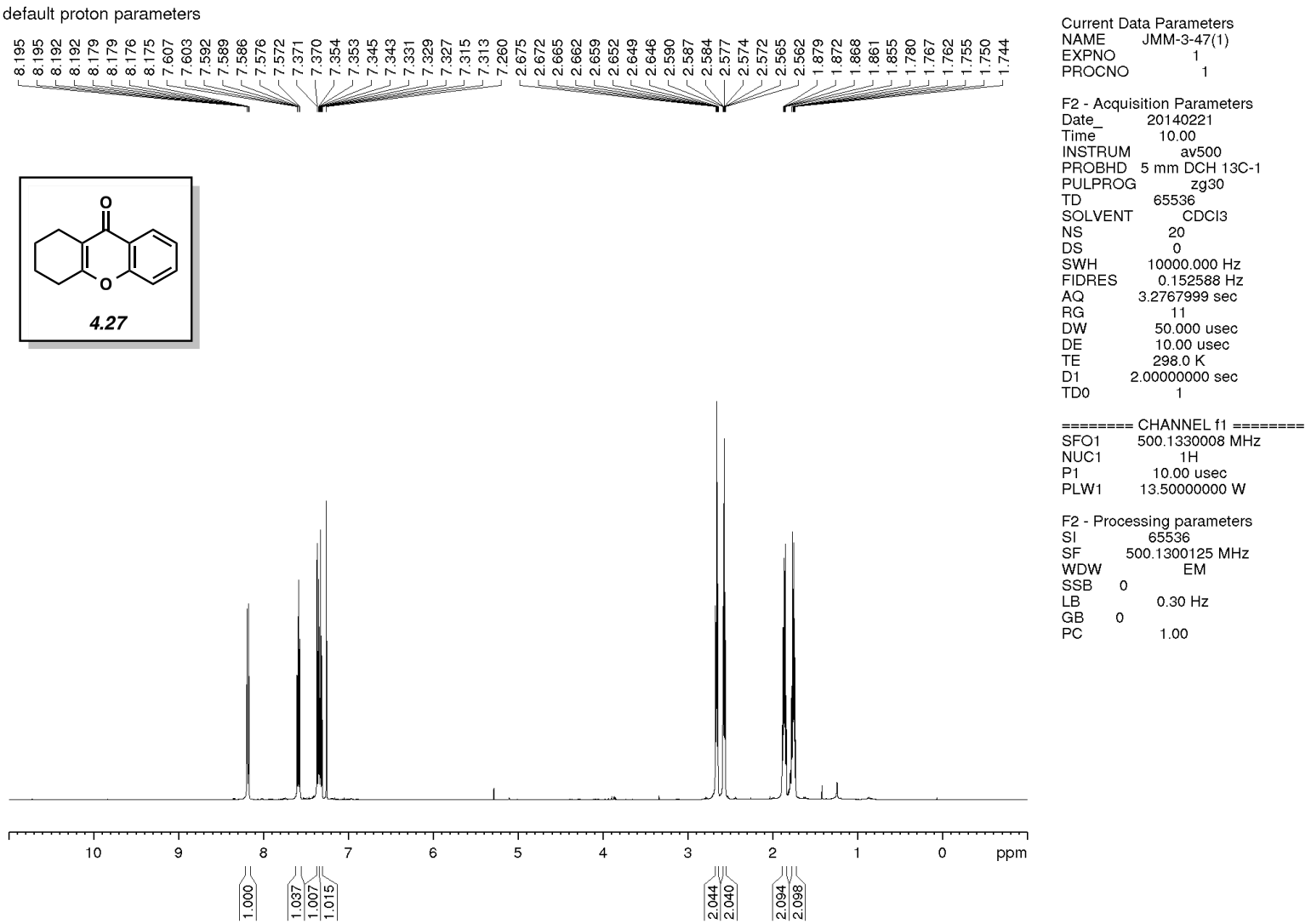

Figure 4.28. ^{1}H NMR (500 MHz, $CDCl_3$) compound **4.27**

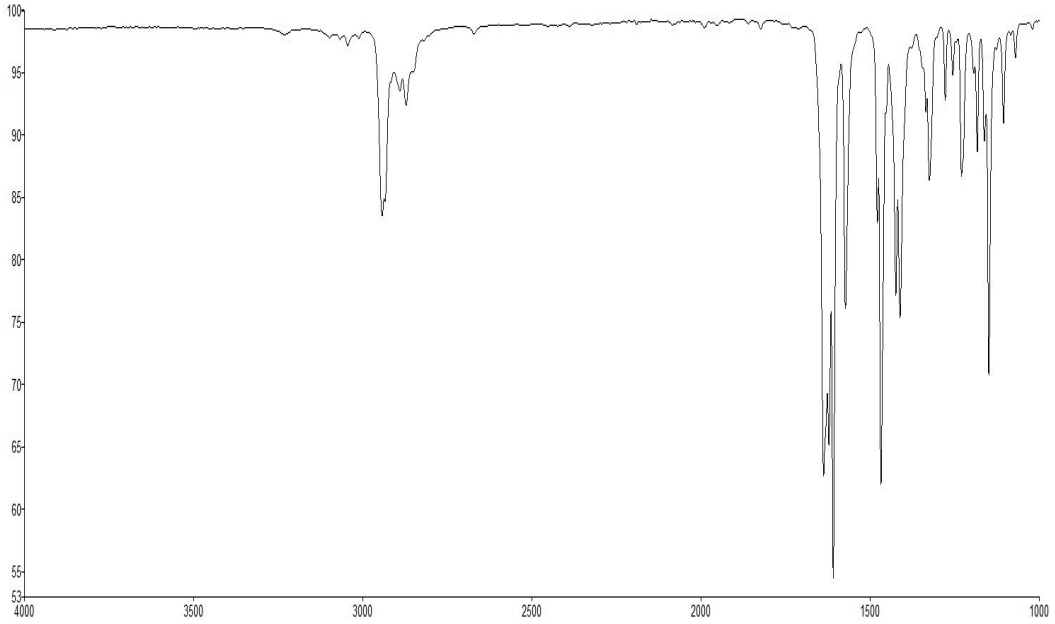

Figure 4.29. Infrared spectrum of compound **4.27**

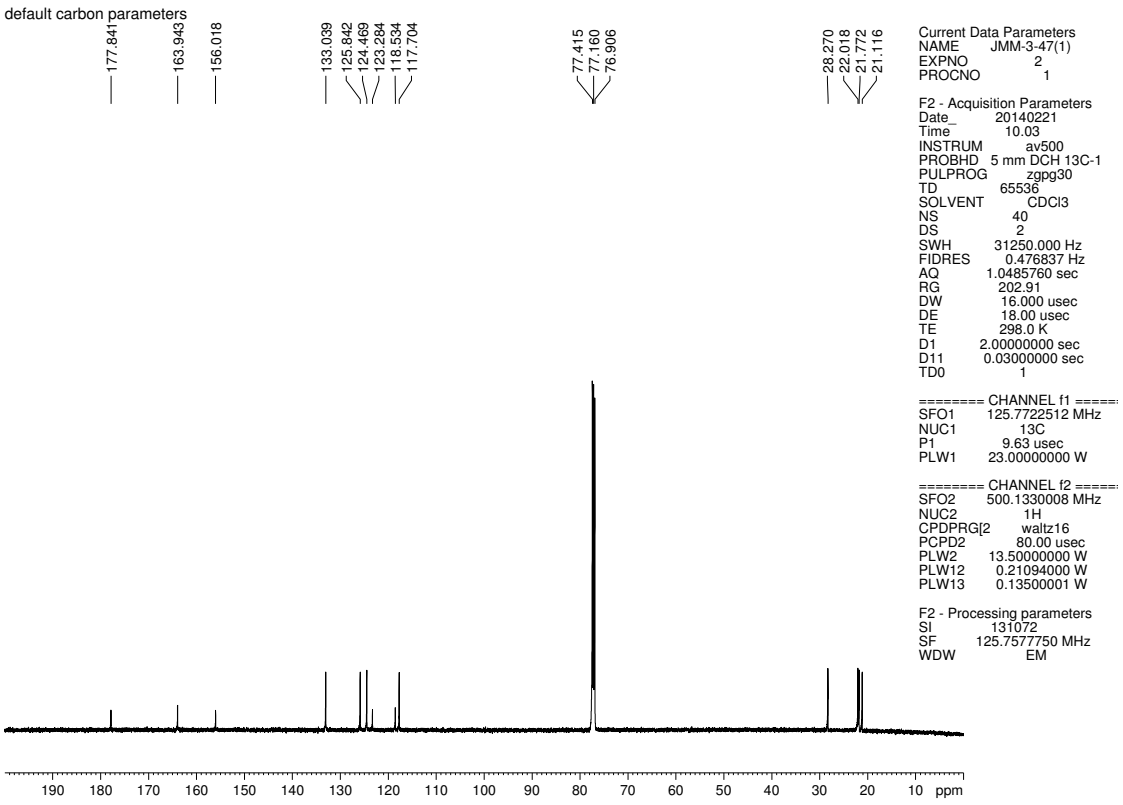

Figure 4.30. ^{13}C NMR (125 MHz, $CDCl_3$) of compound **4.27**

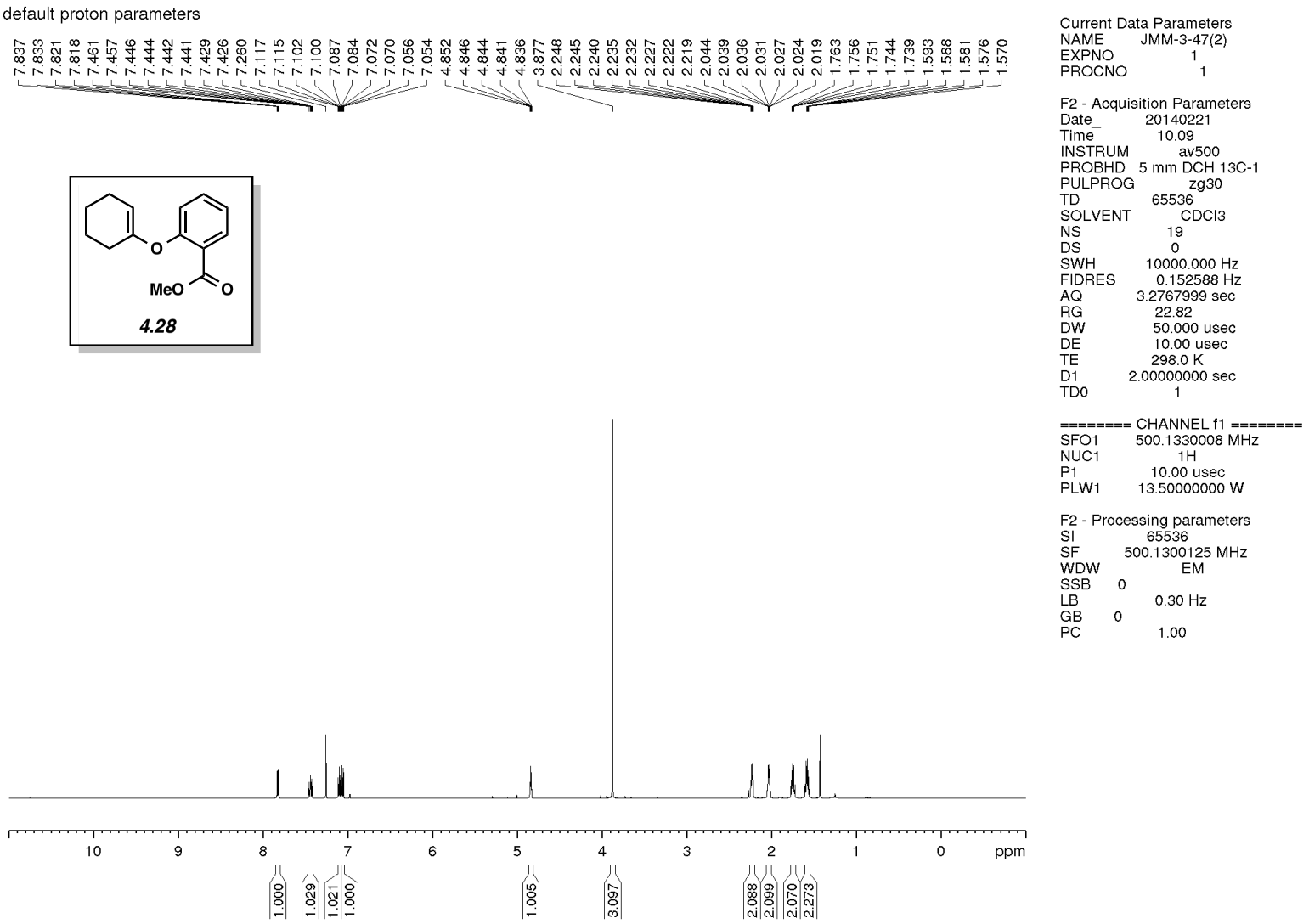

Figure 4.31. ^{1}H NMR (500 MHz, $CDCl_3$) compound **4.28**

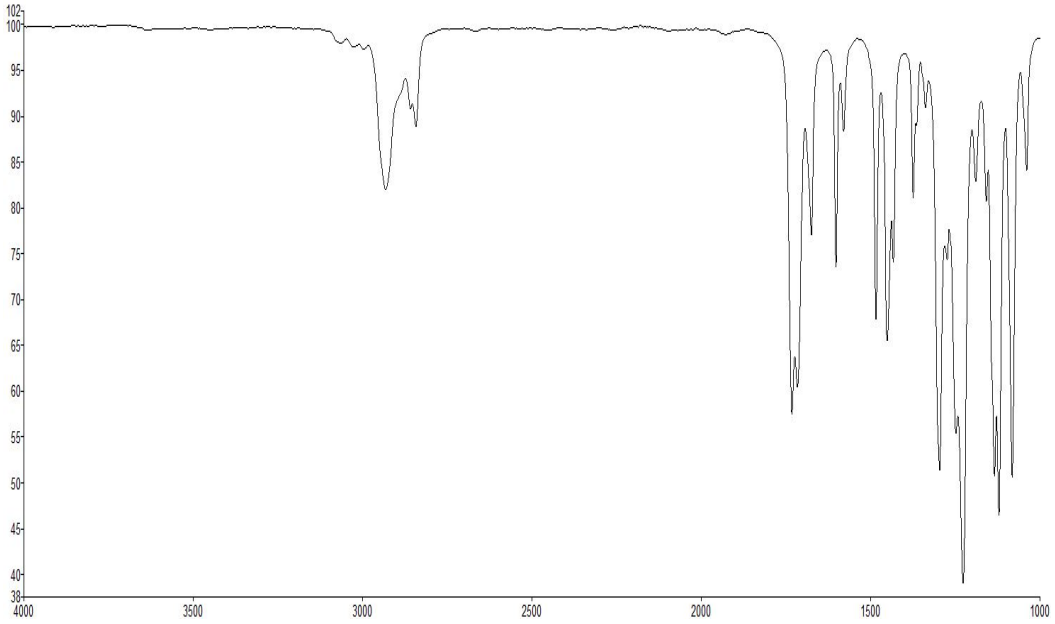

Figure 4.32. Infrared spectrum of compound **4.28**

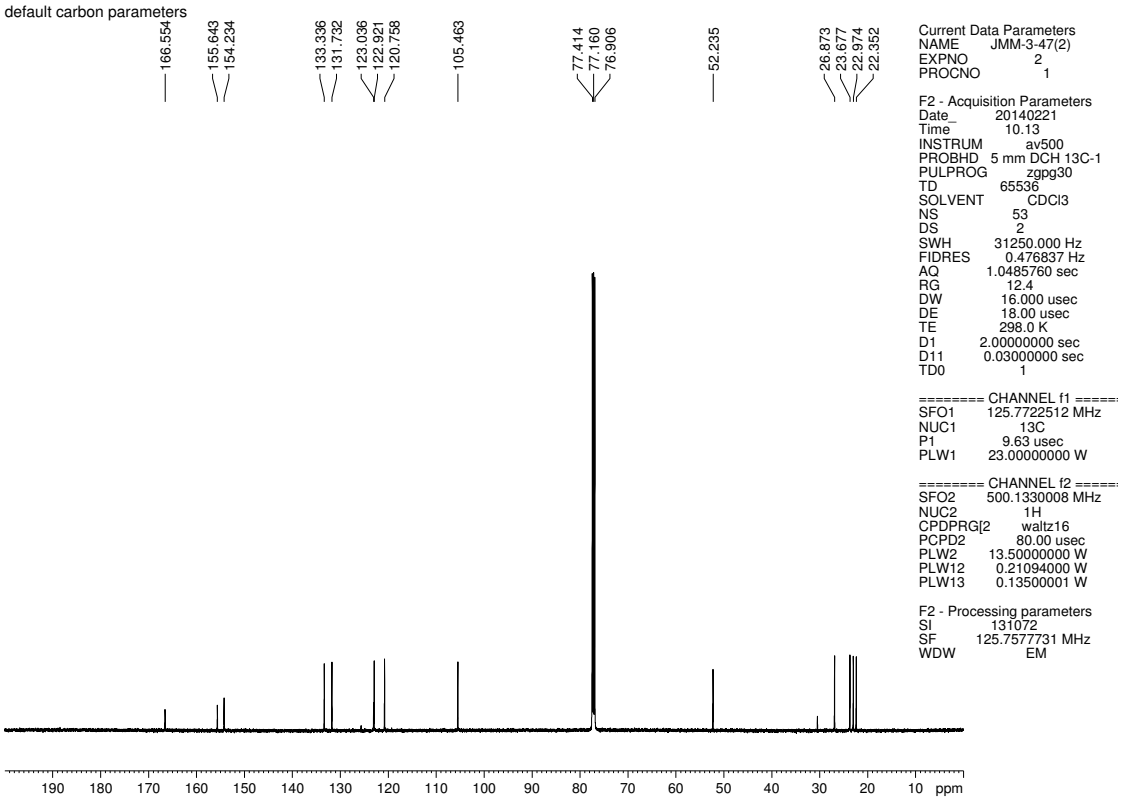

Figure 4.33. ^{13}C NMR (125 MHz, $CDCl_3$) of compound **4.28**

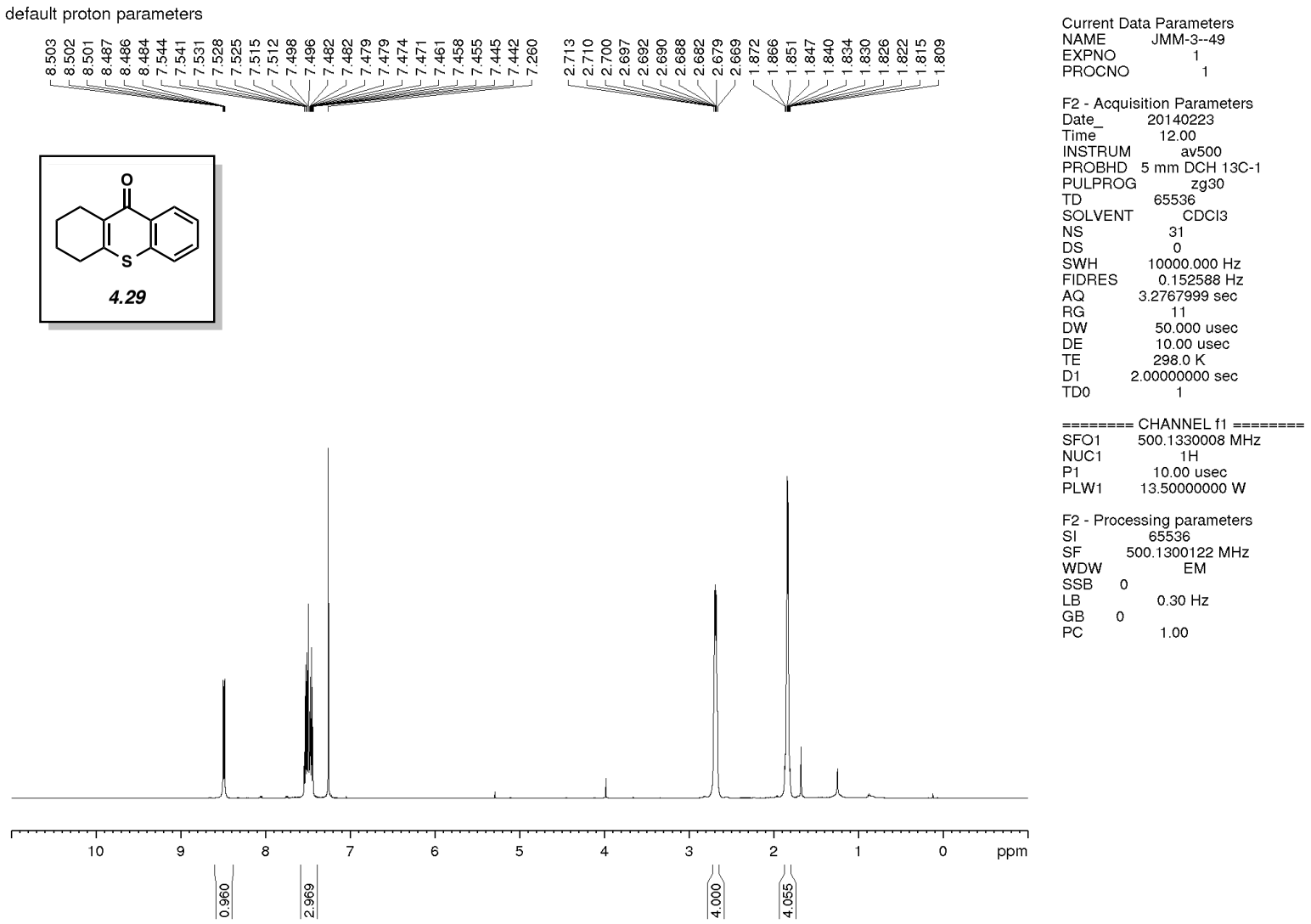

Figure 4.34. ^{1}H NMR (500 MHz, $CDCl_3$) compound **4.29**

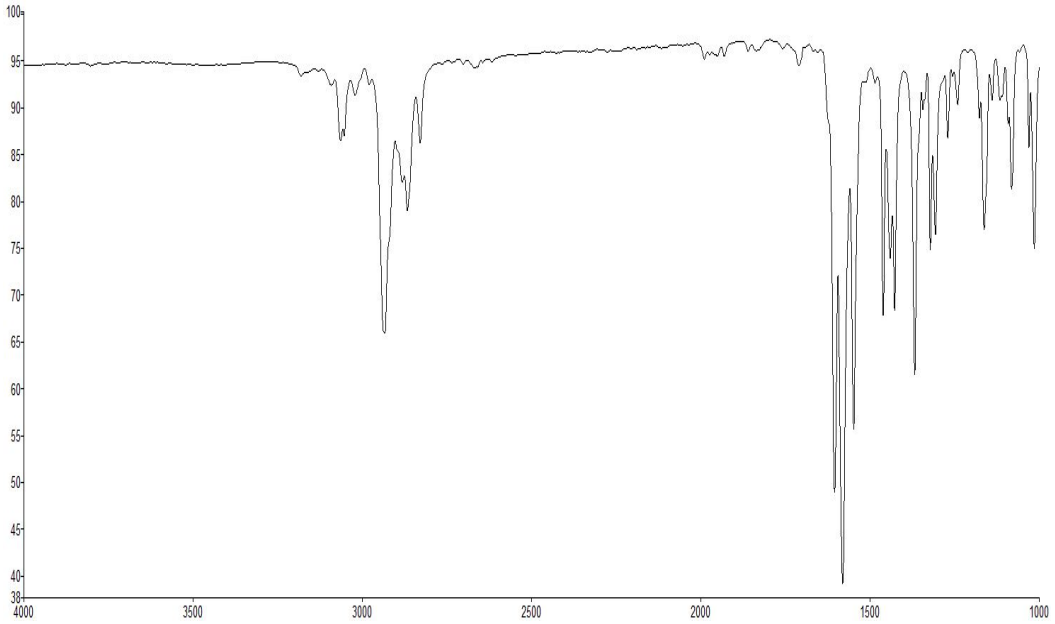

Figure 4.35. Infrared spectrum of compound **4.29**

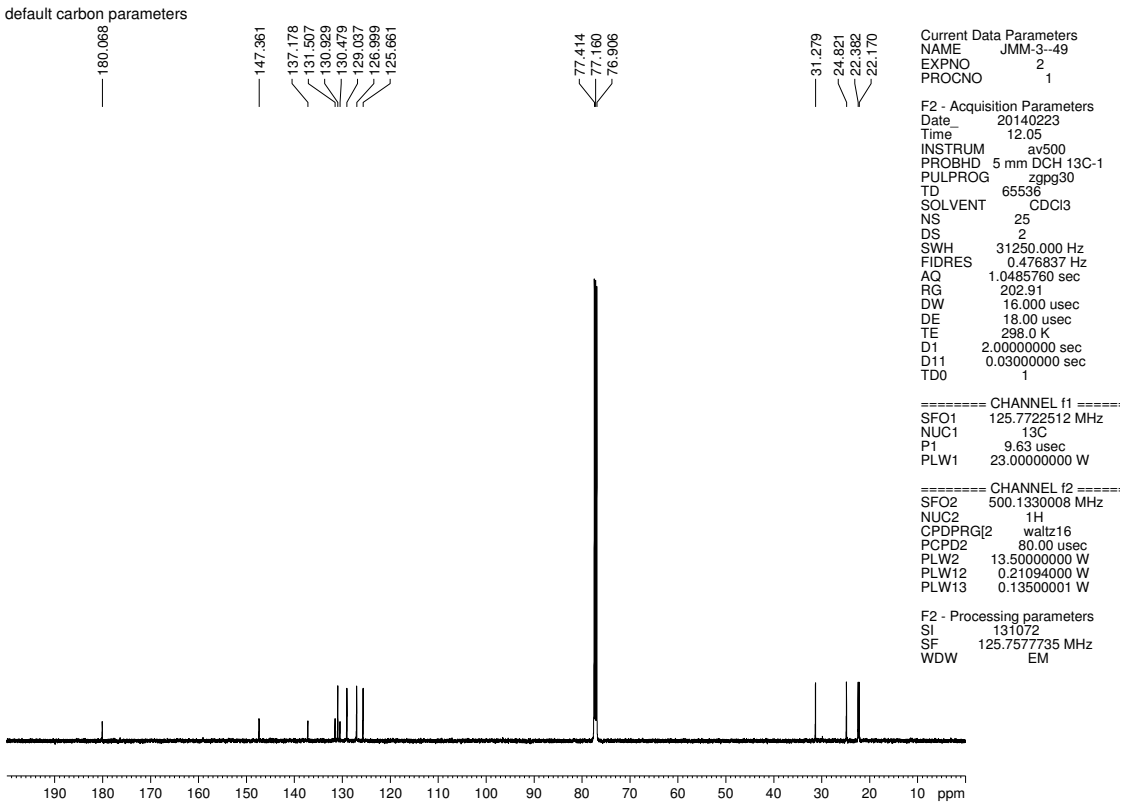

Figure 4.36. ^{13}C NMR (125 MHz, $CDCl_3$) of compound **4.29**

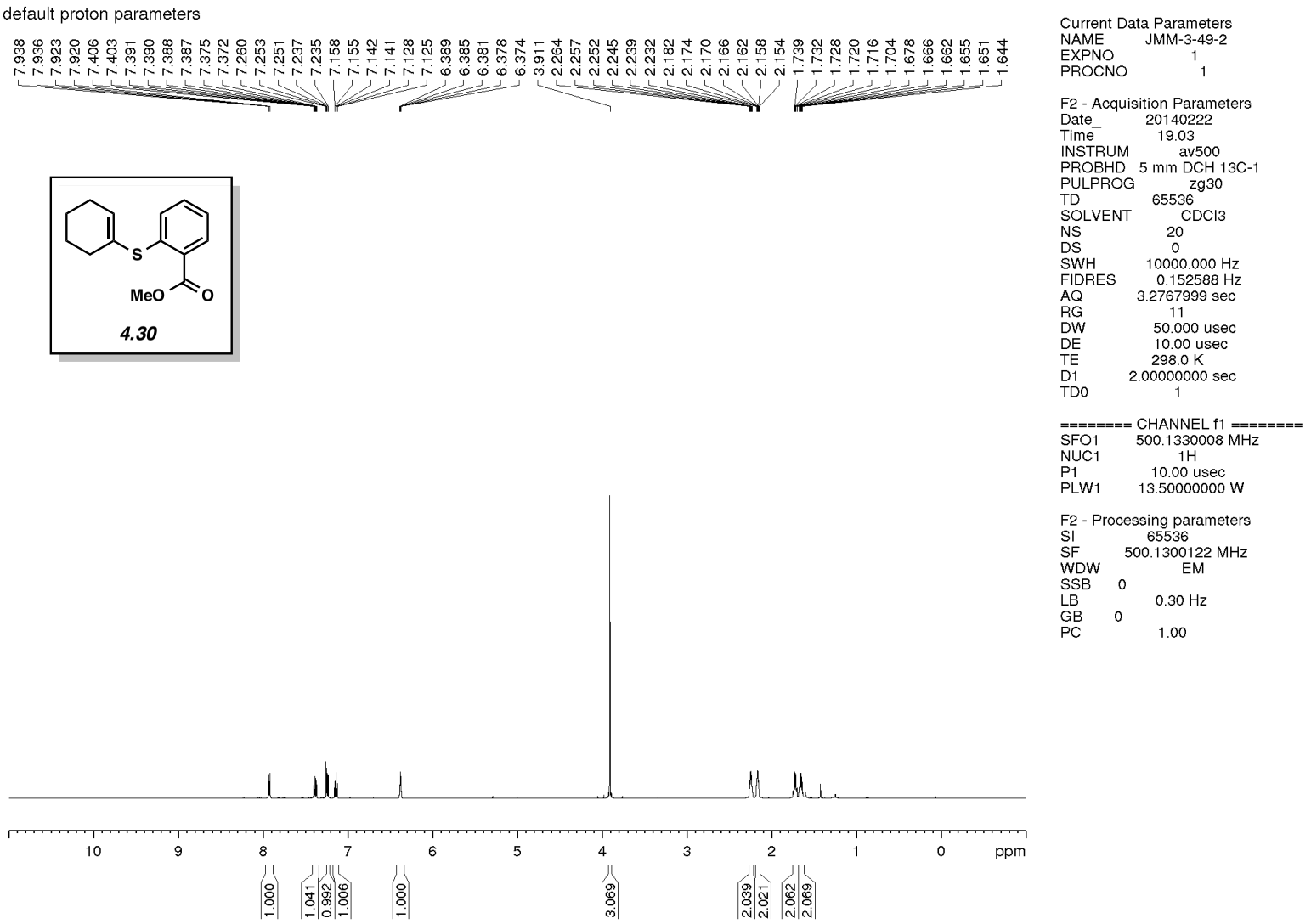

Figure 4.37. ^{1}H NMR (500 MHz, $CDCl_3$) compound **4.30**

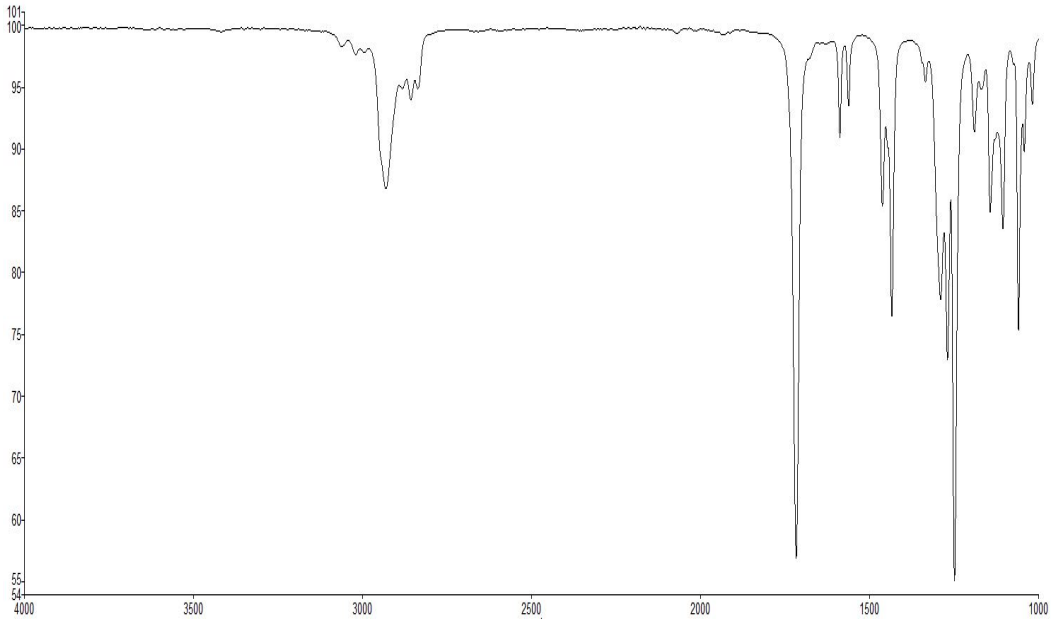

Figure 4.38. Infrared spectrum of compound **4.30**

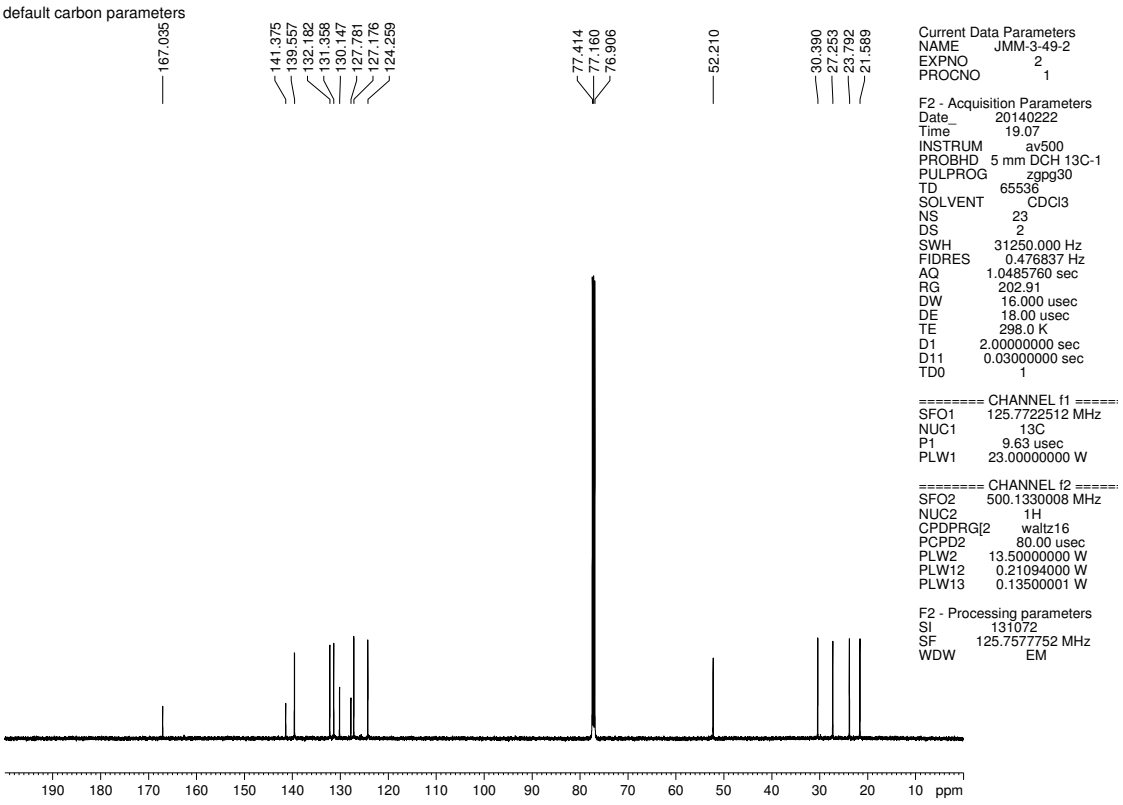

Figure 4.39. ^{13}C NMR (125 MHz, $CDCl_3$) of compound **4.30**

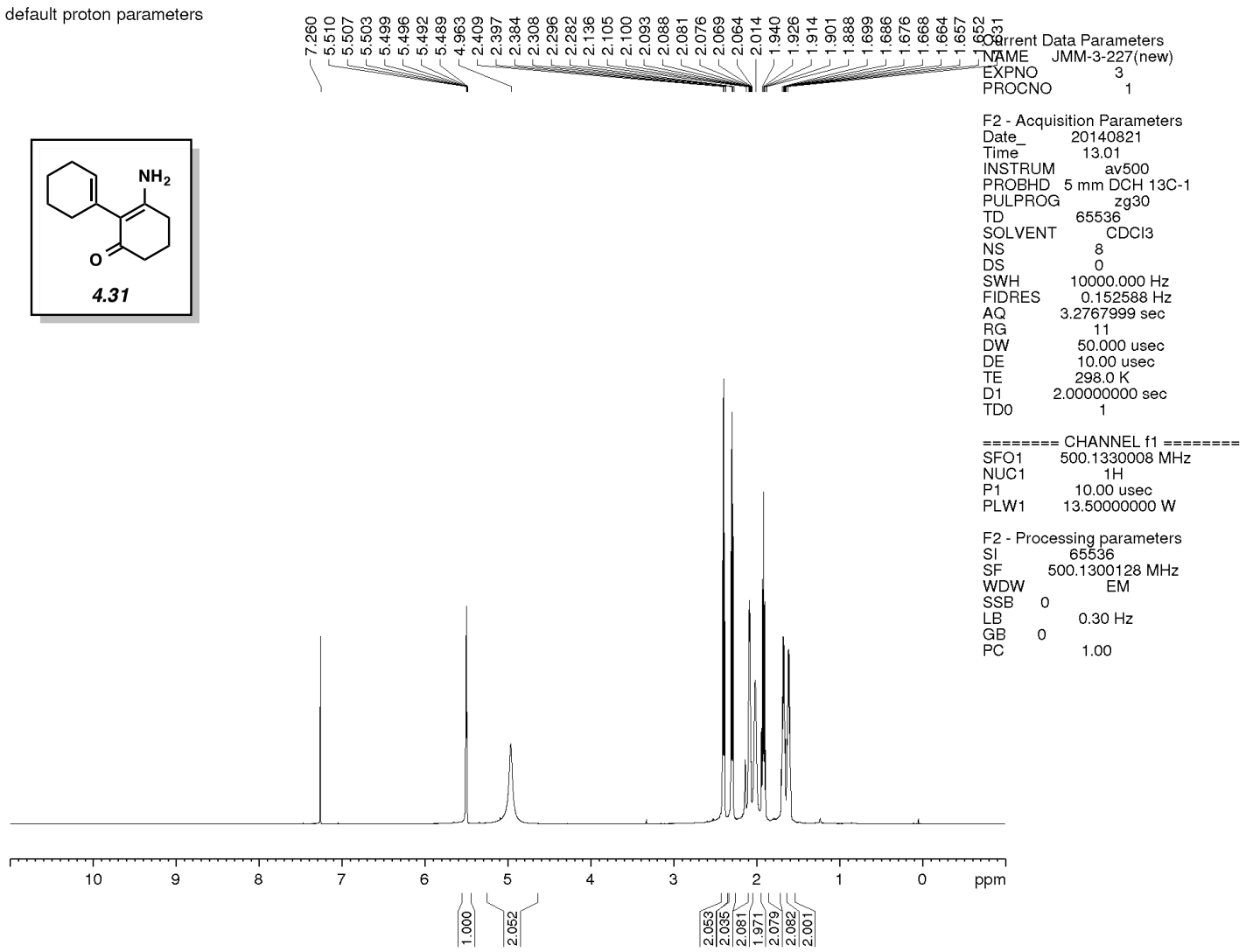

Figure 4.40. ^{1}H NMR (500 MHz, $CDCl_3$) compound **4.31**

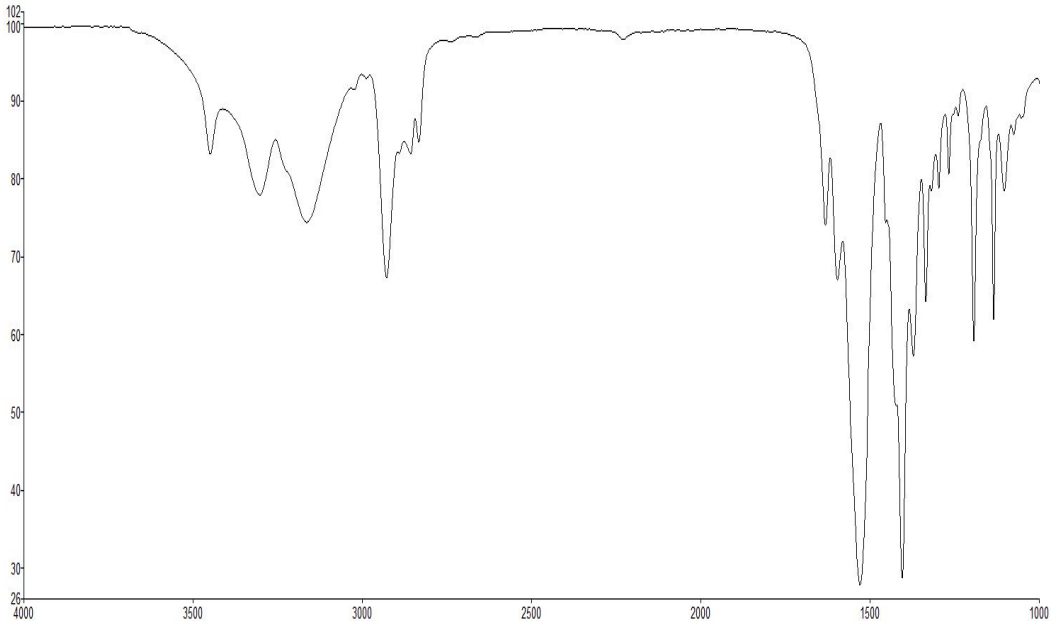

Figure 4.41. Infrared spectrum of compound **4.31**

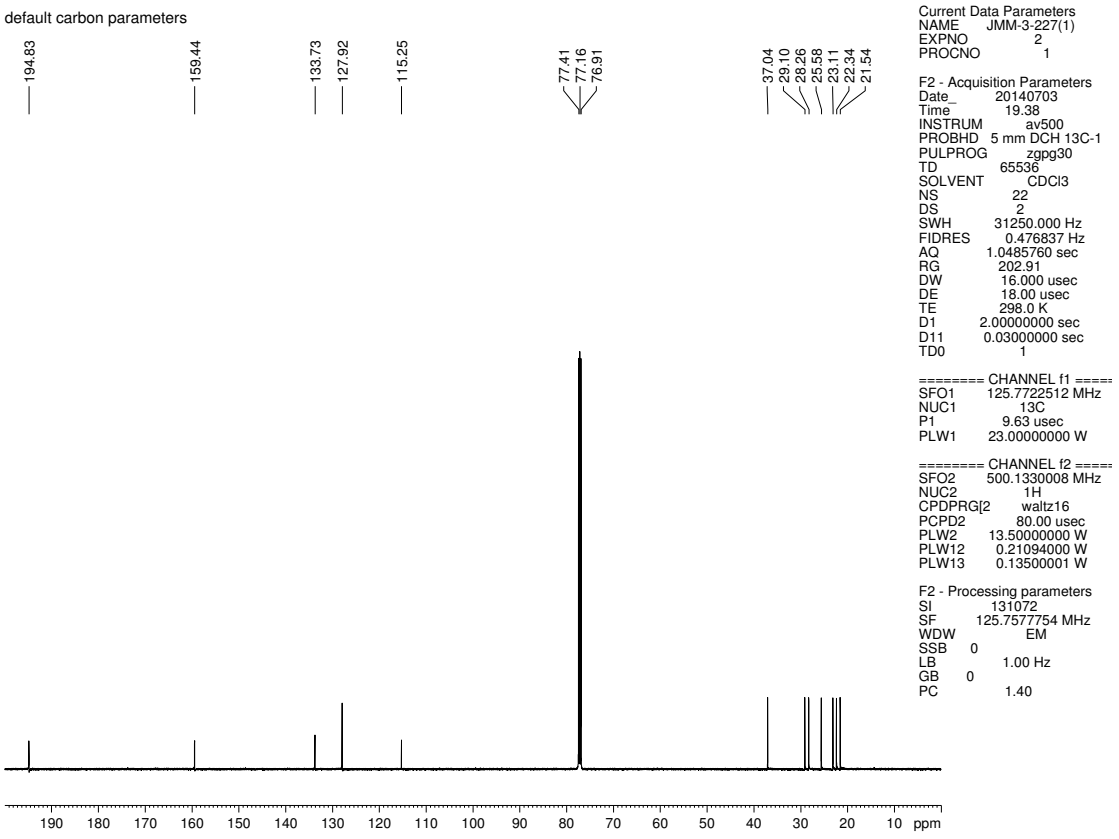

Figure 4.42. ^{13}C NMR (125 MHz, $CDCl_3$) of compound **4.31**

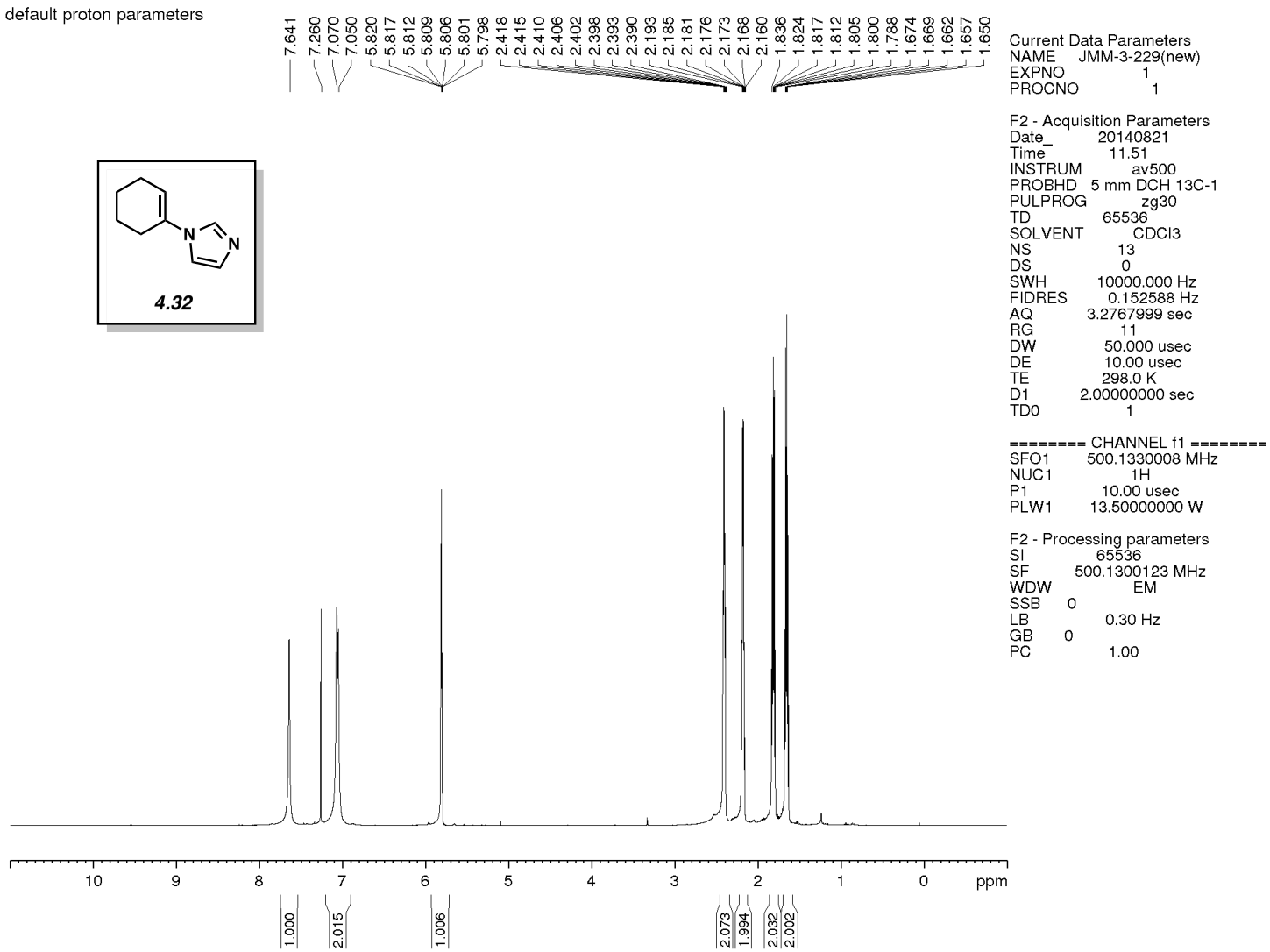

Figure 4.43. ^{1}H NMR (500 MHz, $CDCl_3$) compound **4.32**

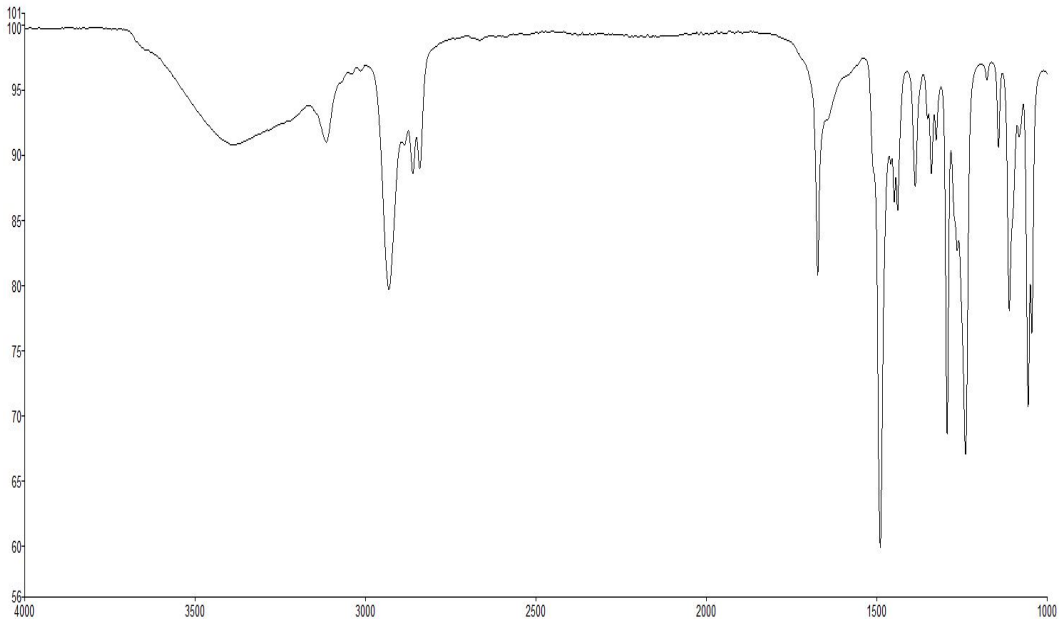

Figure 4.44. Infrared spectrum of compound **4.32**

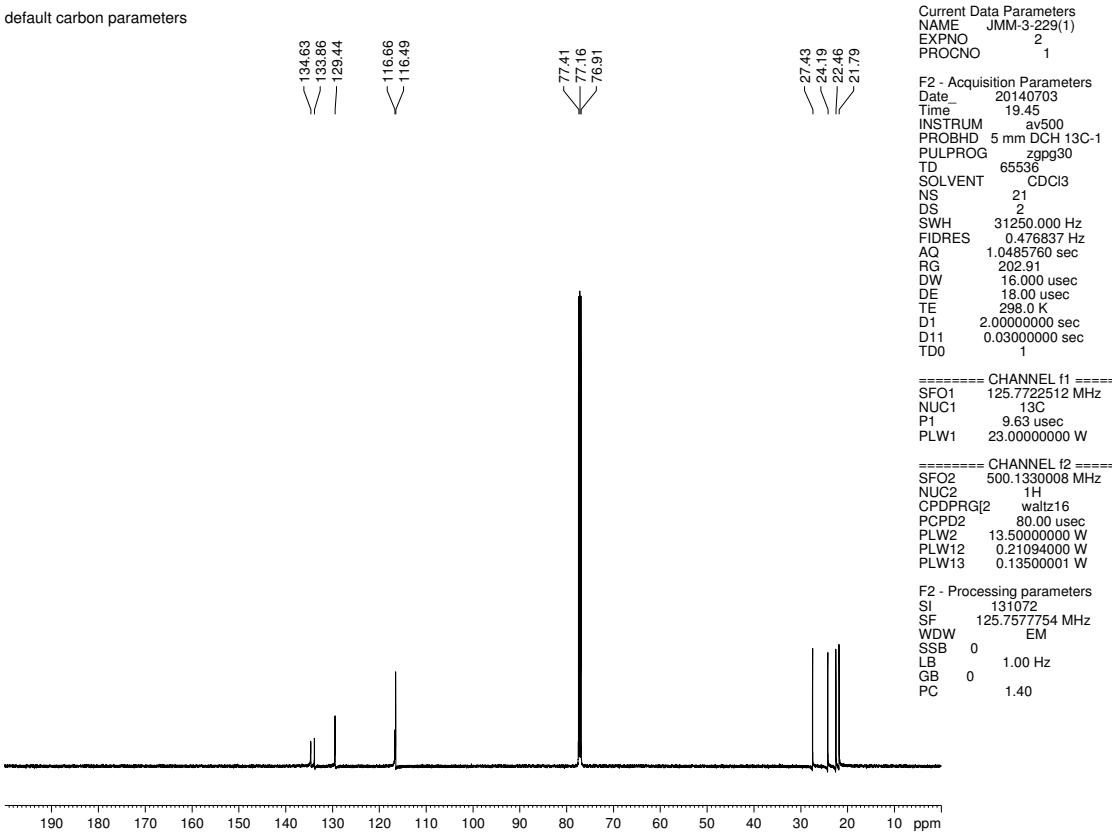

Figure 4.45. ^{13}C NMR (125 MHz, $CDCl_3$) of compound **4.32**

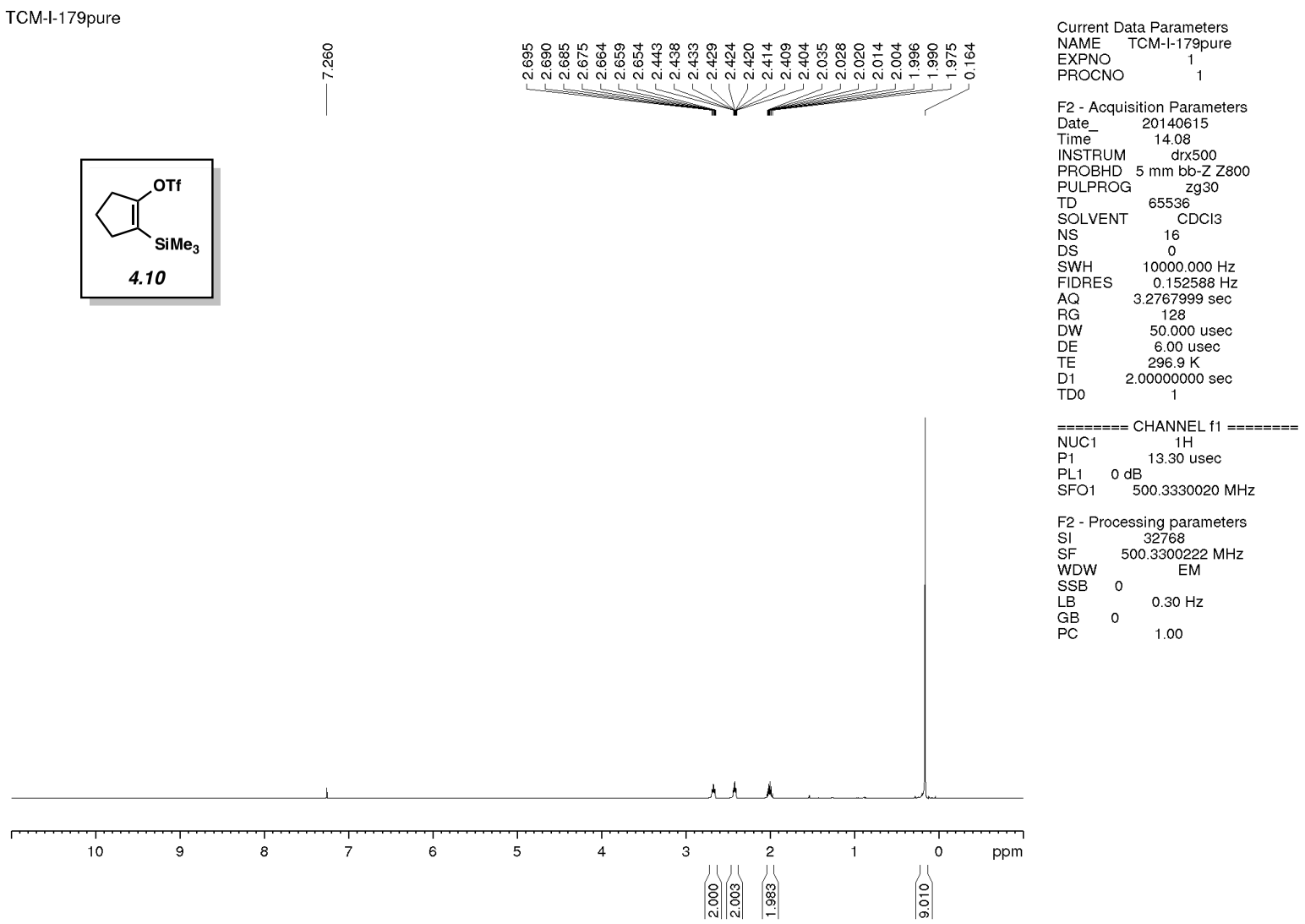

Figure 4.46. ^{1}H NMR (500 MHz, $CDCl_3$) compound **4.10**

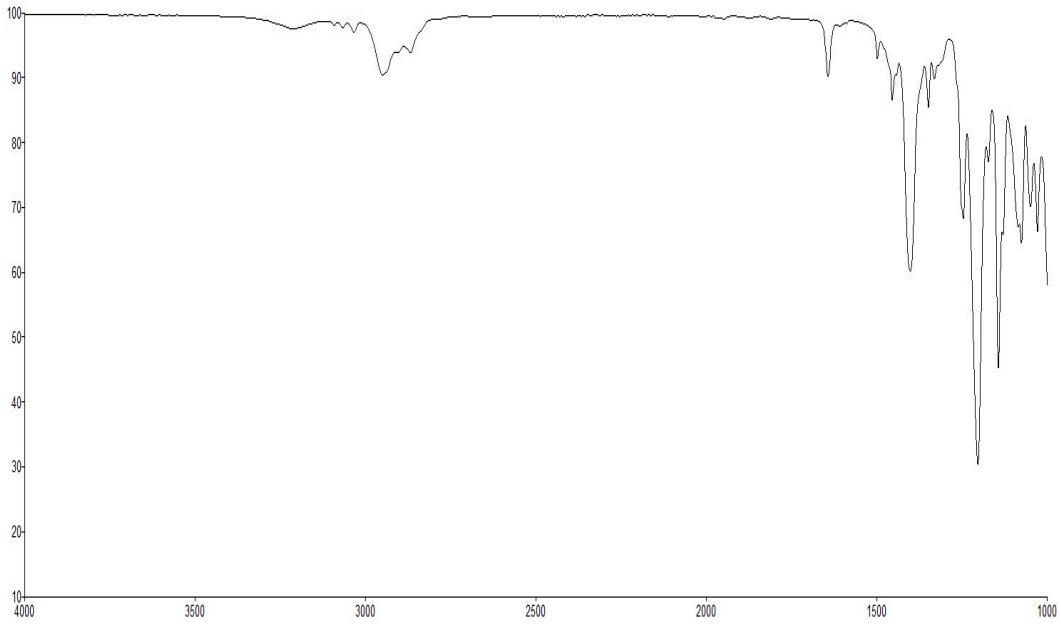

Figure 4.47. Infrared spectrum of compound **4.10**

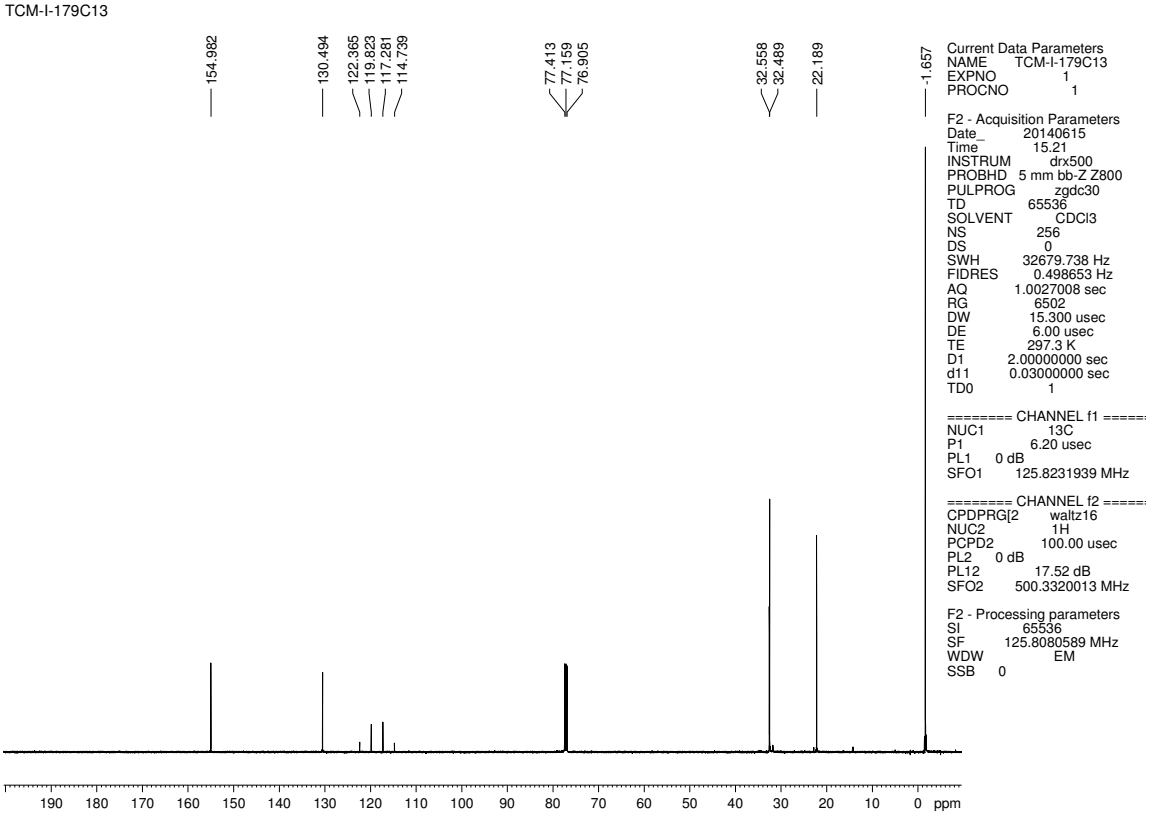

Figure 4.48. ^{13}C NMR (125 MHz, $CDCl_3$) of compound **4.10**

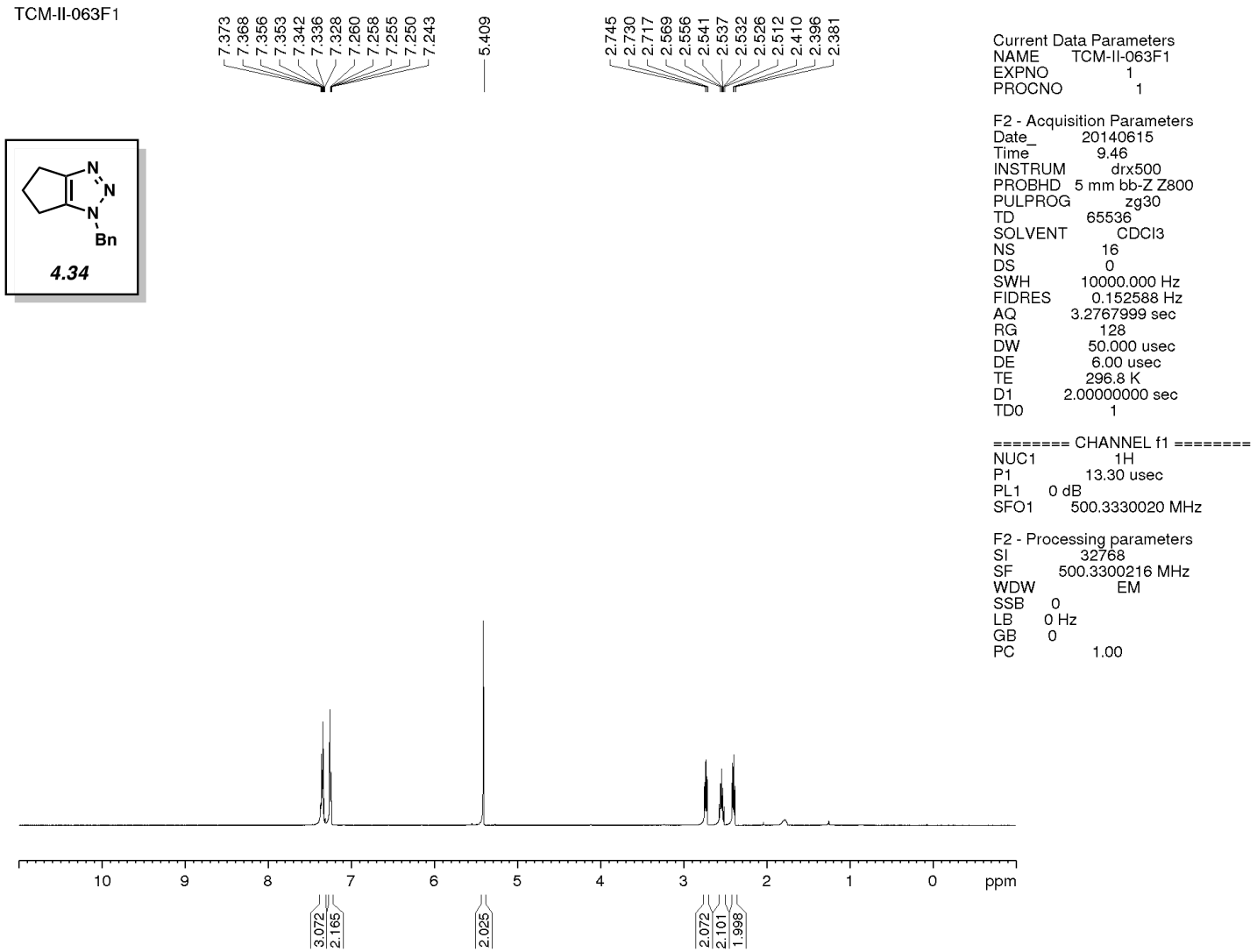

Figure 4.49. ^{1}H NMR (500 MHz, $CDCl_3$) compound **4.34**

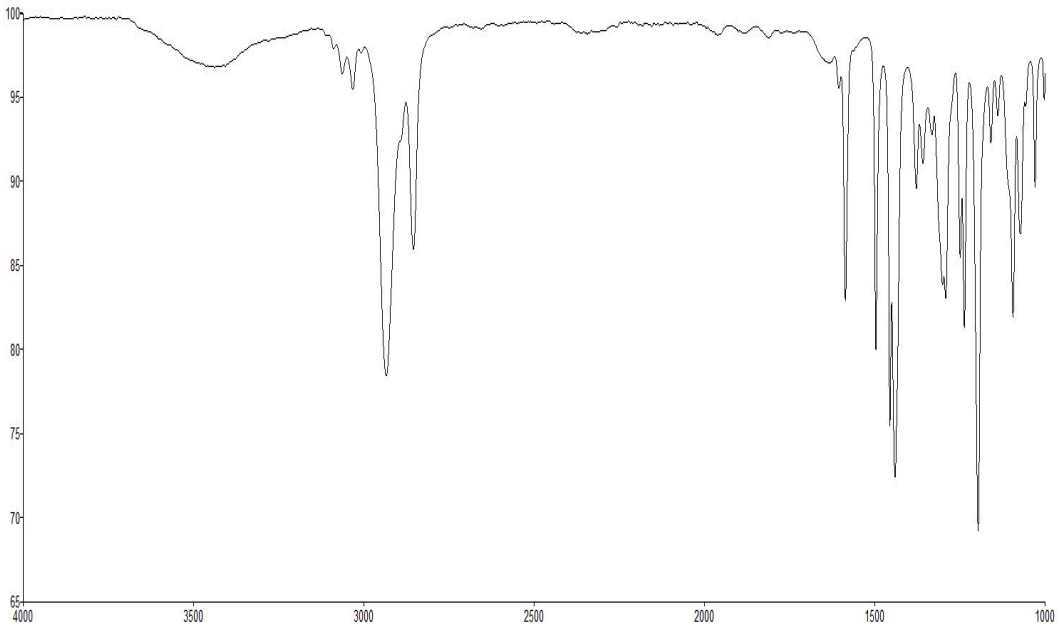

Figure 4.50. Infrared spectrum of compound **4.34**

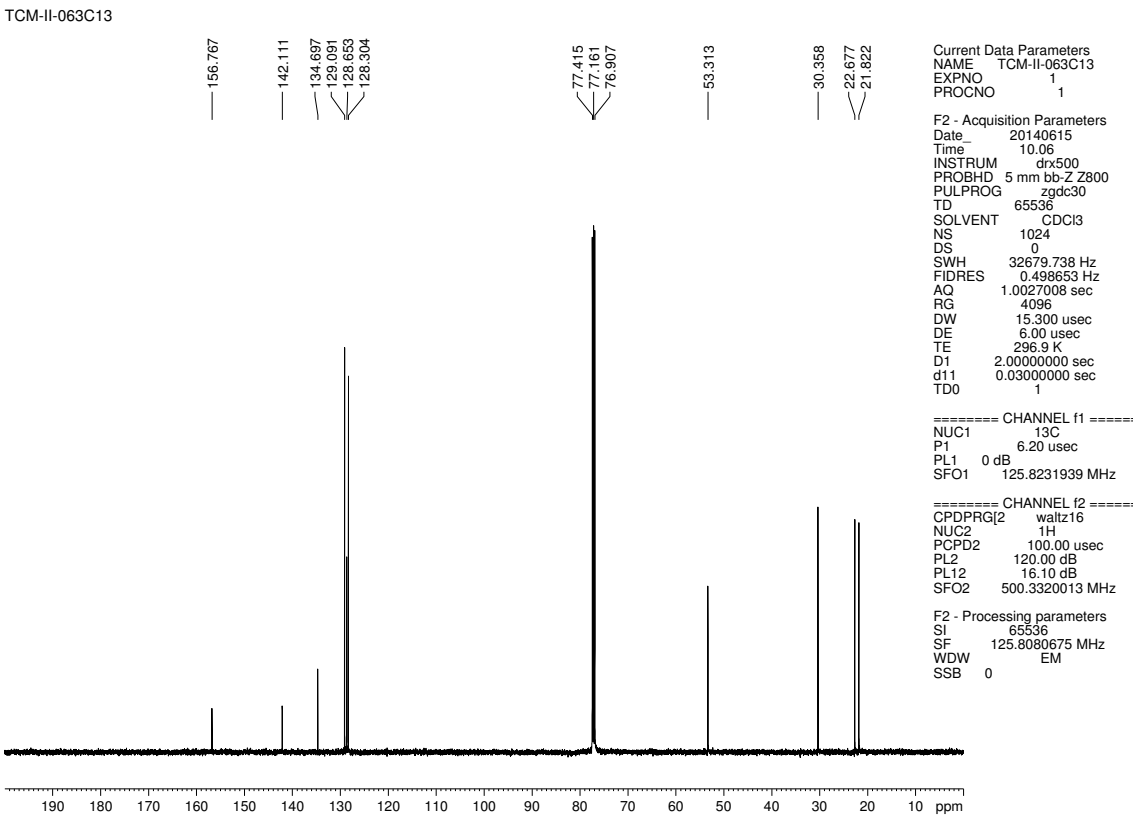

Figure 4.51. ^{13}C NMR (125 MHz, $CDCl_3$) of compound **4.34**

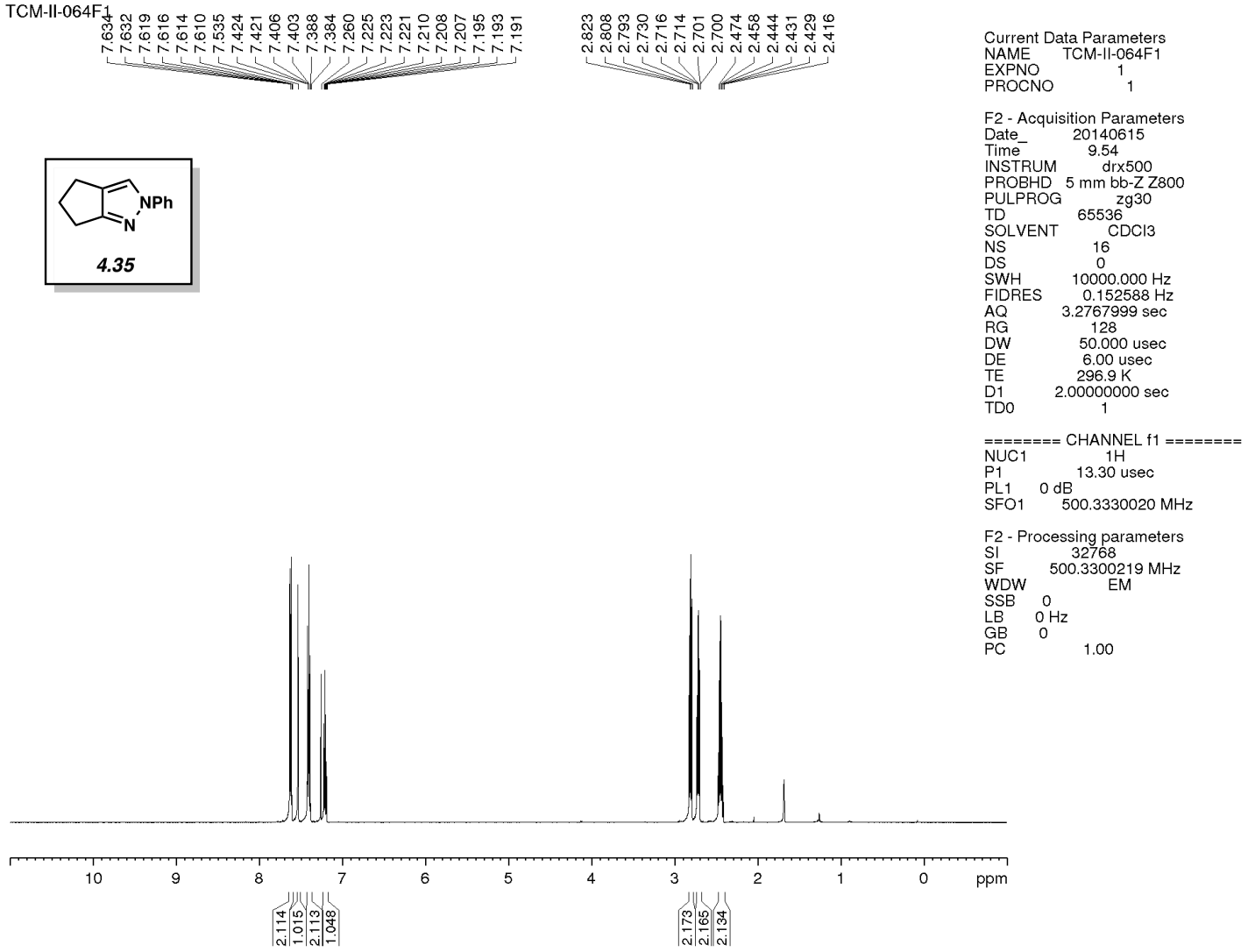

Figure 4.52. ^{1}H NMR (500 MHz, $CDCl_3$) compound **4.35**

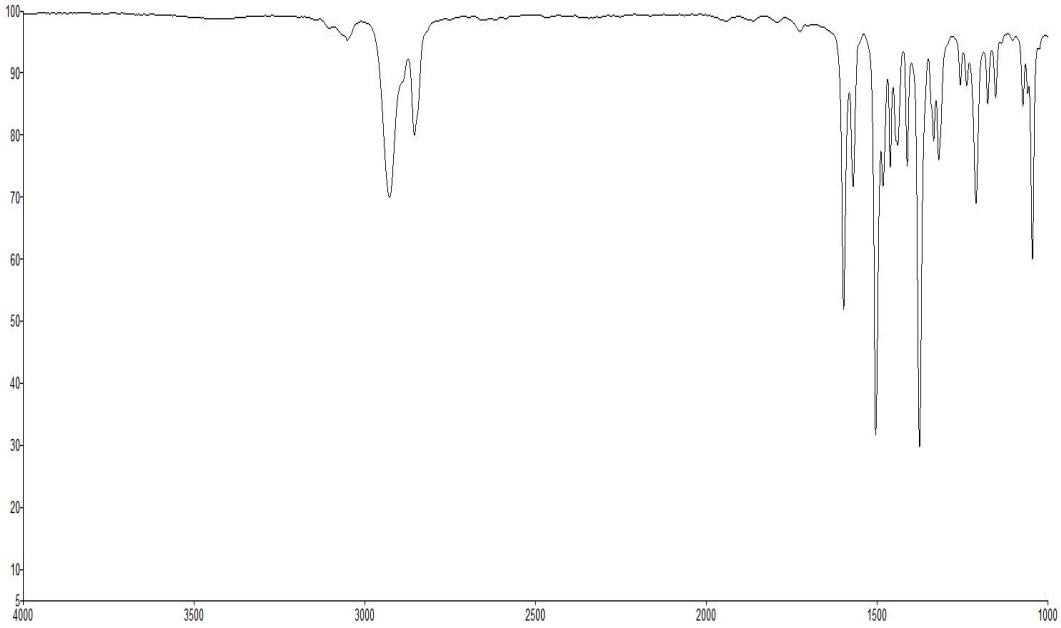

Figure 4.53. Infrared spectrum of compound **4.35**

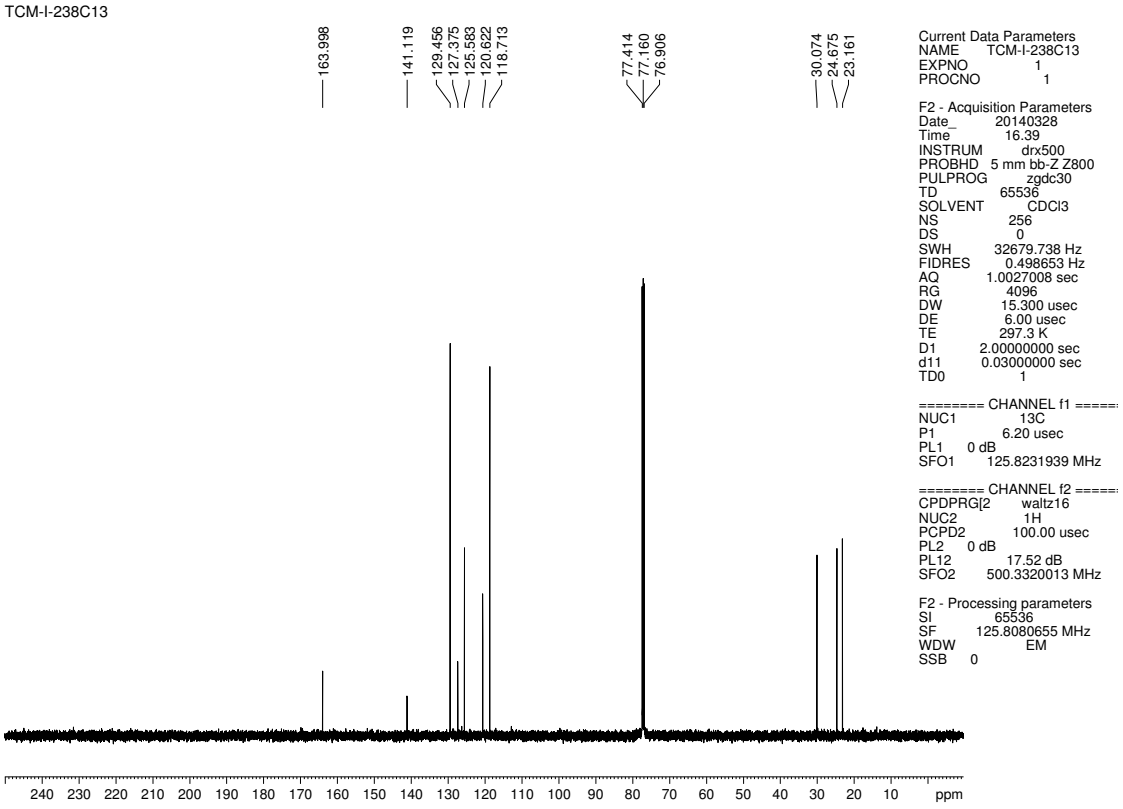

Figure 4.54. ^{13}C NMR (125 MHz, $CDCl_3$) of compound **4.35**

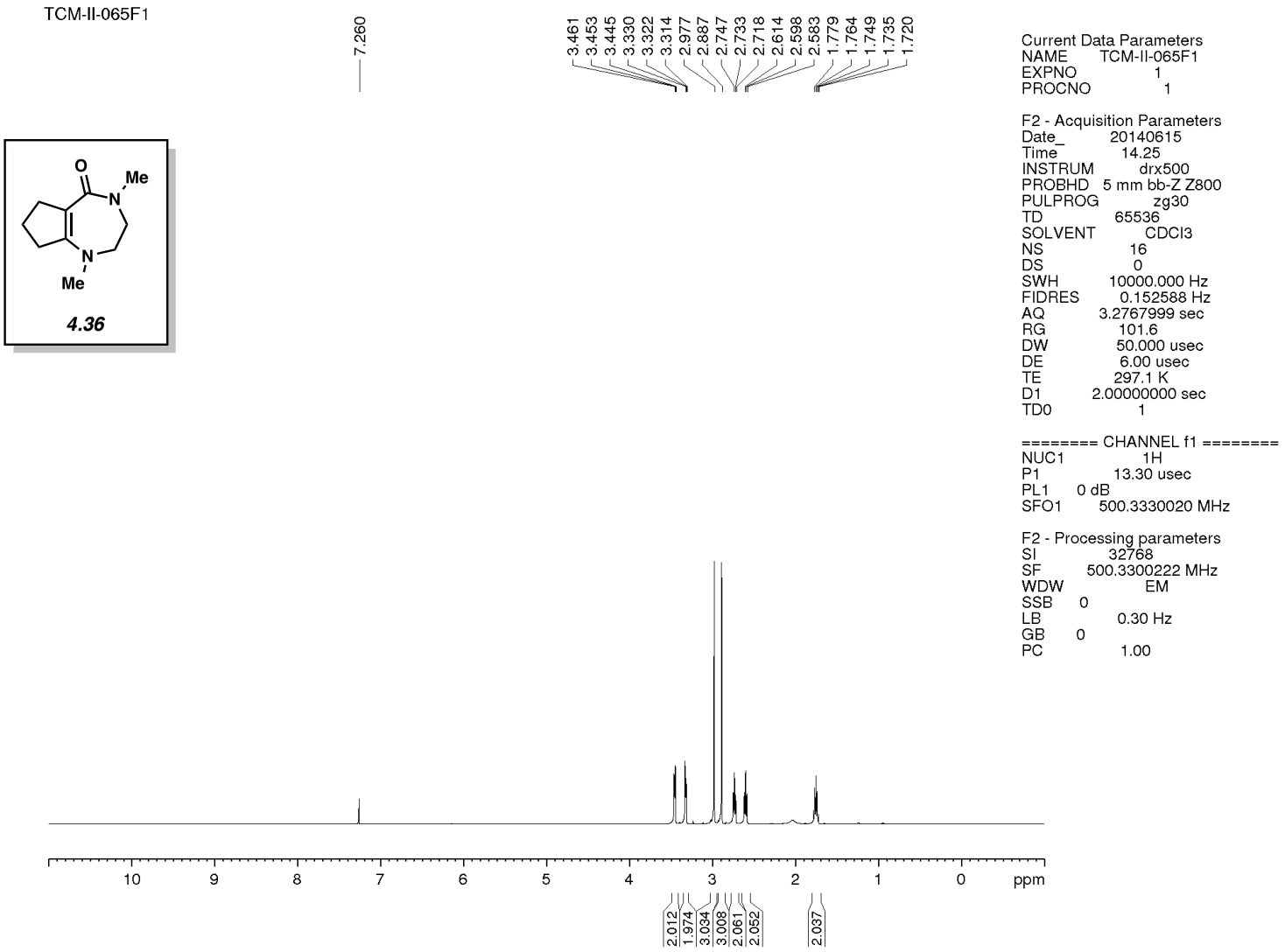

Figure 4.55. ^{1}H NMR (500 MHz, $CDCl_3$) compound **4.36**

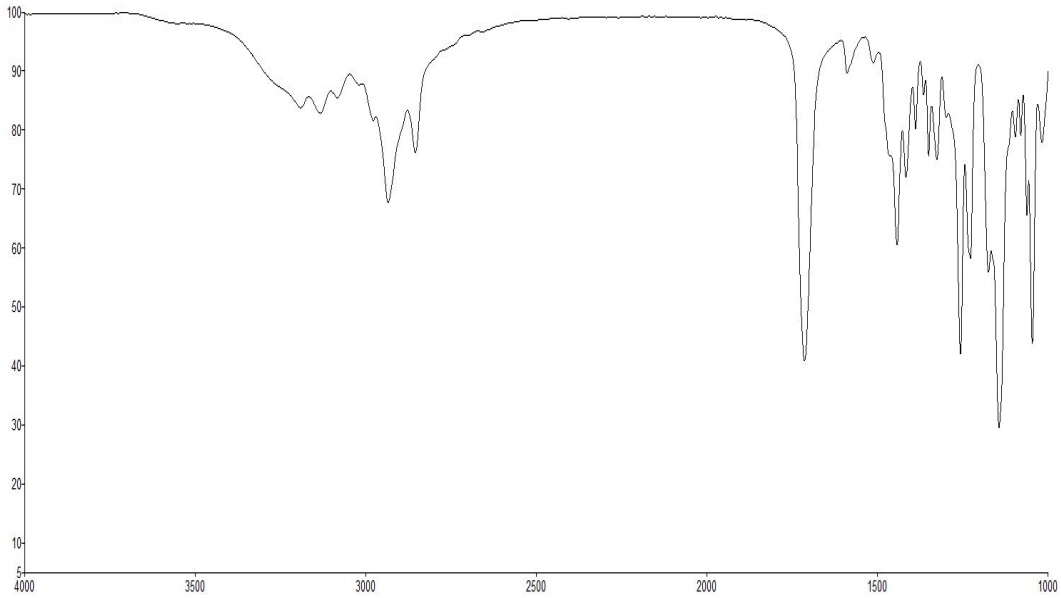

Figure 4.56. Infrared spectrum of compound **4.36**

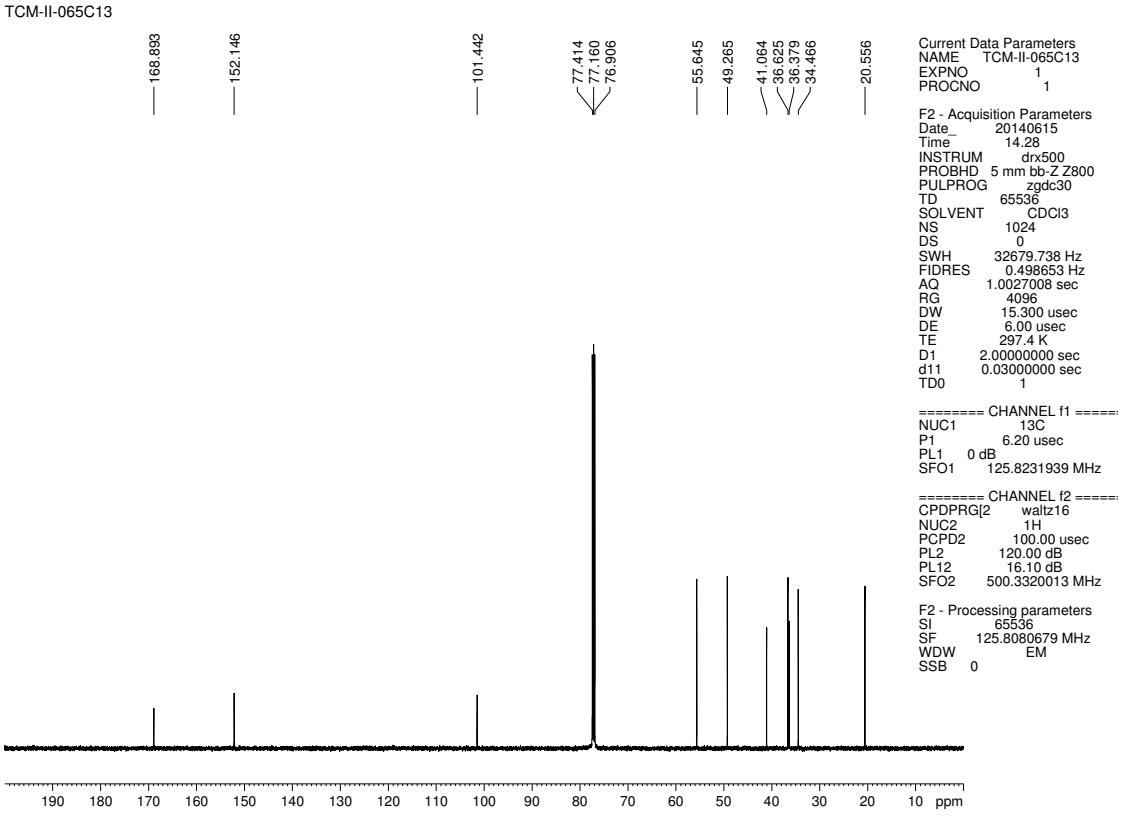

Figure 4.57. ^{13}C NMR (125 MHz, $CDCl_3$) of compound **4.36**

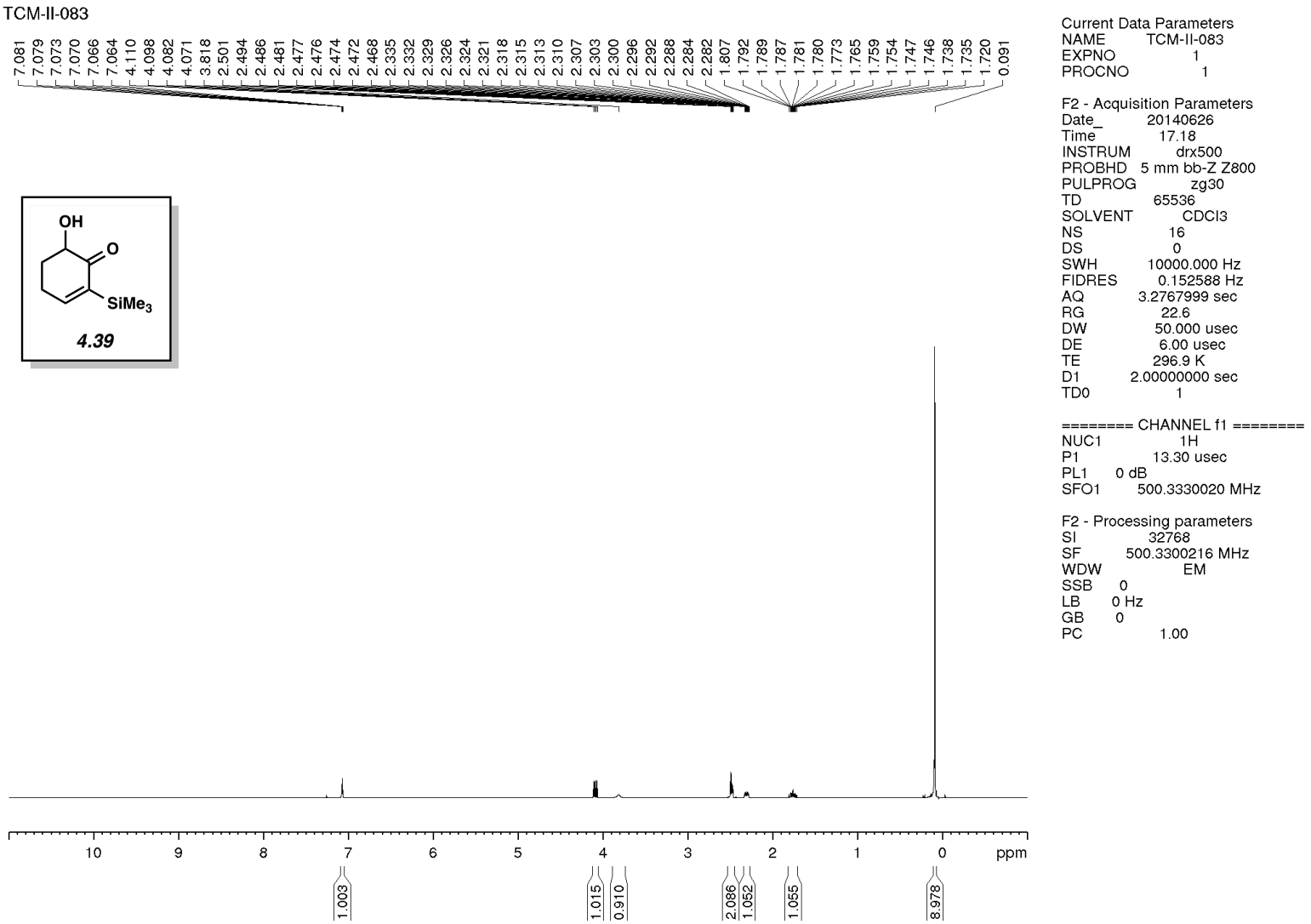

Figure 4.58. ^{1}H NMR (500 MHz, $CDCl_3$) compound **4.39**

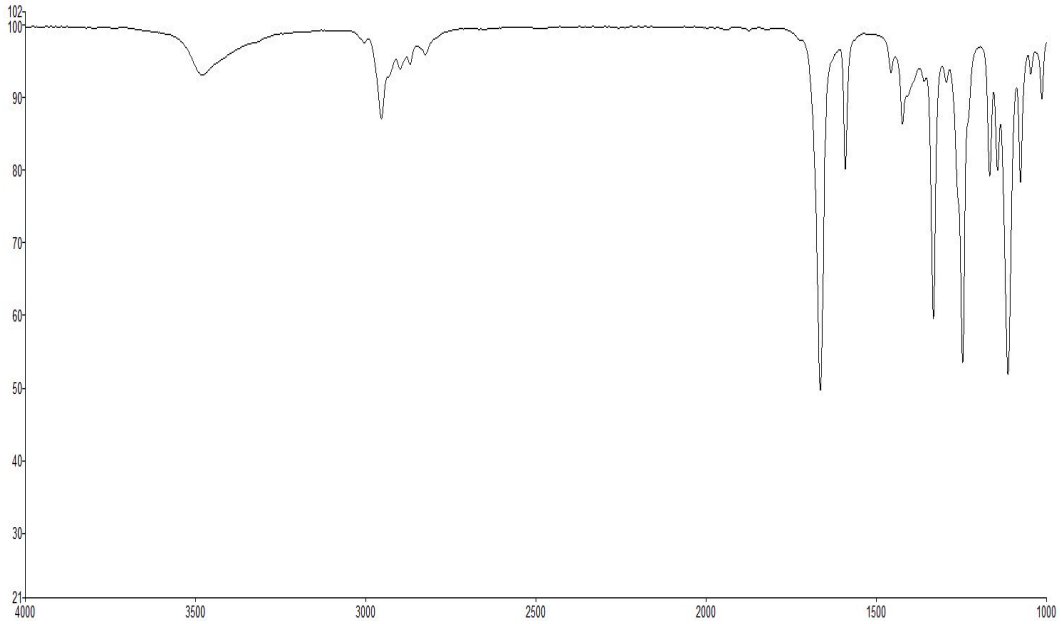

Figure 4.59. Infrared spectrum of compound **4.39**

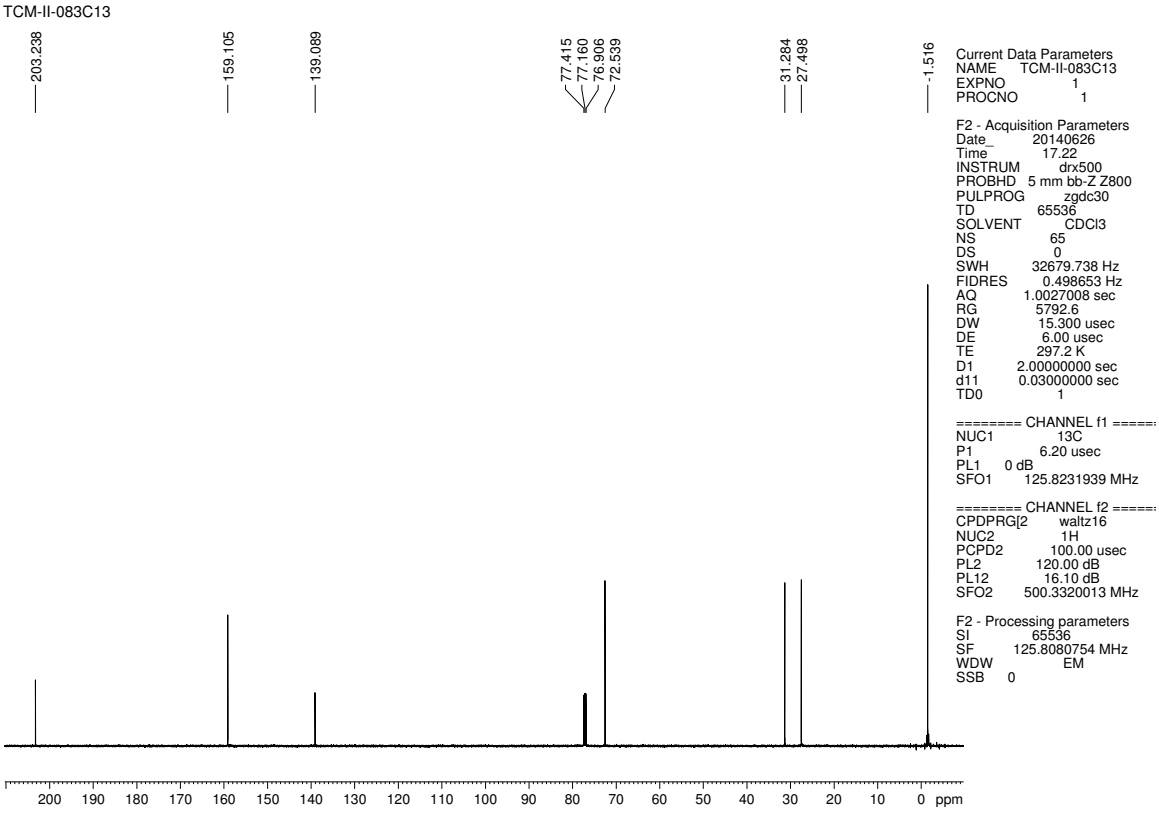

Figure 4.60. ^{13}C NMR (125 MHz, $CDCl_3$) of compound **4.39**

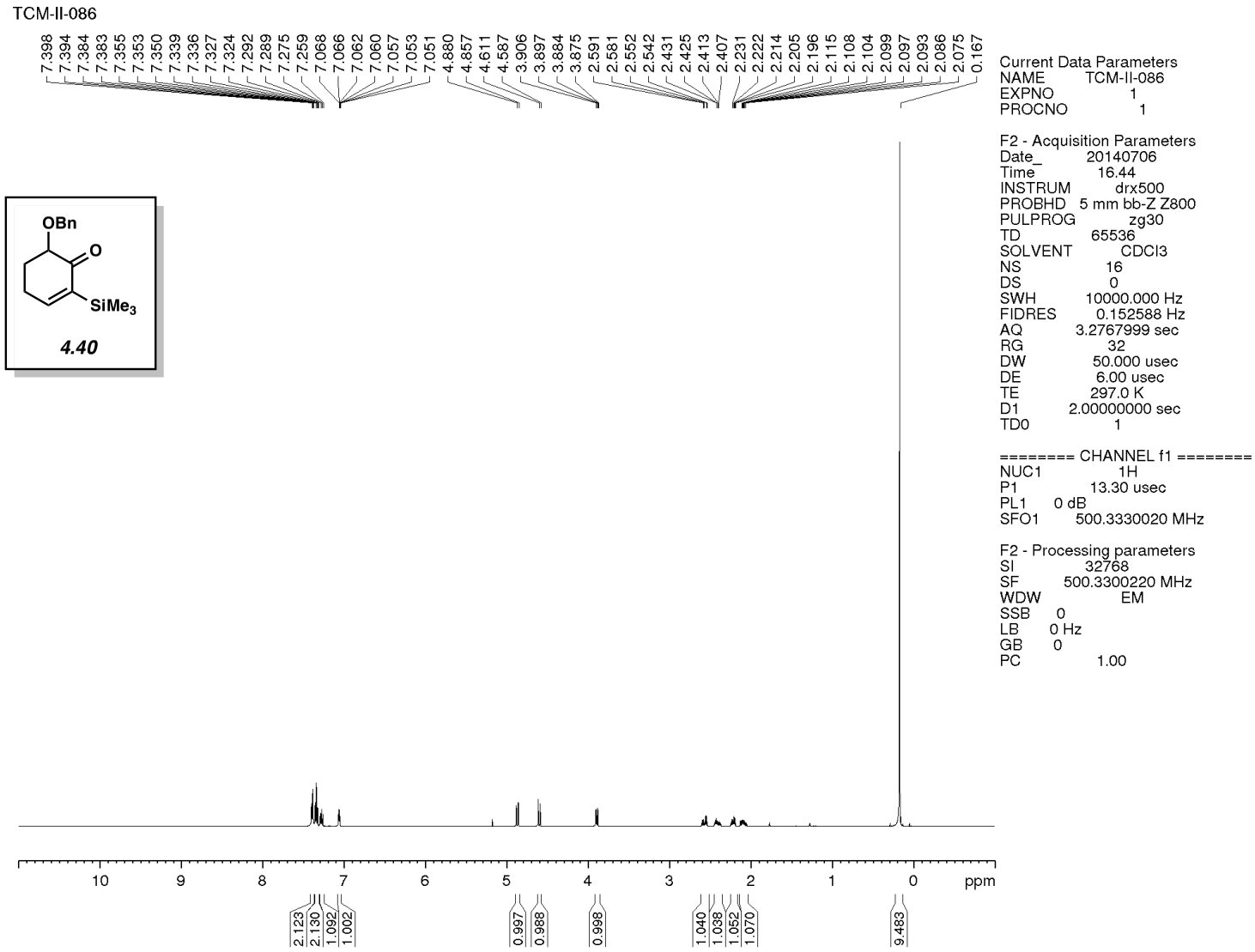

Figure 4.61. ^{1}H NMR (500 MHz, $CDCl_3$) compound **4.40**

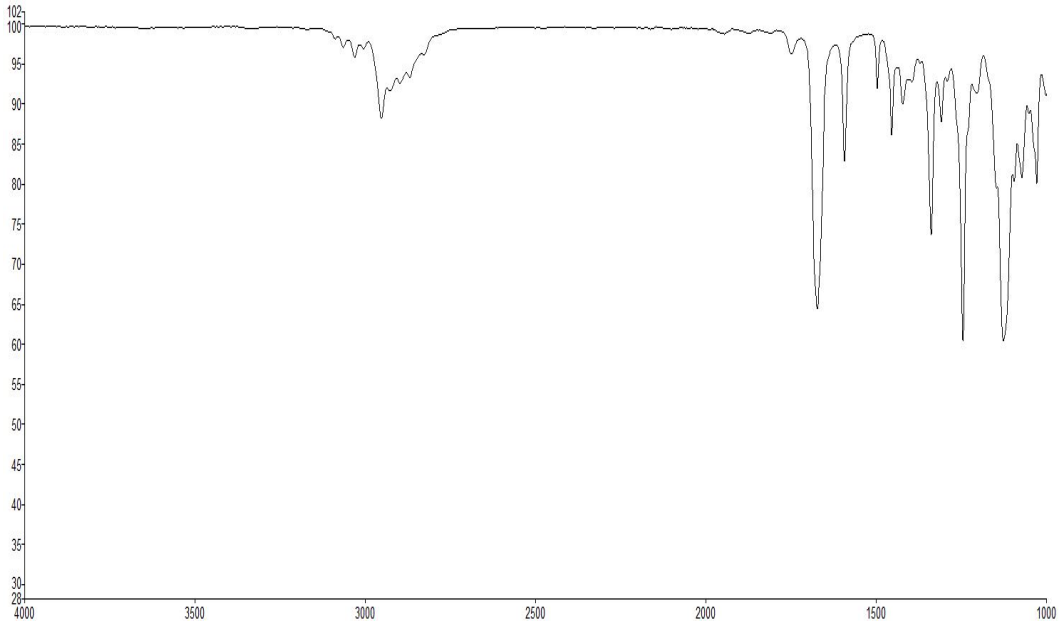

Figure 4.62. Infrared spectrum of compound **4.40**

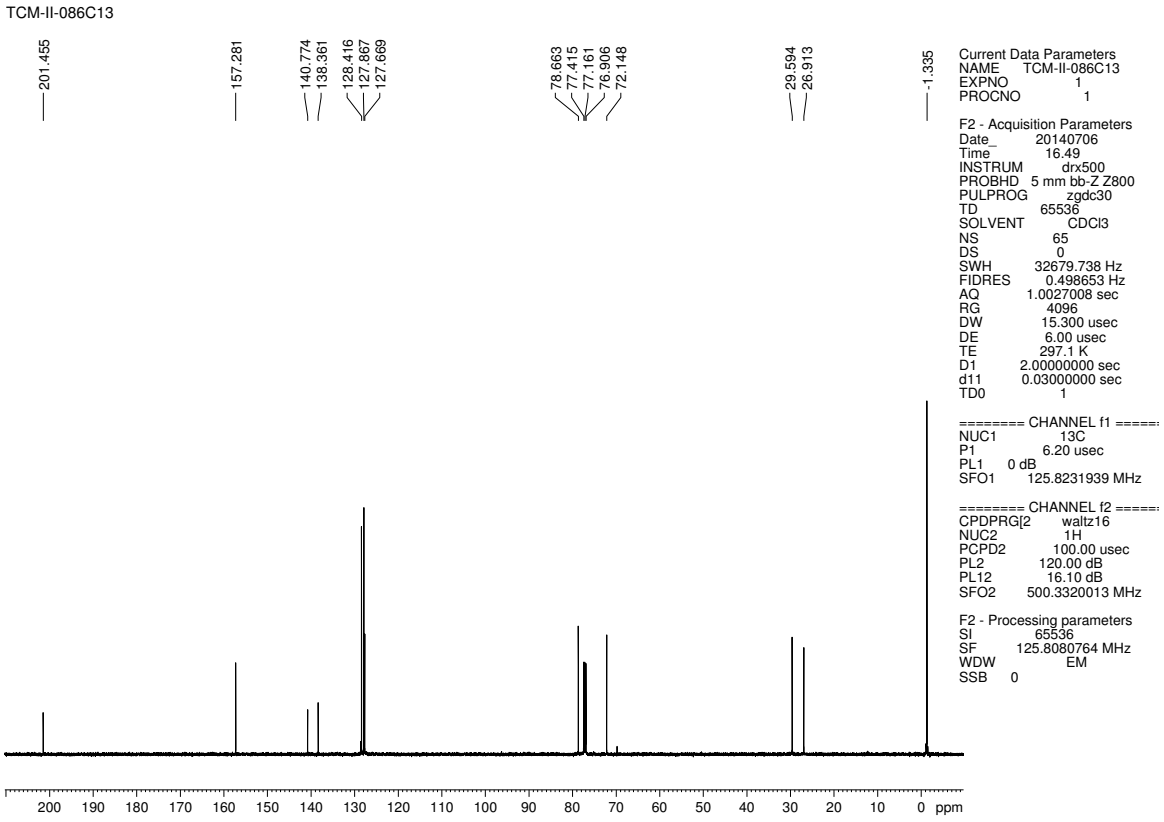

Figure 4.63. ^{13}C NMR (125 MHz, $CDCl_3$) of compound **4.40**

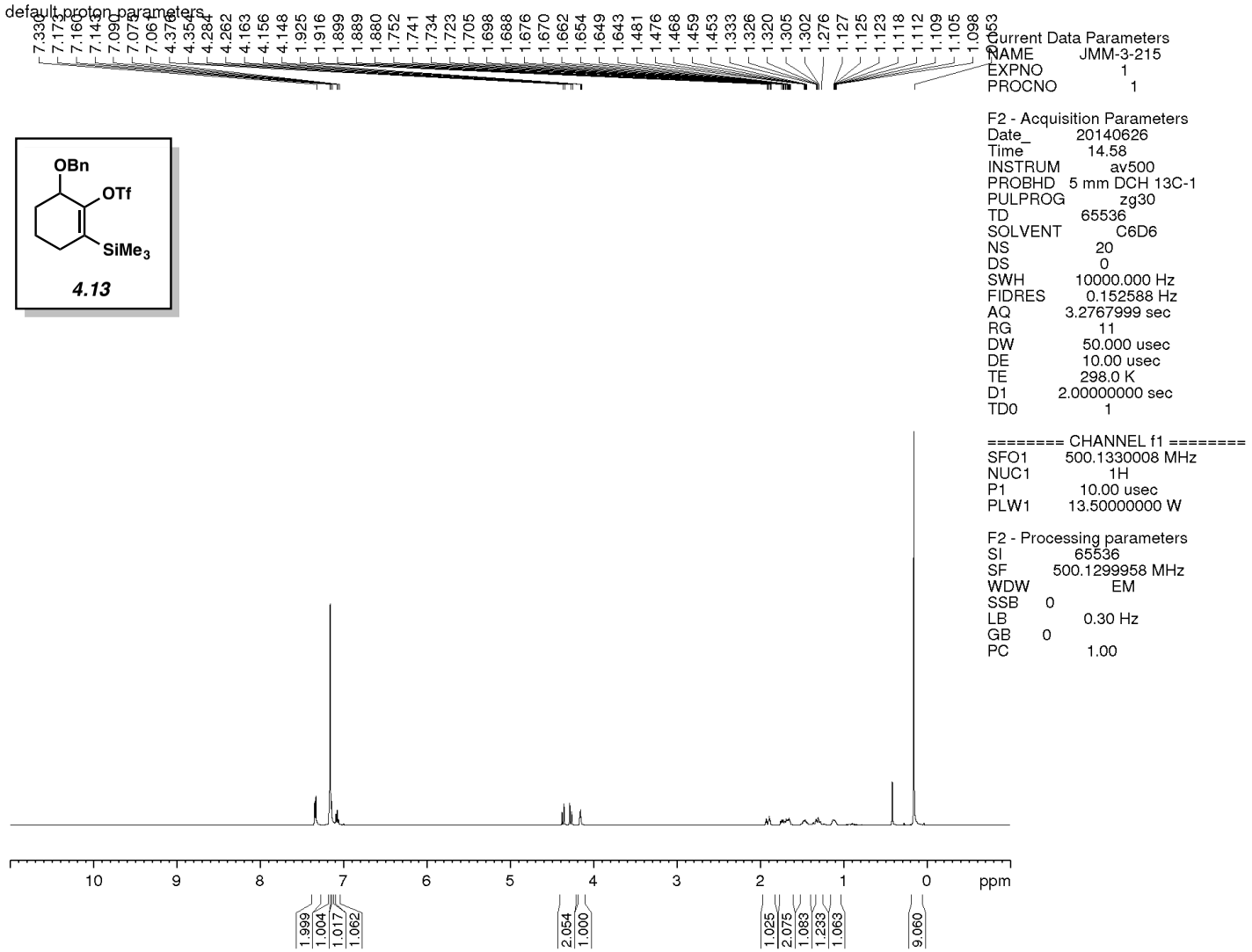

Figure 4.64. ^{1}H NMR (500 MHz, C_6D_6) compound **4.13**

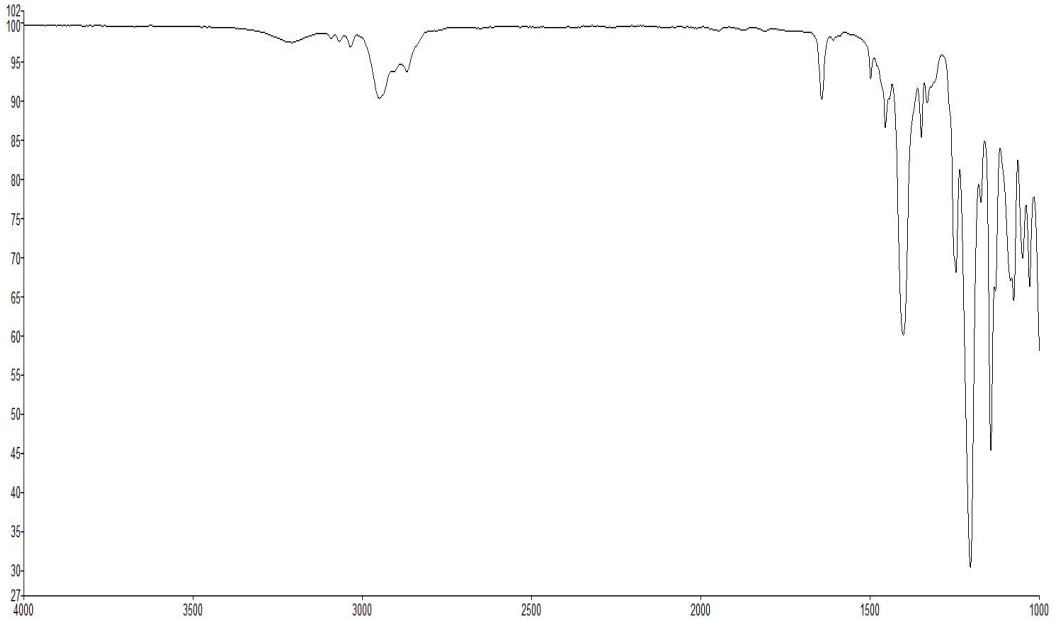

Figure 4.65. Infrared spectrum of compound **4.13**

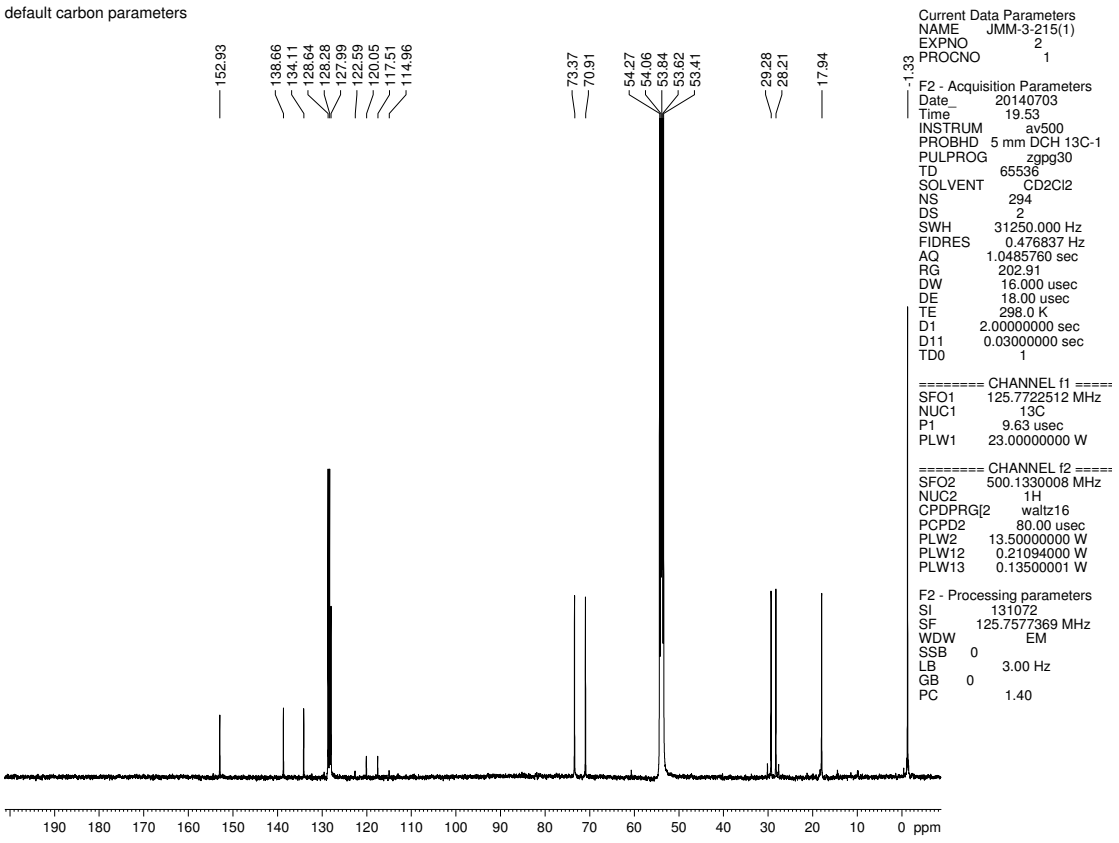

Figure 4.66. ^{13}C NMR (125 MHz, CD_2Cl_2) of compound **4.13**

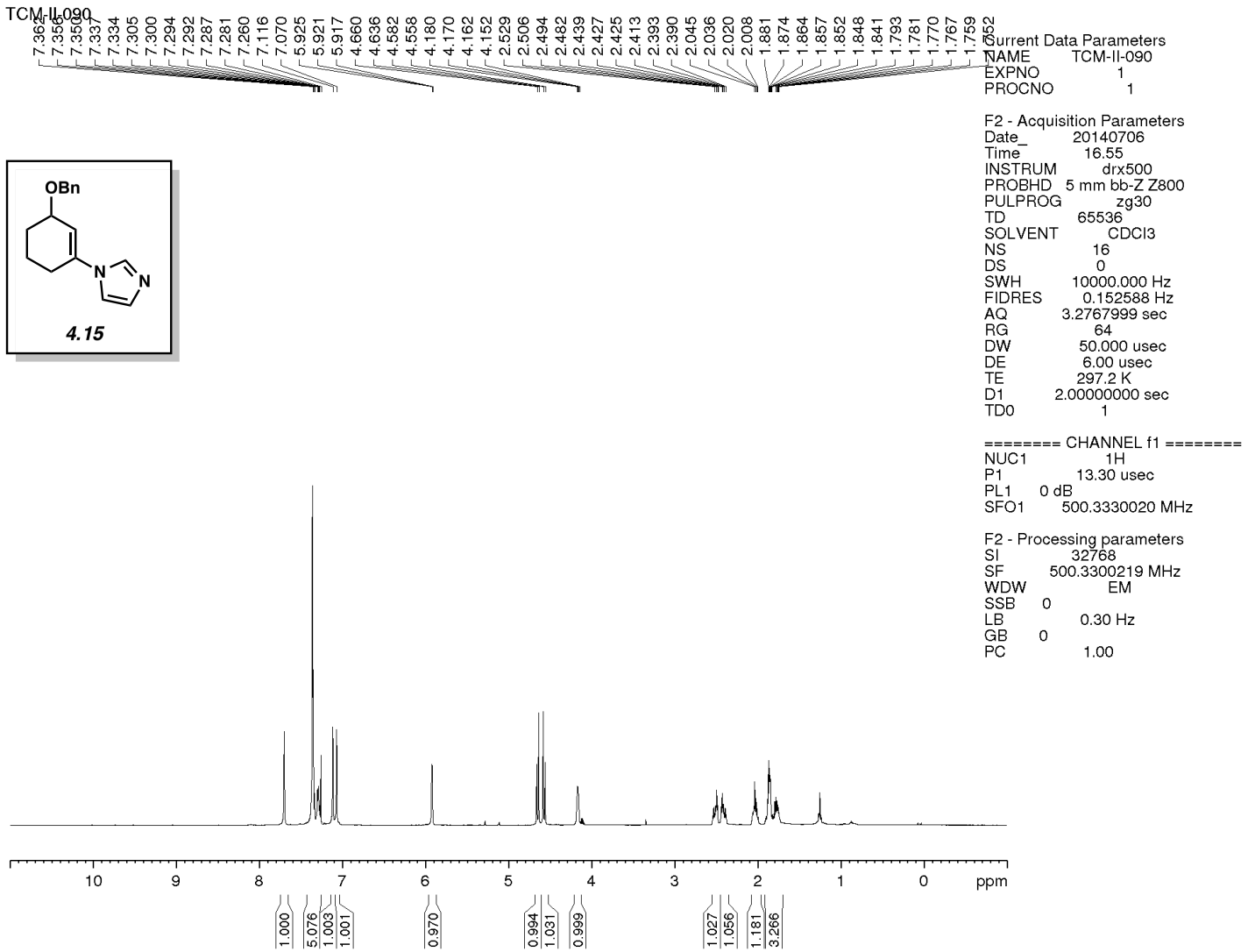

Figure 4.67. ^{1}H NMR (500 MHz, $CDCl_3$) compound **4.15**

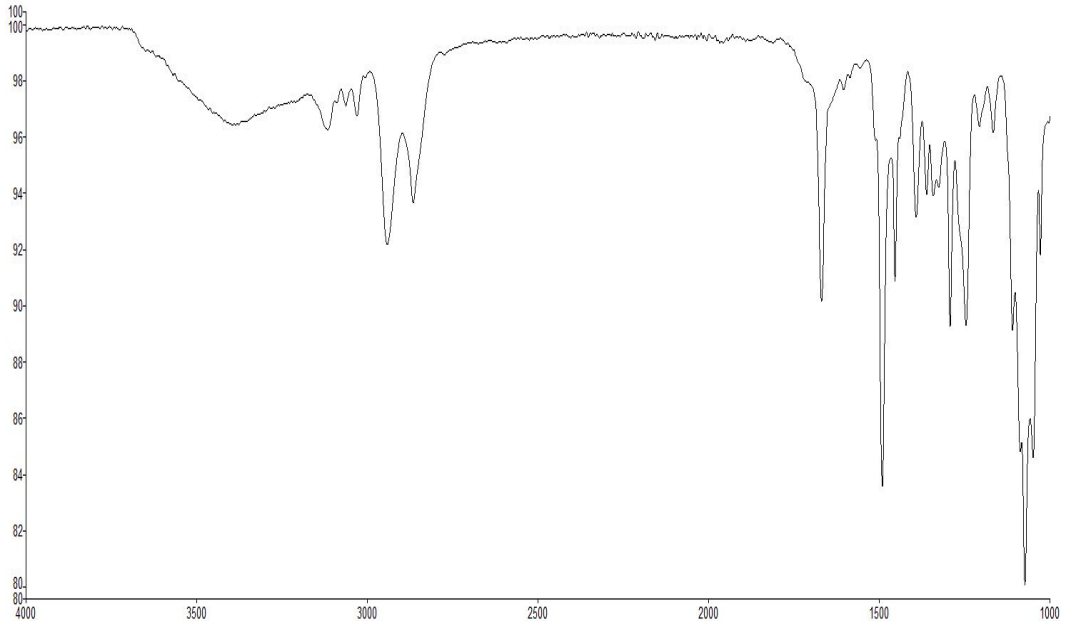

Figure 4.68. Infrared spectrum of compound **4.15**

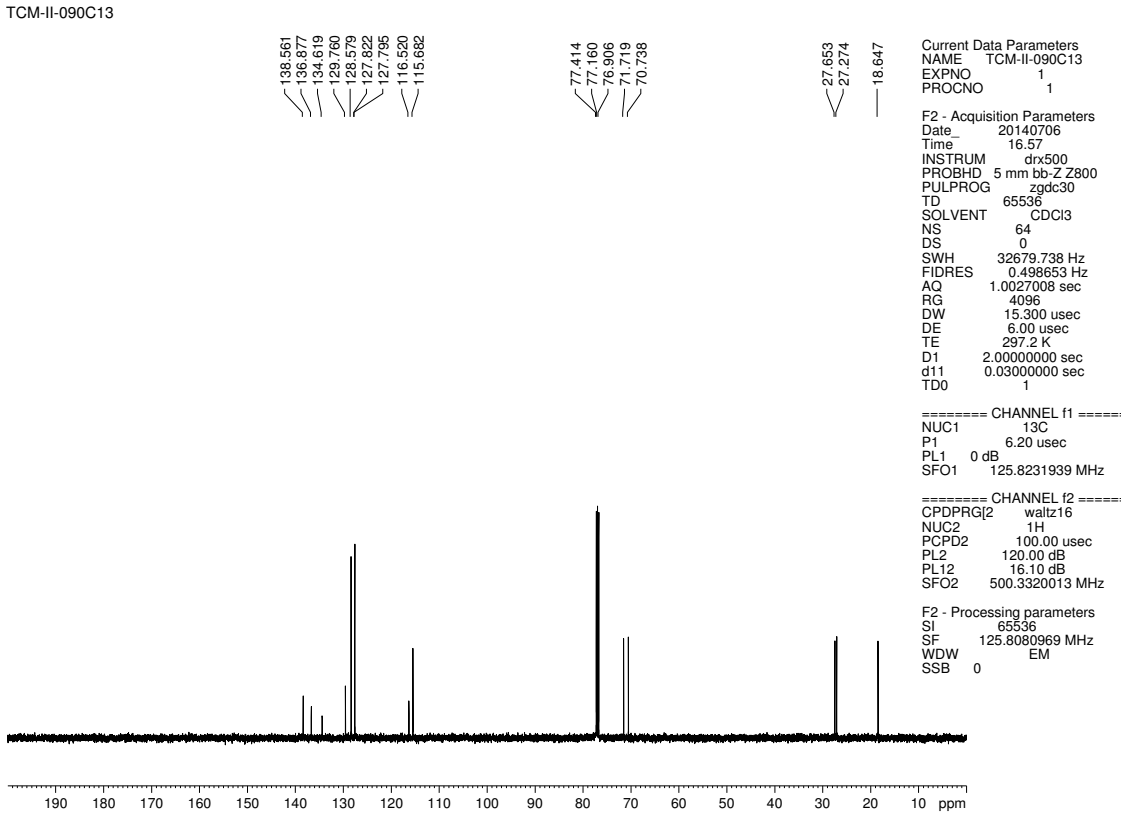

Figure 4.69. ^{13}C NMR (125 MHz, $CDCl_3$) of compound **4.15**

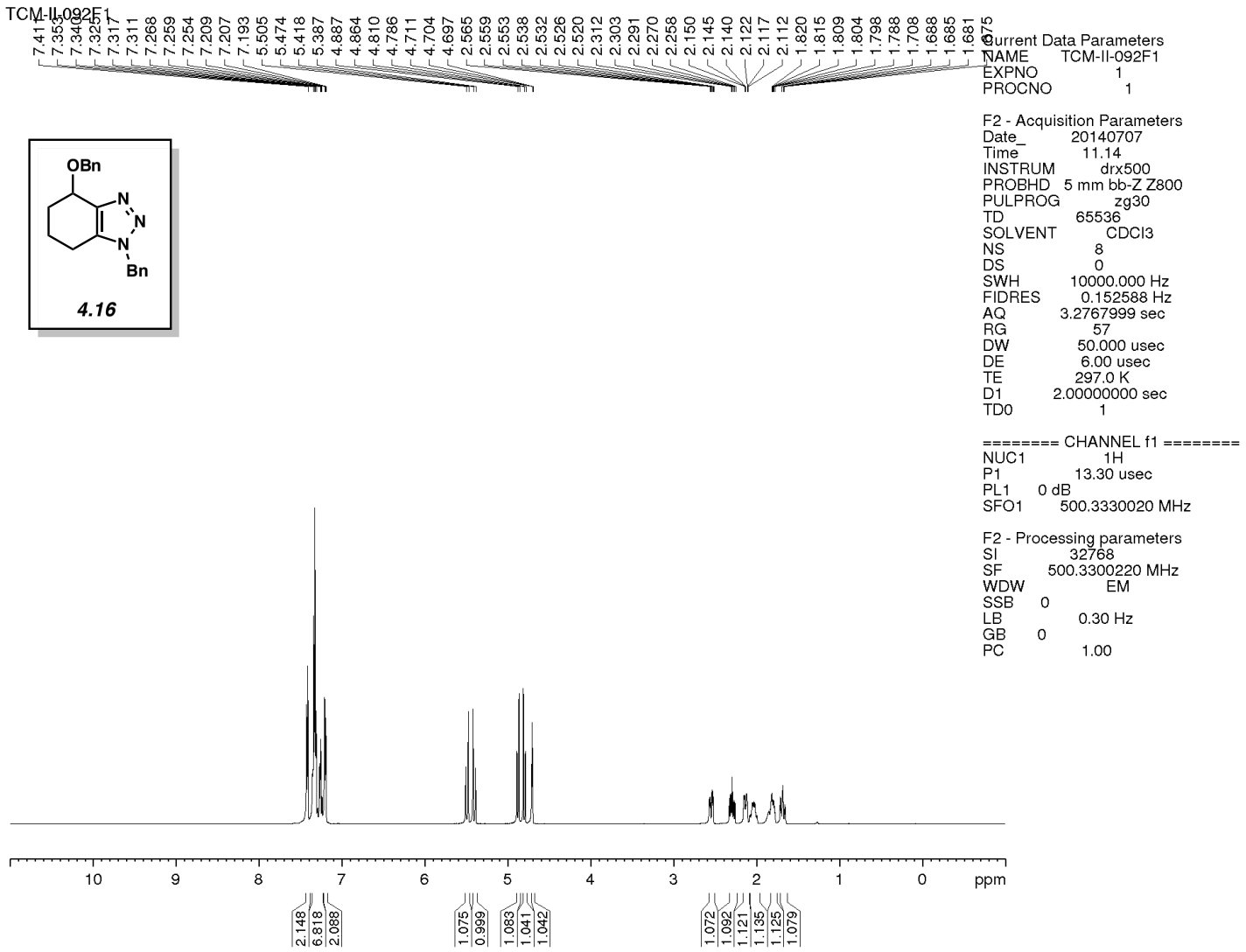

Figure 4.70. ^{1}H NMR (500 MHz, $CDCl_3$) compound **4.16**

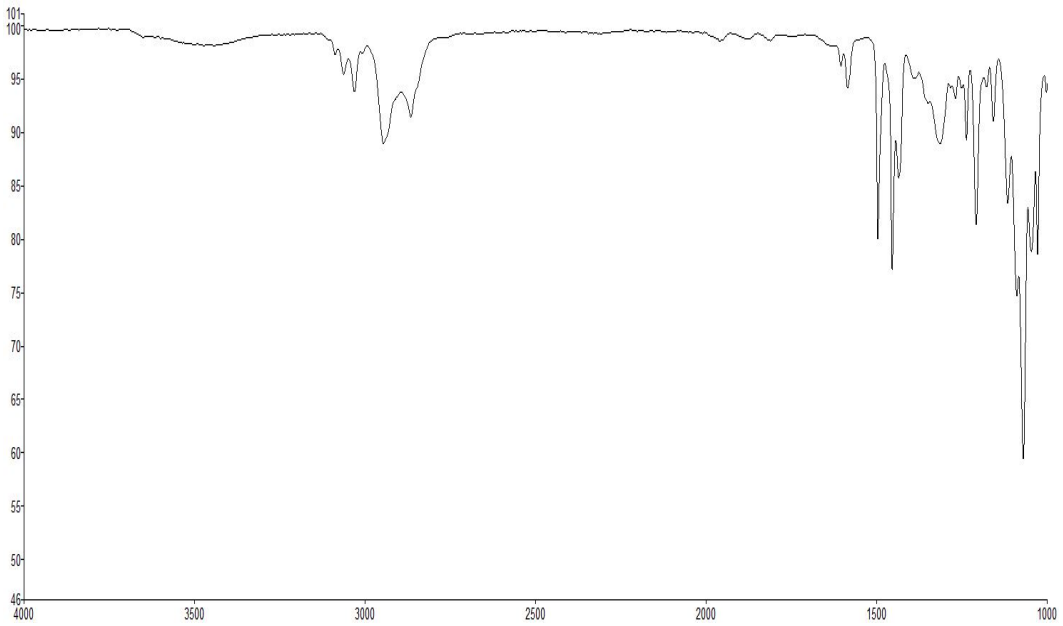

Figure 4.71. Infrared spectrum of compound **4.16**

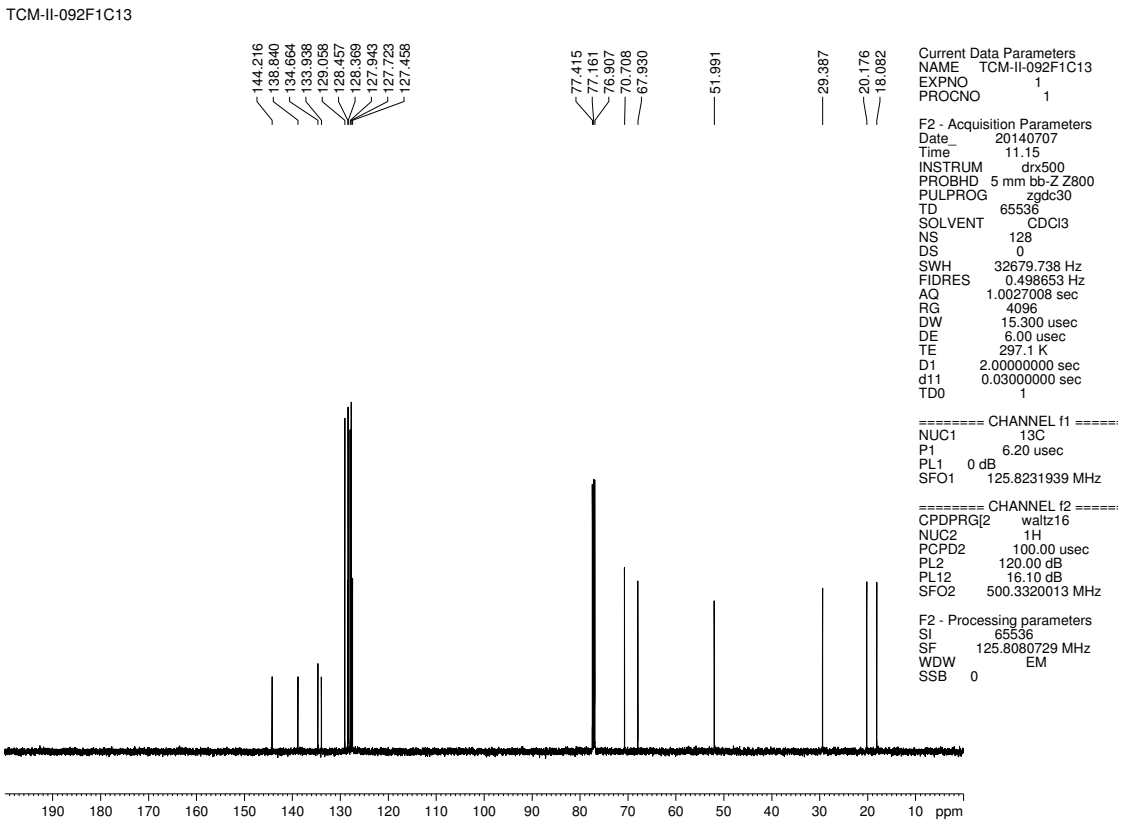

Figure 4.72. ^{13}C NMR (125 MHz, $CDCl_3$) of compound **4.16**

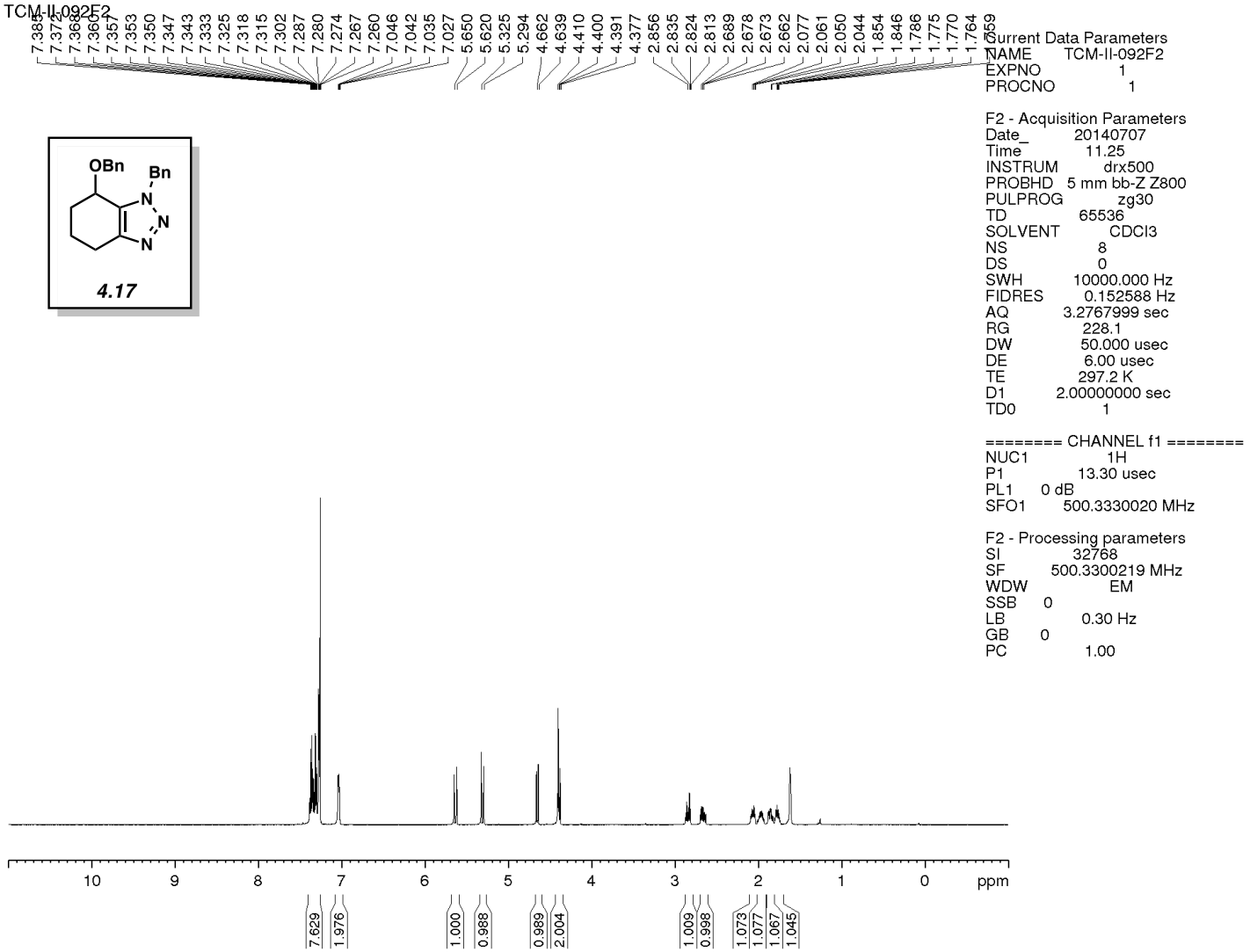

Figure 4.73. ^{1}H NMR (500 MHz, $CDCl_3$) compound **4.17**

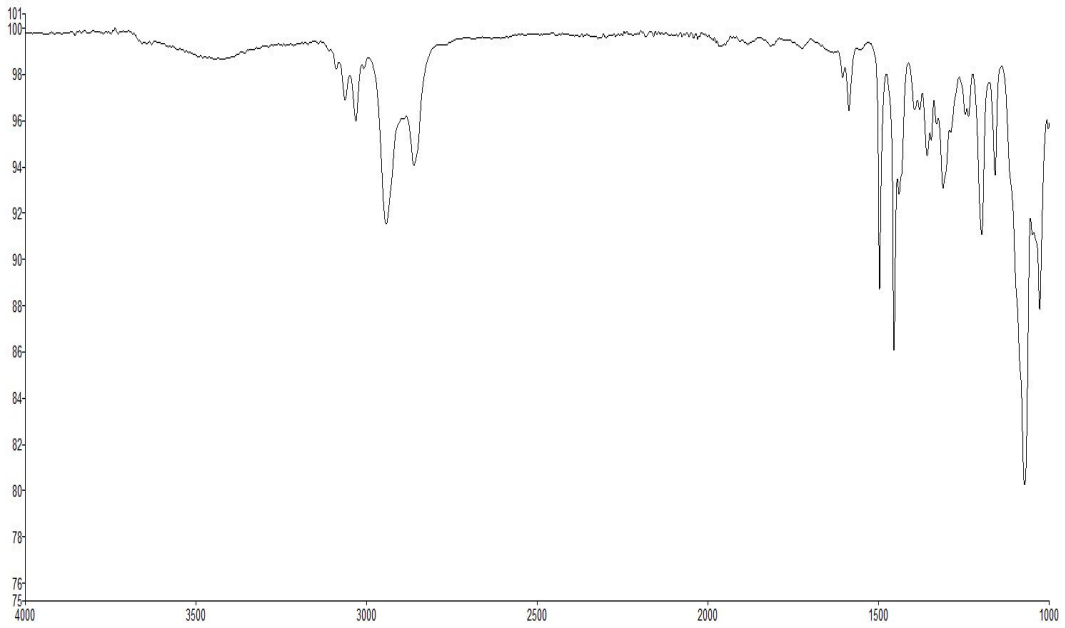

Figure 4.74. Infrared spectrum of compound **4.17**

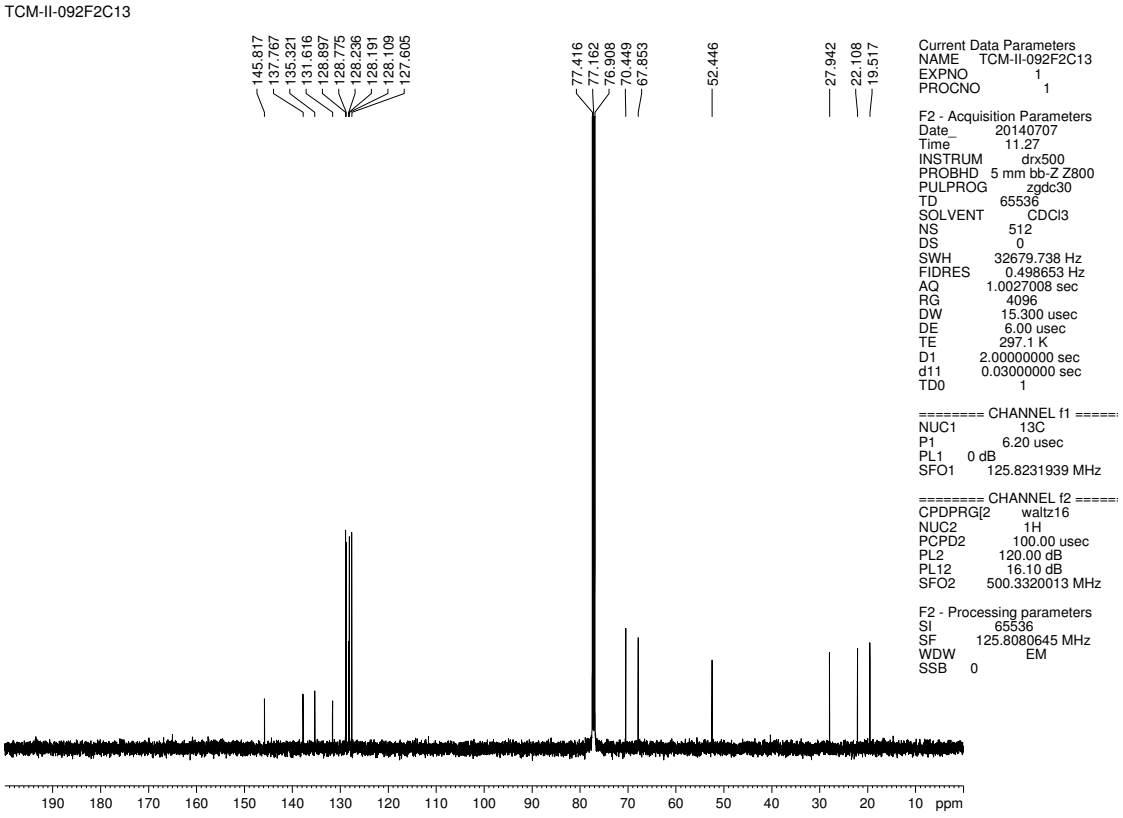

Figure 4.75. ^{13}C NMR (125 MHz, $CDCl_3$) of compound **4.17**

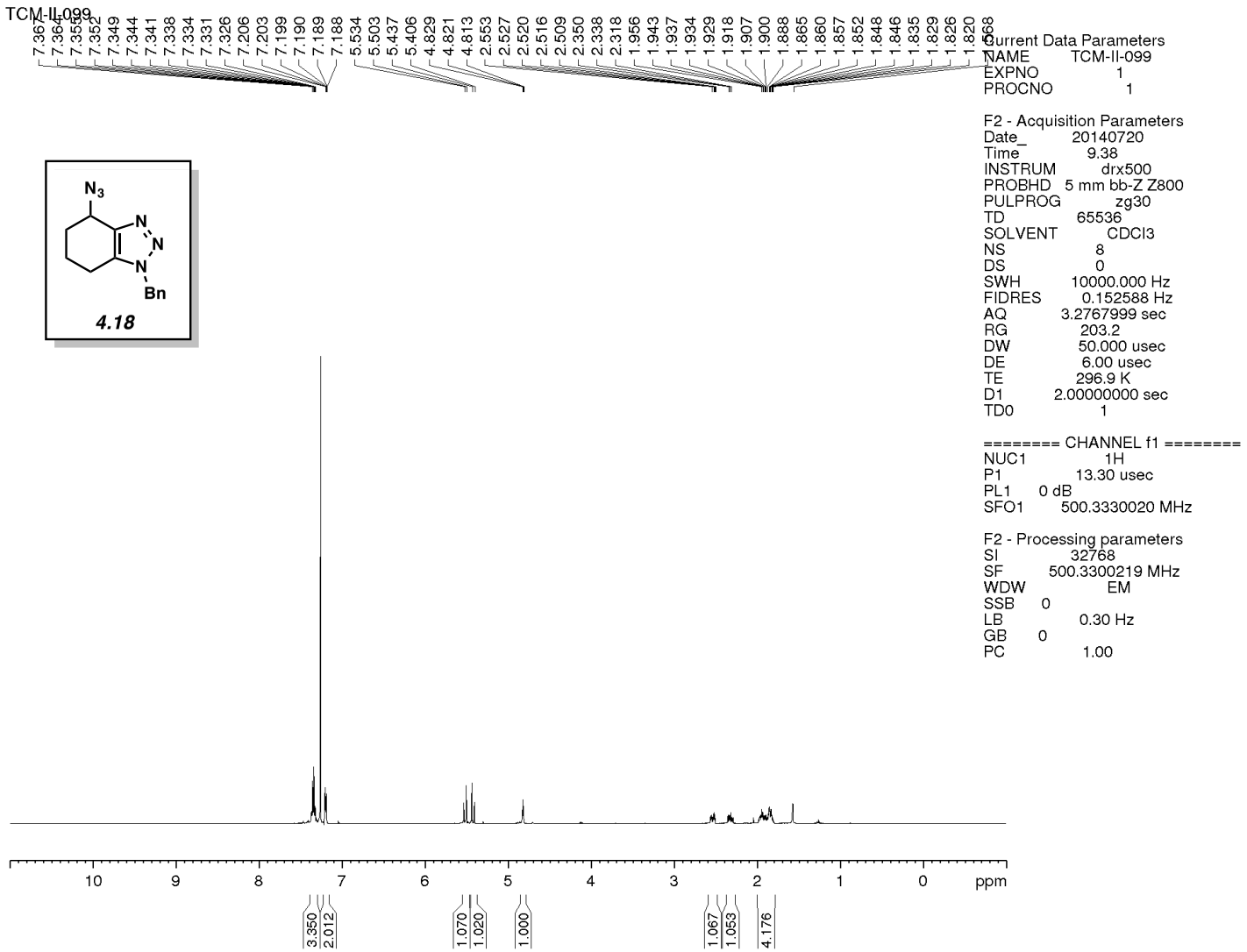

Figure 4.76. ^{1}H NMR (500 MHz, $CDCl_3$) compound **4.18**

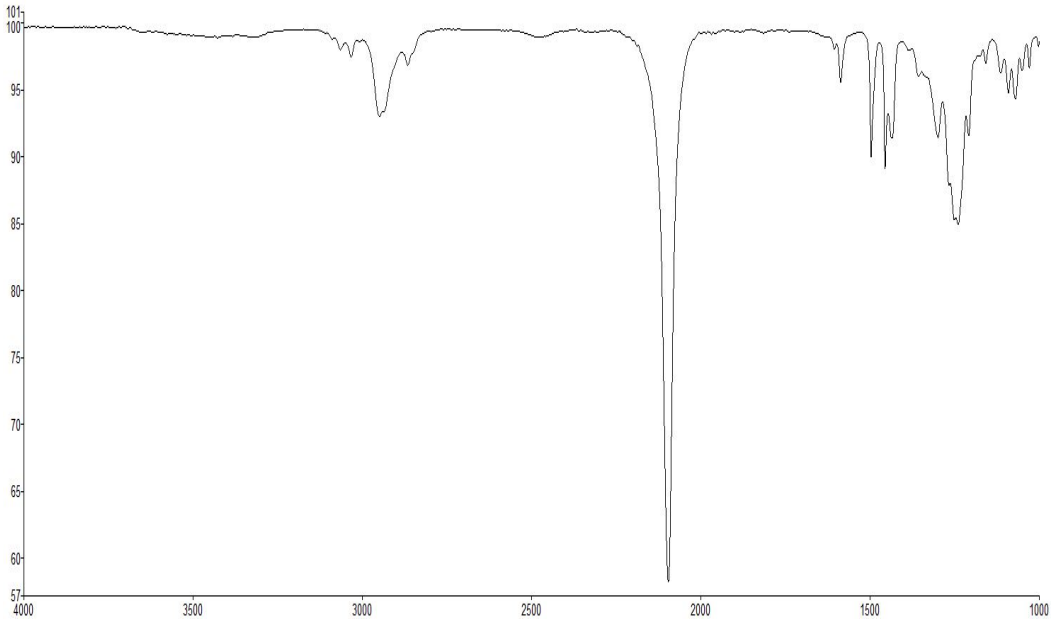

Figure 4.77. Infrared spectrum of compound **4.18**

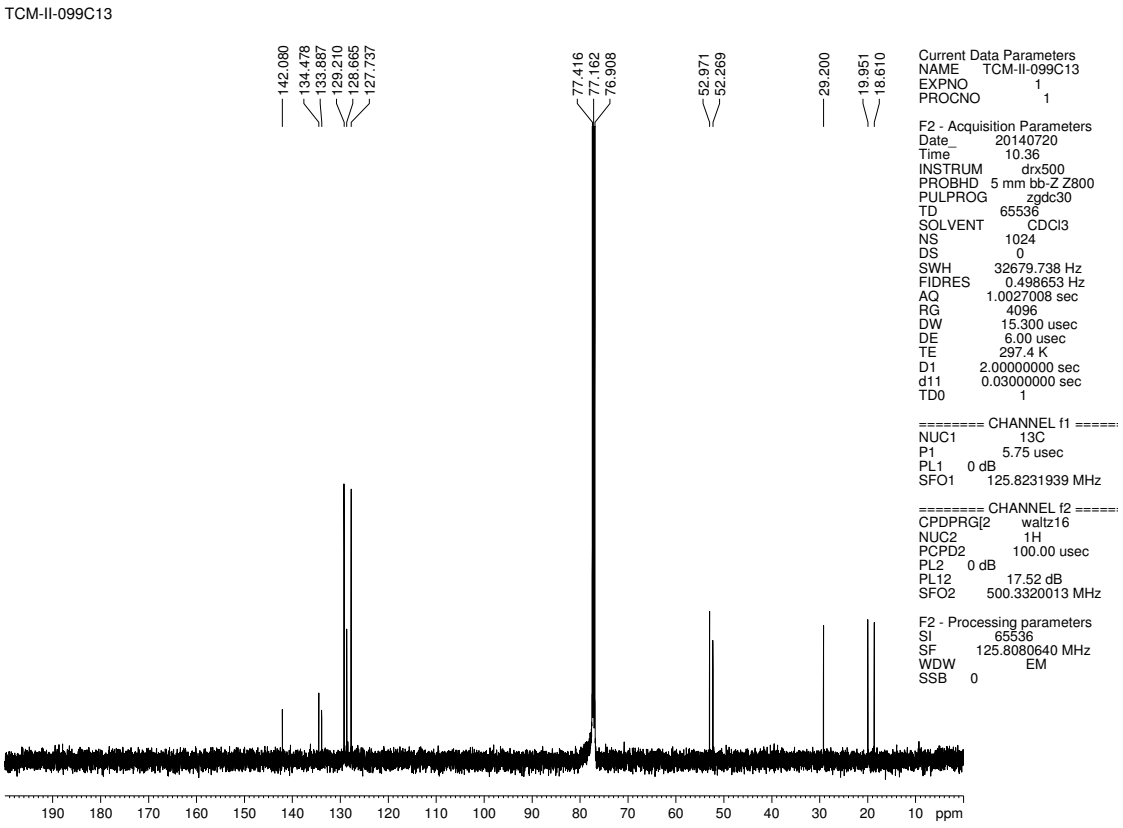

Figure 4.78. ^{13}C NMR (125 MHz, $CDCl_3$) of compound **4.18**

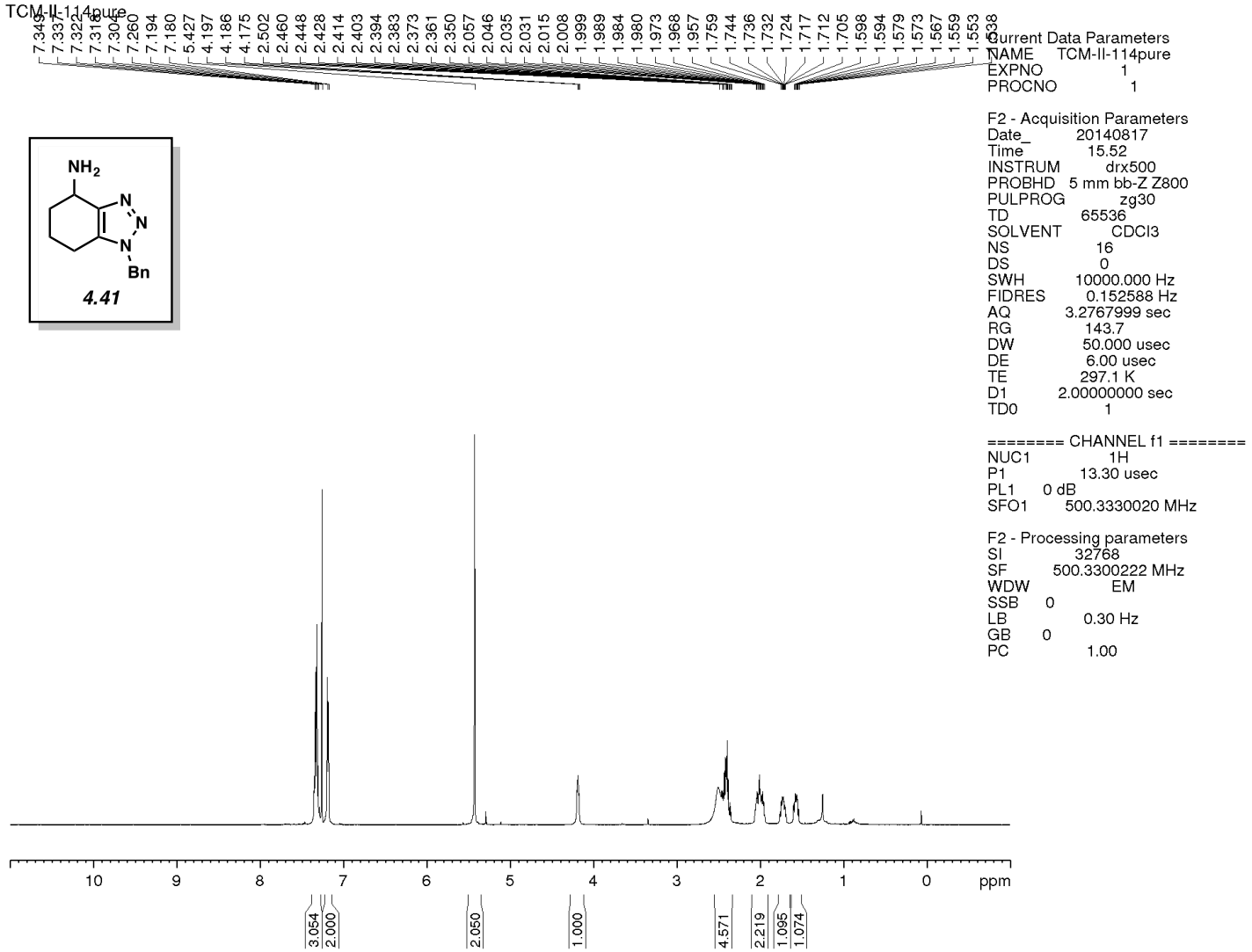

Figure 4.79. ^{1}H NMR (500 MHz, $CDCl_3$) compound **4.41**

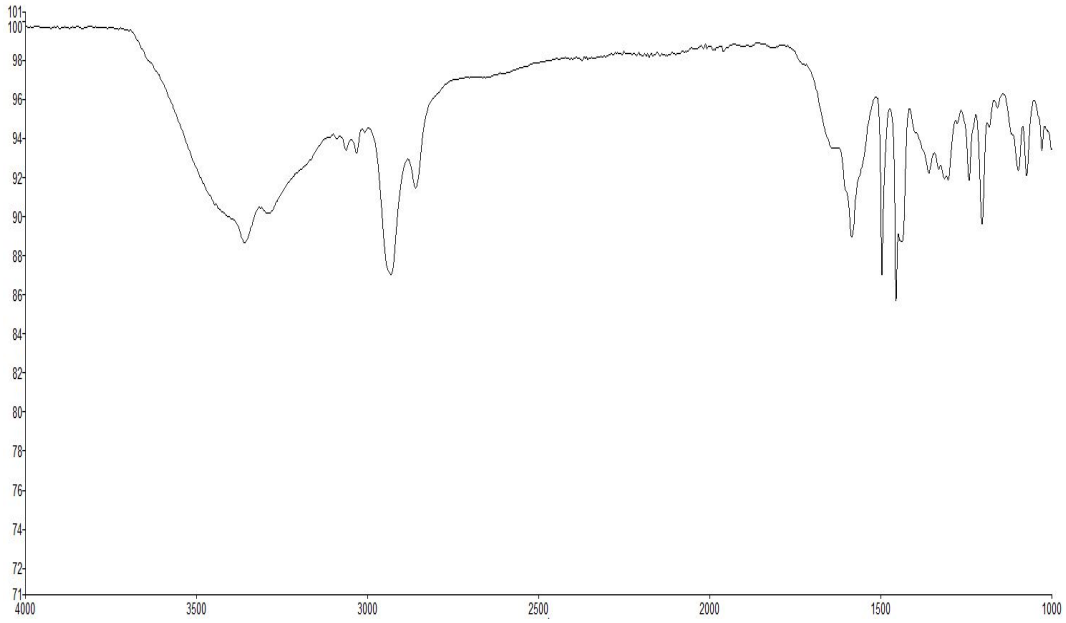

Figure 4.80. Infrared spectrum of compound **4.41**

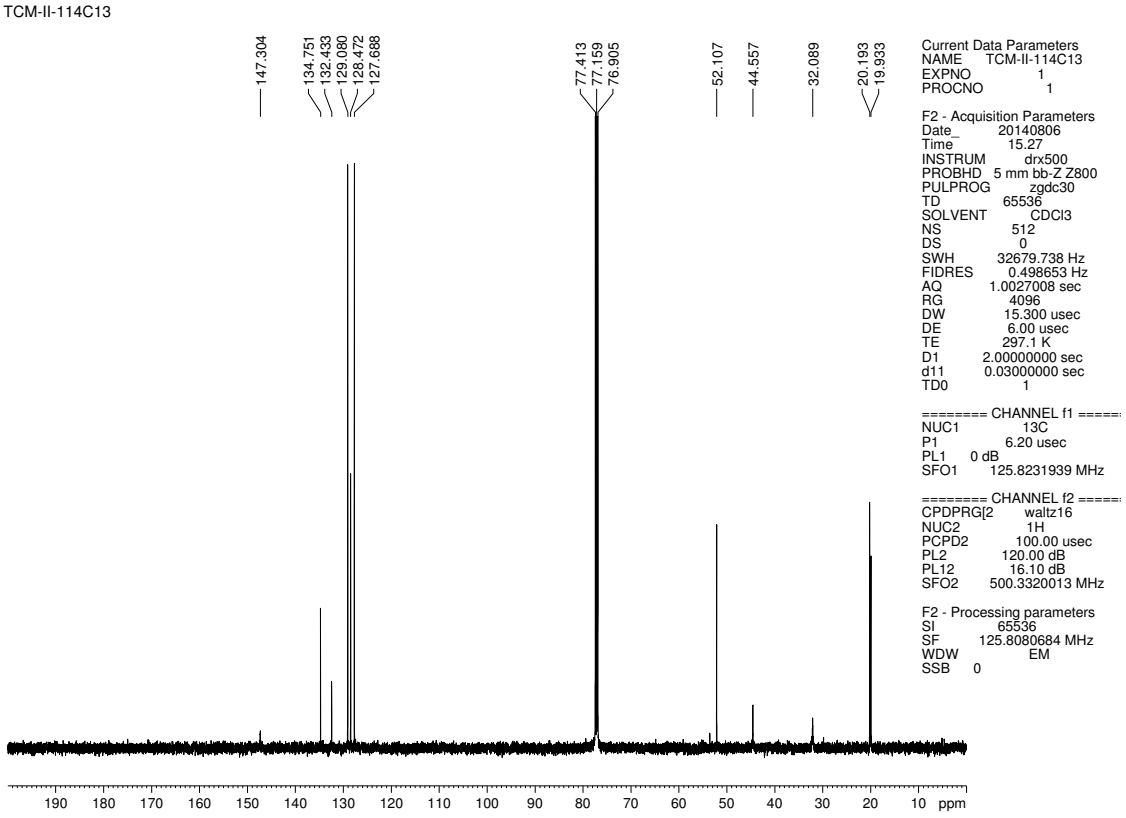

Figure 4.81. ^{13}C NMR (125 MHz, $CDCl_3$) of compound **4.41**

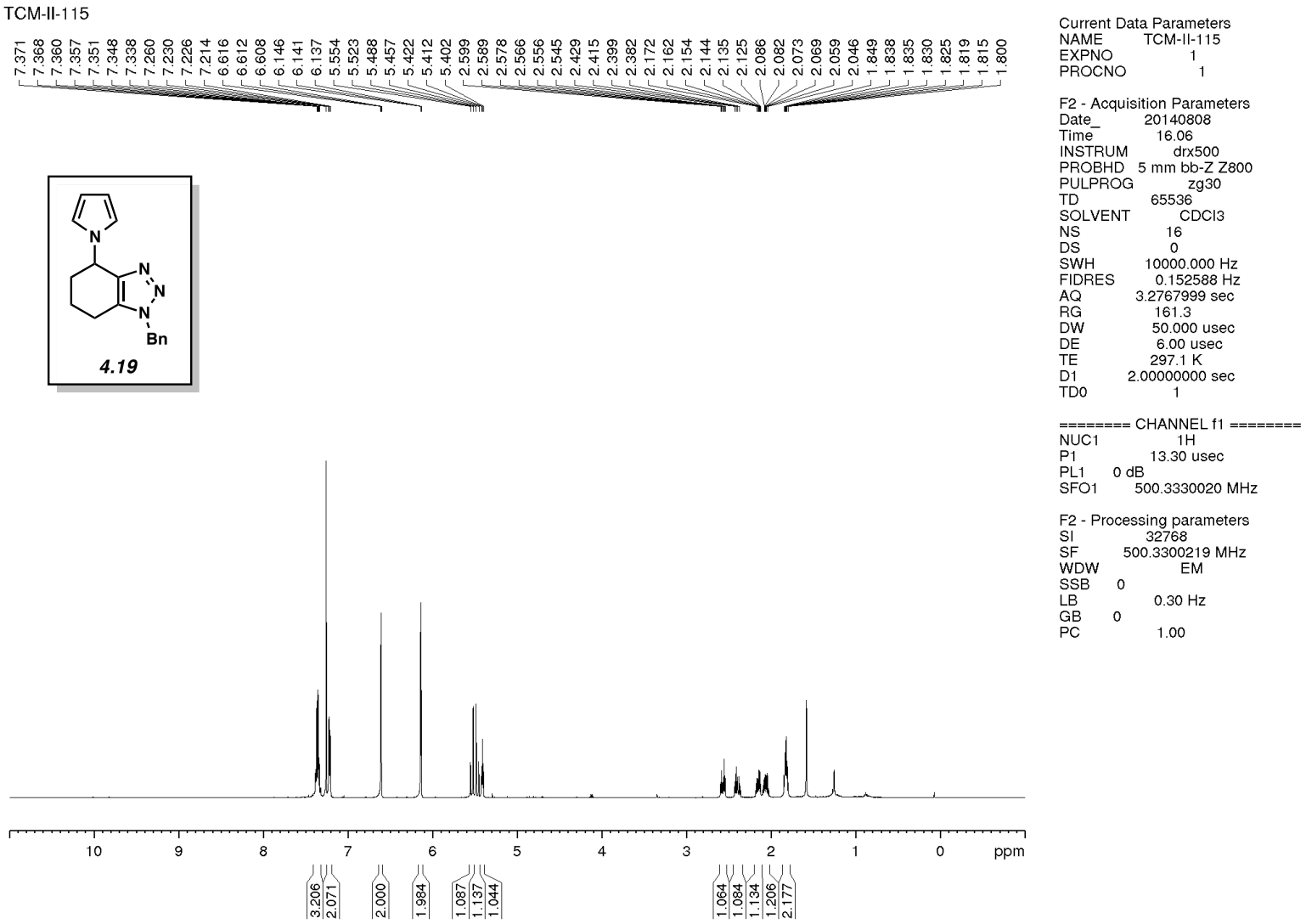

Figure 4.82. ^{1}H NMR (500 MHz, $CDCl_3$) compound **4.19**

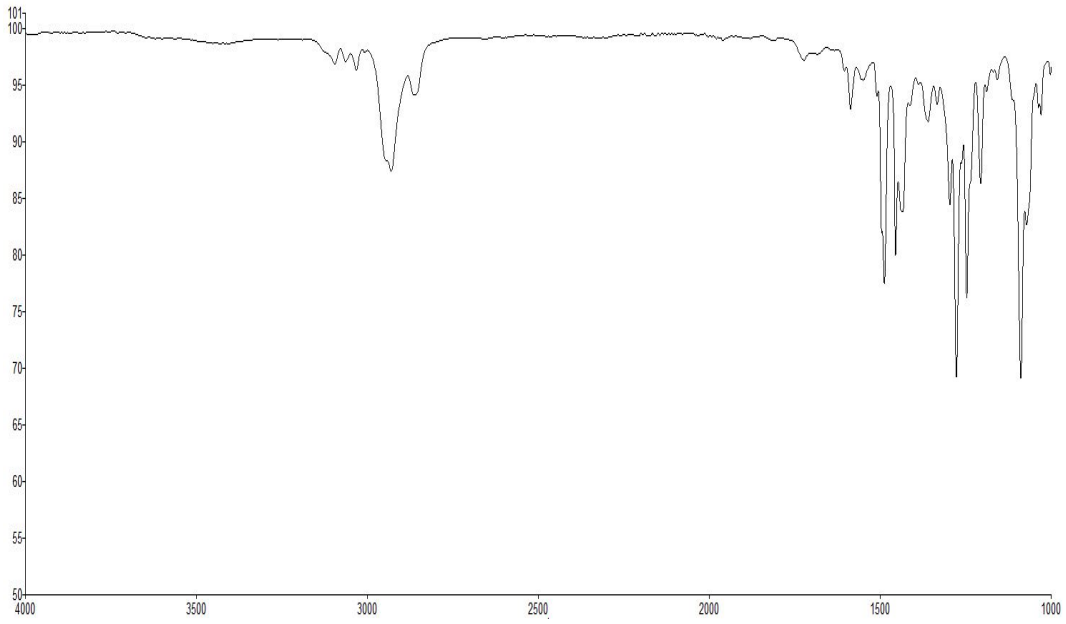

Figure 4.83. Infrared spectrum of compound **4.19**

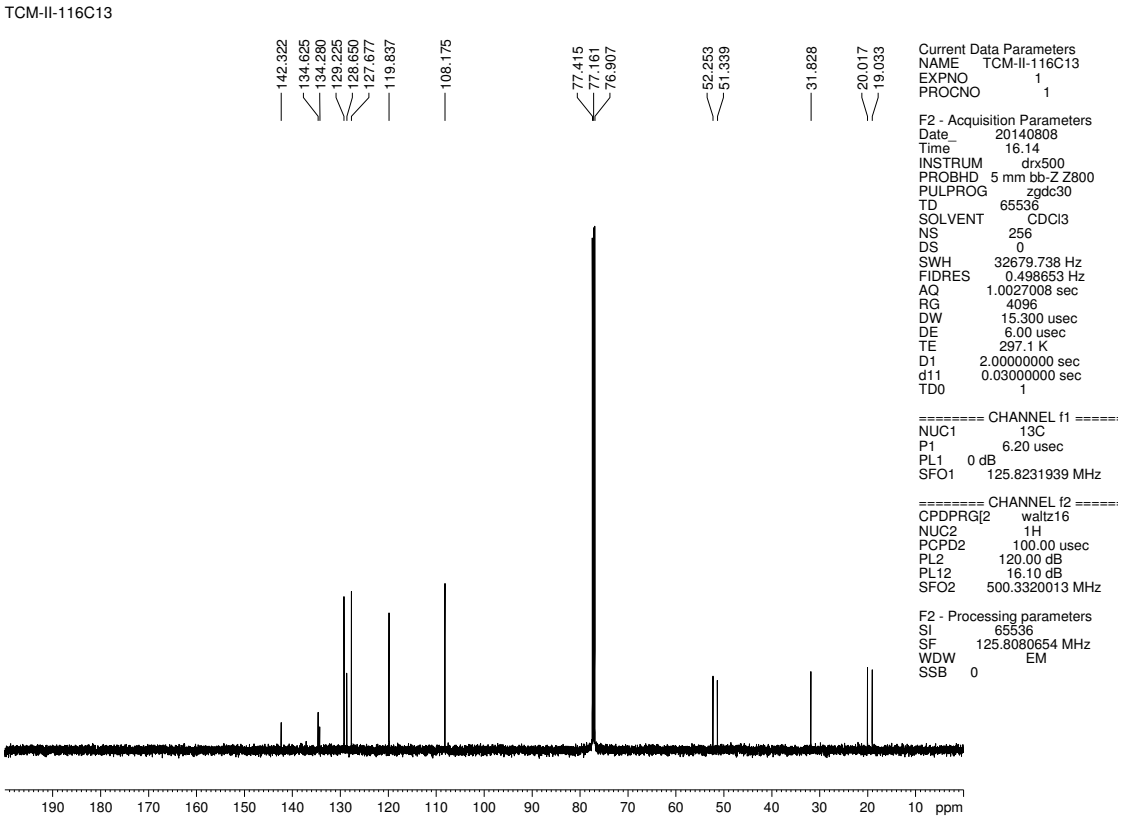

Figure 4.84. ^{13}C NMR (125 MHz, $CDCl_3$) of compound **4.19**

4.7 Notes and References

(1) For pertinent reviews, see: (a) Pellissier, H.; Santelli, M. *Tetrahedron* **2003**, *59*, 701–730. (b) Sanz, R. *Org*. *Prep. Proced. Int*. **2008**, *40*, 215–291. (c) Tadross, P. M.; Stoltz, B. M. *Chem. Rev*. **2012**, *112*, 3550–3577. (d) Gampe, C. M.; Carreira, E. M. *Angew. Chem. Int. Ed*. **2012**, *51*, 3766–3778.

(2) Stoermer, R.; Kahlert, B. *Ber.* **1902**, *35*, 1633–1640.

(3) Roberts, J. D.; Simmons Jr., H. E.; Carlsmith, L. A.; Vaughan, C. W. *J. Am. Chem. Soc.* **1953**, *75*, 3290–3291.

(4) For a pertinent review, see: Sletten, E. M.; Bertozzi, C. R. *Angew. Chem. Int. Ed.* **2009**, *48*, 6974–6998.

(5) For seminal manuscripts regarding cyclohexyne, see: (a) Scardiglia, F.; Roberts, J. D. *Tetrahedron* **1957**, *1*, 343–344. (b) Fixari, B.; Brunet, J. J.; Caubere, P. *Tetrahedron* **1976**, *32*, 927–934. (c) Wentrup, C.; Blanch, R.; Briehl, H.; Gross, G. *J. Am. Chem. Soc*. **1988**, *110*, 1874–1880.

(6) For seminal manuscripts regarding cyclopentyne, see: (a) Wittig, G.; Krebs, A.; Pohlke, R. *Angew. Chem.* **1960**, *72*, 324. (b) Montgomery, L. K.; Applegate, L. E. *J. Am. Chem. Soc*. **1967**, *89*, 5305–5307. (c) Chapman, O. L.; Gano, J.; West, P. R.; Regitz, M.; Maas, G. *J. Am. Chem. Soc.* **1981**, *103*, 7033–7036. (d) Wittig, G.; Heyn, J. *Liebigs Ann. Chem.* **1969**, *726*, 57–68.

(7) (a) Allan, K. M.; Hong, B. D.; Stoltz, B. M. *Org. Biomol. Chem*. **2009**, *7*, 4960–4964. (b) Gampe, C. M.; Boulos, S.; Carreira, E. M. *Angew. Chem. Int. Ed.* **2010**, *49*, 4092–4095. (c) Gampe, C. M.; Carreira, E. M. *Angew. Chem. Int. Ed.* **2011**, *50*, 2962–2965.

(8) For a pertinent computational study, see: Sader, C. A.; Houk, K. N. *J. Org. Chem*. **2012**, *77*, 4939–4948.

(9) (a) Atanes, N.; Escudero, S.; Pérez, D.; Guitián, E.; Castedo, L. *Tetrahedron Lett.* **1998**, *39*, 3039–3040. (b) See reference 31.

(10) For a study pertaining to cyclopentyne, see: Gilbert, J. C.; Hou, D.-R. *Tetrahedron* **2004**, *60*, 469–474; see also references therein.

(11) (a) Dinges, J.; Lamberth, C., Eds. *Bioactive Heterocyclic Compounds Classes: Pharmaceuticals*; Wiley-VCH: Weinheim, 2012. (b) Quin, L. D.; Tyrell, J. *Fundamentals of Heterocyclic Chemistry: Importance in Nature and in the Synthesis of Pharmaceuticals*; Wiley-Interscience: Hoboken, 2010.

(12) For the aryne distortion model, see: (a) Cheong, P. H.-Y.; Paton, R. S.; Bronner, S. M.; Im, G.-Y. J.; Garg, N. K.; Houk, K. N. *J. Am. Chem. Soc.* **2010**, *132*, 1267–1269. (b) Im, G.-Y. J.; Bronner, S. M.; Goetz, A. E.; Paton, R. S.; Cheong, P. H.-Y.; Houk, K. N.; Garg, N. K. *J. Am. Chem. Soc.* **2010**, *132*, 17933–17944. (c) Bronner, S. M.; Goetz, A. E.; Garg, N. K. *J. Am. Chem. Soc.* **2011**, *133*, 3832–3835. (d) Bronner, S. M.; Goetz, A. E.; Garg, N. K. *Synlett* **2011**, *18*, 2599–2604. (e) Goetz, A. E.; Bronner, S. M.; Cisneros, J. D.; Melamed, J. M.; Paton, R. S.; Houk, K. N.; Garg, N. K. *Angew. Chem. Int. Ed.* **2012**, *51*, 2758–2762. (f) Bronner, S. M.; Mackey, J. L.; Houk, K. N.; Garg, N. K. *J. Am. Chem. Soc.* **2012**, *134*, 13966–13969. (g) Goetz, A. E.; Garg, N. K. *Nat. Chem.* **2013**, *5*, 54–60. (h) Goetz, A. E.; Garg, N. K. *J. Org. Chem.* **2014**, *79*, 846–851.

(13) Silyltriflate **4.9** has also been employed in a Pd-catalyzed cyclotrimerization reaction; see reference 18.

(14) For the generation of cyclohexyne (**4.3**) from an iodonium precursor, see: Fujita, M.; Sakanishi, Y.; Kim, W. H.; Okuyama, T. *Chem. Lett.* **2002**, *31*, 908–909.

(15) In the absence of CsF, no reaction occurs, which suggests that a mechanism involving cycloaddition followed by elimination of the silyltriflate is not operative.

(16) (a) Lovering, F.; Bikker, J.; Humblet, C. *J. Med. Chem*. **2009**, *52*, 6752–6756. (b) Ritchie, T. J.; Macdonald, S. J. F. *Drug Discovery Today* **2009**, *14*, 1011–1020.

(17) No identifiable byproducts were obtained from these reactions, thus, we attribute the loss of mass to substantial non-specific decomposition.

(18) Iglesias, B.; Peña, D.; Pérez, D.; Guitián, E.; Castedo, L. *Synlett* **2002**, 486–488.

(19) For the trapping of arynes with dimethylurea, see: Yoshida, H.; Shirakawa, E.; Honda, Y.; Hiyama, T. *Angew. Chem. Int. Ed.* **2002**, *41*, 3247–3249.

(20) Interestingly, the corresponding trapping experiment involving cyclohexyne precursor **4.9** in place of **4.10** failed.

(21) **4.3** and **4.4** have previously been studied computationally (see references 22 and 24); however, our efforts mark the first computational study of a 3-substituted cyclohexyne and regioselectivity predictions.

(22) (a) Johnson, R. P.; Daoust, K. J. *J. Am. Chem. Soc.* **1995**, *117*, 362–367. (b) Olivella, S.; Pericas, M. A.; Riera, A.; Sole, A. *J. Org. Chem.* **1986**, *52*, 4160–4163.

(23) Other stationary points on the potential energy surface of the well-known cyclopentyne to cyclobutylidenecarbene rearrangement were also located. These structures are not relevant for this study, although the moderate yields obtained experimentally suggest competitive processes

in which these carbene-like species could be involved; see: Domingo, L. R.; Pérez, P.; Contreras, R. *Eur. J. Org. Chem.* **2006**, 498–506.

(24) Olivella, S.; Pericas, M. A.; Riera, A.; Sole, A. *J. Am. Chem. Soc.* **1986**, *108*, 6884–6888.

(25) In addition to the minimum energy conformer shown in Figure 4.2, we located another half-chair conformer of **4.12**, which is 0.8 kcal/mol less stable and shows similar distortion with internal angles of 135° and 128° at C1 and C2, respectively.

(26) Bent, H. *Chem. Rev.* **1961**, *61*, 275–311.

(27) See the Experimental Section for details.

(28) Houk, K. N.; Sims, J.; Watts, C. R.; Luskus, L. J. *J. Am. Chem. Soc.* **1973**, *95*, 7301–7315.

(29) Methyl azide is used as a model for benzyl azide; **4.12** is used as a model for **4.14**.

(30) Sawama, Y.; Goto, R.; Nagata, S.; Shishido, Y.; Monguchi, Y.; Sajiki, H. *Chem. Eur. J.* **2014**, *20*, 2631–2636.

(31) Devlin, A. S.; Du Bois, J. *Chem. Sci*. **2013**, *4*, 1059–1063.

(32) Thoman, C. J.; Voaden, D. J. *Org. Synth*. **1965**, *45*, 96.

(33) Dubrovskiy, A. V.; Larock, R. C. *Org. Lett*. **2010**, *12*, 1180–1183.

(34) Shih, C.; Fritzen, E. L.; Swenton, J. S. *J. Org. Chem*. **1980**, *45*, 4462–4471.

(35) Zhao, Y.; Truhlar, D. *Theor. Chem. Acc.* **2008**, *120*, 215–241.

(36) Gaussian 09, Revision D.1., Frisch, M. J.; Trucks, G. W.; Schlegel, H. B.; Scuseria, G. E.; Robb, M. A.; J. R. Cheeseman; Scalmani, G.; Barone, V.; Mennucci, B.; Petersson, G. A.; Nakatsuji, H.; Caricato, M.; Li, X.; Hratchian, H. P.; Izmaylov, A. F.; Bloino, J.; Zheng, G.; Sonnenberg, J. L.; Hada, M.; Ehara, M.; Toyota, K.; Fukuda, R.; Hasegawa, J.; Ishida, M.; Nakajima, T.; Honda, Y.; Kitao, O.; Nakai, H.; Vreven, T.; Montgomery, J. A.; Peralta, J. E.;

Ogliaro, F.; Bearpark, M.; Heyd, J. J.; Brothers, E.; Kudin, K. N.; Staroverov, V. N.; Kobayashi, R.; Normand, J.; Raghavachari, K.; Rendell, A.; Burant, J. C.; Iyengar, S. S.; Tomasi, J.; Cossi, M.; Rega, N.; Millam, J. M.; Klene, M.; Knox, J. E.; Cross, J. B.; Bakken, V.; Adamo, C.; Jaramillo, J.; Gomperts, R.; Stratmann, R. E.; Yazyev, O.; Austin, A. J.; Cammi, R.; Pomelli, C.; Ochterski, J. W.; Martin, R. L.; Morokuma, K.; Zakrzewski, V. G.; Voth, G. A.; Salvador, P.; Dannenberg, J. J.; Dapprich, S.; Daniels, A. D.; Farkas, Ö.; Foresman, J. B.; Ortiz, J. V.; Cioslowski, J.; Fox, D. J. Gaussian, Inc., Wallingford CT, 2009.

(37) (a) Gonzalez, C.; Schlegel, H. B. *J. Chem. Phys.* **1989**, *90*, 2154–2161. (b) Gonzalez, C.; Schlegel, H. B. *J. Phys. Chem.* **1990**, *94*, 5523–5527.

(38) Scalmani, G.; Frisch, M. J. *J. Chem. Phys.* **2010**, *132*, 114110.

(39) Medina, J. M.; McMahon, T. C.; Jimenez-Oses, G.; Houk, K. N.; Garg, N. K. *J. Am. Chem. Soc*. **2014**, *136*, 14706–14709.

CHAPTER FIVE

Generation and Regioselective Trapping of a 3,4-Piperidyne for the Synthesis of Functionalized Heterocycles

Travis C. McMahon, Jose M. Medina, Yun-Fang Yang, Bryan J. Simmons,

K. N. Houk, and Neil K. Garg

J. Am. Chem. Soc. **2015**, *137*, 4082–4085.

5.1 Abstract

We report the generation of the first 3,4-piperidyne and its use as a building block for the synthesis of annulated piperidines. Experimental and computational studies of this intermediate are disclosed, along with comparisons to the well-known 3,4-pyridyne. The distortion/interaction model is used to explain the observed regioselectivities.

5.2 Introduction

Heterocycles containing one or more nitrogen atoms comprise nearly 60% of all small-molecule drugs that have been approved by the U.S. Food and Drug Administration.[1] The most prevalent of *N*-containing heterocycles is the piperidine ring, which is found in 72 currently marketed small-molecule drugs. Notable examples include the blockbuster drugs clopidogrel (Plavix), tadalafil (Cialis), and solifenacin (VESIcare) (Figure 5.1). Given the importance of this medicinally privileged scaffold, new methods to rapidly access annulated piperidines from simple precursors are highly sought after.

With the aim of developing a new method for the synthesis of decorated piperidines, we questioned if the unusual 3,4-piperidyne intermediate **5.1** could be generated and used as a new synthetic building block (Figure 5.1). Notably, 3,4-piperidynes have never been accessed previously. The most closely related studies have involved the isomeric 2,3-piperidyne **5.2**, which has been the subject of two seminal investigations. In 1988, Wentrup and coworkers generated **5.2** (R = H) using flash vacuum pyrolysis.[2] Although **5.2** was deemed unstable above –150 °C and was never utilized in any synthetic application, Wentrup's studies validated the notion that **5.2** could be generated. Additionally, during the preparation of this manuscript, Danheiser disclosed an efficient means to access **5.2** (R = Ts) and performed a series of synthetically useful trapping reactions.[3] Interestingly, whereas piperidynes have been rarely studied,[4] the corresponding aromatic pyridynes **5.3**[5] and **5.4**,[6] along with many other arynes and hetarynes, have been widely pursued for more than half a century.[7,8,9]

Herein we report: (a) the first generation of a 3,4-piperidyne **5.1**; (b) the strategic use of **5.1** to construct a range of functionalized piperidines, many of which possess significant aliphatic character[10] and represent new heterocyclic scaffolds; (c) regioselectivity predictions,

observations, and explanations involving the 3,4-piperidyne, which are in accord with the distortion/interaction model;[7a,7d,8a] and (d) an explanation for the lack of selectivity observed in trapping experiments of the 3,4-pyridyne (**5.3**), which has been unresolved for many decades.

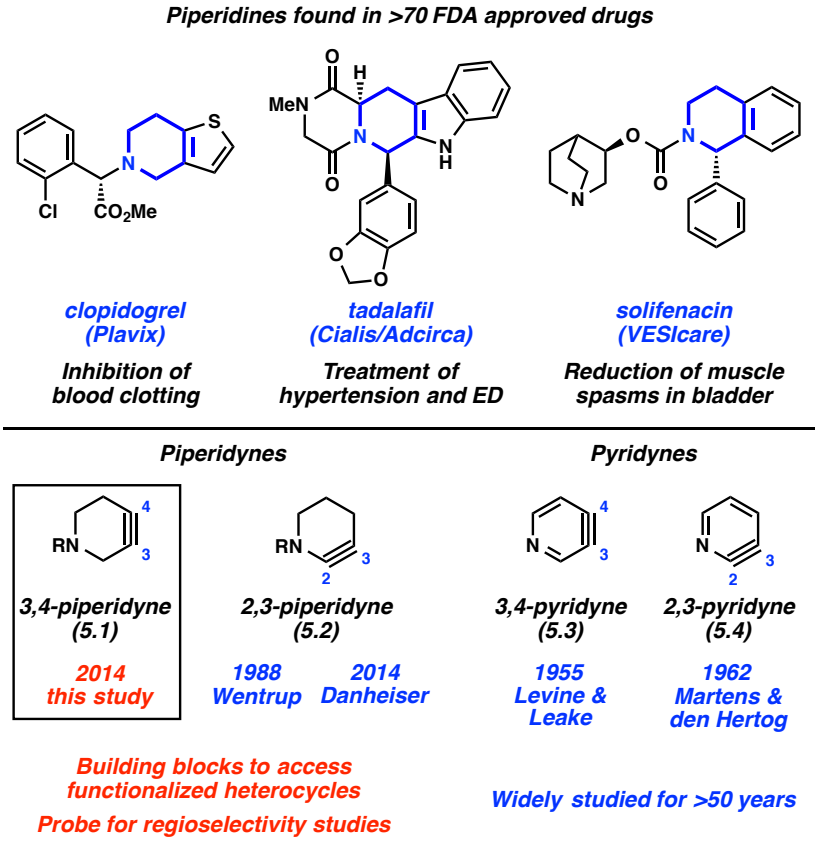

Figure 5.1. Piperidine-containing drugs, piperidynes **5.1** and **5.2**, and pyridynes **5.3** and **5.4**

5.3 Results and Discussion

5.3.1 Prediction of Regioselectivities Based on the Distortion/Interaction Model

We initiated our studies by applying the distortion/interaction model to our targeted piperidyne, Cbz-derivative **5.1a**,[11] in order to assess its likelihood that it would undergo regioselective trapping in reactions with nucleophiles and cycloaddition partners (Figure 5.2). In

previous studies, we have shown that the degree of distortion present in the ground state of arynes and strained alkynes correlates to observed regioselectivities due to the intermediate being pre-distorted toward one of two competing transition states.[7a,7d,8a,9] Geometry optimization using DFT calculations (B3LYP/6-31G(d)) revealed that **5.1a** is significantly distorted (ca. 10° difference in internal angles at C4 and C3) such that nucleophilic addition should occur preferentially at the more linear terminus (C4). As a key point of comparison, we also studied the 3,4-pyridyne (**5.3**), which is well known to react with poor regioselectivity,[7a,7d,8a,12] as alluded to earlier. In contrast to **5.1a**, the geometry-optimized structure of **5.3** shows little unsymmetrical distortion. Given this interesting dichotomy, we envisioned that experimental studies of 3,4-piperidyne **5.1a** would not only test our regioselectivity predictions, but could ultimately also shed light on why the 3,4-pyridyne (**5.3**) is not significantly distorted and, accordingly, reacts with poor regioselectivity.

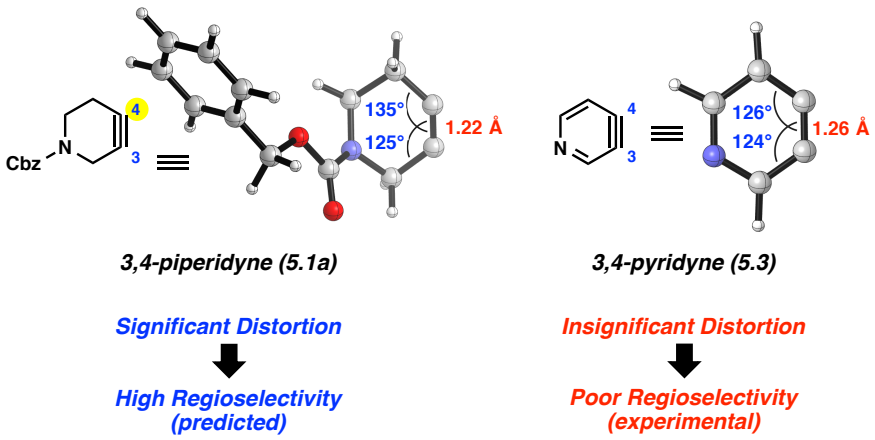

Figure 5.2. Optimized structures of **5.1a** and **5.3** obtained at the B3LYP/6-31G(d) level

5.3.2 Synthesis of Silyl Triflate Precursor

The success of our study would rely on the development of an efficient synthesis of a suitable 3,4-piperidyne precursor. After identifying silyltriflate **5.8** as our target,[11, 13] we developed the robust and scalable three-step route shown in Scheme 5.1. Beginning from commercially available 4-methoxypyridine (**5.5**), a known procedure was employed to effect ortho silylation to yield silyl pyridine **5.6**.[14] Next, a one-pot procedure involving reductive carbamoylation and hydrolysis[15] provided vinylogous amide **5.7** in excellent yield. Finally, conjugate reduction followed by trapping of the resultant enolate with Tf_2O[16] provided silyltriflate **5.8**. The sequence was performed on gram scale and provided **5.8** in 51% overall yield from **5.5**.[17]

Scheme 5.1. Syntheses of Silyl Triflate **5.8**

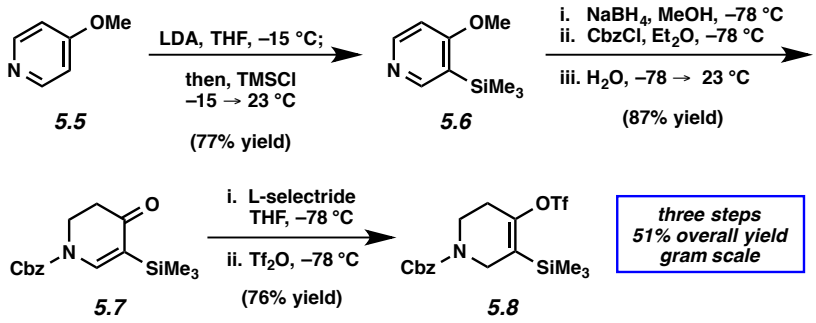

5.3.3 Generation & Trapping of 3,4-Piperidyne 5.1a

To validate that the 3,4-piperidyne could be generated, we performed a series of Diels–Alder trapping experiments to produce a variety of annulated products (Table 5.1). Specifically, silyltriflate **5.8** was treated with CsF in the presence of several trapping agents (3 equiv) in acetonitrile at 60 °C. The use of tetracyclone as the trapping agent delivered a

tetrahydroisoquinoline product in 76% yield via cycloaddition, followed by loss of CO (entry 1). An alternate tetrahydroisoquinoline was accessed upon trapping of the intermediate 3,4-piperidyne with 2-pyrone, by way of a Diels–Alder, retro-Diels–Alder sequence with concomitant loss of CO_2 (entry 2). Additionally, cycloadditions with 2,5-dimethylfuran or *N*-Boc-pyrrole provided the corresponding piperidine-fused [2.2.1]-bridged bicyclic products (entries 3 and 4).

Table 5.1. Diels–Alder Cycloadditions of 3,4-Piperidyne **5.1a**

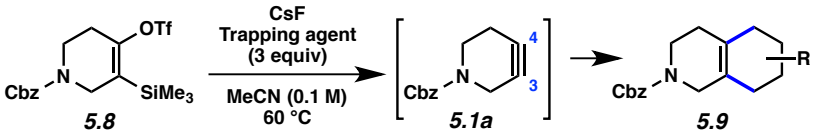

Entry	Trapping agent	Product	Yield[a]
1	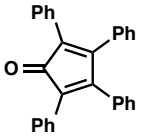	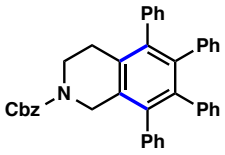	76%
2	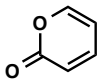		62%
3	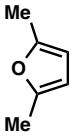	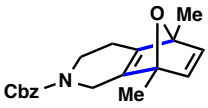	61%
4	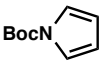	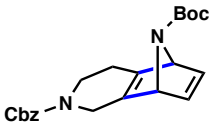	66%

[a] Reported yields are the average of two experiments and are based on the amount of isolated products.

Encouraged by our initial success, we carried out trapping experiments of 3,4-piperidyne **5.1a** with a variety of nucleophiles and unsymmetrical cycloaddition partners (Table 5.2). In

addition to acting as a probe for our regioselectivity predictions, some of the transformations provide access to interesting heterocyclic products. Nucleophilic addition experiments were performed with imidazole and morpholine (entries 1 and 2). In both cases, addition occurred exclusively at C4, consistent with our earlier prediction and differing from the known trends of 3,4-pyridyne reactions. An analogous regiochemical preference was observed in a series of cycloaddition reactions. For example, trapping with a nitrone afforded isoxazoline products in good yield and with a significant regiochemical preference of 12.7 to 1 (entry 3). (3+2) Cycloadditions using either azide or diazo coupling partners provided triazole and pyrazole products, respectively (entries 4 and 5). Pyridine- and *N*-Ph pyrazole-containing annulated products could be obtained as well, albeit with lower selectivities (entries 6 and 7).[18]

Several salient features regarding this methodology and the products shown in Tables 5.1 and 5.2 should be noted. (a) Analogous to known reactions of arynes using silyltriflate precursors, 3,4-piperidyne trapping experiments are operationally trivial to perform and generally do not require the rigorous exclusion of oxygen or moisture. (b) Silyltriflate **5.8**, which is now being commercialized to enable its widespread use in drug discovery,[17] can be used as a single precursor in order to access a variety of annulated piperidines. This stands in contrast to more conventional strategies, which would involve developing independent syntheses of each annulated piperidine desired. (c) Several of the products accessed by our methodology represent new scaffolds, including those unique compounds shown in entries 3 and 4 in Table 5.1 and those highlighted in entries 3 and 6 of Table 5.2.[19] (d) Several of the cycloaddition adducts shown in Table 5.2 are new analogs of known medicinally important scaffolds. For example, compounds related to those in entries 4, 5, and 7 show promise for the treatment of inflammation,[20] diabetes,[21] cancer,[22] hepatitis C,[23] or other illnesses. (e) Finally, with regard to

regioselectivity, it should be emphasized that 3,4-piperidyne **5.1a** uniformly reacts with a preference for initial attack occurring at C4, which is the same trend seen in reactions of the well-studied 3,4-pyridyne (**5.3**). However, the observed selectivities in the case of **5.1a** are generally greater compared to the selectivities seen in the trapping of 3,4-pyridynes.[24]

Table 5.2. Reactions of Silyl Triflate **5.8** with Nucleophiles and Cycloaddition Partners

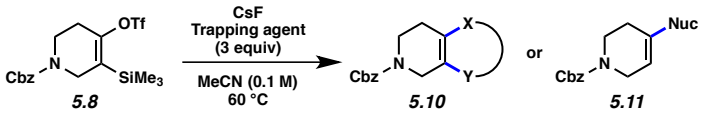

Entry	Trapping agent	Product(s)	Yield[a] (ratio)
1		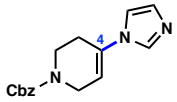	78% (>20:1)
2		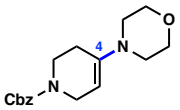	99%[b] (>20:1)
3	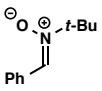	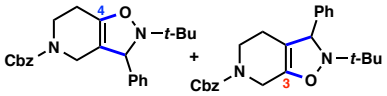	84% (12.7:1)
4		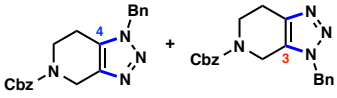	81% (5.3:1)
5		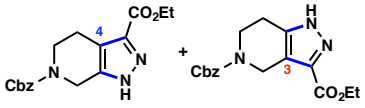	78% (4.6:1)
6	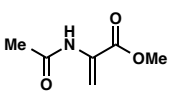	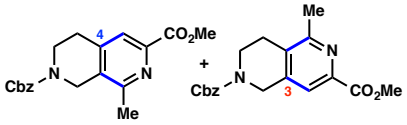	57% (2.1:1)
7	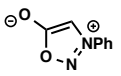	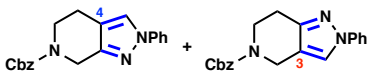	87% (1.3:1)

[a] Reported yields are the average of two experiments and are based on the amount of isolated products. [b] Yield was determined using 1,3,5-trimethoxybenzene as an external standard.

5.3.4 Comparison of Transition States & Distortion Present in 5.1a and 5.3

To understand the disparity in the regioselectivities of the reactions of the 3,4-pyridyne (**5.3**) and 3,4-piperidyne **5.1a**, we used DFT calculations to analyze the competing transition states for the nucleophilic addition of morpholine to **5.3**, and compared the results to the corresponding transition states involving **5.1a** (Figure 5.3). In the reactions of **5.3** with morpholine, the difference in energies for attack at C4 vs C3 (**TS5.1** and **TS5.2**, respectively) is negligible. This is consistent with the low regioselectivity seen experimentally.[24,25] Given that these are very early transition states, the distortion energy (ΔE^{dist}), or the energy required to alter the alkyne geometry toward the transition state, is expected to be small; in fact, we do calculate a slightly greater ΔE^{dist} of the alkyne for **TS5.2** than **TS5.1** (ca. 0.2 kcal/mol). In contrast, the addition of morpholine to C4 of 3,4-piperidyne **5.1a** (**TS5.3**) is predicted to be favored over attack at C3 (**TS5.4**) by roughly 1.7 kcal/mol. Notably, the disparity in distortion energy (ΔE^{dist}) accounts for most of the energetic difference and the resulting high regioselectivity observed experimentally (see Table 5.2, entry 2). These results validate that the distortion/interaction model correctly predicts and explains regioselectivities in reactions of both the 3,4-pyridyne (**5.3**) and 3,4-piperidyne **5.1a**.

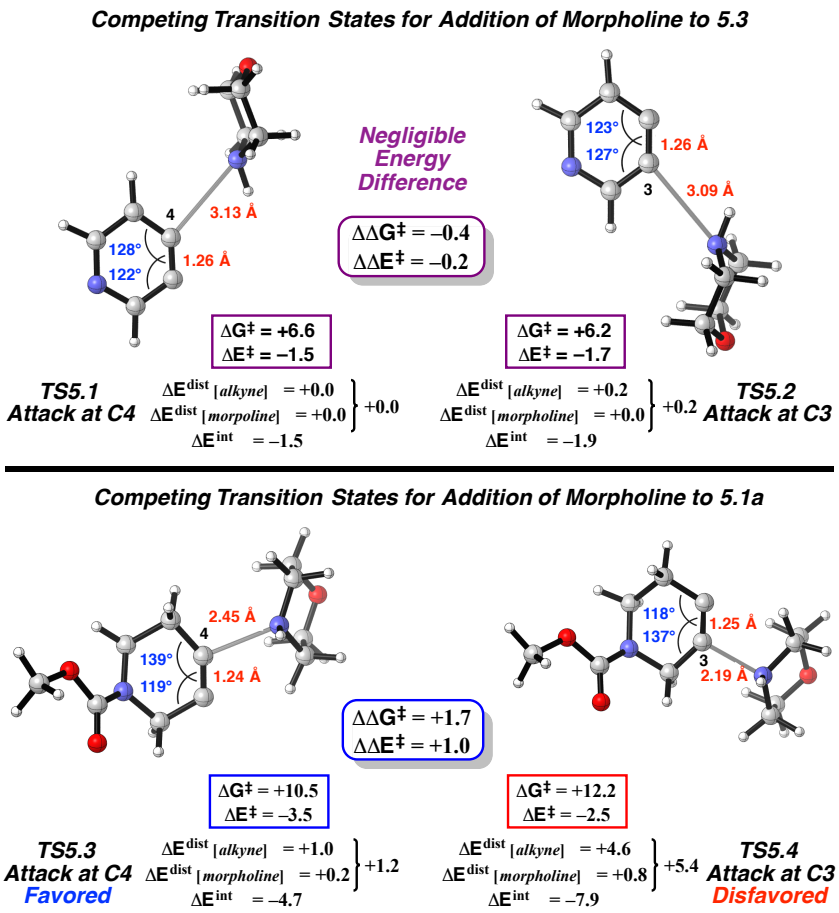

Figure 5.3. Optimized transition states for nucleophilic addition by morpholine to **5.3** and **5.1a** using B3LYP/6-31G(d). Single point energies were calculated at the B3LYP-D3/6-311+G(d,p) level with CPCM solvent model for MeCN. Energies are provided in kcal mol^{-1}

As noted earlier, the lack of regioselectivity seen in reactions of 3,4-pyridynes has been a long-standing problem. Thus, we sought to probe one remaining critical question: why is the 3,4-piperidyne significantly distorted, while the 3,4-pyridyne is not? The explanation is summarized in Figure 5.4. The distortion of 3,4-piperidyne **5.1a** is caused by the electronegativity of the *N*-heteroatom that deforms the triple bond as a result of Bent's rule.[26] The internal bond angle at C3 is decreased, mixing in *p* character at C3 and releasing electron density toward the electronegative *N*-atom. Although the analogous effect is also present in 3,4-pyridyne (**5.3**), it is

offset by the in-plane overlap of the nitrogen lone pair with the π and π* orbitals at C3, which causes C3 to move toward the *N*-atom (for further discussion of these competing effects, see the Experimental Section). Such an effect is not seen in **5.1a**, as the nitrogen lone pair is orthogonal to the π and π* orbitals of the alkyne.

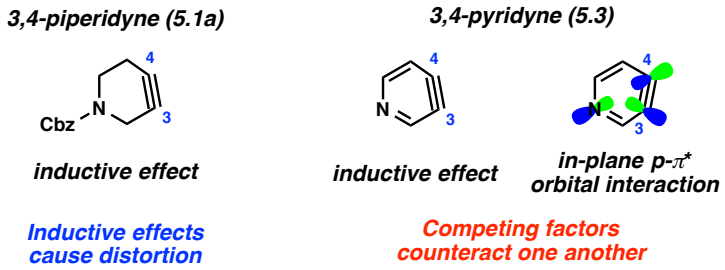

Figure 5.4. Explanation for differing distortion seen in **5.1a** and **5.3**

5.4 Conclusion

In summary, we have synthesized the first 3,4-piperidyne, **5.1a**, and demonstrated that this reactive intermediate can be utilized in a variety of cycloadditions to form annulated piperidine scaffolds. The regioselectivity trends observed in reactions of **5.1a** with nucleophiles and unsymmetrical cycloaddition partners are predicted and rationalized by the distortion/interaction model. Moreover, we have explained the inductive effect that causes the distortion seen in **5.1a**, in addition to the competing inductive effects and orbital interactions that result in the lack of regioselectivity observed in reactions of the well-studied 3,4-pyridyne (**5.3**). Our findings not only provide a new platform to access medicinally-privileged piperidine scaffolds, but also lay the foundation for further studies geared toward strategically harnessing strained heterocyclic alkynes as useful synthetic building blocks.

5.5 Experimental Section

5.5.1 Materials and Methods

Unless stated otherwise, reactions were conducted in flame-dried glassware under an atmosphere of nitrogen using anhydrous solvents (freshly distilled or passed through activated alumina columns). All commercially obtained reagents were used as received unless otherwise specified. Cesium fluoride (CsF) was obtained from Strem Chemicals. Trifluoromethanesulfonic anhydride (Tf_2O) and trimethylsilyl chloride (TMSCl) were obtained from Oakwood Products, Inc. and distilled before use. *N*-tert-butyl-α-phenylnitrone and methyl 2-acetamidoacrylate were obtained from Alfa Aesar. Ethyl diazoacetate, (trimethylsilyl)diazomethane (1 M in Et_2O), tetracyclone, 2,5-dimethylfuran, *N*-Boc-pyrrole, and L-selectride (1 M in THF) were obtained from Sigma Aldrich. Benzyl chloroformate and 2-pyrone were obtained from Acros Organics. Morpholine was obtained from Spectrum Chemical and distilled before use. Reaction temperatures were controlled using an IKAmag temperature modulator and, unless stated otherwise, reactions were performed at room temperature (rt, approximately 23 °C). Thin layer chromatography (TLC) was conducted with EMD gel 60 F254 pre-coated plates (0.25 mm) and visualized using a combination of UV light and potassium permanganate staining. Preparative thin layer chromatography (TLC) was conducted with EMD gel 60 F254 pre-coated plates (0.5 mm) and visualized using UV light. Silicycle Siliaflash P60 (particle size 0.040–0.063 mm) was used for flash column chromatography. ^{1}H NMR and 2D-NOESY spectra were recorded on Bruker spectrometers (500 MHz) and are reported relative to deuterated solvent signals. Data for ^{1}H NMR spectra are reported as follows: chemical shift (δ ppm), multiplicity, coupling constant (Hz) and integration. ^{13}C NMR spectra were recorded on Bruker spectrometers (125 MHz) and are reported relative to deuterated solvent signals. Data for ^{13}C NMR spectra are reported in

terms of chemical shift and, when necessary, multiplicity, and coupling constant (Hz). For mixtures of regioisomers, the major regioisomer is reported with the minor regioisomer in parentheses for both ^{1}H NMR and ^{13}C NMR spectra. IR spectra were obtained using a Perkin-Elmer 100 spectrometer and are reported in terms of frequency absorption (cm^{-1}). High-resolution mass spectra were obtained on Waters LCT Premier with ACQUITY LC and Thermo Scientific™ Exactive Mass Spectrometers with DART ID-CUBE.

5.5.2 Experimental Procedures

5.5.2.1 Synthesis of 3,4-Piperidyne Precursor

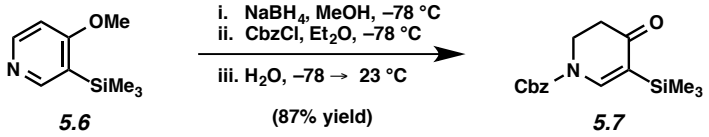

Vinylogous Amide 5.7. To a solution of known silyl pyridine **5.6**[27] (1.00 g, 5.52 mmol, 1 equiv) in MeOH (11 mL) was added $NaBH_4$ (0.230 g, 6.07 mmol, 1.1 equiv) at –78 °C. After stirring for 20 min, benzyl chloroformate (0.87 mL, 6.07 mmol, 1.1 equiv) in Et_2O (1.1 mL) was then added dropwise over 15 min. After stirring for 1 h at –78 °C, H_2O (9.2 mL) was added and the reaction was warmed to room temperature. After 1.5 h, the reaction mixture was diluted with H_2O (20 mL) and extracted with EtOAc (3 × 15 mL). The combined organic layers were washed with H_2O (2 × 20 mL) and brine (20 mL), dried over Na_2SO_4, filtered, and concentrated *in vacuo*. The resulting crude product was purified by flash chromatography (9:1 hexanes : EtOAc) to provide vinylogous amide **5.7** (1.45 g, 87% yield) as a colorless oil. Vinylogous Amide **5.7**: R_f 0.52 (4:1 hexanes : EtOAc); ^{1}H NMR (500 MHz, $CDCl_3$, 55 °C): δ 7.85 (s, 1H), 7.40–7.36 (m, 5H), 5.28 (s, 2H), 4.01 (t, J = 7.4, 2H), 2.52 (t, J = 7.3, 2H), 0.17 (s, 9H); ^{13}C NMR (125 MHz,

$CDCl_3$, 55 °C): δ 196.2, 153.1, 147.3, 135.6, 128.9, 128.8, 128.4, 116.7, 69.0, 42.9, 36.3, –1.24; IR (film): 1723, 1655, 1576, 1391, 1344, 1298 cm^{-1}; HRMS-ESI (*m/z*) $[M + H]^+$ calcd for $C_{16}H_{22}NO_3Si$, 304.1364; found 304.1350.

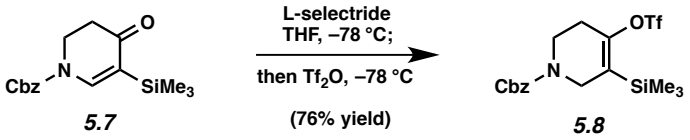

Silyl Triflate 5.8. To a stirred solution of vinylogous amide **5.7** (2.91 g, 9.56 mmol, 1 equiv) in THF (43 mL) was added L-selectride (1.0 M in THF, 10.5 mL, 10.5 mmol, 1.1 equiv) at –78 °C. After stirring for 15 min, Tf_2O (1.26 mL, 10.5 mmol, 1.1 equiv) was added dropwise over 15 min. The reaction was stirred for 20 min at –78 °C and then a saturated aqueous solution of $NaHCO_3$ (30 mL) was added and the reaction was warmed to room temperature. After stirring for 2 h, the layers were separated and the aqueous layer was extracted with EtOAc (3 × 20 mL), washed with brine (1 × 50 mL), dried over Na_2SO_4, filtered, and concentrated *in vacuo*. The resulting crude product was purified by flash chromatography with basic Brockman Grade I 58 Å Al_2O_3 (hexanes), followed by a silica gel column (3:2 hexanes : EtOAc) to give silyl triflate **5.8** (2.60 g, 76% yield) as a colorless oil. Silyl Triflate **5.8**: R_f 0.60 (4:1 hexanes : EtOAc); ^1H NMR (500 MHz, $CDCl_3$, 55 °C): δ 7.37–7.35 (m, 5H), 5.18 (s, 2H), 4.13 (t, J = 2.5, 2H), 3.68 (t, J = 5.9, 2H), 2.57–2.55 (m, 2H), 0.25 (s, 9H); ^{13}C NMR (125 MHz, $CDCl_3$, 55 °C): δ 155.1, 151.8, 136.8, 128.7, 128.3, 128.1, 126.3, 118.6 (q, J = 320.0), 67.7, 45.4, 41.0, 28.9, –1.32; IR (film): 1702, 1656, 1412, 1243, 1204, 1141 cm^{-1}; HRMS-ESI (*m/z*) $[M + H]^+$ calcd for $C_{17}H_{23}NF_3O_5SiS$, 438.1013; found, 438.0992.

5.5.2.2 Trapping Experiments of 3,4-Piperidyne

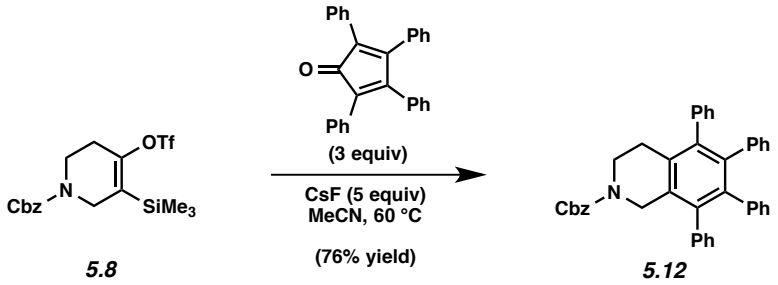

Representative Procedure (Preparation of piperidine 5.12 is used as an example). Piperidine 5.12 (Table 5.1, Entry 1). To a stirred solution of silyltriflate **5.8** (51.6 mg, 0.118 mmol, 1 equiv) and tetracyclone (133 mg, 0.345 mmol, 3.0 equiv) in MeCN (1.2 mL) was added CsF (88.0 mg, 0.575 mmol, 5.0 equiv). The reaction vessel was sealed and placed in a preheated aluminum heating block maintained at 60 °C for 3 h. After cooling to 23 °C, the reaction mixture was filtered over silica gel (EtOAc eluent, 12 mL). Evaporation under reduced pressure and further purification by preparative thin layer chromatography (6:1:1 hexanes : EtOAc : PhH) afforded **5.12** as a pale yellow oil (76% yield, average of two experiments). **5.12**: R_f 0.25 (9:1 hexanes : EtOAc); ^{1}H NMR (500 MHz, C_6D_6, 80 °C): δ 7.12–6.98 (m, 19H), 6.78–6.74 (m, 4H), 6.67–6.64 (m, 2H), 5.11 (s, 2H), 4.55 (s, 2H), 3.53 (m, 2H), 2.58 (t, J = 6.1, 2H); ^{13}C NMR (125 MHz, C_6D_6, 80 °C): δ 155.4, 141.1, 141.0, 140.8, 140.7, 140.2, 139.9, 139.8, 139.6, 137.9, 133.2, 132.3, 131.8, 130.7, 130.5, 128.6, 128.4, 128.2, 128.1, 128.1, 128.0, 127.9, 127.1, 126.9, 126.6, 125.8, 125.8, 67.2, 46.1, 42.2, 28.8; IR (film): 3034, 1702, 1478, 1442, 1428, 1269 cm^{-1}; HRMS-ESI (*m/z*) $[M + H]^+$ calcd for $C_{41}H_{34}NO_2$, 572.2584; found 572.2552.

Any modifications of the conditions shown in this representative procedure are specified in the following schemes, which depict all of the results shown in Tables 5.1 and 5.2

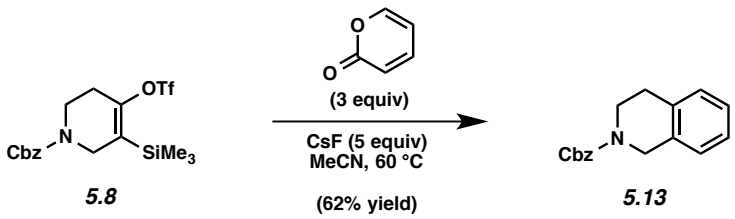

Piperidine 5.13 (Table 5.1, Entry 2). Purification by preparative thin layer chromatography (2:1 hexanes : EtOAc) afforded **5.13** (62% yield, average of two experiments) as a colorless oil. **5.13**: R_f 0.25 (9:1 hexanes : EtOAc); ^{1}H NMR (500 MHz, C_6D_6, 80 °C): δ 7.27 (d, J = 7.6, 2H), 7.14–7.11 (m, 2H), 7.08–7.05 (m, 1H), 6.96–6.92 (m, 2H), 6.81–6.79 (m, 1H), 6.74 (br s, 1H), 5.16 (d, J = 4.4, 2H), 4.50 (s, 2H), 3.46 (br s, 2H), 2.43 (app t, J = 5.3, 2H); ^{13}C NMR (125 MHz, C_6D_6, 80 °C): δ 155.5, 137.8, 135.0, 134.0, 128.9, 128.7, 128.4, 128.1, 126.6, 126.6, 126.5, 67.3, 46.2, 41.9, 29.1; IR (film): 1699, 1452, 1428, 1294, 1226, 1119 cm^{-1}; HRMS-ESI (*m/z*) $[M + H]^+$ calcd for $C_{17}H_{18}NO_2$, 268.1332; found 268.1317.

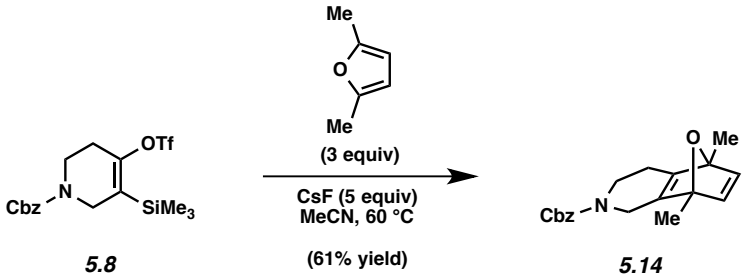

Piperidine 5.14 (Table 5.1, Entry 3). Purification by preparative thin layer chromatography (2:1 hexanes : EtOAc) afforded **5.14** (61% yield, average of two experiments) as a colorless oil. **5.14**: R_f 0.20 (4:1 hexanes : EtOAc); ^{1}H NMR (500 MHz, C_6D_6, 80 °C): δ 7.24 (d, J = 7.6, 2H), 7.11 (d, J = 7.6, 2H), 7.05 (app t, J = 7.3, 1H), 6.58 (m, 2H), 5.14 (s, 2H), 4.17 (dd, J = 15.0, 2.9, 1H), 3.74 (d, J = 17.8, 1H), 3.45–3.42 (m, 1H), 3.30–3.29 (m, 1H), 2.06–2.02 (m, 1H), 1.59–1.54 (m, 1H), 1.41 (s, 3H), 1.38 (s, 3H); ^{13}C NMR (125 MHz, C_6D_6, 80 °C): δ 155.7, 150.9, 149.3, 148.3,

148.2, 137.9, 128.7, 128.4, 128.0, 90.9, 90.3, 67.4, 43.3, 41.4, 23.5, 15.0, 14.9; IR (film): 1701, 1424, 1290, 1234, 1106, 860.1 cm^{-1}; HRMS-ESI (*m/z*) $[M + H]^+$ calcd for $C_{19}H_{22}NO_3$, 312.1594; found 312.1580.

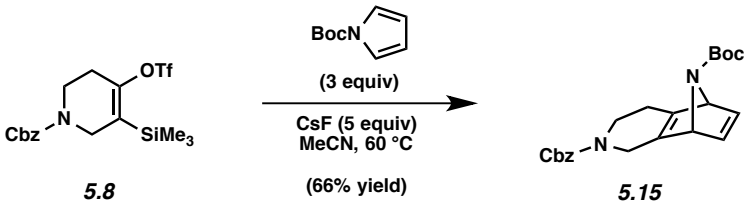

Piperidine 5.15 (Table 5.1, Entry 4). Purification by preparative thin layer chromatography (4:1 hexanes : EtOAc) afforded **5.15** (66% yield, average of two experiments) as a colorless oil. **5.15**: R_f 0.25 (4:1 hexanes : EtOAc); ^{1}H NMR (500 MHz, CD_3CN, 55 °C): δ 7.38–7.31 (m, 5H), 7.02–7.00 (m, 2H), 5.13 (s, 2H), 4.95–4.91 (m, 2H), 4.28 (dt, *J* = 18.0, 3.2, 1H), 3.90 (dt, *J* = 18.0, 3.3, 1H), 3.51–3.48 (m, 2H), 2.47–2.44 (m, 1H), 2.09–2.04 (m, 1H), 1.4 (s, 9H); ^{13}C NMR (125 MHz, CD_3CN, 55 °C): δ 156.9, 156.3, 149.8, 148.0, 144.5, 144.3, 139.1, 129.9, 129.3, 129.2, 81.3, 70.4, 68.9, 68.2, 45.6, 42.7, 29.1, 26.6; IR (film): 1700, 1455, 1423, 1366, 1332, 1228 cm^{-1}; HRMS-ESI (*m/z*) $[M + H]^+$ calcd for $C_{22}H_{27}N_2O_4$, 383.1965; found 383.1947.

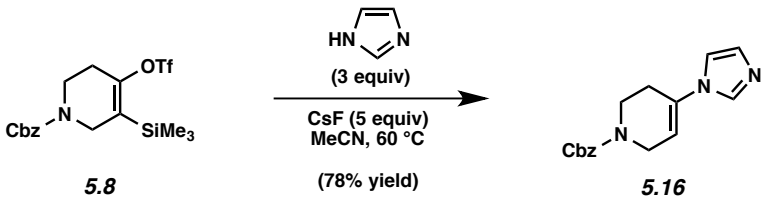

Piperidine 5.16 (Table 5.2, Entry 1). Purification by preparative thin layer chromatography (9:1 CH_2Cl_2 : MeOH) afforded **5.16** (78% yield, average of two experiments) as a colorless oil. **5.16**: R_f 0.41 (9:1 CH_2Cl_2 : MeOH); ^{1}H NMR (500 MHz, CD_3CN, 55 °C): δ 7.67 (s, 1H), 7.42–7.32 (m, 5H), 7.22 (s, 1H), 7.01 (s, 1H), 5.88–5.87 (m, 1H), 5.18 (s, 2H), 4.13 (m, 2H), 3.75 (t, *J* =

3.8, 2H), 2.62–2.58 (m, 2H); ^{13}C NMR (125 MHz, CD_3CN, 55 °C): δ 158.5, 138.8, 136.1, 134.1, 130.7, 139.8, 129.3, 129.0, 125.1, 113.8, 68.2, 43.6, 41.7, 28.4; IR (film): 1699, 1493, 1428, 1233, 1213, 1112 cm^{-1}; HRMS-ESI (*m/z*) $[M + H]^+$ calcd for $C_{16}H_{18}N_3O_2$, 284.1394; found 284.1379.

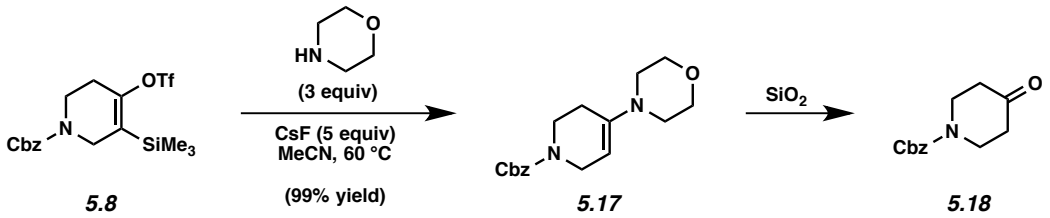

Piperidine 5.17 (Table 5.2, Entry 2). Evaporation under reduced pressure afforded **5.17** (99% yield). The yield was determined by ^{1}H NMR analysis of the crude reaction mixture using trimethoxybenzene (5.6 mg, 0.72 equiv) as an external standard. **5.17** was found to hydrolyze to the corresponding ketone[28] **5.18** upon exposure to silica gel. **5.18**: R_f 0.45 (3:1 PhH : EtOAc). The regioselectivity of the nucleophilic attack was verified by the isolation of **5.18**. **5.17**: ^{1}H NMR (500 MHz, C_6D_6, 80 °C): δ 7.28 (d, J = 7.4, 2H), 7.13 (t. J = 7.5, 2H), 7.07 (t, J = 7.5, 1H), 5.18 (s, 2H), 4.23 (m, 1H), 3.99 (br s, 2H), 3.46 (t, J = 4.8, 6H), 2.41 (t, J = 4.8, 4H), 1.8 (m, 2H); ^{13}C NMR (125 MHz, CD_3CN, 55 °C): δ 146.1, 139.0, 129.8, 129.1, 129.0, 118.3, 97.4, 67.8, 67.8, 49.5, 44.1, 42.2, 41.7, 27.7, 1.88; IR (film): 1699, 1362, 1329, 1290, 1267, 1033 cm^{-1}; HRMS-ESI (*m/z*) $[M + H]^+$ calcd for $C_{17}H_{23}N_2O_3$, 303.1703; found 303.1690.

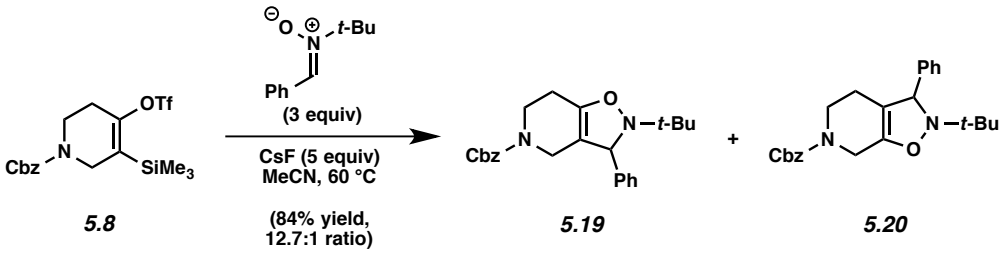

Piperidines 5.19 and 5.20 (Table 5.2, Entry 3). Purification by preparative thin layer chromatography (7:3 hexanes : EtOAc) afforded **5.19** and **5.20** (84% yield, average of two experiments, 12.7:1 ratio) as a colorless oil. **5.19**: R_f 0.63 (7:3 hexanes : EtOAc); ^{1}H NMR (500 MHz, $CDCl_3$, 55 °C): δ 7.36–7.29 (m, 9H), 7.26–7.24 (m, 1H), 5.12 (s, 2H), 5.02 (br s, 1H), 3.95 (app d, J = 15.7, 1H), 3.83 (app dt, J = 13.2, 5.2, 1H), 3.55–3.47 (m, 2H), 2.29 (br s, 2H), 1.14 (s, 9H); ^{13}C NMR (125 MHz, $CDCl_3$, 55 °C): δ 155.8, 147.2, 143.0, 137.1, 128.7, 128.6, 128.1, 128.0, 127.6, 127.3, 104.5, 69.3, 67.4, 60.7, 41.1, 41.1, 25.3, 22.3; IR (film): 1700, 1454, 1423, 1286, 1212, 1132 cm^{-1}; HRMS-ESI (*m/z*) [M + H]$^+$ calcd for $C_{24}H_{29}N_2O_3$, 393.2173; found 393.2154.

The structure of **5.19** was verified by 2D-NOESY, as the following interaction was observed:

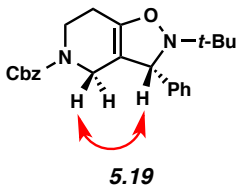

5.19

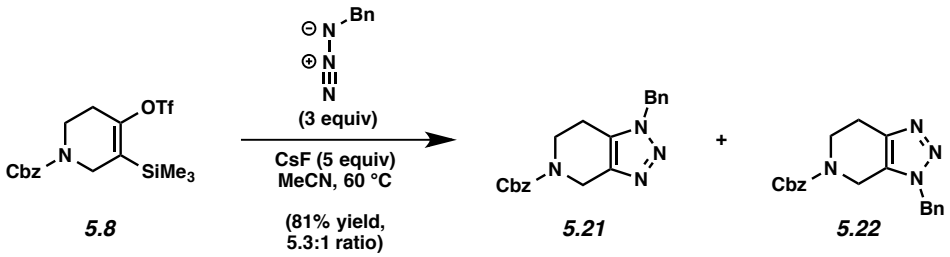

Piperidines 5.21 and 5.22 (Table 5.2, Entry 4). Purification by preparative thin layer chromatography (3:2 EtOAc : hexanes) afforded an inseparable mixture of triazoles **5.21** and **5.22** (81% yield, average of two experiments, 5.3:1 ratio) as a white solid. Compounds **5.21** and **5.22** were characterized as a mixture of regioisomers. R_f 0.40 (3:2 EtOAc : hexanes); ^{1}H NMR (500 MHz, C_6D_6, 80 °C): δ 7.21–7.20 (7.21–7.20) (m, 2H), 7.15 (7.15) (m, 1H), 7.13–7.10 (7.13–7.10) (m, 2H), 7.07–7.06 (7.07–7.06) (m, 1H), 7.01–7.00 (7.01–7.00) (m, 3H), 6.92–6.90 (6.92–6.90) (m, 2H), 5.07 (5.06) (app s, 2H), 4.92 (4.89) (s, 2H), 4.61 (4.11) (s, 2H), 3.30 (3.30) (app t, J = 5.2, 2H), 1.95 (2.56) (app t, J = 5.6, 2H); ^{13}C NMR (125 MHz, $CDCl_3$, 55 °C): δ 155.7, 155.6, 142.4, 141.3, 136.7, 136.6, 134.7, 134.2, 130.6, 129.3, 129.2, 128.8, 128.7, 128.6, 128.6, 128.3, 128.2, 128.2, 128.1, 127.9, 127.7, 127.7, 67.8, 67.7, 52.7, 52.3, 42.1, 42.0, 41.2, 40.3, 22.8, 21.0; IR (film): 1698, 1455, 1424, 1223, 1198, 1100 cm^{-1}; HRMS-ESI (m/z) $[M + H]^+$ calcd for $C_{20}H_{21}N_4O_2$, 349.1659; found 349.1638.

The structure of **5.21** was verified by 2D-NOESY and 2D-HMBC of the mixture, as the following interactions were observed:

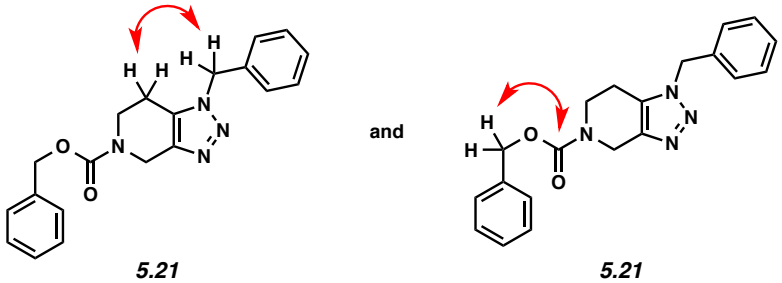

5.21

2D-NOESY

5.21

2D-HMBC

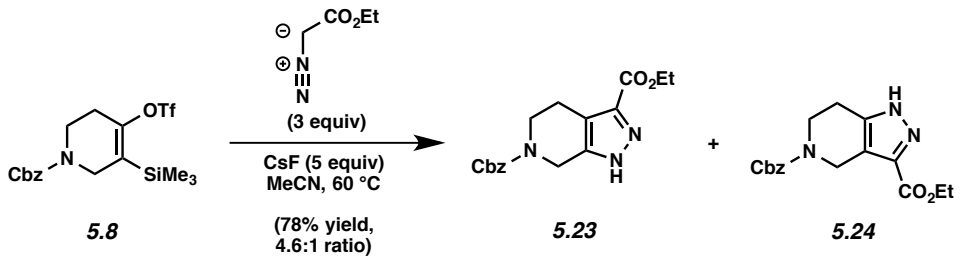

5.8 *5.23* *5.24*

Piperidines 5.23 and 5.24 (Table 5.2, Entry 5). Purification by preparative thin layer chromatography (3:2 EtOAc : hexanes) afforded **5.23** (64% yield, average of two experiments) as a colorless oil and **5.24** (14% yield, average of two experiments) as a colorless oil. **5.23**: R_f 0.43 (3:2 EtOAc : hexanes); ^{1}H NMR (500 MHz, $CDCl_3$, 55 °C): δ 7.37–7.28 (m, 5H), 5.19 (s, 2H), 4.69 (s, 2H), 4.37 (q, J = 7.2, 2H), 3.74 (t, J = 5.8, 2H), 2.87 (t, J = 5.6, 2H), 1.36 (t, J = 7.0, 3H); ^{13}C NMR (125 MHz, $CDCl_3$, 55 °C): δ 160.3, 155.8, 145.9, 136.8, 132.1, 128.6, 128.2, 128.0, 118.2, 67.6, 61.1, 42.5, 42.0, 21.9, 14.4; IR (film): 3219, 2931, 1701, 1470, 1427, 1226 cm^{-1}; HRMS-ESI (*m/z*) $[M + H]^+$ calcd for $C_{17}H_{20}N_3O_4$, 330.1448; found 330.1426. **5.24**: R_f 0.25 (2:3 Hexanes : EtOAc); ^{1}H NMR (500 MHz, $CDCl_3$, 55 °C): δ 7.38–7.30 (m, 5H), 5.20 (s, 2H), 4.74 (s, 2H), 4.39 (q, J = 7.1, 2H), 3.79 (t, J = 5.8, 2H), 2.82 (t, J = 5.7, 2H), 1.38 (t, J = 7.0, 3H); ^{13}C NMR (125 MHz, $CDCl_3$, 55 °C): δ 160.5, 155.9, 145.9, 137.0, 132.6, 128.7, 128.2, 128.1, 117.0, 67.6, 61.3, 41.7, 41.6, 23.3, 14.4; IR (film): 3244, 2957, 1699, 1424, 1269, 1222 cm^{-1}; HRMS-ESI (*m/z*) $[M + H]^+$ calcd for $C_{17}H_{20}N_3O_4$, 330.1448; found 330.1429.

The structures of **5.23** and **5.24** were verified by 2D-HMBC, as the following interactions were observed:

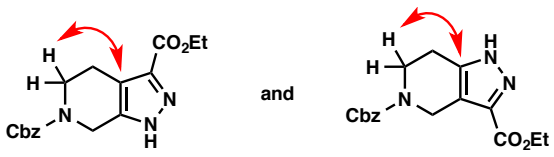

5.23 *5.24*

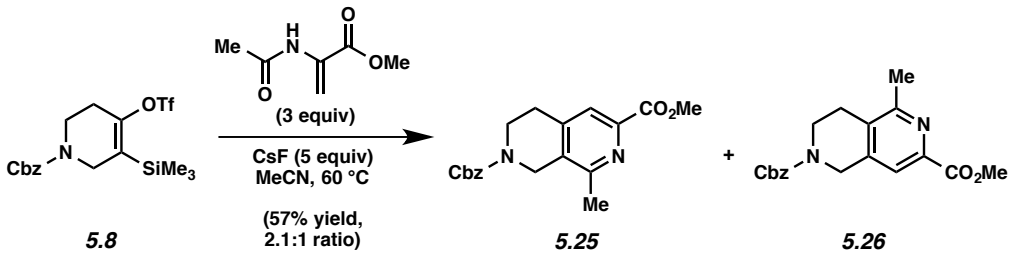

Piperidines 5.25 and 5.26 (Table 5.2, Entry 6). Purification by preparative thin layer chromatography (3:1 PhH : EtOAc) afforded an inseparable mixture of pyridines **5.25** and **5.26** (57% yield, average of two experiments, 2.1:1 ratio) as a colorless oil. Compounds **5.25** and **5.26** were characterized as a mixture of regioisomers. R_f 0.40 (1:1 PhH : EtOAc); ^{1}H NMR (500 MHz, $CDCl_3$, 55 °C): δ 7.76 (7.73) (s, 1H), 7.38–7.36 (7.35–7.32) (m, 5H), 5.21 (5.19) (s, 2H), 4.62 (4.69) (s, 2H), 3.98 (3.98) (s, 3H), 3.75 (3.80) (t, J = 5.9, 2H), 2.89 (2.81) (t, J = 5.7, 2H), 2.54 (2.56) (s, 3H); ^{13}C NMR (125 MHz, $CDCl_3$, 55 °C): δ 166.1, 166.1, 166.1, 166.1, 158.0, 155.9, 155.6, 155.4, 145.6, 145.3, 144.4, 143.1, 136.8, 136.8, 132.4, 13 1.5, 128.8, 128.4, 128.2, 128.2, 123.6, 120.9, 67.8, 67.8, 52.8, 52.7, 45.8, 44.1, 41.2, 40.7, 29.1, 26.2, 22.3, 21.8; IR (film): 1740, 1702, 1433, 1340, 1242, 1217 cm^{-1}; HRMS-ESI (*m/z*) [M + H]$^+$ calcd for $C_{19}H_{21}N_2O_4$, 341.1496; found 341.1482.

The structures of **5.25** and **5.26** were verified by 2D-NOESY, as the following interactions were observed:

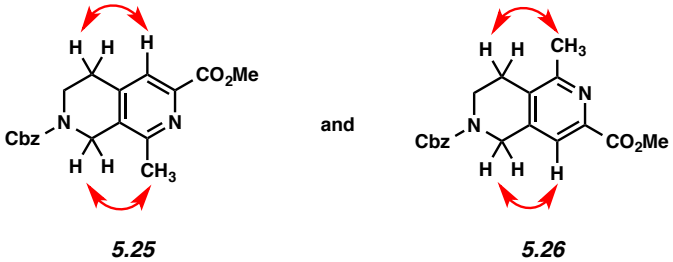

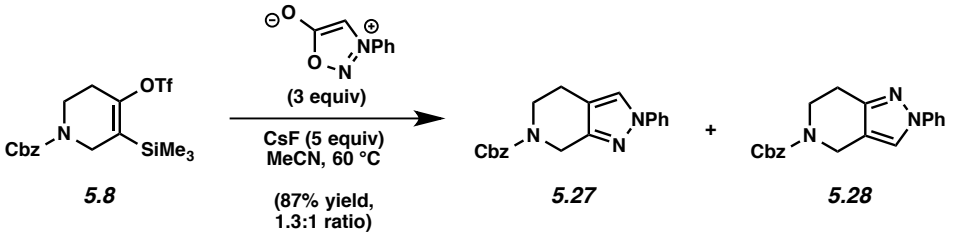

Piperidines 5.27 and 5.28 (Table 5.2, Entry 7). The sydnone trapping agent was synthesized using a known procedure.[29] Purification by preparative thin layer chromatography (9:1 PhH : Et_2O) afforded pyrazoles **5.27** and **5.28** (87% yield, average of two experiments, 1.3:1 ratio) both as amorphous white solids. **5.27**: R_f 0.43 (9:1 PhH : Et_2O); ^{1}H NMR (500 MHz, CD_3CN, 55 °C): δ 7.85 (s, 1H), 7.68–7.66 (m, 2H), 7.46–7.43 (m, 2H), 7.40–7.35 (m, 4H), 7.33–7.29 (m, 1H), 7.27 (t, *J* = 7.5, 1H), 5.15 (s, 2H), 4.64 (s, 2H), 3.72 (t, *J* = 5.8, 2H), 2.69 (t, *J* = 5.8, 2H); ^{13}C NMR (125 MHz, CD_3CN, 55 °C): δ 156.8, 148.9, 141.2, 138.7, 130.7, 129.7, 129.1, 128.9, 127.2, 125.7, 119.8, 117.5, 68.1, 44.0, 43.5, 21.8; IR (film): 2929, 1698, 1599, 1504, 1425, 1385 cm^{-1}; HRMS-ESI (*m/z*) $[M + H]^+$ calcd for $C_{20}H_{20}N_3O_2$, 334.1550; found 334.1537. **5.28**: R_f 0.42 (9:1 PhH : Et_2O); ^{1}H NMR (500 MHz, CD_3CN, 55 °C): δ 7.86 (s, 1H), 7.68–7.66 (m, 2H), 7.45–7.43 (m, 2H), 7.39–7.35 (m, 4H), 7.32–7.29 (m, 1H), 7.26 (t, *J* = 7.4, 1H), 5.15 (s, 2H), 4.58 (s, 2H), 3.78 (t, *J* = 5.8, 2H), 2.79, (t, *J* = 5.9, 2H); ^{13}C NMR (125 MHz, CD_3CN, 55 °C): δ 156.7, 149.8, 141.7, 138.7, 130.7, 129.7, 129.2, 128.9, 127.2, 124.2, 119.7, 116.7, 68.1, 43.3, 41.6, 24.7; IR (film): 1698, 1599, 1505, 1426, 1384, 1223 cm^{-1}; HRMS-ESI (*m/z*) $[M + H]^+$ calcd for $C_{20}H_{20}N_3O_2$, 334.1550; found 334.1530.

The structures of **5.27** and **5.28** were verified by 2D-NOESY, as the following interactions were observed:

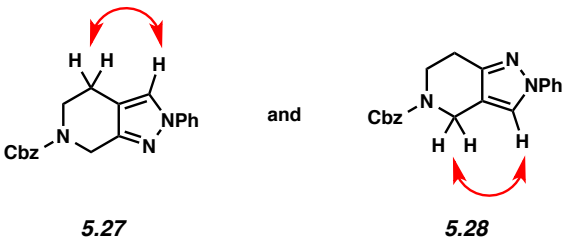

5.27 *5.28*

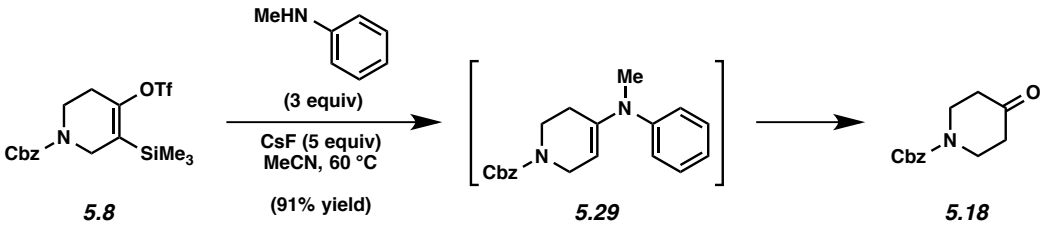

5.8 *5.29* *5.18*

Piperidine 5.29. Evaporation under reduced pressure afforded **5.18** (91% yield). The yield was determined by ^{1}H NMR analysis of the crude reaction mixture using trimethoxybenzene (5.3 mg, 0.75 equiv) as an external standard. **5.29** was not observed; however, its intermediacy was inferred by the isolation of the hydrolysis product, known ketone **5.18**.[28] **5.18**: R_f 0.45 (3:1 PhH : EtOAc). The regioselectivity of the nucleophilic attack was verified by the isolation of **5.18**.

5.5.3 Computational Methods

All calculations were carried out with the Gaussian 09 package.[30] Geometry optimization and energy calculations were performed with B3LYP.[31] The 6-31G (d) basis set[32] was used for all of the atoms. Frequency analysis was conducted at the same level of theory to verify the stationary points to be real minima or saddle points and to obtain the thermodynamic energy corrections. A quasiharmonic correction was applied during the entropy calculation by setting all positive frequencies that are less than 100 cm^{-1} to 100 cm^{-1}.[33] This method has been found to give relatively accurate energetics for cycloadditions. Single point energies were calculated at the

B3LYP-D3[34]/6-311+G(d,p) level. Solvent effect (solvent = acetonitrile) was calculated by using the CPCM[35] solvation model. Computed structures are illustrated using CYLVIEW.[36]

5.5.3.1 Bent´s Rule & Alkyne Distortion Determine Regioselectivity of Nucleophilic Addition

Bent's rule, as stated in 1961, is that *"atomic s character concentrates in orbitals directed toward electropositive substituents"*. In other words, bonds between elements of different electro negativities are polarized in a way such that the electron density will be shifted towards the more electronegative element. Due to the inherent higher stability of *s* orbitals, the hybrid orbitals from the more electronegative atoms will increase their *s* character in order to stabilize the withdrawn electron density. To compensate for this shift in electron density, the less electronegative atoms will direct hybrid orbitals with an increased *p* character toward the more electronegative atoms to which they are bound, without a significant energic penalty. As a result, the hybrid orbitals that constitute these polarized bonds deviate from ideal sp^n (n = 1, 2 or 3) hybridizations, which translates into distorted geometries.

5.5.3.2 *n*→*p interaction in 3,4-pyridyne** The delocalization of the lone pair of electrons (*n*) from the nitrogen atom to the antibonding orbital (*p**) of the alkyne moiety is an attractive electronic interaction that stabilizes 3,4-pyridyne. Figure 5.5 shows this favorable two-electron, two-orbital interaction between the nitrogen lone pair (*n*) and the antibonding orbital (*p**) of the alkyne. The result of this interaction is the formation of a lower energy orbital, (*n*+*p**), and a higher energy orbital, (*n*-*p**). The (*n*+*p**) orbital is computed to be HOMO-2, and it is stabilized by the favorable orbital overlap between the nitrogen lone pair (*n*) and the p orbital at C-3 of the

antibonding orbital (p^*), which is in closer proximity compared with that of C-4. The maximum stabilization occurs in the system when there is greater orbital overlap between *n* and C3. As a result, the alkyne reorients itself in a manner where C3 of the alkyne moves toward the nitrogen atom to maximize this stabilizing interaction. This counteracts the inductive effect of the electronegative nitrogen atom, which would distort the alkyne in the opposite manner in accord with Bent's rule (see: Figure 5.4). It is the sum of these two opposing effects that lead to the two internal angles at C3 and C4 (124° and 126°) being very similar and showing little distortion, and consequently, no significant regioselectivity in nucleophilic additions.

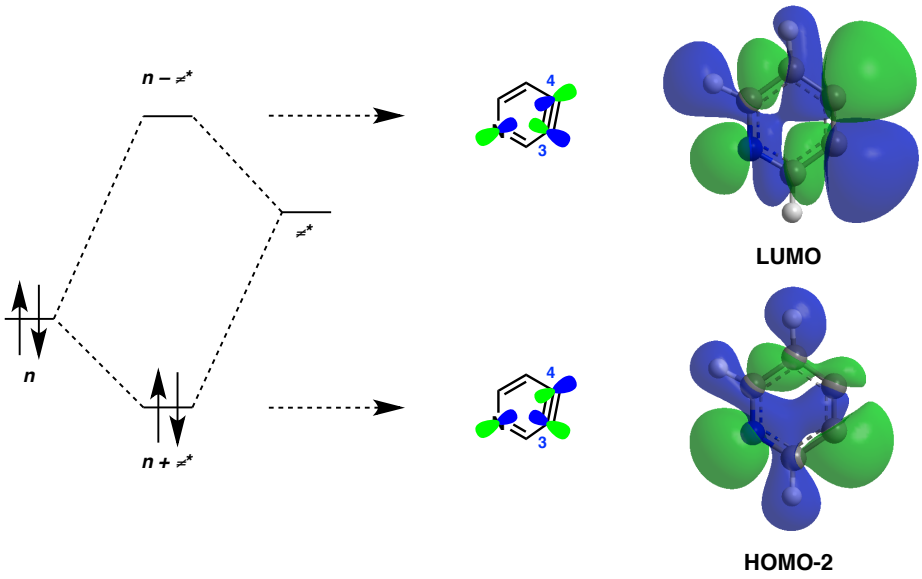

Figure 5.5. *n*→*p** interaction in 3,4-pyridyne

5.5.3.3 Energies, Enthalpies, and Free Energies

Table 5.3. Energies, Enthalpies, and Free Energies of the Structures Calculated at the B3LYP-D3/6-311+G(d,p)(CPCM^{MeCN})//B3LYP/6-31G(d).

Structures	ZPE	DE	DH	DG	E	H	G	Imaginary Frequency
5.3	0.154569	0.164225	0.165169	0.11937	-477.409844	-477.244675	-477.290474	–
TS5.1	0.200137	0.211205	0.212149	0.170824	-534.923275	-534.711126	-534.752451	-41.505
TS5.2	0.200204	0.211238	0.212182	0.163959	-534.923580	-534.711398	-534.759621	-42.130
5.1a	0.063685	0.067966	0.068910	0.036450	-247.022283	-246.953373	-246.985833	–
TS5.3	0.291685	0.307621	0.308565	0.245795	-765.314031	-765.005466	-765.068236	-21.426
TS5.4	0.292273	0.307920	0.308864	0.247304	-765.312285	-765.003421	-765.064981	-68.745

5.5.3.4 Cartesian Coordinates of the Relevant Structures

Cartesian coordinates for the optimized structures have been previously reported.[37]

5.6 Spectra Relevant to Chapter Five:

Generation and Regioselective Trapping of a 3,4-Piperidyne for the Synthesis of Functionalized Heterocycles

Travis C. McMahon, Jose M. Medina, Yun-Fang Yang, Bryan J. Simmons,

K. N. Houk, and Neil K. Garg

J. Am. Chem. Soc. **2015**, *137*, 4082–4085.

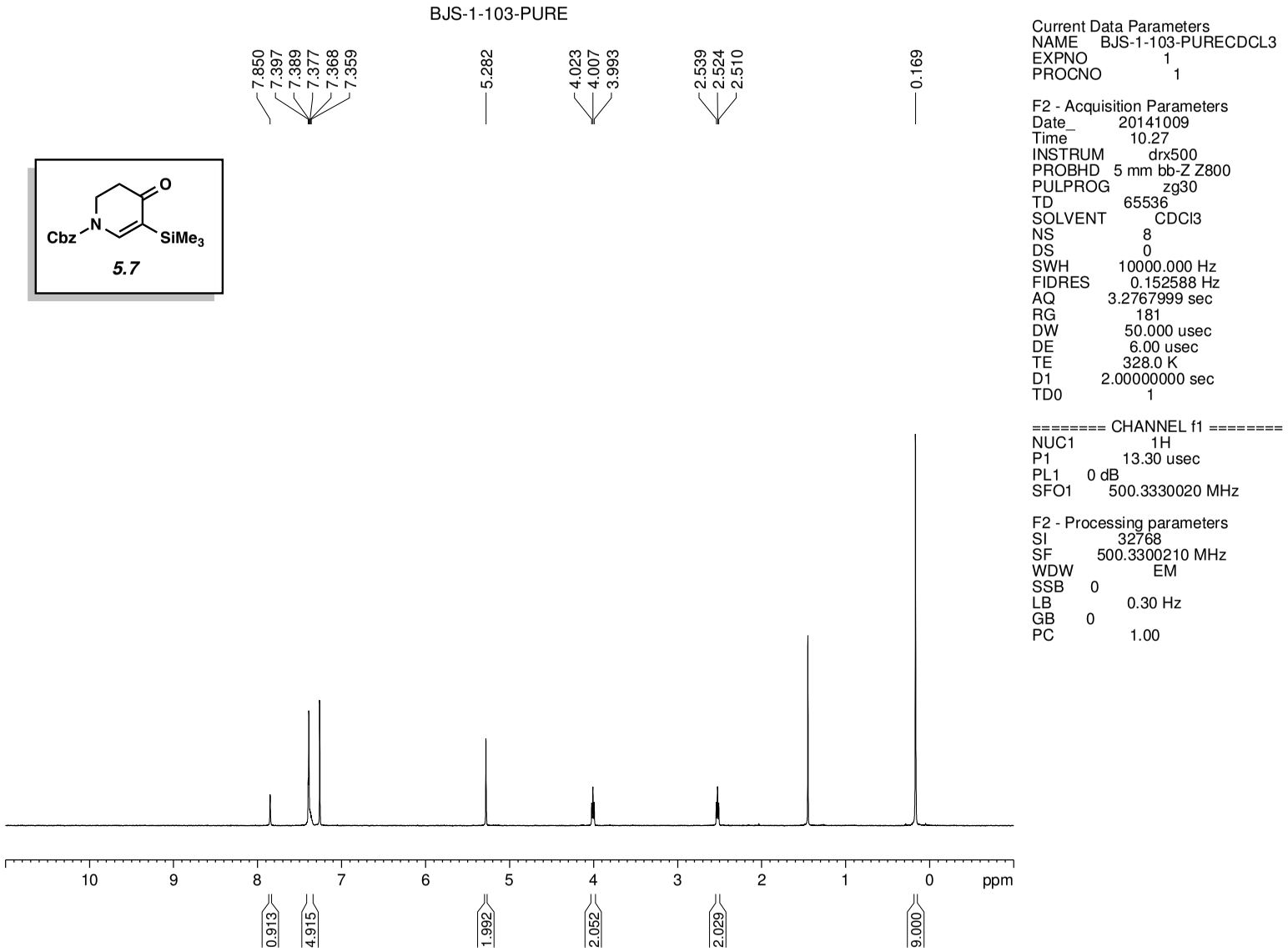

Figure 5.6. ^{1}H NMR (500 MHz, $CDCl_3$) compound **5.7**

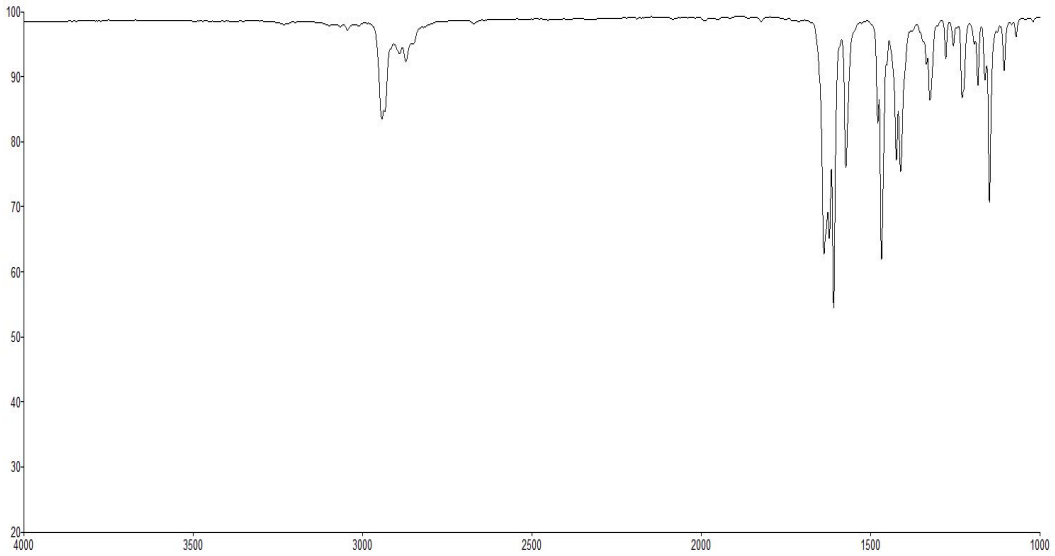

Figure 5.7. Infrared spectrum of compound **5.7**

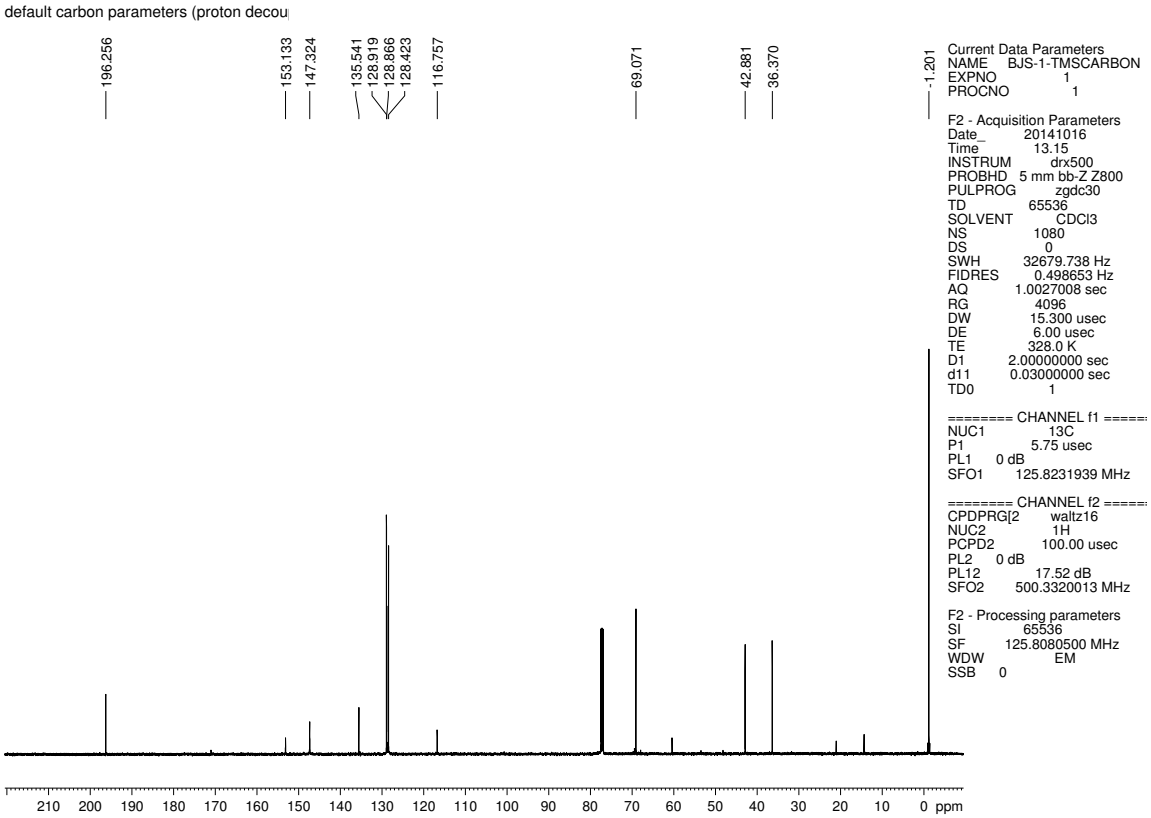

Figure 5.8. ^{13}C NMR (125 MHz, $CDCl_3$) of compound **5.7**

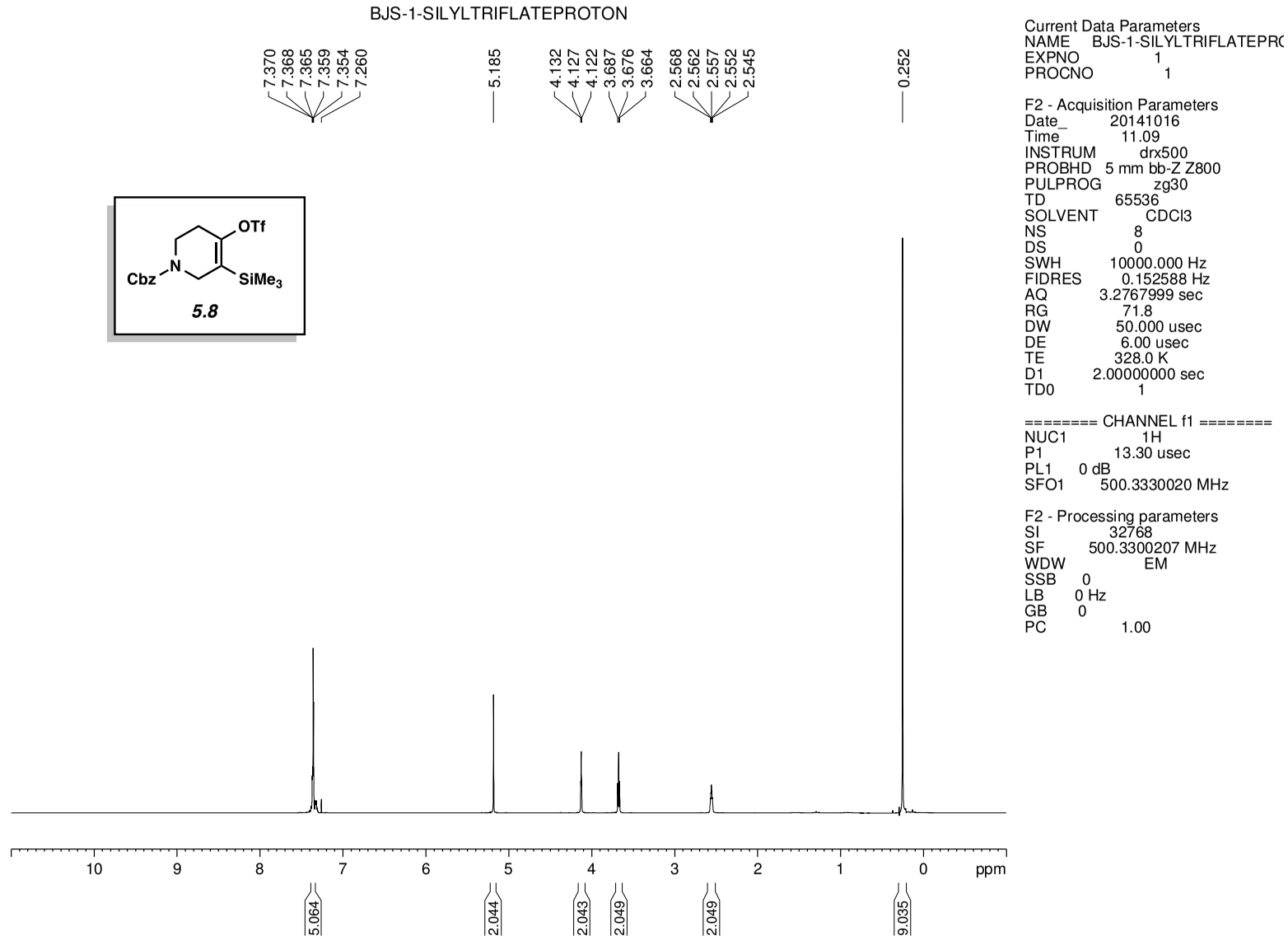

Figure 5.9. ^{1}H NMR (500 MHz, $CDCl_3$) compound **5.8**

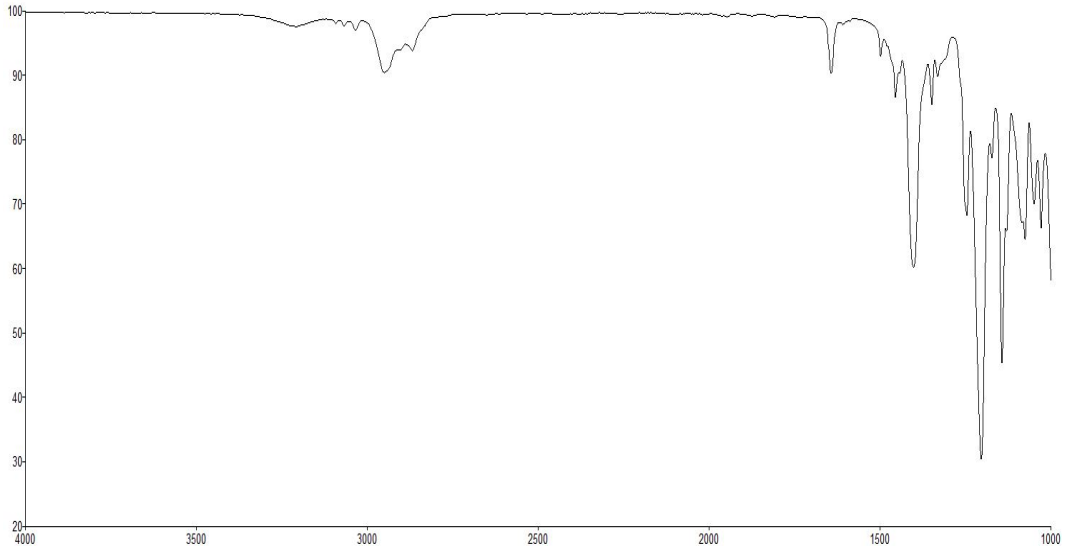

Figure 5.10. Infrared spectrum of compound **5.8**

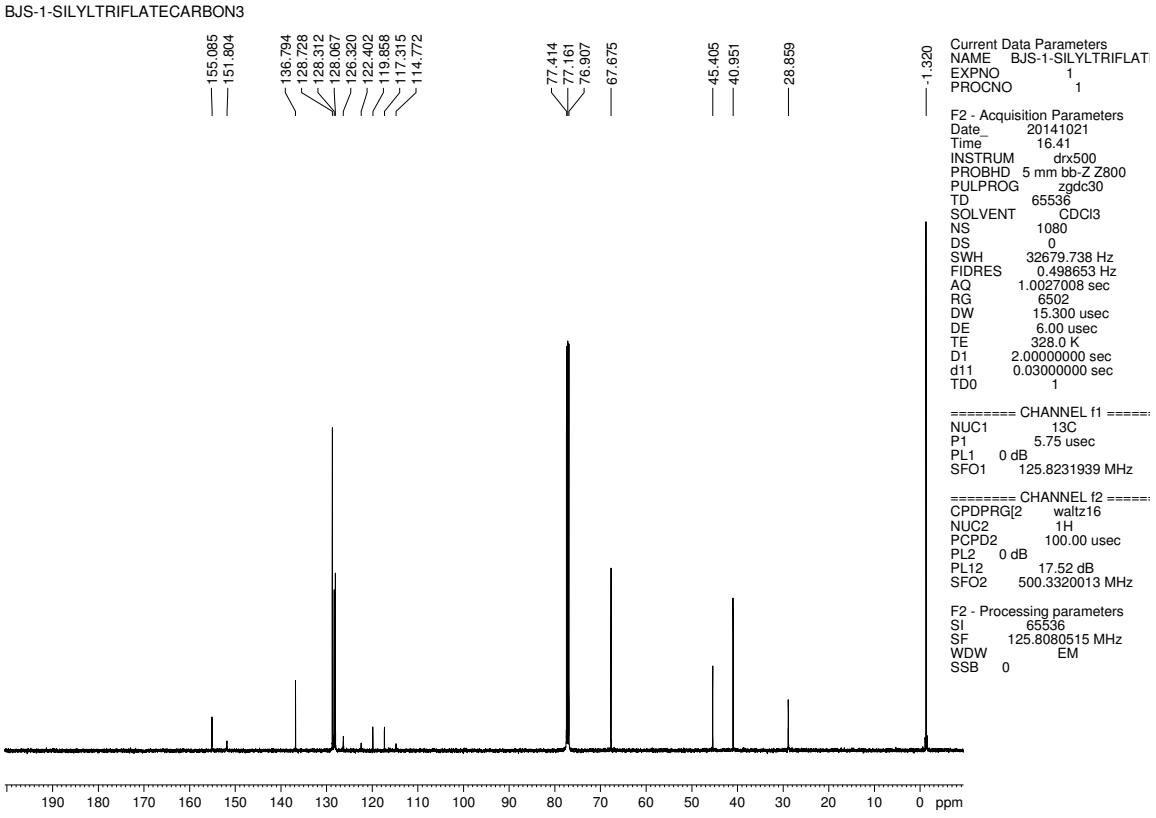

Figure 5.11. ^{13}C NMR (125 MHz, $CDCl_3$) of compound **5.8**

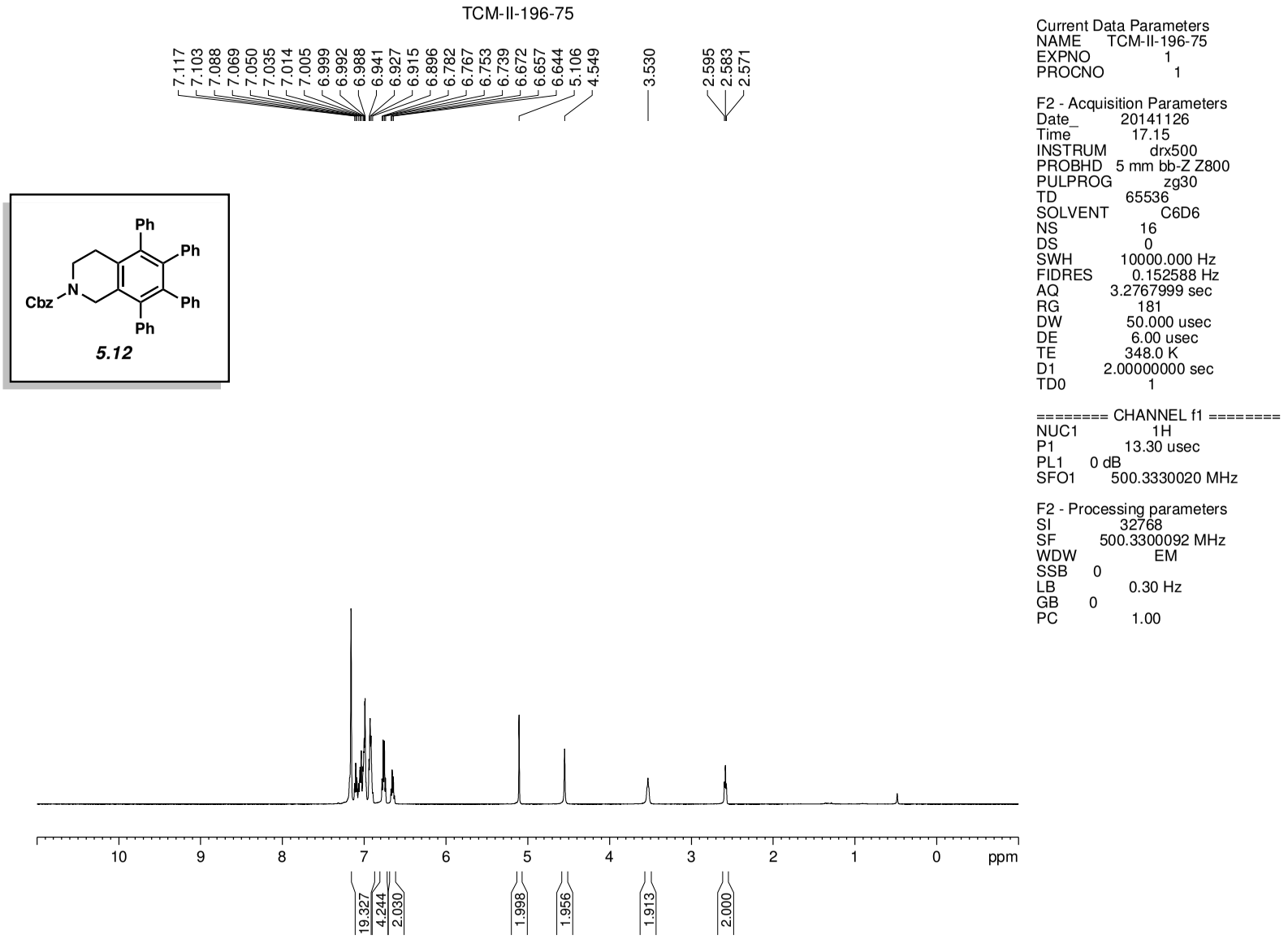

Figure 5.12. ^{1}H NMR (500 MHz, C_6D_6) compound **5.12**

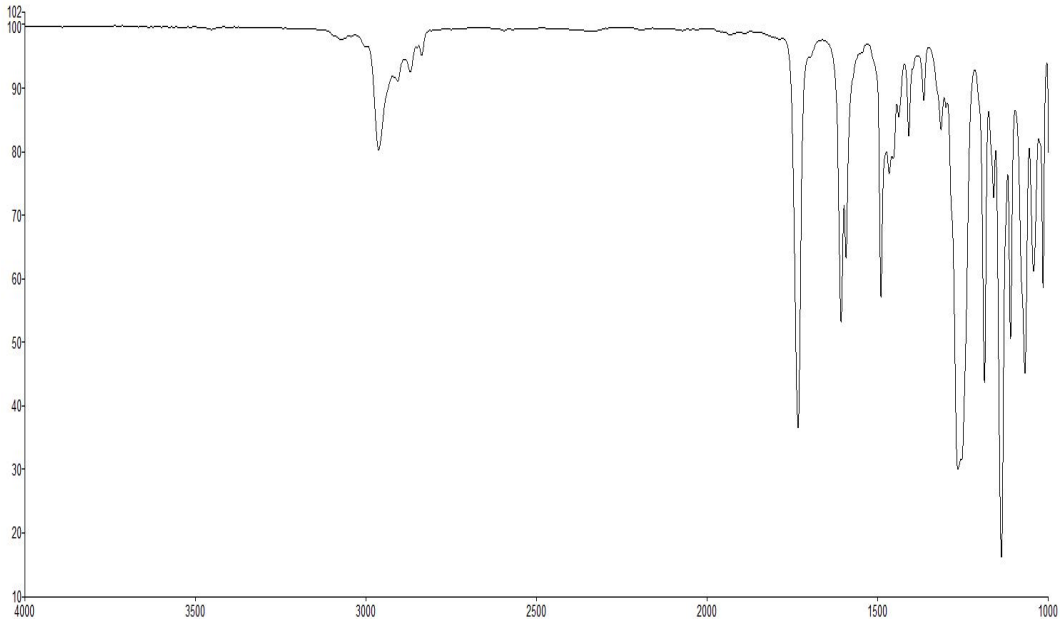

Figure 5.13. Infrared spectrum of compound **5.12**

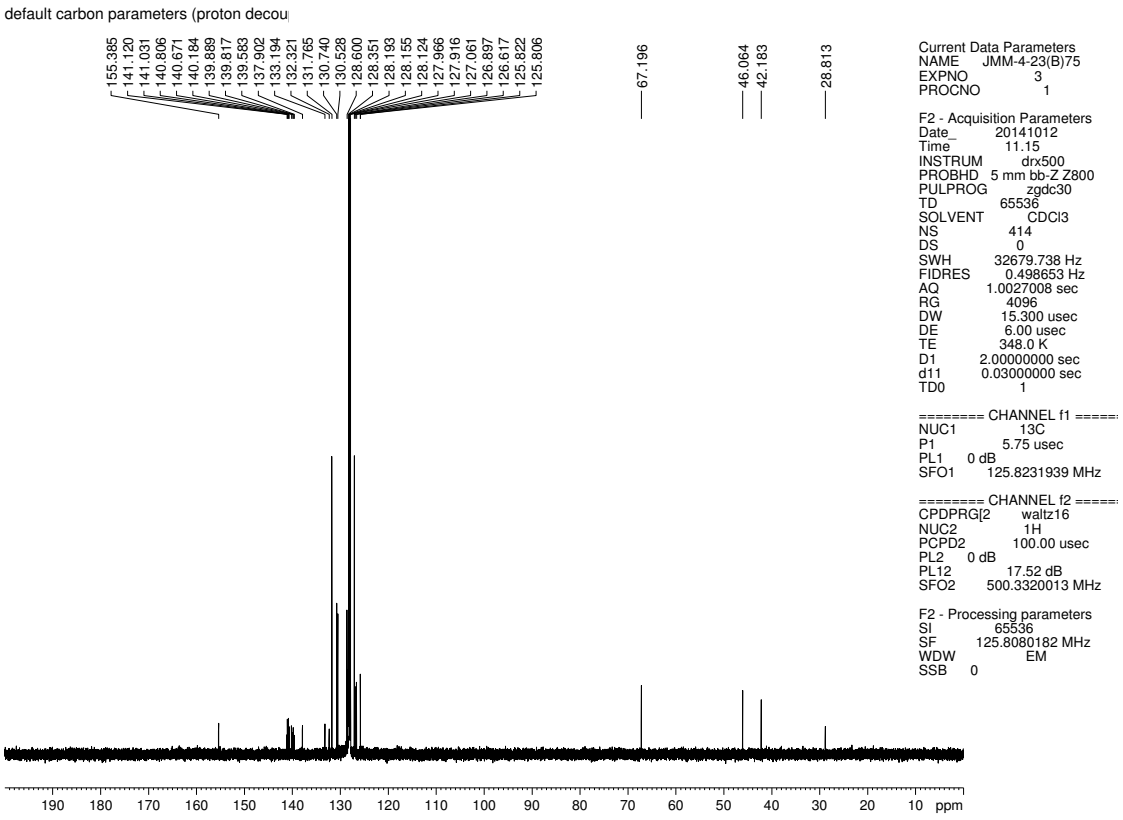

Figure 5.14. ^{13}C NMR (125 MHz, $CDCl_3$) of compound **5.12**

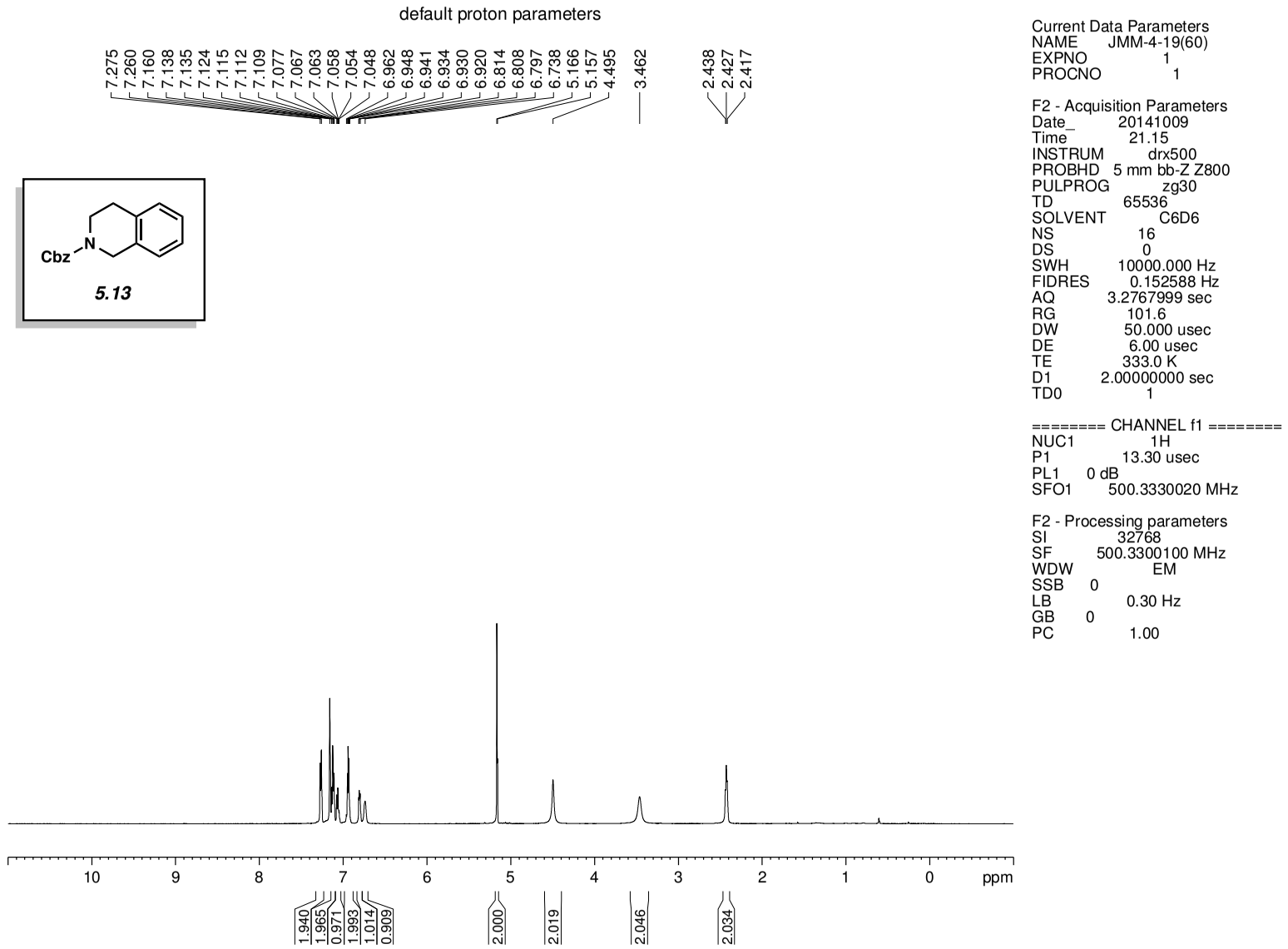

Figure 5.15. ^{1}H NMR (500 MHz, C_6D_6) compound **5.13**

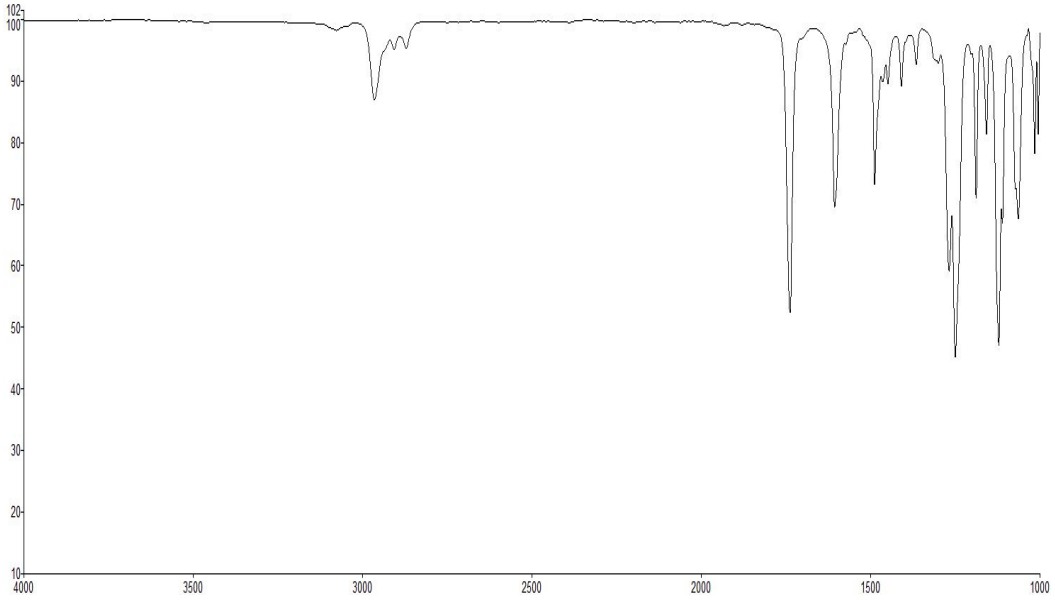

Figure 5.16. Infrared spectrum of compound **5.13**

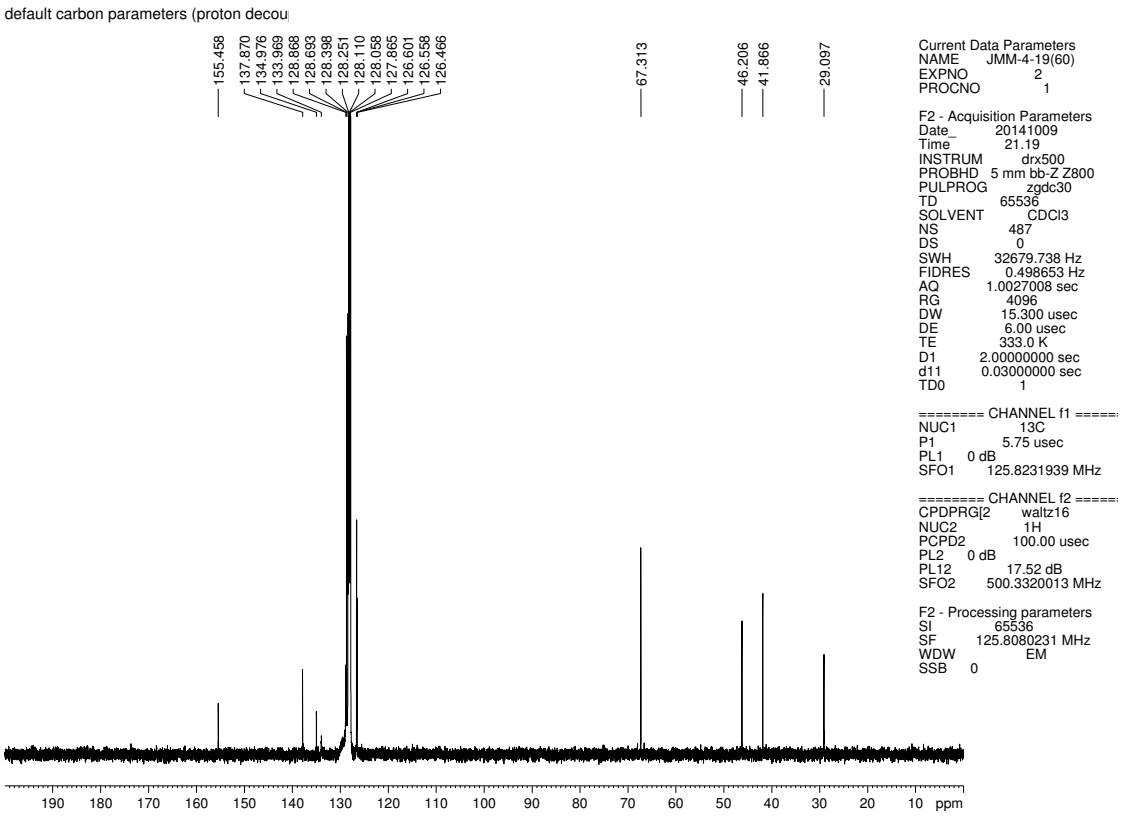

Figure 5.17. ^{13}C NMR (125 MHz, $CDCl_3$) of compound **5.13**

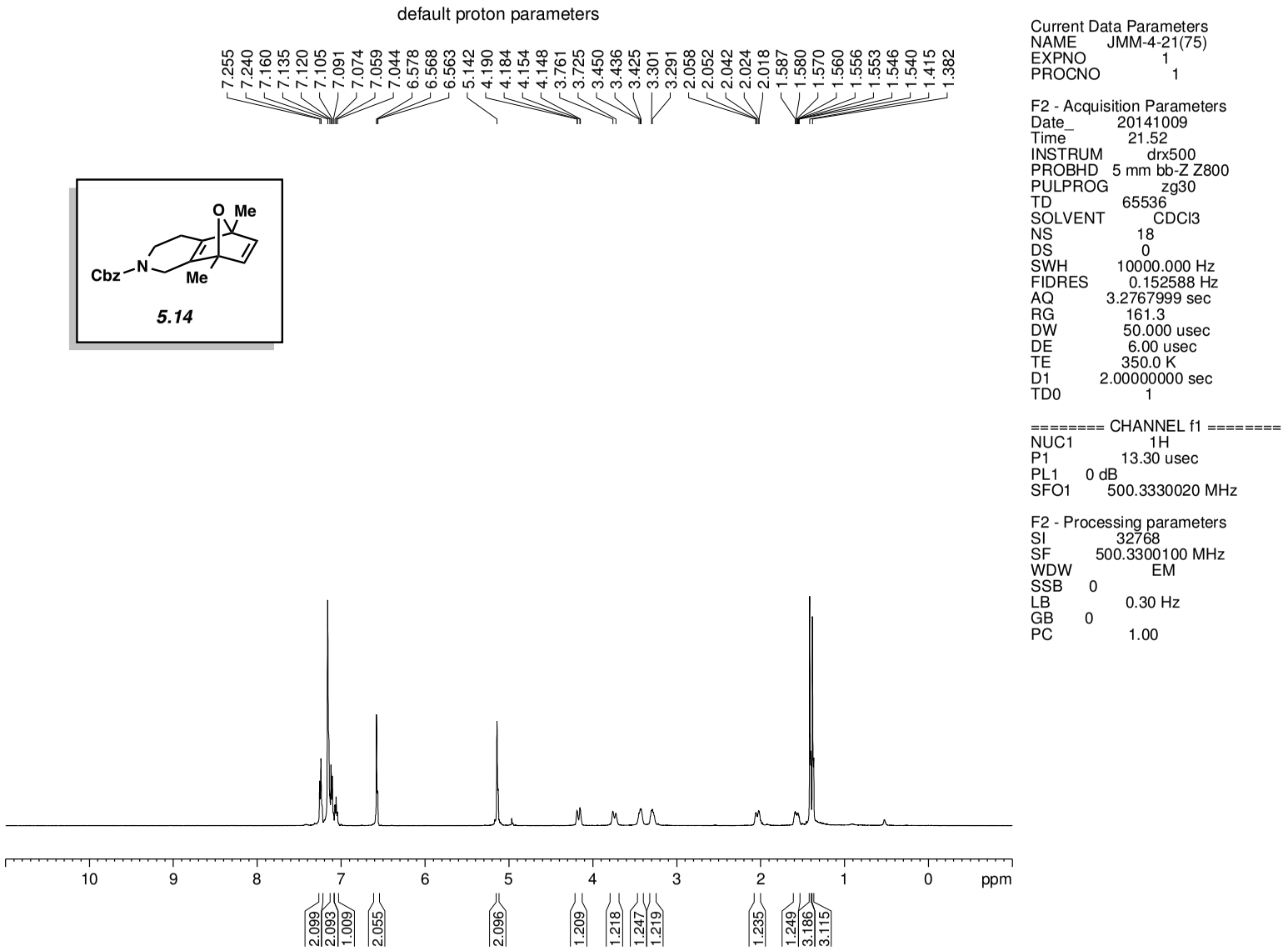

Figure 5.18. ^{1}H NMR (500 MHz, $CDCl_3$) compound **5.14**

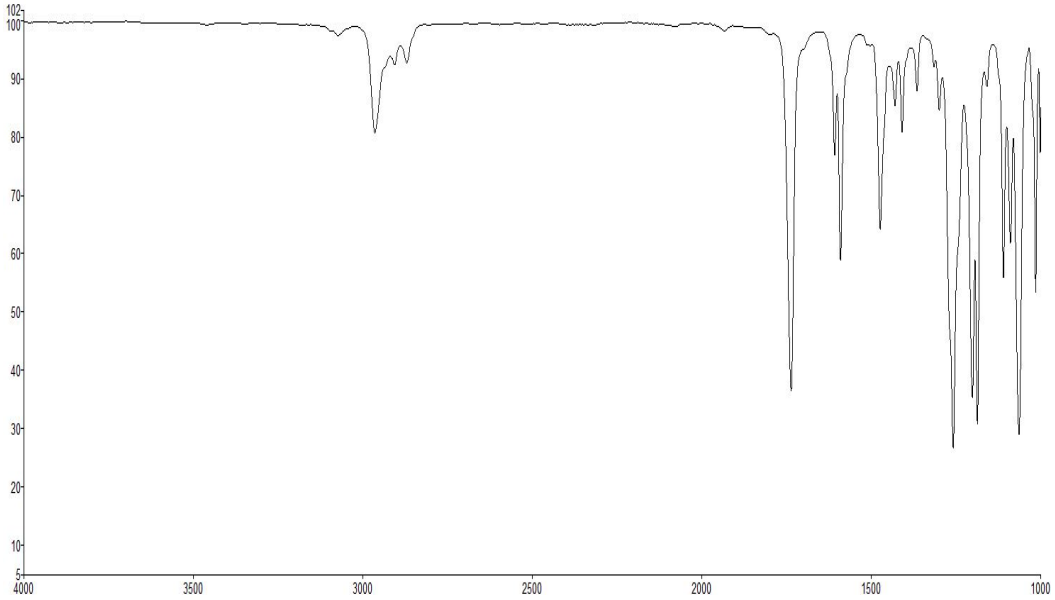

Figure 5.19. Infrared spectrum of compound **5.14**

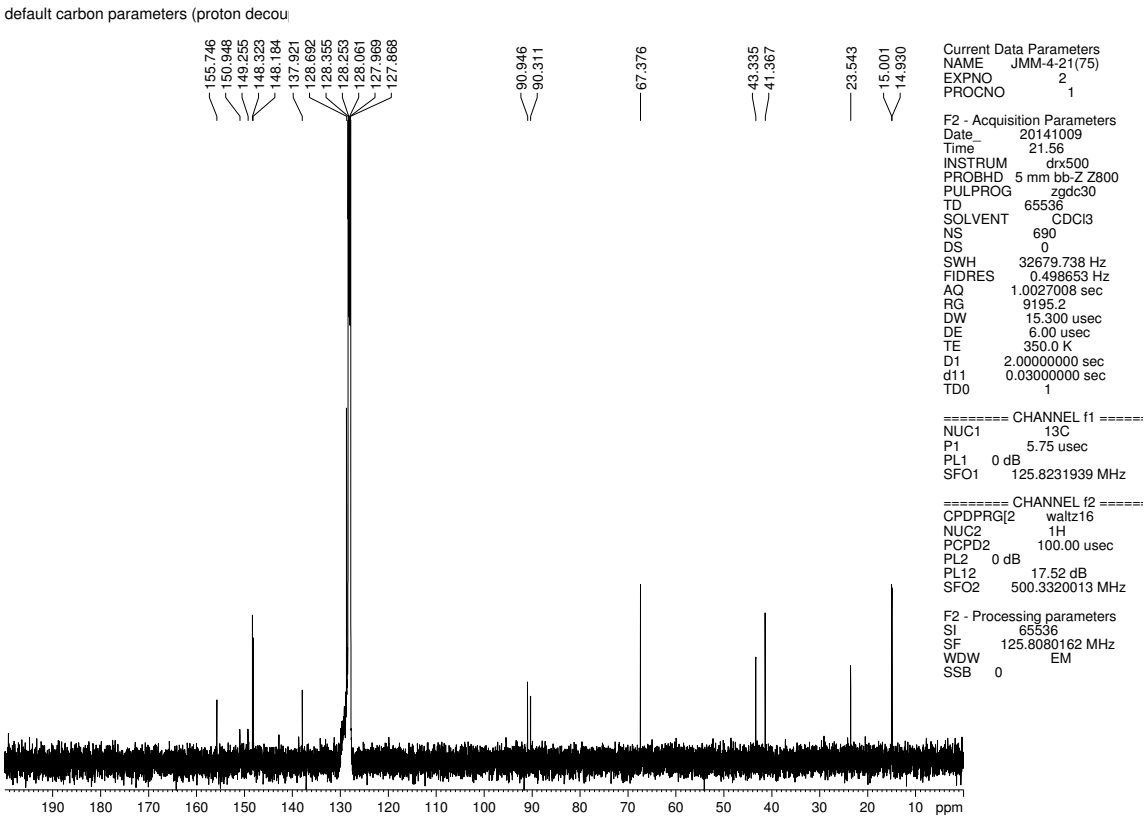

Figure 5.20. ^{13}C NMR (125 MHz, $CDCl_3$) of compound **5.14**

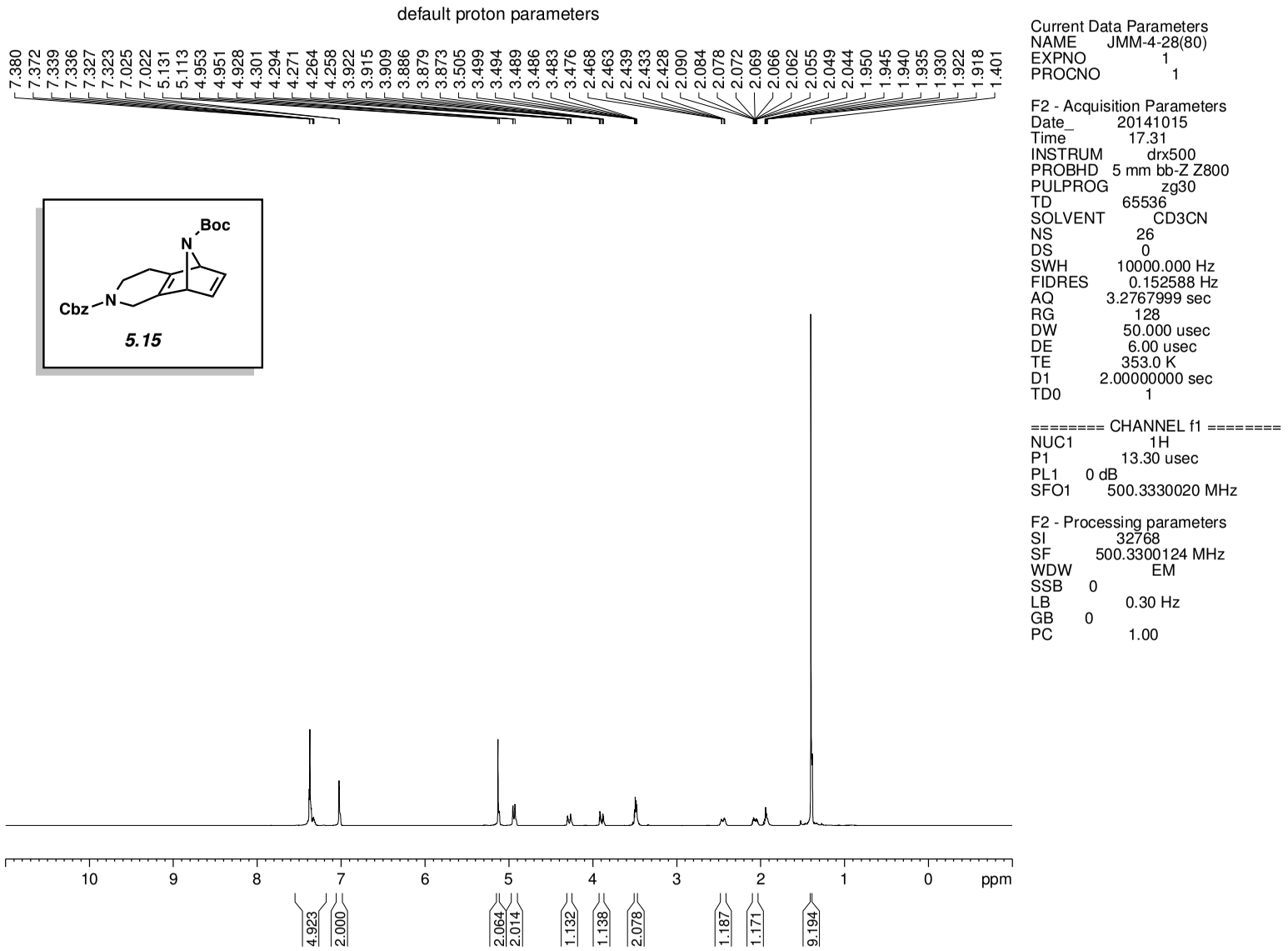

Figure 5.21. ^{1}H NMR (500 MHz, CD_3CN) compound **5.15**

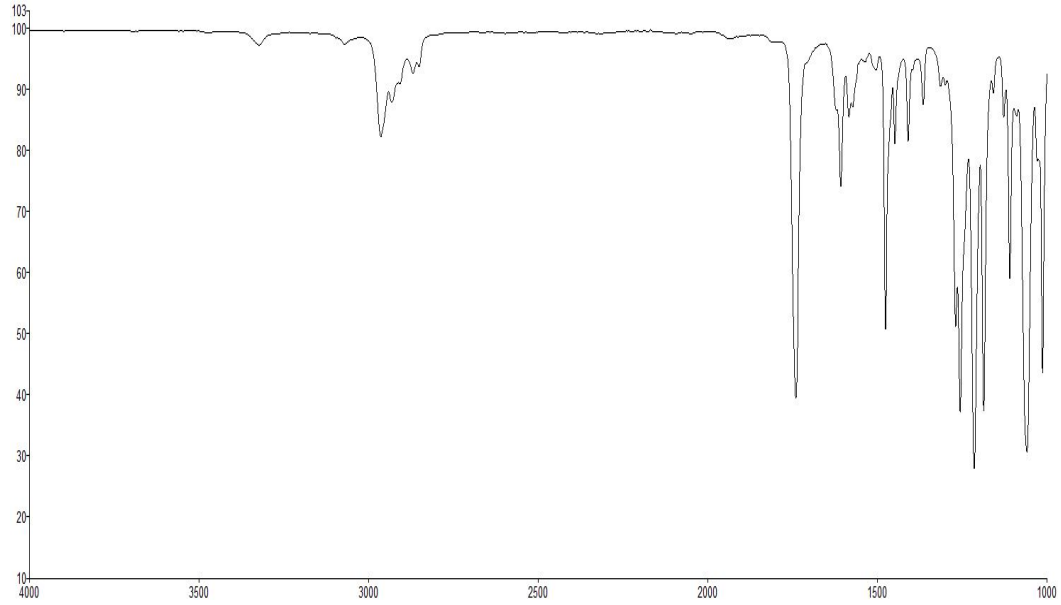

Figure 5.22. Infrared spectrum of compound **5.15**

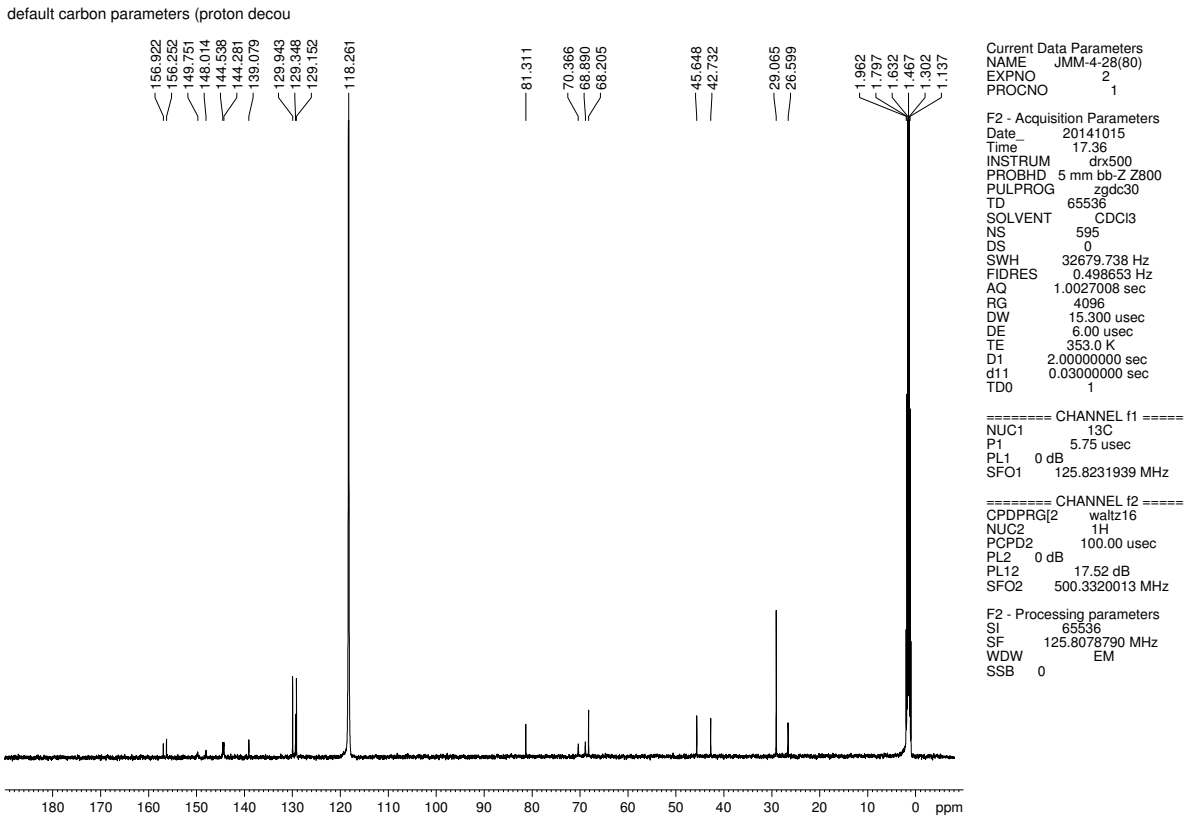

Figure 5.23. ^{13}C NMR (125 MHz, $CDCl_3$) of compound **5.15**

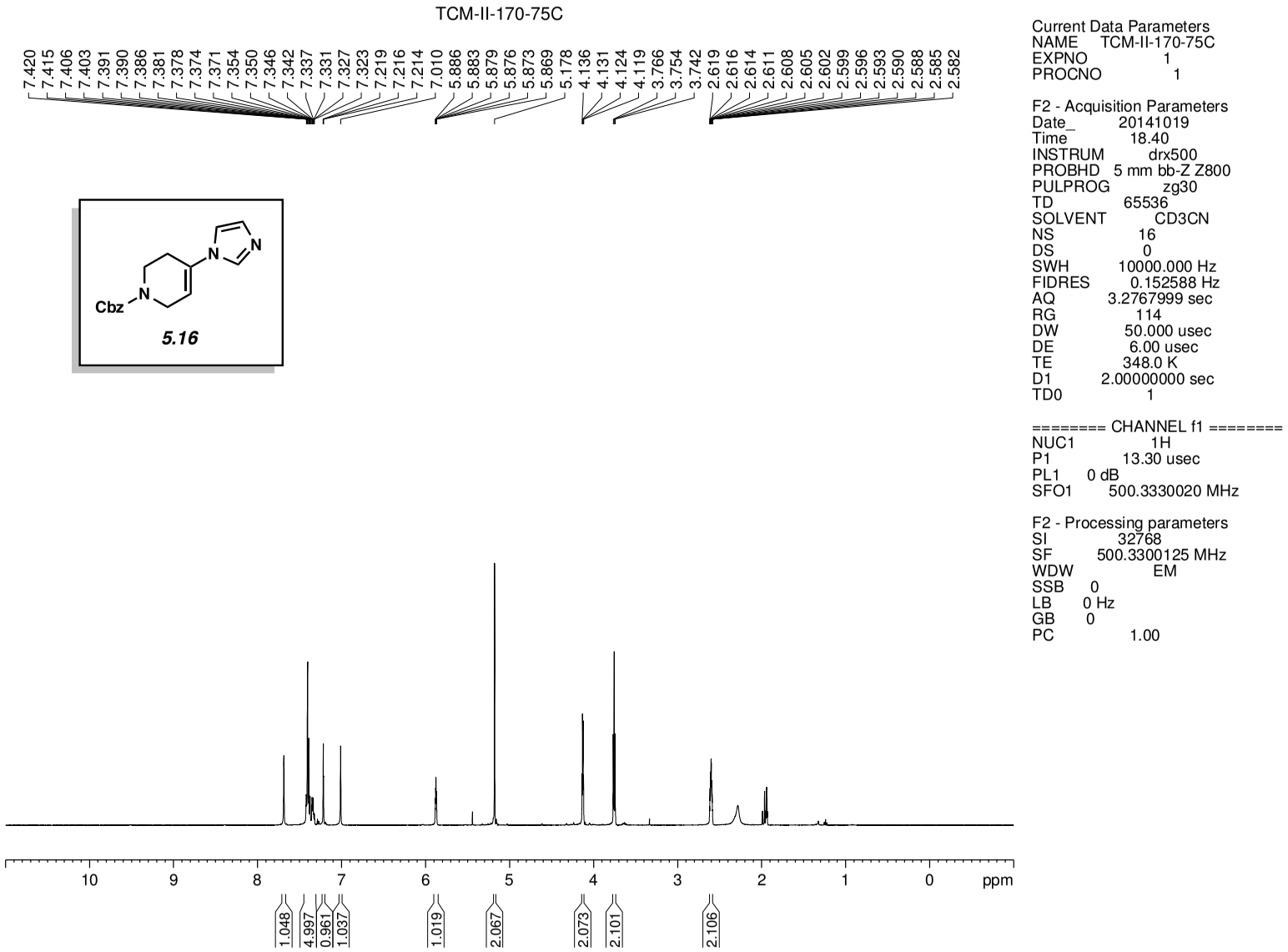

Figure 5.24. ^{1}H NMR (500 MHz, CD_3CN) compound **5.16**

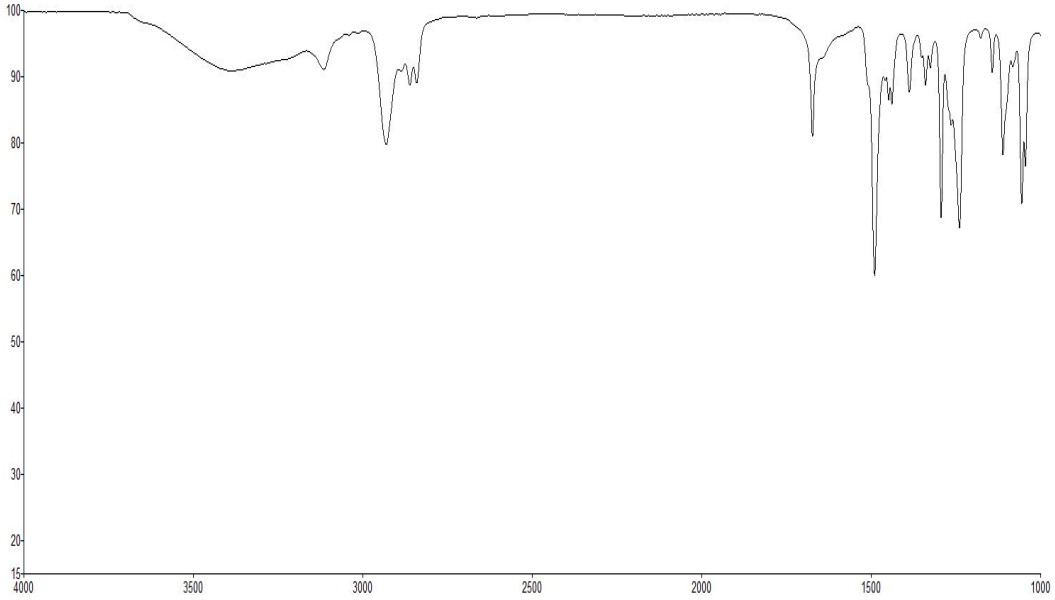

Figure 5.25. Infrared spectrum of compound **5.16**

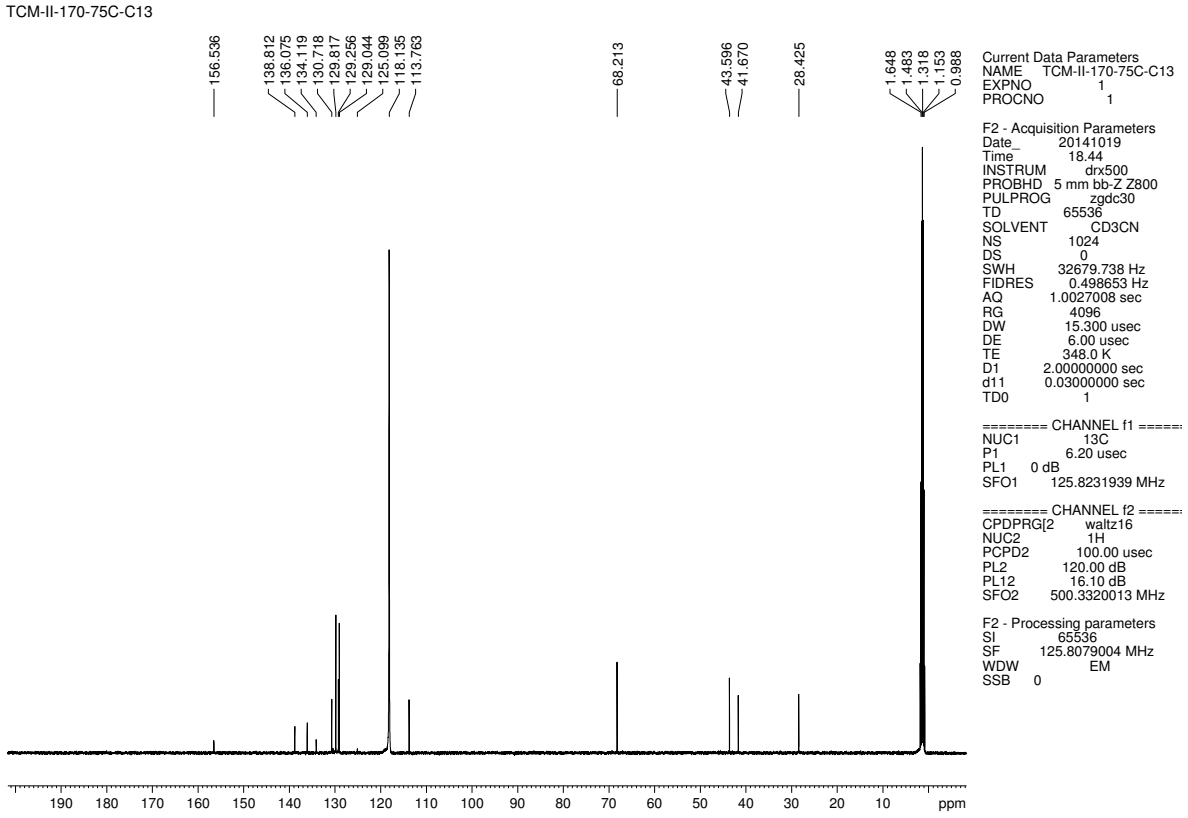

Figure 5.26. ^{13}C NMR (125 MHz, CD_3CN) of compound **5.16**

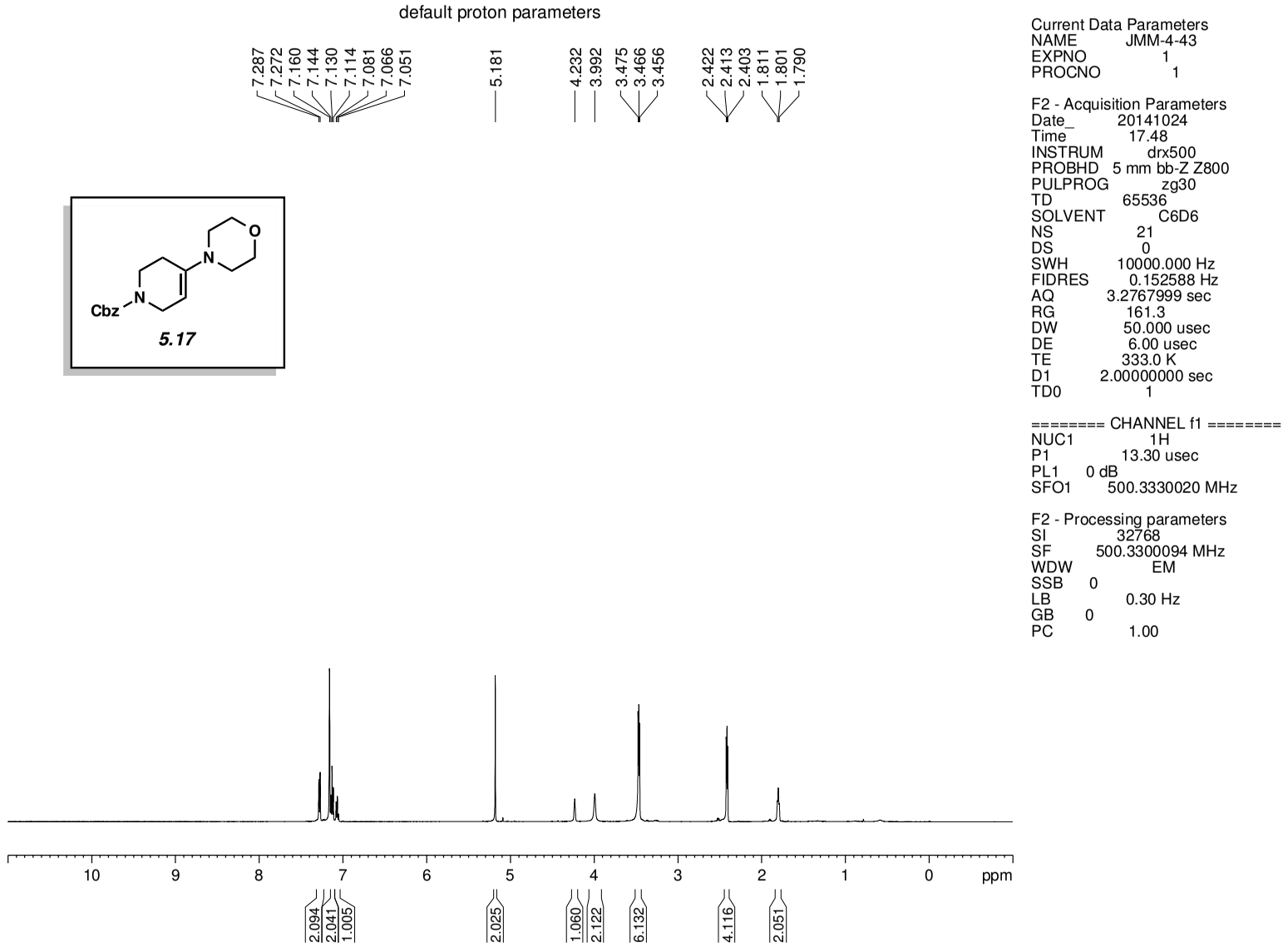

Figure 5.27. ^{1}H NMR (500 MHz, C_6D_6) compound **5.17**

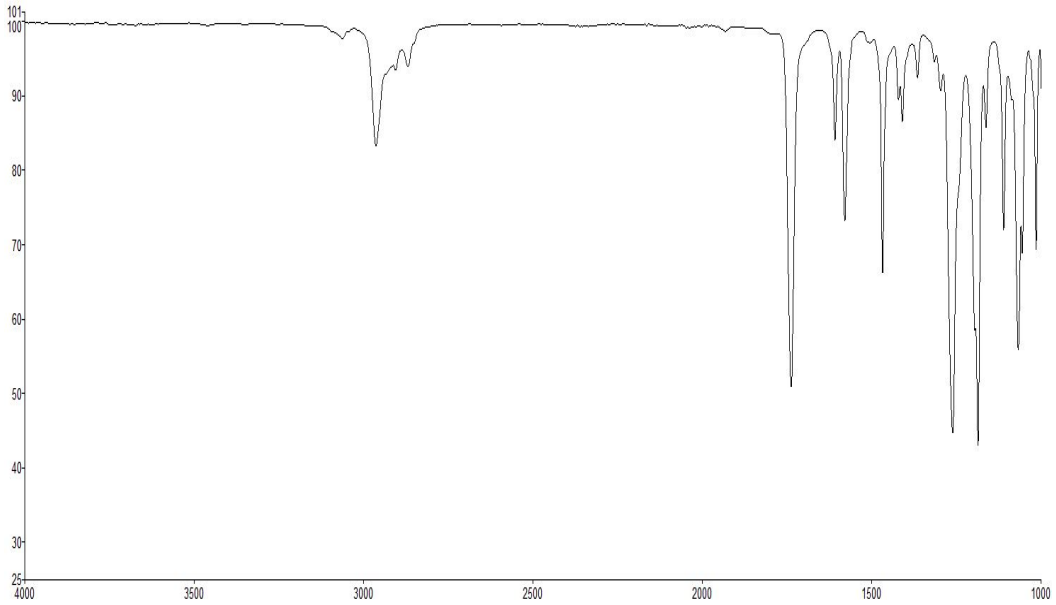

Figure 5.28. Infrared spectrum of compound **5.17**

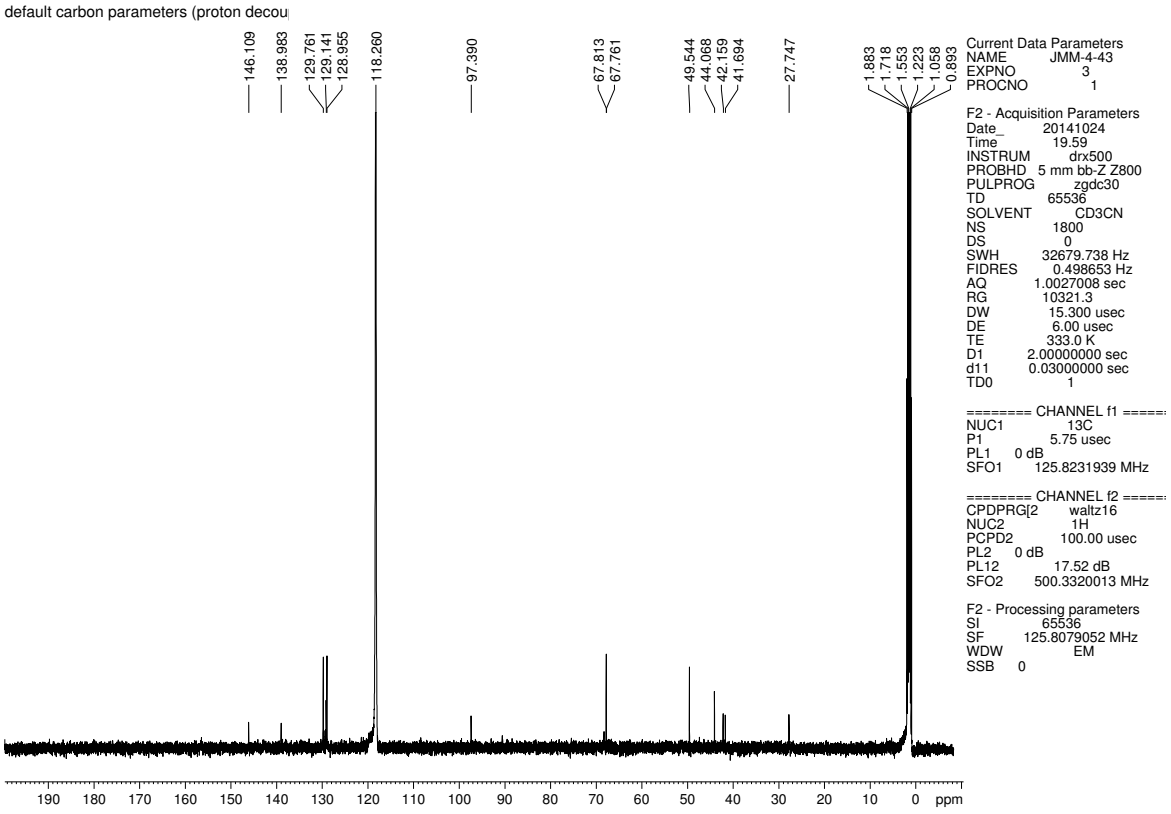

Figure 5.29. ^{13}C NMR (125 MHz, CD_3CN) of compound **5.17**

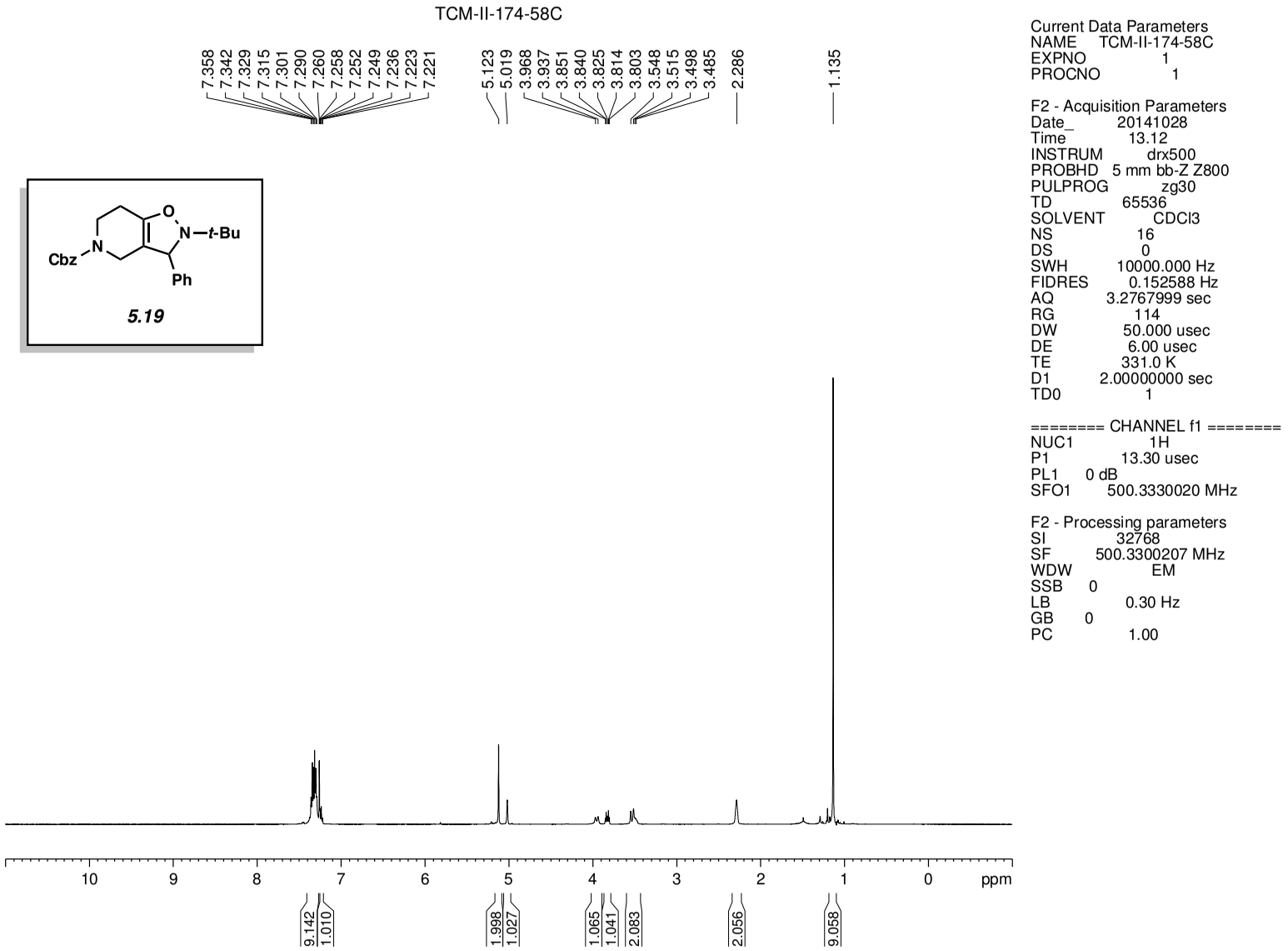

Figure 5.30. ^{1}H NMR (500 MHz, $CDCl_3$) compound **5.19**

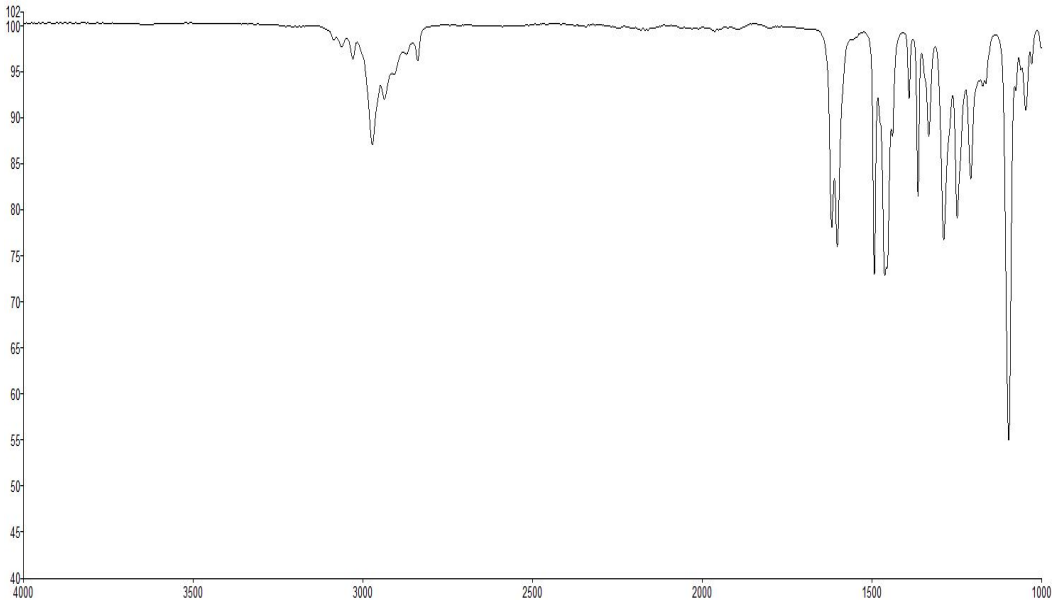

Figure 5.31. Infrared spectrum of compound **5.19**

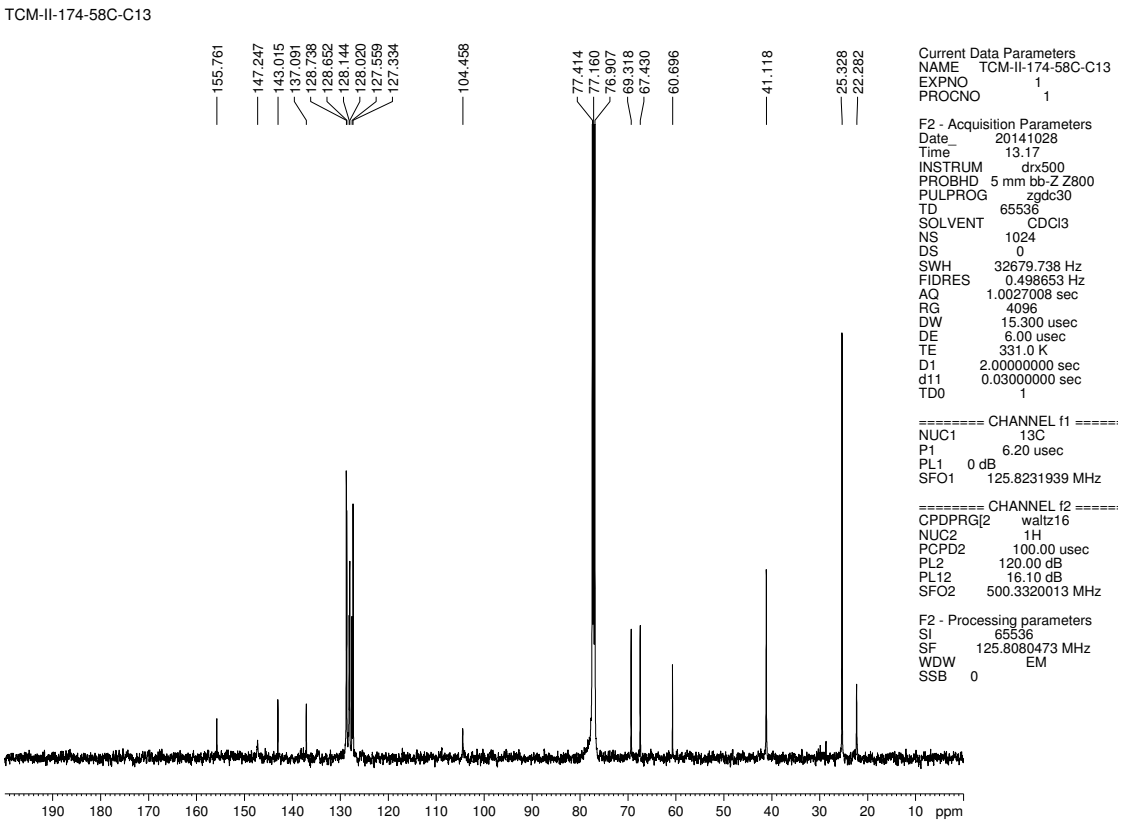

Figure 5.32. ^{13}C NMR (125 MHz, $CDCl_3$) of compound **5.19**

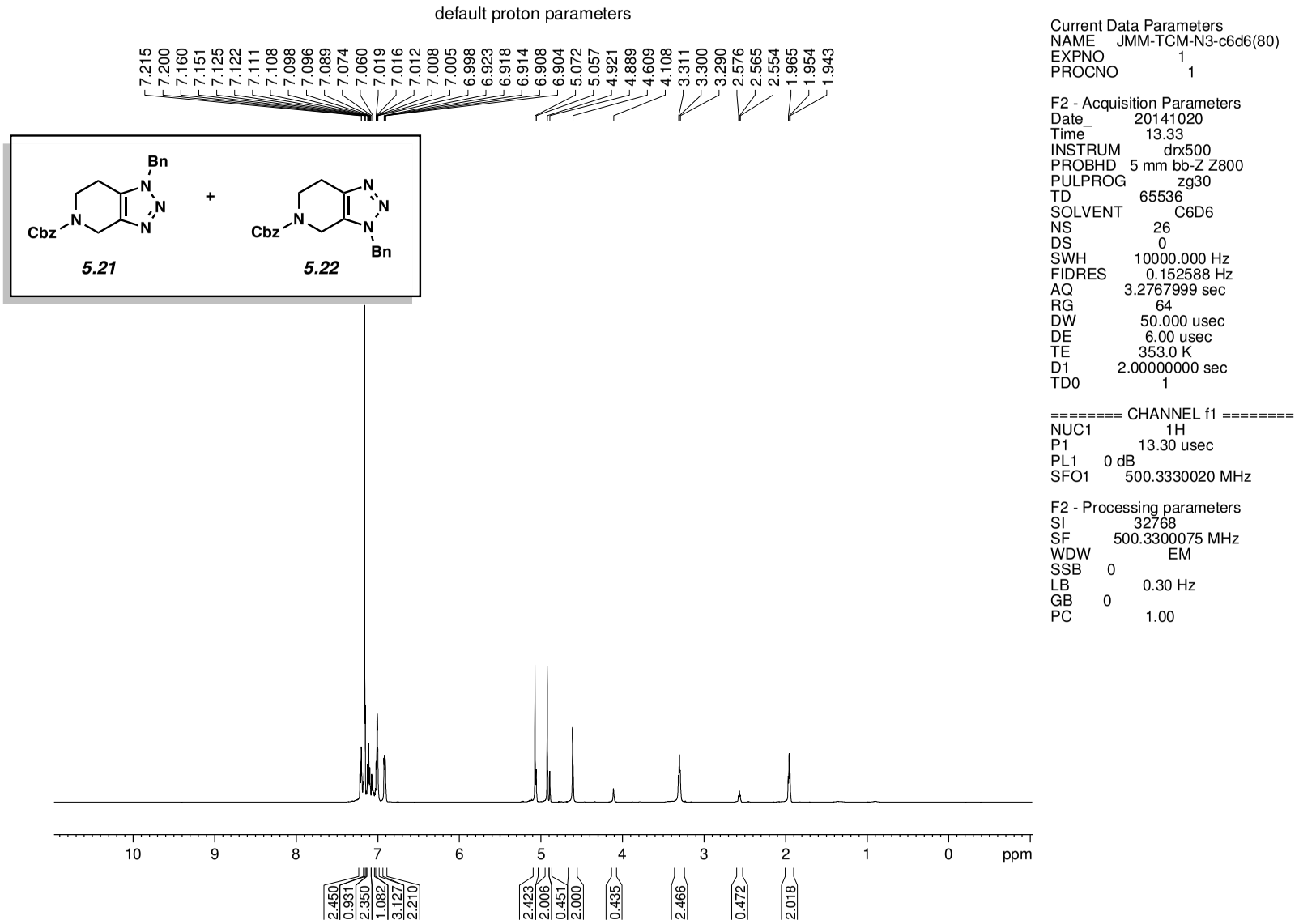

Figure 5.33. ^{1}H NMR (500 MHz, C_6D_6) compounds **5.21** amd **5.22**

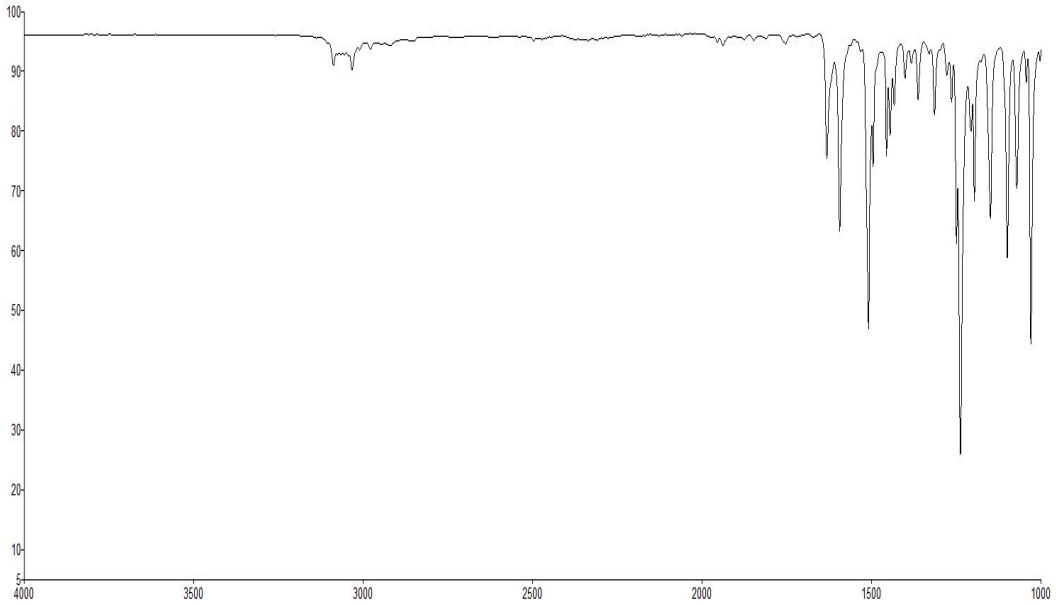

Figure 5.34. Infrared spectrum of compounds **5.21** and **5.22**

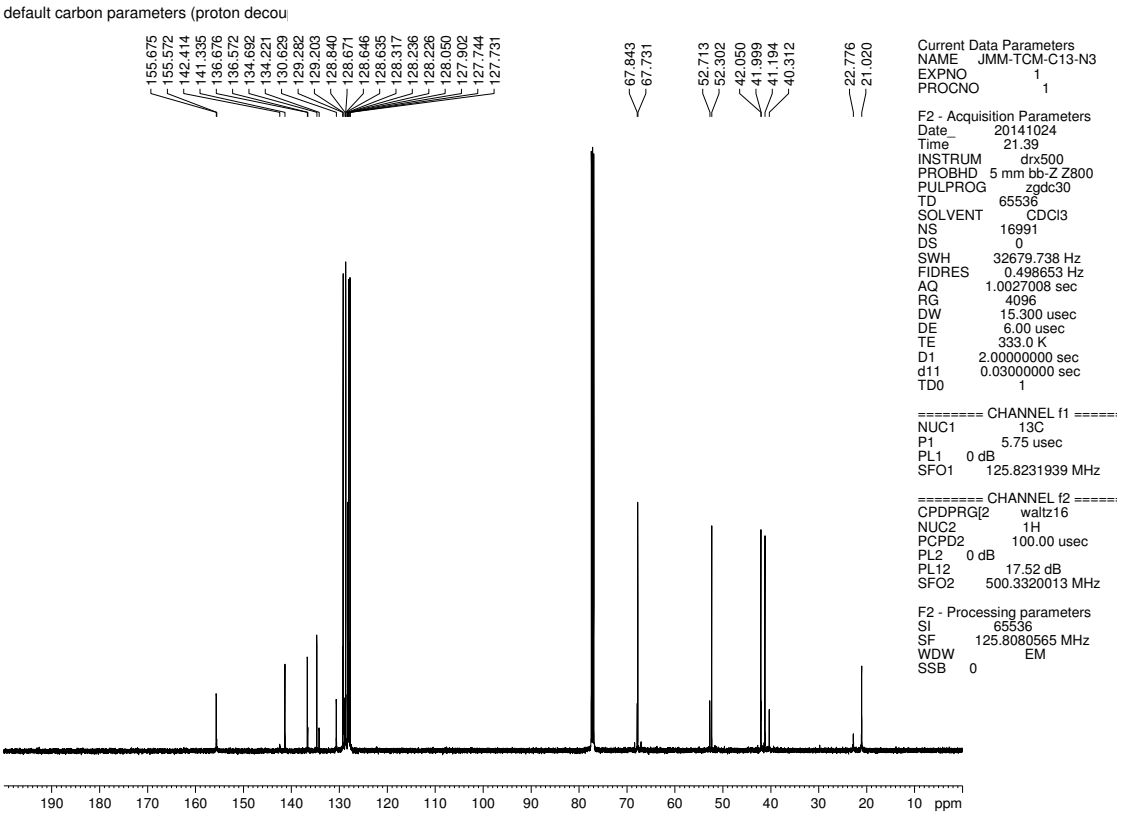

Figure 5.35. ^{13}C NMR (125 MHz, $CDCl_3$) of compounds **5.21** and **5.22**

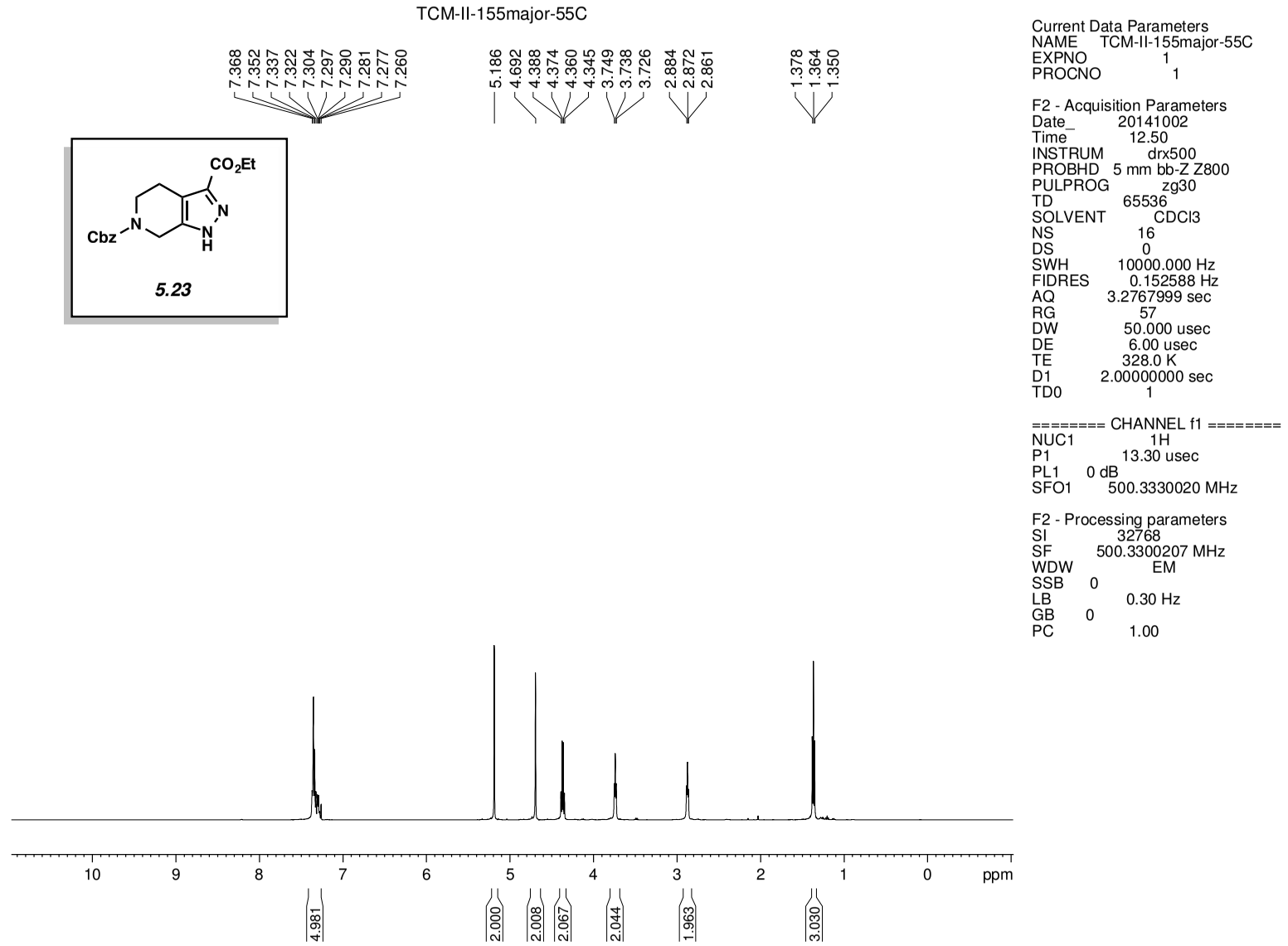

Figure 5.36. ^{1}H NMR (500 MHz, $CDCl_3$) compound **5.23**

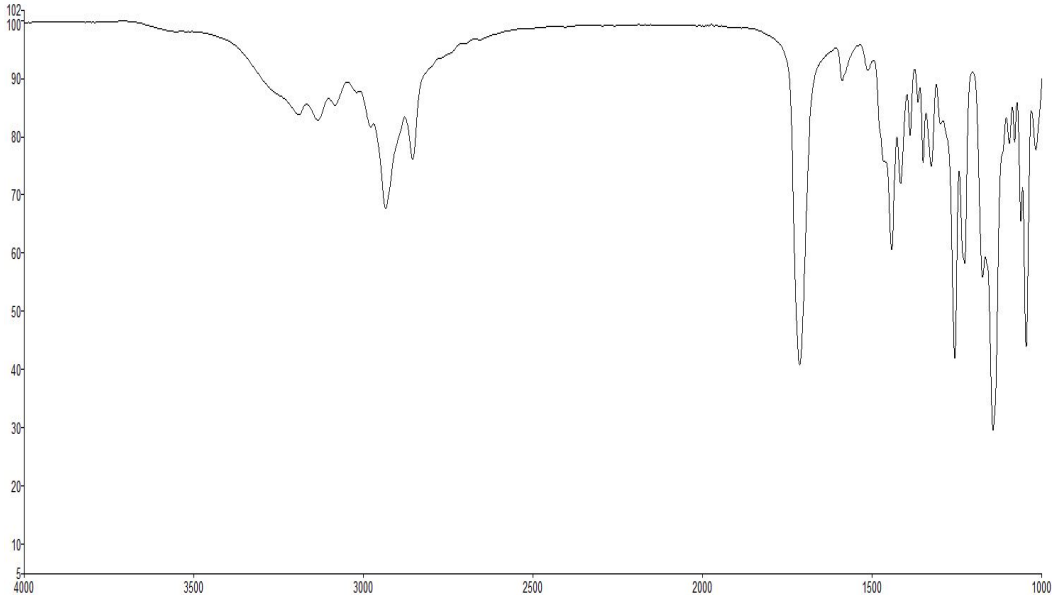

Figure 5.37. Infrared spectrum of compound **5.23**

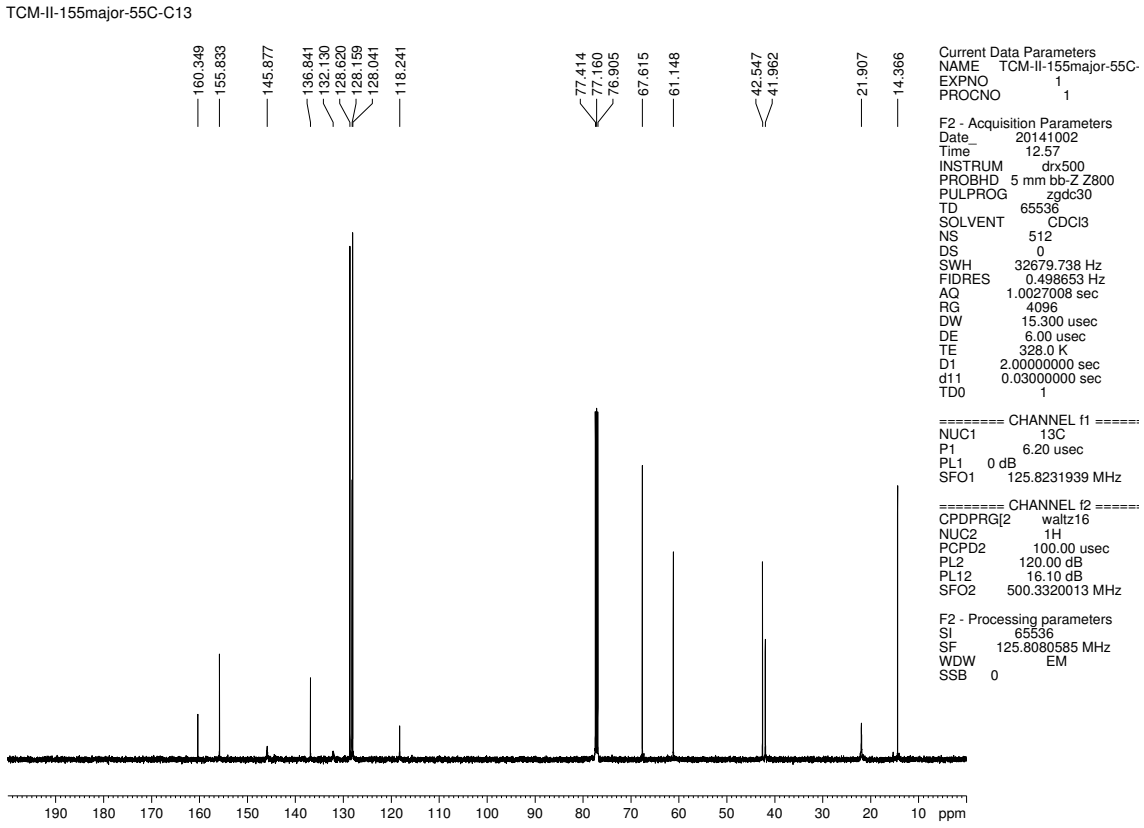

Figure 5.38. ^{13}C NMR (125 MHz, $CDCl_3$) of compound **5.23**

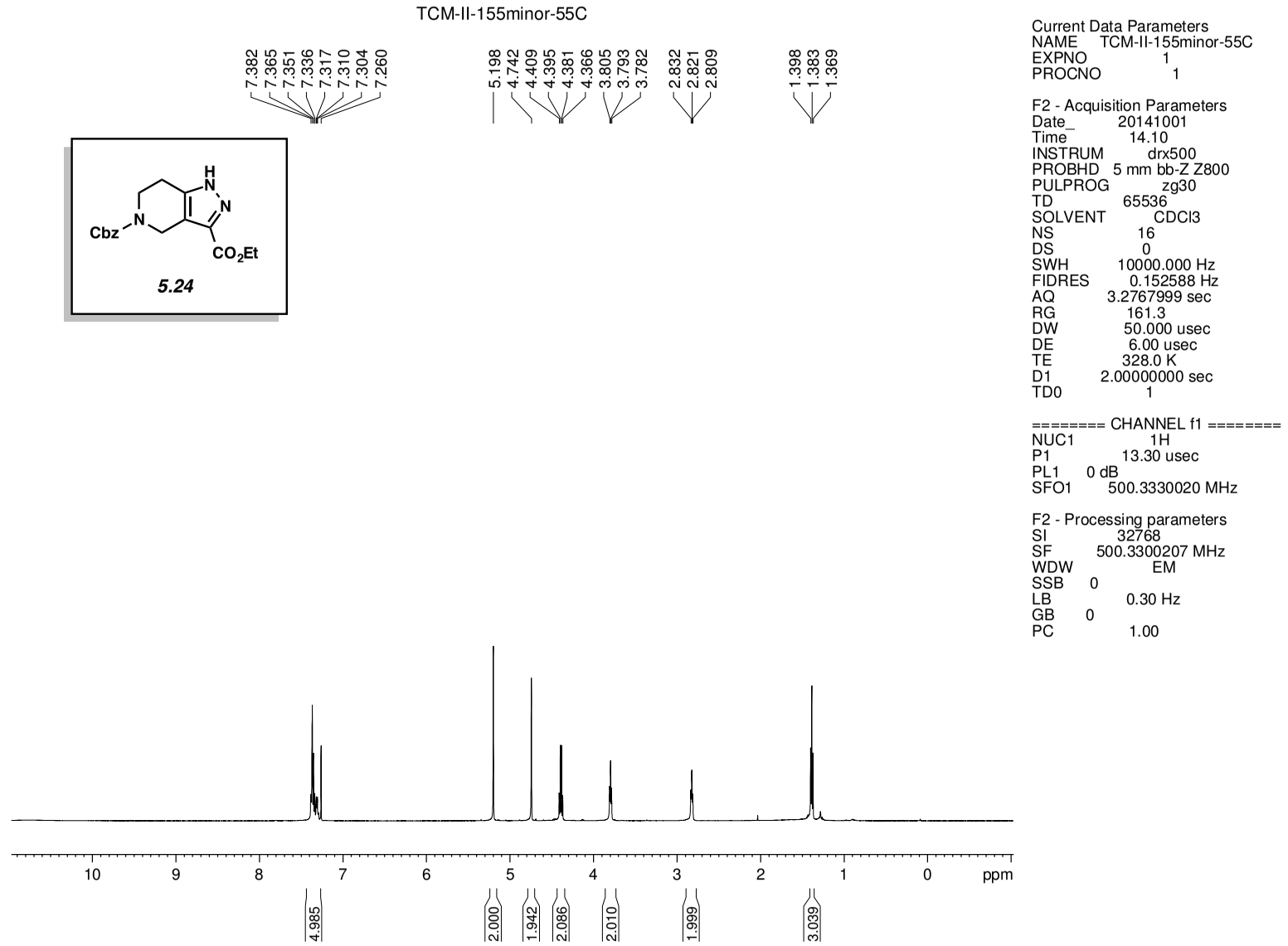

Figure 5.39. ^{1}H NMR (500 MHz, $CDCl_3$) compound **5.24**

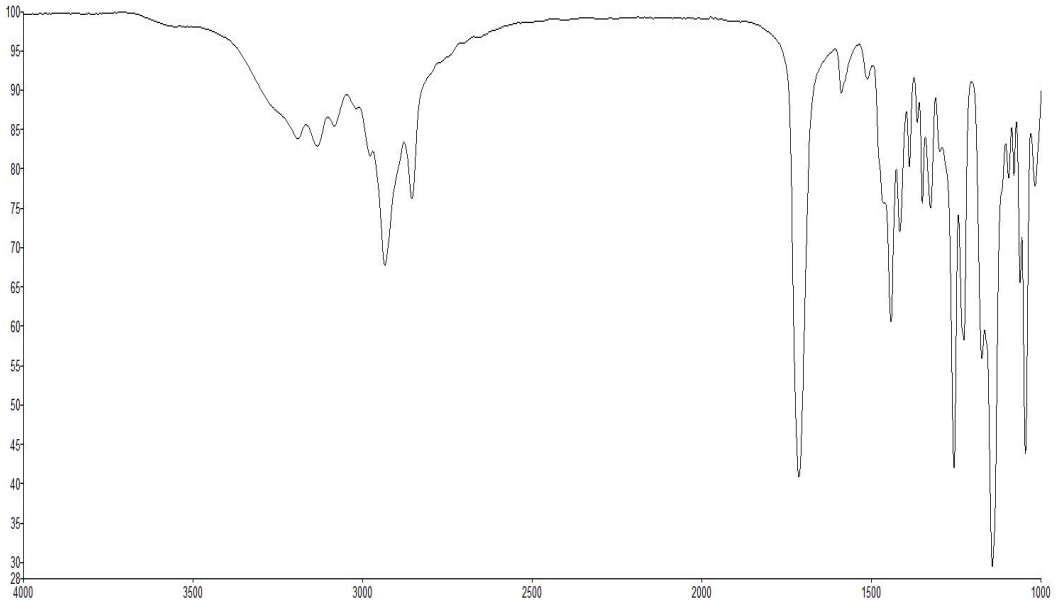

Figure 5.40. Infrared spectrum of compound **5.24**

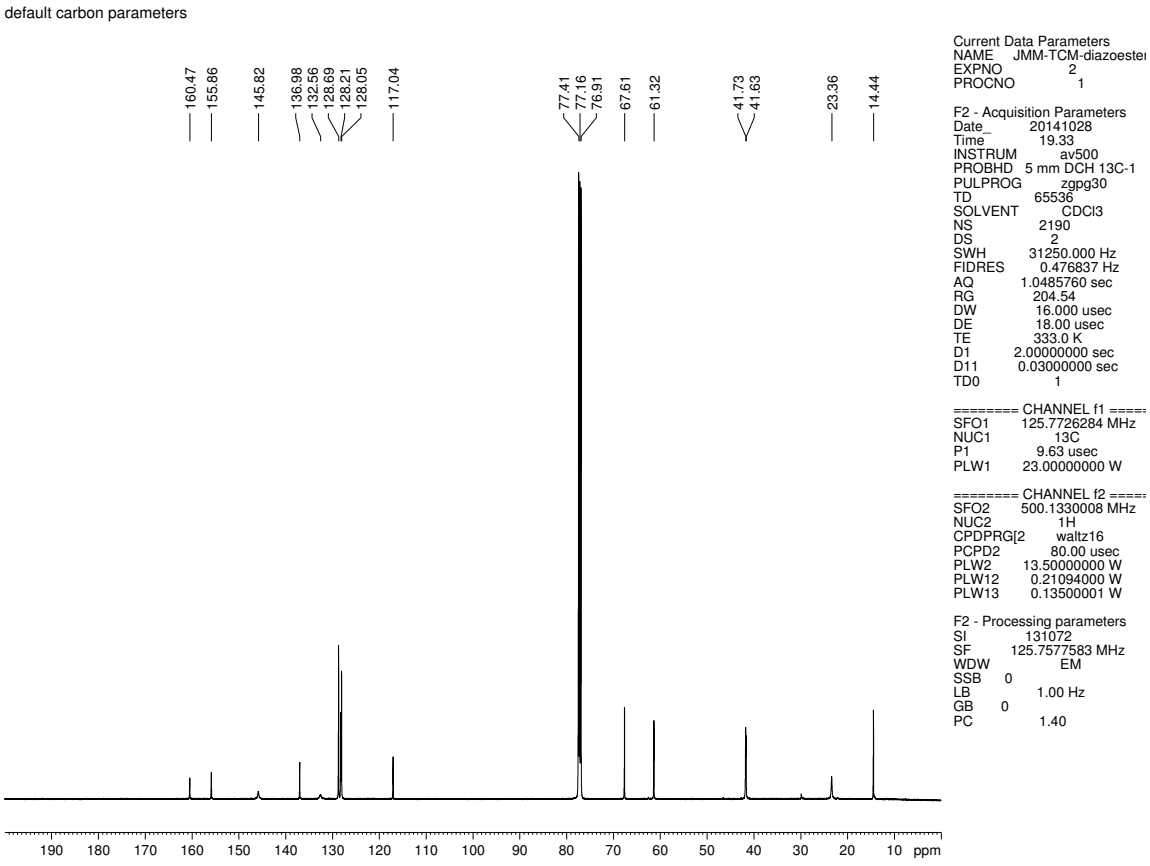

Figure 5.41. ^{13}C NMR (125 MHz, $CDCl_3$) of compound **5.24**

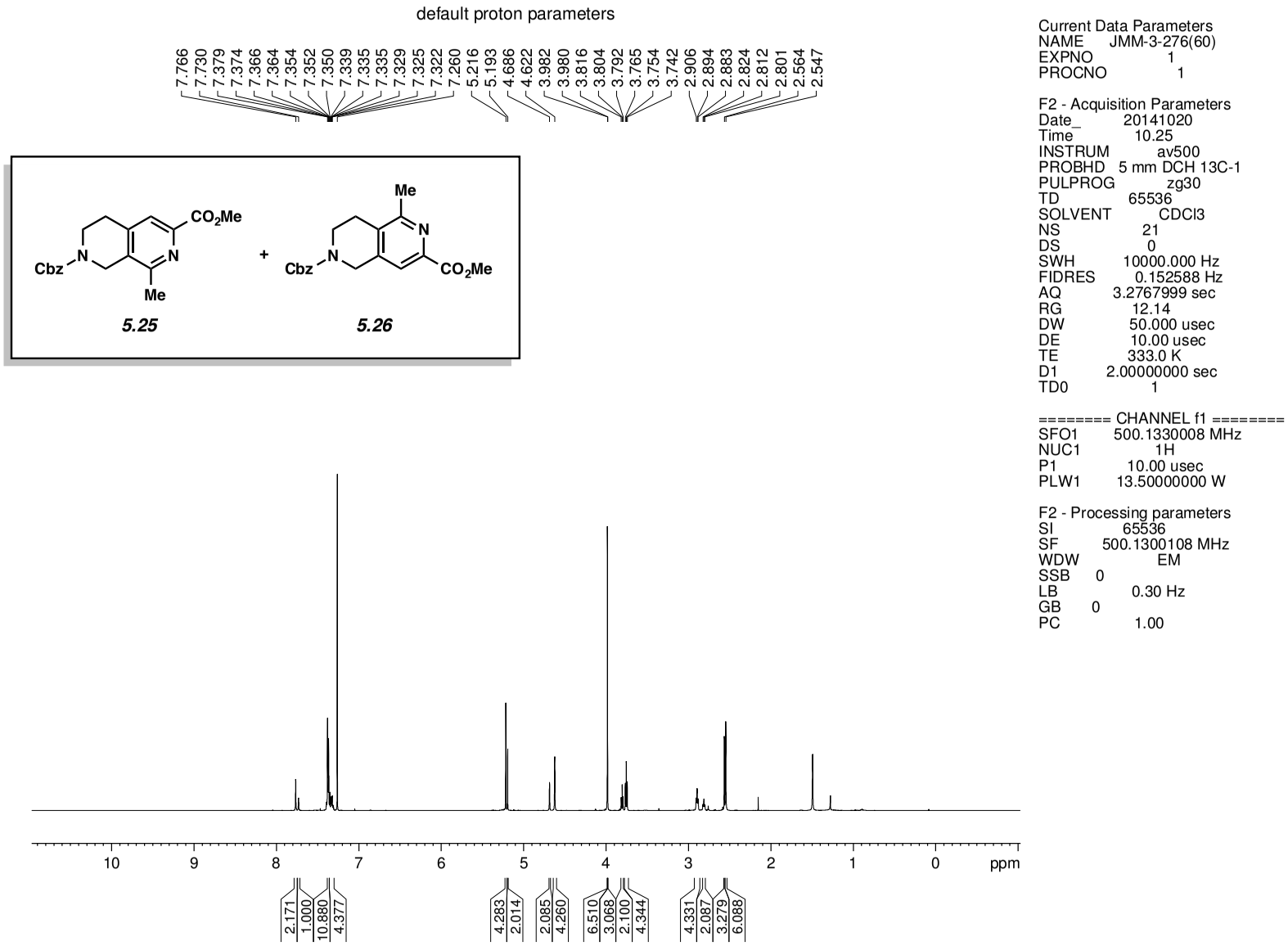

Figure 5.42. ^{1}H NMR (500 MHz, $CDCl_3$) compounds **5.25** and **5.26**

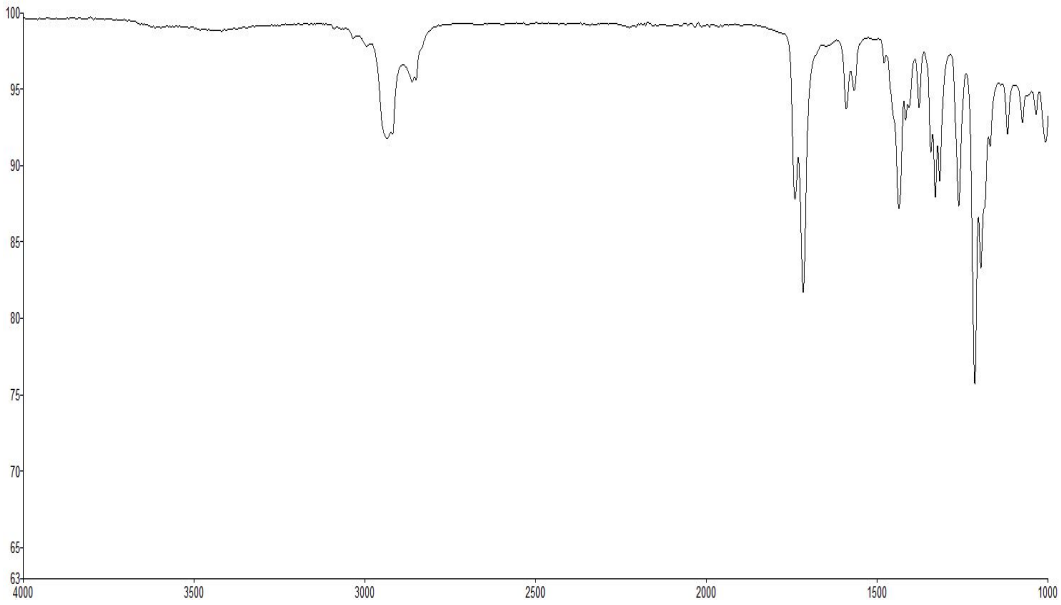

Figure 5.43. Infrared spectrum of compounds **5.25** and **5.26**

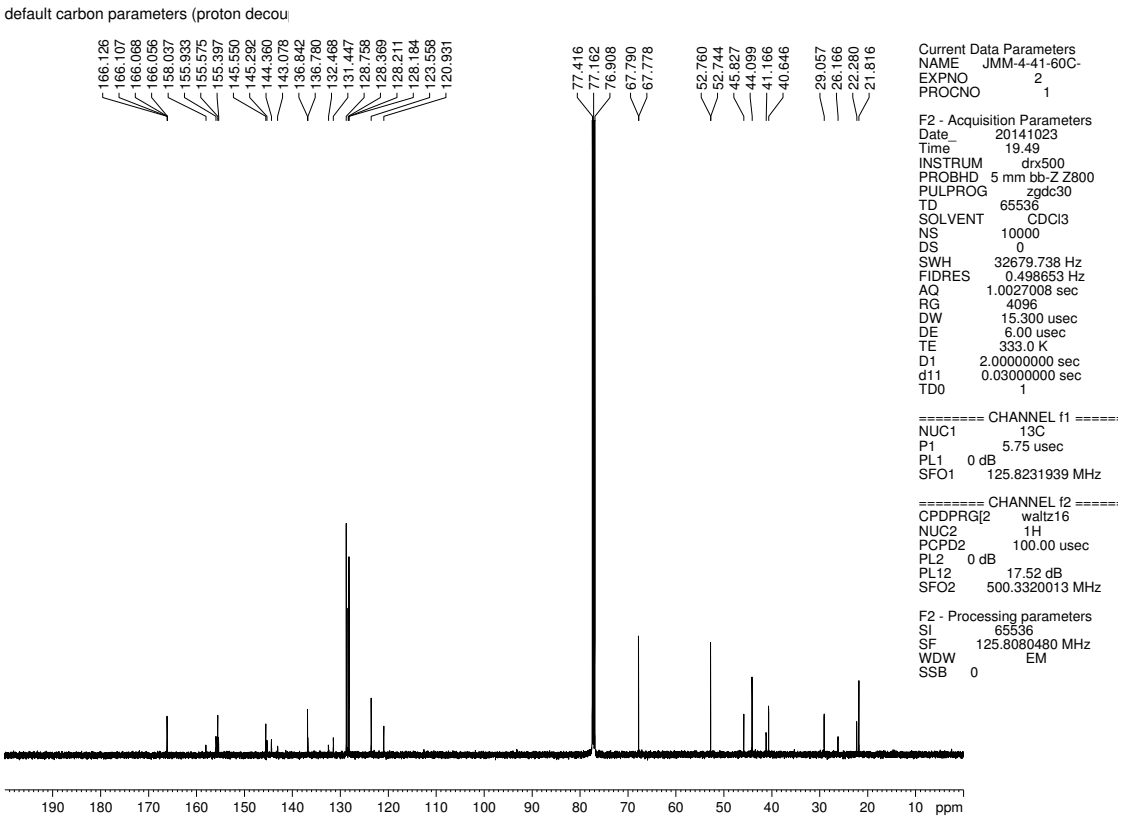

Figure 5.44. ^{13}C NMR (125 MHz, $CDCl_3$) of compounds **5.25** and **5.26**

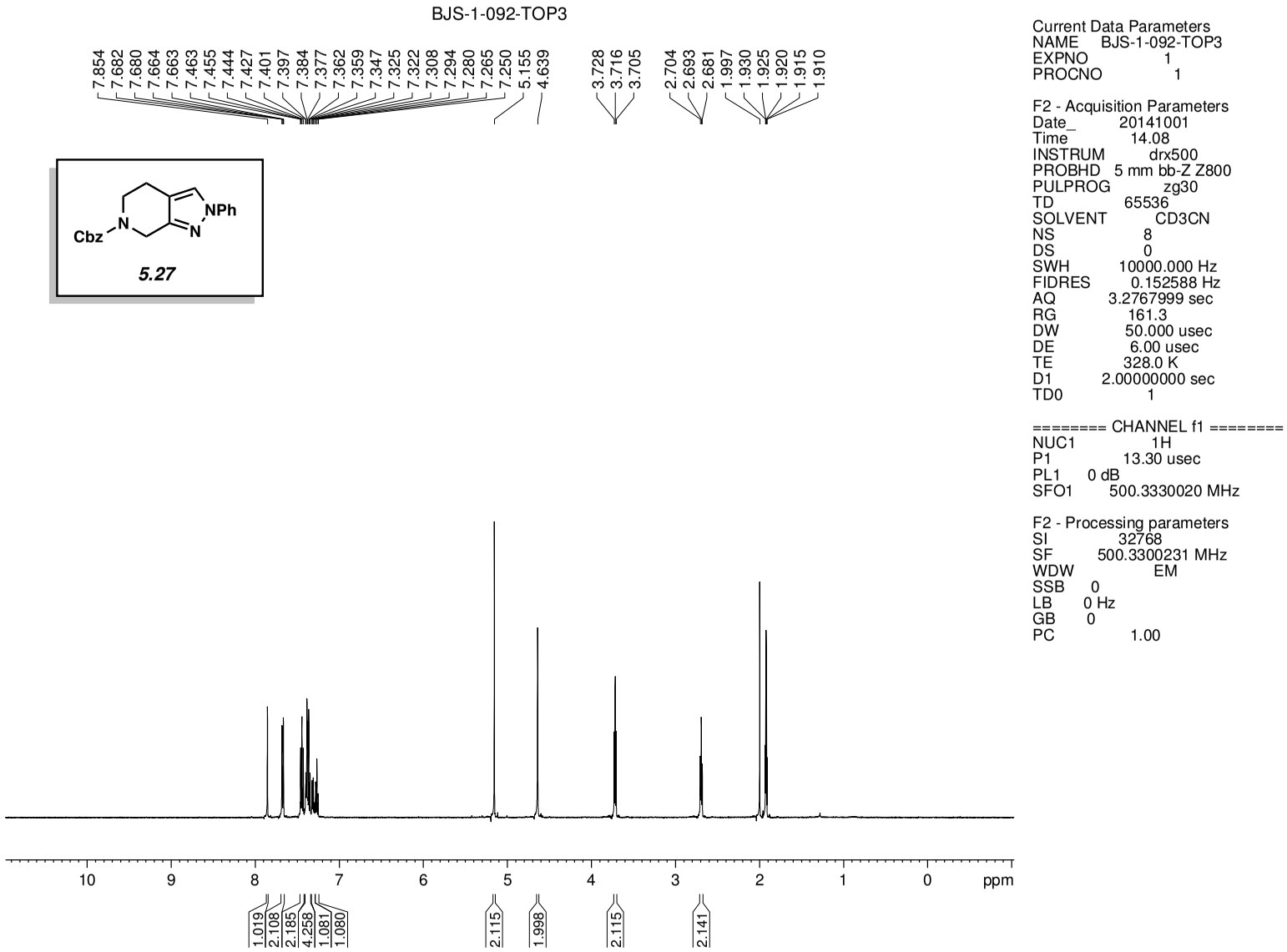

Figure 5.45. ^{1}H NMR (500 MHz, CD_3CN) compound **5.27**

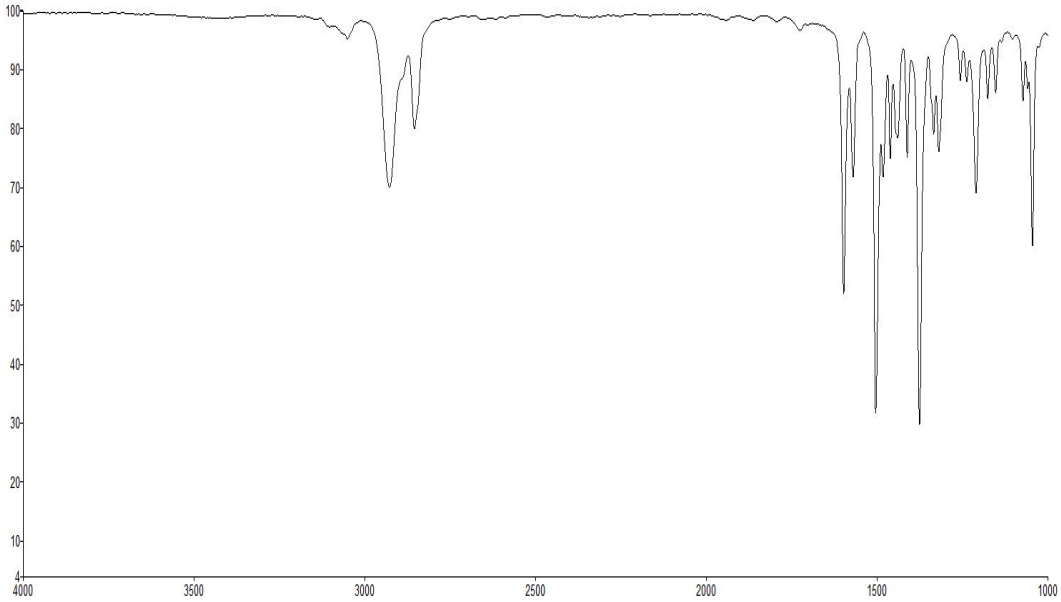

Figure 5.46. Infrared spectrum of compound **5.27**

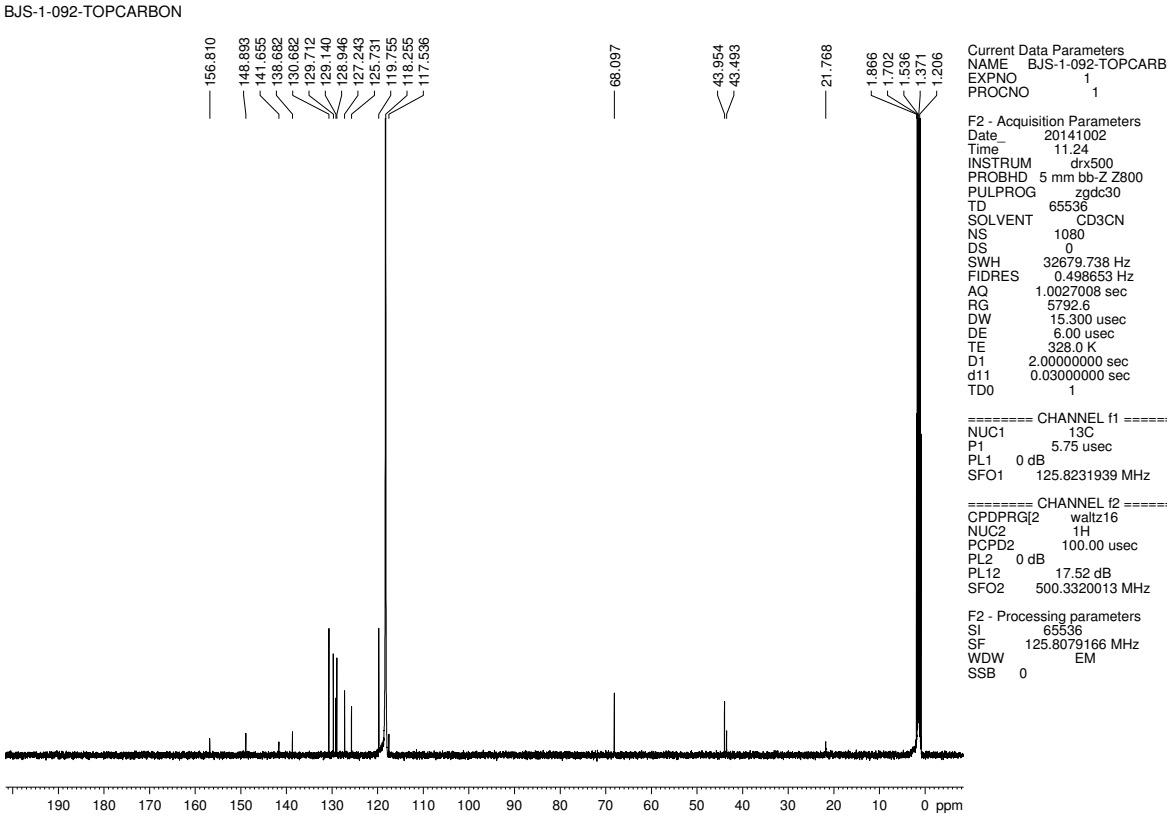

Figure 5.47. ^{13}C NMR (125 MHz, CD_3CN) of compound **5.27**

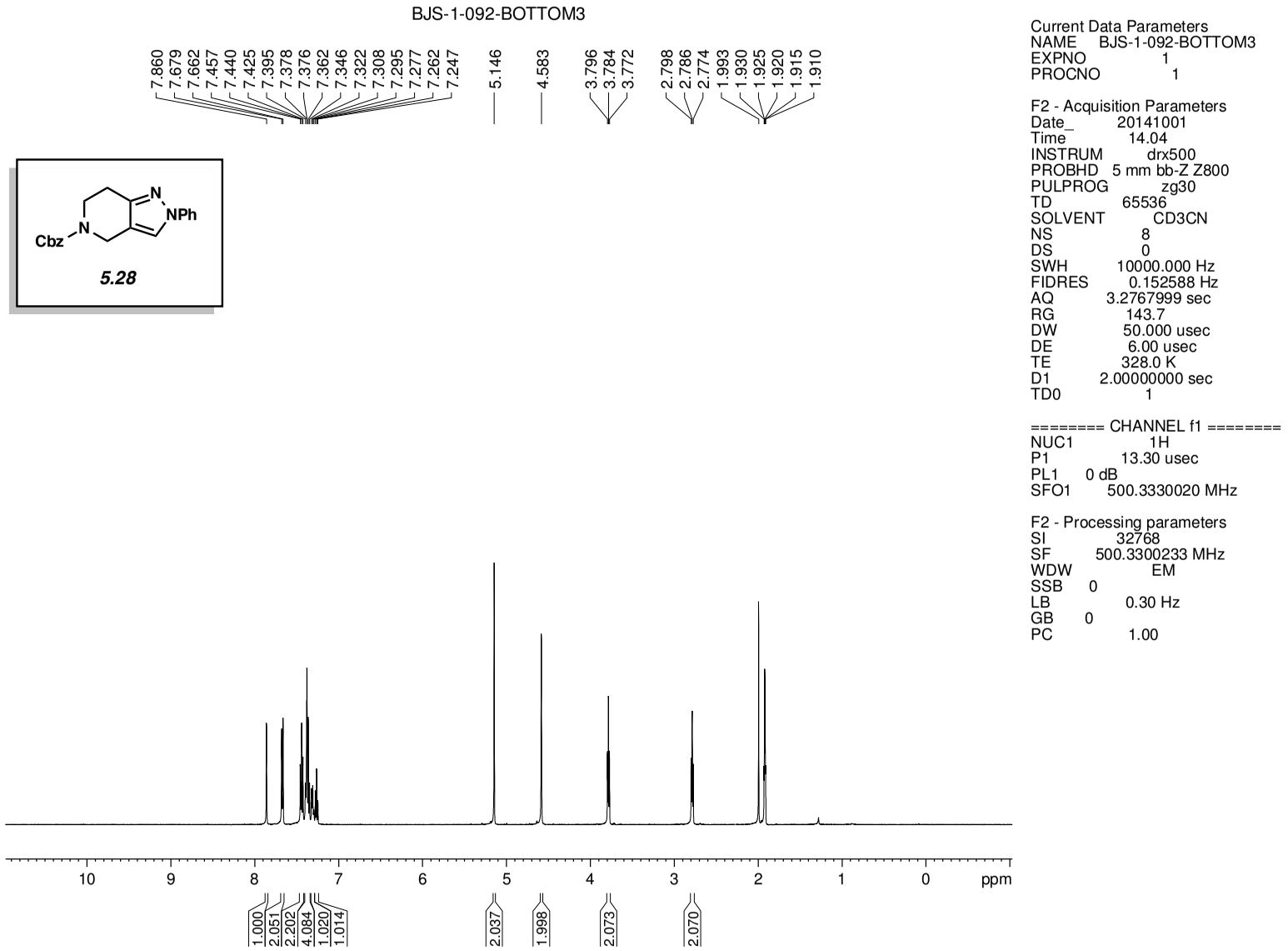

Figure 5.48. ^{1}H NMR (500 MHz, CD_3CN) compound **5.28**

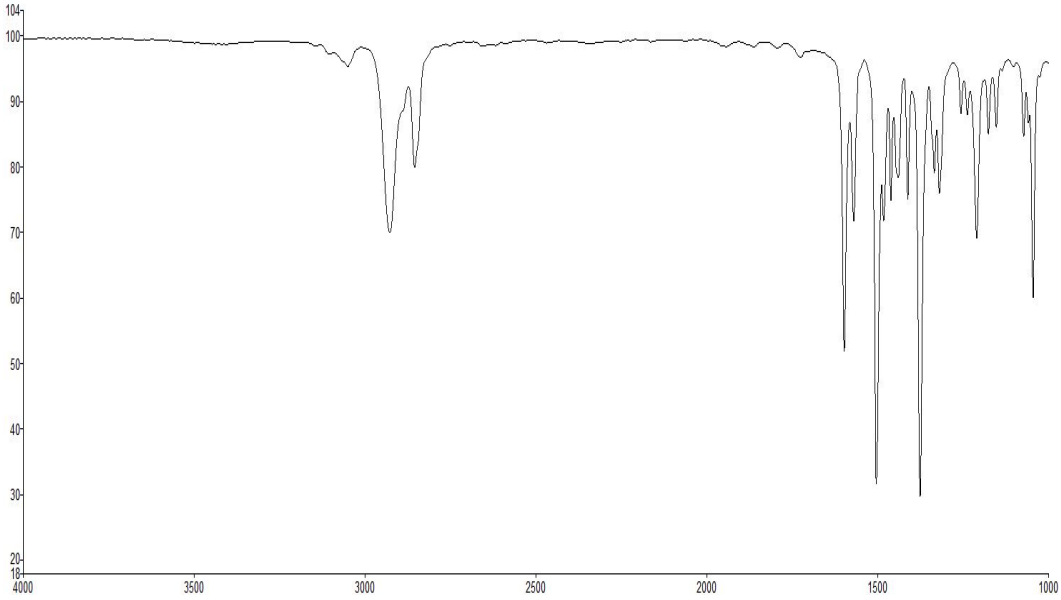

Figure 5.49. Infrared spectrum of compound **5.28**

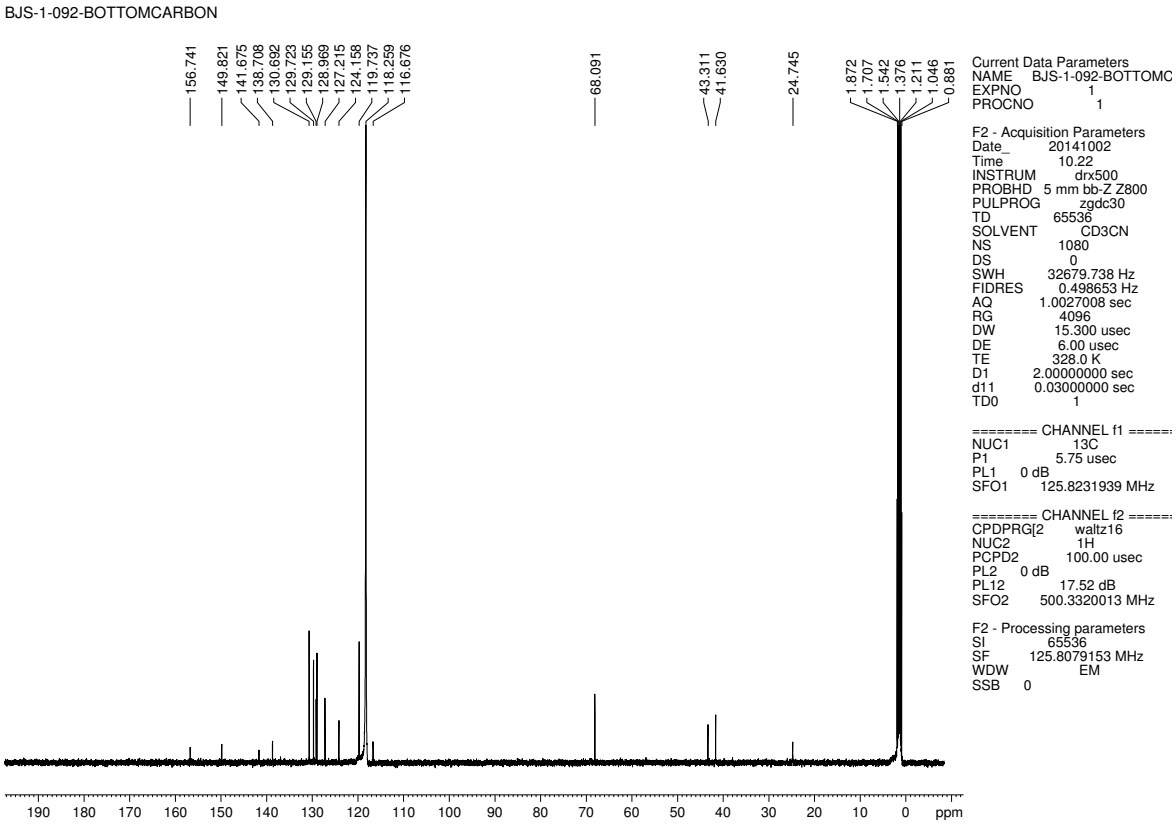

Figure 5.50. ^{13}C NMR (125 MHz, CD_3CN) of compound **5.28**

5.7 Notes and References

(1) Vitaku, E.; Smith, D. T.; Njardarson, J. T. *J. Med. Chem.* **2014**, *57*, 10257.

(2) Wentrup, C.; Blanch, R.; Briehl, H.; Gross, G. *J. Am. Chem. Soc.* **1988**, *110*, 1874.

(3) Tlais, S. F.; Danheiser, R. L. *J. Am. Chem. Soc.* **2014**, *136*, 15489.

(4) Medium sized *N*-containing cycloalkynes have been used in bioorthogonal click chemistry by Bertozzi and others. For a pertinent review, see: Sletten, E. M.; Bertozzi, C. R. *Angew. Chem., Int. Ed.* **2009**, *48*, 6974.

(5) Levine, R.; Leake, W. W. *Science* **1955**, *121*, 780.

(6) Martens, R. J.; den Hertog, H. J. *Tetrahedron Lett.* **1962**, *3*, 643.

(7) For recent reviews of arynes and hetarynes, see: (a) Bronner, S. M.; Goetz, A. E.; Garg, N. K. *Synlett* **2011**, 2599. (b) Tadross, P. M.; Stoltz, B. M. *Chem. Rev.* **2012**, *112*, 3550. (c) Gampe, C. M.; Carreira, E. M. *Angew. Chem., Int. Ed.* **2012**, *51*, 3766. (d) Goetz, A. E.; Garg, N. K. *J. Org. Chem.* **2014**, *79*, 846. (e) Goetz, A. E.; Shah, T. K.; Garg, N. K. *Chem. Commun.* **2015**, *51*, 34.

(8) For recent studies from our laboratory, see: (a) Goetz, A. E.; Garg, N. K. *Nat. Chem.* **2013**, *5*, 54. (b) Medina, J. M.; Mackey, J. L.; Garg, N. K.; Houk, K. N. *J. Am. Chem. Soc.* **2014**, *136*, 15798.

(9) For a recent study of cyclohexynes and cyclopentyne, see: Medina, J. M.; McMahon, T. C.; Jiménez-Osés, G.; Houk, K. N.; Garg, N. K. *J. Am. Chem. Soc.* **2014**, *136*, 14706.

(10) The ability to access heterocyclic scaffolds with significant aliphatic character is an important direction in modern drug discovery; see: (a) Lovering, F.; Bikker, J.; Humblet, C. *J. Med. Chem.* **2009**, *52*, 6752. (b) Ritchie, T. J.; Macdonald, S. J. F. *Drug Discovery Today* **2009**, *14*, 1011.

(11) The carboxybenzyl (Cbz) protecting group was chosen because of its pronounced stability and its ability to be selectively cleaved.

(12) For recent examples of 3,4-pyridyne regioselectivities, see: (a) Enamorado, M. F.; Ondachi, P. W.; Comins, D. L. *Org. Lett.* **2010**, *12*, 4513. (b) Saito, N.; Nakamura, K.-i.; Shibano, S.; Ide, S.; Minami, M.; Sato, Y. *Org. Lett.* **2013**, *15*, 386. (c) Saito, N.; Nakamura, K.-i.; Sato, Y. *Heterocycles* **2014**, *88*, 929.

(13) Given the widespread use of silyltriflates in aryne and cycloalkyne trapping experiments (using mild fluoride-based conditions), we deemed silyltriflate **5.8** an ideal target.

(14) Comins, D. L.; Joseph, S. P.; Goehring, R. R. *J. Am. Chem. Soc.* **1994**, *116*, 4719.

(15) Knapp, S.; Yang, C.; Pabbaraja, S.; Rempel, B.; Reid, S.; Withers, S. G. *J. Org. Chem.* **2005**, *70*, 7715.

(16) Atanes, N.; Escudero, S.; Pérez, D.; Guitián, E.; Castedo, L. *Tetrahedron Lett.* **1998**, *39*, 3039.

(17) Aldrich Chemical Co, Inc. is currently commercializing silyltriflate **5.8**, which will be available by mid 2015.

(18) For entry 6, substantial mass is lost to non-productive reaction pathways, which may render regioselectivity data unreliable. In the case of entry 7, the lack of regioselectivity can be attributed to the sydnone trappings occurring through concerted, highly synchronous transition states, with low activation barriers. Larock and Shi have reported similarly modest regioselectivities using 3-methoxybenzyne with the sydnone trapping agent; see: Fang, Y.; Wu, C.; Larock, R. C.; Shi, F. *J. Org. Chem.* **2011**, *76*, 8840.

(19) Structural similarity searches were performed using SciFinder Scholar. Other scaffolds, including the minor adduct from the diazoester cycloaddition (Table 5.2, entry 5) and the major product from the sydnone cycloaddition (Table 5.2, entry 7) are also difficult to access.

(20) Vaca, M. J. A.; Gil, J. I. A.; Chrovian, C. C.; Coate, H. R.; Angelis, M. D.; Dvorak, C. A.; Gelin, C. F.; Letavic, M. A.; Savall, B. M.; Soyode-Johnson, A.; Stenne, B. M.; Swanson, D. M. P2X7 Modulators, US 20140275015, September 18, 2014.

(21) Ashton, W. T.; Caldwell, C. G.; Mathvink, R. J.; Ok, H. O.; Reigle, L. B.; Weber, A. E. 3-Amino-4-Phenylbutanoic Acid Derivatives as Dipeptidyl Peptidase Inhibitors for the Treatment or Prevention of Diabetes, WO 2004064778, August 05, 2004.

(22) Fabienne, T.; Patrick, M.; Teresa, D.; Pierre, C. M.; Francois, C. New Tetrahydropyrazolo (3,4-c)pyridine Derivatives are Kinase Modulators Used Especially for Treating Cancer, FR 2857362, January 14, 2005.

(23) Blatt, L. M.; Seiwert, S.; Beigelman, L.; Kercher, T.; Kennedym, A. L.; Andrews, S. W. Novel Inhibitors of Hepatitis C Virus Replication, WO 2008005511, January 10, 2008.

(24) Comparative regioselectivity data for the reactions of 3,4-pyridyne (**5.3**) and 3,4-piperidyne **5.1a** are summarized below (C4 attack favored in all cases). For piperidyne regioselectivity data, see: Table 5.2 and the Experimental Section. For pyridyne regioselectivity data: A. E. Goetz, N. K. Garg, Unpublished Results, UCLA; see also ref 8a. For additional pyridyne azide cycloaddition regioselectivity data, see ref 12c.

Reactive Species	*Regioselectivity with Morpholine*	*Regioselectivity with N-Me-Aniline*	*Regioselectivity with Nitrone*	*Regioselectivity with Azide*
5.3	*1.3 : 1*	*1.9 : 1*	*1.9 : 1*	*1.7 : 1*
5.1a	*>20 : 1*	*>20 : 1*	*12.7 : 1*	*5.3 : 1*

(25) Considering the standard error associated with computations and that the transition states are very early with low barriers, we consider the computational and experimental findings to be in reasonable accord.

(26) Bent, H. A. *Chem. Rev.* **1961**, *61*, 275.

(27) Comins, D. L.; Joseph, S. P.; Goehring, R. R. *J. Am. Chem. Soc.* **1994**, *116*, 4719.

(28) The corresponding ketone is a commercially available compound, CAS: 19099-93-5. For known spectral data, see: Sasano, Y.; Nagasawa, S.; Yamazaki, M.; Shibuya, M.; Park, J.; Iwabuchi, Y. *Angew. Chem.* **2014**, *126*, 3300.

(29) Thoman, C. J.; Voaden, D. J. *Org. Synth*. **1965**, *45*, 96.

(30) Frisch, M. J.; Trucks, G. W.; Schlegel, H. B.; Scuseria, G. E.; Robb, M. A.; Cheeseman, J. R.; Scalmani, G.; Barone, V.; Mennucci, B.; Petersson, G. A.; Nakatsuji, H.; Caricato, M.; Li, X.; Hratchian, H. P.; Izmaylov, A. F.; Bloino, J.; Zheng, G.; Sonnenberg, J. L.; Hada, M.; Ehara, M.; Toyota, K.; Fukuda, R.; Hasegawa, J.; Ishida, M.; Nakajima, T.; Honda, Y.; Kitao, O.; Nakai, H.; Vreven, T.; Montgomery, J. A.; Peralta, J. E.; Ogliaro, F.; Bearpark, M.; Heyd, J. J.; Brothers, E.; Kudin, K. N.; Staroverov, V. N.; Kobayashi, R.; Normand, J.; Raghavachari, K.; Rendell, A.; Burant, J. C.; Iyengar, S. S.; Tomasi, J.; Cossi, M.; Rega, N.; Millam, J. M.; Klene, M.; Knox, J. E.; Cross, J. B.; Bakken, V.; Adamo, C.; Jaramillo, J.; Gomperts, R.; Stratmann, R. E.; Yazyev, O.; Austin, A. J.; Cammi, R.; Pomelli, C.; Ochterski, J. W.; Martin, R. L.; Morokuma, K.; Zakrzewski, V. G.; Voth, G. A.; Salvador, P.; Dannenberg, J. J.; Dapprich, S.; Daniels, A. D.; Farkas, Ö.; Foresman, J. B.; Ortiz, J. V.; Cioslowski J.; Fox, D. J. *Gaussian 09, Revision D.01*, *Vol.* Gaussian, Inc., Wallingford CT, 2010.

(31) (a) Becke, A. D. *J. Chem. Phys.* **1993**, *98*, 5648. (b) Lee, C.; Yang, W.; Parr, R. G. *Phys. Rev. B*, **1988**, *37*, 785. (c) Becke, A. D. *J. Chem. Phys.* **1993**, *98*, 1372. (d) Stephens, P. J.; Devlin, F. J.; Chabalowski, C. F.; Frisch, M. J. *J. Phys. Chem.*, **1994**, *98*, 11623.

(32) (a) Ditchfield, R.; Hehre, W. J.; Pople, J. A. *J. Chem. Phys.* **1971**, *54*, 724. (b) Hehre, W. J.; Ditchfield, R.; Pople, J. A. *J. Chem. Phys.* **1972**, *56*, 2257. (c) Hariharan, P. C.; Pople, J. A. *Theor. Chim. Acta.* **1973**, *28*, 213.

(33) (a) Zhao, Y.; Truhlar, D. G. *Phys. Chem. Chem. Phys*. **2008**, *10*, 2813. (b) Ribeiro, R. F.; Marenich, A. V.; Cramer, C. J.; Truhlar, D. G. *J. Phys. Chem. B* **2011**, *115*, 14556.

(34) (a) Grimme, S. *J. Comput. Chem.* **2006**, *27*, 1787. (b) Grimme, S.; Antony, J.; Ehrlich, S.; Krieg, H. *J. Chem. Phys.* **2010**, *132*, 154104.

(35) (a) Barone, V.; Cossi, M. *J. Phys. Chem. A* **1998**, *102*, 1995. (b) Cossi, M.; Rega, N.; Scalmani, G.; Barone, V. *J. Comput. Chem.* **2003**, *24*, 669. (c) Takano, Y.; Houk, K. N. *J. Chem. Theory Comput.* **2005**, *1*, 70.

(36) Legault, C. Y. CYLView, 1.0b; Université de Sherbrooke, Canada, **2009**; http://www.cylview.org

(37) McMahon, T. C.; Medina, J. M.; Yang, Y.-F.; Simmons, B. J.; Houk, K. N.; Garg, N. K. *J. Am. Chem. Soc*. **2015**, *137*, 4082.

CHAPTER SIX

Expanding the Strained Alkyne Toolbox: Generation and Utility of Oxygen-Containing Strained Alkynes

Tejas K. Shah, Jose M. Medina, and Neil K. Garg

J. Am. Chem. Soc. **2016**, *138*, 4948–4954.

6.1 Abstract

We report synthetic methodology that permits access to two oxacyclic strained intermediates, the 4,5-benzofuranyne and the 3,4-oxacyclohexyne. In situ trapping of these intermediates affords an array of heterocyclic scaffolds by the formation of one or more new C–C or C–heteroatom bonds. Experimentally determined regioselectivities were consistent with predictions made using the distortion / interaction model and were also found to be greater compared to selectivities seen in the case of trapping experiments of the corresponding *N*-containing intermediates. These studies demonstrate the synthetic versatility of oxacyclic arynes and alkynes for the synthesis of functionalized heterocycles, while further expanding the scope of the distortion / interaction model. Moreover, these efforts underscore the value of harnessing strained heterocyclic intermediates as a unique approach to building polycyclic heteroatom-containing frameworks.

6.2 Introduction

New approaches for the synthesis of decorated heterocycles remain highly sought after because of the prevalence of heterocycles in drugs, agrochemicals, materials, and natural products.[1] One unique strategy for heterocycle construction involves the trapping of transient heterocyclic arynes or alkynes.[2] For example, pyridynes,[2m,3] indolynes,[4,5,6] and piperidynes[7] (e.g., **6.1**–**6.3**, Figure 6.1) can now be used as building blocks for the synthesis of functionalized heterocycles in a predictable manner using the distortion / interaction model.[8]

Whereas advances in heterocyclic aryne and alkyne chemistry have focused on nitrogen-containing reactive intermediates, the corresponding chemistry of oxacycles has remained underdeveloped. The first aryne ever proposed was the 2,3-benzofuranyne;[9] however, this structural assignment was later called into question.[2b] Subsequent contributions in the area of oxacyclic arynes are limited to scattered examples involving dehydrohalogenation of benzofuran derivatives[10] and access to the 6,7-benzofuranyne using butyllithium reagents.[11] With regard to oxacyclohexynes, even less is known, with only two studies involving metalated oxacyclohexynes in the literature.[12] Silyl triflate precursors to oxacyclic arynes or alkynes have not been synthesized previously; likewise, no general methodologies for oxacyclic aryne or alkyne trapping have been reported to date.

We reasoned that mild methodologies involving the trapping of oxacyclic arynes and alkynes through a multitude of cycloadditions would provide a new avenue for building *O*-containing compounds. Oxygenated heterocycles, such as benzofuran and pyran derivatives, are often seen in natural products and drugs.[13] Notable examples include Saprisartan (treatment of hypertension),[14] hopeafuran (antimicrobial agent),[15] artemisinin (antimalarial drug),[16] rhoeadine (sedative & antitussive),[17] and frenolicin B (kinase inhibitor).[18] Moreover, some oxygen-

containing heterocycles are known bioisosteres for their nitrogen and sulfur-containting counterparts in medicinal chemistry.[19]

In the present study, we describe synthetic methodology to access two oxacyclic strained intermediates: the 4,5-benzofuranyne (**6.4**) and the 3,4-oxacyclohexyne (**6.5**) (Figure 6.1). In addition to establishing synthetic routes to silyl triflate precursors to **6.4** and **6.5** and using these species to build an assortment of functionalized heterocycles, we show that reliable regioselectivity predictions can be made prior to experiment using the distortion / interaction model. Selectivities are compared to those seen in the case of trapping experiments of the corresponding *N*-containing intermediates. Overall, our studies demonstrate that oxacyclic arynes and alkynes can be harnessed to efficiently construct decorated oxygen-containing heterocycles. The methodology is expected to prove useful in the synthesis of new pharmaceuticals and natural products.

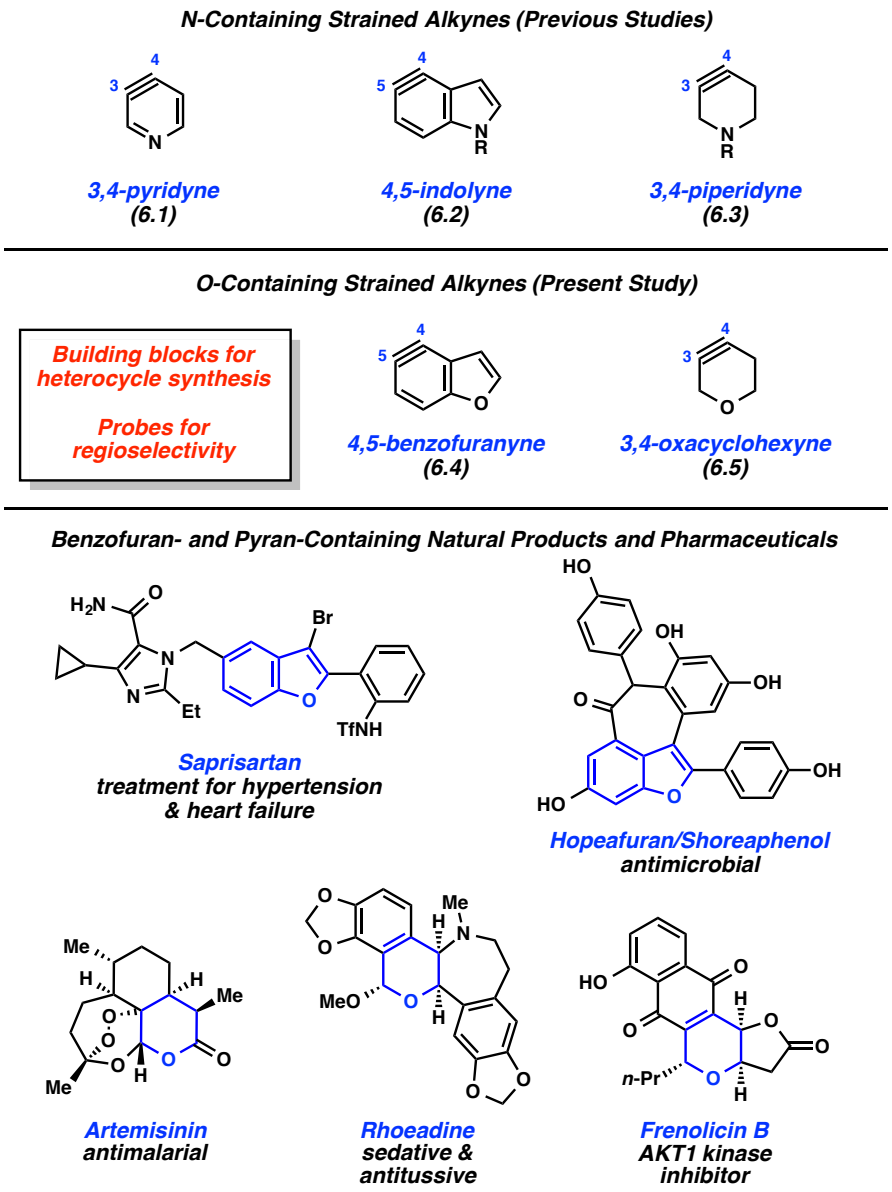

Figure 6.1. Well studied *N*-containing cyclic alkynes **6.1**–**6.3**, *O*–containing strained alkynes **6.4** and **6.5** (present study), and representative drugs and natural products

6.3 Results and Discussion

6.3.1 Prediction of Regioselectivities Based on the Distortion / Interaction Model

An attractive aspect of using strained alkynes as synthetic building blocks is the ability to make reliable regioselectivity predictions prior to experiments using the distortion / interaction

model.[8] Briefly stated, substituted arynes or cyclic alkynes are unsymmetrically distorted in their ground state. Nucleophilic addition occurs at the terminus of the aryne (or alkyne) that is more distorted toward linearity (i.e., the site that possesses a larger internal angle). The geometry of the unsymmetrical aryne or alkyne can readily be determined by performing simple geometry optimization calculations using DFT methods. In addition to revealing the preferred site of attack by nucleophiles, these calculations can also be used to roughly assess the degree of regioselectivities. The greater the difference in internal angles between the two aryne (or alkyne) termini ($\Delta\theta$), the more pronounced regioselectivities are expected.

With the aim of predicting the site of nucleophilic attack on 4,5-benzofuranyne (**6.4**) and 3,4-oxacyclohexyne (**6.5**), while drawing comparisons to the corresponding *N*-containing heterocyclic alkynes **6.6** and **6.7**, we performed geometry optimizations using DFT calculations (B3LYP/6-31G(d)) (Figure 6.2).[20] First, we compared the optimized structures of 4,5-benzofuranyne (**6.4**) and 4,5-indolyne (**6.6**); each is distorted such that nucleophilic addition is expected to occur at C5, which is the more linear terminus. 4,5-Benzofuranyne (**6.4**) was found to be unsymmetrically distorted with the C5–C4 $\Delta\theta$ being 7°. In comparsion, 4,5-indolyne (**6.6**) is less distorted, with the C5–C4 $\Delta\theta$ being 4°.[5e,5f] As the $\Delta\theta$ is greater in the case of 4,5-benzofuranyne (**6.4**), we predicted this species would react with greater regioselectivity compared to 4,5-indolyne (**6.6**). To see if this trend extended to non-aromatic strained alkynes, we compared 3,4-oxacyclohexyne (**6.5**) and 3,4-piperidyne **6.7**. For both cyclic alkynes, nucleophilic attack is preferred to occur at C4, the site further distorted toward linearity. C4–C3 $\Delta\theta$ is 15° in the case of 3,4-oxacyclohexyne (**6.5**), but slightly less (i.e., 12°) for 3,4-piperidyne **6.7**.[7c] As such, we surmised that 3,4-oxacyclohexyne (**6.5**) would react with greater regioselectivities compared to 3,4-piperidyne **6.7**.

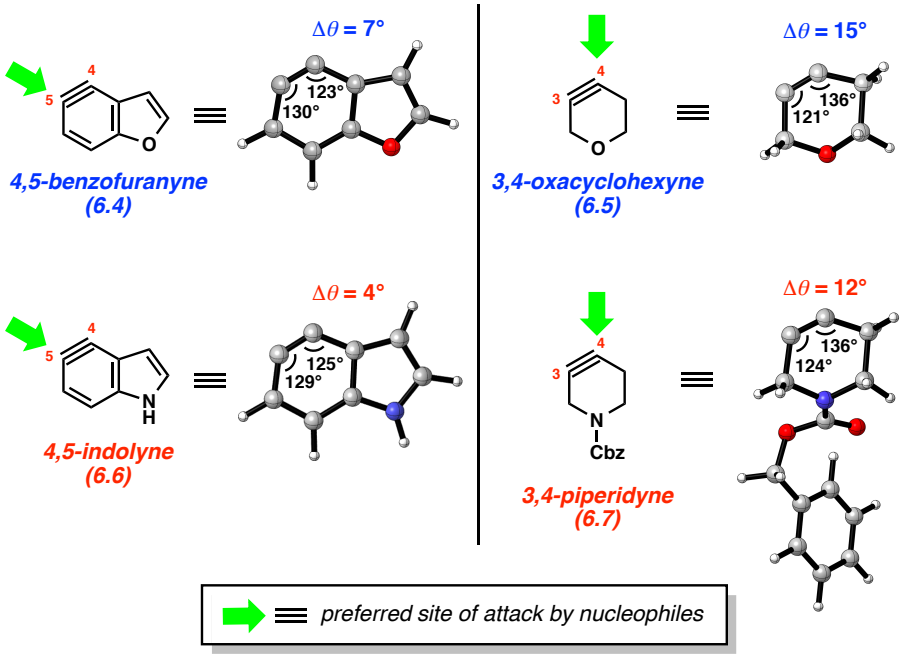

Figure 6.2. Geometry optimized structures of **6.4**–**6.7** obtained at the B3LYP/6-31G(d) level and predicted site of nucleophilic attack. *Δθ* represents the net distortion of the alkyne

6.3.2 Synthesis of Silyl Triflate Precursors

Our study relied on developing efficient syntheses of suitable precursors to 4,5-benzofuranyne (**6.4**) and 3,4-oxacyclohexyne (**6.5**). Given the well-known versatility of silyl triflate precursors to arynes,[21] we targeted silyl triflates **6.10** and **6.14** (Scheme 6.1). The benzofuranyne precursor was derived from 5-hydroxybenzofuran (**6.8**), which is commercially available or readily accessible from hydroquinone.[22] Bromination of **6.8** proceeded smoothly to deliver the known bromoalcohol **6.9**.[23] Subsequent *O*-silylation, followed by retro-Brook rearrangement and triflation, furnished silyl triflate **6.10** in 81% yield. 3,4-Oxacyclohexyne precursor **6.14** could be synthesized in four steps beginning from commercially available 4-oxotetrahydropyran **6.11**. α-Bromination of **6.11** was performed using a known two-step sequence to provide bromoketone **6.12**.[24] Treatment of **6.12** with DABCO and TESCl afforded

silyl enol ether **6.13** in 91% yield. Finally, lithiation, retro-Brook rearrangement, and triflation delivered silyl triflate **6.14**.

Scheme 6.1. Syntheses of Silyl Triflates **6.10** and **6.14**

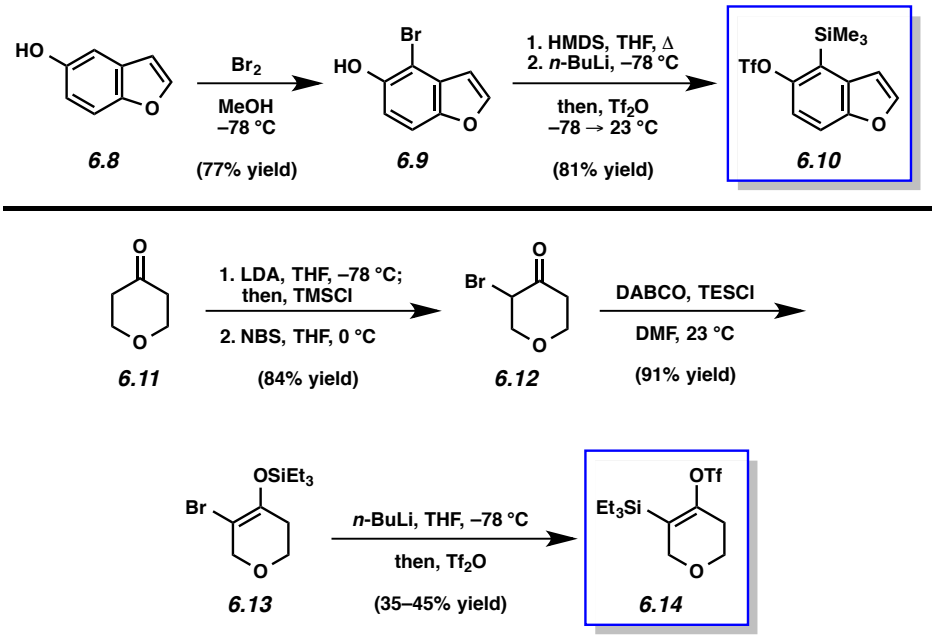

6.3.3 Generation & Trapping of 4,5-Benzofuranyne (6.4)

With the silyl triflate precursors in hand, we first investigated the generation and trapping of the 4,5-benzofuranyne (**6.4**) with symmetrical cycloaddition partners (Table 6.1). Thus, silyl triflate **6.10** was exposed to 2-pyrone and CsF in MeCN at 50 °C; to our delight the desired benzannulated product was obtained via a Diels–Alder / retro-Diels–Alder sequence (entry 1). We also performed trapping experiments with furan and *N*-Boc pyrrole (entries 2 and 3). In each case, the corresponding [2.2.1]-bridged bicyclic adduct was formed in synthetically useful yields. These results not only validated that the 4,5-benzofuranyne (**6.4**) can be generated, but also demonstrated how this intermediate can be used to build two new C–C bonds on the benzofuran

motif in an efficient manner. In the latter case, the two linkages formed are sp^2–sp^3 C–C bonds, which would be difficult to introduce by known means.

Table 6.1. Diels–Alder Cycloadditions of 4,5-Benzofuranyne (**6.4**)

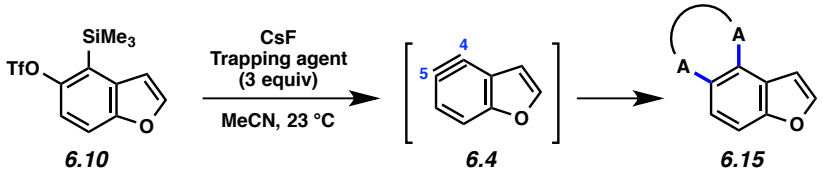

6.10 *6.4* *6.15*

Entry	*Trapping agent*	*Product*	*Yield*[a]
1	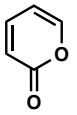	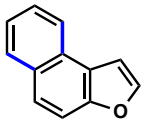	*68%*[b]
2		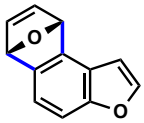	*96%*
3		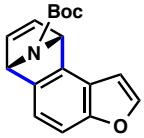	*75%*

[a] Reported yields are the average of two experiments and are based on the amount of isolated products. [b] Reaction performed at 50 °C.

With the aim of probing regioselectivity trends and accessing functionalized benzofurans, we shifted our attention to trapping benzofuranyne **6.4** with nucleophiles and unsymmetrical cycloaddition partners (Table 6.2). We found that *p*-cresol, morpholine, and *N*-Me-aniline could be employed as trapping agents,[25] to furnish benzofuranyne adducts in good yields (entries 1–3). In all cases, the major product was indicative of nucleophilic attack occurring at C5, consistent with the prediction made by the distortion / interaction model. To access more unique scaffolds and further examine regioselectivities, we surveyed trapping agents that would allow for the

appendage of seven-, six-, or five-membered heterocycles on the benzofuran motif. In situ trapping of **6.4** with 1,3-dimethyl-2-imidazolidinone[26] furnished the corresponding product of formal C–N bond insertion in 90% yield (entry 4). Only one constitutional isomer was observed in this case, although the subsequent trappings led to mixtures with a preference for initial bond formation also occurring at C5. The use of an amido acrylate trapping agent[27] allowed for the appendage of substituted pyridine rings to the benzofuran unit (entry 5). With regard to the formation of 5-membered rings, several trapping agents were deemed successful and could be used to forge C–C, C–O, and C–N bonds (entries 6–11).[28–33] In all cases, synthetically useful yields of substituted heterocycles were prepared with the expected regioselectivities. Thus, with access to a single new aryne precursor (i.e., **6.10**), one can build arrays of decorated benzofurans using this methodology.

Table 6.2. Reactions of Silyl Triflate **6.10** with Nucleophiles and Cycloaddition Partners

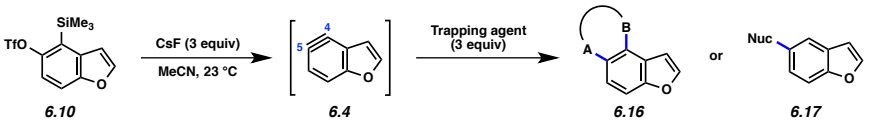

Entry	Trapping agent	Product(s)	Yield[a] (ratio)
1	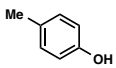	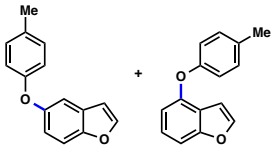	73% (8.5:1)
2		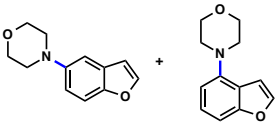	78% (4.2:1)
3		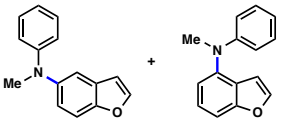	83% (10:1)
4	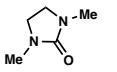	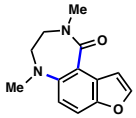	90%[b]
5	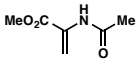	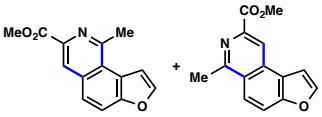	51% (2.9:1)
6	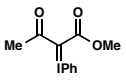	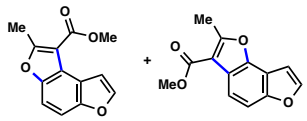	66% (12:1)
7		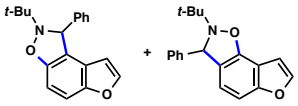	82% (5.4:1)
8	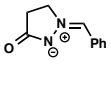	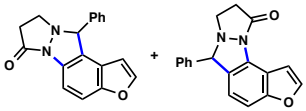	64% (4.5:1)
9		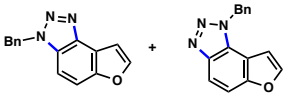	71% (6.2:1)
10	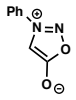	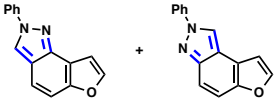	85% (1.3:1)
11		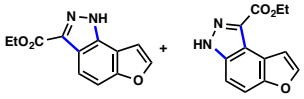	65% (2.5:1)

[a] Reported yields are the average of two experiments and are based on the amount of isolated products. [b] Reaction performed neat with 1,3-dimethyl-2-imidazolidinone (10 equiv) at 50 °C with yield determined by ^{1}H NMR analysis using 1,3,5-trimethoxybenzene as an external standard.

6.3.4 Generation & Trapping of 3,4-Oxacyclohexyne (6.5)

Efforts were also put forth to generate and trap 3,4-oxacyclohexyne (**6.5**). To confirm the in situ formation of the strained alkyne, we first examined trappings with dienes to give Diels–Alder adducts (Table 6.3). Thus, silyl triflate **6.14** was treated with CsF in the presence of 3 equivalents of tetracyclone in THF at 60 °C. This furnished the desired benzannulated product in quantitative yield (entry 1). Trapping with 2-pyrone, delivered the expected benzannulated product (entry 2). To arrive at more complex, heterocyclic adducts, Diels–Alder trappings were

performed with 2,5-dimethylfuran and *N*-Boc-pyrrole. In each case, the desired [2.2.1]-bicycles, which would arguably be difficult to make by other means, were formed (entries 3 and 4).

Table 6.3. Diels–Alder Cycloadditions of 3,4-Oxacyclohexyne (**6.5**)

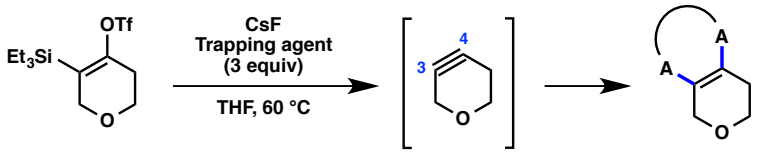

6.14 *6.5* *6.18*

Entry	*Trapping agent*	*Product*	*Yield*[a]
1	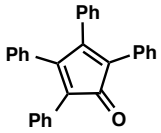	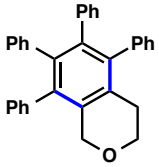	*100%*
2	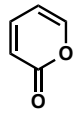	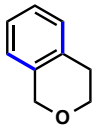	*49%*
3	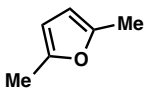	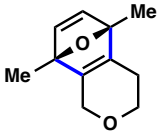	*50%*
4			*48%*

[a] Reported yields are the average of two experiments and are based on the amount of isolated products.

Analogous to our studies involving the 4,5-benzofuranyne (**6.4**), we tested the generation and trapping of 3,4-oxacyclohexyne (**6.5**) with nucleophiles and unsymmetrical cycloaddition partners (Table 6.4). Trapping with imidazole was examined primarily as a means to probe regioselectivity (entry 1). In this case, the 4-substituted adduct was obtained in >20:1

regiochemical preference. Addition at C4 was also seen in a variety of other trapping experiments, consistent with the predictions made by the distortion / interaction model. For example, interception of **6.5** with methyl salicylate[34] gave two products, both indicative of the same regioselectivity trend (entry 2). We also performed the trapping with an amido acrylate species,[27] which led to the appendage of pyridine motifs, albeit with modest selectivity (entry 3). Several efforts to annulate the oxacyclohexyne with 5-membered heterocycles were also put forth. Trapping with an iodoniun ylide[28] led to the introduction of a furan (entry 4), whereas nitrone trapping[29] gave the expected isoxazoline product (entry 5). Similarly, an azide cycloaddition[31] proceeded smoothly to give triazole-containing products (entry 6). In two additional examples, pyrazole derivatives could be obtained by trapping the oxacyclohexyne intermediate with either a sydnone[32] or diazoester[33] (entries 7 and 8). With this methodology, a variety of annulated oxacycles can be readily accessed from silyl triflate **6.14**, with good to excellent control of regioselectivity. It should be noted that the products obtained from these trapping studies possess significant sp^3 character. The generation of such sp^3-rich heterocyclic frameworks is an important direction in modern drug discovery.[35]

Table 6.4. Reactions of Silyl Triflate **6.14** with Nucleophiles and Cycloaddition Partners

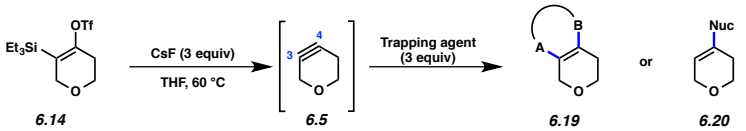

Entry	Trapping agent	Product(s)	Yield[a] (ratio)	Entry	Trapping agent	Product(s)	Yield[a] (ratio)
1		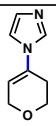	59% (>20:1)	5		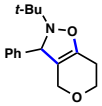	73% (>20:1)
2		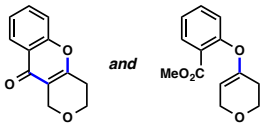	79% (>20:1)	6		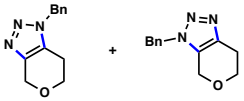	69% (7.2:1)
3	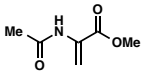	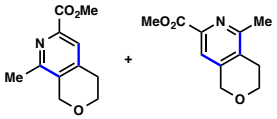	71% (2.6:1)	7	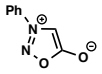	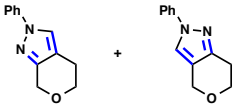	88% (1.5:1)
4	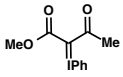	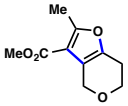	70%[b] (>20:1)	8		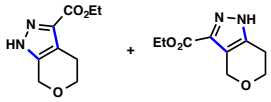	64% (6.1:1)

[a] Reported yields are average of two experiments and are based on the amount of isolated products. [b] Reaction performed with MeCN as the solvent.

6.3.5 Comparison of Regioselectivities for *N*- and *O*-Containing Strained Alkynes

As noted earlier, we predicted that the 4,5-benzofuranyne (**6.4**) and the 3,4-oxacyclohexyne (**6.5**) would react with significant regioselectivities to give nucleophilic addition preferentially at C5 and C4, respectively. These predictions were verified, as described above. Additionally, we predicted that **6.4** and **6.5** would undergo trapping with more significant regioselectivities in comparison to their *N*-containing analogs, **6.22** and **6.7**.

Table 6.5 shows a comparison of regioselectivities for trapping experiments of 4,5-benzofuranyne (**6.4**) and *N*-Me-4,5-indolyne (**6.22**). When *p*-cresol was used as the nucleophile (entry 1), the indolyne reacted to furnish the C5- and C4-substituted adducts in a 3.0 : 1 ratio. In the case of benzofuranyne **6.4**, a higher degree of selectivity was observed (8.5 : 1). Similarly, in

the trapping of the arynes with benzylazide (entry 2), selectivity was greater in the case of the benzofuranyne (2.4 : 1 vs 6.2 : 1), consistent with predictions.

Table 6.5. Comparison of 4,5-Indolyne and 4,5-Benzofuranyne Regioselectivities

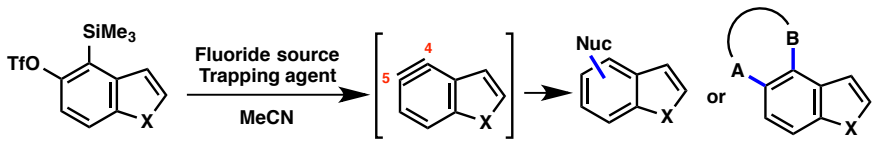

6.21; X = NMe
6.10; X = O

6.22; X = NMe
6.4; X = O

X = NMe or O

Entry	*Trapping agent*	*Products*	*Ratio (Yield) X = NMe*	*Ratio (Yield) X = O*
1	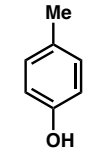	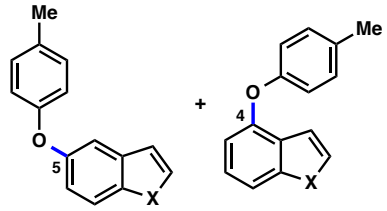	*3.0 : 1*[a] *(80%)*	*8.5 : 1*[b] *(73%)*
2	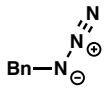	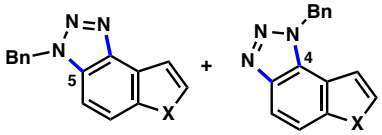	*2.4 : 1*[c] *(86%)*	*6.2 : 1*[b] *(71%)*

[a] Reaction performed with *p*-cresol (1.5 equiv) and CsF (3 equiv) at 50 °C.
[b] Reactions performed with trapping agent (3 equiv) and CsF (3 equiv) at 23 °C.
[c] Reaction performed with benzyl azide (5 equiv) and TBAF (2 equiv) at 23 °C.

Similar comparisons were made between the 3,4-oxacyclohexyne (**6.5**) and the corresponding *N*-Cbz-protected piperidyne **6.7** using cycloaddition reactions (Table 6.6). In the case of nitrone trapping (entry 1), the piperidyne undergoes cycloaddition to give a 12.7 : 1 ratio of products. However, use of the oxacyclic variant gave >20:1 selectivity. Likewise, slightly higher selectivities were seen in the trapping of oxacyclohexyne **6.5** with benzyl azide, compared to the trapping of piperidyne **6.7** (entry 2). The more pronounced selectivities seen in the case of the 4,5-benzofuranyne (**6.4**) and the 3,4-oxacyclohexyne (**6.5**), compared to their nitrogen-

containing counterparts, can be attributed to the greater electronegativity of oxygen. The oxygen atom has a stronger inductive effect that leads to increased distortion,[36] which in turn parlays into the more significant selectivities observed.

Table 6.6. Comparison of Oxacyclohexyne and Piperidyne Regioselectivities

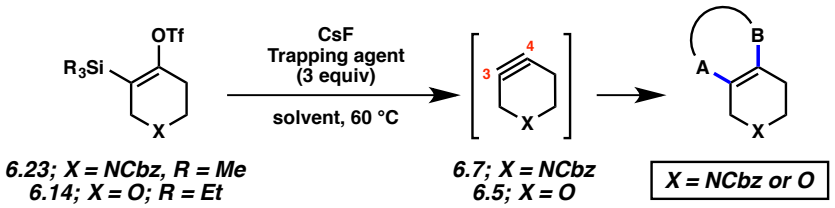

6.23; X = NCbz, R = Me
6.14; X = O; R = Et

6.7; X = NCbz
6.5; X = O

X = NCbz or O

Entry	*Trapping agent*	*Products*	*Ratio (Yield)[a] X = NCbz*	*Ratio (Yield)[b] X = O*
1	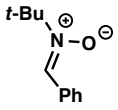	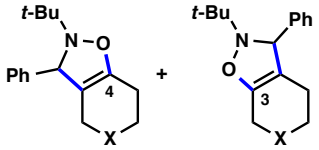	*12.7:1 (84%)*	*>20:1 (73%)*
2	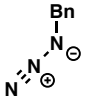	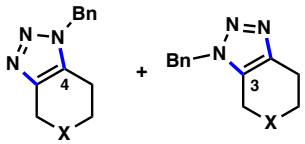	*5.3:1 (81%)*	*7.2:1 (69%)*

[a] Reaction performed with MeCN as the solvent. [b] Reactions performed with THF as the solvent.

6.4 Conclusion

In summary, we have developed methodology that allows for the generation and trapping of two oxacyclic strained intermediates, the 4,5-benzofuranyne and the 3,4-oxacyclohexyne. Interception of these species by nucleophiles and cycloaddition partners provides a new means to prepare arrays of heterocyclic scaffolds by the formation of one or more new C–C or C–heteroatom bonds. The distortion / interaction model was used to make regioselectivity predictions about the preferred sites of reactivity, which were validated by experiments.

Moreover, greater selectivities were seen in the trapping of the oxacyclic strained intermediates compared to the corresponding *N*-containing compounds, also consistent with computational predictions. Our studies demonstrate that oxacyclic arynes and alkynes can be generated from silyl triflate precursors and strategically harnessed to build decorated oxygen-containing heterocycles. Given the abundance of aryne trapping reactions available in the literature, this methodology is expected to find utility in the synthesis of medicinal substances and natural products.

6.5 Experimental Section

6.5.1 Materials and Methods

Unless stated otherwise, reactions were conducted in flame-dried glassware under an atmosphere of nitrogen using anhydrous solvents (freshly distilled or passed through activated alumina columns). All commercially obtained reagents were used as received unless otherwise specified. Cesium fluoride (CsF) was obtained from Strem Chemicals. Trifluoromethanesulfonic anhydride (Tf_2O) and Triethylsilyl chloride (TESCl) were obtained from Oakwood Products, Inc. and distilled before use. Furan, *N*-*tert*-butyl-α-phenylnitrone, methyl 2-acetamidoacrylate, and methyl salicylate were obtained from Alfa Aesar. Hexamethyldisilane, *N*-Boc-pyrrole, *N*-methylaniline, 1,3-dimethyl-2-imidazolidinone, ethyl diazoacetate, tetracyclone, and 2,5-dimethylfuran were obtained from Sigma Aldrich. 2-Pyrone, *p*-cresol was obtained from Acros Organics. Morpholine was obtained from Spectrum Chemical and distilled before use. Reaction temperatures were controlled using an IKAmag temperature modulator and, unless stated otherwise, reactions were performed at room temperature (rt, approximately 23 °C). Thin layer chromatography (TLC) was conducted with EMD gel 60 F254 pre-coated plates (0.25 mm) and

visualized using a combination of UV light and potassium permanganate staining. Preparative thin layer chromatography (TLC) was conducted with EMD gel 60 F254 pre-coated plates (0.5 mm) and visualized using UV light. Silicycle Siliaflash P60 (particle size 0.040–0.063 mm) was used for flash column chromatography. ^{1}H NMR and 2D-NOESY spectra were recorded on Bruker spectrometers (500 MHz) and are reported relative to deuterated solvent signals. Data for ^{1}H NMR spectra are reported as follows: chemical shift (δ ppm), multiplicity, coupling constant (Hz) and integration. ^{13}C NMR spectra were recorded on Bruker spectrometers (125 MHz) and are reported relative to deuterated solvent signals. Data for ^{13}C NMR spectra are reported in terms of chemical shift and, when necessary, multiplicity, and coupling constant (Hz). IR spectra were obtained using a Perkin-Elmer UATR Two FT-IR spectrometer and are reported in terms of frequency absorption (cm^{-1}). High-resolution mass spectra were obtained on Waters LCT Premier with ACQUITY LC and Thermo Scientific™ Exactive Mass Spectrometers with DART ID-CUBE. Images in Figure 6.2 were created using CYLview.[37]

6.5.2 Experimental Procedures

6.5.2.1 Synthesis of 4,5-Benzofuranyne Precursor

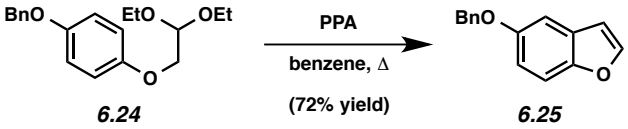

6.24 *6.25*

5-Benzyloxybenzofuran (6.25). To a solution of known diethylacetal[22] **6.24** (13.0 g, 41.1 mmol) in benzene (550 mL, 0.075 M) was added polyphosphoric acid (13.0 g, 1 equiv by weight). The flask was topped with a water condenser and the system placed under N_2. The reaction was heated to reflux and stirred for 2 h. After cooling, the reaction mixture was diluted with H_2O

(150 mL) and EtOAc (150 mL). The layers were separated, and the aqueous layer was extracted with EtOAc (3 x 150 mL). The organic layers were combined and dried over $MgSO_4$. Evaporation under reduced pressure and further purification by flash chromatography (20:1 Hexanes:EtOAc) afforded known 5-benzyloxybenzofuran (**6.25**)[22] (6.6 g, 72% yield) as an off white solid.

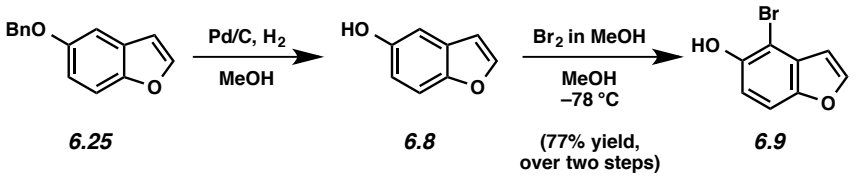

4-Bromo-5-hydroxybenzofuran (6.9). To a solution of 5-benzyloxybenzofuran (**6.25**) (3.08 g, 13.73 mmol) in MeOH (137 mL, 0.1 M) was added 10% Pd/C (146 mg, 0.137 mmol, 1.0 mol% Pd). The mixture was placed under an atmosphere of hydrogen (double-balloon), stirred for 4 h at 23 °C, and then filtered over celite (EtOAc eluent). Evaporation of the solvent under reduced pressure afforded crude product **6.8**[38] as an off white solid, which was used in the subsequent step without further purification.

To a stirred solution of 5-hydroxybenzofuran (**6.8**) (1.8 g, 13.73 mmol) in MeOH (274 mL, 0.05 M) at –78 °C was added a solution of Br_2 in MeOH (14.4 mL, 1.0 M, 13.73 mmol, 1 equiv) dropwise over 30 min. The resulting mixture was stirred at –78 °C for 2 h, quenched with sat. $NaHCO_3$ (50 mL), and then diluted with EtOAc (100 mL). The layers were separated, and the aqueous layer was extracted with EtOAc (3 x 100 mL). The organic layers were combined and dried over $MgSO_4$. Evaporation under reduced pressure and further purification by flash chromatography (20:1 Hexanes:Et_2O) afforded known 4-bromo-5-hydroxybenzofuran[23] (**6.9**) as a yellow solid (2.3 g, 77% yield).

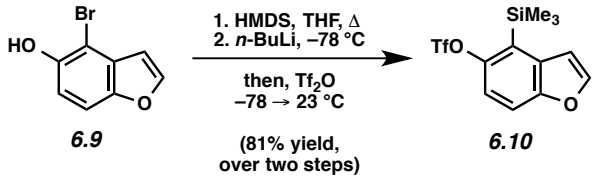

Silyl Triflate 6.10. To a solution of 4-bromo-5-hydroxybenzofuran (**6.9**) (900 mg, 4.22 mmol) in THF (7.7 mL, 0.55 M) was added hexamethyldisilane (1.9 mL, 9.3 mmol, 2.2 equiv). The flask was fitted with a reflux condenser, flushed with N_2, and then heated to reflux. After 12 h, the reaction mixture was cooled to room temperature. Evaporation of the volatiles under reduced pressure afforded the silyl ether, which was used in the subsequent step without further purification.

To the crude material was added THF (8.5 mL, 0.5 M) at –78 °C, followed by *n*-BuLi (2.9 mL, 1.75 M in hexanes, 5.07 mmol, 1.2 equiv) dropwise over 5 min. The resulting solution was stirred at –78 °C for an additional 20 min, and then neat Tf_2O (0.85 mL, 5.07 mmol, 1.2 equiv) was added dropwise over 5 min. The resulting mixture was stirred at –78 °C for 2 h and allowed to warm to 23 °C over 12 h. The reaction was quenched with sat. $NaHCO_3$ (5 mL) and then diluted with EtOAc (10 mL). The layers were separated and the aqueous layer was extracted with EtOAc (3 x 30 mL). The organic layers were combined and dried over $MgSO_4$. Evaporation under reduced pressure and further purification by flash chromatography (50:1 Hexanes:Et_2O) afforded silyl triflate **6.10** as a colorless oil (1.2 g, 81% yield). Silyl triflate **6.10**: R_f 0.6 (20:1 Hexanes:EtOAc); ^{1}H NMR (500 MHz, $CDCl_3$): δ 7.74 (d, J = 2.3, 1H), 7.53 (dd, J = 9.0, 0.9, 1H), 7.26 (d, J = 9.0, 1H), 6.96 (dd, J = 2.3, 0.9, 1H), 0.50 (s, 9H); ^{13}C NMR (125 MHz, $CDCl_3$): δ 152.7, 150.4, 147.0, 133.2, 125.9, 118.7 (q, J = 320.0, CF_3), 116.8, 113.6, 108.5, 0.9; IR (film): 2960, 1398, 1205 cm^{-1}; HRMS-APCI (*m/z*) $[M - H]^-$ calcd for $C_{12}H_{12}F_3O_4SSi$, 337.01722; found, 337.01828.

6.5.2.2 Synthesis of 3,4-Oxacyclohexyne Precursor

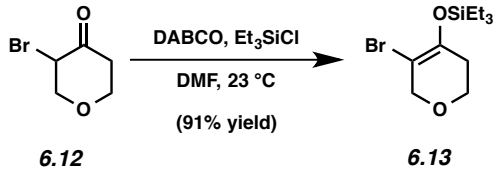

6.12 *6.13*

Silyl Enol Ether 6.13. To a stirred solution of known bromoketone **6.12**[24] (2.31 g, 12.88 mmol) and DABCO (3.34 g, 29.62 mmol, 2.3 equiv) in DMF (12.0 mL, 1.1 M) was added Et_3SiCl (3.55 mL, 20.61 mmol, 1.6 equiv). The reaction vessel was purged with N_2 gas and sealed. The solution was stirred for 24 h, and then quenched with saturated $NaHCO_3$ (20 mL). The layers were separated, and the aqueous layer was extracted with EtOAc (3 x 50 mL). The organic layers were combined and dried over $MgSO_4$. Evaporation under reduced pressure and further purification by flash chromatography (95:5 Hexanes:EtOAc) afforded silyl enol ether **6.13** as a faint yellow oil (3.4 g, 91% yield). Silyl enol ether **6.13**: R_f 0.72 (9:1 Hexanes:EtOAc); ^{1}H NMR (500 MHz, C_6D_6): δ 4.16 (t, *J* = 2.3, 2H), 3.43 (t, *J* = 5.5, 2H), 1.96–1.91 (m, 2H), 0.99 (t, *J* = 8.1, 9H), 0.63 (q, *J* = 8.1, 6H); ^{13}C NMR (125 MHz, C_6D_6): δ 145.1, 98.1, 69.9, 64.8, 32.9, 7.0, 6.0; IR (film): 2954, 2907, 2874, 1673, 1457, 1246 cm^{-1}; HRMS-APCI (*m/z*) $[M + H]^+$ calcd for $C_{11}H_{22}BrO_2Si$, 293.05670; found, 293.05675

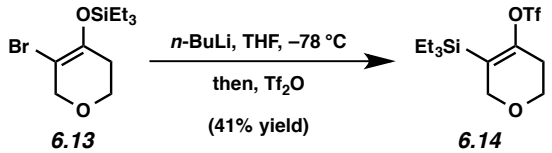

6.13 *6.14*

Silyl Triflate 6.14. To a stirred solution of silyl enol ether **6.13** (250 mg, 0.85 mmol) in THF (8.5 mL, 0.1 M) at –78 °C was added *n*-BuLi (1.06 mL, 2.16 M in hexanes, 2.30 mmol, 2.7 equiv) dropwise over 5 min. The resulting solution was stirred at –78 °C for an additional 15 min, and then neat Tf_2O (186 μL, 1.02 mmol, 1.2 equiv) was added dropwise over 2 min. The

resulting mixture was stirred at –78 °C for 1 h, quenched with saturated NH_4Cl (10 mL), and allowed to warm to 23 °C over 30 min. The layers were separated, and the aqueous layer was extracted with EtOAc (3 x 20 mL). The organic layers were combined and dried over $MgSO_4$. Evaporation under reduced pressure and further purification by flash chromatography (95:5 Hexanes:Et_2O) afforded silyl triflate **6.14** as a colorless oil (120 mg, 41% yield). Silyl triflate **6.14**: R_f 0.55 (9:1 Hexanes:Et_2O); ^{1}H NMR (500 MHz, C_6D_6): δ 4.03 (t, J = 2.7, 2H), 3.31 (t, J = 5.5, 2H), 2.15 (sept, J = 2.7, 2H), 0.87 (t, J = 8.1, 9H), 0.63 (q, J = 8.1, 6H); ^{13}C NMR (125 MHz, C_6D_6): δ 151.5, 125.7, 118.8 (q, J = 319.9, CF_3), 68.0, 64.0, 28.9, 7.3, 2.9; IR (film): 2958, 2879, 1654, 1415, 1213, 1138 cm^{-1}; HRMS-APCI (*m/z*) $[M + H]^+$ calcd for $C_{12}H_{22}F_3O_4SSi$, 347.09547; found, 347.09571.

6.5.2.3 Trapping Experiments of 4,5-Benzofuranyne

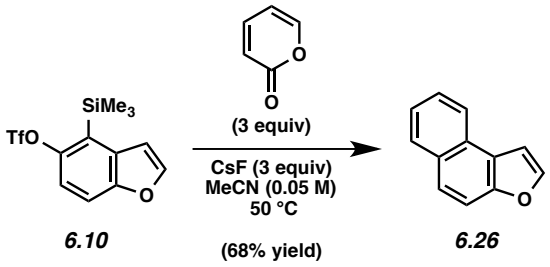

Representative Procedure (Preparation of Benzofuran 6.26 is used as an example).

Benzofuran 6.26 (Table 6.1, Entry 1). To a stirred solution of silyl triflate **6.10** (50.0 mg, 0.148 mmol) and 2-pyrone (35 μL, 0.443 mmol, 3.0 equiv) in MeCN (2.9 mL, 0.05 M) was added CsF (67.3 mg, 0.443 mmol, 3.0 equiv). The reaction vessel was purged with N_2 gas, sealed, and placed in a preheated aluminum heating block maintained at 50 °C for 12 h. After cooling to 23 °C, the reaction mixture was filtered over silica gel (EtOAc eluent, 10 mL). Evaporation under reduced pressure and further purification by preparative thin layer chromatography (20:1

Hexanes:EtOAc) afforded known benzofuran **6.26**[39] as a white solid (68% yield, average of two experiments).

Any modifications of the conditions shown in this representative procedure are specified in the following schemes, which depict all of the results shown in Tables 6.1 and 6.2

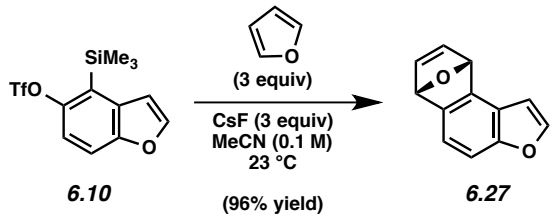

Benzofuran 6.27 (Table 6.1, Entry 2). Purification by preparative thin layer chromatography (10:1 Hexanes:EtOAc) afforded benzofuran **6.27** as a white solid (96% yield, average of two experiments). Benzofuran **6.27**: R_f 0.25 (10:1 Hexanes:EtOAc); ^{1}H NMR (500 MHz, $CDCl_3$): δ 7.60 (d, *J* = 2.9, 1H), 7.24 (d, *J* = 7.9, 1H), 7.16–7.08 (m, 3H), 6.72 (dd, *J* = 2.3, 0.9, 1H), 5.96 (app t, *J* = 0.9, 1H), 5.83 (dd, *J* = 1.7, 0.7, 1H; ^{13}C NMR (125 MHz, $CDCl_3$): δ 153.9, 146.5, 144.8, 144.1, 142.9, 142.7, 122.2, 116.5, 106.5, 104.0, 82.9, 81.7; IR (film): 3309, 3013, 1278, 864 cm^{-1}; HRMS-APCI (*m/z*) $[M + H]^+$ calcd for $C_{12}H_8O_2$, 185.06025; found, 185.05825.

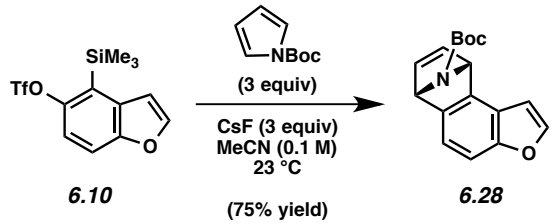

Benzofuran 6.28 (Table 6.1, Entry 3). Purification by preparative thin layer chromatography (20:1 Hexanes:EtOAc) afforded benzofuran **6.28** as a tan solid (75% yield, average of two

experiments). Benzofuran **6.28**: R_f 0.21 (20:1 Hexanes:EtOAc); ^{1}H NMR (500 MHz, $CDCl_3$, 50 °C): δ 7.62–7.54 (br s, 3H), 7.23 (d, *J* = 7.8, 1H), 7.15–6.96 (m, 3H), 6.74 (br s, 1H), 5.73 (br s, 1H), 5.58 (br s, 1H), 1.38 (s, 9H); ^{13}C NMR (125 MHz, $CDCl_3$, 52 °C): δ 155.2, 154.1, 146.4, 144.7, 143.7, 142.8, 142.1, 122.8, 117.1, 106.5, 104.1, 80.7, 67.2, 65.9, 28.4; IR (film): 2977, 1701, 1338, 1163 cm^{-1}; HRMS-APCI (*m/z*) $[M + H]^+$ calcd for $C_{17}H_{18}NO_3$, 284.12867; found, 284.12601.

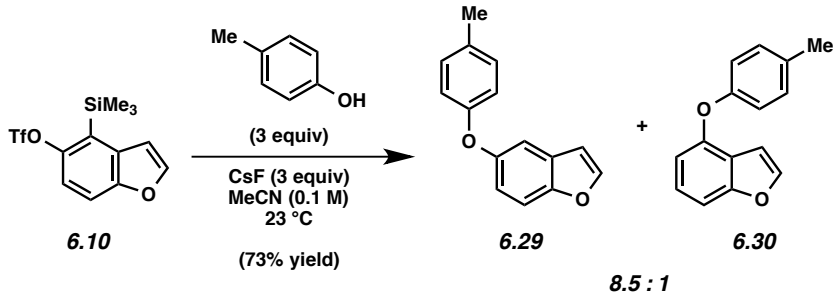

Ethers 6.29 and 6.30 (Table 6.2, Entry 1). Purification by preparative thin layer chromatography (20:1 Hexanes:EtOAc) afforded ether **6.29** (65% yield, average of two experiments) as a colorless oil and ether **6.30** (8% yield, average of two experiments) as a colorless oil. Ether **6.29**: R_f 0.42 (20:1 Hexanes:EtOAc); ^{1}H NMR (500 MHz, $CDCl_3$): δ 7.63 (d, *J* = 1.9, 1H), 7.45 (d, *J* = 8.8, 1H), 7.19 (d, *J* = 2.4, 1H), 7.12 (d, *J* = 8.4, 2H), 7.01 (dd, *J* = 8.8, 2.4, 1H), 6.89 (d, *J* = 8.4, 2H), 6.70 (app t, *J* = 1.1, 1H), 2.33 (s, 3H); ^{13}C NMR (125 MHz, $CDCl_3$): δ 156.1, 153.1, 151.3, 146.1, 132.2, 130.2, 128.3, 118.1, 116.6, 112.0, 110.8, 106.8, 20.7; IR (film): 3030, 2925, 1595, 1505, 1460, 1218 cm^{-1}; HRMS-APCI (*m/z*) $[M + H]^+$ calcd for $C_{15}H_{13}O_2$, 225.09101; found, 225.08969. Ether **6.30**: R_f 0.48 (20:1 Hexanes:EtOAc); ^{1}H NMR (500 MHz, CD_3CN): δ 7.67 (d, *J* = 2.2, 1H), 7.31 (dt, *J* = 8.3, 0.9, 1H), 7.26 (t, *J* = 8.0, 1H), 7.22–7.17 (m, 2H), 6.96–6.92 (m, 2H), 6.75 (dd, *J* = 7.8, 0.8, 1H), 6.64 (dd, *J* = 2.2, 0.9, 1H), 2.32 (s, 3H); ^{13}C NMR (125 MHz, CD_3CN): δ 156.7, 154.9, 150.8, 145.0, 133.3, 130.3, 125.1,

119.3, 118.6, 111.2, 106.4, 103.8, 19.7; IR (film): 3030, 2855, 1596, 1506, 1481, 1242 cm^{-1}; HRMS-APCI (*m/z*) $[M - H]^-$ calcd for $C_{15}H_{11}O_2$, 223.07536; found, 223.07630.

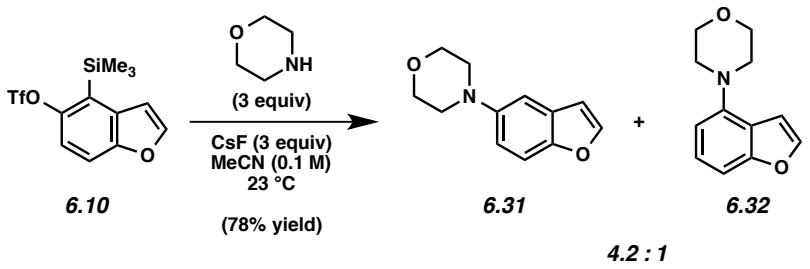

Amines 6.31 and 6.32 (Table 6.2, Entry 2). Purification by preparative thin layer chromatography (10:1 Hexanes:Et_2O) afforded amine **6.31** (63% yield, average of two experiments) as a brown solid and amine **6.32** (15% yield, average of two experiments) as a white amorphous solid. Amine **6.31**: R_f 0.27 (10:1 Hexanes:EtOAc); ^1H NMR (500 MHz, $CDCl_3$): δ 7.58 (d, *J* = 2.2, 1H), 7.41 (dt, *J* = 8.8, 0.7, 1H), 7.10 (d, *J* = 2.4, 1H), 6.99 (dd, *J* = 8.8, 2.4, 1H), 6.69 (dd, *J* = 2.2, 0.9, 1H), 3.93–3.87 (m, 4H), 3.17–3.10 (m, 4H); ^{13}C NMR (125 MHz, $CDCl_3$): δ 150.3, 148.1, 145.5, 128.0, 115.8, 111.6, 107.9, 106.7, 67.1, 51.5; IR (film): 3123, 2958, 2828, 1592, 1447, 1266, 1119, 736 cm^{-1}; HRMS-APCI (*m/z*) $[M + H]^+$ calcd for $C_{14}H_{14}NO_2$, 204.10245; found, 204.10179. Amine **6.32**: R_f 0.36 (10:1 Hexanes:EtOAc); ^1H NMR (500 MHz, $CDCl_3$): δ 7.58 (d, *J* = 2.2, 1H), 7.24–7.16 (m, 2H), 6.78 (d, *J* = 1.6, 1H), 6.71 (d, *J* = 7.2, 1H), 3.98–3.89 (m, 4H), 3.26–3.16 (m, 4H); ^{13}C NMR (125 MHz, $CDCl_3$): δ 156.3, 146.4, 143.7, 125.1, 120.3, 109.7, 106.1, 105.3, 67.3, 51.8; IR (film): 2960, 2854, 1604, 1490, 1240, 1118, 749 cm^{-1}; HRMS-APCI (*m/z*) $[M + H]^+$ calcd for $C_{14}H_{14}NO_2$, 204.10245; found, 204.10192.

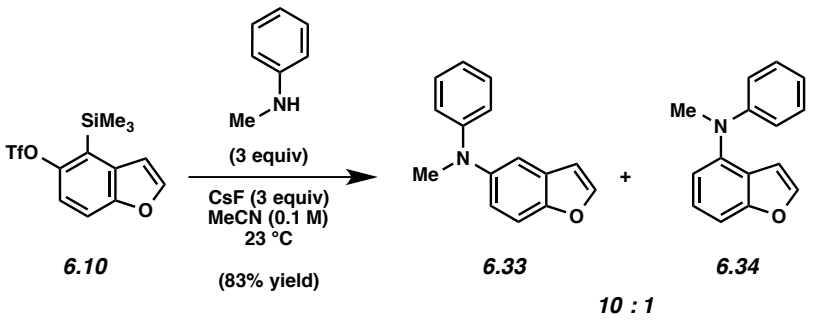

Amines 6.33 and 6.34 (Table 6.2, Entry 3). Purification by preparative thin layer chromatography (10:1 Benzene:Et_2O) afforded amine **6.33** (75% yield, average of two experiments) as a white amorphous solid and amine **6.34** (8% yield, average of two experiments) as a colorless oil. Amine **6.33**: R_f 0.46 (20:1 Hexanes:EtOAc); ^{1}H NMR (500 MHz, $CDCl_3$): δ 7.63 (d, J = 2.2, 1H), 7.47 (d, J = 8.8, 1H), 7.38 (d, J = 2.2, 1H), 7.24–7.19 (m, 2H), 7.11 (dd, J = 8.8, 2.2, 1H), 6.86–6.79 (m, 3H), 6.73 (dd, J = 2.1, 0.8, 1H), 3.33 (s, 3H); ^{13}C NMR (125 MHz, $CDCl_3$): δ 152.2, 150.1, 145.8, 144.8, 129.1, 128.5, 122.5, 118.7, 117.3, 116.2, 112.3, 106.8, 41.0; IR (film): 3060, 2873, 2809, 1597, 1495, 1216 cm^{-1}; HRMS-APCI (*m/z*) $[M + H]^+$ calcd for $C_{15}H_{14}NO$, 224.10754; found, 224.10671. Amine **6.34**: R_f 0.52 (20:1 Hexanes:EtOAc); ^{1}H NMR (500 MHz, CD_3CN): δ 7.56 (d, J = 2.2, 1H), 7.35–7.25 (m, 2H), 7.25–7.20 (m, 2H), 7.02 (dd, J = 7.4, 1.1, 1H), 6.91–6.94 (m, 3H), 6.20 (dd, J = 2.3, 0.9, 1H), 3.38 (s, 3H); ^{13}C NMR (125 MHz, CD_3CN): δ 157.0, 150.3, 145.1, 143.4, 129.9, 126.2, 123.3, 121.0, 119.0, 117.4, 107.6, 106.5, 41.1; IR (film): 3025, 2872, 2808, 1597, 1495, 1216 cm^{-1}; HRMS-APCI (*m/z*) $[M + H]^+$ calcd for $C_{15}H_{14}NO$, 224.10754; found, 224.10675.

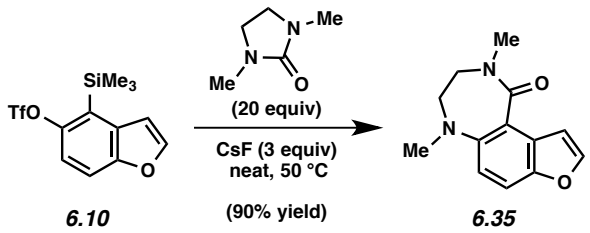

6.10 *6.35*

Benzofuran 6.35 (Table 6.2, Entry 4). The yield was determined by ^{1}H NMR analysis of the crude reaction mixture using 1,3,5-trimethoxybenzene as an external standard (90% yield of **6.35**, average of two experiments). The crude reaction mixture was placed under reduced pressure until most of the DMI was removed, and then purified by preparative thin layer chromatography (100% EtOAc) to give analytical sample of benzofuran **6.35**. Benzofuran **6.35**: R_f 0.54 (100% EtOAc); ^{1}H NMR (500 MHz, $CDCl_3$): δ 7.60 (d, J = 2.1, 1H), 6.47 (dd, J = 8.7, 0.9, 1H), 7.01 (dd, J = 2.2, 0.9, 1H), 6.87 (d, J = 8.8, 1H), 3.42 (t, J = 5.8, 2H), 3.30 (t, J = 5.8, 2H), 3.26 (s, 3H), 2.86 (s, 3H); ^{13}C NMR (125 MHz, $CDCl_3$): δ 169.4, 151.1, 146.5, 142.9, 128.2, 121.3, 114.8, 113.9, 107.4, 55.9, 48.4, 40.9, 34.4; IR (film): 2939, 1628, 1485, 1438, 1253, 1033 cm^{-1}; HRMS-APCI (*m/z*) $[M + H]^+$ calcd for $C_{13}H_{15}N_2O_2$, 231.11280; found, 231.11300.

The structure of **6.35** was verified by 2D-NOESY, as the following interaction was observed:

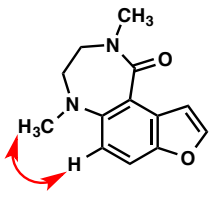

6.35

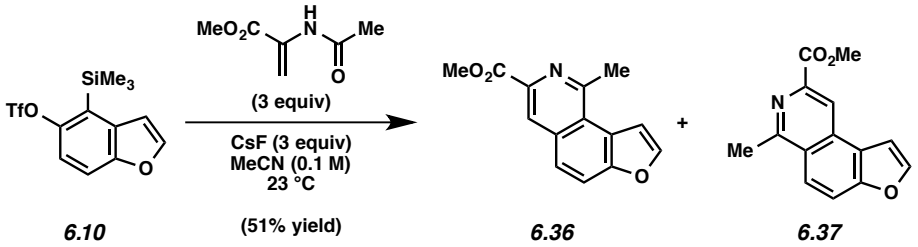

Pyridines 6.36 and 6.37 (Table 6.2, Entry 5). Purification by preparative thin layer chromatography (2:1 Hexanes:EtOAc) afforded an inseparable mixture of pyridines **6.36** and **6.37** (51% yield, average of two experiments) as a white amorphous solid. **6.36** and **6.37**: R_f 0.13 (2:1 Hexanes:EtOAc); ^{1}H NMR (500 MHz, $CDCl_3$): **6.36** (major isomer): δ 8.59 (s, 1H), 7.97 (d, J = 8.3, 1H), 7.93 (d, J = 2.2, 1H), 7.86 (d, J = 8.8, 1H), 7.48 (d, J = 1.9, 1H), 4.07 (s, 3H), 3.25 (s, 3H); **6.37** (minor isomer): ^{1}H NMR (500 MHz, $CDCl_3$): δ 8.76 (s, 1H), 8.09 (d, J = 9.1, 1H), 7.91–7.88 (m, 2H), 7.37 (d, J = 1.9, 1H), 4.08 (s, 3H), 3.11 (s, 3H); ^{13}C NMR (125 MHz, $CDCl_3$): δ 166.8, 166.7, 157.7, 154.8, 154.7, 146.1, 145.6, 141.0, 139.9, 134.0, 131.2, 126.0, 125.7, 124.5, 123.7, 123.6, 122.7, 122.3, 119.3, 117.5, 115.6, 109.0, 106.1, 53.1, 53.0, 27.0, 23.6; IR (film): 3704, 2969, 2864, 1705, 1365, 1275, 1033, 1012 cm^{-1}; HRMS-APCI (*m/z*) [M + H]$^+$ calcd for $C_{14}H_{12}NO_3$, 242.08172; found, 242.07926.

The structure of **6.36** and **6.37** was verified by 2D-NOESY, as the following interactions were observed:

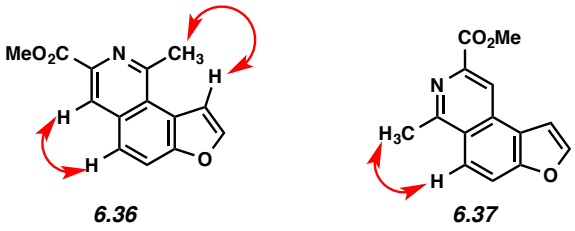

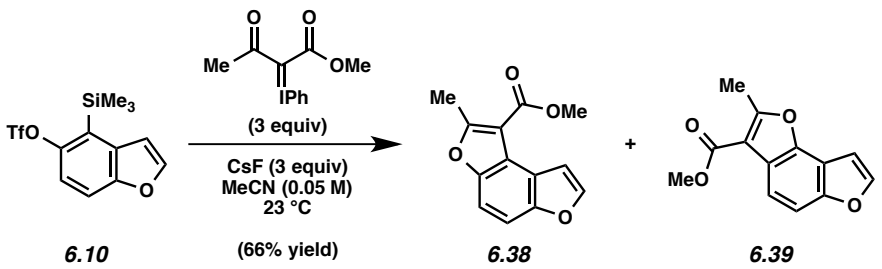

Furans 6.38 and 6.39 (Table 6.2, Entry 6). Purification by preparative thin layer chromatography (20:1 Hexanes:EtOAc) afforded an inseparable mixture of furan adducts **6.38** and **6.39** (66% yield, average of two experiments) as a white solid. Furan **6.38**: R_f 0.45 (20:1 Hexanes:EtOAc); ^{1}H NMR (500 MHz, $CDCl_3$): δ 7.88 (d, J = 8.7, 1H), 6.67 (d, J = 2.2, 1H), 7.49 (dd, J = 8.7, 0.9, 1H), 7.00 (dd, J = 2.2, 0.9, 1H), 3.97 (s, 3H), 2.81 (s, 3H); ^{13}C NMR (125 MHz, $CDCl_3$): δ 165.2, 162.5, 154.3, 146.2, 145.1, 120.8, 117.3, 112.7, 109.6, 108.2, 102.8, 51.6, 14.6; IR (film): 3145, 2953, 1714, 1597, 1444, 1261, 1099, 746 cm^{-1}; HRMS-APCI (*m/z*) $[M + H]^+$ calcd for $C_{13}H_{11}O_4$, 231.06519; found, 231.06430.

The structure of **6.38** was verified by 2D-NOESY, as the following interaction was observed:

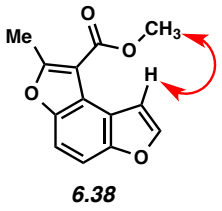

6.38

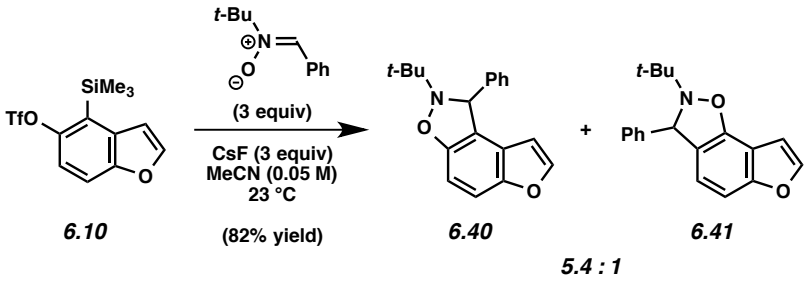

Isoxazolines 6.40 and 6.41 (Table 6.2, Entry 7). Purification by preparative thin layer chromatography (50:1:1 Hexanes:Benzene:Et_2O) afforded isoxazoline **6.40** (69% yield, average of two experiments) as a yellow solid and isoxazoline **6.41** (13% yield, average of two experiments) as an off white solid. Isoxazoline **6.40**: R_f 0.61 (50:1:1 Hexanes:Benzene:Et_2O); ^{1}H NMR (500 MHz, $CDCl_3$): δ 7.48 (d, *J* = 2.1, 1H), 7.48–7.42 (m, 2H), 7.36–7.29 (m, 3H), 7.28–7.23 (m, 1H), 6.79 (d, *J* = 8.7, 1H), 6.27 (dd, *J* = 2.2, 0.9, 1H), 5.80 (s, 1H), 1.21 (s, 9H); ^{13}C NMR (125 MHz, $CDCl_3$): δ 152.6, 151.3, 146.4, 143.3, 128.7, 127.8, 127.7, 123.1, 119.4, 111.1, 103.9, 103.8, 67.4, 61.2, 25.6; IR (film): 2973, 1607, 1478, 1432, 1223, 759, 697 cm^{-1}; HRMS-APCI (*m/z*) $[M + H]^+$ calcd for $C_{19}H_{20}NO_2$, 294.14886; found, 294.14917. Isoxazoline **6.41**: R_f 0.66 (50:1:1 Hexanes:Benzene:Et_2O); ^{1}H NMR (500 MHz, $CDCl_3$): δ 7.56 (d, *J* = 2.2, 1H), 7.45–7.37 (m, 2H), 7.36–7.29 (m, 2H), 7.26–7.22 (m, 1H), 6.98 (dd, *J* = 8.3, 0.7, 1H), 6.80 (dd, *J* = 2.2, 0.8, 1H), 6.78 (d, *J* = 8.3, 1H), 5.69 (s, 1H), 1.22 (s, 9H); ^{13}C NMR (125 MHz, CD_3CN): δ 157.7, 149.9, 146.3, 145.8, 129.5, 128.2, 128.0, 123.7, 120.1, 110.6, 104.8, 103.8, 67.5, 62.0, 25.4; IR (film): 2974, 1601, 1473, 1210, 1050, 754, 699 cm^{-1}; HRMS-APCI (*m/z*) $[M + H]^+$ calcd for $C_{19}H_{20}NO_2$, 294.14886; found, 294.14895.

The structure of **6.41** was verified by 2D-NOESY, as the following interaction was observed:

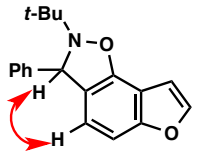

6.41

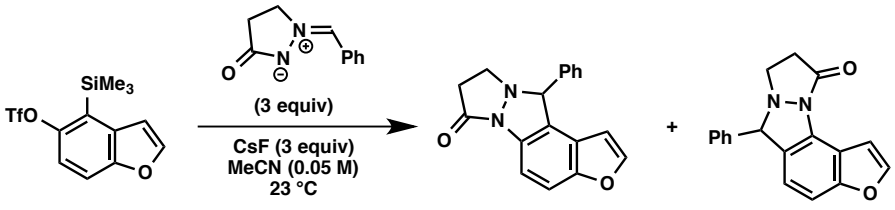

6.10 (66% yield) ***6.42*** ***6.43***

4.5 : 1

Diazolidines 6.42 and 6.43 (Table 6.2, Entry 8). Purification by preparative thin layer chromatography (9:1 Benzene:Acetone) afforded diazolidine **6.42** (54% yield, average of two experiments) as a yellow solid and diazolidine **6.43** (12% yield, average of two experiments) as a orange solid. Diazolidine **6.42**: R_f 0.40 (9:1 Benzene:Acetone); ^{1}H NMR (500 MHz, CD_3CN): δ 7.64 (d, J = 2.2, 1H), 7.56–7.47 (m, 4H), 7.46–7.40 (m, 3H), 6.08 (dd, J = 2.2, 0.7, 1H), 5.48 (s, 1H), 3.55 (dt, J = 8.7, 1.6, 1H), 3.27 (ddd, J = 12.6, 8.8, 8.0, 1H), 3.04–2.94 (m, 1H), 2.76–2.68 (ddd, J = 16.3, 7.8, 1.6, 1H); ^{13}C NMR (125 MHz, CD_3CN): δ 164.2, 154.0, 148.4, 140.0, 131.4, 129.7, 129.7, 130.0, 127.0, 124.5, 112.0, 109.8, 104.7, 74.8, 52.8, 36.8, 36.8; IR (film): 3114, 3032, 2834, 1682, 1438, 1070, 702 cm^{-1}; HRMS-APCI (*m/z*) $[M + H]^+$ calcd for $C_{18}H_{15}N_2O_2$, 291.11280; found, 291.11424. Diazolidine **6.43**: R_f 0.52 (9:1 Benzene:Acetone); ^{1}H NMR (500 MHz, CD_3CN): δ 7.74 (d, J = 2.2, 1H), 7.51–7.46 (m, 2H), 7.46–7.41 (m, 2H), 7.41–7.36 (m, 1H), 7.26 (dd, J = 2.2, 0.9, 1H), 7.22 (dd, J = 8.4, 0.8, 1H), 6.75 (dd, J = 8.4, 0.8, 1H), 5.34 (s, 1H), 3.56 (dt, J = 8.6, 1.5, 1H), 3.32–3.23 (m, 1H), 3.10–3.00 (m, 1H), 2.80–2.72 (ddd, J = 16.2, 7.8, 1.6, 1H); ^{13}C NMR (125 MHz, CD_3CN): δ 163.9, 157.2, 146.5, 140.5, 129.7, 129.6, 129.3,

129.3, 127.6, 120.4, 115.2, 108.3, 107.8, 74.9, 52.9, 36.8; IR (film): 3124, 3032, 2836, 1691, 1477, 1098, 704 cm^{-1}; HRMS-APCI (*m/z*) $[M + H]^+$ calcd for $C_{18}H_{15}N_2O_2$, 291.11280; found, 291.11346.

The structure of **6.43** was verified by 2D-NOESY, as the following interaction was observed:

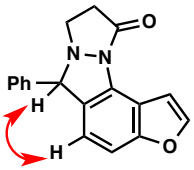

6.43

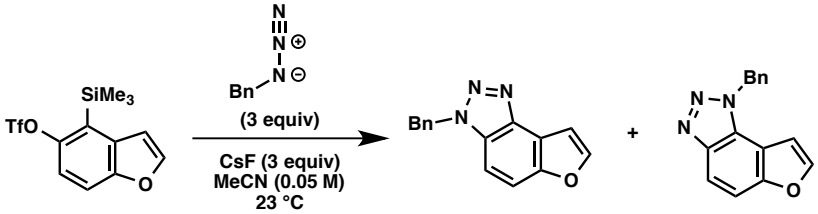

6.10 ***6.44*** ***6.45***

6.2 : 1

Triazoles 6.44 and 6.45 (Table 6.2, Entry 9). Purification by preparative thin layer chromatography (10:1 Benzene:Et_2O) afforded triazole **6.44** (61% yield, average of two experiments) as an off white solid and triazole **6.45** (10% yield, average of two experiments) as an off white solid. Triazole **6.44**: R_f 0.43 (10:1 Benzene:Et_2O); ^1H NMR (500 MHz, $CDCl_3$): δ 7.80 (d, *J* = 2.1, 1H), 7.59 (dd, *J* = 9.0, 0.9, 1H), 7.38 (dd, *J* = 2.1, 0.8, 1H), 7.35–7.26 (m, 5H), 7.21 (d, *J* = 9.0, 1H), 5.90 (s, 2H); ^{13}C NMR (125 MHz, $CDCl_3$): δ 152.5, 146.1, 140.4, 134.9, 130.3, 129.2, 128.6, 127.6, 117.9, 113.2, 105.5, 105.4, 52.7; IR (film): 3118, 3033, 1597, 1499, 1457, 1249, 1144, 1059, 721 cm^{-1}; HRMS-APCI (*m/z*) $[M + H]^+$ calcd for $C_{15}H_{12}N_3O$, 250.09804; found, 250.09552. Triazole **6.45**: R_f 0.48 (10:1 Benzene:Et_2O); ^1H NMR (500 MHz,

$CDCl_3$): δ 7.96 (d, *J* = 9.1, 1H), 7.67 (d, *J* = 2.2, 1H), 7.56 (dd, *J* = 9.2, 0.8, 1H), 7.37–7.29 (m, 3H), 7.26–7.19 (m, 2H), 6.71 (dd, *J* = 2.1, 0.9, 1H), 6.03 (s, 2H); ^{13}C NMR (125 MHz, $CDCl_3$): δ 154.5, 145.3, 143.5, 135.1, 129.1, 128.5, 127.3, 126.9, 115.8, 110.3, 110.1, 104.4, 52.9; IR (film): 3116, 3033, 1637, 1499, 1455, 1242, 1147, 1052, 730 cm^{-1}; HRMS-APCI (*m/z*) $[M + H]^+$ calcd for $C_{15}H_{12}N_3O$, 250.09804; found, 250.09587.

The structure of **6.44** was verified by 2D-NOESY, as the following interaction was observed:

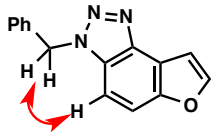

6.44

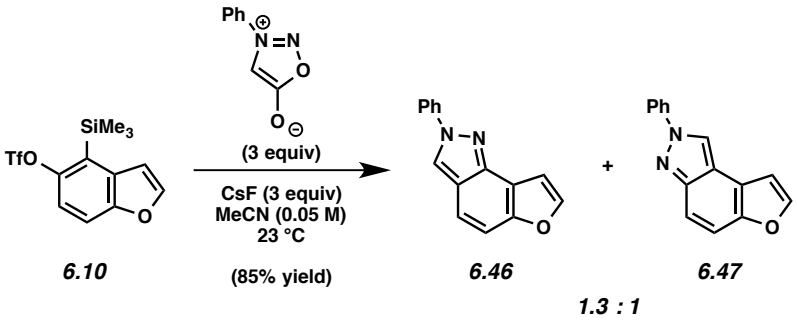

Pyrazoles 6.46 and 6.47 (Table 6.2, Entry 10). Purification by preparative thin layer chromatography (20:1 Hexanes:Et_2O) afforded pyrazole **6.46** (48% yield, average of two experiments) as a black solid and pyrazole **6.47** (37% yield, average of two experiments) as a dark green solid. Pyrazole **6.46**: R_f 0.21 (20:1 Hexanes:EtOAc); ^{1}H NMR (500 MHz, $CDCl_3$): δ 8.46 (s, 1H), 7.94–7.90 (m, 2H), 7.71 (d, *J* = 2.0, 1H), 7.58–7.51 (m, 3H), 7.43–7.36 (m, 2H), 7.30 (dd, *J* = 2.0, 0.8, 1H); ^{13}C NMR (125 MHz, $CDCl_3$): δ 154.5, 144.8, 143.7, 140.7, 129.7, 127.8, 121.7, 121.0, 120.2, 116.6, 115.1, 111.0, 105.8; IR (film): 3123, 2923, 1635, 1599, 1519,

1415, 1043, 735 cm^{-1}; HRMS-APCI (*m/z*) $[M + H]^+$ calcd for $C_{15}H_{11}N_2O$, 235.08714; found, 235.08663. Pyrazole **6.47**: R_f 0.21 (20:1 Hexanes:EtOAc); ^1H NMR (500 MHz, $CDCl_3$): δ 8.54 (s, 1H), 7.96–7.60 (m, 2H), 7.71 (d, *J* = 2.0, 1H), 7.60 (d, *J* = 9.3, 1H), 7.59–7.50 (m, 3H), 7.40 (t, *J* = 7.4, 1H), 7.01 (dd, *J* = 2.0, 0.8, 1H); ^{13}C NMR (125 MHz, $CDCl_3$): δ 151.3, 148.5, 144.2, 140.8, 129.8, 127.8, 120.9, 118.9, 116.8, 116.7, 114.9, 114.8, 106.7; IR (film): 3120, 3070, 1600, 1517, 1504, 1387, 1062, 754 cm^{-1}; HRMS-APCI (*m/z*) $[M + H]^+$ calcd for $C_{15}H_{11}N_2O$, 235.08714; found, 235.08643.

The structure of **6.46** was verified by 2D-NOESY, as the following interaction was observed:

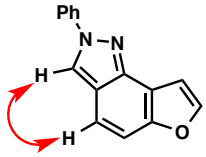

6.46

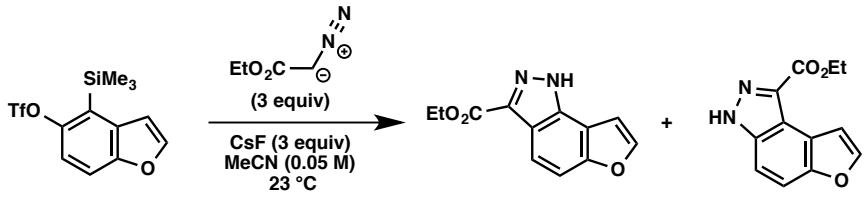

6.10 ***6.48*** ***6.49***

2.5 : 1

Pyrazoles 6.48 and 6.49 (Table 6.2, Entry 11). Purification by preparative thin layer chromatography (3:1:1 Hexanes:CH_2Cl_2:Et_2O) afforded pyrazole **6.48** (46% yield, average of two experiments) as a white solid and pyrazole **6.49** (19% yield, average of two experiments) as a white solid. Pyrazole **6.48**: R_f 0.48 (20:1 Hexanes:EtOAc); ^1H NMR (500 MHz, $CDCl_3$): δ 8.04 (d, *J* = 9.0, 1H), 7.71 (d, *J* = 2.1, 1H), 7.51 (dd, *J* = 9.0, 0.7, 1H), 7.17 (dd, *J* = 2.8, 0.8, 1H), 4.48 (q, *J* = 7.2, 2H) 1.39 (t, *J* = 7.2, 3H); ^{13}C NMR (125 MHz, $CDCl_3$): δ 163.3, 155.0 144.5,

136.9, 135.8, 118.8, 117.7, 111.2, 109.8, 104.7, 61.3, 14.4; IR (film): 3195, 3123, 2980, 1714, 1485, 1251, 1150, 740 cm^{-1}; HRMS-APCI (*m/z*) $[M + H]^+$ calcd for $C_{12}H_{11}N_2O_3$, 231.07697; found, 231.07500. Pyrazole **6.49**: R_f 0.48 (20:1 Hexanes:EtOAc); ^1H NMR (500 MHz, $CDCl_3$): δ 7.79 (d, *J* = 2.0, 1H), 7.67 (d, *J* = 9.1, 1H), 7.64 (d, *J* = 1.9, 1H), 7.56 (d, *J* = 9.1, 1H), 4.59 (q, *J* = 7.1, 2H), 1.51 (t, *J* = 7.1, 3H); ^{13}C NMR (125 MHz, $CDCl_3$): δ 162.9, 152.0, 145.0, 139.4, 136.3, 119.1, 116.2, 113.4, 108.7, 107.3, 61.5, 14.7; IR (film): 3246, 3168, 2980, 1710, 1447, 1227, 1148, 768 cm^{-1}; HRMS-APCI (*m/z*) $[M - H]^-$ calcd for $C_{12}H_9N_2O_3$, 229.06132; found, 229.06117.

The structure of **6.48** was verified by 2D-NOESY, as the following interaction was observed:

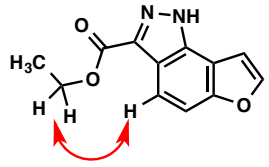

6.48

6.5.2.4 Trapping Experiments of 3,4-Oxacyclohexyne

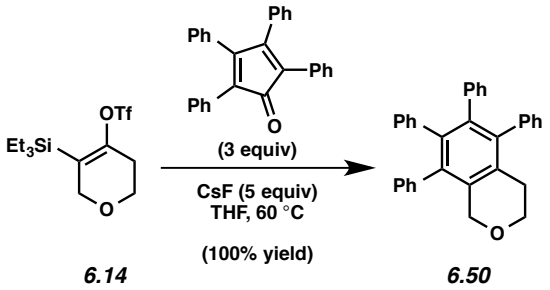

6.14 ***6.50***

Representative Procedure (Preparation of Pyran 6.50 is used as an example).

Pyran 6.50 (Table 6.3, Entry 1). To a stirred solution of silyl triflate **6.14** (50.2 mg, 0.145 mmol) and tetracyclone (168 mg, 0.434 mmol, 3.0 equiv) in THF (5.0 mL, 0.03 M) was added

CsF (100 mg, 0.725 mmol, 5.0 equiv). The reaction vessel was purged with N_2 gas, sealed, and placed in a preheated aluminum heating block maintained at 60 °C for 24 h. After cooling to 23 °C, the reaction mixture was filtered over silica gel (EtOAc eluent, 12 mL). Evaporation under reduced pressure and further purification by preparative thin layer chromatography (1:1 Benzene:Hexanes) afforded pyran **6.50** as a faint yellow amorphous solid (100% yield, average of two experiments). Pyran **6.50**: R_f 0.52 (9:1 Hexanes:EtOAc); ^{1}H NMR (500 MHz, $CDCl_3$): δ 7.21–7.17 (m, 4H), 7.14–7.06 (m, 6H), 6.85–6.77 (m, 10H), 4.55 (s, 2H), 3.91 (t, J = 5.8, 2H), 2.64 (t, J = 5.8, 2H); ^{13}C NMR (125 MHz, $CDCl_3$) [24/33 carbons were discernable]: δ 140.7, 140.2, 139.9, 139.8, 139.4, 139.0, 138.8, 137.8, 132.3, 131.4, 131.3, 131.1, 130.3, 130.0, 127.9, 127.8, 126.7, 126.6, 126.4, 125.4, 125.3, 68.2, 65.4, 28.6; IR (film): 3080, 3057, 2244, 1950, 1809, 1603 cm^{-1}; HRMS-APCI (*m/z*) $[M + H]^+$ calcd for $C_{33}H_{27}O$, 439.20564; found, 439.19306.

Any modifications of the conditions shown in this representative procedure are specified in the following schemes, which depict all of the results shown in Tables 6.3 and 6.4

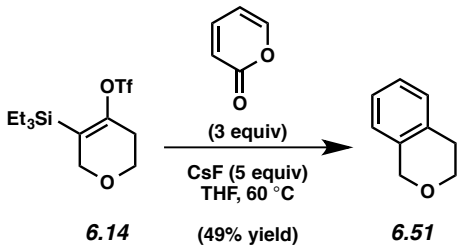

Isochroman (6.51) (Table 6.3, Entry 2). Purification by preparative thin layer chromatography (2:1 Hexanes:EtOAc) afforded isochroman (**6.51**) as a colorless oil (49% yield, average of two experiments). Isochroman (**6.51**): R_f 0.50 (9:1 Hexanes:Et_2O); ^{1}H NMR (500 MHz, $CDCl_3$): δ 7.18–7.10 (m, 3H), 6.99–6.96 (m, 1H), 4.78 (s, 2H), 3.99 (t, J = 5.7, 2H), 2.87 (t, J = 5.7, 2H);

^{13}C NMR (125 MHz, $CDCl_3$): δ 135.1, 133.4, 129.1, 126.5, 126.1, 124.5, 68.1, 65.5, 28.5; IR (film): 3061, 2930, 2832, 1649, 1495, 1452 cm^{-1}; HRMS-APCI (*m/z*) $[M + H]^+$ calcd for $C_9H_{11}O$, 135.08044; found, 135.07911.

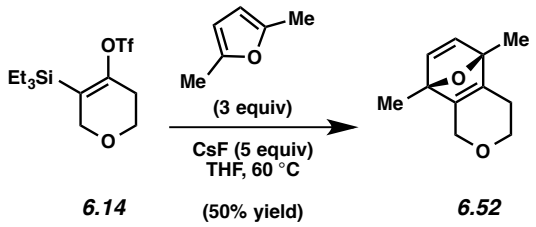

6.14 (50% yield) *6.52*

Pyran 6.52 (Table 6.3, Entry 3). Purification by preparative thin layer chromatography (1:1 Hexanes:EtOAc) afforded pyran **6.52** as a colorless oil (50% yield, average of two experiments). Pyran **6.52**: R_f 0.25 (9:1 Hexanes:Et_2O); ^{1}H NMR (500 MHz, $CDCl_3$): δ 6.86 (s, 2H), 4.46 (app. dt, *J* = 16.3, 3.7, 1H), 3.97 (app. ddd, *J* = 16.3, 3.7, 0.8, 1H), 3.68–3.65 (m, 2H), 2.39–2.31 (m, 1H), 2.00–1.92 (m, 1H), 1.64 (s, 3H), 1.61 (s, 3H); ^{13}C NMR (125 MHz, $CDCl_3$): δ 150.0, 149.6, 148.1, 147.7, 91.0, 90.1, 64.7, 63.8, 24.1, 15.4, 15.1; IR (film): 2972, 2930, 2898, 1715, 1668, 1387 cm^{-1}; HRMS-APCI (*m/z*) $[M + H]^+$ calcd for $C_{11}H_{15}O_2$, 179.10666; found, 179.10518.

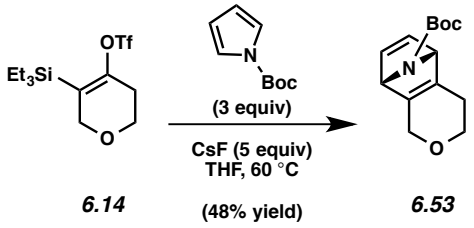

6.14 (48% yield) *6.53*

Pyran 6.53 (Table 6.3, Entry 4). Purification by preparative thin layer chromatography (1:1 Hexanes:EtOAc) afforded pyran **6.53** as a faint orange oil (48% yield, average of two experiments). Pyran **6.53**: R_f 0.78 (1:1 Hexanes:EtOAc); ^{1}H NMR (500 MHz, $CDCl_3$, 60 °C): δ 7.00 (br s, 2H), 4.97 (app. d, *J* = 9.6, 2H), 4.49 (app. d, *J* = 15.8, 1H), 4.02 (dt, *J* = 16.4, 3.2, 1H),

3.70–3.65 (m ,1H), 3.64–3.59 (m, 1H), 2.44 (app. d, J = 16.4, 1H), 2.12–2.04 (m, 1H), 1.41 (s, 9H); ^{13}C NMR (125 MHz, $CDCl_3$, 60 °C): δ 154.9, 147.3, 146.8, 143.3, 143.0, 80.5, 68.8, 66.8, 66.0, 64.1, 28.4, 26.4; IR (film): 2977, 2921, 1701, 1368, 1335, 1255 cm^{-1}; HRMS-APCI (*m/z*) [M + H]$^+$ calcd for $C_{14}H_{20}NO_3$, 250.14377; found, 250.14157.

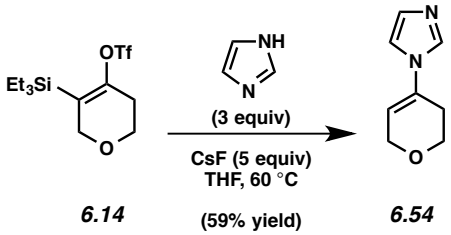

6.14 ***6.54***

Pyran 6.54 (Table 6.4, Entry 1). Purification by preparative thin layer chromatography (5:4:1 Benzene:EtOAc:Et_3N) afforded pyran **6.54** as a colorless oil (59% yield, average of two experiments). Pyran **6.54**: R_f 0.35 (5:4:1 Benzene:EtOAc:Et_3N); ^{1}H NMR (500 MHz, C_6D_6): δ 7.44 (s, 1H), 7.25 (s, 1H), 6.64 (s, 1H), 4.94 (sept, J = 1.5, 1H), 3.79 (q, J = 2.7, 2H), 3.35 (t, J = 5.5, 2H), 1.73–1.68 (m, 2H); ^{13}C NMR (125 MHz, C_6D_6): δ 134.3, 131.1, 130.5, 115.7, 112.2, 64.2, 63.5, 26.8; IR (film): 3381, 2930, 2841, 1678, 1495, 1382 cm^{-1}; HRMS-APCI (*m/z*) [M + H]$^+$ calcd for $C_8H_{11}N_2O$, 151.08659; found, 151.08530.

The structure of **6.54** was verified by 2D-NOESY, as the following interaction was observed:

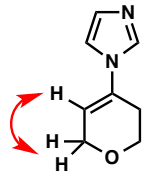

6.54

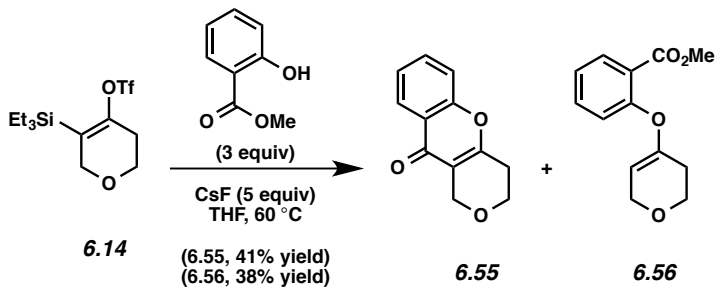

Pyrone 6.55 and Enol Ether 6.56 (Table 6.4, Entry 2). Purification by preparative thin layer chromatography (9:1 Benzene:EtOAc) afforded adduct **6.55** (41% yield, average of two experiments) as a white amorphous solid and **6.56** (38% yield, average of two experiments) as a colorless oil. Pyrone **6.55**: R_f 0.20 (9:1 Benzene:EtOAc); ^{1}H NMR (500 MHz, $CDCl_3$): δ 8.17 (dd, *J* = 8.0, 1.5, 1H), 7.66–7.60 (m, 1H), 7.40 (app. dd, *J* = 8.4, 0.5, 1H), 7.38–7.33 (m, 1H), 4.65 (t, *J* = 1.8, 2H), 4.00 (t, *J* = 5.7, 2H), 2.77 (tt, *J* = 5.7, 1.8, 2H); ^{13}C NMR (125 MHz, $CDCl_3$): δ 175.8, 160.9, 156.1, 133.5, 125.7, 125.0, 123.6, 117.9, 117.2, 63.9, 62.7, 27.7; IR (film): 3066, 2855, 1649, 1607, 1471, 1429 cm^{-1}; HRMS-APCI (*m/z*) $[M + H]^+$ calcd for $C_{12}H_{11}O_3$, 203.07027; found, 203.06829. Enol ether **6.56**: R_f 0.40 (9:1 Benzene:EtOAc); ^{1}H NMR (500 MHz, $CDCl_3$): δ 7.88 (dd, *J* = 7.7, 1.7, 1H), 7.49 (ddd, *J* = 8.1, 7.7, 1.7, 1H), 7.19 (dt, *J* = 7.7, 1.1, 1H), 7.12 (dd, *J* = 8.1, 1.1, 1H), 4.62 (sept, *J* = 1.1, 1H), 4.13 (q, *J* = 2.5, 2H), 3.90 (t, *J* = 5.6, 2H), 3.89 (s, 3H), 2.44–2.39 (m, 2H); ^{13}C NMR (125 MHz, C_6D_6): δ 165.7, 154.9, 153.1, 133.3, 132.2, 124.6, 124.1, 122.7, 101.0, 64.5, 64.4, 51.7, 28.2; IR (film): 2949, 2836, 1729, 1678, 1603, 1485 cm^{-1}; HRMS-APCI (*m/z*) $[M + H]^+$ calcd for $C_{13}H_{15}O_4$, 235.09649; found, 235.09445.

The structure of **6.56** was verified by 2D-NOESY, as the following interaction was observed:

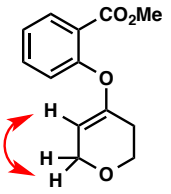

6.56

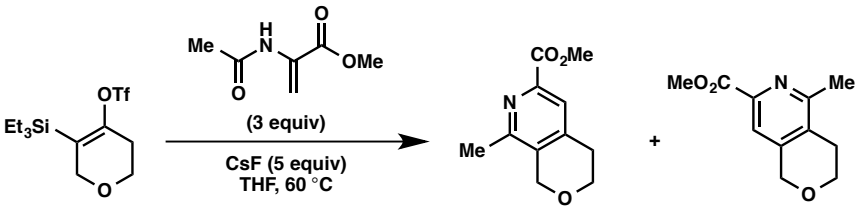

6.14 *6.57* *6.58*

2.6 : 1

Pyridines 6.57 and 6.58 (Table 6.4, Entry 3). Purification by preparative thin layer chromatography (9:1 Benzene:Acetone) afforded an inseparable mixture of pyridine adducts **6.57** and **6.58** (71% yield, average of two experiments) as a white amorphous solid. Pyridines **6.57** and **6.58**: R_f 0.50 (9:1 Benzene:Acetone); ^{1}H NMR (500 MHz, $CDCl_3$): **6.57** (major isomer): δ 7.75 (s, 1H), 4.72 (s, 2H), 3.96 (s, 3H), 3.93 (t, J = 5.8, 2H), 2.87 (t, J = 5.8, 2H), 2.42 (s, 3H); **6.58** (minor isomer): ^{1}H NMR (500 MHz, $CDCl_3$): δ 7.63 (s, 1H), 4.73 (s, 2H), 4.00 (t, J = 5.8, 2H), 3.95 (s, 3H), 2.76 (t, J = 5.8, 2H), 2.53 (s, 3H); ^{13}C NMR (125 MHz, $CDCl_3$): **6.57** (major isomer): δ 166.1, 154.5, 145.0, 143.6, 133.1, 123.7, 65.7, 64.1, 53.0, 28.2, 21.3; **6.58** (minor isomer): δ 166.1, 157.8, 144.6, 144.4, 131.7, 119.2, 67.2, 64.9, 53.0, 25.8, 22.0; IR (film): 3451, 2949, 2850, 1715, 1598, 1433 cm^{-1}; HRMS-APCI (*m/z*) $[M + H]^+$ calcd for $C_{11}H_{14}NO_3$, 208.09682; found, 208.09521.

The structure of **6.57** was verified by 2D-NOESY, as the following interaction was observed:

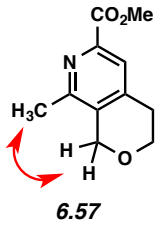

6.57

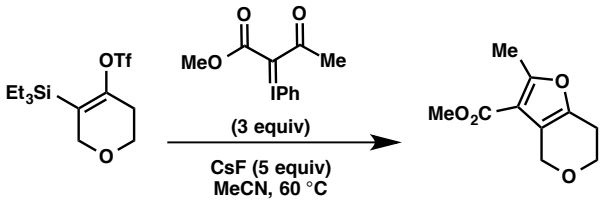

6.14 ***6.59***

The solvent used in this reaction was acetonitrile. The solubility of the trapping agent prevented the use of tetrahydrofuran.

Furan 6.59 (Table 6.4, Entry 4). Purification by preparative thin layer chromatography (9:1 Hexanes:EtOAc) afforded furan **6.59** (70% yield, average of two experiments) as a colorless oil. Furan **6.59**: R_f 0.52 (9:1 Benzene:EtOAc); ^{1}H NMR (500 MHz, $CDCl_3$): δ 4.55 (s, 2H), 3.86 (t, *J* = 5.5, 2H), 3.81 (s, 3H), 2.75–2.71 (m, 2H), 2.55 (s, 3H); ^{13}C NMR (125 MHz, $CDCl_3$): δ 165.1, 158.6, 146.2, 115.3, 112.7, 65.4, 63.2, 51.3, 23.9, 14.0; IR (film): 2954, 2846, 1715, 1584, 1443, 1293 cm^{-1}; HRMS-APCI (*m/z*) $[M + H]^+$ calcd for $C_{10}H_{13}O_4$, 197.08084; found, 197.07904.

The structure of **6.59** was verified by 2D-NOESY, as the following interaction was observed:

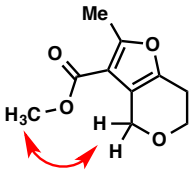

6.59

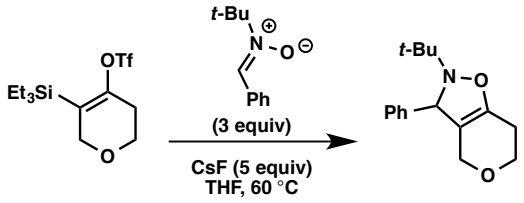

6.14 ***6.60***

Isoxazoline 6.60 (Table 6.4, Entry 5). Purification by preparative thin layer chromatography (1:1 Hexanes:EtOAc) afforded isoxazoline **6.60** (73% yield, average of two experiments) as a colorless oil. Isoxazoline **6.60**: R_f 0.95 (1:1 Hexanes:EtOAc); ^{1}H NMR (500 MHz, C_6D_6): δ 7.37 (app. d, J = 8.1, 2H), 7.18 (app. d, J = 7.6, 2H), 7.07 (tt, J = 7.0, 1.3, 1H), 4.90 (s, 1H), 4.01 (d, J = 14.1, 1H), 3.84 (d, J = 14.1, 1H), 3.51–3.46 (m, 1H), 3.34–3.28 (m, 1H), 2.05–1.89 (m, 2H), 1.11 (s, 9H); ^{13}C NMR (125 MHz, C_6D_6): δ 146.0, 143.6, 128.4, 127.1, 127.0, 105.2, 68.3, 63.4, 62.9, 60.0, 24.9, 23.0; IR (film): 2972, 2902, 1729, 1457, 1363, 1232 cm^{-1}; HRMS-APCI (*m/z*) $[M + H]^+$ calcd for $C_{16}H_{22}NO_2$, 260.16451; found, 260.16226.

The structure of **6.60** was verified by 2D-NOESY, as the following interaction was observed:

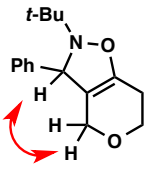

6.60

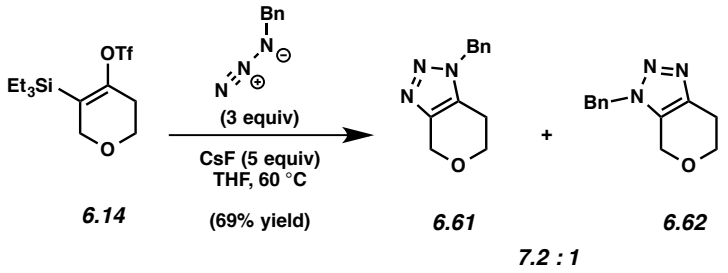

Triazoles 6.61 and 6.62 (Table 6.4, Entry 6). Purification by preparative thin layer chromatography (4:1 EtOAc:Hexanes) afforded an inseparable mixture of triazoles **6.61** and **6.62** (69% yield, average of two experiments) as a white amorphous solid. Triazoles **6.61** and **6.62**: R_f 0.30 (4:1 EtOAc:Hexanes); ^{1}H NMR (500 MHz, $CDCl_3$): **6.61** (major isomer): δ 7.37–7.31 (m, 3H), 7.22–7.17 (m, 2H), 5.48 (s, 2H), 4.80 (t, J = 1.2, 2H), 3.86 (t, J = 5.5, 2H), 2.54 (tt, J = 5.5, 1.2, 2H); **6.62** (minor isomer): δ 7.37–7.31 (m, 3H), 7.22–7.17 (m, 2H), 5.43 (s, 2H), 4.40 (t, J = 1.2, 2H), 3.85 (t, J = 5.5, 2H), 2.88 (tt, J = 5.5, 1.2, 2H); ^{13}C NMR (125 MHz, $CDCl_3$): **6.61** (major isomer): δ 142.3, 134.5, 129.7, 129.2, 128.7, 127.7, 64.2, 64.0, 52.3, 21.9; **6.62** (minor isomer): δ 141.3, 134.0, 130.4, 129.3, 128.9, 127.9, 65.2, 61.8, 52.9, 23.5; IR (film): 3446, 2925, 2855, 2353, 1499, 1189 cm^{-1}; HRMS-APCI (*m/z*) $[M + H]^+$ calcd for $C_{12}H_{14}N_3O$, 216.11314; found, 216.11143.

The structure of **6.61** was verified by 2D-NOESY, as the following interaction was observed:

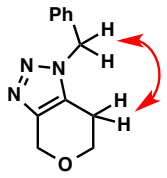

6.61

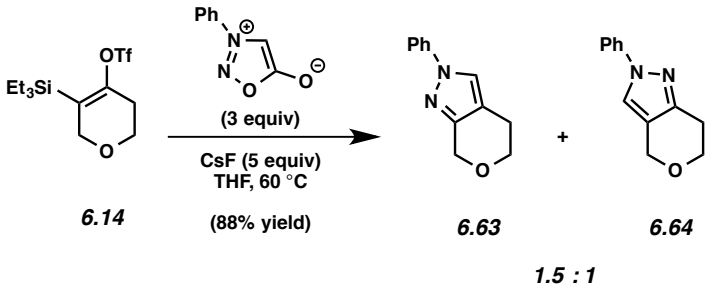

6.14 *6.63* *6.64*

1.5 : 1

Pyrazoles 6.63 and 6.64 (Table 6.4, Entry 7). Purification by preparative thin layer chromatography (4:1 Benzene:EtOAc) afforded pyrazole **6.63** (53% yield, average of two experiments) as a yellow oil and pyrazole **6.64** (35% yield, average of two experiments) as a yellow oil. Pyrazole **6.63**: R_f 0.65 (4:1 Benzene:EtOAc); ^{1}H NMR (500 MHz, $CDCl_3$): δ 7.69 (s, 1H), 7.62 (dd, *J* = 8.7, 1.9, 2H), 7.42 (tt, *J* = 7.5, 1.2, 2H), 7.24 (dd, *J* = 8.7, 7.5, 1H), 4.85 (s, 2H), 3.92 (t, *J* = 5.6, 2H), 2.76 (t, *J* = 5.6, 2H); ^{13}C NMR (125 MHz, $CDCl_3$): δ 149.0, 140.4, 129.5, 126.2, 124.0, 118.9, 115.0, 65.6, 65.2, 21.8; IR (film): 3113, 3052, 2841, 1598, 1504, 1391 cm^{-1}; HRMS-APCI (*m/z*) $[M + H]^+$ calcd for $C_{12}H_{13}N_2O$, 201.10224; found, 201.10053. Pyrazole **6.64**: R_f 0.55 (4:1 Benzene:EtOAc); ^{1}H NMR (500 MHz, $CDCl_3$): δ 7.65–7.61 (m, 3H), 7.45–7.39 (m, 2H), 7.27–7.23 (m, 1H), 4.77 (s, 2H), 4.00 (t, *J* = 5.8, 2H), 2.91 (t, *J* = 5.8, 2H); ^{13}C NMR (125 MHz, $CDCl_3$): δ 147.8, 140.4, 129.5, 126.2, 121.4, 119.0, 116.6, 65.6, 63.3, 24.5; IR (film): 2944, 2846, 1598, 1570, 1509, 1377 cm^{-1}; HRMS-APCI (*m/z*) $[M + H]^+$ calcd for $C_{12}H_{13}N_2O$, 201.10224; found, 201.10039.

The structure of **6.63** was verified by 2D-NOESY, as the following interaction was observed:

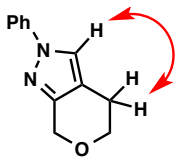

6.63

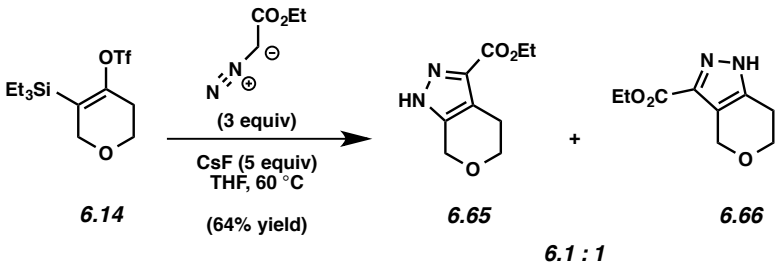

Pyrazoles 6.65 and 6.66 (Table 6.4, Entry 8). Purification by preparative thin layer chromatography (9:1 Benzene:MeOH) afforded an inseparable mixture of pyrazoles **6.65** and **6.66** (64% yield, average of two experiments) as a yellow oil. Pyrazoles **6.65** and **6.66**: R_f 0.45 (9:1 Benzene:MeOH); ^{1}H NMR (500 MHz, C_6D_6): **6.65** (major isomer): δ 4.93 (s, 2H), 4.01 (q, J = 7.2, 2H), 3.61 (t, J = 5.7, 2H), 2.70 (t, J = 5.7, 2H), 0.95 (t, J = 7.2, 3H); **6.66** (minor isomer): δ 4.89 (s, 2H), 3.94 (q, J = 7.2, 2H), 3.62 (t, J = 5.7, 2H), 2.77 (t, J = 5.7, 2H), 0.89 (t, J = 7.2, 3H); ^{13}C NMR (125 MHz, C_6D_6): **6.65** (major isomer): δ 161.5, 144.9, 134.9, 116.6, 64.9, 64.3, 60.6, 23.3, 14.2; **6.66** (minor isomer): δ 161.7, 142.3, 134.9, 117.9, 64.3, 64.2, 60.7, 23.8, 14.1; IR (film): 3212, 2958, 2850, 1720, 1448, 1255 cm^{-1}; HRMS-APCI (m/z) $[M + H]^+$ calcd for $C_9H_{13}N_2O_3$, 197.09207; found, 197.09016.

The structure of **6.65** was verified by 2D-NOESY, as the following interaction was observed:

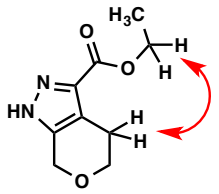

6.65

6.5.3 Computational Methods

All computations were carried out using Spartan '10 Parallel Suite for Mac unless otherwise noted.[40] All structures were minimized using Molecular Mechanics, and then further minimized using Density Functional Theory B3LYP/6–31G*. Computational data for structures **6.6** and **6.7** have previously been reported.[5e, 5f, 7c, 8a]

6.5.3.1 Cartesian Coordinates of Strained Alkynes

Structure **6.4**

C	-0.915310	-1.508769	-0.000000
C	-1.136055	1.214394	0.000000
C	0.309699	-0.842830	-0.000000
C	-2.014499	-0.917769	0.000000
C	-2.312414	0.443151	0.000000
C	0.110164	0.568133	0.000000
H	-3.298649	0.893331	0.000000
H	-1.185215	2.298979	0.000000
C	1.732086	-1.043564	-0.000000
H	2.270565	-1.980214	-0.000000
O	1.328037	1.193936	0.000000
C	2.274967	0.201642	-0.000000
H	3.297172	0.550090	-0.000000

Structure **6.5**

H	-2.395709	-0.204146	0.568566
C	-1.552912	-0.184770	-0.132100
C	0.647654	-1.340220	0.041322
C	1.506487	-0.118244	0.081443
C	-0.574405	-1.258131	-0.000894
C	-0.610478	1.052425	0.236791
H	1.897936	0.043069	1.096118
H	-0.560416	1.106573	1.334921
H	-1.951206	-0.099172	-1.149939
H	2.342505	-0.121492	-0.622200
H	-1.059463	1.971018	-0.152238
O	0.680025	0.996295	-0.325870

6.5.3.2 Energies of Strained Alkynes

Structure	Energy (hartrees)	Energy (kcal/mol)
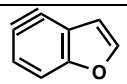 *6.4*	–382.332940	–239917.743

Structure	Energy (hartrees)	Energy (kcal/mol)
 *6.5*	–269.218809	–168937.494

6.6 Spectra Relevant to Chapter Six:

Expanding the Strained Alkyne Toolbox: Generation and Utility of Oxygen-Containing Strained Alkynes

Tejas K. Shah, Jose M. Medina, and Neil K. Garg

J. Am. Chem. Soc. **2016**, *138*, 4948–4954.

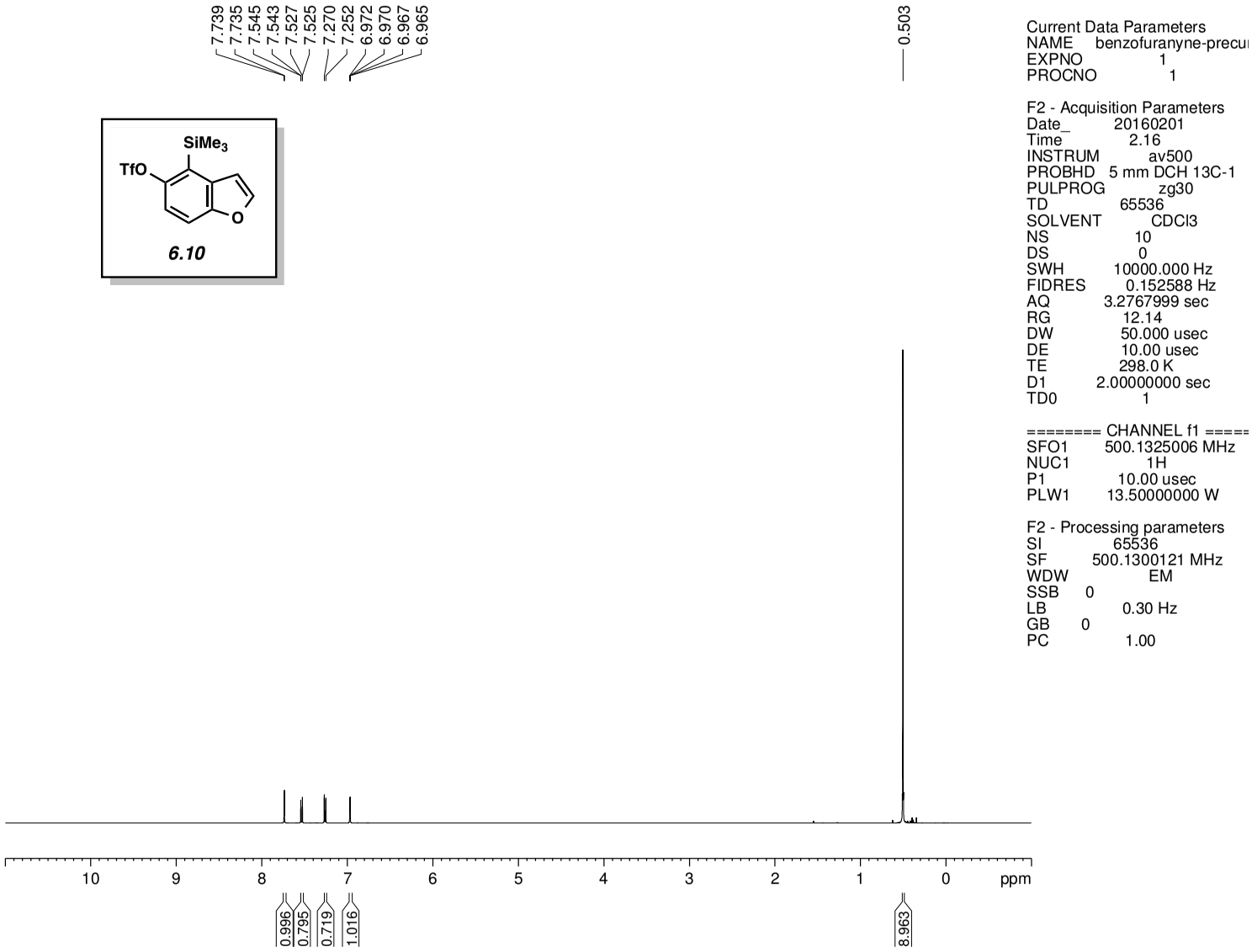

Figure 6.3. ^{1}H NMR (500 MHz, $CDCl_3$) compound **6.10**

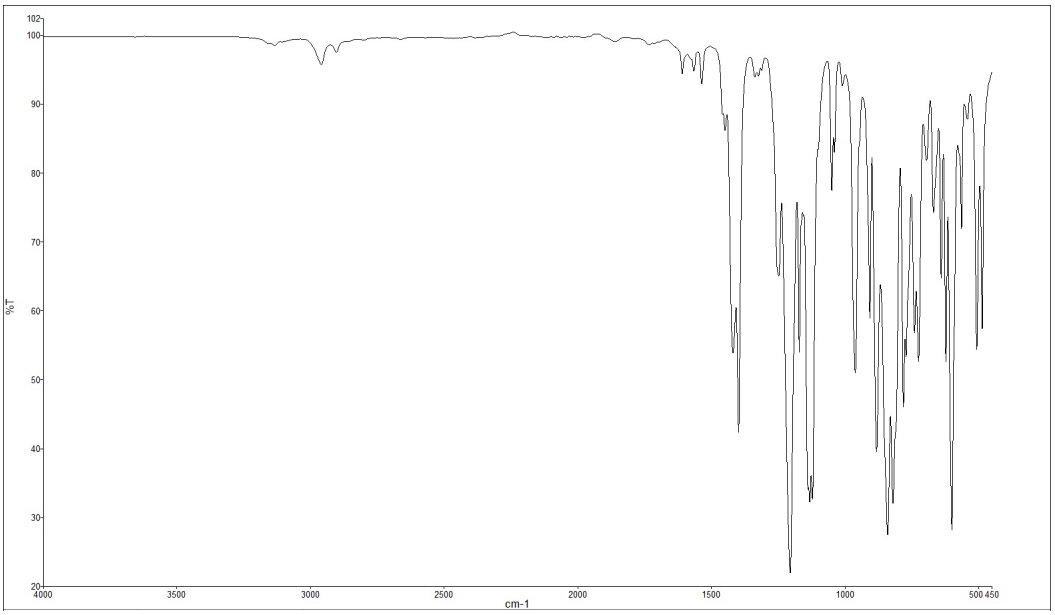

Figure 6.4. Infrared spectrum of compound **6.10**

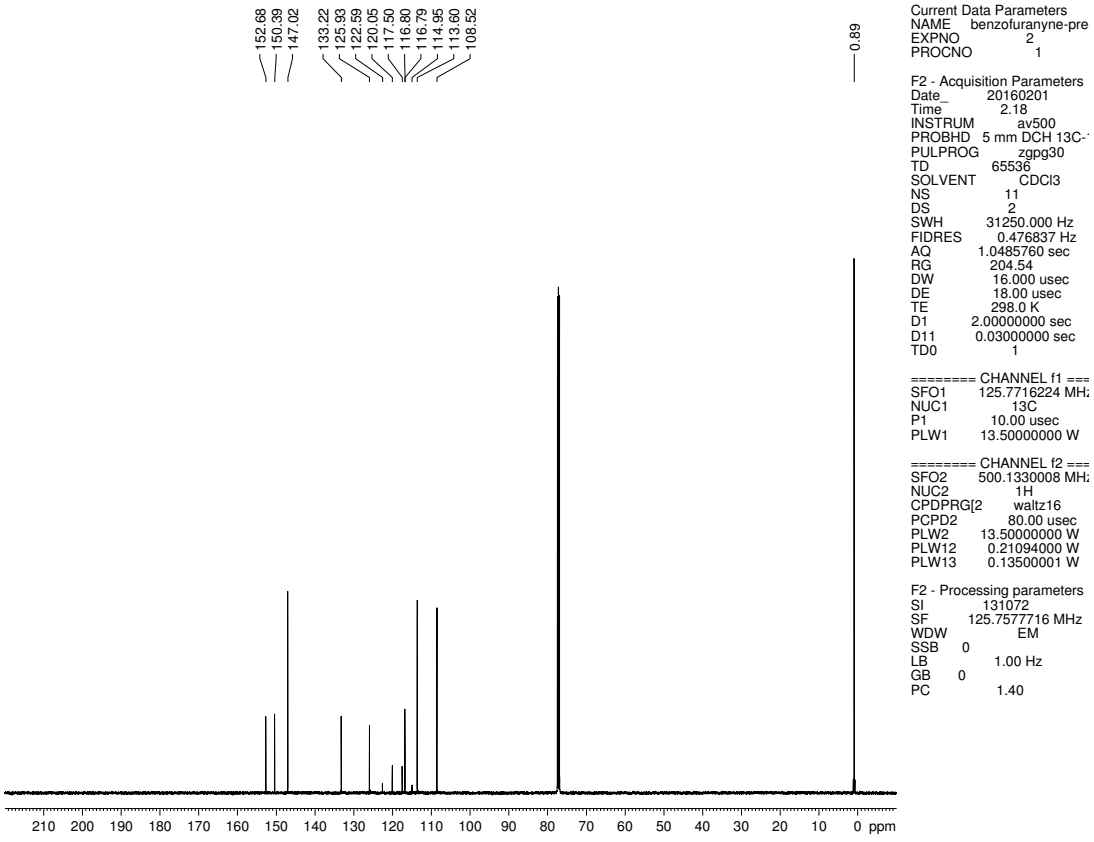

Figure 6.5. ^{13}C NMR (125 MHz, $CDCl_3$) of compound **6.10**

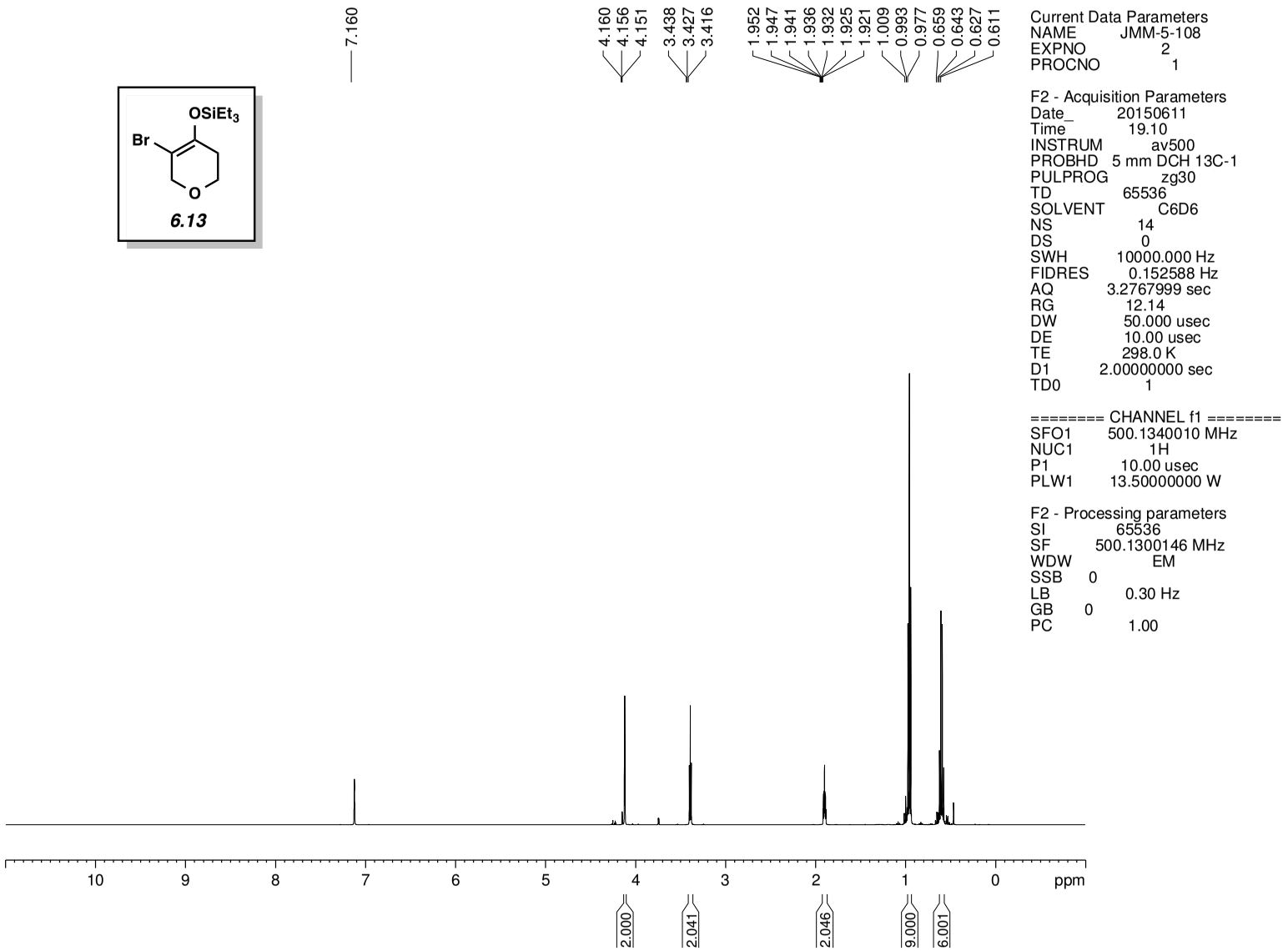

Figure 6.6. ^{1}H NMR (500 MHz, C_6D_6) compound **6.13**

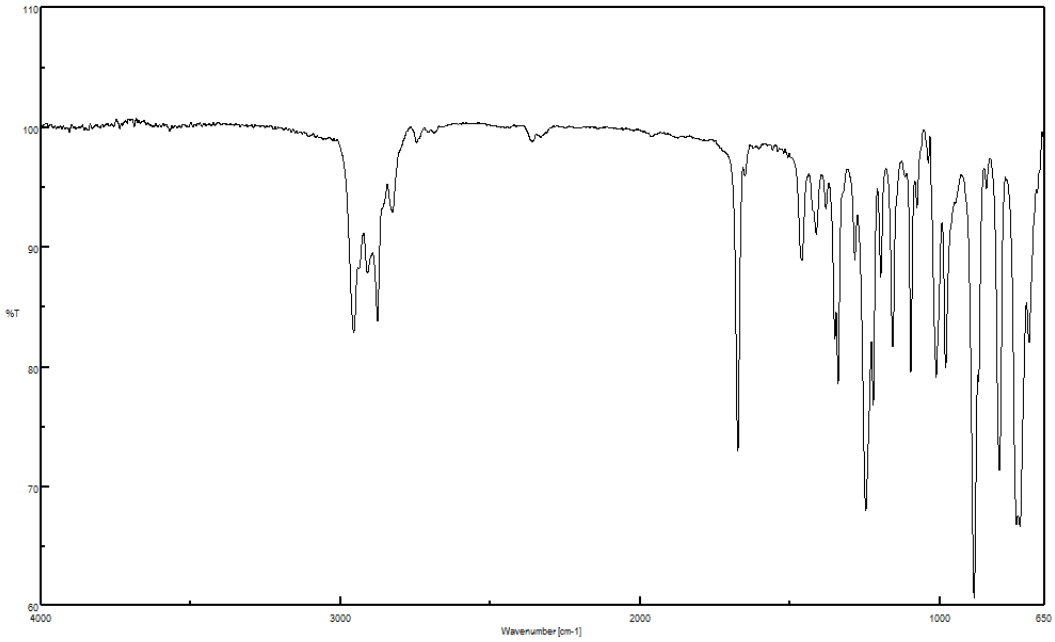

Figure 6.7. Infrared spectrum of compound **6.13**

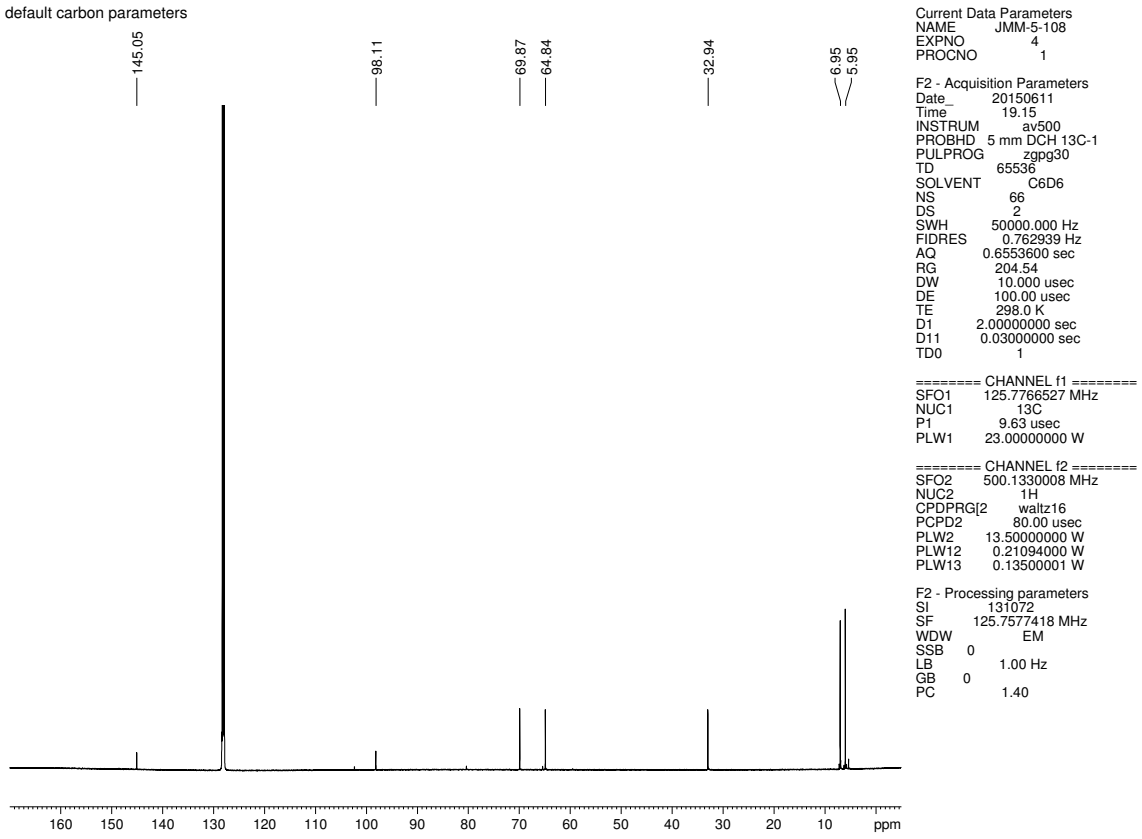

Figure 6.8. ^{13}C NMR (125 MHz, C_6D_6) of compound **6.13**

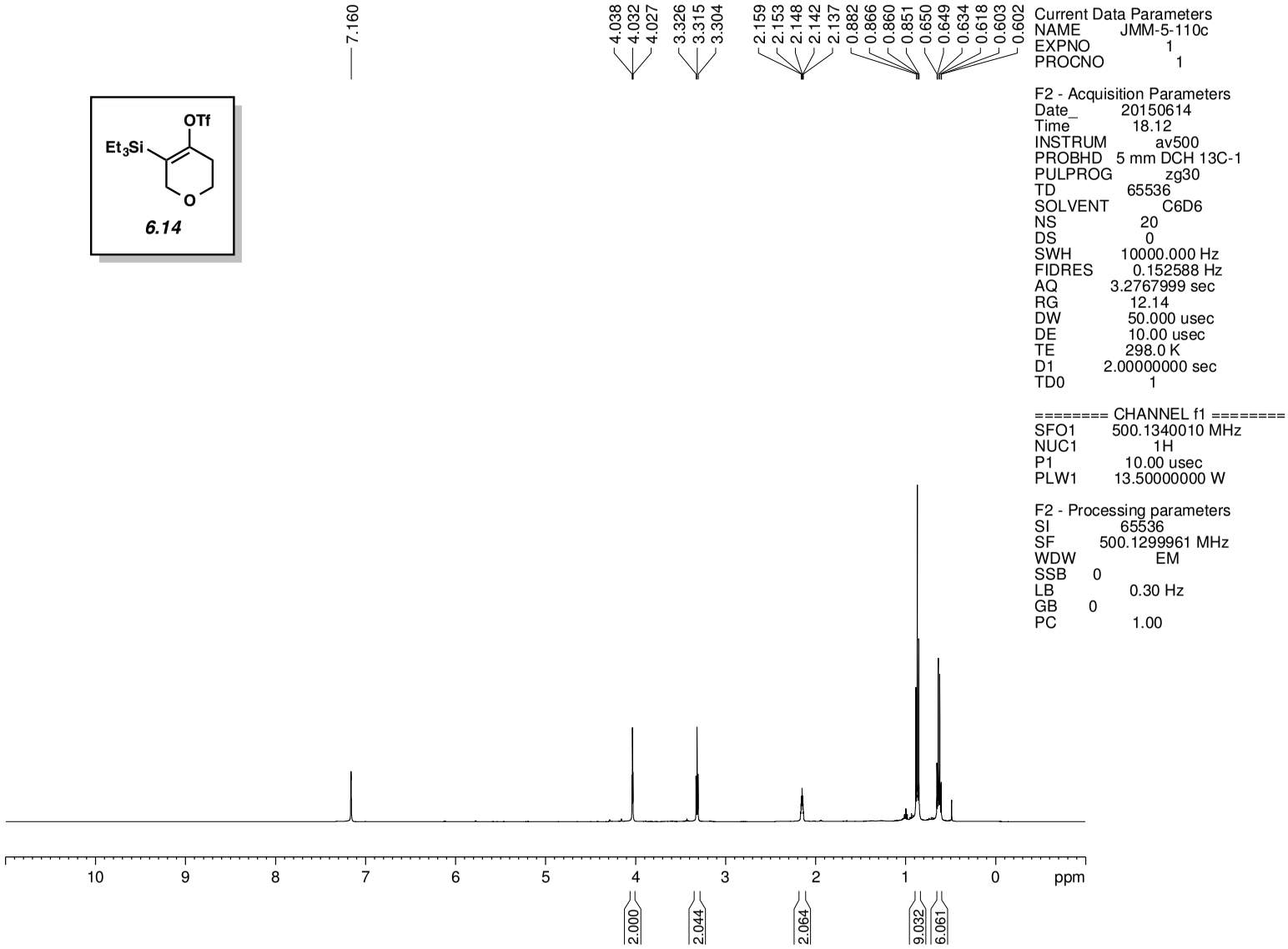

Figure 6.9. ^{1}H NMR (500 MHz, C_6D_6) compound **6.14**

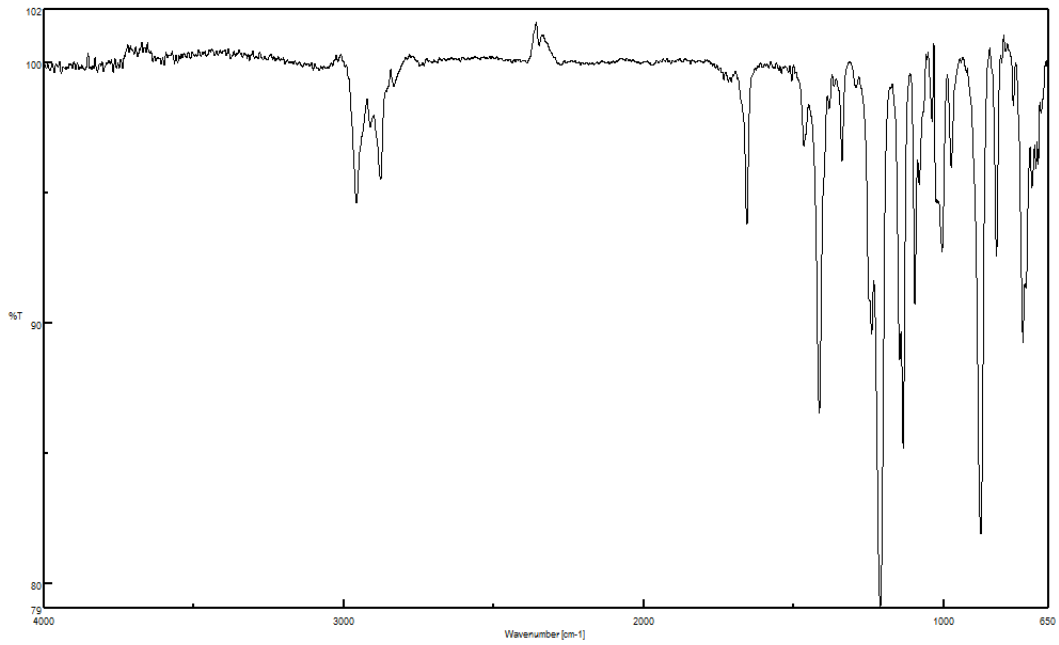

Figure 6.10. Infrared spectrum of compound **6.14**

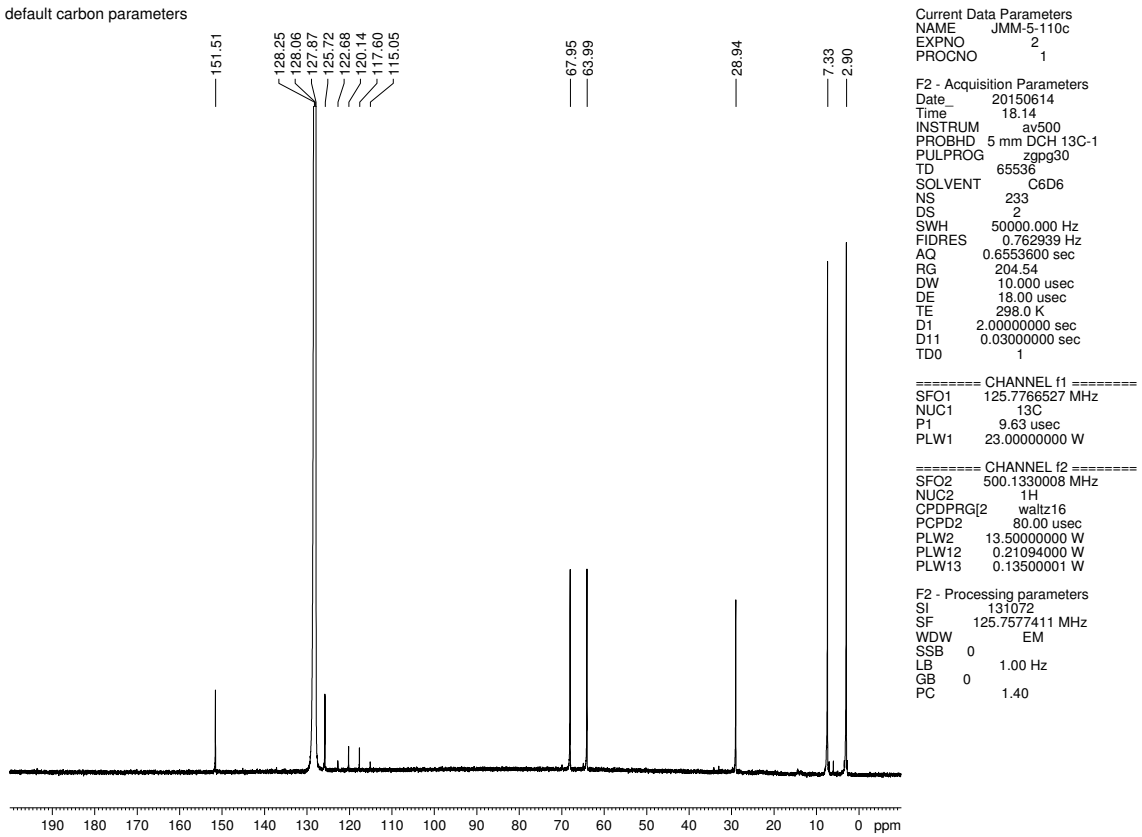

Figure 6.11. ^{13}C NMR (125 MHz, C_6D_6) of compound **6.14**

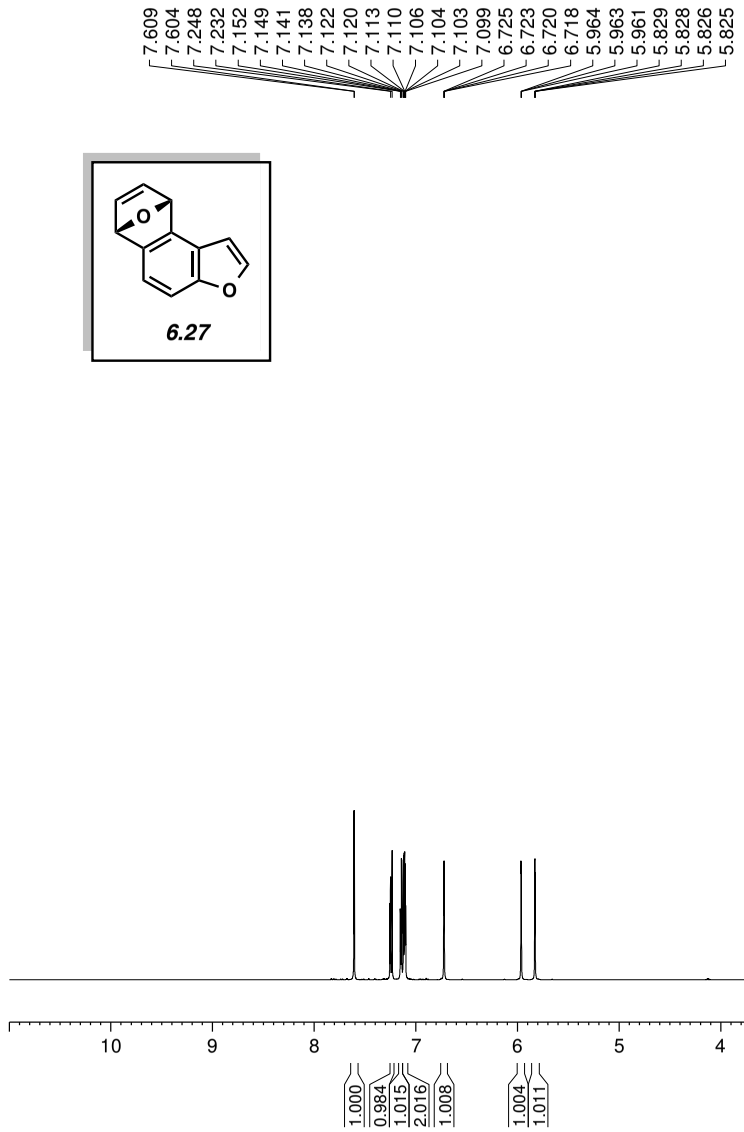

Figure 6.12. ^{1}H NMR (500 MHz, $CDCl_3$) compound **6.27**

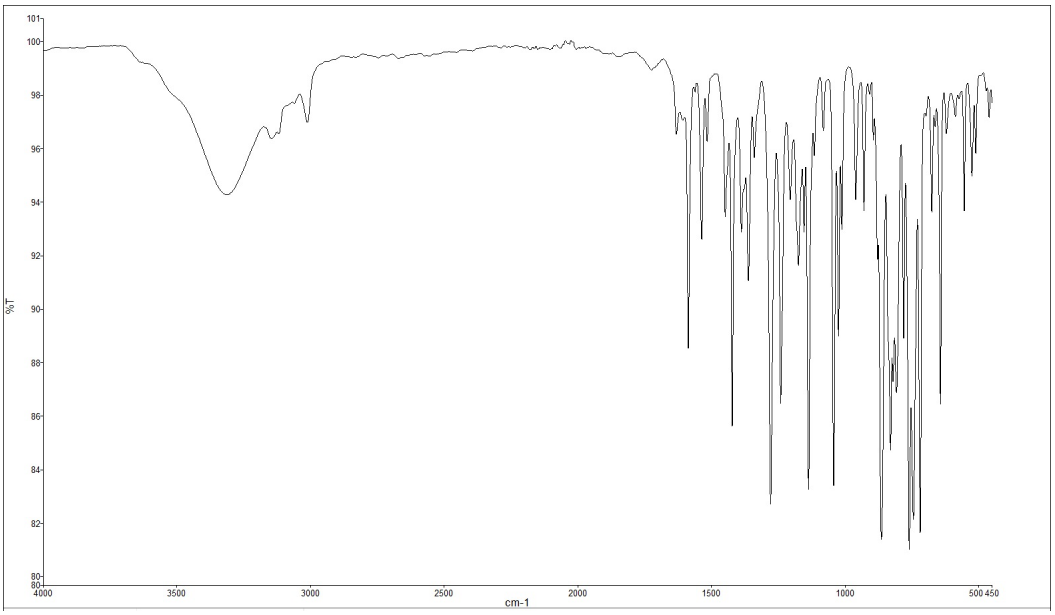

Figure 6.13. Infrared spectrum of compound **6.27**

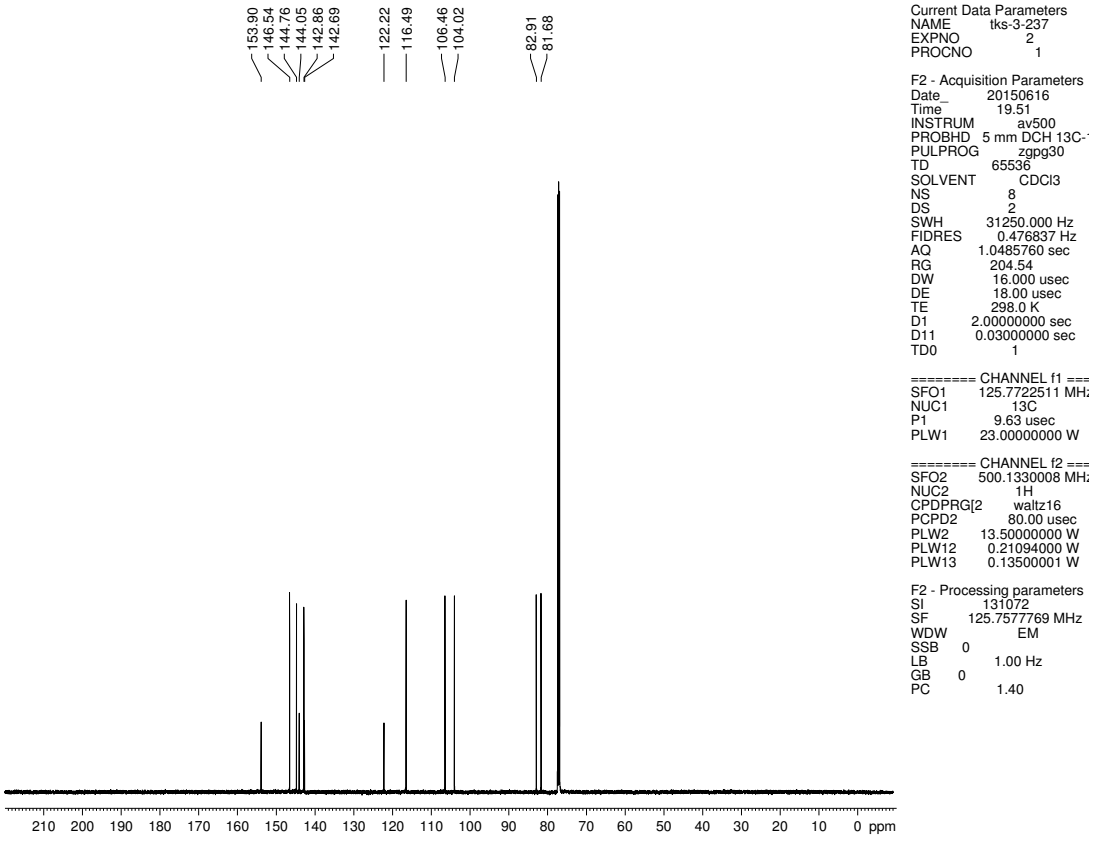

Figure 6.14. ^{13}C NMR (125 MHz, $CDCl_3$) of compound **6.27**

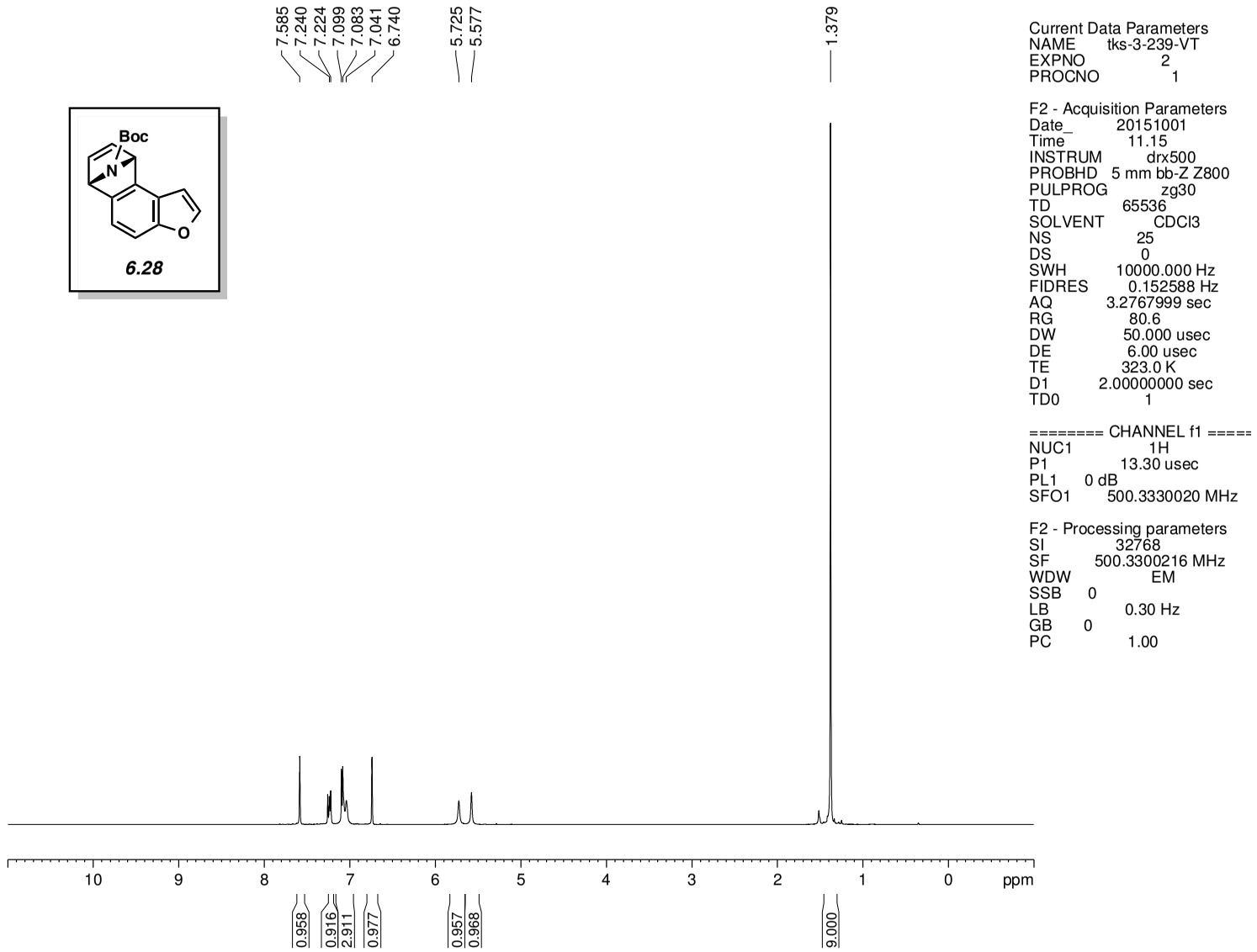

Figure 6.15. ^{1}H NMR (500 MHz, $CDCl_3$) compound **6.28**

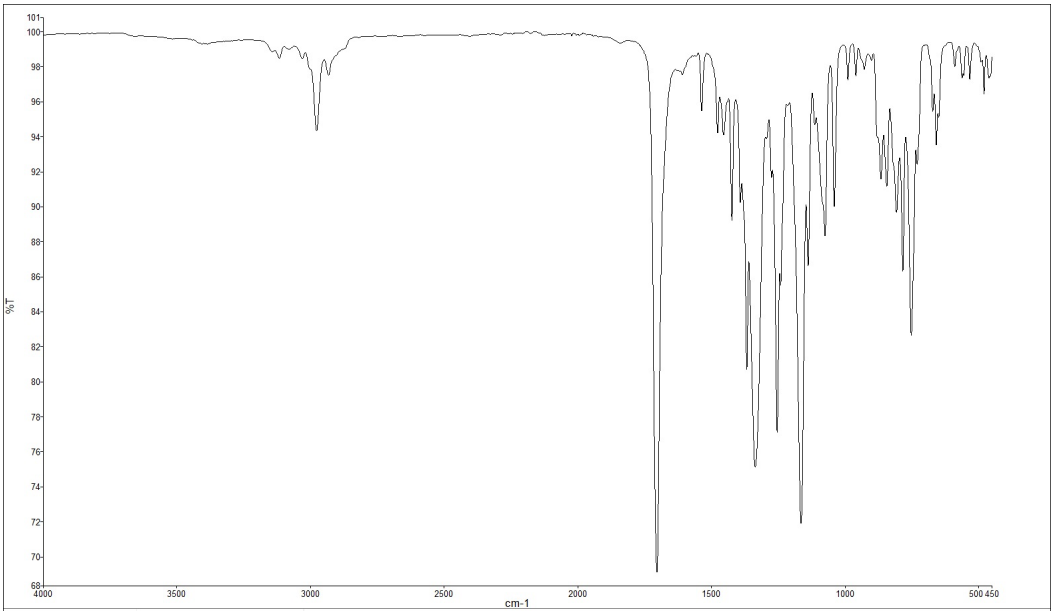

Figure 6.16. Infrared spectrum of compound **6.28**

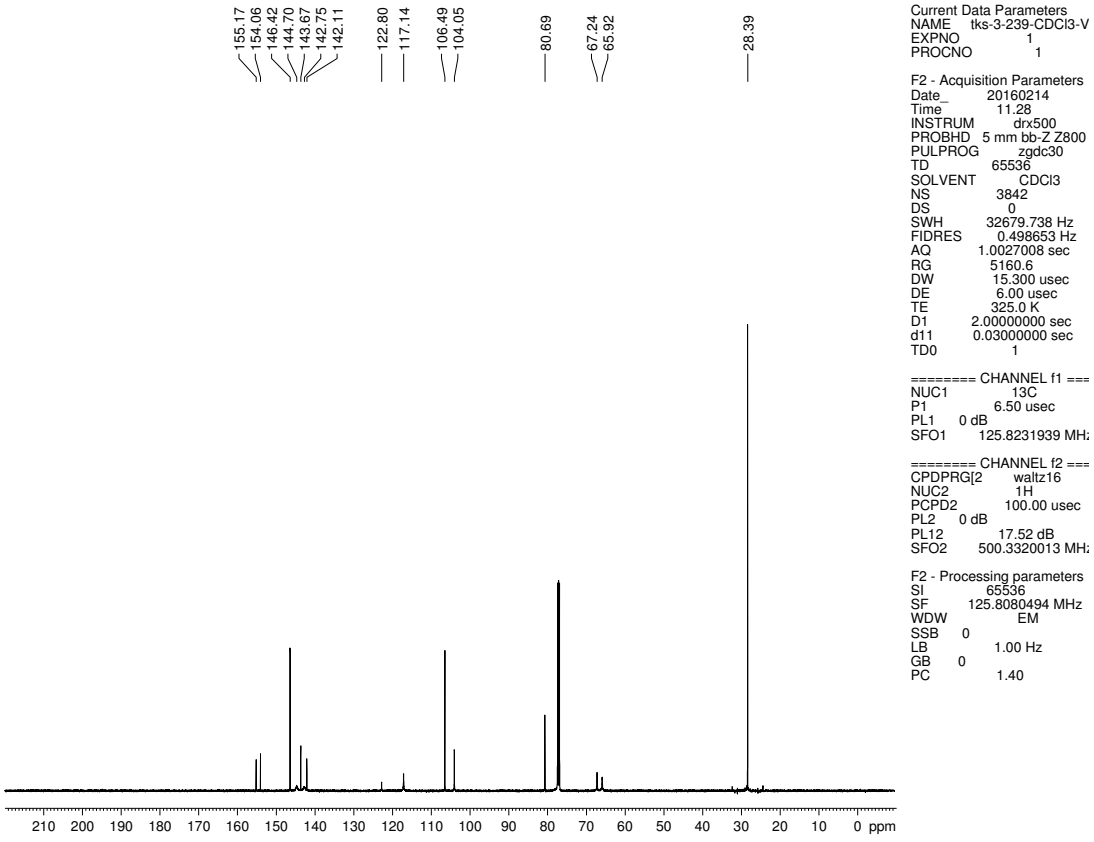

Figure 6.17. ^{13}C NMR (125 MHz, $CDCl_3$) of compound **6.28**

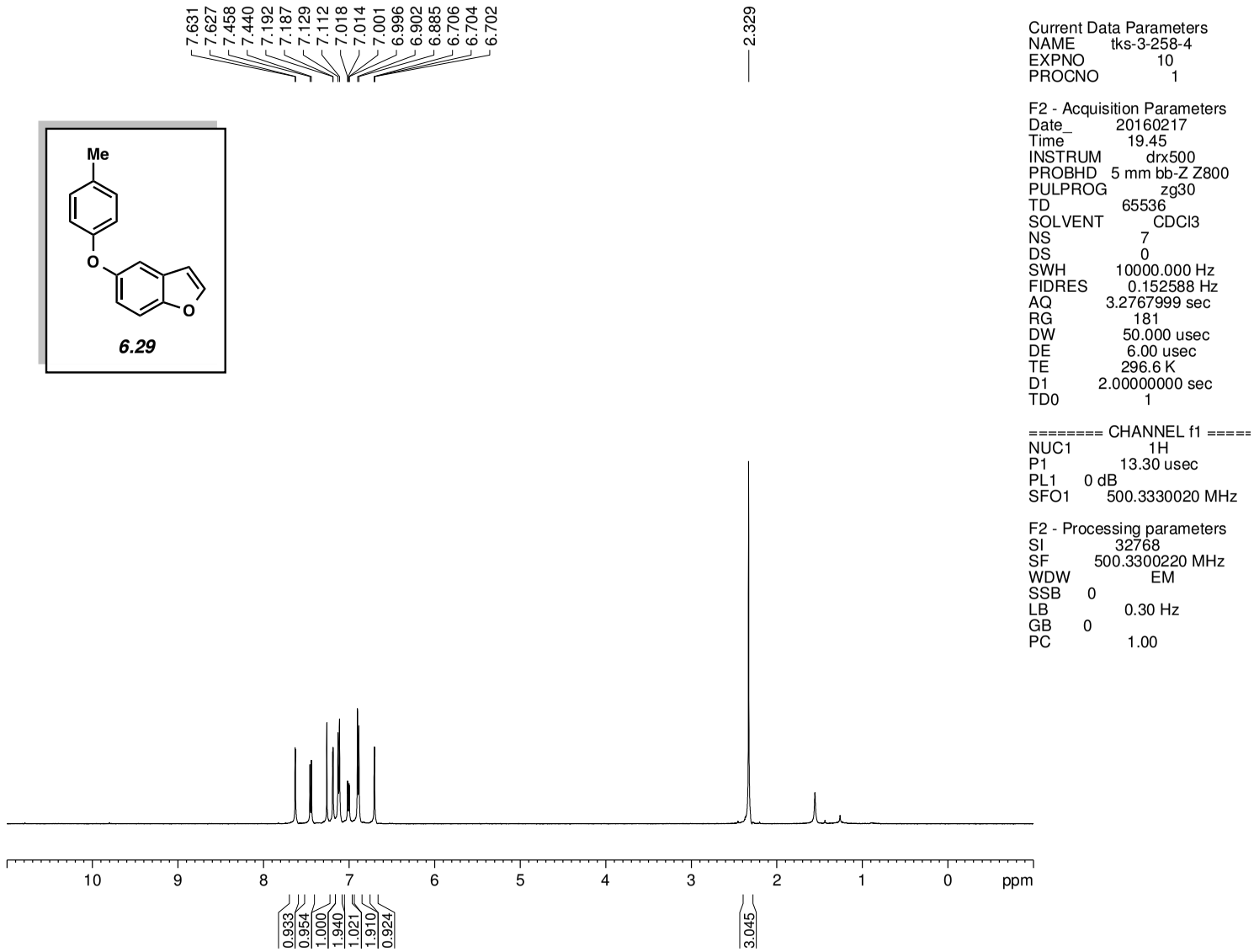

Figure 6.18. ^{1}H NMR (500 MHz, $CDCl_3$) compound **6.29**

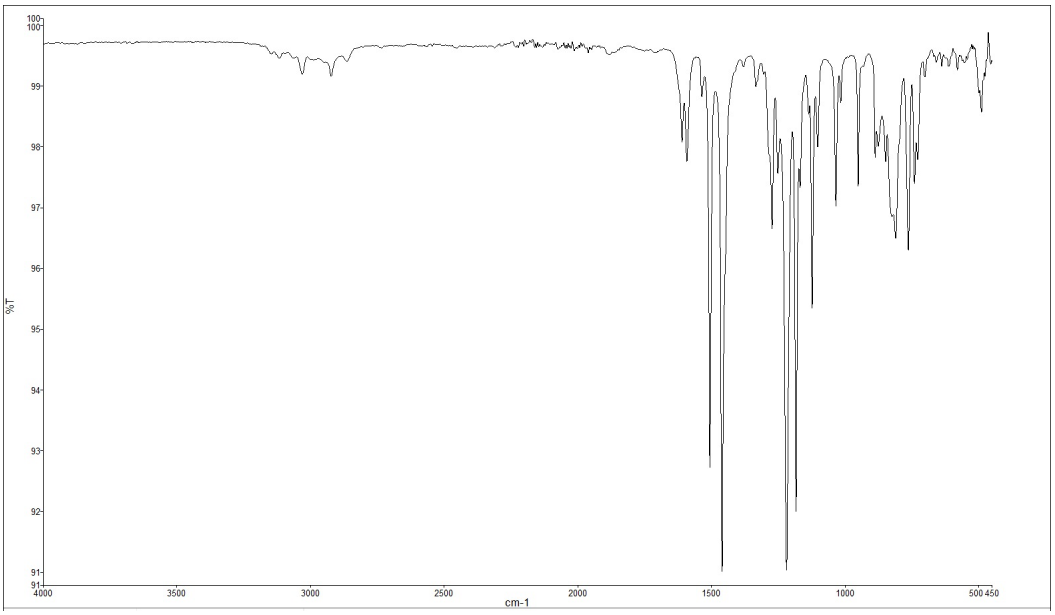

Figure 6.19. Infrared spectrum of compound **6.29**

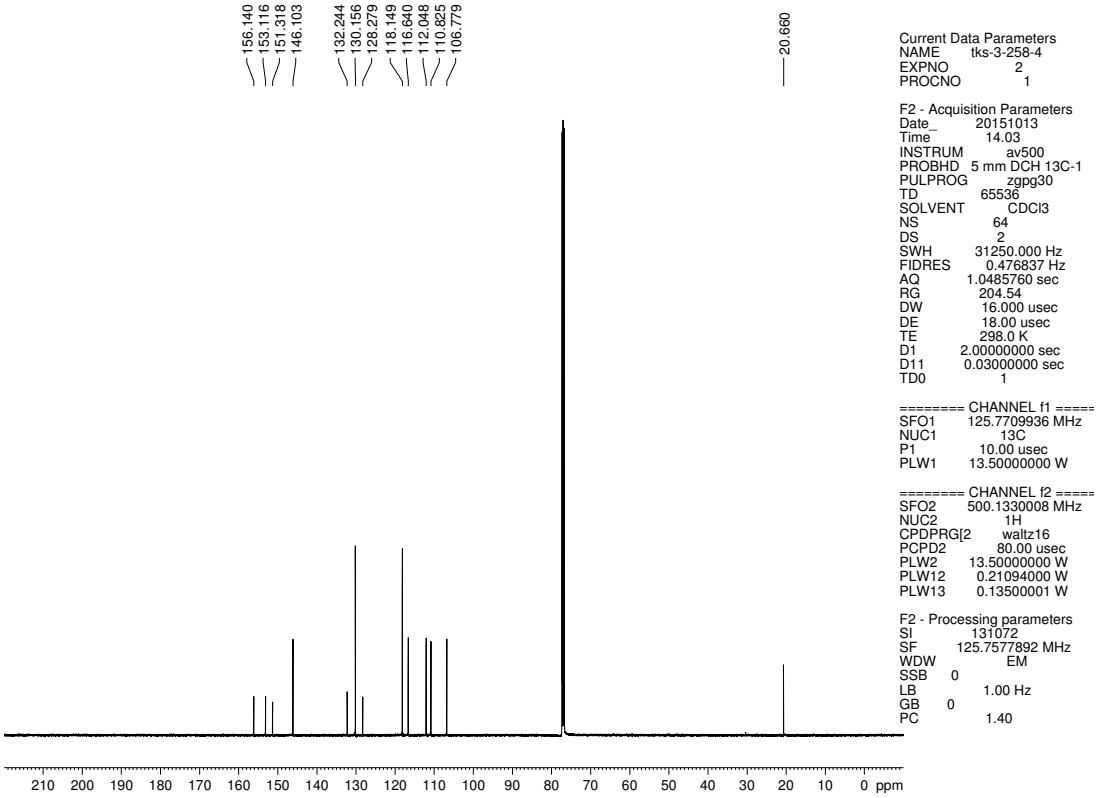

Figure 6.20. ^{13}C NMR (125 MHz, $CDCl_3$) of compound **6.29**

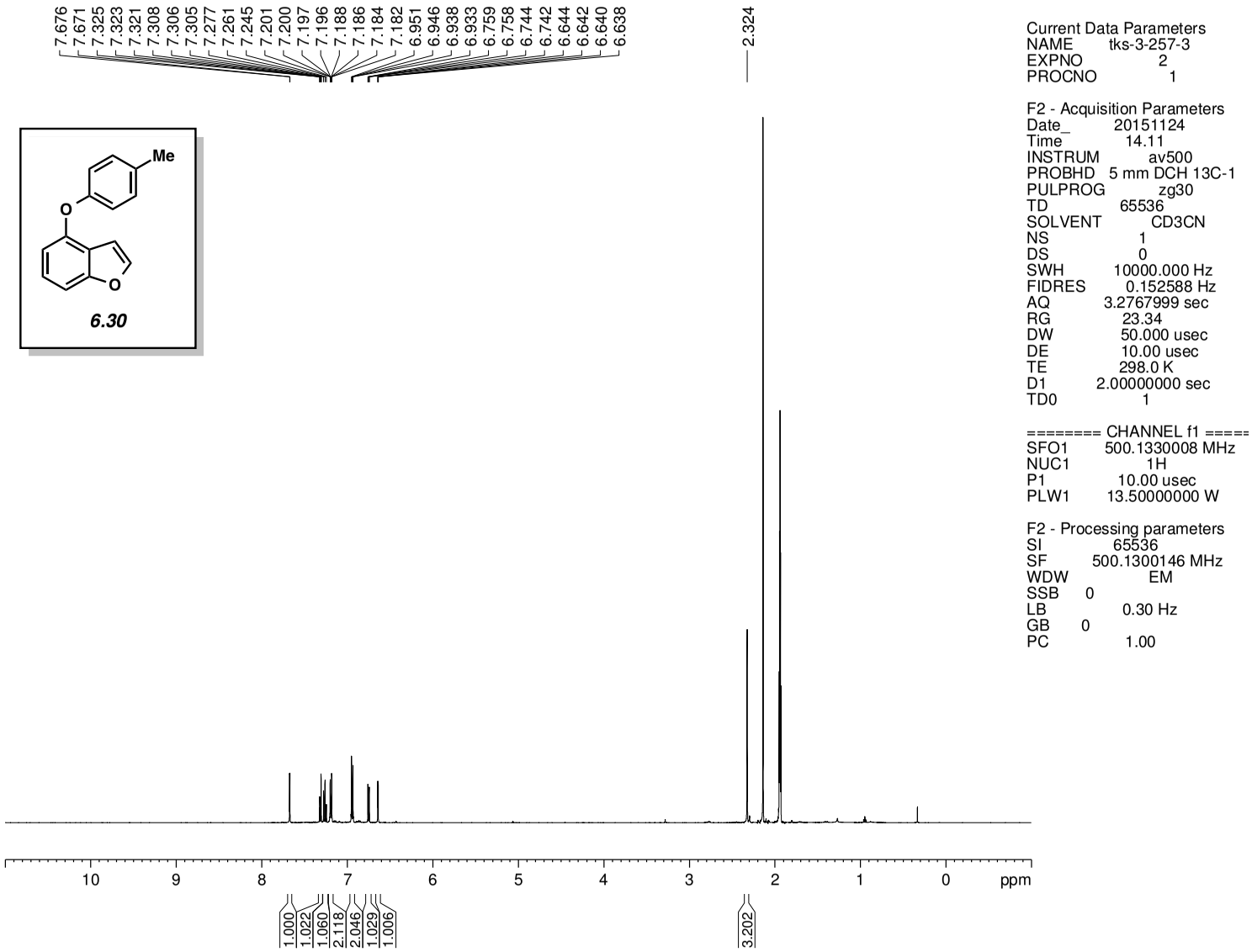

Figure 6.21. ^{1}H NMR (500 MHz, CD_3CN) compound **6.30**

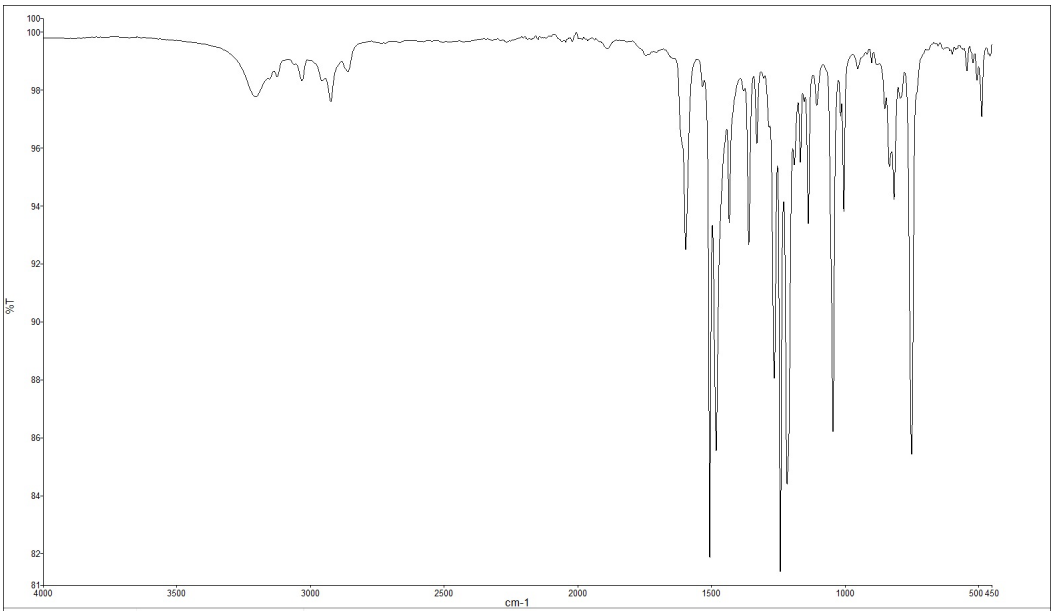

Figure 6.22. Infrared spectrum of compound **6.30**

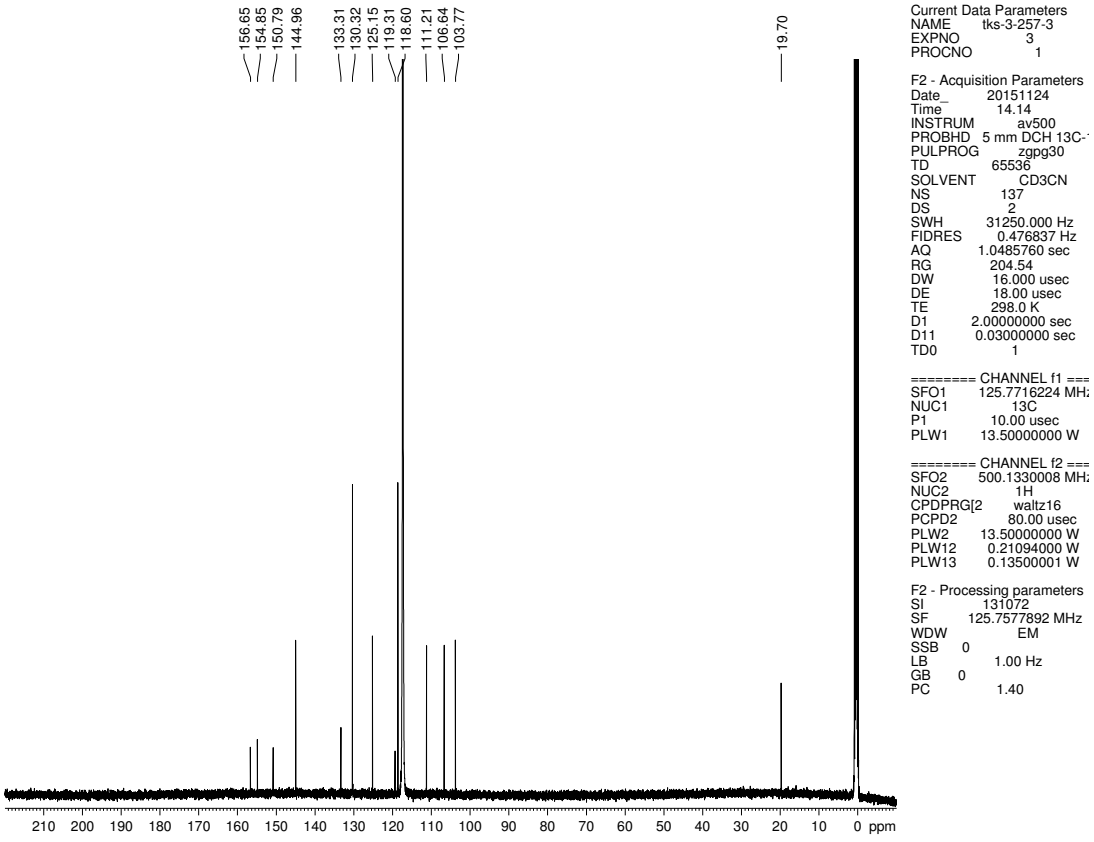

Figure 6.23. ^{13}C NMR (125 MHz, CD_3CN) of compound **6.30**

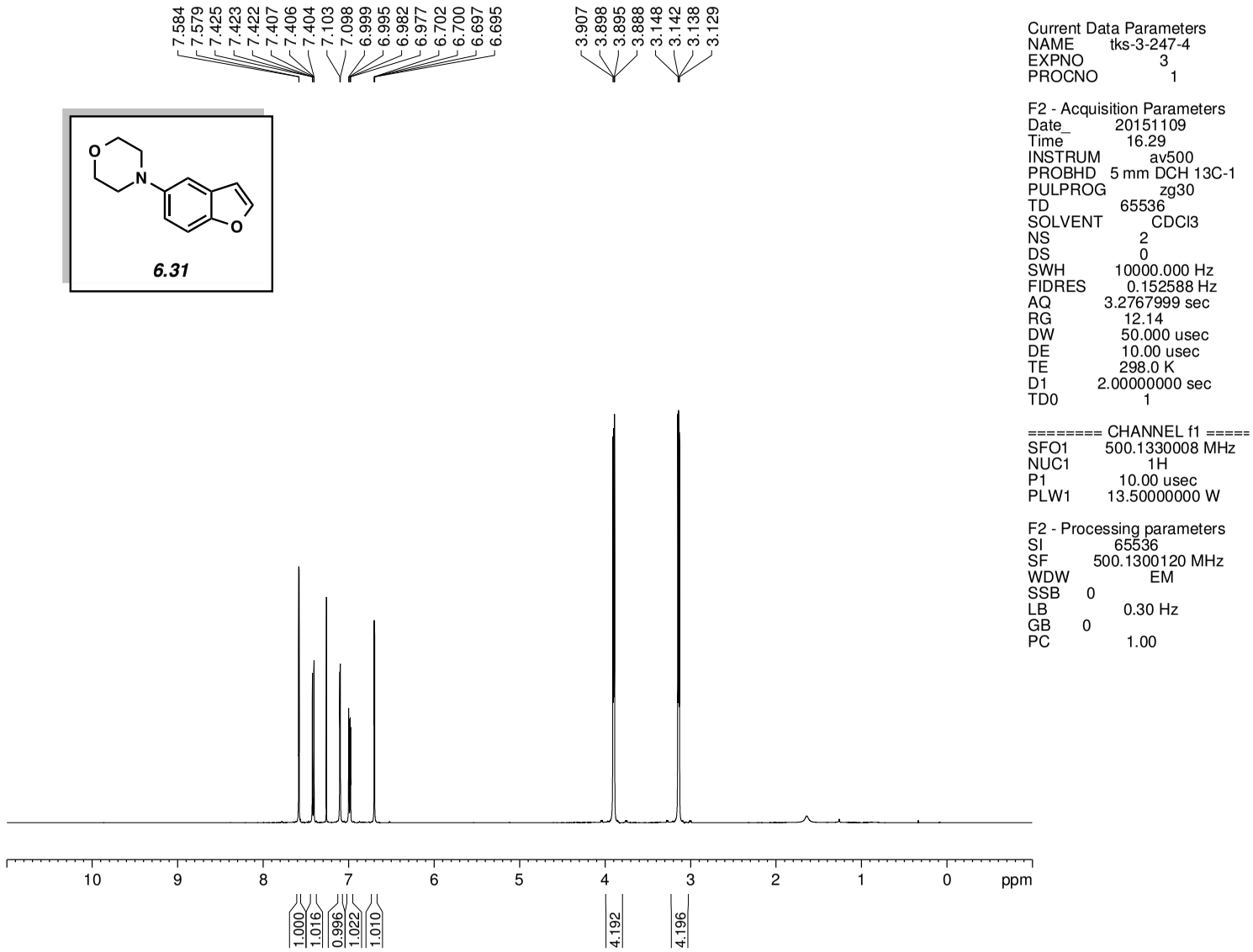

Figure 6.24. ^{1}H NMR (500 MHz, $CDCl_3$) compound **6.31**

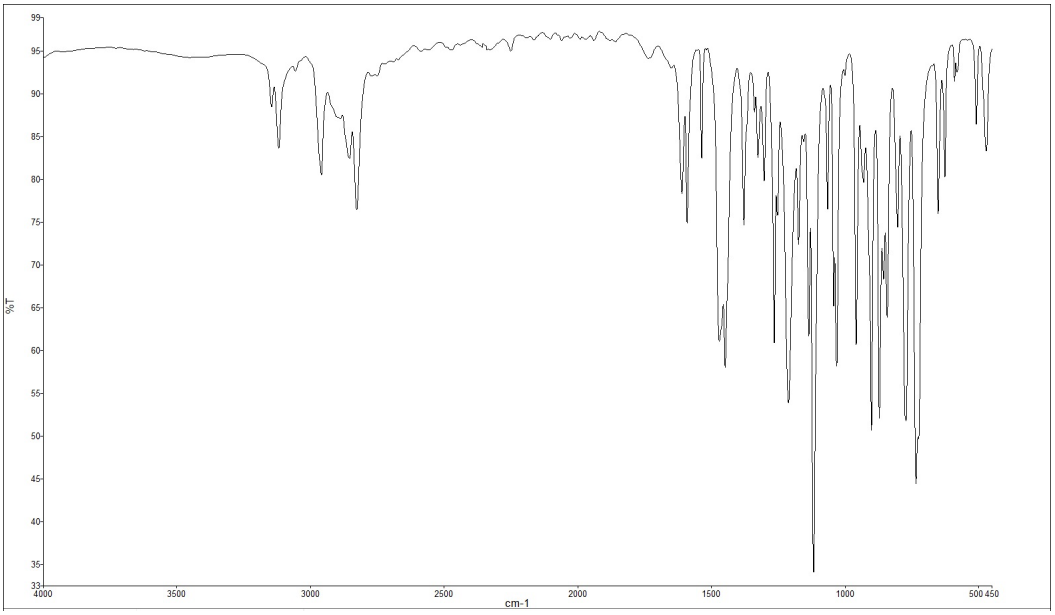

Figure 6.25. Infrared spectrum of compound **6.31**

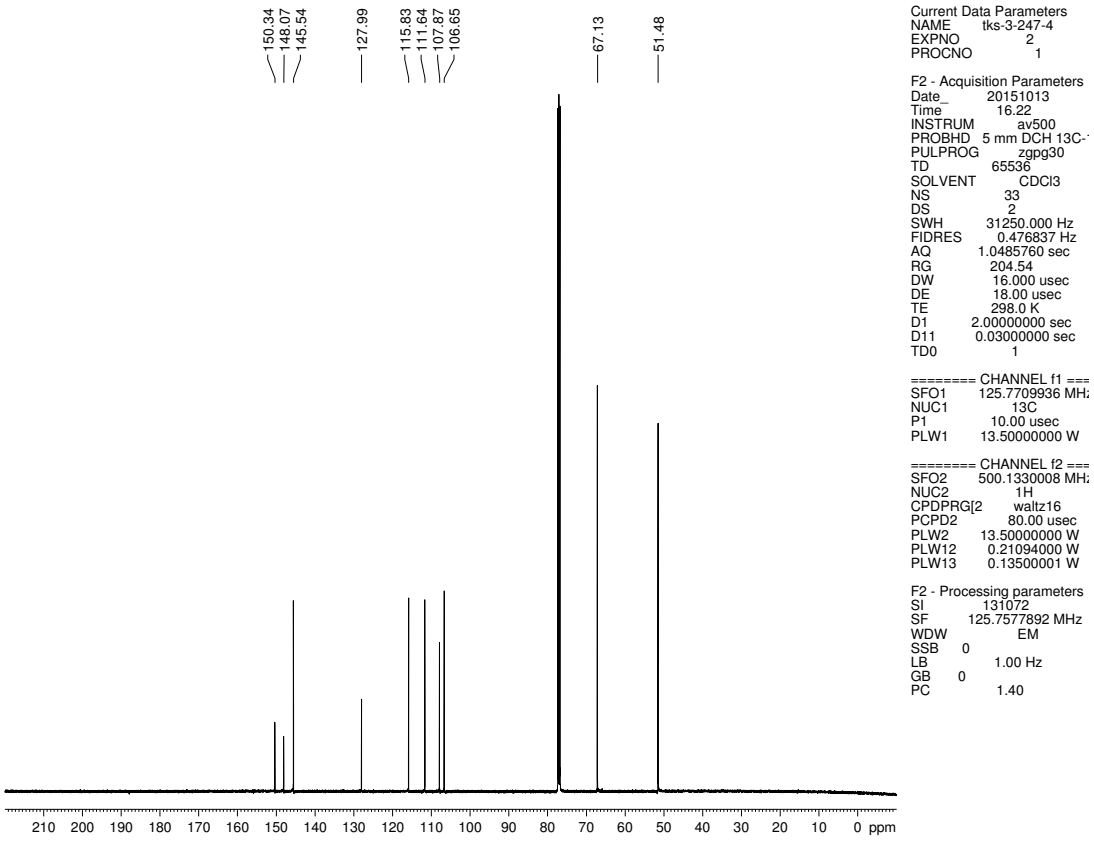

Figure 6.26. ^{13}C NMR (125 MHz, $CDCl_3$) of compound **6.31**

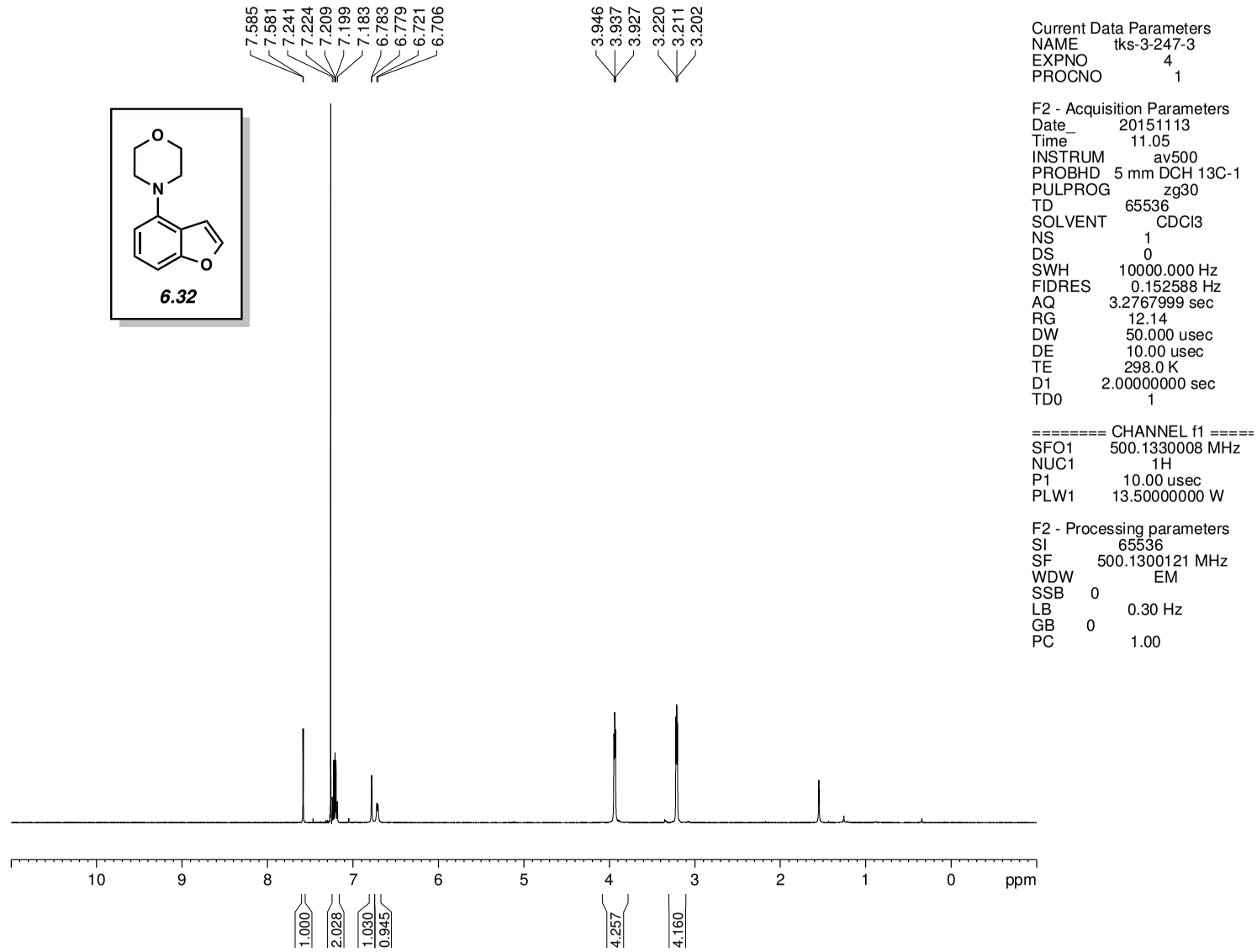

Figure 6.27. ^{1}H NMR (500 MHz, $CDCl_3$) compound **6.32**

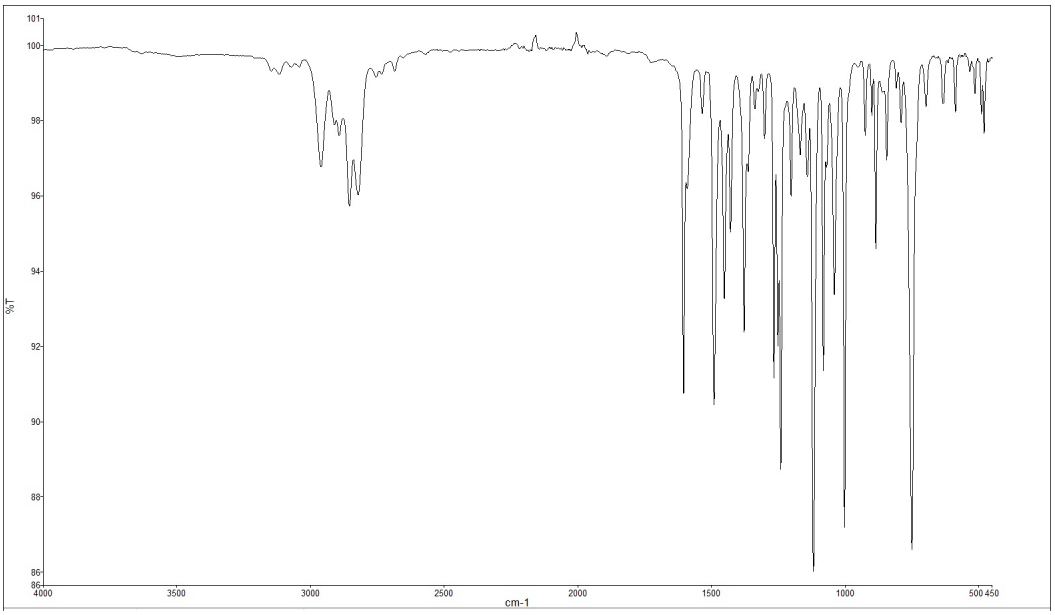

Figure 6.28. Infrared spectrum of compound **6.32**

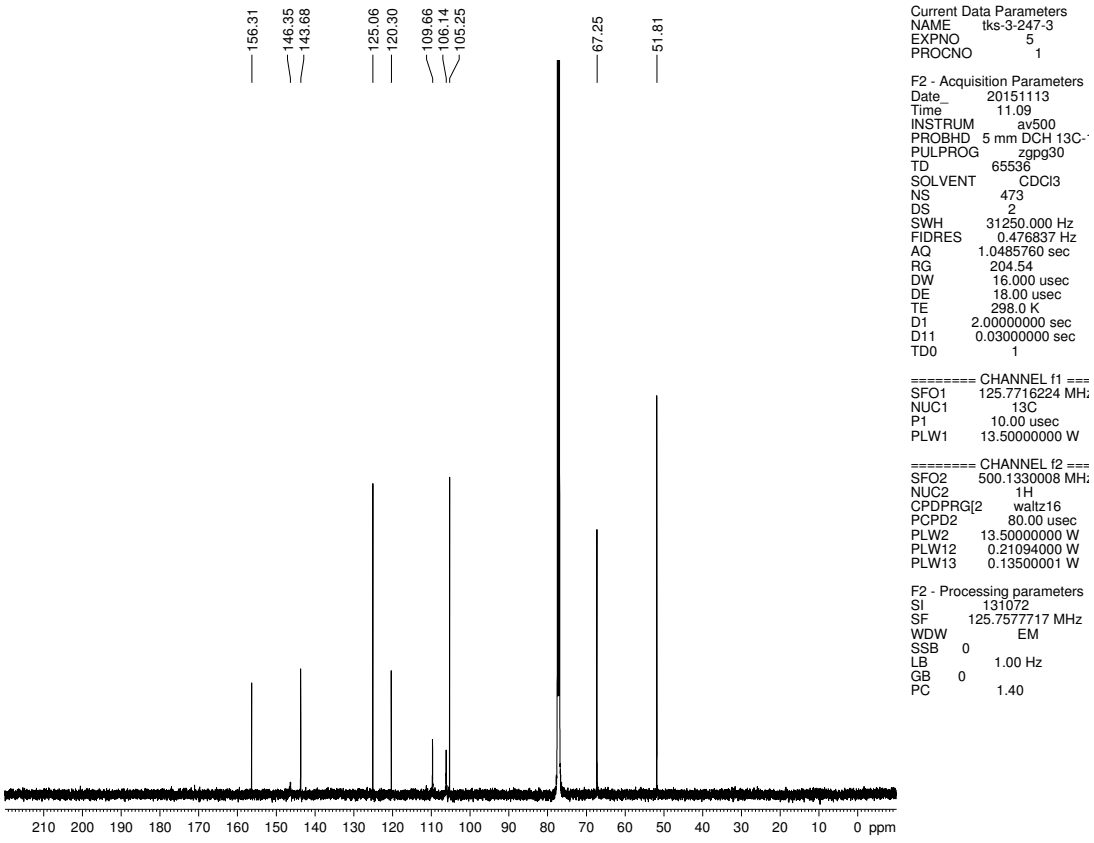

Figure 6.29. ^{13}C NMR (125 MHz, $CDCl_3$) of compound **6.32**

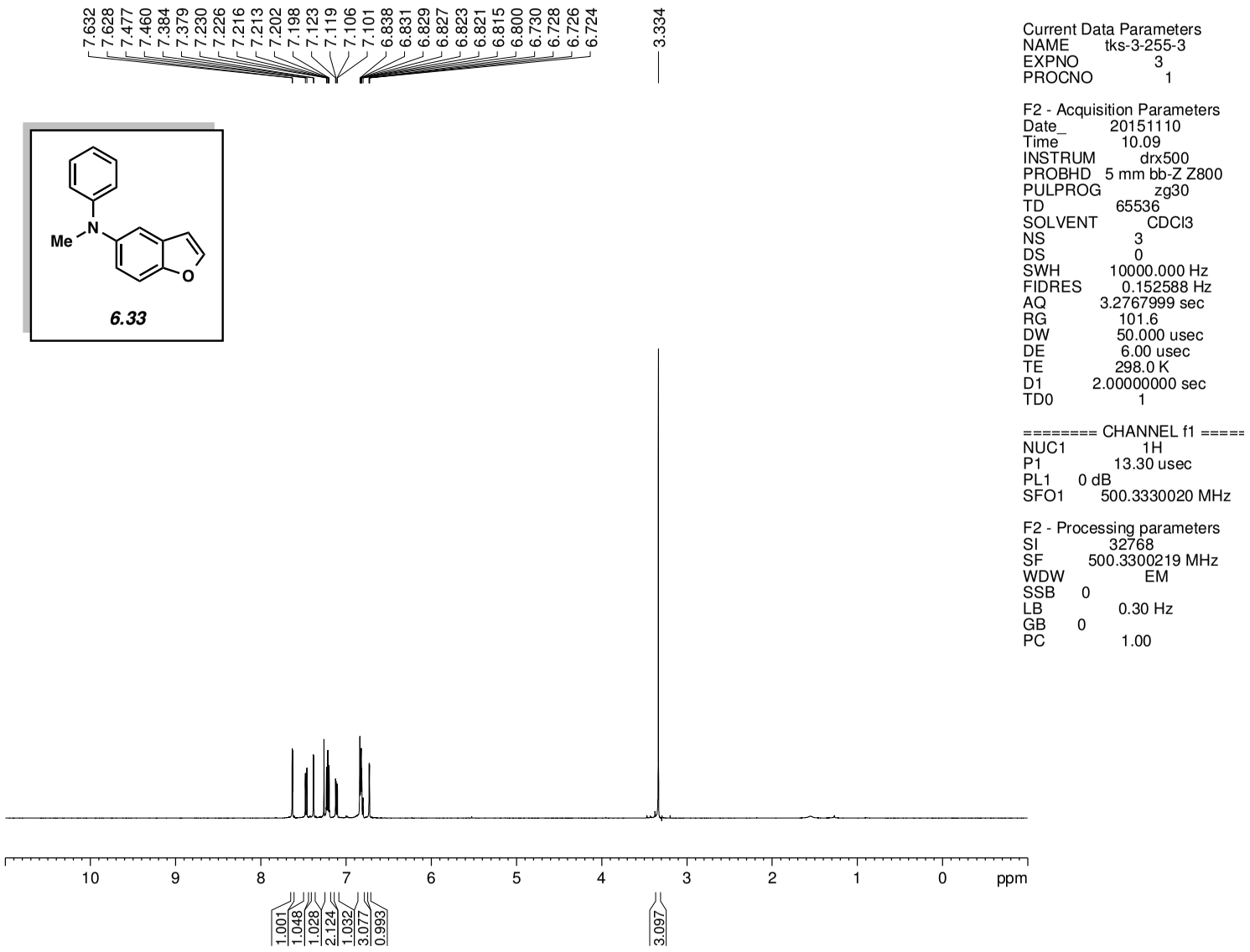

Figure 6.30. ^{1}H NMR (500 MHz, $CDCl_3$) compound **6.33**

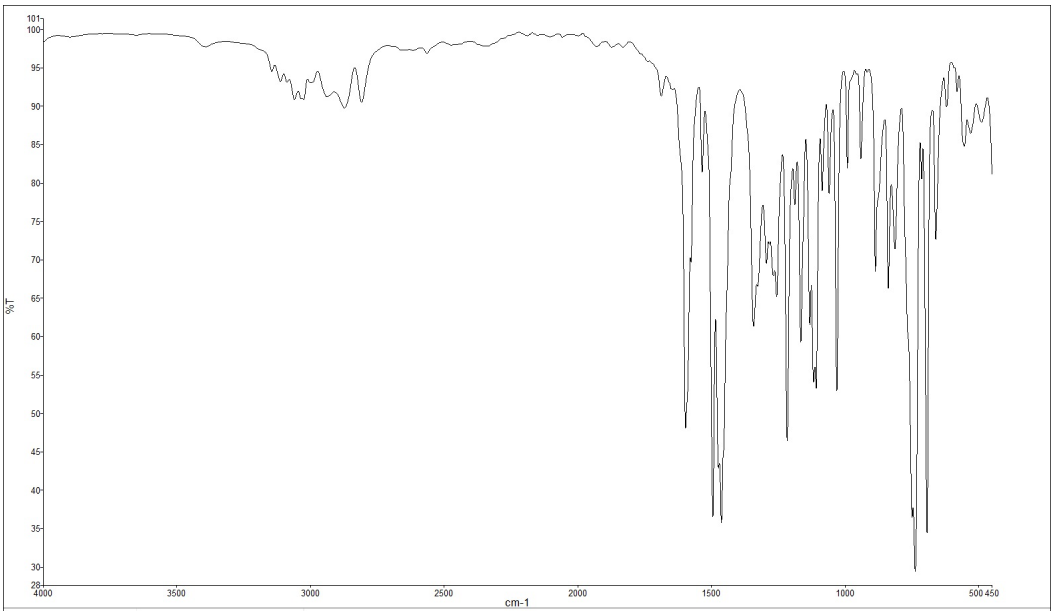

Figure 6.31. Infrared spectrum of compound **6.33**

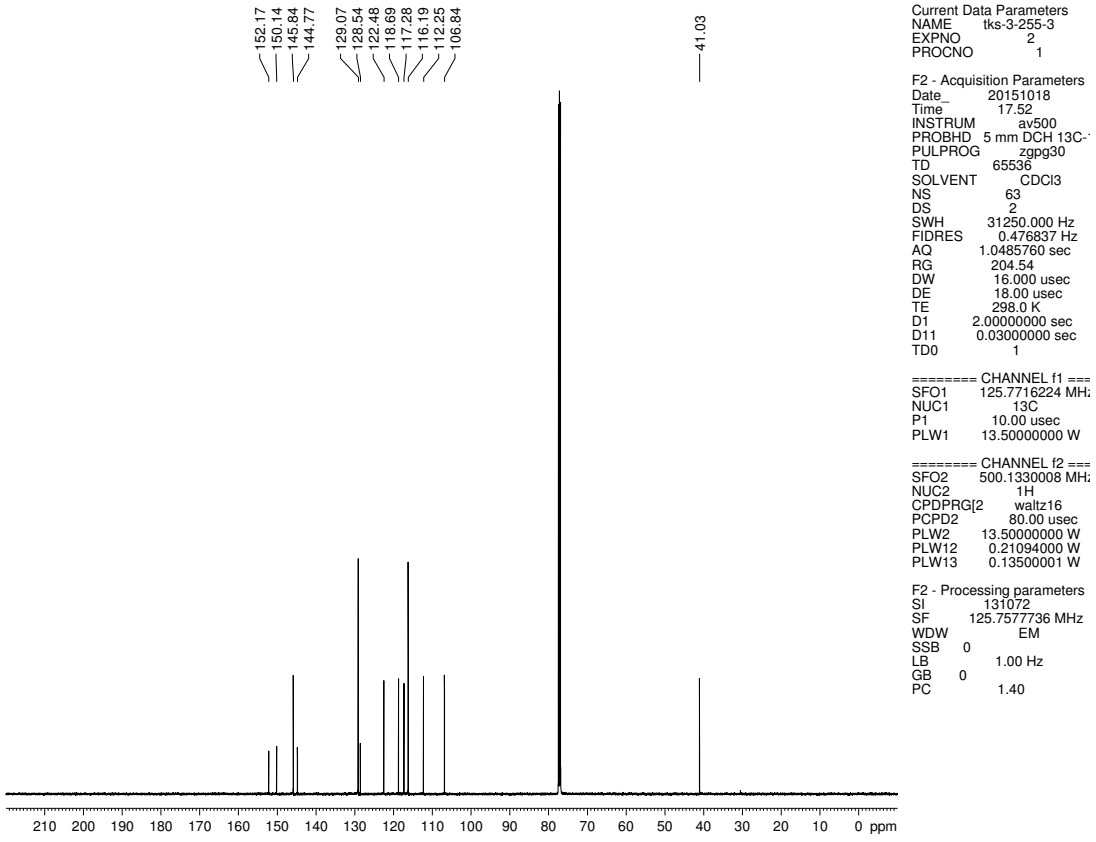

Figure 6.32. ^{13}C NMR (125 MHz, $CDCl_3$) of compound **6.33**

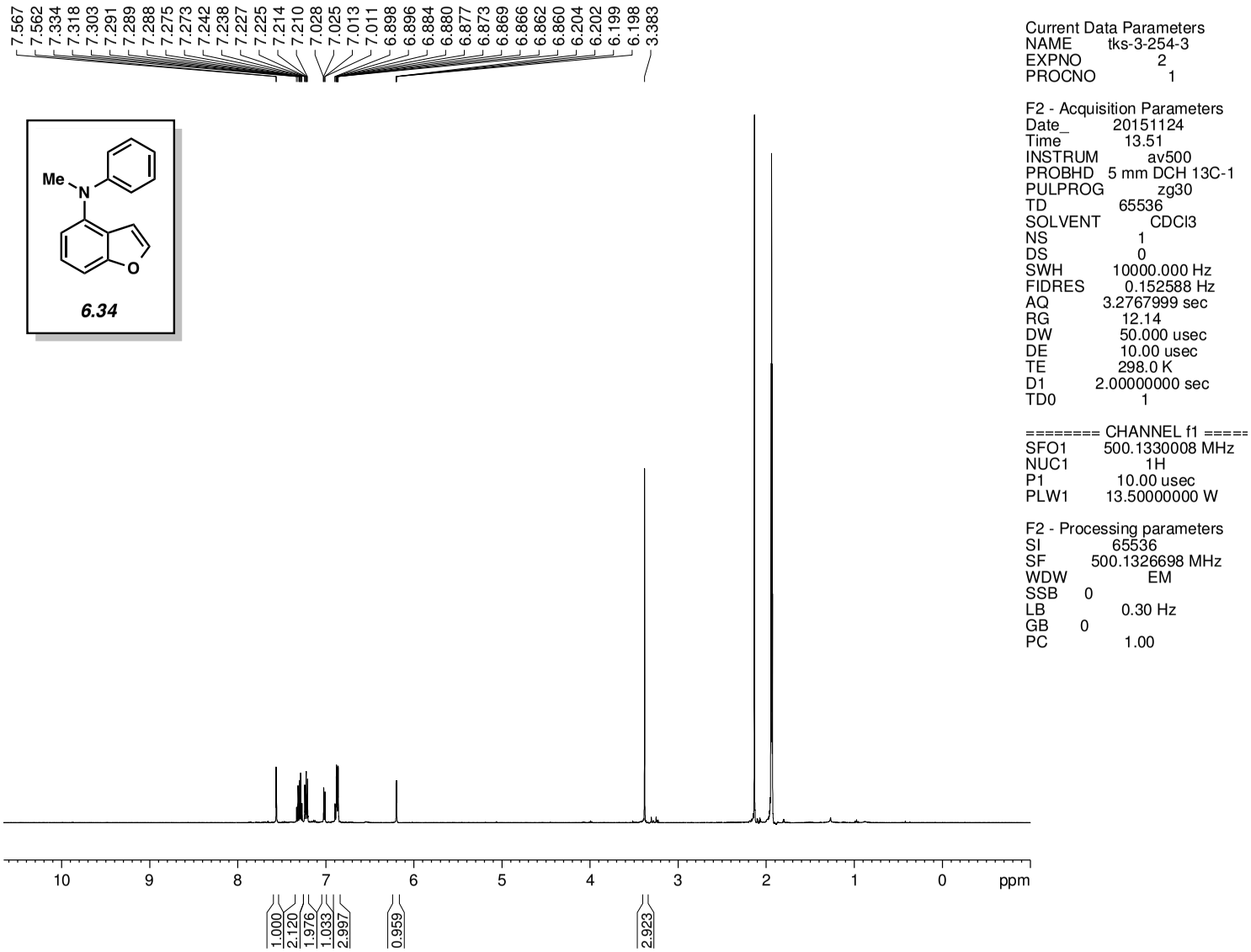

Figure 6.33. ^{1}H NMR (500 MHz, CD_3CN) compound **6.34**

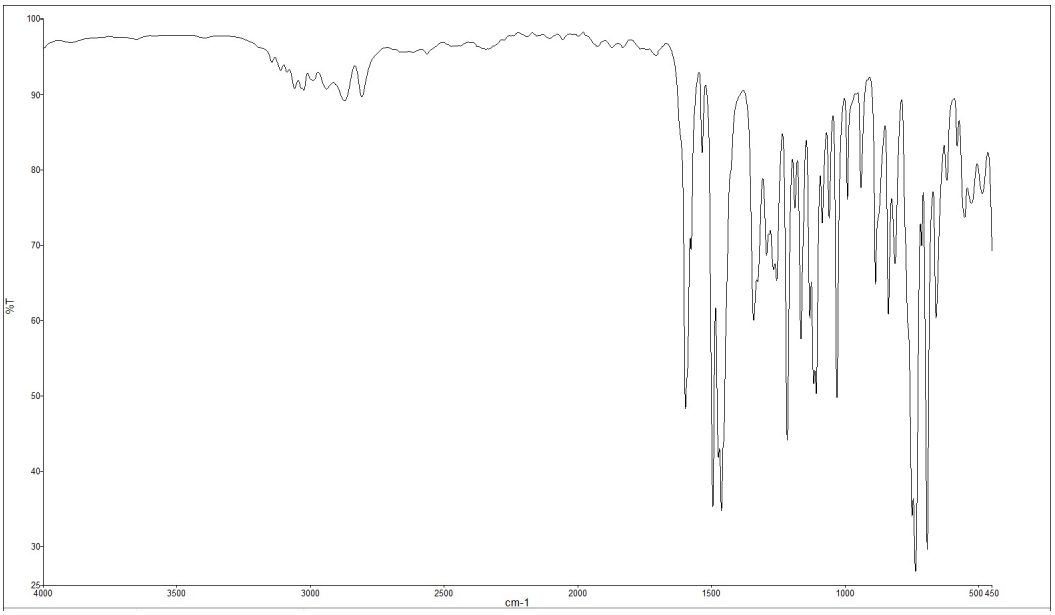

Figure 6.34. Infrared spectrum of compound **6.34**

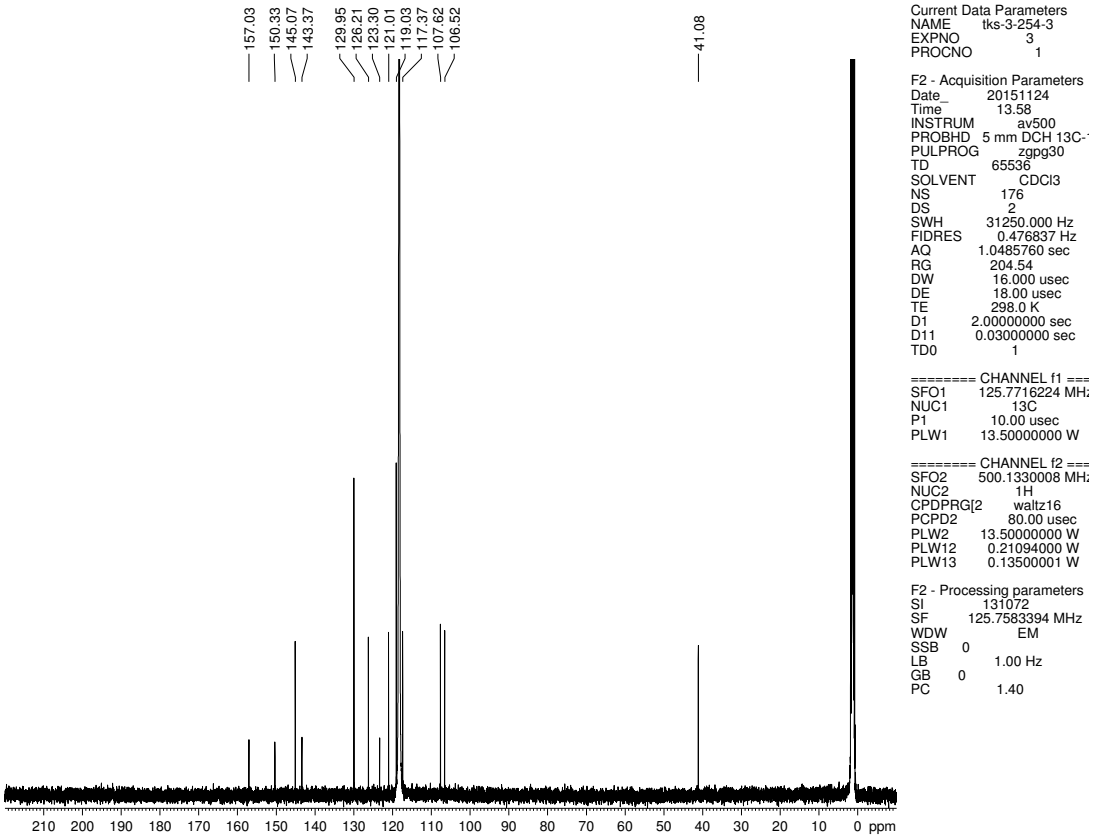

Figure 6.35. ^{13}C NMR (125 MHz, CD_3CN) of compound **6.34**

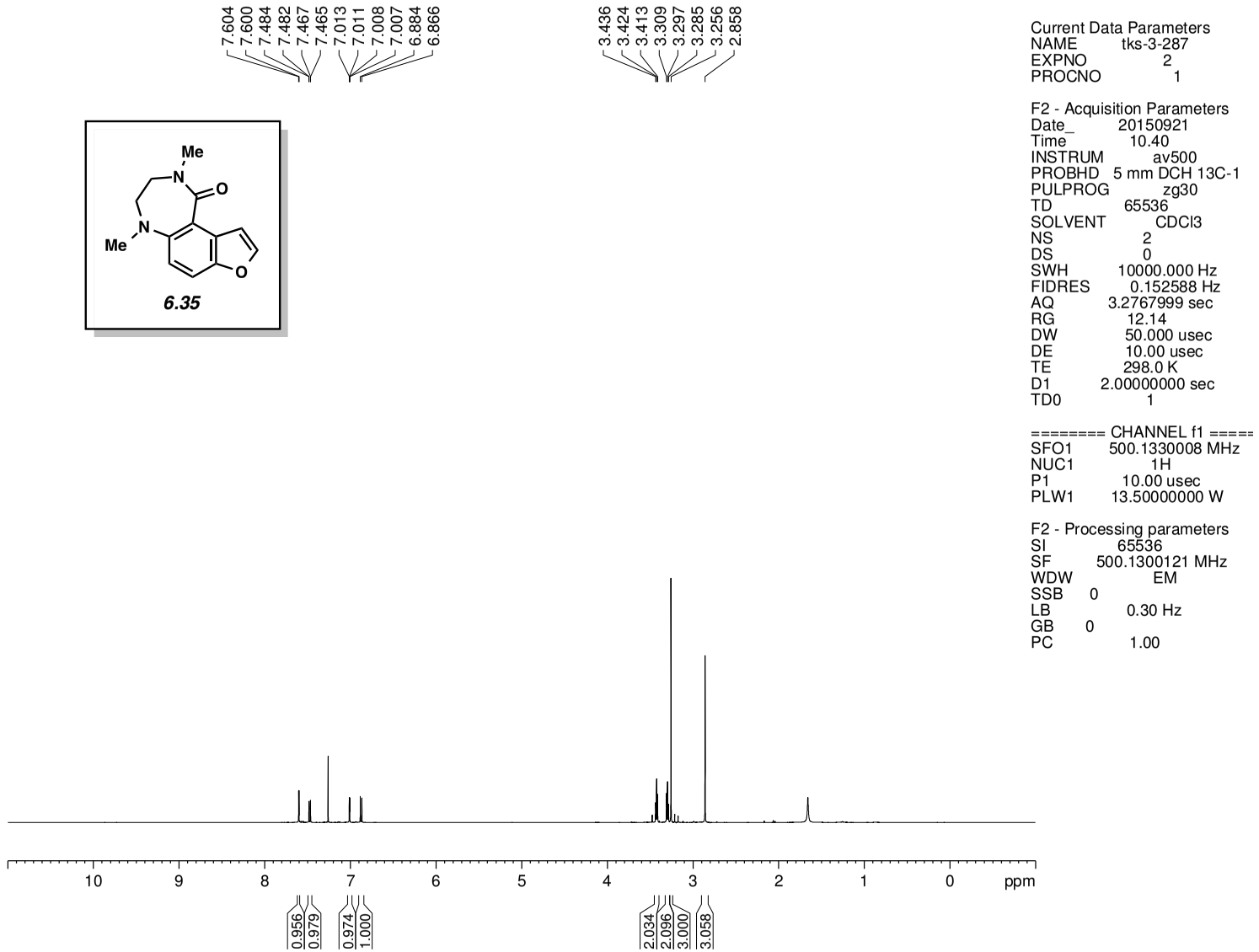

Figure 6.36. ^{1}H NMR (500 MHz, $CDCl_3$) compound **6.35**

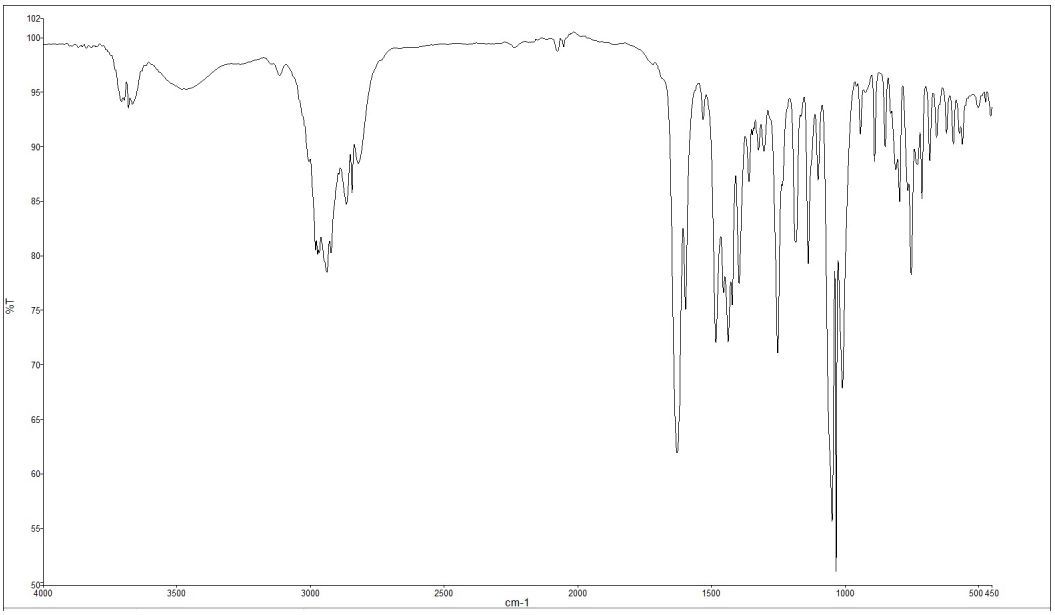

Figure 6.37. Infrared spectrum of compound **6.35**

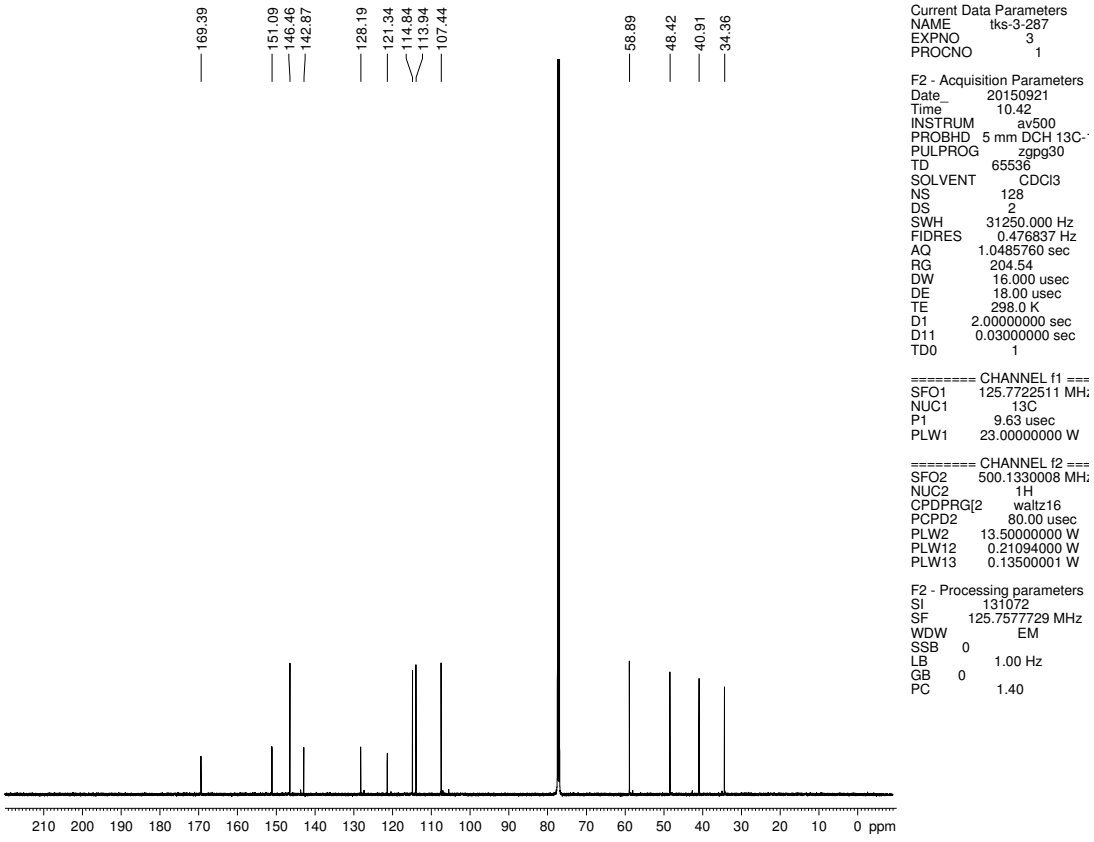

Figure 6.38. ^{13}C NMR (125 MHz, $CDCl_3$) of compound **6.35**

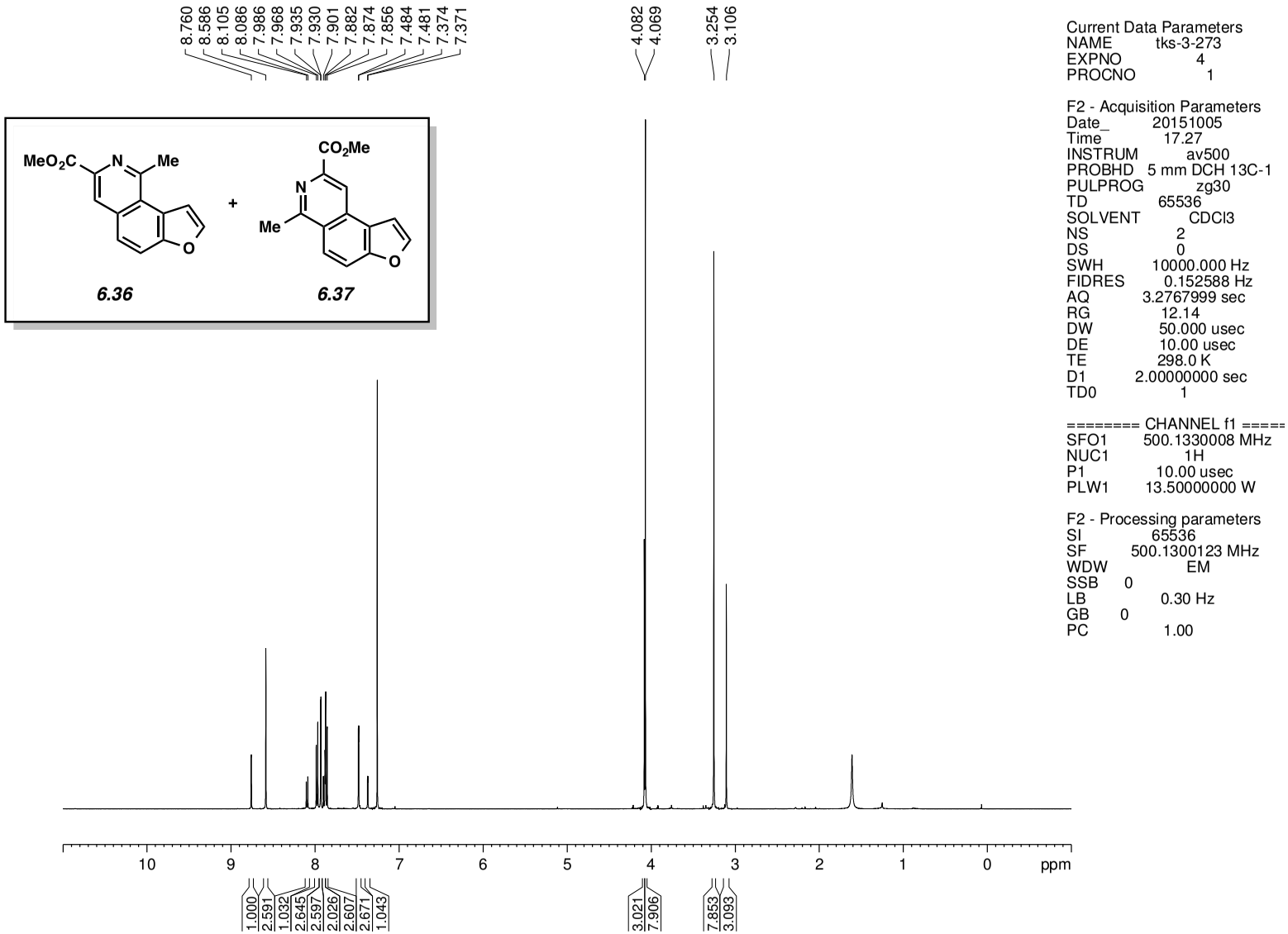

Figure 6.39. ^{1}H NMR (500 MHz, $CDCl_3$) compounds **6.36** & **6.37**

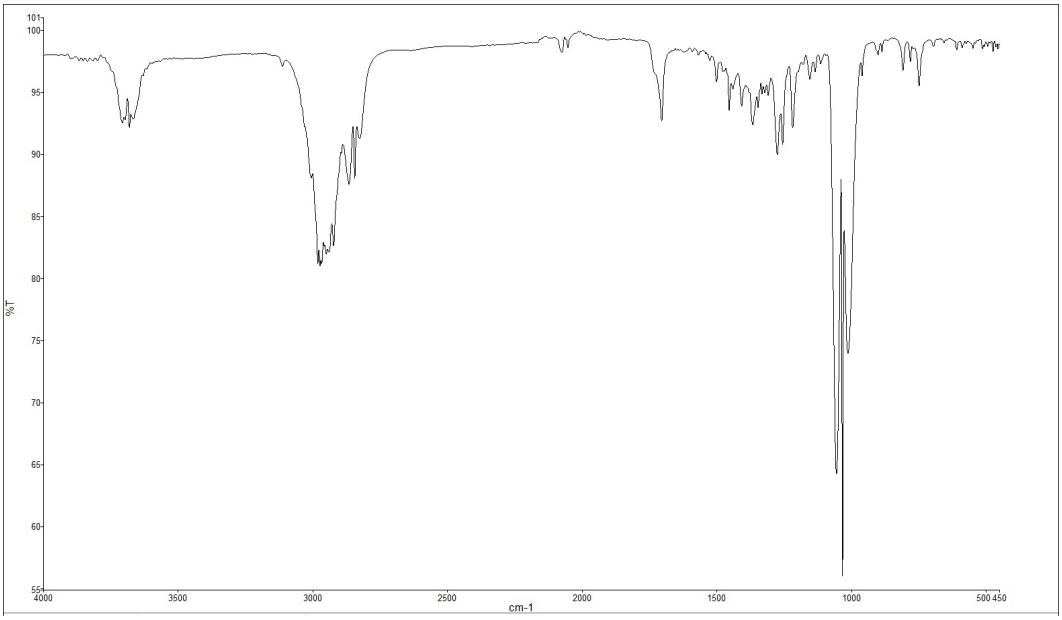

Figure 6.40. Infrared spectrum of compounds **6.36** & **6.37**

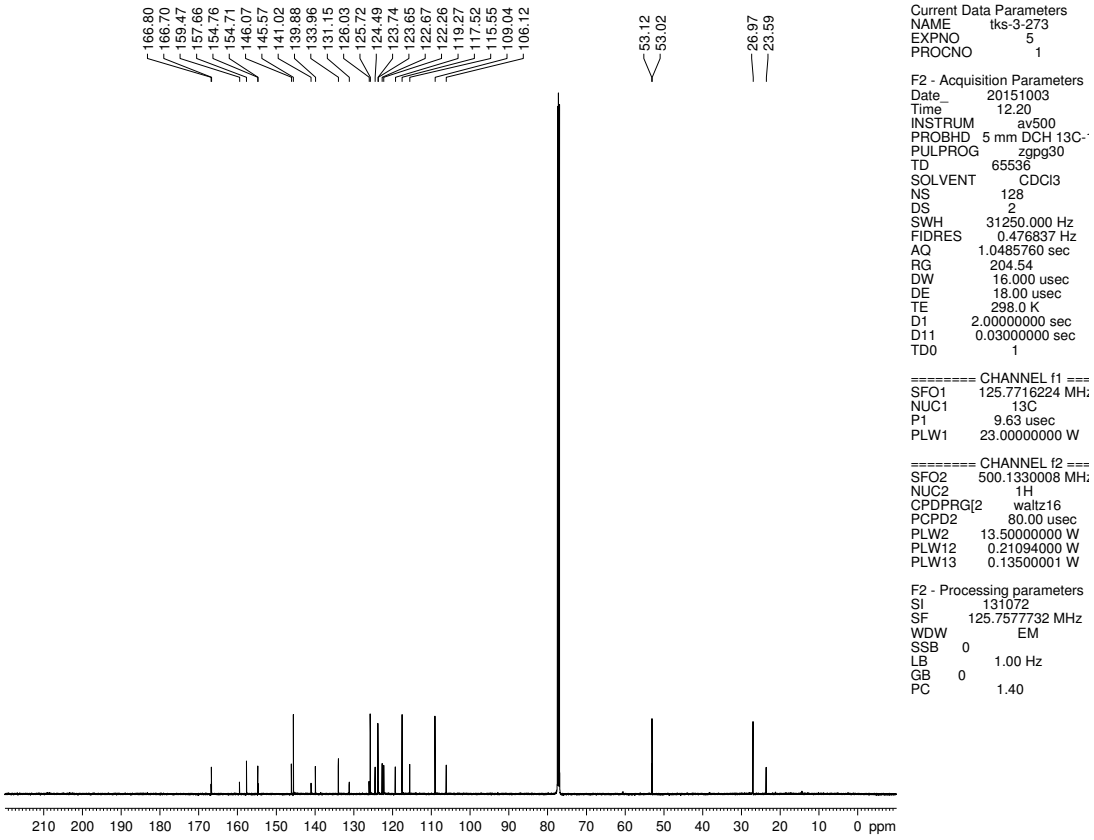

Figure 6.41. ^{13}C NMR (125 MHz, $CDCl_3$) of compounds **6.36** & **6.37**

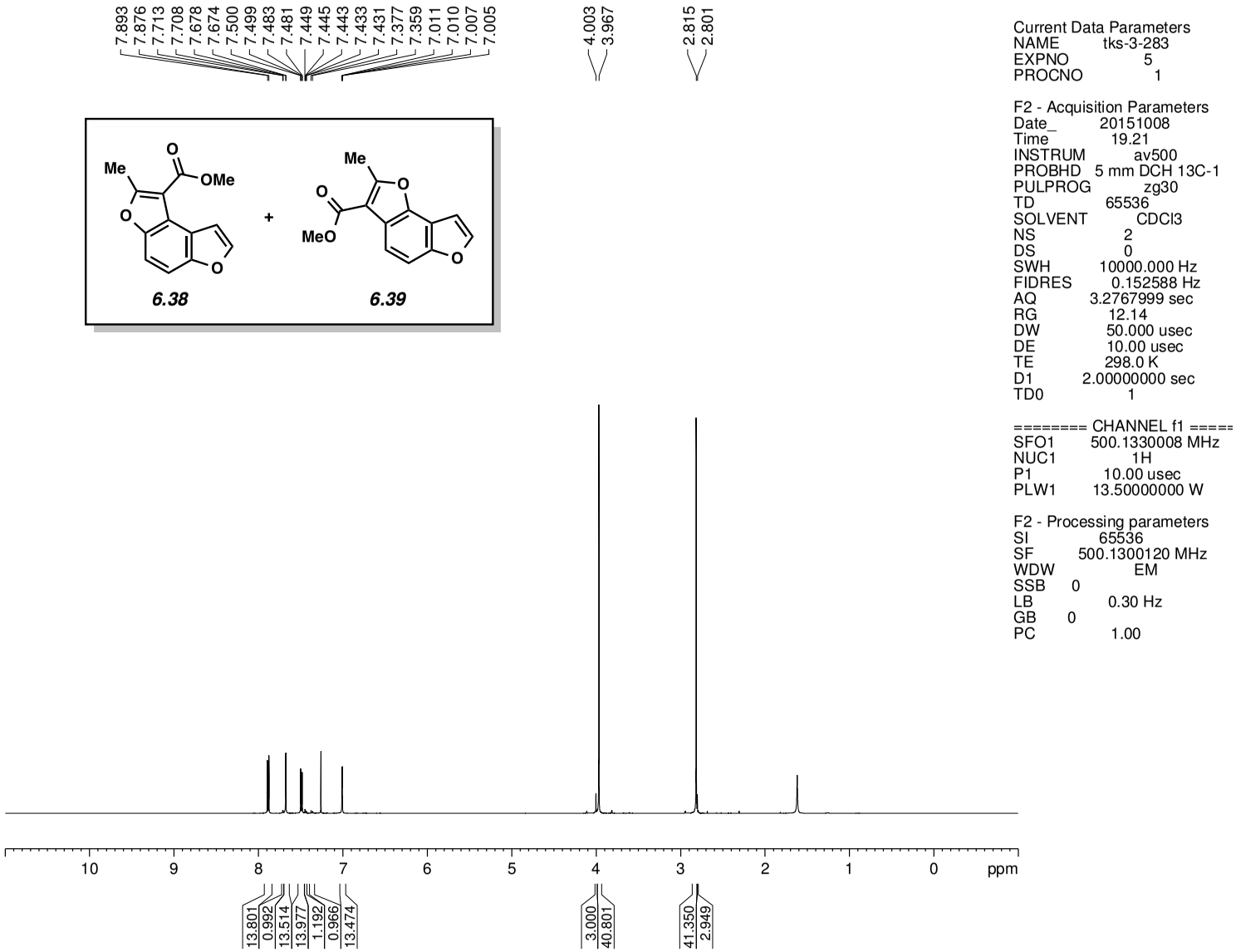

Figure 6.42. ^{1}H NMR (500 MHz, $CDCl_3$) compounds **6.38** & **6.39**

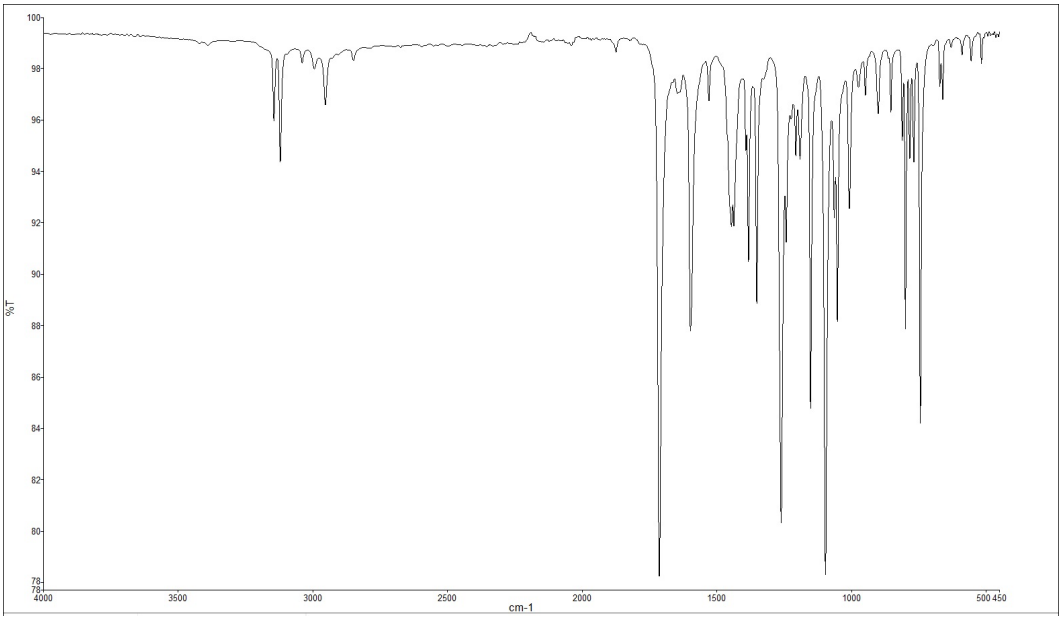

Figure 6.43. Infrared spectrum of compound **6.38** & **6.39**

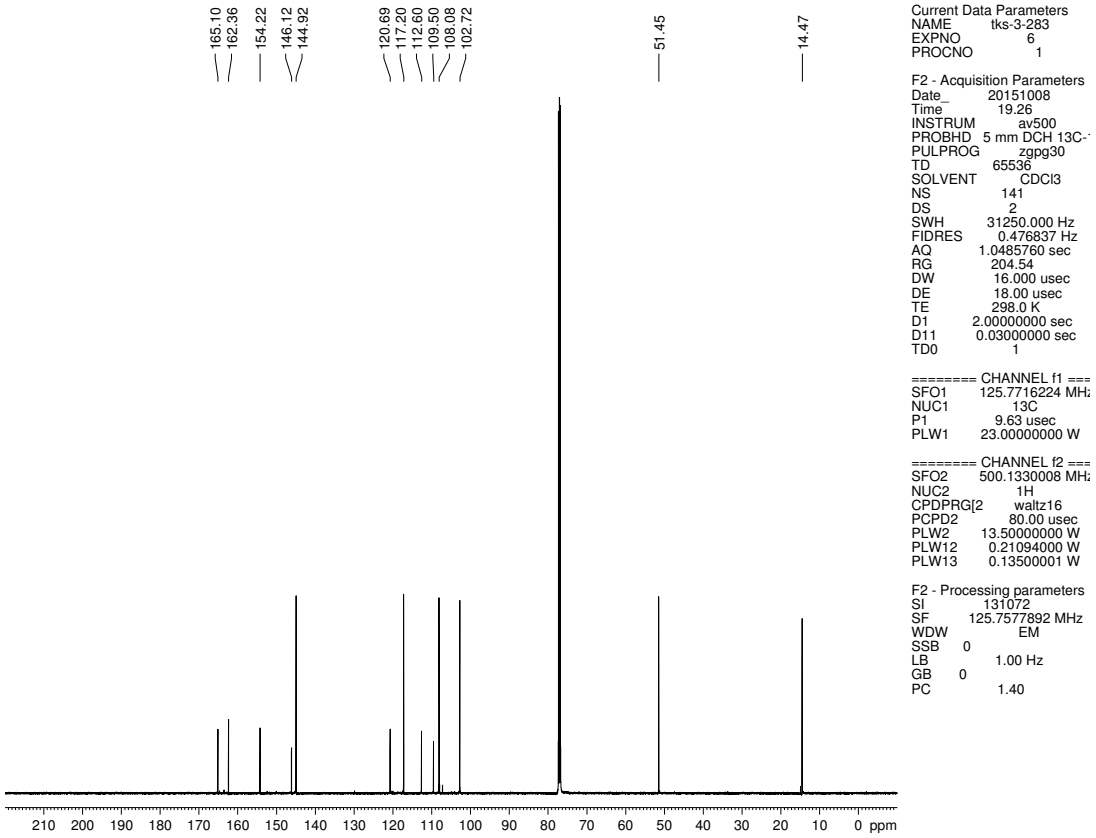

Figure 6.44. ^{13}C NMR (125 MHz, $CDCl_3$) of compounds **6.38** & **6.39**

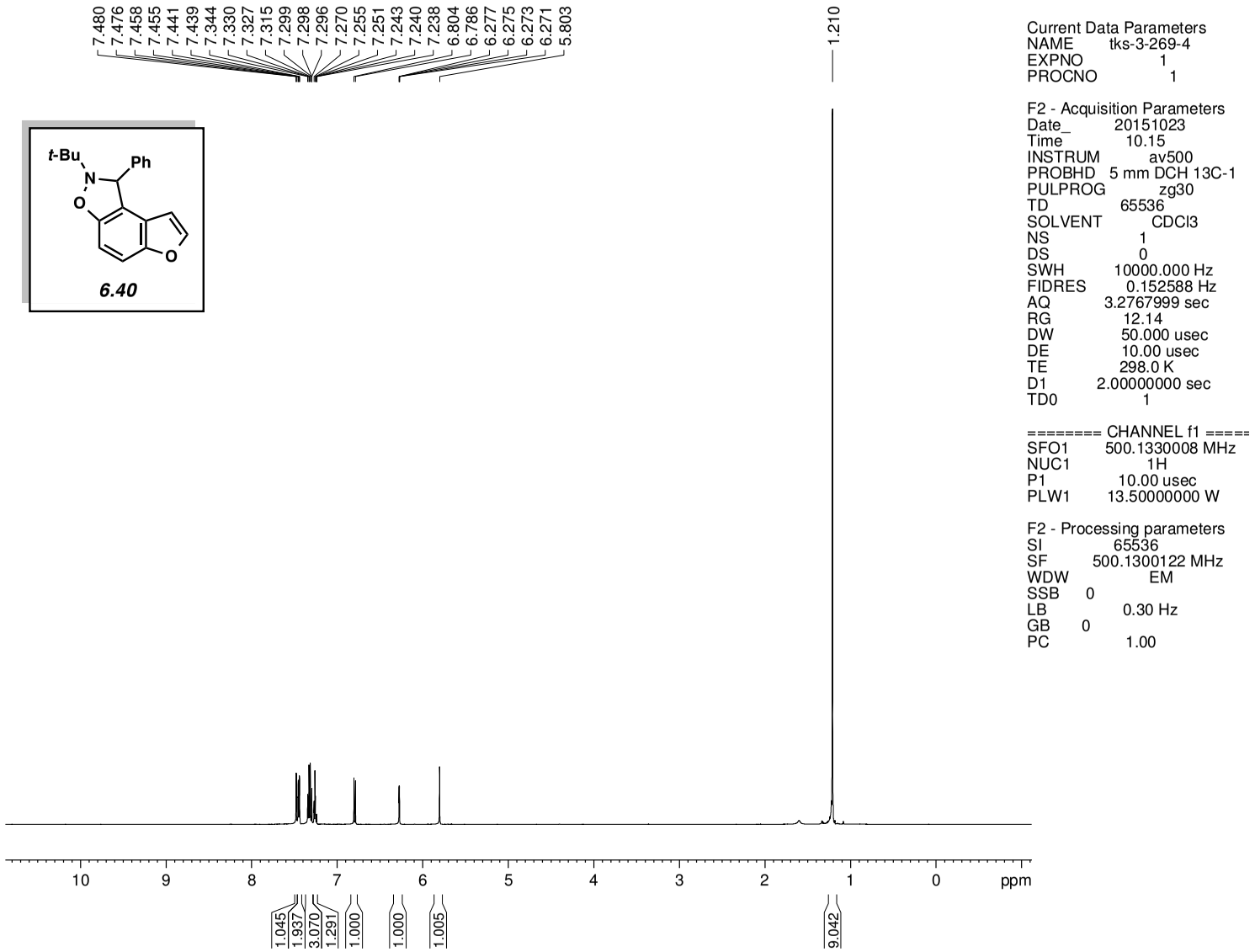

Figure 6.45. ^{1}H NMR (500 MHz, $CDCl_3$) compound **6.40**

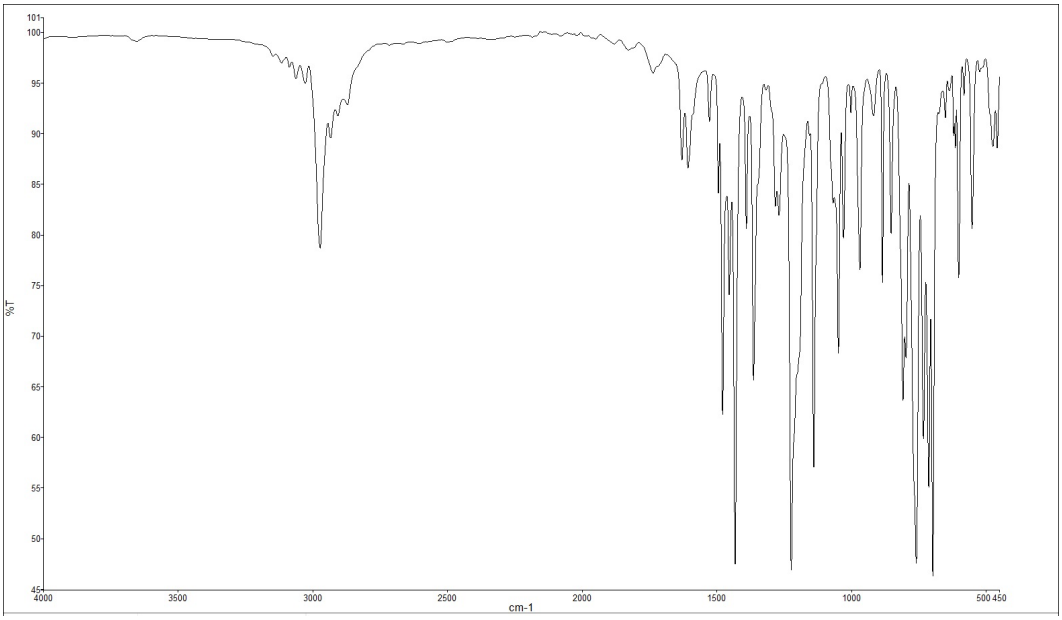

Figure 6.46. Infrared spectrum of compound **6.40**

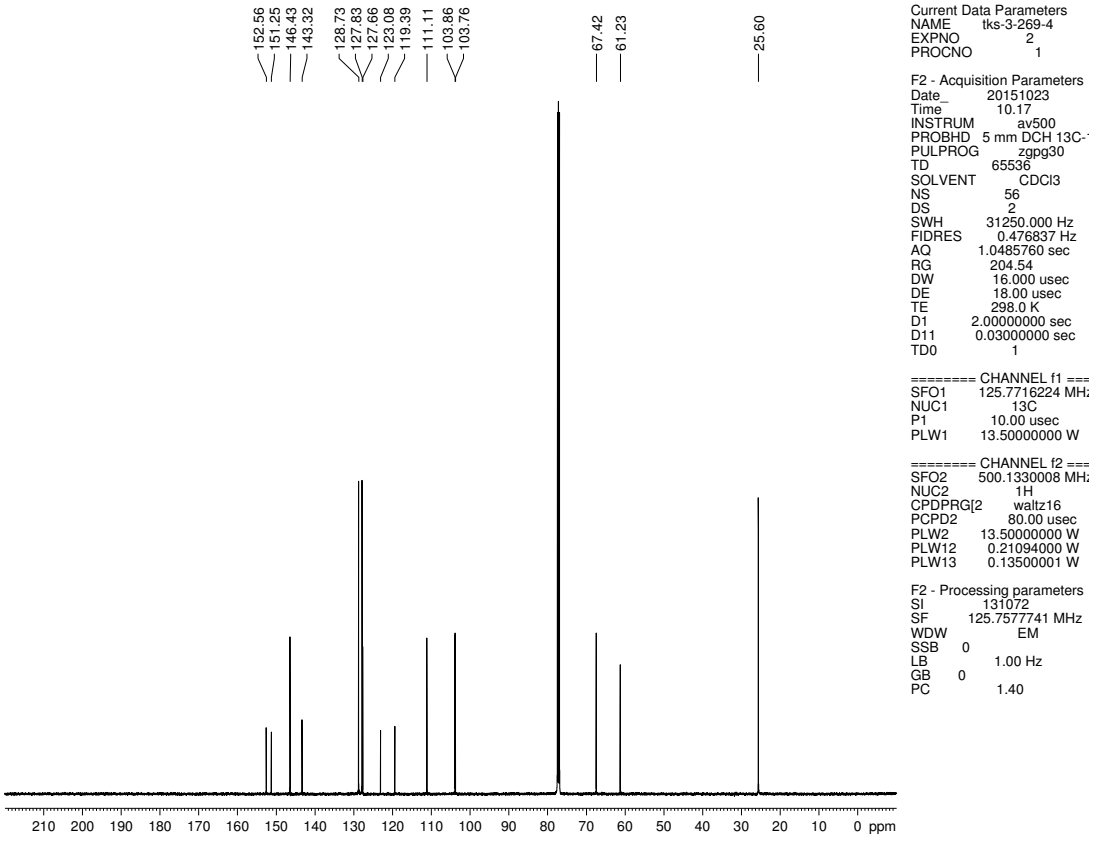

Figure 6.47. ^{13}C NMR (125 MHz, $CDCl_3$) of compound **6.40**

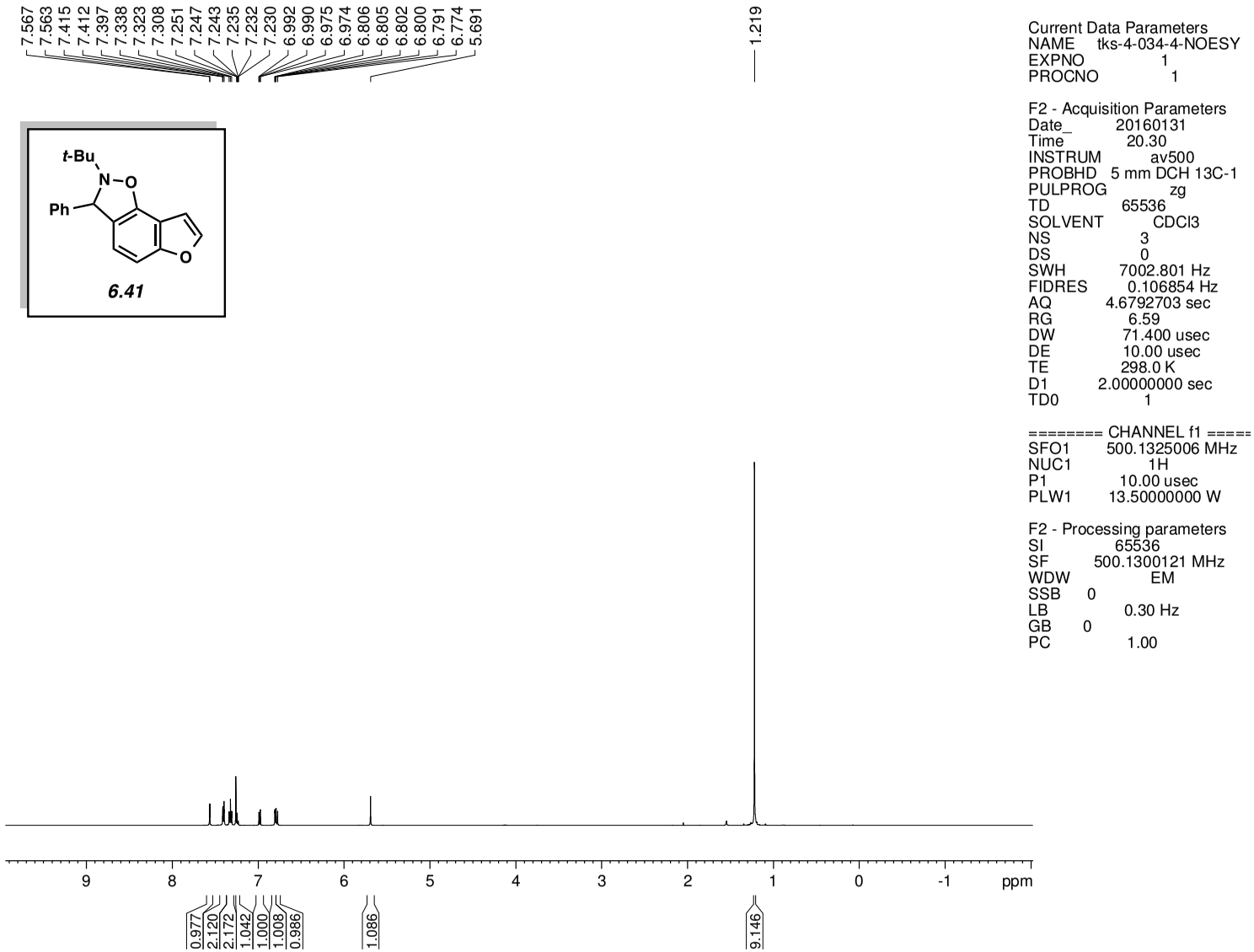

Figure 6.48. ^{1}H NMR (500 MHz, $CDCl_3$) compound **6.41**

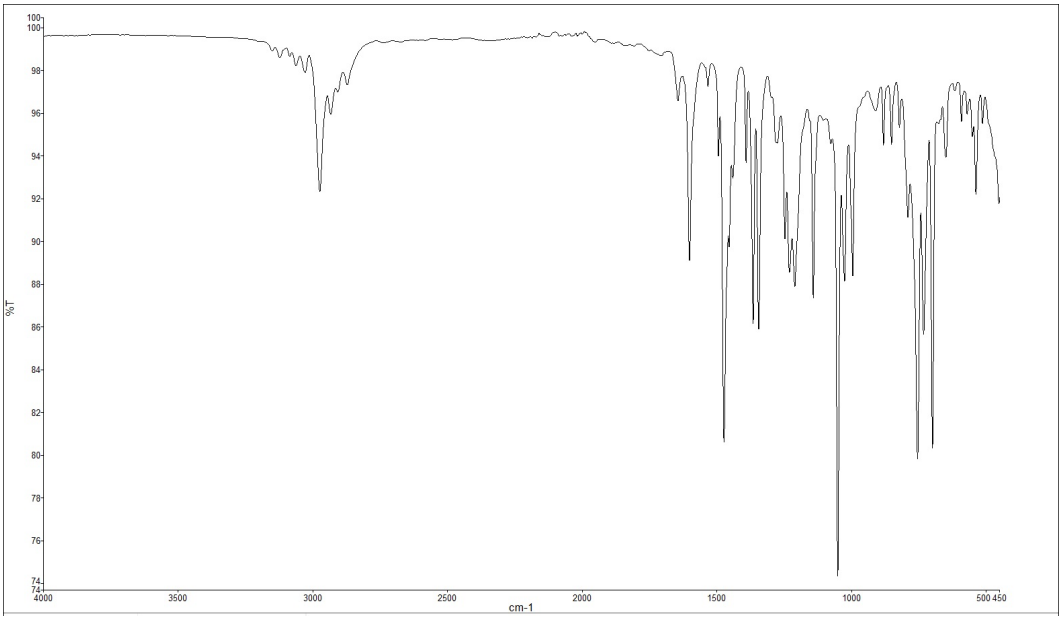

Figure 6.49. Infrared spectrum of compound **6.41**

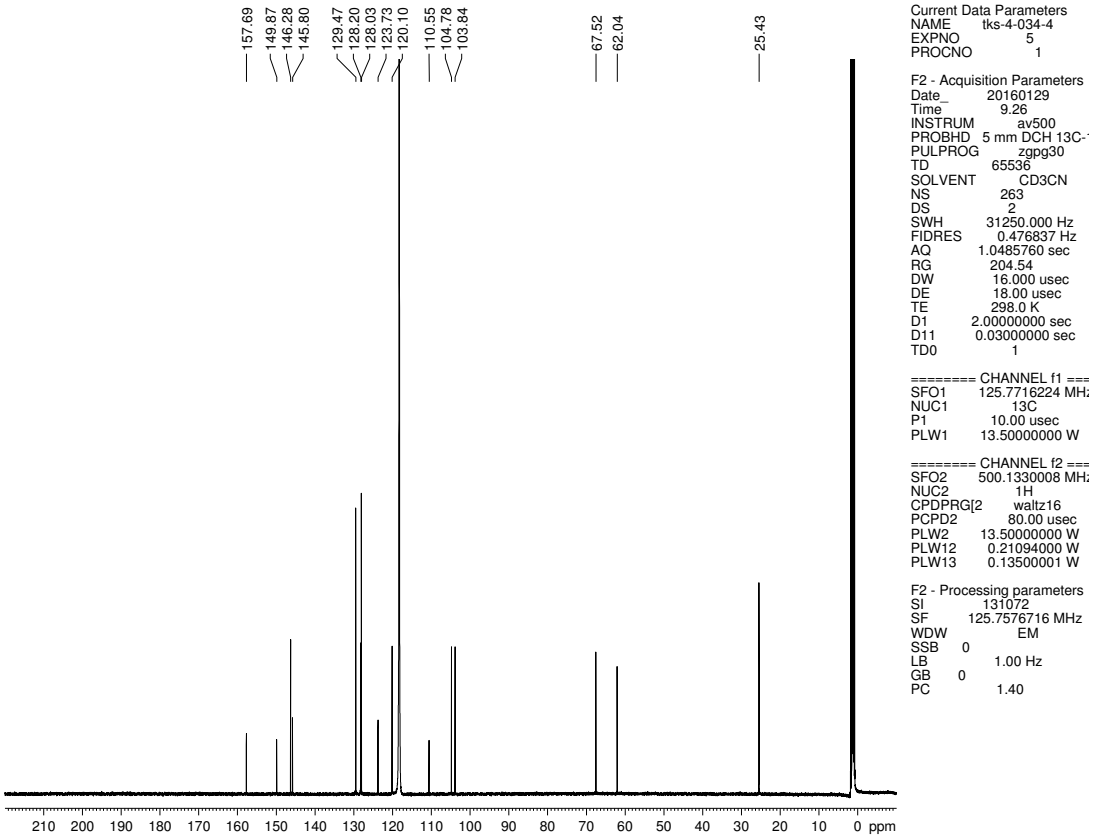

Figure 6.50. ^{13}C NMR (125 MHz, CD_3CN) of compound **6.41**

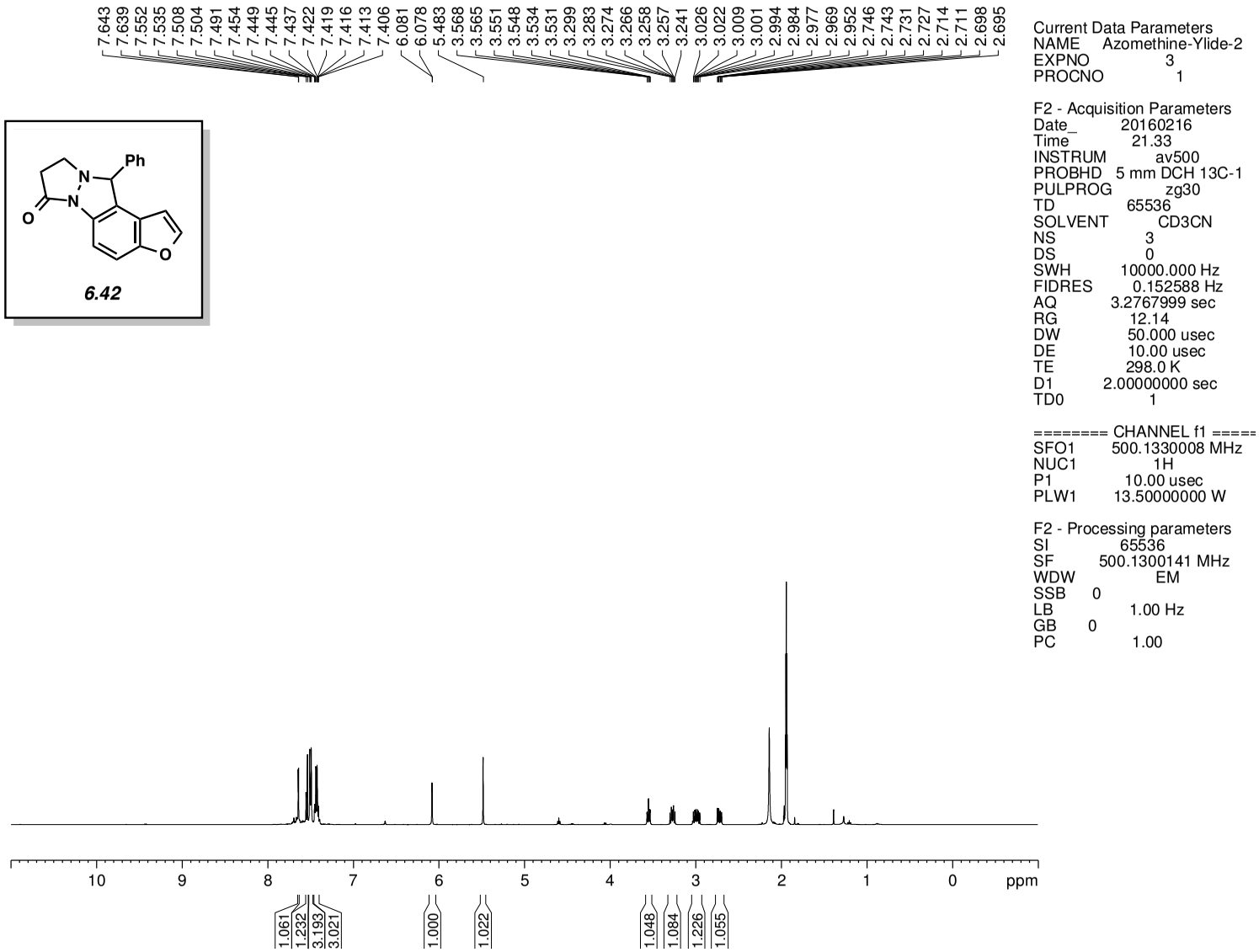

Figure 6.51. ^{1}H NMR (500 MHz, CD_3CN) compound **6.42**

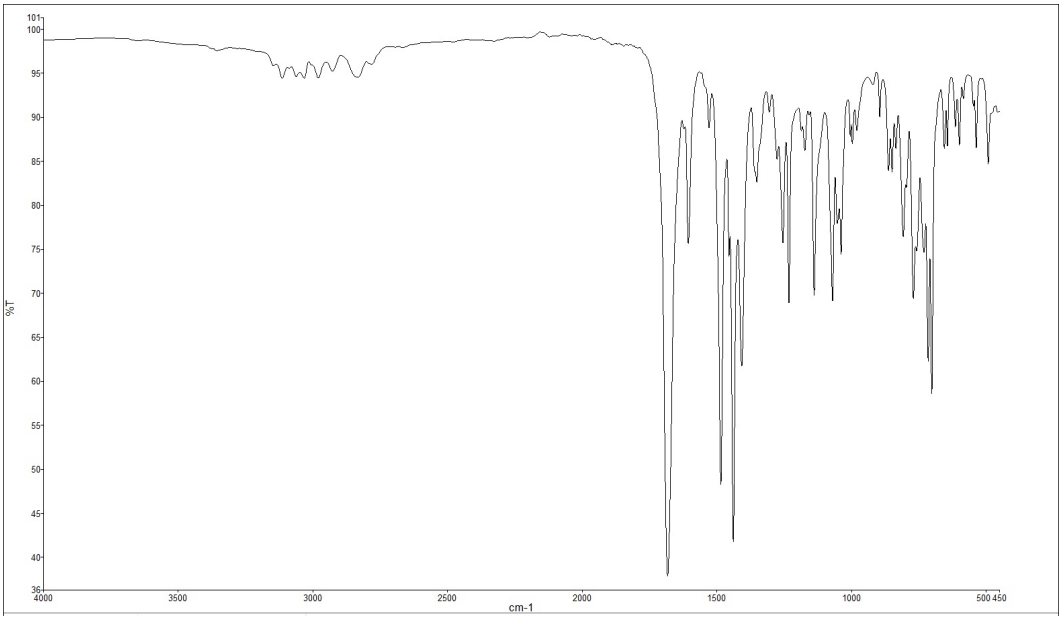

Figure 6.52. Infrared spectrum of compound **6.42**

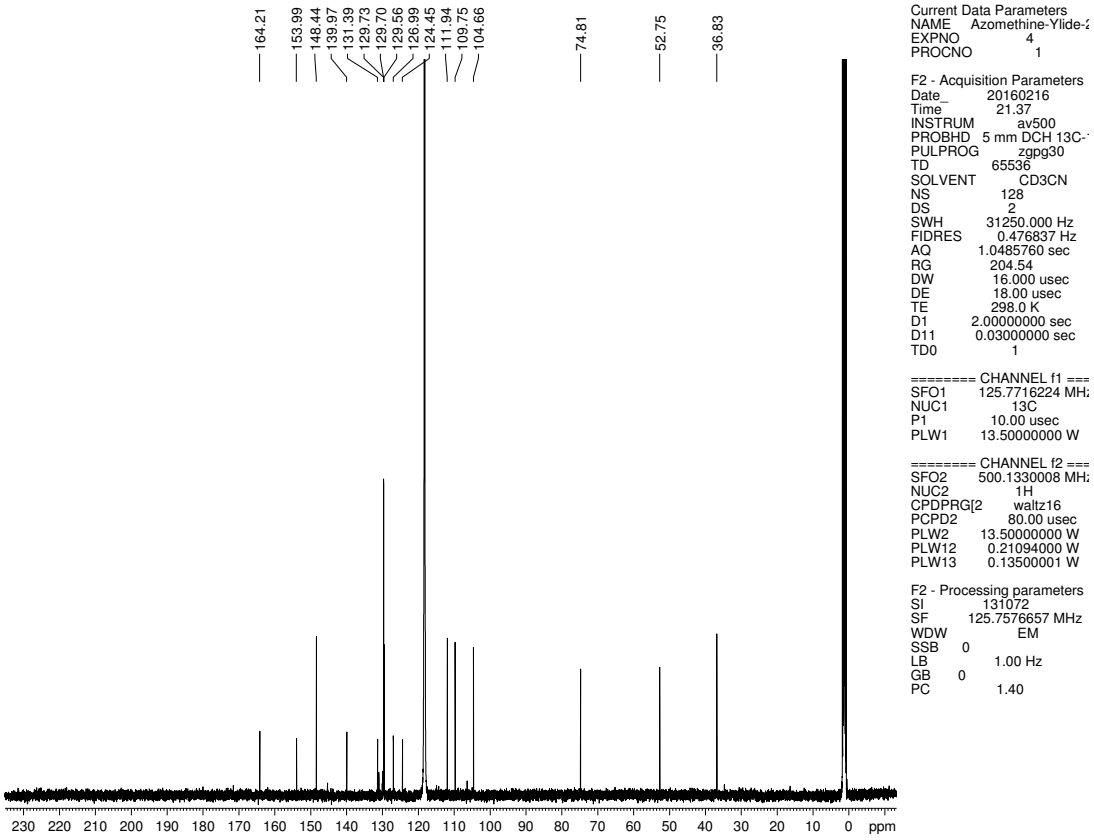

Figure 6.53. ^{13}C NMR (125 MHz, CD_3CN) of compound **6.42**

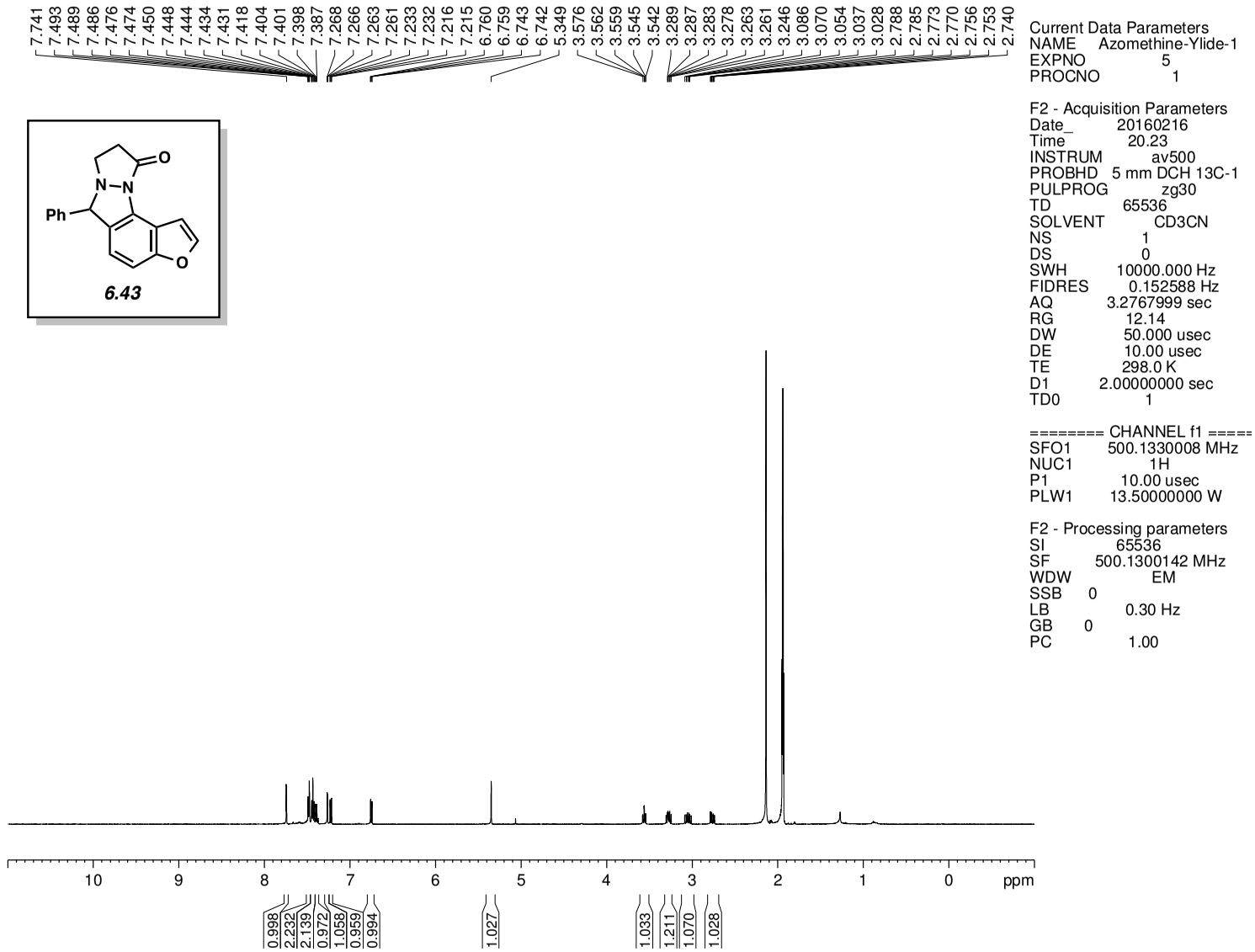

Figure 6.54. ^{1}H NMR (500 MHz, CD_3CN) compound **6.43**

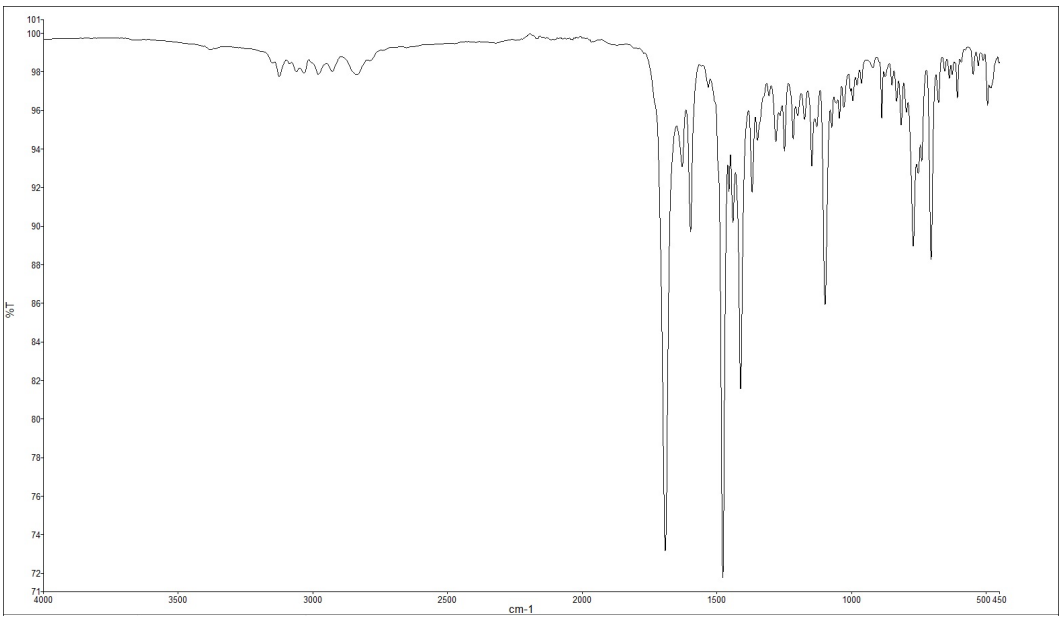

Figure 6.55. Infrared spectrum of compound **6.43**

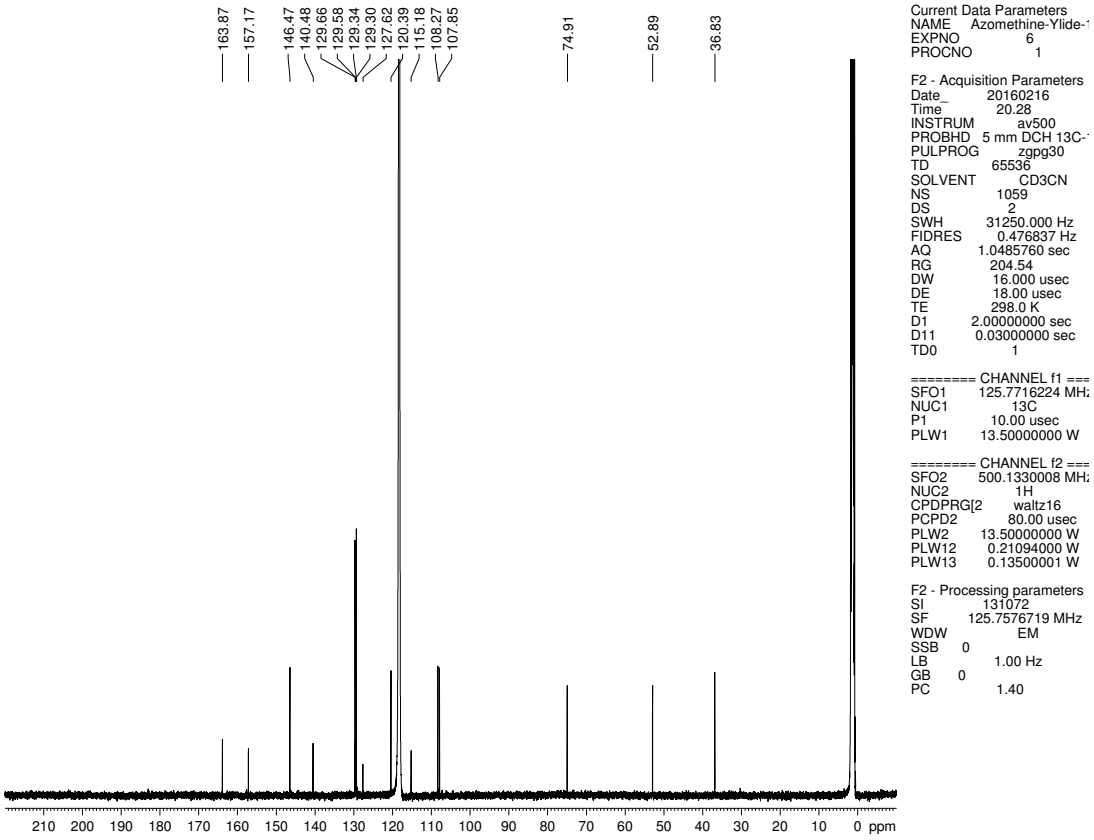

Figure 6.56. ^{13}C NMR (125 MHz, CD_3CN) of compound **6.43**

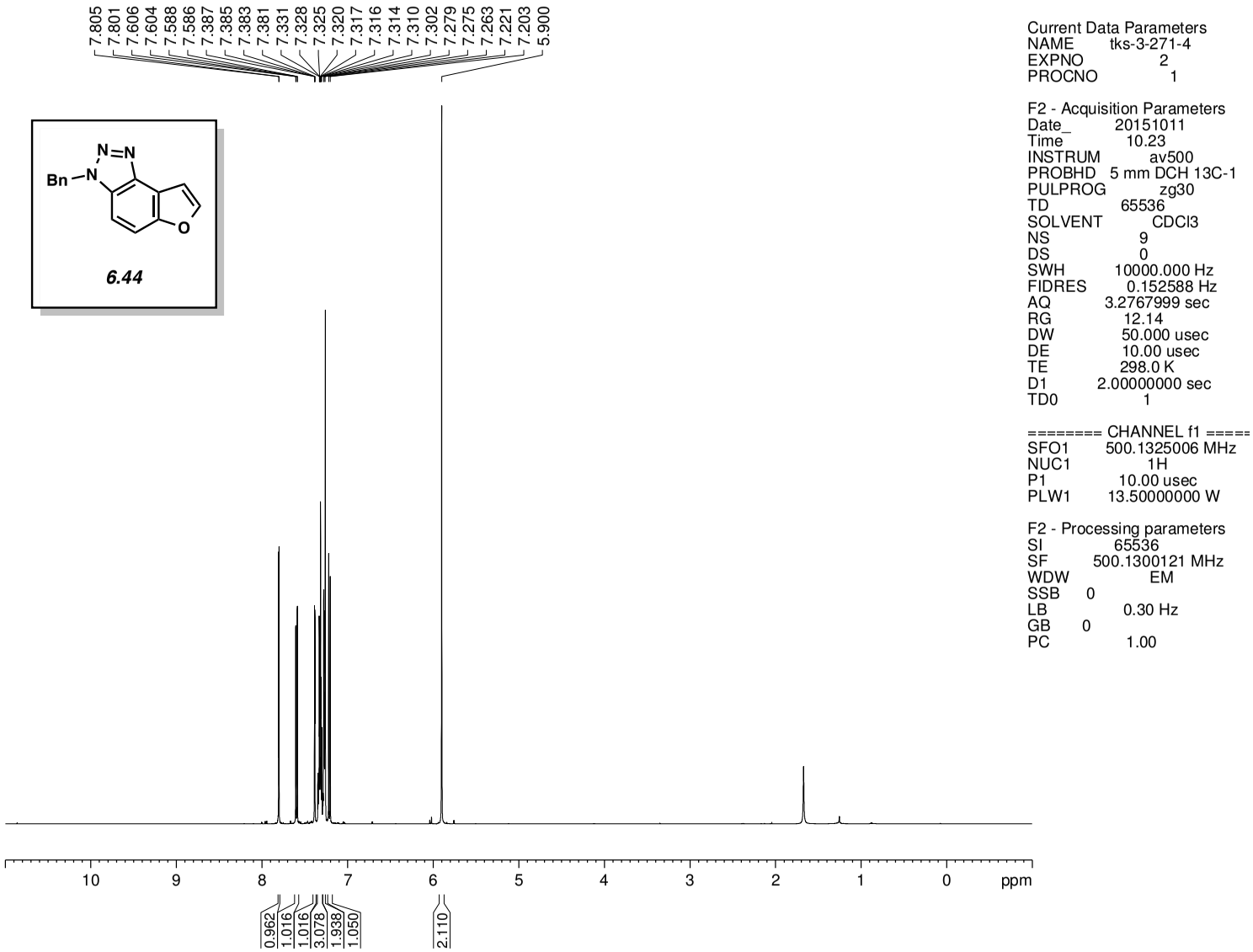

Figure 6.57. ^{1}H NMR (500 MHz, $CDCl_3$) compound **6.44**

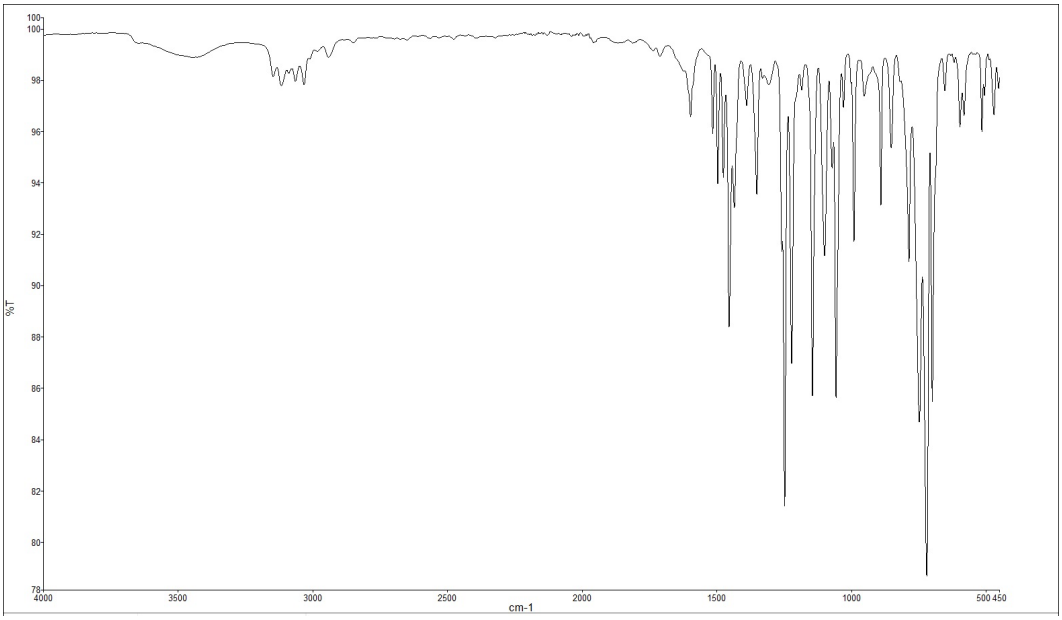

Figure 6.58. Infrared spectrum of compound **6.44**

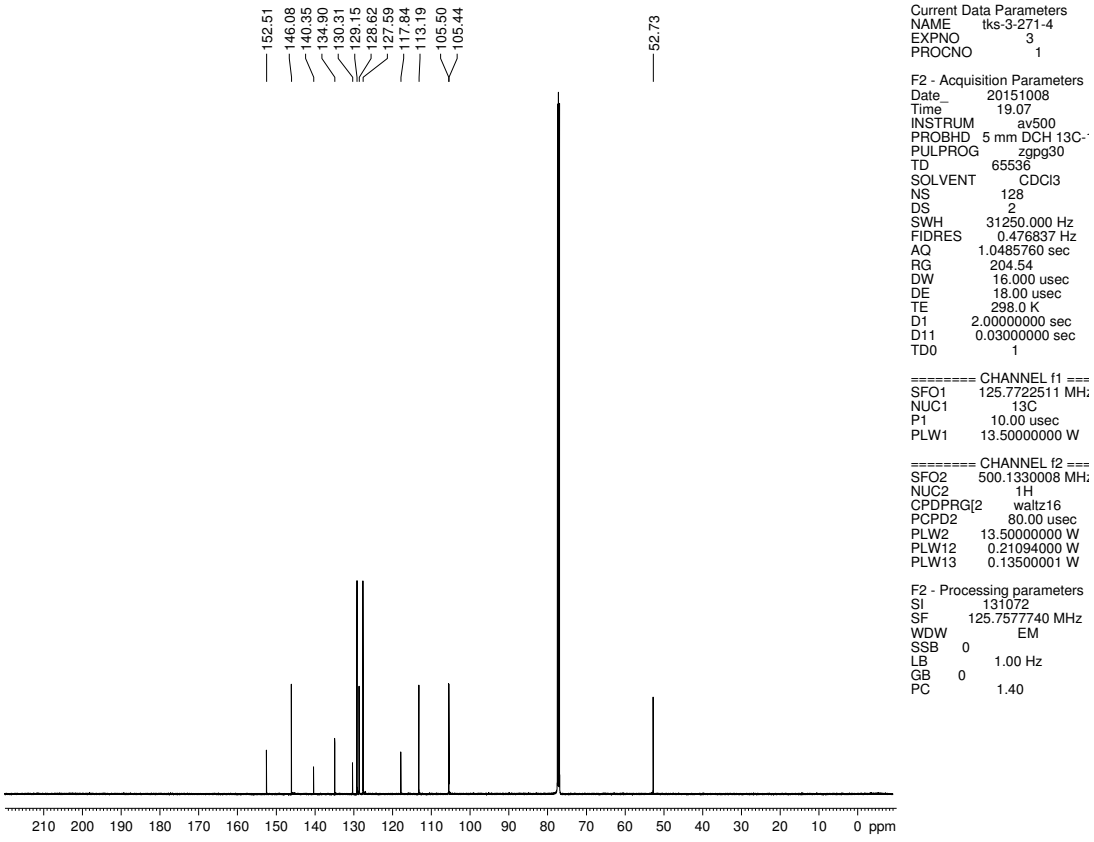

Figure 6.59. ^{13}C NMR (125 MHz, $CDCl_3$) of compound **6.44**

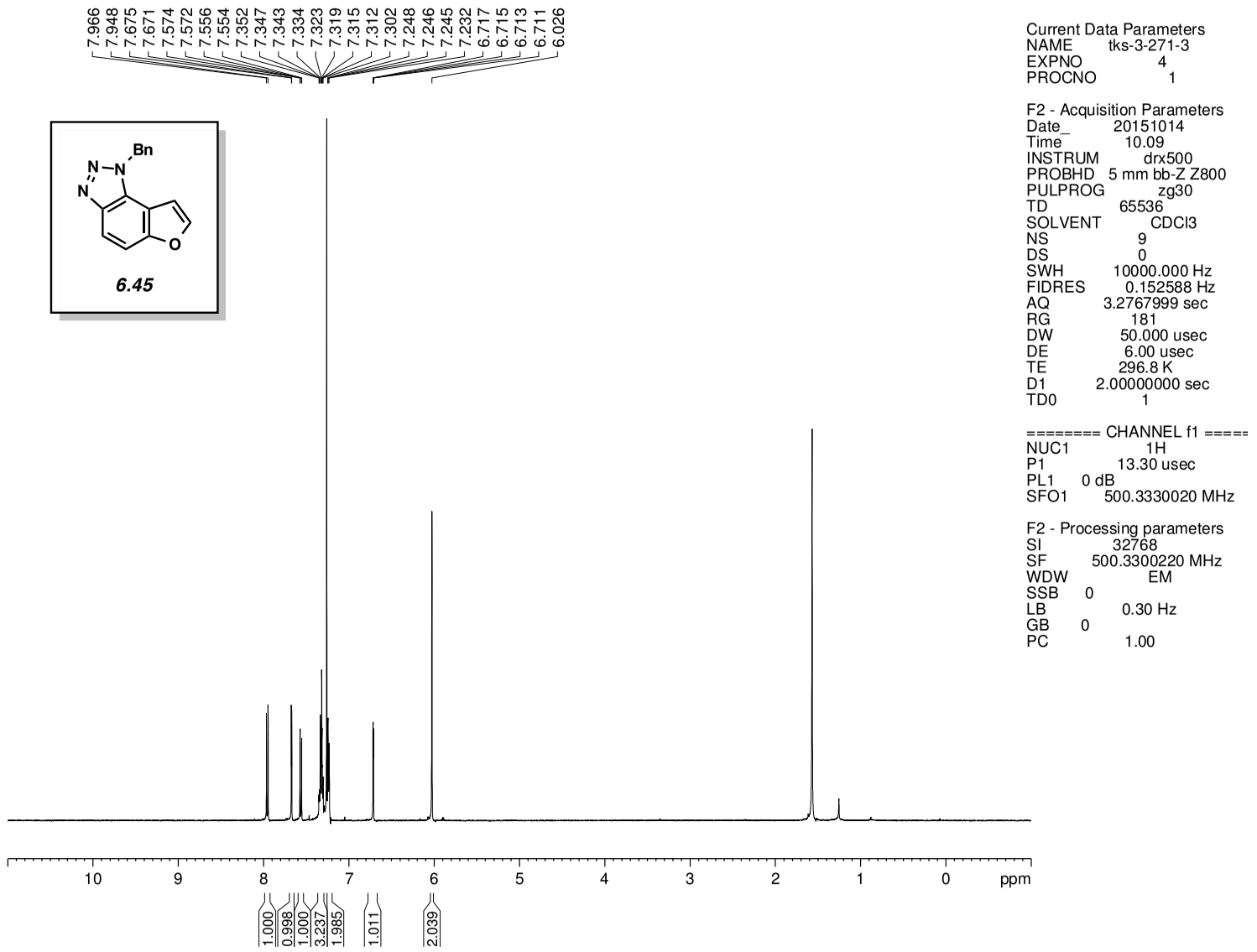

Figure 6.60. ^{1}H NMR (500 MHz, $CDCl_3$) compound **6.45**

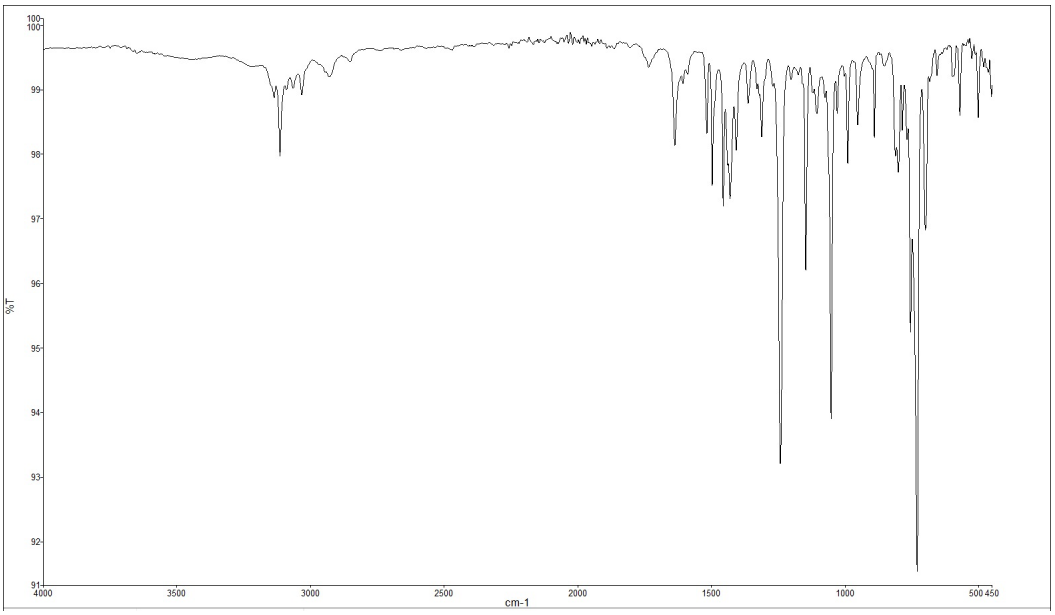

Figure 6.61. Infrared spectrum of compound **6.45**

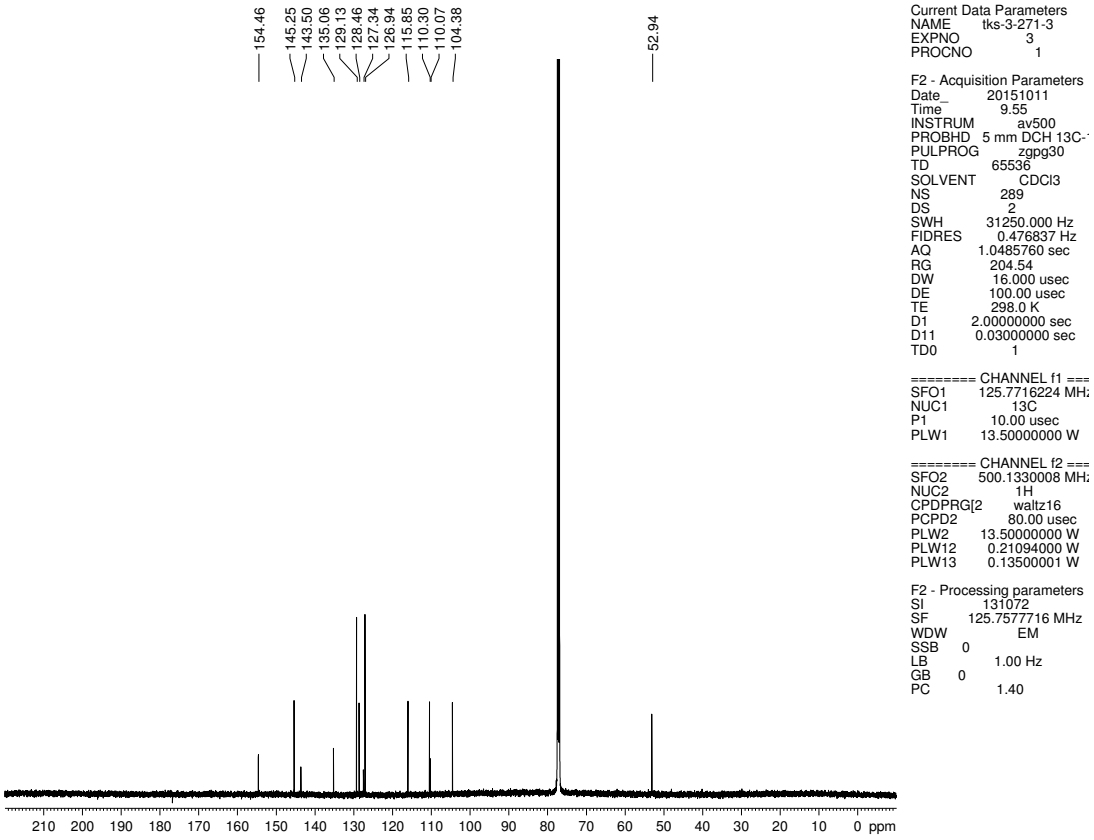

Figure 6.62. ^{13}C NMR (125 MHz, $CDCl_3$) of compound **6.45**

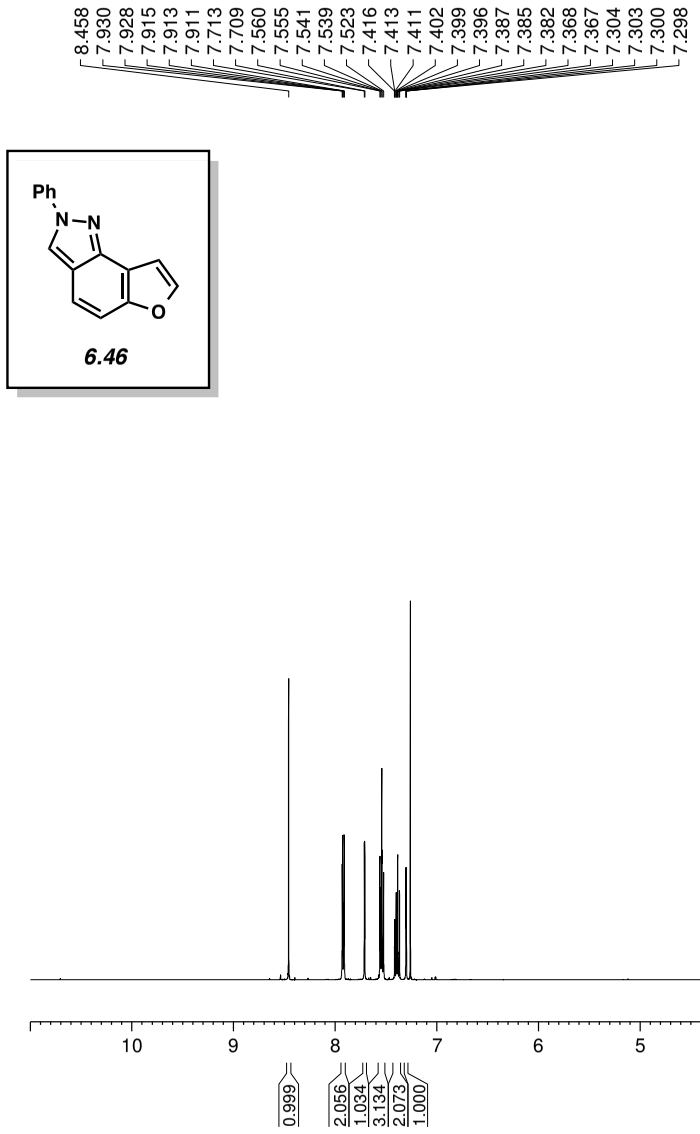

Figure 6.63. ^{1}H NMR (500 MHz, $CDCl_3$) compound **6.46**

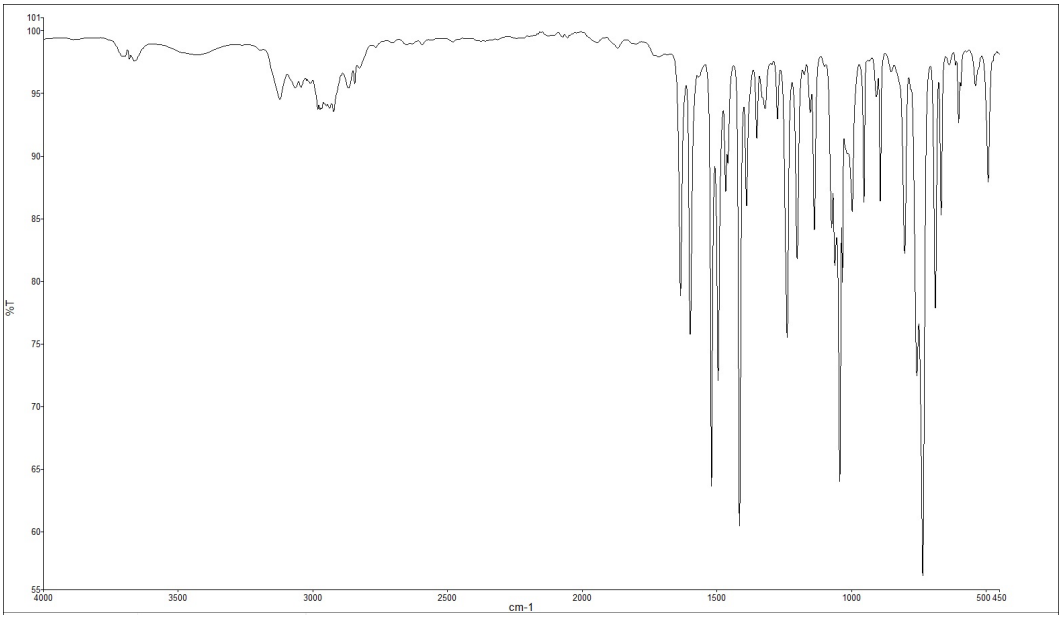

Figure 6.64. Infrared spectrum of compound **6.46**

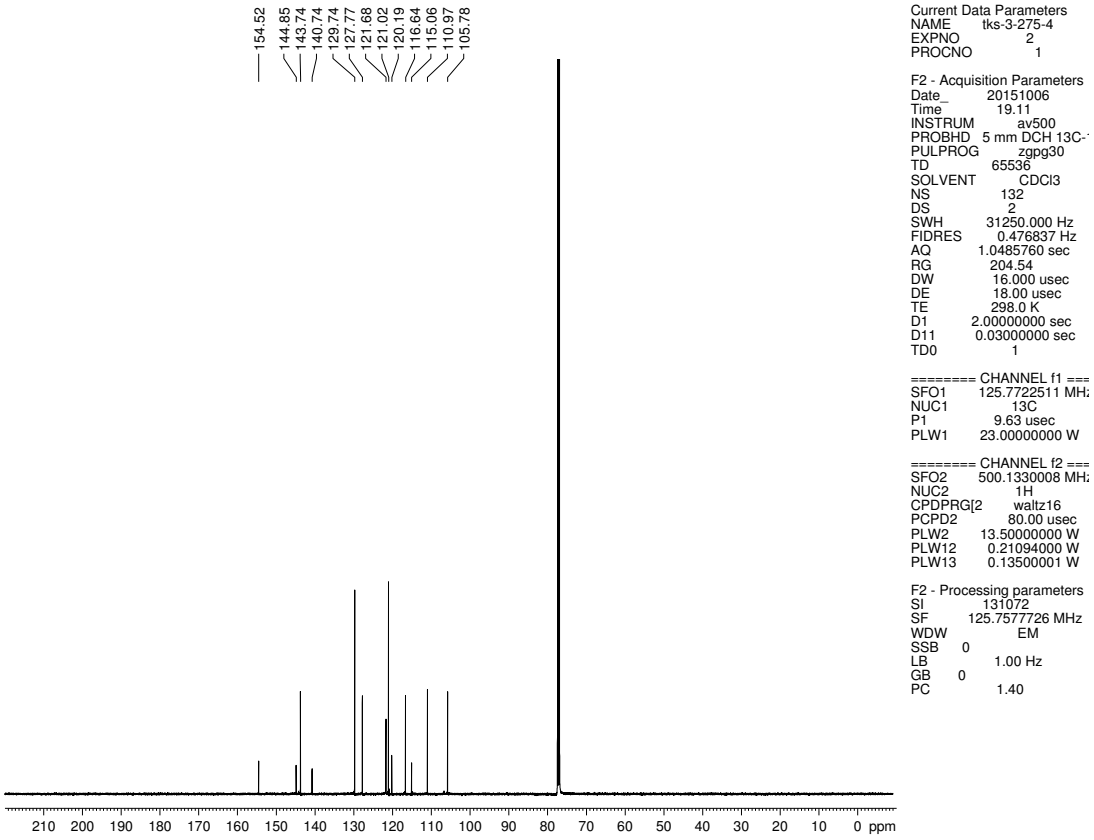

Figure 6.65. ^{13}C NMR (125 MHz, $CDCl_3$) of compound **6.46**

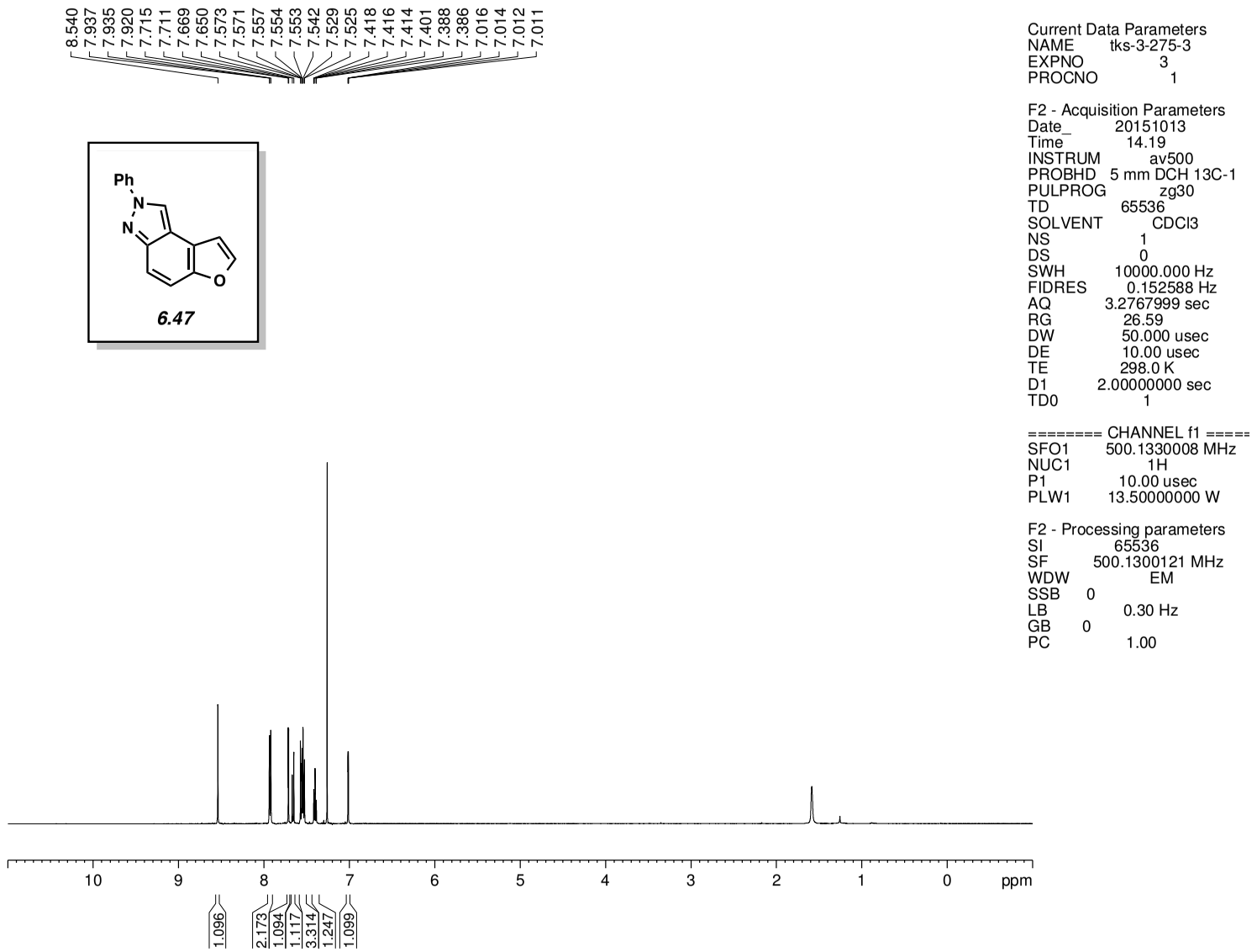

Figure 6.66. ^{1}H NMR (500 MHz, $CDCl_3$) compound **6.47**

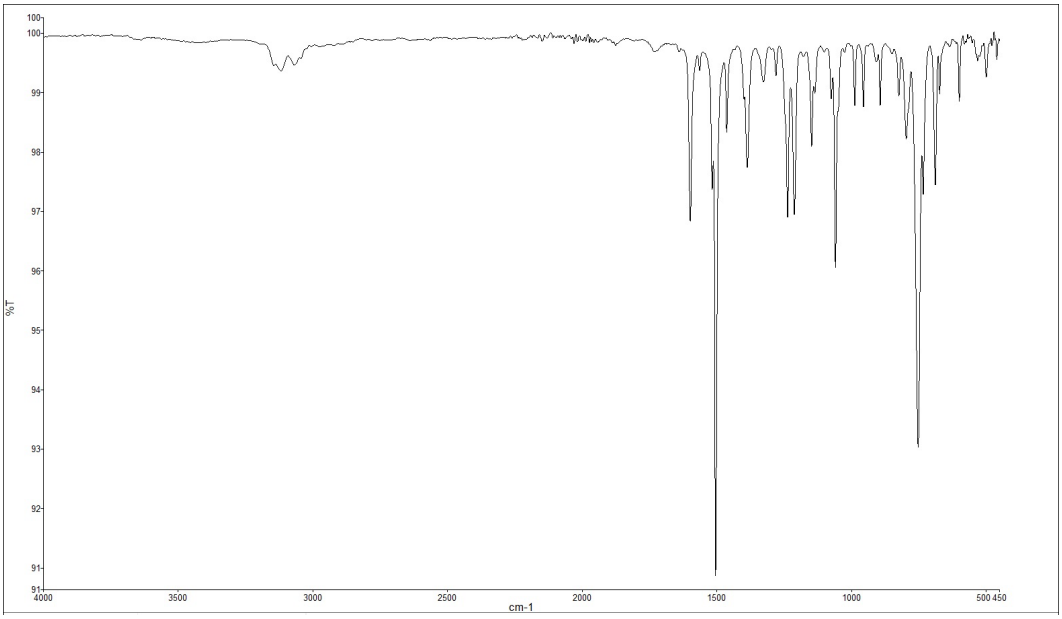

Figure 6.67. Infrared spectrum of compound **6.47**

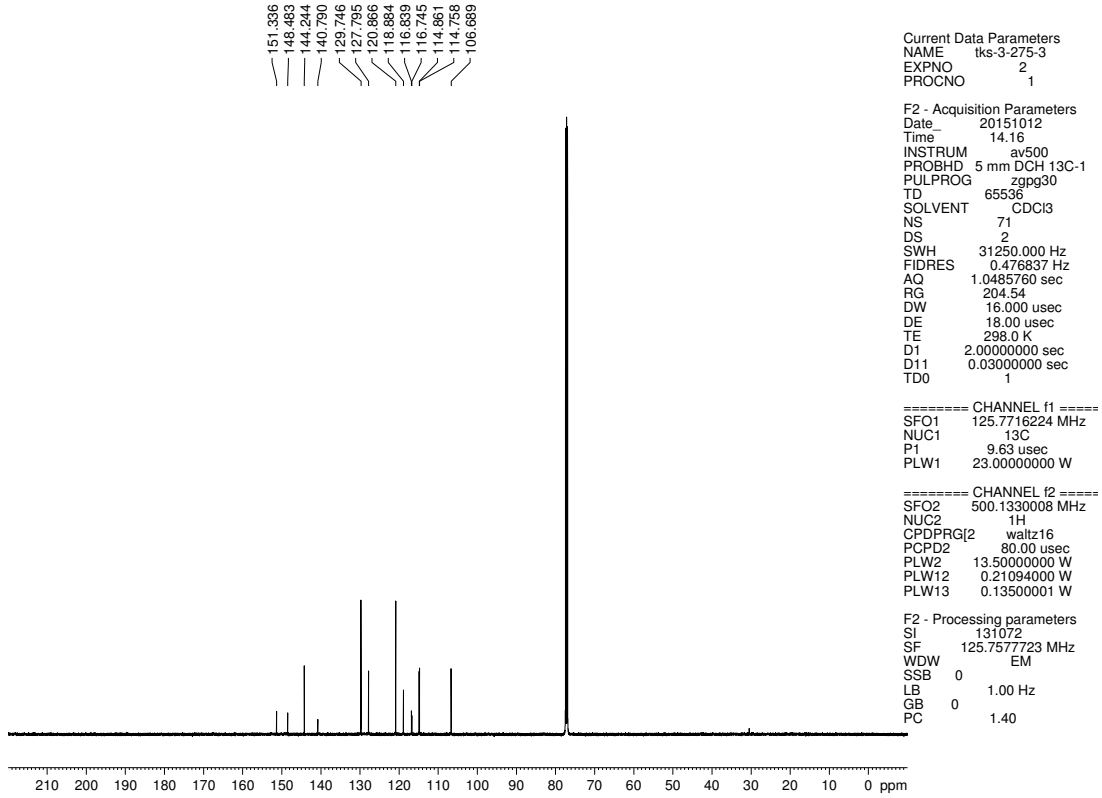

Figure 6.68. ^{13}C NMR (125 MHz, $CDCl_3$) of compound **6.47**

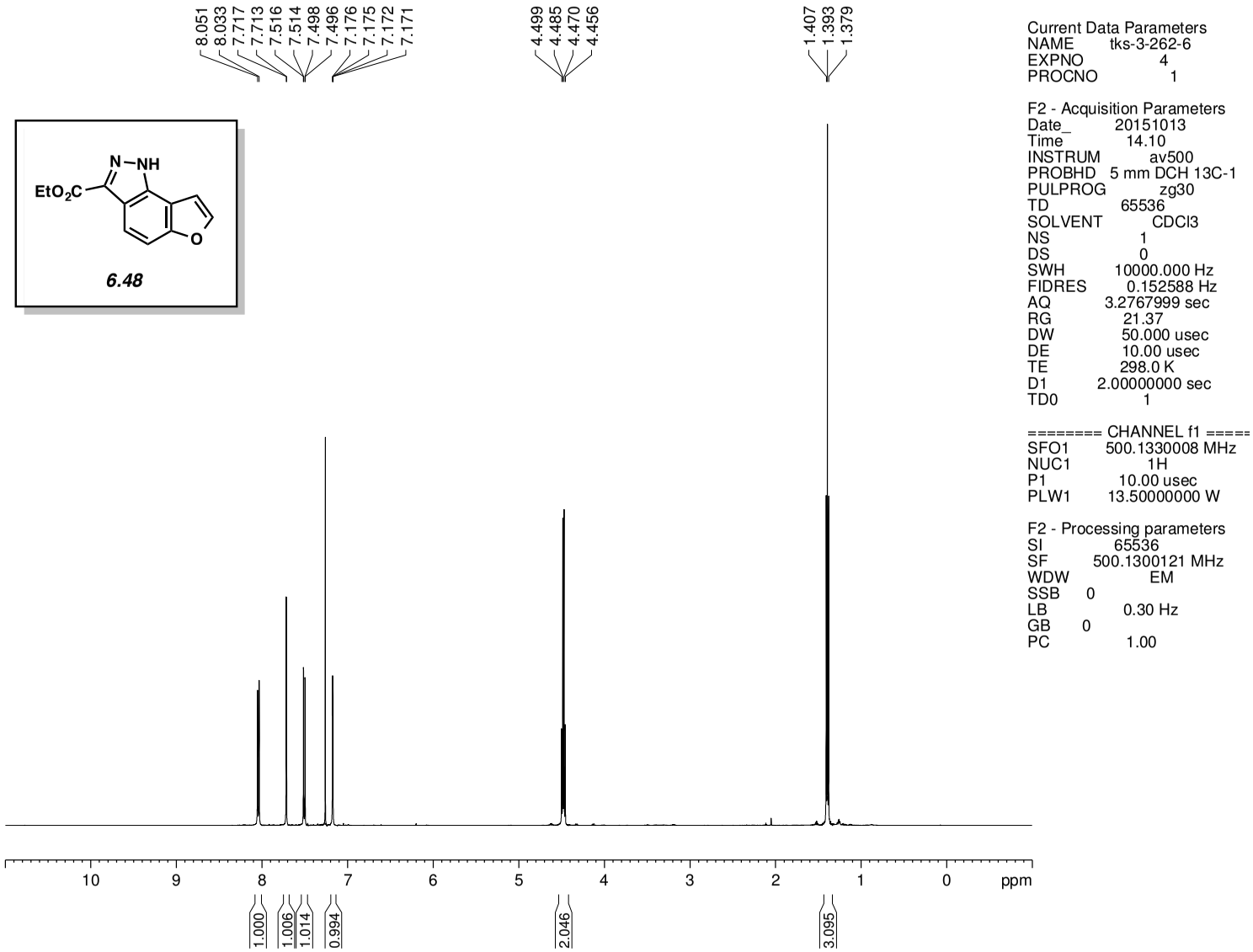

Figure 6.69. ^{1}H NMR (500 MHz, $CDCl_3$) compound **6.48**

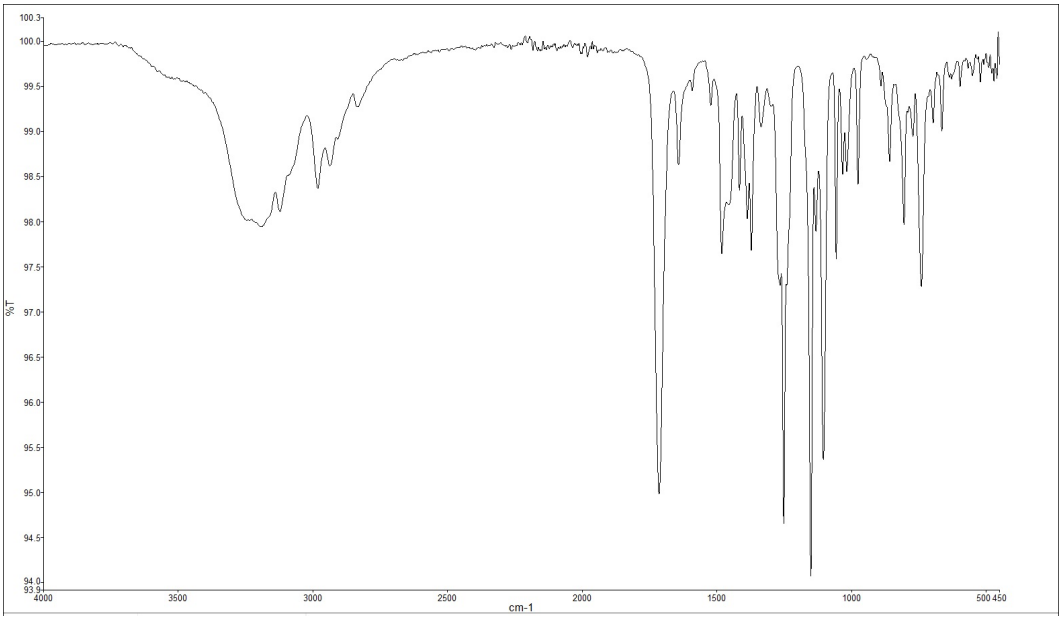

Figure 6.70. Infrared spectrum of compound **6.48**

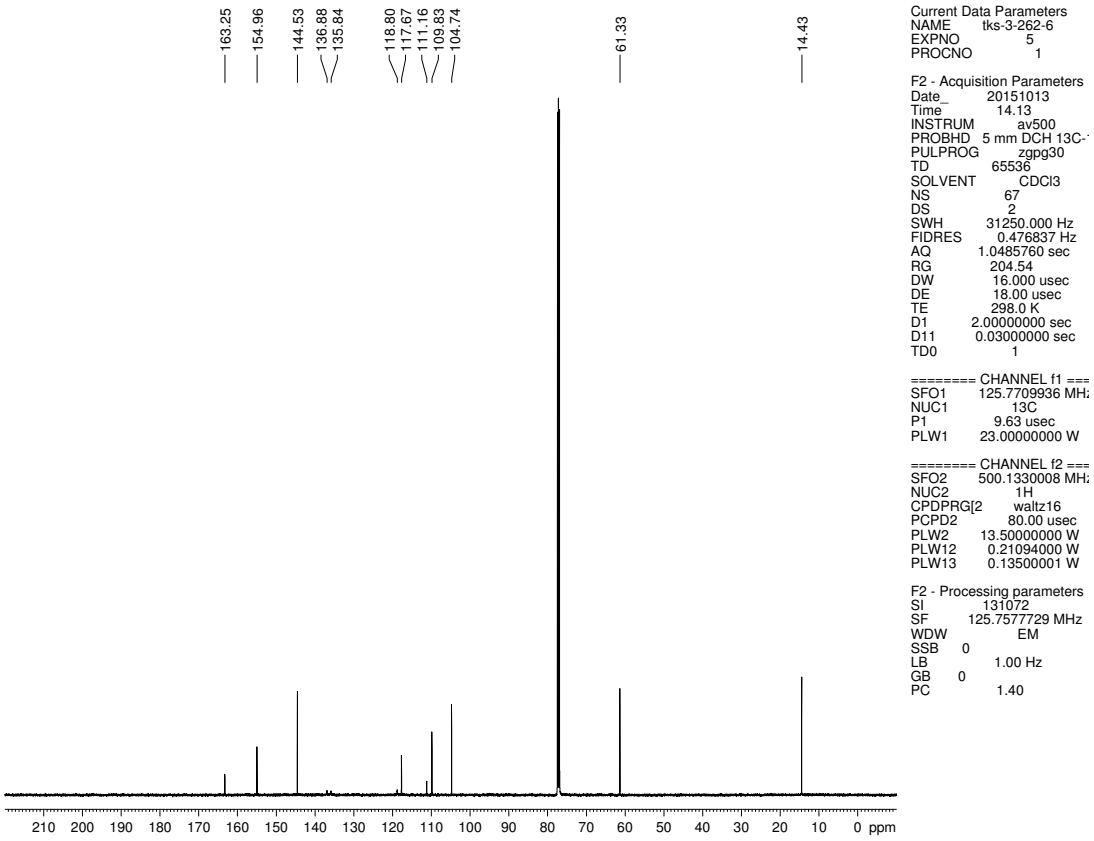

Figure 6.71. ^{13}C NMR (125 MHz, $CDCl_3$) of compound **6.48**

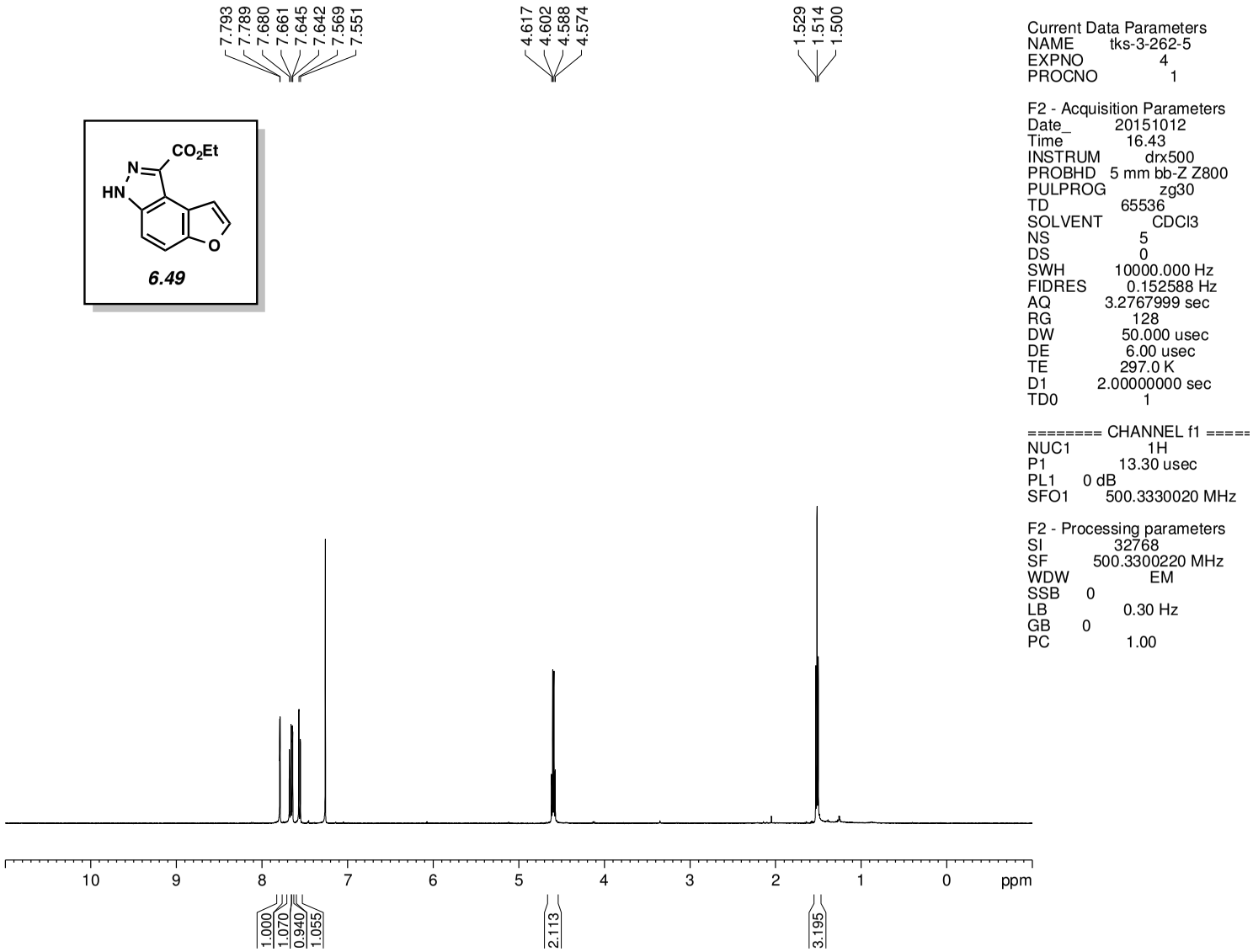

Figure 6.72. ^{1}H NMR (500 MHz, $CDCl_3$) compound **6.49**

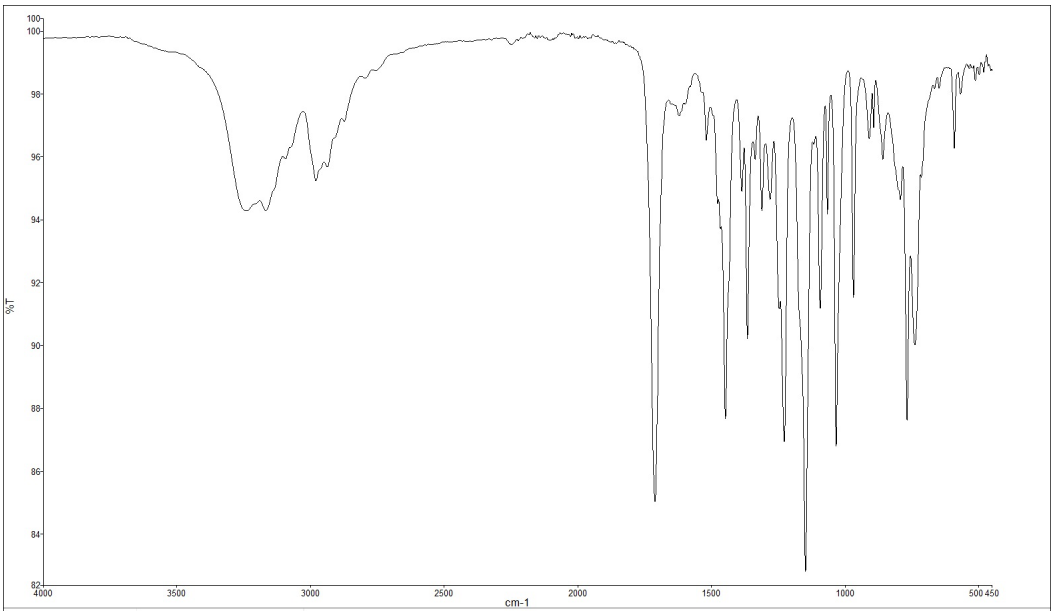

Figure 6.73. Infrared spectrum of compound **6.49**

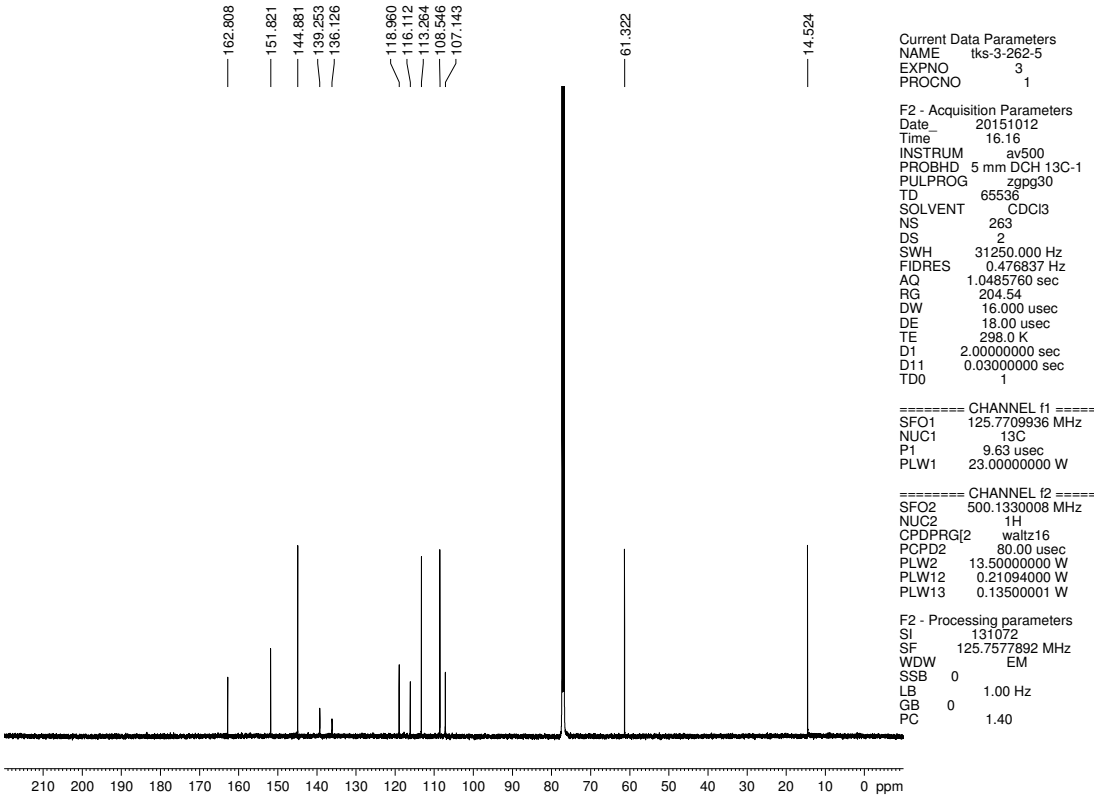

Figure 6.74. ^{13}C NMR (125 MHz, $CDCl_3$) of compound **6.49**

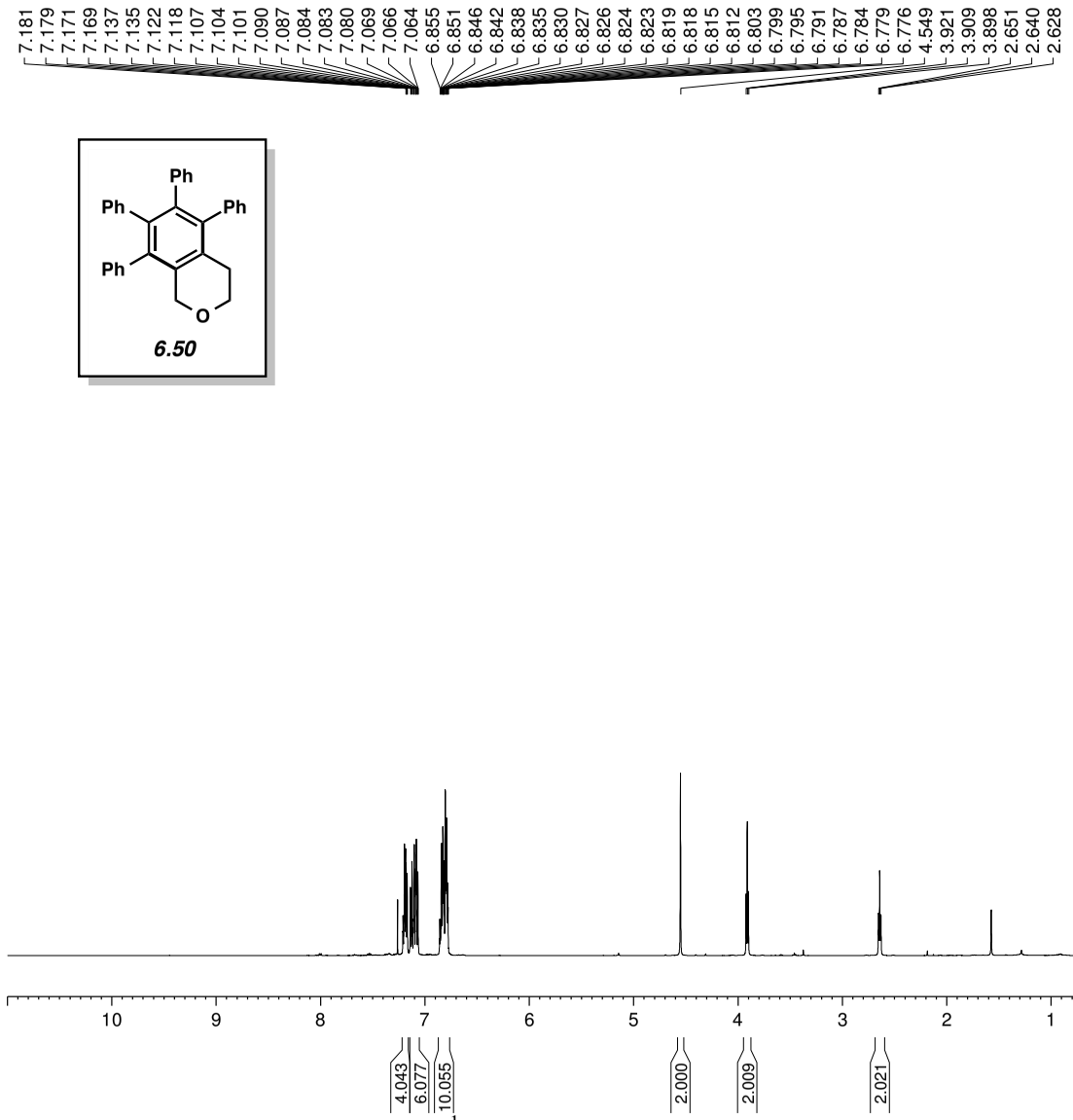

Figure 6.75. ^{1}H NMR (500 MHz, $CDCl_3$) compound **6.50**

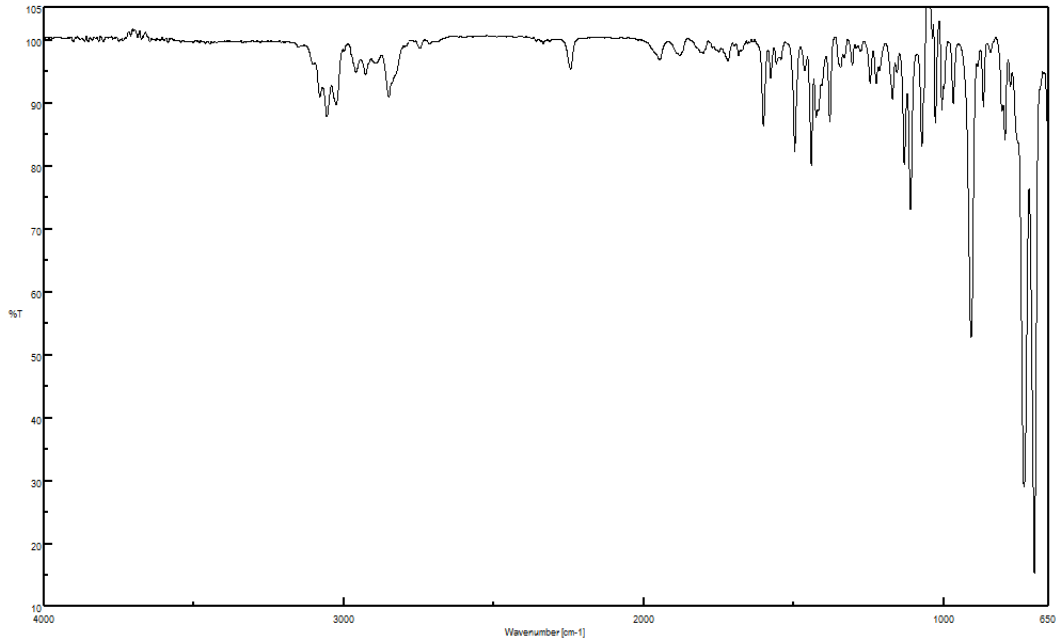

Figure 6.76. Infrared spectrum of compound **6.50**

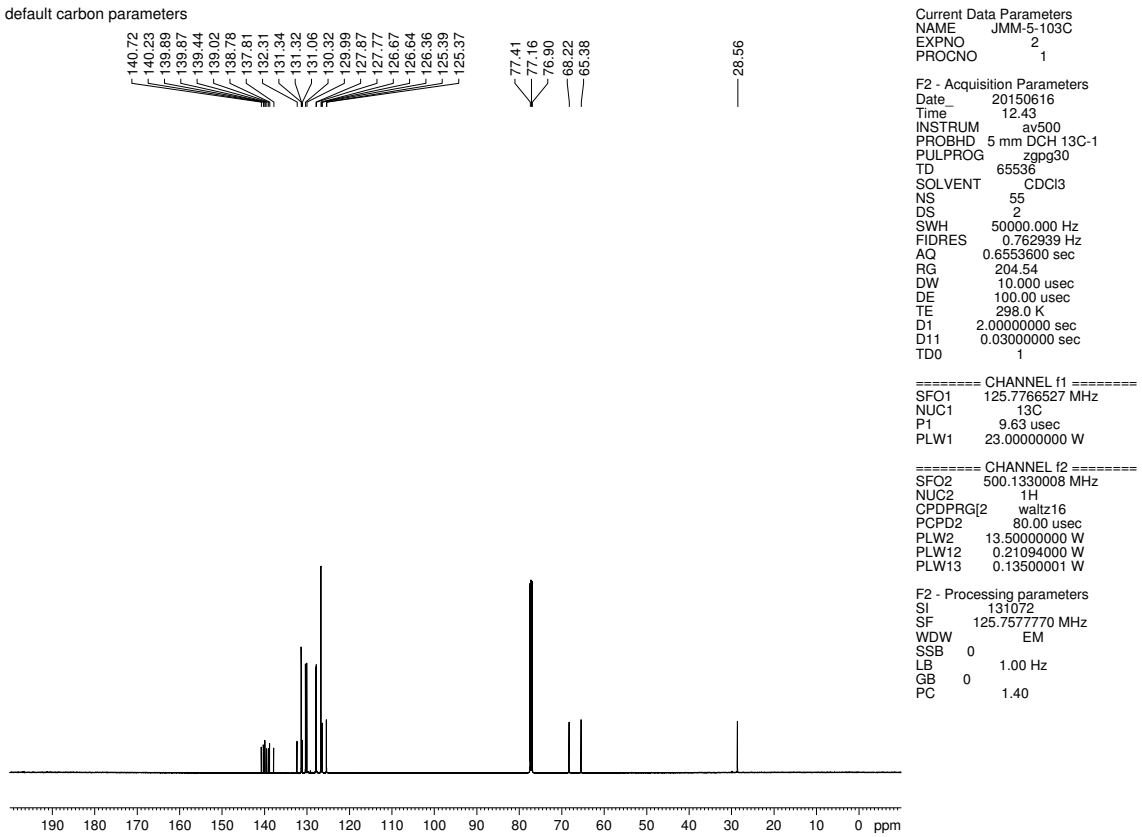

Figure 6.77. ^{13}C NMR (125 MHz, $CDCl_3$) of compound **6.50**

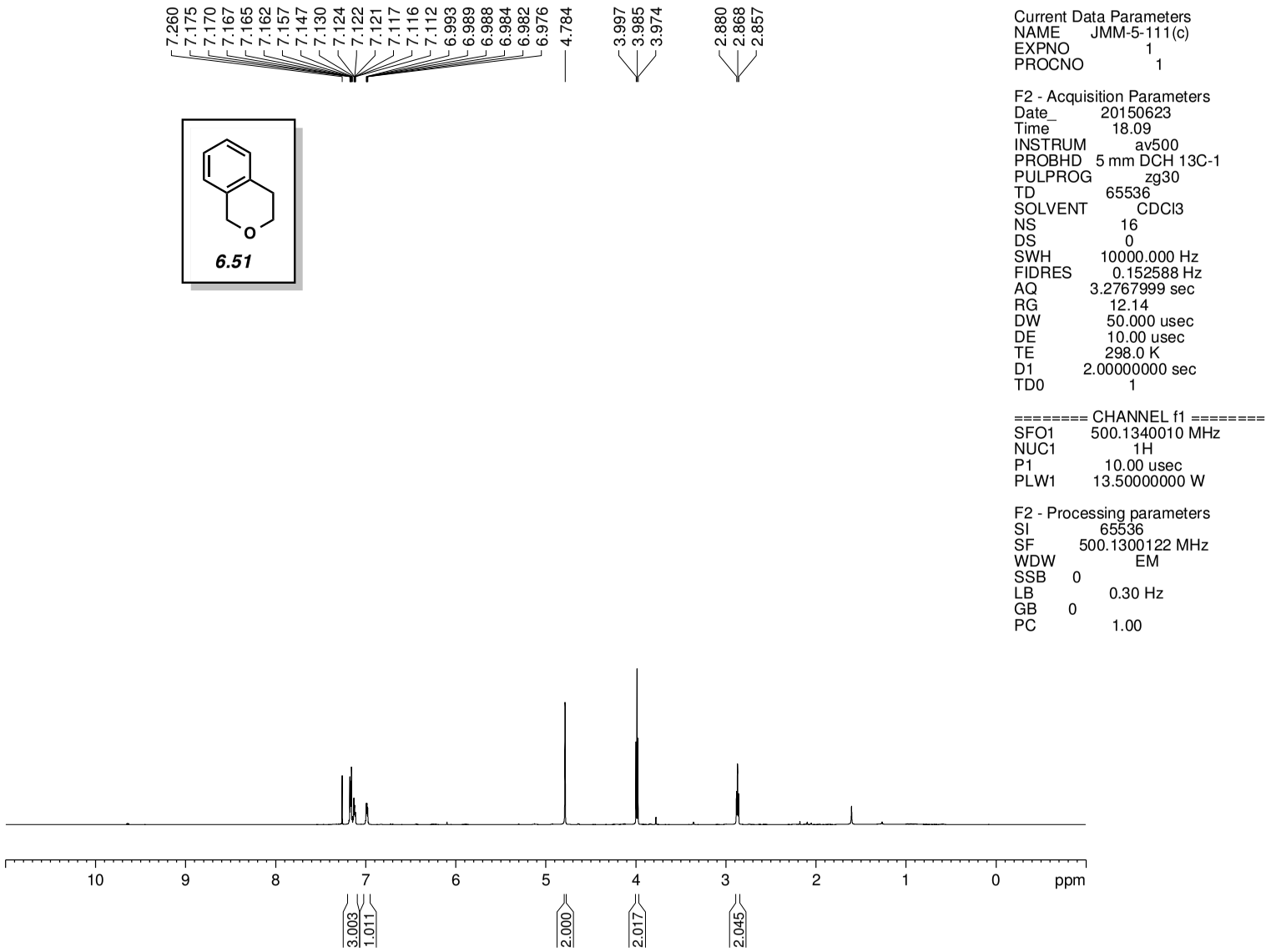

Figure 6.78. ^{1}H NMR (500 MHz, $CDCl_3$) compound **6.51**

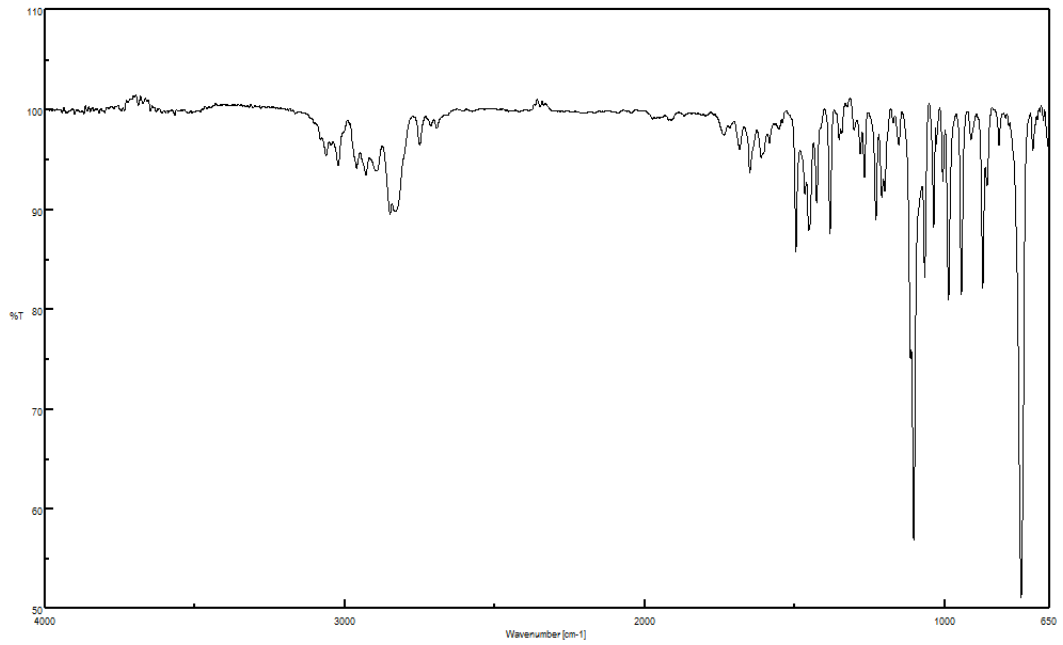

Figure 6.79. Infrared spectrum of compound **6.51**

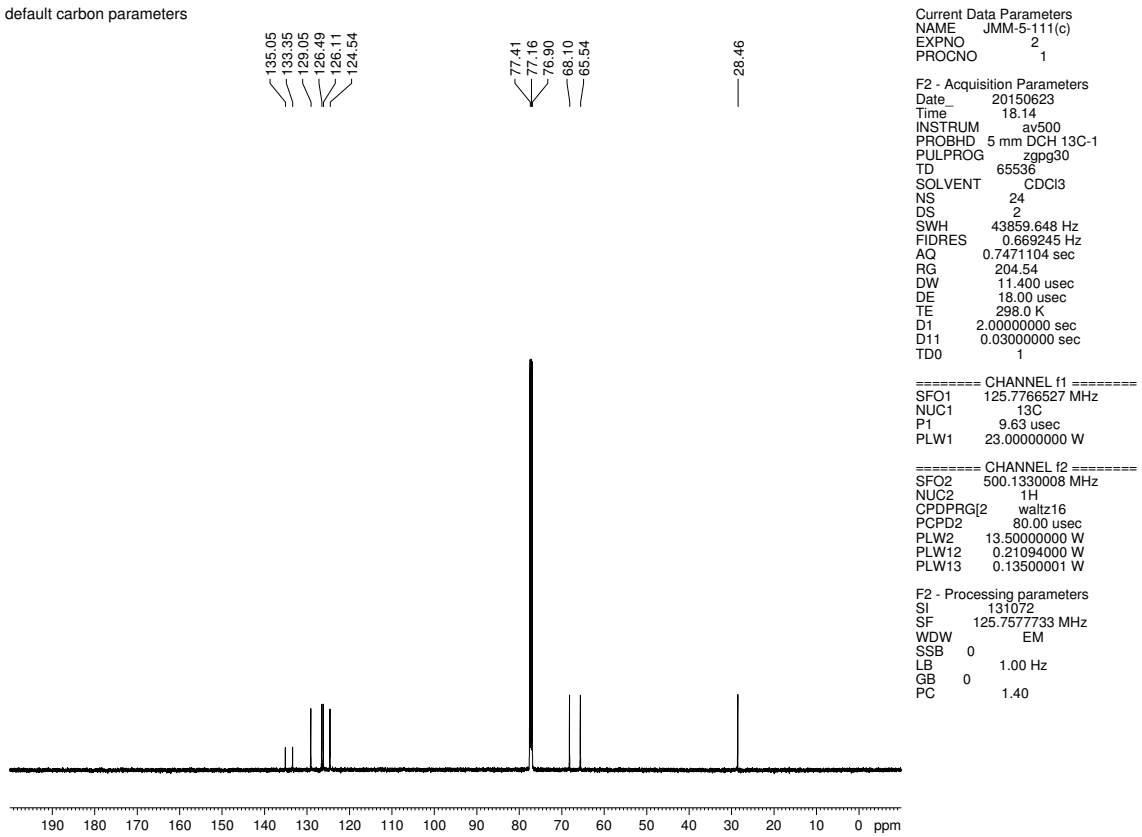

Figure 6.80. ^{13}C NMR (125 MHz, $CDCl_3$) of compound **6.51**

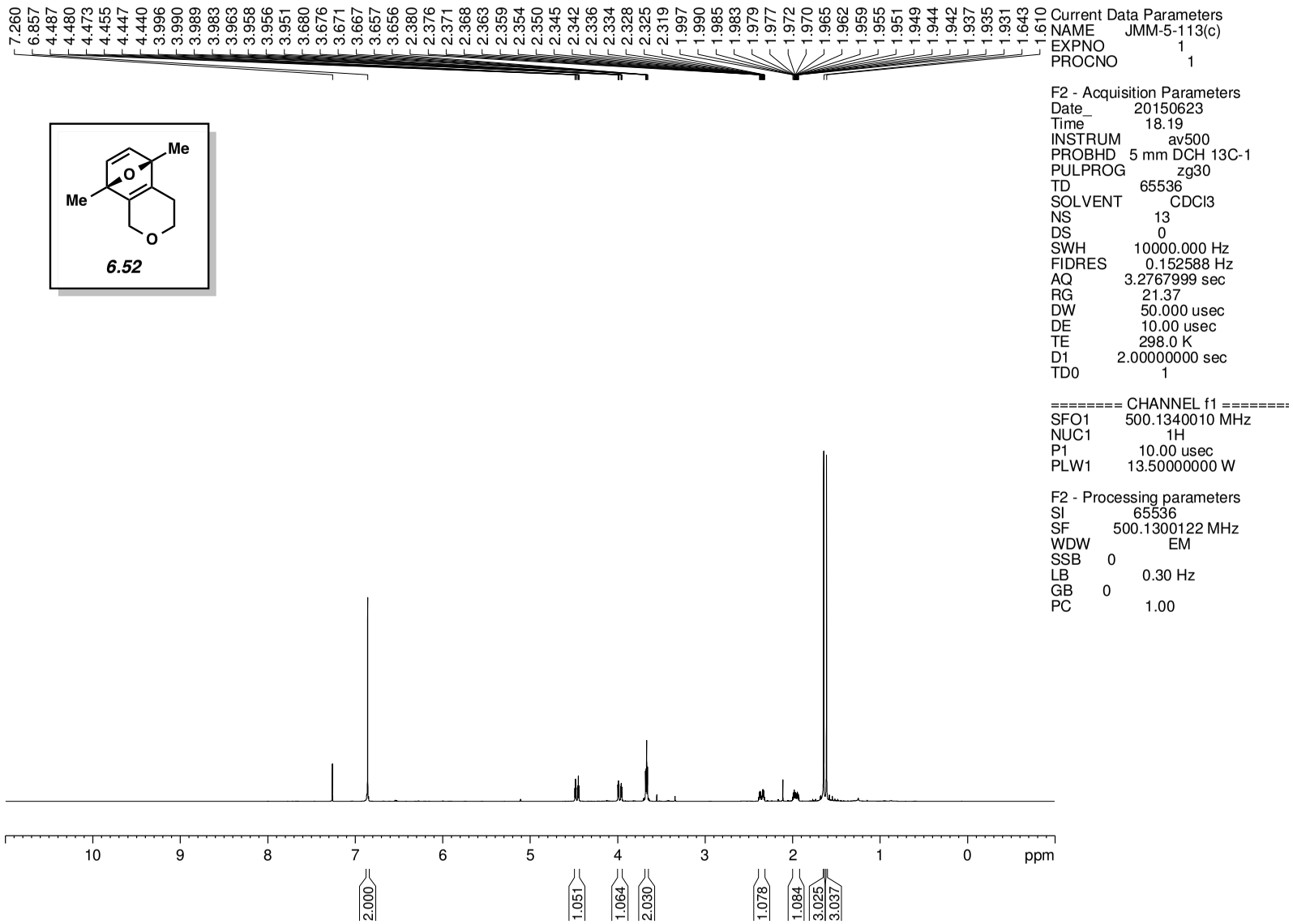

Figure 6.81. ^{1}H NMR (500 MHz, $CDCl_3$) compound **6.52**

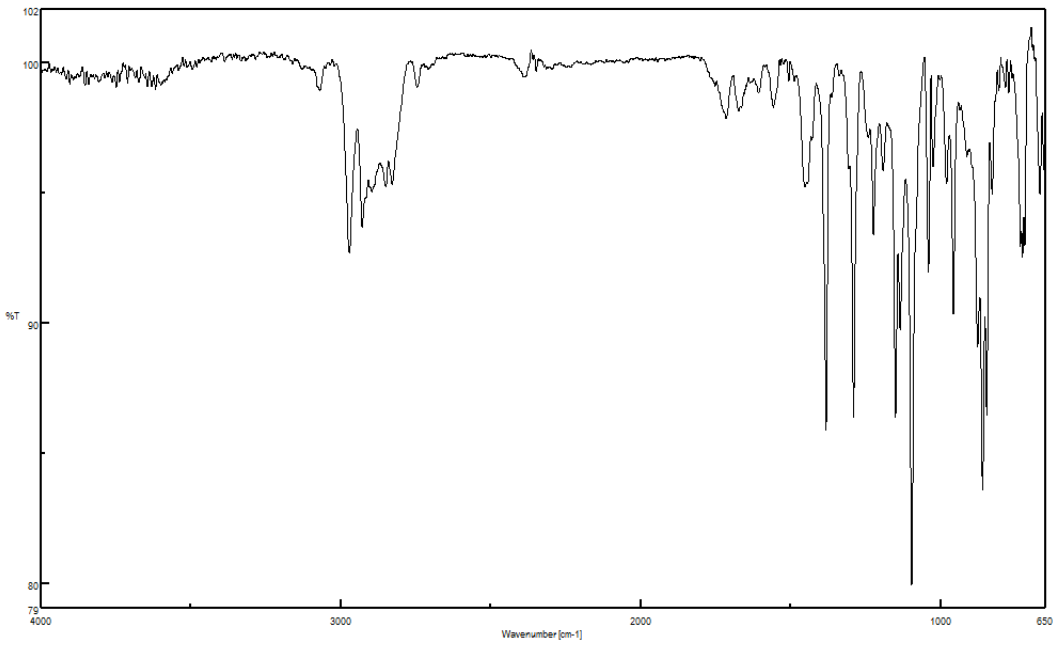

Figure 6.82. Infrared spectrum of compound **6.52**

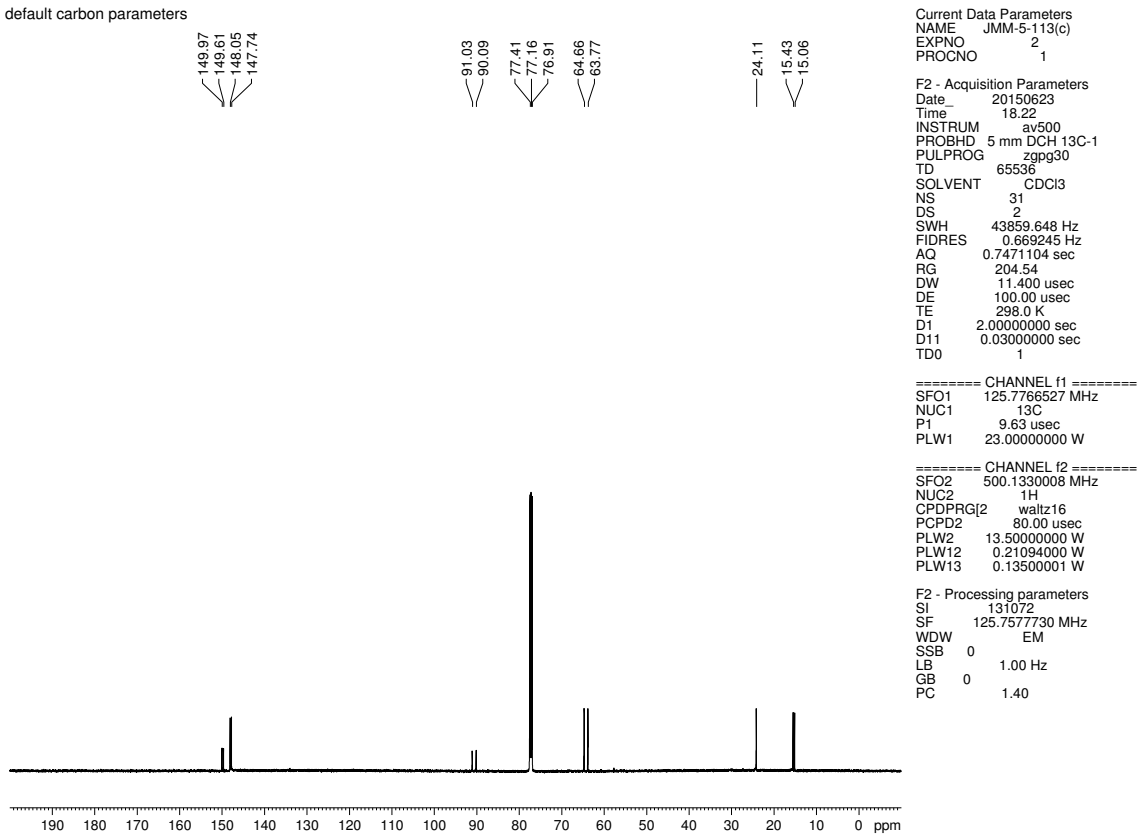

Figure 6.83. ^{13}C NMR (125 MHz, $CDCl_3$) of compound **6.52**

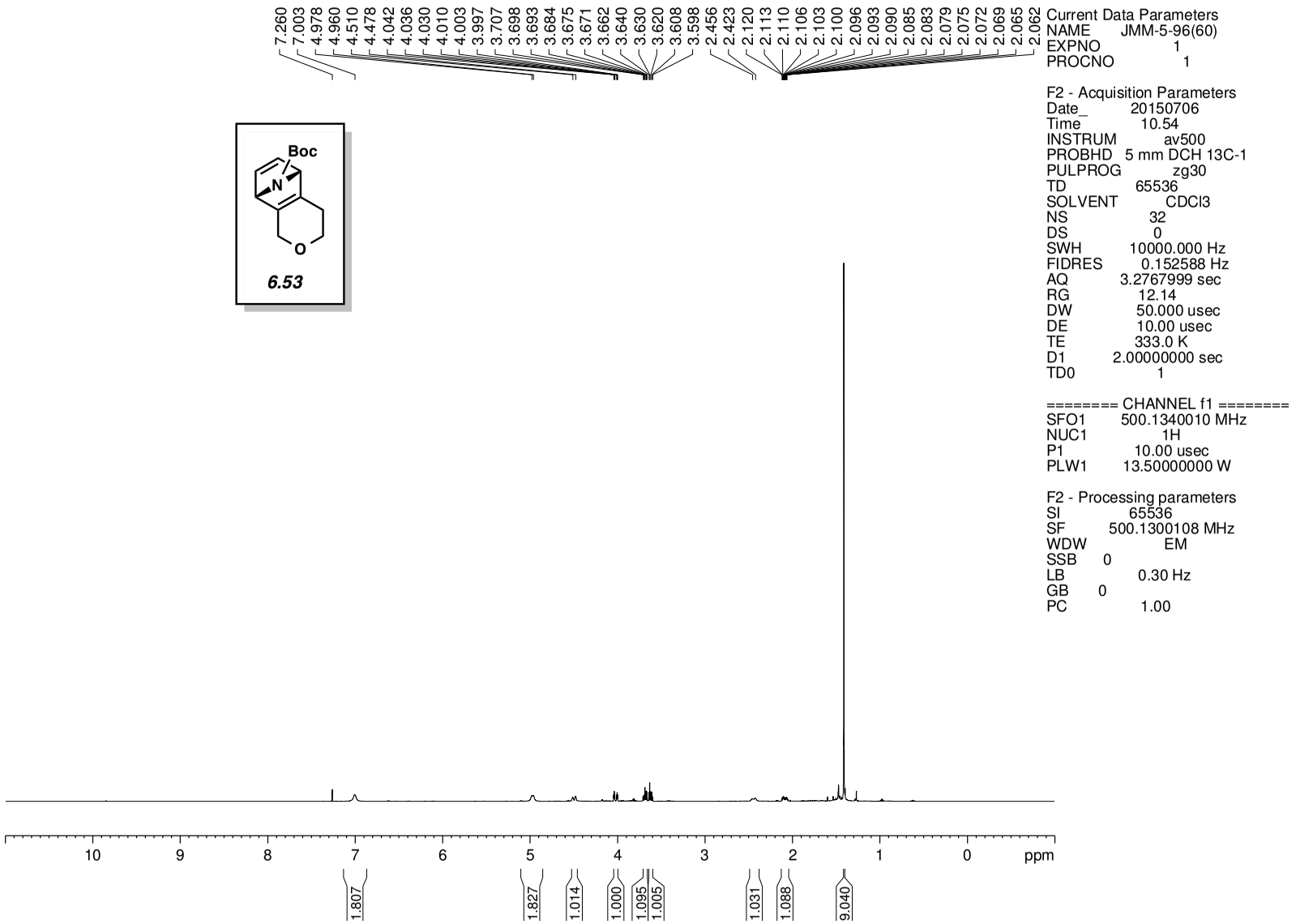

Figure 6.84. ^{1}H NMR (500 MHz, $CDCl_3$) compound **6.53**

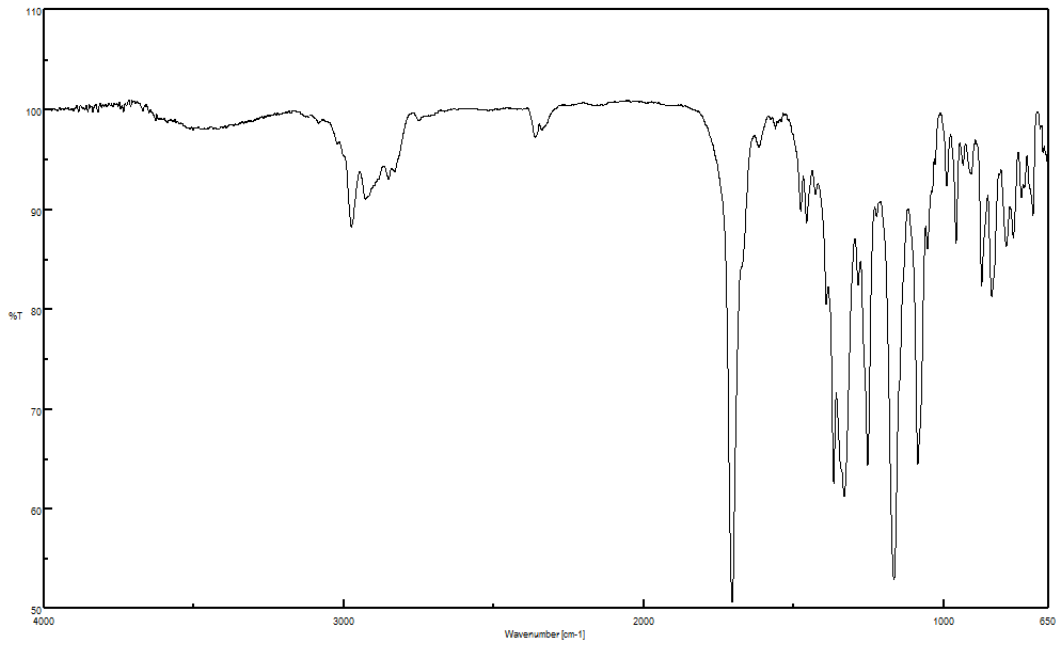

Figure 6.85. Infrared spectrum of compound **6.53**

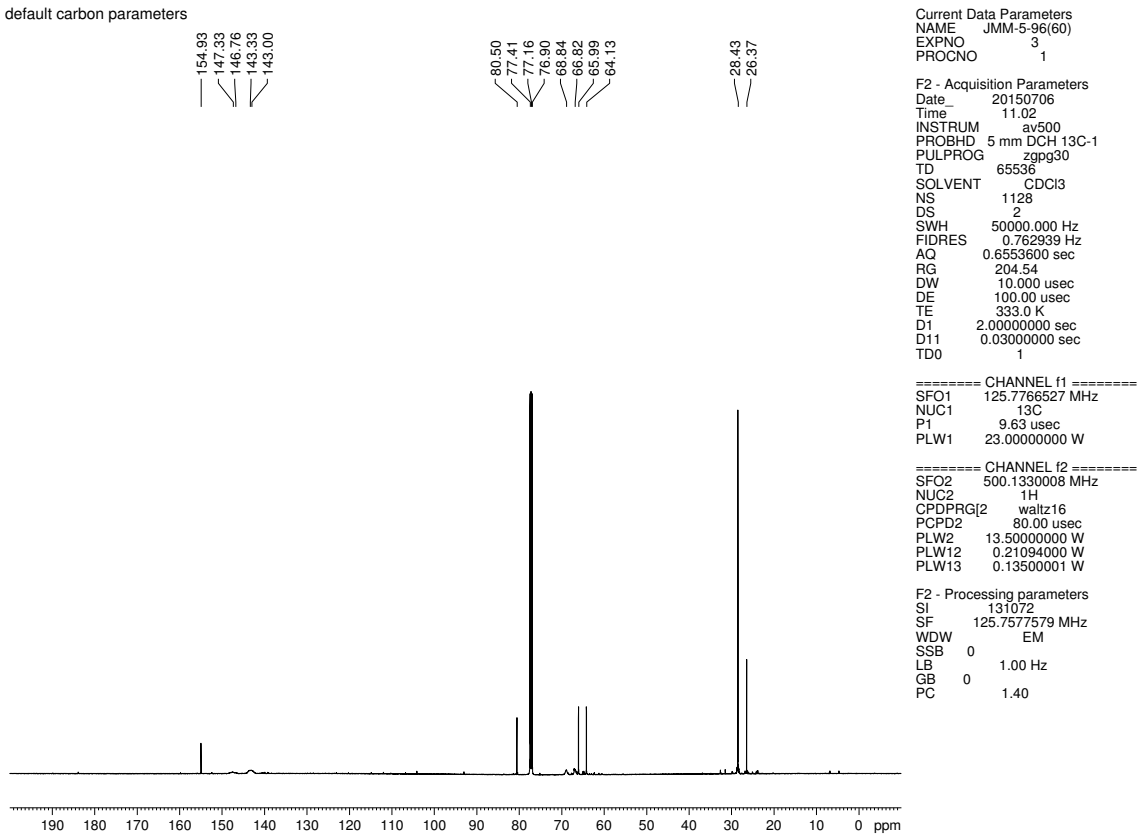

Figure 6.86. ^{13}C NMR (125 MHz, $CDCl_3$) of compound **6.53**

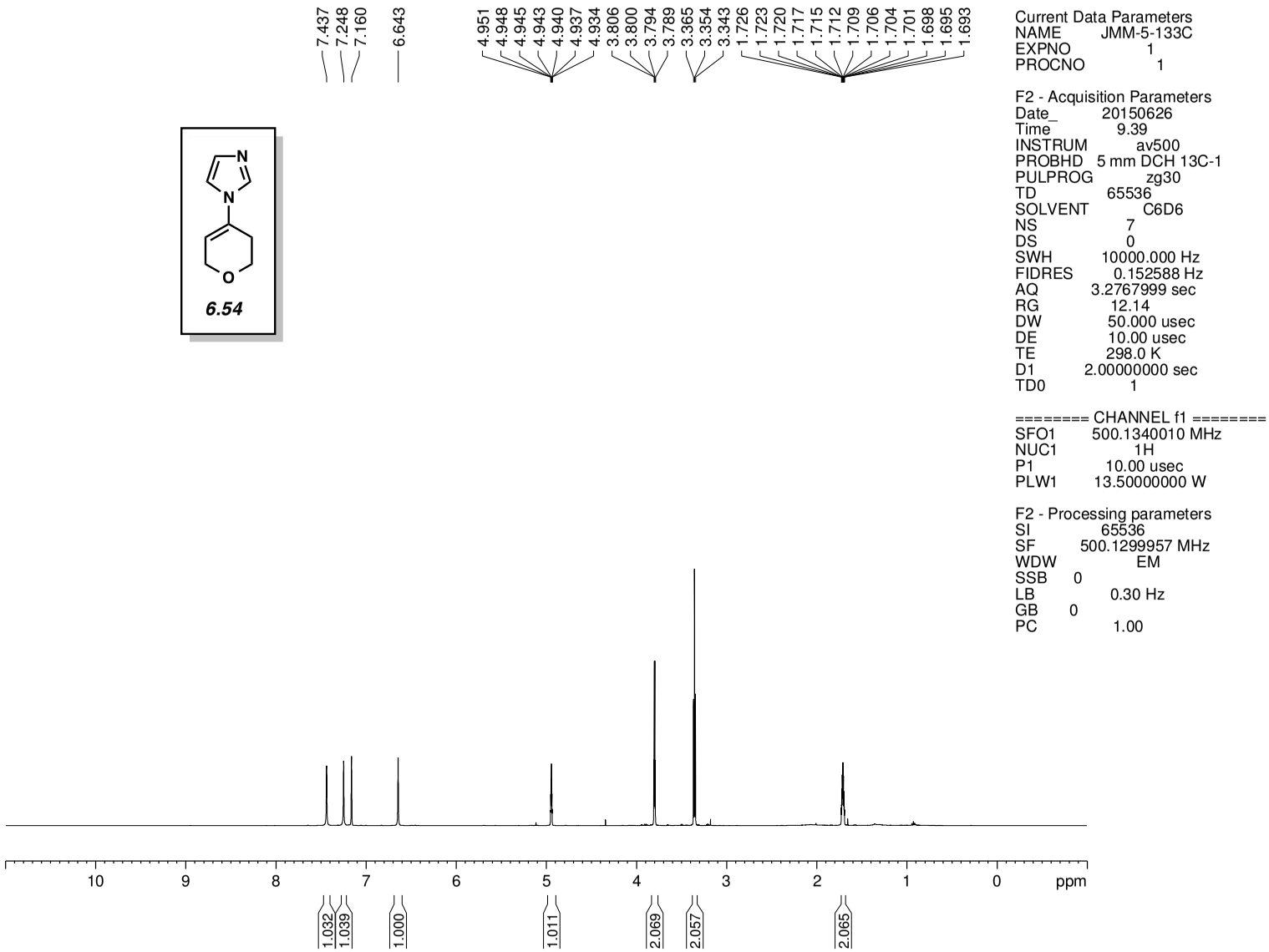

Figure 6.87. ^{1}H NMR (500 MHz, C_6D_6) compound **6.54**

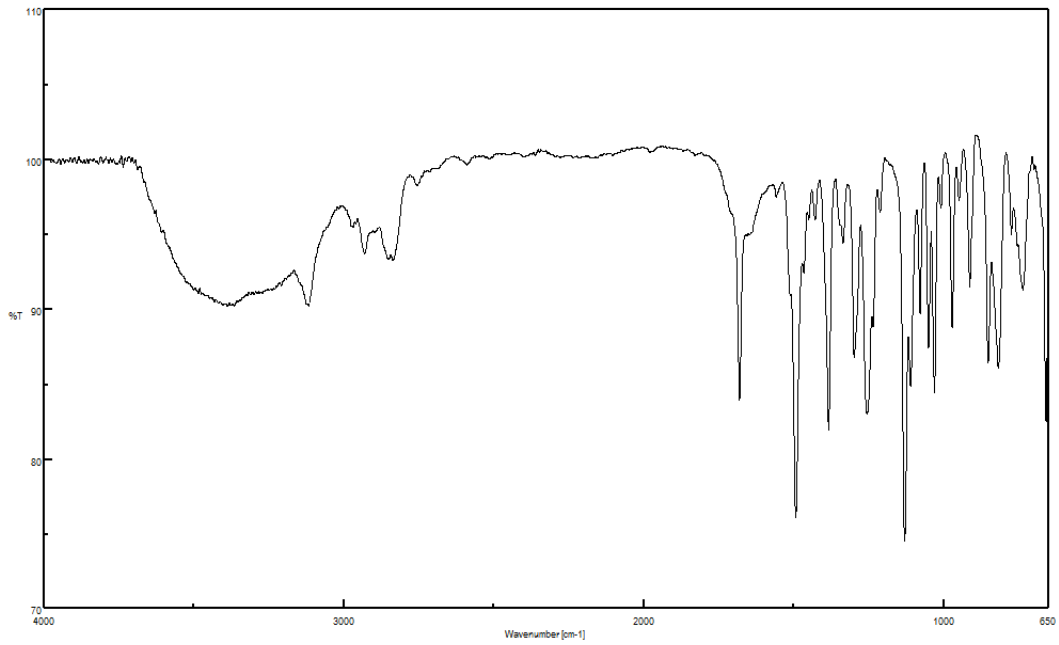

Figure 6.88. Infrared spectrum of compound **6.54**

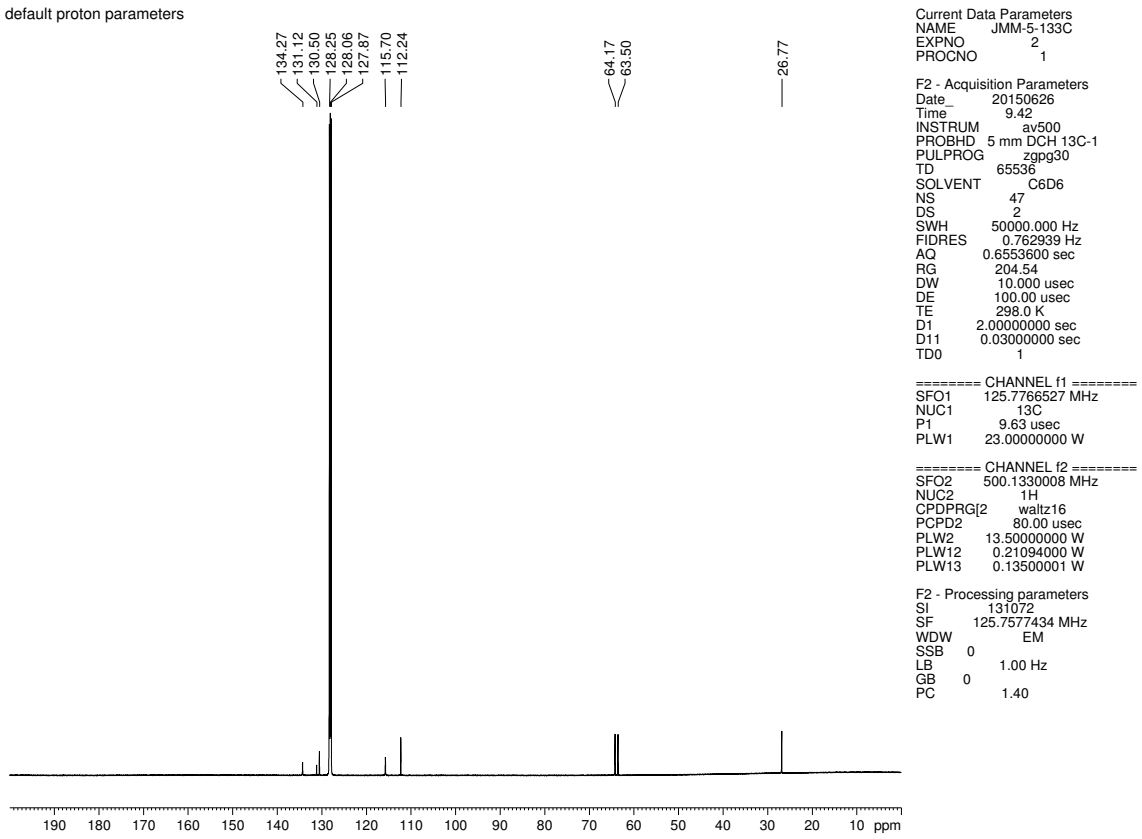

Figure 6.89. ^{13}C NMR (125 MHz, C_6D_6) of compound **6.54**

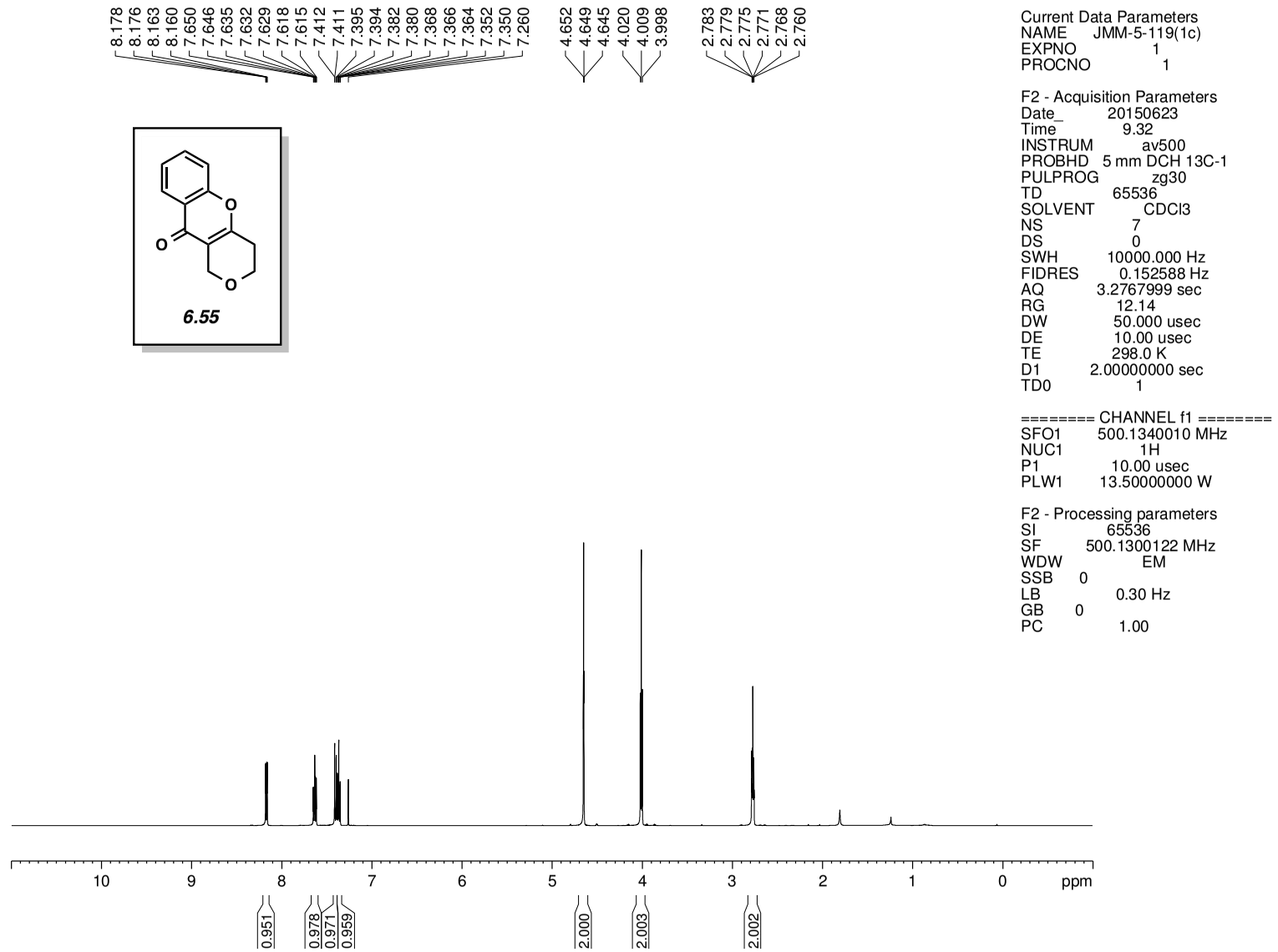

Figure 6.90. ^{1}H NMR (500 MHz, $CDCl_3$) compound **6.55**

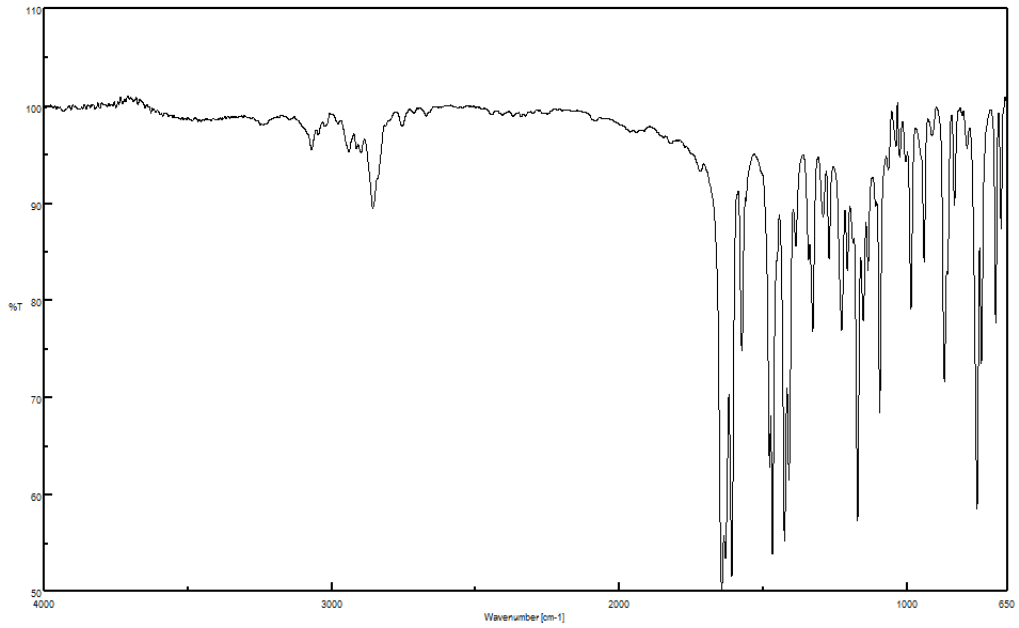

Figure 6.91. Infrared spectrum of compound **6.55**

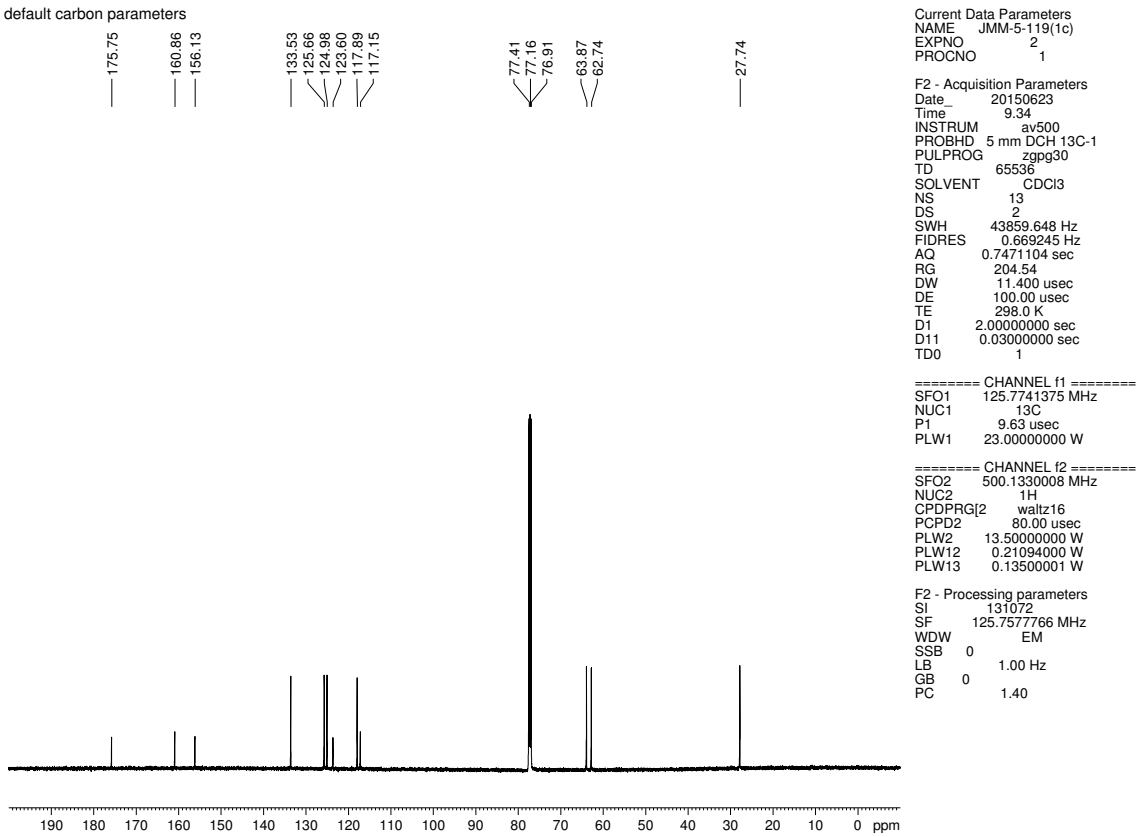

Figure 6.92. ^{13}C NMR (125 MHz, $CDCl_3$) of compound **6.55**

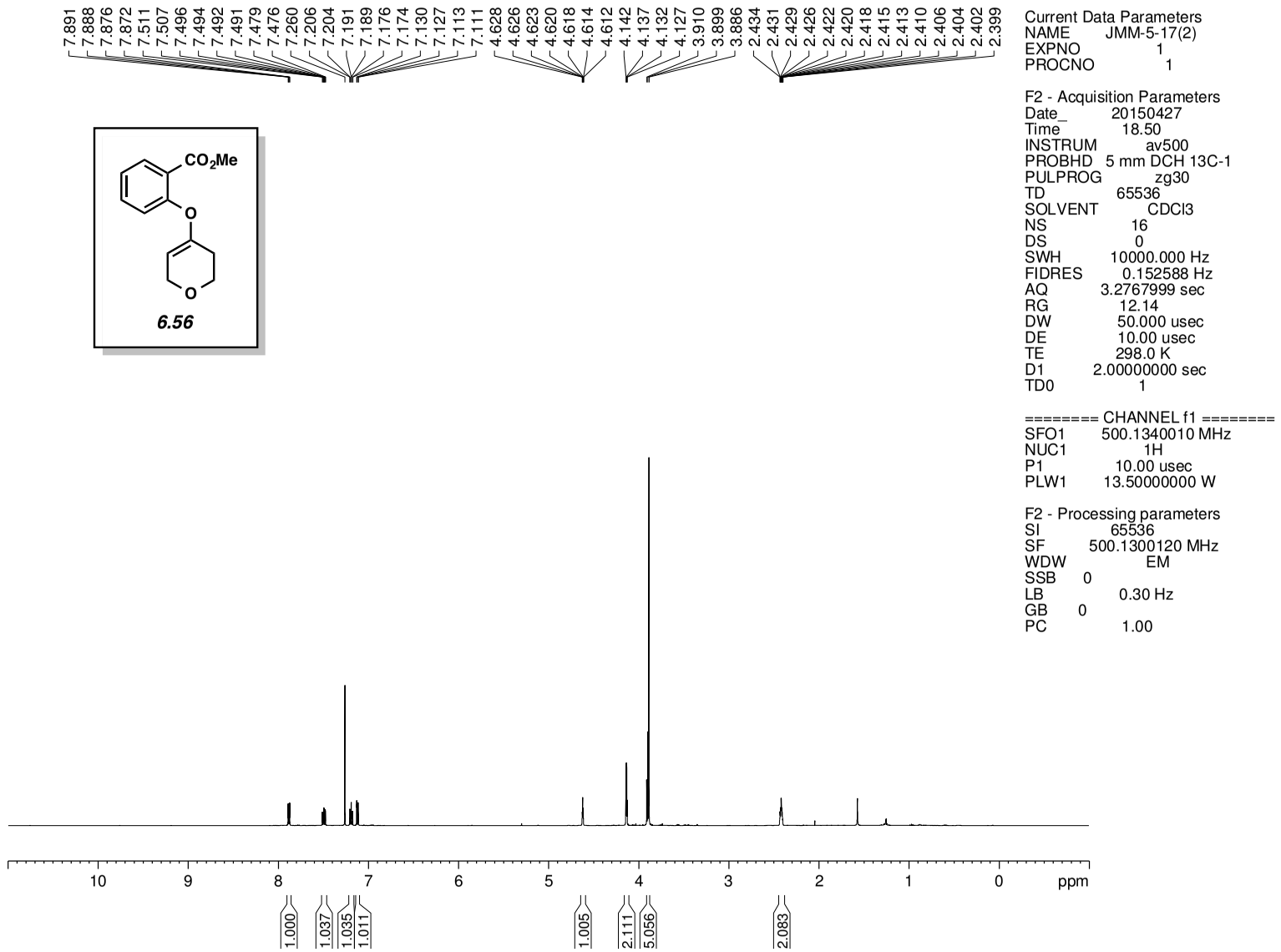

Figure 6.93. ^{1}H NMR (500 MHz, $CDCl_3$) compound **6.56**

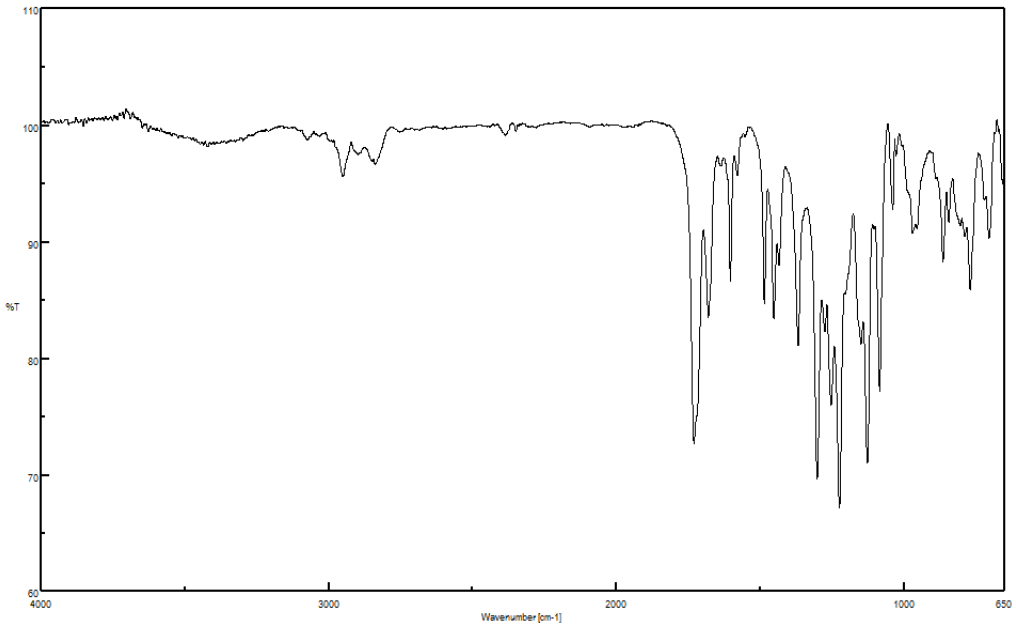

Figure 6.94. Infrared spectrum of compound **6.56**

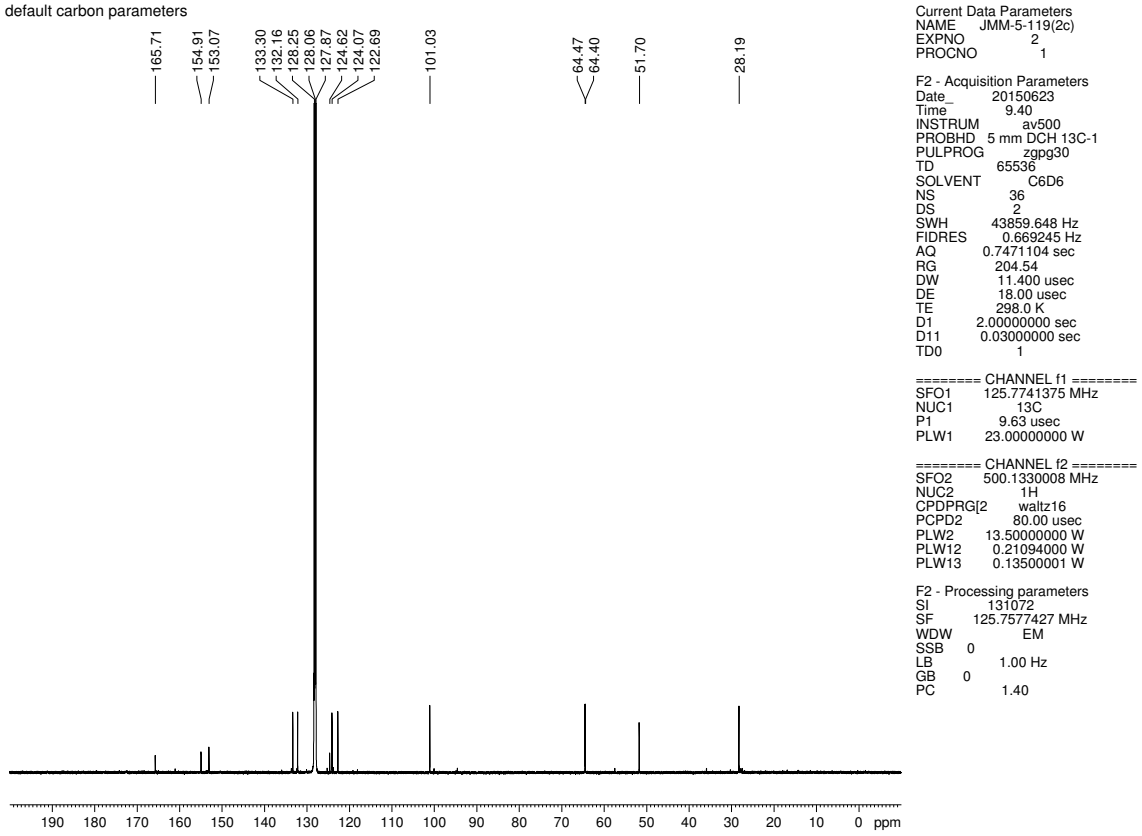

Figure 6.95. ^{13}C NMR (125 MHz, C_6D_6) of compound **6.56**

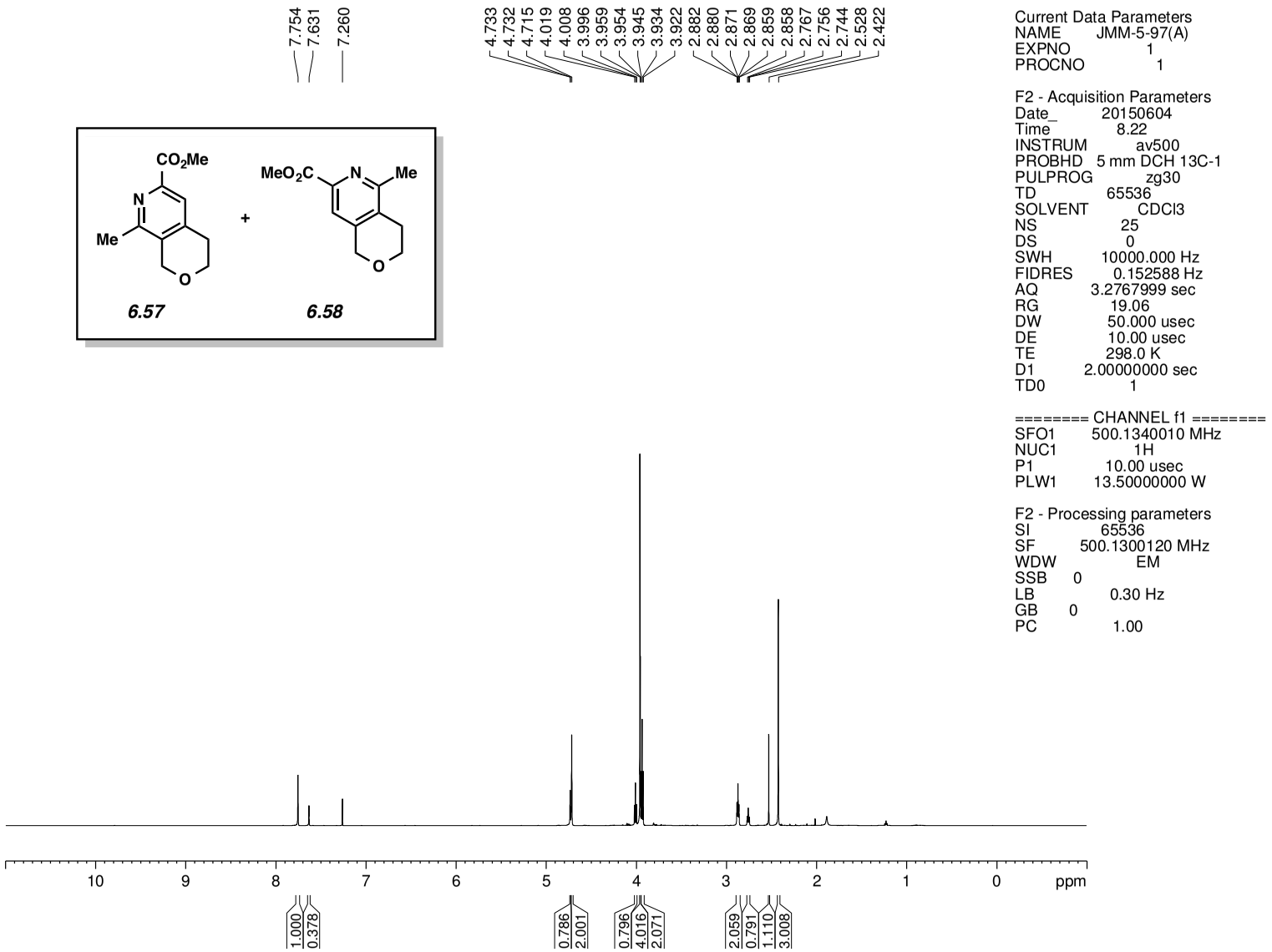

Figure 6.96. ^{1}H NMR (500 MHz, $CDCl_3$) compound **6.57** & **6.58**

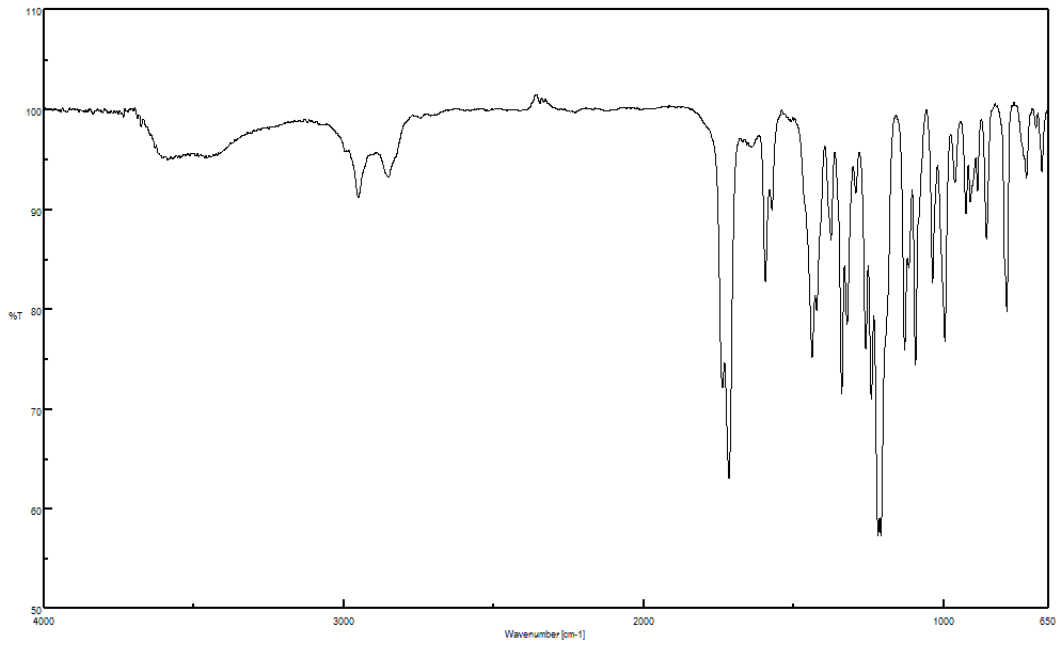

Figure 6.97. Infrared spectrum of compound **6.57** & **6.58**

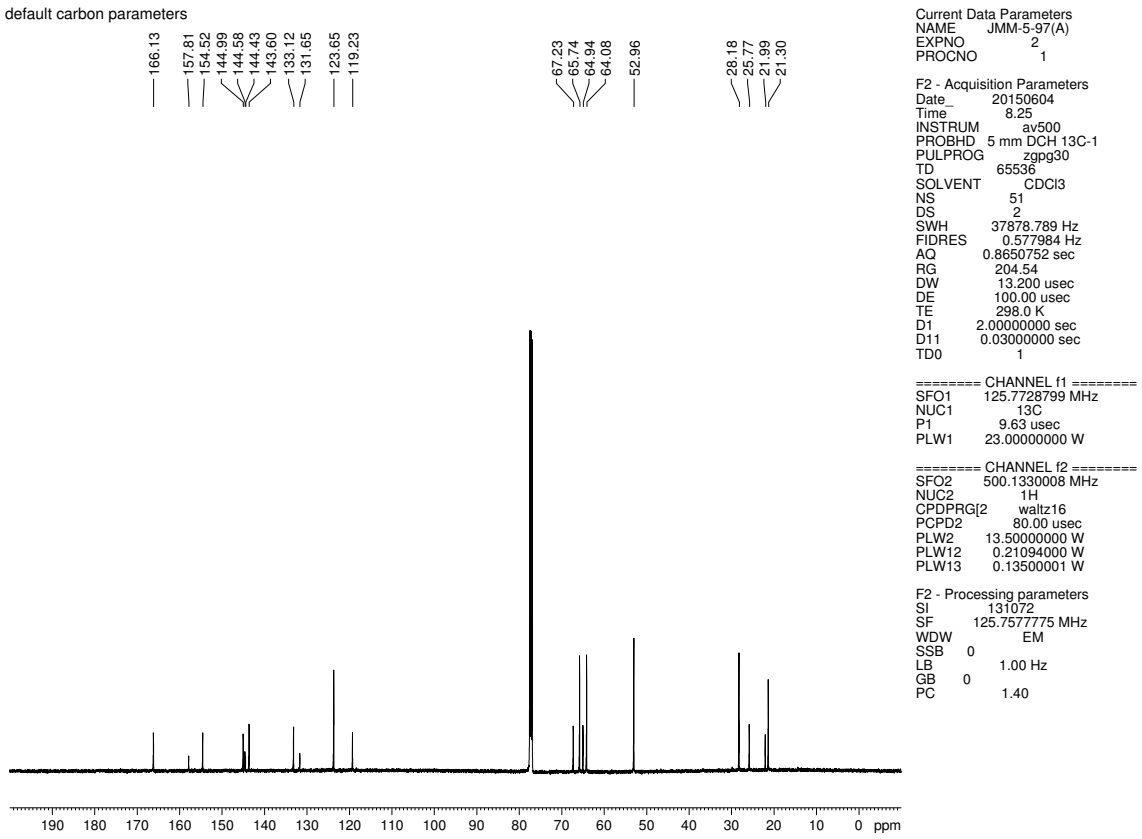

Figure 6.98. ^{13}C NMR (125 MHz, $CDCl_3$) of compound **6.57** & **6.58**

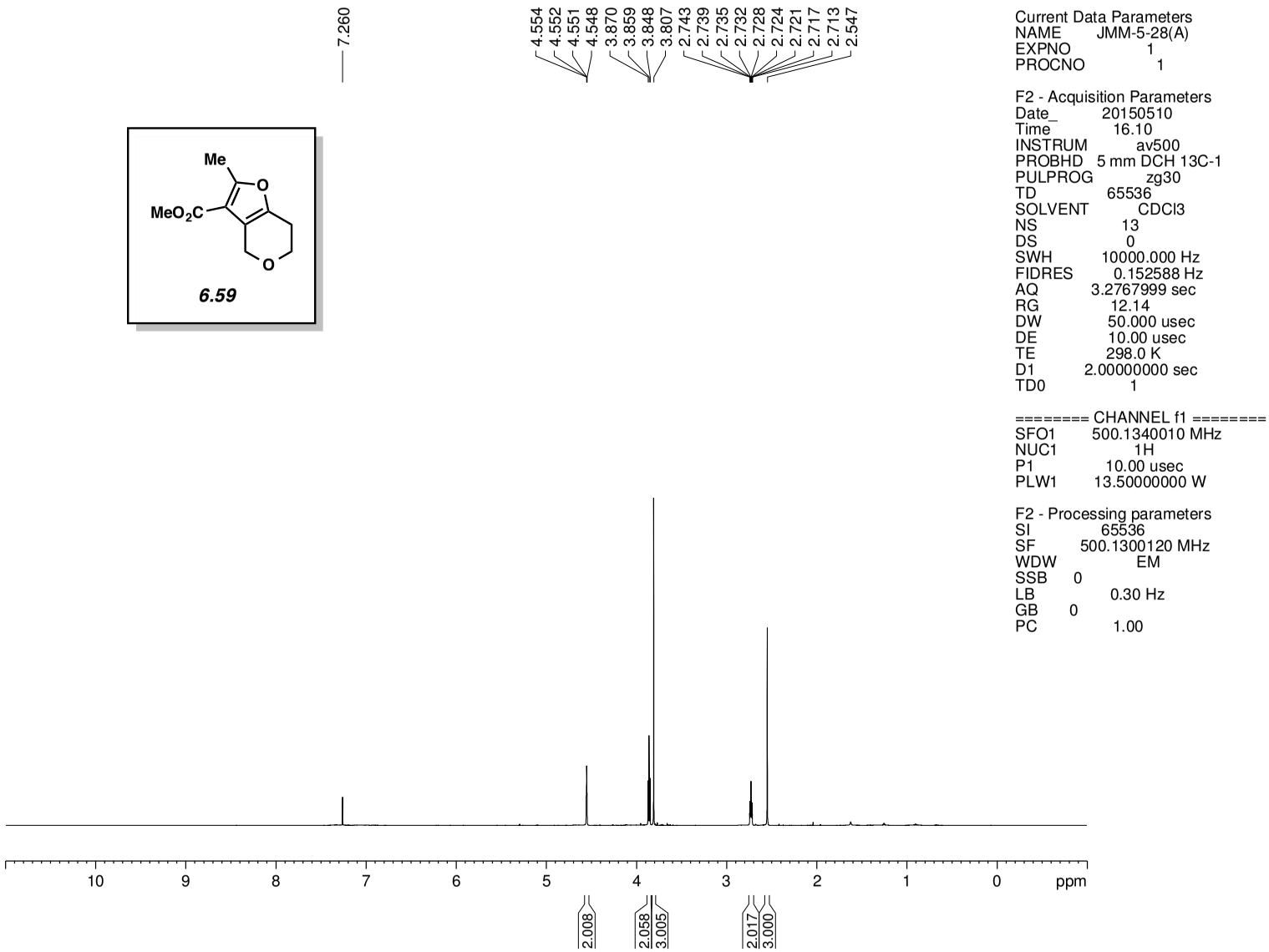

Figure 6.99. ^{1}H NMR (500 MHz, $CDCl_3$) compound **6.59**

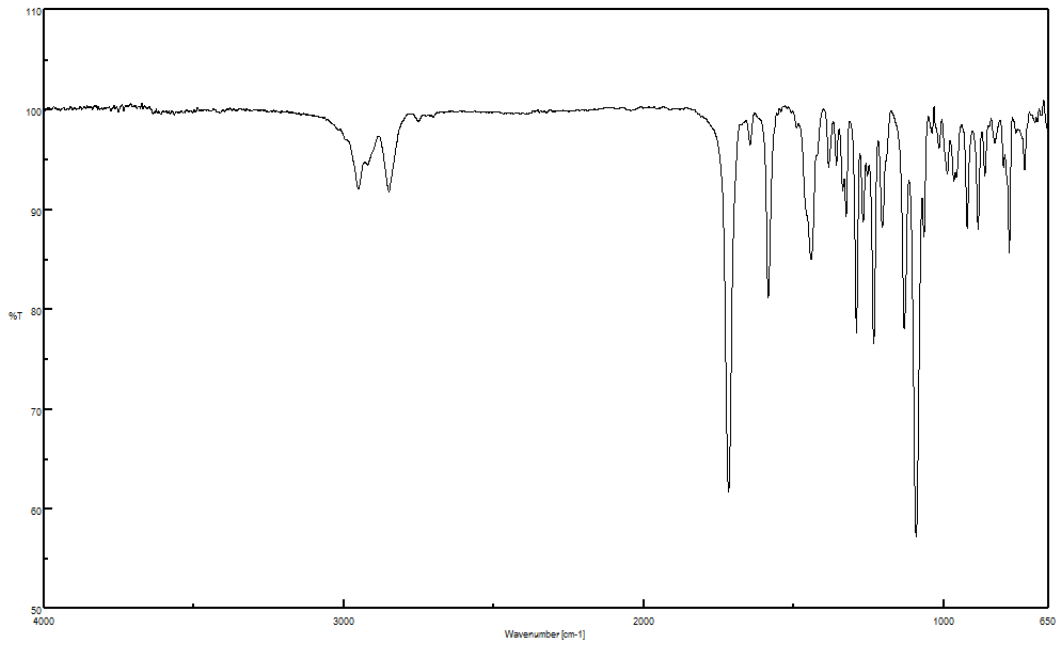

Figure 6.100. Infrared spectrum of compound **6.59**

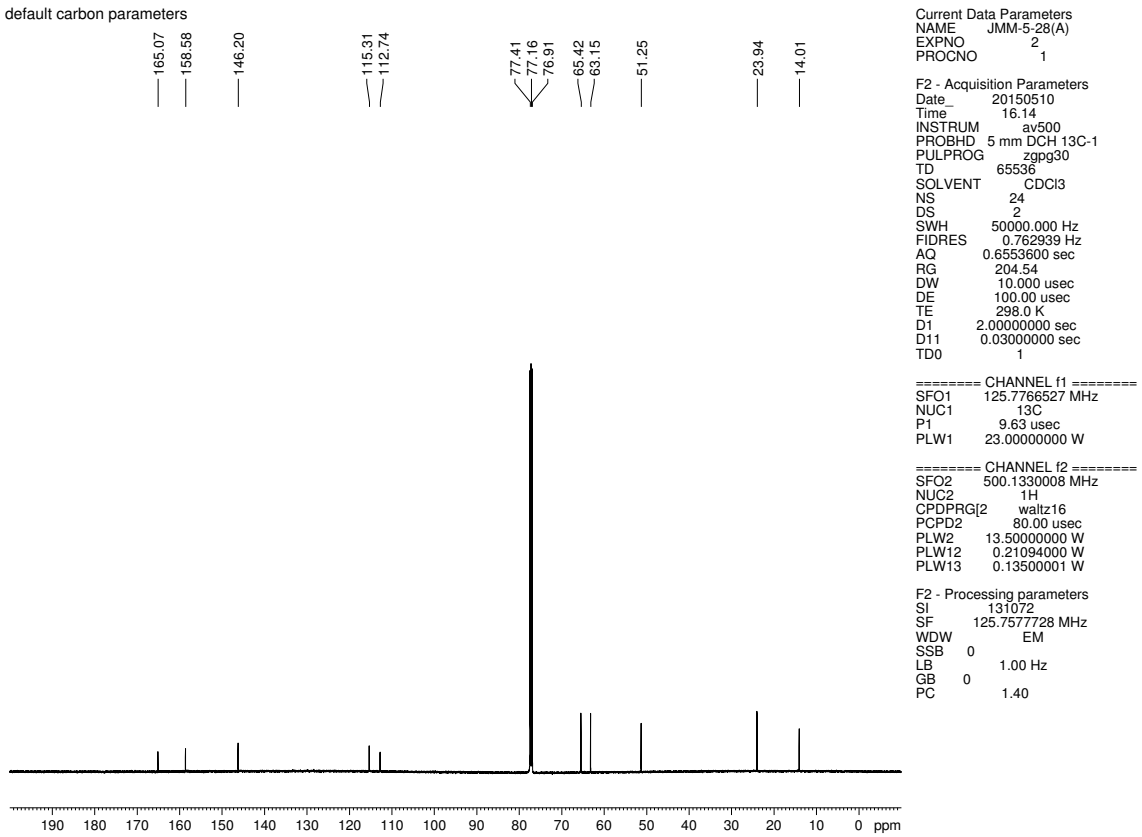

Figure 6.101. ^{13}C NMR (125 MHz, $CDCl_3$) of compound **6.59**

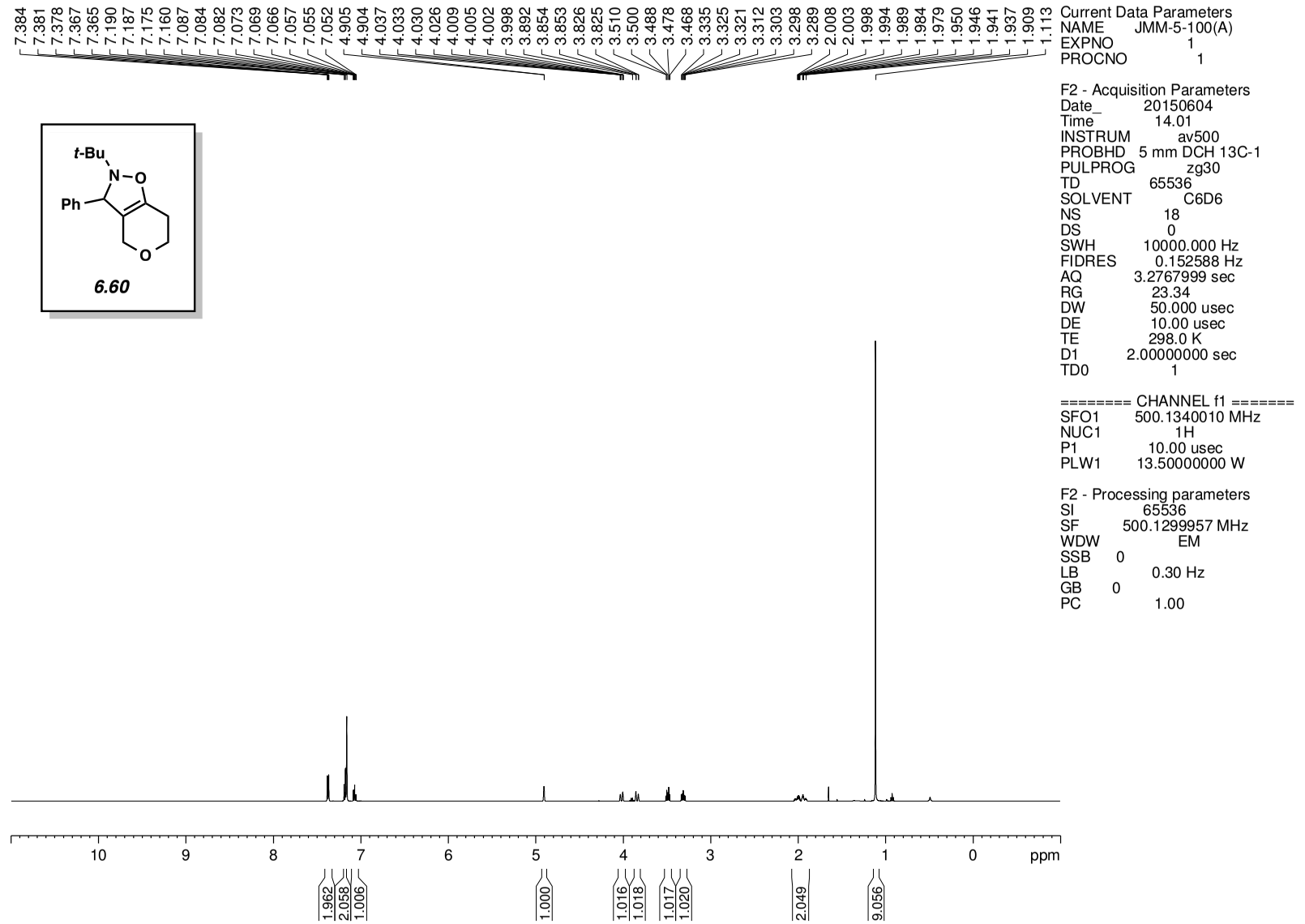

Figure 6.102. ^{1}H NMR (500 MHz, C_6D_6) compound **6.60**

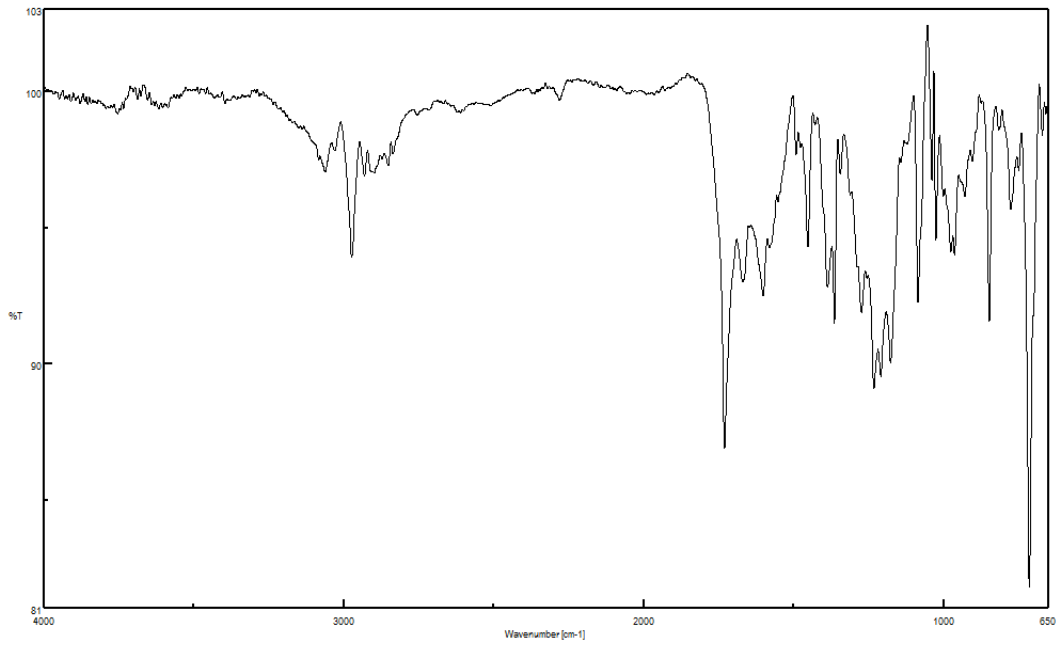

Figure 6.103. Infrared spectrum of compound **6.60**

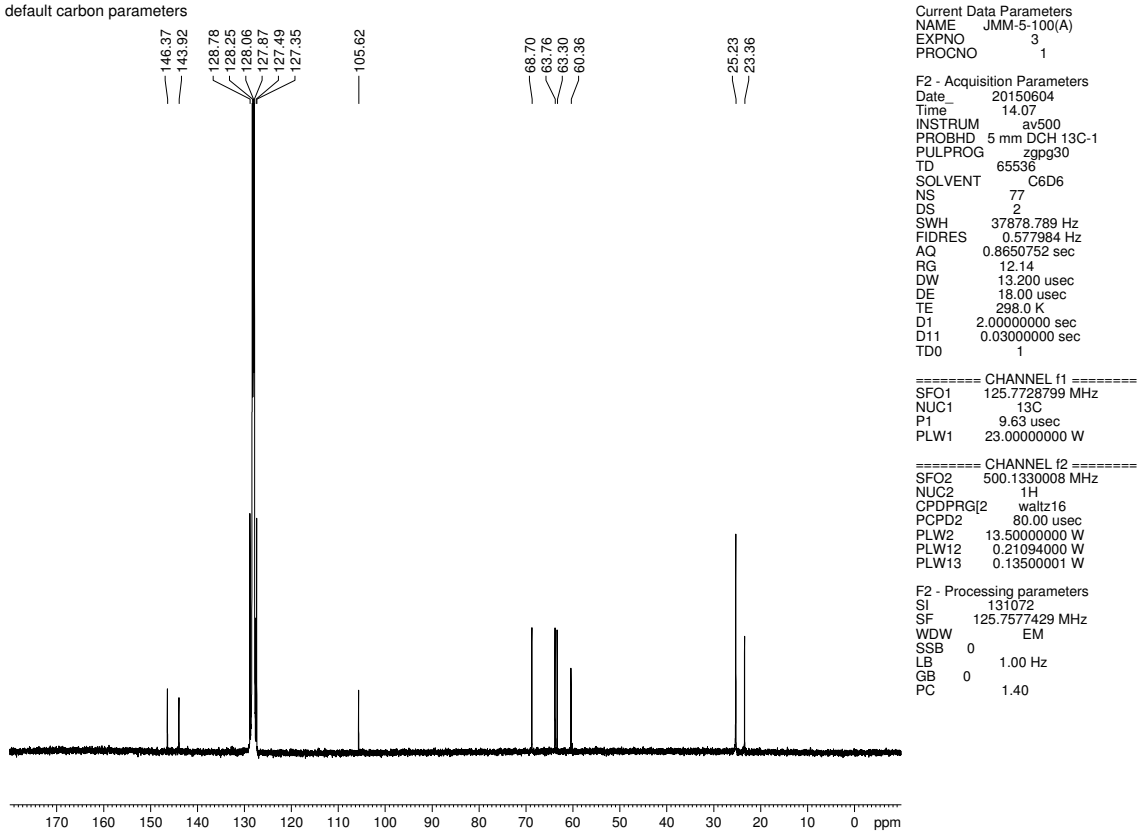

Figure 6.104. ^{13}C NMR (125 MHz, C_6D_6) of compound **6.60**

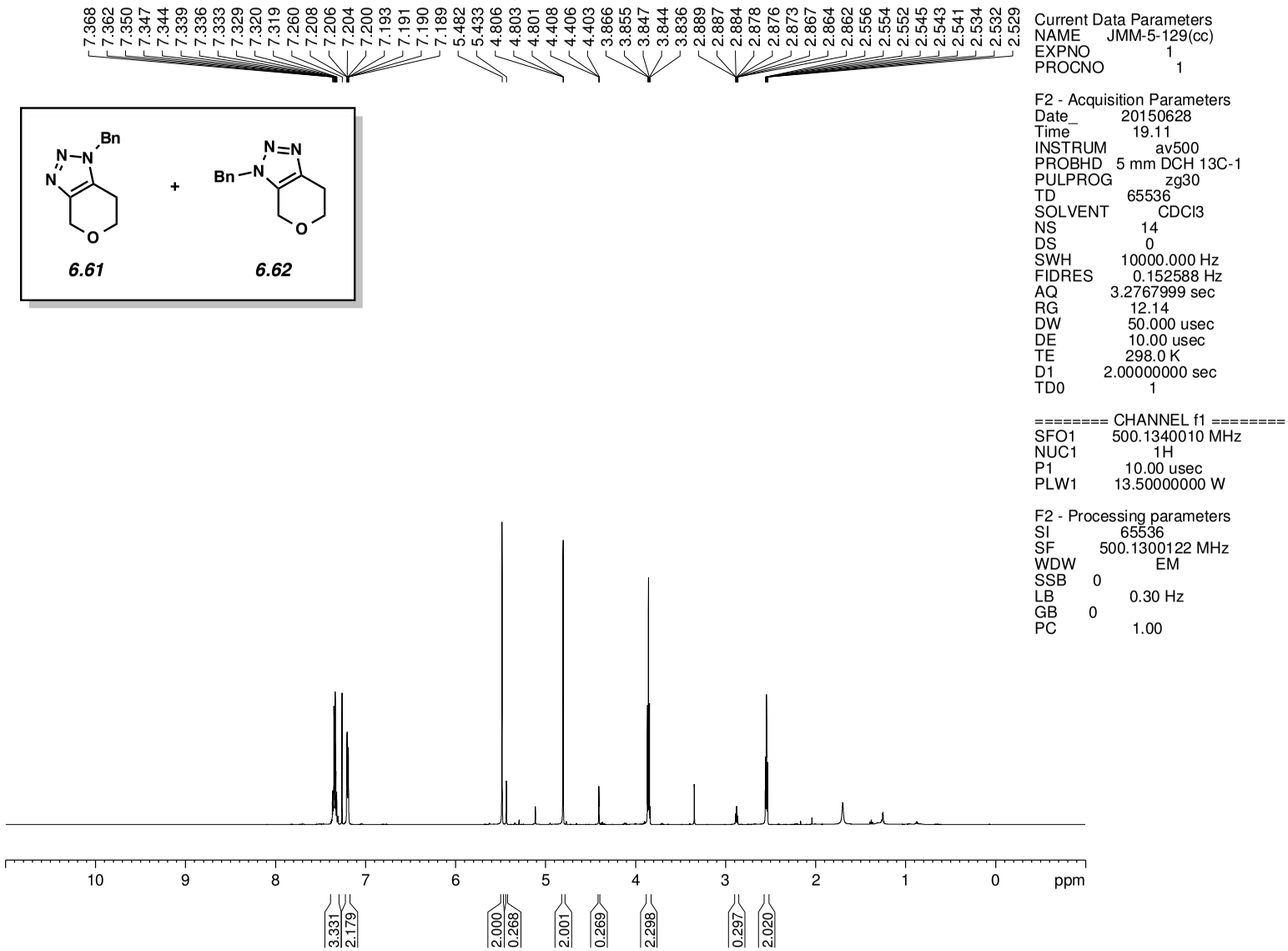

Figure 6.105. ^{1}H NMR (500 MHz, $CDCl_3$) compounds **6.61** & **6.62**

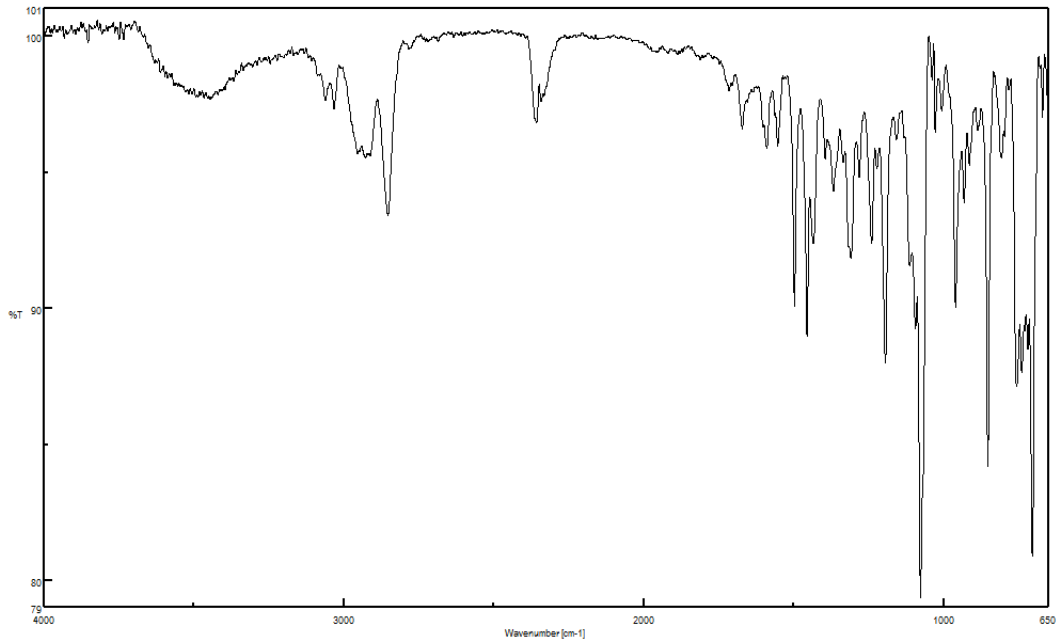

Figure 6.106. Infrared spectrum of compounds **6.61** & **6.62**

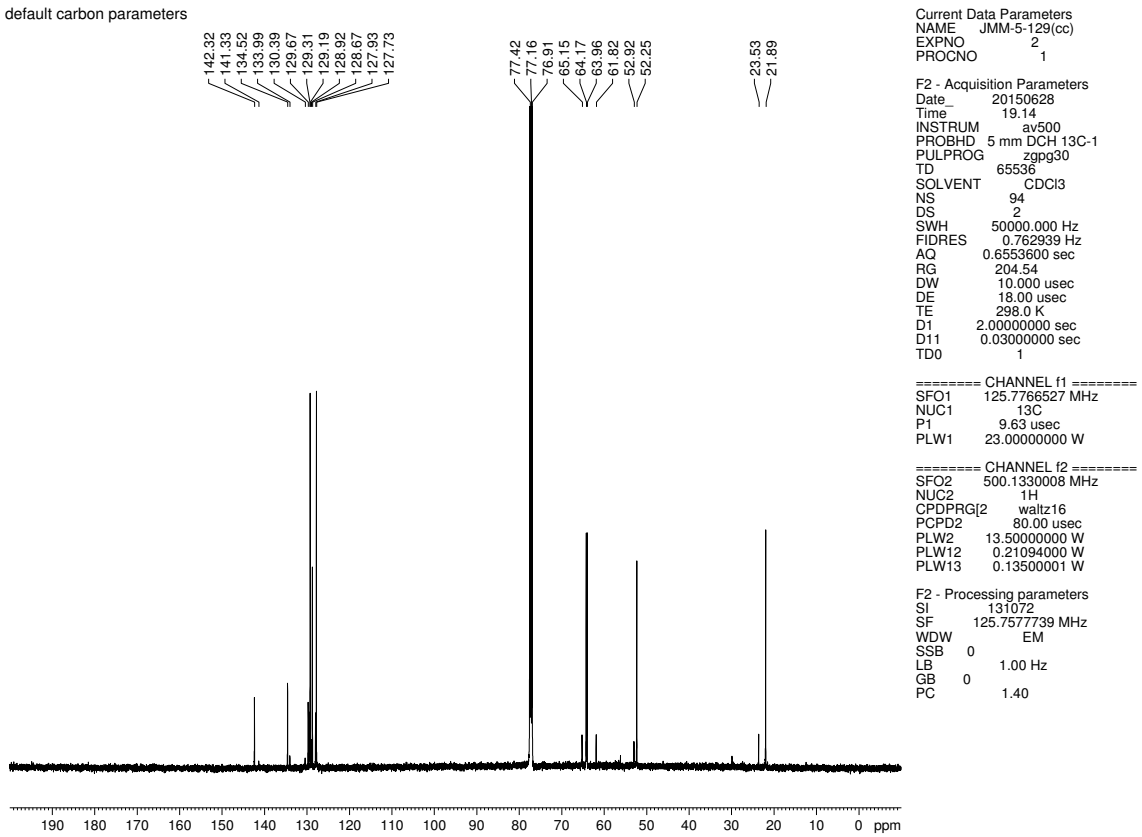

Figure 6.107. ^{13}C NMR (125 MHz, $CDCl_3$) of compounds **6.61** & **6.62**

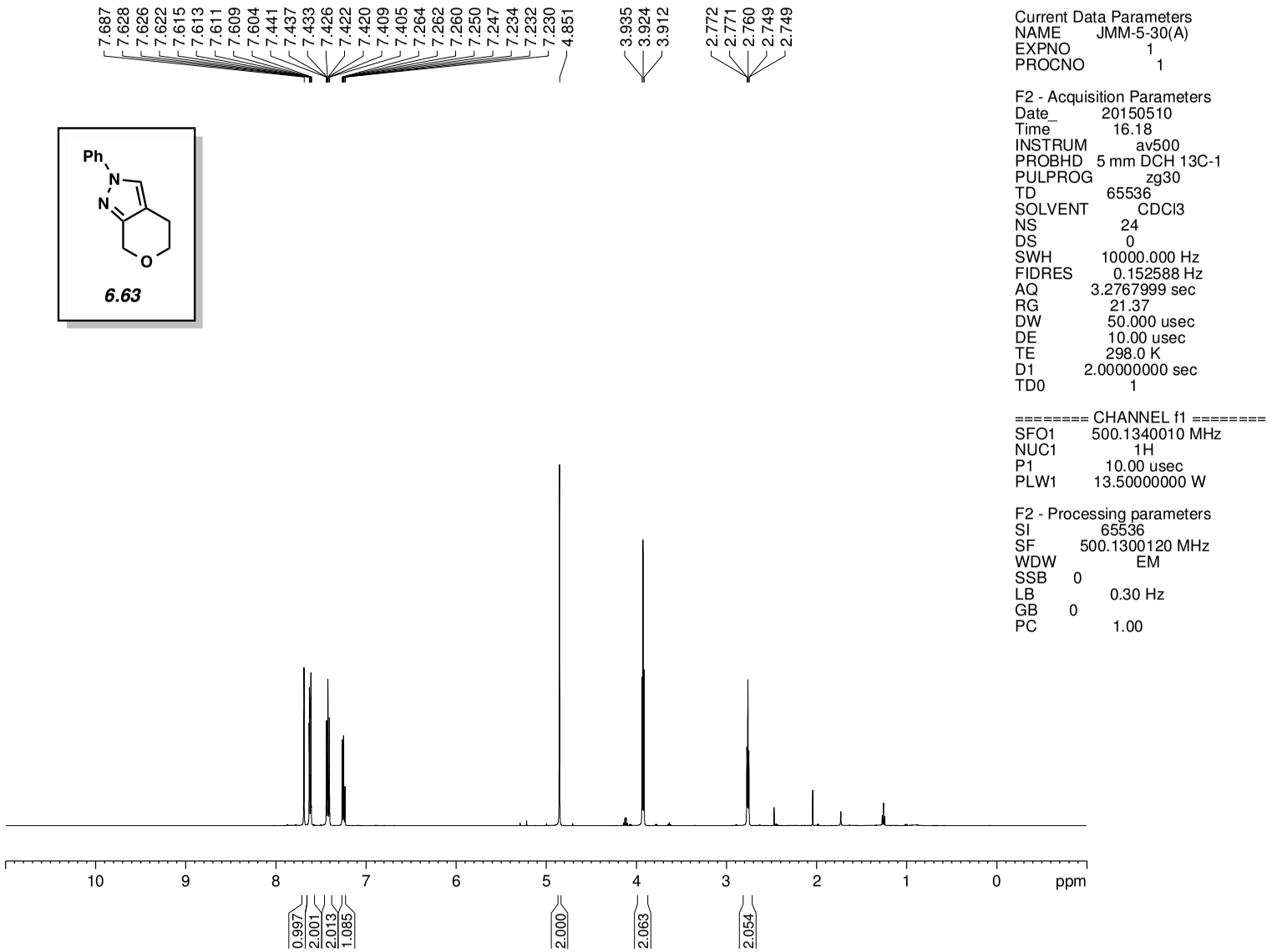

Figure 6.108. ^{1}H NMR (500 MHz, $CDCl_3$) compound **6.63**

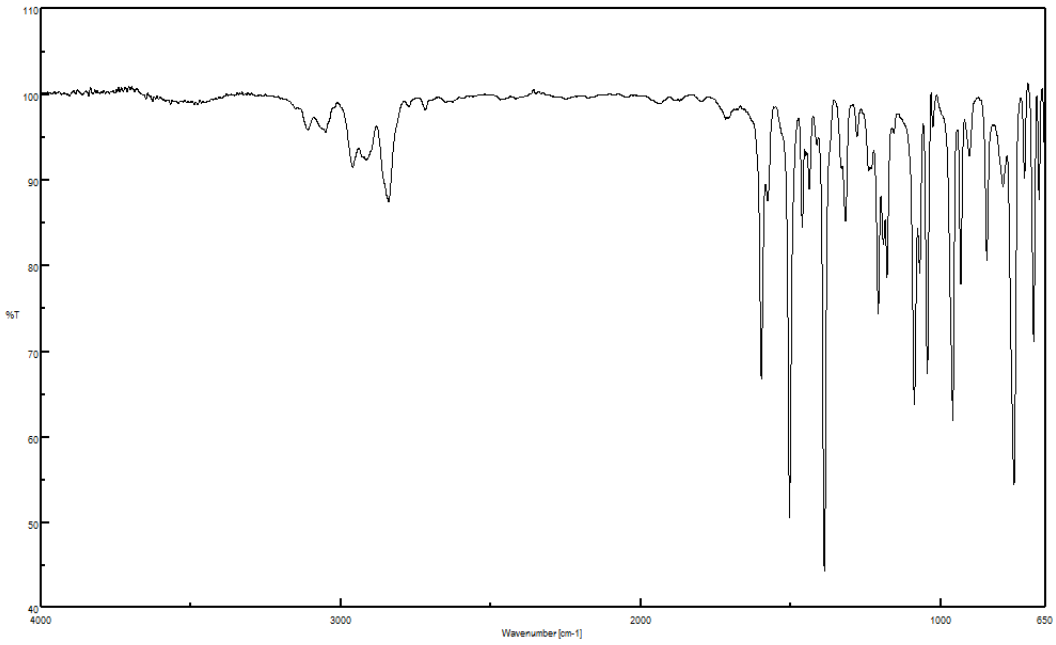

Figure 6.109. Infrared spectrum of compound **6.63**

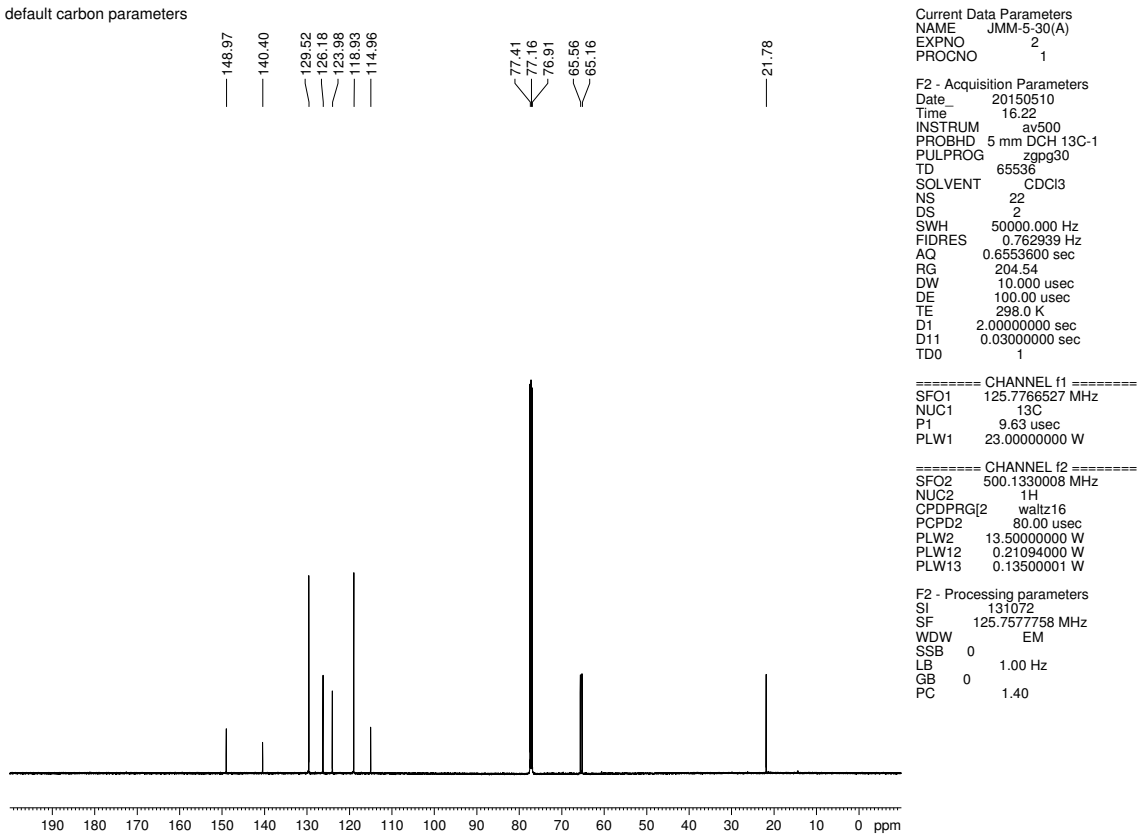

Figure 6.110. ^{13}C NMR (125 MHz, $CDCl_3$) of compound **6.63**

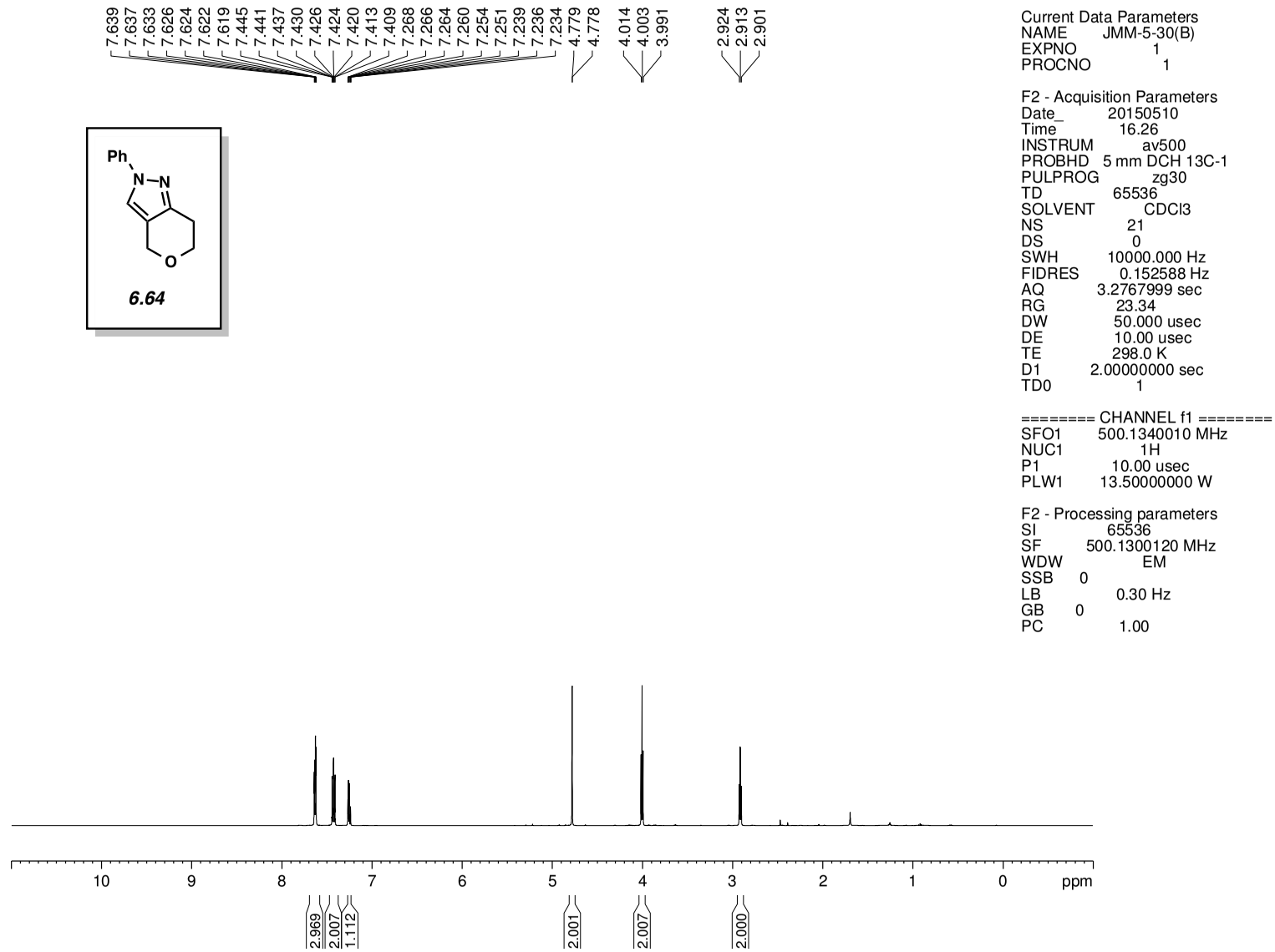

Figure 6.111. ^{1}H NMR (500 MHz, $CDCl_3$) compound **6.64**

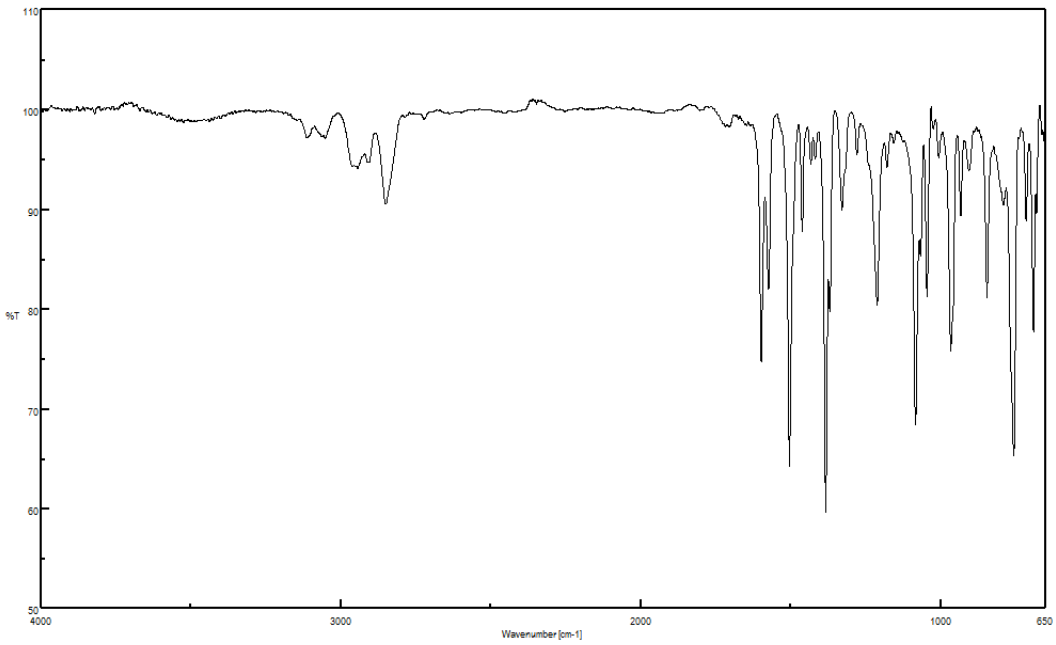

Figure 6.112. Infrared spectrum of compound **6.64**

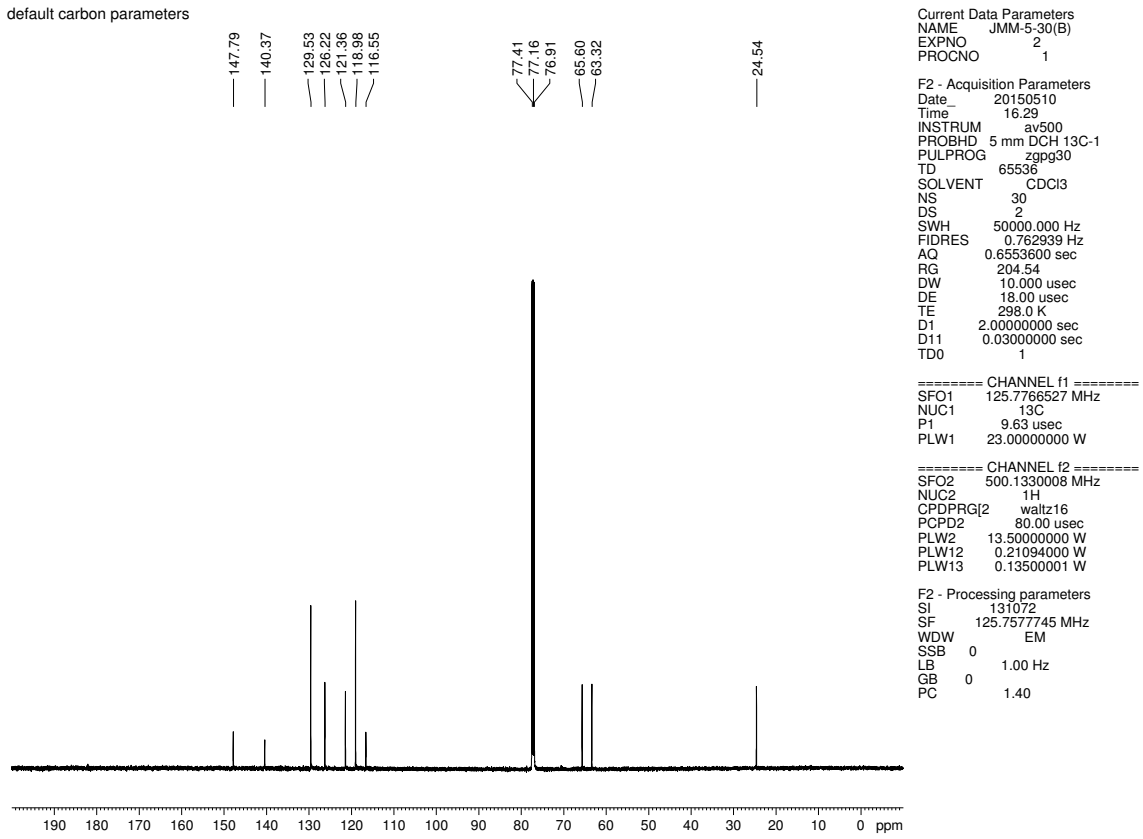

Figure 6.113. ^{13}C NMR (125 MHz, $CDCl_3$) of compound **6.64**

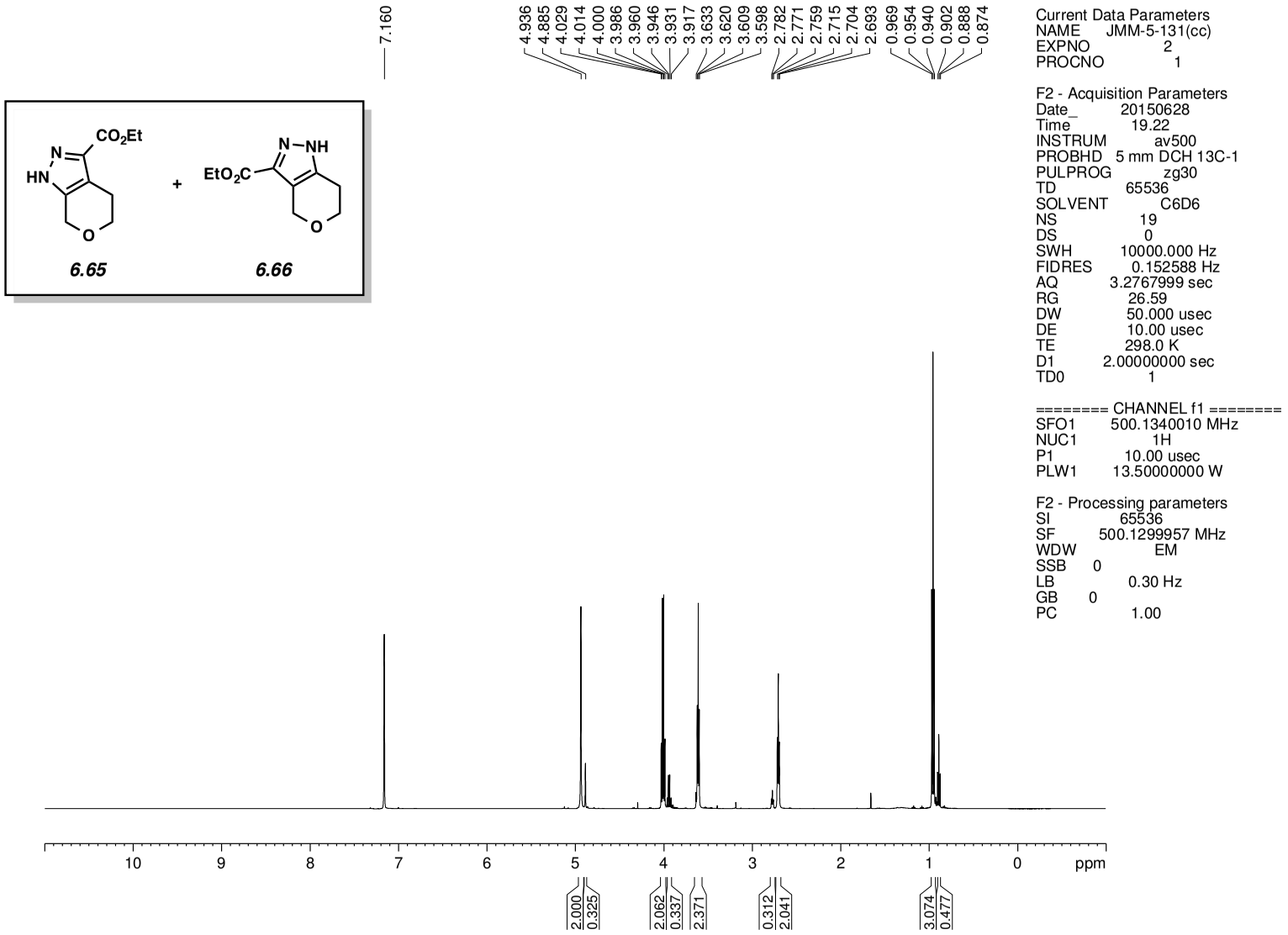

Figure 6.114. ^{1}H NMR (500 MHz, C_6D_6) compounds **6.65** & **6.66**

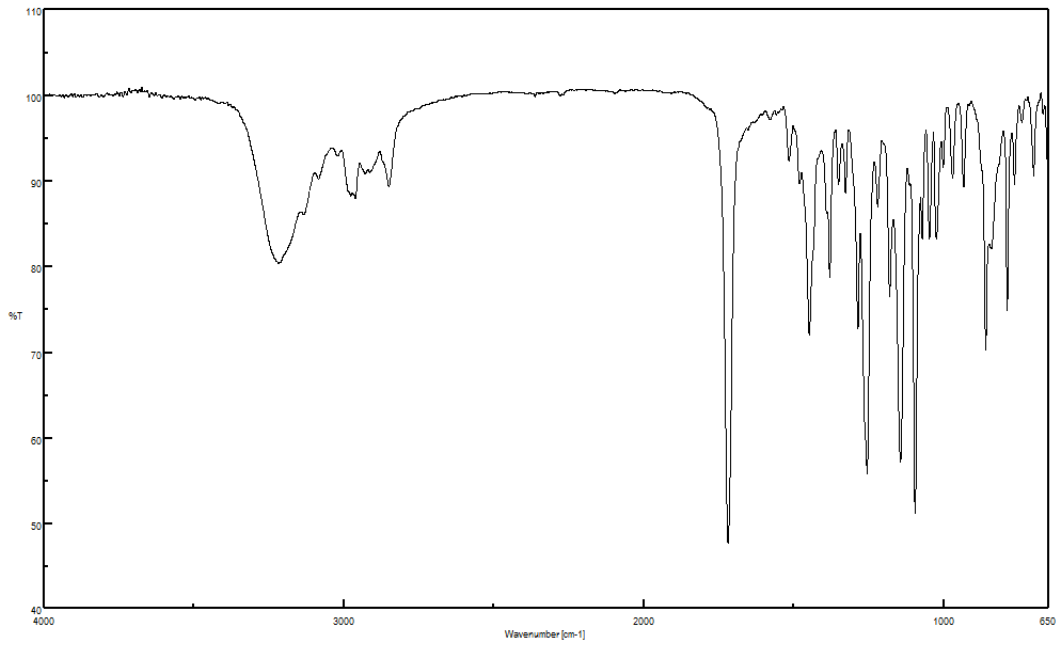

Figure 6.115. Infrared spectrum of compounds **6.65** & **6.66**

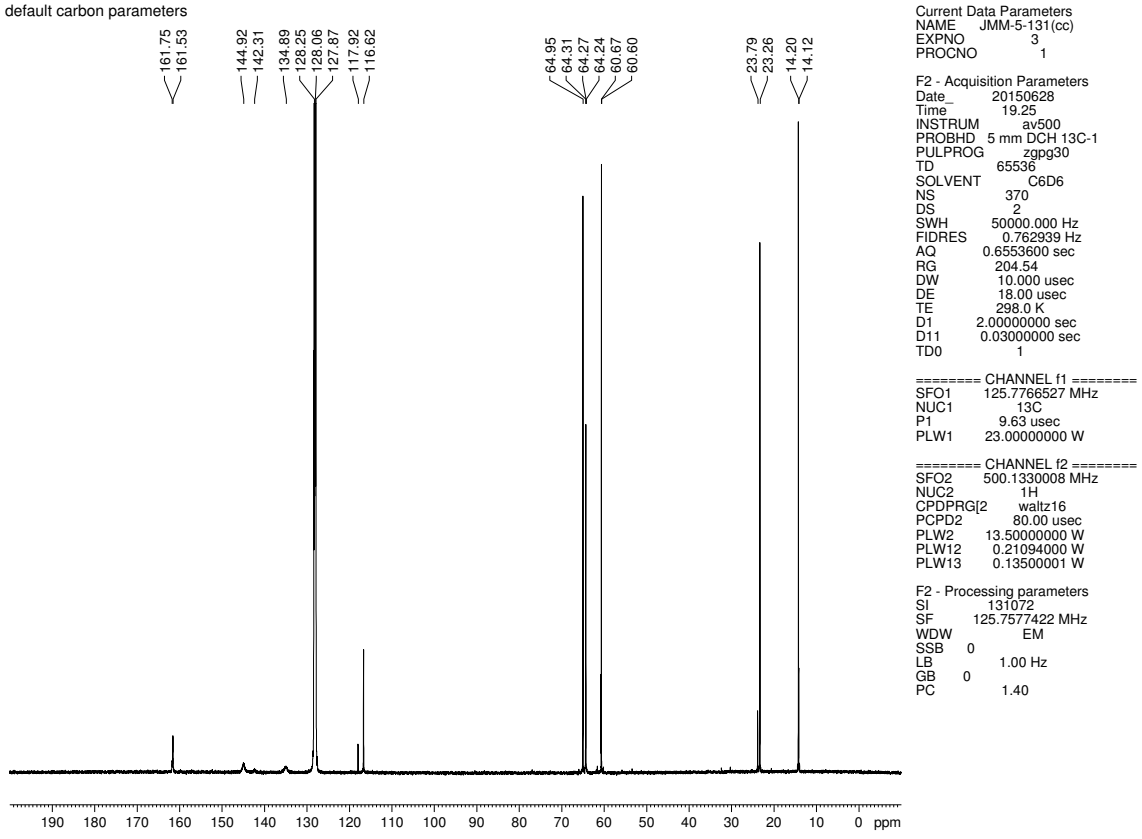

Figure 6.116. ^{13}C NMR (125 MHz, C_6D_6) of compounds **6.65** & **6.66**

6.7 Notes and References

(1) (a) Vitaku, E.; Smith, B. R.; Smith, D. T.; Njardarson, J. T. http://njardarson.lab.arizona.edu/sites/njardarson.lab.arizona.edu/files/Top%20US%20Pharmaceutical%20Products%20of%202013.pdf (accessed February 9, 2016). (b) McGrath, N. A.; Brichacek, M.; Njardarson, J. T. *J. Chem. Educ.* **2010**, *87*, 1348–1349. (c) Dinges, J., Lamberth, C., Eds. *Bioactive Heterocyclic Compounds Classes: Agrochemicals*; Wiley-VCH: Weinheim, Germany, 2012. (d) Gilchrist, T. L. *J. Chem. Soc., Perkin Trans. 1* **1999**, 2849–2866.

(2) For reviews of arynes and hetarynes, see: (a) Kauffmann, T. *Angew. Chem. Int. Ed. Engl.* **1965**, *4*, 543–618. (b) Reinecke, M. G. *Tetrahedron* **1982**, *38*, 427–498. (c) Pellissier, H.; Santelli, M. *Tetrahedron* **2003**, *59*, 701–730. (d) Wenk, H. H.; Winkler, M.; Sander, W. *Angew. Chem. Int. Ed.* **2003**, *42*, 502–528. (e) Sanz, R. *Org. Prep. Proced. Int.* **2008**, *40*, 215–291. (f) Bronner, S. M.; Goetz, A. E.; Garg, N. K. *Synlett* **2011**, 2599–2604. (g) Tadross, P. M.; Stoltz, B. M. *Chem. Rev.* **2012**, *112*, 3550–3557. (h) Gampe, C. M.; Carreira, E. M. *Angew. Chem. Int. Ed.* **2012**, *51*, 3766–3778. (i) Bhunia, A.; Yetra, S. R.; Biju, A. T. *Chem. Soc. Rev.* **2012**, *41*, 3140–3152. (j) Yoshida, H.; Takaki, K. *Synlett* **2012**, 1725–1732. (k) Dubrovskiy, A. V.; Markina, N. A.; Larock, R. C. *Org. Biomol. Chem.* **2013**, *11*, 191–218. (l) Wu, C.; Shi, F. *Asian J. Org. Chem.* **2013**, *2*, 116–125. (m) Goetz, A. E.; Garg, N. K. *J. Org. Chem.* **2014**, *79*, 846–851. (n) Goetz, A. E.; Shah, T. K.; Garg, N. K. *Chem. Commun*. **2015**, *51*, 34–45.

(3) For a recent example from our laboratory, see: Goetz, A. E.; Garg, N. K. *Nat. Chem*. **2013**, *5*, 54–60.

(4) (a) Julia, M.; Goffic, F. L.; Igolen, J.; Baillarge, M. *C. R. Acad. Sci., Ser. C* **1967**, *264*, 118–120. (b) Julia, M.; Huang, Y.; Igolen, J. *C. R. Acad. Sci., Ser. C* **1967**, *265*, 110–112. (c) Igolen, J.; Kolb, A. *C. R. Acad. Sci., Ser. C* **1969**, *269*, 54–56. (d) Julia, M.; Igolen, J.; Kolb, M. *C. R. Acad. Sci., Ser. C* **1971**, *273*, 1776–1777.

(5) (a) Buszek, K. R.; Luo, D.; Kondrashov, M.; Brown, N. VanderVelde, D. *Org. Lett.* **2007**, *9*, 4135–4137. (b) Brown, N.; Luo, D.; VanderVelde, D.; Yang, S.; Brassfield, A.; Buszek, K. R. *Tetrahedron Lett.* **2009**, *50*, 63–65. (c) Bronner, S. M.; Bahnck, K. B.; Garg, N. K. *Org. Lett.* **2009**, *11*, 1007–1010. (d) Garr, A. N.; Luo, D.; Brown, N.; Cramer, C. J.; Buszek K. R.; VanderVelde, D. *Org. Lett.* **2010**, *12*, 96–99. (e) Cheong, P. H.-Y.; Paton, R. S.; Bronner, S. M.; Im, G.-Y. J.; Garg, N. K.; Houk, K. N. *J. Am. Chem. Soc.* **2010**, *132*, 1267–1269. (f) Im, G.-Y. J.; Bronner, S. M.; Goetz, A. E.; Paton, R. S.; Cheong, P. H.-Y.; Houk, K. N.; Garg, N. K. *J. Am. Chem. Soc.* **2010**, *132*, 17933–17944. (g) Thornton, P. D.; Brown, N.; Hill, D.; Neuenswander, B.; Lushington, G. H.; Santini, C.; Buszek, K. R. *ACS Comb. Sci.* **2011**, *13*, 443–448. (h) Candito, D. A.; Dobrovolsky, D.; Lautens, M. *J. Am. Chem. Soc.* **2012**, *134*, 15572–15580. (i) Nerurkar, A.; Chandrasoma, N.; Maina, L.; Brassfield, A.; Luo, D.; Brown, N. Buszek, K. R. *Synthesis* **2013**, *45*, 1843–1852. (j) Picazo, E.; Houk, K. N.; Garg, N. K. *Tetrahedron Lett.* **2015**, *56*, 3511–3514.

(6) For the recent use of indolynes and related species in total synthesis, see: (a) Julia, M.; Le Goffic, F.; Igolen, J.; Baillarge, M. *Tetrahedron Lett.* **1969**, *10*, 1569–1572. (b) Iwao, M.; Motoi, O.; Fukuda, T.; Ishibashi, F. *Tetrahedron* **1998**, *54*, 8999–9010. (c) Moro-oka, Y.; Fukuda, T.; Iwao, M. *Tetrahedron Lett.* **1999**, *40*, 1713–1716. (d) Buszek, K. R.; Brown, N.; Luo, D. *Org. Lett.* **2009**, *11*, 201–204. (*e*) Tian, X.; Huters, A. D.; Douglas, C. J.; Garg, N. K.

Org. Lett. **2009**, *11*, 2349–2351. (f) Brown, N.; Luo, D.; Decapo, J. A.; Buszek, K. R. *Tetrahedron Lett.* **2009**, *50*, 7113–7115. (g) Bronner, S. M.; Goetz, A. E.; Garg, N. K. *J. Am. Chem. Soc.* **2011**, *133*, 3832–3835. (h) Huters, A. D.; Quasdorf, K. W.; Styduhar, E. D.; Garg, N. K. *J. Am. Chem. Soc.* **2011**, 133, 15797–15799. (i) Quasdorf, K. W.; Huters, A. D.; Lodewyk, M. W.; Tantillo, D. J.; Garg, N. K. *J. Am. Chem. Soc.* **2012**, *134*, 1396–1399. (j) Styduhar, E. D.; Huters, A. D.; Weires, N. A.; Garg, N. K. *Angew. Chem. Int. Ed.* **2013**, *52*, 12422–12425. (k) Chandrasome, N.; Brown, N.; Brassfield, A.; Nerukar, A.; Suarez, S.; Buszek, K. R. *Tetrahedron Lett.* **2013**, *54*, 913–917. (l) Fine Nathel, N. F.; Shah, T. K.; Bronner, S. M.; Garg, N. K. *Chem. Sci.* **2014**, *5*, 2184–2190. (m) Goetz, A. E.; Silberstein, A. L.; Corsello, M. A.; Garg, N. K. *J. Am. Chem. Soc.* **2014**, *136*, 3036–3039. (n) Weires, N. A.; Styduhar, E. D.; Baker, E. L.: Garg, N. K. *J. Am. Chem. Soc.* **2014**, *136*, 14710–14713. (o) Chandrasome, N.; Pathmanathan, S.; Buszek, K. R. *Tetrahedron Lett.* **2015**, *56*, 3507–3510.

(7) (a) Wentrup, C.; Blanch, R.; Briehl, H.; Gross, G. *J. Am. Chem. Soc.* **1988**, *110*, 1874–1880. (b) Tlais, S. F.; Danheiser, R. L. *J. Am. Chem. Soc*. **2014**, *136*, 15489–15492. (c) McMahon, T. C.; Medina, J. M.; Yang, Y.–F.; Simmons, B. J.; Houk, K. N.; Garg, N. K. *J. Am. Chem. Soc*. **2015**, *137*, 4082–4085.

(8) For our collaborative studies with Houk et al. on the distortion/interaction model, see references 2m, 3, 5e, 5f, 5j, 6g, 6l, 7c, and the following: (a) Goetz, A. E.; Bronner, S. M.; Cisneros, J. D.; Melamed, J. M.; Paton, R. S.; Houk, K. N.; Garg, N. K. *Angew. Chem. Int. Ed.* **2012**, *51*, 2758–2762. (b) Bronner, S. M.; Mackey, J. L.; Houk, K. N.; Garg, N. K. *J. Am. Chem. Soc.* **2012**, *134*, 13966–13969. (c) Medina, J. M.; Mackey, J. L.; Garg, N. K.; Houk, K.

N. *J. Am. Chem. Soc*. **2014**, *136*, 15798–15805. (d) Medina, J. M.; McMahon, T. C.; Jimenez-Osés, G.; Houk, K. N. Garg, N. K. *J. Am. Chem. Soc.* **2014**, *136*, 14706–14709.

(9) Stoermer, R.; Kahlert, B. *Ber.* **1902**, *35*, 1633–1640.

(10) (a) Townsend, C. A.; Whittamore, P. R. O.; Brobst, S. W. *J. Chem. Soc. Chem. Commun.* **1988**, 726–728. (b) Graybill, T. L.; Casillas, E. G.; Pal, K.; Townsend, C. A. *J. Am. Chem. Soc.* **1999**, *121*, 7729–7746. (c) Gilman, H.; Willis, H. B.; Swislowsky, J. *J. Am. Chem. Soc.* **1939**, *61*, 1371–1373.

(11) For studies on 6,7-benzofuranyne, see: Brown, N.; Buszek, K. R. *Tetrahedron Lett.* **2012**, *53*, 4022–4025.

(12) (a) Harris, M. C. J.; Whitby, R. J.; Blagg, J. *Synlett* **1993**, 705–707. (b) Closser, K. D.; Quintal, M. M.; Shea, K. M. *J. Org. Chem*. **2009**, *74*, 3680–3688.

(13) (a) Miyabe, H.; Miyata, O.; Naito, T. Pyran and its derivatives. In Heterocycles in Natural Product Synthesis; Majumdar, K. C., Chattopadhyay, S. K., Eds.; Wiley-VCH: Weinheim, Germany, 2011; pp. 153–186. (b) Kaur, P.; Arora, R.; Gill, N.S. *Indo Am. J. Pharm. Res.* **2013**, *3*, 9067–9084. (c) Atul, G.; Amit, K.; Ashutosh, R. *Chem. Rev.* **2013**, *113*, 1614–1640. (d) Radadiya, A.; Shah, A. *Eur. J. Med. Chem.* **2015**, *97*, 356–376.

(14) (a) Aukakh, G. K.; Sodhi, R. K.; Singh, M. *Life Sci.* **2007**, *81*, 615–639. (b) Hilditch, A.; Hunt, A. A.; Travers, A.; Polley, J.; Drew, G. M.; Middlemiss, D.; Judd, D. B.; Ross, B. C.; Robertson, M. J. *J. Pharmacol. Exp. Ther.* **1995**, *272*, 750–757.

(15) (a) Tanaka, T.; Ito, T.; Ido, Y.; Nakaya, K.-i.; Iinuma, M.; Chelladurai, V. *Chem. Pharm. Bull.* **2001**, *49*, 785–787. (b) Ge, H. M.; Huang, B.; Tan, S. H.; Shi, D. H.; Song, Y. C.; Tan,

R. X. *J. Nat. Prod.* **2006**, *69*, 1800–1802. (c) Kim, I.; Choi, J. *Org. Biomol. Chem.* **2009**, *7*, 2788–2795.

(16) (a) Klayman, D. L. *Science* **1985**, *228*, 1049–1055. (b) Dondorp, A. M.; Nosten, F.; Yi, P.; Das, D.; Phyo, A. P.; Tarning, J.; Lwin, K. M.; Ariey, F.; Hanpithakpong, W.; Lee, S. J.; Ringwald, P.; Silamut, K.; Imwong, M.; Chotivanich, K.; Lim, P.; Herdman, T.; An, S. S.; Yeung, S.; Singhasivanon, P.; Day, N. P. J.; Lindegardh, N.; Socheat, D.; White, N. J. *N. Engl. J. Med*. **2009**, *361*, 455–467.

(17) Montgomery, C. T.; Cassels, B. K.; Shamma, M. *J. Nat. Prod*. **1983**, *46*, 441–453.

(18) Salaski, E. J.; Krishnamurthy, G.; Ding, W.-D.; Yu, K.; Insaf, S. S.; Eid, C.; Shim, J.; Levin, J. I.; Tabei, K.; Toral-Barza, L.; Zhang, W.-G.; McDonald, L. A.; Honores, E.; Hanna, C.; Yamashita, A.; Johnson, B.; Li, Z.; Laakso, L.; Powell, D.; Mansour, T. S. *J. Med. Chem*. **2009**, *52*, 2181–2184.

(19) (a) Tomaszewski, Z.; Johnson, M. P.; Huang, X.; Nichols, D. E. *J. Med. Chem*. **1992**, *35*, 2061–2064. (b) Marugán, J. J.; Manthey, C.; Anaclerio, B.; Lafrance, L.; Lu, T.; Markotan, T.; Leonard, K. A.; Crysler, C.; Eisennagel, S.; Dasgupta, M.; Tomczuk, B. *J. Med. Chem*. **2005**, *48*, 926–934. (c) Nevagi, R. J.; Dighe, S. N.; Dighe, S. N. *Eur. J. Med. Chem*. **2015**, *97*, 561–581. (d) Zhang, S.; Zhen, J.; Reith, M. E. A.; Dutta, A. K. *Bioorg. Med. Chem*. **2004**, *12*, 6301–6315. (e) Zhang, S.; Reith, M. E. A.; Dutta, A. K. *Bioorg. Med. Chem. Lett*. **2003**, *13*, 1591–1595.

(20) We have previously demonstrated that DFT calculations (B3LYP/6-31G(d)) are well suited for the aryne distortion model, although ab initio methods (MP2/6-311+G**) can also be used; see reference 8a.

(21) Arynes and cyclic alkynes can be generated from silyl triflates using mild fluoride-based conditions. In turn, an array of trapping experiments can be carried out in synthetically useful yields (see references 2c–2n). For the initial use of silyl triflates as aryne precursors, see: Himeshima, Y.; Sonoda, T.; Kobayashi, H. *Chem. Lett.* **1983**, *12*, 1211–1214.

(22) (a) For benzylation of hydroquinone, see: Frlan, R.; Gobec, S.; Kikelj, D. *Tetrahedron* **2007**, *63*, 10698–10708. (b) For formation of diethyl acetal and subsequent benzofuran, see: Hisashi, S.; Takao, I.; Hideki, Y. US Patent 6410561 B1, 2002.

(23) Fliri, A. J.; O'Donnell, C. J.; Claffey, M.; Gallaschun; R. J. US Patent 0058361 A1, 2006

(24) Smith III, A. B.; Empfield, J. R.; Vaccaro, H. A. *Tetrahedron Lett*. **1989**, *30*, 7325–7328.

(25) Liu, Z.; Larock, R. C. *J. Org. Chem.* **2006**, *71*, 3198–3209.

(26) Yoshida, H.; Shirakawa, E.; Honda, Y.; Hiyama, T. *Angew. Chem. Int. Ed.* **2002**, *41*, 3247–3249.

(27) Gilmore, C. D.; Allan, K. M.; Stoltz, B. M. *J. Am. Chem. Soc.* **2008**, *130*, 1558–1559.

(28) For the trapping of arynes with iodonium ylides, see: Huang, X.-C.; Liu, Y.-L.; Liang, Y.; Pi, S.-F.; Wang, F.; Li, J.-H. *Org. Lett.* **2008**, *10*, 1525–1528.

(29) For the trapping of arynes with nitrones, see: Lu, C.; Dubrovskiy, A. V.; Larock, R. C. *J. Org. Chem*. **2012**, *77*, 2279–2284.

(30) For the trapping of arynes with azomethine imines, see: Shi, F.; Mancuso, R.; Larock, R. C. *Tetrahedron Lett*. **2009**, *50*, 4067–4070.

(31) For the trapping of arynes with azides, see: Shi, F.; Waldo, J. P.; Chen, Y.; Larock, R. C. *Org. Lett*. **2008**, *10*, 2409–2412.

(32) For the trapping of arynes with sydnones, see: Wu, C.; Fang, Y.; Larock, R. C.; Shi, F. *Org. Lett*. **2010**, *12*, 2234–2237.

(33) For the trapping of arynes with diazoesters, see: Jin, T.; Yamamoto, Y. *Angew. Chem. Int. Ed*. **2007**, *46*, 3323–3325.

(34) Zhao, J.; Larock, R. C. *Org. Lett*. **2005**, *7*, 4273–4275.

(35) The ability to access heterocyclic scaffolds with significant aliphatic character is an important direction in modern drug discovery; see: (a) Lovering, F.; Bikker, J.; Humblet, C. *J. Med. Chem.* **2009**, *52*, 6752–6756. (b) Ritchie, T. J.; Macdonald, S. J. F. *Drug Discovery Today* **2009**, *14*, 1011–1020.

(36) Bent, H. *Chem. Rev.* **1961**, *61*, 275-311.

(37) Legault, C. Y. CYLview, 1.0b; Université de Sherbrooke: Québec, Montreal, Canada, 2009; http://www.cylview.org.

(38) Also commercially available from Combi Blocks, Inc.

(39) Liu, Y.; Park, S. K.; Xiao, Y.; Chae, J. *Org. Biomol. Chem.* **2014**, *12*, 4747–4753.

(40) Spartan ’10; Wavefunction, Inc: Irvine, CA, 2010.

CHAPTER SEVEN

Mizoroki–Heck Cyclizations of Amide Derivatives for the Introduction of Quaternary Centers

Jose M. Medina, Jesus Moreno, Sophie Racine, Shuaijing Du, and Neil K. Garg

Angew. Chem., Int. Ed. [Online early access]. DOI: 10.1002/anie.201703174R1.

7.1 Abstract

We report the first non-decarbonylative Mizoroki–Heck reactions of amide derivatives. The transformation relies on the use of nickel catalysis and proceeds using sterically hindered tri- and tetrasubstituted olefins to give products containing quaternary centers. The resulting polycyclic or spirocyclic products can be obtained in good yields. Moreover, a diastereoselective variant of this methodology demonstrates its value for accessing adducts bearing vicinal, highly substituted sp^3 stereocenters. Our results demonstrate that amide derivatives can be used as building blocks for the assembly of complex scaffolds.

7.2 Introduction

The introduction of quaternary carbon centers remains a popular topic in modern chemical synthesis.[1] Such motifs are often difficult to access due to the steric challenge associated with constructing a fully substituted carbon center. One attractive means to install quaternary centers is via the intramolecular Mizoroki–Heck reaction.[2] Most notably, the Pd-catalyzed Mizoroki–Heck cyclization of *aryl* halides and triflates has been the subject of intense investigation for decades and has been utilized to assemble many sterically demanding scaffolds. On the other hand, the corresponding Mizoroki–Heck cyclization of *acyl* electrophiles to furnish ketone products bearing quaternary carbons has not been reported.

Considering the aforementioned deficiency concerning the Mizoroki–Heck cyclization of acyl electrophiles, we pursued the transformation shown in Figure 7.1. In the presence of an appropriate nickel catalyst, imide **7.1**, derived from the corresponding secondary amide upon Boc-activation, would be converted to cyclized products **7.2**, bearing the desired quaternary centers. Mechanistically, the conversion would proceed by a sequence akin to classical Mizoroki–Heck chemistry involving oxidative addition (**7.1**→**7.3**), olefin coordination and insertion (**7.3**→**7.4**), followed by β-hydride elimination[3] (**7.4**→**7.2**). It should be noted that amide derivatives have recently been employed in Pd- and Ni-catalyzed couplings for carbon–heteroatom[4] and carbon–carbon[5,6,7] bond formation, although never for the synthesis of quaternary centers.[8] Moreover, precedent for the desired olefin insertion is available from Stambuli's Pd-catalyzed Mizoroki–Heck cyclization of benzoic anhydrides, albeit without quaternary stereocenter formation,[9,10] and Pd-catalyzed carbonylative Mizoroki–Heck reactions of aryl halides and triflates.[11] Herein, we describe the development and scope of the Ni-catalyzed

Mizoroki–Heck cyclization of amide derivatives.[12] The transformation provides a new means to build complex scaffolds using non-precious metal catalysis.[13]

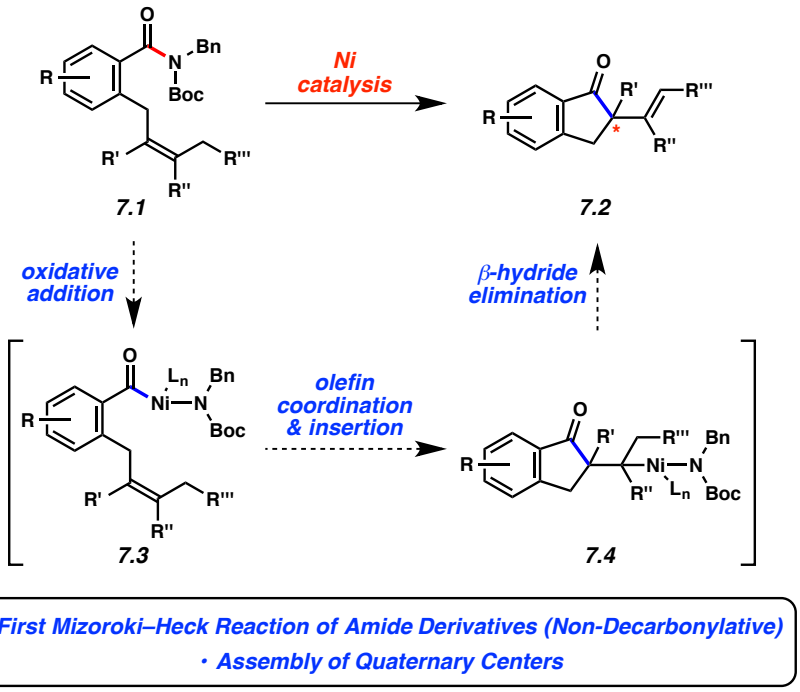

Figure 7.1. Designed nickel-catalyzed Mizoroki–Heck reaction of amide derivatives to forge quaternary centers

7.3 Results and Discussion

7.3.1 Optimization of Reaction Conditions

After some initial experimentation, we arrived at **7.5** as a suitable test substrate (Table 7.1).[14] This substrate contains the *N*-Bn,Boc imide-type motif,[15] which we have previously found to be reactive using Ni/SIPr (**7.7**) combinations,[4,5] in addition to a sterically encumbered tetrasubstituted olefin. The Mizoroki–Heck cyclization of **7.5** was attempted under a variety of reaction conditions,[16] with a selection of key results using $Ni(cod)_2$, NHC ligands, and toluene as solvent at 100 °C depicted. Unfortunately, attempts to conduct the desired cyclization using SIPr•HCl (**7.7**) in the presence of NaO*t*Bu were unsuccessful (entry 1). However, by switching to

NHC precursor **7.8** the Mizoroki–Heck product **7.6** was obtained, albeit in modest yield (entry 2). Further improvements were seen when benzimidazolium salt **7.9** was employed,[17] which gave rise to the desired product **7.6** in 76% yield (entry 3). We also probed the Ni to ligand ratio and found that employing a 1:1 ratio of $Ni(cod)_2$ to **7.9** (rather than a 1:2 ratio), led to diminished yields (entry 4). Efforts to optimize the Ni loading were also undertaken. Although using 10 mol% $Ni(cod)_2$ gave the desired product (entry 5), the use of 15 mol% $Ni(cod)_2$ gave excellent yields (entry 6) and was found more generally effective across a range of substrates studied subsequently. During the course of our studies, we also evaluated a series of additives used previously in Ni-catalyzed couplings.[18] These efforts demonstrated that the reaction temperature could be lowered to 60 °C, provided that *t*-amyl alcohol was employed as the additive, to deliver product **7.6** in 95% yield (entry 7).[19] It should be noted that: (a) Ni-catalyzed Mizoroki–Heck reactions to form quaternary centers are rare,[20] (b) there are no prior examples of Ni-catalyzed Mizoroki–Heck reactions involving tetrasubstituted olefins in the literature,[21] and (c) decarbonylation products were not observed during reaction development.

Table 7.1. Evaluation of ligand effects and reaction conditions for the conversion of **7.5** to Mizoroki–Heck cyclization product **7.6**, bearing a quaternary center[a]

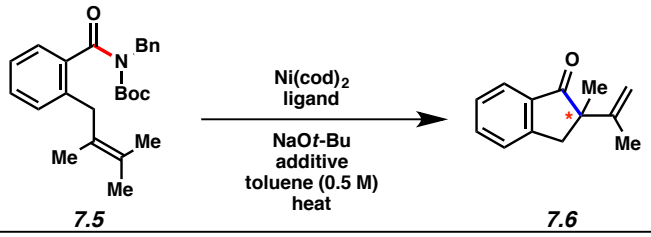

7.5 *7.6*

Entry	*Ni(cod)$_2$ (loading)*	*Ligand (loading)*	*Additive*	*Temp.*	*Yield*[b]
1	20 mol%	***7.7*** (40 mol%)	none	100 °C	0%
2	20 mol%	***7.8*** (40 mol%)	none	100 °C	24%
3	20 mol%	***7.9*** (40 mol%)	none	100 °C	76%
4	20 mol%	***7.9*** (20 mol%)	none	100 °C	67%
5	10 mol%	***7.9*** (20 mol%)	none	100 °C	51%
6	15 mol%	***7.9*** (30 mol%)	none	100 °C	91%
7	15 mol%	***7.9*** (30 mol%)	*t*-amyl alcohol[c]	60 °C	95%

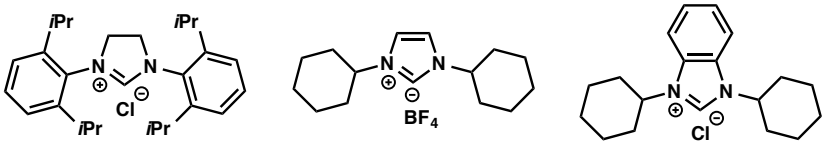

SIPr·HCl (7.7) *ICy·HBF$_4$ (7.8)* *Benz-ICy·HCl (7.9)*

[a] Conditions unless otherwise stated: **7.5** (1.0 equiv, 0.1 mmol), Ni(cod)$_2$ (mol% as shown), **7.7**–**7.9** (mol% as shown), toluene (0.5 M), NaO*t*Bu (1.1x ligand loading) heated at the specified temperature for 24 h in a sealed vial. [b] Yields reflect an average of two experiments and were determined by ^{1}H NMR analysis using hexamethylbenzene as an internal standard. [c] 3.0 equiv of *t*-amyl alcohol was used.

7.3.2 Evaluation of Substrate Scope

Having identified conditions to achieve the nickel-catalyzed cyclization, we evaluated the scope with respect to the tethered alkene (Table 7.2).[22,23] It was found that a trisubstituted olefin[24] analog of our parent substrate could be employed to furnish terminal olefin product **7.10** in 71% yield (entry 1). We also examined substrates in which the trisubstituted olefin was embedded in a ring. Using both 5- and 6-membered ring substrates, the desired Mizoroki–Heck cyclization proceeded smoothly to give the corresponding spirocyclic products, **7.11** and **7.12**, respectively, as mixtures of olefin isomers (entries 2 and 3).[25] Returning to the more challenging

tetrasubstituted olefins, a series of substrates bearing exocyclic olefins were prepared and evaluated. Whereas utilization of a substrate containing a 5-membered ring led to product **7.13** in 51% yield (entry 4), the use of 6- and 7-membered ring-containing substrates furnished products **7.14** and **7.15**, respectively, in good yields (entries 5 and 6). Lastly, two heterocyclic substrates were examined. We were delighted to find that our methodology proved tolerant of a tetrahydropyran and a protected piperidine, thus giving rise to tricycles **7.16** and **7.17**, respectively, in excellent yields (entries 7 and 8).

As shown in Figure 7.2, the methodology is also tolerant of substituents on the arene. For example, use of substrates containing the fluoride or trifluoromethyl group, both of which are critical in medicinal chemistry,[26] gave rise to products **7.18** and **7.19**, respectively. The methoxy group was also well tolerated, as shown by the formation of **7.20** and **7.21**. As demonstrated by the synthesis of **7.22** and **7.23**, substrates bearing a methyl group could also be utilized. In the latter case, it is notable that the presence of a methyl group *ortho* to the tethered alkene did not hinder reactivity.

Table 7.2. Mizoroki–Heck cyclization of a variety of tri- and tetrasubstituted olefin substrates

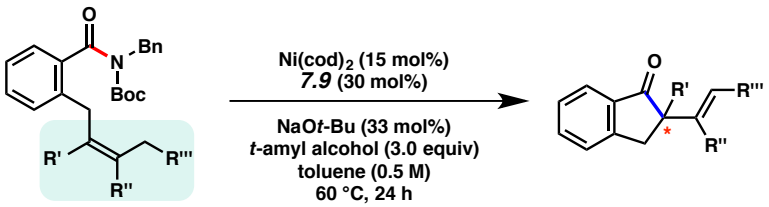

Entry	Alkene	Product	Yield[a]
1	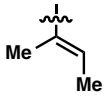	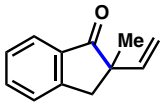 7.10	71%[b]
2		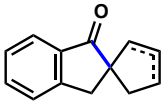 7.11	92%[b]
3	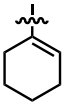	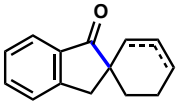 7.12	75%[b]
4	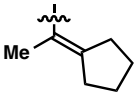	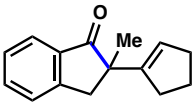 7.13	51%
5	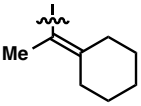	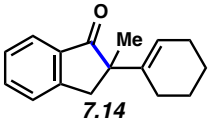 7.14	96%
6	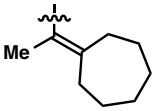	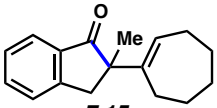 7.15	80%
7	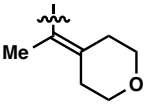	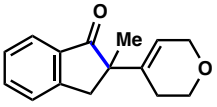 7.16	91%
8	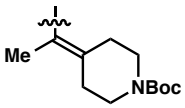	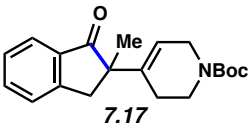 7.17	93%

[a] Yields shown reflect the average of two isolation experiments. [b] Reaction performed at 100 °C in the absence of *t*-amyl alcohol.

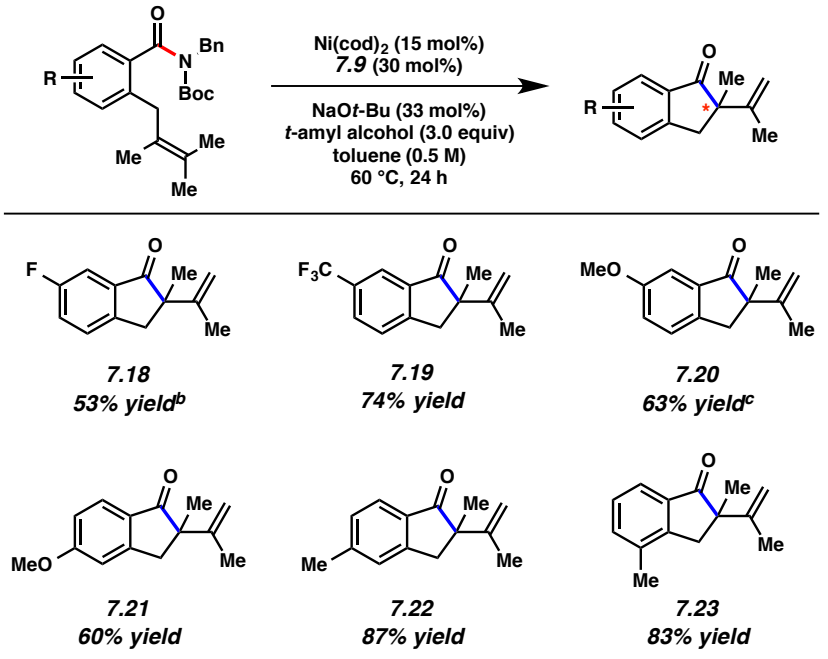

[a] Yields shown reflect the average of two isolation experiments. [b] Yield determined by ^{1}H NMR analysis using hexamethylbenzene as an external standard. [c] Reaction performed at 100 °C in the absence of *t*-amyl alcohol.

Figure 7.2. Substituents on the arene motif[a]

7.3.3 Diastereoselective Application to Build Vicinal sp^3 Stereocenters

As a further test, we questioned if this methodology could be performed in a diastereoselective sense (Figure 7.3). Trisubstituted olefin **7.24**,[27] which bears an allylic methyl group, was treated under our optimal reaction conditions. This reaction delivered ketone **7.25** in 80% yield, as a 92:8 ratio of diastereomers. Of note, **7.25** contains vicinal sp^3 stereocenters, both of which are highly substituted. Prior transition metal-catalyzed methods for the synthesis of 2-vinylindanones[22] have not been demonstrated for the construction of such complexity. The diastereoselectivity seen in the conversion of **7.24** to **7.25** can be rationalized by considering the two competing olefin insertion transition states, **TS7.1** and **TS7.2**. In both cases, the olefin insertion event is thought to occur via a standard 4-centered transition state, which in turn, prompts allylic strain arguments.[28] In **TS7.1**, A(1,3) strain between the two highlighted

hydrogens is minimal and the methyl group rests in a pseudo-equatorial disposition. As such, **TS7.1** is favorable and leads to the major diastereomer of **7.25** shown, with the methyl groups residing in a cis fashion. On the other hand, the minor diastereomer of **7.25** (not depicted) is thought to arise from **TS7.2**, which displays a less favorable A(1,3) interaction between the highlighted hydrogen and methyl substituents.

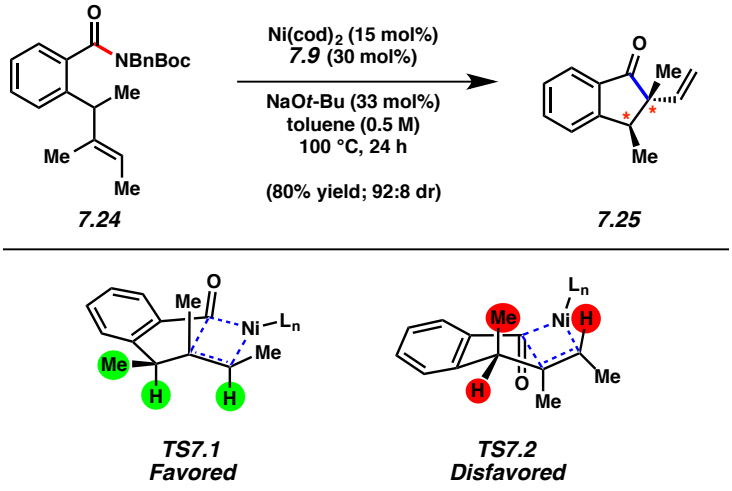

[a] Yields shown reflect the average of two isolation experiments.

Figure 7.3. Diastereoselective Heck cyclization for the introduction of vicinal sp^3 stereocenters[a]

7.4 Conclusion

We have developed the Mizoroki–Heck cyclization of amide derivatives to access ketones containing quaternary centers. The transformation is tolerant of variation on both the alkene and aryl moieties, and most notably, proceeds using sterically hindered tetrasubstituted olefins. As a result, polycyclic, spirocyclic, and heteroatom-containing products can be synthesized using this methodology. Moreover, we have demonstrated that a diastereoselective Mizoroki–Heck cyclization proceeds for the controlled formation of an adduct bearing vicinal, highly substituted sp^3 stereocenters. In addition to providing a rare Ni-catalyzed Mizoroki–Heck cyclization methodology for accessing quaternary centers and the first Mizoroki–Heck

cyclizations of amide derivatives, our results demonstrate that amides, despite once being viewed as unreactive, can be used as building blocks for the preparation of complex scaffolds.

7.5 Experimental Section

7.5.1 Materials and Methods

Unless stated otherwise, reactions were conducted in flame-dried glassware under an atmosphere of nitrogen and commercially obtained reagents were used as received. Non-commercially available substrates were synthesized following protocols specified in Section 7.7.2.1. Prior to use, toluene was purified by distillation and taken through three freeze-pump-thaw cycles. 2-Halobenzoic acids derivatives **7.31, 7.33, 7.35** were obtained from Combi-Blocks; **7.29** and **7.26** were obtained from Oakwood; **7.37** was obtained from AstaTech; and **7.41** was obtained from Ark Pharm. $Ni(cod)_2$ and Benz-ICy•HCl (**7.9**) were obtained from Strem Chemicals. Reductive coupling ligands **7.60**[14c] and **7.66**[14d] were prepared from known literature procedures. Reaction temperatures were controlled using an IKAmag temperature modulator, and unless stated otherwise, reactions were performed at room temperature (approximately 23 °C). Thin-layer chromatography (TLC) was conducted with EMD gel 60 F254 pre-coated plates (0.25 mm for analytical chromatography and 0.50 mm for preparative chromatography) and visualized using a combination of UV, anisaldehyde, iodine, and potassium permanganate staining techniques. Silicycle Siliaflash P60 (particle size 0.040–0.063 mm) was used for flash column chromatography. ^{1}H NMR spectra were recorded on Bruker spectrometers (at 400 and 500 MHz) and are referenced to the residual solvent peak 7.26 ppm for $CDCl_3$. Data for ^{1}H NMR spectra are reported as follows: chemical shift (δ ppm), multiplicity, coupling constant (Hz), integration.^{13}C NMR spectra were recorded on Bruker spectrometers (at 125 MHz) and are

referenced to the residual solvent peak 77.16 ppm for $CDCl_3$. Data for ^{13}C NMR are reported as follows: chemical shift (δ ppm), multiplicity, and coupling constant (Hz). ^{19}F NMR spectra were recorded on Bruker spectrometers (at 376 MHz) and are reported in terms of chemical shift in $CDCl_3$. IR spectra were recorded on a Perkin-Elmer 100 spectrometer and are reported in terms of frequency absorption (cm^{-1}). High-resolution mass spectra were obtained on a Waters Micromass LCT Premier TOF Mass Spectrometer (Waters) equipped with a ZSpray source for electrospray ionization (ESI) and a time-of-flight (TOF) analyzer. The instrument was controlled by Waters MassLynx 4.0. The analyte was injected as a solution using acetonitrile as the solvent. Additionally, DART-MS spectra were collected on a Thermo Exactive Plus MSD (Thermo Scientific) equipped with an ID-CUBE ion source and a Vapur Interface (IonSense Inc.). Both the source and MSD were controlled by Excalibur software v. 3.0. The analyte was spotted onto OpenSpot sampling cards (IonSense Inc.) using dichloromethane as the solvent. Ionization was accomplished using UHP He (Airgas Inc.) plasma with no additional ionization agents. The mass calibration was carried out using Pierce LTQ Velos ESI (+) and (–) Ion calibration solutions (Thermo Fisher Scientific).

7.5.2 Experimental Procedures

7.5.2.1 Syntheses of Heck Cyclization Substrates

7.5.2.1.1 Synthesis of Imide 7.5 for Reaction Discovery

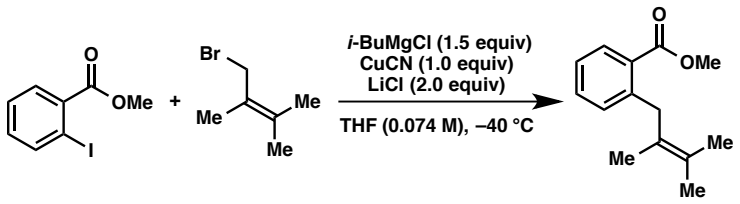

7.26 *7.27* (31% yield) *7.28*

Ester 7.28. Following a modification of the general procedure reported by Querolle and co-workers,[29] a flask containing a stir bar was charged with CuCN (1.03 g, 11.5 mmol, 1.0 equiv) and LiCl (971 mg, 22.9 mmol, 2.0 equiv) in the glovebox. The flask was removed from the glovebox, and the solids were suspended in THF (39 mL). The resulting mixture was stirred vigorously until a completely dissolved solution of CuCN•2LiCl was formed. In a separate flask containing a solution of methyl-2-iodobenzoate (**7.26**) (3.02 g, 11.45 mmol, 1.0 equiv) in THF (115 mL) at –40 °C was added *i*-BuMgCl (8.6 mL of a 2.0 M solution in THF, 17.2 mmol, 1.5 equiv) dropwise over 1 min. After this mixture was stirred at –40 °C for 1 h, the solution of CuCN•2LiCl was added via cannula. The combined mixture stirred at –40 °C for an additional 15 min, at which point bromide **7.27** (4.65 g, 28.6 mmol, 2.5 equiv) was added dropwise over 1 min. After stirring at –40 °C for an additional hour, the reaction was poured into 9:1 sat. aq. NH_4Cl:NH_4OH (150 mL). The layers were separated and the aqueous layer was extracted with EtOAc (3 x 100 mL). The organic layers were combined, dried over $MgSO_4$, and concentrated under reduced pressure. The crude mixture was purified via flash chromatography (4:1 Benzene:Hexanes) to afford ester **7.28** (767 mg, 31% yield) as a colorless oil. Ester **7.28**: R_f 0.63

(3:1 Hexanes:EtOAc); ^{1}H NMR (500 MHz, $CDCl_3$): δ 7.83 (dd, *J* = 7.7, 1.3, 1H), 7.40 (td, *J* = 7.5, 1.5, 1H), 7.23 (t, *J* = 7.5, 1H), 7.20 (d, *J* = 7.7, 1H), 3.89 (s, 3H), 3.78 (s, 2H) 1.76 (s, 3H), 1.71 (s, 3H), 1.57 (s, 3H); ^{13}C NMR (125 MHz, $CDCl_3$): δ 168.7, 142.1, 131.9, 130.6, 130.3, 129.2, 127.1, 125.73, 125.66, 52.0, 37.7, 20.73, 20.69, 18.6; IR (film): 2916, 1720, 1433, 1262, 1246, 1121, 1076 cm^{-1}; HRMS–APCI (m/z) $[M + H]^+$ calcd for $C_{14}H_{19}O_7^+$, 219.13796; found 219.13784.

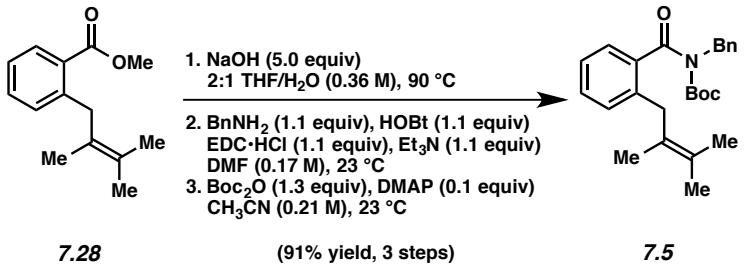

7.28 **(91% yield, 3 steps)** ***7.5***

Imide 7.5. To a solution of ester **7.28** (767 mg, 3.51 mmol, 1.0 equiv) in THF (6.6 mL) was added a solution of NaOH (703 mg, 17.6 mmol, 5.0 equiv) in H_2O (3.3 mL). The reaction was heated to 90 °C and stirred for 12 h. After cooling to room temperature, the reaction mixture was poured into deionized water (25 mL) and diluted with EtOAc (25 mL). The layers were separated and the aqueous layer was acidified to pH ~4 with 1 N HCl (15 mL) and extracted with EtOAc (3 x 25 mL). The organic layers were combined, washed with deionized water (300 mL), dried over $MgSO_4$, and concentrated under reduced pressure to afford the corresponding carboxylic acid, which was used in the subsequent step without further purification.

To a solution of the crude carboxylic acid, HOBt (591 mg, 3.86 mmol, 1.1 equiv from **7.28**), and EDC•HCl (740 mg, 3.86 mmol, 1.1 equiv from **7.28**) in DMF (21 mL) was added $BnNH_2$ (0.42 mL, 3.86 mmol, 1.1 equiv from **7.28**) and Et_3N (0.5 mL, 3.86 mmol, 1.1 equiv from **7.28**). After stirring for 7 h, the reaction mixture was poured into deionized water (100 mL) and diluted with

EtOAc (50 mL). The layers were separated and the aqueous layer was extracted with EtOAc (2 x 50 mL). The organic layers were combined, washed with deionized water (100 mL), dried over $MgSO_4$, and concentrated under reduced pressure to afford the corresponding amide, which was used in the subsequent step without further purification.

To a solution of the crude amide in CH_3CN (17 mL) was added DMAP (43 mg, 0.351 mmol, 0.1 equiv from **7.28**) and Boc_2O (996 mg, 4.56 mmol, 1.3 equiv from **7.28**). After stirring for 7 h, the reaction mixture was concentrated under reduced pressure and purified by flash chromatography (99:1 Hexanes:EtOAc) to yield imide **7.5** (1.26 g, 91% yield, three steps) as a white solid. Imide **7.5**: mp: 65–67 °C; R_f 0.60 (3:1 Hexanes:EtOAc); ^{1}H NMR (500 MHz, $CDCl_3$): δ 7.43 (d, *J* = 7.9, 2H), 7.34 (d, *J* = 7.4, 2H), 7.31–7.25 (m, 2H), 7.16 (t, *J* = 7.4, 1H), 7.11 (d, *J* = 7.9, 2H), 5.03 (s, 2H), 3.43 (s, 2H), 1.75 (s, 3H), 1.70 (s, 3H), 1.58 (s, 3H), 1.11 (s, 9H); ^{13}C NMR (125 MHz, $CDCl_3$): δ 172.6, 153.0, 138.7, 138.0, 137.7, 129.5, 128.6, 128.40, 128.36, 127.5, 127.2, 125.9, 125.44, 125.37, 83.4, 48.0, 36.8, 27.5, 20.76, 20.75, 18.8; IR (film): 2981, 2922, 1728, 1670, 1368, 1333, 1229, 1138 cm^{-1}; HRMS–APCI (m/z) $[M + H]^+$ calcd for $C_{25}H_{32}NO_3^+$, 394.23767; found 394.23462.

7.5.2.1.2 Syntheses of Halo-Imide Coupling Partners

Representative Procedure (synthesis of imide 7.30 is used as an example).

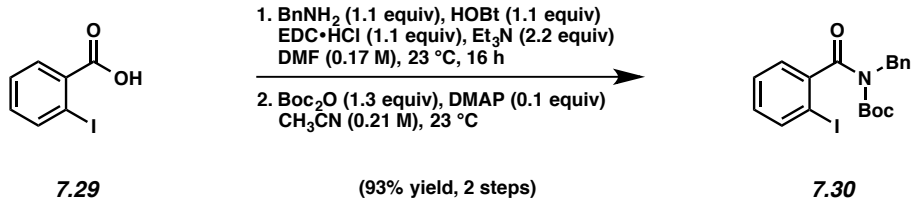

7.29 (93% yield, 2 steps) *7.30*

Iodo-imide 7.30. To a mixture of 2-iodo-benzoic acid (**7.29**) (10.0 g, 40.4 mmol, 1.0 equiv), EDC•HCl (8.5 g, 44 mmol, 1.1 equiv), HOBt (6.0 g, 44 mmol, 1.1 equiv) and Et_3N (6.2 mL, 88 mmol, 2.2 equiv) in DMF (238 mL) was added $BnNH_2$ (5.0 mL, 44 mmol, 1.1 equiv). The resulting mixture was stirred for 16 h, and then diluted with deionized water (100 mL). The layers were separated and the aqueous layer was extracted with EtOAc (3 x 100 mL). The combined organic layers were washed with 0.1 N HCl (100 mL), sat. aq. $NaHCO_3$ (100 mL), and brine (100 mL), dried over Na_2SO_4, and filtered. Concentration under reduced pressure afforded the crude amide, which was used in the subsequent step without further purification.

To the vessel containing the crude amide was added DMAP (0.5 g, 4 mmol, 0.1 equiv from **7.29**), followed by acetonitrile (192 mL). Boc_2O (11.5 g, 52.5 mmol, 1.3 equiv from **7.29**) was added in one portion and the reaction vessel was flushed with N_2. The reaction mixture was allowed to stir for 16 h. The reaction was concentrated under reduced pressure and the resulting crude residue was purified by flash chromatography (9:1 Hexanes:EtOAc) to yield iodo-imide **7.30** (16.4 g, 93% yield, two steps) as a white solid. Iodo-imide **7.30**: mp: 100–101 ºC; R_f 0.54 (4:1 Hexanes:EtOAc); ^{1}H NMR (500 MHz, $CDCl_3$): δ 7.79 (d, J = 8.0, 1H), 7.47 (d, J = 8.0, 2H), 7.37–7.32 (m, 3H), 7.30–7.27 (m, 1H), 7.18–7.15 (m, 1H), 7.10–7.05 (m, 1H), 5.05 (s, 2H), 1.14 (s, 9H); ^{13}C NMR (125 MHz, $CDCl_3$): δ 171.7, 152.1, 144.6, 139.2, 137.5, 130.3, 128.6,

128.5, 127.9, 127.6, 127.0, 91.7, 83.9, 48.0, 27.6; IR (film): 2979, 1731, 1668, 1228, 741 cm^{-1}; HRMS–APCI (m/z) $[M + H]^+$ calcd for $C_{19}H_{21}INO_3^+$, 438.05606; found 438.05536.

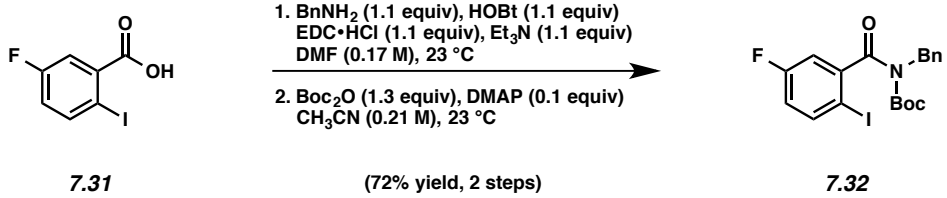

7.31 (72% yield, 2 steps) *7.32*

Iodo-imide 7.32. Following the representative procedure with 2-iodo-5-fluorobenzoic acid (**7.31**) (2.0 g, 7.52 mmol), purification by flash chromatography (99:1 Pentane:Et_2O → 19:1 Pentane:Et_2O) afforded iodo-imide **7.32** (2.46 g, 72% yield, two steps) as a white solid. Iodo-imide **7.32**: mp: 61–63 °C; R_f 0.60 (3:1 Hexanes:EtOAc); ^1H NMR (500 MHz, $CDCl_3$): δ 7.72 (dd, *J* = 8.7, 5.2, 1H), 7.46 (d, *J* = 7.3, 2H), 7.34 (tt, *J* = 7.1, 1.4, 2H), 7.28 (tt, *J* = 7.3, 1.4, 1H), 6.93 (dd, *J* = 8.5, 3.1, 1H), 6.83 (dt, *J* = 8.5, 3.1, 1H), 5.04 (s, 2H), 1.20 (s, 9H); ^{13}C NMR (125 MHz, $CDCl_3$): δ 170.3 (d, *J* = 2.2), 162.7 (d, *J* = 246), 151.8, 146.2 (d, *J* = 7.2), 140.6 (d, *J* = 7.7), 137.2, 128.63, 128.56, 127.7, 117.7 (d, *J* = 22), 114.7 (d, *J* = 24), 84.6 (d, *J* = 3.6), 84.3, 48.0, 27.6; ^{19}F NMR (376 MHz, $CDCl_3$): δ –113.7, (s, 1F); IR (film): 2981, 1736, 1671, 1369, 1350, 1331, 1232, 1149 cm^{-1}; HRMS–APCI (m/z) $[M + H]^+$ calcd for $C_{19}H_{20}FINO_3^+$ 456.04664; found 456.04664.

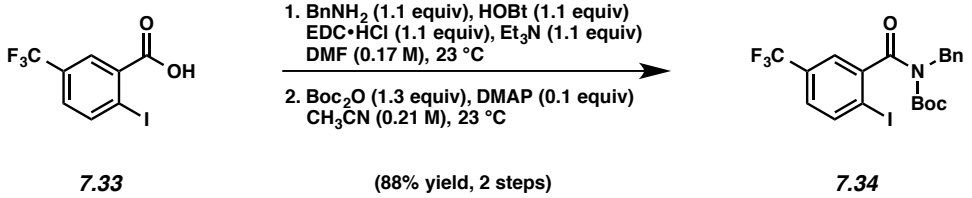

7.33 (88% yield, 2 steps) *7.34*

Iodo-imide 7.34. Following the representative procedure with 2-iodo-5-(trifluoromethyl)benzoic acid (**7.33**) (1.98 g, 6.27 mmol), purification by flash chromatography (99:1 Pentane:Et_2O →

19:1 Pentane:Et_2O) afforded iodo-imide **7.34** (2.79 g, 88% yield, two steps) as an off-white solid. Iodo-imide **7.34**: mp: 60–62 °C; R_f 0.70 (3:1 Hexanes:EtOAc); ^{1}H NMR (500 MHz, $CDCl_3$): δ 7.93 (d, *J* = 8.3, 1H), 7.48 (d, *J* = 7.3, 2H), 7.41 (d, *J* = 2.0, 1H), 7.35 (tt, *J* = 7.6, 1.5, 2H), 7.33–7.28 (m, 2H), 5.07 (s, 2H), 1.15 (s, 9H); ^{13}C NMR (125 MHz, $CDCl_3$): δ 170.4, 151.7, 145.5, 139.8, 137.1, 130.8 (q, *J* = 33), 128.7, 128.6, 127.8, 126.5 (q, *J* = 3.6), 123.68 (q, *J* = 273), 123.67 (q, *J* = 3.8), 95.8, 84.4, 48.0, 27.5; ^{19}F NMR (376 MHz, $CDCl_3$): δ –63.0, (s, 3F); IR (film): 2982, 1737, 1669, 1317, 1225, 1126, 1079 cm^{-1}; HRMS–APCI (m/z) $[M + H]^+$ calcd for $C_{20}H_{20}F_3INO_3^+$ 506.04345; found 506.04387.

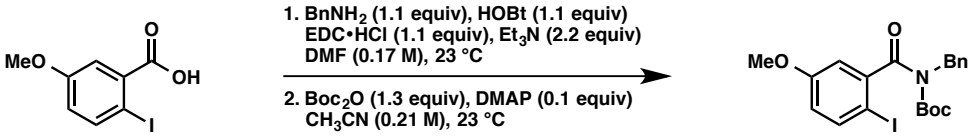

7.35 (87% yield, 2 steps) *7.36*

Iodo-imide 7.36. Following the representative procedure with 2-iodo-5-methoxybenzoic acid (**7.35**) (1.0 g, 3.6 mmol), 2-iodo-imide **7.36** (1.5 g, 87% yield, two steps) was obtained as a colorless oil. Iodo-imide **7.36**: R_f 0.24 (4:1 Hexanes:EtOAc); ^{1}H NMR (400 MHz, $CDCl_3$): δ 7.62 (d, *J* = 8.8, 1H), 7.48–7.45 (m, 2H), 7.36–7.32 (m, 2H), 7.30–7.26 (m, 1H), 6.73 (d, *J* = 3.1, 1H), 6.66 (dd, *J* = 8.7, 3.1, 1H), 5.04 (s, 2H), 3.76, (s, 3H), 1.17 (s, 9H); ^{13}C NMR (125 MHz, $CDCl_3$): δ 171.3, 159.6, 151.9, 145.1, 139.7, 137.3, 128.5, 128.4, 127.4, 116.8, 112.8, 83.7, 80.0, 55.5, 47.9, 27.4; IR (film): 2979, 1735, 1466, 1144, 848, 699 cm^{-1}; HRMS–APCI (m/z) $[M + H]^+$ calcd for $C_{20}H_{23}INO_4^+$, 468.06663; found 468.06671.

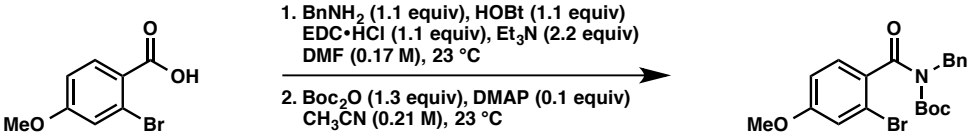

7.37 (quantitative yield, 2 steps) *7.38*

Bromo-imide 7.38. Following the representative procedure with 2-bromo-4-methoxybenzoic acid (**7.37**) (0.46 g, 2.0 mmol), 2-bromo-imide **7.38** (0.86 g, quantitative yield, two steps) was obtained as a yellow oil. Bromo-imide **7.38**: R_f 0.25 (9:1 Hexanes:EtOAc); ^{1}H NMR (500 MHz, $CDCl_3$): δ 7.46–7.44 (m, 2H), 7.35–7.31 (m, 2H), 7.32–7.29 (m, 1H), 7.22 (d, J = 8.7, 1H), 7.07 (d, J = 2.5, 1H), 6.86 (dd, J = 8.7, 2.5, 1H), 5.02 (s, 2H), 3.81, (s, 3H), 1.19 (s, 9H); ^{13}C NMR (125 MHz, $CDCl_3$): δ 170.5, 160.8, 152.5, 137.7, 132.7, 129.3, 128.5 (4 carbons), 127.5, 119.8, 118.1, 113.2, 83.5, 55.8, 48.2, 27.6; IR (film): 2979, 1731, 1599, 1227, 848, 558 cm^{-1}; HRMS–APCI (m/z) $[M + H]^+$ calcd for $C_{20}H_{23}BrNO_4^+$, 420.08050; found 420.08082.

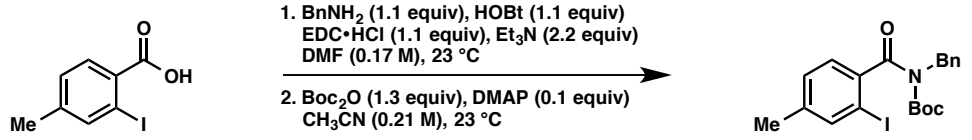

7.39 (92% yield, 2 steps) *7.40*

Iodo-imide 7.40. Following the representative procedure with 2-iodo-4-methylbenzoic acid (**7.39**) (2.0 g, 7.6 mmol), iodo-imide **7.40** (3.3 g, 92% yield, two steps) was obtained as a colorless oil. Iodo-imide **7.40**: R_f 0.34 (9:1 Hexanes:EtOAc); ^{1}H NMR (500 MHz, $CDCl_3$): δ 7.65 (d, J = 7.8, 1H), 7.48–7.45 (m, 2H), 7.35–7.31 (m, 2H), 7.29–7.25 (m, 1H), 7.00 (d, J = 2.1, 1H), 6.89 (ddd, J = 8.1, 2.1, 0.8, 1H), 5.04 (s, 2H), 2.29 (s, 3H), 1.15 (s, 9H); ^{13}C NMR (125 MHz, $CDCl_3$): δ 171.7, 152.1, 144.2, 138.8, 138.0, 137.4, 131.2, 128.5, 128.4, 127.8, 127.4, 87.4, 83.6, 47.9, 27.4, 20.8; IR (film): 2979, 1731, 1668, 1141, 848, 698 cm^{-1}; HRMS–APCI (m/z) $[M + H]^+$ calcd for $C_{20}H_{23}INO_3^+$, 452.07171; found 452.07080.

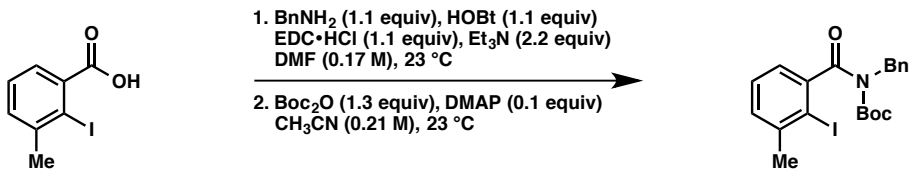

7.41 (85% yield, 2 steps) *7.42*

Iodo-imide 7.42. Following the representative procedure with 2-iodo-3-methylbenzoic acid (**7.41**) (3.0 g, 12 mmol), iodo-imide **7.42** (4.4 g, 85% yield, two steps) was obtained as a white solid. Iodo-imide **7.42**: mp: 87–89 ºC; R_f 0.62 (4:1 Hexanes:EtOAc); ^{1}H NMR (500 MHz, $CDCl_3$): δ 7.48 (d, J = 7.8, 2H), 7.36–7.32 (m, 2H), 7.29–7.26 (m, 1H), 7.24–7.20 (m, 2H), 6.90 (dd, J = 6.7, 2.4, 1H), 5.07 (s, 2H), 2.46 (s, 3H), 1.11 (s, 9H); ^{13}C NMR (125 MHz, $CDCl_3$): δ 171.9, 152.0, 145.7, 142.2, 137.4, 129.5, 128.42, 128.36, 127.9, 127.4, 123.7, 98.5, 83.6, 47.7, 28.8, 27.4; IR (film): 2979, 1732, 1338, 1145, 849, 699 cm^{-1}; HRMS–APCI (m/z) $[M + H]^+$ calcd for $C_{20}H_{23}INO_3^+$, 452.07171; found 452.07177.

7.5.2.1.3 Syntheses of Carbonate Coupling Partners

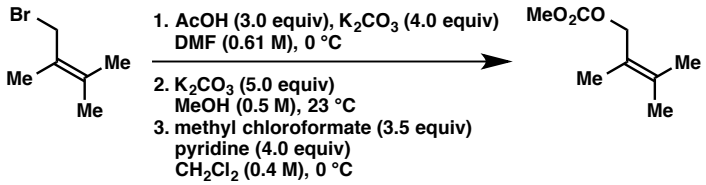

7.27 (41% yield, 3 steps) *7.43*

Carbonate 7.43. To a suspension of K_2CO_3 (39.0 g, 0.282 mol, 4.0 equiv) in DMF (116 mL) was added AcOH (12 mL, 0.212 mol, 3.0 equiv). The mixture was cooled to 0 °C. After stirring for 5 min, bromide **7.27**[30] (11.5 g, 0.0705 mol, 1.0 equiv) was added. After stirring vigorously at 0 °C for 2 h, the reaction mixture was poured into deionized water (300 mL) and diluted with Et_2O (150 mL). The layers were separated and the aqueous layer was extracted with Et_2O (2 x 150 mL). The organic layers were combined, washed with deionized water (300 mL), dried over

$MgSO_4$, and concentrated under reduced pressure (~100 mbar, at room temperature) to afford the corresponding acetate, which was used in the subsequent step without further purification.

To a solution of the crude acetate in MeOH (141 mL) was added K_2CO_3 (48.7 g, 0.353 mol, 4.0 equiv from **7.27**). After stirring vigorously for 12 h, the reaction mixture was poured into deionized water (300 mL) and diluted with Et_2O (150 mL). The layers were separated and the aqueous layer was extracted with Et_2O (2 x 150 mL). The organic layers were combined, washed with deionized water (300 mL), dried over $MgSO_4$, and concentrated under reduced pressure (~100 mbar, at room temperature) to afford the corresponding alcohol, which was used in the subsequent step without further purification.

To a solution of the crude alcohol in CH_2Cl_2 (176 mL) was added pyridine (17.0 mL, 0.212 mol, 3.0 equiv from **7.27**). The reaction was cooled to 0 °C. After stirring for 5 min, methyl chloroformate (11 mL, 0.141 mol, 2.0 equiv from **7.27**) was added dropwise over 1 min. The reaction was stirred for 6 h, and allowed to warm to room temperature, at which point additional pyridine (8.50 mL, 0.141 mol, 1.0 equiv from **7.27**) and methyl chloroformate (5.5 ml, 0.106 mol, 1.5 equiv from **7.27**) was added. After stirring for an additional 12 h, the reaction mixture was poured into brine (200 mL) and diluted with Et_2O (150 mL). The layers were separated and the aqueous layer was extracted with Et_2O (2 x 150 mL). The organic layers were combined, washed with 1 N HCl (300 mL), dried over $MgSO_4$, and concentrated under reduced pressure (~100 mbar, at room temperature). The crude mixture was purified via flash chromatography (99:1 Pentane:Et_2O → 15:1 Pentane:Et_2O) to afford carbonate **7.43** (4.62 g, 41% yield, three steps) as a colorless oil. Carbonate **7.43**: R_f 0.61 (3:1 Hexanes:EtOAc); ^{1}H NMR (500 MHz, $CDCl_3$): δ 4.63 (s, 2H), 3.74 (s, 3H), 1.75–1.73 (m, 3H), 1.70–1.68 (m, 3H), 1.67 (s, 3H); ^{13}C NMR (125 MHz, $CDCl_3$): δ 156.1, 132.8, 122.4, 69.3, 54.7, 20.9, 20.3, 16.7; IR

(film): 2988, 2919, 1744, 1442, 1246 cm^{-1}; HRMS–ESI (m/z) $[M + Na]^+$ calcd for $C_8H_{14}NaO_3^+$, 181.0841; found 181.0843.

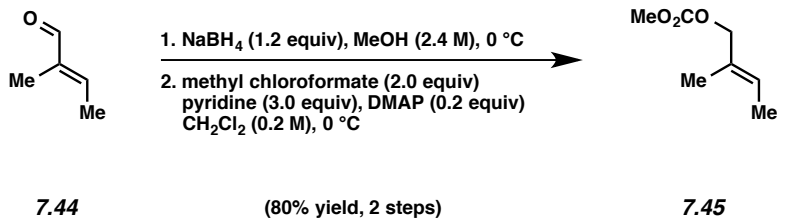

7.44 (80% yield, 2 steps) *7.45*

Carbonate 7.45. To a solution of tiglic aldehyde (**7.44**) (3.0 g, 36 mmol, 1.0 equiv) in MeOH (15 mL) at 0 °C was added $NaBH_4$ (1.6 g, 43 mmol, 1.2 equiv) in 10 portions over 5 min at 0 °C. After 3 h of stirring at room temperature, the mixture was poured into deionized water (50 mL) and diluted with CH_2Cl_2 (50 mL). The layers were separated and the aqueous layer was extracted with CH_2Cl_2 (2 x 50 mL). The organic layers were combined, washed with brine (50 mL), dried over $MgSO_4$, and concentrated under reduced pressure to afford the corresponding alcohol, which was used in the subsequent step without further purification.

To a solution of the crude alcohol in CH_2Cl_2 (180 mL) was added pyridine (2.57 mL, 31.9 mmol, 3.0 equiv from **7.44**) and DMAP (0.86 g, 7.1 mmol, 0.2 equiv). The reaction was cooled to 0 °C. After stirring for 5 min, methyl chloroformate (0.87 mL, 11.3 mmol, 2.0 equiv from **7.44**) was added dropwise over 20 min. The reaction was allowed to warm to room temperature. After stirring for 1 h, the reaction mixture was poured into brine (50 mL) and diluted with CH_2Cl_2 (50 mL). The layers were separated and the aqueous layer was extracted with CH_2Cl_2 (2 x 50 mL). The organic layers were combined, washed with 1 N HCl (50 mL), dried over $MgSO_4$, and concentrated under reduced pressure. The crude mixture was purified via flash chromatography (9:1 Pentane:Et_2O) to afford carbonate **7.45** (4.6 g, 80% yield, two steps) as a colorless oil. Carbonate **7.45**: R_f 0.61 (4:1 Hexanes:EtOAc); ^1H NMR (500 MHz, $CDCl_3$): δ

5.59 (q, J = 7.0, 1H), 4.51 (s, 2H), 3.77 (s, 3H), 1.67 (s, 3H), 1.63 (d, J = 7.0, 3H); ^{13}C NMR (125 MHz, $CDCl_3$): δ 156.0, 130.4, 125.2, 74.0, 54.8, 13.7, 13.4; IR (film): 2957, 1745, 1442, 1250, 935, 792 cm^{-1}; HRMS–ESI (m/z) $[M + Na]^+$ calcd for $C_8H_{14}O_3Na$ 181.0843; found 181.0841.

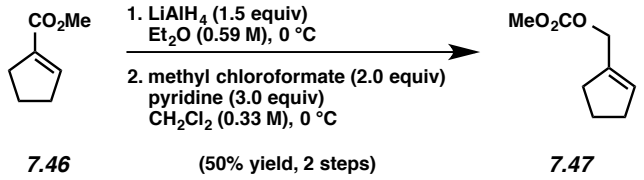

Carbonate 7.47. To a solution of methyl ester **7.46** (1.26 g, 10.0 mmol, 1.0 equiv) in Et_2O (17 mL) at 0 °C was added $LiAlH_4$ (570 mg, 15.0 mmol, 1.5 equiv) at 0 °C. After stirring for 4 h, deionized water (3 mL) was added dropwise over 5 min at 0 °C. The resulting heterogeneous mixture was filtered through a plug of celite® (50 mL of Et_2O eluent) and the filtrate was diluted with deionized water (50 mL). The layers were separated and the aqueous layer was extracted with Et_2O (3 x 50 mL). The organic layers were combined, dried over $MgSO_4$, and concentrated under reduced pressure (~100 mbar, at room temperature) to afford the corresponding alcohol, which was used in the subsequent step without further purification.

To a solution of the crude alcohol in CH_2Cl_2 (30 mL) was added pyridine (2.50 mL, 30.0 mmol, 3.0 equiv from **7.46**). The reaction was cooled to 0 °C. After stirring for 5 min, methyl chloroformate (1.55 mL, 20.0 mmol, 2.0 equiv from **7.46**) was added dropwise over 1 min. The reaction was allowed to warm to room temperature. After stirring for 15 h, the reaction mixture was poured into brine (150 mL) and diluted with CH_2Cl_2 (50 mL). The layers were separated and the aqueous layer was extracted with CH_2Cl_2 (3 x 50 mL). The organic layers were combined, washed with 1 N HCl (50 mL), dried over $MgSO_4$, and concentrated under reduced pressure (~100 mbar, at room temperature). The crude mixture was purified via flash chromatography

(98:2 Hexanes:Et_2O) to afford carbonate **7.47** (792 mg, 50% yield, two steps) as a colorless oil. Carbonate **7.47**: R_f 0.48 (9:1 Hexanes:EtOAc); ^1H NMR (500 MHz, $CDCl_3$): δ 5.72 (s, 1H), 4.69 (s, 2H), 3.79 (s, 3H), 2.38–2.31 (m, 4H), 1.92 (quint, J =7.7, 2H); ^{13}C NMR (125 MHz, $CDCl_3$): δ 156.0, 138.6, 129.6, 66.9, 54.9, 32.9, 32.6, 23.4; IR (film): 2960, 2918, 2848, 1750, 1447, 1263, 949 cm^{-1}; HRMS–ESI (m/z) $[M + Na]^+$ calcd for $C_8H_{12}O_3Na$, 179.0684; found 179.0677.

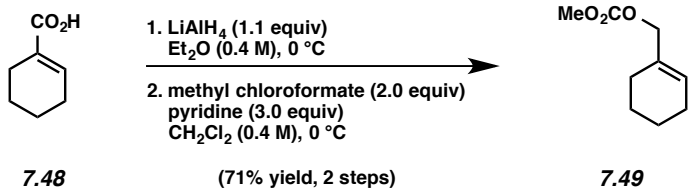

Carbonate 7.49. To a solution of carboxylic acid **7.48** (2.00 g, 16.5 mmol, 1.0 equiv) in Et_2O (40 mL) at 0 °C was added $LiAlH_4$ (18.2 mL of a 1.0 M solution in Et_2O, 18.2 mmol, 1.1 equiv) dropwise over 5 min at 0 °C. After stirring for 15 min, deionized water (5 mL) was added dropwise at 0 °C. The resulting heterogeneous mixture was filtered through a plug of celite® (25 mL of Et_2O eluent) and the filtrate was diluted with deionized water (50 mL). The layers were separated and the aqueous layer was extracted with Et_2O (2 x 50 mL). The organic layers were combined, dried over $MgSO_4$, and concentrated under reduced pressure (~100 mbar, at room temperature) to afford the corresponding alcohol, which was used in the subsequent step without further purification.

To a solution of the crude alcohol in CH_2Cl_2 (40 mL) was added pyridine (2.55 mL, 49.5 mmol, 3.0 equiv from **7.48**). The reaction was cooled to 0 °C. After stirring for 5 min, methyl chloroformate (2.6 mL, 33.0 mmol, 2.0 equiv from **7.48**) was added dropwise over 1 min. The reaction was allowed to warm to room temperature. After stirring for 4 h, the reaction mixture was poured into brine (50 mL) and diluted with CH_2Cl_2 (50 mL). The layers were separated and

the aqueous layer was extracted with CH_2Cl_2 (2 x 50 mL). The organic layers were combined, washed with 1 N HCl (50 mL), dried over $MgSO_4$, and concentrated under reduced pressure (~100 mbar, at room temperature). The crude mixture was purified via flash chromatography (99:1 Pentane:Et_2O → 49:1 Pentane:Et_2O) to afford carbonate **7.49** (2.00 g, 71% yield, two steps) as a colorless oil. Carbonate **7.49**: R_f 0.86 (1:1 Hexanes:EtOAc); ^{1}H NMR (500 MHz, $CDCl_3$): δ 5.78 (m, 1H), 4.49 (s, 2H), 3.78 (s, 3H), 2.02 (m, 4H), 1.64 (m, 2H), 1.57 (m, 2H); ^{13}C NMR (125 MHz, $CDCl_3$): δ 156.0, 132.5, 127.5, 72.7, 54.8, 25.9, 25.1, 22.4, 22.2; IR (film): 2930, 1744, 1441, 1250 cm^{-1}; HRMS–ESI (m/z) $[M + Na]^+$ calcd for $C_9H_{14}NaO_3^+$, 193.0841; found 193.0839.

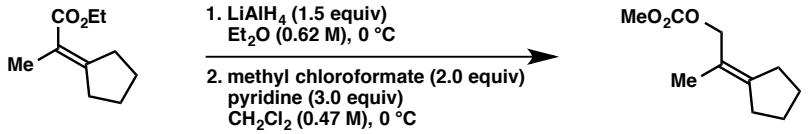

7.50 (61% yield, 2 steps) *7.51*

Carbonate 7.51. To a solution of known ester **7.50**[31] (3.15 g, 18.7 mmol, 1.0 equiv) in Et_2O (30 mL) at 0 °C was added $LiAlH_4$ (1.07 g, 28.1 mmol, 1.5 equiv) at 0 °C. After stirring for 4 h, deionized water (3 mL) was added dropwise over 5 min at 0 °C. The resulting heterogeneous mixture was filtered through a plug of celite® (25 mL of Et_2O eluent) and the filtrate was diluted with deionized water (25 mL). The layers were separated and the aqueous layer was extracted with Et_2O (2 x 50 mL). The organic layers were combined, dried over $MgSO_4$, and concentrated under reduced pressure (~100 mbar, at room temperature) to afford the corresponding alcohol, which was used in the subsequent step without further purification.

To a solution of the crude alcohol in CH_2Cl_2 (40 mL) was added pyridine (4.65 mL, 56.1 mmol, 3.0 equiv from **7.50**). The reaction was cooled to 0 °C. After stirring for 5 min, methyl

chloroformate (2.9 mL, 37.4 mmol, 2.0 equiv from **7.50**) was added dropwise over 1 min. The reaction was allowed to warm to room temperature. After stirring for 15 h, the reaction mixture was poured into brine (100 mL) and diluted with Et_2O (50 mL). The layers were separated and the aqueous layer was extracted with Et_2O (3 x 50 mL). The organic layers were combined, washed with 1 N HCl (25 mL), dried over $MgSO_4$, and concentrated under reduced pressure. The crude mixture was purified via flash chromatography (95:5 Hexanes:Et_2O) to afford carbonate **7.51** (2.09 g, 61% yield, two steps) as a colorless oil. Carbonate **7.51**: R_f 0.45 (9:1 Hexanes:EtOAc); ^{1}H NMR (500 MHz, $CDCl_3$): δ 4.63 (s, 2H), 3.78 (s, 3H), 2.33 (s, 2H), 2.22 (s, 2H), 1.70–1.63 (m, 7H); ^{13}C NMR (125 MHz, $CDCl_3$): δ 156.2, 145.0, 119.6, 70.6, 54.8, 31.3, 30.4, 27.0, 26.4, 17.2; IR (film): 2956, 2867, 1748, 1442, 1373, 1256, 942 cm^{-1}; HRMS–APCI (m/z) $[M + H]^+$ calcd for $C_{10}H_{17}O_3^+$, 185.11722; found 185.11700.

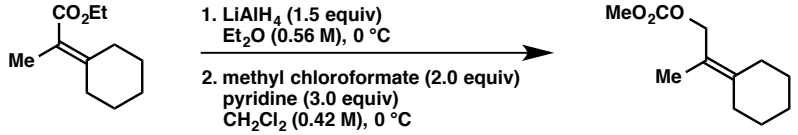

7.52 **(54% yield, 2 steps)** ***7.53***

Carbonate 7.53. To a solution of known ester **7.52**[3] (3.08 g, 16.9 mmol, 1.0 equiv) in Et_2O (30 mL) at 0 °C was added $LiAlH_4$ (965 mg, 25.4 mmol, 1.5 equiv). After stirring for 1 h, deionized water (3 mL) was added dropwise over 5 min at 0 °C. The resulting heterogeneous mixture was filtered through a plug of celite® (25 mL of Et_2O eluent) and the filtrate was diluted with deionized water (25 mL). The layers were separated and the aqueous layer was extracted with Et_2O (2 x 50 mL). The organic layers were combined, dried over $MgSO_4$, and concentrated under reduced pressure (~100 mbar, at room temperature) to afford the corresponding alcohol, which was used in the subsequent step without further purification.

To a solution of the crude alcohol in CH_2Cl_2 (40 mL) was added pyridine (4.21 mL, 50.7 mmol, 3.0 equiv from **7.52**). The reaction was cooled to 0 °C. After stirring for 5 min, methyl chloroformate (2.6 mL, 33.8 mmol, 2.0 equiv from **7.52**) was added dropwise over 1 min. The reaction was allowed to warm to room temperature. After stirring for 15 h, the reaction mixture was poured into brine (100 mL) and diluted with Et_2O (50 mL). The layers were separated and the aqueous layer was extracted with Et_2O (3 x 50 mL). The organic layers were combined, washed with 1 N HCl (25 mL), dried over $MgSO_4$, and concentrated under reduced pressure. The crude mixture was purified via flash chromatography (95:5 Hexanes:Et_2O) to afford carbonate **7.53** (1.83 g, 54% yield, two steps) as a colorless oil. Carbonate **7.53**: R_f 0.45 (9:1 Hexanes:EtOAc); ^{1}H NMR (500 MHz, $CDCl_3$): δ 4.68 (s, 2H), 3.77 (s, 3H), 2.28–2.22 (m, 2H), 2.21–2.15 (m, 2H), 1.73 (s, 3H), 1.60–1.48 (m, 6H); ^{13}C NMR (125 MHz, $CDCl_3$): δ 156.2, 141.4, 119.1, 69.0, 54.8, 31.0, 30.7, 28.4, 27.9, 26.8, 16.5; IR (film): 2925, 2854, 1744, 1443, 1373, 1247, 937 cm^{-1}; HRMS–APCI (m/z) $[M + H]^+$ calcd for $C_{11}H_{19}O_3^+$, 199.13287; found 199.13247.

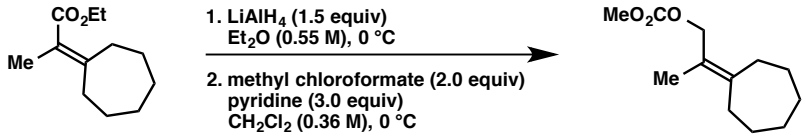

7.54 (64% yield, 2 steps) *7.55*

Carbonate 7.55. To a solution of known ester **7.54**[32] (2.15 g, 10.9 mmol, 1.0 equiv) in Et_2O (20 mL) at 0 °C was added $LiAlH_4$ (626 mg, 16.4 mmol, 1.5 equiv). After stirring for 1 h, deionized water (3 mL) was added dropwise over 5 min at 0 °C. The resulting heterogeneous mixture was filtered through a plug of celite® (25 mL of Et_2O eluent) and the filtrate was diluted with deionized water (25 mL). The layers were separated and the aqueous layer was extracted with

Et_2O (2 x 50 mL). The organic layers were combined, dried over $MgSO_4$, and concentrated under reduced pressure (~100 mbar, at room temperature) to afford the corresponding alcohol, which was used in the subsequent step without further purification.

To a solution of the crude alcohol in CH_2Cl_2 (30 mL) was added pyridine (2.80 mL, 32.9 mmol, 3.0 equiv from **7.54**). The reaction was cooled to 0 °C. After stirring for 5 min, methyl chloroformate (1.7 mL, 21.9 mmol, 2.0 equiv from **7.54**) was added dropwise over 1 min. The reaction was allowed to warm to room temperature. After stirring for 15 h, the reaction mixture was poured into brine (100 mL) and diluted with Et_2O (50 mL). The layers were separated and the aqueous layer was extracted with Et_2O (3 x 50 mL). The organic layers were combined, washed with 1 N HCl (25 mL), dried over $MgSO_4$, and concentrated under reduced pressure. The crude mixture was purified via flash chromatography (95:5 Hexanes:Et_2O) to afford carbonate **7.55** (1.49 g, 64% yield, two steps) as a colorless oil. Carbonate **7.55**: R_f 0.52 (9:1 Hexanes:EtOAc); ^{1}H NMR (500 MHz, $CDCl_3$): δ 4.67 (s, 2H), 3.77 (s, 3H), 2.33 (t, J = 6.0, 2H), 2.26 (t, J = 6.0, 2H), 1.71 (s, 3H), 1.60–1.53 (m, 4H), 1.51–1.44 (m, 4H); ^{13}C NMR (125 MHz, $CDCl_3$): δ 156.1, 142.2, 122.4, 69.1, 54.6, 32.3, 31.2, 28.9, 28.6, 28.2, 26.8, 16.4; IR (film): 2922, 2854, 1748, 1443, 1374, 1256, 936 cm^{-1}; HRMS–ESI (m/z) [M + Na]$^+$ calcd for $C_{12}H_{20}O_3Na^+$, 235.1310; found 235.1301.

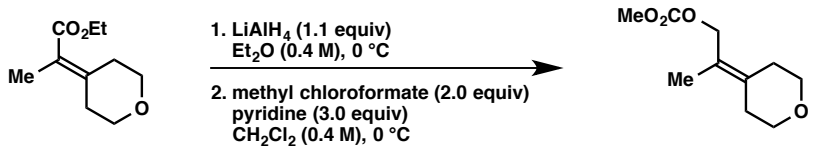

7.56 (71% yield, 2 steps) *7.57*

Carbonate 7.57. To a solution of ester **7.56**[33] (1.47 g, 8.0 mmol, 1.0 equiv) in Et_2O (20 mL) at 0 °C was added $LiAlH_4$ (8.8 mL of a 1.0 M solution in Et_2O, 8.8 mmol, 1.1 equiv) dropwise over 5

min. After stirring for 1 h, deionized water (1 mL) was added dropwise over 5 min at 0 °C. The resulting heterogeneous mixture was filtered through a plug of celite® (25 mL of Et_2O eluent) and the filtrate was diluted with deionized water (25 mL). The layers were separated and the aqueous layer was extracted with Et_2O (2 x 50 mL). The organic layers were combined, dried over $MgSO_4$, and concentrated under reduced pressure (~100 mbar, at room temperature) to afford the corresponding alcohol, which was used in the subsequent step without further purification.

To a solution of the crude alcohol in CH_2Cl_2 (20 mL) was added pyridine (1.93 mL, 24.0 mmol, 3.0 equiv from **7.56**). The reaction was cooled to 0 °C. After stirring for 5 min, methyl chloroformate (1.24 mL, 16.0 mmol, 2.0 equiv from **7.56**) was added dropwise over 1 min. The reaction was allowed to warm to room temperature. After stirring for 12 h, the reaction mixture was poured into brine (25 mL) and diluted with Et_2O (25 mL). The layers were separated and the aqueous layer was extracted with Et_2O (2 x 50 mL). The organic layers were combined, washed with 1 N HCl (25 mL), dried over $MgSO_4$, and concentrated under reduced pressure. The crude mixture was purified via flash chromatography (9:1 Hexanes:EtOAc → 5:1 Hexanes:EtOAc) to afford carbonate **7.57** (1.14 g, 71% yield, two steps) as a colorless oil. Carbonate **7.57**: R_f 0.73 (1:1 Hexanes:EtOAc); ^{1}H NMR (500 MHz, $CDCl_3$): δ 4.66 (s, 2H), 3.78 (s, 3H), 3.67 (app ddd, *J* = 13.2, 7.7, 5.5, 4H), 2.39 (t, *J* = 5.5, 2H), 2.32 (t, *J* = 5.5, 2H) 1.75 (s, 3H); ^{13}C NMR (125 MHz, $CDCl_3$): δ 156.1, 135.6, 121.5, 68.9–68.2 (2 carbons), 54.9, 31.3 & 31.1 (1 carbon), 16.3; IR (film): 2958, 2847, 1743, 1442, 1251 cm^{-1}; HRMS–APCI (m/z) $[M + H]^+$ calcd for $C_{10}H_{17}O_7^+$, 201.11214; found 201.11059.

*Note: The data for carbonate **7.57** represents empirically observed chemical shifts from the ^{13}C NMR spectrum, presumably due to the oxygen-containing heterocycle.*

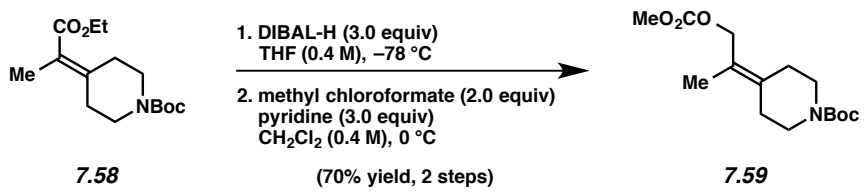

7.58 (70% yield, 2 steps) *7.59*

Carbonate 7.59. To a solution of ester **7.58**[34] (1.60 g, 5.65 mmol, 1.0 equiv) in THF (14 mL) at 0 °C was added DIBAL-H (11.3 mL of a 1.0 M solution in THF, 11.3 mmol, 2.0 equiv) dropwise over 5 min. The reaction was stirred for 3 h, and allowed to warm to room temperature, at which point additional DIBAL-H (5.65 mL of a 1.0 M solution in THF, 5.65 mmol, 1.0 equiv) was added. After stirring for an additional hour, the reaction mixture was poured into water (50 mL) and diluted with Et_2O (50 mL). The resulting heterogeneous mixture was filtered through a plug of celite® (100 mL of Et_2O eluent). The layers of the resulting filtrate were separated and the aqueous layer was extracted with Et_2O (1 x 50 mL). The organic layers were combined, dried over $MgSO_4$, and concentrated under reduced pressure to afford the corresponding alcohol, which was used in the subsequent step without further purification.

To a solution of the crude alcohol in CH_2Cl_2 (14 mL) was added pyridine (2.57 mL, 31.9 mmol, 3.0 equiv from **7.58**). The reaction was cooled to 0 °C. After stirring for 5 min, methyl chloroformate (0.87 mL, 11.3 mmol, 2.0 equiv from **7.58**) was added dropwise over 1 min. The reaction was allowed to warm to room temperature. After stirring for 1 h, the reaction mixture was poured into brine (50 mL) and diluted with CH_2Cl_2 (50 mL). The layers were separated and the aqueous layer was extracted with CH_2Cl_2 (2 x 50 mL). The organic layers were combined, washed with 1 N HCl (50 mL), dried over $MgSO_4$, and concentrated under reduced pressure. The crude mixture was purified via flash chromatography (9:1 Hexanes:EtOAc) to afford carbonate **7.59** (1.18 g, 70% yield, two steps) as a colorless oil. Carbonate **7.59**: R_f 0.78 (1:1 Hexanes:EtOAc); ^{1}H NMR (500 MHz, $CDCl_3$): δ 4.66 (s, 2H), 3.77 (s, 3H), 3.40 (app q, J = 6.8,

4H), 2.35 (t, J = 5.6, 2H), 2.28 (t, J = 5.6, 2H) 1.75 (s, 3H), 1.45 (s, 9H); ^{13}C NMR (125 MHz, $CDCl_3$): δ 156.0, 154.9, 136.2, 122.3, 79.6, 68.3, 54.9, 29.9, 29.5, 28.6, 16.5; IR (film): 2974, 1745, 1691, 1441, 1420, 1365, 1250, 1228, 1164 cm^{-1}; HRMS–APCI (m/z) $[M + H]^+$ calcd for $C_{15}H_{26}NO_5^+$, 300.18055; found 300.17829.

7.5.2.1.4 Reductive Coupling of Imides and Carbonates

Representative Procedure (synthesis of imide 7.5 is used as an example).

Reductive couplings were performed using a modification of the procedure reported by Gong and co-workers for the coupling of aryl bromides with substituted allylic acetates.[14c]

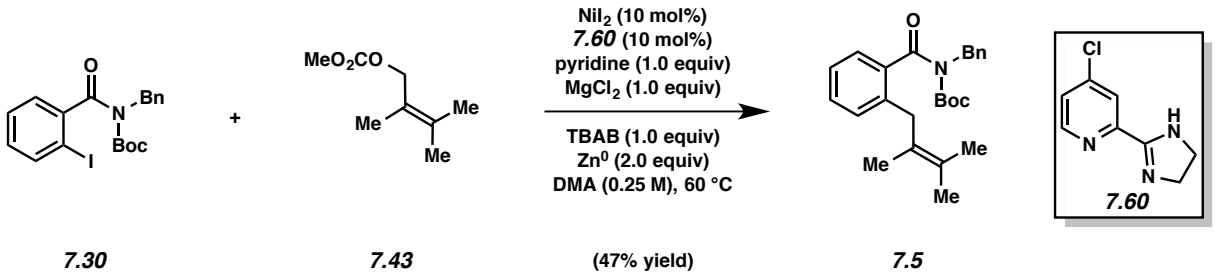

Imide 7.5. A scintillation vial containing imide **7.30** (219 mg, 0.50 mmol, 1.0 equiv), ligand **7.60** (9.1 mg, 0.050 mmol, 10 mol%), and a magnetic stir bar was sequentially charged with NiI_2 (15.6 mg, 0.050 mmol, 10 mol%), $MgCl_2$ (47.6 mg, 0.50 mmol, 1.0 equiv), TBAB (161 mg, 0.50 mmol, 1.0 equiv) and Zn^0 (65.4 mg, 1.0 mmol, 2.0 equiv) in the glovebox. The vial was removed from the glovebox, at which point DMA (2.0 mL), pyridine (40 μL, 0.5 mmol, 1.0 equiv), and carbonate **7.43** (158 mg, 1.0 mmol, 2.0 equiv) were added. The vial was quickly sealed with a teflon-lined screw cap, and stirred at 60 °C for 14 h. After cooling to room temperature, the mixture was passed through a column of silica gel and flushed (5:2 Hexanes:EtOAc) until TLC indicated the desired product had eluted. The volatiles were removed under reduced pressure and

the crude mixture was further purified by flash chromatography (99:1 Hexanes:EtOAc) to yield imide **7.5** (92 mg, 47% yield) as a white solid. Spectral data matched what is reported in Section 7.5.2.1.1.

Any modifications of the conditions shown in the representative procedures above are specified in the following schemes.

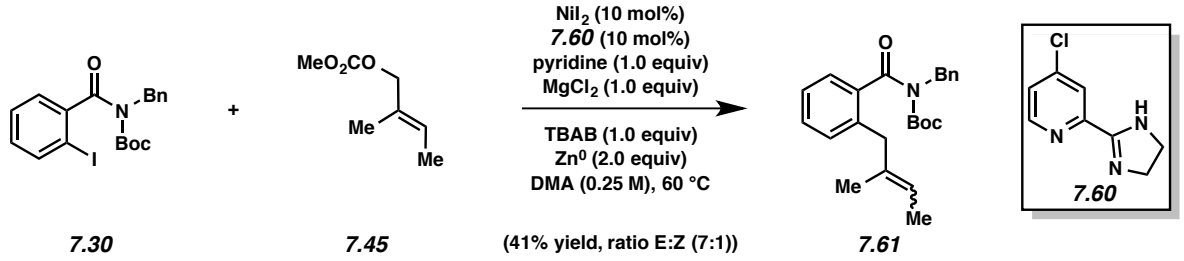

Imide 7.61. Following the representative procedure with iodo-imide **7.30** (218 mg, 0.5 mmol, 1.0 equiv), purification by flash chromatography (9:1 Hexanes:EtOAc) yielded **7.61** as an inseparable mixture of olefin isomers (79 mg, 41% yield, 7:1 isomer ratio E:Z) and as a colorless oil. Configurational isomers of imide **7.61** were analyzed as a mixture: **7.61** (**Major (*E*)-isomer**): ^{1}H NMR (500 MHz, $CDCl_3$): δ 7.45–7.41 (m, 2H), 7.36–7.32 (m, 2H), 7.31–7.26 (m, 1H), 7.21–7.12 (m, 4H), 5.24 (q, *J* = 6.8, 1H), 5.01 (s, 2H), 3.34 (s, 2H), 1.57 (d, *J* = 6.8, 3H), 1.53 (s, 3H), 1.10 (s, 9H); ^{13}C NMR (125 MHz, $CDCl_3$): δ 172.5, 153.0, 138.6, 138.1, 137.5, 134.2, 130.0, 129.4, 127.5, 126.4, 125.8, 121.7, 83.4, 48.1, 42.8, 27.6, 16.0, 13.7; **7.61** (**Minor (*Z*)-isomer**): ^{1}H NMR (500 MHz, $CDCl_3$): (20 of 29 signals observed) δ 5.45 (q, *J* = 6.8, 1H), 5.07–5.03 (m, 1H), 4.90–4.85 (m, 1H), 3.41 (s, 2H), 1.63 (d, *J* = 6.8, 3H), 1.61 (s, 3H), 1.11 (s, 9H); ^{13}C NMR (125 MHz, $CDCl_3$): δ 172.6, 153.1, 138.7, 138.0, 137.0, 133.8, 129.7, 129.6, 127.6, 126.1, 125.7, 121.9, 83.5, 48.1, 34.2, 27.7, 23.8, 13.8; Imide **7.61** (**mixture**): R_f 0.62 (4:1 Hexanes:EtOAc) IR

(film): 2979, 1726, 1669, 1228, 1137, 739 cm^{-1}; HRMS–APCI (m/z) $[M + H]^+$ calcd for $C_{24}H_{30}NO_3$ 380.22202; found 380.22186.

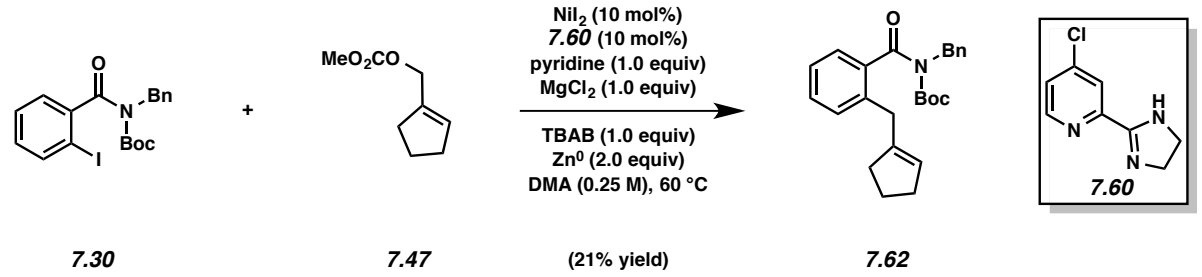

7.30 *7.47* (21% yield) *7.62*

Imide 7.62. Following the representative procedure with iodo-imide **7.30** (874 mg, 2.0 mmol, 1.0 equiv), imide **7.62** (165 mg, 21% yield) was obtained as a colorless oil. Imide **7.62**: R_f 0.48 (9:1 Hexanes:EtOAc); ^{1}H NMR (500 MHz, $CDCl_3$): δ 7.43 (d, *J* = 7.4, 2H), 7.35–7.24 (m, 4H), 7.22–7.13 (m, 3H), 5.32 (s, 1H), 5.01 (s, 2H), 3.45 (s, 2H), 2.32–2.24 (m, 2H), 2.20–2.14 (m, 2H), 1.83 (quint, *J* = 7.7, 2H), 1.10 (s, 9H); ^{13}C NMR (125 MHz, $CDCl_3$): δ 172.4, 152.9, 142.6, 138.2, 138.0, 137.3, 130.1, 129.4, 128.5, 128.4, 127.5, 126.7, 126.4, 125.7, 83.3, 48.1, 35.1, 34.9, 32.6, 27.5, 23.6; IR (film): 2933, 1728, 1671, 1369, 1334, 1229, 1139 cm^{-1}; HRMS–APCI (m/z) $[M + H]^+$ calcd for $C_{25}H_{30}NO_3^+$, 392.22202; found 392.21992.

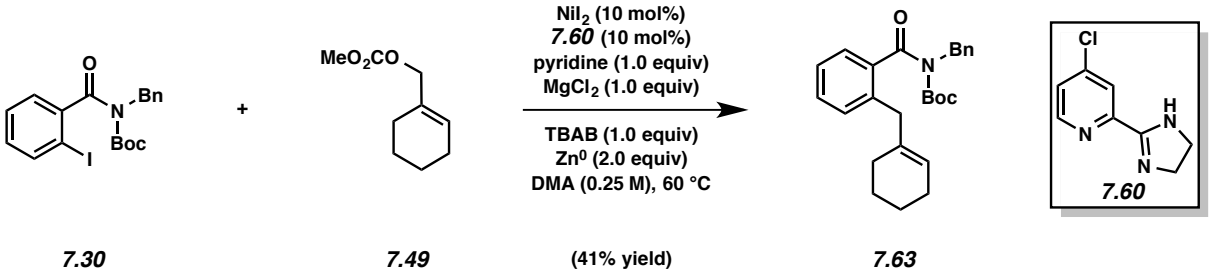

7.30 *7.49* (41% yield) *7.63*

Imide 7.63. Following the representative procedure with iodo-imide **7.30** (1.09 g, 2.5 mmol, 1.0 equiv), imide **7.63** (417 mg, 41% yield) was obtained as a colorless oil. Imide **7.63**: R_f 0.66 (3:1 Hexanes:EtOAc); ^{1}H NMR (500 MHz, $CDCl_3$): δ 7.43 (d, *J* = 7.1, 2H), 7.33 (t, *J* = 7.6, 2H), 7.31–7.24 (m, 2H), 7.23–7.13 (m, 3H), 5.43 (m, 1H), 5.01 (s, 2H), 3.31 (s, 2H), 1.98 (s, 2H),

1.83 (s, 2H), 1.55 (m, 4H), 1.11 (s, 9H); ^{13}C NMR (125 MHz, $CDCl_3$): δ 172.5, 152.9, 138.4, 138.0, 137.4, 136.2, 129.9, 129.4, 128.6, 128.4, 127.5, 126.4, 125.7, 124.2, 83.3, 48.1, 41.4, 28.3, 27.5, 25.5, 23.0, 22.4; IR (film): 2929, 1728, 1671, 1334, 1230, 1140 cm^{-1}; HRMS–APCI (m/z) $[M + H]^+$ calcd for $C_{26}H_{32}NO_3^+$, 406.23767; found 406.23493.

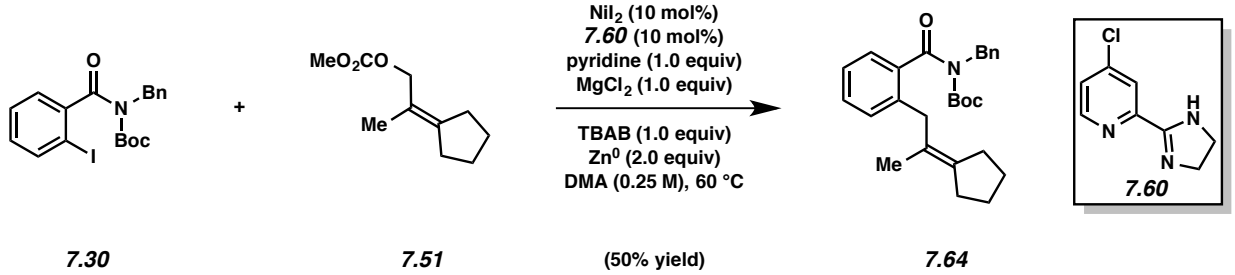

Imide 7.64. Following the representative procedure with iodo-imide **7.30** (874 mg, 2.0 mmol), imide **7.64** (418 mg, 50% yield) was obtained as a colorless oil. Imide **7.64**: R_f 0.45 (9:1 Hexanes:EtOAc); ^{1}H NMR (500 MHz, $CDCl_3$): δ 7.44 (d, J = 7.7, 2H), 7.33 (t, J = 7.2, 2H), 7.31–7.25 (m, 2H), 7.18–7.10 (m, 3H), 5.03 (s, 2H), 3.39 (s, 2H), 2.25 (m, 4H), 1.67 (m, 4H), 1.55 (m, 3H), 1.10 (s, 9H); ^{13}C NMR (125 MHz, $CDCl_3$): δ 172.6, 153.0, 139.7, 138.7, 138.0, 137.5, 129.5, 128.59, 128.57, 128.4, 127.5, 126.1, 125.5, 122.9, 83.4, 48.0, 38.1, 31.0, 30.9, 27.5, 27.2, 27.0, 19.3 ; IR (film): 2938, 1729, 1672, 1335, 1229, 1139 cm^{-1}; HRMS–APCI (m/z) $[M + H]^+$ calcd for $C_{27}H_{34}NO_3^+$, 420.25332; found 420.25300.

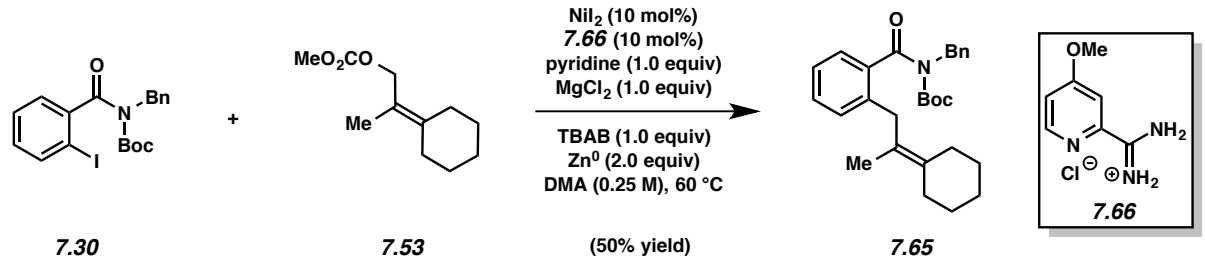

Imide 7.65. Following the representative procedure with iodo-imide **7.30** (0.44 g, 1.0 mmol, 1.0 equiv), imide **7.65** (0.22 g, 50% yield) was obtained as a colorless oil. Imide **7.65**: R_f 0.45 (9:1 Hexanes:EtOAc); ^{1}H NMR (500 MHz, $CDCl_3$): δ 7.45–7.42 (m, 2H), 7.46–7.43 (m, 2H), 7.36–7.32 (m, 2H), 7.18–7.10 (m, 3H), 5.04 (s, 2H), 3.44 (s, 2H), 2.25 (t, J = 5.8, 2H), 2.17 (t, J = 5.8, 2H), 1.60 (s, 3H), 1.59–1.54 (m, 4H), 1.52–1.46 (m, 2H), 1.10 (s, 9H); ^{13}C NMR (125 MHz, $CDCl_3$): δ 172.6, 153.0, 138.7, 138.0, 137.8, 135.9, 129.5, 128.6, 128.4, 128.3, 127.5, 125.9, 125.4, 121.8, 83.4, 48.0, 36.2, 30.84, 30.78, 28.5, 28.3, 27.5, 27.1, 18.4; IR (film): 2922, 1728, 1368, 1137, 740, 672 cm^{-1}; HRMS–APCI (m/z) $[M + H]^+$ calcd for $C_{28}H_{36}NO_3^+$, 434.26897; found 434.26866.

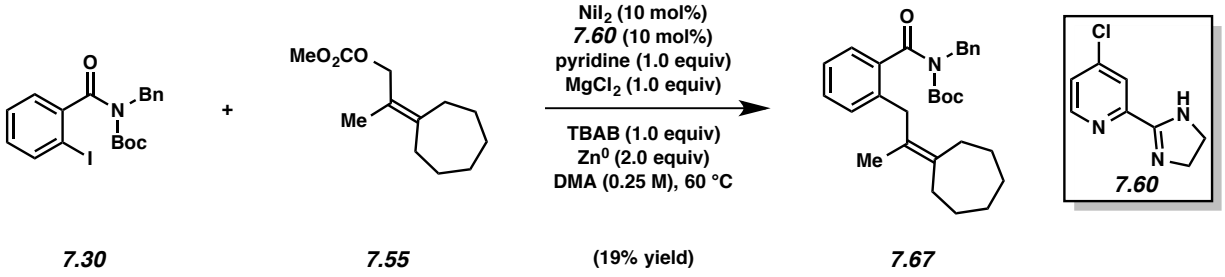

Imide 7.67. Following the representative procedure with iodo-imide **7.30** (874 mg, 2.0 mmol, 1.0 equiv), purification by flash chromatography (199:1 Hexanes:EtOAc) yielded imide **7.67** (172 mg, 19% yield) was obtained as a colorless oil. Imide **7.67**: R_f 0.50 (9:1 Hexanes:EtOAc); ^{1}H NMR (500 MHz, $CDCl_3$): δ 7.44 (d, J = 7.8, 2H), 7.33 (t, J = 7.2, 2H), 7.31–7.25 (m, 2H), 7.18–7.10 (m, 3H), 5.04 (s, 2H), 3.42 (s, 2H), 2.31 (t, J = 5.9, 2H), 2.25 (t, J = 5.9, 2H), 1.65–

1.59 (m, 2H), 1.58 (s, 3H), 1.57–1.47 (m, 6H), 1.11 (s, 9H); ^{13}C NMR (125 MHz, $CDCl_3$): δ 172.6, 153.0, 138.7, 138.0, 137.7, 137.0, 129.5, 128.6, 128.4, 128.2, 127.5, 126.0, 125.4, 125.3, 83.4, 48.0, 36.4, 32.0, 31.8, 29.4, 29.0, 28.1, 27.8, 27.5, 18.6; IR (film): 2921, 1730, 1673, 1335, 1229, 1138 cm^{-1}; HRMS–APCI (m/z) $[M + H]^+$ calcd for $C_{29}H_{38}NO_3^+$, 448.28462; found 448.28241.

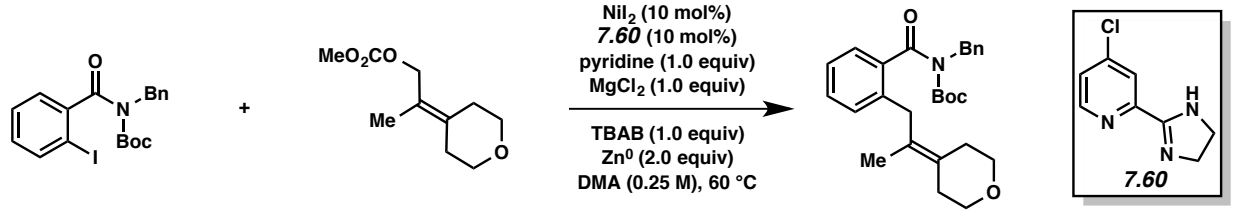

7.30 ***7.57*** **(46% yield)** ***7.68***

Imide 7.68. After following the representative procedure with iodo-imide **7.30** (1.16 g, 2.66 mmol, 1.0 equiv), the crude reaction mixture was vigorously stirred with 1:1 1 N NaOH/THF (26 mL) solution for 4 h to remove residual carbonate **7.57**. Purification by flash chromatography (49:1 Hexanes:EtOAc → 9:1 Hexanes:EtOAc) afforded imide **7.68** (536 mg, 46% yield) as a colorless oil. Imide **7.68**: R_f 0.49 (3:1 Hexanes:EtOAc); ^{1}H NMR (500 MHz, $CDCl_3$): δ 7.43 (d, J = 7.7, 2H), 7.34 (t, J = 7.7, 2H), 7.29 (dt, J = 7.7, 1.3, 2H), 7.17 (t, J = 7.7, 1H), 7.13 (t, J = 8.0, 2H), 5.03 (s, 2H), 3.71 (d, J = 5.5, 2H), 3.64 (d, J = 5.5, 2H), 3.45 (s, 2H), 2.38 (d, J = 5.5, 2H), 2.30 (d, J = 5.5, 2H), 1.63 (s, 3H), 1.11 (s, 9H); ^{13}C NMR (125 MHz, $CDCl_3$): δ 172.5, 153.0, 138.6, 137.9, 137.3, 130.3, 129.6, 128.6, 128.4, 128.2, 127.6, 126.0, 125.6, 124.5, 83.5, 69.2 & 69.1 (1 carbon), 48.1, 35.9, 31.3 & 31.2 (1 carbon), 27.6, 18.3; IR (film): 2962, 2845, 1728, 1669, 1369, 1333, 1228, 1137, 1101 cm^{-1}; HRMS–APCI (m/z) $[M + H]^+$ calcd for $C_{27}H_{34}NO_4^+$, 436.24824; found 436.24824.

*Note: The data for imide **7.68** represents empirically observed chemical shifts from the ^{13}C NMR spectrum, presumably due to the oxygen-containing heterocycle.*

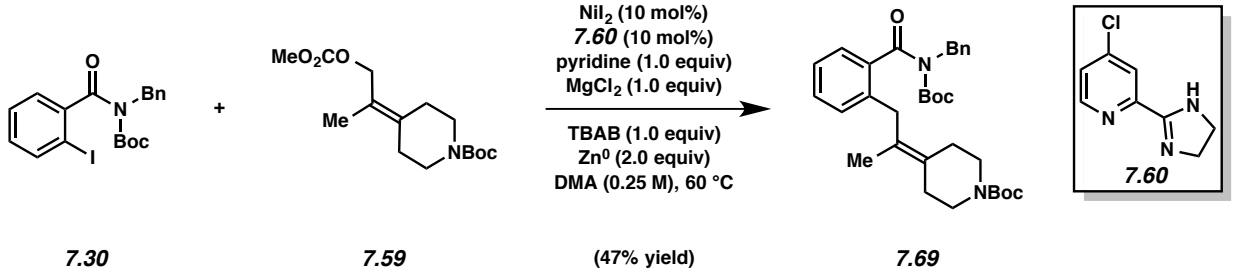

Imide 7.69. After following the representative procedure with iodo-imide **7.30** (1.08 g, 2.47 mmol, 1.0 equiv), the crude reaction mixture was vigorously stirred with 2:1 1 N NaOH/THF (30 mL) solution for 22 h to remove residual carbonate **7.59**. Purification by flash chromatography (199:1 Benzene:EtOAc → 24:1 Benzene:EtOAc) afforded imide **7.69** (622 mg, 47% yield) as a colorless oil. Imide **7.69**: R_f 0.49 (3:1 Hexanes:EtOAc); ^1H NMR (500 MHz, $CDCl_3$): δ 7.44 (d, J = 7.9, 2H), 7.34 (tt, J = 7.6, 1.4, 2H), 7.32–7.27 (m, 2H), 7.16 (td, J = 7.6, 1.0, 1H), 7.11 (td, J = 7.4, 1.3, 2H), 5.03 (s, 2H), 3.45 (s, 4H), 3.37 (s, 2H), 2.34 (t, J = 5.6, 2H), 2.27 (s, 2H), 1.63 (s, 3H), 1.47 (s, 9H) 1.11 (s, 9H); ^{13}C NMR (125 MHz, $CDCl_3$): δ 172.5, 155.1, 153.0, 138.6, 137.9, 137.2, 130.9, 129.6, 128.6, 128.4, 128.2, 127.6, 126.0, 125.7, 125.3, 83.5, 79.5, 48.1, 45.0 & 44.4 (1 carbon), 36.2, 29.8 & 29.7 (1 carbon), 28.6, 27.6, 18.5; IR (film): 2976, 1730, 1692, 1672, 1367, 1231, 1164, 1141 cm^{-1}; HRMS–APCI (m/z) $[M + H]^+$ calcd for $C_{32}H_{43}N_2O_5^+$, 535.31665; found 535.31392.

*Note: The data for imide **7.69** represents empirically observed chemical shifts from the ^{13}C NMR spectrum, presumably due to the nitrogen-containing heterocycle.*

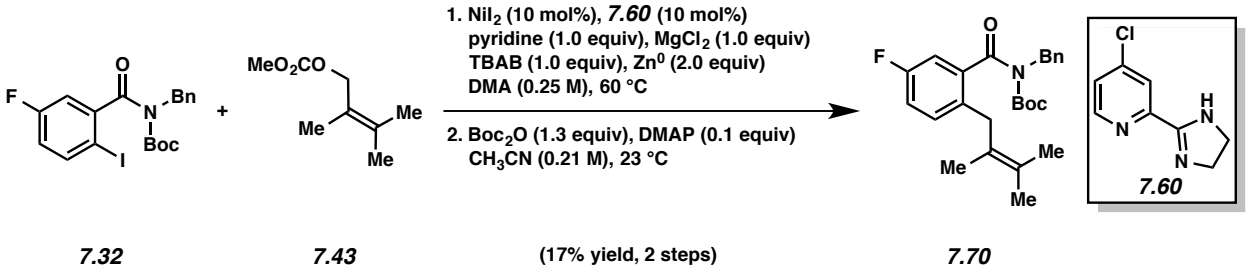

Imide 7.70. Following the representative procedure with iodo-imide **7.32** (1.82g, 4.0 mmol) led to appreciable amounts of des-Boc coupled product. As such, the mixture was re-subjected to the general conditions used to install a boc group described in the synthesis of **7.5** (Section 7.5.2.1.1). Purification by flash chromatography (99:1 Pentane:Et_2O → 49:1 Pentane:Et_2O) afforded imide **7.70** (275 mg, 17% yield, two steps) as an off-white oil. Imide **7.70**: R_f 0.64 (3:1 Hexanes:EtOAc); ^{1}H NMR (500 MHz, $CDCl_3$): δ 7.42 (d, *J* = 7.8, 2H), 7.34 (tt, *J* = 7.2, 1.4, 2H), 7.28 (tt, *J* = 7.4, 1.4, 1H), 7.06 (dd, *J* = 8.6, 5.6, 1H), 6.98 (dt, *J* = 8.4, 2.7, 1H), 6.84 (dd, *J* = 8.6, 2.7, 1H) 5.02 (s, 2H), 3.34 (s, 2H), 1.74 (s, 3H), 1.68 (s, 3H), 1.56 (s, 3H), 1.16 (s, 9H); ^{13}C NMR (125 MHz, $CDCl_3$): δ 171.2 (d, *J* = 2.4), 160.7 (d, *J* = 246), 152.6, 139.9 (d, *J* = 6.8), 137.7, 133.0 (d, *J* = 3.3), 130.0 (d, *J* = 7.6), 128.6, 128.3, 127.6, 127.5, 125.2, 116.1 (d, *J* = 21), 113.0 (d, *J* = 23), 83.8, 48.0, 36.1, 27.6, 20.8, 20.7, 18.7; ^{19}F NMR (376 MHz, $CDCl_3$): δ –117.9, (s, 1F); IR (film): 2982, 2920, 1734, 1673, 1369, 1331, 1229, 1149 cm^{-1}; HRMS–APCI (m/z) $[M + H]^+$ calcd for $C_{25}H_{31}FNO_3^+$, 412.22825; found 412.22781.

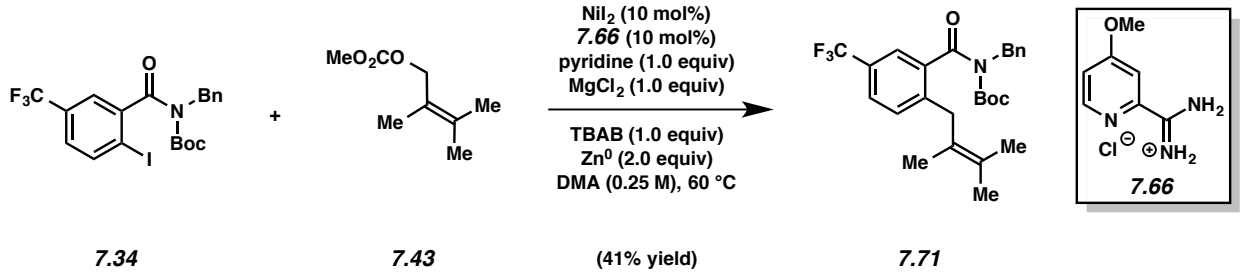

Imide 7.71. Following the representative procedure with iodo-imide **7.34** (455 mg, 0.9 mmol), purification by flash chromatography (199:1 Benzene:EtOAc) yielded imide **7.71** (169 mg, 41% yield) as a yellow oil. Imide **7.71**: R_f 0.75 (3:1 Hexanes:EtOAc); ^{1}H NMR (500 MHz, $CDCl_3$): δ 7.54 (dd, *J* = 8.2, 1.4, 1H), 7.43 (d, *J* = 8.0, 2H), 7.37 (d, *J* = 1.5, 1H), 7.35 (tt, *J* = 7.8, 1.4, 2H), 7.29 (tt, *J* = 7.4, 1.3, 1H), 7.24 (d, *J* = 8.1, 1H) 5.05 (s, 2H), 3.44 (s, 2H), 1.76 (s, 3H), 1.69 (s, 3H), 1.58 (s, 3H), 1.12 (s, 9H); ^{13}C NMR (125 MHz, $CDCl_3$): δ 171.2, 152.4, 141.7, 139.3, 137.6, 128.9, 128.7, 128.4 128.3, 128.2, 127.7, 125.9 (q, *J* = 3.7), 124.4, 124.1 (q, *J* = 274), 122.8 (q, *J* = 3.7), 84.0, 48.1, 36.9, 27.5, 20.78, 20.75, 18.9; ^{19}F NMR (376 MHz, $CDCl_3$): δ –62.4, (s, 3F); IR (film): 2983, 1736, 1672, 1318, 1141, 1123 cm^{-1}; HRMS–APCI (m/z) $[M + H]^+$ calcd for $C_{26}H_{31}F_3NO_3^+$, 462.22505; found 462.22240.

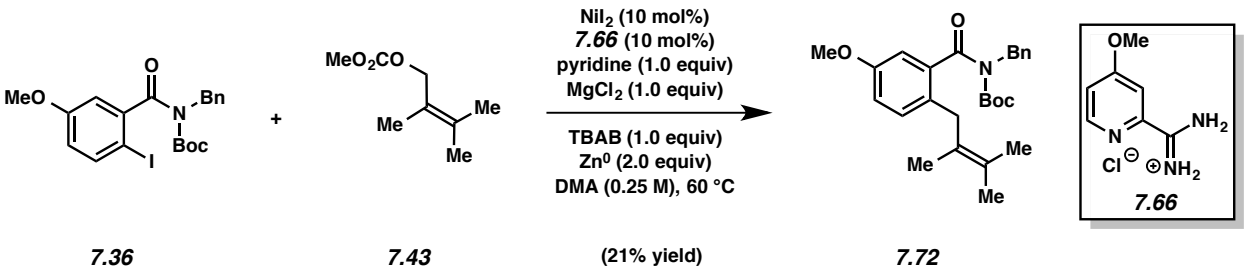

Imide 7.72. Following the representative procedure with iodo-imide **7.36** (0.42 g, 0.9 mmol), purification by flash chromatography (99:1 Hexanes:EtOAc) yielded imide **7.72** (79 mg, 21% yield) as a colorless oil. Imide **7.72**: R_f 0.52 (4:1 Hexanes:EtOAc); ^{1}H NMR (500 MHz, $CDCl_3$): δ 7.45–7.42 (m, 2H), 7.36–7.31 (m, 2H), 7.29–7.25 (m, 1H), 7.00 (d, *J* = 8.6, 1H), 6.84 (dd, *J* =

8.6, 2.8, 1H), 6.66 (d, J = 2.8, 1H), 5.02 (s, 2H), 3.74 (s, 3H), 3.33 (s, 2H), 1.73 (s, 3H), 1.69 (s, 3H), 1.56 (s, 3H), 1.13 (s, 9H); ^{13}C NMR (125 MHz, $CDCl_3$): δ 172.4, 157.5, 153.0, 139.4, 138.0, 129.60, 129.57, 128.7, 128.5, 127.6, 127.0, 125.8, 115.3, 111.5, 83.5, 55.6, 48.1, 36.0, 27.7, 20.84, 20.81, 18.8; IR (film): 2980, 1730, 1672, 1142, 1039, 851 cm^{-1}; HRMS–APCI (m/z) $[M + H]^+$ calcd for $C_{26}H_{34}NO_4^+$, 424.24824; found 424.24803.

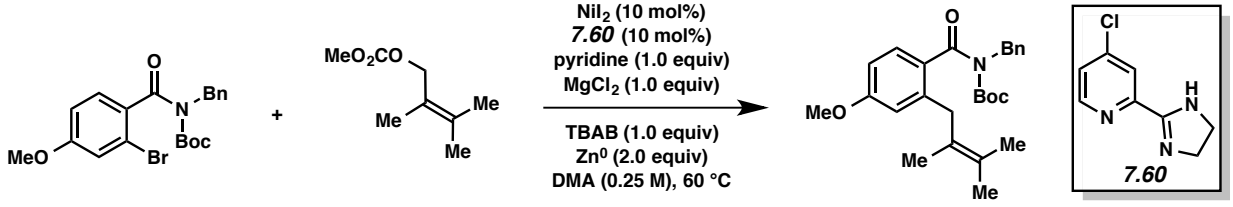

Imide 7.73: Following the representative procedure with bromo-imide **7.38** (0.84 g, 2.0 mmol), purification by flash chromatography (98:2 Hexanes:EtOAc) yielded imide **7.73** (0.24 g, 28% yield) as a colorless oil. Imide **7.73**: R_f 0.40 (9:1 Hexanes:EtOAc); ^{1}H NMR (500 MHz, $CDCl_3$): δ 7.44–7.42 (m, 2H), 7.35–7.32 (m, 2H), 7.28–7.24 (m, 1H), 7.13–7.10 (m, 1H), 6.69–6.66 (m, 2H), 5.00 (s, 2H), 3.78 (s, 3H), 3.47 (s, 2H), 1.75 (s, 3H), 1.70 (s, 3H), 1.59 (s, 3H), 1.15 (s, 9H); ^{13}C NMR (125 MHz, $CDCl_3$): (20 of 21 signals observed) δ 172.5, 160.9, 153.3, 140.7, 138.1, 131.0, 128.6, 128.34, 128.30, 127.4, 125.3, 114.7, 109.7, 83.0, 55.4, 48.4, 37.0, 27.7, 20.8, 18.9; IR (film): 2979, 1726, 1328, 1227, 966, 626 cm^{-1}; HRMS–APCI (m/z) $[M + H]^+$ calcd for $C_{26}H_{34}NO_4^+$, 424.24824; found 424.24858.

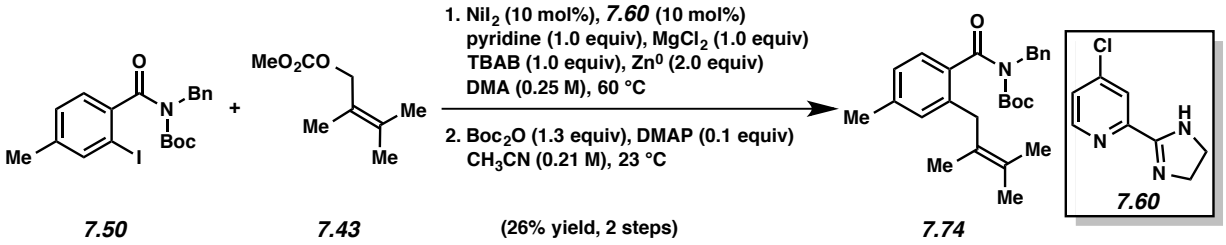

Imide 7.74. Following the representative procedure with iodo-imide **7.50** (2.1 g, 4.5 mmol) led to appreciable amounts of des-Boc coupled product. As such, the mixture was re-subjected to the general conditions used to install a boc group described in the synthesis of **7.5** (Section 7.5.2.1.1). Purification by flash chromatography (9:1 Hexanes:EtOAc) afforded imide **7.74** (0.48 g, 26% yield, two steps) as a colorless oil. Imide **7.74**: R_f 0.51 (9:1 Hexanes:EtOAc); ^{1}H NMR (500 MHz, $CDCl_3$): δ 7.42–7.39 (m, 2H), 7.33–7.29 (m, 2H), 7.27–7.22 (m, 1H), 7.01 (d, J = 7.7, 1H), 6.94 (d, J = 7.7, 1H), 6.88 (s, 1H), 5.00 (s, 2H), 3.41 (s, 2H), 2.30 (s, 3H), 1.73 (s, 3H), 1.69 (s, 3H), 1.56 (s, 3H), 1.11 (s, 9H); ^{13}C NMR (125 MHz, $CDCl_3$): δ 172.6, 153.0, 139.4, 137.9, 137.7, 135.5, 129.0, 128.4, 128.1, 127.2, 126.7, 126.1, 125.9, 125.4, 83.0, 47.9, 36.6, 27.4, 21.5, 20.6, 18.6; IR (film): 2980, 1728, 1670, 1229, 1142, 969 cm^{-1}; HRMS–APCI (m/z) $[M + H]^+$ calcd for $C_{26}H_{33}NO_3^+$, 408.25332; found 408.25332.

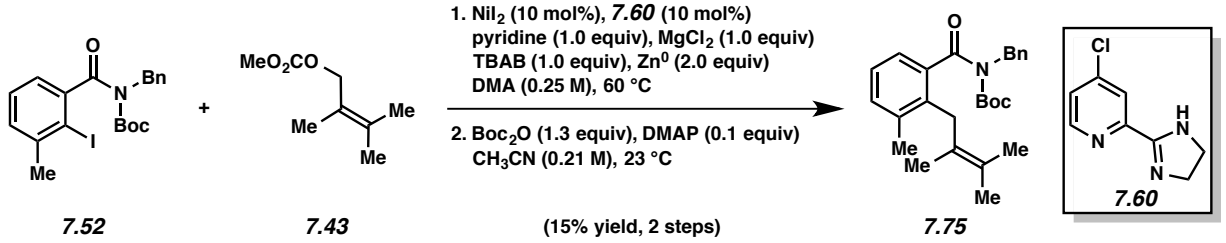

Imide 7.75. Following the representative procedure with iodo-imide **7.52** (0.93 g, 2.0 mmol, 1.0 equiv) led to appreciable amounts of des-Boc coupled product. As such, the mixture was re-subjected to the general conditions used to install a boc group described in the synthesis of **7.5** (Section 7.5.2.1.1). Purification by flash chromatography (9:1 Hexanes:EtOAc) afforded imide

7.75 (102 mg, 15% yield, two steps) as a colorless oil. Imide **7.75**: R_f 0.57 (4:1 Hexanes:EtOAc); ^{1}H NMR (500 MHz, $CDCl_3$): δ 7.42–7.39 (m, 2H), 7.34–7.30 (m, 2H), 7.28–7.24 (m, 1H), 7.13 (d, *J* = 8.0, 1H), 7.06 (t, *J* = 8.0, 1H), 6.95 (d, *J* = 8.0, 1H), 5.00 (s, 2H), 3.43 (br s, 2H), 2.21 (s, 3H), 1.74 (s, 3H), 1.67 (s, 3H), 1.39 (s, 3H), 1.10 (s, 9H); ^{13}C NMR (125 MHz, $CDCl_3$): δ 173.1, 153.0, 139.6, 138.3, 138.2, 136.5, 131.2, 128.6, 128.4, 127.5, 125.7, 125.3, 125.1, 123.8, 83.8, 48.0, 34.8, 27.6, 21.1, 20.7, 19.8, 16.9; IR (film): 2979, 1729, 1674, 1368, 1144, 698 cm^{-1}; HRMS–APCI (m/z) $[M + H]^+$ calcd for $C_{26}H_{34}NO_3^+$, 408.25332; found 408.25311.

7.5.2.2 Initial Evaluation of Reaction Conditions

Representative Procedure for the Nickel-Catalyzed Heck Cyclization of Imides

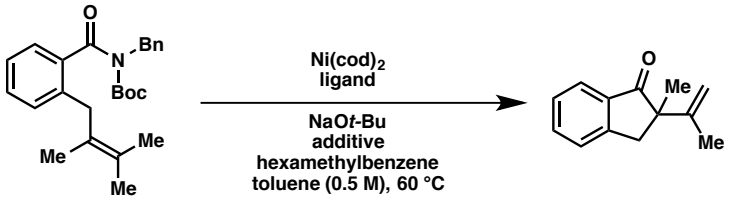

7.5 *7.6*

Indanone 7.6 (Table 7.1). A dram vial containing imide **7.5** (39.3 mg, 0.10 mmol, 1.0 equiv), hexamethylbenzene, and a magnetic stir bar was sequentially charged with the appropriate ligand, $Ni(cod)_2$, and NaO*t*-Bu in a glovebox. Subsequently, toluene (0.20 mL) and the additive (when applicable) were added. The vial was sealed with a Teflon-lined screw cap, removed from the glove box, wrapped with Teflon tape, and stirred at the appropriate temperature for 24 h. After cooling to room temperature, the mixture was diluted with Hexanes (1.0 mL) and filtered through a plug of silica gel (10 mL of EtOAc eluent). The volatiles were removed under reduced pressure, and the yield was determined by ^{1}H NMR analysis with hexamethylbenzene as the internal standard.

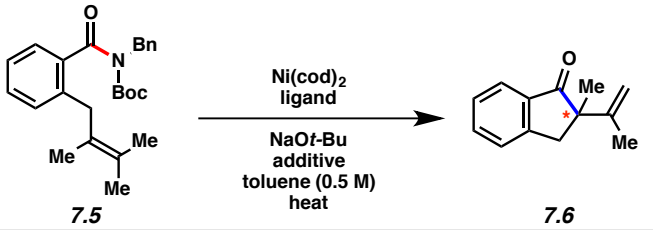

Entry	$Ni(cod)_2$ (loading)	Ligand (loading)	Additive	Temp.	Yield[b]
1	20 mol%	*7.7* (40 mol%)	none	100 °C	0%
2	20 mol%	*7.8* (40 mol%)	none	100 °C	24%
3	20 mol%	*7.9* (40 mol%)	none	100 °C	76%
4	20 mol%	*7.9* (20 mol%)	none	100 °C	67%
5	10 mol%	*7.9* (20 mol%)	none	100 °C	51%
6	15 mol%	*7.9* (30 mol%)	none	100 °C	91%
7	15 mol%	*7.9* (30 mol%)	*t*-amyl alcohol[c]	60 °C	95%

SIPr·HCl (7.7) *ICy·HBF$_4$ (7.8)* *Benz-ICy·HCl (7.9)*

7.5.2.3 Scope of Methodology

Representative Procedure for the Nickel-Catalyzed Heck Cyclization of Imides (synthesis of indanone 7.6 is used as an example).

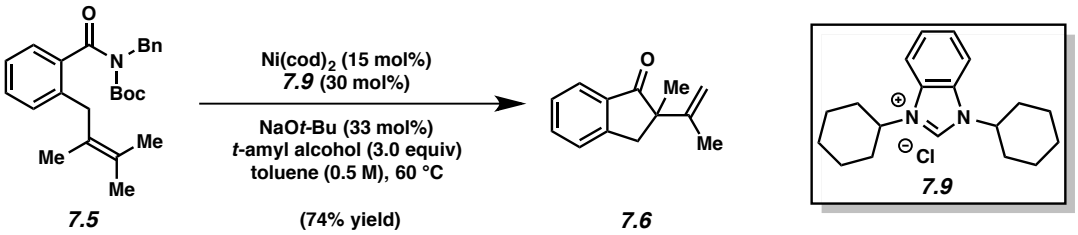

7.5 (74% yield) *7.6*

Indanone 7.6 (Table 7.2). A dram vial containing imide **7.5** (39.3 mg, 0.10 mmol, 1.0 equiv) and a magnetic stir bar was sequentially charged with **7.9** (9.6 mg, 0.030 mmol, 30 mol%), $Ni(cod)_2$ (4.1 mg, 0.015 mmol, 15 mol%), and NaO*t*-Bu (3.2 mg, 0.033 mmol, 33 mol%) in a glovebox. Subsequently, toluene (0.20 mL) and then *t*-amyl alcohol (32 µL, 0.30 mmol, 3.0

equiv) were added. The vial was sealed with a Teflon-lined screw cap, removed from the glovebox, and stirred at 60 °C for 24 h. After cooling to room temperature, the mixture was diluted with hexanes (1.0 mL) and filtered through a plug of silica gel (10 mL of EtOAc eluent). The volatiles were removed under reduced pressure. ^{1}H NMR analysis of the crude reaction mixture indicated a 95% yield (average of two experiments) of ketone **7.6** relative to a hexamethylbenzene external standard. Purification by preparative thin-layer chromatography (3:1 Hexanes:EtOAc) afforded indanone **7.6** (74% yield, average of two experiments) as a colorless oil. The diminished isolated yields of **7.6** can be attributed to the volatility of the neat compound. Indanone **7.6**: R_f 0.59 (3:1 Hexanes:EtOAc); ^{1}H NMR (500 MHz, $CDCl_3$): δ 7.78 (d, J = 7.7, 1H), 7.61 (td, J = 7.5, 1.1, 1H), 7.45 (dt, J = 7.7, 0.9, 1H), 7.38 (td, J = 7.5, 0.7, 1H), 4.95 (m, 2H), 3.33 (d, J = 17.4, 1H), 2.95 (d, J = 17.4, 1H), 1.65 (s, 3H), 1.38 (s, 3H); ^{13}C NMR (125 MHz, $CDCl_3$): δ 209.2, 152.7, 145.9, 135.9, 135.0, 127.6, 126.5, 124.6, 112.1, 54.5, 41.3, 22.7, 19.9; IR (film): 2966, 2928, 1710, 1604, 1464, 1277 cm^{-1}; HRMS–APCI (m/z) $[M + H]^+$ calcd for $C_{13}H_{15}O$, 187.11174; found 187.11130.

Any modifications of the conditions shown in the representative procedure above are specified in the following schemes, which depict all of the results shown in Table 7.2 and Figure 7.2.

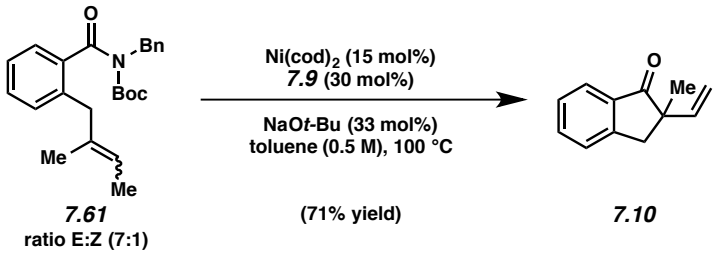

Indanone 7.10 (Table 7.2). Purification by preparative thin-layer chromatography (9:1 Hexanes:EtOAc) afforded indanone **7.10** (71% yield, average of two experiments) as a colorless

oil. Indanone **7.10**: R_f 0.59 (4:1 Hexanes:EtOAc); ^{1}H NMR (500 MHz, $CDCl_3$): δ 7.77 (d, J = 7.8, 1H), 7.60 (td, J = 7.5, 1.2, 1H), 7.45 (dt, J = 7.7, 0.9, 1H), 7.38 (t, J = 7.8, 1H), 5.95 (dd, J = 7.5, 10.6, 1H), 5.20–5.11 (m, 2H), 3.32 (d, J = 17.0, 1H), 3.02 (d, J = 17.0, 1H), 1.37 (s, 3H); ^{13}C NMR (125 MHz, $CDCl_3$): δ 208.0, 152.0, 140.6, 135.2, 134.9, 127.5, 126.4, 124.6, 113.9, 52.3, 40.7, 23.2; IR (film): 2966, 1714, 1465, 1279, 738 cm^{-1}; HRMS–APCI (m/z) $[M + H]^+$ calcd for $C_{12}H_{13}O^+$, 173.09609; found 173.09618.

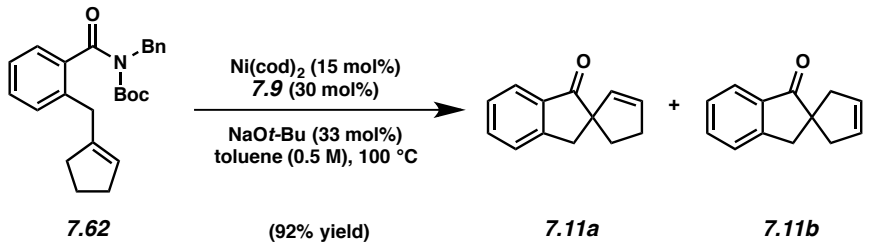

Indanones 7.11a and 7.11b (Table 7.2). Purification by preparative thin-layer chromatography (95:5 Benzene:CH_3CN) afforded indanones **7.11a** and **7.11b** (92% combined yield, average of two experiments) as a ~1:1 mixture of olefin isomers. Iterative purification by preparative thin-layer chromatography (Benzene) afforded analytical samples of indanones **7.11a** and **7.11b** as colorless oils. Spectral data match those previously reported.[35]

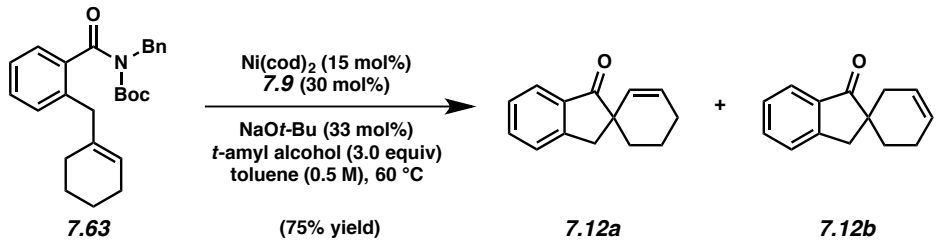

Indanones 7.12a and 7.12b (Table 7.2). Purification by preparative thin-layer chromatography (19:1 Benzene:CH_3CN) afforded indanones **7.12a** and **7.12b** (75% combined yield, average of two experiments) as a ~1:1 mixture of olefin isomers. Iterative purification by preparative thin-

layer chromatography (Benzene) afforded analytical samples of **7.12a** and **7.12b** as colorless oils. Indanone **7.12a**: R_f 0.47 (benzene); ^{1}H NMR (500 MHz, $CDCl_3$): δ 7.77 (d, *J* = 7.6, 1H) 7.59 (td, *J* = 7.6, 1.1, 1H), 7.43 (d, *J* = 7.6, 1H), 7.37 (t, *J* = 7.6, 1H), 6.00 (ddd, *J* = 7.5, 4.2, 3.3, 1H), 5.45 (d, *J* = 9.9, 1H), 3.14 (d, *J* = 17.1, 1H), 3.07 (d, *J* = 17.1, 1H), 2.22–2.13 (m, 1H), 2.13–2.04 (m, 1H), 2.04–1.96 (m, 1H), 1.90 (td, *J* = 11.6, 2.7, 1H), 1.69–1.57 (m, 2H); ^{13}C NMR (125 MHz, $CDCl_3$): δ 210.1, 152.6, 135.9, 135.0, 130.2, 128.3, 127.7, 126.7, 124.7, 51.4, 42.6, 32.8, 24.6, 19.5; IR (film): 3019, 2930, 1712, 1605, 1464, 1282 cm^{-1}; HRMS–APCI (m/z) $[M + H]^+$ calcd for $C_{14}H_{15}O^+$, 199.11174; found 199.11026. Indanone **7.12b**: R_f 0.50 (benzene); ^{1}H NMR (500 MHz, $CDCl_3$): δ 7.77 (d, *J* = 7.7, 1H) 7.59 (td, *J* = 7.6, 0.9, 1H), 7.44 (d, *J* = 7.5, 1H), 7.38 (t, *J* = 7.5, 1H), 5.79 (m, 2H), 3.06 (d, *J* = 17.3, 1H), 2.93 (d, *J* = 17.3, 1H), 2.48 (dquint *J* = 17.7, 2.5, 1H), 2.30–2.14 (m, 2H), 1.91 (ddd, *J* = 17.5, 11.1, 6.6, 1H), 1.79 (dt, *J* = 17.7, 2.5, 1H), 1.50 (dt, *J* = 17.5, 2.7, 1H); ^{13}C NMR (125 MHz, $CDCl_3$): δ 211.3, 153.0, 136.0, 135.0, 127.6, 126.81, 126.76, 125.3, 124.5, 48.5, 39.2, 34.1, 28.7, 22.8; IR (film): 3026, 2925, 2840, 1712, 1608, 1284 cm^{-1}; HRMS–APCI (m/z) $[M + H]^+$ calcd for $C_{14}H_{15}O^+$, 199.11174; found 199.11028.

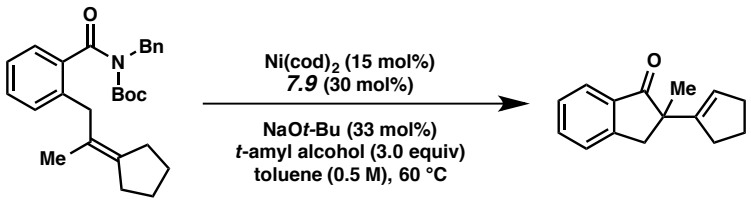

7.64 **(51% yield)** ***7.13***

Indanone 7.13 (Table 7.2). Purification by preparative thin-layer chromatography (97:3 Benzene:CH_3CN) afforded indanone **7.13** (51% yield, average of two experiments) as a colorless oil. Indanone **7.13**: R_f 0.25 (9:1 Hexane:EtOAc); ^{1}H NMR (500 MHz, $CDCl_3$): δ 7.77 (d, *J* = 7.7,

1H), 7.60 (dt, *J* = 7.5, 1.2, 1H), 7.44 (td, *J* = 7.7, 0.9, 1H), 7.37 (dt, *J* = 7.5, 0.9, 1H), 5.57 (quint, *J* = 2.2, 1H), 3.32 (d, *J* = 17.2, 1H), 2.97 (d, *J* = 17.2, 1H), 2.34–2.20 (m, 3H), 2.15–2.06 (m, 1H), 1.88–1.78 (m, 2H), 1.41 (s, 3H); ^{13}C NMR (125 MHz, $CDCl_3$): δ 208.9, 152.7, 145.5, 135.8, 135.0, 127.6, 126.6, 125.7, 124.7, 51.6, 41.4, 32.4, 32.2, 23.6, 22.9; IR (film): 2956, 2929, 2846, 1713, 1608, 1464, 1280 cm^{-1}; HRMS–APCI (m/z) $[M + H]^+$ calcd for $C_{15}H_{17}O^+$, 213.12739; found 213.12580.

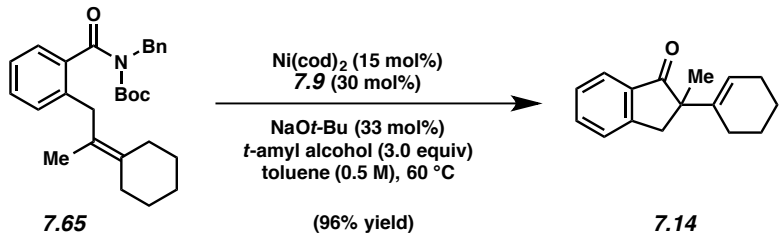

Indanone 7.14 (Table 7.2). Purification by preparative thin-layer chromatography (9:1 Benzene:CH_3CN) afforded indanone **7.14** (96% yield, average of two experiments) as a colorless oil. Indanone **7.14**: R_f 0.48 (9:1 Hexanes:EtOAc); ^{1}H NMR (500 MHz, $CDCl_3$): δ 7.76 (d, *J* = 7.6, 1H), 7.59 (td, *J* = 7.6, 1.2, 1H), 7.43 (dt, *J* = 7.6, 0.9, 1H), 7.39–7.34 (m, 1H), 5.65 (d, *J* = 17.6, 1H), 3.29 (d, *J* = 17.4, 1H), 2.91 (d, *J* = 17.4, 1H), 2.13–1.99 (m, 2H), 1.92–1.83 (m, 1H), 1.79–1.70 (m, 1H), 1.63–1.50 (m, 4H), 1.33 (s, 3H); ^{13}C NMR (125 MHz, $CDCl_3$): δ 210.2, 153.1, 138.5, 136.3, 134.9, 127.5, 126.6, 124.5, 122.4, 54.6, 41.7, 25.5 (two carbons), 23.1, 22.32, 22.28; IR (film): 2928, 1712, 1464, 1153, 736 cm^{-1}; HRMS–APCI (m/z) $[M + H]^+$ calcd for $C_{16}H_{19}O^+$, 227.14304; found 227.14236.

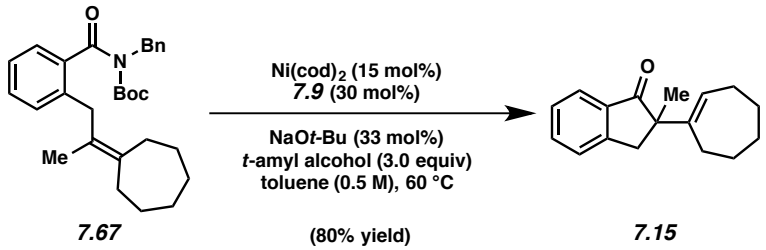

Indanone 7.15 (Table 7.2). Purification by preparative thin-layer chromatography (97:3 Benzene:CH_3CN) afforded indanone **7.15** (80% yield, average of two experiments) as a colorless oil. Indanone **7.15**: R_f 0.48 (9:1 Hexane:EtOAc); ^{1}H NMR (500 MHz, $CDCl_3$): δ 7.78 (d, J = 7.7, 1H), 7.60 (dt, J = 7.5, 1.2, 1H), 7.44 (td, J = 7.7, 0.9, 1H), 7.37 (dt, J = 7.5, 0.9, 1H), 5.86 (t, J = 6.8, 1H), 3.26 (d, J = 17.4, 1H), 2.89 (d, J = 17.4, 1H), 2.22–2.10 (m, 2H), 1.98 (ddd, J = 14.9, 9.5, 1.7, 1H), 1.89 (ddd, J = 14.9, 8.9, 1.7, 1H), 1.78–1.64 (m, 2H), 1.55–1.45 (m, 2H) 1.45–1.30 (m, 2H), 1.29 (s, 3H); ^{13}C NMR (125 MHz, $CDCl_3$): δ 210.0, 153.1, 145.0, 136.4, 134.9. 127.5, 127.4, 126.7, 124.6, 55.9, 40.9, 33.0, 31.1, 28.5, 27.4, 26.9, 22.7; IR (film): 2920, 2947, 1710, 1607, 1463, 1440, 1750 cm^{-1}; HRMS–APCI (m/z) $[M + H]^+$ calcd for $C_{17}H_{21}O^+$, 241.15869; found 241.15748.

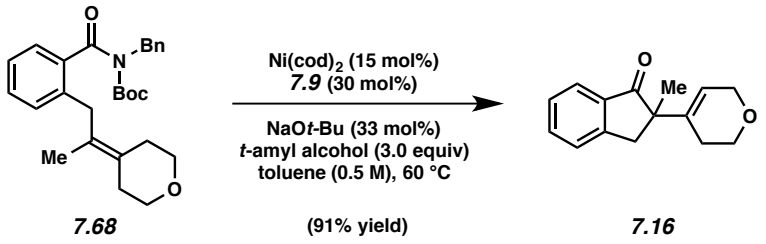

Indanone 7.16 (Table 7.2). Purification by preparative thin-layer chromatography (2:1 Hexanes:EtOAc) afforded indanone **7.16** (91% yield, average of two experiments) as a colorless oil. Indanone **7.16**: R_f 0.34 (3:1 Hexanes:EtOAc); ^{1}H NMR (400 MHz, $CDCl_3$): δ 7.77 (d, J = 7.8, 1H), 7.61 (td, J = 7.6, 1.3, 1H), 7.45 (dt, J = 7.8, 1.0, 1H), 7.39 (t, J = 7.6, 1H), 5.65 (app sext, J = 1.4, 1H), 4.19 (app tquint, J = 16.4, 2.6, 2H), 3.73 (td, J = 5.0, 1.1, 2H), 3.34 (d, J =

17.3, 1H), 2.95 (d, J = 17.3, 1H), 2.12 (m, 1H), 1.86 (m, 1H), 1.37 (s, 3H); ^{13}C NMR (125 MHz, $CDCl_3$): δ 209.0, 152.8, 136.4, 136.0, 135.2, 127.8, 126.6, 124.7, 121.4, 65.9, 64.3, 54.0, 41.0, 25.6, 22.1; IR (film): 2961, 2927, 2850, 1709, 1606, 1464, 1277, 1127 cm^{-1}; HRMS–APCI (m/z) $[M + H]^+$ calcd for $C_{15}H_{17}O_2^+$, 229.12231; found 229.12094.

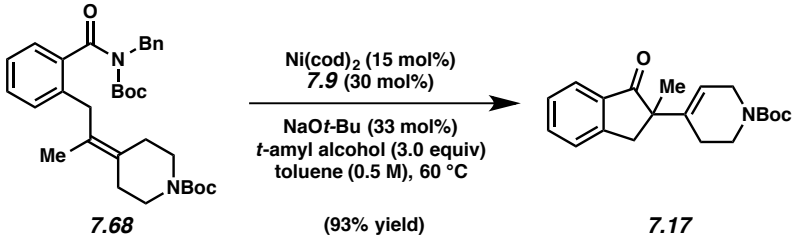

7.68 (93% yield) *7.17*

Indanone 7.17 (Table 7.2). Purification by preparative thin-layer chromatography (2:1 Hexanes:EtOAc) afforded indanone **7.17** (93% yield, average of two experiments) as a colorless oil. Indanone **7.17**: R_f 0.37 (3:1 Hexanes:EtOAc); ^{1}H NMR (400 MHz, $CDCl_3$): δ 7.77 (d J = 7.6, 1H) 7.61 (td, J = 7.6, 1.1, 1H), 7.45 (d, J = 7.7, 1H), 7.39 (t, J = 7.7, 1H), 5.61 (br s, 1H), 3.93 (s, 2H), 3.43 (t, J = 4.7, 2H), 3.30 (d, J = 17.4, 1H), 2.95 (d, J = 17.4, 1H), 2.06 (m, 1H), 1.87 (m, 1H), 1.45 (s, 9H), 1.36 (s, 3H); ^{13}C NMR (125 MHz, $CDCl_3$): δ 209.1, 154.9, 152.7, 137.5, 135.9, 135.2, 127.8, 126.6, 124.7, 119.6, 79.7, 54.1, 43.5, 41.0, 39.7, 28.6, 25.7, 22.3; IR (film): 2975, 2931, 1695, 1419, 1365, 1241, 1171 cm^{-1}; HRMS–ESI (m/z) $[M + Na]^+$ calcd for $C_{20}H_{25}NNaO_3^+$, 350.1732; found 350.1736.

*Note: The data for indanone **7.17** represents empirically observed chemical shifts from the ^{13}C NMR spectrum, presumably due to the nitrogen-containing heterocycle.*

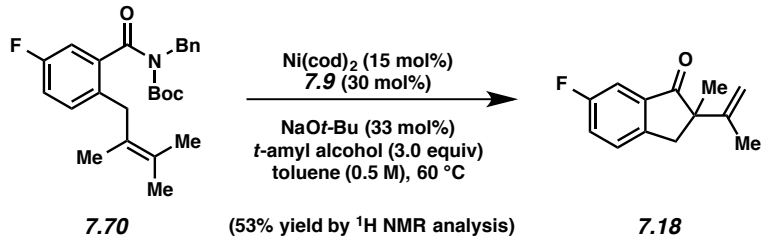

7.70 (53% yield by ^{1}H NMR analysis) *7.18*

Indanone 7.18 (Figure 7.2). ^{1}H NMR analysis of the crude reaction mixture indicated a 53% yield (average of two experiments) of ketone **7.18** relative to a hexamethylbenzene external standard. Purification by preparative thin-layer chromatography (97:3 Benzene: CH_3CN) afforded an analytical sample of **7.18** as an off-white oil. Diminished isolated yields (i.e. <50%) for **7.18** were observed and can be attributed to the volatility of the neat compound. Indanone **7.18**: R_f 0.59 (3:1 Hexanes:EtOAc); ^{1}H NMR (500 MHz, $CDCl_3$): δ 7.44–7.39 (m, 2H), 7.32 (td, J = 8.6, 2.4, 1H), 4.94 (m, 2H), 3.29 (d, J = 17.8, 1H), 2.91 (d, J = 17.8, 1H), 1.65 (q, J = 0.7, 3H), 1.38 (s, 3H); ^{13}C NMR (125 MHz, $CDCl_3$): δ 208.3 (d, J = 2.6), 162.5 (d, J = 248), 148.1 (d, J = 2.1), 145.6, 137.7 (d, J = 7.0), 128.0 (d, J = 7.9), 122.8 (d, J = 24), 112.4, 110.4 (d, J = 22), 55.7, 40.8, 22.7, 20.0; ^{19}F NMR (376 MHz, $CDCl_3$): δ –114.3 (s, 1F); IR (film): 2970, 2929, 1712, 1484, 1447, 1263 cm^{-1}; HRMS–APCI (m/z) $[M + H]^+$ calcd for $C_{13}H_{14}FO^+$, 205.10232; found 205.10239.

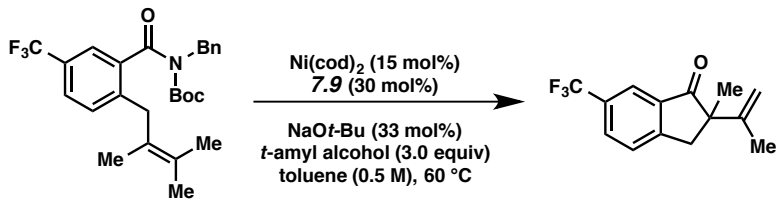

7.71 (74% yield) *7.19*

Indanone 7.19 (Figure 7.2). Purification by preparative thin-layer chromatography (4:1 Hexanes:EtOAc) afforded indanone **7.19** (74% yield, average of two experiments) as a yellow oil. Indanone **7.19**: R_f 0.69 (3:1 Hexanes:EtOAc); ^{1}H NMR (500 MHz, $CDCl_3$): δ 8.05 (s, 1H),

7.32 (dd, J = 7.9, 1.3, 1H), 7.59 (d, J = 7.9, 1H), 4.97 (quint, J = 1.1, 1H), 4.95 (s, 1H), 3.40 (d, J = 18.0, 1H), 3.02 (d, J = 18.0, 1H), 1.67 (q, J = 0.7, 3H), 1.40 (s, 3H); ^{13}C NMR (125 MHz, $CDCl_3$): δ 207.9, 156.0, 145.2, 136.4, 131.5 (q, J = 3.5), 130.6 (q, J = 33), 127.3, 123.9 (q, J = 273), 122.0 (d, J = 3.9), 112.8, 55.2, 41.4, 22.7, 20.0; ^{19}F NMR (376 MHz, $CDCl_3$): δ –62.5 (s, 3F); IR (film): 2972, 2936, 1722, 1625, 1332, 1257, 1184, 1128 cm^{-1}; HRMS–APCI (m/z) [M + H]$^+$ calcd for $C_{14}H_{14}F_3O^+$, 255.09913; found 255.09744.

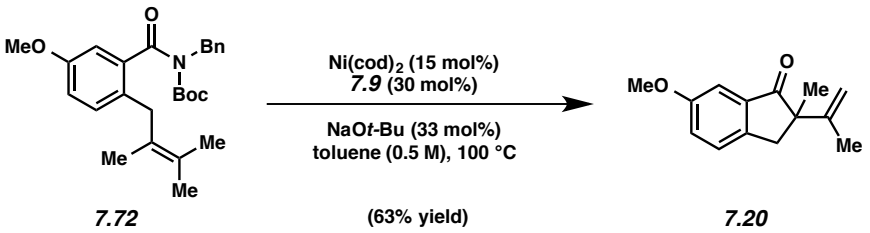

Indanone 7.20 (Figure 7.2). Purification by preparative thin-layer chromatography (99:1 Benzene:CH_3CN) afforded indanone **7.20** (63% yield, average of two experiments) as a white crystalline solid. Indanone **7.20**: mp: 41–43 ºC; R_f 0.32 (10:1 Hexanes:EtOAc); ^{1}H NMR (500 MHz, $CDCl_3$): δ 7.33 (d, J = 8.0, 1H), 7.23–7.18 (m, 2H), 4.95 (m, 2H), 3.84 (s, 3H), 3.24 (d, J = 17.4, 1H), 2.87 (d, J = 17.4, 1H), 1.64 (s, 3H), 1.37 (s, 3H); ^{13}C NMR (125 MHz, $CDCl_3$): δ 209.2, 159.5, 145.9, 145.5, 137.0, 127.2, 124.5, 112.0, 105.5, 55.6, 40.6, 22.7, 19.8; IR (film): 2964, 1707, 1275, 1280, 894 cm^{-1}; HRMS–APCI (m/z) [M + H]$^+$ calcd for $C_{14}H_{17}O_2^+$, 217.12231; found 217.12123.

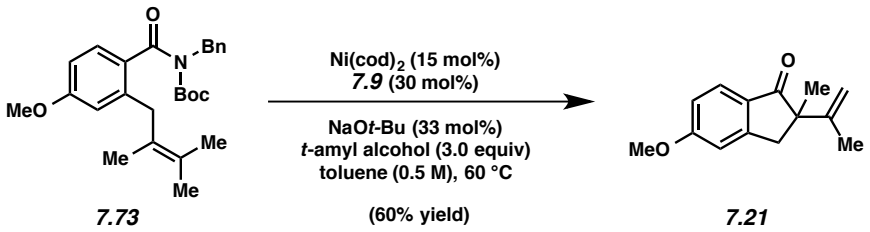

7.73 (60% yield) *7.21*

Indanone 7.21 (Figure 7.2). Purification by preparative thin-layer chromatography (9:1 Hexanes:Et_3N) afforded indanone **7.21** (60% yield, average of two experiments). Spectral data match those previously reported.[11b]

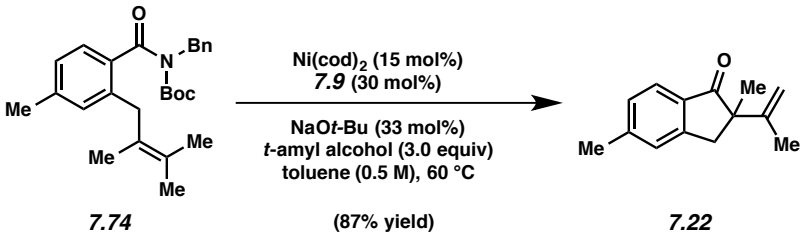

7.74 (87% yield) *7.22*

Indanone 7.22 (Figure 7.2). Purification by preparative thin-layer chromatography (9:1 Hexanes:EtOAc) afforded indanone **7.22** (87% yield, average of two experiments) as a colorless oil. Indanone **7.22**: R_f 0.43 (9:1 Hexanes:EtOAc); ^{1}H NMR (500 MHz, $CDCl_3$): δ 7.67 (d, J = 7.8, 1H), 7.25–7.23 (m, 1H), 7.20–7.18 (m, 1H), 4.95–4.93 (m, 2H), 3.27 (d, J = 17.6, 1H), 2.89 (d, J = 17.4, 1H), 2.44 (s, 3H), 1.63 (s, 3H), 1.36 (s, 3H); ^{13}C NMR (125 MHz, $CDCl_3$): δ 208.8, 153.3, 146.3, 146.1, 133.7, 128.9, 126.9, 124.5, 112.0, 54.7, 41.2, 22.8, 22.2, 19.9; IR (film): 2965, 1705, 1608, 1322, 585 cm^{-1}; HRMS–APCI (m/z) $[M + H]^+$ calcd for $C_{14}H_{17}O^+$, 201.12739; found 201.12719.

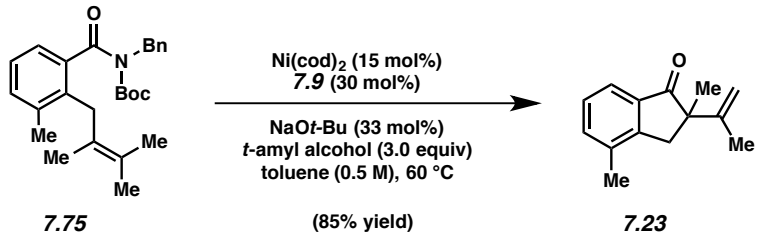

Indanone 7.23 (Figure 7.2). Purification by preparative thin-layer chromatography (9:1 Hexanes:EtOAc) afforded indanone **7.23** (85% yield, average of two experiments) as a colorless oil. Indanone **7.23**: R_f 0.38 (10:1 Hexanes:EtOAc); ^{1}H NMR (500 MHz, $CDCl_3$): δ 7.63 (d, J = 7.4, 1H), 7.43 (d, J = 7.4, 1H), 7.31 (t, J = 7.4, 1H), 4.97–4.94 (m, 2H), 3.21 (d, J = 17.5, 1H), 2.84 (d, J = 17.4, 1H), 2.35 (s, 3H), 1.65 (s, 3H), 1.39 (s, 3H); ^{13}C NMR (125 MHz, $CDCl_3$): δ 209.5, 151.6, 146.0, 135.67, 135.66, 135.4, 127.8, 122.0, 112.0, 54.5, 40.3, 22.8, 19.9, 17.8; IR (film): 2966, 1708, 1591, 1268, 893 cm^{-1}; HRMS–APCI (m/z) $[M + H]^+$ calcd for $C_{14}H_{17}O^+$, 201.12739; found 201.12701.

7.5.2.4 Diastereoselective Heck Cyclization

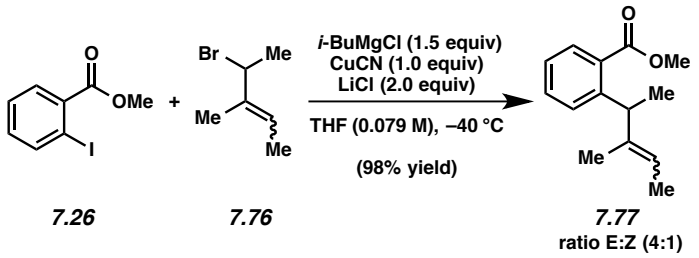

Ester 7.77. Following a modification of the general procedure reported by Querolle and co-workers,[29] a flask containing a stir bar was charged CuCN (680 mg, 7.50 mmol, 1.0 equiv) and LiCl (650 mg, 15.0 mmol, 2.0 equiv) in the glovebox. The flask was removed from the glovebox, and the solids were suspended in THF (25 mL). The resulting mixture was stirred vigorously until a completely dissolved solution of CuCN•2LiCl was formed. In a separate flask containing a solution of methyl-2-iodobenzoate (**7.26**) (1.97 g, 7.50 mmol, 1.0 equiv) in THF (70 mL) at –

40 °C was added *i*-BuMgCl (5.60 mL of a 2.0 M solution in THF, 11.3 mmol, 1.5 equiv) dropwise over 1 min at –40 °C. After this mixture was stirred at –40 °C for 1 h, the solution of CuCN•2LiCl was added via cannula. The combined mixture was stirred at –40 °C for an additional 15 min, at which point known bromide **7.76**[36] (2.43 g, 15.0 mmol, 2.0 equiv) was added dropwise over 1 min. After stirring at –40 °C for an additional hour, the reaction was poured into 9:1 sat. aq. NH_4Cl:NH_4OH (100 mL). The layers were separated and the aqueous layer was extracted with EtOAc (3 x 75 mL). The organic layers were combined, dried over $MgSO_4$, and concentrated under reduced pressure. The crude mixture was purified via flash chromatography (97:3 Hexanes:EtOAc) to afford ester **7.77** (1.61 g, 98% yield) as an inseparable mixture of olefin isomers and as a colorless oil (4:1 mixture of alkene isomers). Configurational isomers of ester **7.77** were analyzed as a mixture. **7.77** (**Major (*E*)-isomer**): ^{1}H NMR (500 MHz, $CDCl_3$): δ 7.71 (dd, *J* = 7.7, 1.5, 1H), 7.40 (dt, *J* = 7.8, 1.6, 1H), 7.30 (dd, *J* = 8.0, 1.24, 1H), 7.22 (dt, *J* = 7.7, 1.6, 1H), 5.38 (tq, *J* = 6.7, 1.6, 1H), 4.23 (q, *J* = 7.1, 1H), 3.88 (s, 3H), 1.63 (dt, *J* = 6.8, 1.2, 3H), 1.45 (br s, 3H), 1.33 (d, *J* = 7.0, 3H); **7.77** (**Minor (*Z*)-isomer**): δ 7.60 (dd, *J* = 7.8, 1.3, 1H), 7.45–7.38 (m, 2H), 7.23 (dt, *J* = 7.6, 1.7, 1H), 5.25 (tq, *J* = 6.9, 0.8, 1H), 4.78 (q, *J* = 7.2, 1H), 3.84 (s, 3H), 1.61 (q, *J* = 1.5, 3H), 1.40 (quint, *J* = 1.5, 3H), 1.35 (d, *J* = 7.3, 3H); Ester **7.77** (**mixture**): R_f 0.55 (9:1 Hexanes:EtOAc); ^{13}C NMR (125 MHz, $CDCl_3$): (27 of 28 signals observed) δ 169.4, 169.1, 146.9, 145.1, 139.3, 138.9, 131.7, 131.6, 131.1, 130.9, 129.8, 129.4, 127.8, 127.6, 125.8, 120.3, 118.3, 52.3, 52.1, 42.7, 35.3, 20.3, 20.2, 18.3, 16.0, 13.6, 13.3; IR (film): 2968, 1721, 1601, 1576, 1485, 1446, 1371 cm^{-1}; HRMS–APCI (m/z) $[M + H]^+$ calcd for $C_{14}H_{19}O_2^+$, 219.13796; found 219.13794.

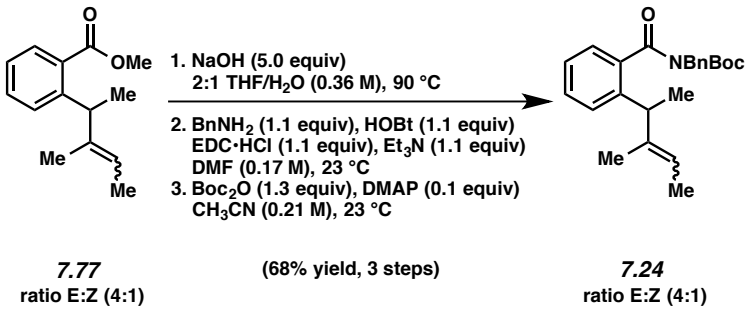

Imide 7.24. To a solution of ester **7.77** (1.61 g, 7.40 mmol, 1.0 equiv) in THF (35 mL) was added a solution of NaOH (1.48 g, 37.0 mmol, 5.0 equiv) in H_2O (35 mL). The reaction was heated to 90 °C and stirred for 12 h. After cooling to room temperature, the reaction mixture was poured into deionized water (25 mL) and diluted with EtOAc (25 mL). The layers were separated and the aqueous layer was acidified to pH ~2 with 1 N HCl (100 mL) and extracted with EtOAc (3 x 50 mL). The organic layers were combined, washed with deionized water (300 mL), dried over $MgSO_4$, and concentrated under reduced pressure to afford the corresponding carboxylic acid, which was used in the subsequent step without further purification.

To a solution of the crude carboxylic acid, HOBt (1.08 g, 7.80 mmol, 1.1 equiv from **7.77**), and EDC•HCl (1.53 g, 7.80 mmol, 1.1 equiv from **7.77**) in DMF (40 mL) was added $BnNH_2$ (0.90 mL, 7.80 mmol, 1.1 equiv from **7.77**) and Et_3N (1.17 mL, 7.80 mmol, 1.1 equiv from **7.77**). After stirring for 15 h, the reaction mixture was poured into deionized water (300 mL) and diluted with EtOAc (50 mL). The layers were separated and the aqueous layer was extracted with EtOAc (3 x 50 mL). The organic layers were combined, washed with deionized water (100 mL), dried over $MgSO_4$, and concentrated under reduced pressure to afford the corresponding amide, which was used in the subsequent step without further purification.

To a solution of the crude amide in CH_3CN (45 mL) was added DMAP (82 mg, 0.65 mmol, 0.1 equiv from **7.77**) and Boc_2O (1.85 g, 8.50 mmol, 1.3 equiv from **7.77**). After stirring for 15 h, the reaction mixture was concentrated under reduced pressure and purified by flash

chromatography (99:1 Hexanes:EtOAc) to yield imide **7.24** (1.97 g, 68% yield, three steps) as an inseparable mixture of olefin isomers and as a colorless oil (4:1 mixture of alkene isomers). Configurational isomers of imide **7.24** were analyzed as a mixture **7.24** (**Major (*E*)-isomer**): ^{1}H NMR (500 MHz, $CDCl_3$): δ 7.43 (d, *J* = 7.5, 2H), 7.37–7.31 (m, 3H), 7.29–7.22 (m, 2H), 7.16 (dt, *J* = 7.7, 1.4, 1H), 7.12–7.08 (m, 1H), 5.36 (tq, *J* = 6.8, 1.3, 1H), 5.06 (s, 2H), 3.67 (q, *J* = 6.9, 1H), 1.60 (d, *J* = 6.7, 3H), 1.48 (s, 3H), 1.30 (d, *J* = 7.0, 3H), 1.13 (s, 9H); **7.24** (**Minor (*Z*)-isomer**) δ 7.45–7.37 (m, 2H), 7.37–7.31 (m, 3H), 7.29–7.22 (m, 2H), 7.18 (dt, *J* = 7.5, 1.3, 1H), 7.12–7.08 (m, 1H), 5.22 (br s, 1H), 4.99 (br s, 2H), 4.34 (br s, 1H), 1.57 (d, *J* = 6.9, 3H), 1.53 (t, *J* = 1.4, 3H), 1.34 (d, *J* = 7.2, 3H), 1.11 (s, 9H); Imide **7.24** (**mixture**): R_f 0.52 (9:1 Hexanes:EtOAc); ^{13}C NMR (125 MHz, $CDCl_3$): δ 172.4, 152.8, 142.8, 141.3, 138.9, 138.6, 138.1, 138.04, 138.02, 129.4, 129.0, 128.5, 128.3, 127.5, 127.4, 126.3, 126.2, 125.4, 120.0, 118.6, 83.5, 48.0, 43.2, 27.7, 27.6, 20.2, 18.7, 15.5, 13.5, 13.3; IR (film): 2973, 1728, 1670, 1456, 1369, 1335, 1228 cm^{-1}; HRMS–APCI (m/z) $[M + H]^+$ calcd for $C_{25}H_{32}NO_3^+$, 394.23767; found 394.23814.

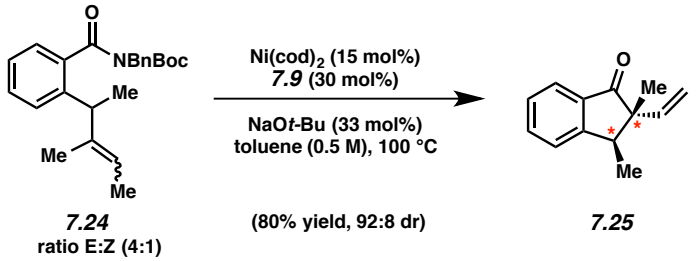

Indanone 7.25 (Figure 7.3). Following the representative procedure described in 7.5.2.1.3, purification by preparative thin-layer chromatography (98:2 Benzene:CH_3CN) afforded indanone **7.25** (80% yield, 92:8 dr, average of two experiments) as a colorless oil. Indanone **7.25**: R_f 0.48 (9:1 Hexane:EtOAc); ^{1}H NMR (500 MHz, $CDCl_3$): δ 7.75 (d, *J* = 7.7, 1H), 7.62 (dt, *J* = 7.7, 1.2,

1H), 7.49 (dd, *J* = 7.8, 0.9, 1H), 7.38 (tt, *J* = 7.5, 0.9, 1H), 5.94 (dd, *J* = 17.4, 10.6, 1H), 5.23–5.15 (m, 2H), 3.40 (q, *J* = 7.5, 1H), 1.32 (d, *J* = 7.4, 3H), 1.19 (s, 3H); ^{13}C NMR (125 MHz, $CDCl_3$): δ 208.4, 157.2, 141.0, 135.1, 134.5, 127.8, 125.1, 124.5, 114.6, 56.2, 43.1, 18.5, 15.1; IR (film): 2972, 1712, 1606, 1466, 1328, 1285, 1226 cm^{-1}; HRMS–APCI (m/z) $[M + H]^+$ calcd for $C_{13}H_{15}O^+$, 187.11174; found 187.11180.

*The stereochemistry of indanone **7.25** was verified by NOESY (500 MHz, $CDCl_3$), as the following correlation was observed:*

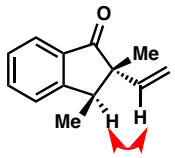

7.25

7.6 Spectra Relevant to Chapter Seven:

Mizoroki–Heck Cyclizations of Amide Derivatives for the Introduction of Quaternary Centers

Jose M. Medina, Jesus Moreno, Sophie Racine, Shuaijing Du, and Neil K. Garg

Angew. Chem., Int. Ed. [Online early access]. DOI: 10.1002/anie.201703174R1.

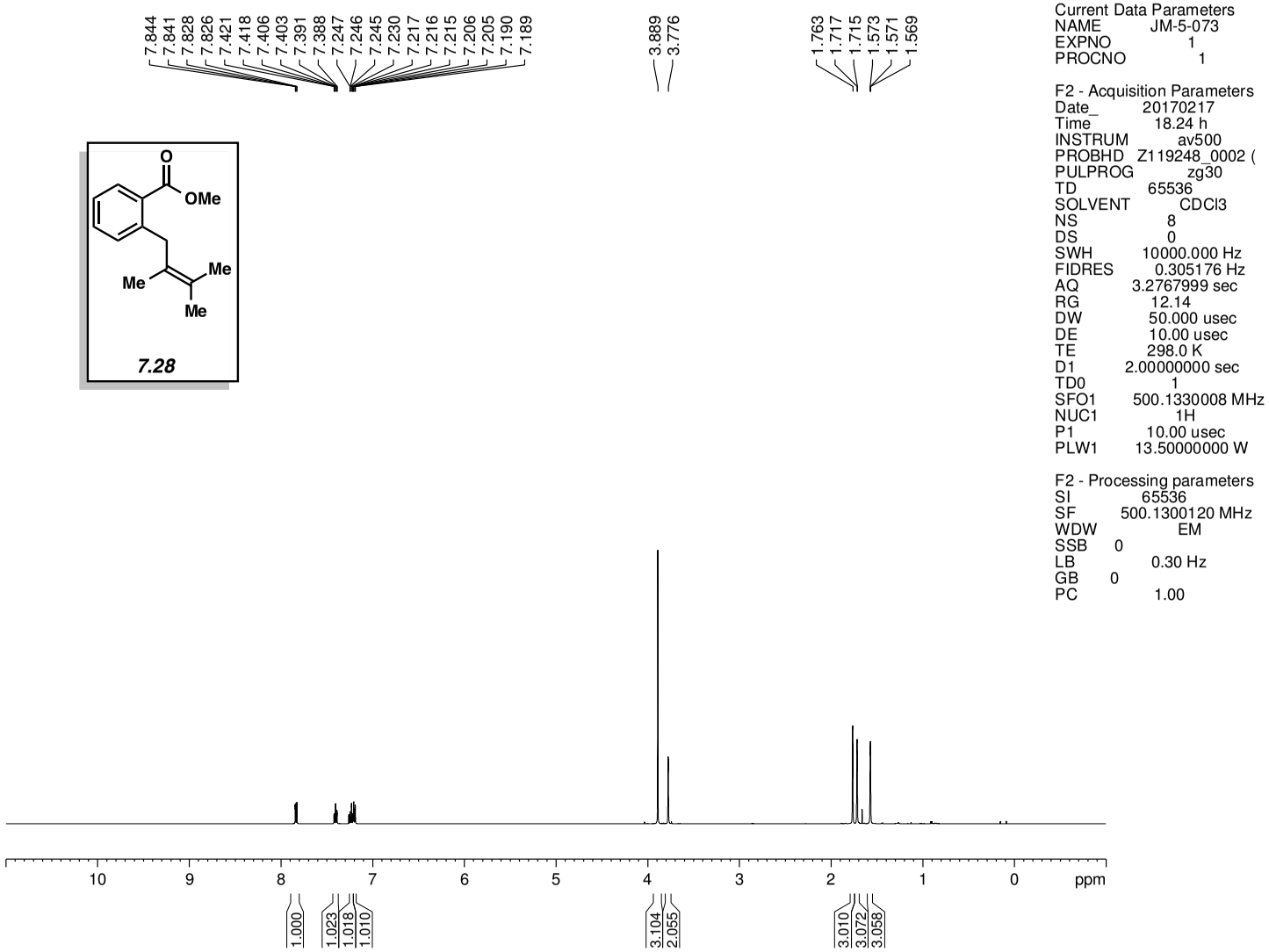

Figure 7.4 ^{1}H NMR (500 MHz, $CDCl_3$) of compound **7.28**

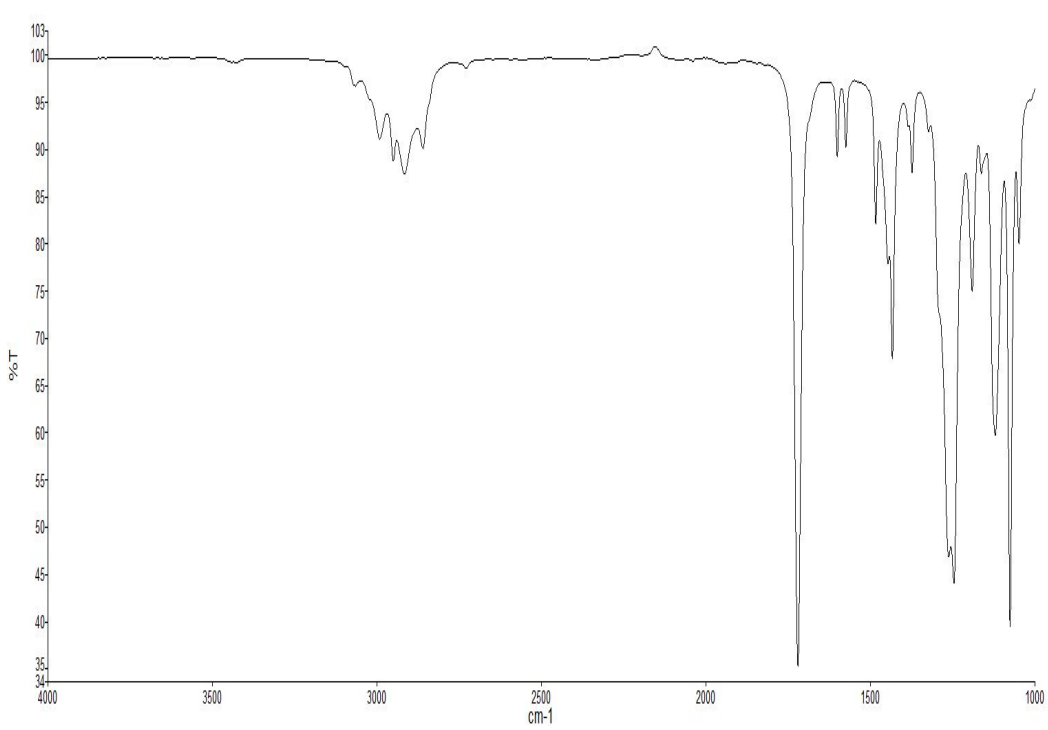

Figure 7.5 Infrared spectrum of compound **7.28**

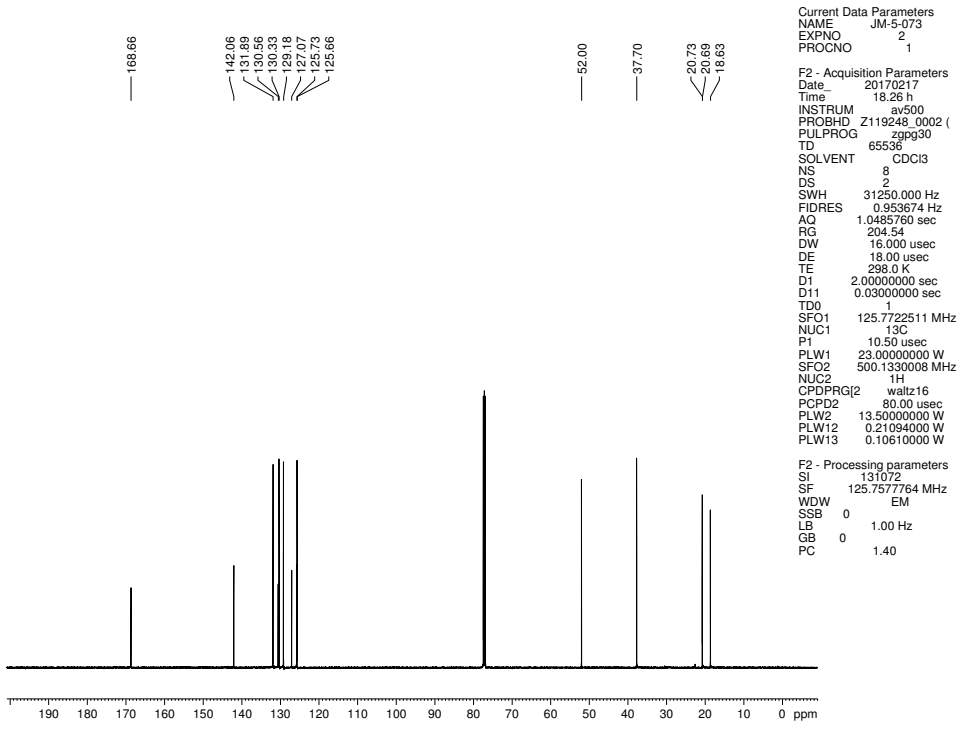

Figure 7.6 ^{13}C NMR (125 MHz, $CDCl_3$) of compound **7.28**

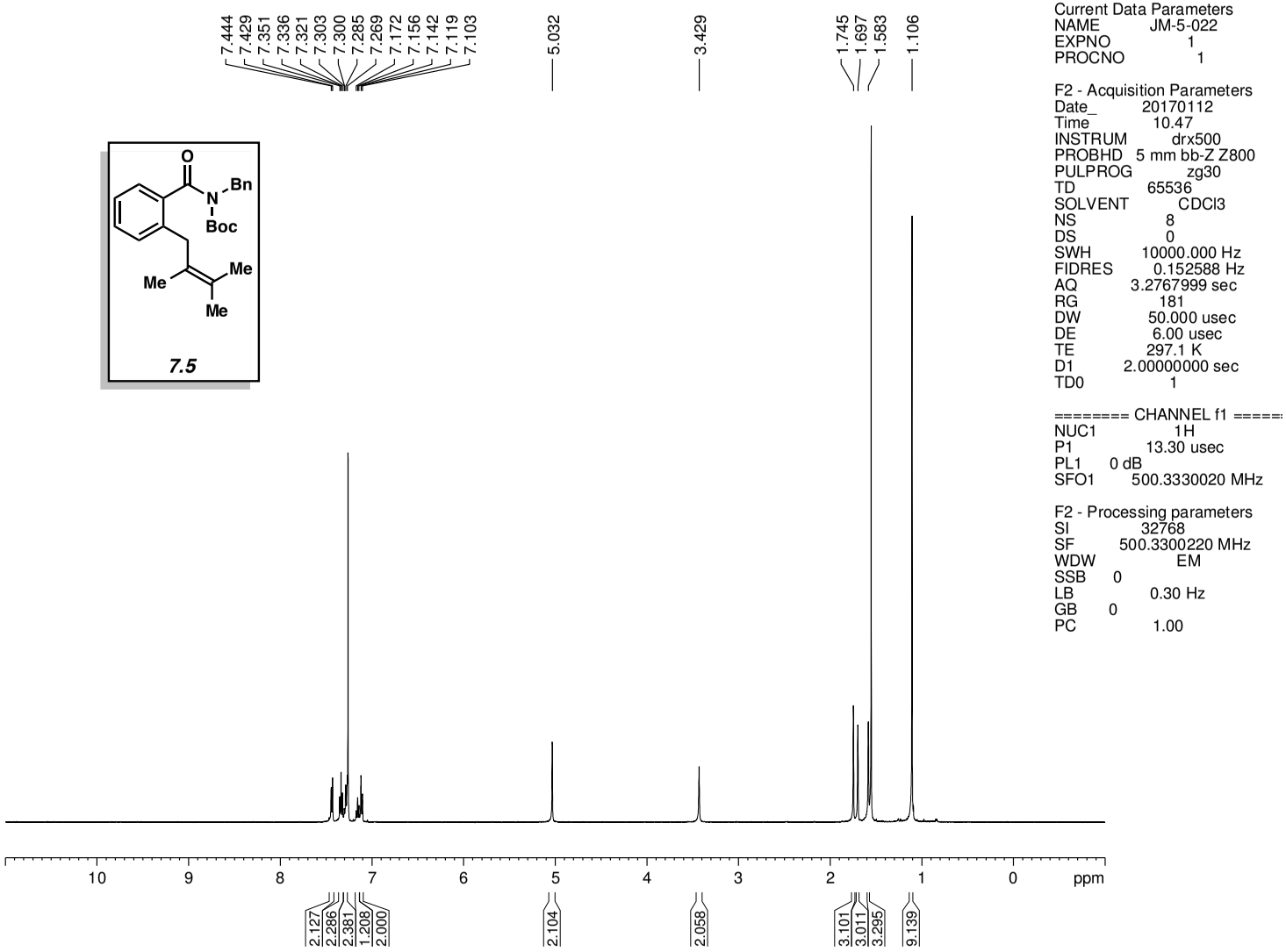

Figure 7.7 ^{1}H NMR (500 MHz, $CDCl_3$) of compound **7.5**

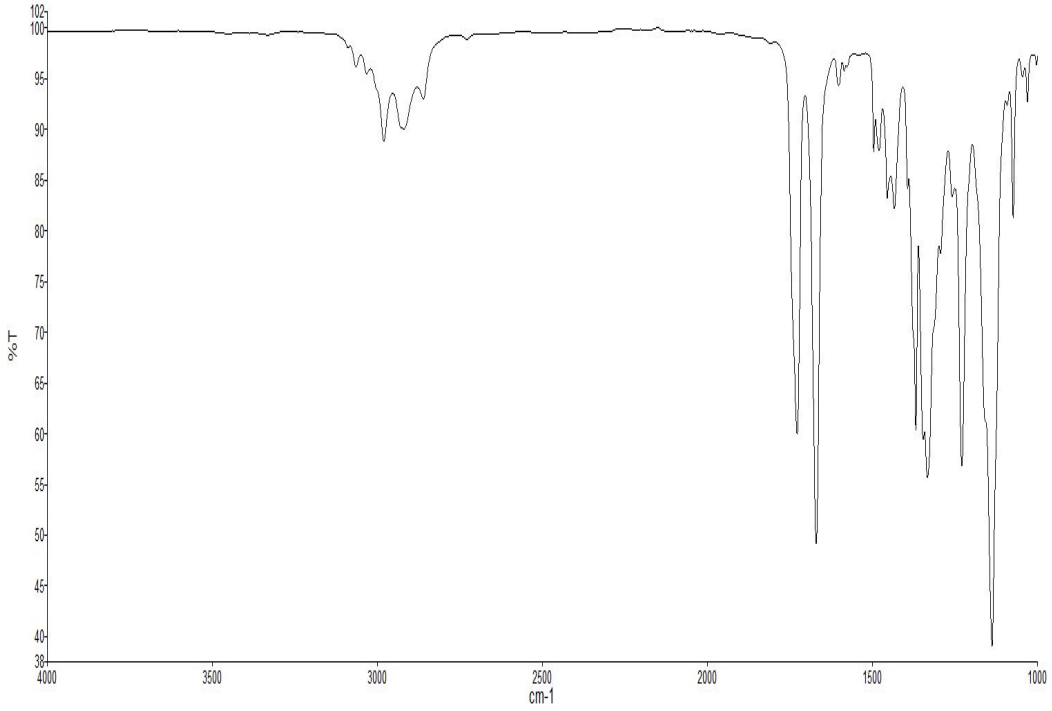

Figure 7.8 Infrared spectrum of compound **7.5**

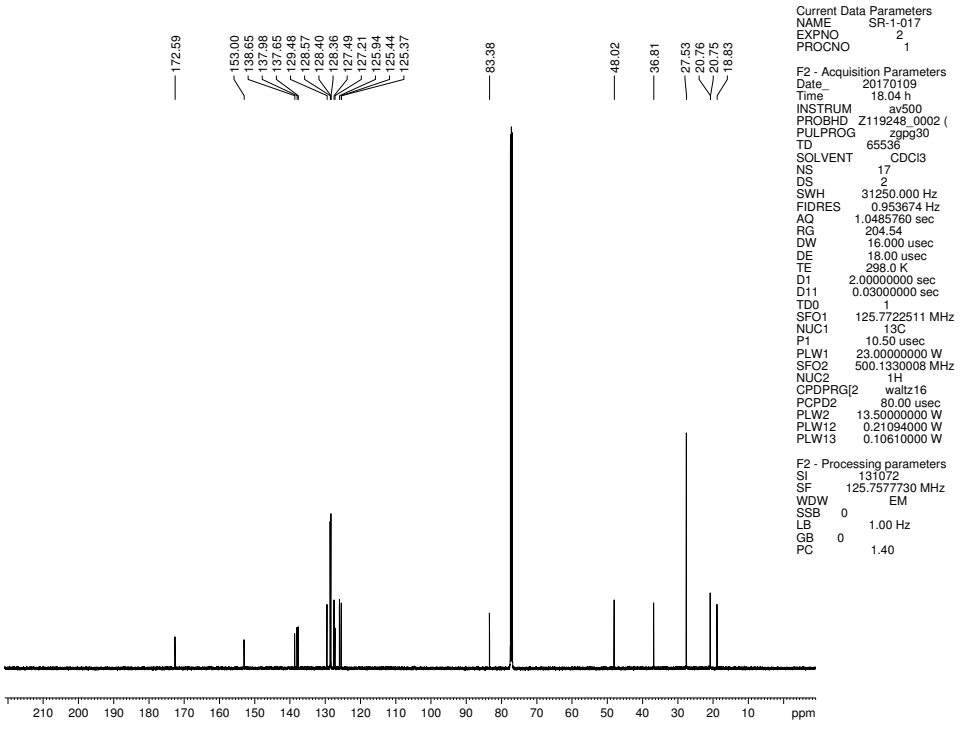

Figure 7.9 ^{13}C NMR (125 MHz, $CDCl_3$) of compound **7.5**

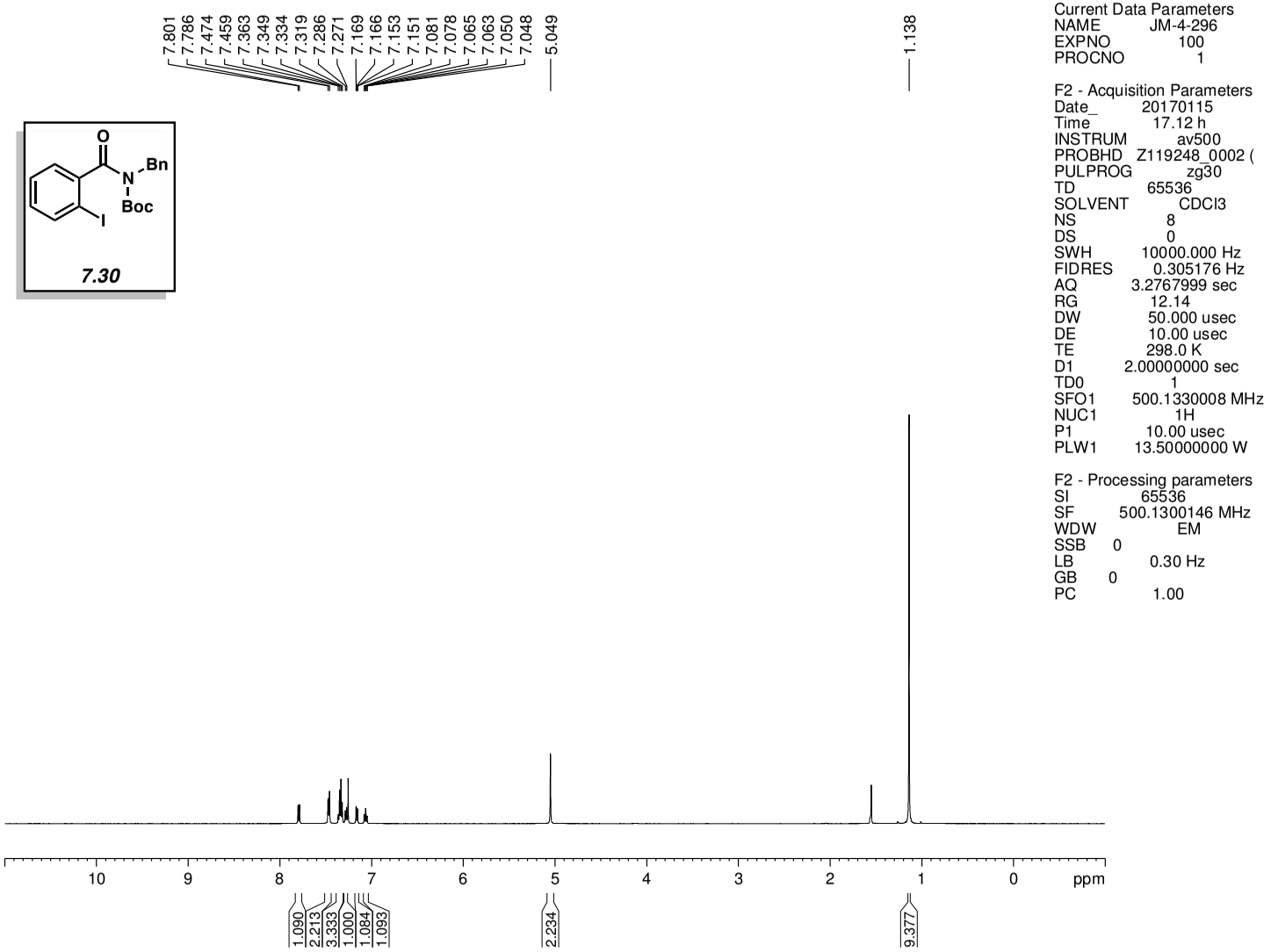

Figure 7.10 ^{1}H NMR (500 MHz, $CDCl_3$) of compound **7.30**

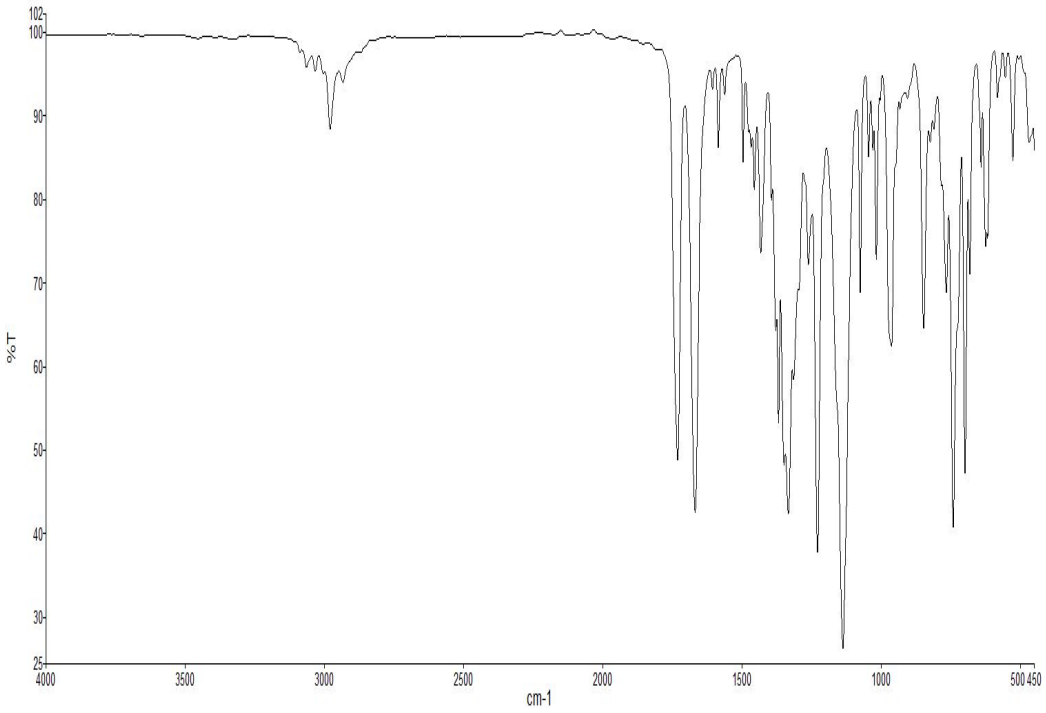

Figure 7.11 Infrared spectrum of compound **7.30**

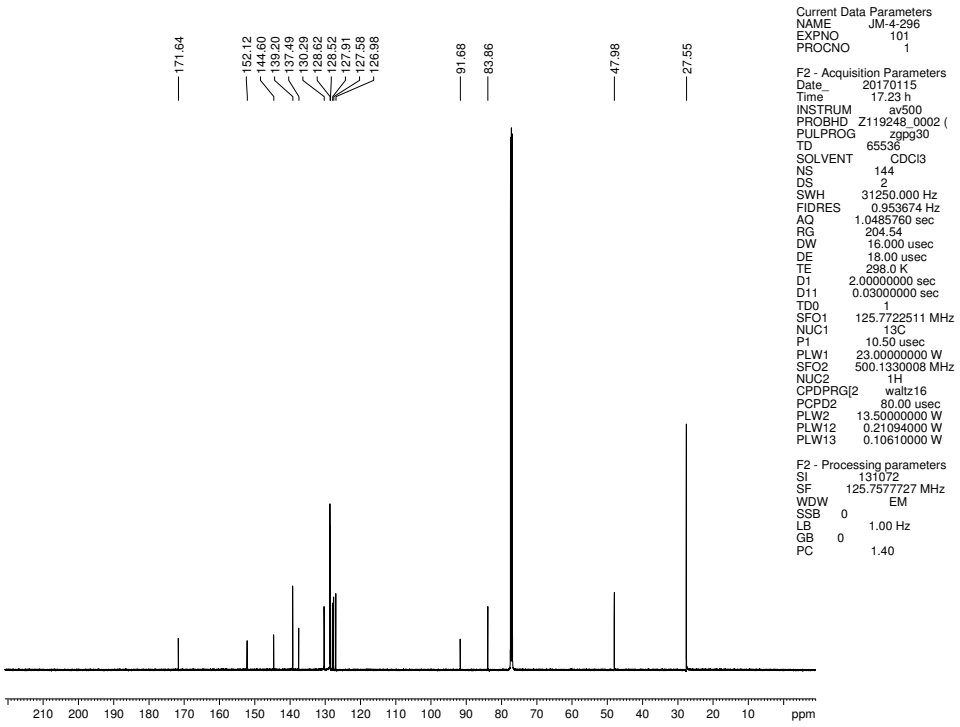

Figure 7.12 ^{13}C NMR (125 MHz, $CDCl_3$) of compound **7.30**

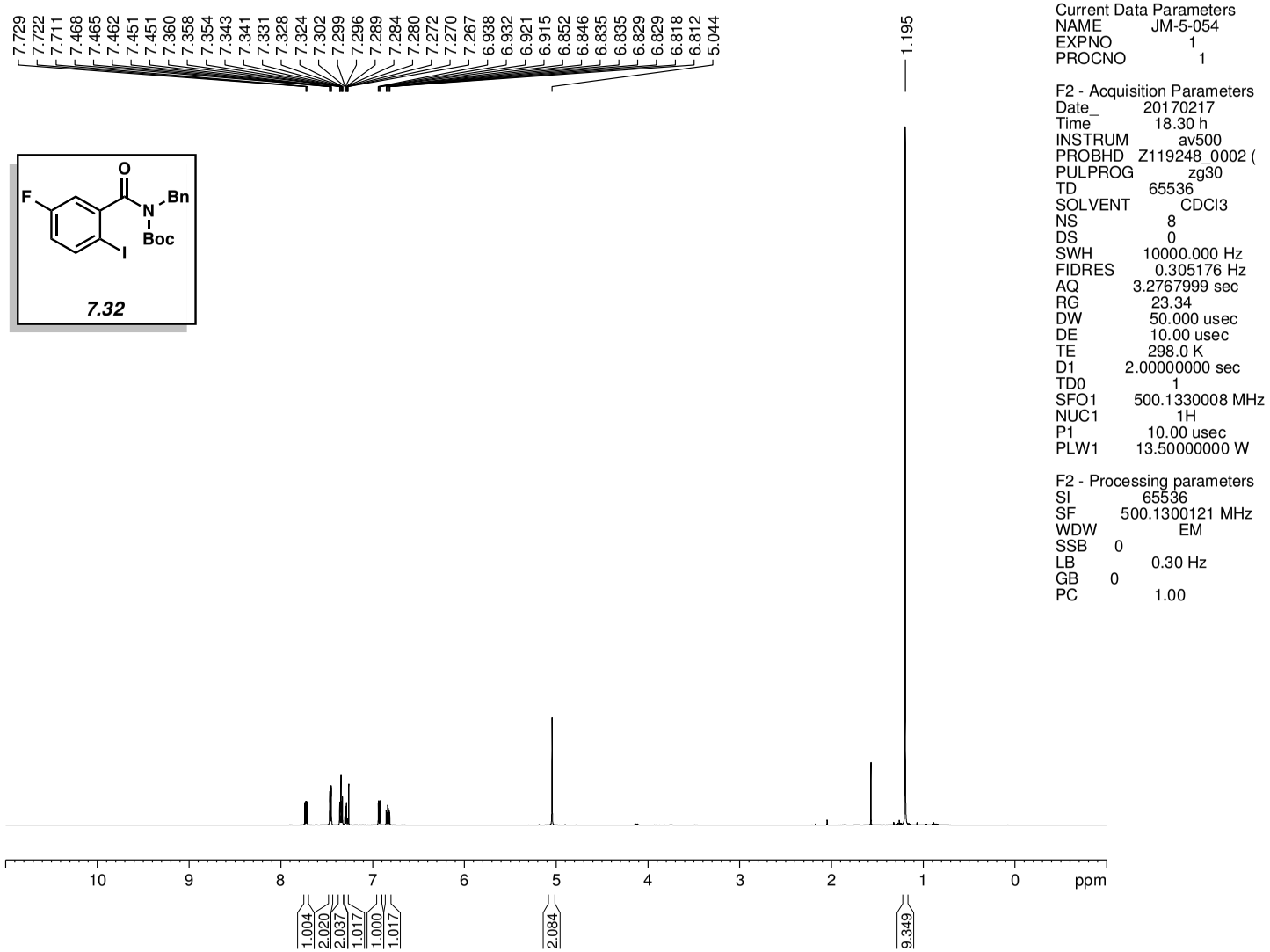

Figure 7.13 ^{1}H NMR (500 MHz, $CDCl_3$) of compound **7.32**

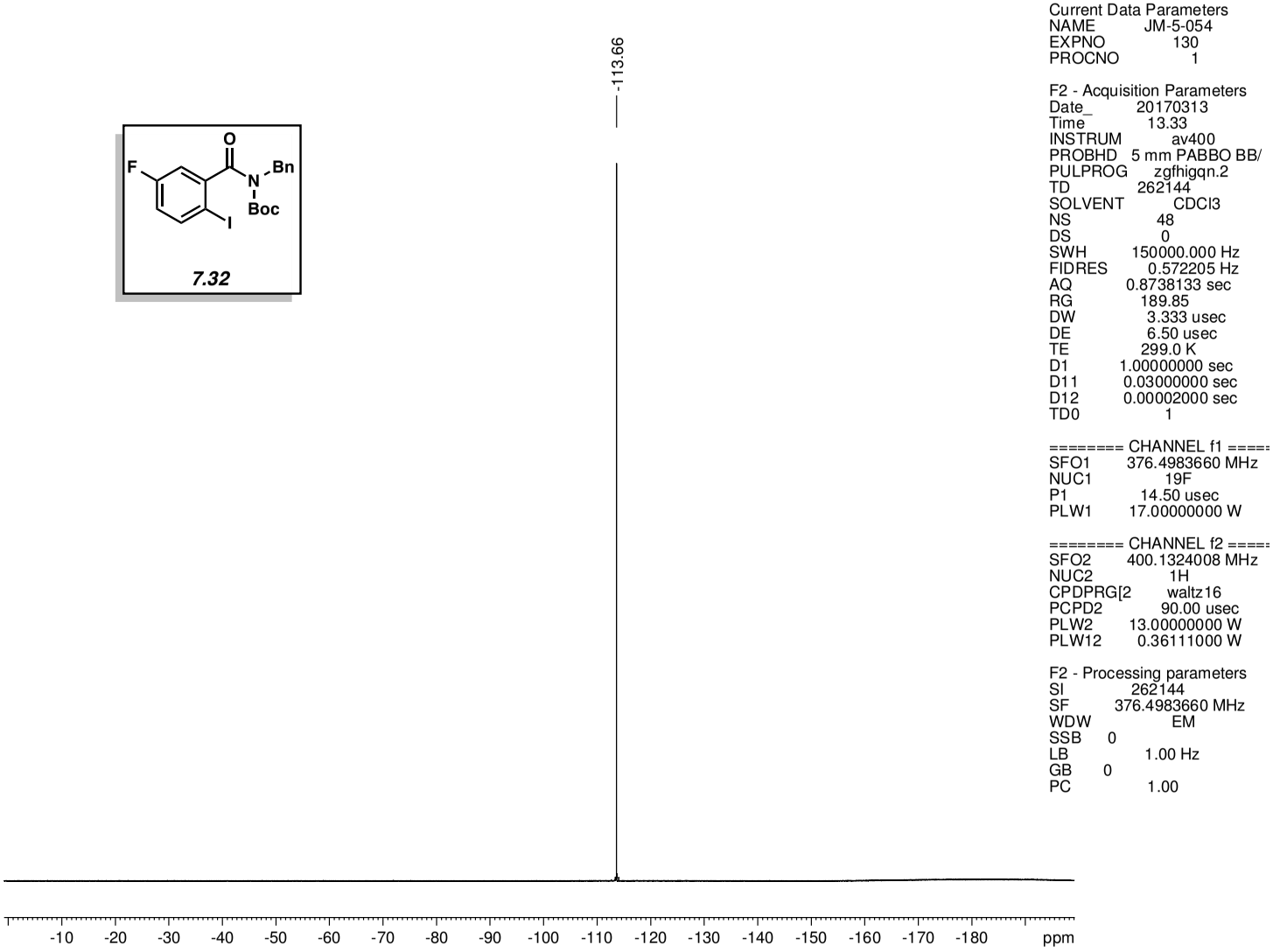

Figure 7.14 ^{19}F NMR (376 MHz, $CDCl_3$) of compound **7.32**

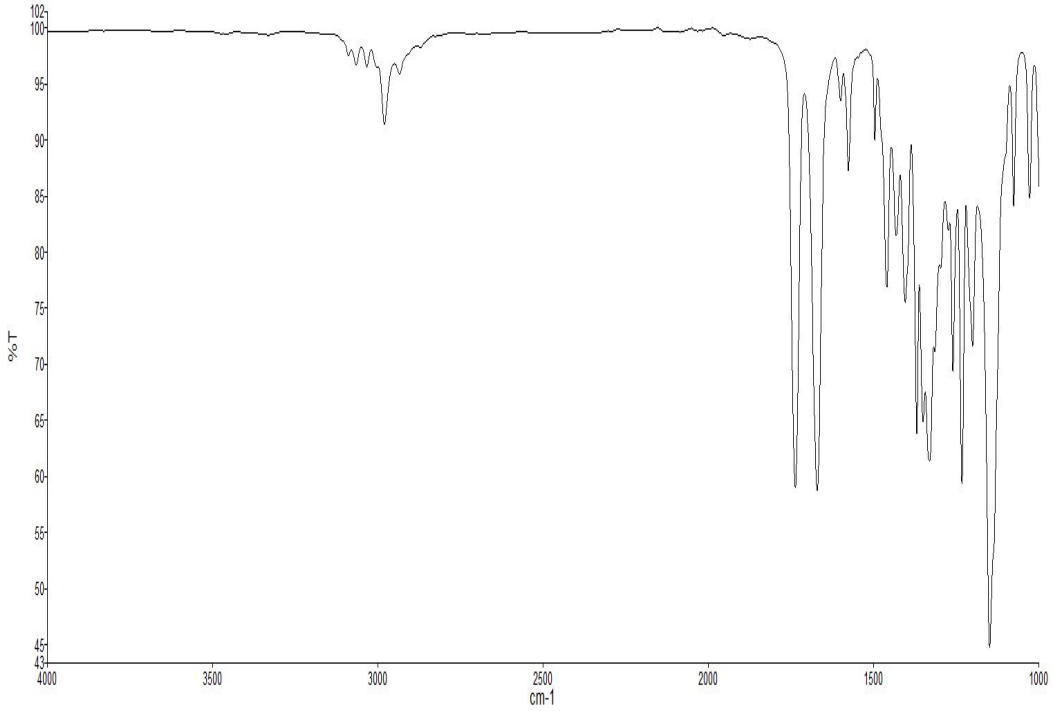

Figure 7.15 Infrared spectrum of compound **7.32**

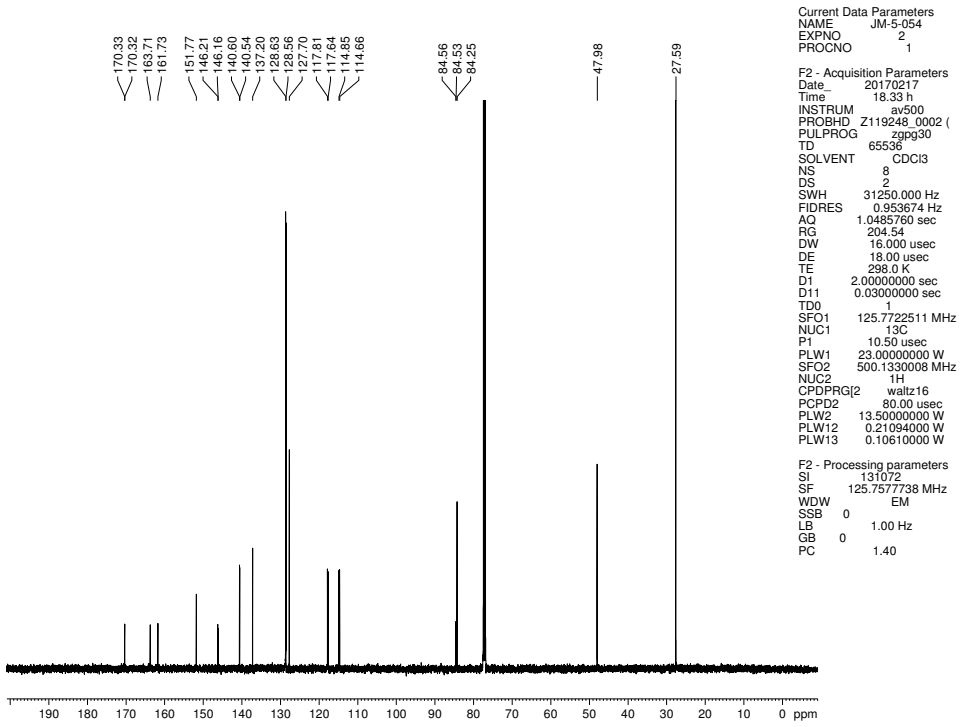

Figure 7.16 ^{13}C NMR (125 MHz, $CDCl_3$) of compound **7.32**

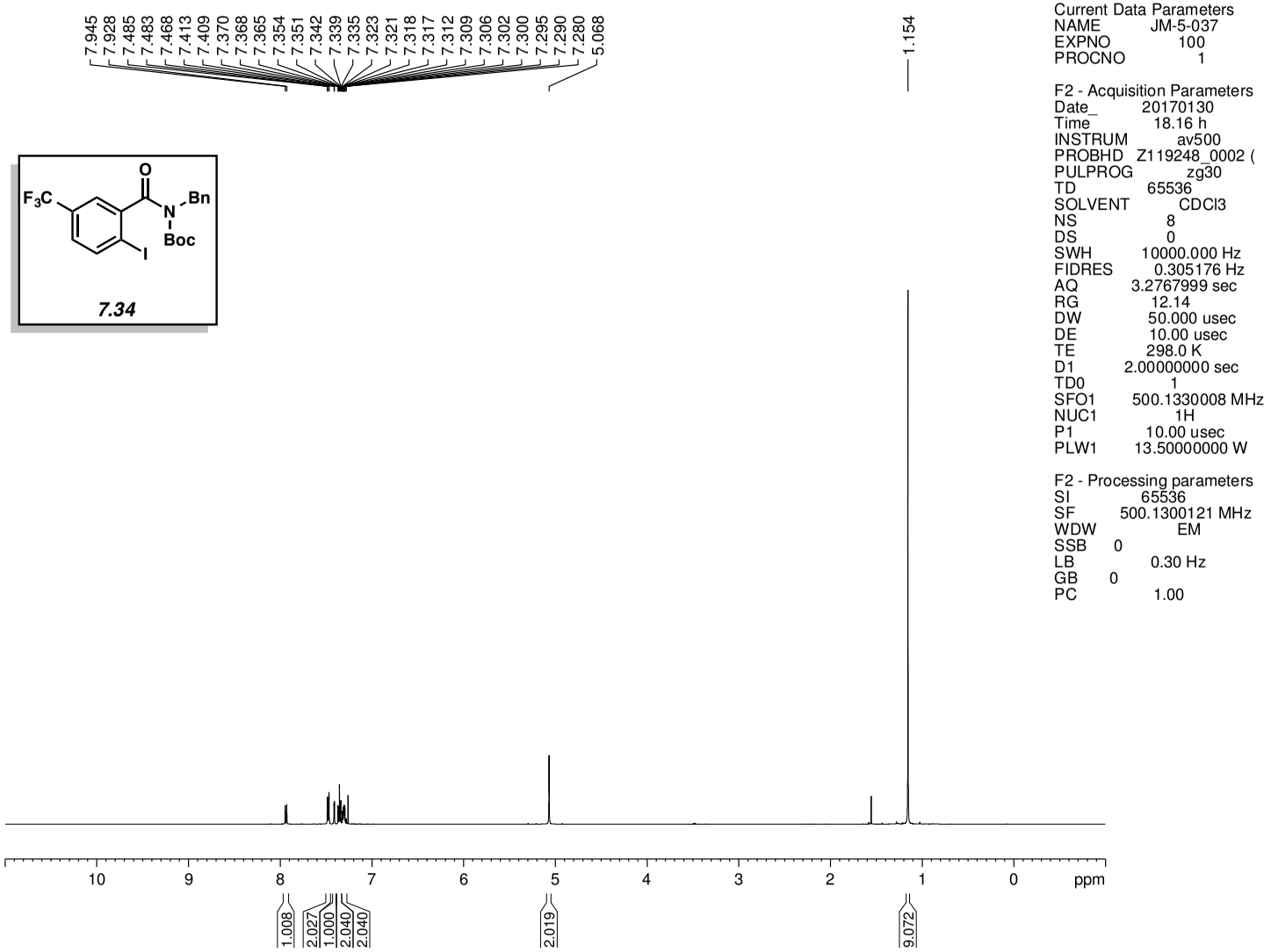

Figure 7.17 ^{1}H NMR (500 MHz, $CDCl_3$) of compound **7.34**

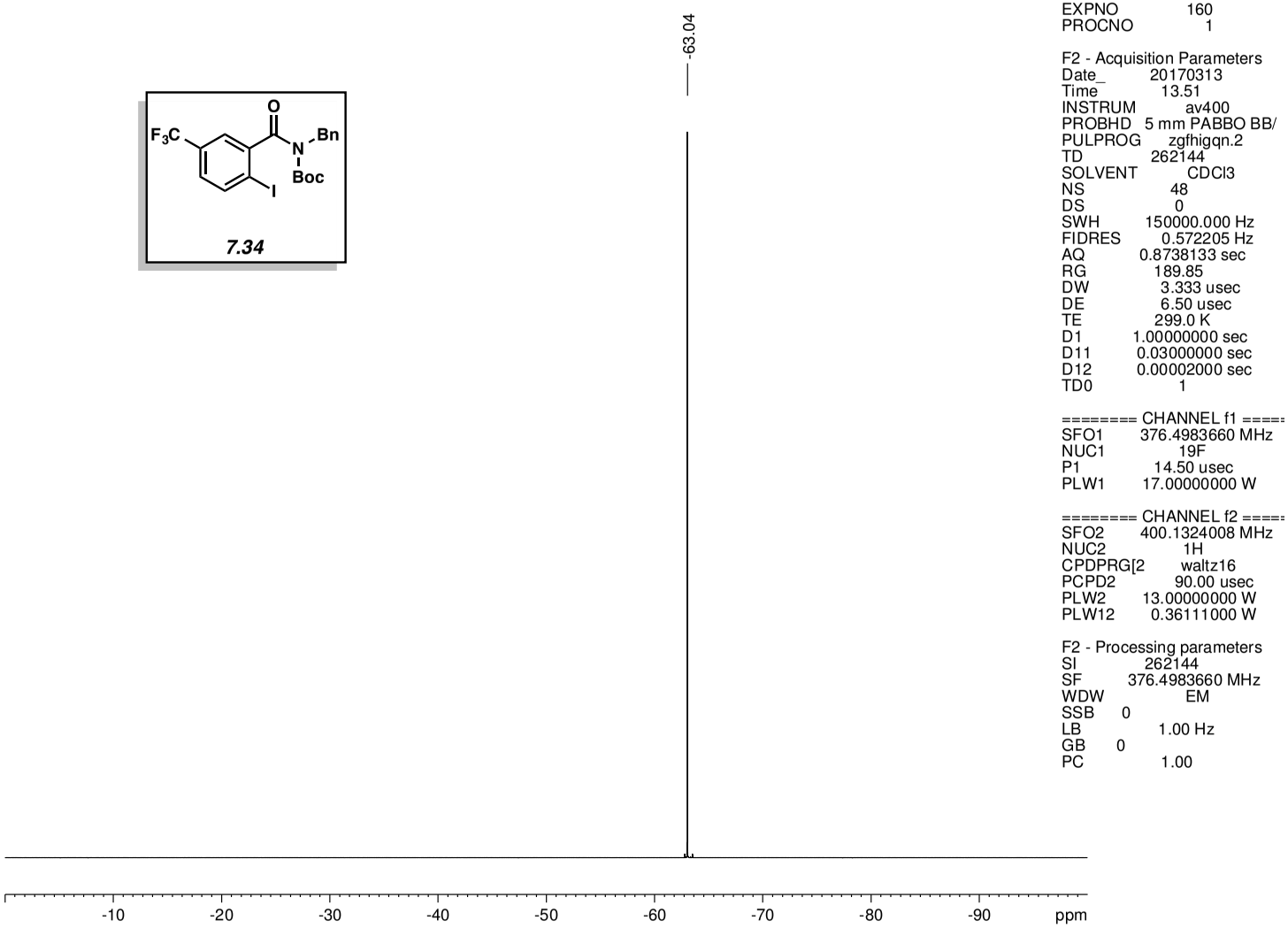

Figure 7.18 ^{19}F NMR (376 MHz, $CDCl_3$) of compound **7.34**

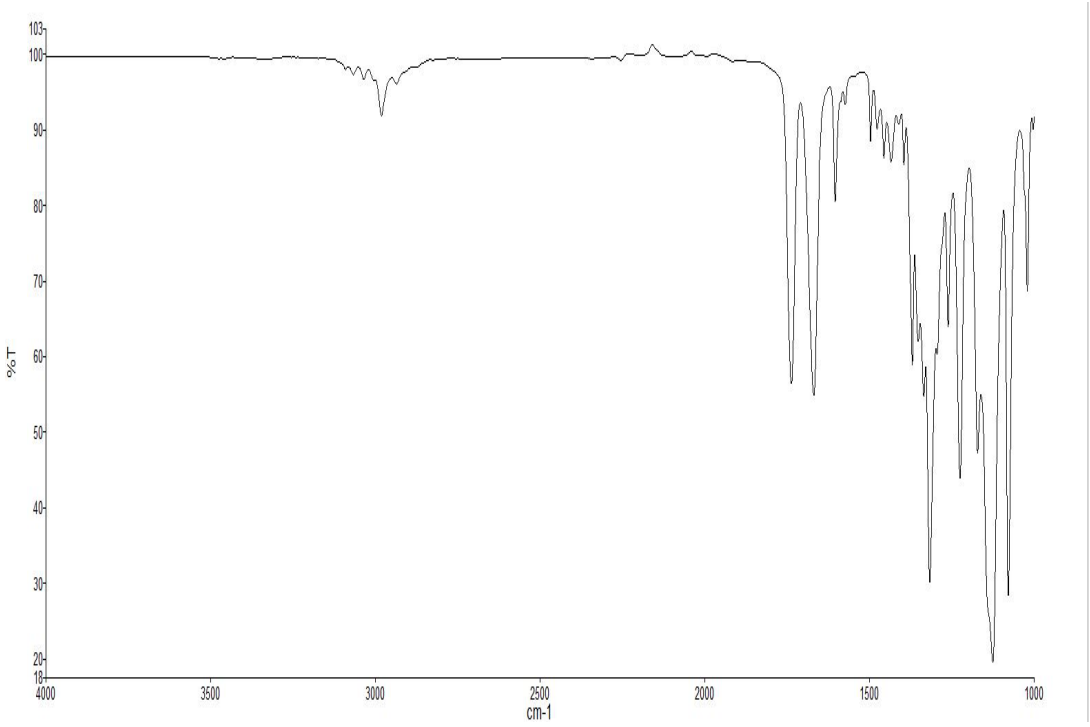

Figure 7.19 Infrared spectrum of compound **7.34**

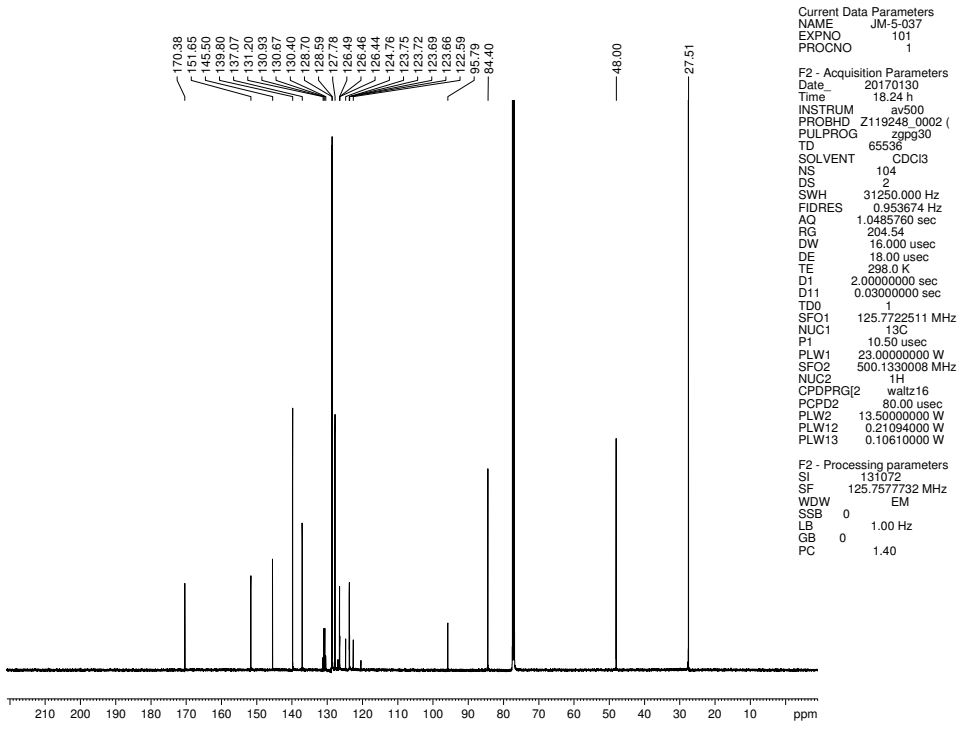

Figure 7.20 ^{13}C NMR (125 MHz, $CDCl_3$) of compound **7.34**

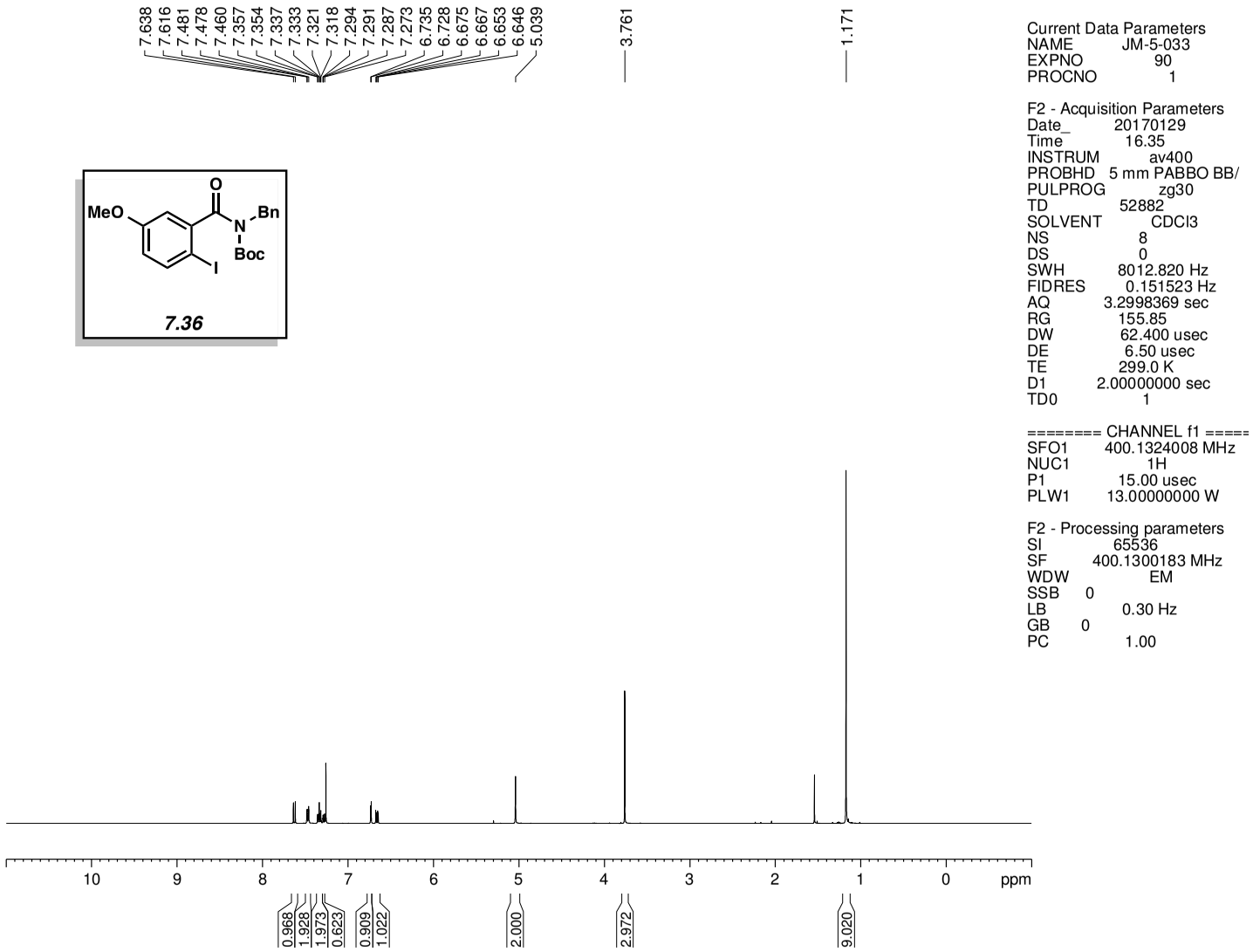

Figure 7.21 ^{1}H NMR (500 MHz, $CDCl_3$) of compound **7.36**

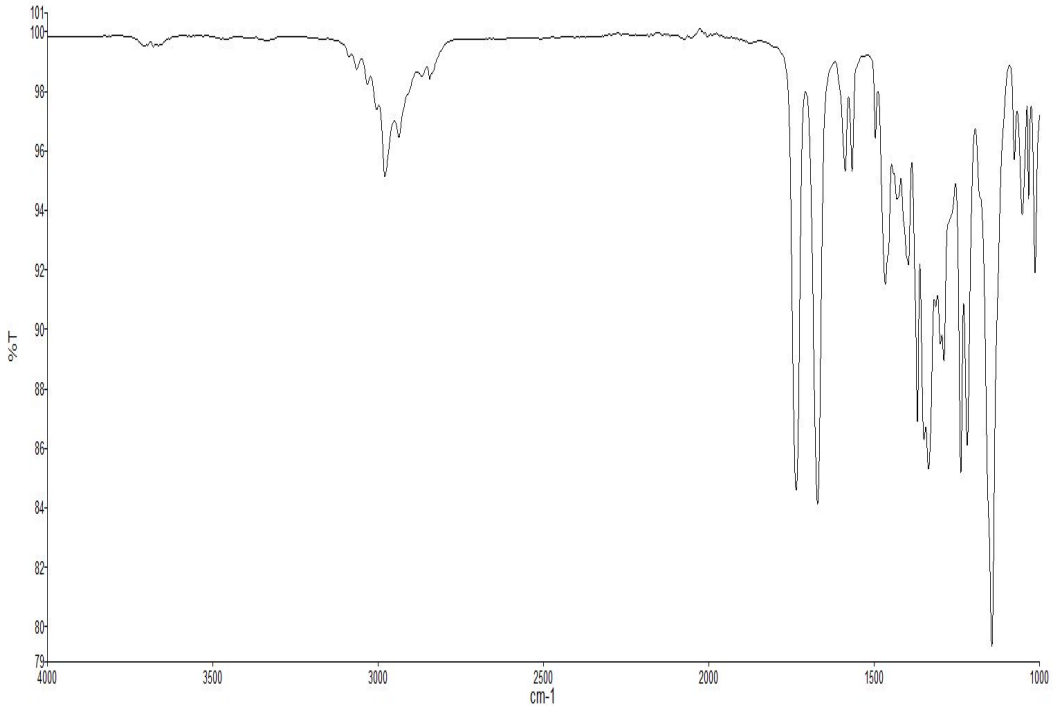

Figure 7.22 Infrared spectrum of compound **7.36**

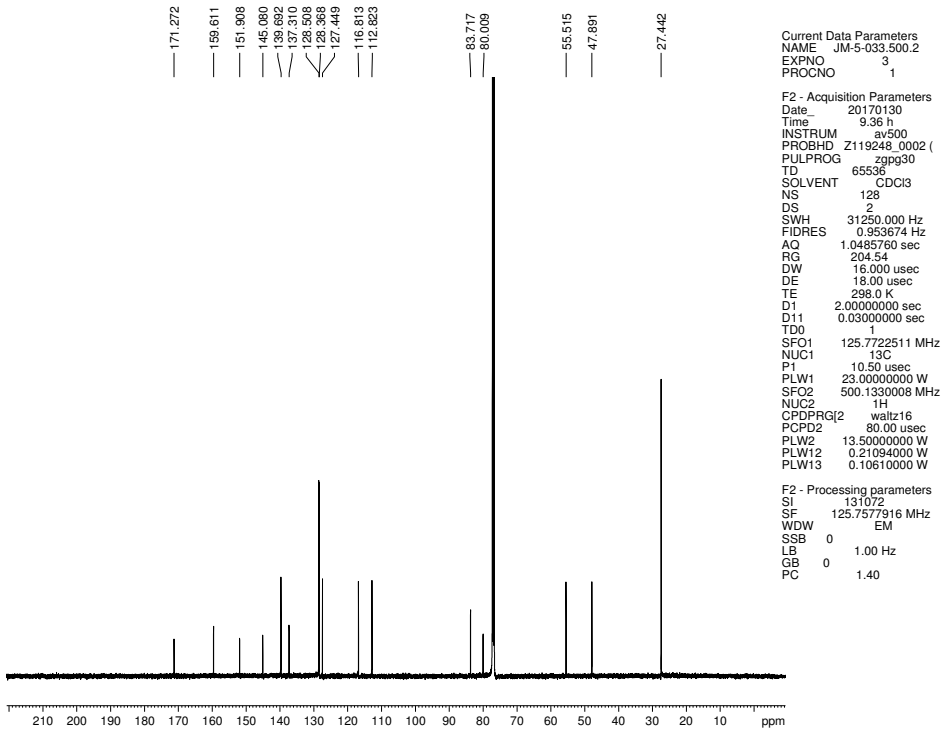

Figure 7.23 ^{13}C NMR (125 MHz, $CDCl_3$) of compound **7.36**

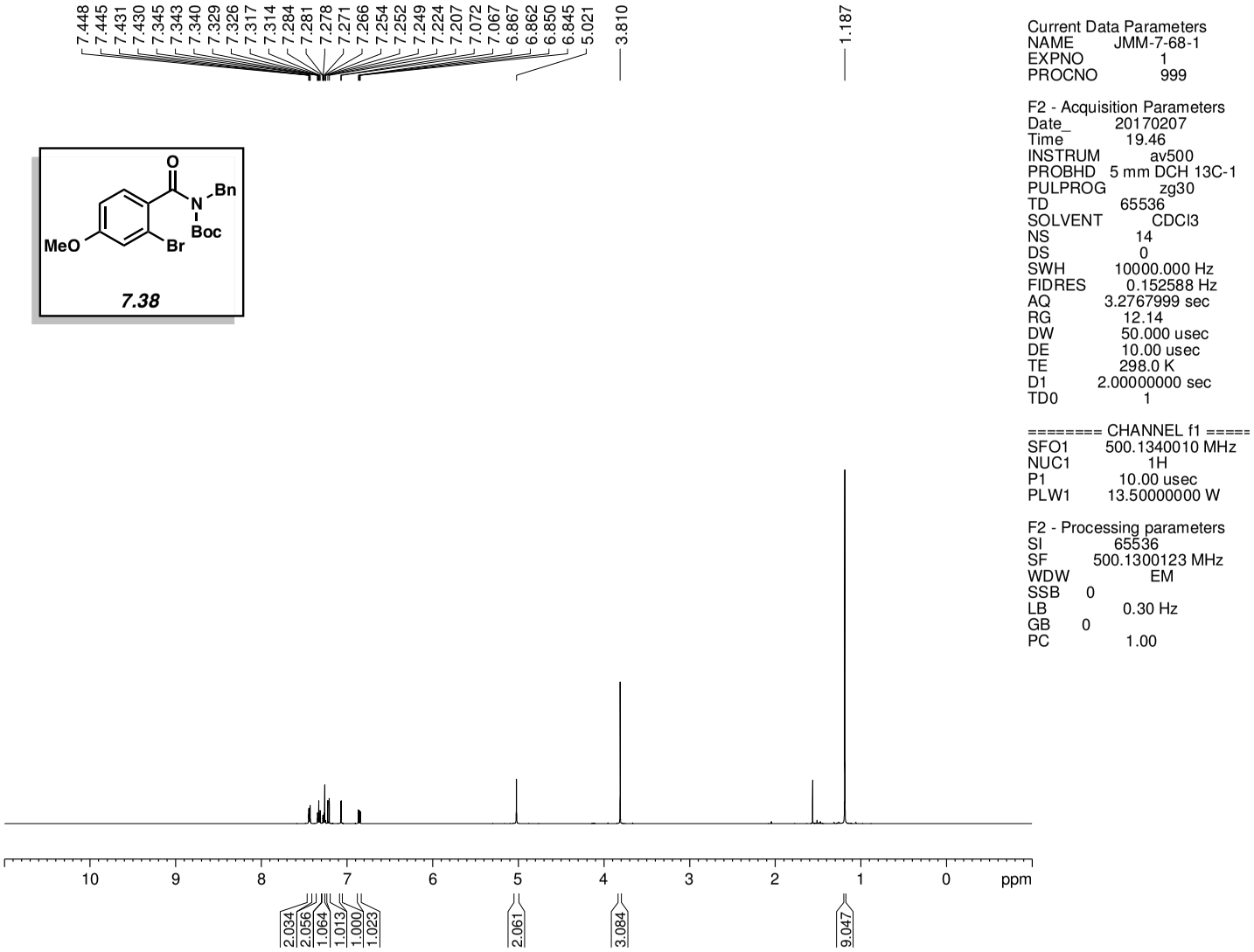

Figure 7.24 ^{1}H NMR (500 MHz, $CDCl_3$) of compound **7.38**

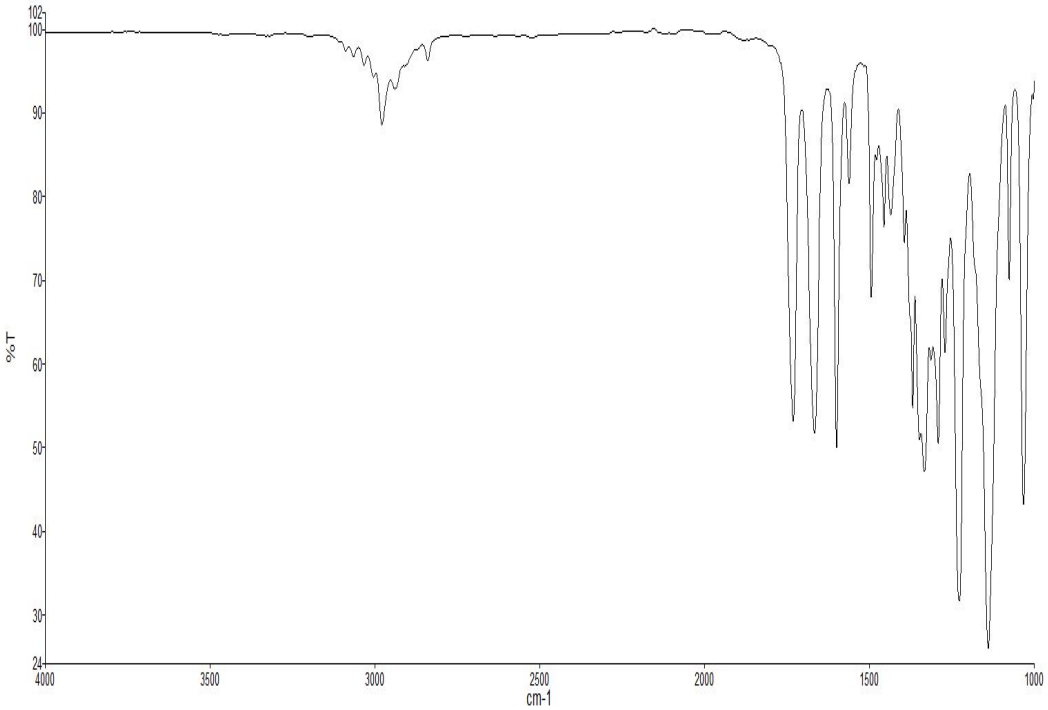

Figure 7.25 Infrared spectrum of compound **7.38**

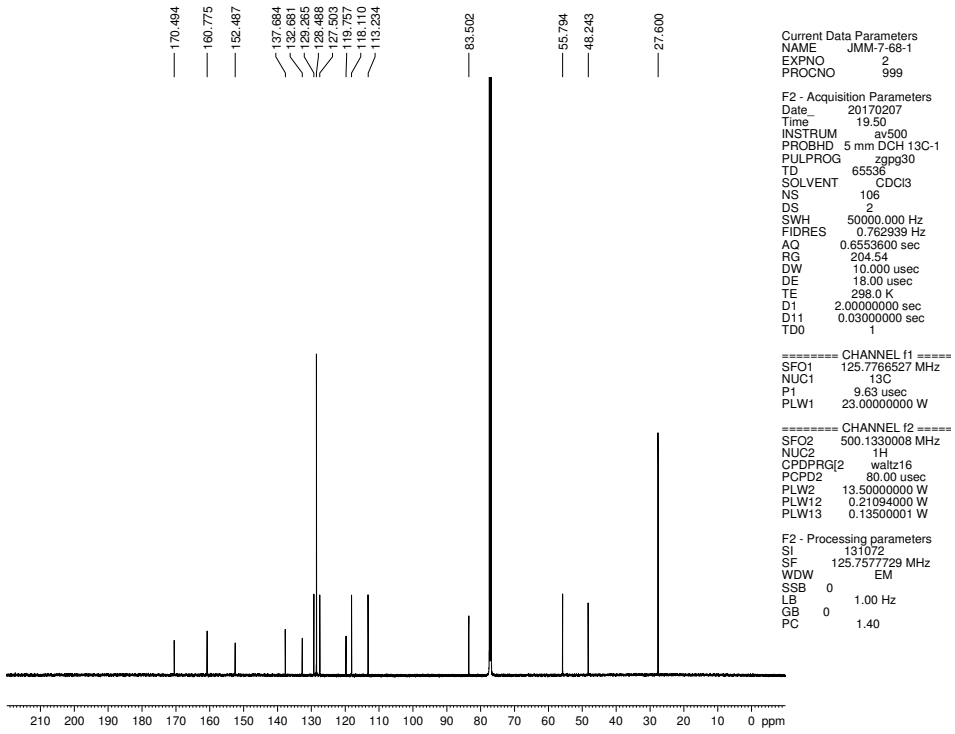

Figure 7.26 ^{13}C NMR (125 MHz, $CDCl_3$) of compound **7.38**

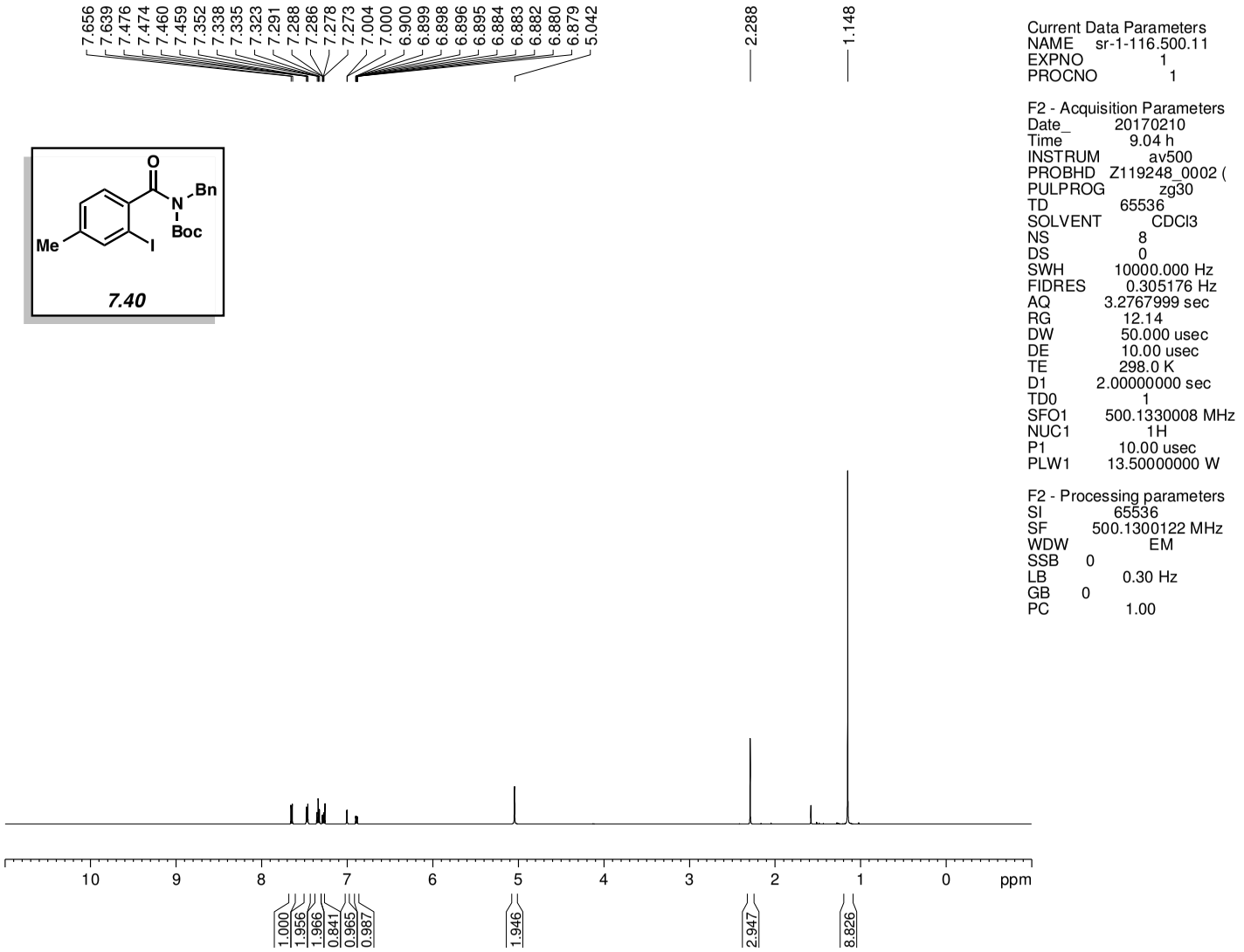

Figure 7.27 ^{1}H NMR (500 MHz, $CDCl_3$) of compound **7.40**

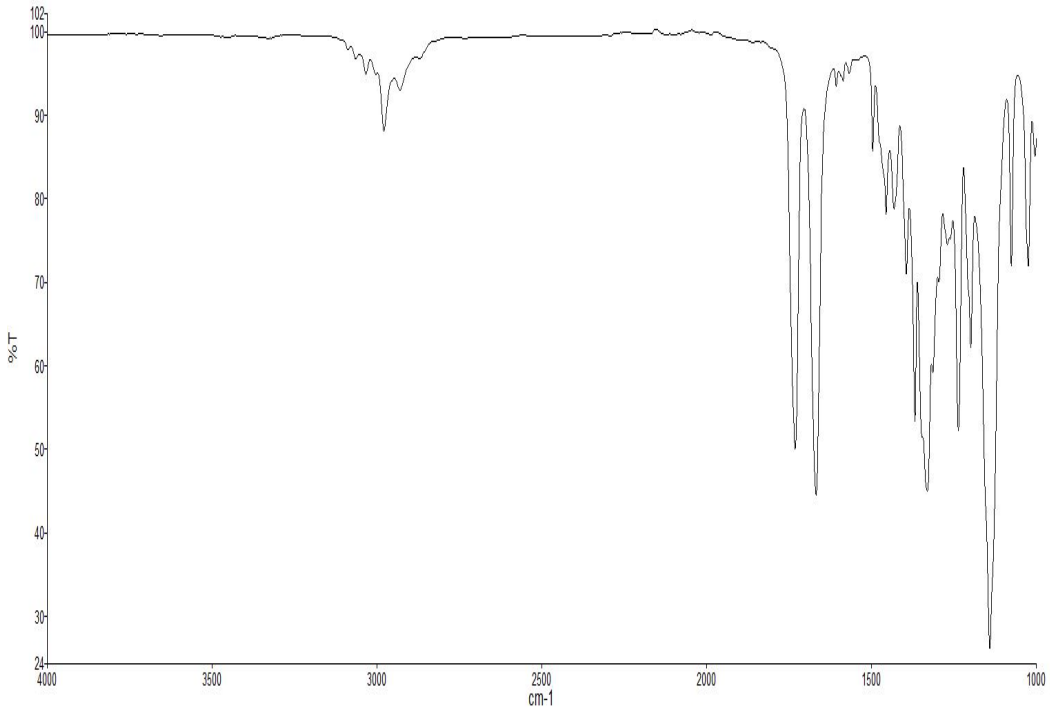

Figure 7.28 Infrared spectrum of compound **7.40**

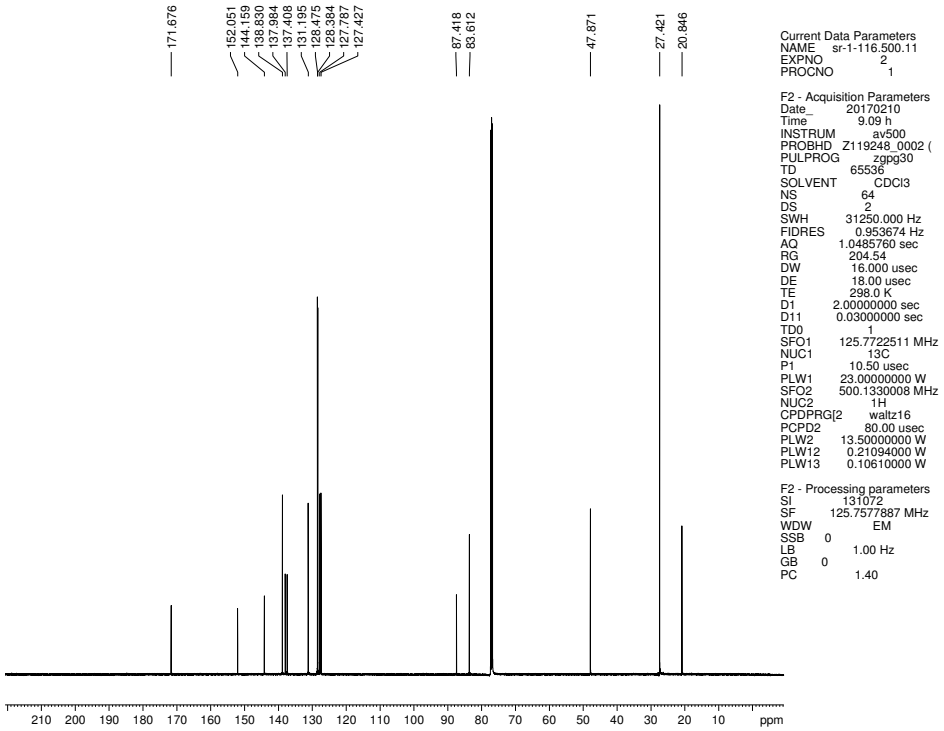

Figure 7.29 ^{13}C NMR (125 MHz, $CDCl_3$) of compound **7.40**

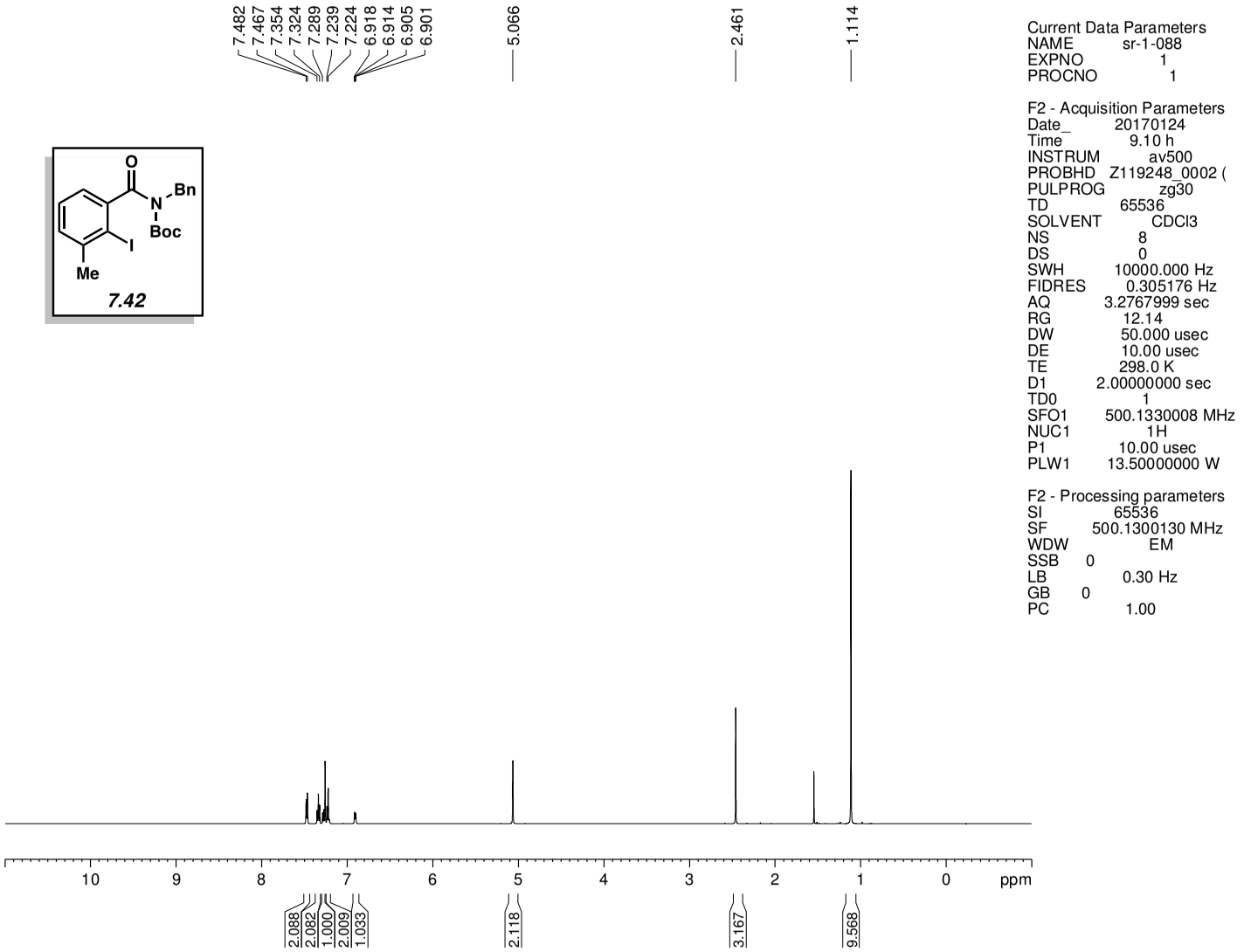

Figure 7.30 ^{1}H NMR (500 MHz, $CDCl_3$) of compound **7.42**

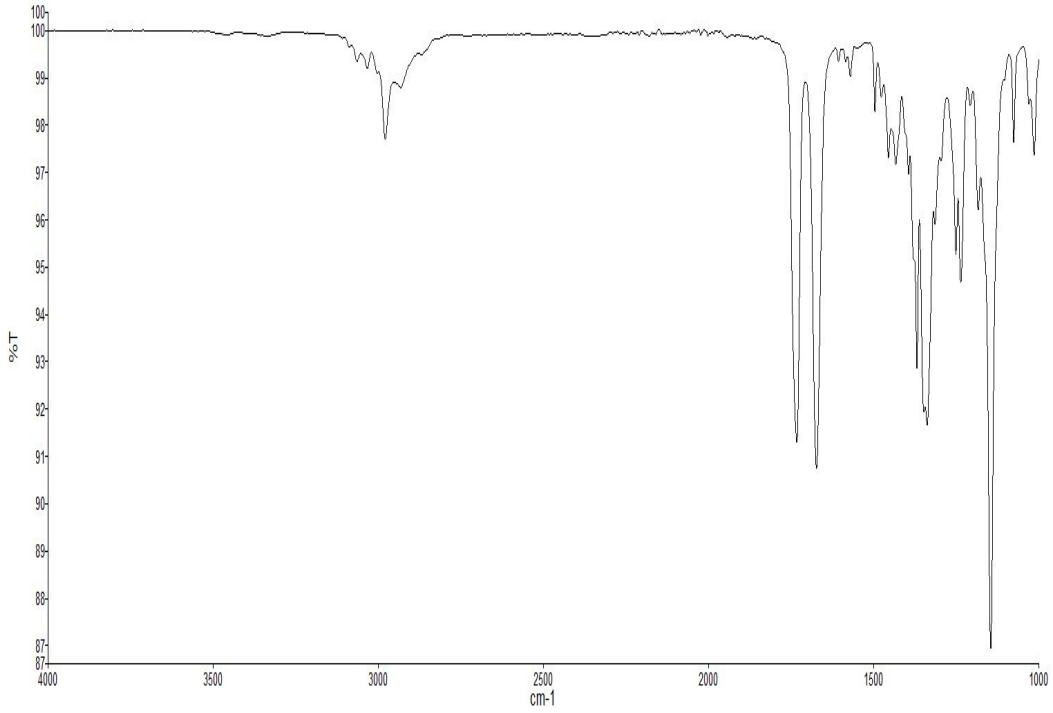

Figure 7.31 Infrared spectrum of compound **7.42**

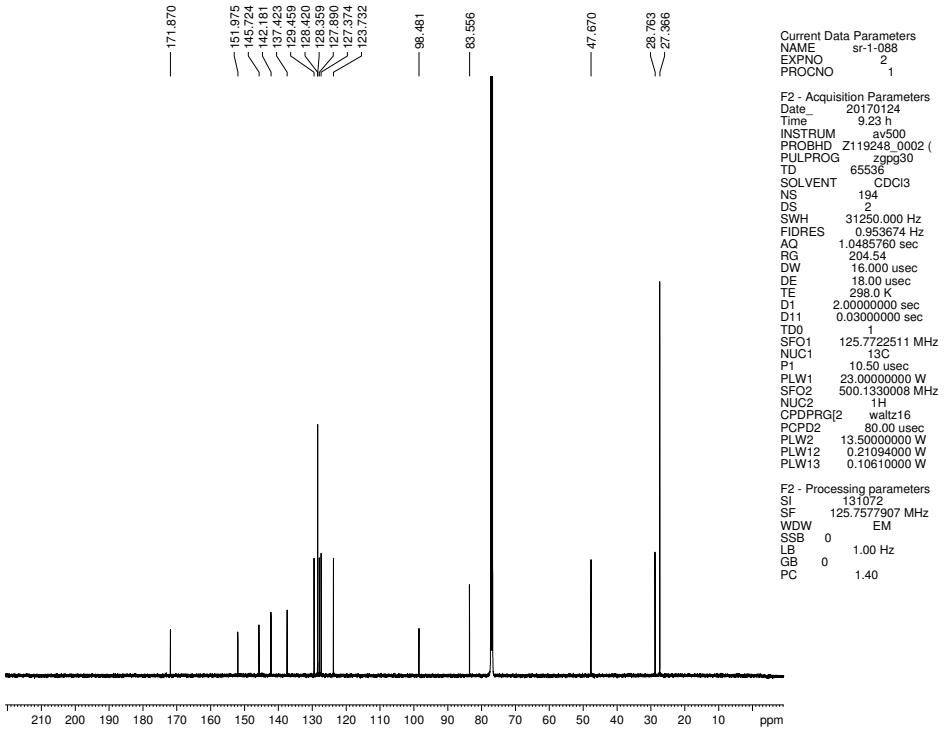

Figure 7.32 ^{13}C NMR (125 MHz, $CDCl_3$) of compound **7.42**

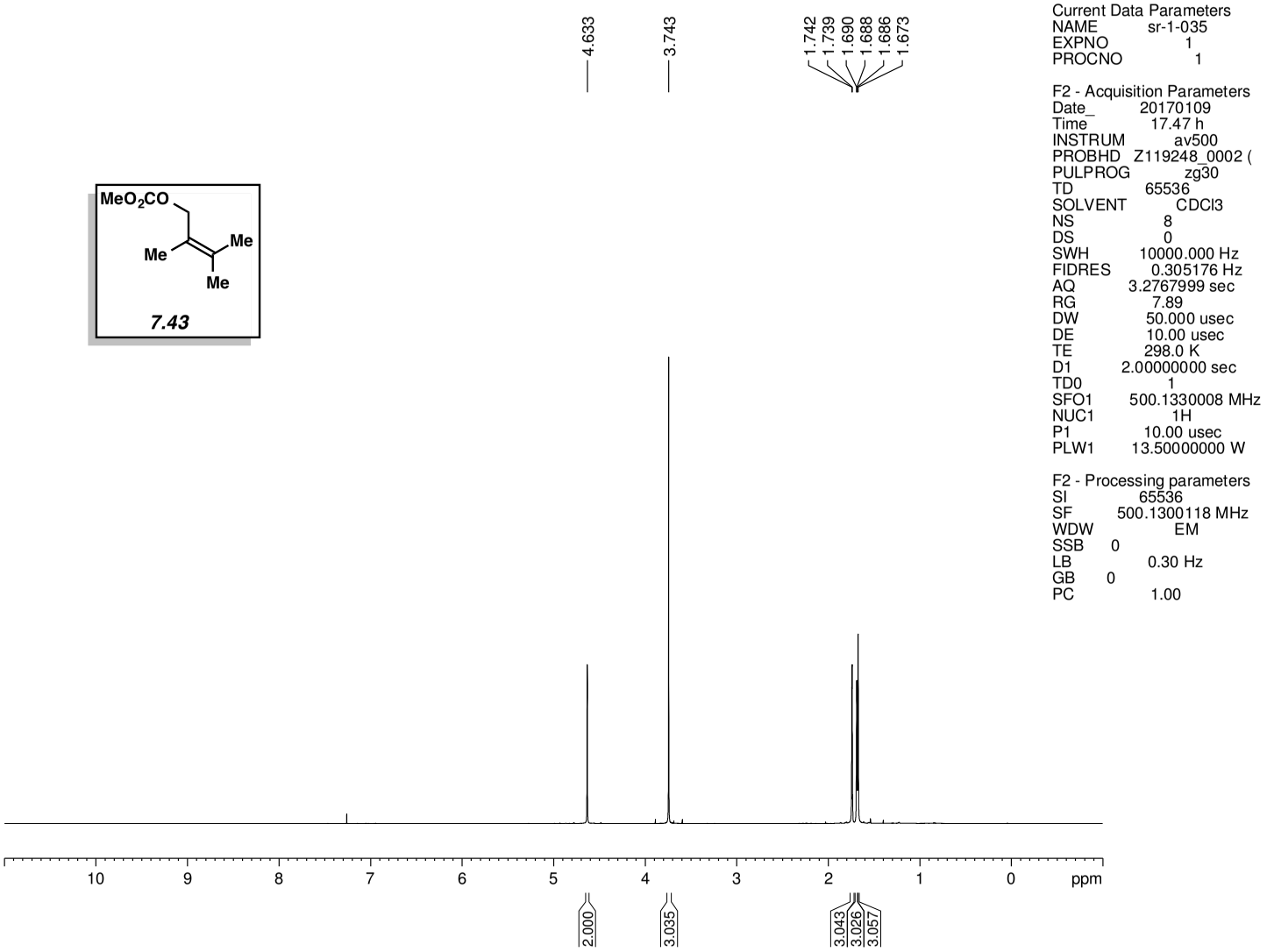

Figure 7.33 ^{1}H NMR (500 MHz, $CDCl_3$) of compound **7.43**

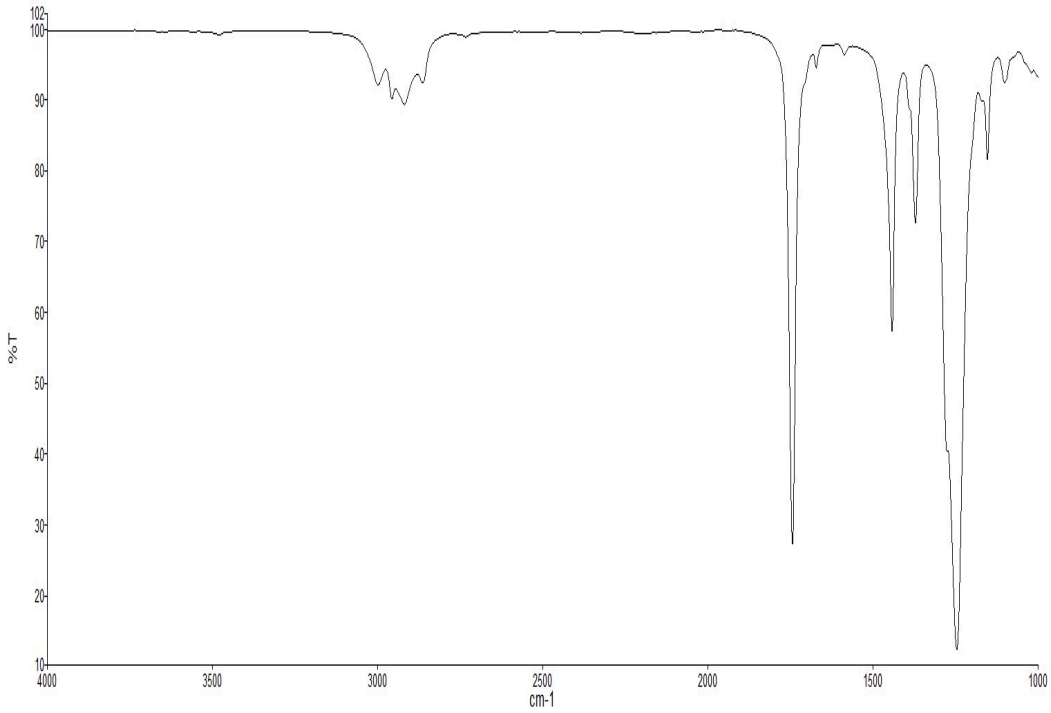

Figure 7.34 Infrared spectrum of compound **7.43**

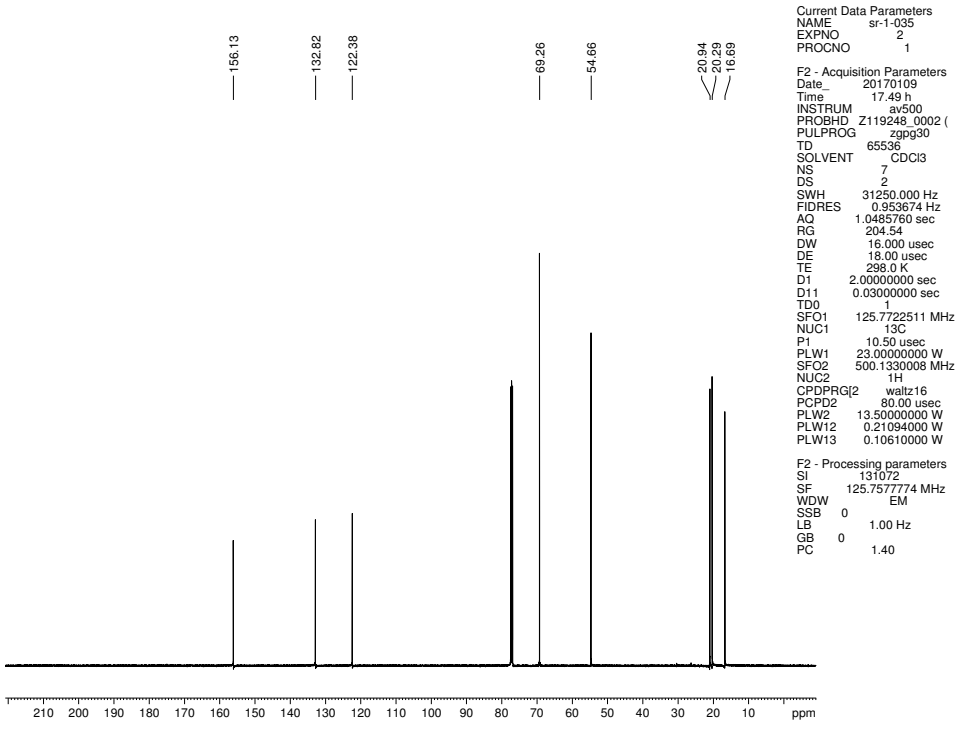

Figure 7.35 ^{13}C NMR (125 MHz, $CDCl_3$) of compound **7.43**

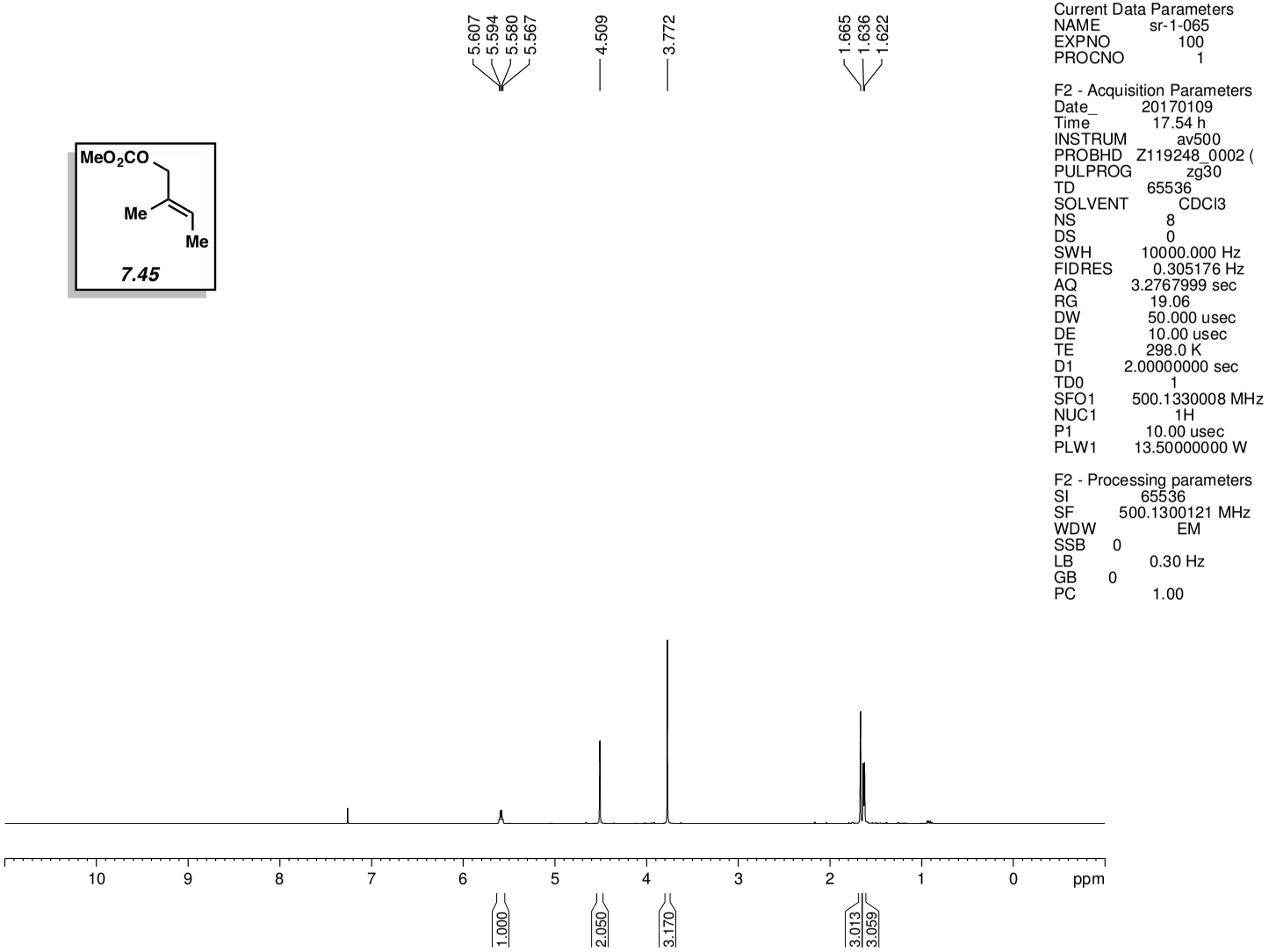

Figure 7.36 ^{1}H NMR (500 MHz, $CDCl_3$) of compound **7.45**

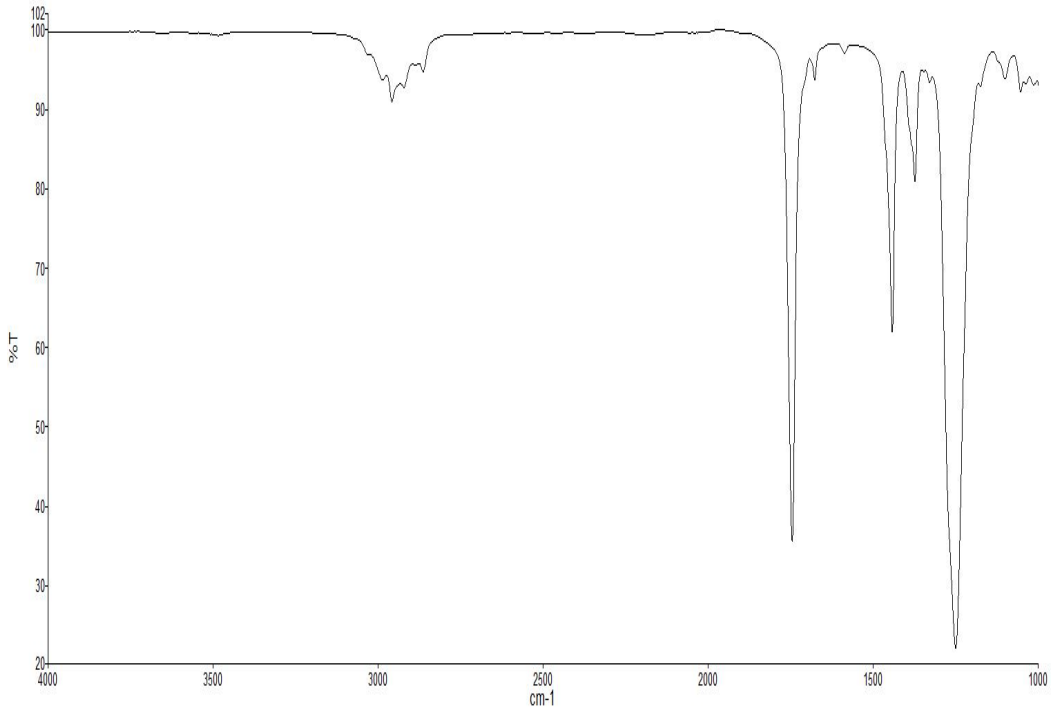

Figure 7.37 Infrared spectrum of compound **7.45**

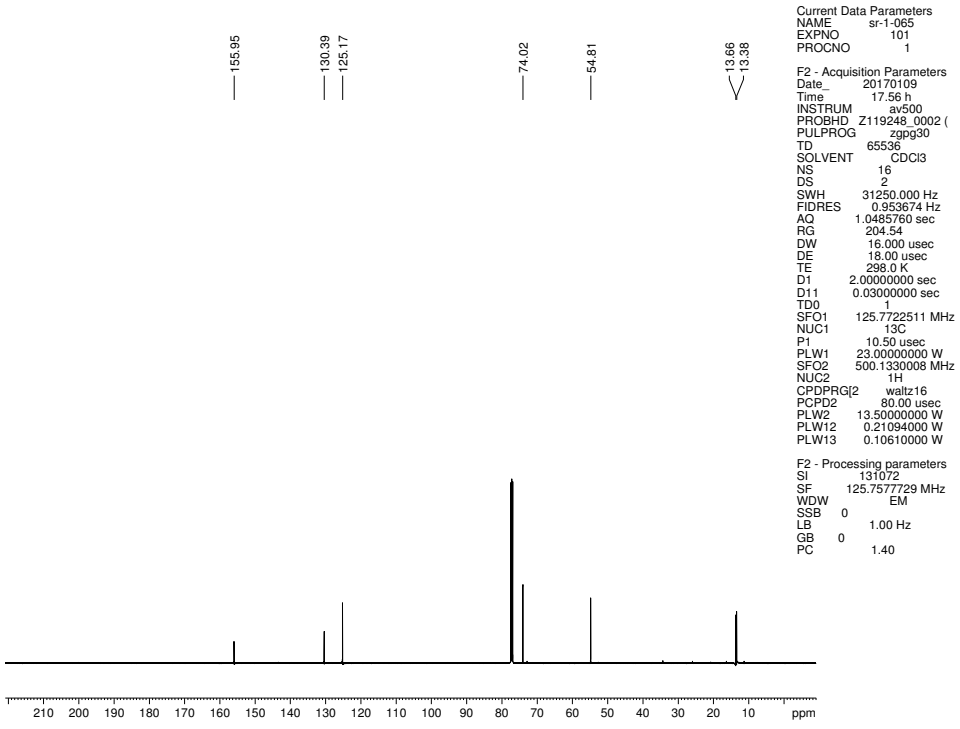

Figure 7.38 ^{13}C NMR (125 MHz, $CDCl_3$) of compound **7.45**

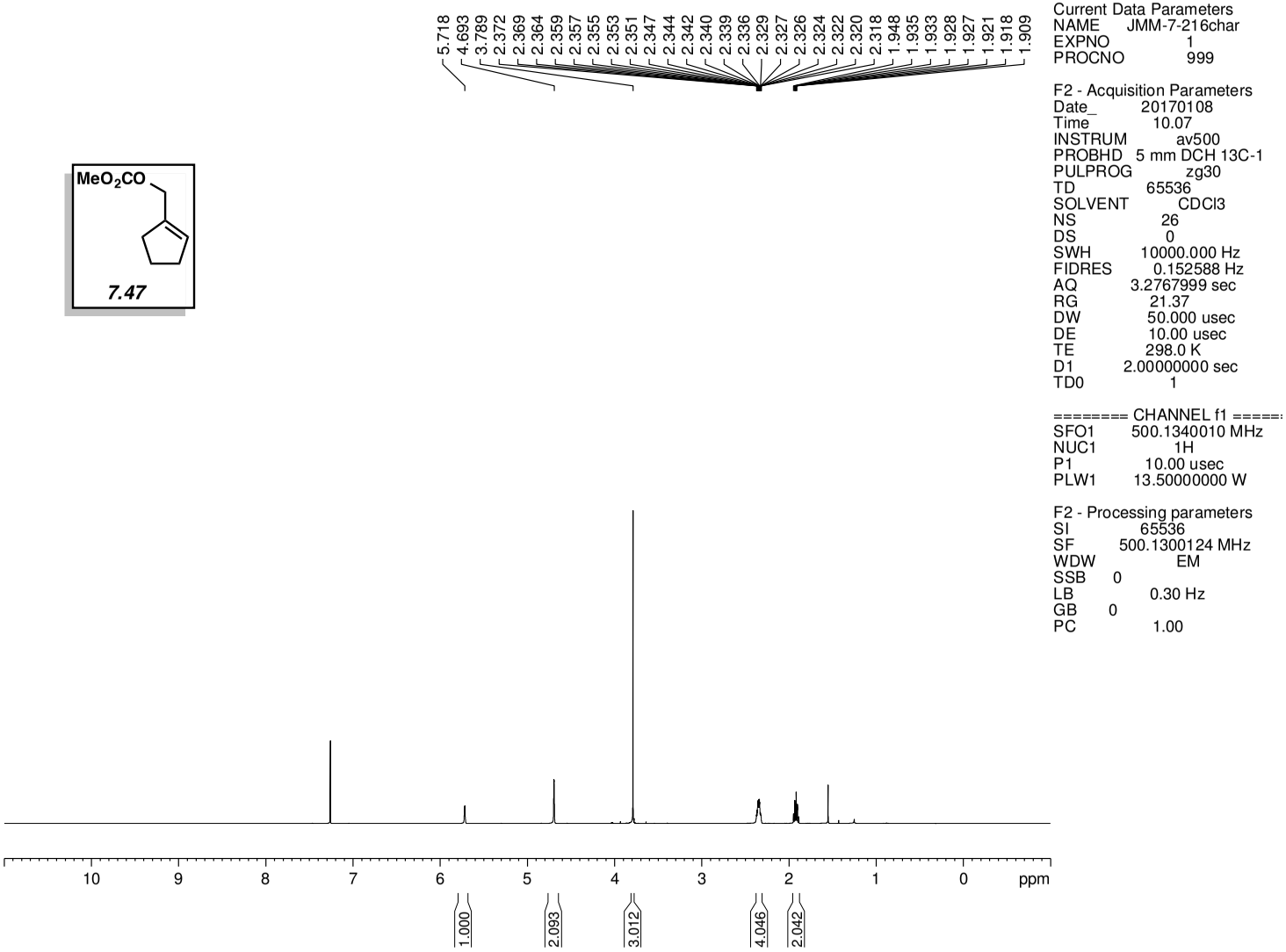

Figure 7.39 ^{1}H NMR (500 MHz, $CDCl_3$) of compound **7.47**

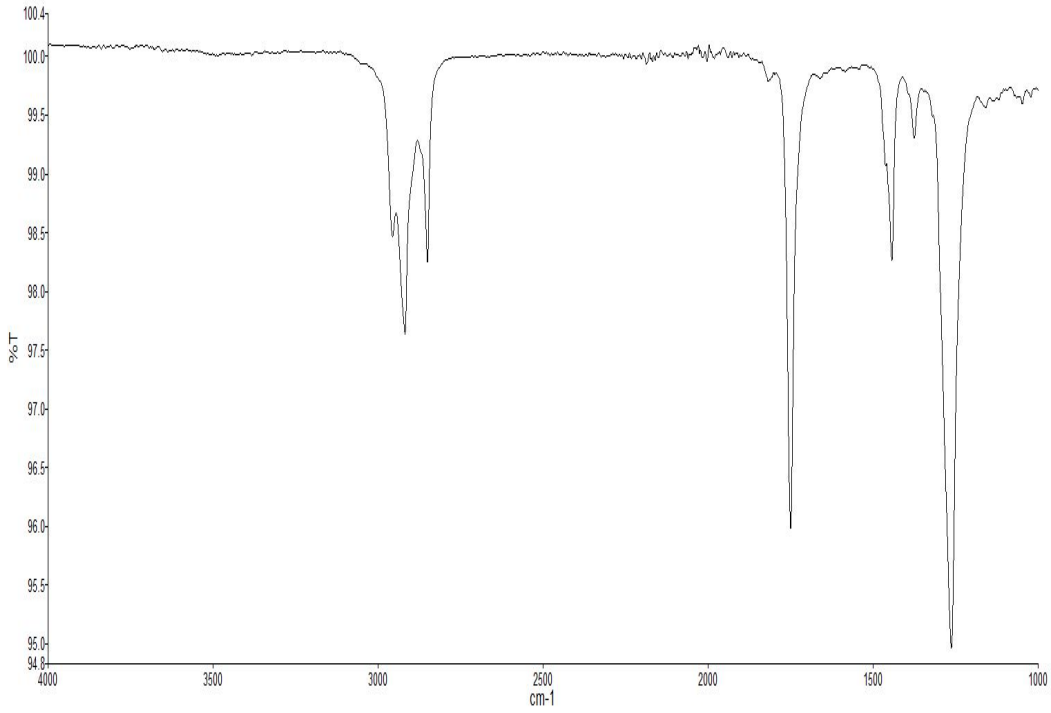

Figure 7.40 Infrared spectrum of compound **7.47**

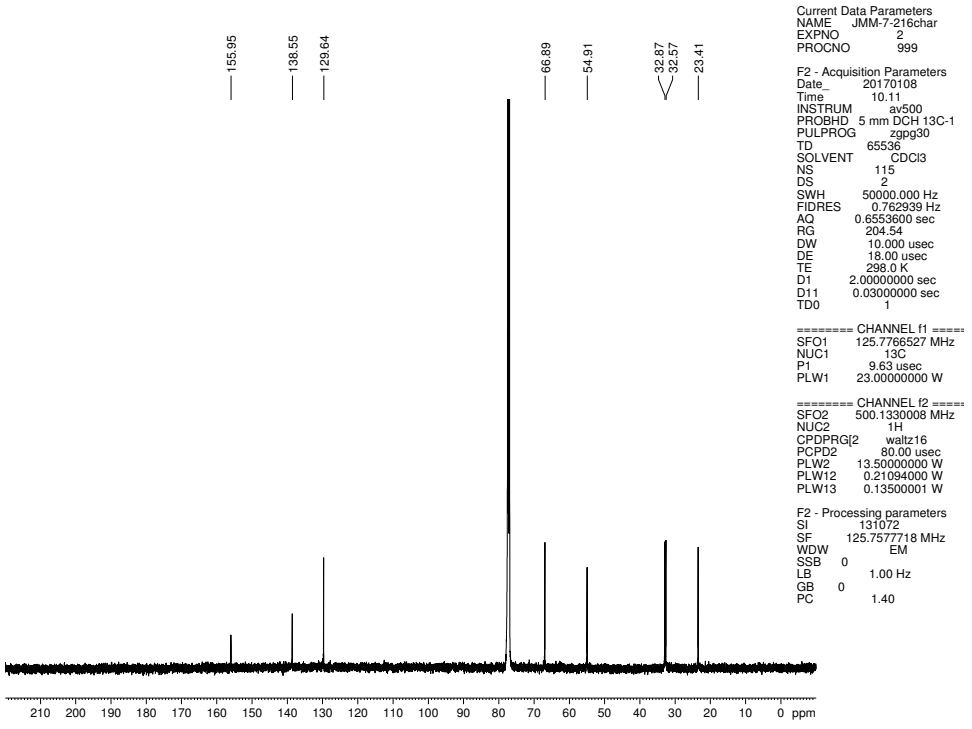

Figure 7.41 ^{13}C NMR (125 MHz, $CDCl_3$) of compound **7.47**

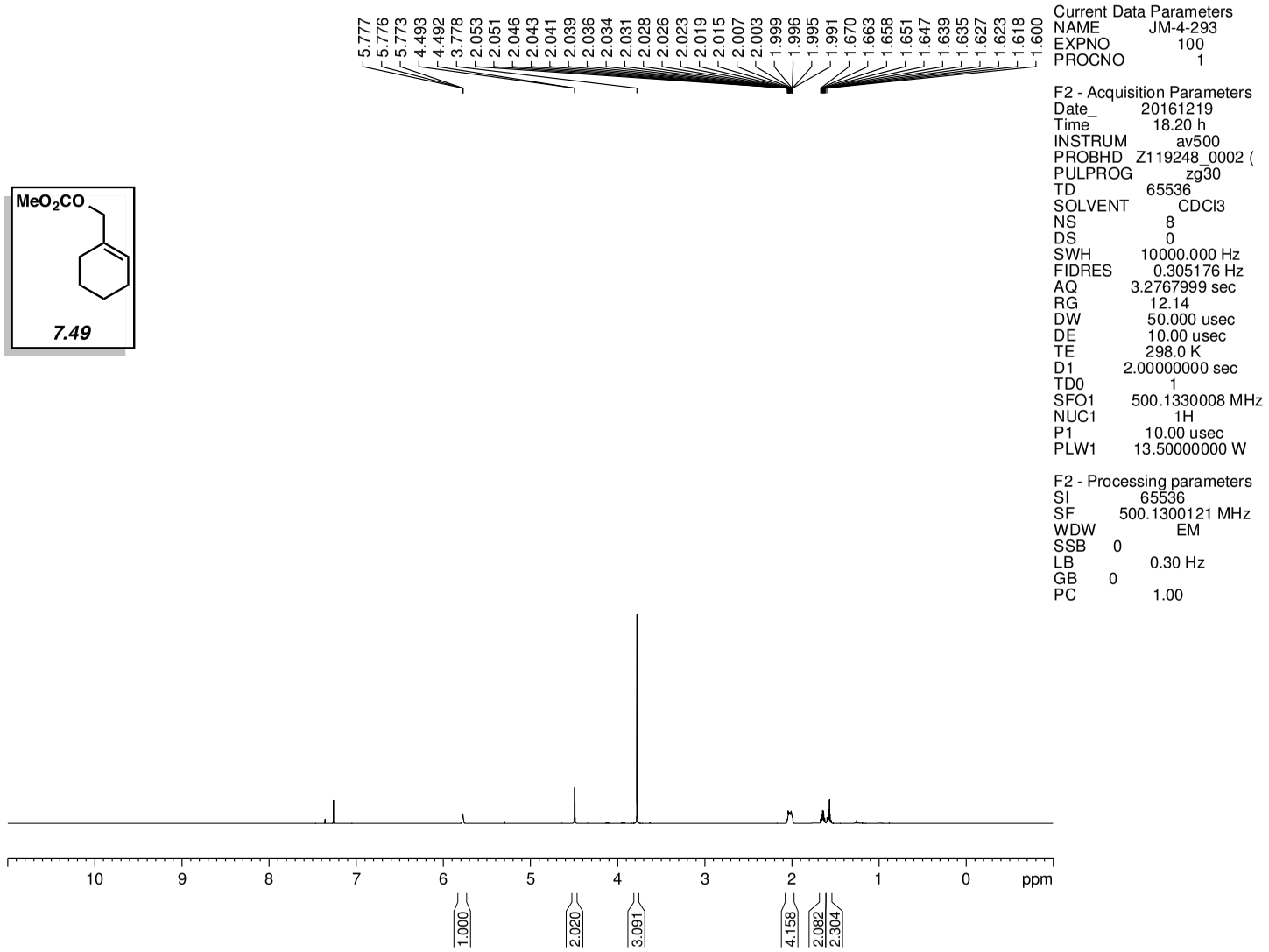

Figure 7.42 ^{1}H NMR (500 MHz, $CDCl_3$) of compound **7.49**

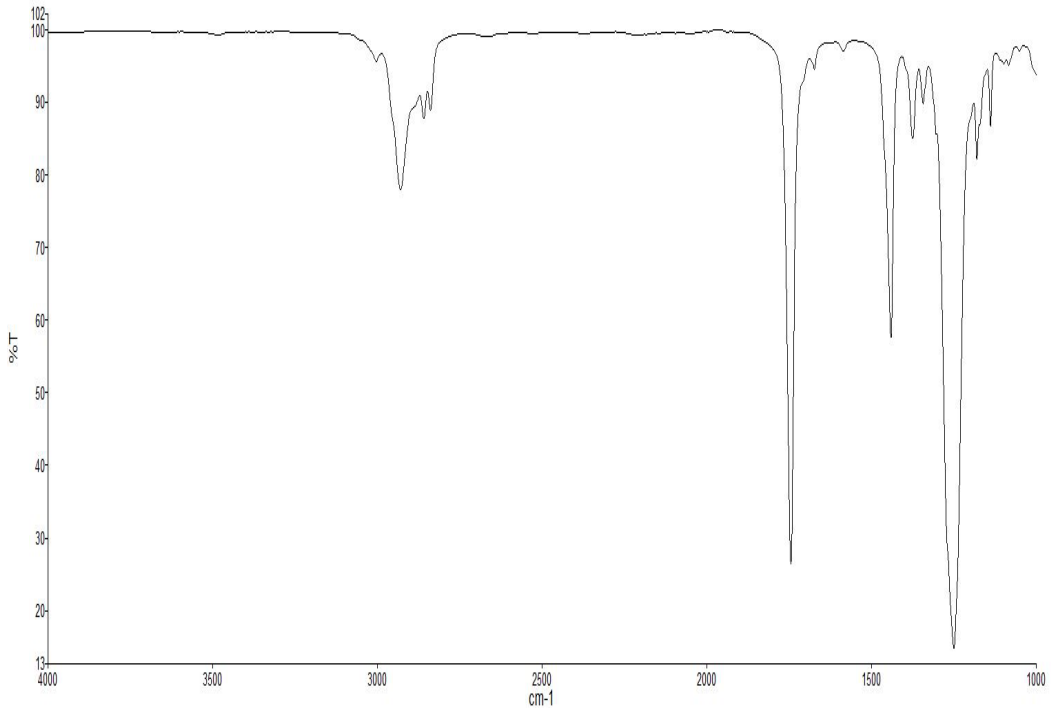

Figure 7.43 Infrared spectrum of compound **7.49**

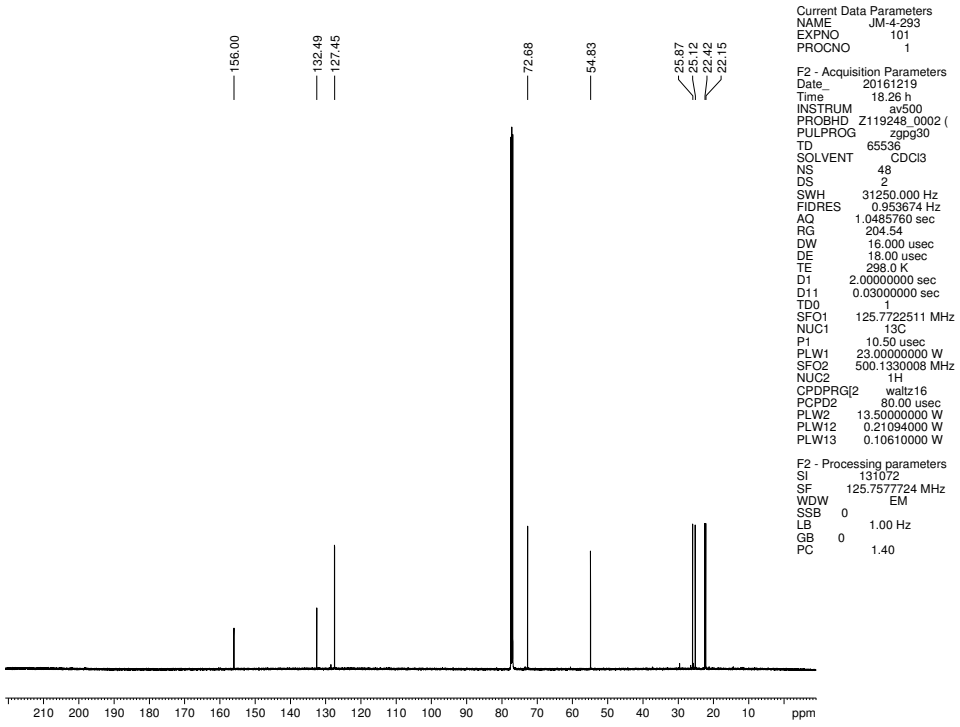

Figure 7.44 ^{13}C NMR (125 MHz, $CDCl_3$) of compound **7.49**

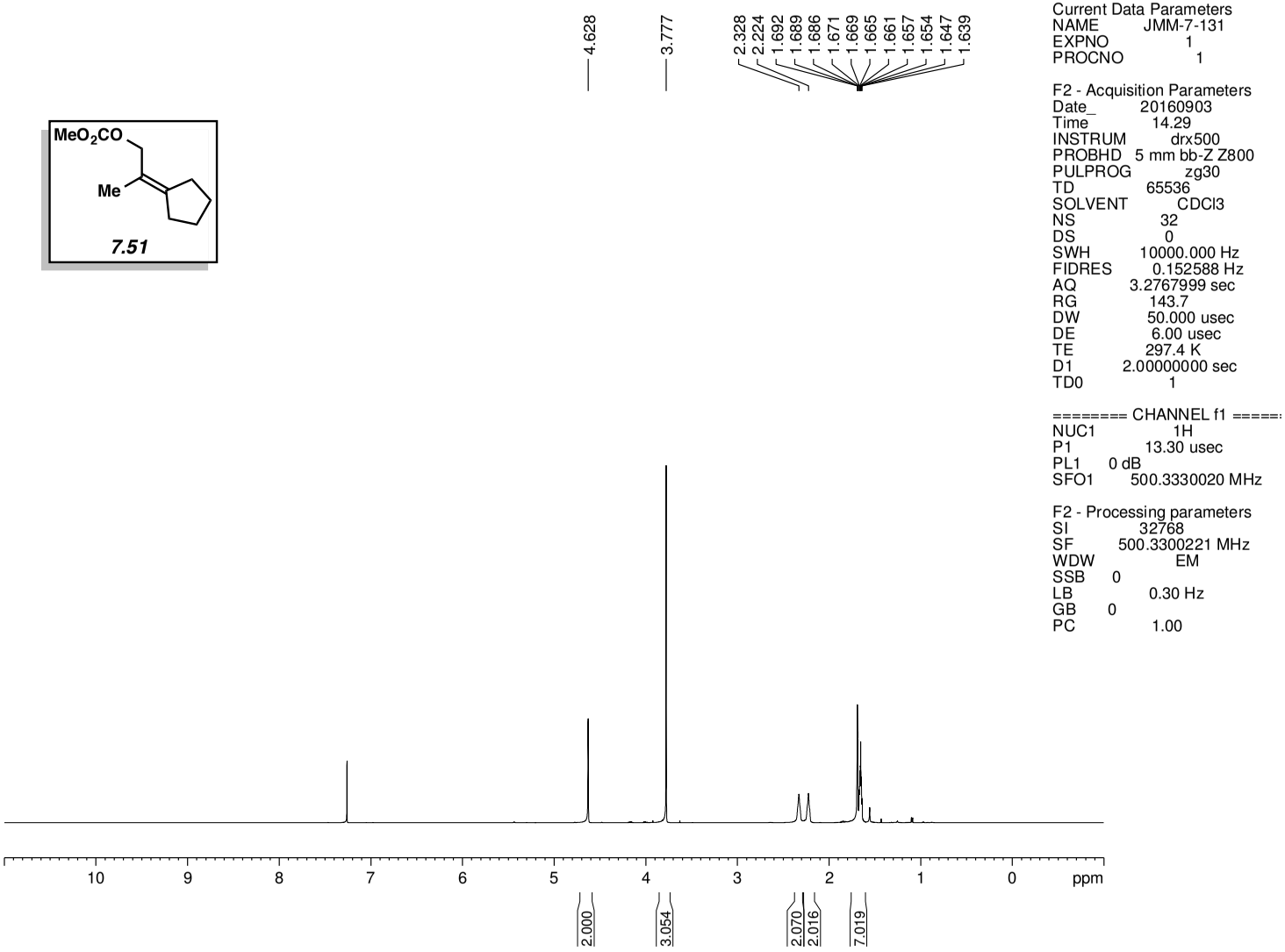

Figure 7.45 ^{1}H NMR (500 MHz, $CDCl_3$) of compound **7.51**

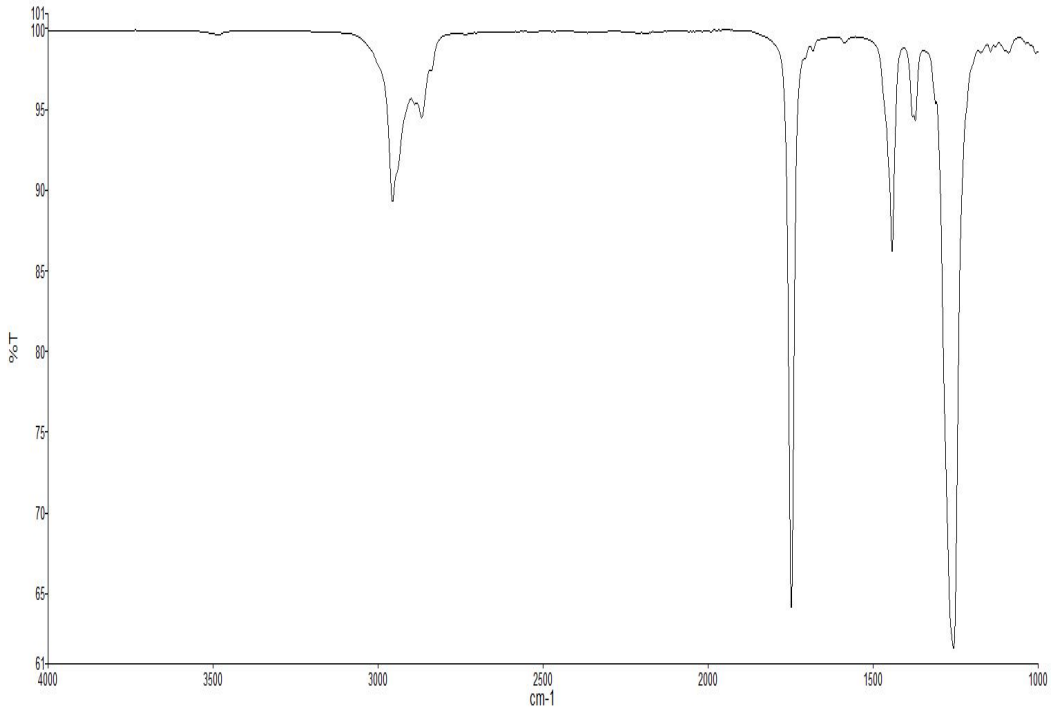

Figure 7.46 Infrared spectrum of compound **7.51**

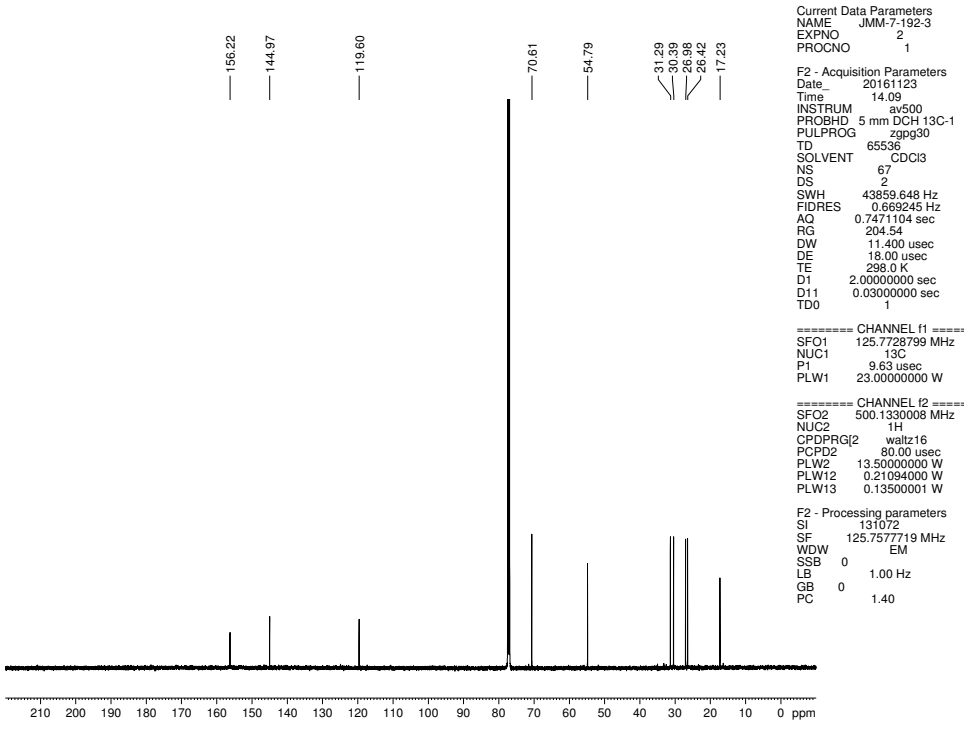

Figure 7.47 ^{13}C NMR (125 MHz, $CDCl_3$) of compound **7.51**

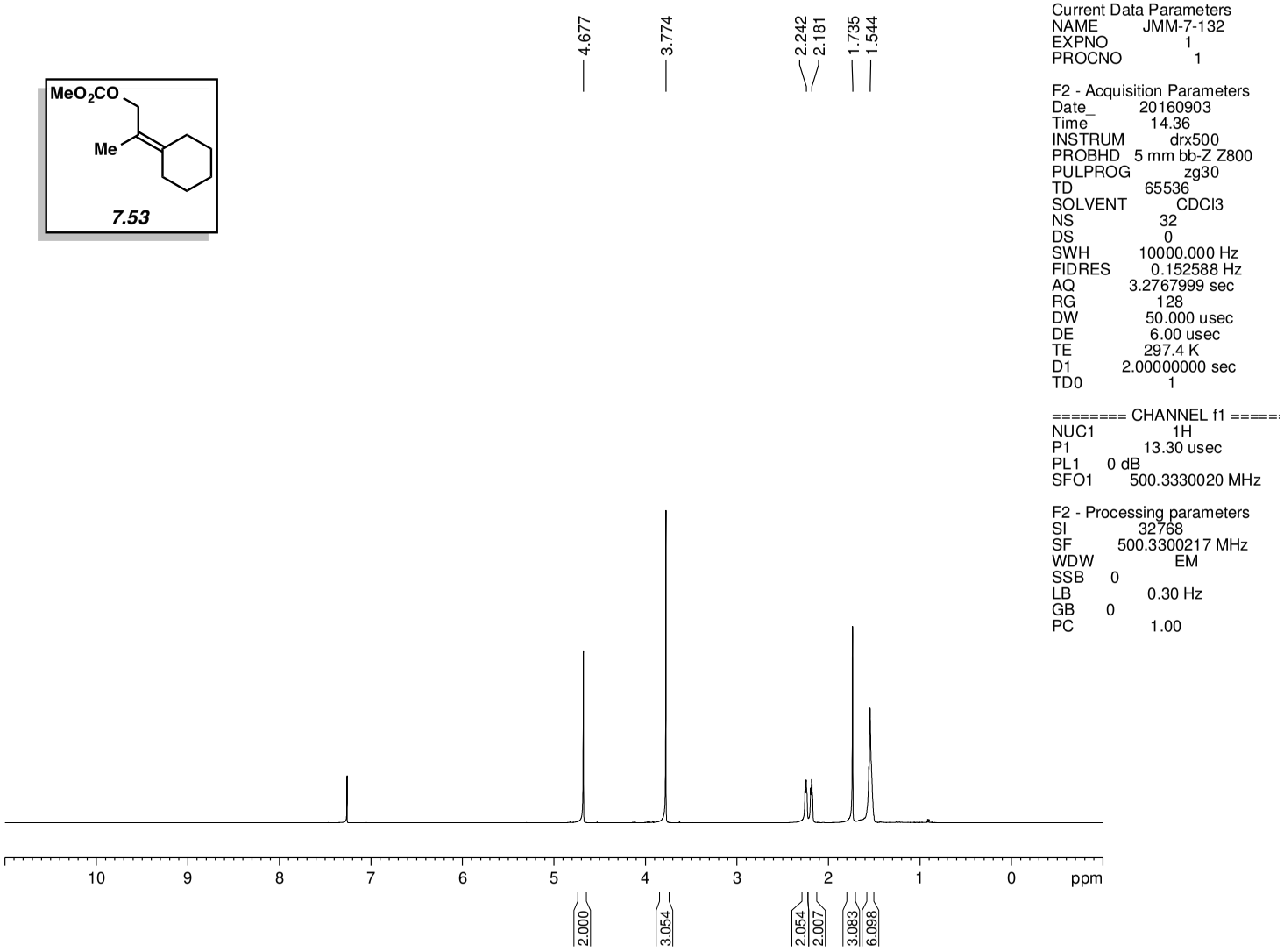

Figure 7.48 ^{1}H NMR (500 MHz, $CDCl_3$) of compound **7.53**

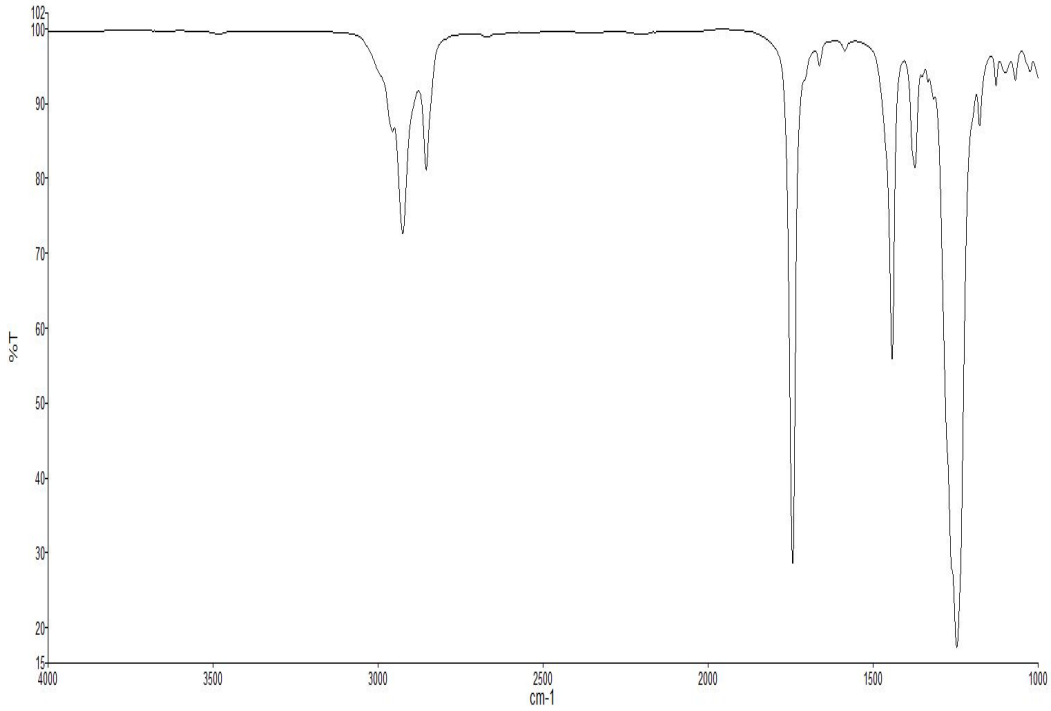

Figure 7.49 Infrared spectrum of compound **7.53**

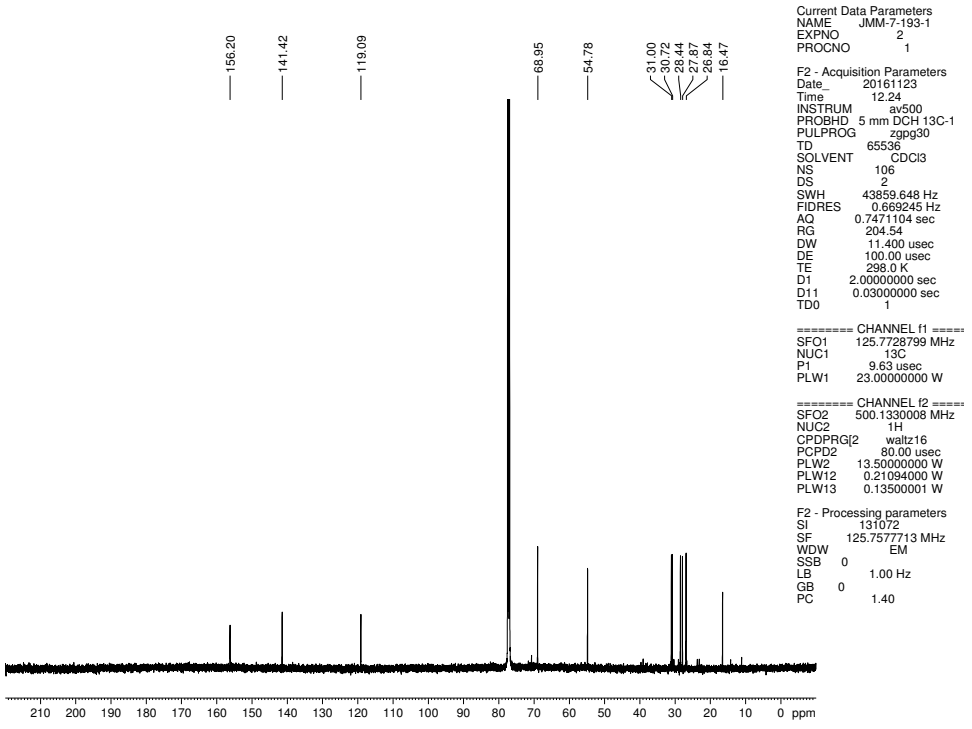

Figure 7.50 ^{13}C NMR (125 MHz, $CDCl_3$) of compound **7.53**

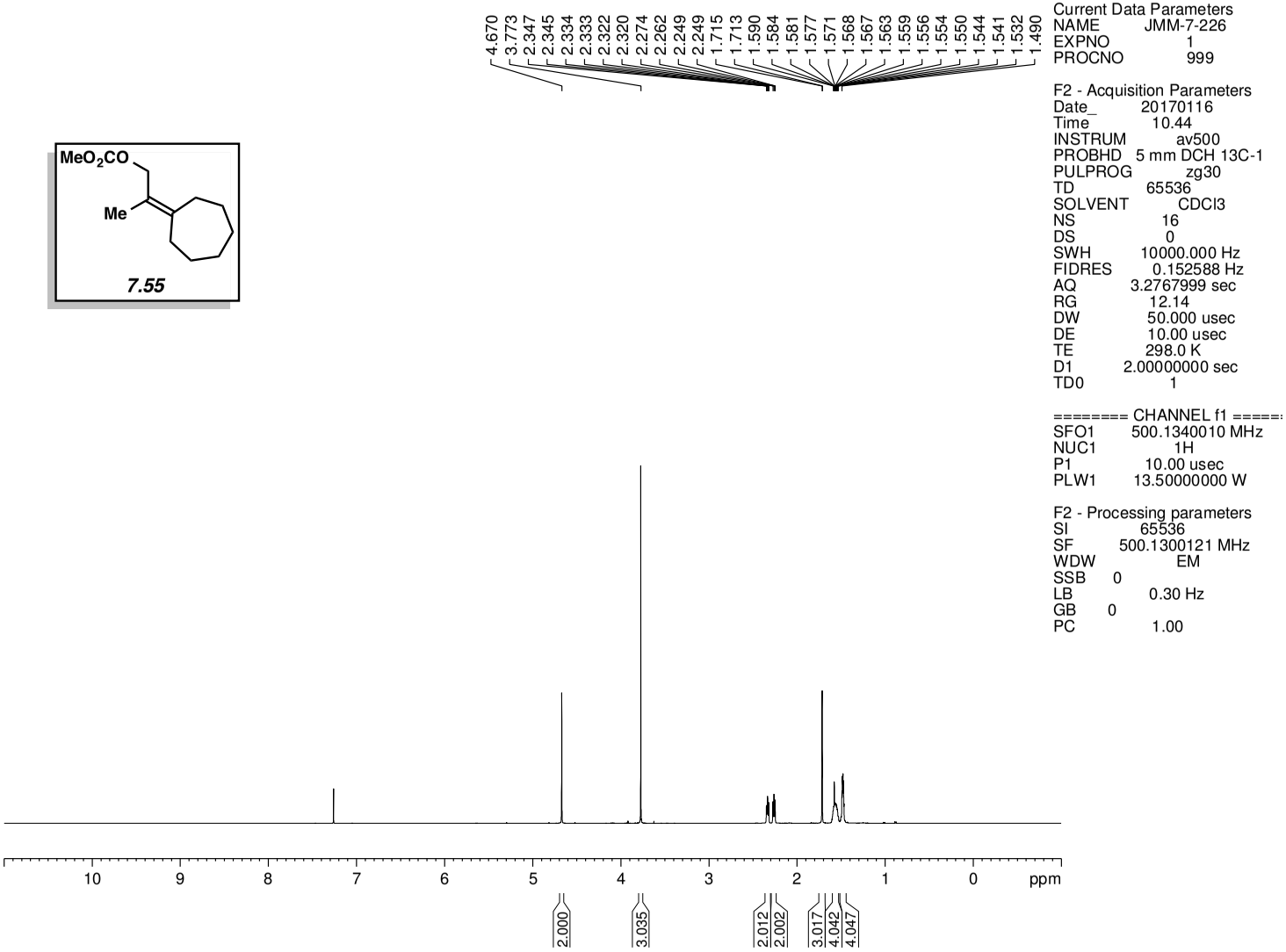

Figure 7.51 ^{1}H NMR (500 MHz, $CDCl_3$) of compound **7.55**

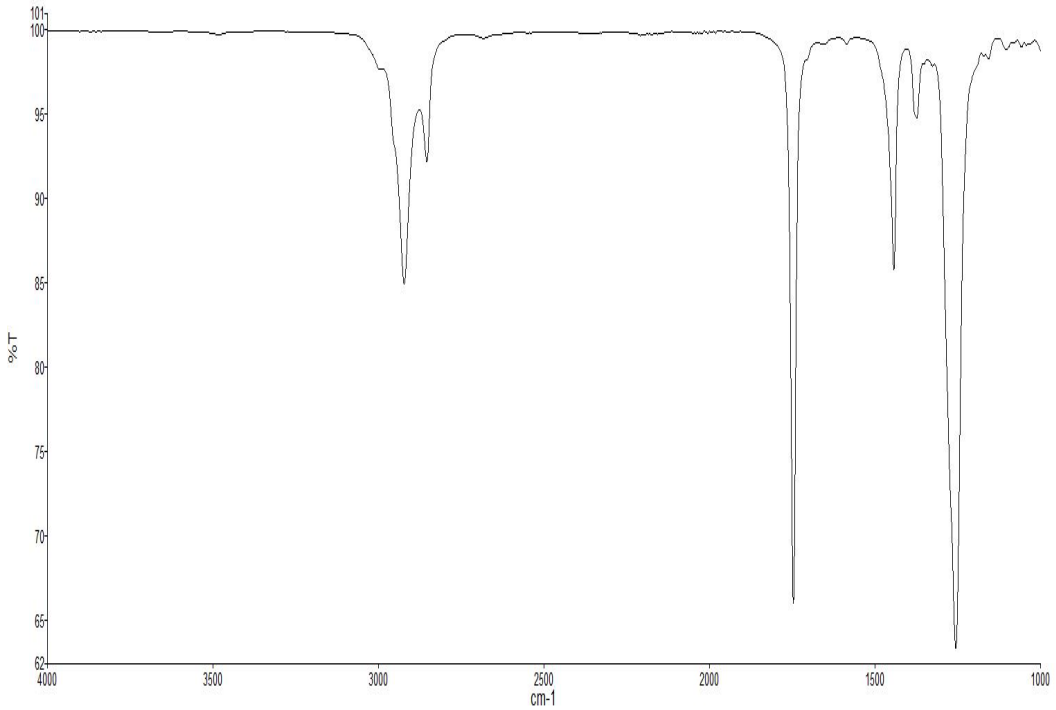

Figure 7.52 Infrared spectrum of compound **7.55**

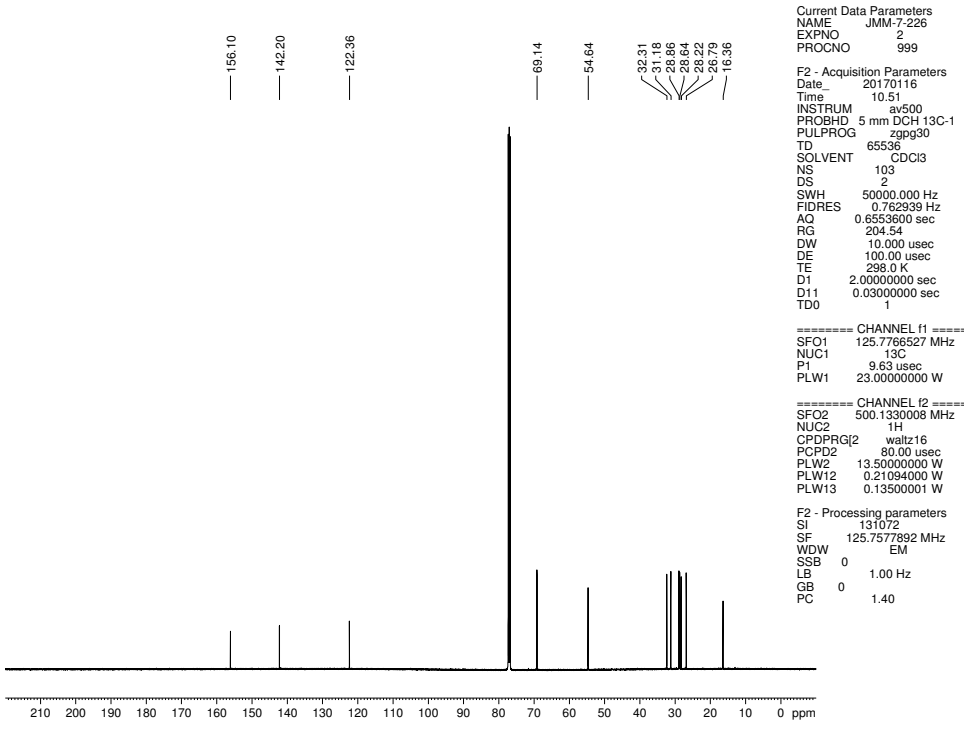

Figure 7.53 ^{13}C NMR (125 MHz, $CDCl_3$) of compound **7.55**

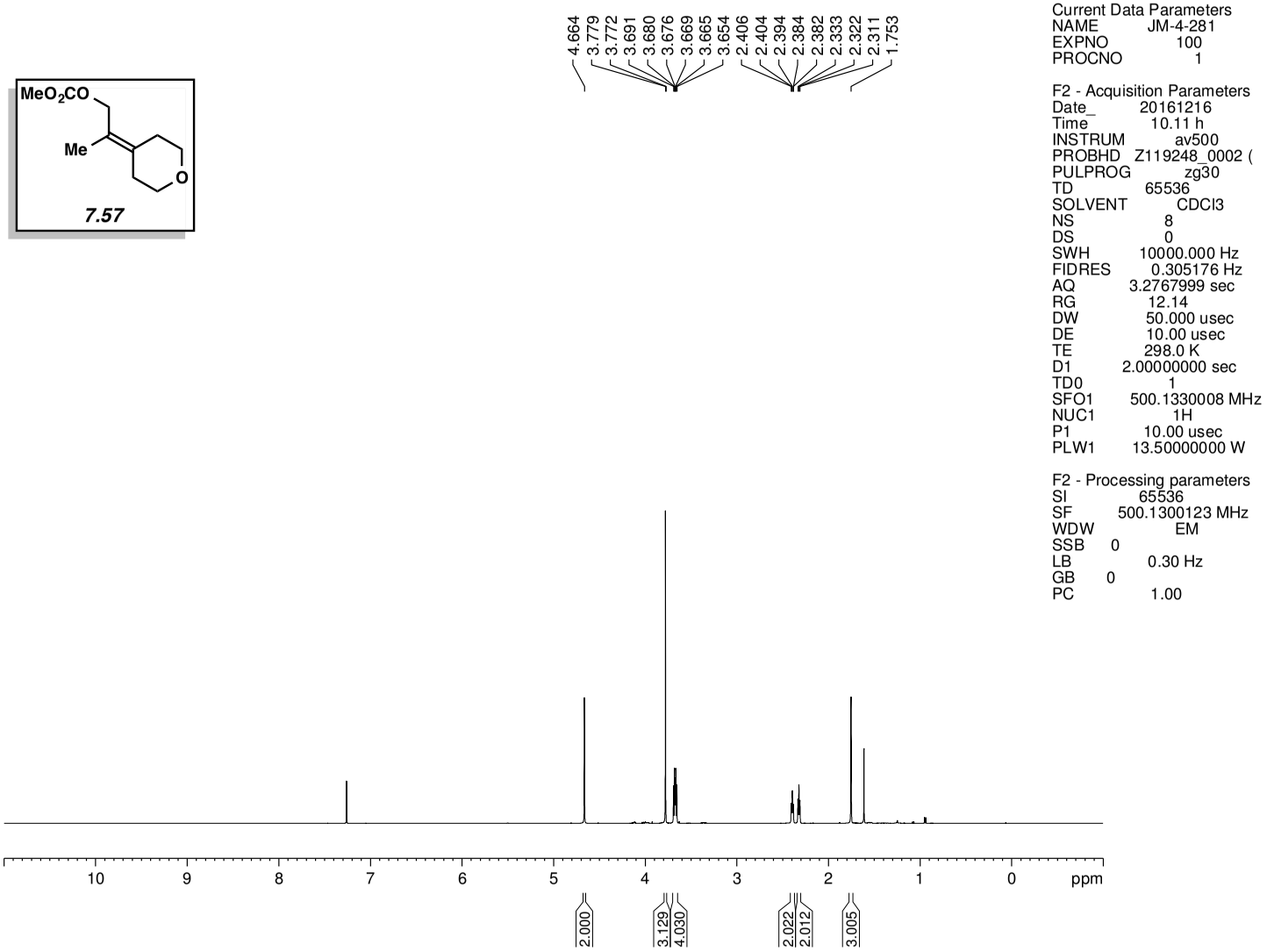

Figure 7.54 ^{1}H NMR (500 MHz, $CDCl_3$) of compound **7.57**

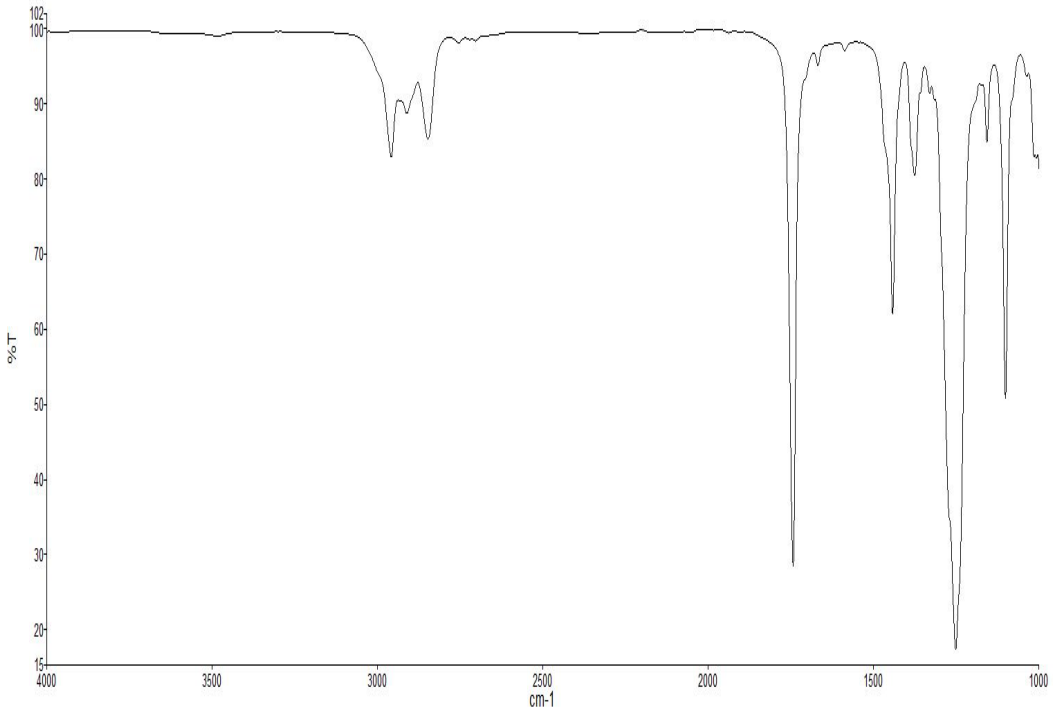

Figure 7.55 Infrared spectrum of compound **7.57**

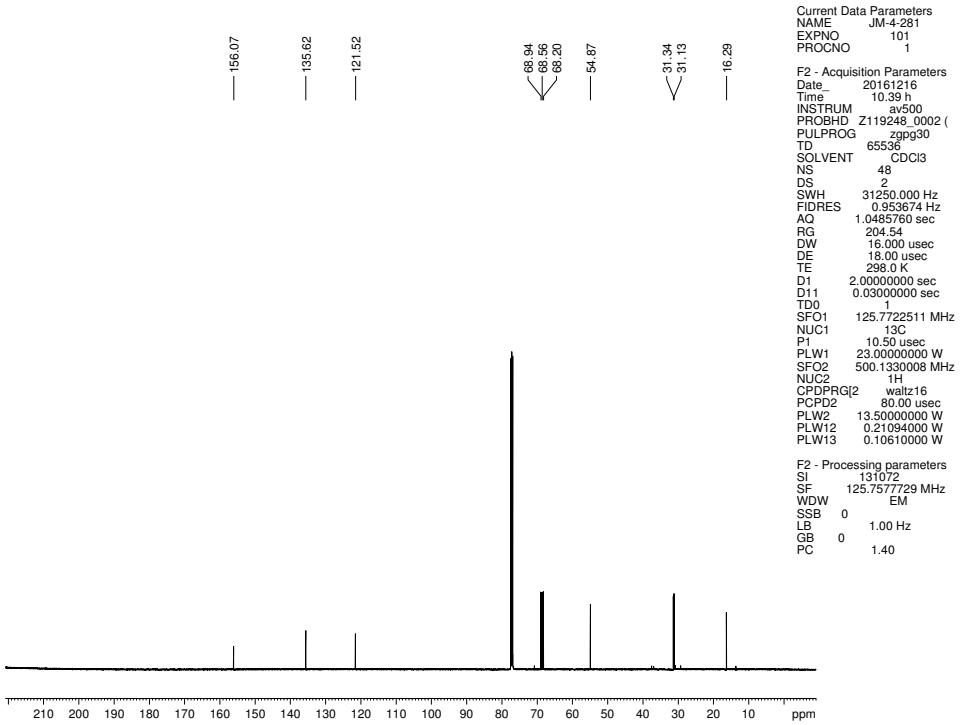

Figure 7.56 ^{13}C NMR (125 MHz, $CDCl_3$) of compound **7.57**

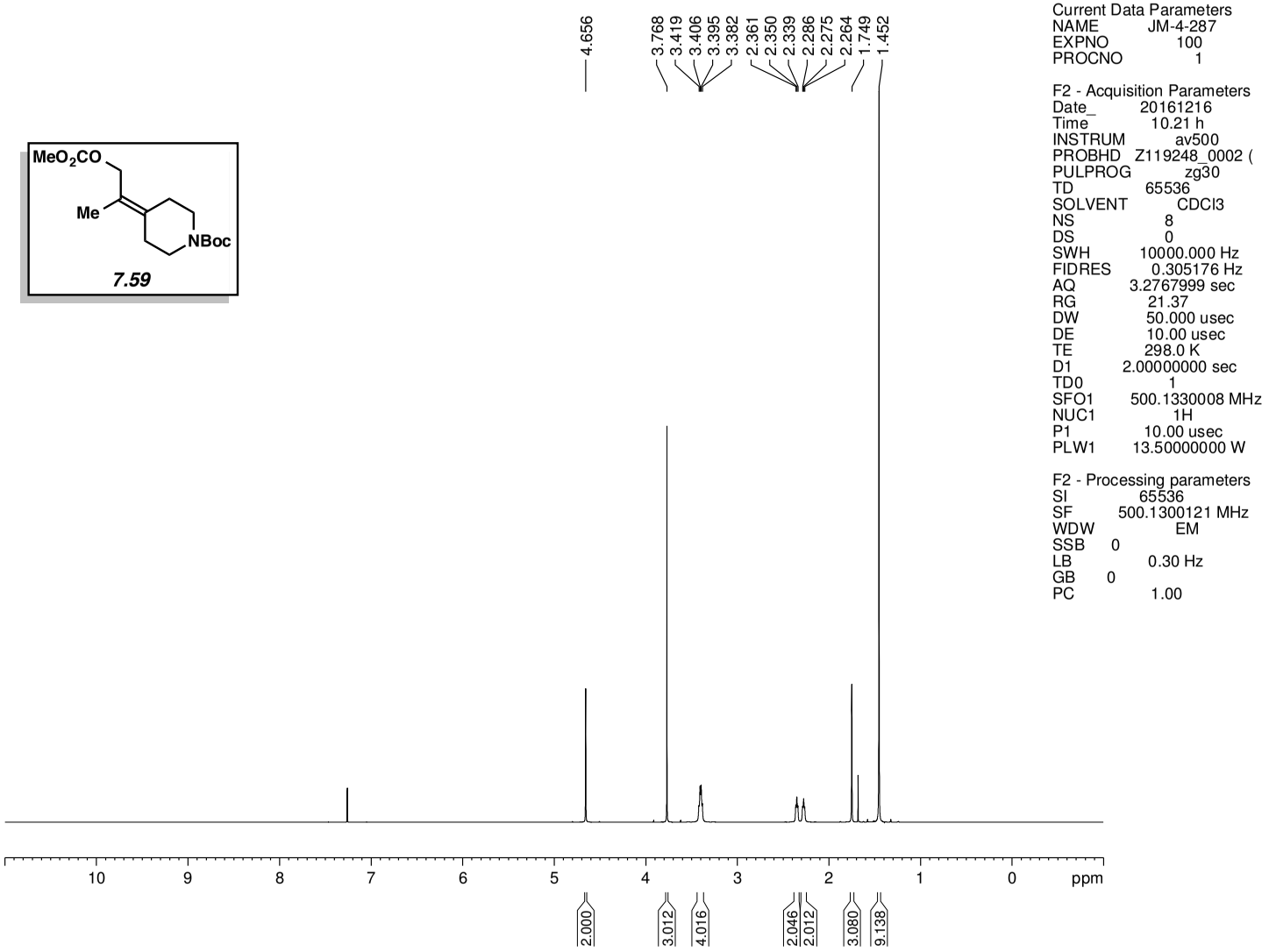

Figure 7.57 ^{1}H NMR (500 MHz, $CDCl_3$) of compound **7.59**

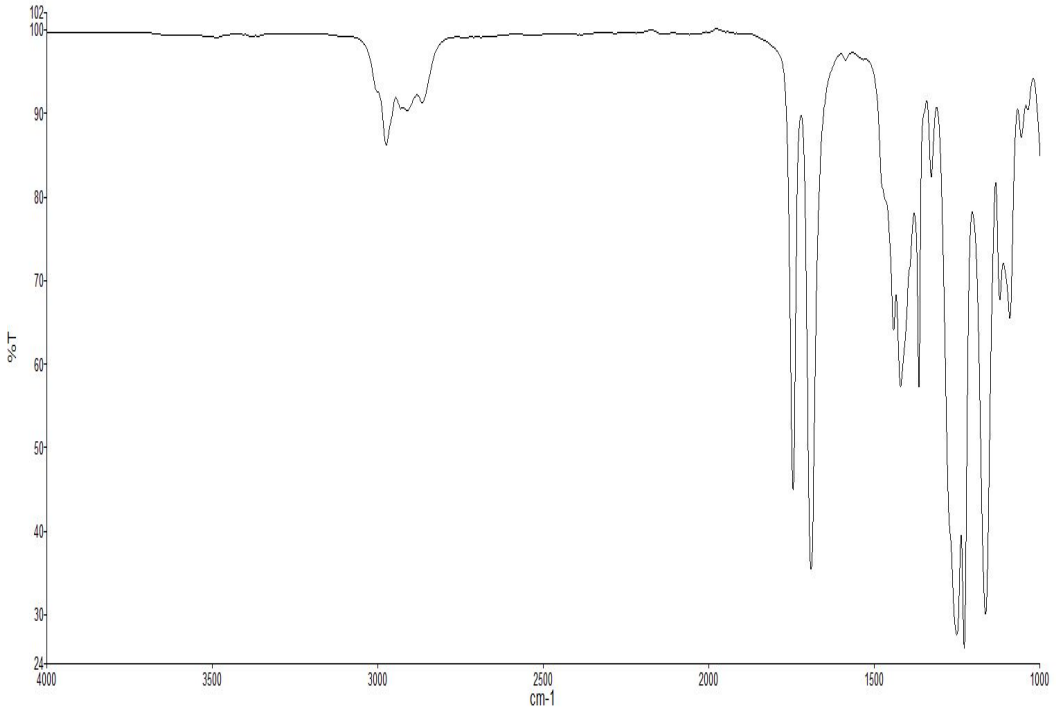

Figure 7.58 Infrared spectrum of compound **7.59**

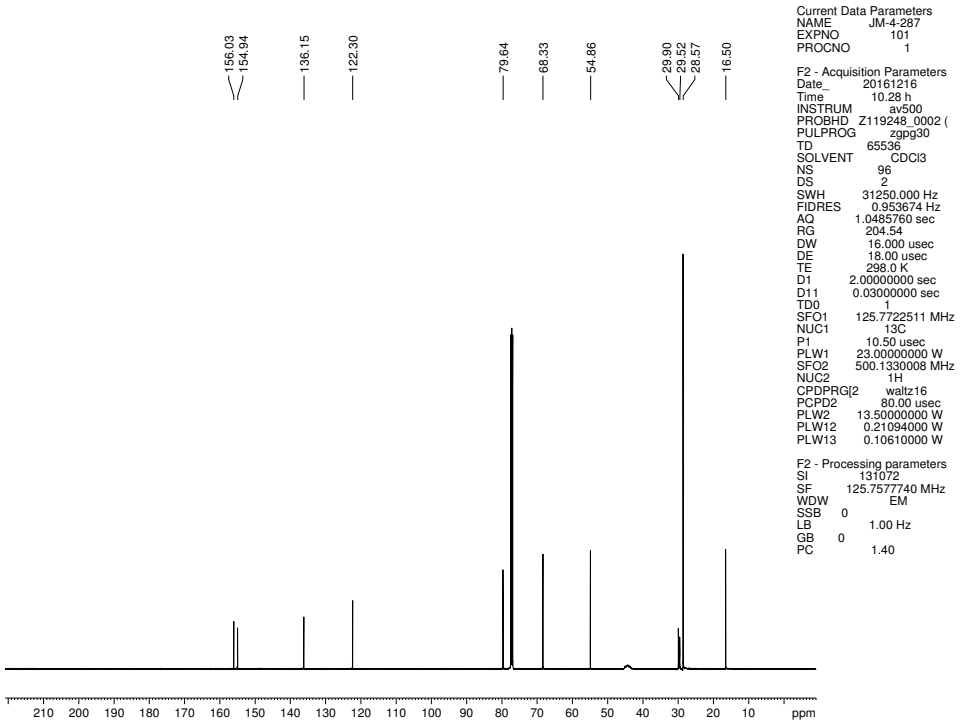

Figure 7.59 ^{13}C NMR (125 MHz, $CDCl_3$) of compound **7.59**

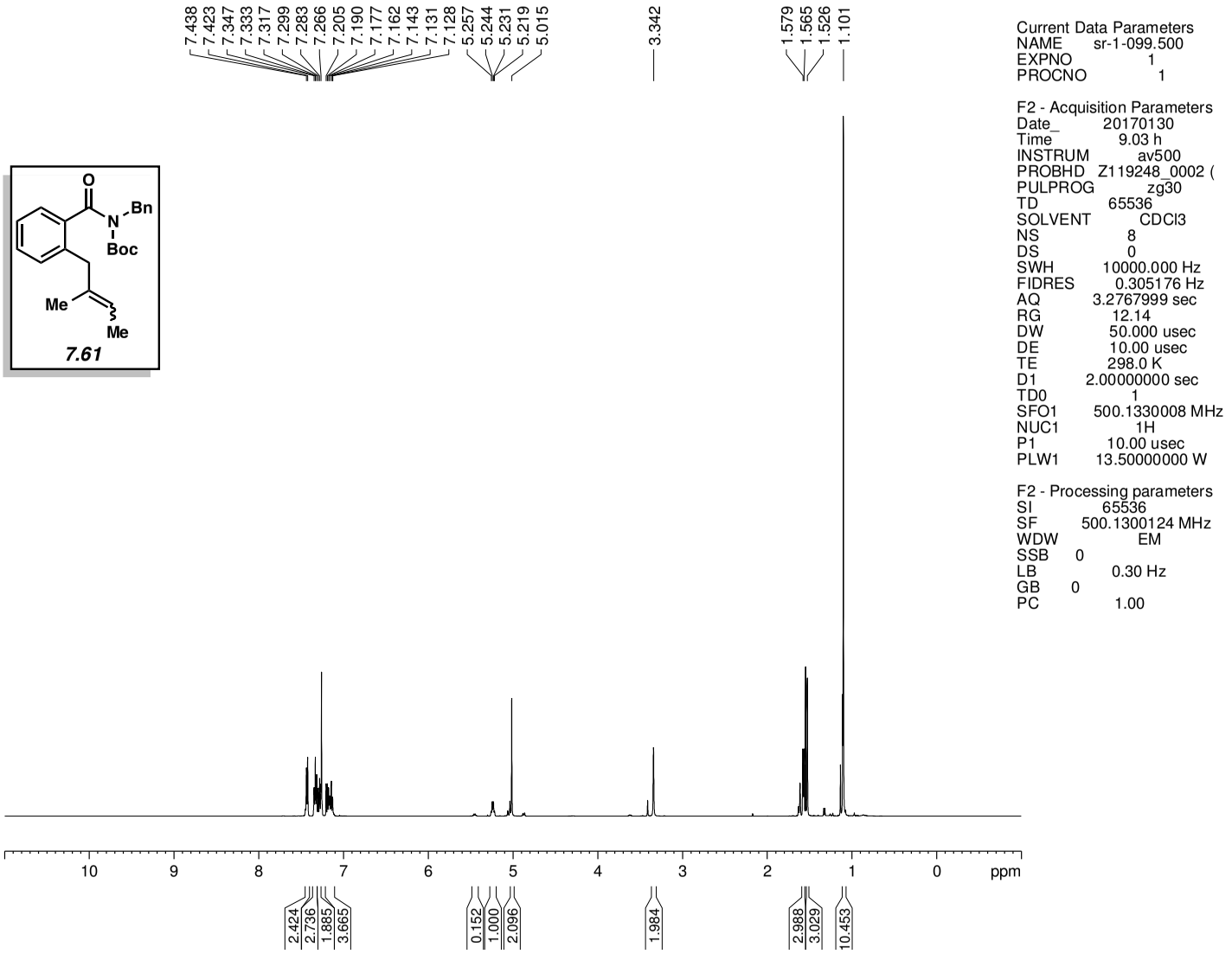

Figure 7.60 ^{1}H NMR (500 MHz, $CDCl_3$) of compound **7.61**

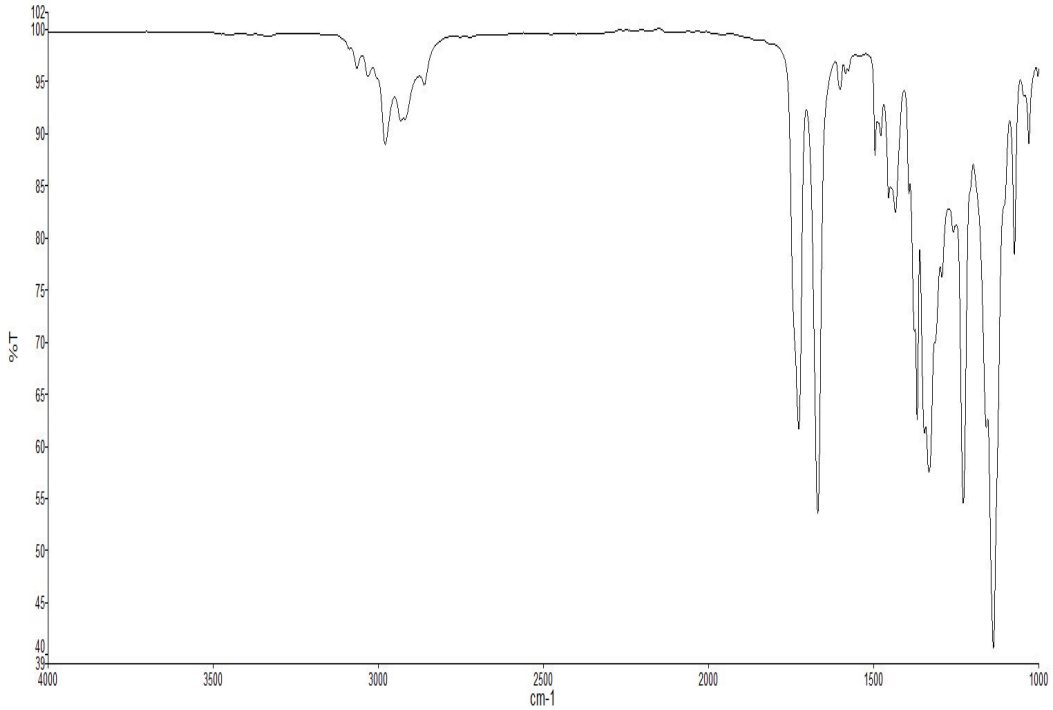

Figure 7.61 Infrared spectrum of compound **7.61**

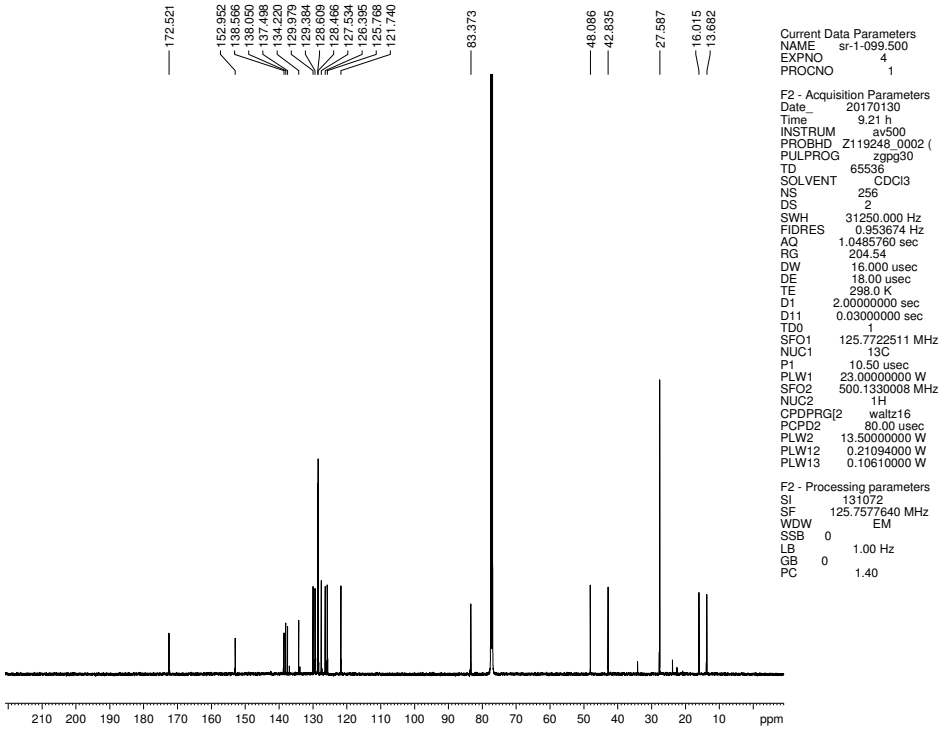

Figure 7.62 ^{13}C NMR (125 MHz, $CDCl_3$) of compound **7.61**

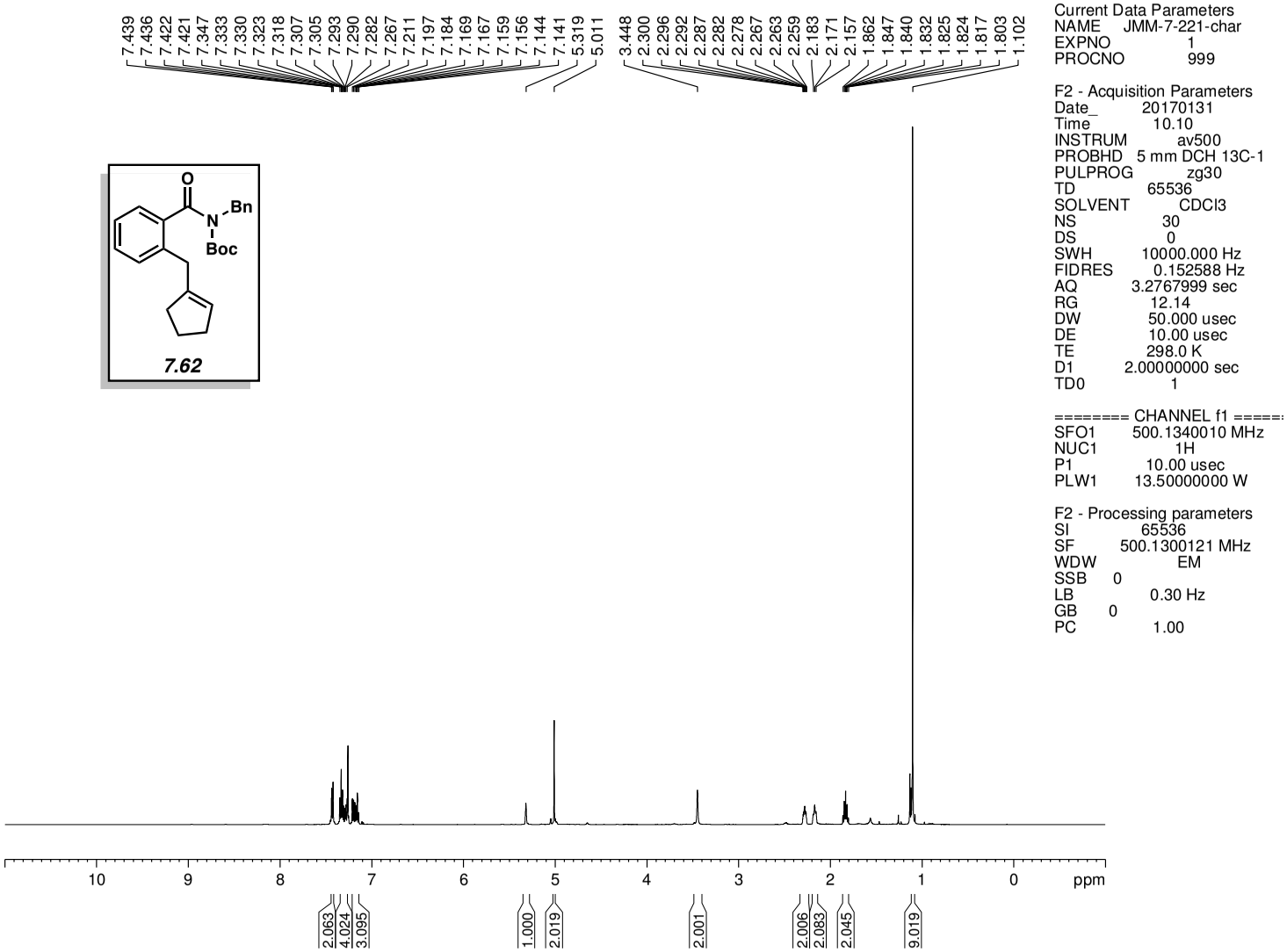

Figure 7.63 ^{1}H NMR (500 MHz, $CDCl_3$) of compound **7.62**

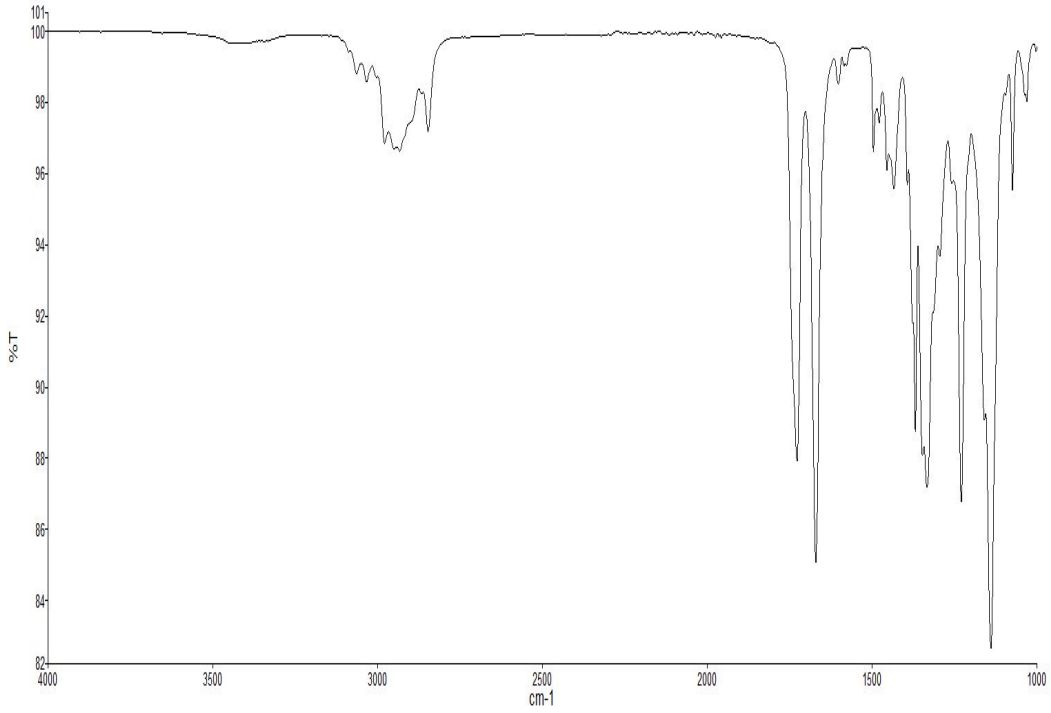

Figure 7.64 Infrared spectrum of compound **7.62**

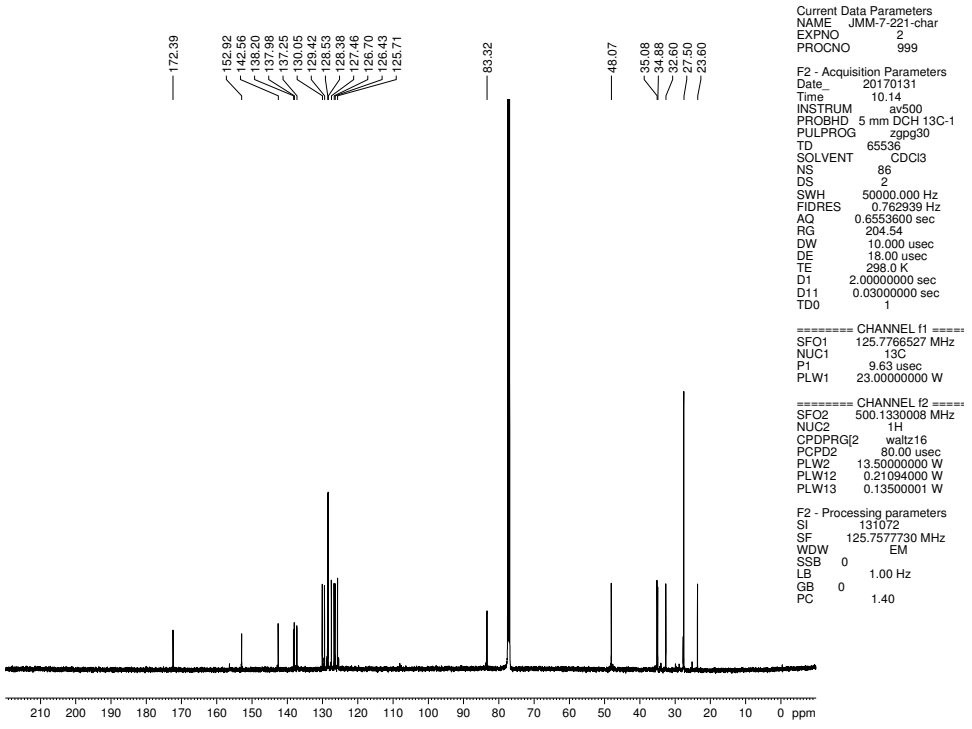

Figure 7.65 ^{13}C NMR (125 MHz, $CDCl_3$) of compound **7.62**

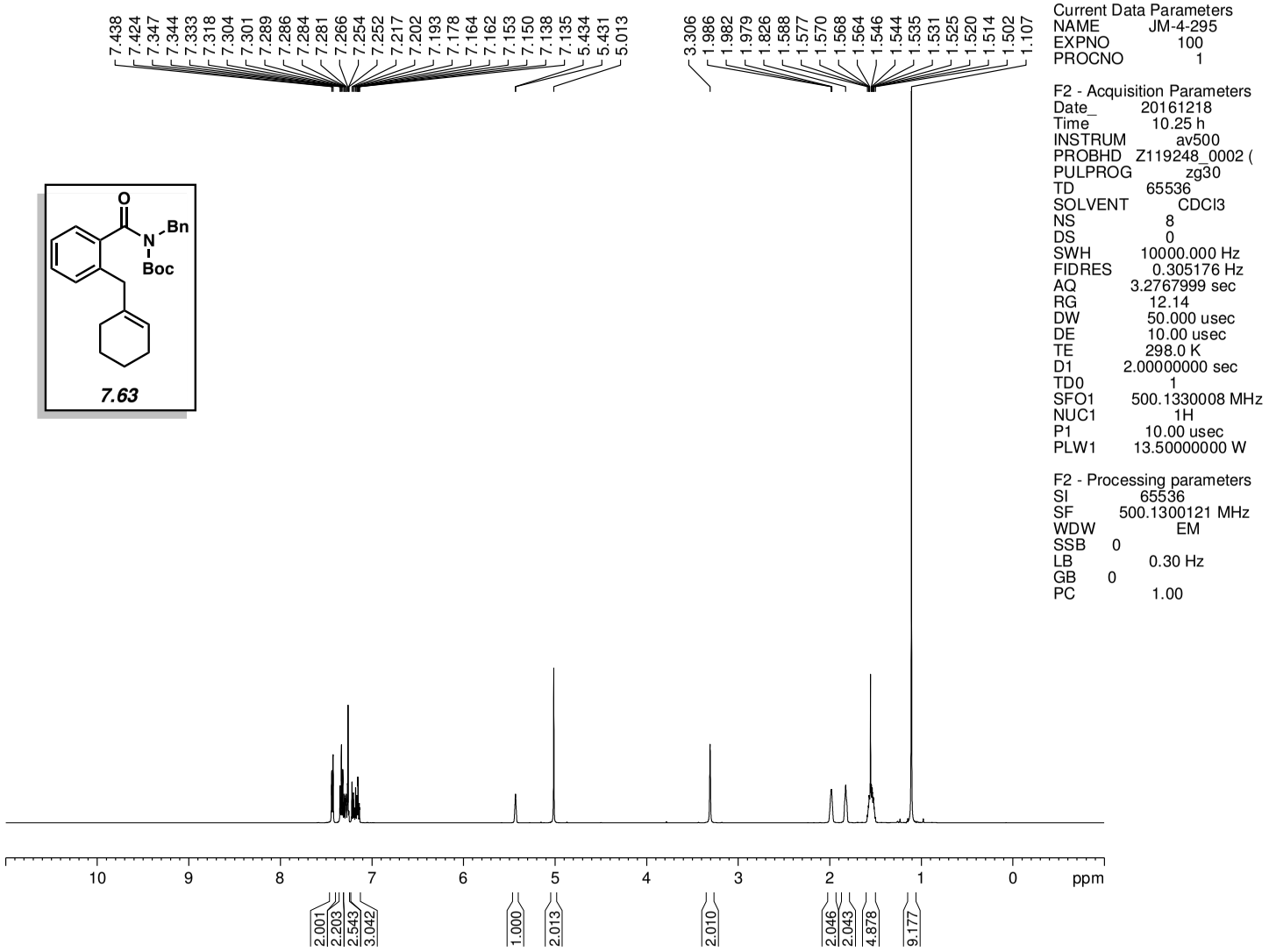

Figure 7.66 ^{1}H NMR (500 MHz, $CDCl_3$) of compound **7.63**

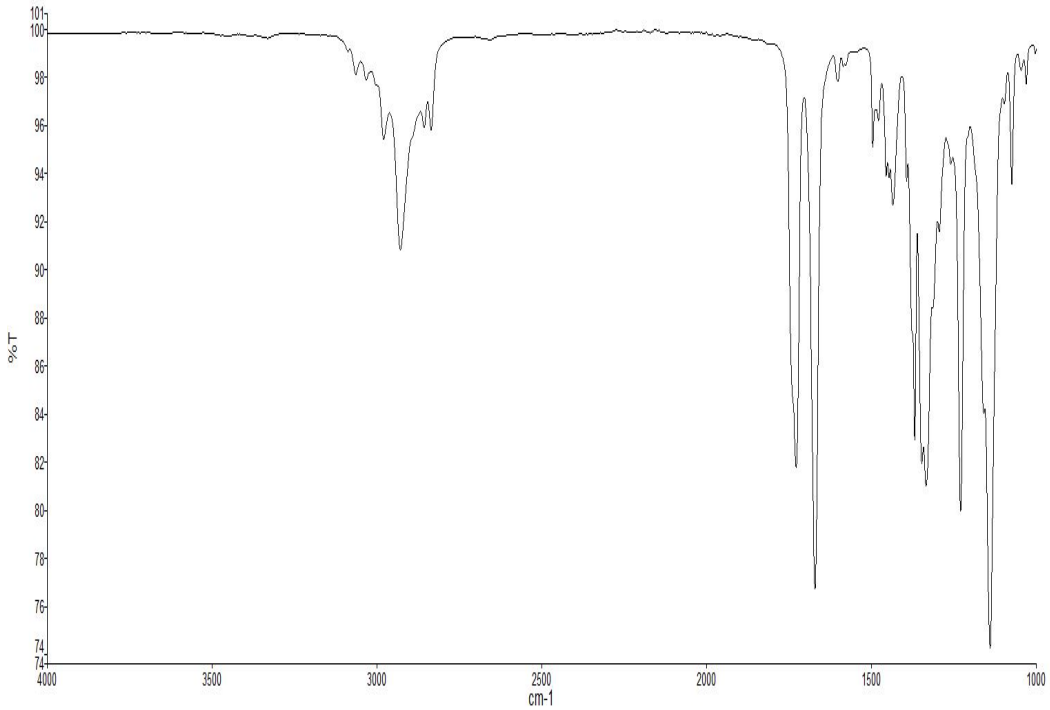

Figure 7.67 Infrared spectrum of compound **7.63**

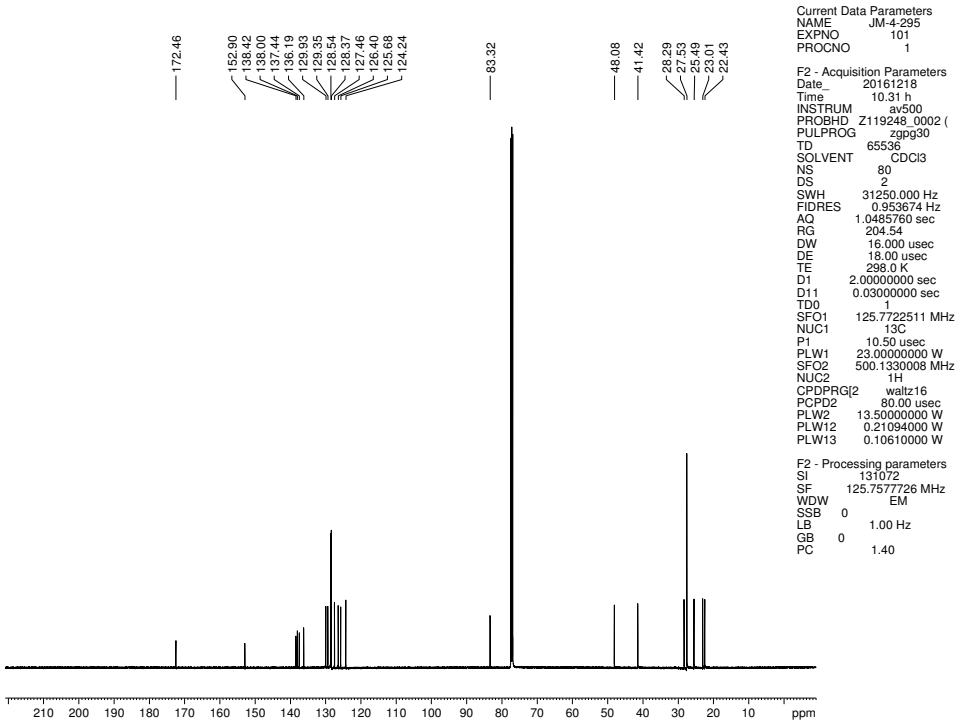

Figure 7.68 ^{13}C NMR (125 MHz, $CDCl_3$) of compound **7.63**

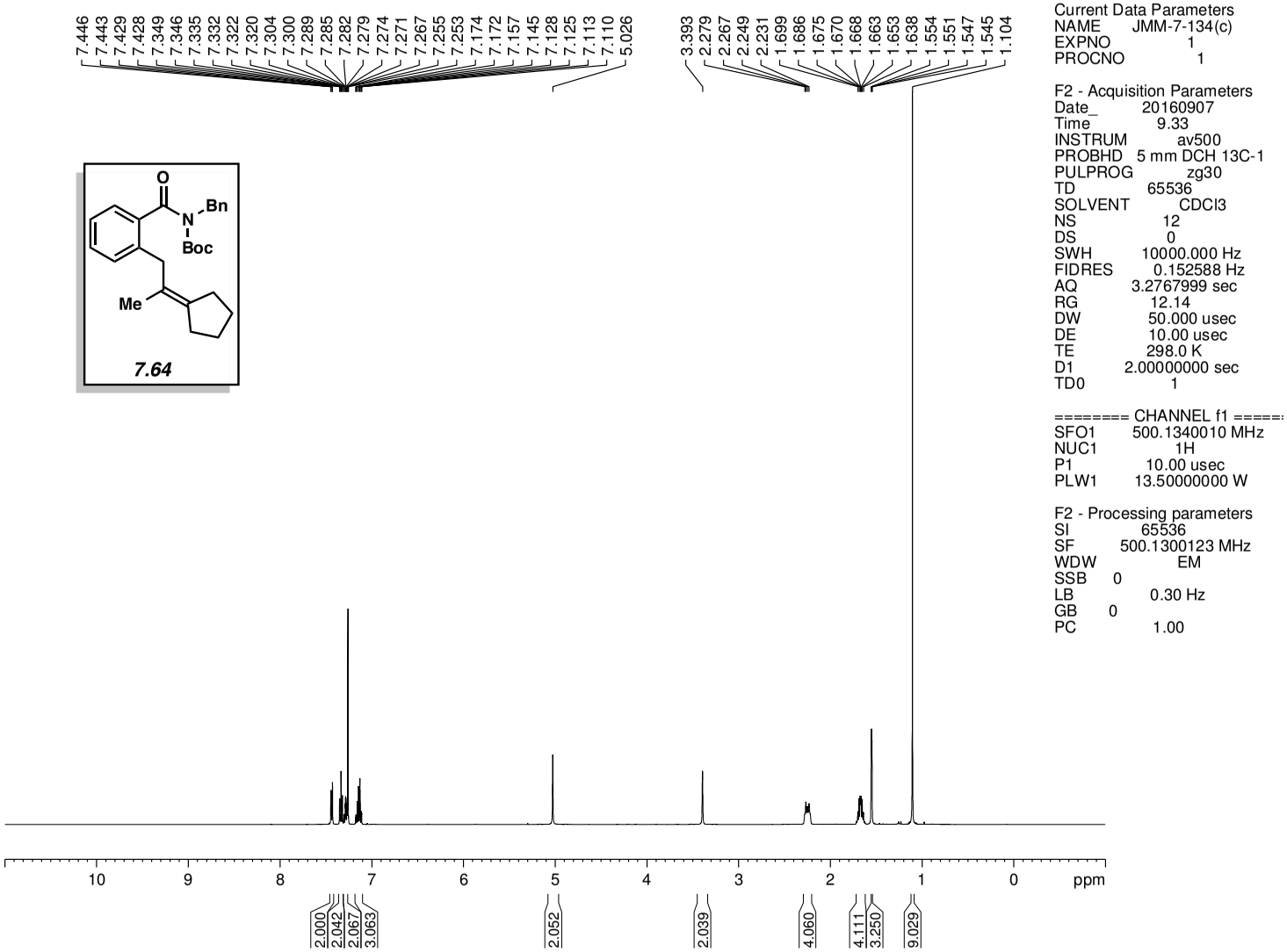

Figure 7.69 ^{1}H NMR (500 MHz, $CDCl_3$) of compound **7.64**

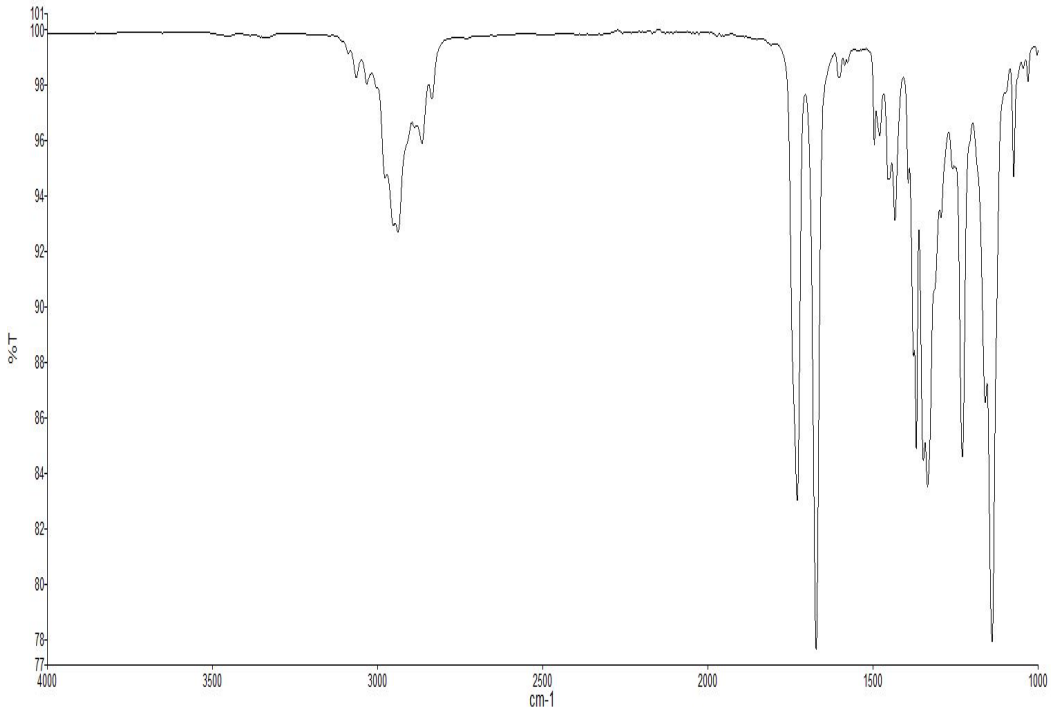

Figure 7.70 Infrared spectrum of compound **7.64**

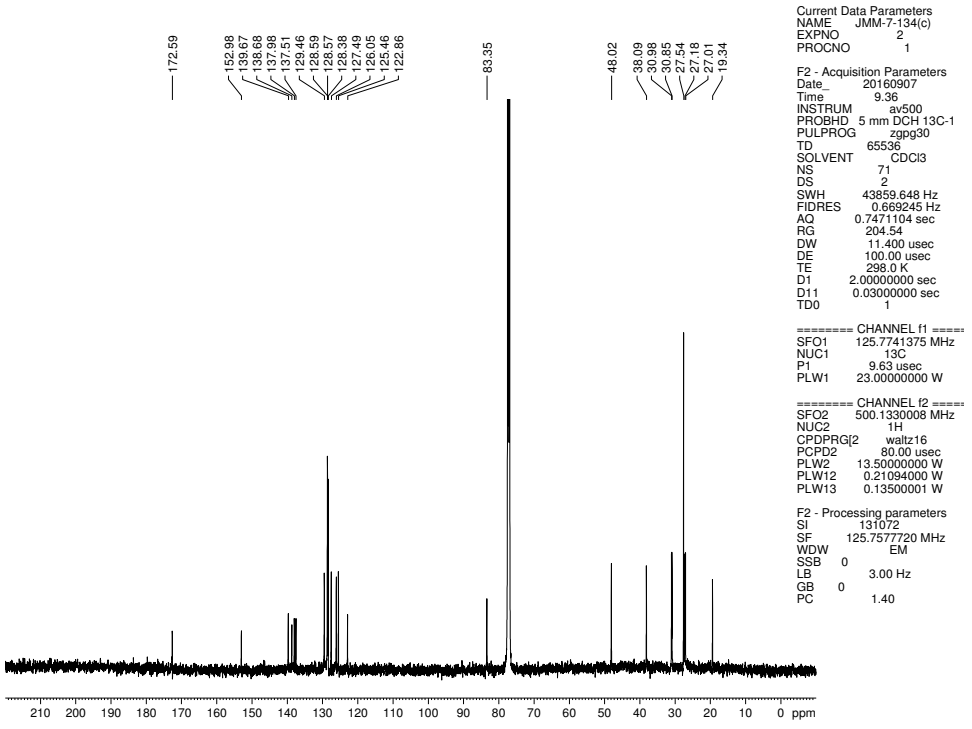

Figure 7.71 ^{13}C NMR (125 MHz, $CDCl_3$) of compound **7.64**

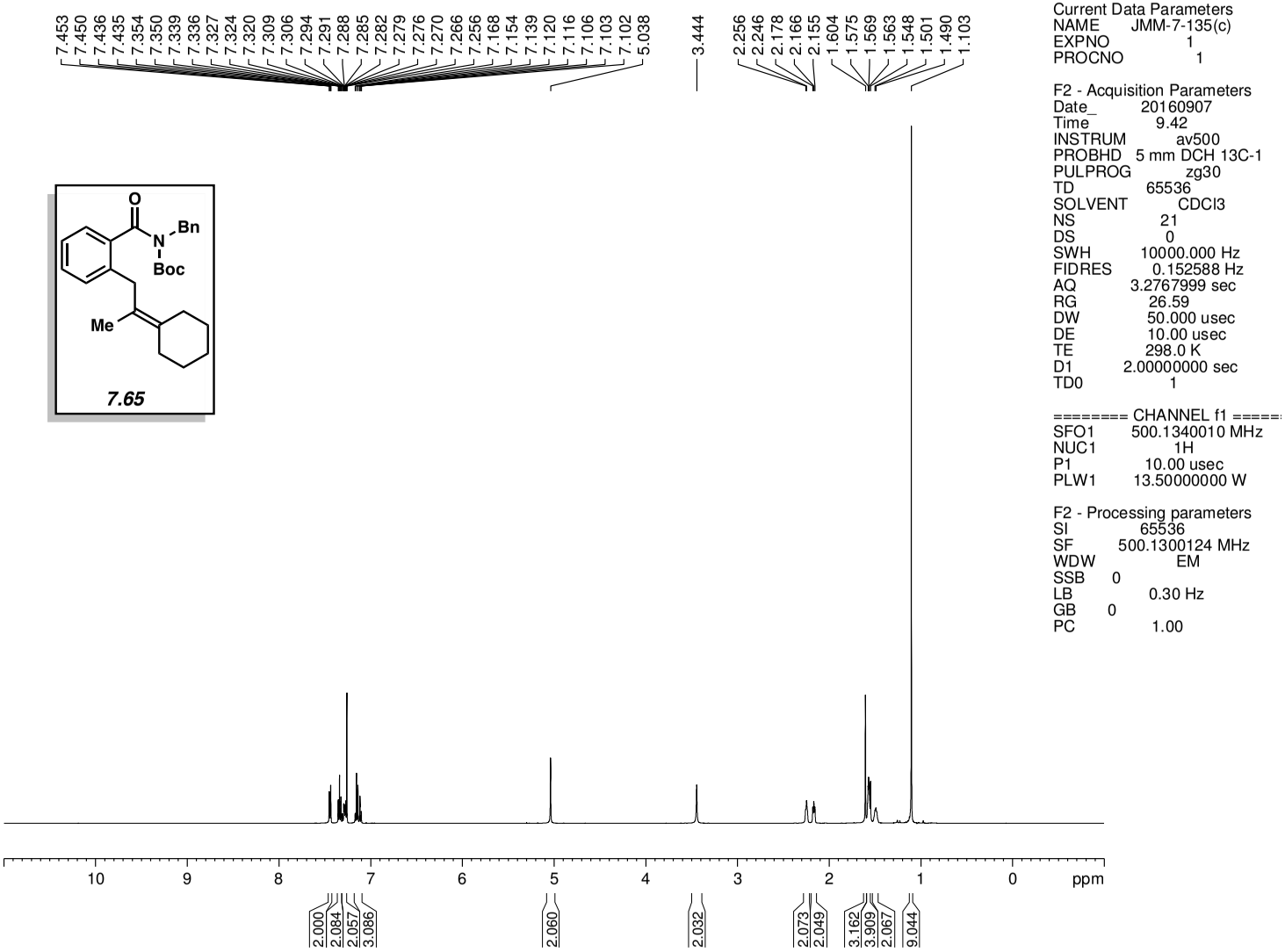

Figure 7.72 ^{1}H NMR (500 MHz, $CDCl_3$) of compound **7.65**

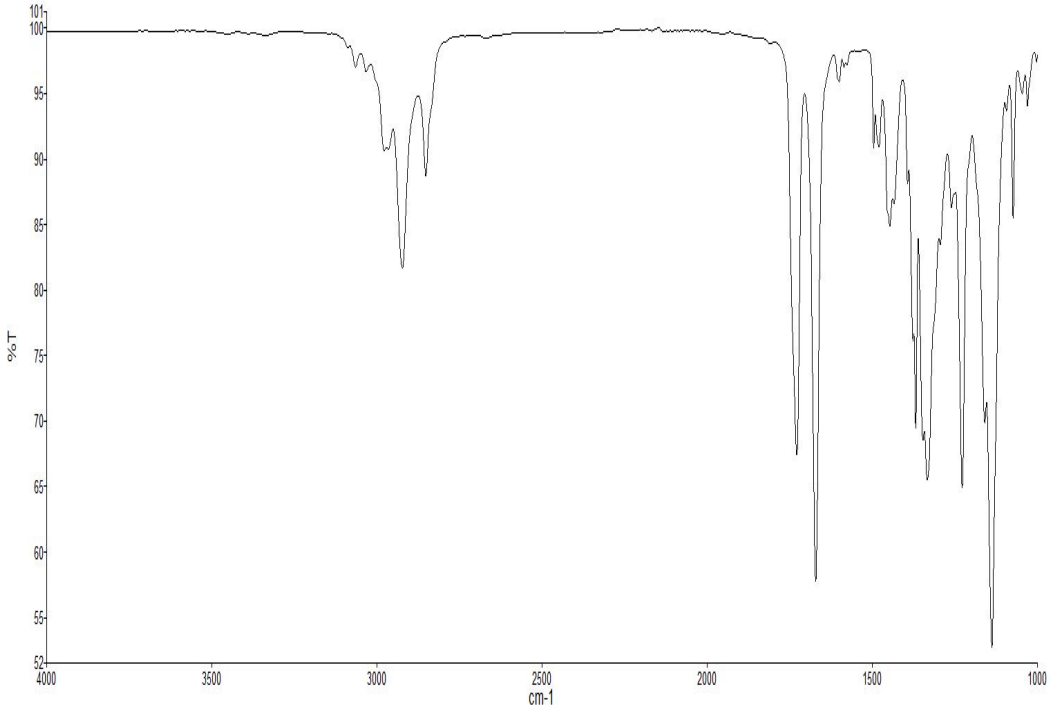

Figure 7.73 Infrared spectrum of compound **7.65**

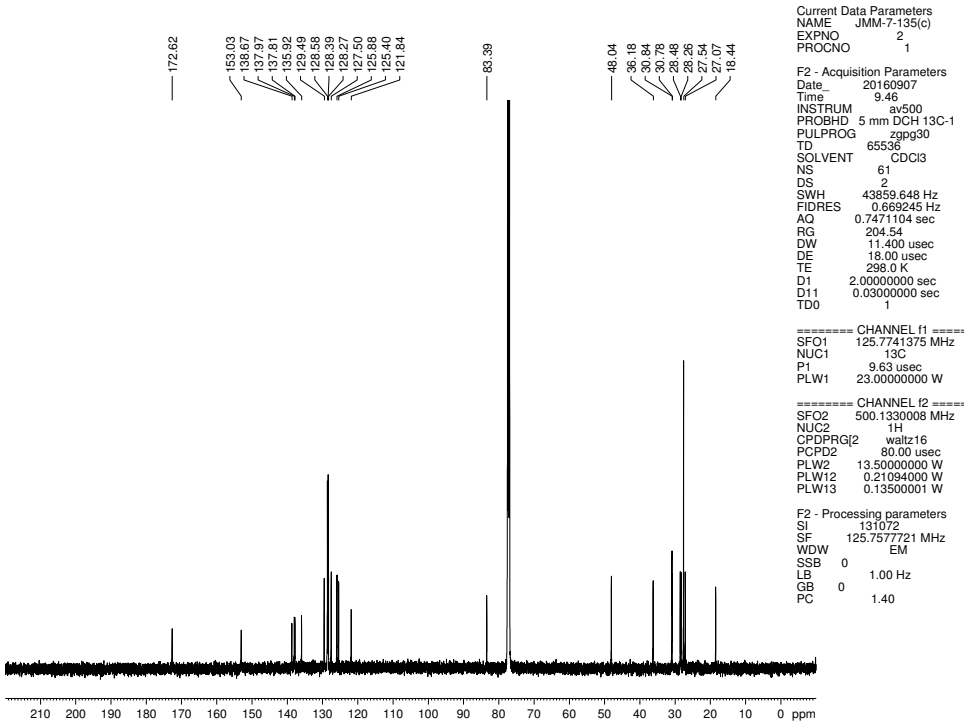

Figure 7.74 ^{13}C NMR (125 MHz, $CDCl_3$) of compound **7.65**

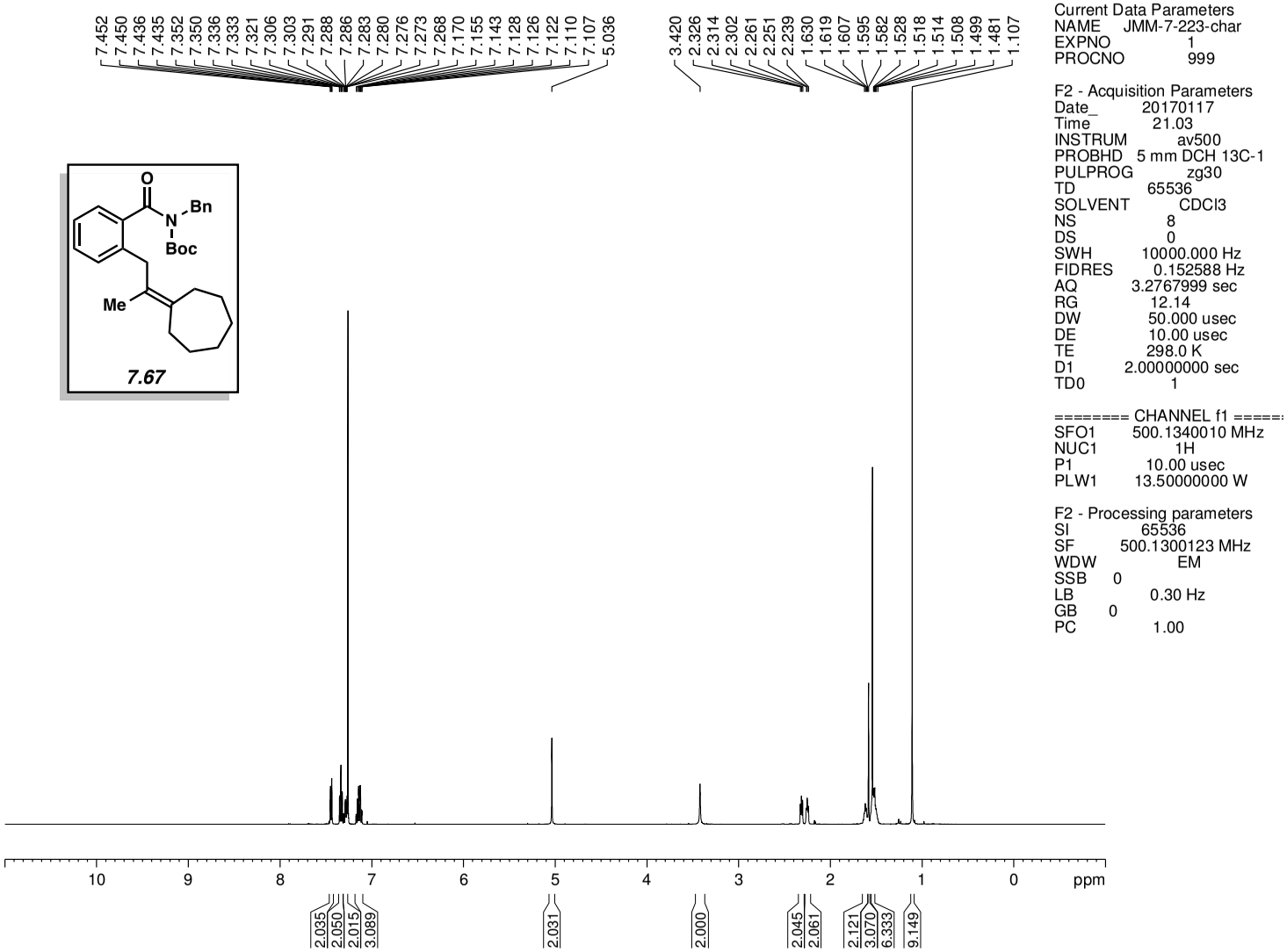

Figure 7.75 ^{1}H NMR (500 MHz, $CDCl_3$) of compound **7.67**

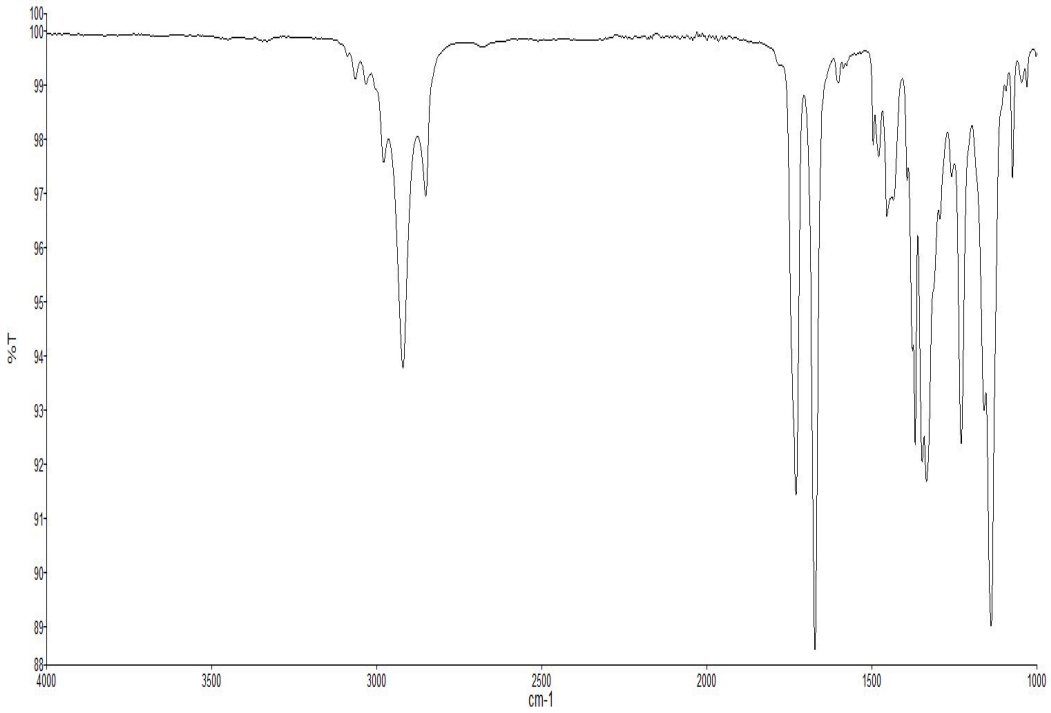

Figure 7.76 Infrared spectrum of compound **7.67**

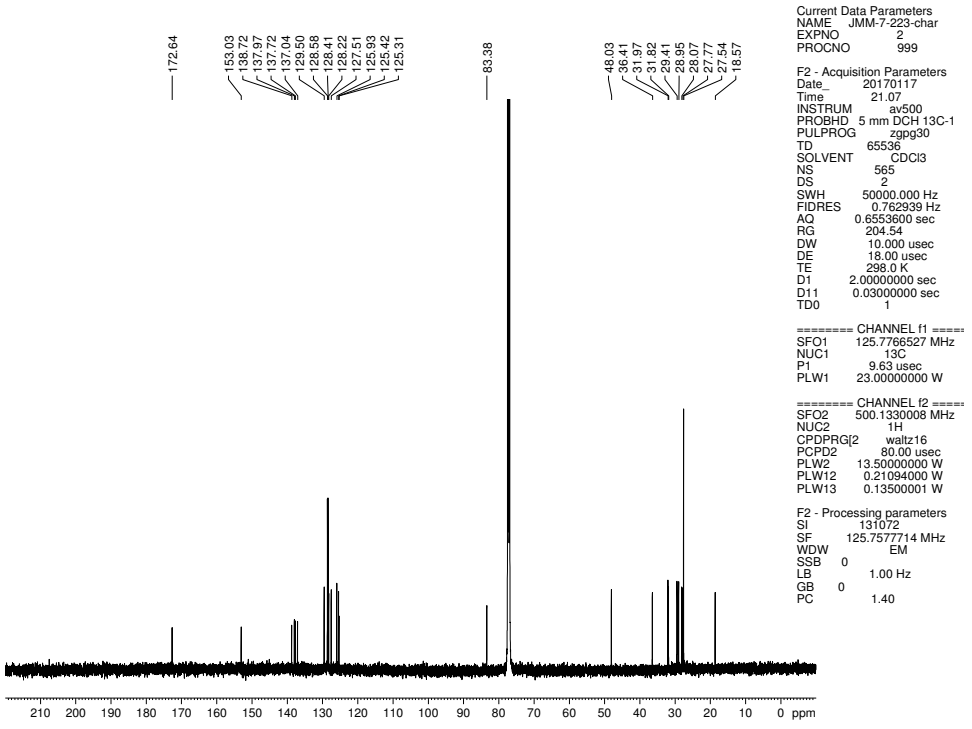

Figure 7.77 ^{13}C NMR (125 MHz, $CDCl_3$) of compound **7.67**

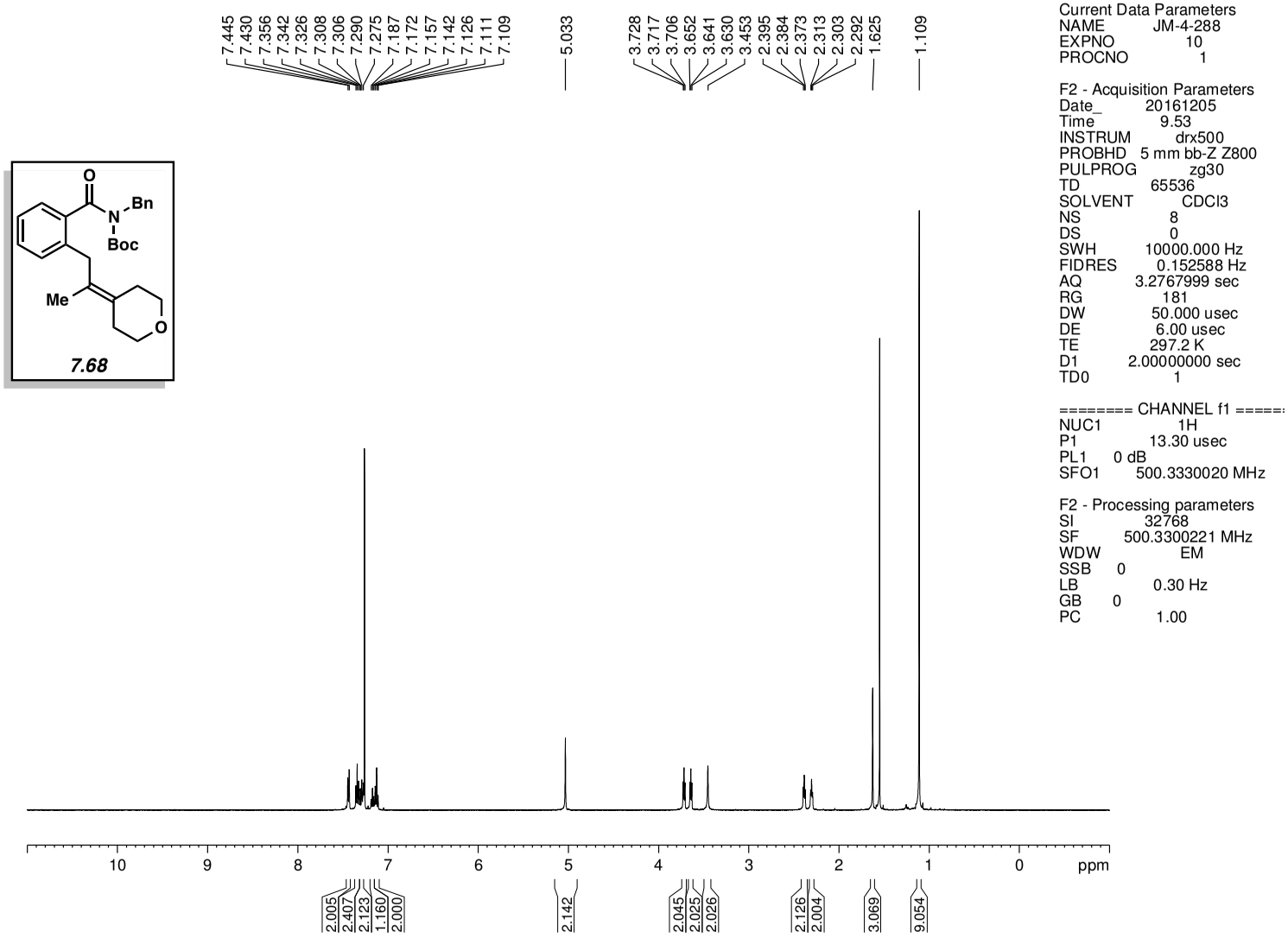

Figure 7.78 ^{1}H NMR (500 MHz, $CDCl_3$) of compound **7.68**

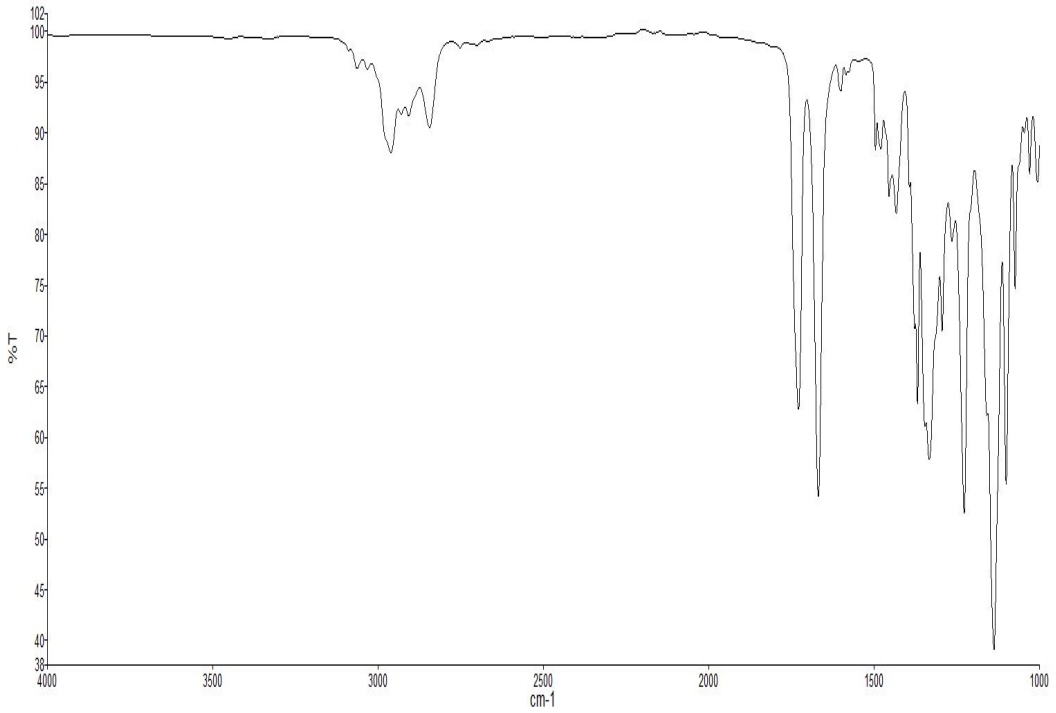

Figure 7.79 Infrared spectrum of compound **7.68**

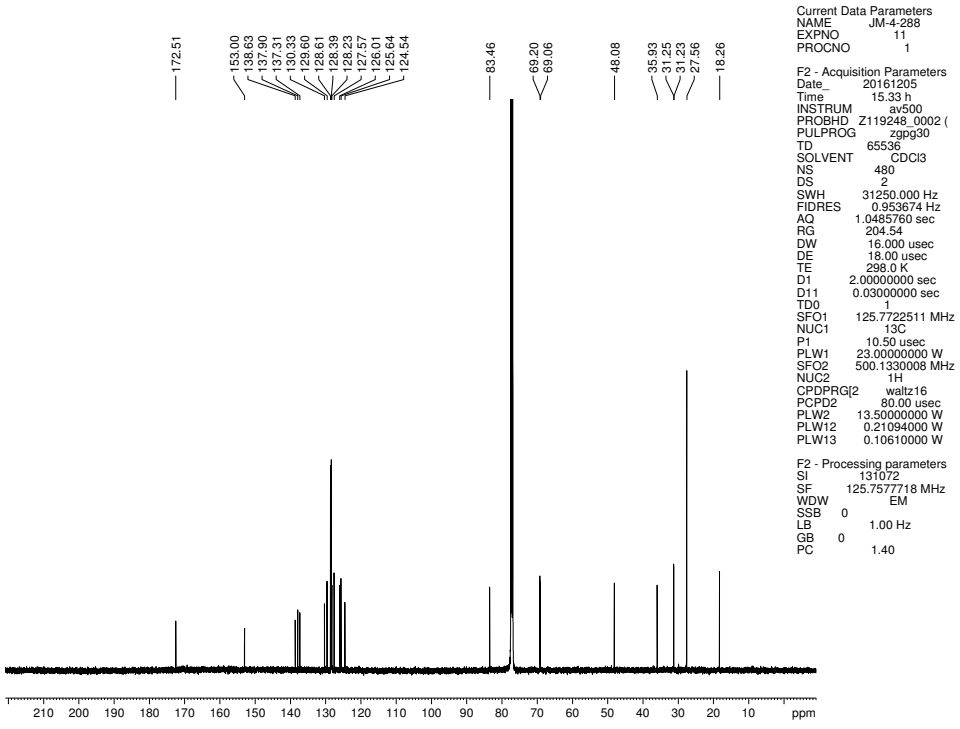

Figure 7.80 ^{13}C NMR (125 MHz, $CDCl_3$) of compound **7.68**

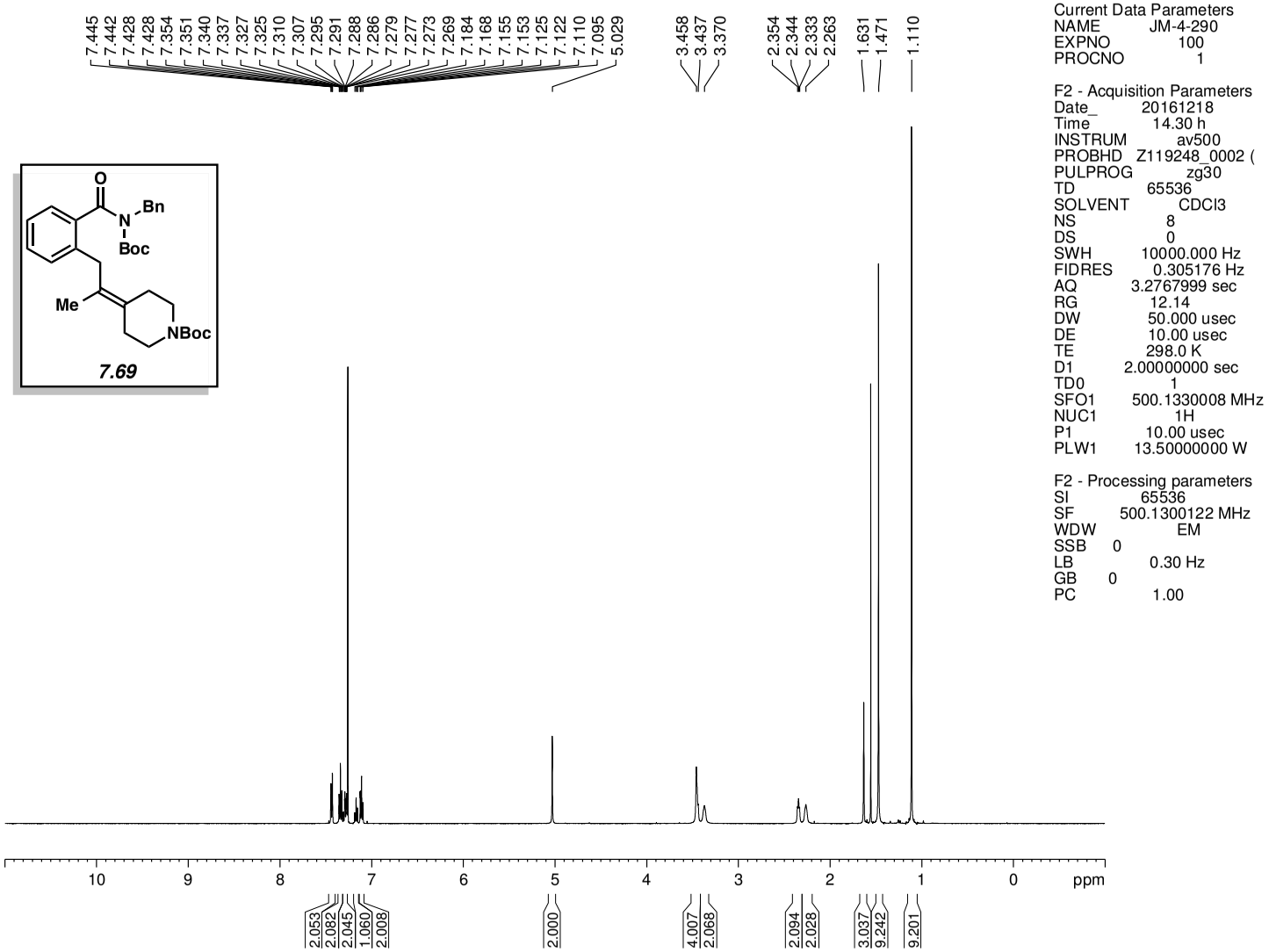

Figure 7.81 ^{1}H NMR (500 MHz, $CDCl_3$) of compound **7.69**

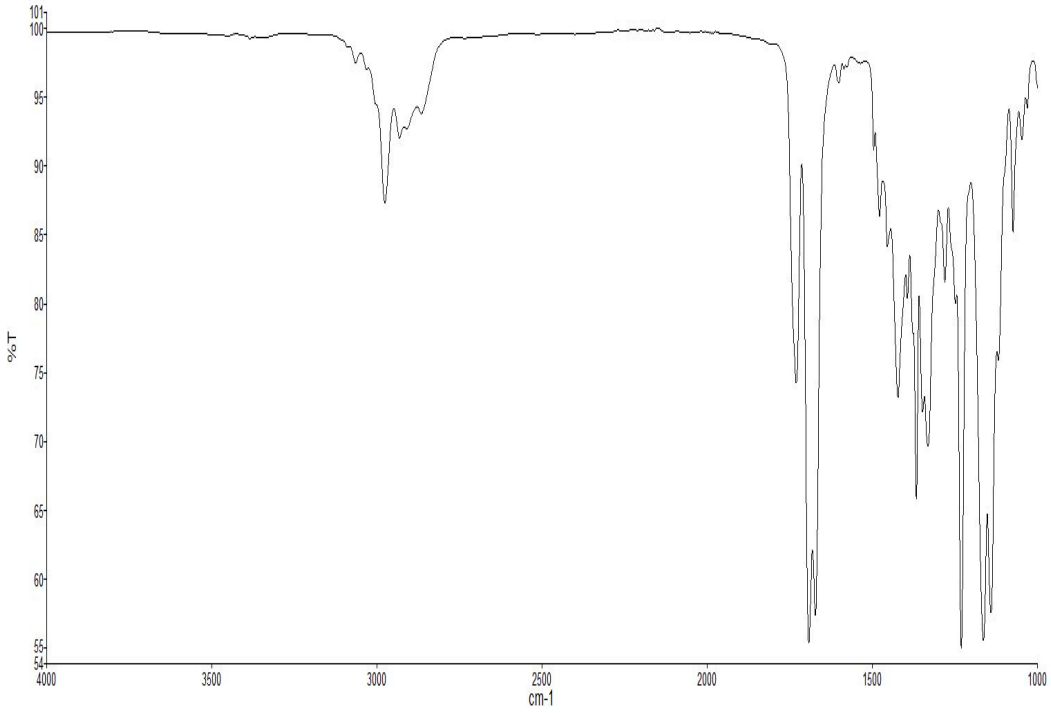

Figure 7.82 Infrared spectrum of compound **7.69**

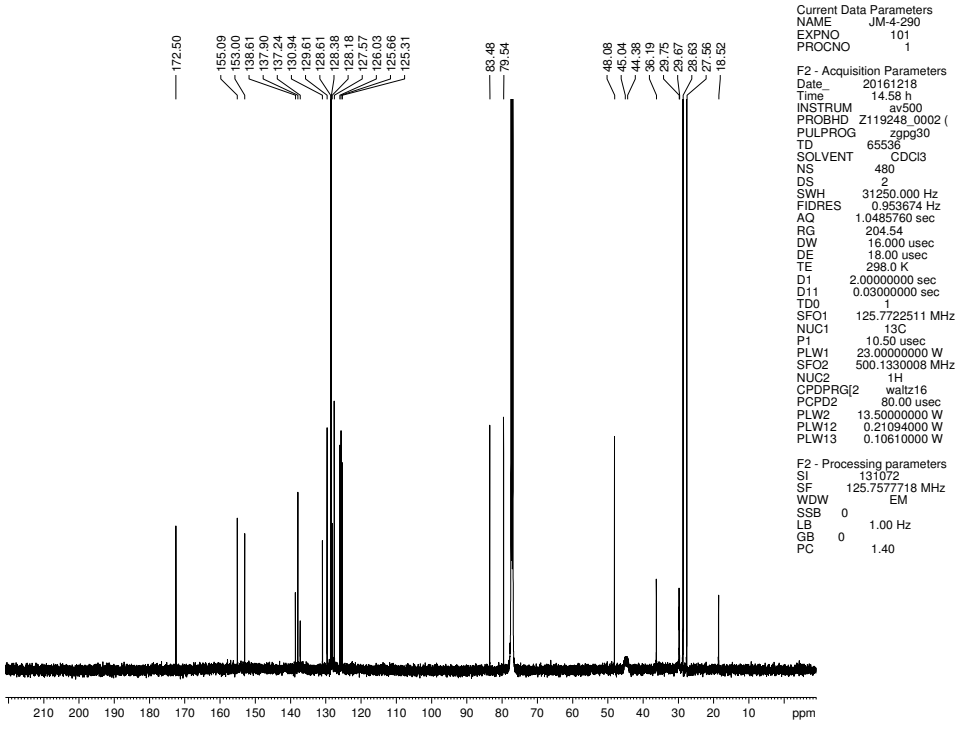

Figure 7.83 ^{13}C NMR (125 MHz, $CDCl_3$) of compound **7.69**

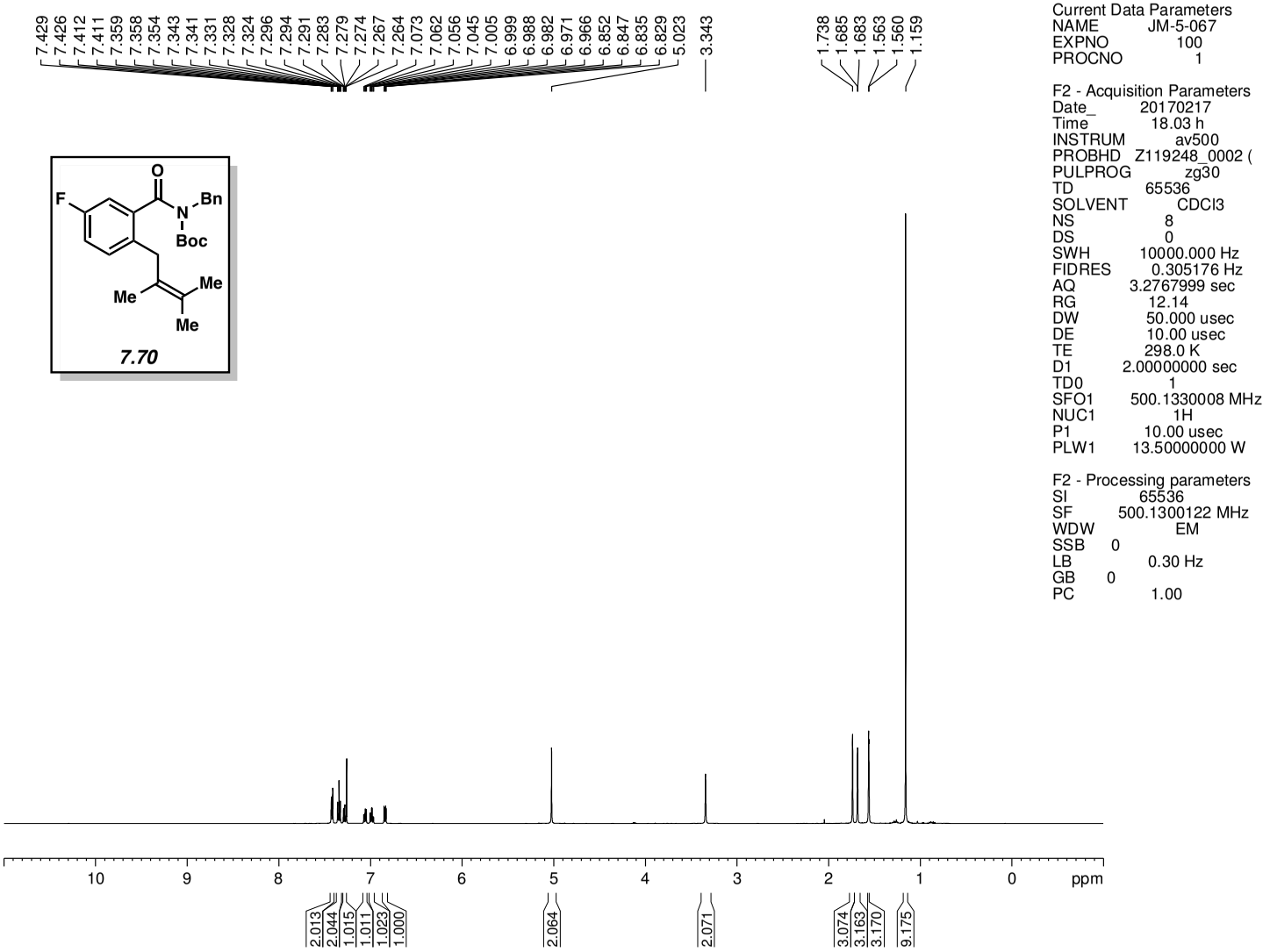

Figure 7.84 ^{1}H NMR (500 MHz, $CDCl_3$) of compound **7.70**

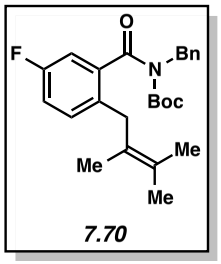

Current Data Parameters
NAME JM-5-067
EXPNO 140
PROCNO 1

F2 - Acquisition Parameters
Date_ 20170313
Time 13.39
INSTRUM av400
PROBHD 5 mm PABBO BB/
PULPROG zgfhigqn.2
TD 262144
SOLVENT CDCl3
NS 48
DS 0
SWH 150000.000 Hz
FIDRES 0.572205 Hz
AQ 0.8738133 sec
RG 189.85
DW 3.333 usec
DE 6.50 usec
TE 299.0 K
D1 1.00000000 sec
D11 0.03000000 sec
D12 0.00002000 sec
TD0 1

======== CHANNEL f1 =====
SFO1 376.4983660 MHz
NUC1 19F
P1 14.50 usec
PLW1 17.00000000 W

======== CHANNEL f2 =====
SFO2 400.1324008 MHz
NUC2 1H
CPDPRG[2 waltz16
PCPD2 90.00 usec
PLW2 13.00000000 W
PLW12 0.36111000 W

F2 - Processing parameters
SI 262144
SF 376.4983660 MHz
WDW EM
SSB 0
LB 1.00 Hz
GB 0
PC 1.00

Figure 7.85 ^{19}F NMR (376 MHz, $CDCl_3$) of compound **7.70**

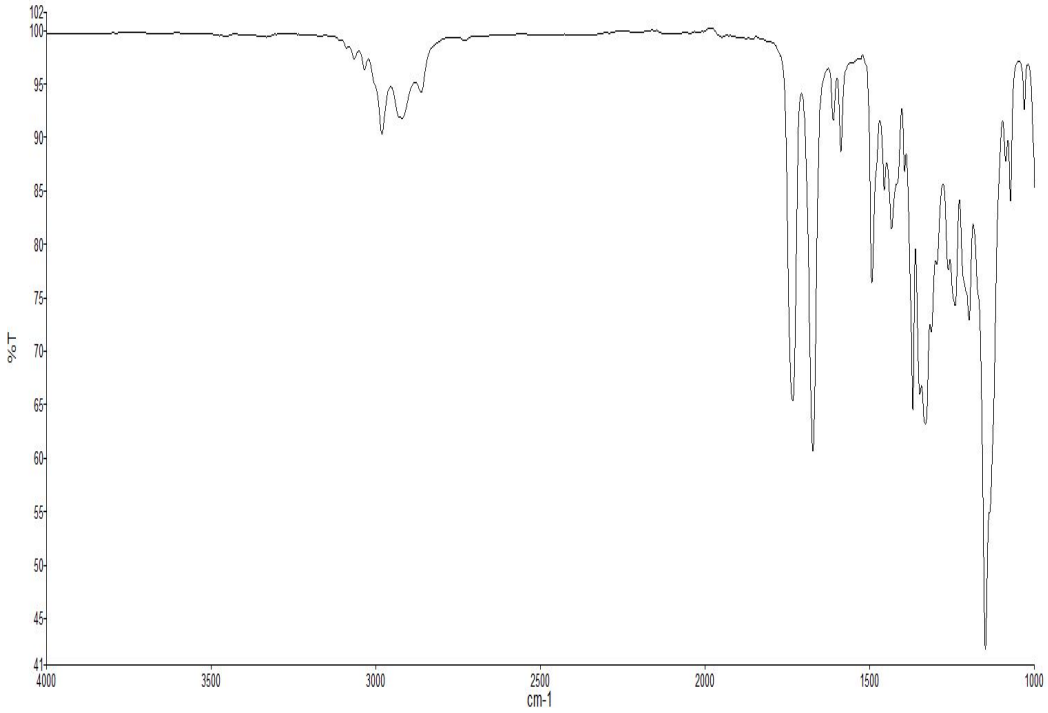

Figure 7.86 Infrared spectrum of compound **7.70**

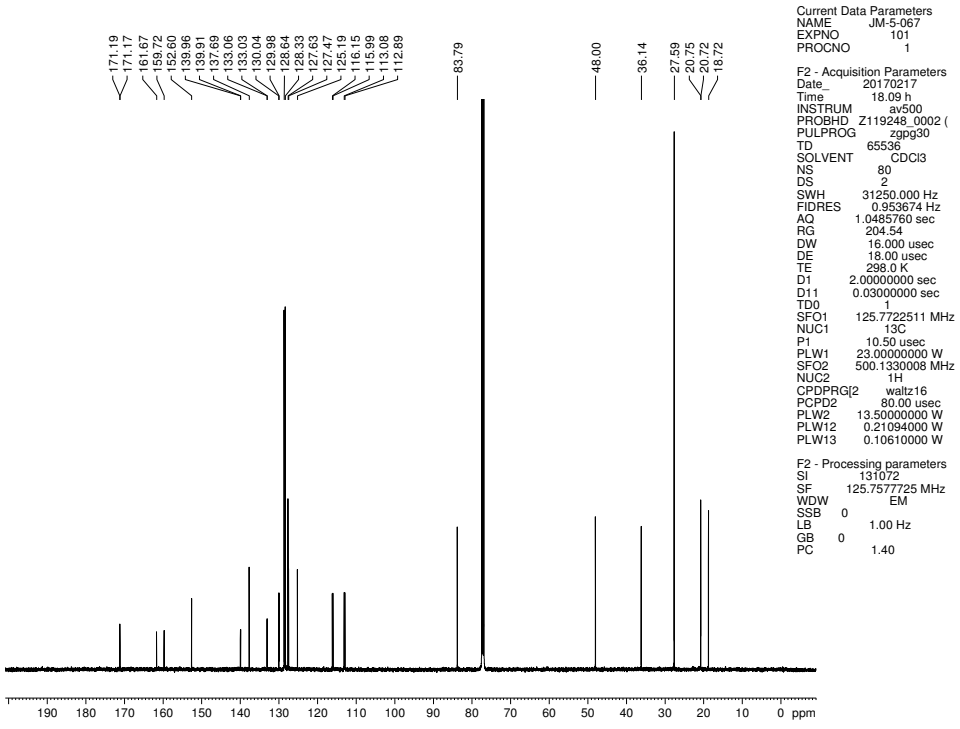

Figure 7.87 ^{13}C NMR (125 MHz, $CDCl_3$) of compound **7.70**

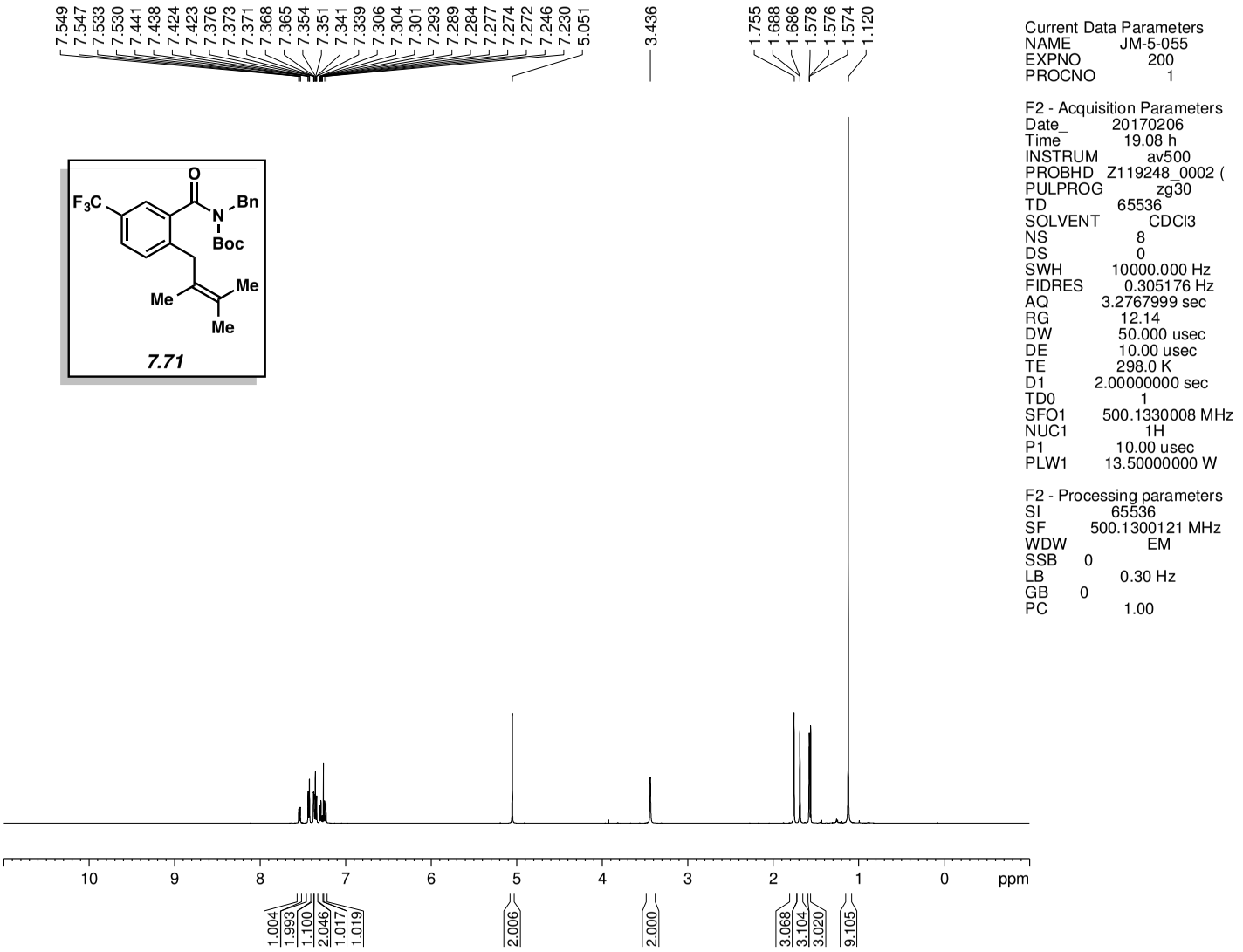

Figure 7.88 ^{1}H NMR (500 MHz, $CDCl_3$) of compound **7.71**

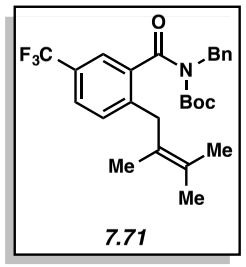

7.71

Current Data Parameters
NAME JM-5-055
EXPNO 170
PROCNO 1

F2 - Acquisition Parameters
Date_ 20170313
Time 13.57
INSTRUM av400
PROBHD 5 mm PABBO BB/
PULPROG zgfhigqn.2
TD 262144
SOLVENT CDCl3
NS 48
DS 0
SWH 150000.000 Hz
FIDRES 0.572205 Hz
AQ 0.8738133 sec
RG 189.85
DW 3.333 usec
DE 6.50 usec
TE 299.0 K
D1 1.00000000 sec
D11 0.03000000 sec
D12 0.00002000 sec
TD0 1

======== CHANNEL f1 =====
SFO1 376.4983660 MHz
NUC1 19F
P1 14.50 usec
PLW1 17.00000000 W

======== CHANNEL f2 =====
SFO2 400.1324008 MHz
NUC2 1H
CPDPRG[2 waltz16
PCPD2 90.00 usec
PLW2 13.00000000 W
PLW12 0.36111000 W

F2 - Processing parameters
SI 262144
SF 376.4983660 MHz
WDW EM
SSB 0
LB 1.00 Hz
GB 0
PC 1.00

Figure 7.89 ^{19}F NMR (376 MHz, $CDCl_3$) of compound **7.71**

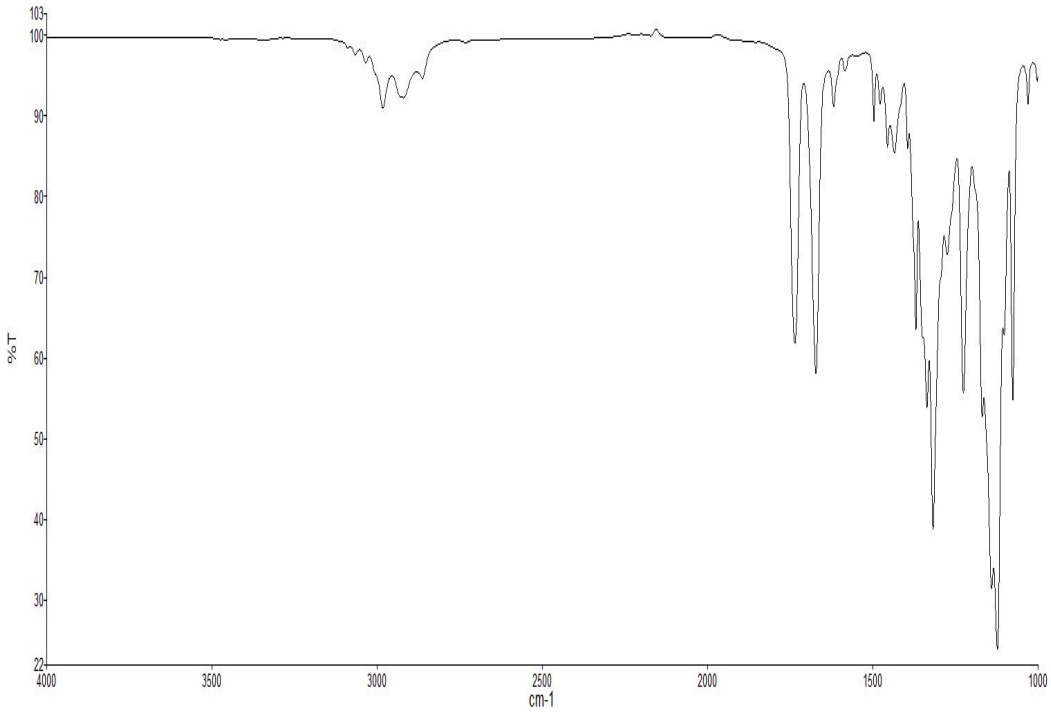

Figure 7.90 Infrared spectrum of compound **7.71**

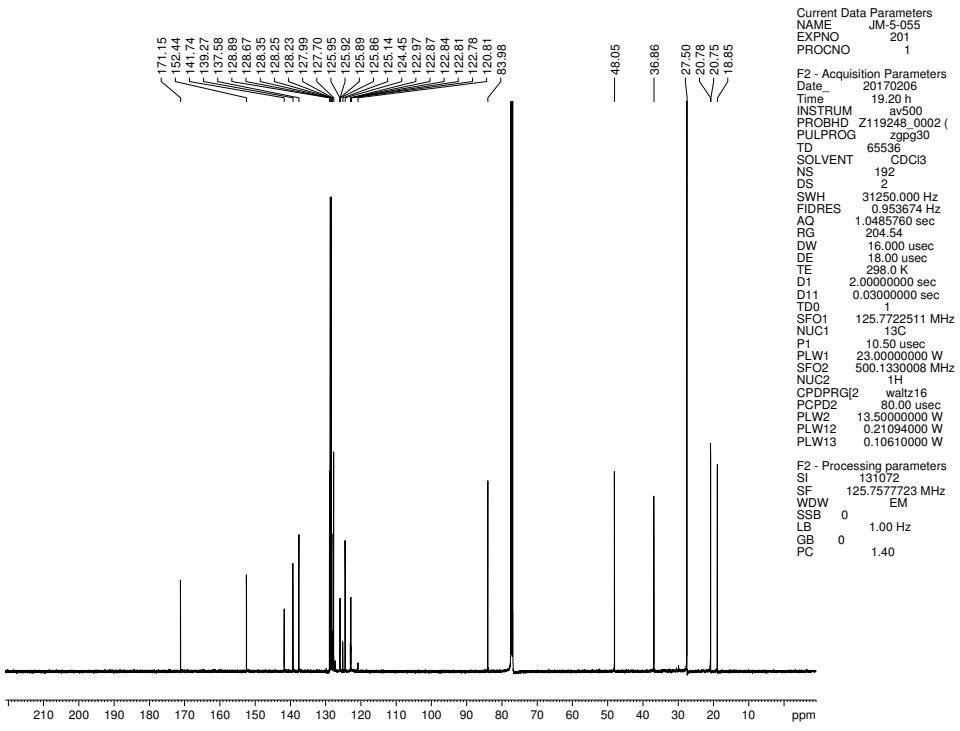

Figure 7.91 ^{13}C NMR (125 MHz, $CDCl_3$) of compound **7.71**

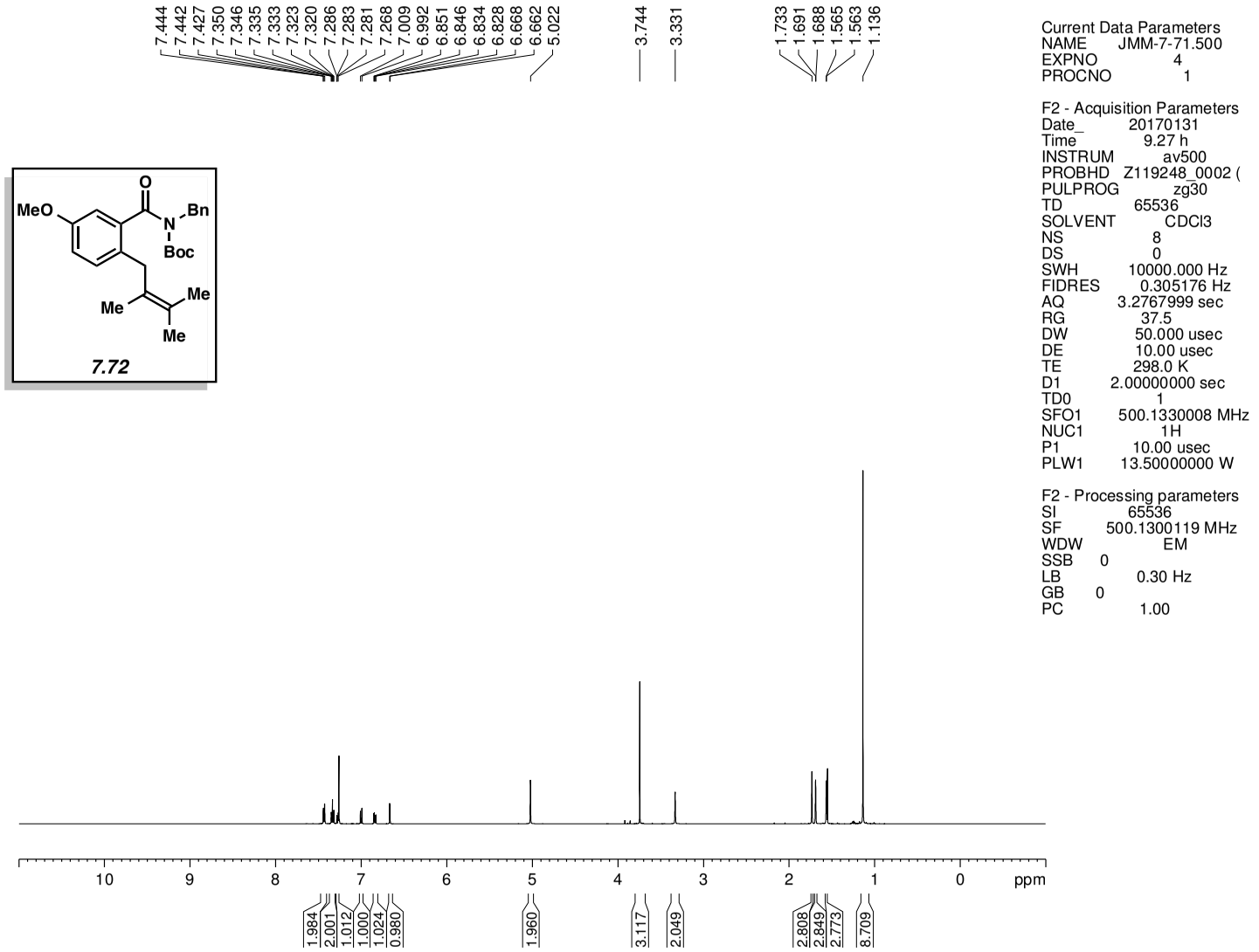

Figure 7.92 ^{1}H NMR (500 MHz, $CDCl_3$) of compound **7.72**

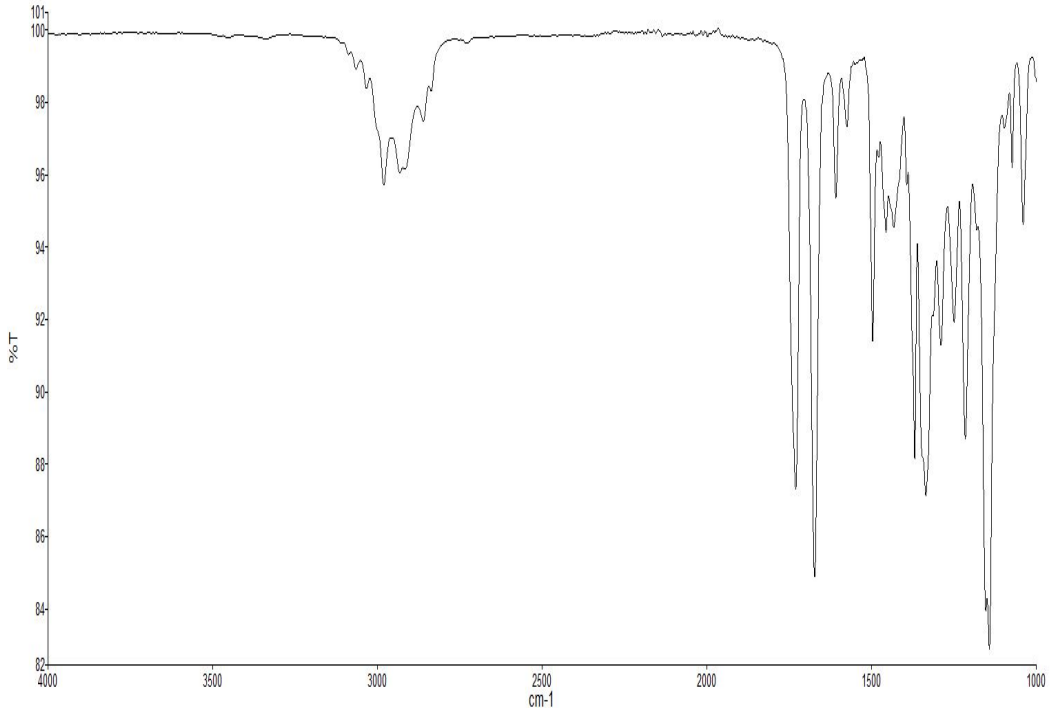

Figure 7.93 Infrared spectrum of compound **7.72**

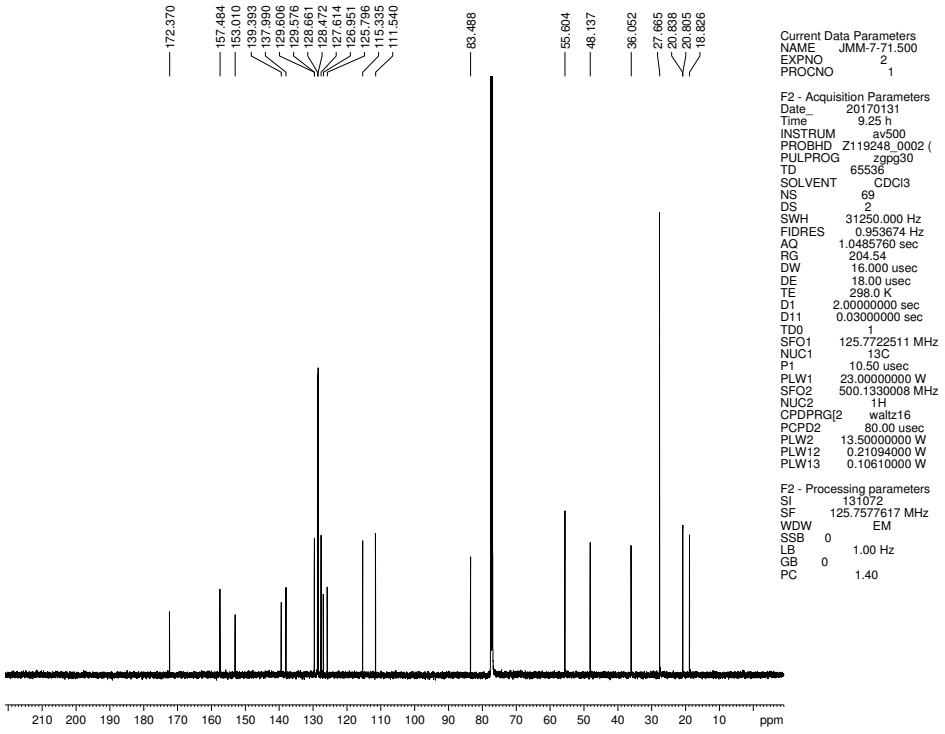

Figure 7.94 ^{13}C NMR (125 MHz, $CDCl_3$) of compound **7.72**

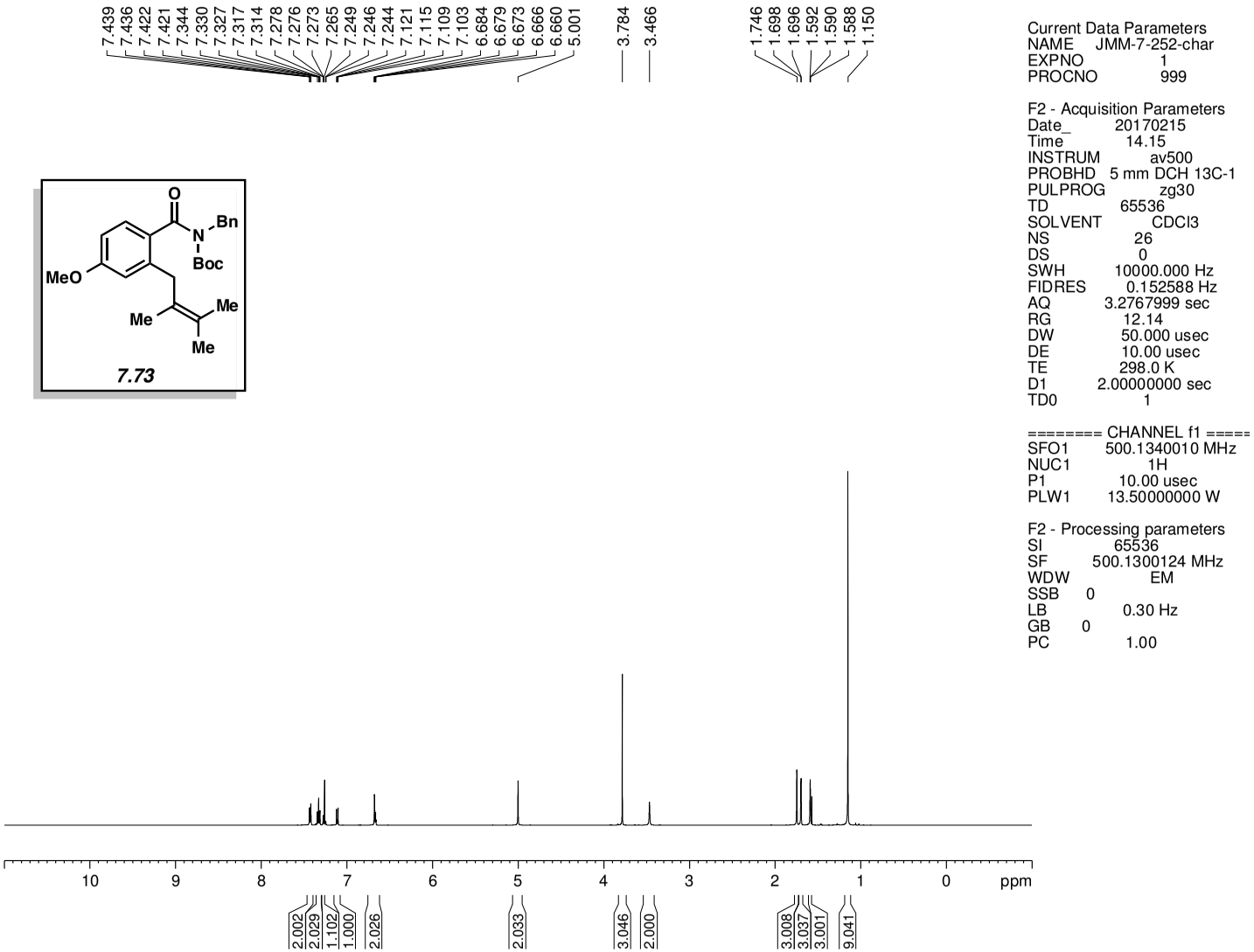

Figure 7.95 ^{1}H NMR (500 MHz, $CDCl_3$) of compound **7.73**

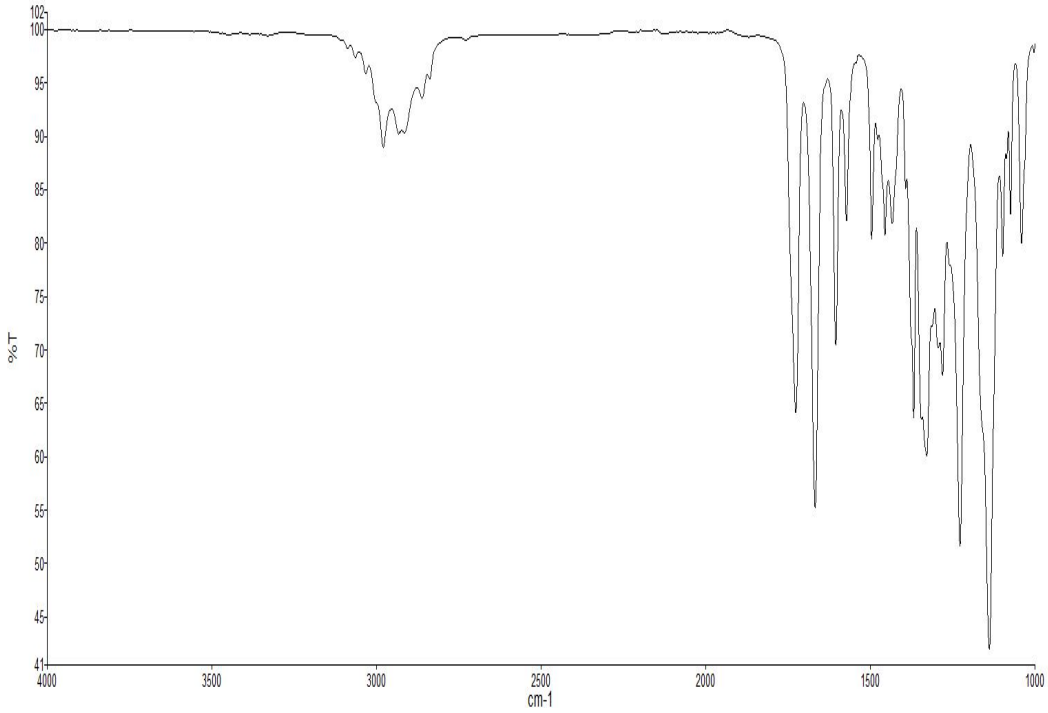

Figure 7.96 Infrared spectrum of compound **7.73**

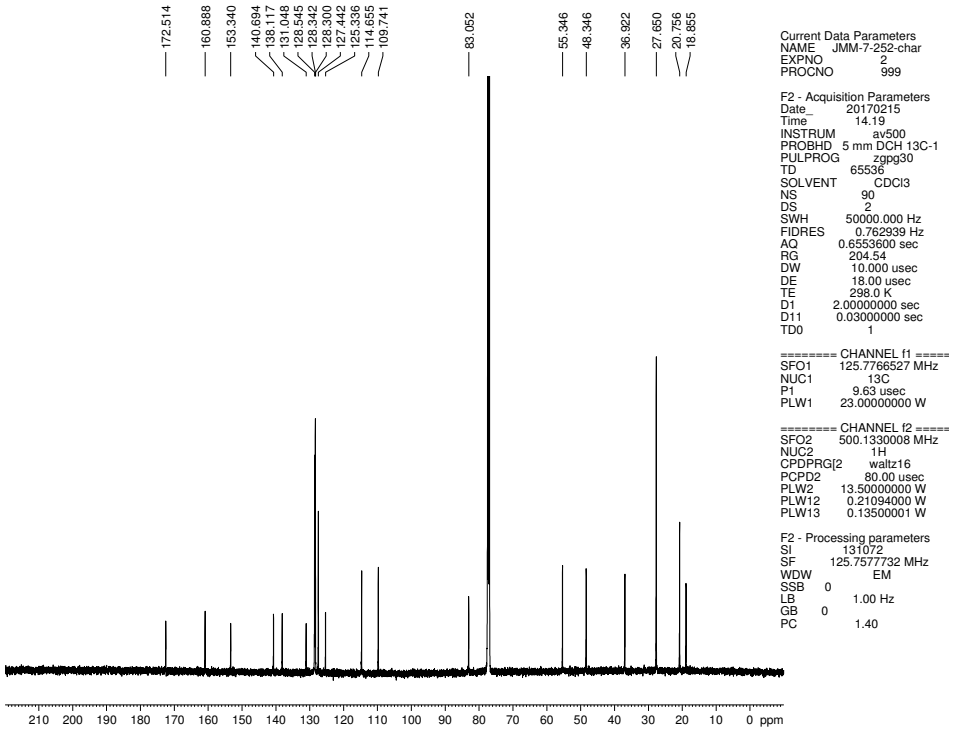

Figure 7.97 ^{13}C NMR (125 MHz, $CDCl_3$) of compound **7.73**

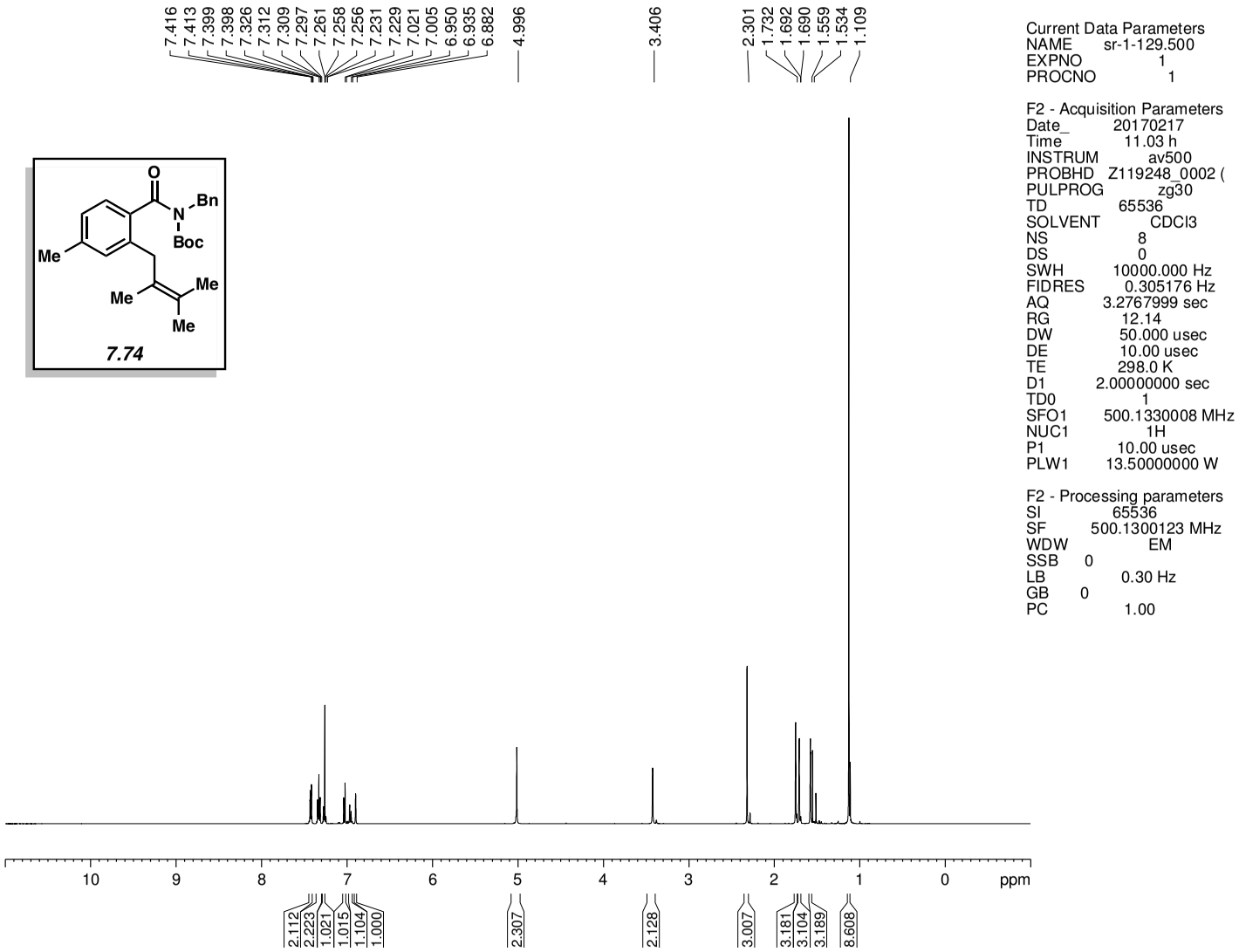

Figure 7.98 ^{1}H NMR (500 MHz, $CDCl_3$) of compound **7.74**

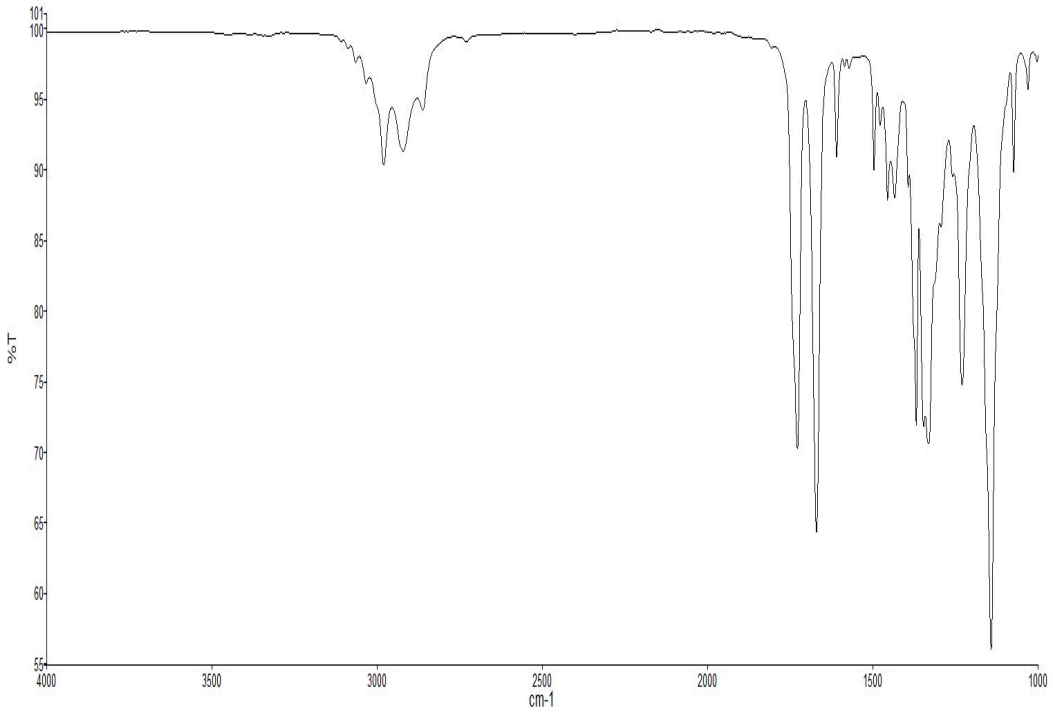

Figure 7.99 Infrared spectrum of compound **7.74**

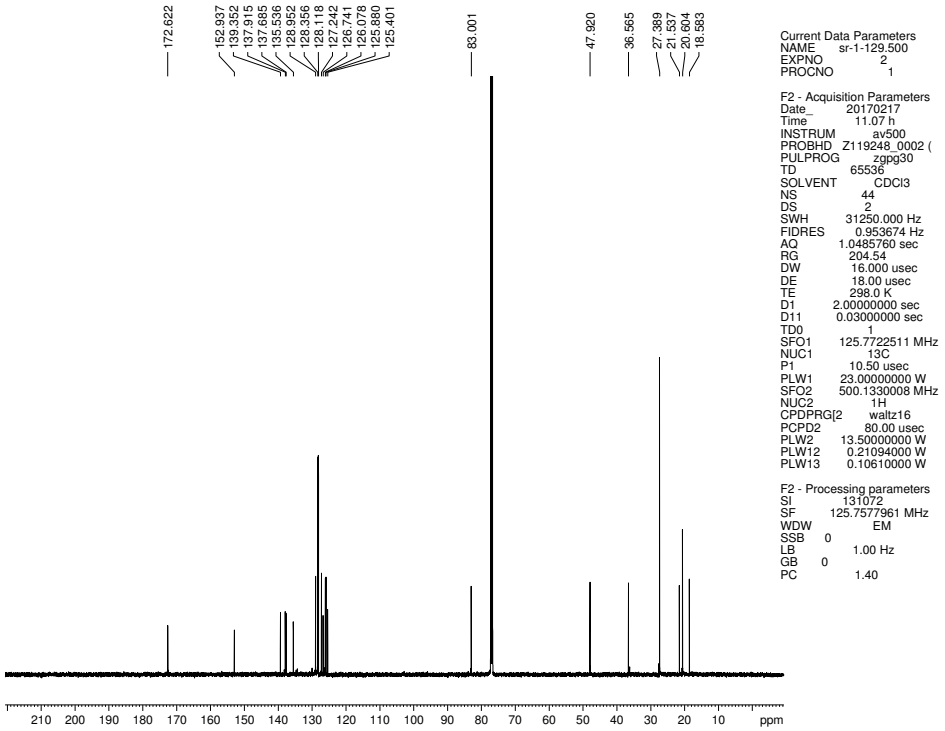

Figure 7.100 ^{13}C NMR (125 MHz, $CDCl_3$) of compound **7.74**

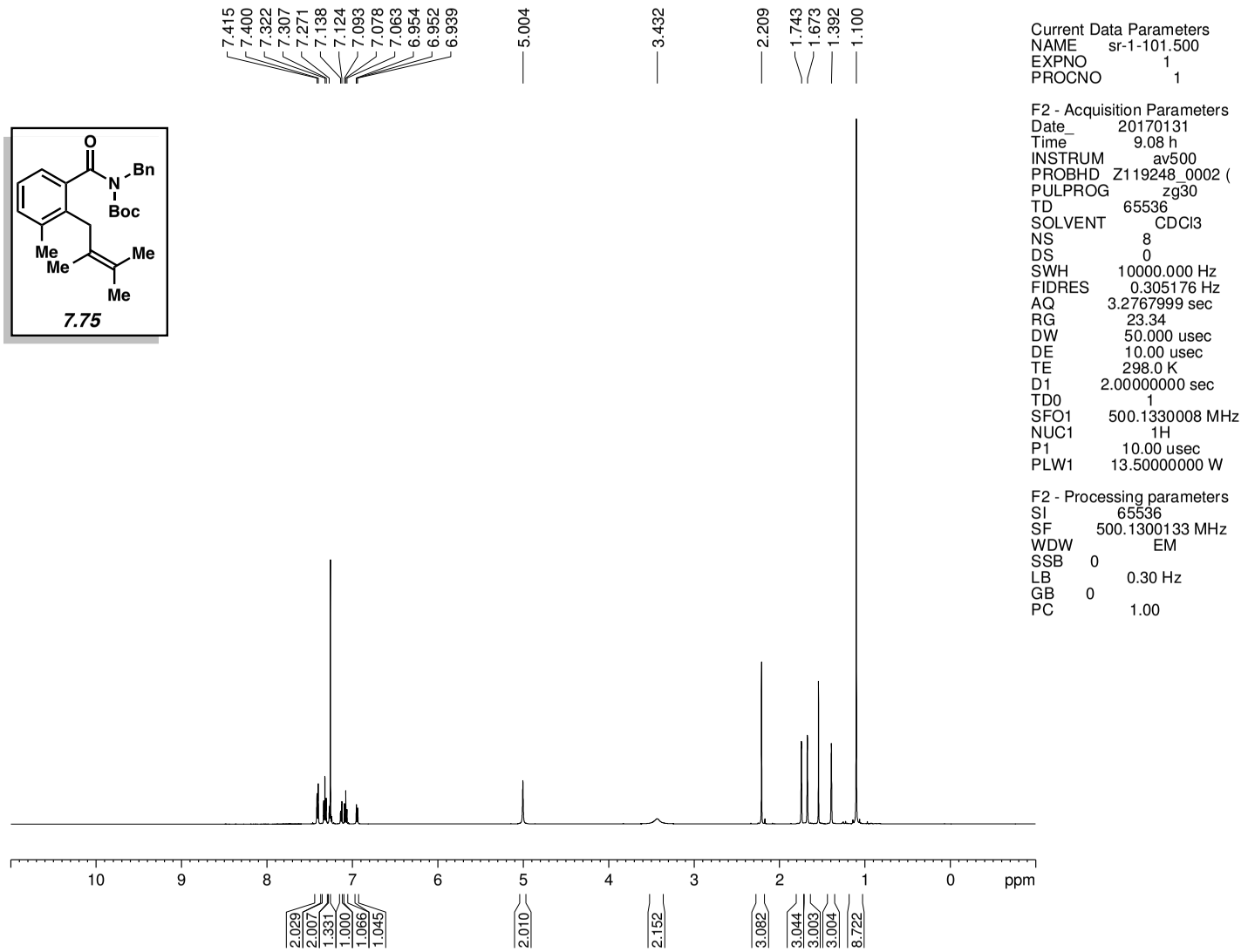

Figure 7.101 ^{1}H NMR (500 MHz, $CDCl_3$) of compound **7.75**

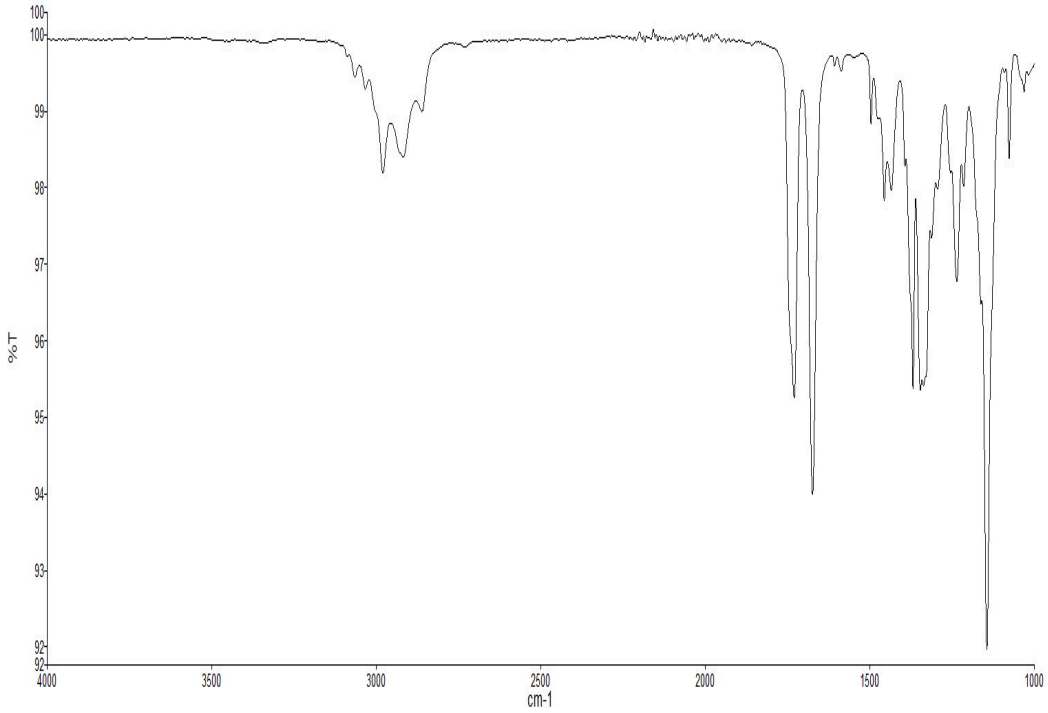

Figure 7.102 Infrared spectrum of compound **7.75**

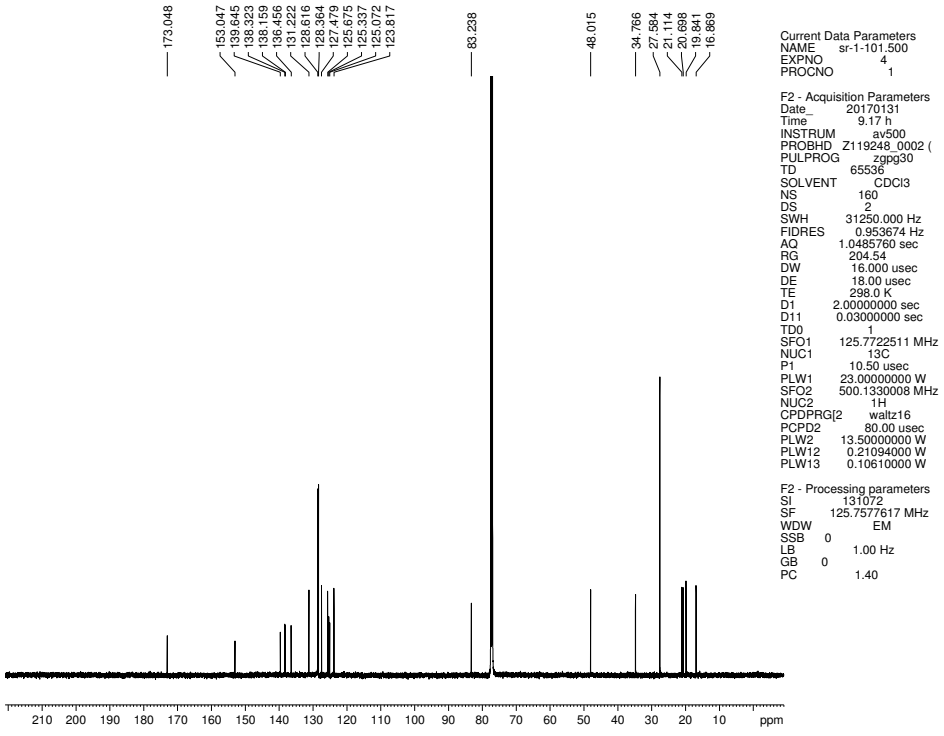

Figure 7.103 ^{13}C NMR (125 MHz, $CDCl_3$) of compound **7.75**

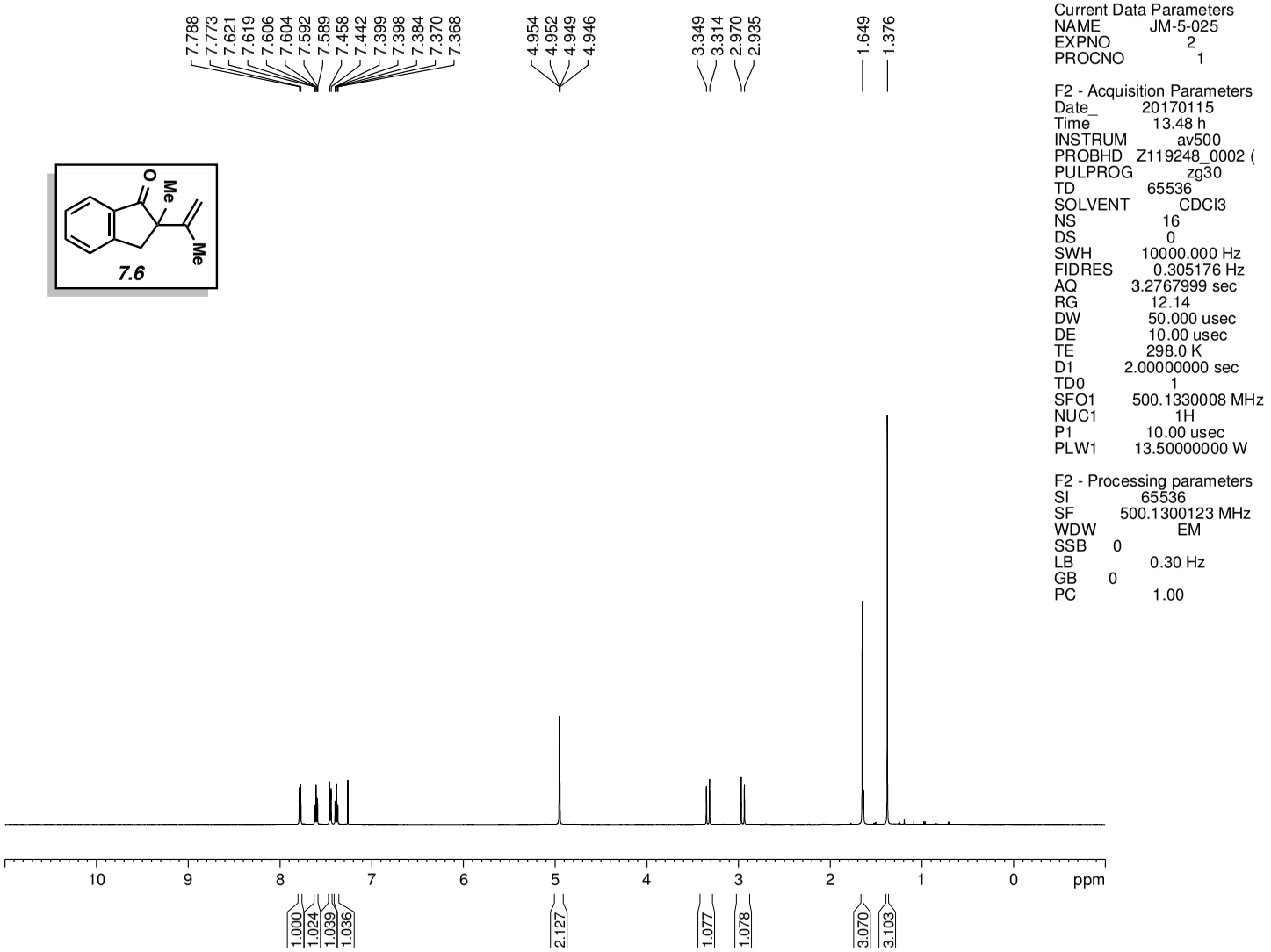

Figure 7.104 ^{1}H NMR (500 MHz, $CDCl_3$) of compound **7.6**

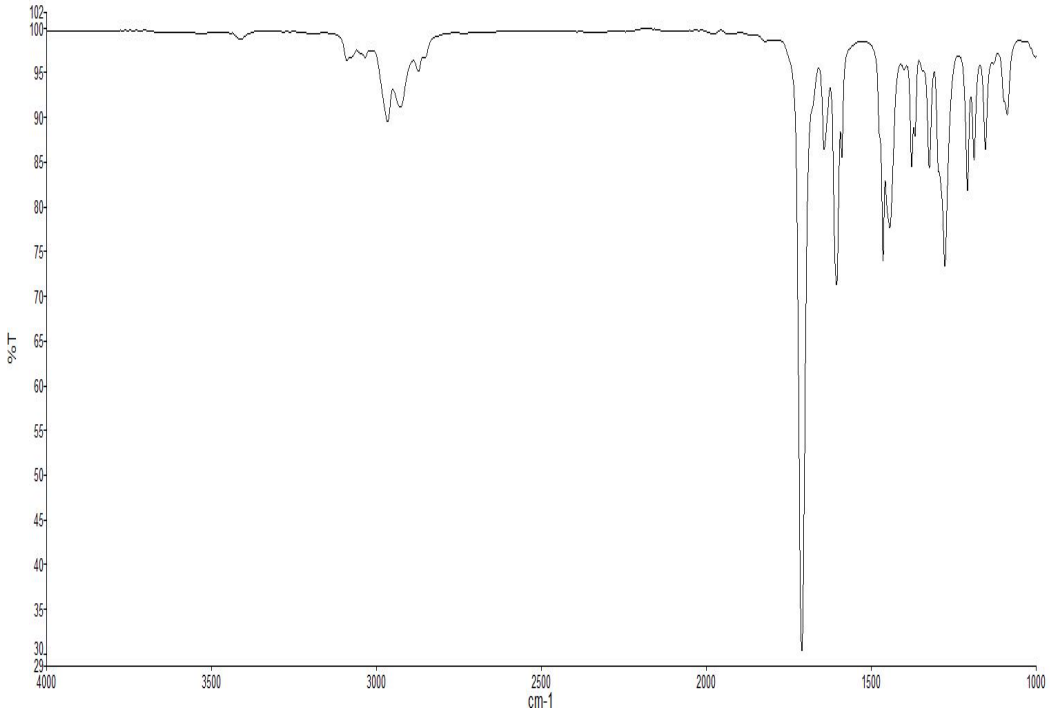

Figure 7.105 Infrared spectrum of compound **7.6**

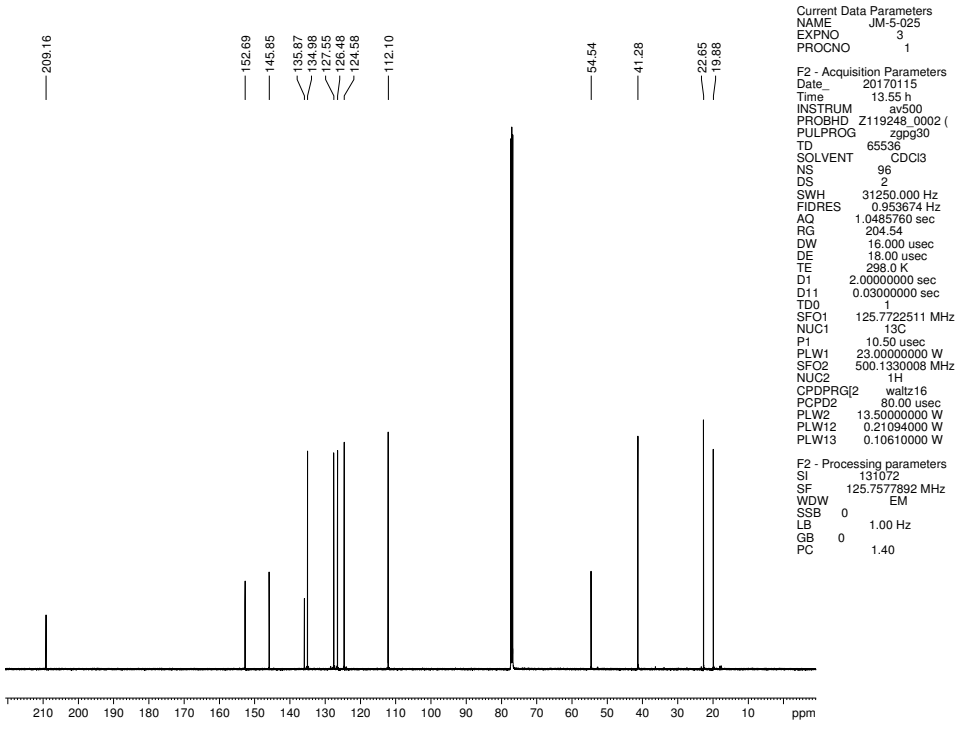

Figure 7.106 ^{13}C NMR (125 MHz, $CDCl_3$) of compound **7.6**

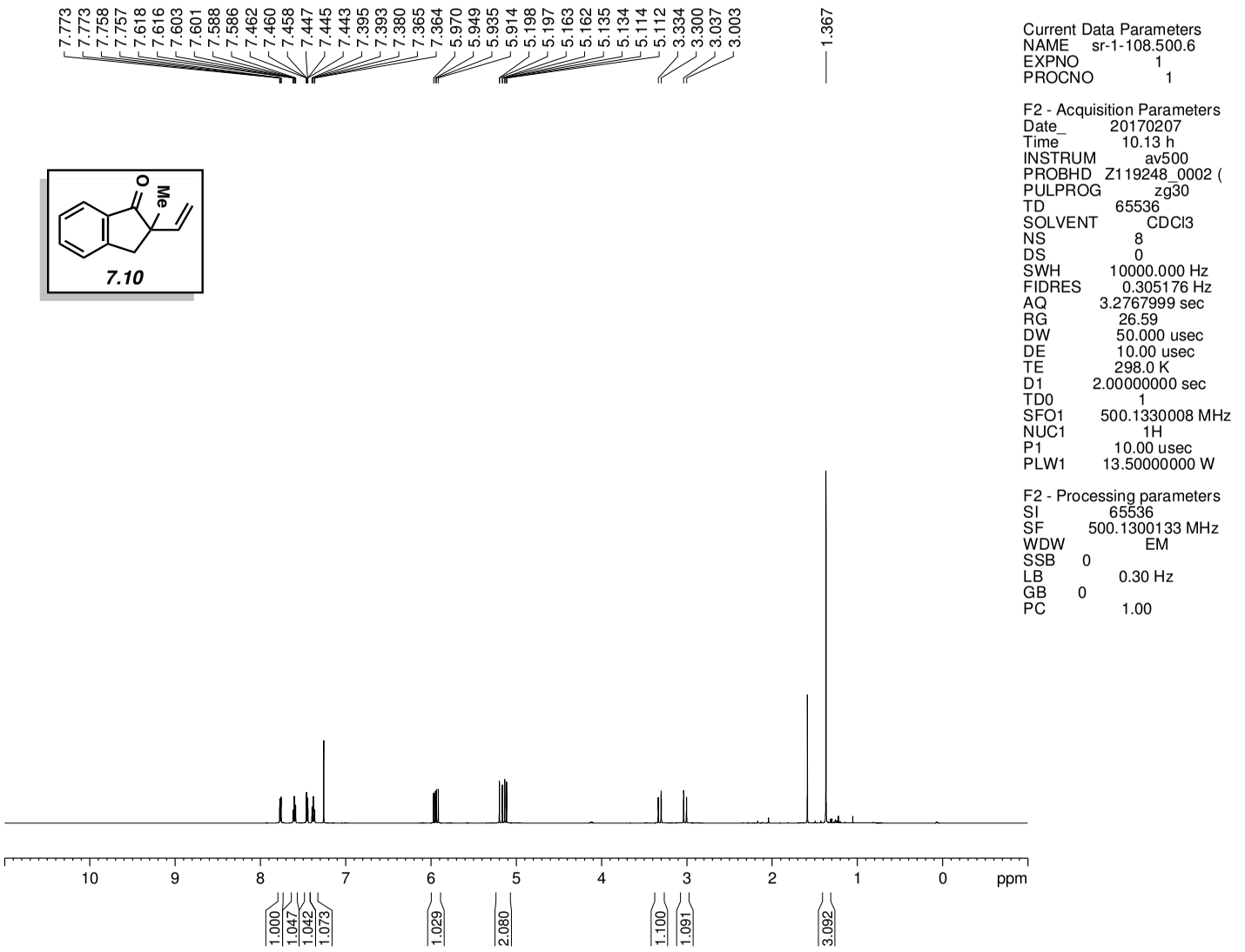

Figure 7.107 ^{1}H NMR (500 MHz, $CDCl_3$) of compound **7.10**

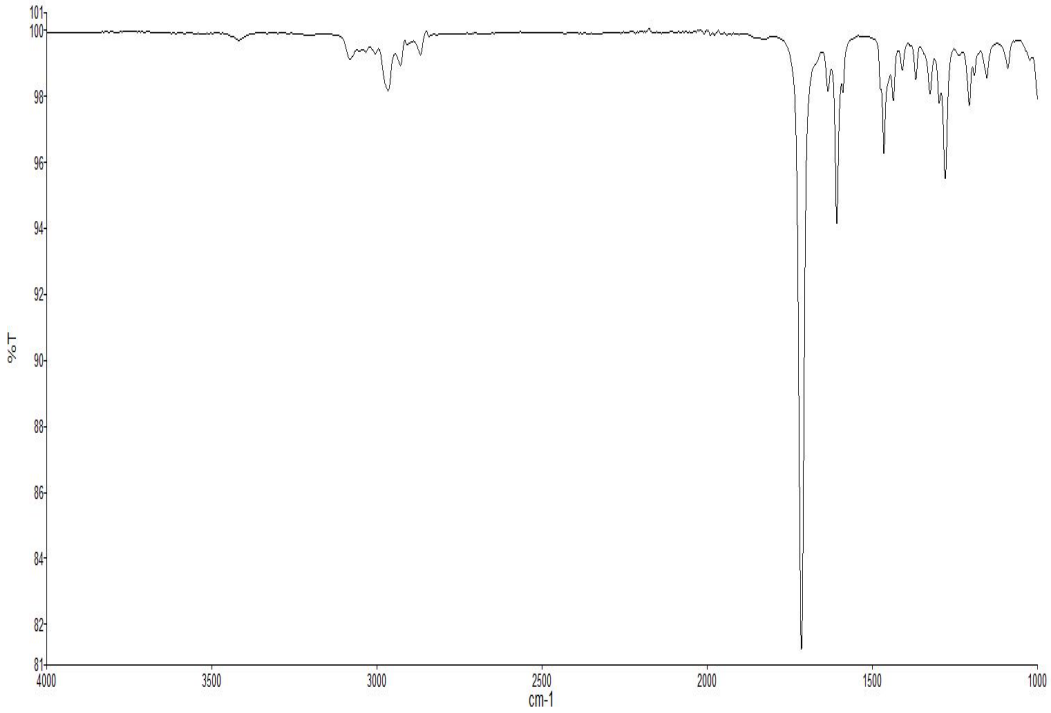

Figure 7.108 Infrared spectrum of compound **7.10**

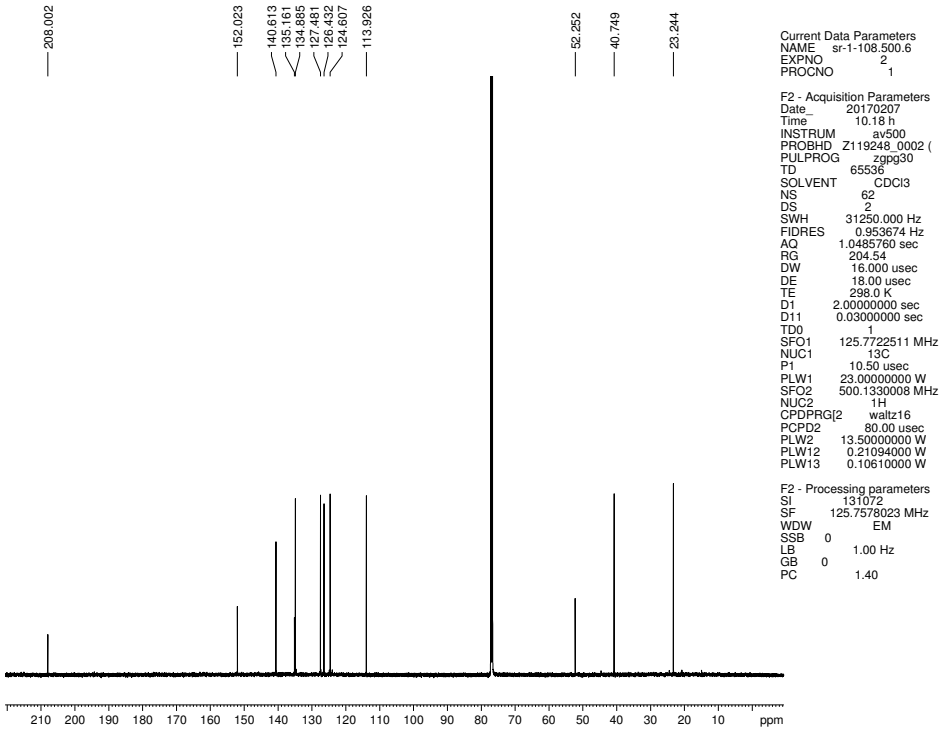

Figure 7.109 ^{13}C NMR (125 MHz, $CDCl_3$) of compound **7.10**

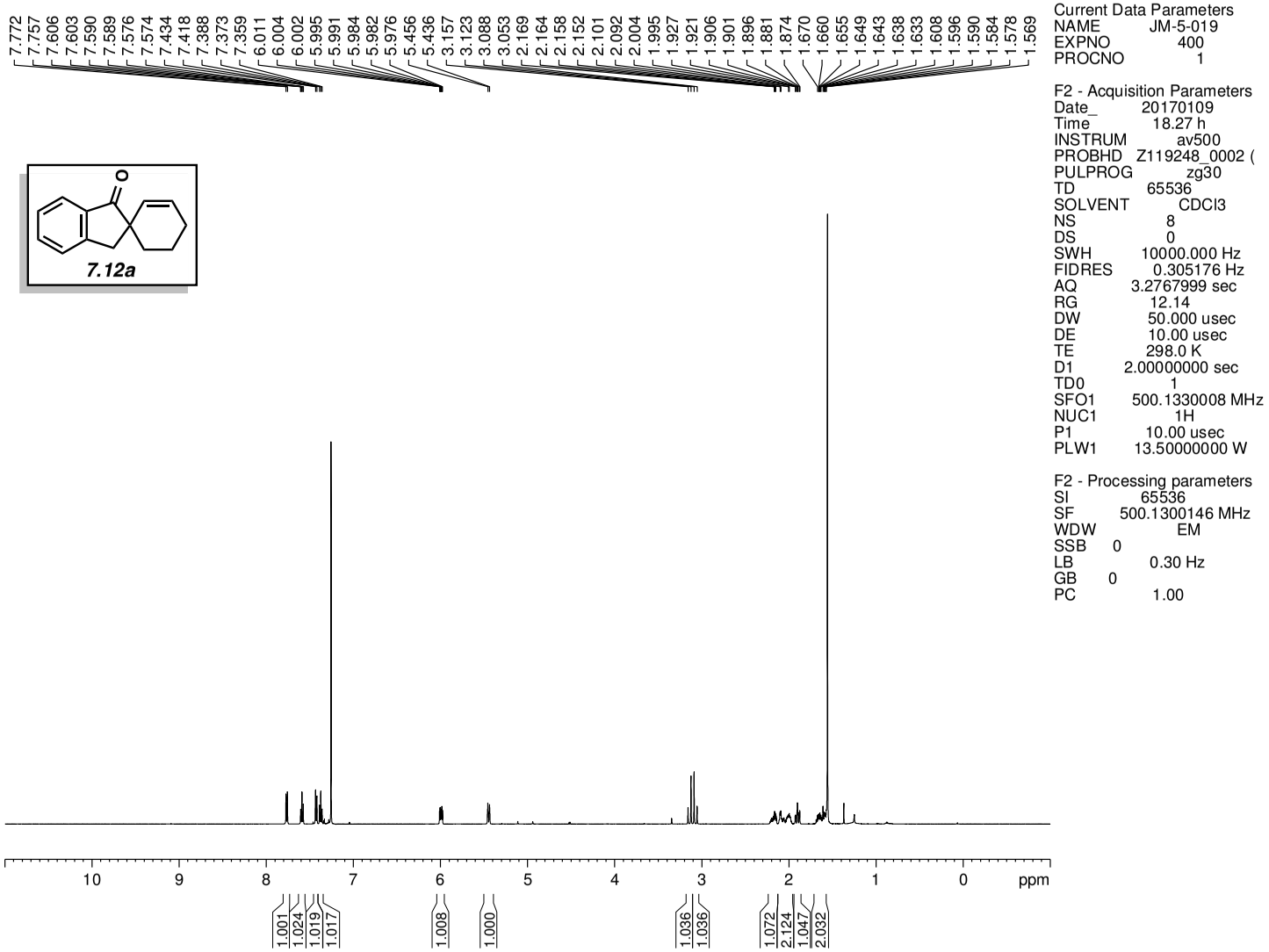

Figure 7.110 ^{1}H NMR (500 MHz, $CDCl_3$) of compound **7.12a**

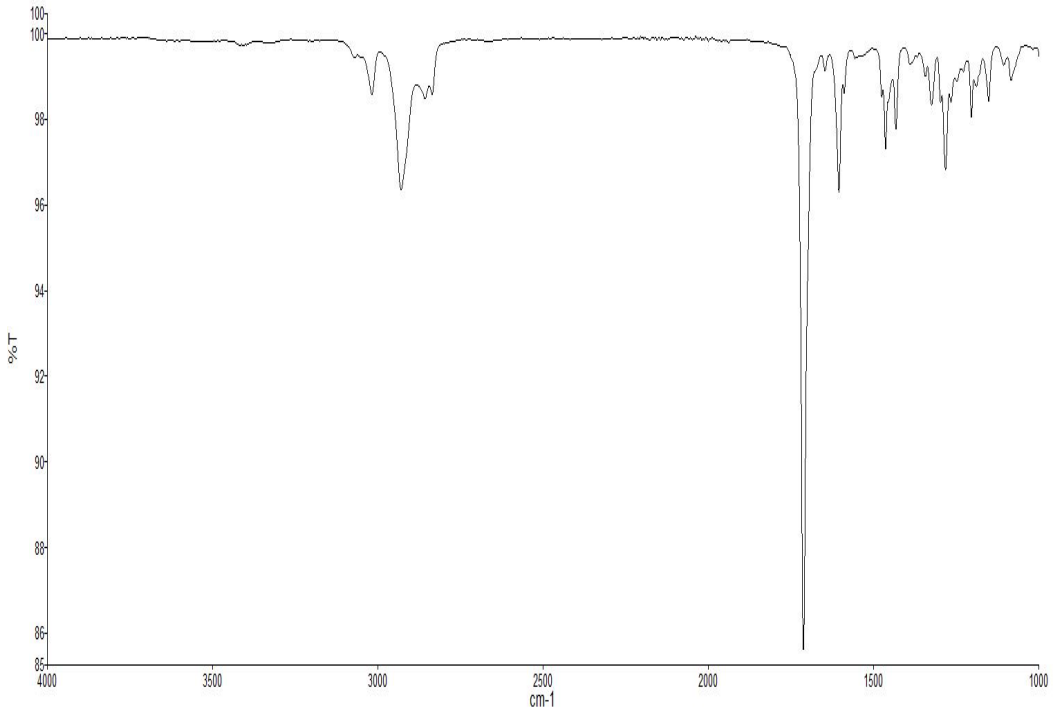

Figure 7.111 Infrared spectrum of compound **7.12a**

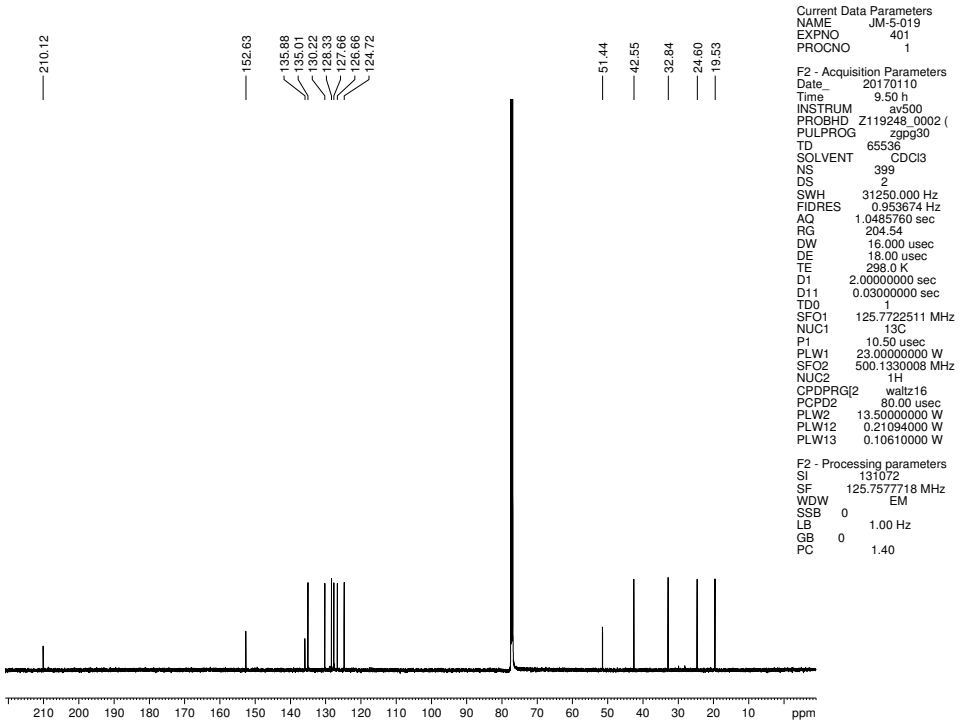

Figure 7.112 ^{13}C NMR (125 MHz, $CDCl_3$) of compound **7.12a**

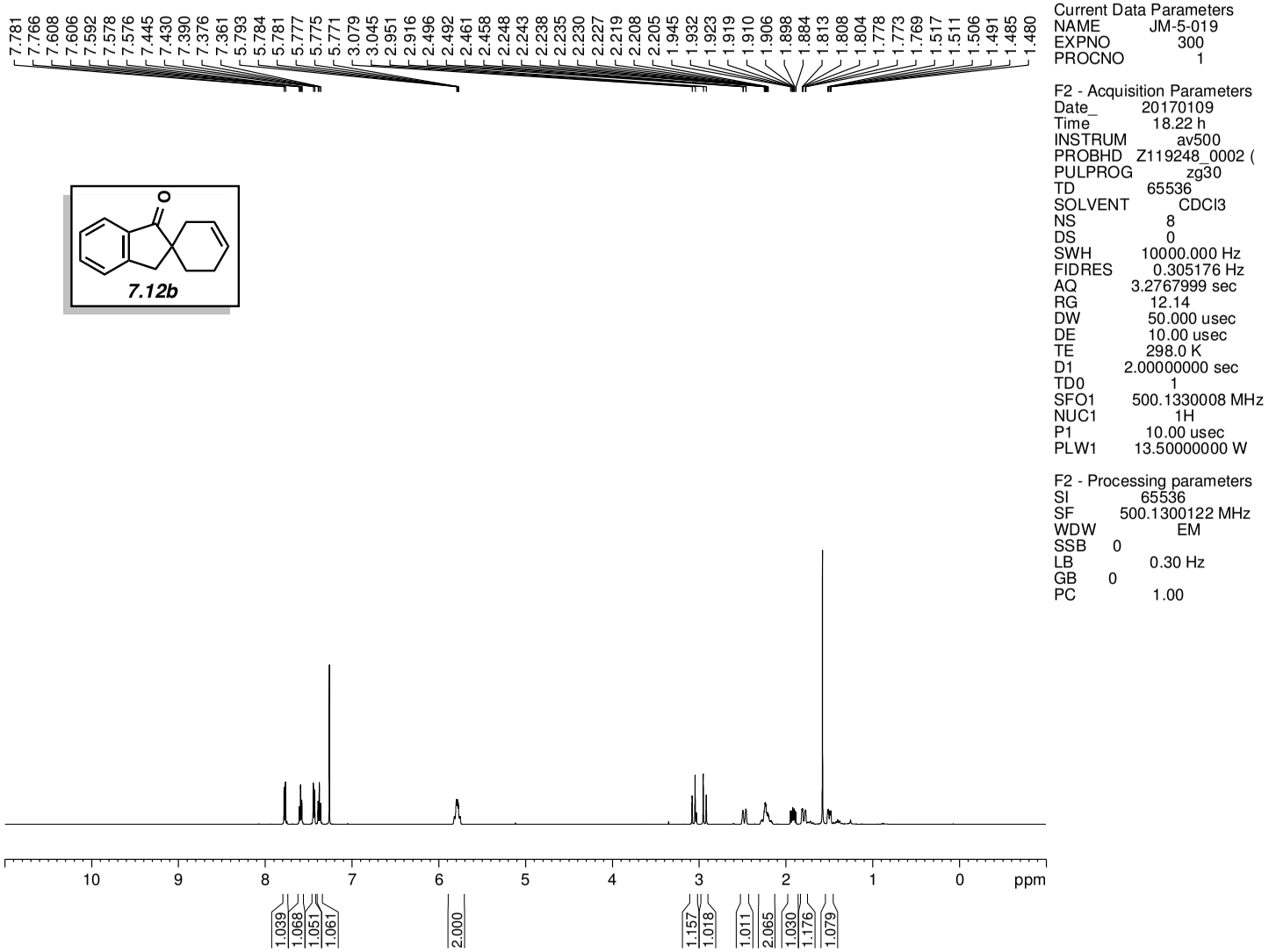

Figure 7.113 ^{1}H NMR (500 MHz, $CDCl_3$) of compound **7.12b**

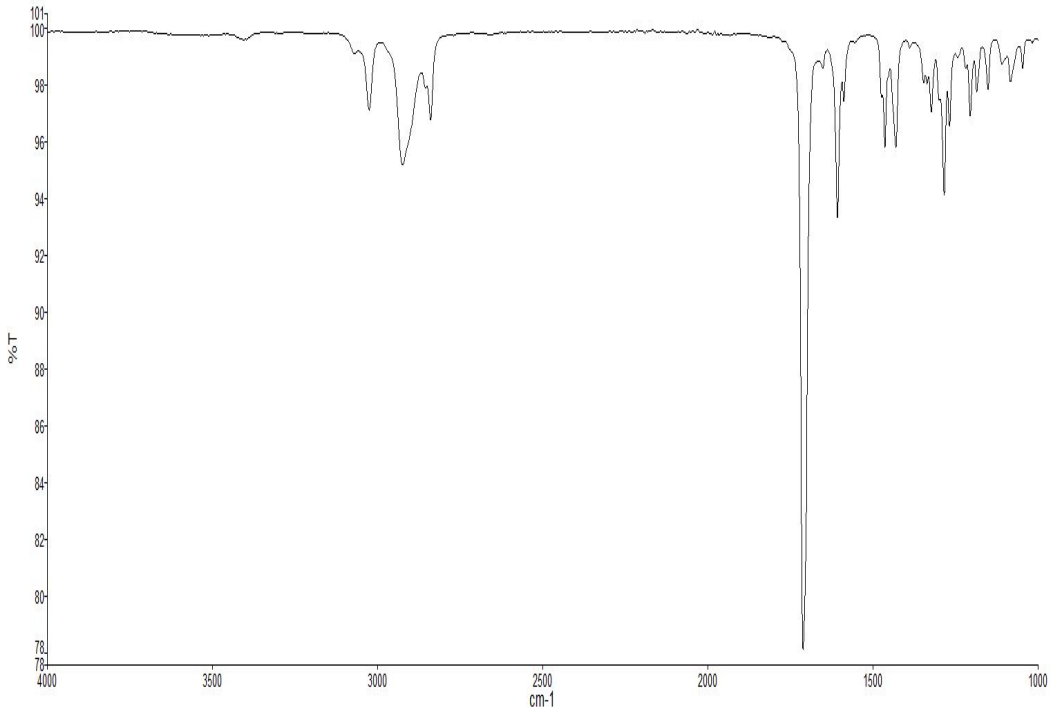

Figure 7.114 Infrared spectrum of compound **7.12b**

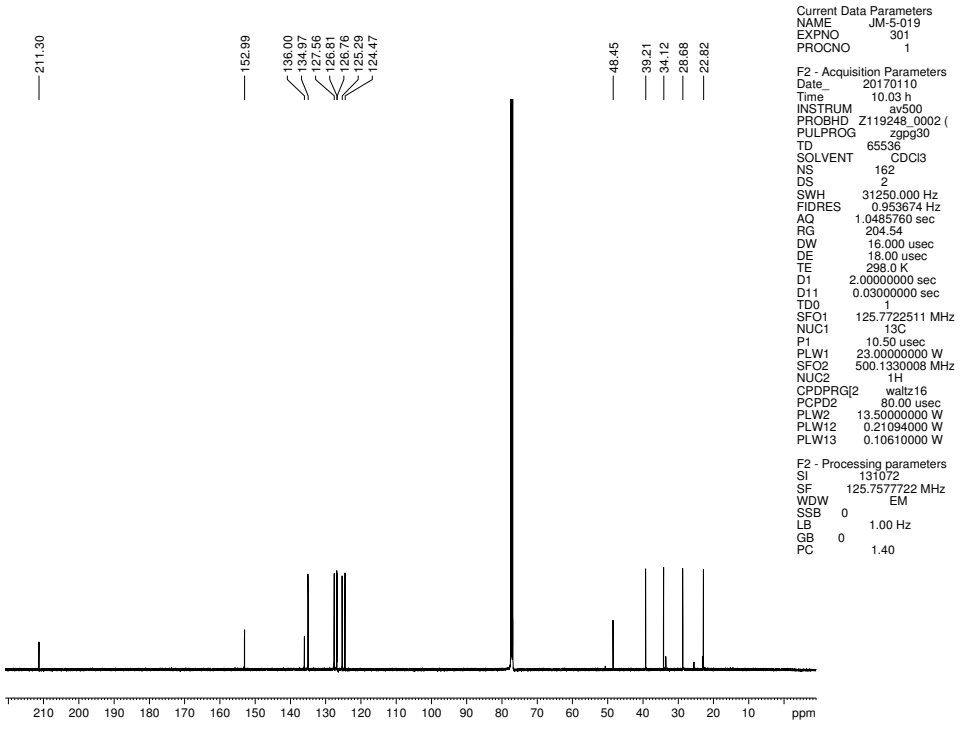

Figure 7.115 ^{13}C NMR (125 MHz, $CDCl_3$) of compound **7.12b**

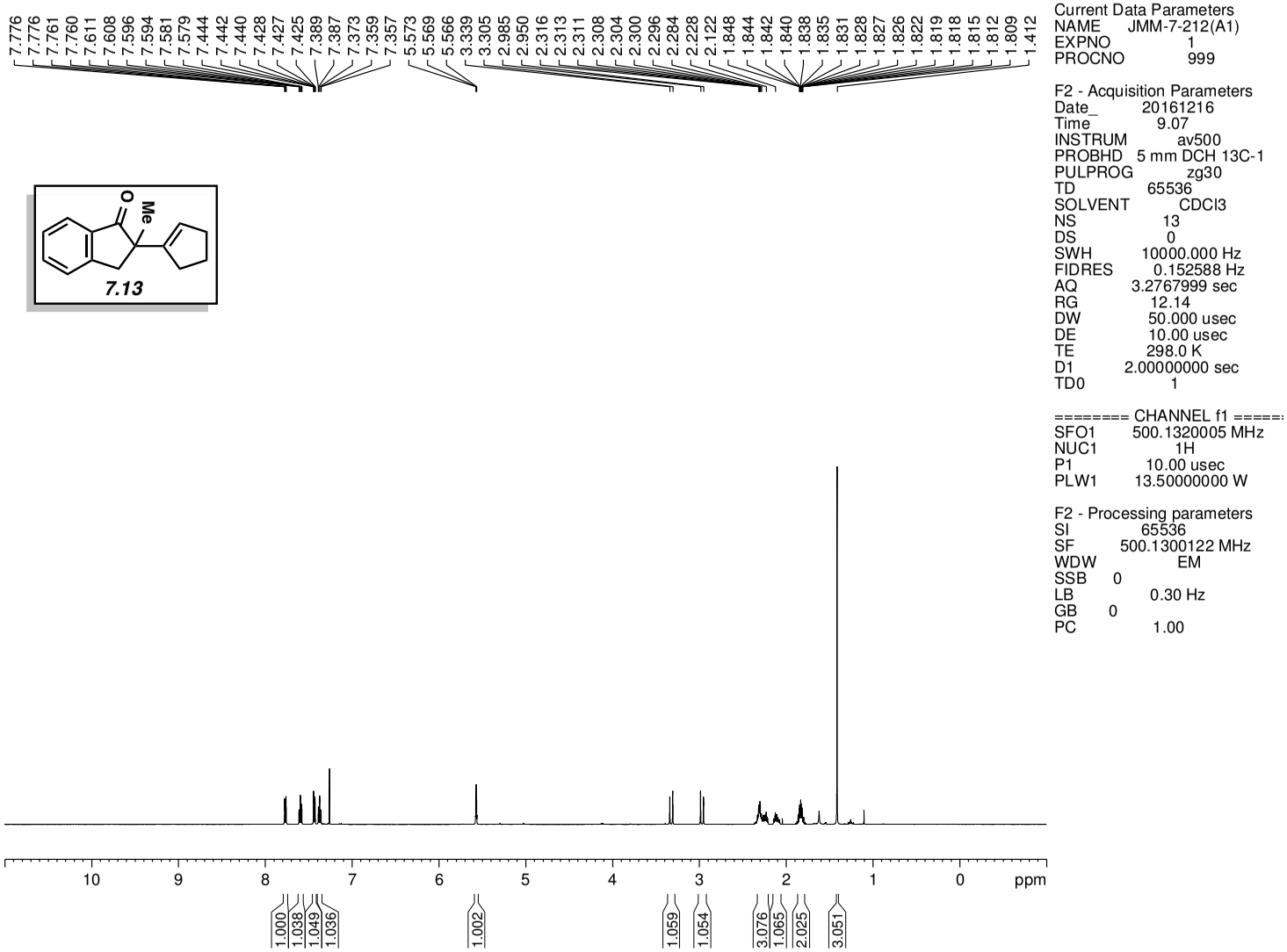

Figure 7.116 ^{1}H NMR (500 MHz, $CDCl_3$) of compound **7.13**

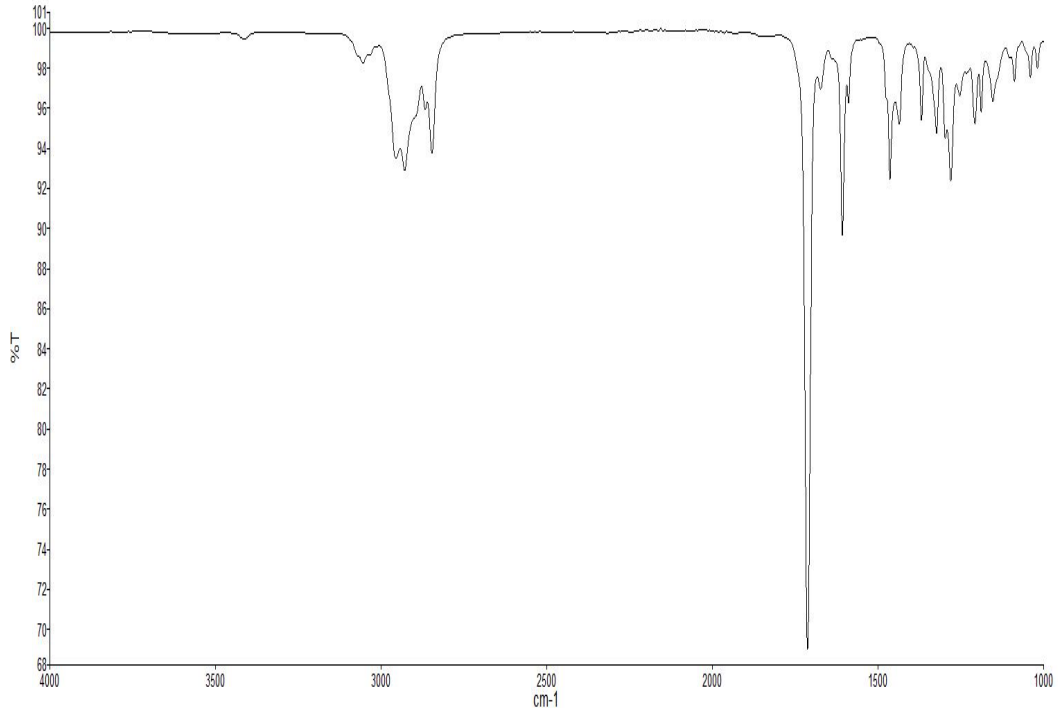

Figure 7.117 Infrared spectrum of compound **7.13**

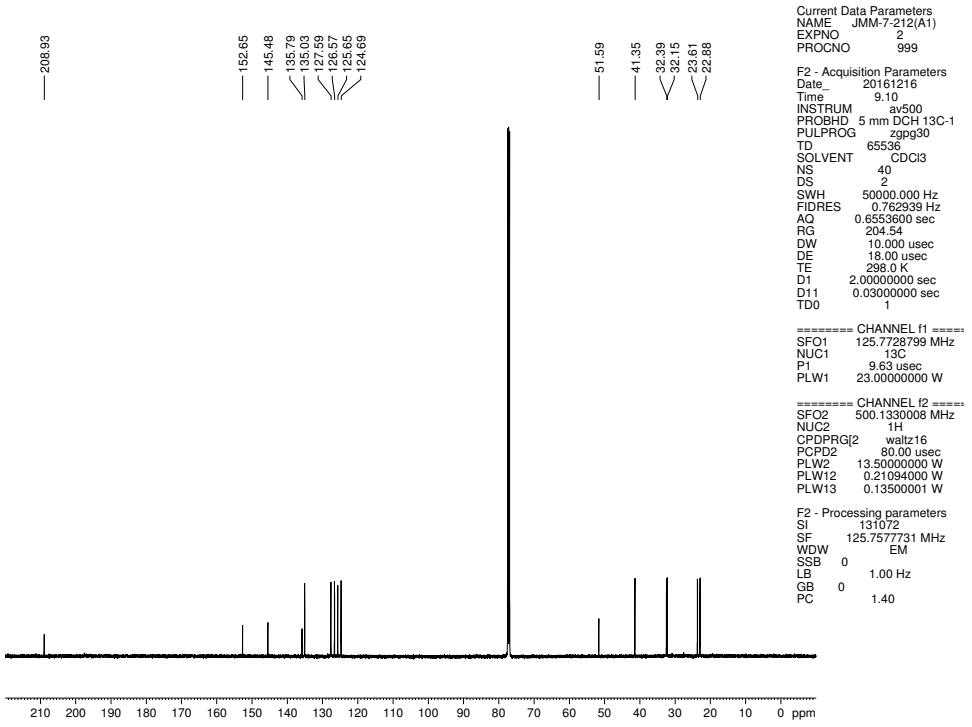

Figure 7.118 ^{13}C NMR (125 MHz, $CDCl_3$) of compound **7.13**

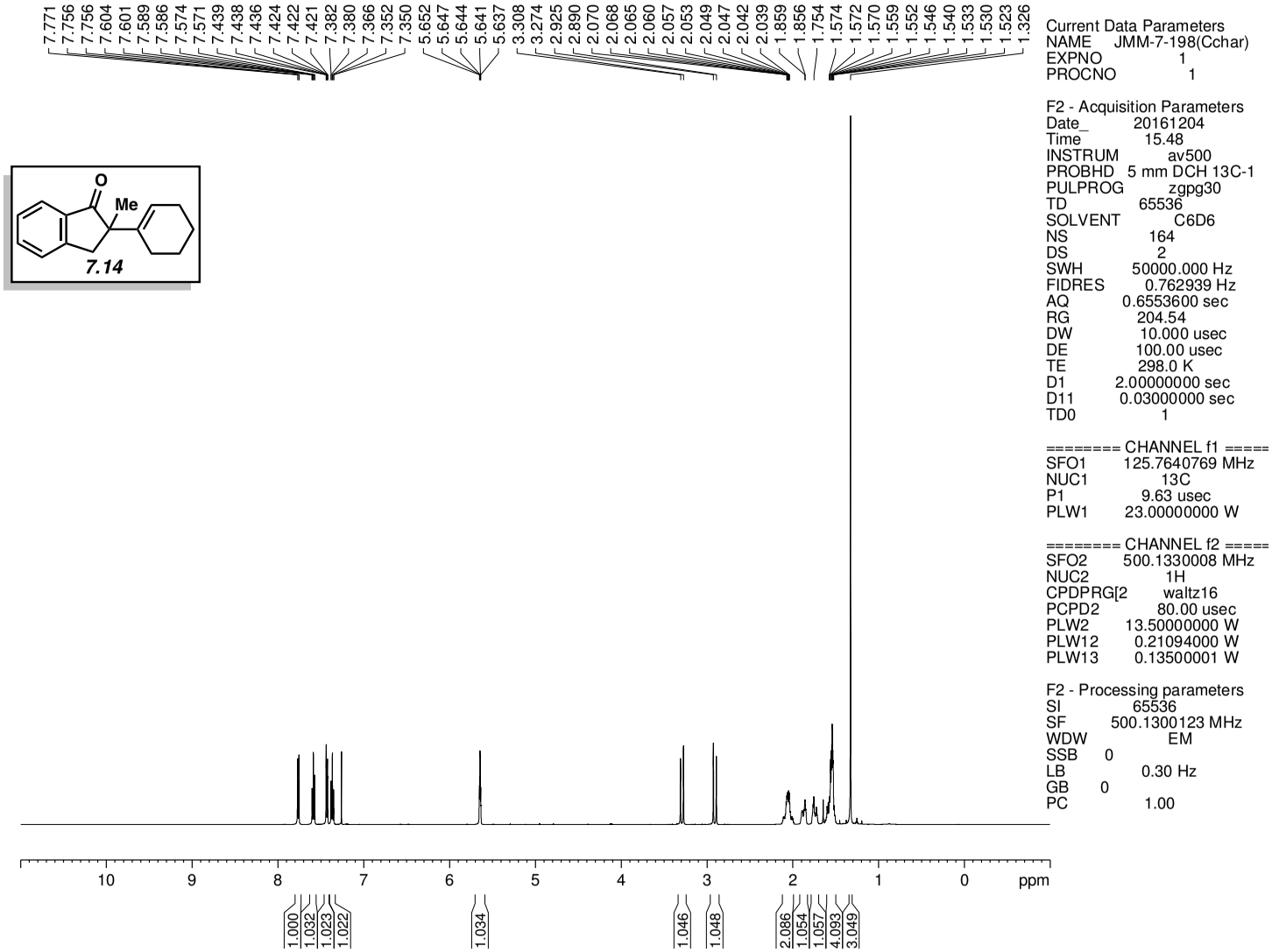

Figure 7.119 ^{1}H NMR (500 MHz, $CDCl_3$) of compound **7.14**

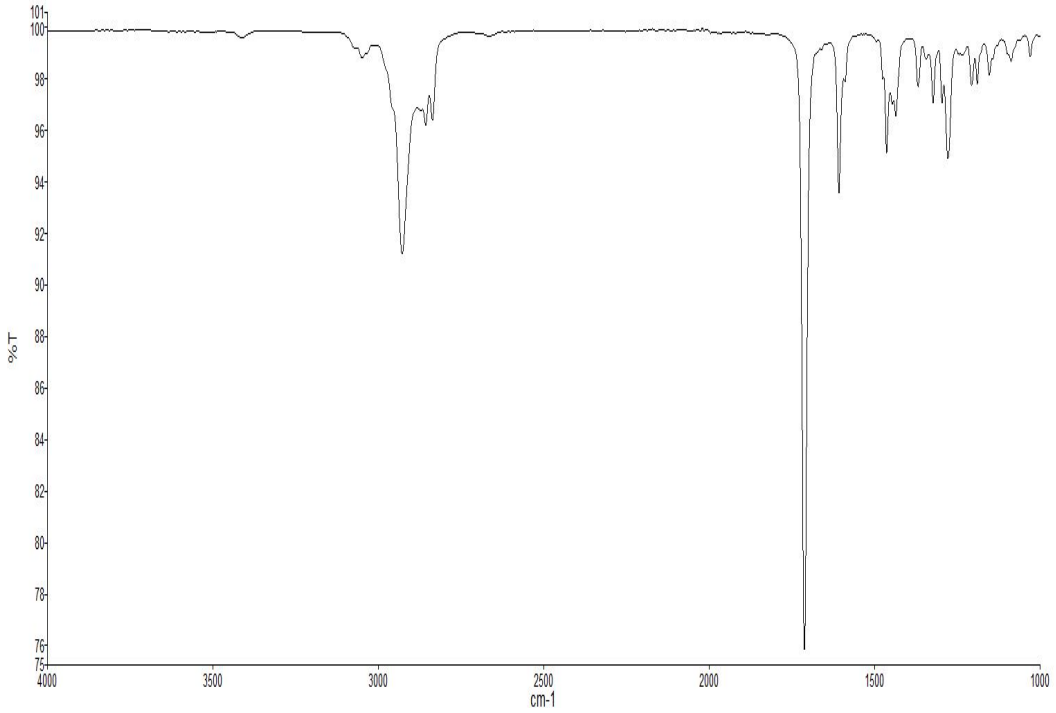

Figure 7.120 Infrared spectrum of compound **7.14**

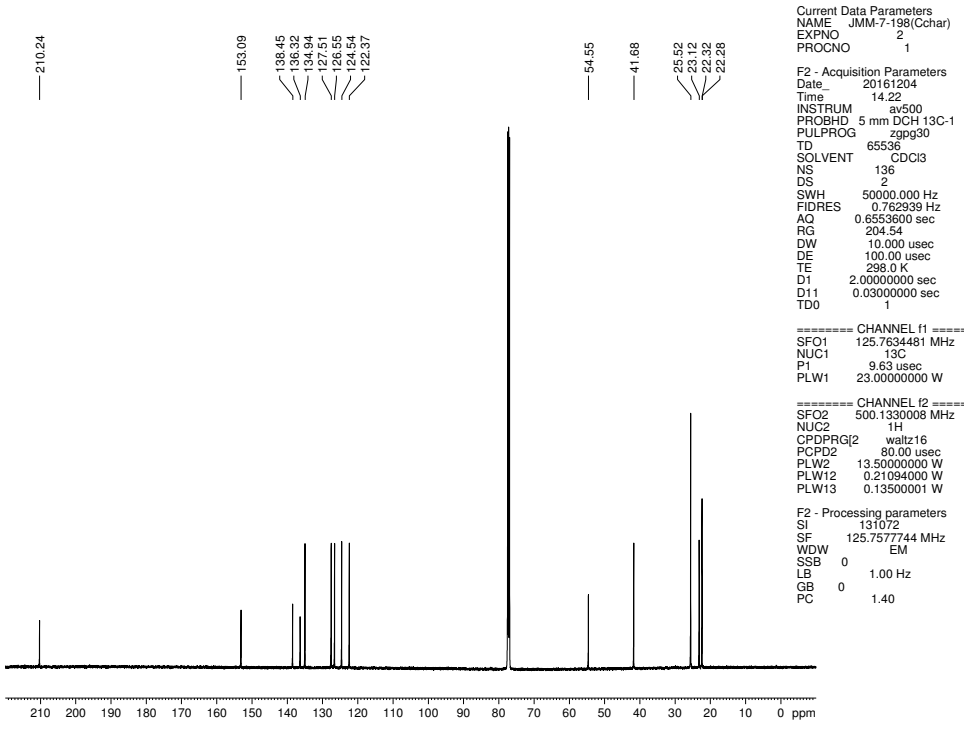

Figure 7.121 ^{13}C NMR (125 MHz, $CDCl_3$) of compound **7.14**

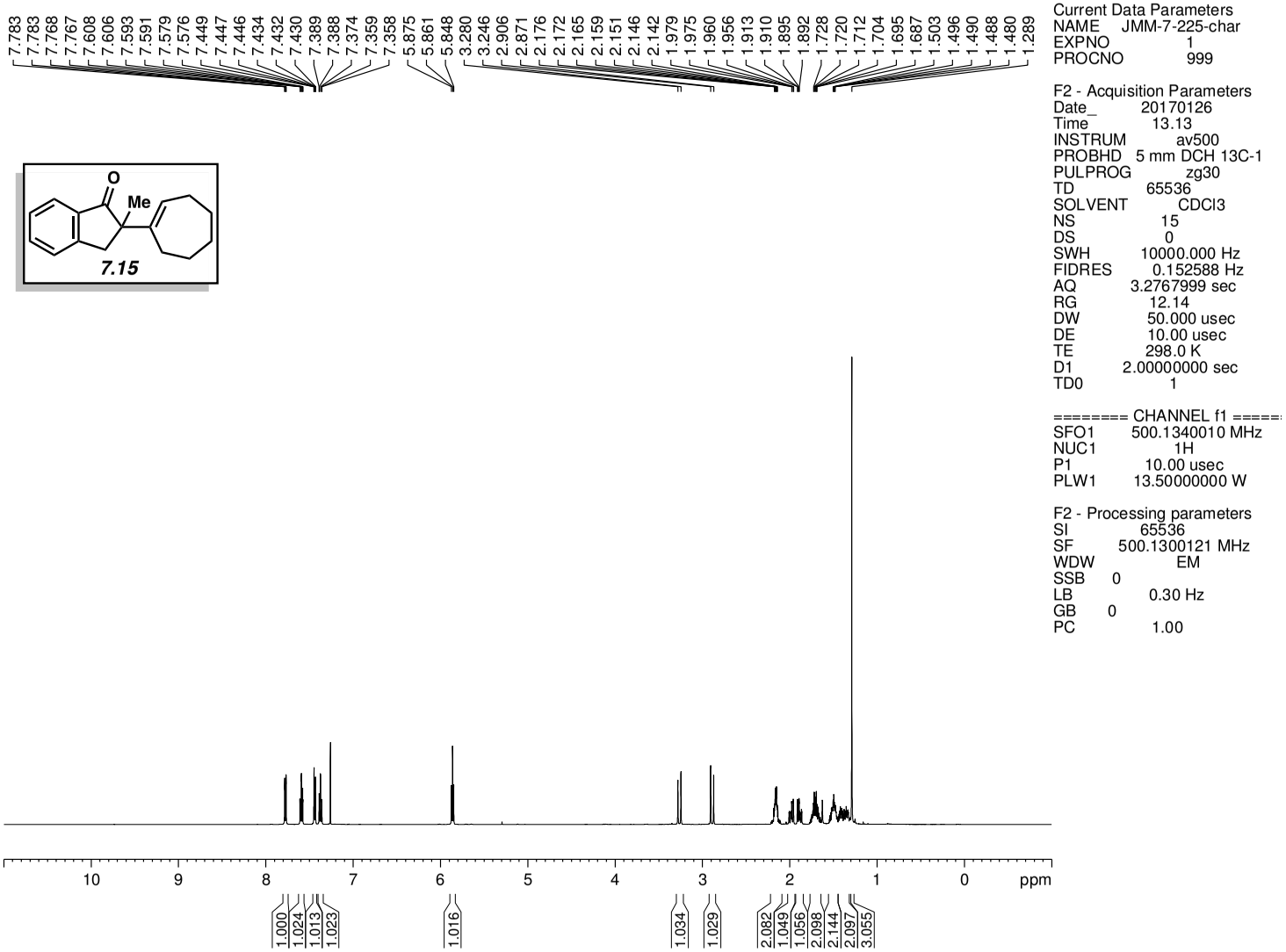

Figure 7.122 ^{1}H NMR (500 MHz, $CDCl_3$) of compound **7.15**

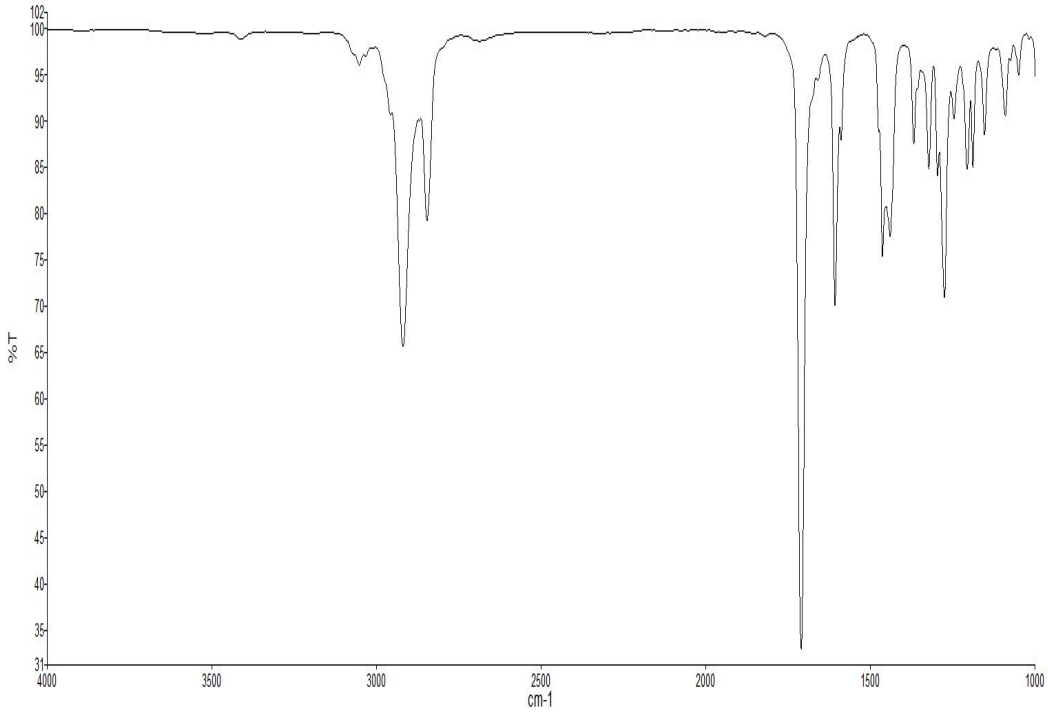

Figure 7.123 Infrared spectrum of compound **7.15**

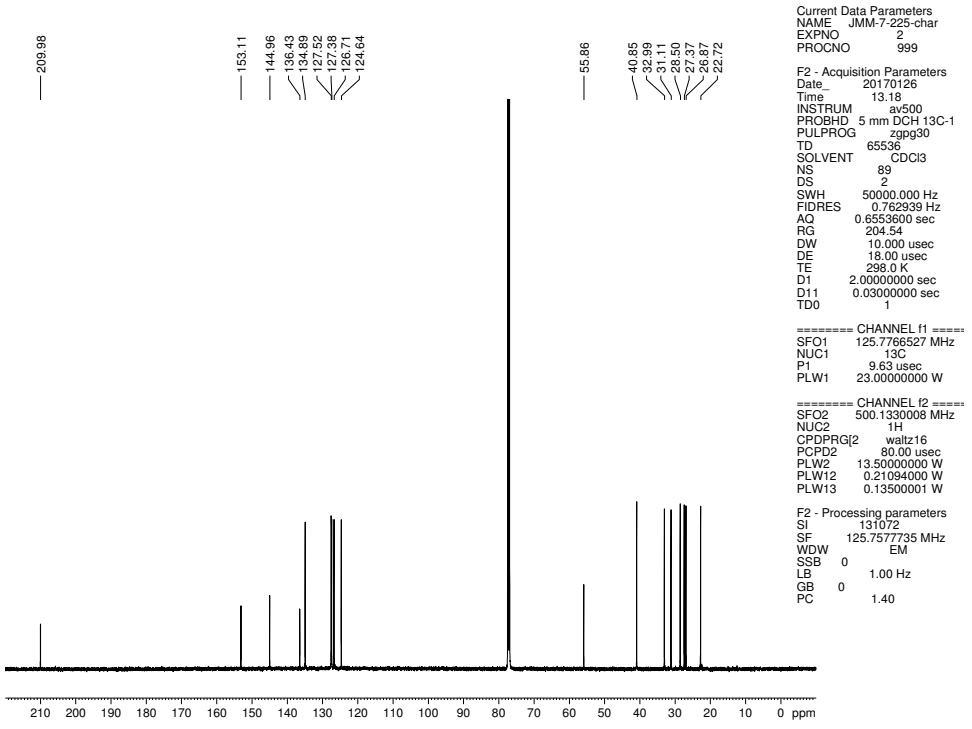

Figure 7.124 ^{13}C NMR (125 MHz, $CDCl_3$) of compound **7.15**

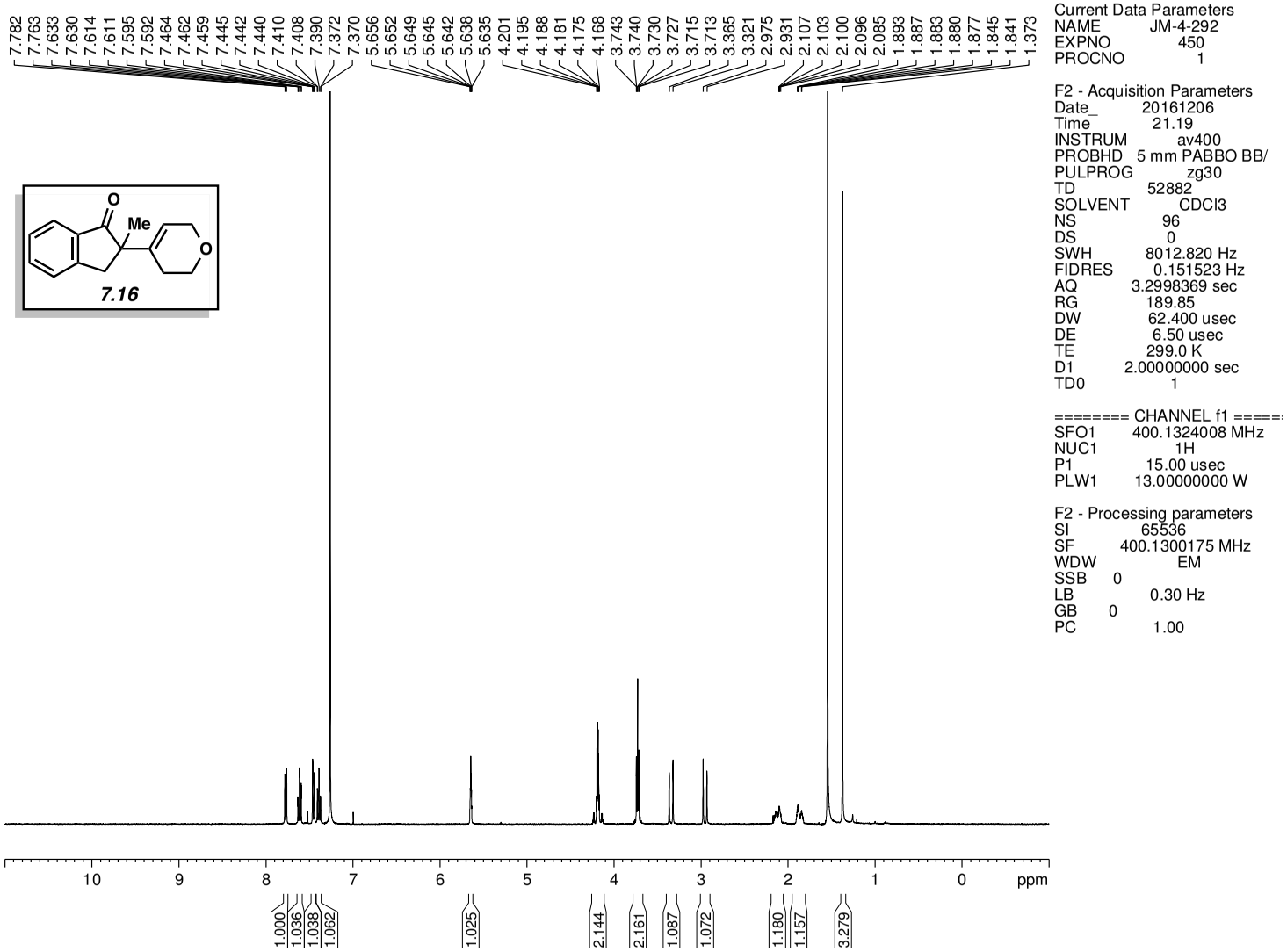

Figure 7.125 ^{1}H NMR (500 MHz, $CDCl_3$) of compound **7.16**

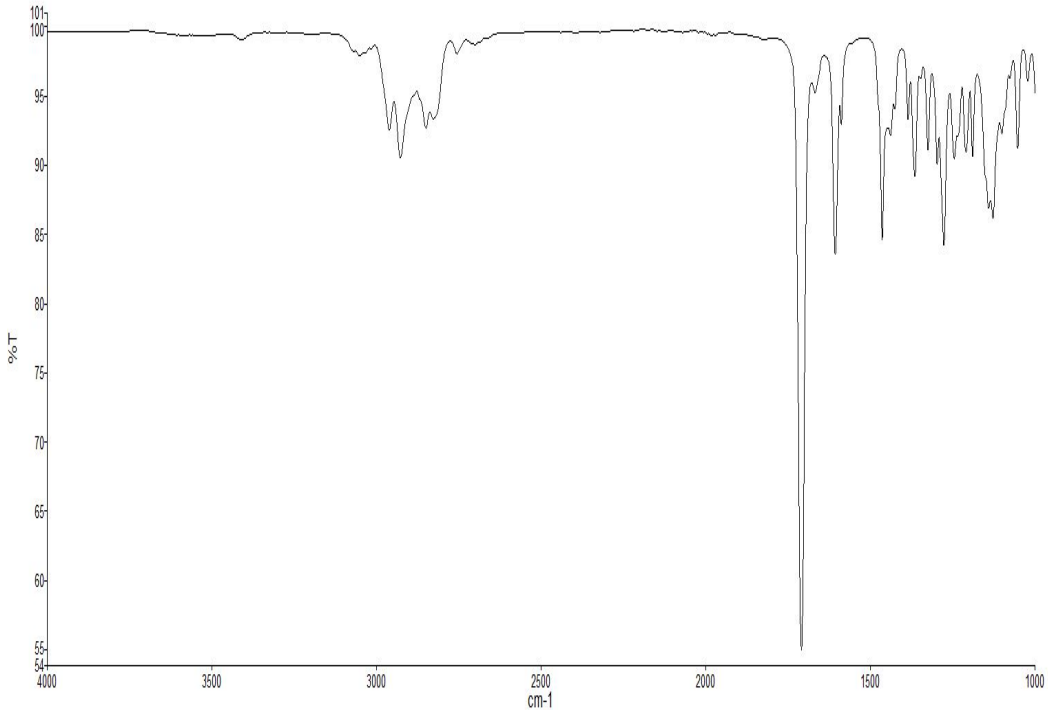

Figure 7.126 Infrared spectrum of compound **7.16**

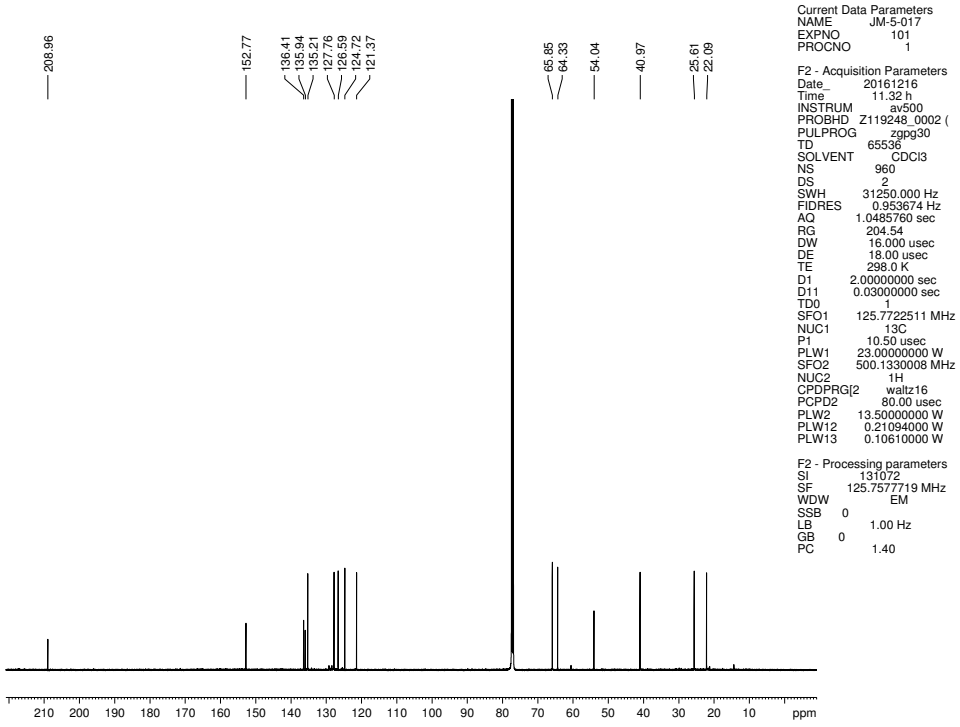

Figure 7.127 ^{13}C NMR (125 MHz, $CDCl_3$) of compound **7.16**

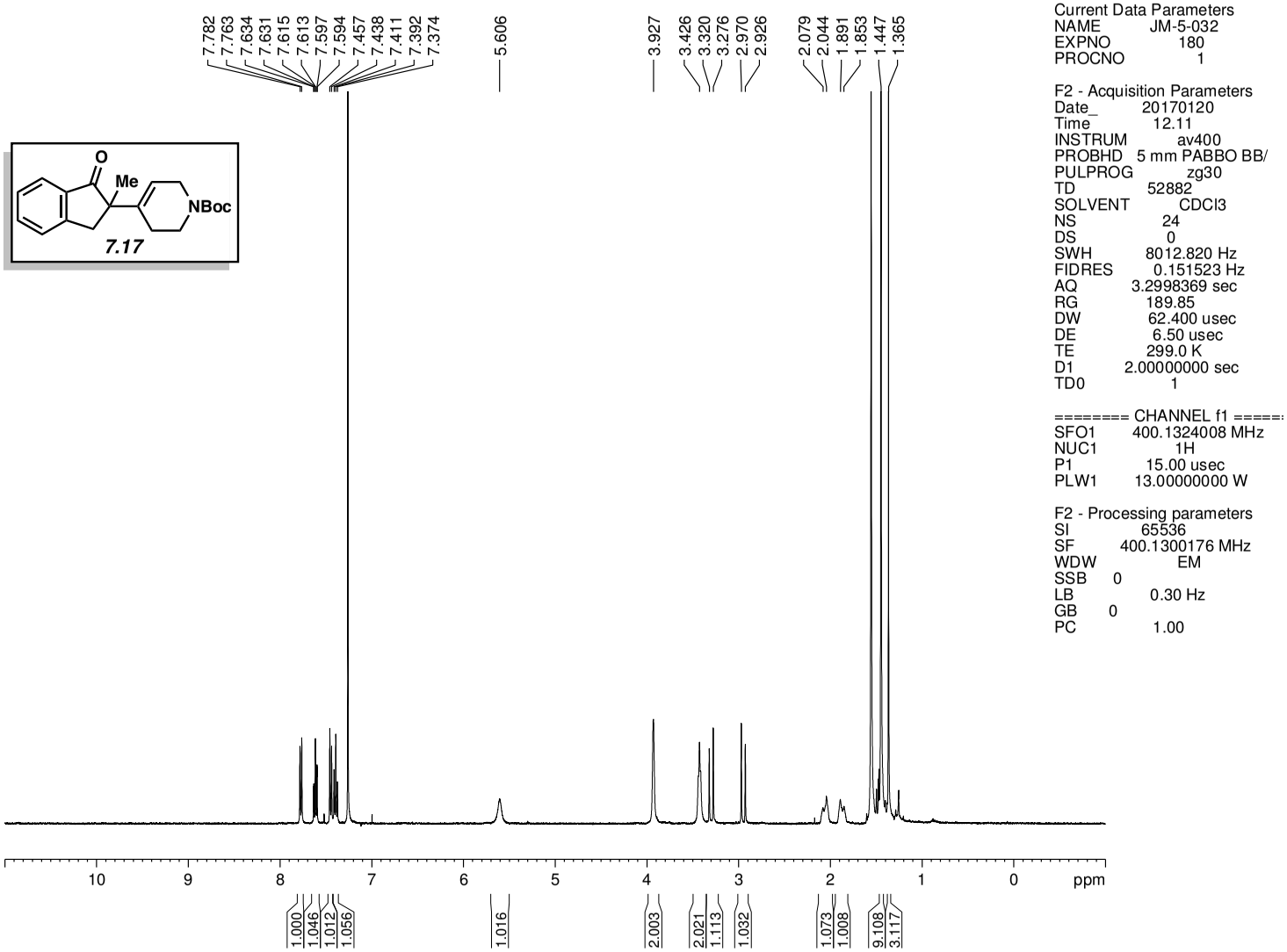

Figure 7.128 ^{1}H NMR (500 MHz, $CDCl_3$) of compound **7.17**

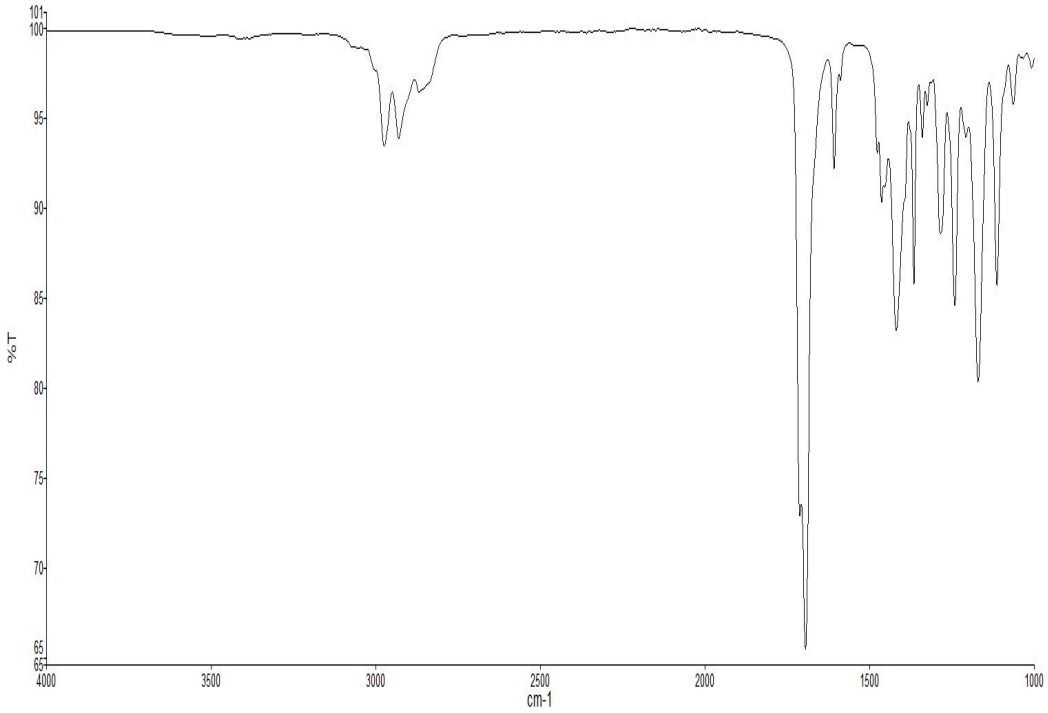

Figure 7.129 Infrared spectrum of compound **7.17**

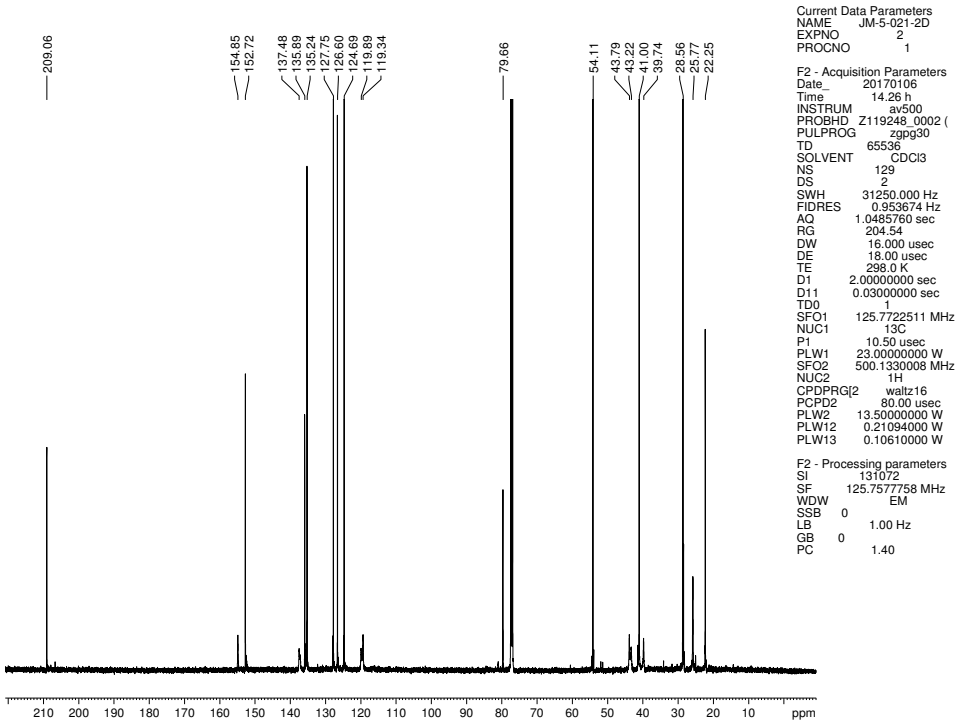

Figure 7.130 ^{13}C NMR (125 MHz, $CDCl_3$) of compound **7.17**

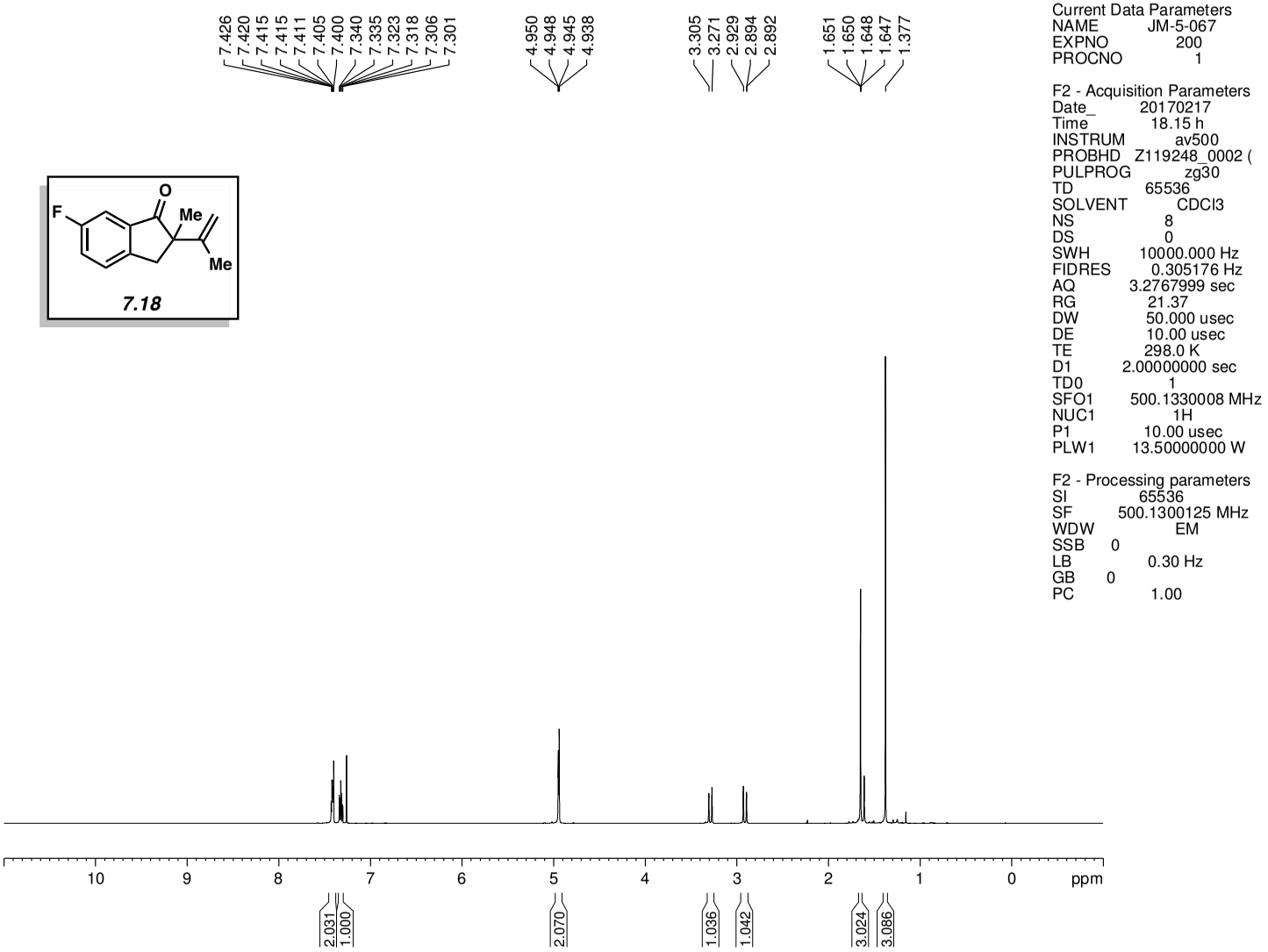

Figure 7.131 ^{1}H NMR (500 MHz, $CDCl_3$) of compound **7.18**

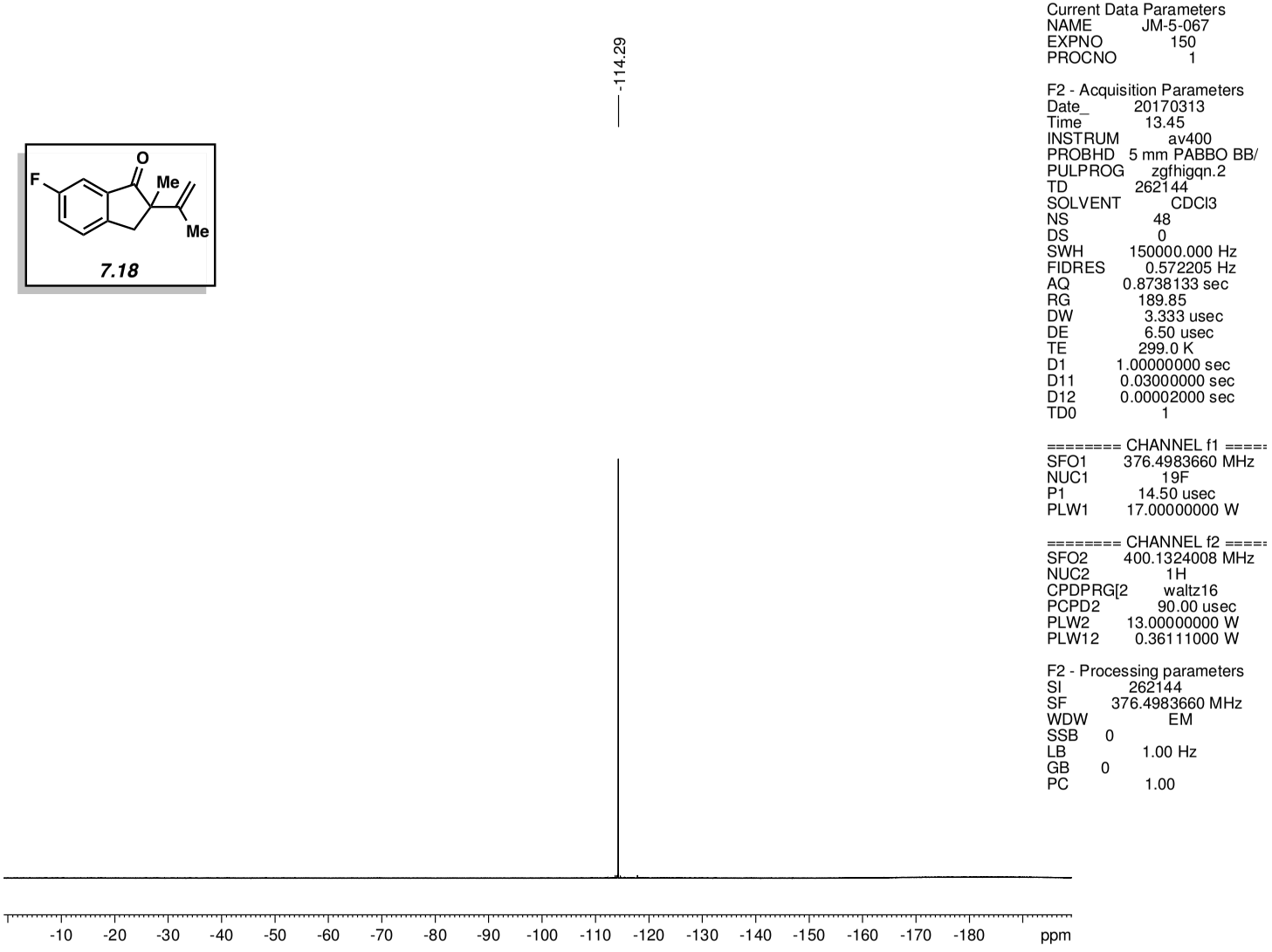

Figure 7.132 ^{19}F NMR (376 MHz, $CDCl_3$) of compound **7.18**

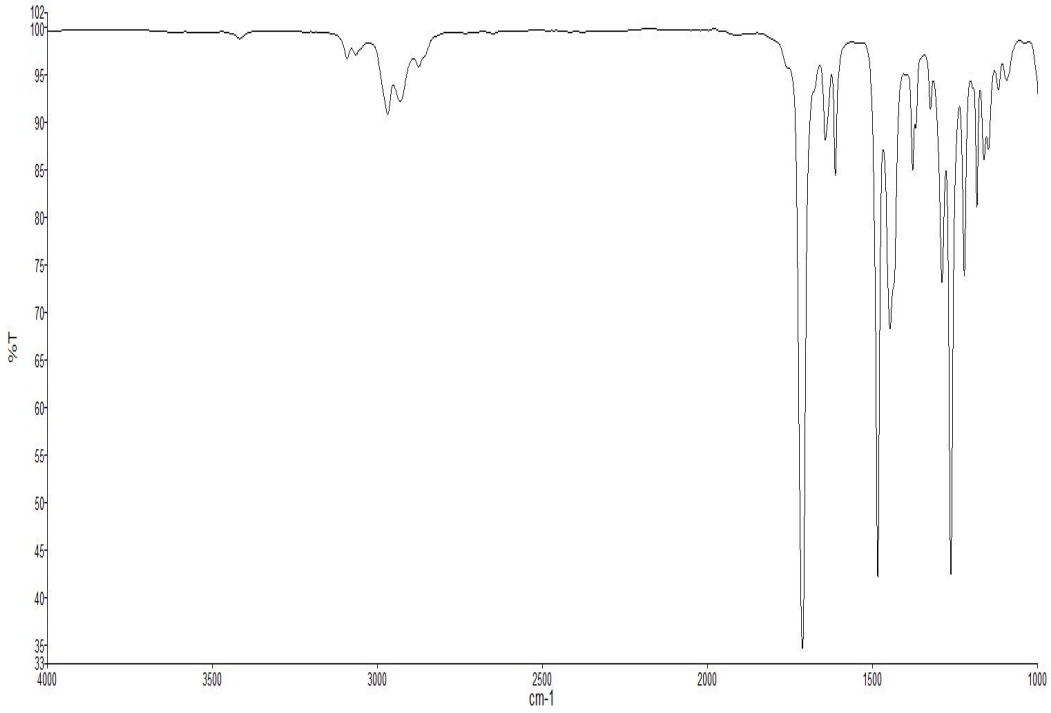

Figure 7.133 Infrared spectrum of compound **7.18**

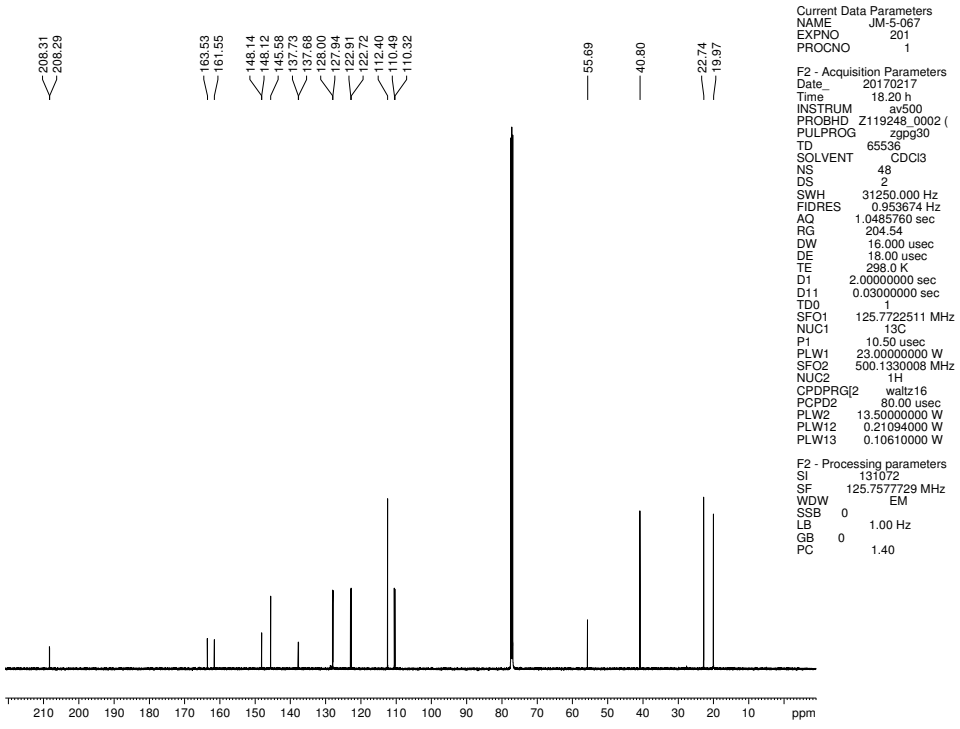

Figure 7.134 ^{13}C NMR (125 MHz, $CDCl_3$) of compound **7.18**

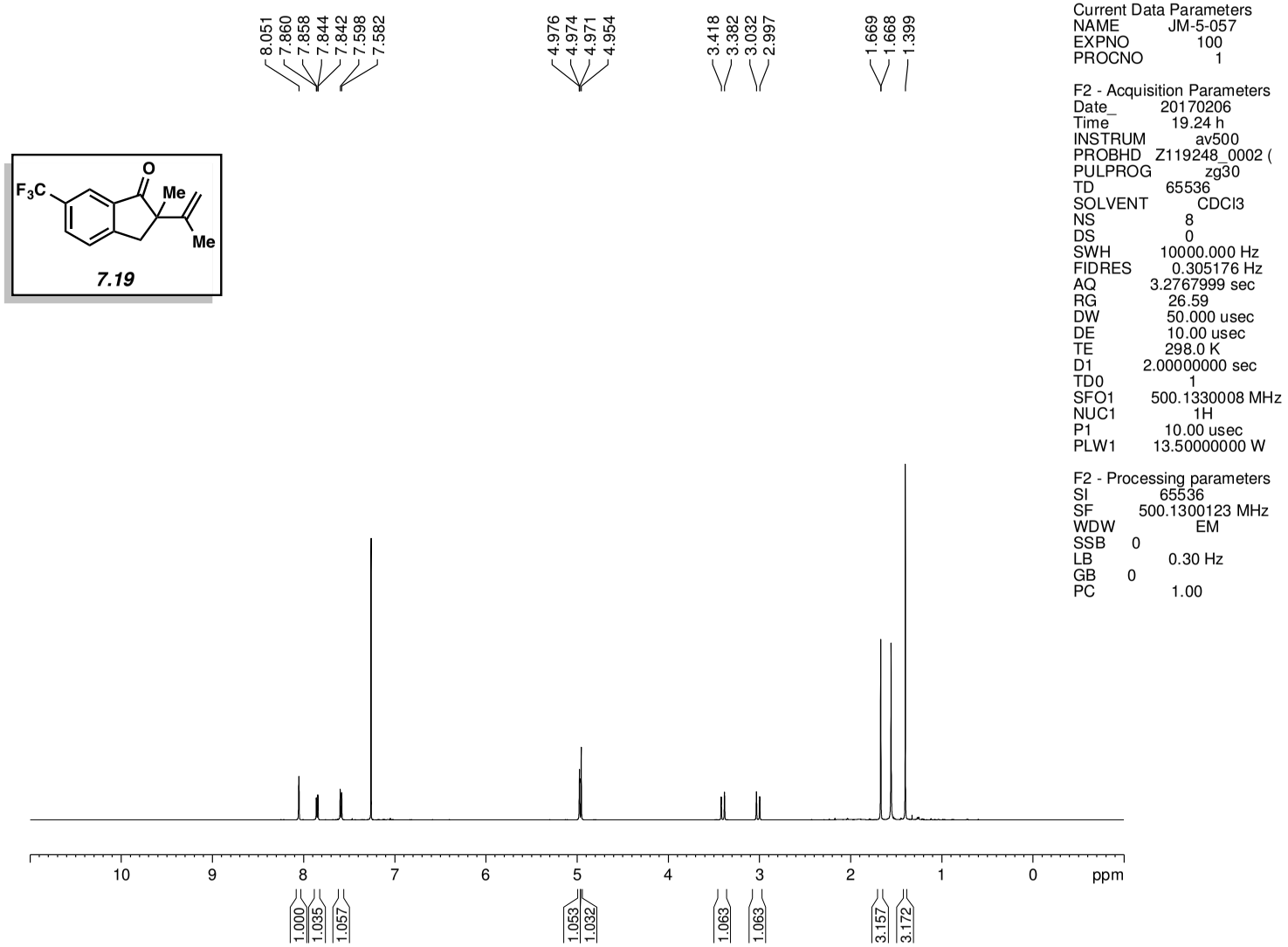

Figure 7.135 ^{1}H NMR (500 MHz, $CDCl_3$) of compound **7.19**

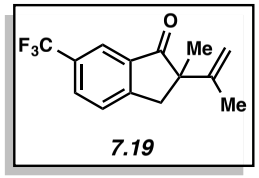

Current Data Parameters
NAME JM-5-057
EXPNO 180
PROCNO 1

F2 - Acquisition Parameters
Date_ 20170313
Time 14.03
INSTRUM av400
PROBHD 5 mm PABBO BB/
PULPROG zgfhigqn.2
TD 262144
SOLVENT CDCl3
NS 48
DS 0
SWH 150000.000 Hz
FIDRES 0.572205 Hz
AQ 0.8738133 sec
RG 189.85
DW 3.333 usec
DE 6.50 usec
TE 299.0 K
D1 1.00000000 sec
D11 0.03000000 sec
D12 0.00002000 sec
TD0 1

======== CHANNEL f1 =====
SFO1 376.4983660 MHz
NUC1 19F
P1 14.50 usec
PLW1 17.00000000 W

======== CHANNEL f2 =====
SFO2 400.1324008 MHz
NUC2 1H
CPDPRG[2 waltz16
PCPD2 90.00 usec
PLW2 13.00000000 W
PLW12 0.36111000 W

F2 - Processing parameters
SI 262144
SF 376.4983660 MHz
WDW EM
SSB 0
LB 1.00 Hz
GB 0
PC 1.00

Figure 7.136 ^{19}F NMR (376 MHz, $CDCl_3$) of compound **7.19**

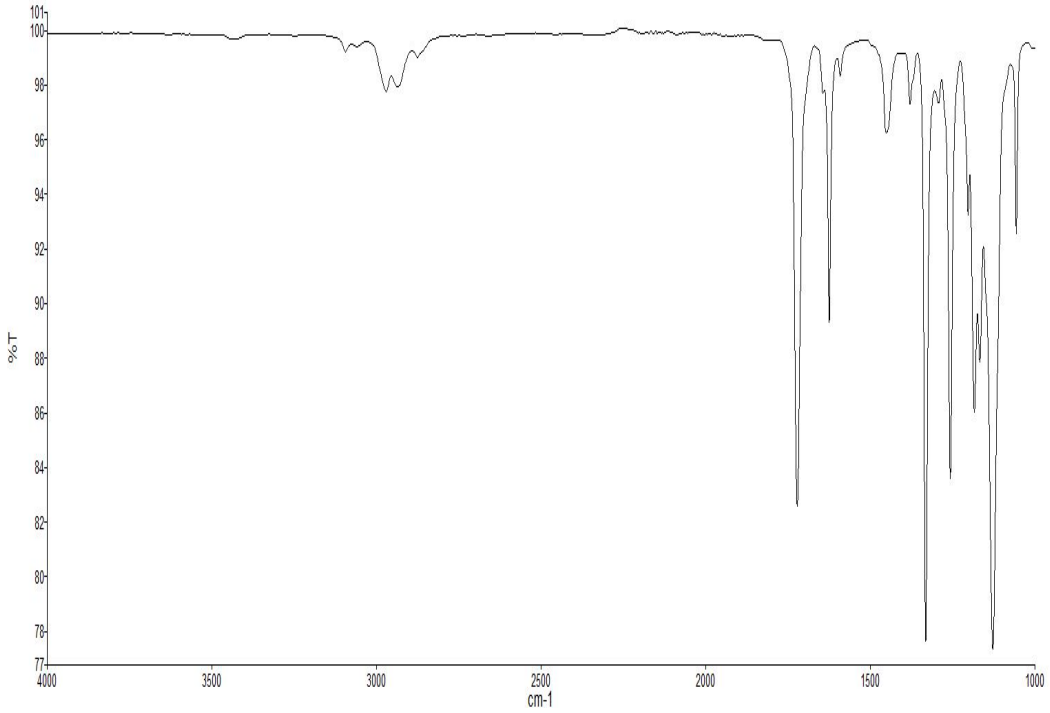

Figure 7.137 Infrared spectrum of compound **7.19**

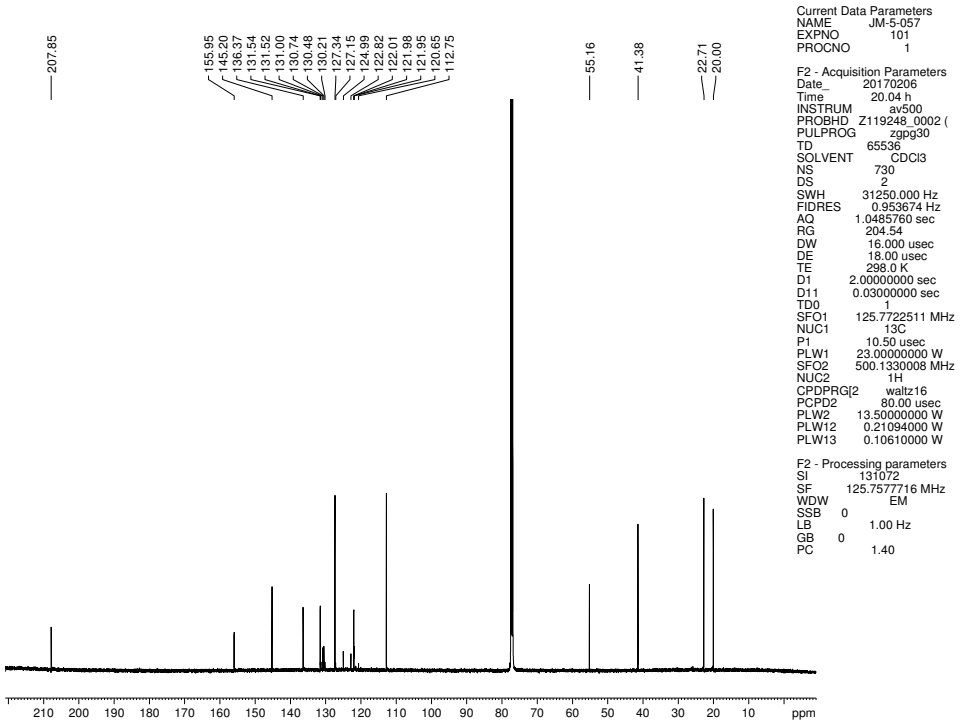

Figure 7.138 ^{13}C NMR (125 MHz, $CDCl_3$) of compound **7.19**

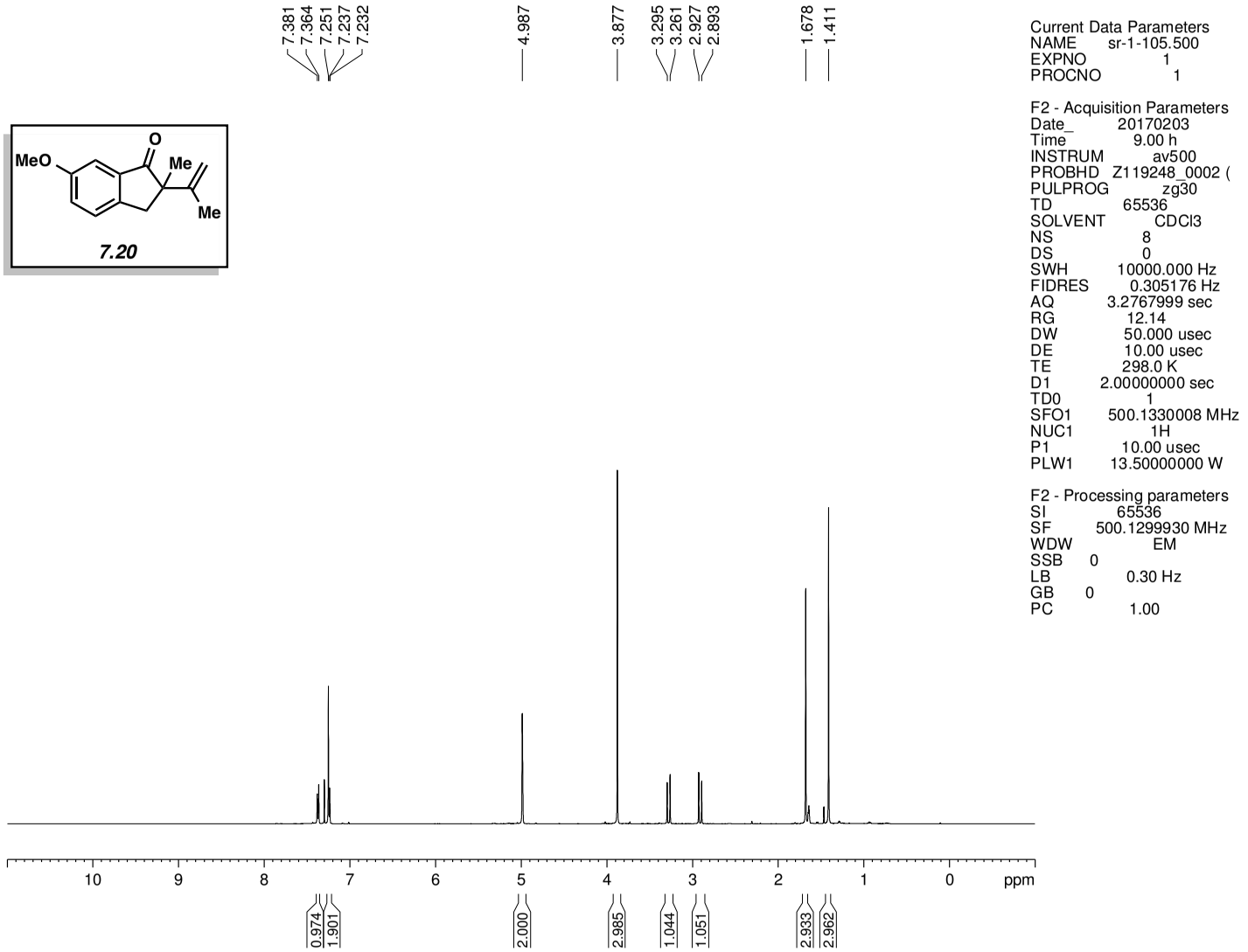

Figure 7.139 ^{1}H NMR (500 MHz, $CDCl_3$) of compound **7.20**

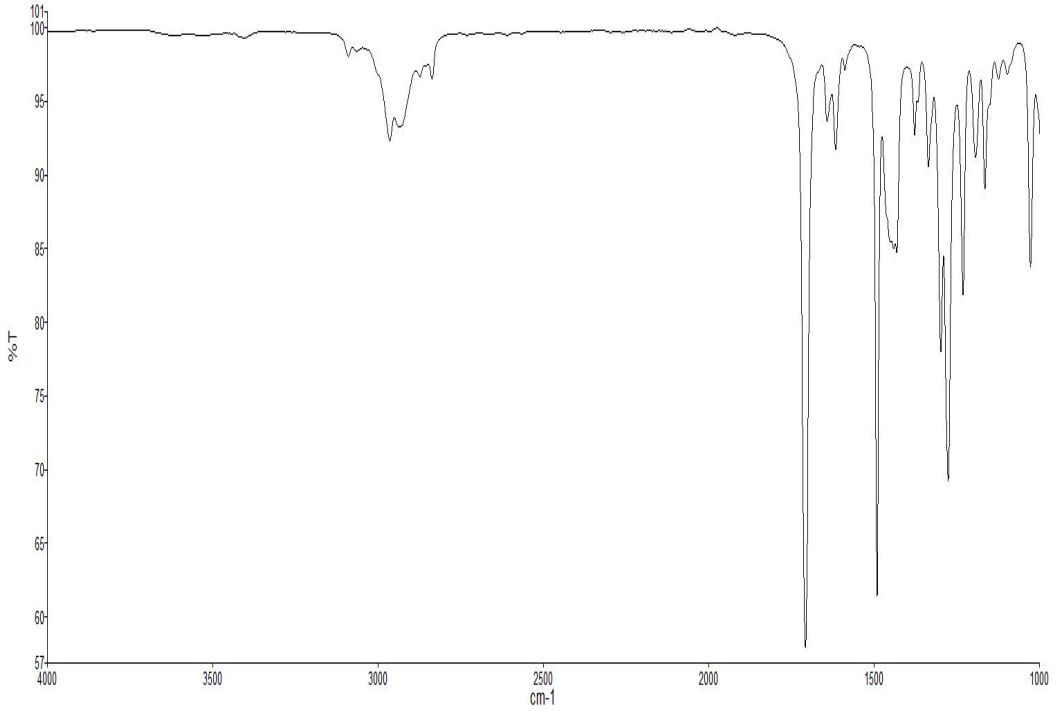

Figure 7.140 Infrared spectrum of compound **7.20**

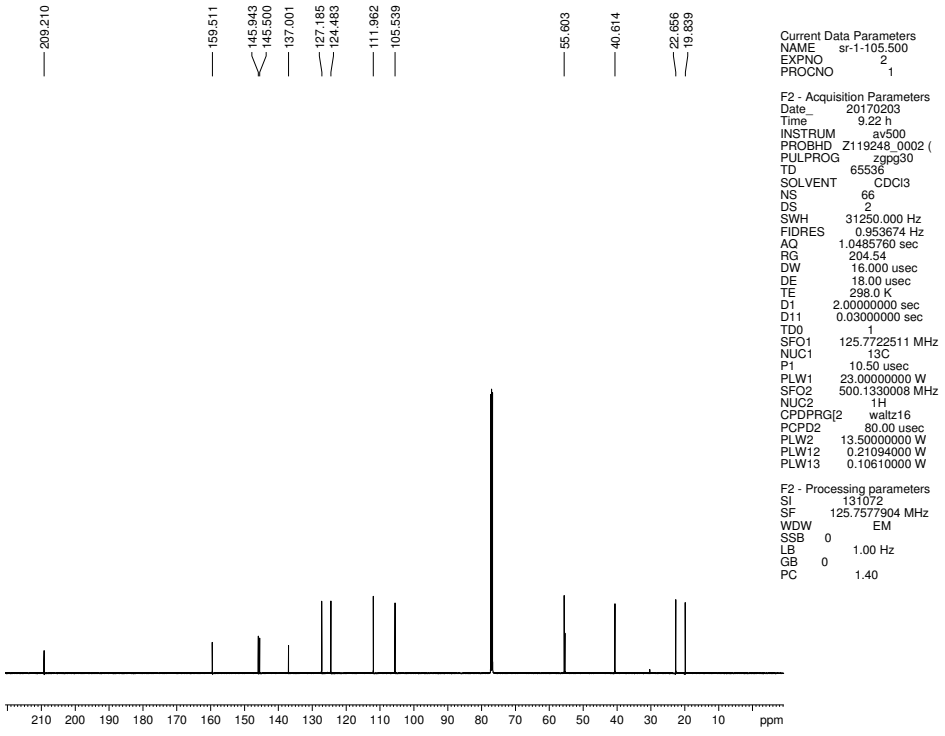

Figure 7.141 ^{13}C NMR (125 MHz, $CDCl_3$) of compound **7.20**

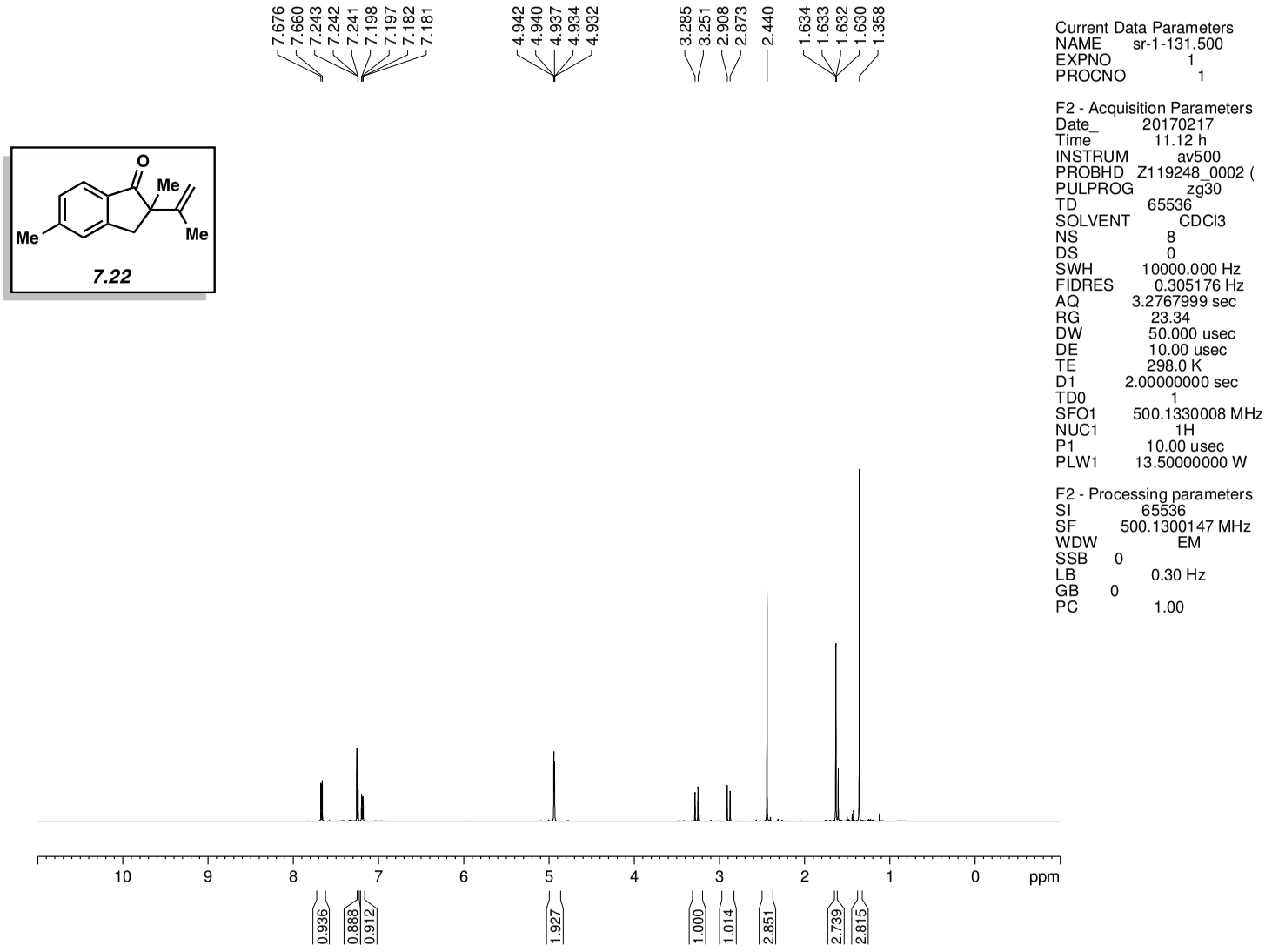

Figure 7.142 ^{1}H NMR (500 MHz, $CDCl_3$) of compound **7.22**

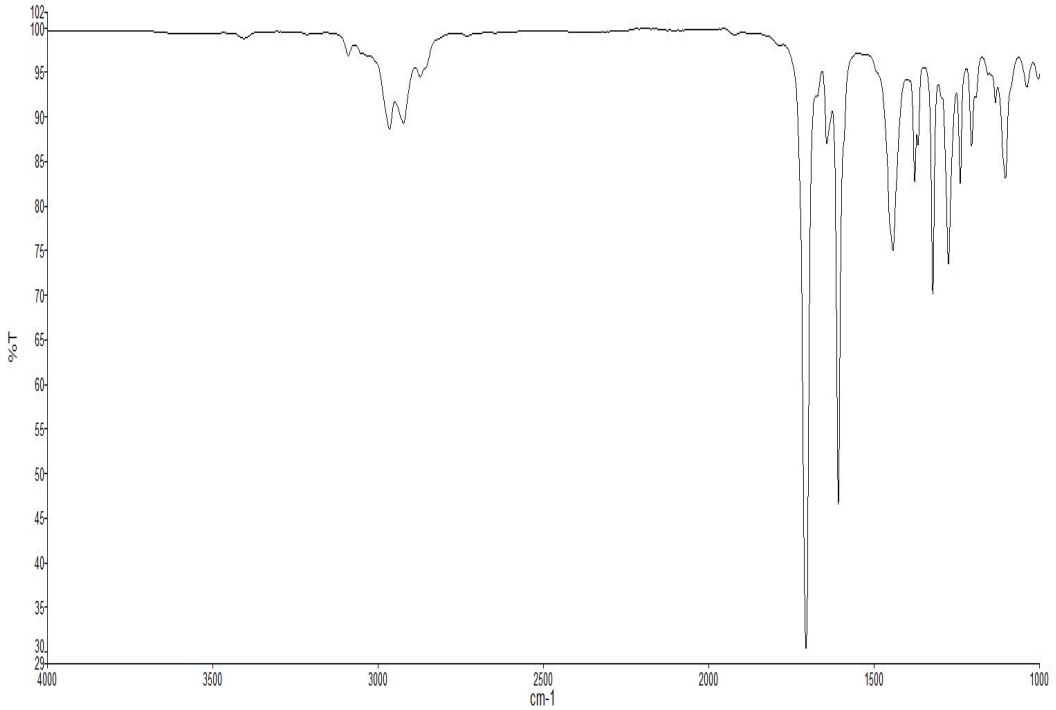

Figure 7.143 Infrared spectrum of compound **7.22**

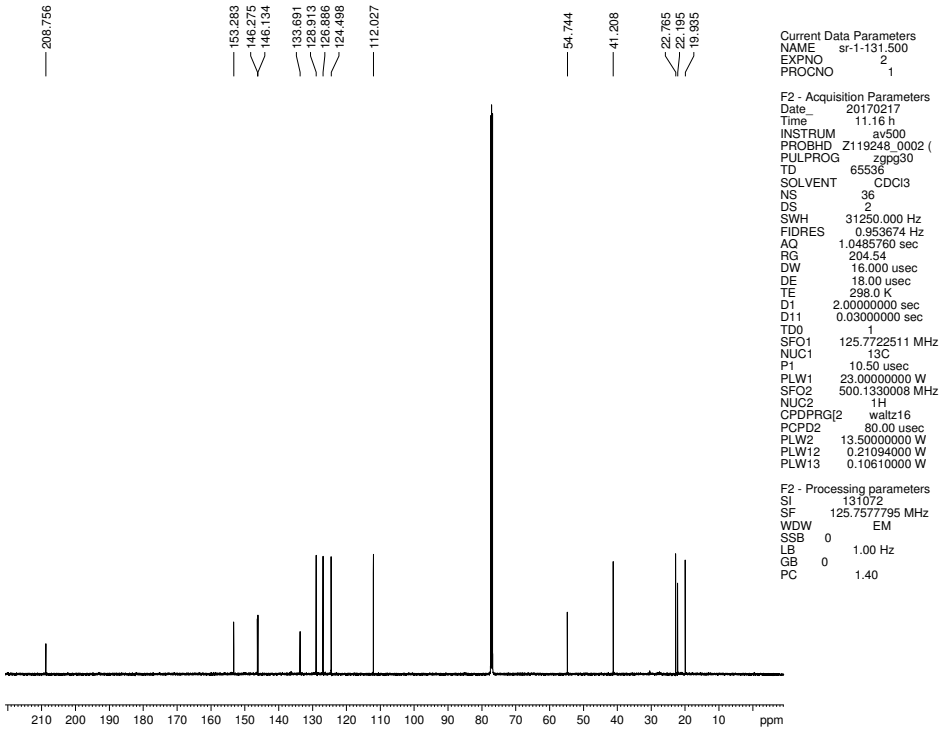

Figure 7.144 ^{13}C NMR (125 MHz, $CDCl_3$) of compound **7.22**

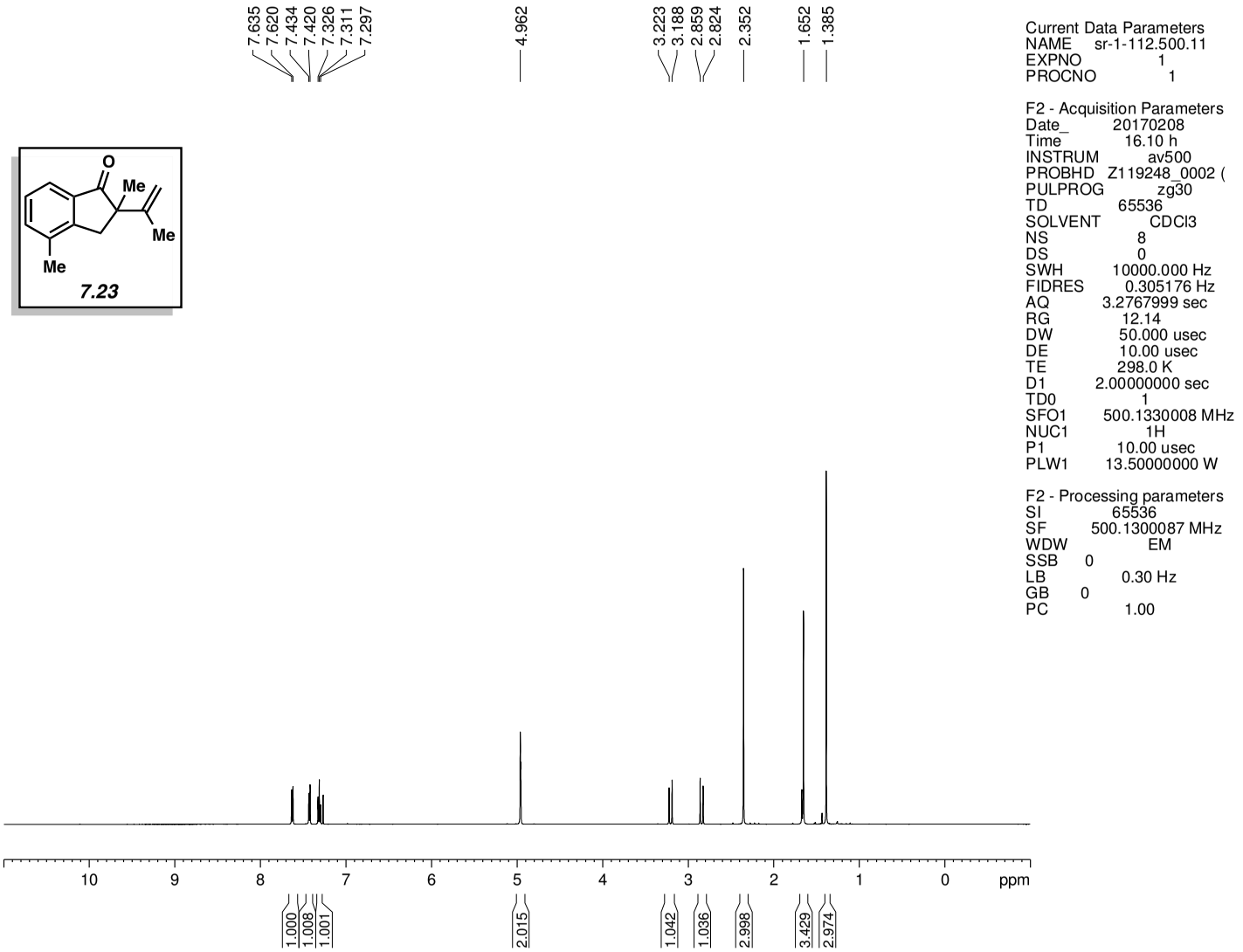

Figure 7.145 ^{1}H NMR (500 MHz, $CDCl_3$) of compound **7.23**

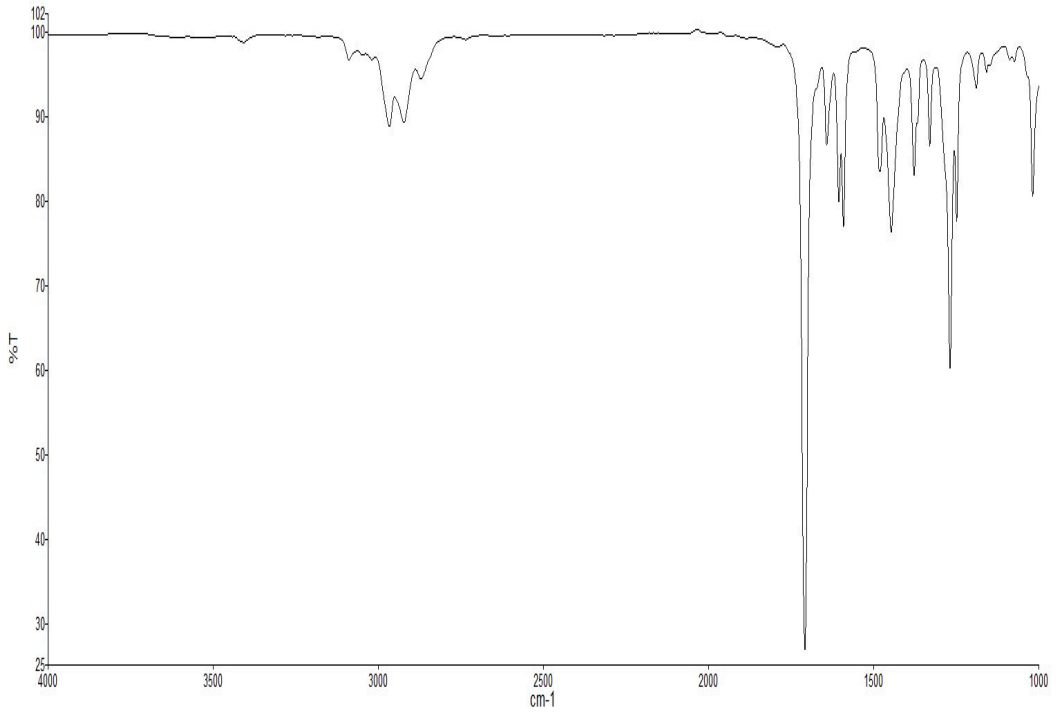

Figure 7.146 Infrared spectrum of compound **7.23**

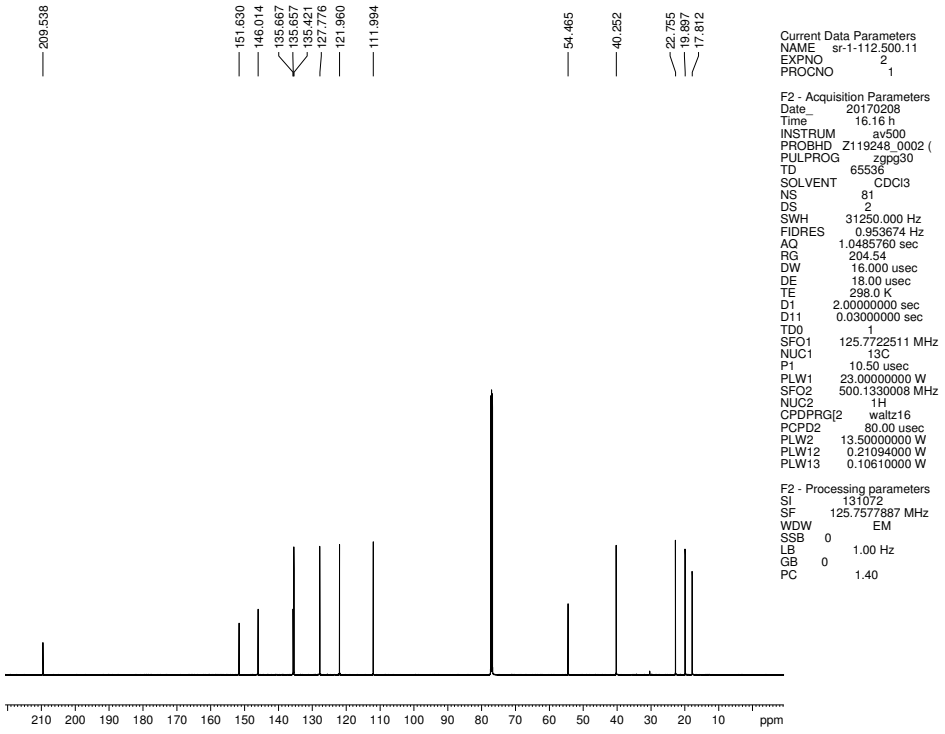

Figure 7.147 ^{13}C NMR (125 MHz, $CDCl_3$) of compound **7.23**

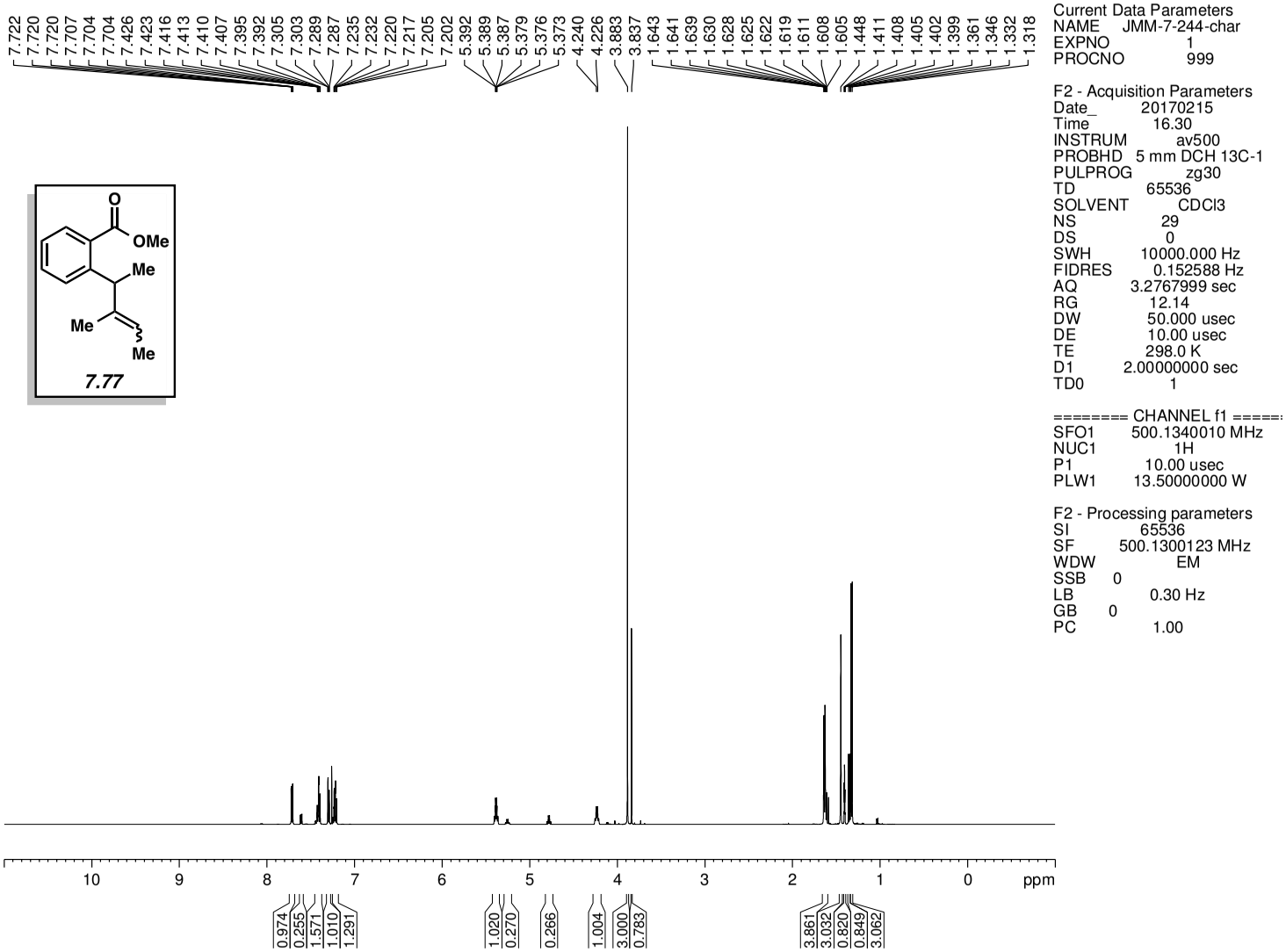

Figure 7.148 ^{1}H NMR (500 MHz, $CDCl_3$) of compound **7.77**

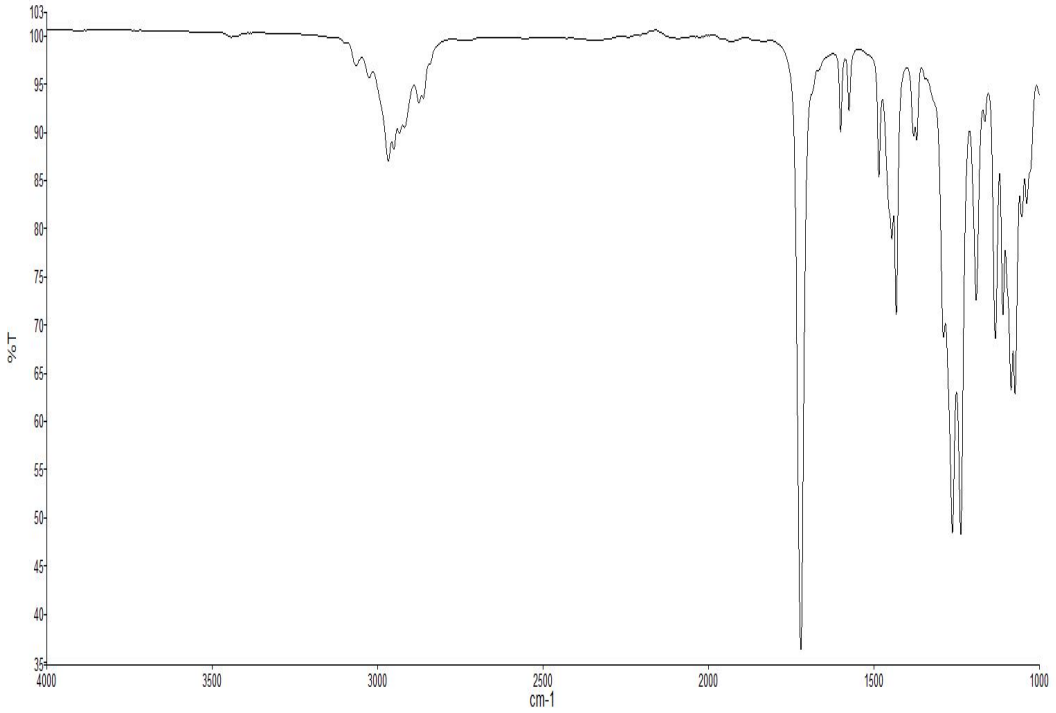

Figure 7.149 Infrared spectrum of compound **7.77**

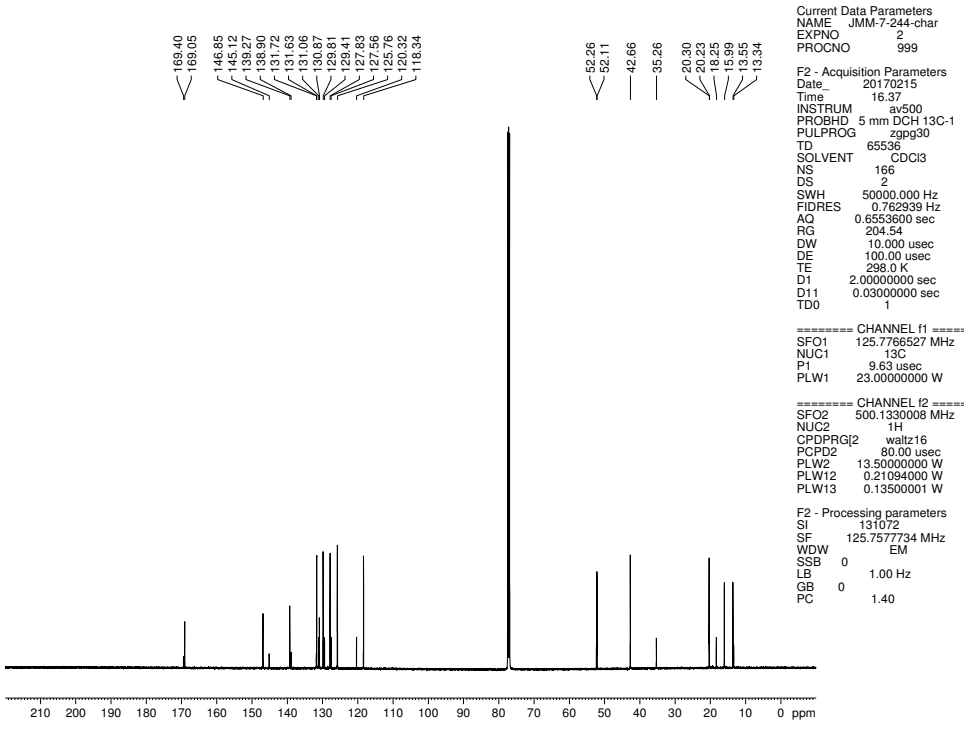

Figure 7.150 ^{13}C NMR (125 MHz, $CDCl_3$) of compound **7.77**

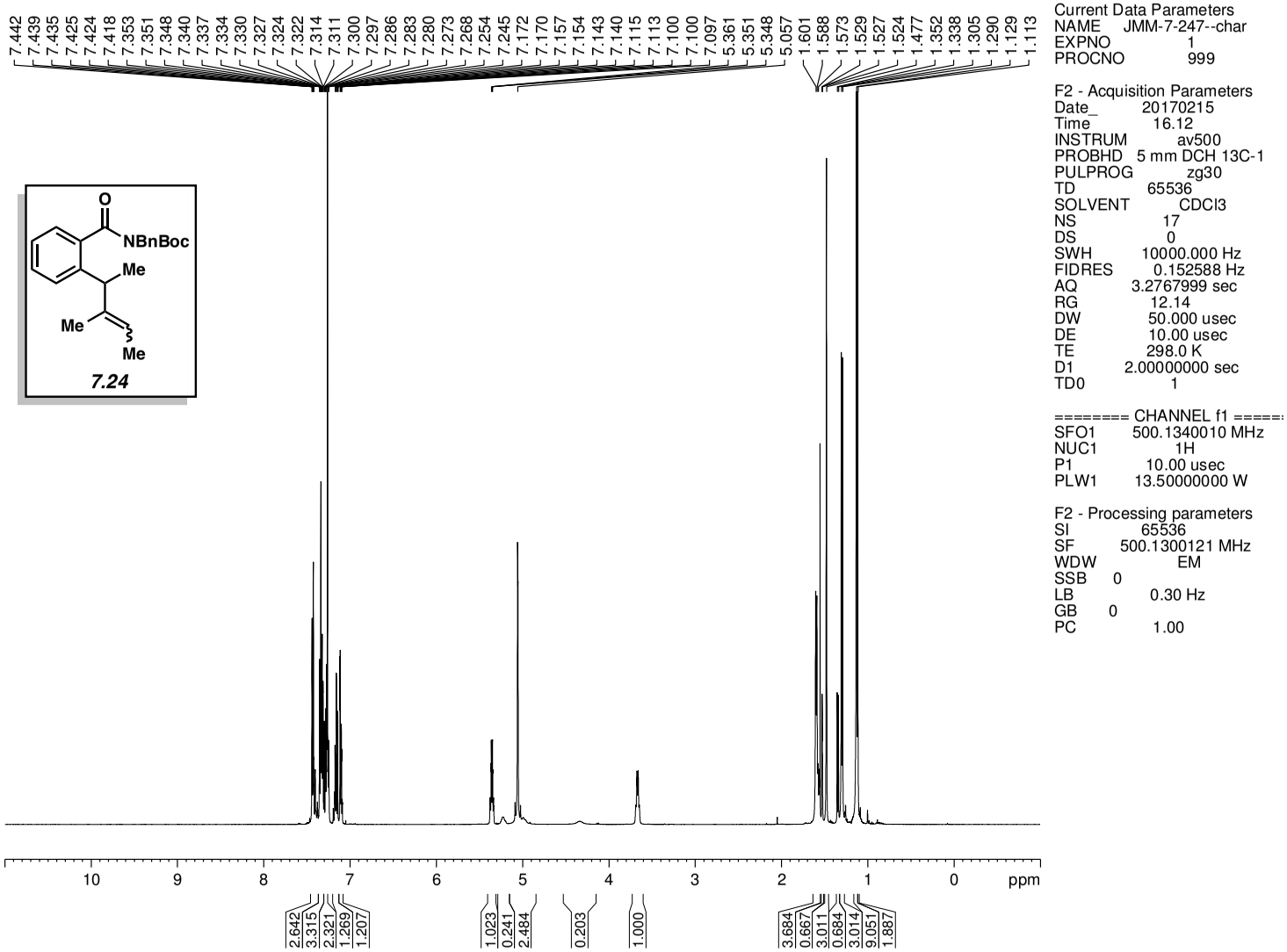

Figure 7.151 ^{1}H NMR (500 MHz, $CDCl_3$) of compound **7.24**

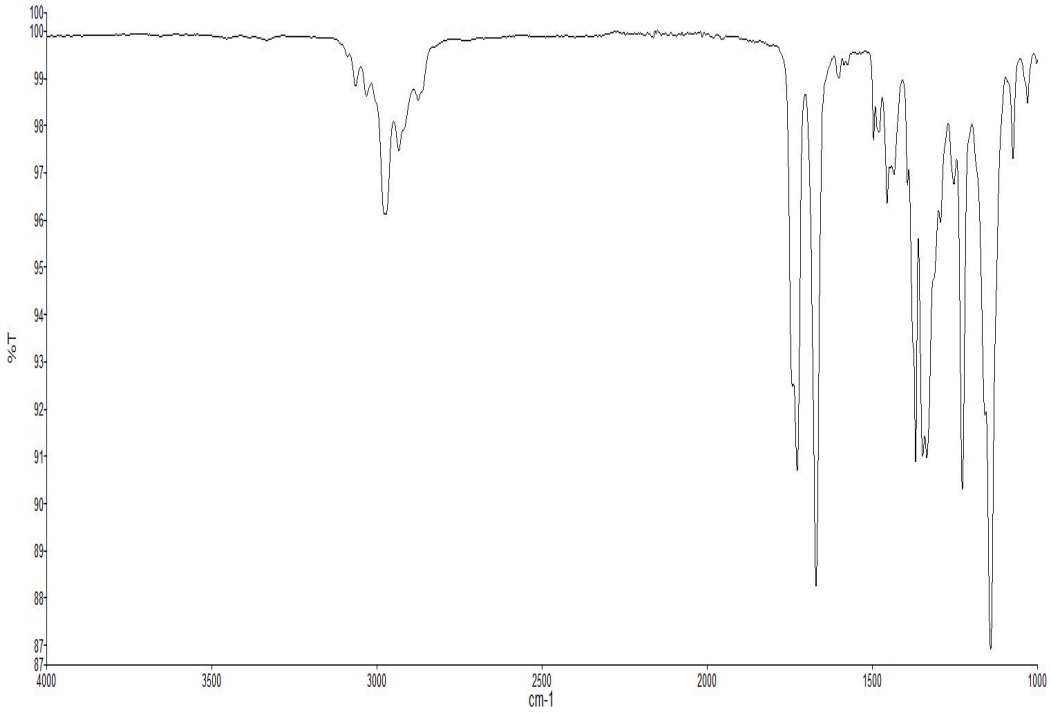

Figure 7.152 Infrared spectrum of compound **7.24**

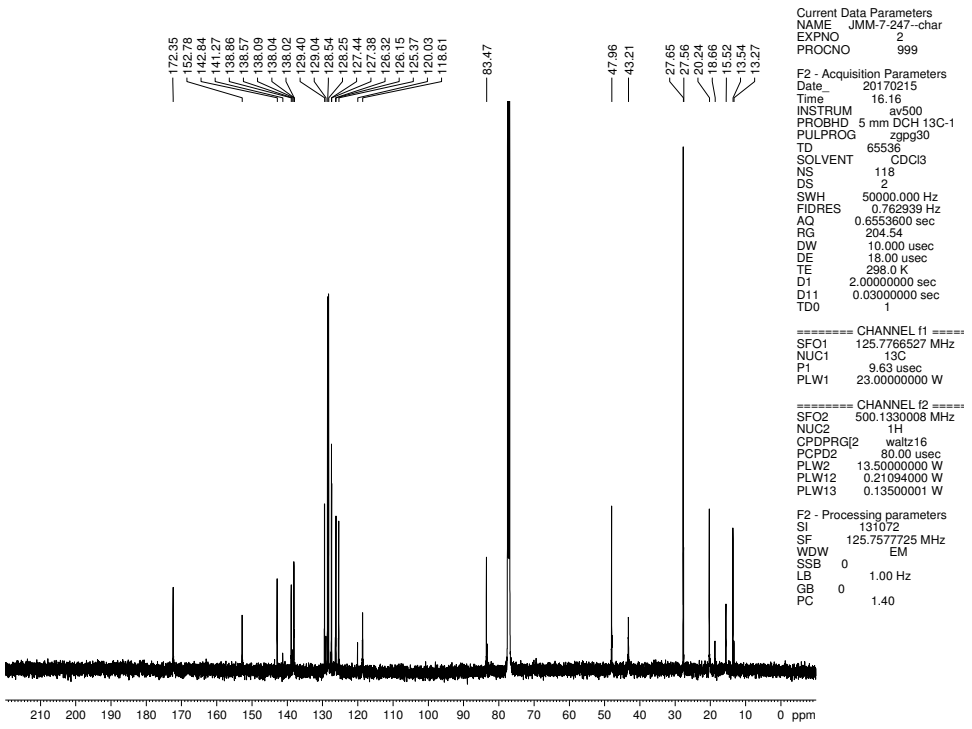

Figure 7.153 ^{13}C NMR (125 MHz, $CDCl_3$) of compound **7.24**

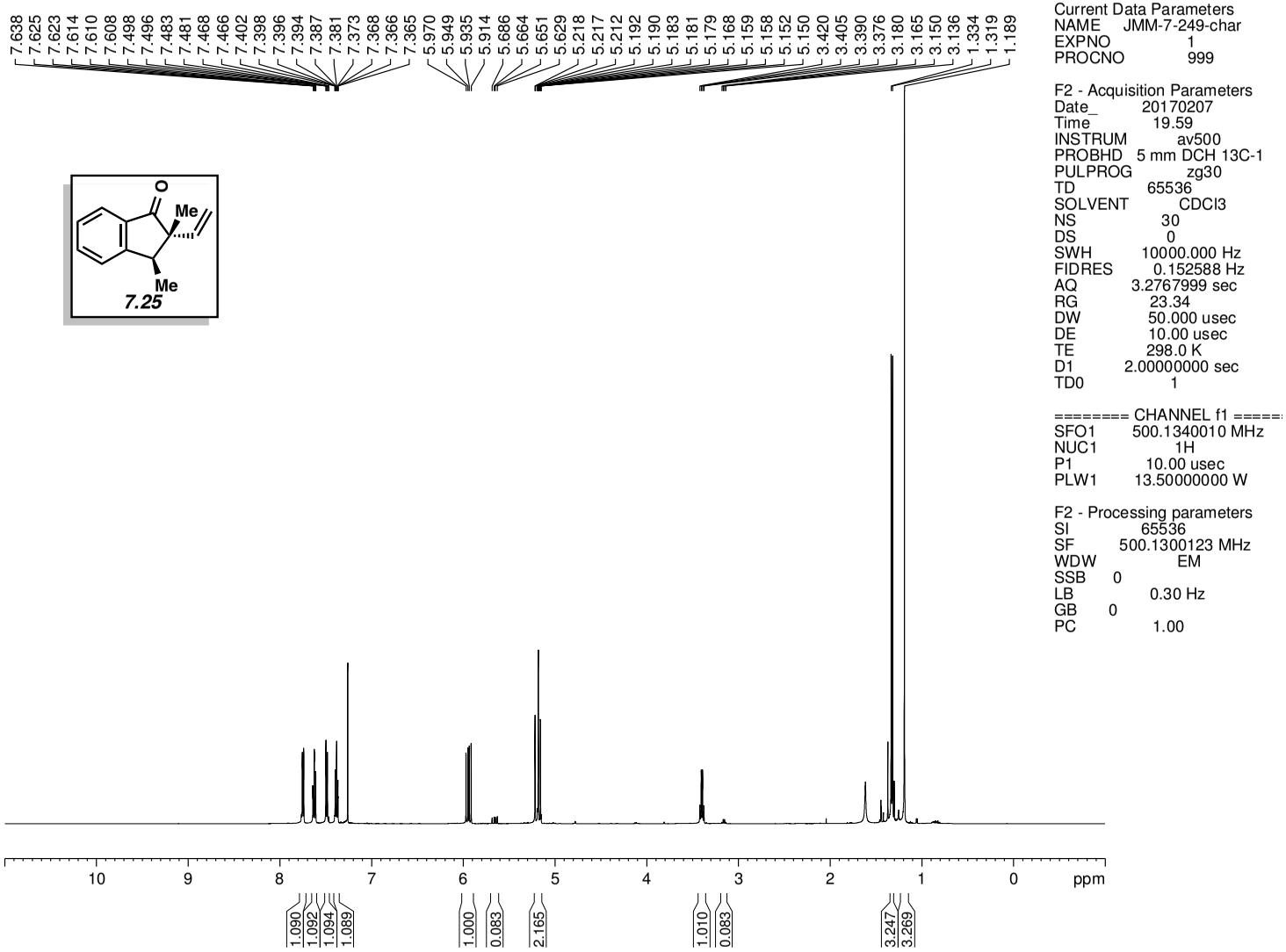

Figure 7.154 ^{1}H NMR (500 MHz, $CDCl_3$) of compound **7.25**

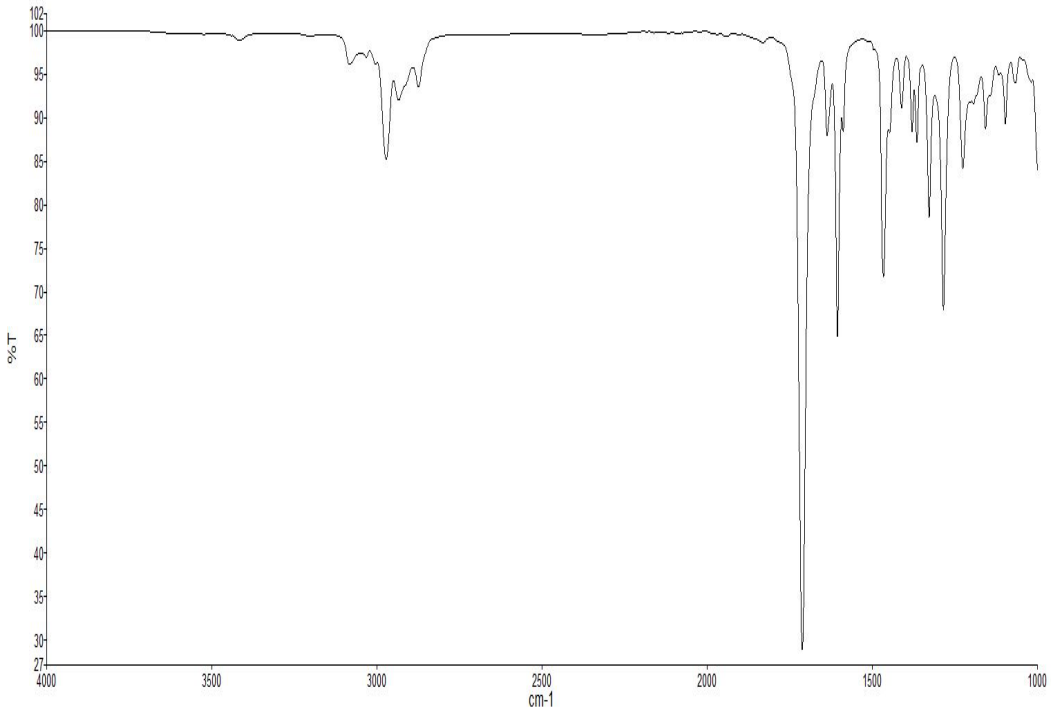

Figure 7.155 Infrared spectrum of compound **7.25**

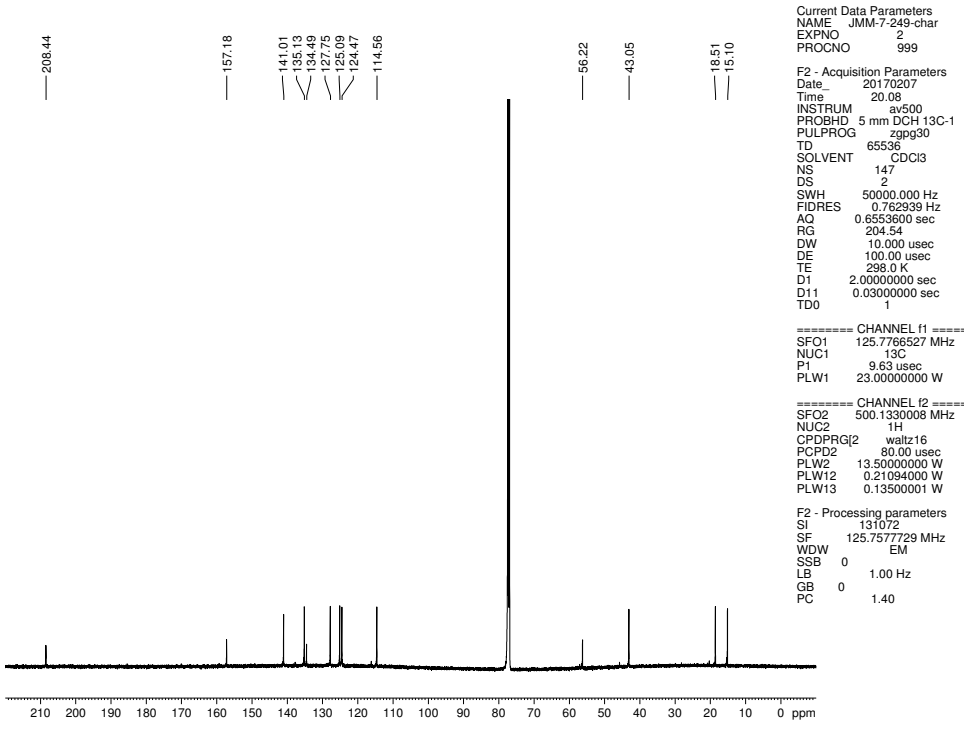

Figure 7.156 ^{13}C NMR (125 MHz, $CDCl_3$) of compound **7.25**

7.7 Notes and References

(1) For reviews on quaternary stereocenters, see: (a) Christoffers, J.; Baro, A. *Adv. Synth. Catal.* **2005**, *347*, 1473–1482. (b) Trost, B. M.; Jiang, C. *Synthesis* **2006**, *3*, 369–396. (c) Quasdorf, K. W.; Overman, L. E. *Nature* **2014**, *516*, 181–191. (d) Marek, I.; Minko, Y.; Pasco, M.; Mejuch, T.; Gilboa, N.; Chechik, H.; Das, J. P. *J. Am. Chem. Soc.* **2014**, *136*, 2682–2694. (e) Liu, Y.; Han, S.-J.; Liu, W.-B.; Stoltz, B. M. *Acc. Chem. Res.* **2015**, *48*, 740–751. (f) Long, R.; Huang, J.; Gong, J.; Yang, Z. *Nat. Prod. Rep.* **2015**, *32*, 1584–1601. (g) Zeng, X.-P.; Cao, Z.-Y.; Wang, Y.-H.; Zhou, F.; Zhou, J. *Chem. Rev.* **2016**, *116*, 7330–7396. (h) Christoffers, J.; Baro, A. John Wiley & Sons. *Quaternary stereocenters: challenges and solutions for organic synthesis*; Wiley-VCH: Weinheim, **2005**.

(2) (a) Beletskaya, I. P.; Cheprakov, A. V. *Chem. Rev.* **2000**, *100*, 3009–3066. (b) Whitcombe, N. J.; Hii, K. K.; Gibson, S. E. *Tetrahedron* **2001**, *57*, 7449–7476. (c) Dounay, A. B.; Overman, L. E. *Chem. Rev.* **2003**, *103*, 2945–2964. (d) Shibasaki, M.; Vogl, E. M.; Ohshima, T. *Adv. Synth. Catal.* **2004**, *346*, 1533–1552. (e) Oestreich, M. *Top. Organomet. Chem.* **2007**, *24*, 169–192. (f) Shibasaki, M.; Ohshima, T.; Itano, W. *Sci. Synth.* **2011**, *3*, 483–512. (g) Mc Cartney, D.; Guiry, P. J. *Chem. Soc. Rev.* **2011**, *40*, 5122–5150. (h) Le Bras, J.; Muzart, J. *Chem. Rev.* **2011**, *111*, 1170–1214. (i) Jones, A. C.; May, J. A.; Sarpong, R.; Stoltz, B. M. *Angew. Chem., Int. Ed.* **2014**, *53*, 2556–2591.

(3) β-hydride elimination of Ni(II) intermediates is known to be challenging; see: Lin, B.-L.; Liu, L.; Fu, Y.; Luo, S.-W.; Chen, Q.; Guo, Q.-X. *Organometallics* **2004**, *23*, 2114–2123.

(4) For Ni-catalyzed reactions of amide derivatives to build C–O or C–N bonds, see: (a) Hie, L.; Fine Nathel, N. F.; Shah, T.; Baker, E. L.; Hong, X.; Yang, Y.-F.; Liu, P.; Houk, K. N.; Garg, N. K. *Nature* **2015**, *524*, 79–83. (b) Baker, E. L.; Yamano, M. M.; Zhou, Y.; Anthony, S. M.; Garg,

N. K. *Nat. Commun*. **2016**, *7*, 11554. (c) Hie, L.; Baker, E. L.; Anthony, S. M.; Desrosiers, J.-N.; Senanayake, C.; Garg, N. K. *Angew. Chem., Int. Ed.* **2016**, *55*, 15129–15132.

(5) For Ni-catalyzed reactions of amide derivatives to build C–C bonds, see: (a) Weires, N. A.; Baker, E. L.; Garg, N. K. *Nat. Chem*. **2016**, *8*, 75–79. (b) Simmons, B. J.; Weires, N. A.; Dander, J. E.; Garg, N. K. *ACS Catal*. **2016**, *6*, 3176–3179. (c) Dander, J. E.; Weires, N. A.; Garg, N. K. *Org. Lett*. **2016**, *18*, 3934–3936. (d) Shi, S.; Szostak, M. *Chem. Eur. J.* **2016**, *22*, 10420–10424. (e) Liu, L.; Chen, P.; Sun, Y.; Wu, Y.; Chen, S.; Zhu, J.; Zhao, Y. *J. Org. Chem.* **2016**, *81*, 11686–11696.

(6) For Pd-catalyzed reactions of amide derivatives to build C–C bonds, see: (a) Li, X.; Zou, G. *Chem. Commun.* **2015**, *51*, 5089–5092. (b) Li, X.; Zou, G. *J. Organomet. Chem.* **2015**, *794*, 136–145. (c) Yada, A.; Okajima, S.; Murakami, M. *J. Am. Chem. Soc.* **2015**, *137*, 8708–8711. (d) Meng, G.; Szostak, M. *Org. Lett.* **2015**, *17*, 4364–4367. (e) Meng, G.; Szostak, M. *Org. Biomol. Chem.* **2016**, *14*, 5690–5705. (f) Liu, C.; Meng, G.; Liu, Y.; Liu, R.; Lalancette, R.; Szostak, R.; Szostak, M. *Org. Lett.* **2016**, *18*, 4194–4197. (g) Meng, G.; Shi, S.; Szostak, M. *ACS Catal.* **2016**, *6*, 7335–7339. (h) Cui, M.; Wu, H.; Jian, J.; Wang, H.; Liu, C.; Daniel, S.; Zeng, Z. *Chem. Commun.* **2016**, *52*, 12076–12079.

(7) For decarbonylative couplings of amide derivatives, see: (a) Meng, G.; Szostak, M. *Angew. Chem., Int. Ed.* **2015**, *54*, 14518–14522. (b) Hu, J.; Zhao, Y.; Zhang, Y.; Shi, Z. *Angew. Chem., Int. Ed.* **2016**, *55*, 8718–8722. (c) Shi, S.; Meng, G.; Szostak, M. *Angew. Chem., Int. Ed.* **2016**, *55*, 6959–6963. (d) Shi, S.; Szostak, M. *Org. Lett.* **2016**, *18*, 5872–5875. (e) Liu, C.; Meng, G.; Szostak, M. *J. Org. Chem.* **2016**, *81*, 12023–12030. (f) Yue, H.; Guo, L.; Liao, H.-H.; Cai, Y.; Zhu, C.; Rueping, M. *Angew. Chem., Int. Ed.* **2017**, *56*, 4282–4285.

(8) For pertinent reviews, see: (a) Meng, G.; Shi, S.; Szostak, M. *Synlett* **2016**, *27*, 2530–2540. (b) Dander, J. E.; Garg, N. K. *ACS Catal.* **2017**, *7*, 1413–1423. (c) Liu, C.; Szostak, M. *Chem. Eur. J.* [Online early access]. DOI: 10.1002/chem.201605012.

(9) Miles, K. C.; Le, C. C.; Stambuli, J. P. *Chem. Eur. J.* **2014**, *20*, 11336–11339.

(10) For the Pd-catalyzed Mizoroki–Heck cyclization of thioesters to give ortho-quinone methide products, see: Thottumkara, A. P.; Kurokawa, T.; Du Bois, J. *Chem. Sci.* **2013**, *4*, 2686-2689.

(11) (a) Negishi, E.-I.; Copéret, C.; Ma, S.; Mita, T.; Sugihara, T.; Tour, J. M. *J. Am. Chem. Soc.* **1996**, *118*, 5904–5918. (b) Hayashi, T.; Tang, J.; Kato, K. *Org. Lett.* **1999**, *1*, 1487–1489. (c) Wu, X.-F.; Neumann, H.; Spannenberg, A.; Schulz, T.; Jiao, H.; Beller, M. *J. Am. Chem. Soc.* **2010**, *132*, 14596–14602. (d) Goegsig, T. M.; Nielsen, D. U.; Lindhardt, A. T.; Skrydstrup, T. *Org. Lett.* **2012**, *14*, 2536–2539.

(12) Amide derivatives are considered to be ideally suited for use as synthons in chemical synthesis because of their directing group ability and stability to a variety of reaction conditions.

(13) For pertinent reviews concerning nickel catalysis, see: (a) Rosen, B. M.; Quasdorf, K. W.; Wilson, D. A.; Zhang, N.; Resmerita, A.-M.; Garg, N. K.; Percec, V. *Chem. Rev.* **2011**, *111*, 1346−1416. (b) Tasker, S. Z.; Standley, E. A.; Jamison, T. F. *Nature* **2014**, *509*, 299−309. (c) Mesganaw, T.; Garg, N. K. *Org. Process Res. Dev.* **2013**, *17*, 29−39. (d) Ananikov, V. P. *ACS Catal*. **2015**, *5*, 1964−1971.

(14) Substrates described in this manuscript were derived from commercially available 2-halobenzoic acid derivatives and readily available allylic electrophiles, either via lithiation/displacement or reductive coupling methodologies (see the Experimental Section). For reductive couplings, see: (a) Weix, D. J.; *Acc. Chem. Res.* **2015**, *48*, 1767–1775. (b) Anka-Lufford, L. L.; Prinsell, M. R.; Weix, D. J. *J. Org. Chem.* **2012**, *77*, 9989–10000. (c) Cui, X.;

Wang, S.; Zhang, Y.; Deng, W.; Qian, Q.; Gong, H. *Org. Biomol. Chem.* **2013**, *11*, 3094–3097. (d) Hansen, E. C.; Pedro, D. J.; Wotal, A. C.; Gower, N. J.; Nelson, J. D.; Caron, S.; Weix, D. J. *Nat. Chem.* **2016**, *8*, 1226–1230.

(15) Other classes of amide derivatives were also evaluated, such as *N*-Me,Ph, *N*-Me,Ts, *N*-Ph,Boc, *N*-Ph,Ts. However, these efforts either led to no product or the Mizoroki–Heck cyclization product in diminished yields. Similarly, efforts to generate 6- or 7-membered ring products were unsuccessful.

(16) Extensive variations in bases (e.g. Cs_2CO_3, K_3PO_4, NaH), ligands (e.g. terpyridine, IMes, Benz-I*t*Bu), solvents (DME, DMA, $PhCF_3$), Ni and ligand loadings, and temperature were explored.

(17) NHC precursors **7.7**–**7.9** are commercially available.

(18) Additives such as morpholine, aniline, Et_2NH, and 1-hexanol were also tested. Of all additives examined, *t*-amyl alcohol proved most successful. For the use of alcohols as additives in Ni-catalyzed cross couplings, see: Harris, M. R.; Hanna, L. E.; Greene, M. A.; Moore, C. E.; Jarvo, E. R. *J. Am. Chem. Soc.* **2013**, *135*, 3303–3306.

(19) (a) Using entry 7 conditions, cyclized product **7.6** was obtained in 74% isolated yield, respectively. Product **7.6** is volatile as described in the Experimental Section. (b) Product **7.6** could also be obtained in comparable yield by Mizoroki–Heck cyclization of the *N*-*n*Bu,Boc derivative of **7.5**, thus demonstrating that this methodology is not restricted to *N*-benzyl amide derivatives.

(20) For the Ni-catalyzed Mizoroki–Heck cyclization of *aryl* halides, albeit without tetrasubstituted olefins, see: Desrosiers, J.-N.; Hie, L.; Biswas, S.; Zatalochnaya, O. V.;

Rodriguez, S.; Lee, H.; Grinberg, N.; Haddad, N.; Yee, N. K.; Garg, N. K.; Senanayake, C. *Angew. Chem., Int. Ed.* **2016**, *55*, 11921–11924; see also references therein.

(21) For examples of Mizoroki–Heck reactions involving tetrasubstituted olefins, see: (a) Shuler, S. A.; Yin, G.; Krause, S. B.; Vesper, C. M.; Watson, D. A. *J. Am. Chem. Soc*. **2016**, *138*, 13830–13833. (b) Seo, J. H.; Liu, P.; Weinreb, S. M. *J. Org. Chem*. **2010**, *75*, 2667–2680. (c) Liu, P.; Seo, J. H.; Weinreb, S. M. *Angew. Chem., Int. Ed*. **2010**, *49*, 2000–2003. (d) Abelman, M. M.; Oh, T.; Overman, L. E. *J. Org. Chem*. **1987**, *52*, 4130–4133. (e) Madin, A.; O'Donnell, C. J.; Oh, T.; Old, D. W.; Overman, L. E.; Sharp, M. J. *J. Am. Chem. Soc*. **2005**, *127*, 18054–18065.

(22) 2-Vinylindanones bearing quaternary stereocenters can also be synthesized by the Pd- or Ni-catalyzed α-vinylation of lithium enolates; see (a) Huang, J.; Bunel, E.; Faul, M. M. *Org. Lett*. **2007**, *9*, 4343–4346. (b) Grigalunas, M.; Ankner, T.; Norrby, P.-O.; Wiest, O.; Helquist, P. *Org. Lett.* **2014**, *16*, 3970–3973. (c) Grigalunas, M.; Ankner, T.; Norrby, P.-O.; Wiest, P. Helquist, O. *J. Am. Chem. Soc*. **2015**, *137*, 7019–7022. (d) Chieffi, A.; Kamikawa, K.; Ahman, J.; Fox, J. M.; Buchwald, S. L. *Org. Lett*. **2001**, *3*, 1897–1900.

(23) A substrate containing a phenyl (Ph) group at the R' position was also tested, but was deemed unreactive.

(24) This substrate was employed as a 7:1 mixture of *E* to *Z* olefins.

(25) See the Experimental Section for details.

(26) (a) Böhm, H.-J.; Banner, D.; Bendels, S.; Kansy, M.; Kuhn, B.; Müller, K.; Obst-Sander, U.; Stahl, M. *ChemBioChem*, **2004**, *5*, 637–643. (b) Wang, J.; Sánchez-Roselló, M.; Aceña, J. L.; del Pozo, C.; Sorochinsky, A. E.; Fustero, S.; Soloshonok, V. A.; Liu, H. *Chem. Rev.* **2014**, *114*,

2432–2506. (c) Gillis, E. P.; Eastman, K. J.; Hill, M. D.; Donnelly, D. J.; Meanwell, N. A. *J. Med. Chem.* **2015**, *58*, 8315–8359.

(27) This substrate was employed as a 4:1 mixture of *E* to *Z* olefins.

(28) Based on calculated rotational energies for conformers of 3-methyl-1-butene and allylic strain arguments, **TS7.2** is estimated to be roughly 0.7 kcal/mol higher in energy compared to **TS7.1**. For a review, see: Hoffmann, R. W. *Chem. Rev.* **1989**, *89*, 1841–1860.

(29) Querolle, O.; Dubois, J.; Thoret, S.; Roussi, F.; Guéritte, F.; Guénard, D. *J. Med. Chem.* **2004**, *47*, 5937–5944.

(30) Clennan, E. L.; Chen, X. *J. Am. Chem. Soc.* **1989**, *111*, 5787–5792.

(31) Tanaka, K.; Uneme, H.; Ono, N.; Kaji, A. *Chem. Lett*. **1979**, *9*, 1039–1040.

(32) Friese, A.; Hell-Momeni, K.; Zundorf, I.; Winckler, T.; Dingermann, T.; Dannhardt, G. *J. Med. Chem*. **2002**, *45*, 1535–1542.

(33) Shimano, M.; Kamei, N.; Tanaka, T.; Harada, T.; Haino, M.; Okuyama, A.; Arakawa, Y. Murakami, Y. Reverse Hydroxamic Acid Derivatives. Eur. Pat. Appl. 1431285. June 23rd, 2004.

(34) Sato, K.; Sugimoto, H.; Rikimaru, K.; Imoto, H.; Kamaura, M.; Negoro, N.; Tsujihata, Y.; Miyashita, H.; Odani, T.; Murata, T. *Bioorg. Med. Chem.* **2014**, *22*, 1649–1666.

(35) (a) Mori, M.; Kaneta, N.; Isono, N.; Shibasaki, M. *J. Organomet. Chem*. **1993**, *455*, 255–260. (b) Kotha, S.; Mandal, K.; Tiwari, A.; Mobin, S. M. *Chem. Eur. J*. **2006**, *12*, 8024–8038.

(36) Van Zyl. C. M.; McKeeby, J. L.; Van Dort, P. C.; Larson, E. J.; Silver, M. E. *Inorg. Chim. Acta*. **1987**, *133*, 289–294.